Evolution of Protoplanetary Disks in the Orion A Star-Forming Region

by

Kyoung Hee Kim

Submitted in Partial Fulfillment
of the Requirements for the Degree

Doctor of Philosophy

Supervised by
Prof. Dan M. Watson

Department of Physics and Astronomy
Arts, Sciences and Engineering
School of Arts and Sciences

University of Rochester
Rochester, New York

2013

Dedication

To my family, my friends, my colleagues, and to the Universe.

Biographical Sketch

Kyoung Hee Kim was born in Incheon, Republic of Korea. She attended Kongju National University, and graduated with a Bachelor of Science degree in Earth science education. She entered as a junior at Korea University and achieved another Bachelor of Science degree in Physics. She majored in High energy particle physics in the Master's program at Korea University and graduated with a Master of Science degree in February, 2002. After taking the M.S. degree, she received a fellowship for the Research Intern Program awarded from the Korea Science and Engineering Foundation in 2002. She began doctoral studies in Physics and Astronomy at the University of Rochester in 2003. She received the Master of Science degree from the University of Rochester in 2005. She pursued her research in Astrophysics under the direction of Prof. Dan M. Watson.

The following publications were a result of work conducted during doctoral study:

- "Transitional disks and their origins: an infrared spectroscopic survey of Orion A", **Kim, K. H.**, Watson, Dan M., Manoj, P., et al. 2013, ApJ, 769, 149

• "A Spitzer IRS Survey of NGC 1333: Insights into disk evolution from a very young cluster", Arnold, L. A., Watson, Dan M., **Kim, K. H.**, Manoj, P., Remming, I., et al. 2012, ApJS, 201, 12A

• "The Spitzer Infrared Spectrograph Survey of T Tauri Stars in Taurus", Furlan, E., Luhman, K. L., Espaillat, C., D'Alessio, P., Adame, L., Manoj, P., **Kim, K. H.**, et al. 2011, ApJS, 195, 3

• "Spitzer Infrared Spectrograph survey of young stars in the Chamaeleon I star-forming region", Manoj, P., **Kim, K. H.**, Furlan, E., McClure, M. K., Luhman, K. L., et al. 2011, ApJS, 193, 11

• "GGD 37: An Extreme Protostellar Outflow", Green, J. D., et al. 2011, ApJ, 726L, 1

• "V819 Tau: A Rare Weak-lined T Tauri Star with A Weak Infrared Excess", Furlan, E., Forrest, W. J., Sargent, B. A., Manoj, P., **Kim, K. H.**, et al. 2009, ApJ, 706, 1194

• "Disk Evolution in the Three Nearby Star-forming Regions of Taurus, Chamaeleon, and Ophiuchus", Furlan, E., et al. 2009, ApJ, 703, 1164

• "Mid-infrared Spectra of Transitional DIsks in the Chamaeleon I Cloud", **Kim, K. H.**, Watson, Dan M., Manoj, P., et al. 2009, ApJ, 700, 1017

• "Dust Processing and Grain Growth in Protoplanetary Disks in the Taurus-Auriga Star-Forming Region", Sargent, B. A., et al. 2009, ApJS, 182, 477

• "Crystalline Silicates and Dust Processing in the Protoplanetary Disks of the Taurus Young Cluster", Watson, Dan M., et al. 2009, ApJS, 180, 84

• "Silica in Protoplanetary Disks" Sargent, B. A., et al. 2009, ApJ, 690, 1193

• "Erratum: "Spitzer IRS Spectroscopy of IRAS-Discovered Debris Disks" (ApJS, 166, 351, [2006])", Chen, C. H., Sargent, B. A., Bohac, C., **Kim, K. H.**, et al. 2008, ApJS, 177, 417

• "The Dust and Gas Around β Pictoris", Chen, C. H., Li, A., Bohac, C., **Kim, K. H.**, et al. 2007, ApJ, 666, 466

• "The development of a protoplanetary disk from its natal envelope", Watson, Dan M., et al. 2007, Nature, 448, 1026

• "Spitzer Observations of HH 54 and HH 7-11: Mapping the H_2 Ortho-to-Para Ratio in Shocked Molecular Gas", Neufeld, D. A., et al. 2006, ApJ, 649, 816

• "Spitzer IRS Spectroscopy of IRAS-discovered Debris Disks", Chen, C. H., Sargent, B. A., Bohac, C., **Kim, K. H.**, et al. 2006, ApJS, 166, 351

• "Dust Processing in Disks around T Tauri Stars", Sargent, B. A., et al. 2006, ApJ, 645, 395

• "Spitzer Space Telescope Studies of the Fomalhaut Debris Disk. II. Resolving the Ring at 70 μm", Stapelfeldt, K. R., et al. 2005, prpl.conf, V, 8620

• "Grain Processing in T Tauri Disks", Forrest, W. J., et al. 2005, IAUS, 235P, 110F

Acknowledgments

I thank my parents who always stay in my heart, for they let me grow freely but responsibly. Even though they were humble farmers who did not have a chance to undertake high-level education, their wisdom, creativity, and love stimulated me to grow into a person who follows her own dreams.

I thank my advisor, Prof. Dan Watson, who patiently supported me for ten years. Without his support and encouragement, especially when I was in doubt of my future research capability due to pregnancy and being a student mom, I would have not been able to finish the Ph.D. He always encouraged me and guided me to be a good researcher as well as allowed me freedom to step forward to grow as an independent researcher. I, also, thank Prof. Bill Forrest for his guidance and continuous support. I learned so many things from his sincere and enthusiastic attitude to scientific study and learning. I would like to thank Dr. Joan Najita who not only has shared valuable discussions and ideas but also has encouraged and supported my search for the next step in my research career. I also want to give my thanks to Dr. Elise Furlan and Dr. Benjamin Sargent for many suggestions and comments through my work. I learned a lot not only from their comments but also from their diligent manner and reliability. I would like to thank Dr. Manoj Puravankara for his enormous

practical help shown as a postdoc, as well as his friendship. I would also like to thank Dr. Joel Green and Melissa McClure, with whom I worked closely when they were at the University of Rochester. I appreciate Patrick Sheehan and Ian Remming, who helped me a lot to improve data reduction for the work in this thesis. Many thanks go to Laura Arnold who spent many nights at the Mauna Kea observatory with me, not only for her time but also her humanity and friendship. I would like to thank many members of the IRS Disks team for their help and advice: Prof. Catherine Espaillat, Prof. Nuria Calvet, Dr. James Muzerolle, and Prof. Tom Megeath. I also thank Prof. John Tarduno, Prof. Adam Frank, Prof. Eric Mamajek, and Prof. Alice Quillen for serving on my qualifying exam and Ph.D defense committees.

I thank the members of Korean Catholic Church Community in Rochester for generosity and warmth. Special thanks go to the staff and teachers at the Children's Center of Brighton for taking care of my daughter Bona for 5 years. Without their consistent care for Bona, I would not have been able to finish this work even in ten years.

I thank my sincere friends, Sunyoung and Jeongim, in Korea. And I thank my brothers, Seunghoi and Myunghoi, and my sister, Jihee, who have always had confident in me. I am deeply grateful to my parents-in-law who always pray for me, Hyup Woo, and Bona.

Finally, I express my love and thanks to my family. Some say that this work would have been done three years faster without them. However, I cannot imagine my life without my family. I thank Hyup Woo and Bona for struggling through some tough times together and for sharing many happy moments of

life.

Abstract

In this dissertation we investigate the characteristics of Class II protoplanetary disks in Orion A star-forming region. Our major goal is to analyze a large sample of protoplanetary disks with near- and mid-IR spectra, by statistical approaches, to understand protoplanetary disk evolution in Orion A. The topics with which we deal include the following: (1) Environmental and age effects on the evolution of protoplanetary disks; (2) Giant planet formation in the transitional disks of Orion A: a statistical study of correlations among disk and stellar properties; (3) The impact of extreme UV radiation on the protoplanetary disks near the Trapezium. For this work, 303 protoplanetary disks in Orion A region observed by IRS/Spitzer and the follow-up observation of 120 objects from SpeX/IRTF are used to reveal the characteristics of Class II disks in Orion A.

For clues on environmental effects on disk evolution and planet formation, we compare the disk properties and dust properties of Orion A disks to that of Taurus disks and examine trends with respect to position within Orion A. We extract spectral indices, equivalent widths, and integrated fluxes from IRS spectra of Class II objects in Orion A which pertain to disk structure and dust composition. We measure mass accretion rates using hydrogen recombination

lines in SpeX spectra of our targets. Utilizing the properties, we analyze the general distribution of properties of disks in ONC, L1641, and Taurus from their histograms.

Our main findings are as follows:

• Transitional disks – those protoplanetary disks for which deficits of infrared excess signify sharp-edged gaps in the dust distribution – are produced gravitationally by companions to the central star. The vast majority of the companions (<10 M_J) must be of giant-planetary mass, rather than stellar- or brown-dwarf mass.

• Orion A is the youngest large nearby association of YSOs surveyed with *Spitzer*. However, its disks have vertical structure similar to those of Taurus, Ophiuchus and Chamaeleon, which range up to five times the age of Orion A. The transitional-disk fraction is at least as large in Orion as in any association in the 0.5–5 Myr age range obtained by main-sequence fitting. Thus giant-planet formation and dust sedimentation is well under way, if not complete, even in the youngest Class II objects.

• Less grain processing – crystallization and growth of grains to diameter of 1–10 μm – has occurred among the dust grains in the Orion A disks than in Taurus. The time scales for dust processing must therefore lie in the range of ages of the nearby clouds like Orion, NGC 1333, Taurus, Ophiuchus and Chamaeleon.

• As others have found for the Trapezium region of Orion, the disks of the surrounding Orion Nebular Cluster suffer reduced emission at long infrared wavelengths. The reduction tracks distance from the most luminous Trapez-

ium star, θ^1 Ori C, so this appears to be the effect of UV oblation of the outer part of the disks. In contrast, the parts of L1641 more distant from θ^1 Ori C have long-λ colors, and thus radial extent, similar to the disks of the fiducial Taurus association.

• Even low-mass and low-luminosity young stars (M type) have abundant complex organic molecular material in their surrounding disks. We see this material *via* PAH emission at 6–14 μm, excited externally by UV from the Trapezium stars. As is the case for PAHs in the disks around Ae stars, these molecules' emission features differ from those of interstellar PAHs, in ways that many indicate that they have recently been released from ice mantles of large grains. They appear to be excited by single UV photon absorption, as is the case for PAH features arising in other environments.

Contributors and Funding Sources

This work was supervised by Professor Dan M. Watson (advisor) and Professor William J. Forrest in the Department of Physics and Astronomy. This work is based on observations made with the *Spitzer Space Telescope*, which is operated by the Jet Propulsion Laboratory, California Institute of Technology under NASA contract 1407. Support for this work was provided by NASA through Contract Number 1257184 issued by JPL/Caltech, and Cornell subcontracts 31419-5714 to the University of Rochester. The author was a visiting astronomer at the Infrared Telescope Facility, which is operated by the University of Hawaii under Cooperative Agreement no. NNX-08AE38A with the National Aeronautics and Space Administration, Science Mission Directorate, Planetary Astronomy Program. Part of analyzed IRS data used in Chapter 4 were borrowed from our team's analysis by McClure et al. (2010) for data in Ophiuchus, and Furlan et al. (2011), Manoj et al. (2011), and Arnold et al. (2012) for data in Taurus, Chamaeleon I, and NGC 1333, the articles which are listed in the Biographical Sketch. All other work conducted for the dissertation, beside described above and the following acknowledgments for adopting photometry data, was completed by the author independently.

• The UKIDSS project is defined in Lawrence et al (2007). UKIDSS uses the UKIRT Wide Field Camera (WFCAM; Casali et al, 2007). The photometric system is described in Hewett et al (2006), and the calibration is described in Hodgkin et al. (2009). The pipeline processing and science archive are described in Irwin et al (2009, in prep) and Hambly et al (2008).

• Funding for SDSS-III has been provided by the Alfred P. Sloan Foundation, the Participating Institutions, the National Science Foundation, and the U.S. Department of Energy Office of Science. The SDSS-III web site is http://www.sdss3.org/.

SDSS-III is managed by the Astrophysical Research Consortium for the Participating Institutions of the SDSS-III Collaboration including the University of Arizona, the Brazilian Participation Group, Brookhaven National Laboratory, University of Cambridge, Carnegie Mellon University, University of Florida, the French Participation Group, the German Participation Group, Harvard University, the Instituto de Astrofisica de Canarias, the Michigan State/Notre Dame/JINA Participation Group, Johns Hopkins University, Lawrence Berkeley National Laboratory, Max Planck Institute for Astrophysics, Max Planck Institute for Extraterrestrial Physics, New Mexico State University, New York University, Ohio State University, Pennsylvania State University, University of Portsmouth, Princeton University, the Spanish Participation Group, University of Tokyo, University of Utah, Vanderbilt University, University of Virginia, University of Washington, and Yale University.

• This publication makes use of data products from the Wide-field Infrared Survey Explorer, which is a joint project of the University of California, Los

Angeles, and the Jet Propulsion Laboratory/California Institute of Technology, funded by the National Aeronautics and Space Administration.

• This publication makes use of data products from the Two Micron All Sky Survey, which is a joint project of the University of Massachusetts and the Infrared Processing and Analysis Center/California Institute of Technology, funded by the National Aeronautics and Space Administration and the National Science Foundation.

• The DENIS project has been partly funded by the SCIENCE and the HCM plans of the European Commission under grants CT920791 and CT940627. It is supported by INSU, MEN and CNRS in France, by the State of Baden-Württemberg in Germany, by DGICYT in Spain, by CNR in Italy, by FFwF-BWF in Austria, by FAPESP in Brazil, by OTKA grants F-4239 and F-013990 in Hungary, and by the ESO C&EE grant A-04-046.

Jean Claude Renault from IAP was the Project manager. Observations were carried out thanks to the contribution of numerous students and young scientists from all involved institutes, under the supervision of P. Fouqué, survey astronomer resident in Chile.

"This research has made use of the VizieR catalogue access tool, CDS, Strasbourg, France". The original description of the VizieR service was published in Ochsenbein et al. (2000).

The production of the XMM catalogue is a collaborative project involving the whole SSC Consortium:

University of Leicester, UK Mullard Space Science Laboratory, University College London, UK Institute of Astronomy, Cambridge, UK Max-Planck

Institut fu"r extraterrestrische Physik, Germany Astrophysikalisches Institut Potsdam, Germany Service d'Astrophysique, CEA/DSM/DAPNIA, Saclay, France Centre d'Etude Spatiale des Rayonnements, Toulouse, France Observatoire Astronomique de Strasbourg, France Instituto de Fisica de Cantabria, Santander, Spain Osservatorio Astronomico di Brera, Milan, Italy

The SSC team is pleased to acknowledge the contributions to the SAS software, on which the catalogue processing is based, made by ESA's Science Operations Centre staff. Significant contributions to the earlier-mission software and data-processing activities were also made by NASA Goddard Space Flight Centre HEASARC staff resident for a substantial time at the University of Leicester. The quality of the pipeline products and the catalogue itself were ensured by the dedicated and sustained efforts of the screening team: Hermann Brunner (MPE), Marcella Brusa (MPE), Maite Ceballos (IFCA), Stephanie Dupuy (CESR), Sean Farrell (CESR), Federico Fraschetti (CEA), Georg Lamer (AIP), Anja Schroeder (LUX), Mark Simpson (LUX), Giorgia Sironi (OAB, LUX), Ann-Marie Stobbart (LUX).

Table of Contents

Dedication **ii**

Biographical Sketch **iii**

Acknowledgments **vi**

Abstract **ix**

Contributors and Funding Sources **xii**

List of Tables **xx**

List of Figures **xliii**

1 Introduction **1**

2 Observation and Data Reduction **8**

2.1 IRS/Spitzer 8

2.2 SpeX/IRTF 44

3 Properties of Protoplanetary Disks in Orion A **51**

3.1 Basic Characteristics 51

3.2 Disk Properties 75
3.3 The Degree of Dust Processing 81
3.4 Comparison of Disk and Dust Features by Sub-Regions to Taurus 84
3.5 Median Spectra 94
3.6 Summary 97

4 Transitional Disks and their Origin 98
4.1 Introduction 98
4.2 Transitional Disks: Selection Criteria and their Variety 102
4.3 Radial Properties of Transitional Disks: R_{wall} 123
4.4 Frequency 131
4.5 Distribution and Trends among Properties 136
4.6 Mechanisms for the Origins of Transitional Disks and Constraints158
4.7 Summary and Conclusions 167

5 Disk Evolution 169
5.1 Comparisons of the distribution of properties between FD and TD 169
5.2 Correlations 182
5.3 Summary 203

6 The Evolution of Protoplanetary Disks in an OB Association 205
6.1 Introduction 205
6.2 Disks in Subsections 207
6.3 Summary 230

7 Polycyclic Aromatic Hydrocarbon (PAH) Molecules in the Disks around Low Mass Stars 231

7.1 Introduction 231

7.2 The Objects with PAHs 233

7.3 Analysis 234

7.4 Discussion 242

7.5 Summary 251

References 253

A Appendix to Chapter 3 269

A.1 SEDs of Class II disks in Orion A: observed in full IRS wavelength range, 5-35 μm 269

A.2 SEDs of Class II disks in Orion A: observed in partial IRS wavelength coverage, 5-14 μm 301

A.3 Tables 308

B Appendix to Chapter 4 360

B.1 Consideration of $\dot{M}$ and $\dot{M}_W$ from XPE 360

B.2 Trends of TDs in Orion A 363

C Appendix to Chapter 5 366

C.1 Trends 366

C.2 Significant Correlations 757

D Appendix to Chapter 6 759

D.1 Distribution of EW10, F_{10}, and $F_{11.3}/F_{9.8}$ by Distance from θ^1 Ori C 759

E Appendix to Chapter 7 **766**

E.1 Relative Integrated Fluxes vs. T_{eff} and Distance (d) from θ^1 Ori C 766

List of Tables

2.1 Observation and Reduction Log of IRS Spectra 16
2.1 Observation and Reduction Log of IRS Spectra 17
2.1 Observation and Reduction Log of IRS Spectra 18
2.1 Observation and Reduction Log of IRS Spectra 19
2.1 Observation and Reduction Log of IRS Spectra 20
2.1 Observation and Reduction Log of IRS Spectra 21
2.1 Observation and Reduction Log of IRS Spectra 22
2.1 Observation and Reduction Log of IRS Spectra 23
2.1 Observation and Reduction Log of IRS Spectra 24
2.1 Observation and Reduction Log of IRS Spectra 25
2.1 Observation and Reduction Log of IRS Spectra 26
2.1 Observation and Reduction Log of IRS Spectra 27
2.1 Observation and Reduction Log of IRS Spectra 28
2.1 Observation and Reduction Log of IRS Spectra 29
2.1 Observation and Reduction Log of IRS Spectra 30
2.1 Observation and Reduction Log of IRS Spectra 31
2.1 Observation and Reduction Log of IRS Spectra 32

2.2 Identifications of the Objects 33
2.2 Identifications of the Objects 34
2.2 Identifications of the Objects 35
2.2 Identifications of the Objects 36
2.2 Identifications of the Objects 37
2.2 Identifications of the Objects 38
2.2 Identifications of the Objects 39
2.2 Identifications of the Objects 40
2.2 Identifications of the Objects 41
2.2 Identifications of the Objects 42
2.2 Identifications of the Objects 43
2.3 Observation log of SpeX spectra 46
2.3 Observation log of SpeX spectra 47
2.3 Observation log of SpeX spectra 48
2.3 Observation log of SpeX spectra 49
2.3 Observation log of SpeX spectra 50

3.1 Spectral Type and Extinction 58
3.2 K-S test for the visual extinction distribution 59
3.3 Basic Stellar Properties I 73
3.4 Median of $\log L_X$ 73
3.5 Basic Stellar Properties II 74
3.6 Wavelength Ranges of Anchors for Spectral Indices 76
3.7 Spectral Indices 77
3.8 Grain Properties 83

4.1 Subclassification of TDs 120
4.1 Subclassification of TDs 121
4.1 Subclassification of TDs 122
4.2 Stellar and Disk Properties 126
4.2 Stellar and Disk Properties 127
4.2 Stellar and Disk Properties 128
4.2 Stellar and Disk Properties 129
4.2 Stellar and Disk Properties 130
4.3 number of transitional disks and age trend 133
4.4 Correlation summary I 155
4.5 Correlation summary II: details by subtypes of TDs 156
4.5 Correlation summary II: details by subtypes of TDs 157

5.1 Distribution of Properties: FD versus TD 171
5.2 Distribution of Properties Comparison to Taurus:FD and TD 181
5.3 Significance of correlations I: disks in ONC with known spectral types 189
5.4 Significance of correlations II: disks in L1641 with known spectral types 190
5.5 Group A. Properties with Significant Correlation in Any Case (Known Spectral types only) 191
5.6 Group B. Properties with Significant Correlation in both TD and FD dominantly in one of L1641 or ONC (Known Spectral types only) 193

5.7 Group C. Properties observed Correlation Changes between FD and TD in both L1641 and ONC (Known Spectral types only) 195

5.8 Group D. Properties observed Correlation Changes between FD and TD dominantly one of L1641 and ONC (Known Spectral types only) 199

6.1 n_{20-31} and d from θ^1 Ori C 220

6.1 n_{20-31} and d from θ^1 Ori C 221

6.1 n_{20-31} and d from θ^1 Ori C 222

6.1 n_{20-31} and d from θ^1 Ori C 223

6.1 n_{20-31} and d from θ^1 Ori C 224

6.1 n_{20-31} and d from θ^1 Ori C 225

6.1 n_{20-31} and d from θ^1 Ori C 226

6.1 n_{20-31} and d from θ^1 Ori C 227

6.1 n_{20-31} and d from θ^1 Ori C 228

6.1 n_{20-31} and d from θ^1 Ori C 229

7.1 List of Objects 235

7.2 Integrated Fluxes 239

7.3 Center Positions of PAH features 241

A.1 Spectral Type and Extinction 309

A.1 Spectral Type and Extinction 310

A.1 Spectral Type and Extinction 311

A.1 Spectral Type and Extinction 312

A.1 Spectral Type and Extinction 313
A.1 Spectral Type and Extinction 314
A.1 Spectral Type and Extinction 315
A.1 Spectral Type and Extinction 316
A.2 Basic Stellar Properties 319
A.2 Basic Stellar Properties 320
A.2 Basic Stellar Properties 321
A.2 Basic Stellar Properties 322
A.2 Basic Stellar Properties 323
A.2 Basic Stellar Properties 324
A.2 Basic Stellar Properties 325
A.2 Basic Stellar Properties 326
A.3 Basic Stellar Properties 327
A.3 Basic Stellar Properties 328
A.3 Basic Stellar Properties 329
A.3 Basic Stellar Properties 330
A.3 Basic Stellar Properties 331
A.3 Basic Stellar Properties 332
A.3 Basic Stellar Properties 333
A.4 Basic Stellar Properties 334
A.4 Basic Stellar Properties 335
A.4 Basic Stellar Properties 336
A.4 Basic Stellar Properties 337
A.4 Basic Stellar Properties 338

A.4 Basic Stellar Properties 339
A.4 Basic Stellar Properties 340
A.4 Basic Stellar Properties 341
A.4 Basic Stellar Properties 342
A.4 Basic Stellar Properties 343
A.4 Basic Stellar Properties 344
A.4 Basic Stellar Properties 345
A.4 Basic Stellar Properties 346
A.4 Basic Stellar Properties 347
A.4 Basic Stellar Properties 348
A.5 Basic Stellar Properties 349
A.5 Basic Stellar Properties 350
A.5 Basic Stellar Properties 351
A.5 Basic Stellar Properties 352
A.5 Basic Stellar Properties 353
A.5 Basic Stellar Properties 354
A.5 Basic Stellar Properties 355
A.5 Basic Stellar Properties 356
A.5 Basic Stellar Properties 357
A.5 Basic Stellar Properties 358
A.5 Basic Stellar Properties 359

B.1 Correlation summary III: TDs in Orion A 364
B.2 Correlation summary IV: details by subtypes of TDs in Orion A 365

C.1 $M_\star$ vs. $L_\star$ (I) 368
C.2 $M_\star$ vs. $L_\star$ (II) 368
C.3 n_{K-6} vs. n_{6-13} (I) 370
C.4 n_{K-6} vs. n_{6-13} (II) 370
C.5 n_{K-6} vs. n_{13-31} (I) 372
C.6 n_{K-6} vs. n_{13-31} (II) 372
C.7 n_{K-6} vs. EW10μm (I) 374
C.8 n_{K-6} vs. EW10μm (II) 374
C.9 n_{K-6} vs. $EW20(\mu\mathrm{m})$ (I) 376
C.10 n_{K-6} vs. $EW20(\mu\mathrm{m})$ (II) 376
C.11 n_{K-6} vs. $EW33(\mu\mathrm{m})$ (I) 378
C.12 n_{K-6} vs. $EW33(\mu\mathrm{m})$ (II) 378
C.13 n_{K-6} vs. $F_{11.3}/F_{9.8}$ (I) 380
C.14 n_{K-6} vs. $F_{11.3}/F_{9.8}$ (II) 380
C.15 n_{K-6} vs. F_{20}/F_{10} (I) 382
C.16 n_{K-6} vs. F_{20}/F_{10} (II) 382
C.17 n_{K-6} vs. $\log F_{10}$ (I) 384
C.18 n_{K-6} vs. $\log F_{10}$ (II) 384
C.19 n_{K-6} vs. $\log F_{20}$ (I) 386
C.20 n_{K-6} vs. $\log F_{20}$ (II) 386
C.21 n_{K-6} vs. $\log L_\star$ (I) 388
C.22 n_{K-6} vs. $\log L_\star$ (II) 388
C.23 n_{K-6} vs. $M_\star$ (I) 390
C.24 n_{K-6} vs. $M_\star$ (II) 390

C.25 n_{6-13} vs. n_{13-31} (I) 392
C.26 n_{6-13} vs. n_{13-31} (II) 392
C.27 n_{6-13} vs. EW10 (μm) (I) 394
C.28 n_{6-13} vs. EW10 (μm) (II) 394
C.29 n_{6-13} vs. EW20 (μm) (I) 396
C.30 n_{6-13} vs. EW20 (μm) (II) 396
C.31 n_{6-13} vs. EW33 (μm) (I) 398
C.32 n_{6-13} vs. EW33 (μm) (II) 398
C.33 n_{6-13} vs. $F_{11.3}/F_{9.8}$ (I) 400
C.34 n_{6-13} vs. $F_{11.3}/F_{9.8}$ (II) 400
C.35 n_{6-13} vs. F_{20}/F_{10} (I) 402
C.36 n_{6-13} vs. F_{20}/F_{10} (II) 402
C.37 n_{6-13} vs. $\log F_{10}$ (I) 404
C.38 n_{6-13} vs. $\log F_{10}$ (II) 404
C.39 n_{6-13} vs. $\log F_{20}$ (I) 406
C.40 n_{6-13} vs. $\log F_{20}$ (II) 406
C.41 n_{6-13} vs. $\log L_\star$ (I) 408
C.42 n_{6-13} vs. $\log L_\star$ (II) 408
C.43 n_{6-13} vs. $\log M_\star$ (I) 410
C.44 n_{6-13} vs. $\log M_\star$ (II) 410
C.45 n_{13-31} vs. EW10 (μm) (I) 412
C.46 n_{13-31} vs. EW10 (μm) (II) 412
C.47 n_{13-31} vs. EW20 (μm) (I) 414
C.48 n_{13-31} vs. EW20 (μm) (II) 414

C.49 n_{13-31} vs. EW33 (μm) (I) 416
C.50 n_{13-31} vs. EW33 (μm) (II) 416
C.51 n_{13-31} vs. $F_{11.3}/F_{9.8}$ (I) 418
C.52 n_{13-31} vs. $F_{11.3}/F_{9.8}$ (II) 418
C.53 n_{13-31} vs. F_{20}/F_{10} (I) 420
C.54 n_{13-31} vs. F_{20}/F_{10} (II) 420
C.55 n_{13-31} vs. $\log F_{10}$ (I) 422
C.56 n_{13-31} vs. $\log F_{10}$ (II) 422
C.57 n_{13-31} vs. $\log F_{20}$ (I) 424
C.58 n_{13-31} vs. $\log F_{20}$ (II) 424
C.59 n_{13-31} vs. $L_\star$ (I) 426
C.60 n_{13-31} vs. $\log L_\star$ (II) 426
C.61 n_{13-31} vs. $\log M_\star$ (I) 428
C.62 n_{13-31} vs. $\log M_\star$ (II) 428
C.63 EW10 vs. EW20 (I) 430
C.64 EW10 vs. EW20 (II) 430
C.65 EW10 vs. EW33 (I) 432
C.66 EW10 vs. EW33 (II) 432
C.67 EW10 vs. $F_{11.3}/F_{9.8}$ (I) 434
C.68 EW10 vs. $F_{11.3}/F_{9.8}$ (II) 434
C.69 EW10 vs. F_{20}/F_{10} (I) 436
C.70 EW10 vs. F_{20}/F_{10} (II) 436
C.71 EW10 vs. $\log F_{10}$ (I) 438
C.72 EW10 vs. $\log F_{10}$ (II) 438

C.73 EW10 vs. $\log F_{20}$ (I) 440
C.74 EW10 vs. $\log F_{20}$ (II) 440
C.75 EW10 vs. $\log L_\star$ (I) 442
C.76 EW10 vs. $\log L_\star$ (II) 442
C.77 EW10 vs. $M_\star$ (I) 444
C.78 EW10 vs. $M_\star$ (II) 444
C.79 EW20 vs. EW33 (I) 446
C.80 EW20 vs. EW33 (II) 446
C.81 EW20 vs $F_{11.3}/F_{9.8}$ (I) 448
C.82 EW20 vs $F_{11.3}/F_{9.8}$ (II) 448
C.83 EW20 vs. F_{20}/F_{10} (I) 450
C.84 EW20 vs. F_{20}/F_{10} (II) 450
C.85 EW20 vs. $\log F_{10}$ (I) 452
C.86 EW20 vs. $\log F_{10}$ (II) 452
C.87 EW20 vs. $\log F_{20}$ (I) 454
C.88 EW20 vs. $\log F_{20}$ (II) 454
C.89 EW20 vs. $\log L_\star$ (I) 456
C.90 EW20 vs. $\log L_\star$ (II) 456
C.91 EW20 vs. $\log M_\star$ (I) 458
C.92 EW20 vs. $\log M_\star$ (II) 458
C.93 EW33 vs. $F_{11.3}/F_{9.8}$ (I) 460
C.94 EW33 vs. $F_{11.3}/F_{9.8}$ (II) 460
C.95 EW33 vs. F_{20}/F_{10} (I) 462
C.96 EW33 vs. F_{20}/F_{10} (II) 462

C.97 EW33 vs. $\log F_{10}$ (I) 464
C.98 EW33 vs. $\log F_{10}$ (II) 464
C.99 EW33 vs. $\log F_{20}$ (I) 466
C.100 EW33 vs. $\log F_{20}$ (II) 466
C.101 EW33 vs. $\log L_\star$ (I) 468
C.102 EW33 vs. $\log L_\star$ (II) 468
C.103 EW33 vs. $\log M_\star$ (I) 470
C.104 EW33 vs. $\log M_\star$ (II) 470
C.105 $F_{11.3}/F_{9.8}$ vs. F_{20}/F_{10} (I) 472
C.106 $F_{11.3}/F_{9.8}$ vs. F_{20}/F_{10} (II) 472
C.107 $F_{11.3}/F_{9.8}$ vs. $\log F_{10}$ (I) 474
C.108 $F_{11.3}/F_{9.8}$ vs. $\log F_{10}$ (II) 474
C.109 $F_{11.3}/F_{9.8}$ vs. $\log F_{20}$ (I) 476
C.110 $F_{11.3}/F_{9.8}$ vs. $\log F_{20}$ (II) 476
C.111 $F_{11.3}/F_{9.8}$ vs. $\log L_\star$ (I) 478
C.112 $F_{11.3}/F_{9.8}$ vs. $\log L_\star$ (II) 478
C.113 $F_{11.3}/F_{9.8}$ vs. $\log M_\star$ (I) 480
C.114 $F_{11.3}/F_{9.8}$ vs. $\log M_\star$ (II) 480
C.115 F_{20}/F_{10} vs. $\log F_{10}$ (I) 482
C.116 F_{20}/F_{10} vs. $\log F_{10}$ (II) 482
C.117 F_{20}/F_{10} vs. $\log F_{20}$ (I) 484
C.118 F_{20}/F_{10} vs. $\log F_{20}$ (II) 484
C.119 F_{20}/F_{10} vs. $\log L_\star$ (I) 486
C.120 F_{20}/F_{10} vs. $\log L_\star$ (II) 486

C.121 F_{20}/F_{10} vs. $\log M_\star$ (I) 488
C.122 F_{20}/F_{10} vs. $\log M_\star$ (II) 488
C.123 $\log F_{10}$ vs. $\log F_{20}$ (I) 490
C.124 $\log F_{10}$ vs. $\log F_{20}$ (II) 490
C.125 $\log F_{10}$ vs. $\log L_\star$ (I) 492
C.126 $\log F_{10}$ vs. $\log L_\star$ (II) 492
C.127 $\log F_{10}$ vs. $\log M_\star$ (I) 494
C.128 $\log F_{10}$ vs. $\log M_\star$ (II) 494
C.129 $\log F_{20}$ vs. $\log L_\star$ (I) 496
C.130 $\log F_{20}$ vs. $\log L_\star$ (II) 496
C.131 $\log F_{20}$ vs. $\log M_\star$ (I) 498
C.132 $\log F_{20}$ vs. $\log M_\star$ (II) 498
C.133 $F_{11.3}$ vs. n_{K-6} (I) 500
C.134 $F_{11.3}$ vs. n_{K-6} (II) 500
C.135 $F_{11.3}$ vs. n_{6-13} (I) 502
C.136 $F_{11.3}$ vs. n_{6-13} (II) 502
C.137 $F_{11.3}$ vs. n_{13-31} (I) 504
C.138 $F_{11.3}$ vs. n_{13-31} (II) 504
C.139 $F_{11.3}$ vs. EW10 (I) 506
C.140 $F_{11.3}$ vs. EW10 (II) 506
C.141 $F_{11.3}$ vs. EW20 (I) 508
C.142 $F_{11.3}$ vs. EW20 (II) 508
C.143 $F_{11.3}$ vs. EW33 (I) 510
C.144 $F_{11.3}$ vs. EW33 (II) 510

C.145 $F_{11.3}$ vs. $F_{11.3}/F_{9.8}$ (I) 512
C.146 $F_{11.3}$ vs. $F_{11.3}/F_{9.8}$ (II) 512
C.147 $F_{11.3}$ vs. F_{20}/F_{10} (I) 514
C.148 $F_{11.3}$ vs. F_{20}/F_{10} (II) 514
C.149 $F_{11.3}$ vs. $\log F_{10}$ (I) 516
C.150 $F_{11.3}$ vs. $\log F_{10}$ (II) 516
C.151 $F_{11.3}$ vs. $\log F_{20}$ (I) 518
C.152 $F_{11.3}$ vs. $\log F_{20}$ (II) 518
C.153 $F_{11.3}$ vs. $\log L_{\star}$ (I) 520
C.154 $F_{11.3}$ vs. $\log L_{\star}$ (II) 520
C.155 $F_{11.3}$ vs. $\log M_{\star}$ (I) 522
C.156 $F_{11.3}$ vs. $\log M_{\star}$ (II) 522
C.157 $F_{9.8}$ vs. $F_{11.3}$ (I) 524
C.158 $F_{9.8}$ vs. $F_{11.3}$ (II) 524
C.159 $F_{9.8}$ vs. n_{K-6} (I) 526
C.160 $F_{9.8}$ vs. n_{K-6} (II) 526
C.161 $F_{9.8}$ vs. n_{6-13} (I) 528
C.162 $F_{9.8}$ vs. n_{6-13} (II) 528
C.163 $F_{9.8}$ vs. n_{13-31} (I) 530
C.164 $F_{9.8}$ vs. n_{13-31} (II) 530
C.165 $F_{9.8}$ vs. EW10 (I) 532
C.166 $F_{9.8}$ vs. EW10 (II) 532
C.167 $F_{9.8}$ vs. EW20 (I) 534
C.168 $F_{9.8}$ vs. EW20 (II) 534

C.169 $F_{9.8}$ vs. EW33 (I) 536
C.170 $F_{9.8}$ vs. EW33 (II) 536
C.171 $F_{9.8}$ vs. $F_{11.3}/F_{9.8}$ (I) 538
C.172 $F_{9.8}$ vs. $F_{11.3}/F_{9.8}$ (II) 538
C.173 $F_{9.8}$ vs. F_{20}/F_{10} (I) 540
C.174 $F_{9.8}$ vs. F_{20}/F_{10} (II) 540
C.175 $F_{9.8}$ vs. $\log F_{10}$ (I) 542
C.176 $F_{9.8}$ vs. $\log F_{10}$ (II) 542
C.177 $F_{9.8}$ vs. $\log F_{20}$ (I) 544
C.178 $F_{9.8}$ vs. $\log F_{20}$ (II) 544
C.179 $F_{9.8}$ vs. $\log L_{\star}$ (I) 546
C.180 $F_{9.8}$ vs. $\log L_{\star}$ (II) 546
C.181 $F_{9.8}$ vs. $\log M_{\star}$ (I) 548
C.182 $F_{9.8}$ vs. $\log M_{\star}$ (II) 548
C.183 n_{K-6} vs. $\log \dot{M}$ (I) 550
C.184 n_{K-6} vs. $\log \dot{M}$ (II) 550
C.185 n_{6-13} vs. $\log \dot{M}$ (I) 552
C.186 n_{6-13} vs. $\log \dot{M}$ (II) 552
C.187 n_{13-31} vs. $\log \dot{M}$ (I) 554
C.188 n_{13-31} vs. $\log \dot{M}$ (II) 554
C.189 EW10 vs. $\log \dot{M}$ (I) 556
C.190 EW10 vs. $\log \dot{M}$ (II) 556
C.191 EW20 vs. $\log \dot{M}$ (I) 558
C.192 EW20 vs. $\log \dot{M}$ (II) 558

C.193 EW33 vs. $\log \dot{M}$ (I) 560
C.194 EW33 vs. $\log \dot{M}$ (II) 560
C.195 $F_{11.3}/F_{9.8}$ vs. $\log \dot{M}$ (I) 562
C.196 $F_{11.3}/F_{9.8}$ vs. $\log \dot{M}$ (II) 562
C.197 $F_{11.3}$ vs. $\log \dot{M}$ (I) 564
C.198 $F_{11.3}$ vs. $\log \dot{M}$ (II) 564
C.199 $F_{9.8}$ vs. $\log \dot{M}$ (I) 566
C.200 $F_{9.8}$ vs. $\log \dot{M}$ (II) 566
C.201 F_{20}/F_{10} vs. $\log \dot{M}$ (I) 568
C.202 F_{20}/F_{10} vs. $\log \dot{M}$ (II) 568
C.203 $\log F_{10}$ vs. $\log \dot{M}$ (I) 570
C.204 $\log F_{10}$ vs. $\log \dot{M}$ (II) 570
C.205 $\log F_{20}$ vs. $\log \dot{M}$ (I) 572
C.206 $\log F_{20}$ vs. $\log \dot{M}$ (II) 572
C.207 $\log L_\star$ vs. $\log \dot{M}$ (I) 574
C.208 $\log L_\star$ vs. $\log \dot{M}$ (II) 574
C.209 $\log M_\star$ vs. $\log \dot{M}$ (I) 576
C.210 $\log M_\star$ vs. $\log \dot{M}$ (II) 576
C.211 n_{K-6} vs. $\log L_X 8$ (I) 578
C.212 n_{K-6} vs. $\log L_X 8$ (II) 578
C.213 n_{6-13} vs. $\log L_X 8$ (I) 580
C.214 n_{6-13} vs. $\log L_X 8$ (II) 580
C.215 n_{13-31} vs. $\log L_X 8$ (I) 582
C.216 n_{13-31} vs. $\log L_X 8$ (II) 582

C.217 EW10 vs. $\log L_X8$ (I) 584
C.218 EW10 vs. $\log L_X8$ (II) 584
C.219 EW20 vs. $\log L_X8$ (I) 586
C.220 EW20 vs. $\log L_X8$ (II) 586
C.221 EW33 vs. $\log L_X8$ (I) 588
C.222 EW33 vs. $\log L_X8$ (II) 588
C.223 $F_{11.3}/F_{9.8}$ vs. $\log L_X8$ (I) 590
C.224 $F_{11.3}/F_{9.8}$ vs. $\log L_X8$ (II) 590
C.225 $F_{11.3}$ vs. $\log L_X8$ (I) 592
C.226 $F_{11.3}$ vs. $\log L_X8$ (II) 592
C.227 $F_{9.8}$ vs. $\log L_X8$ (I) 594
C.228 $F_{9.8}$ vs. $\log L_X8$ (II) 594
C.229 F_{20}/F_{10} vs. $\log L_X8$ (I) 596
C.230 F_{20}/F_{10} vs. $\log L_X8$ (II) 596
C.231 $\log F_{10}$ vs. $\log L_X8$ (I) 598
C.232 $\log F_{10}$ vs. $\log L_X8$ (II) 598
C.233 $\log F_{20}$ vs. $\log L_X8$ (I) 600
C.234 $\log F_{20}$ vs. $\log L_X8$ (II) 600
C.235 $\log L_\star$ vs. $\log L_X8$ (I) 602
C.236 $\log L_\star$ vs. $\log L_X8$ (II) 602
C.237 $\log M_\star$ vs. $\log L_X8$ (I) 604
C.238 $\log M_\star$ vs. $\log L_X8$ (II) 604
C.239 n_{K-6} vs. $\log L_X1$ (I) 606
C.240 n_{K-6} vs. $\log L_X1$ (II) 606

C.241 n_{6-13} vs. $\log L_X 1$ (I) 608
C.242 n_{6-13} vs. $\log L_X 1$ (II) 608
C.243 n_{13-31} vs. $\log L_X 1$ (I) 610
C.244 n_{13-31} vs. $\log L_X 1$ (II) 610
C.245 EW10 vs. $\log L_X 1$ (I) 612
C.246 EW10 vs. $\log L_X 1$ (II) 612
C.247 EW20 vs. $\log L_X 1$ (I) 614
C.248 EW20 vs. $\log L_X 1$ (II) 614
C.249 EW33 vs. $\log L_X 1$ (I) 616
C.250 EW33 vs. $\log L_X 1$ (II) 616
C.251 $F_{11.3}/F_{9.8}$ vs. $\log L_X 1$ (I) 618
C.252 $F_{11.3}/F_{9.8}$ vs. $\log L_X 1$ (II) 618
C.253 $F_{11.3}$ vs. $\log L_X 1$ (I) 620
C.254 $F_{11.3}$ vs. $\log L_X 1$ (II) 620
C.255 $F_{9.8}$ vs. $\log L_X 1$ (I) 622
C.256 $F_{9.8}$ vs. $\log L_X 1$ (II) 622
C.257 F_{20}/F_{10} vs. $\log L_X 1$ (I) 624
C.258 F_{20}/F_{10} vs. $\log L_X 1$ (II) 624
C.259 $\log F_{10}$ vs. $\log L_X 1$ (I) 626
C.260 $\log F_{10}$ vs. $\log L_X 1$ 626
C.261 $\log F_{20}$ vs. $\log L_X 1$ (I) 628
C.262 $\log F_{20}$ vs. $\log L_X 1$ (II) 628
C.263 $\log L_\star$ vs. $\log L_X 1$ (I) 630
C.264 $\log L_\star$ vs. $\log L_X 1$ (II) 630

C.265 $\log M_\star$ vs. $\log L_X1$ (I) 632
C.266 $\log M_\star$ vs. $\log L_X1$ (II) 632
C.267 n_{K-6} vs. $\log L_X2$ (I) 634
C.268 n_{K-6} vs. $\log L_X2$ (II) 634
C.269 n_{6-13} vs. $\log L_X2$ (I) 636
C.270 n_{6-13} vs. $\log L_X2$ (II) 636
C.271 n_{13-31} vs. $\log L_X2$ (I) 638
C.272 n_{13-31} vs. $\log L_X2$ (II) 638
C.273 EW10 vs. $\log L_X2$ (I) 640
C.274 EW10 vs. $\log L_X2$ (II) 640
C.275 EW20 vs. $\log L_X2$ (I) 642
C.276 EW20 vs. $\log L_X2$ (II) 642
C.277 EW33 vs. $\log L_X2$ (I) 644
C.278 EW33 vs. $\log L_X2$ (II) 644
C.279 $F_{11.3}/F_{9.8}$ vs. $\log L_X2$ (I) 646
C.280 $F_{11.3}/F_{9.8}$ vs. $\log L_X2$ (II) 646
C.281 $F_{11.3}$ vs. $\log L_X2$ (I) 648
C.282 $F_{11.3}$ vs. $\log L_X2$ (II) 648
C.283 $F_{9.8}$ vs. $\log L_X2$ (I) 650
C.284 $F_{9.8}$ vs. $\log L_X2$ (II) 650
C.285 F_{20}/F_{10} vs. $\log L_X2$ (I) 652
C.286 F_{20}/F_{10} vs. $\log L_X2$ (II) 652
C.287 $\log F_{10}$ vs. $\log L_X2$ (I) 654
C.288 $\log F_{10}$ vs. $\log L_X2$ (II) 654

C.289 $\log F_{20}$ vs. $\log L_X 2$ (I) 656
C.290 $\log F_{20}$ vs. $\log L_X 2$ (II) 656
C.291 $\log L_\star$ vs. $\log L_X 2$ (I) 658
C.292 $\log L_\star$ vs. $\log L_X 2$ (II) 658
C.293 $\log M_\star$ vs. $\log L_X 2$ (I) 660
C.294 $\log M_\star$ vs. $\log L_X 2$ (II) 660
C.295 n_{K-6} vs. $\log L_X 3$ (I) 662
C.296 n_{K-6} vs. $\log L_X 3$ (II) 662
C.297 n_{6-13} vs. $\log L_X 3$ (I) 664
C.298 n_{6-13} vs. $\log L_X 3$ (II) 664
C.299 n_{13-31} vs. $\log L_X 3$ (I) 666
C.300 n_{13-31} vs. $\log L_X 3$ (II) 666
C.301 EW10 vs. $\log L_X 3$ (I) 668
C.302 EW10 vs. $\log L_X 3$ (II) 668
C.303 EW20 vs. $\log L_X 3$ (I) 670
C.304 EW20 vs. $\log L_X 3$ (II) 670
C.305 EW33 vs. $\log L_X 3$ (I) 672
C.306 EW33 vs. $\log L_X 3$ (II) 672
C.307 $F_{11.3}/F_{9.8}$ vs. $\log L_X 3$ (I) 674
C.308 $F_{11.3}/F_{9.8}$ vs. $\log L_X 3$ (II) 674
C.309 $F_{11.3}$ vs. $\log L_X 3$ (I) 676
C.310 $F_{11.3}$ vs. $\log L_X 3$ (II) 676
C.311 $F_{9.8}$ vs. $\log L_X 3$ (I) 678
C.312 $F_{9.8}$ vs. $\log L_X 3$ (II) 678

C.313 F_{20}/F_{10} vs. $\log L_X3$ (I) 680
C.314 F_{20}/F_{10} vs. $\log L_X3$ (II) 680
C.315 $\log F_{10}$ vs. $\log L_X3$ (I) 682
C.316 $\log F_{10}$ vs. $\log L_X3$ (II) 682
C.317 $\log F_{20}$ vs. $\log L_X3$ (I) 684
C.318 $\log F_{20}$ vs. $\log L_X3$ (II) 684
C.319 $\log L_\star$ vs. $\log L_X3$ (I) 686
C.320 $\log L_\star$ vs. $\log L_X3$ (II) 686
C.321 $\log M_\star$ vs. $\log L_X3$ (I) 688
C.322 $\log M_\star$ vs. $\log L_X3$ (II) 688
C.323 n_{K-6} vs. $\log L_X4$ (I) 690
C.324 n_{K-6} vs. $\log L_X4$ (II) 690
C.325 n_{6-13} vs. $\log L_X4$ (I) 692
C.326 n_{6-13} vs. $\log L_X4$ (II) 692
C.327 n_{13-31} vs. $\log L_X4$ (I) 694
C.328 n_{13-31} vs. $\log L_X4$ (II) 694
C.329 EW10 vs. $\log L_X4$ (I) 696
C.330 EW10 vs. $\log L_X4$ (II) 696
C.331 EW20 vs. $\log L_X4$ (I) 698
C.332 EW20 vs. $\log L_X4$ (II) 698
C.333 EW33 vs. $\log L_X4$ (I) 700
C.334 EW33 vs. $\log L_X4$ (II) 700
C.335 $F_{11.3}/F_{9.8}$ vs. $\log L_X4$ (I) 702
C.336 $F_{11.3}/F_{9.8}$ vs. $\log L_X4$ (II) 702

C.337 $F_{11.3}$ vs. $\log L_X4$ (I) 704
C.338 $F_{11.3}$ vs. $\log L_X4$ (II) 704
C.339 $F_{9.8}$ vs. $\log L_X4$ (I) 706
C.340 $F_{9.8}$ vs. $\log L_X4$ (II) 706
C.341 F_{20}/F_{10} vs. $\log L_X4$ (I) 708
C.342 F_{20}/F_{10} vs. $\log L_X4$ (II) 708
C.343 $\log F_{10}$ vs. $\log L_X4$ (I) 710
C.344 $\log F_{10}$ vs. $\log L_X4$ (II) 710
C.345 $\log F_{20}$ vs. $\log L_X4$ (I) 712
C.346 $\log F_{20}$ vs. $\log L_X4$ (II) 712
C.347 $\log L_\star$ vs. $\log L_X4$ (I) 714
C.348 $\log L_\star$ vs. $\log L_X4$ (II) 714
C.349 $\log M_\star$ vs. $\log L_X4$ (I) 716
C.350 $\log M_\star$ vs. $\log L_X4$ (II) 716
C.351 n_{K-6} vs. $\log L_X5$ (I) 718
C.352 n_{K-6} vs. $\log L_X5$ (II) 718
C.353 L_X5 vs. n_{6-13} (I) 720
C.354 n_{6-13} vs. $\log L_X5$ (II) 720
C.355 n_{13-31} vs. $\log L_X5$ (I) 722
C.356 n_{13-31} vs. $\log L_X5$ (II) 722
C.357 EW10 vs. $\log L_X5$ (I) 724
C.358 EW10 vs. $\log L_X5$ (II) 724
C.359 EW20 vs. $\log L_X5$ (I) 726
C.360 EW20 vs. $\log L_X5$ (II) 726

C.361 EW33 vs. $\log L_X5$ (I) 728
C.362 EW33 vs. $\log L_X5$ (II) 728
C.363 $F_{11.3}/F_{9.8}$ vs. $\log L_X5$ (I) 730
C.364 $F_{11.3}/F_{9.8}$ vs. $\log L_X5$ (II) 730
C.365 $F_{11.3}$ vs. $\log L_X5$ (I) 732
C.366 $F_{11.3}$ vs. $\log L_X5$ (II) 732
C.367 $F_{9.8}$ vs. $\log L_X5$ (I) 734
C.368 $F_{9.8}$ vs. $\log L_X5$ (II) 734
C.369 F_{20}/F_{10} vs. $\log L_X5$ (I) 736
C.370 F_{20}/F_{10} vs. $\log L_X5$ (II) 736
C.371 $\log F_{10}$ vs. $\log L_X5$ (I) 738
C.372 $\log F_{10}$ vs. $\log L_X5$ (II) 738
C.373 $\log F_{20}$ vs. $\log L_X5$ (I) 740
C.374 $\log F_{20}$ vs. $\log L_X5$ (II) 740
C.375 $\log L_\star$ vs. $\log L_X5$ (I) 742
C.376 $\log L_\star$ vs. $\log L_X5$ (II) 742
C.377 $\log M_\star$ vs. $\log L_X5$ (I) 744
C.378 $\log M_\star$ vs. $\log L_X5$ (II) 744
C.379 $\log L_X8$ vs $\log \dot{M}$ (I) 746
C.380 $\log L_X8$ vs $\log \dot{M}$ (II) 746
C.381 $\log L_X1$ vs $\log \dot{M}$ (I) 748
C.382 $\log L_X1$ vs $\log \dot{M}$ (II) 748
C.383 $\log L_X2$ vs $\log \dot{M}$ (I) 750
C.384 $\log L_X2$ vs $\log \dot{M}$ (II) 750

C.385 $\log L_X 3$ vs $\log \dot{M}$ (I) 752

C.386 $\log L_X 3$ vs $\log \dot{M}$ (II) 752

C.387 $\log L_X 4$ vs $\log \dot{M}$ (I) 754

C.388 $\log L_X 4$ vs $\log \dot{M}$ (II) 754

C.389 $\log L_X 5$ vs $\log \dot{M}$ (I) 756

C.390 $\log L_X 5$ vs $\log \dot{M}$ (II) 756

C.391 Significance of correlations III: disks in ONC regardless of spectral type information 757

C.392 Significance of correlations IV: disks in L1641regardless of spectral type information 758

List of Figures

1.1 YSO Classification 2

1.2 Spitzer's images of Orion A 5

2.1 Targets in ONC 13

2.2 Targets in L1641 14

2.3 Targets in Trapezium 15

3.1 Spectral typing from SpeX spectra 53

3.2 Spectral type distribution 55

3.3 $J - H$ vs. $H - K$ color-color diagram 57

3.4 A_V distribution 60

3.5 De-reddened SEDs (SLLL) 64

3.6 De-reddened SEDs of disks (SL only) 65

3.7 Histogram of $L_\star$ 66

3.8 Evolutionary Track 67

3.9 Histogram of $M_\star$ 68

3.10 Example of $\dot{M}$ measurement 70

3.11 Histogram of $\dot{M}$ 71

3.12 Histograms of L_X 72
3.13 n_{5-12}-n_{K-25} 79
3.14 n_{5-12}-n_{12-20} 80
3.15 Histogram of n_{K-6} 86
3.16 Histogram of n_{6-13} 87
3.17 Histogram of EW10 88
3.18 Histogram of $F_{11.3}/F_{9.8}$ 89
3.19 Histograms of n_{13-31} 90
3.20 Histograms of EW20 and EW33 91
3.21 Histogram of $F_{9.8}$ and $F_{11.3}$ 92
3.22 Histogram of F_{10}, F_{20}, and F_{20}/F_{10} 93
3.23 Median spectra compared to Taurus median. 96

4.1 TD selection: Orion A 105
4.2 TD selection: other region 107
4.3 SEDs of TDs in Orion A 108
4.3 Figure 4.3 109
4.3 Figure 4.3 110
4.3 Figure 4.3 111
4.3 Figure 4.3 112
4.4 Ternary plot of n_{K-6}, n_{13-31}, and EW10 116
4.5 n_{13-31} and EW10 vs. IDEF 117
4.6 TD selection criteria from literature 119
4.7 Skeptical diagram of R_{wall} 125
4.8 Example of R_{wall} estimation 125

4.9 Fraction of TDs 132
4.10 Spectral types of TDs 134
4.11 R_{wall} distribution of TDs 135
4.12 $\dot{M}$ distribution of TDs 139
4.13 Trends among $M_\star$, $\dot{M}$ and L_X 144
4.14 Trends related to R_{wall} 145
4.15 $\dot{M}$–$M_\star$ and L_X–$M_\star$ 146
4.16 $\dot{M}$-R_{wall} 149
4.17 L_X-R_{wall} 150
4.18 $\dot{M}$-L_X 151
4.19 $\dot{M}$ and R_{wall} under a constant R_{wall} 154
4.20 TDs over the predictions by X-ray photoevaporation I 161
4.21 TDs over the predictions by X-ray photoevaporation II . . . 162

5.1 Distribution of $M_\star$ and $L_\star$ (FD vs. TD) 174
5.2 Distribution of spectral indices (FD vs. TD) 175
5.3 Distribution of equivalent widths (FD vs. TD) 176
5.4 Distribution of integrated fluxes (FD vs. TD) 177
5.5 Distribution of grain progression index (FD vs. TD) 178
5.6 Distribution of $\dot{M}$ (FD vs. TD) 179
5.7 Distribution of L_X (FD vs. TD) 180
5.8 n_{K-6} between OriA and Taurus 182
5.9 n_{6-13} between OriA and Taurus 183
5.10 n_{13-31} between OriA and Taurus 184
5.11 EW10 between OriA and Taurus 185

5.12 $F_{11.3}/F_{9.8}$ between OriA and Taurus 186
5.13 Group A. 192
5.14 Group B. 194
5.15 Group C. 196
5.15 Figure 5.15 197
5.16 Group D. 200
5.16 Figure 5.16 201
5.16 Figure 5.16 202

6.1 Subsections of ONC 206
6.2 Subsections of L1641 207
6.3 Grid of the median spectra (Full) 209
6.4 Grid of the median spectra (Part) 210
6.5 Histograms of n_{20-31} in each subsection 212
6.6 n_{20-31} versus D 213
6.7 Histograms of n_{13-31} in each subsection 214
6.8 n_{13-31} versus D 215
6.9 Histograms of EW20 in each subsection 216
6.10 EW20 versus D 217
6.11 Histograms of F_{20}in each subsection 218
6.12 F_{20} versus D 219

7.1 Objects of PAHs in disks on IRAC ch2 image 234
7.2 PAH disk continuum 236
7.3 PAH disk continuum 2 237

7.4 PAH features 238
7.5 PAH classification 240
7.6 Comparison to other sources1 243
7.7 Comparison to other sources2 244
7.8 I_{PAH} vs. T_{eff} 245
7.9 I_{PAH} vs. d 246
7.10 PAH center positions 248
7.11 PAH Relative Flux Ratio 250
7.12 Flux Ratio vs. T_{eff} and D 252

A.1 De-reddened SEDs (SLLL) 270
A.1 Figure A.1 cont. 271
A.1 Figure A.1 cont. 272
A.1 Figure A.1 cont. 273
A.1 Figure A.1 cont. 274
A.1 Figure A.1 cont. 275
A.1 Figure A.1 cont. 276
A.1 Figure A.1 cont. 277
A.1 Figure A.1 cont. 278
A.1 Figure A.1 cont. 279
A.1 Figure A.1 cont. 280
A.1 Figure A.1 cont. 281
A.1 Figure A.1 cont. 282
A.1 Figure A.1 cont. 283
A.1 Figure A.1 cont. 284

A.1 Figure A.1 cont. 285
A.1 Figure A.1 cont. 286
A.1 Figure A.1 cont. 287
A.1 Figure A.1 cont. 288
A.1 Figure A.1 cont. 289
A.1 Figure A.1 cont. 290
A.1 Figure A.1 cont. 291
A.1 Figure A.1 cont. 292
A.1 Figure A.1 cont. 293
A.1 Figure A.1 cont. 294
A.1 Figure A.1 cont. 295
A.1 Figure A.1 cont. 296
A.1 Figure A.1 cont. 297
A.1 Figure A.1 cont. 298
A.1 Figure A.1 cont. 299
A.1 Figure A.1 cont. 300
A.2 De-reddened SEDs of disks (SL only) 302
A.2 Figure A.2 cont. 303
A.2 Figure A.2 cont. 304
A.2 Figure A.2 cont. 305
A.2 Figure A.2 cont. 306
A.2 Figure A.2 cont. 307

B.1 $\dot{M}$ vs. L_X of TDs versus M_W vs. L_X from XPE 362

C.1 $M_\star$ vs. $L_\star$ 367
C.2 n_{K-6} vs. n_{6-13} 369
C.3 n_{K-6} vs. n_{13-31} 371
C.4 n_{K-6} vs. EW10μm 373
C.5 n_{K-6} vs. $EW20(\mu\mathrm{m})$ 375
C.6 n_{K-6} vs. EW33 (μm) 377
C.7 n_{K-6} vs. $F_{11.3}/F_{9.8}$ 379
C.8 n_{K-6} vs. F_{20}/F_{10} 381
C.9 n_{K-6} vs. $\log F_{10}$ 383
C.10 n_{K-6} vs. $\log F_{20}$ 385
C.11 n_{K-6} vs. $\log L_\star$ 387
C.12 n_{K-6} vs. $\log M_\star$ 389
C.13 n_{6-13} vs. n_{13-31} 391
C.14 n_{6-13} vs. EW10 (μm) 393
C.15 n_{6-13} vs. EW20 (μm) 395
C.16 n_{6-13} vs. EW33 (μm) 397
C.17 n_{6-13} vs. $F_{11.3}/F_{9.8}$ 399
C.18 n_{6-13} vs. F_{20}/F_{10} 401
C.19 n_{6-13} vs. $\log F_{10}$ 403
C.20 n_{6-13} vs. $\log F_{20}$ 405
C.21 n_{6-13} vs. $\log L_\star$ 407
C.22 n_{6-13} vs. $\log M_\star$ 409
C.23 n_{13-31} vs. EW10 (μm) 411
C.24 n_{13-31} vs. EW20 (μm) 413

C.25 n_{13-31} vs. EW33 (μm) 415
C.26 n_{13-31} vs. $F_{11.3}/F_{9.8}$ 417
C.27 n_{13-31} vs. F_{20}/F_{10} 419
C.28 n_{13-31} vs. $\log F_{10}$ 421
C.29 n_{13-31} vs. $\log F_{20}$ 423
C.30 n_{13-31} vs. $\log L_{\star}$ 425
C.31 n_{13-31} vs. $\log M_{\star}$ 427
C.32 EW10 vs. EW20 429
C.33 EW10 vs. EW33 431
C.34 EW10 vs. $F_{11.3}/F_{9.8}$ 433
C.35 EW10 vs. F_{20}/F_{10} 435
C.36 EW10 vs. $\log F_{10}$ 437
C.37 EW10 vs. $\log F_{20}$ 439
C.38 EW10 vs. $L_{\star}$ 441
C.39 EW10 vs. $M_{\star}$ 443
C.40 EW20 vs. EW33 445
C.41 EW20 vs $\mathrm{F_{11.3}/F_{9.8}}$ 447
C.42 EW20 vs. $\mathrm{F_{20}/F_{10}}$ 449
C.43 EW20 vs. $\log F_{10}$ 451
C.44 EW20 vs. $\log F_{20}$ 453
C.45 EW20 vs. $\mathrm{logL_{\star}}$ 455
C.46 EW20 vs. $\mathrm{logM_{\star}}$ 457
C.47 EW33 vs. $\mathrm{F_{11.3}/F_{9.8}}$ 459
C.48 EW33 vs. $\mathrm{F_{20}/F_{10}}$ 461

C.49 EW33 vs. $\log F_{10}$ 463
C.50 EW33 vs. $\log F_{20}$ 465
C.51 EW33 vs. $\log L_\star$ 467
C.52 EW33 vs. $\log M_\star$ 469
C.53 $F_{11.3}/F_{9.8}$ vs. F_{20}/F_{10} 471
C.54 $F_{11.3}/F_{9.8}$ vs. $\log F_{10}$ 473
C.55 $F_{11.3}/F_{9.8}$ vs. $\log F_{20}$ 475
C.56 $F_{11.3}/F_{9.8}$ vs. $\log L_\star$ 477
C.57 $F_{11.3}/F_{9.8}$ vs. $\log M_\star$ 479
C.58 F_{20}/F_{10} vs. $\log F_{10}$ 481
C.59 F_{20}/F_{10} vs. $\log F_{20}$ 483
C.60 F_{20}/F_{10} vs. $\log L_\star$ 485
C.61 F_{20}/F_{10} vs. $\log M_\star$ 487
C.62 $\log F_{10}$ vs. $\log F_{20}$ 489
C.63 $\log F_{10}$ vs. $\log L_\star$ 491
C.64 $\log F_{10}$ vs. $\log M_\star$ 493
C.65 $\log F_{20}$ vs. $\log L_\star$ 495
C.66 $\log F_{20}$ vs. $\log M_\star$ 497
C.67 $F_{11.3}$ vs. n_{K-6} 499
C.68 $F_{11.3}$ vs. n_{6-13} 501
C.69 $F_{11.3}$ vs. n_{13-31} 503
C.70 $F_{11.3}$ vs. EW10 505
C.71 $F_{11.3}$ vs. EW20 507
C.72 $F_{11.3}$ vs. EW33 509

C.73 $F_{11.3}$ vs. $F_{11.3}/F_{9.8}$ 511
C.74 $F_{11.3}$ vs. F_{20}/F_{10} 513
C.75 $F_{11.3}$ vs. F_{10} 515
C.76 $F_{11.3}$ vs. F_{20} 517
C.77 $F_{11.3}$ vs. $L_\star$ 519
C.78 $F_{11.3}$ vs. $M_\star$ 521
C.79 $F_{9.8}$ vs. $F_{11.3}$ 523
C.80 $F_{9.8}$ vs. n_{K-6} 525
C.81 $F_{9.8}$ vs. n_{6-13} 527
C.82 $F_{9.8}$ vs. n_{13-31} 529
C.83 $F_{9.8}$ vs. EW10 531
C.84 $F_{9.8}$ vs. EW20 533
C.85 $F_{9.8}$ vs. EW33 535
C.86 $F_{9.8}$ vs. $F_{11.3}/F_{9.8}$ 537
C.87 $F_{9.8}$ vs. F_{20}/F_{10} 539
C.88 $F_{9.8}$ vs. F_{10} 541
C.89 $F_{9.8}$ vs. $\log F_{20}$ 543
C.90 $F_{9.8}$ vs. $L_\star$ 545
C.91 $F_{9.8}$ vs. $M_\star$ 547
C.92 n_{K-6} vs. $\dot{M}$ 549
C.93 n_{6-13} vs. $\dot{M}$ 551
C.94 n_{13-31} vs. $\dot{M}$ 553
C.95 EW10 vs. $\dot{M}$ 555
C.96 EW20 vs. $\dot{M}$ 557

C.97 EW33 vs. $\dot{M}$ 559
C.98 $F_{11.3}/F_{9.8}$ vs. $\dot{M}$ 561
C.99 $F_{11.3}$ vs. $\dot{M}$ 563
C.100 $F_{9.8}$ vs. $\dot{M}$ 565
C.101 F_{20}/F_{10} vs. $\dot{M}$ 567
C.102 F_{10} vs. $\dot{M}$ 569
C.103 F_{20} vs. $\dot{M}$ 571
C.104 $L_\star$ vs. $\dot{M}$ 573
C.105 $M_\star$ vs. $\dot{M}$ 575
C.106 n_{K-6} vs. L_X8 577
C.107 n_{6-13} vs. L_X8 579
C.108 n_{13-31} vs. L_X8 581
C.109 EW10 vs. L_X8 583
C.110 EW20 vs. L_X8 585
C.111 EW33 vs. L_X8 587
C.112 $F_{11.3}/F_{9.8}$ vs. L_X8 589
C.113 $F_{11.3}$ vs. L_X8 591
C.114 $F_{9.8}$ vs. L_X8 593
C.115 F_{20}/F_{10} vs. L_X8 595
C.116 F_{10} vs. L_X8 597
C.117 F_{20} vs. L_X8 599
C.118 $L_\star$ vs. L_X8 601
C.119 $M_\star$ vs. L_X8 603
C.120 n_{K-6} vs. L_X1 605

C.121 n_{6-13} vs. L_X1 607
C.122 n_{13-31} vs. L_X1 609
C.123 EW10 vs. L_X1 611
C.124 EW20 vs. L_X1 613
C.125 EW33 vs. L_X1 615
C.126 $F_{11.3}/F_{9.8}$ vs. L_X1 617
C.127 $F_{11.3}$ vs. L_X1 619
C.128 $F_{9.8}$ vs. L_X1 621
C.129 F_{20}/F_{10} vs. L_X1 623
C.130 F_{10} vs. L_X1 625
C.131 F_{20} vs. L_X1 627
C.132 $L_\star$ vs. L_X1 629
C.133 $M_\star$ vs. L_X1 631
C.134 n_{K-6} vs. L_X2 633
C.135 n_{6-13} vs. L_X2 635
C.136 n_{13-31} vs. L_X2 637
C.137 EW10 vs. L_X2 639
C.138 EW20 vs. L_X2 641
C.139 EW33 vs. L_X2 643
C.140 $F_{11.3}/F_{9.8}$ vs. L_X2 645
C.141 $F_{11.3}$ vs. L_X2 647
C.142 $F_{9.8}$ vs. L_X2 649
C.143 F_{20}/F_{10} vs. L_X2 651
C.144 F_{10} vs. L_X2 653

C.145 F_{20} vs. L_X2 655
C.146 $L_\star$ vs. L_X2 657
C.147 $M_\star$ vs. L_X2 659
C.148 n_{K-6} vs. L_X3 661
C.149 n_{6-13} vs. L_X3 663
C.150 n_{13-31} vs. L_X3 665
C.151 EW10 vs. L_X3 667
C.152 EW20 vs. L_X3 669
C.153 EW33 vs. L_X3 671
C.154 $F_{11.3}/F_{9.8}$ vs. L_X3 673
C.155 $F_{11.3}$ vs. L_X3 675
C.156 $F_{9.8}$ vs. L_X3 677
C.157 F_{20}/F_{10} vs. L_X3 679
C.158 F_{10} vs. L_X3 681
C.159 F_{20} vs. L_X3 683
C.160 $L_\star$ vs. L_X3 685
C.161 $M_\star$ vs. L_X3 687
C.162 n_{K-6} vs. L_X4 689
C.163 n_{6-13} vs. L_X4 691
C.164 n_{13-31} vs. L_X4 693
C.165 EW10 vs. L_X4 695
C.166 EW20 vs. L_X4 697
C.167 EW33 vs. L_X4 699
C.168 $F_{11.3}/F_{9.8}$ vs. L_X4 701

C.169 $F_{11.3}$ vs. L_X4 703
C.170 $F_{9.8}$ vs. L_X4 705
C.171 F_{20}/F_{10} vs. L_X4 707
C.172 F_{10} vs. L_X4 709
C.173 F_{20} vs. L_X4 711
C.174 $L_\star$ vs. L_X4 713
C.175 $M_\star$ vs. L_X4 715
C.176 n_{K-6} vs. L_X5 vs. n_{K-6} 717
C.177 n_{6-13} vs. L_X5 719
C.178 n_{13-31} vs. L_X5 721
C.179 EW10 vs. L_X5 723
C.180 EW20 vs. L_X5 725
C.181 EW33 vs. L_X5 727
C.182 $F_{11.3}/F_{9.8}$ vs. L_X5 729
C.183 $F_{11.3}$ vs. L_X5 731
C.184 $F_{9.8}$ vs. L_X5 733
C.185 F_{20}/F_{10} vs. L_X5 735
C.186 F_{10} vs. L_X5 737
C.187 F_{20} vs. L_X5 739
C.188 $L_\star$ vs. L_X5 741
C.189 $M_\star$ vs. L_X5 743
C.190 L_X8 vs $\dot{M}$ 745
C.191 L_X1 vs $\dot{M}$ 747
C.192 L_X2 vs $\dot{M}$ 749

C.193 L_X3 vs $\dot{M}$ 751

C.194 L_X4 vs $\dot{M}$ 753

C.195 L_X5 vs $\dot{M}$ 755

D.1 distribution of nk6 by subsection 760

D.2 distribution of EW10 by subsection 761

D.3 distribution of F_{10} by subsection 762

D.4 distribution of $F_{11.3}/F_{9.8}$ by subsection 763

D.5 n_{K-6} versus d 764

D.6 EW10 versus d 764

D.7 F_{10} versus d 765

D.8 $F_{11.3}/F_{9.8}$ versus d 765

E.1 $F_{6.2}/F_{8.6}$ vs. T_{eff} and distance from θ^1 Ori C. 767

E.2 $F_{6.2}/F_{8.6}$ vs. T_{eff} and distance from θ^1 Ori C. 768

E.3 $F_{6.2}/F_{11.2}$ vs. T_{eff} and distance from θ^1 Ori C. 769

E.4 $F_{7.7}/F_{8.6}$ vs. T_{eff} and distance from θ^1 Ori C. 770

E.5 $F_{7.7}/F_{11.2}$ vs. T_{eff} and distance from θ^1 Ori C. 771

E.6 $F_{8.6}/F_{11.2}$ vs. T_{eff} and distance from θ^1 Ori C. 772

E.7 $F_{12.7}/F_{11.2}$ vs. T_{eff} and distance from θ^1 Ori C. 773

1 Introduction

How do planets form? From the well established star-formation scenario, we now understand that there is a protoplanetary disk around each newly forming, growing central star and the protoplanetary disk is the birth place of planets. Encrypted in the **evolution** of these disks is the story of the origin of planets.

Protoplanetary disks evolve from optically thick flared disks toward optically thin, flat, tenuous disks. The infrared based classification of the spectral energy distributions (SEDs) of young stellar objects (YSOs) by Lada (1987) divides the spectral evolution into three stages, Class I-II-III. These classifications are based on the spectral slope (α) of SEDs between the near- (2 μm) and mid- (25 μm) infrared. Class I objects ($\alpha > 0$) have SEDs with increasing infrared emission dominated by envelope, as expected from protostars (Figure 1.1). Class II objects (-2 $< \alpha <$ 0) have relatively flat or negative SED slopes, corresponding to excess emission over infrared wavelength ranges produced by a dusty and optically thick disks around a pre-main sequence star (Figure 1.1). Class III objects ($\alpha <$ -2) have SEDs with very little or no disk emission at infrared wavelengths indicating that dust in the disk has been

processed and has settled toward to the midplane with large sized grains.

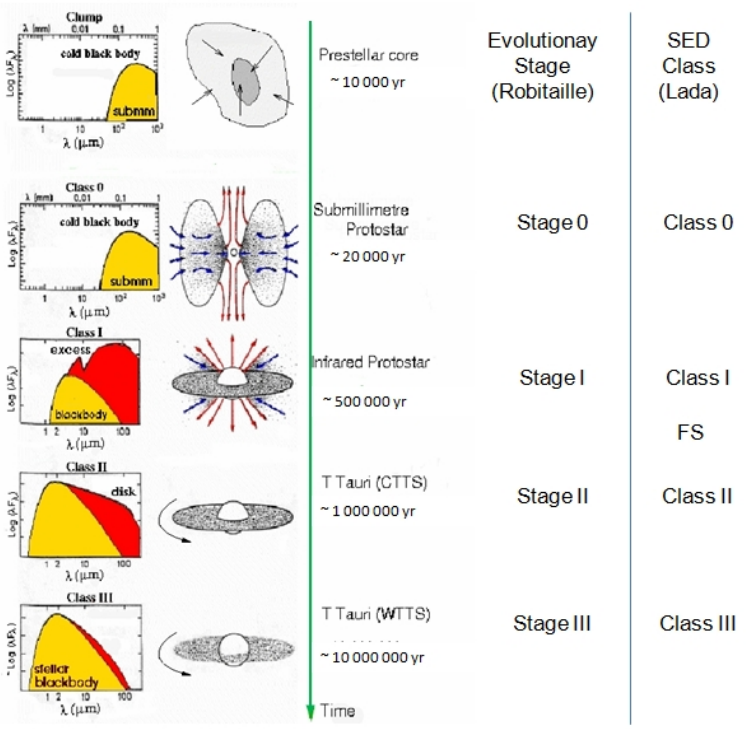


Figure 1.1 Evolutionary classification of Young Stellar Objects. (The original image (Image Credit: http://astro.kent.ac.uk/mds/Origin/birth.html) is modified in order to help the evolutionary classification)

Andre et al. (1993) extended the classification to an earlier Class 0 based on millimeter wavelength emission, and Greene et al. (1994) introduced flat spectrum sources as those with spectral slopes between Class I and II. The SED classes are close, though not perfect, matches to evolutionary stages (cf. Robitaille et al., 2006). Classes 0, I and FS correspond to the progress of the accretion and dispersal of the protostellar envelope, and the monotonic reduction of the central star's accretion rate through the range 10^{-4}–10^{-7} $M_{\odot}yr^{-1}$. Class II corresponds to the evolution and dispersal of the disk's gaseous and

small-grain components, and to the central star's accretion rate through the range 10^{-7}–10^{-10} $M_{\odot}yr^{-1}$. Effects of orientation can make an object from one *evolutionary* stage appear in a different SED class; for example, an envelope-less protoplanetary disk viewed edge on may belong to the Class I SED type.

YSOs with different stellar spectral type and mass evolve quite differently. A young star called a Herbig Ae/Be star has spectral type of A or B, and it masses between 2 and 10 $M_{\odot}$. A young star referred to a T Tauri star has spectral type between F and M, and its mass is less than 2 $M_{\odot}$. The more massive Herbig Ae/Be stars, and their disks, evolve much faster than T Tauri stars, and their surrounding protoplanetary disks. T Tauri stars will end up as stars of mass similar to that of the Sun.

Mass accretion is important to the disk evolution and star- and planet-formation. Throughout a disk's life, its material is accreted toward the central star. A classification based on the accretion indicators (for instance, H_{α} equivalent width being greater/less than 10 Å) divides T Tauri stars into classical T Tauri stars (CTTS) and weak-lined T Tauri stars (WTTS), which generally correspond closely to Class II and Class III, respectively.

In this thesis, we focus on Class II T Tauri stars because planets are thought to be formed in dusty and massive disks during the Class II stage. We note that we sometimes cite CTTS and WTTS for Class II and Class III depending on context; the pairs of terms are generally considered synonymous (Evans et al., 2009).

Some disks have distinctive SEDs that do not fit neatly in the classes of Class I, II, or III. They have the appearance of Class III in some wavelength

range, Class II in others. These transitional disks (TDs) are protoplanetary disks around young stars which are optically thick and gas-rich, but which have AU-scale radial gaps or central clearings in their dust distribution. Usually the gap, which is depleted of small dust grains, is revealed as a deficit in the host T Tau star's infrared excess, with respect to its siblings. Such disks are often thought to represent an evolutionary stage between Class II and Class III young stellar objects (YSOs). Strom et al. (1989) first drew attention to these objects, using examples with small — almost photospheric — infrared excess at short mid-infrared ($5 - 50\mu$m) wavelengths which switch sharply to large and strong excess at longer wavelengths. There have been debates about the origin of TDs, but recent observations (Forrest et al., 2004; D'Alessio et al., 2005; Calvet et al., 2005; Brown et al., 2007; Espaillat et al., 2007a,b, 2008; Kim et al., 2009) support that the early giant planet formation plays a major role in the gap/hole formation of transitional disks.

The entire Orion A cloud appears to be a filament which is roughly perpendicular to the line of sight; its parts are all the same distance from us. We take that distance to be 414 pc, as derived from geometric parallax of H_2O masers in the Orion A molecular cloud (Menten et al., 2007). Fits to stellar-evolution models by the color-magnitude diagrams of their young stars give ages <1 Myr (Hillenbrand, 1997) and ∼1 Myr for L1641 (Gâlfalk & Olofsson, 2008). Age is a fraught subject for YSO associations; we will assume that the ages of the young clusters addressed in this dissertation lie in the range 0.5–5 Myr, and that the color-magnitude diagrams correctly rank the typical ages, with ONC, L1641 and NGC 1333 the youngest, Ophiuchus and Chamaeleon

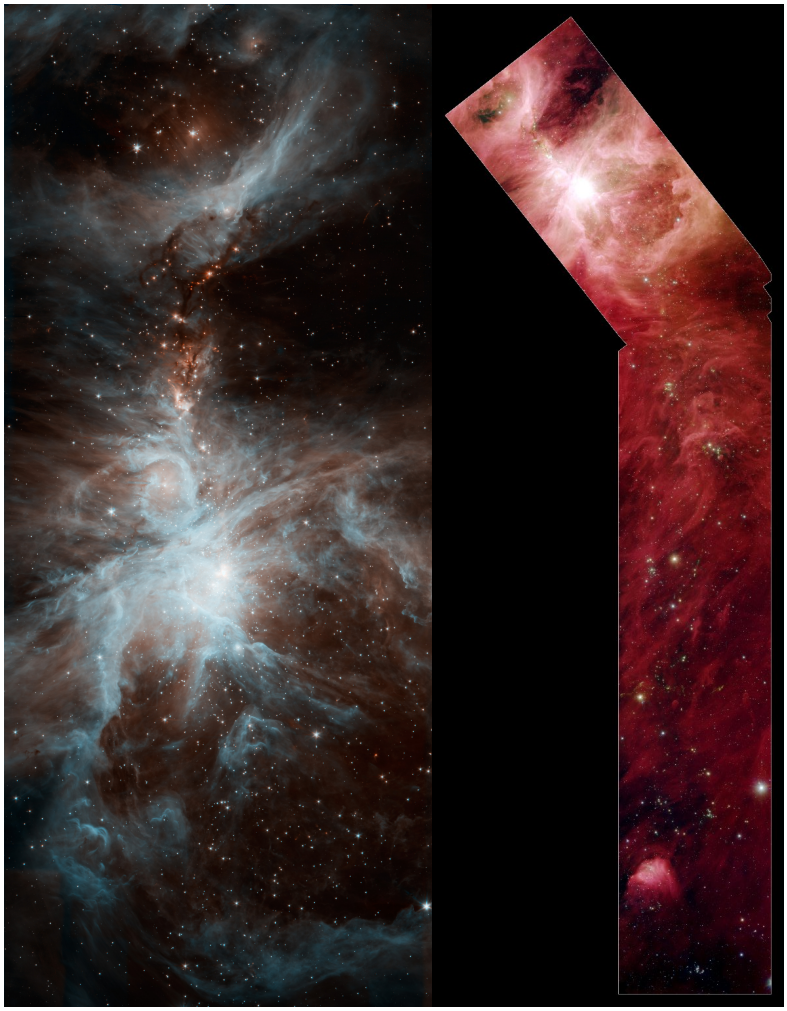


Figure 1.2 Infrared images of Orion A star-forming region (Left: ONC; Right: ONC and L1641). The left image is the composite images taken at 3.6 (blue) μm and 4.5 (orange)μm by IRAC at *Spitzer* Space Telescope. The right image is the composite image taken at 3.6 (blue), 4.5 (green), 5.8 (orange), and 8 (red) μm by IRAC. (Image credit: NASA/JPL-Caltech/S. T. Megeath (University of Toledo))

on the oldest, and Taurus in between.

In this dissertation we will explore the characteristics of Class II disks in Orion A star-forming region. The IRS/Spitzer observation of 303 protoplanetary disks in Orion A and the follow-up observation of 120 objects with SpeX/IRTF are used to reveal the characteristics of Class II disks in Orion A. To study the environmental effects on disk evolution and planet formation, we frequently compare the structural and dust properties of Orion A disks to those of the fiducial Taurus association (Furlan et al., 2006, 2007, 2009, 2011).

In Chapter 2, we describe the observations and data reduction process.

In Chapter 3, we report the disk properties derived from IRS spectra of Class II objects in Orion A. We describe how to measure mass accretion rate from SpeX spectra. We discuss the general distribution of properties of disks and stars in ONC, L1641, and Taurus.

In Chapter 4[1], we focus on the properties of Transitional disks (TDs). In particular, we search for several trends to reveal the origin of TDs. We also include TDs from Taurus, Chamaeleon I, Ophiuchus, and NGC 1333 in this analysis. From the total of 105 transitional disks we establish the empirical selection criteria and sub-classification of type of TDs. We test theoretical mechanisms of the formation of TDs with the properties and trends we found.

In Chapter 5, we examine in more detail the spectral and stellar-system properties by their disk structures (radially continuous disks or transitional disks) and by star-forming regions, revealing how certain properties change in the course of disk evolution. We search for correlations among stellar, disk,

[1]Most of the material presented in this chapter appears in Kim et al. 2013

and dust properties we measured.

Orion A differs from other nearby YSO associations studied with Spitzer, in that it is the only one that harbors an OB association (ONC). Yet it also includes regions in L1641 with stellar density and UV intensity as small as in the fiducial low-mass star-formation region, Taurus. In Chapter 6, we discuss how the evolution of protoplanetary disks is affected by the star-forming environment, by comparing disk properties by the distance from θ^1 Ori C which emits very strong UV radiation.

In Chapter 7, we report the first detection of Polycyclic Aromatic Hydrocarbons (PAHs) features of protoplanetary disks around low-mass T Tauri stars which are excited by the UV illumination from a near-by OB association.

2 Observation and Data Reduction

2.1 IRS/Spitzer

2.1.1 Observations

We observed 303 Class II objects in the Orion A star-forming region as part of the *Spitzer* IRS Guaranteed Time Observation (GTO) program, PID 30706 (PI: J. Houck) between November 2006 and October 2007 during IRS campaigns 36, 39, 40, and 44. These sources were selected based on the identification of young stars with disks by IRAC/2MASS color-color diagrams (Megeath et al., 2012). We observed 241 objects (114 in L1641; 127 in ONC) with the IRS with full IRS wavelength coverage of 5-37 μm in the low resolution mode ($\lambda/\Delta\lambda \sim 90$; Short-Low (SL):5.3-14 μm; Long-Low (LL): 14-38 μm), and 62 objects located close to Trapezium region with partial wavelength coverage (5-14 μm; SL only) because the detectors for the longer wavelengths would have been saturated by bright background emission. Each object was observed at two nod positions separated by one-third the length of the slit in the staring

mode. The IRS targets in ONC, L1641, and the Trapezium are indicated in Figure 2.1, Figure 2.2, and Figure 2.3, respectively.

2.1.2 Data Reduction

We began with version S15.3 of the basic calibrated data (BCD) product from the Spitzer Science Center IRS pipeline for both SL and LL.

To fix bad, hot and rogue detector-array pixels before extracting objects from the 2D spectral images, we generated a set of "grand rogue masks" for Orion A data. A grand rogue mask for the general data reduction process is generated by combining rogue mask files available up to a recent IRS campaign supplied from the Spitzer Science Center, and adding additionally identified rogue pixels from data images. However, we applied additional special treatment to make LL grand rogue masks for these data because (1) the LL array exposure to cosmic rays had increased continuously up to campaign 44 [1], which caused the S/N to decrease and the number of rogue pixels and hot pixels to increase, (2) fluxes from our objects are fainter than similar sources in other nearby star-forming regions due to the greater distance to Orion A, (3) the large number of rogue pixels and hot pixels severely degraded the signal-to-noise ratio of our targets, and introduced spectral artifacts when many rogue pixels were grouped in clusters. To avoid rejection of too many pixels which might be perfectly good, we chose only the rogue pixels which appear in the campaign rogue masks more than 10 times through campaign 44. To these we added hot pixels selected by eye from LL 2D images from campaign 39 and

[1] In IRS campaign 45 the bias voltage on the Long Low array was reduced from 1.8 to 1.6 volts and the array temperature was reduced from 4.4 to 4.1 K)

campaign 44. The usage of grand mask files including rogue pixels and hot pixels cannot perfectly clean bad pixels. However, we tested several versions of grand rogue masks for our LL data and chose a set of grand rogue masks to apply for all of Orion A ClassII data. We fixed those rogue pixels in the grand rogue mask (and the permanently bad pixels) by interpolation in the spectral direction from nearest-neighbor good pixels.

Spectral extraction of Class II YSOs in Orion A is generally much more challenging than in other nearby star-forming regions. This is due not only to the source faintness but also to the range of spatial structure in sky emission from the Orion HII regions, and the high stellar density. We used four source extraction methods to derive the final point-source spectra, choosing among them to optimize the rejection of emission from the sky and other nearby point sources.

As a first, basic source extraction step, we used an automated extractor ("auto") based upon the IRS instrument team's Spectral Modeling, Analysis and Reduction Tool (SMART; Higdon et al., 2004). In auto we extracted sources from the uniformly-weighted signal along a tapered column, 3-5 pixels wide. In this step we used two versions of background-subtracted images: one prepared by subtraction of the two nods ("off-nod"), and the other by subtraction of the sky spectrum in each grating order obtained while the target was being observed in the other order ("off-order"). If there were no serious sky background issues or no additional sources in the 2D images, the spectra taken from images subtracted by off-order or off-nods backgrounds are very similar. We examined each sky-subtracted image and the resulting spectra.

If large sky-subtraction artifacts (e.g. spectral lines in the sky, contamination from nearby point sources) remained in both auto products, we re-reduced the data in SMART by using the same tapered column extraction as before, but with sky removed by fitting and subtracting a 0th- or 1st order polynomial to emission outside the span of the target. We designate the tapered column extraction with subtraction of a polynomial (constant or linear) sky selected manually as "man".

Usually one of three tapered column extractions gave artifact-free results even when the sky emission had complicated structure, but issues remained for targets with a neighbor closer than four pixels away along the slit. In those cases, we resorted to optimal point-source extraction, using both the AdOpt script in SMART (Lebouteiller et al., 2010) and another routine, OPSE, developed separately from SMART (Tayrien & Forrest, 2013, in preparation). They are complementary: AdOpt employs an empirical point response function (PRF) and can fit multiple objects along the slit; OPSE uses an analytical PRF and can make corrections to the spectrum for pointing errors, and thus was useful for extracting our target sources, as it can account other sources in a image.

For the flux calibration of the spectra, we multiplied relative spectral response functions (RSRFs), which were generated by dividing a template spectrum by a calibrator's spectrum, extracted in the same way as the target spectrum. Our photometric standards were α Lac (A1V; M. Cohen 2003, private communication) for SL, ξ Dra (K2III; ibid) for LL, and Mrk 231 (J.Marshall 2007, private communication) for LL wavelength greater than 32 μm.

We compared the spectra from all different versions of source extraction for each object, then we selected the final spectrum based upon freedom from artifacts. During the process, we combined spectra from different versions of methods if necessary to get the best spectra. For example, we use the combined spectrum for OriA-19: SL from AdOpt and LL from OPSE. Reduction choices for the final selection of spectra are noted in Table 2.1.

We list the selected identifications of the targets in Table 2.2.

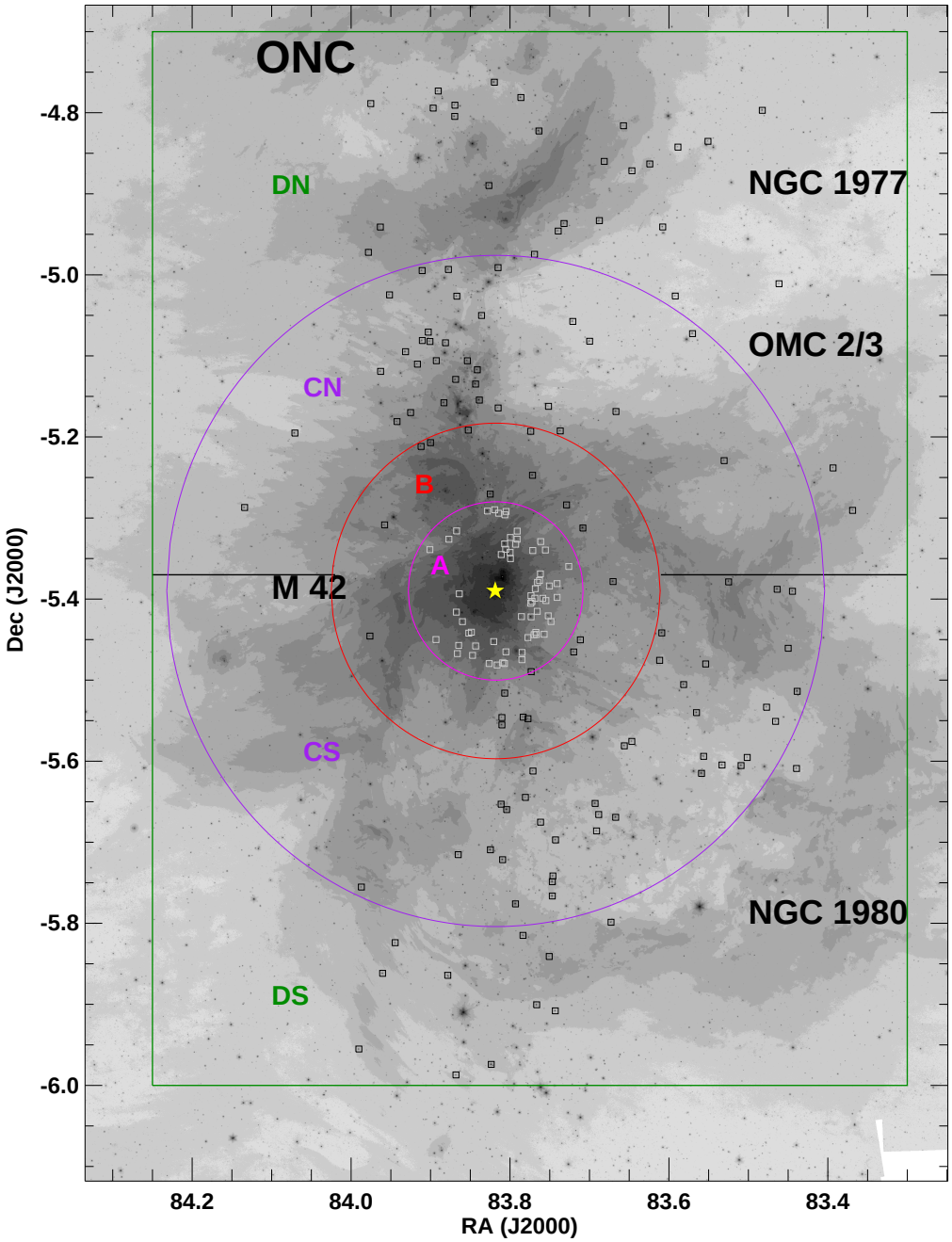


Figure 2.1 IRS targets in ONC over the IRAC/Spitzer ch2 (4.5 μm) image. Subsections of ONC separated by the projected distance (d) from θ^1 Ori C (yellow star) are indicated. The criteria of subsections: A: $d \leq 0.7$ pc; B: 0.7 pc $< d \leq 1.5$ pc; C: 1.5 pc $< d \leq 2.5$ pc; D: $d > 2.5$ pc and DEC > -6^o. Subsection B, C, and D are also separated by N and S from the DEC of θ^1 Ori C.

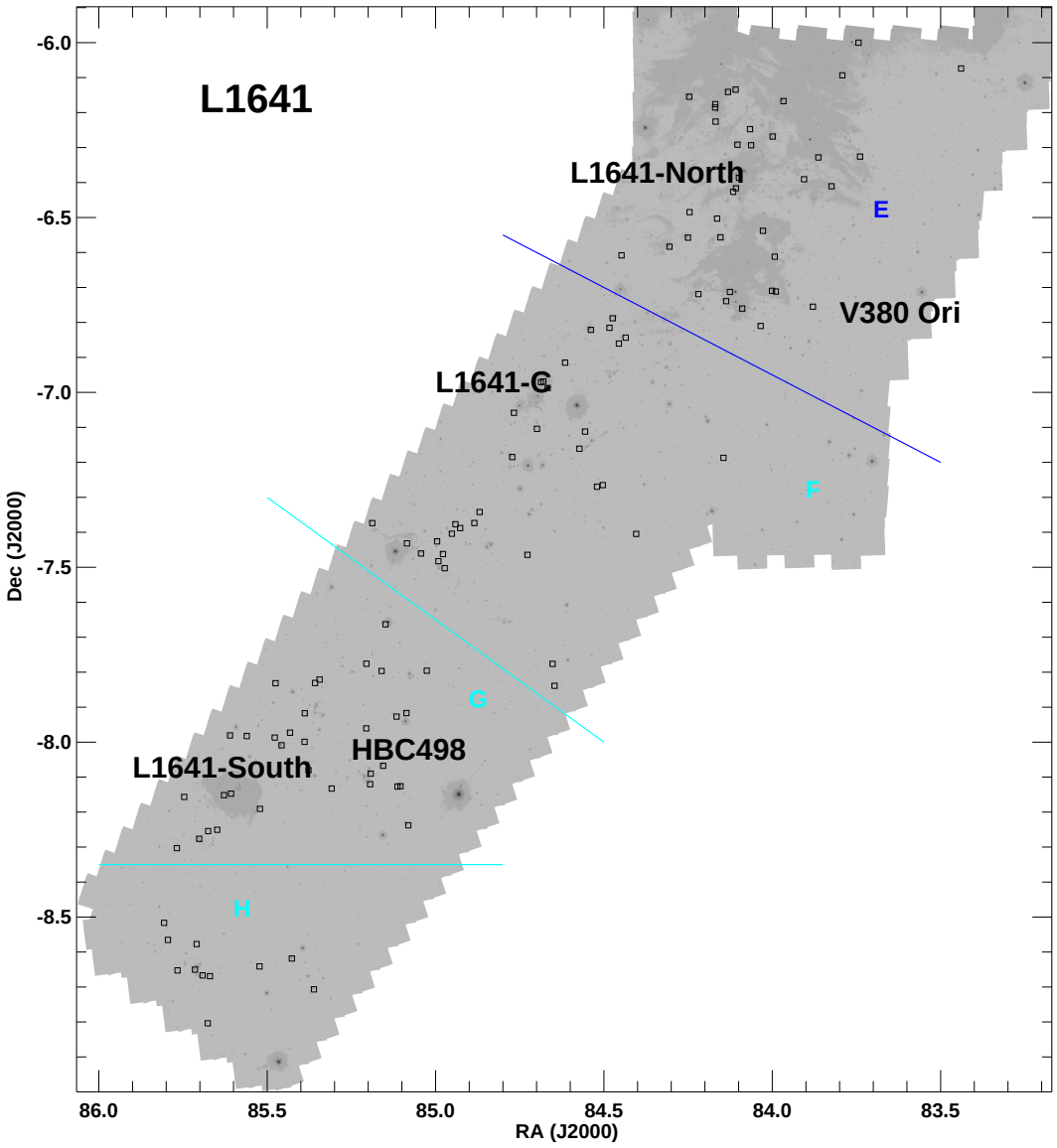


Figure 2.2 IRS targets in L1641 over the RAC/Spitzer ch2 (4.5 μm) image.

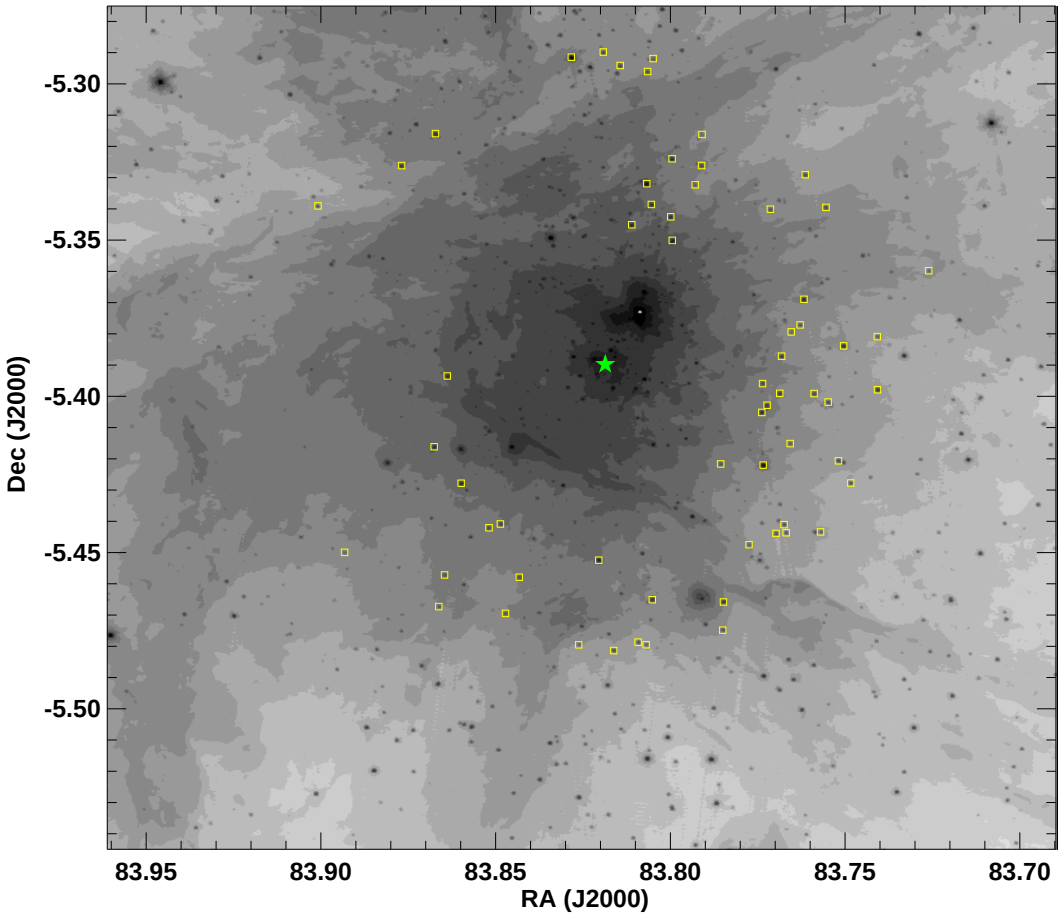


Figure 2.3 Close up of Section A (Trapezium region) in Fig 2.1. θ^1 Ori C is indicated with a green star.

Table 2.1. Observation and Reduction Log of IRS Spectra

Num. (1)	IRS name (2)	RA (J2000) (3)	DEC (J2000) (4)	AORID (5)	IRS Camp. (6)	Date observed (7)	modules (8)	region (9)	reduction (10)
1	8336884-5290	5 33 28.52	-5 17 26.16	18804224	39	2007 Mar 12	SLLL	ONC	AdOpt
2	8339347-5238	5 33 34.43	-5 14 17.7	18843904	39	2007 Mar 12	SLLL	ONC	AdOpt
3	8343858-5513	5 33 45.26	-5 30 49.75	18825472	39	2007 Mar 12	SLLL	ONC	AdOpt
4	8343917-6073	5 33 45.4	-6 4 25.86	18848000	39	2007 Mar 09	SLLL	L1641	man
5	8343944-5609	5 33 45.47	-5 36 32.54	18833152	39	2007 Mar 12	SLLL	ONC	opse/AdOpt [a]
6	8344455-5390	5 33 46.69	-5 23 25.44	18802944	39	2007 Mar 24	SLLL	ONC	opse
7	8344987-5460	5 33 47.97	-5 27 38.56	18780672	44	2007 Oct 05	SLLL	ONC	man
8	8346141-5010	5 33 50.74	-5 0 39.46	18781952	39	2007 Mar 22	SLLL	ONC	AdOpt
9	8346378-5387	5 33 51.31	-5 23 16.62	18849536	39	2007 Mar 12	SLLL	ONC	man/AdOpt [b]
10	8346581-5550	5 33 51.79	-5 33 3.35	18830848	39	2007 Mar 12	SLLL	ONC	man
11	8347711-5533	5 33 54.51	-5 32 0.42	18844416	39	2007 Mar 12	SLLL	ONC	AdOpt
12	8348250-4797	5 33 55.8	-4 47 49.34	18832896	39	2007 Mar 24	SLLL	ONC	man
13	8350150-5595	5 34 0.36	-5 35 43.51	18778880	39	2007 Mar 12	SLLL	ONC	man
14	8350916-5605	5 34 2.2	-5 36 19.48	18811648	39	2007 Mar 12	SLLL	ONC	AdOpt
15	8352483-5378	5 34 5.96	-5 22 43.72	18817280	39	2007 Mar 12	SLLL	ONC	AdOpt
16	8353051-5229	5 34 7.32	-5 13 45.12	18801408	39	2007 Mar 22	SLLL	ONC	AdOpt
17	8353319-5604	5 34 7.97	-5 36 17.06	18838272	39	2007 Mar 09	SLLL	ONC	opse
18	8355083-4835	5 34 12.2	-4 50 7.12	18810624	39	2007 Mar 24	SLLL	ONC	AdOpt

Table 2.1 (cont'd)

Num. (1)	IRS name (2)	RA (J2000) (3)	DEC (J2000) (4)	AORID (5)	IRS Camp. (6)	Date observed (7)	modules (8)	region (9)	reduction (10)
19	8355371-5480	5 34 12.89	-5 28 48.29	18779904	44	2007 Oct 05	SLLL	ONC	Adopt/opse [c]
20	8355629-5594	5 34 13.51	-5 35 38.58	18840320	39	2007 Mar 12	SLLL	ONC	man
21	8355898-5615	5 34 14.16	-5 36 54.14	18832640	39	2007 Mar 12	SLLL	ONC	Adopt/man [d]
22	8356531-5540	5 34 15.67	-5 32 24.43	18820608	39	2007 Mar 12	SLLL	ONC	AdOpt
23	8357031-5072	5 34 16.87	-5 4 21.14	18836736	39	2007 Mar 22	SLLL	ONC	man
24	8358147-5505	5 34 19.55	-5 30 19.84	18812928	39	2007 Mar 24	SLLL	ONC	AdOpt
25	8358862-4842	5 34 21.27	-4 50 32.68	18776576	44	2007 Oct 11	SLLL	ONC	AdOpt
26	8359203-5026	5 34 22.09	-5 1 34.21	18776320	39	2007 Mar 22	SLLL	ONC	AdOpt
27	8360781-4940	5 34 25.87	-4 56 27.35	18830592	39	2007 Mar 22	SLLL	ONC	AdOpt
28	8360900-5441	5 34 26.16	-5 26 30.26	18837760	39	2007 Mar 24	SLLL	ONC	AdOpt
29	8361167-5475	5 34 26.8	-5 28 32.09	18778624	44	2007 Oct 05	SLLL	ONC	AdOpt
30	8362406-4863	5 34 29.77	-4 51 47.56	18809600	39	2007 Mar 24	SLLL	ONC	AdOpt
31	8364658-4871	5 34 35.18	-4 52 17.9	18836992	39	2007 Mar 24	SLLL	ONC	AdOpt
32	8364671-5575	5 34 35.21	-5 34 32.23	18823424	39	2007 Mar 27	SLLL	ONC	AdOpt
33	8365614-5581	5 34 37.47	-5 34 51.78	18840064	39	2007 Mar 27	SLLL	ONC	AdOpt
34	8365722-4816	5 34 37.73	-4 48 57.85	18781440	44	2007 Oct 11	SLLL	ONC	man
35	8366668-5168	5 34 40	-5 10 7	18815488	39	2007 Mar 22	SLLL	ONC	AdOpt
36	8366704-5669	5 34 40.09	-5 40 9.3	18844160	39	2007 Mar 12	SLLL	ONC	man

Table 2.1 (cont'd)

Num. (1)	IRS name (2)	RA (J2000) (3)	DEC (J2000) (4)	AORID (5)	IRS Camp. (6)	Date observed (7)	modules (8)	region (9)	reduction (10)
37	8367030-5378	5 34 40.87	-5 22 42.28	18812160	39	2007 Mar 27	SLLL	ONC	AdOpt
38	8367284-5798	5 34 41.48	-5 47 55.46	18838528	39	2007 Mar 24	SLLL	ONC	AdOpt
39	8368137-4860	5 34 43.53	-4 51 36.25	18778368	44	2007 Oct 05	SLLL	ONC	AdOpt
40	8368755-4933	5 34 45.01	-4 55 59.2	18809088	39	2007 Mar 24	SLLL	ONC	AdOpt
41	8368837-5665	5 34 45.21	-5 39 57.02	18838784	39	2007 Mar 12	SLLL	ONC	man
42	8369106-5686	5 34 45.85	-5 41 9.78	18840832	39	2007 Mar 12	SLLL	ONC	AdOpt
43	8369290-5652	5 34 46.3	-5 39 7.74	18841600	39	2007 Mar 27	SLLL	ONC	man
44	8369980-5081	5 34 47.95	-5 4 54.88	18817792	39	2007 Mar 22	SLLL	ONC	AdOpt
45	8370827-5312	5 34 49.98	-5 18 44.5	18852352	39	2007 Mar 22	SLLL	ONC	man/opse [e]
46	8371143-5450	5 34 50.74	-5 27 1.12	18810112	39	2007 Mar 27	SLLL	ONC	AdOpt
47	8371984-5465	5 34 52.76	-5 27 54.9	18843648	39	2007 Mar 09	SLLL	ONC	AdOpt
48	8372100-5057	5 34 53.04	-5 3 27	18803968	39	2007 Mar 22	SLLL	ONC	AdOpt
49	8372608-5359	5 34 54.26	-5 21 35.28	18782464	39	2007 Mar 12	SL	Trapezium	AdOpt
50	8372885-5283	5 34 54.92	-5 17 1.86	18847744	39	2007 Mar 22	SLLL	ONC	AdOpt
51	8373201-4936	5 34 55.68	-4 56 12.12	18806016	39	2007 Mar 27	SLLL	ONC	AdOpt
52	8373676-5192	5 34 56.82	-5 11 33.11	18828032	36	2006 Nov 10	SLLL	ONC	AdOpt
53	8373930-6325	5 34 57.43	-6 19 33.02	18781696	39	2007 Mar 09	SLLL	L1641	man
54	8373936-4946	5 34 57.45	-4 56 45.64	18808064	39	2007 Mar 26	SLLL	ONC	AdOpt

Table 2.1 (cont'd)

Num. (1)	IRS name (2)	RA (J2000) (3)	DEC (J2000) (4)	AORID (5)	IRS Camp. (6)	Date observed (7)	modules (8)	region (9)	reduction (10)
55	8374073-5397	5 34 57.78	-5 23 52.44	18782720	39	2007 Mar 12	SL	Trapezium	AdOpt
56	8374080-5380	5 34 57.79	-5 22 51.24	18782976	39	2007 Mar 22	SL	Trapezium	AdOpt/man [m]
57	8374271-5697	5 34 58.25	-5 41 49.74	18842368	39	2007 Mar 12	SLLL	ONC	man
58	8374301-5908	5 34 58.32	-5 54 28.84	18808320	39	2007 Mar 12	SLLL	ONC	AdOpt
59	8374388-6000	5 34 58.53	-6 0 0.43	18820864	44	2007 Oct 05	SLLL	L1641	man
60	8374599-5741	5 34 59.04	-5 44 29.8	18813952	39	2007 Mar 12	SLLL	ONC	AdOpt
61	8374677-5748	5 34 59.22	-5 44 55.32	18806272	39	2007 Mar 12	SLLL	ONC	man/opse [e]
62	8374677-5766	5 34 59.22	-5 45 58.72	18810880	39	2007 Mar 12	SLLL	ONC	opse
63	8374839-5427	5 34 59.61	-5 25 39.83	18783232	39	2007 Mar 24	SL	Trapezium	AdOpt
64	8375041-5383	5 35 0.1	-5 23 1.86	18783488	39	2007 Mar 22	SL	Trapezium	man
65	8375063-5840	5 35 0.15	-5 50 27.38	18839040	39	2007 Mar 12	SLLL	ONC	AdOpt
66	8375158-5162	5 35 0.38	-5 9 43.99	18779648	44	2007 Oct 05	SLLL	ONC	AdOpt
67	8375190-5420	5 35 0.46	-5 25 14.3	18783744	39	2007 Mar 24	SL	Trapezium	AdOpt
68	8375484-5401	5 35 1.16	-5 24 6.66	18784000	39	2007 Mar 24	SL	Trapezium	AdOpt
69	8375546-5339	5 35 1.31	-5 20 22.24	18784256	39	2007 Mar 22	SL	Trapezium	failed
70	8375702-5443	5 35 1.68	-5 26 36.24	18784512	39	2007 Mar 24	SL	Trapezium	AdOpt
71	8375886-5399	5 35 2.13	-5 23 56.76	18784768	39	2007 Mar 21	SL	Trapezium	AdOpt
72	8376139-5329	5 35 2.73	-5 19 44.54	18785024	39	2007 Mar 22	SL	Trapezium	failed

Table 2.1 (cont'd)

Num. (1)	IRS name (2)	RA (J2000) (3)	DEC (J2000) (4)	AORID (5)	IRS Camp. (6)	Date observed (7)	modules (8)	region (9)	reduction (10)
73	8376154-5675	5 35 2.77	-5 40 30.86	18834944	40	2007 Apr 18	SLLL	ONC	AdOpt
74	8376176-5368	5 35 2.82	-5 22 8.18	18785280	39	2007 Mar 22	SL	Trapezium	AdOpt
75	8376287-5377	5 35 3.09	-5 22 37.7	18785536	39	2007 Mar 22	SL	Trapezium	AdOpt
76	8376356-4822	5 35 3.25	-4 49 21	18803456	39	2007 Mar 24	SLLL	ONC	AdOpt
77	8376541-5379	5 35 3.7	-5 22 45.77	18785792	39	2007 Mar 22	SL	Trapezium	AdOpt
78	8376571-5415	5 35 3.77	-5 24 54.4	18786048	39	2007 Mar 24	SL	Trapezium	AdOpt
79	8376643-5900	5 35 3.94	-5 54 1.84	18812416	39	2007 Mar 12	SLLL	ONC	AdOpt
80	8376687-5443	5 35 4.05	-5 26 37.18	18786304	39	2007 Mar 24	SL	Trapezium	AdOpt
81	8376747-5441	5 35 4.19	-5 26 27.82	18786560	39	2007 Mar 24	SL	Trapezium	AdOpt
82	8376817-5387	5 35 4.36	-5 23 13.7	18786816	39	2007 Mar 22	SL	Trapezium	AdOpt
83	8376871-5399	5 35 4.49	-5 23 56.51	18787072	39	2007 Mar 24	SL	Trapezium	AdOpt
84	8376918-4974	5 35 4.6	-4 58 28.92	18805760	39	2007 Mar 26	SLLL	ONC	AdOpt
85	8376976-5443	5 35 4.74	-5 26 37.93	18787328	39	2007 Mar 24	SL	Trapezium	AdOpt
86	8377111-5612	5 35 5.07	-5 36 43.78	18851328	40	2007 Apr 18	SLLL	ONC	AdOpt
87	8377137-5340	5 35 5.13	-5 20 24.4	18787584	39	2007 Mar 22	SL	Trapezium	failed
88	8377167-5247	5 35 5.2	-5 14 50.28	18802176	39	2007 Mar 24	SLLL	ONC	AdOpt
89	8377232-5402	5 35 5.36	-5 24 10.3	18787840	39	2007 Mar 22	SL	Trapezium	AdOpt
90	8377335-5489	5 35 5.6	-5 29 22.31	18828544	39	2007 Mar 25	SLLL	ONC	AdOpt

Table 2.1 (cont'd)

Num. (1)	IRS name (2)	RA (J2000) (3)	DEC (J2000) (4)	AORID (5)	IRS Camp. (6)	Date observed (7)	modules (8)	region (9)	reduction (10)
91	8377345-5422	5 35 5.63	-5 25 19.24	18788096	39	2007 Mar 22	SL	Trapezium	AdOpt/man [m]
92	8377361-5395	5 35 5.67	-5 23 45.31	18788352	39	2007 Mar 22	SL	Trapezium	AdOpt
93	8377383-5405	5 35 5.72	-5 24 18.54	18788608	39	2007 Mar 24	SL	Trapezium	AdOpt
94	8377392-5193	5 35 5.74	-5 11 34.94	18831872	39	2007 Mar 22	SLLL	ONC	AdOpt
95	8377737-5547	5 35 6.57	-5 32 51.4	18814976	39	2007 Mar 27	SLLL	ONC	AdOpt
96	8377749-5447	5 35 6.6	-5 26 50.96	18788864	39	2007 Mar 24	SL	Trapezium	AdOpt
97	8378059-5644	5 35 7.34	-5 38 40.96	18816512	39	2007 Mar 27	SLLL	ONC	AdOpt
98	8378345-5545	5 35 8.03	-5 32 44.34	18846464	39	2007 Mar 27	SLLL	ONC	AdOpt
99	8378366-5814	5 35 8.08	-5 48 53.78	18839296	39	2007 Mar 12	SLLL	ONC	AdOpt
100	8378481-5465	5 35 8.35	-5 27 56.95	18789120	39	2007 Mar 24	SL	Trapezium	AdOpt
101	8378503-5474	5 35 8.41	-5 28 29.42	18789376	39	2007 Mar 24	SL	Trapezium	AdOpt
102	8378561-5421	5 35 8.55	-5 25 17.9	18789632	39	2007 Mar 24	SL	Trapezium	AdOpt
103	8378630-4781	5 35 8.71	-4 46 52.46	18833920	39	2007 Mar 24	SLLL	ONC	man
104	8379094-5316	5 35 9.83	-5 18 58.28	18789888	39	2007 Mar 24	SL	Trapezium	failed
105	8379108-5326	5 35 9.86	-5 19 34.07	18790144	39	2007 Mar 22	SL	Trapezium	failed
106	8379192-6093	5 35 10.06	-6 5 36.42	18844672	39	2007 Mar 09	SLLL	L1641	man
107	8379289-5332	5 35 10.29	-5 19 56.24	18790400	39	2007 Mar 22	SL	Trapezium	failed
108	8379312-5776	5 35 10.35	-5 46 33.82	18850560	39	2007 Mar 12	SLLL	ONC	man

Table 2.1 (cont'd)

Num. (1)	IRS name (2)	RA (J2000) (3)	DEC (J2000) (4)	AORID (5)	IRS Camp. (6)	Date observed (7)	modules (8)	region (9)	reduction (10)
109	8379945-5350	5 35 11.87	-5 21 0.36	18790656	39	2007 Mar 22	SL	Trapezium	failed
110	8379950-5323	5 35 11.88	-5 19 26.29	18790912	39	2007 Mar 22	SL	Trapezium	failed
111	8379990-5342	5 35 11.98	-5 20 33.14	18791168	39	2007 Mar 22	SL	Trapezium	failed
112	8380422-5659	5 35 13.01	-5 39 34.99	18824960	40	2007 Apr 18	SLLL	ONC	AdOpt
113	8380493-5291	5 35 13.18	-5 17 30.84	18791424	39	2007 Mar 22	SL	Trapezium	failed
114	8380518-5465	5 35 13.24	-5 27 54.36	18791680	39	2007 Mar 24	SL	Trapezium	AdOpt
115	8380544-5338	5 35 13.31	-5 20 18.92	18791936	39	2007 Mar 22	SL	Trapezium	failed
116	8380651-5296	5 35 13.56	-5 17 45.74	18792192	39	2007 Mar 22	SL	Trapezium	failed
117	8380667-5516	5 35 13.6	-5 30 57.67	18819840	40	2007 Apr 18	SLLL	ONC	AdOpt
118	8380675-5331	5 35 13.62	-5 19 55.02	18792448	39	2007 Mar 22	SL	Trapezium	failed
119	8380695-5479	5 35 13.67	-5 28 46.27	18792704	39	2007 Mar 24	SL	Trapezium	AdOpt
120	8380923-5478	5 35 14.22	-5 28 43.21	18792960	39	2007 Mar 24	SL	Trapezium	AdOpt
121	8380932-5721	5 35 14.24	-5 43 17.58	18845440	39	2007 Mar 12	SLLL	ONC	AdOpt
122	8381019-5555	5 35 14.45	-5 33 18.94	18851840	39	2007 Mar 27	SLLL	ONC	AdOpt
123	8381020-5546	5 35 14.45	-5 32 46.36	18809856	39	2007 Mar 27	SLLL	ONC	AdOpt
124	8381104-5345	5 35 14.65	-5 20 42.29	18793216	39	2007 Mar 22	SL	Trapezium	failed
125	8381120-5653	5 35 14.69	-5 39 10.94	18832128	39	2007 Mar 22	SLLL	ONC	AdOpt
126	8381436-5294	5 35 15.45	-5 17 38.8	18793472	39	2007 Mar 22	SL	Trapezium	failed

Table 2.1 (cont'd)

Num. (1)	IRS name (2)	RA (J2000) (3)	DEC (J2000) (4)	AORID (5)	IRS Camp. (6)	Date observed (7)	modules (8)	region (9)	reduction (10)
127	8381491-5164	5 35 15.58	-5 9 51.26	18834688	39	2007 Mar 22	SLLL	ONC	AdOpt
128	8381501-4991	5 35 15.6	-4 59 27.96	18799360	39	2007 Mar 26	SLLL	ONC	AdOpt
129	8381622-5481	5 35 15.89	-5 28 52.93	18793728	39	2007 Mar 09	SL	Trapezium	AdOpt
130	8381919-5289	5 35 16.61	-5 17 23.28	18793984	39	2007 Mar 22	SL	Trapezium	failed
131	8381971-4762	5 35 16.73	-4 45 44.5	18852096	39	2007 Mar 24	SLLL	ONC	man
132	8382048-5452	5 35 16.92	-5 27 8.78	18794240	39	2007 Mar 24	SL	Trapezium	AdOpt
133	8382359-5974	5 35 17.66	-5 58 26.76	18799616	40	2007 Apr 18	SLLL	ONC	AdOpt
134	8382412-6410	5 35 17.79	-6 24 38.34	18845952	39	2007 Mar 09	SLLL	L1641	man
135	8382467-5709	5 35 17.92	-5 42 33.48	18802688	39	2007 Mar 12	SLLL	ONC	AdOpt
136	8382490-5270	5 35 17.98	-5 16 13.91	18827776	39	2007 Mar 24	SLLL	ONC	AdOpt
137	8382623-5479	5 35 18.3	-5 28 46.34	18794496	39	2007 Mar 12	SL	Trapezium	AdOpt
138	8382655-4889	5 35 18.37	-4 53 23.46	18849024	39	2007 Mar 26	SLLL	ONC	AdOpt
139	8382835-5291	5 35 18.8	-5 17 29.18	18794752	36	2006 Nov 11	SL	Trapezium	AdOpt
140	8383581-5050	5 35 20.59	-5 3 0.58	18851072	39	2007 Mar 25	SLLL	ONC	AdOpt
141	8383861-5154	5 35 21.27	-5 9 16.2	18803712	39	2007 Mar 25	SLLL	ONC	AdOpt
142	8384113-5117	5 35 21.87	-5 7 1.74	18842112	39	2007 Mar 25	SLLL	ONC	AdOpt
143	8384325-5457	5 35 22.38	-5 27 28.48	18795008	39	2007 Mar 24	SL	Trapezium	AdOpt
144	8384331-5134	5 35 22.39	-5 8 4.99	18824704	39	2007 Mar 25	SLLL	ONC	man/AdOpt [b]

Table 2.1 (cont'd)

Num. (1)	IRS name (2)	RA (J2000) (3)	DEC (J2000) (4)	AORID (5)	IRS Camp. (6)	Date observed (7)	modules (8)	region (9)	reduction (10)
145	8384717-5469	5 35 23.32	-5 28 10.09	18795264	39	2007 Mar 24	SL	Trapezium	AdOpt
146	8384864-5440	5 35 23.67	-5 26 27.06	18795520	39	2007 Mar 24	SL	Trapezium	AdOpt
147	8385190-5442	5 35 24.46	-5 26 31.45	18795776	39	2007 Mar 09	SL	Trapezium	AdOpt
148	8385255-5191	5 35 24.61	-5 11 29.8	18813696	39	2007 Mar 25	SLLL	ONC	man
149	8385365-5106	5 35 24.88	-5 6 21.6	18798592	39	2007 Mar 25	SLLL	ONC	AdOpt
150	8385988-5427	5 35 26.37	-5 25 40.12	18796032	39	2007 Mar 22	SL	Trapezium	AdOpt
151	8386322-6328	5 35 27.17	-6 19 41.88	18802432	39	2007 Mar 09	SLLL	L1641	man
152	8386383-5393	5 35 27.32	-5 23 36.56	18796288	39	2007 Mar 22	SL	Trapezium	AdOpt
153	8386462-5457	5 35 27.51	-5 27 25.81	18796544	39	2007 Mar 24	SL	Trapezium	AdOpt
154	8386523-5715	5 35 27.66	-5 42 55.08	18801664	39	2007 Mar 12	SLLL	ONC	AdOpt
155	8386627-5467	5 35 27.9	-5 28 2.24	18796800	39	2007 Mar 24	SL	Trapezium	AdOpt
156	8386694-5026	5 35 28.07	-5 1 34.82	18835456	39	2007 Mar 26	SLLL	ONC	opse
157	8386722-5315	5 35 28.13	-5 18 57.28	18797056	39	2007 Mar 22	SL	Trapezium	failed
158	8386759-5416	5 35 28.22	-5 24 58.1	18797312	39	2007 Mar 22	SL	Trapezium	AdOpt
159	8386804-5987	5 35 28.33	-5 59 13.38	18841088	40	2007 Apr 18	SLLL	ONC	AdOpt
160	8386841-5129	5 35 28.42	-5 7 44.44	18808576	39	2007 Mar 25	SLLL	ONC	AdOpt
161	8386935-4790	5 35 28.64	-4 47 26.59	18823680	39	2007 Mar 24	SLLL	ONC	AdOpt
162	8386957-4804	5 35 28.7	-4 48 16.31	18828288	39	2007 Mar 24	SLLL	ONC	man

Table 2.1 (cont'd)

Num. (1)	IRS name (2)	RA (J2000) (3)	DEC (J2000) (4)	AORID (5)	IRS Camp. (6)	Date observed (7)	modules (8)	region (9)	reduction (10)
163	8387691-5326	5 35 30.46	-5 19 34.1	18797568	36	2006 Nov 11	SL	Trapezium	AdOpt
164	8387753-4993	5 35 30.61	-4 59 36.02	18835200	39	2007 Mar 26	SLLL	ONC	opse/AdOpt [f]
165	8387832-5864	5 35 30.8	-5 51 51.19	18821632	40	2007 Apr 18	SLLL	ONC	AdOpt
166	8387937-6755	5 35 31.05	-6 45 18.18	18840576	39	2007 Mar 09	SLLL	L1641	AdOpt
167	8388119-5083	5 35 31.49	-5 5 1.75	18825216	39	2007 Mar 25	SLLL	ONC	AdOpt
168	8388316-5157	5 35 31.96	-5 9 28.08	18807552	39	2007 Mar 25	SLLL	ONC	AdOpt
169	8389033-4773	5 35 33.68	-4 46 23.52	18775040	39	2007 Mar 24	SLLL	ONC	AdOpt
170	8389275-5105	5 35 34.26	-5 6 21.38	18839552	39	2007 Mar 27	SLLL	ONC	AdOpt
171	8389323-5449	5 35 34.38	-5 26 59.75	18797824	36	2006 Nov 10	SL	Trapezium	failed
172	8389673-4794	5 35 35.22	-4 47 39.52	18810368	39	2007 Mar 24	SLLL	ONC	man
173	8390003-5207	5 35 36.01	-5 12 25.27	18820096	39	2007 Mar 25	SLLL	ONC	AdOpt
174	8390073-5082	5 35 36.18	-5 4 56.03	18826752	39	2007 Mar 26	SLLL	ONC	AdOpt
175	8390083-5339	5 35 36.2	-5 20 20.58	18798080	39	2007 Mar 22	SL	Trapezium	AdOpt
176	8390285-5070	5 35 36.68	-5 4 14.56	18815744	39	2007 Mar 26	SLLL	ONC	AdOpt
177	8390554-6390	5 35 37.33	-6 23 26.23	18780928	39	2007 Mar 12	SLLL	L1641	AdOpt
178	8391040-5081	5 35 38.5	-5 4 51.67	18819584	39	2007 Mar 26	SLLL	ONC	AdOpt
179	8391058-4994	5 35 38.54	-4 59 41.1	18846976	39	2007 Mar 26	SLLL	ONC	AdOpt
180	8391196-5211	5 35 38.87	-5 12 42.16	18816000	39	2007 Mar 25	SLLL	ONC	AdOpt/opse [c]

Table 2.1 (cont'd)

Num. (1)	IRS name (2)	RA (J2000) (3)	DEC (J2000) (4)	AORID (5)	IRS Camp. (6)	Date observed (7)	modules (8)	region (9)	reduction (10)
181	8391648-5110	5 35 39.96	-5 6 36.72	18800640	39	2007 Mar 27	SLLL	ONC	AdOpt
182	8392509-5169	5 35 42.02	-5 10 11.68	18819328	39	2007 Mar 27	SLLL	ONC	AdOpt
183	8393152-5094	5 35 43.56	-5 5 41.35	18825728	39	2007 Mar 27	SLLL	ONC	AdOpt
184	8394216-5181	5 35 46.12	-5 10 51.71	18825984	39	2007 Mar 27	SLLL	ONC	AdOpt
185	8394454-5823	5 35 46.69	-5 49 26.08	18818048	39	2007 Mar 25	SLLL	ONC	AdOpt
186	8395167-5024	5 35 48.4	-5 1 28.96	18816256	39	2007 Mar 27	SLLL	ONC	AdOpt
187	8395780-5308	5 35 49.87	-5 18 30.64	18813184	36	2006 Nov 11	SLLL	ONC	AdOpt
188	8396035-5861	5 35 50.48	-5 51 42.26	18838016	44	2007 Oct 05	SLLL	ONC	AdOpt
189	8396285-5119	5 35 51.08	-5 7 8.83	18821120	39	2007 Mar 27	SLLL	ONC	AdOpt
190	8396319-4941	5 35 51.17	-4 56 27.71	18826240	39	2007 Mar 26	SLLL	ONC	AdOpt
191	8396679-6167	5 35 52.03	-6 10 1.56	18800128	39	2007 Mar 09	SLLL	L1641	man
192	8397522-4788	5 35 54.05	-4 47 19.5	18847232	39	2007 Mar 24	SLLL	ONC	AdOpt
193	8397632-5445	5 35 54.32	-5 26 44.3	18837504	39	2007 Mar 27	SLLL	ONC	AdOpt
194	8397818-4972	5 35 54.76	-4 58 20.06	18834432	39	2007 Mar 26	SLLL	ONC	AdOpt
195	8398707-5755	5 35 56.9	-5 45 19.08	18801920	39	2007 Mar 25	SLLL	ONC	AdOpt/opse [g]
196	8398936-6711	5 35 57.45	-6 42 41.9	18837248	39	2007 Mar 09	SLLL	L1641	AdOpt
197	8399022-5955	5 35 57.65	-5 57 18.36	18799872	40	2007 Apr 18	SLLL	ONC	opse/AdOpt [f]
198	8399269-6612	5 35 58.25	-6 36 43.2	18798336	39	2007 Mar 12	SLLL	L1641	man

Table 2.1 (cont'd)

Num. (1)	IRS name (2)	RA (J2000) (3)	DEC (J2000) (4)	AORID (5)	IRS Camp. (6)	Date observed (7)	modules (8)	region (9)	reduction (10)
199	8399902-6268	5 35 59.76	-6 16 6.64	18813440	39	2007 Mar 12	SLLL	L1641	man
200	8400080-6709	5 36 0.19	-6 42 33.98	18836480	39	2007 Mar 09	SLLL	L1641	opse
201	8402765-6538	5 36 6.64	-6 32 17.16	18800384	39	2007 Mar 12	SLLL	L1641	man
202	8403455-6810	5 36 8.29	-6 48 36.36	18799104	39	2007 Mar 09	SLLL	L1641	man
203	8406280-6293	5 36 15.07	-6 17 36.78	18845696	39	2007 Mar 12	SLLL	L1641	AdOpt
204	8406609-6247	5 36 15.86	-6 14 50.6	18777088	39	2007 Mar 12	SLLL	L1641	AdOpt
205	8407074-5195	5 36 16.98	-5 11 42.72	18801152	39	2007 Mar 25	SLLL	ONC	AdOpt
206	8408920-6760	5 36 21.41	-6 45 36.9	18842880	39	2007 Mar 12	SLLL	L1641	AdOpt
207	8409911-6386	5 36 23.79	-6 23 11.08	18811904	39	2007 Mar 12	SLLL	L1641	AdOpt
208	8410334-6291	5 36 24.8	-6 17 30.48	18806784	39	2007 Mar 09	SLLL	L1641	man
209	8410779-6416	5 36 25.87	-6 24 58.82	18835712	39	2007 Mar 12	SLLL	L1641	AdOpt
210	8410886-6134	5 36 26.13	-6 8 3.84	18803200	39	2007 Mar 11	SLLL	L1641	man
211	8411618-6426	5 36 27.88	-6 25 35.9	18780160	39	2007 Mar 12	SLLL	L1641	man
212	8412592-6712	5 36 30.22	-6 42 46.19	18830080	39	2007 Mar 12	SLLL	L1641	man/AdOpt [b]
213	8413152-6141	5 36 31.56	-6 8 27.82	18849792	39	2007 Mar 09	SLLL	L1641	man
214	8413399-5287	5 36 32.16	-5 17 13.42	18850816	39	2007 Mar 27	SLLL	ONC	opse
215	8413704-6739	5 36 32.89	-6 44 20.94	18842624	39	2007 Mar 12	SLLL	L1641	opse
216	8414490-7187	5 36 34.78	-7 11 13.7	18778112	39	2007 Mar 09	SLLL	L1641	man

Table 2.1 (cont'd)

Num. (1)	IRS name (2)	RA (J2000) (3)	DEC (J2000) (4)	AORID (5)	IRS Camp. (6)	Date observed (7)	modules (8)	region (9)	reduction (10)
217	8415394-6556	5 36 36.95	-6 33 23.87	18829312	39	2007 Mar 12	SLLL	L1641	AdOpt
218	8416389-6503	5 36 39.33	-6 30 11.27	18781184	39	2007 Mar 12	SLLL	L1641	man
219	8416834-6225	5 36 40.4	-6 13 33.35	18775808	39	2007 Mar 09	SLLL	L1641	man
220	8416914-6175	5 36 40.59	-6 10 33.42	18849280	39	2007 Mar 09	SLLL	L1641	AdOpt/ECO [h]
221	8416978-6185	5 36 40.75	-6 11 8.16	18804992	39	2007 Mar 11	SLLL	L1641	AdOpt
222	8421949-6718	5 36 52.68	-6 43 8.18	18839808	40	2007 Apr 18	SLLL	L1641	AdOpt
223	8424570-6484	5 36 58.97	-6 29 4.85	18780416	39	2007 Mar 12	SLLL	L1641	AdOpt
224	8424689-6154	5 36 59.25	-6 9 16.6	18814720	39	2007 Mar 11	SLLL	L1641	man
225	8425038-6557	5 37 0.09	-6 33 27.4	18815232	39	2007 Mar 12	SLLL	L1641	man
226	8430527-6583	5 37 13.26	-6 35 0.38	18835968	39	2007 Mar 09	SLLL	L1641	AdOpt
227	8440418-7404	5 37 37	-7 24 16.6	18814464	39	2007 Mar 09	SLLL	L1641	AdOpt/ECO [i]
228	8443530-6843	5 37 44.47	-6 50 36.64	18812672	40	2007 Apr 16	SLLL	L1641	man
229	8444779-6608	5 37 47.47	-6 36 29.63	18776064	39	2007 Mar 12	SLLL	L1641	AdOpt
230	8445558-6860	5 37 49.34	-6 51 37.26	18777600	44	2007 Oct 06	SLLL	L1641	AdOpt
231	8447398-6788	5 37 53.76	-6 47 17.2	18809344	39	2007 Mar 09	SLLL	L1641	opse/AdOpt [f]
232	8448350-6815	5 37 56.04	-6 48 55.15	18822144	39	2007 Mar 09	SLLL	L1641	opse/AdOpt/man [j]
233	8450343-7265	5 38 0.82	-7 15 54.04	18807808	39	2007 Mar 09	SLLL	L1641	opse/man [k]
234	8452061-7269	5 38 4.95	-7 16 10.56	18805504	39	2007 Mar 09	SLLL	L1641	opse/man [k]

Table 2.1 (cont'd)

Num. (1)	IRS name (2)	RA (J2000) (3)	DEC (J2000) (4)	AORID (5)	IRS Camp. (6)	Date observed (7)	modules (8)	region (9)	reduction (10)
235	8453876-6821	5 38 9.3	-6 49 16.46	18834176	39	2007 Mar 09	SLLL	L1641	man
236	8455602-7112	5 38 13.44	-7 6 43.42	18850048	39	2007 Mar 09	SLLL	L1641	man
237	8457266-7161	5 38 17.44	-7 9 39.74	18831360	39	2007 Mar 09	SLLL	L1641	man
238	8461533-6914	5 38 27.68	-6 54 53.68	18818304	39	2007 Mar 09	SLLL	L1641	man
239	8464666-7838	5 38 35.2	-7 50 19.72	18817536	39	2007 Mar 09	SLLL	L1641	man
240	8465247-7776	5 38 36.59	-7 46 34.39	18821888	40	2007 Apr 16	SLLL	L1641	man
241	8466711-6987	5 38 40.11	-6 59 14.75	18827520	39	2007 Mar 09	SLLL	L1641	AdOpt
242	8468002-6969	5 38 43.2	-6 58 8.98	18851584	39	2007 Mar 09	SLLL	L1641	AdOpt
243	8468729-6970	5 38 44.95	-6 58 14.59	18823936	39	2007 Mar 09	SLLL	L1641	AdOpt
244	8469891-7104	5 38 47.74	-7 6 14.94	18841856	39	2007 Mar 09	SLLL	L1641	man
245	8472719-7464	5 38 54.53	-7 27 51.91	18822656	39	2007 Mar 09	SLLL	L1641	man
246	8476732-7058	5 39 4.16	-7 3 29.92	18811392	39	2007 Mar 12	SLLL	L1641	AdOpt
247	8477229-7184	5 39 5.35	-7 11 5.32	18816768	39	2007 Mar 09	SLLL	L1641	man
248	8486920-7342	5 39 28.61	-7 20 31.34	18831616	39	2007 Mar 09	SLLL	L1641	man
249	8488472-7373	5 39 32.33	-7 22 24.42	18844928	39	2007 Mar 09	SLLL	L1641	AdOpt
250	8492690-7387	5 39 42.46	-7 23 16.48	18818816	40	2007 Apr 16	SLLL	L1641	man
251	8494096-7377	5 39 45.83	-7 22 37.2	18798848	40	2007 Apr 16	SLLL	L1641	opse/man [k]
252	8495155-7404	5 39 48.37	-7 24 14.9	18833664	40	2007 Apr 16	SLLL	L1641	man

Table 2.1 (cont'd)

Num. (1)	IRS name (2)	RA (J2000) (3)	DEC (J2000) (4)	AORID (5)	IRS Camp. (6)	Date observed (7)	modules (8)	region (9)	reduction (10)
253	8497290-7502	5 39 53.5	-7 30 9.43	18823168	39	2007 Mar 12	SLLL	L1641	AdOpt/opse [g]
254	8497797-7462	5 39 54.71	-7 27 44.1	18843136	39	2007 Mar 09	SLLL	L1641	opse/man [k]
255	8499151-7482	5 39 57.96	-7 28 57.54	18846208	39	2007 Mar 09	SLLL	L1641	AdOpt
256	8499541-7426	5 39 58.9	-7 25 33.71	18826496	39	2007 Mar 09	SLLL	L1641	opse/man [k]
257	8502614-7795	5 40 6.27	-7 47 44.59	18779136	44	2007 Oct 07	SLLL	L1641	man
258	8504327-7460	5 40 10.38	-7 27 38.16	18804736	39	2007 Mar 09	SLLL	L1641	man
259	8508083-8237	5 40 19.4	-8 14 16.26	18848768	36	2006 Nov 10	SLLL	L1641	man
260	8508501-7431	5 40 20.4	-7 25 54.16	18779392	44	2007 Oct 07	SLLL	L1641	man
261	8508648-7916	5 40 20.76	-7 55 0.23	18829824	36	2006 Nov 14	SLLL	L1641	man
262	8510403-8125	5 40 24.97	-8 7 33.28	18818560	36	2006 Nov 13	SLLL	L1641	man
263	8511308-8126	5 40 27.14	-8 7 36.48	18807040	36	2006 Nov 10	SLLL	L1641	opse/man [k]
264	8511602-7926	5 40 27.84	-7 55 36.66	18848256	39	2007 Mar 12	SLLL	L1641	opse/man [k]
265	8514861-7663	5 40 35.67	-7 39 46.94	18832384	39	2007 Mar 12	SLLL	L1641	man
266	8515568-8067	5 40 37.36	-8 4 2.78	18836224	36	2006 Nov 10	SLLL	L1641	man
267	8516031-7796	5 40 38.47	-7 47 47.15	18827264	39	2007 Mar 12	SLLL	L1641	AdOpt/man [d]
268	8518798-7373	5 40 45.12	-7 22 25.07	18829056	39	2007 Mar 12	SLLL	L1641	man
269	8519260-8090	5 40 46.22	-8 5 24.4	18808832	36	2006 Nov 10	SLLL	L1641	man
270	8519428-8120	5 40 46.63	-8 7 12.79	18821376	36	2006 Nov 10	SLLL	L1641	man

Table 2.1 (cont'd)

Num. (1)	IRS name (2)	RA (J2000) (3)	DEC (J2000) (4)	AORID (5)	IRS Camp. (6)	Date observed (7)	modules (8)	region (9)	reduction (10)
271	8520557-7775	5 40 49.34	-7 46 32.56	18777856	44	2007 Oct 07	SLLL	L1641	man
272	8520580-7960	5 40 49.39	-7 57 38.16	18804480	36	2006 Nov 14	SLLL	L1641	man
273	8530851-8132	5 41 14.04	-8 7 57.4	18814208	36	2006 Nov 10	SLLL	L1641	opse
274	8534457-7821	5 41 22.7	-7 49 16.1	18833408	36	2006 Nov 14	SLLL	L1641	AdOpt
275	8535781-7830	5 41 25.87	-7 49 50.88	18806528	36	2006 Nov 13	SLLL	L1641	man
276	8536129-8706	5 41 26.71	-8 42 24.48	18807296	36	2006 Nov 09	SLLL	L1641	man
277	8537742-8080	5 41 30.58	-8 4 48.14	18831104	36	2006 Nov 10	SLLL	L1641	man
278	8538844-7917	5 41 33.23	-7 55 2.35	18822400	36	2006 Nov 14	SLLL	L1641	AdOpt
279	8538911-7999	5 41 33.39	-7 59 56.47	18820352	36	2006 Nov 13	SLLL	L1641	man
280	8542681-8618	5 41 42.43	-8 37 7.14	18846720	36	2006 Nov 09	SLLL	L1641	man
281	8543224-7972	5 41 43.74	-7 58 22.26	18847488	36	2006 Nov 13	SLLL	L1641	opse/man [k]
282	8545724-8008	5 41 49.74	-8 0 32.08	18819072	36	2006 Nov 13	SLLL	L1641	man
283	8547523-7831	5 41 54.06	-7 49 53.22	18777344	36	2006 Nov 13	SLLL	L1641	man
284	8547770-7986	5 41 54.65	-7 59 12.52	18817024	36	2006 Nov 13	SLLL	L1641	opse
285	8552157-8190	5 42 5.18	-8 11 26.59	18824192	36	2006 Nov 15	SLLL	L1641	opse
286	8552280-8641	5 42 5.47	-8 38 28.32	18800896	36	2006 Nov 12	SLLL	L1641	man
287	8556074-7982	5 42 14.58	-7 58 57.79	18824448	36	2006 Nov 13	SLLL	L1641	man
288	8560743-8147	5 42 25.78	-8 8 50.03	18827008	39	2007 Mar 12	SLLL	L1641	AdOpt

Table 2.1 (cont'd)

Num. (1)	IRS name (2)	RA (J2000) (3)	DEC (J2000) (4)	AORID (5)	IRS Camp. (6)	Date observed (7)	modules (8)	region (9)	reduction (10)
289	8561044-7980	5 42 26.51	-7 58 50.63	18829568	36	2006 Nov 13	SLLL	L1641	man
290	8562845-8151	5 42 30.83	-8 9 5.47	18822912	36	2006 Nov 13	SLLL	L1641	AdOpt
291	8564835-8250	5 42 35.6	-8 15 1.84	18775296	44	2007 Oct 07	SLLL	L1641	man
292	8567003-8669	5 42 40.81	-8 40 8.58	18841344	36	2006 Nov 09	SLLL	L1641	opse/man [k]
293	8567545-8254	5 42 42.11	-8 15 15.3	18843392	36	2006 Nov 13	SLLL	L1641	AdOpt
294	8567670-8803	5 42 42.41	-8 48 13.79	18830336	36	2006 Nov 09	SLLL	L1641	man
295	8569204-8666	5 42 46.09	-8 40 0.66	18848512	36	2006 Nov 09	SLLL	L1641	man
296	8570200-8276	5 42 48.48	-8 16 34.72	18811136	39	2007 Mar 12	SLLL	L1641	man
297	8570949-8577	5 42 50.28	-8 34 38.1	18782208	36	2006 Nov 09	SLLL	L1641	man
298	8571439-8650	5 42 51.45	-8 39 1.98	18845184	36	2006 Nov 09	SLLL	L1641	man
299	8574645-8156	5 42 59.15	-8 9 23.76	18805248	36	2006 Nov 14	SLLL	L1641	AdOpt/man [l]
300	8576640-8652	5 43 3.94	-8 39 9.47	18828800	36	2006 Nov 15	SLLL	L1641	opse/man [k]
301	8576836-8303	5 43 4.41	-8 18 11.02	18850304	36	2006 Nov 15	SLLL	L1641	man
302	8579480-8565	5 43 10.75	-8 33 55.22	18775552	36	2006 Nov 09	SLLL	L1641	man
303	8580634-8516	5 43 13.52	-8 31 0.05	18776832	39	2007 Mar 12	SLLL	L1641	man

Note. — Column (1) Num.: the numbers are from the number sequence of 303 Class II objects observed in the IRS program ID 30706. We use these numbers to identify objects easily. This number sequence will be used consistently in other future papers dealing with the objects in the PID 30706.
Column (2) IRS name: sometimes IRS name indicated as in the column are used to identify objects. The IRS names are came from the position of each object.
Column (10) reduction: it indicates the methods of source extraction to get the SEDs in Figure A.1 and Figure A.2 in Appendix A. ECO: an automated tapered column extraction in SMART with off-nod or off-order sky subtraction; man: a manual tapered column extraction in SMART with a constant or linear sky subtraction; AdOpt: an optimal source extraction using an empirical point response function (PRF) in SMART; opse: an optimal source extraction using an analytical PRF.

Table 2.2. Identifications of the Objects

Num.	IRS name	2MASS name	other names selected
1	8336884-5290	05332852-0517262	V719 Ori, [FHM2008] F22-ap40, Parenago 1190
2	8339347-5238	05333443-0514177	[FHM2008] S1-ap78
3	8343858-5513	05334525-0530498	VZ Ori, [FHM2008] S3-ap68, HBC 106, Parenago 1260
4	8343917-6073	05334537-0604253	V1006 Ori, HBC 108, Parenago 1267
5	8343944-5609	05334545-0536323	V726 Ori, [FHM2008] S1-ap42
6	8344455-5390	05334668-0523256	V1897 Ori, [FHM2008] S2-ap3
7	8344987-5460	05334797-0527385	[FHM2008] S2-ap6
8	8346141-5010	05335074-0500394	V1902 Ori, [FHM2008] F11-ap39
9	8346378-5387	05335131-0523164	V1903 Ori, [FHM2008] S2-ap5
10	8346581-5550	05335179-0533035	V1905 Ori
11	8347711-5533	05335450-0532003	[FHM2008] S3-ap64
12	8348250-4797	05335580-0447497	SU Ori, [FHM2008] S2-ap66, HBC 110, Parenago 1301
13	8350150-5595	05340034-0535434	Parenago 1327
14	8350916-5605	05340217-0536195	II Ori, [FHM2008] S3-ap58, Parenago 1333
15	8352483-5378	05340595-0522435	V1922 Ori, [FHM2008] S2-ap8
16	8353051-5229	05340731-0513454	WX Ori, HBC 111, Parenago 1352
17	8353319-5604	05340797-0536170	V396 Ori, [FHM2008] S1-ap33
18	8355083-4835	05341221-0450072	BT Ori, Parenago 1373
19	8355371-5480	05341289-0528482	Parenago 1382
20	8355629-5594	05341351-0535386	V1935 Ori
21	8355898-5615	05341416-0536542	[FHM2008] S3-ap41, HBC 442, Parenago 1394
22	8356531-5540	05341566-0532241	WY Ori, [FHM2008] S2-ap238, Parenago 1396
23	8357031-5072	05341687-0504210	BU Ori, [FHM2008] F22-ap62, Parenago 1403
24	8358147-5505	05341954-0530198	WZ Ori, [FHM2008] S3-ap65, Parenago 1424
25	8358862-4842	05342125-0450326	[FHM2008] S2-ap63
26	8359203-5026	05342207-0501342	[FHM2008] F22-ap69
27	8360781-4940	05342587-0456274	IP Ori, [FHM2008] S2-ap64, Parenago 1452
28	8360900-5441	05342616-0526304	V1956 Ori, [FHM2008] S2-ap239
29	8361167-5475	05342679-0528321	Parenago 1465
30	8362406-4863	05342978-0451477	V1970 Ori, [FHM2008] S2-ap72

Table 2.2 (cont'd)

Num.	IRS name	2MASS name	other names selected
31	8364658-4871	05343516-0452179	V1987 Ori
32	8364671-5575	05343519-0534322	V1988 Ori, [FHM2008] S1-ap32; [FHM2008] F22-ap234
33	8365614-5581	05343746-0534519	IV Ori, [FHM2008] S3-ap52, Parenago 1527
34	8365722-4816	05343772-0448577	
35	8366668-5168	05343999-0510070	Parenago 1539
36	8366704-5669	05344007-0540094	V398 Ori, [FHM2008] S3-ap40, Parenago 1553
37	8367030-5378	05344086-0522423	IX Ori, [FHM2008] S2-ap234, HBC 118, Parenago 1552
38	8367284-5798	05344146-0547561	V764 Ori, Parenago 1571
39	8368137-4860	05344351-0451364	[FHM2008] F11-ap50
40	8368755-4933	05344500-0455593	[FHM2008] S2-ap76, Parenago 1574
41	8368837-5665	05344521-0539571	V2021 Ori
42	8369106-5686	05344587-0541097	V1447 Ori, [FHM2008] F21-ap30
43	8369290-5652	05344629-0539077	V474 Ori, [FHM2008] S3-ap34, Parenago 1601
44	8369980-5081	05344794-0504550	V550 Ori, [FHM2008] F22-ap80, Parenago 1599
45	8370827-5312	05344998-0518447	V2056 Ori, [FHM2008] S1-ap67, Parenago 1623
46	8371143-5450	05345073-0527010	[FHM2008] S1-ap37
47	8371984-5465	05345275-0527545	NA;V551 Ori, NA; [FHM2008] S3-ap92
48	8372100-5057	05345304-0503271	YZ Ori, [FHM2008] S1-ap101, HBC 120, Parenago 1648
49	8372608-5359	05345424-0521353	
50	8372885-5283	05345494-0517017	V2073 Ori, [FHM2008] S1-ap80
51	8373201-4936	05345566-0456117	V2079 Ori, [FHM2008] S2-ap71
52	8373676-5192	05345681-0511330	KN Ori, [FHM2008] S3-ap118, HBC 123, Parenago 1665
53	8373930-6325	05345744-0619331	
54	8373936-4946	05345745-0456454	[FHM2008] S1-ap115
55	8374073-5397	05345776-0523522	
56	8374080-5380	05345778-0522511	V402 Ori, [FHM2008] S3-ap109,
57	8374271-5697	05345825-0541498	V2091 Ori
58	8374301-5908	05345833-0554288	BX Ori, [FHM2008] S3-ap7, Parenago 1688
59	8374388-6000	05345852-0600004	
60	8374599-5741	05345908-0544303	KT Ori, [FHM2008] S3-ap12, Parenago 1687

Table 2.2 (cont'd)

Num.	IRS name	2MASS name	other names selected
61	8374677-5748	05345923-0544553	V1712 Ori
62	8374677-5766	05345923-0545588	V2097 Ori
63	8374839-5427	05345962-0525399	V1477 Ori, [FHM2008] S3-ap106, Parenago 1686
64	8375041-5383	05350011-0523019	KR Ori, [FHM2008] S2-ap222, HBC 125, Parenago 1684
65	8375063-5840	05350015-0550274	
66	8375158-5162	05350039-0509441	[FHM2008] S2-ap7
67	8375190-5420	05350046-0525143	V2102 Ori
68	8375484-5401	05350117-0524067	[FHM2008] S2-ap211, Parenago 1694
69	8375546-5339	05350133-0520221	V2109 Ori, [FHM2008] S1-ap55
70	8375702-5443	05350167-0526363	V2114 Ori
71	8375886-5399	05350213-0523569	V2121 Ori
72	8376139-5329	05350274-0519444	V2123 Ori
73	8376154-5675	05350278-0540310	
74	8376176-5368	05350284-0522082	V2125 Ori
75	8376287-5377	05350309-0522378	V404 Ori, [FHM2008] S3-ap114
76	8376356-4822	05350326-0449209	V1718 Ori, [FHM2008] S2-ap83, Parenago 1701; Parenago 1702
77	8376541-5379	05350370-0522457	
78	8376571-5415	05350378-0524543	V375 Ori, Parenago 1713
79	8376643-5900	05350395-0554019	V2135 Ori, [FHM2008] S3-ap8
80	8376687-5443	05350406-0526371	V1482 Ori, [FHM2008] F22-ap222
81	8376747-5441	05350419-0526278	V1322 Ori
82	8376817-5387	05350437-0523138	V1274 Ori
83	8376871-5399	05350450-0523565	V2140 Ori, Parenago 1737
84	8376918-4974	05350460-0458289	V554 Ori, Parenago 1723
85	8376976-5443	05350475-0526380	V2143 Ori, [FHM2008] S1-ap27
86	8377111-5612	05350506-0536438	V2148 Ori, [FHM2008] S1-ap19
87	8377137-5340	05350513-0520244	V479 Ori
88	8377167-5247	05350519-0514503	V2149 Ori, [FHM2008] S1-ap95, Parenago 1736
89	8377232-5402	05350537-0524105	V2150 Ori, [FHM2008] S1-ap36
90	8377335-5489	05350561-0529223	V407 Ori

Table 2.2 (cont'd)

Num.	IRS name	2MASS name	other names selected
91	8377345-5422	05350563-0525195	LL Ori, [FHM2008] S1-ap25, HBC 126, 1746
92	8377361-5395	05350567-0523452	V2156 Ori
93	8377383-5405	05350572-0524184	V480 Ori
94	8377392-5193	05350572-0511350	V2157 Ori, [FHM2008] S1-ap107
95	8377737-5547	05350656-0532515	V2168 Ori
96	8377749-5447	05350660-0526509	
97	8378059-5644	05350732-0538409	V2172 Ori
98	8378345-5545	05350801-0532442	LN Ori, [FHM2008] S3-ap69, HBC 128, Parenago 1766
99	8378366-5814	05350807-0548539	V2179 Ori
100	8378481-5465	05350834-0527569	V2182 Ori
101	8378503-5474	05350838-0528293	V1397 Ori
102	8378561-5421	05350853-0525179	V2184 Ori
103	8378630-4781	05350869-0446523	V555 Ori, Parenago 1753
104	8379094-5316	05350982-0518583	V2192 Ori
105	8379108-5326	05350985-0519339	
106	8379192-6093	05351004-0605364	V2195 Ori
107	8379289-5332	05351029-0519563	[FHM2008] F21-ap127
108	8379312-5776	05351033-0546335	AA Ori, [FHM2008] S1-ap1, HBC 130, Parenago 1787
109	8379945-5350	05351188-0521032	V2220 Ori
110	8379950-5323	05351188-0519261	
111	8379990-5342	05351197-0520331	V2221 Ori
112	8380422-5659	05351299-0539348	LX Ori, [FHM2008] S1-ap14, HBC 133, Parenago 1828
113	8380493-5291	05351317-0517307	V2233 Ori
114	8380518-5465	05351324-0527541	V2237 Ori
115	8380544-5338	05351330-0520189	V2238 Ori
116	8380651-5296	05351356-0517457	V2244 Ori
117	8380667-5516	05351360-0530575	V488 Ori, HBC 134, Parenago 1827
118	8380675-5331	05351362-0519548	
119	8380695-5479	05351365-0528462	v1495 Ori
120	8380923-5478	05351419-0528434	V2256 Ori

Table 2.2 (cont'd)

Num.	IRS name	2MASS name	other names selected
121	8380932-5721	05351423-0543175	AB Ori, [FHM2008] S3-ap231, HBC 135, Parenago 1848
122	8381019-5555	05351444-0533190	V2660 Ori
123	8381020-5546	05351444-0532464	V1498 Ori
124	8381104-5345	05351465-0520424	
125	8381120-5653	05351467-0539108	MO Ori, Parenago 1876
126	8381436-5294	05351545-0517383	V2271 Ori
127	8381491-5164	05351556-0509512	[FHM2008] S1-ap122
128	8381501-4991	05351559-0459278	V2273 Ori
129	8381622-5481		V2277 Ori
130	8381919-5289	05351661-0517234	V2291 Ori
131	8381971-4762	05351673-0445444	TT Ori, HBC 136, Parenago 1856
132	8382048-5452	05351691-0527087	V2296 Ori
133	8382359-5974	05351767-0558265	V1812 Ori, HBC 138, Parenago 1931
134	8382412-6410	05351780-0624384	V794 Ori
135	8382467-5709	05351790-0542340	V2318 Ori, Parenago 1929
136	8382490-5270	05351799-0516136	
137	8382623-5479	05351829-0528461	
138	8382655-4889	05351838-0453234	V2329 Ori
139	8382835-5291	05351880-0517291	V2338 Ori, [FHM2008] S1-ap104
140	8383581-5050	05352061-0503008	V2369 Ori
141	8383861-5154	05352125-0509161	MX Ori, [FHM2008] S3-ap124, HBC 462, Parenago 1953
142	8384113-5117	05352187-0507018	V415 Ori, [FHM2008] S2-ap157, Parenago 1952
143	8384325-5457	05352237-0527283	V1340 Ori
144	8384331-5134	05352240-0508051	V492 Ori, [FHM2008] S2-ap165
145	8384717-5469	05352331-0528100	V1530 Ori
146	8384864-5440		V2411 Ori
147	8385190-5442	05352445-0526314	V1283 Ori
148	8385255-5191	05352459-0511296	V2427 Ori
149	8385365-5106	05352486-0506216	
150	8385988-5427	05352634-0525401	AK Ori, [FHM2008] S1-ap233, HBC 468, Parenago 2032

Table 2.2 (cont'd)

Num.	IRS name	2MASS name	other names selected
151	8386322-6328	05352716-0619420	V799 Ori
152	8386383-5393	05352730-0523366	V2463 Ori
153	8386462-5457	05352749-0527259	V1287 Ori, [FHM2008] F21-ap240
154	8386523-5715	05352765-0542551	V2468 Ori, Parenago 2059
155	8386627-5467	05352788-0528020	V1542 Ori
156	8386694-5026	05352805-0501349	V2470 Ori
157	8386722-5315	05352812-0518572	
158	8386759-5416		V420 Ori, Parenago 2046
159	8386804-5987	05352831-0559132	V1546 Ori, [FHM2008] F31-ap113
160	8386841-5129	05352849-0507465	
161	8386935-4790	05352864-0447265	V1547 Ori, [FHM2008] F11-ap13, Parenago 2041
162	8386957-4804	05352868-0448163	V418 Ori, Parenago 2042
163	8387691-5326	05353046-0519340	V2489 Ori
164	8387753-4993	05353060-0459360	V2493 Ori
165	8387832-5864	05353080-0551509	
166	8387937-6755	05353105-0645181	TW Ori, HBC 145, Parenago 2105
167	8388119-5083	05353149-0505016	V422 Ori, [FHM2008] F21-ap146, Parenago 2072
168	8388316-5157	05353195-0509279	V360 Ori, [FHM2008] S2-ap163, HBC 144, Parenago 2084
169	8389033-4773	05353369-0446237	V2528 Ori, Parenago 2092
170	8389275-5105	05353428-0506212	HD 37060, Parenago 2102
171	8389323-5449	05353437-0526596	[FHM2008] F22-ap173
172	8389673-4794	05353522-0447396	V2544 Ori, [FHM2008] F11-ap153
173	8390003-5207	05353601-0512253	NY Ori, [FHM2008] S1-ap148, HBC 148, Parenago 2119
174	8390073-5082	05353620-0504559	V2549 Ori
175	8390083-5339	05353621-0520204	V2550 Ori
176	8390285-5070	05353668-0504145	V424 Ori, [FHM2008] S2-ap135, Parenago 2116
177	8390554-6390	05353733-0623263	
178	8391040-5081	05353851-0504515	
179	8391058-4994	05353852-0459411	V1572 Ori, [FHM2008] S2-ap113
180	8391196-5211	05353885-0512419	V426 Ori, [FHM2008] S1-ap143, Parenago 2144

Table 2.2 (cont'd)

Num.	IRS name	2MASS name	other names selected
181	8391648-5110	05353995-0506368	V1578 Ori, [FHM2008] S2-ap143
182	8392509-5169	05354201-0510115	V2573 Ori, [FHM2008] S1-ap147
183	8393152-5094	05354355-0505414	AO Ori, [FHM2008] S2-ap145, Parenago 2171
184	8394216-5181	05354612-0510517	V808 Ori, [FHM2008] F22-ap120
185	8394454-5823	05354669-0549262	CF Ori, [FHM2008] F31-ap126, Parenago 2218
186	8395167-5024	05354838-0501287	CE Ori, [FHM2008] S2-ap136, HBC 152, Parenago 2203
187	8395780-5308	05354987-0518308	V2605 Ori, [FHM2008] S2-ap187
188	8396035-5861	05355047-0551422	OU Ori, [FHM2008] S3-ap224, Parenago 2254
189	8396285-5119	05355109-0507088	V575 Ori, [FHM2008] S2-ap156, Parenago 2243
190	8396319-4941	05355118-0456276	V2610 Ori, [FHM2008] S2-ap122
191	8396679-6167	05355202-0610016	V1296 Ori
192	8397522-4788	05355405-0447193	AS Ori, [FHM2008] S2-ap114, Parenago 2255
193	8397632-5445	05355433-0526444	OW Ori, [FHM2008] S1-ap215, Parenago 2269
194	8397818-4972	05355476-0458200	V2620 Ori, [FHM2008] S2-ap129, Parenago 2262
195	8398707-5755	05355690-0545191	V1589 Ori, [FHM2008] S1-ap239
196	8398936-6711	05355745-0642418	V577 Ori, HBC 158, Parenago 2299
197	8399022-5955	05355765-0557183	AU Ori, [FHM2008] S3-ap226, HBC 157, Parenago 2285
198	8399269-6612	05355825-0636431	OY Ori, Parenago 2297
199	8399902-6268	05355975-0616065	V1178 Ori, Parenago 2307
200	8400080-6709	05360017-0642339	AV Ori, HBC 159;HBC 481, Parenago 2312
201	8402765-6538	05360665-0632171	V823 Ori
202	8403455-6810	05360828-0648363	AY Ori, Parenago 2350
203	8406280-6293	05361506-0617369	BB Ori, Parenago 2369
204	8406609-6247	05361584-0614507	V1076 Ori, [FHM2008] F31-ap197
205	8407074-5195	05361698-0511427	AZ Ori, [FHM2008] S1-ap165, HBC 162, Parenago 2368
206	8408920-6760	05362140-0645366	V2669 Ori, HBC 483
207	8409911-6386	05362378-0623113	V2674 Ori
208	8410334-6291	05362499-0617324	PR Ori, Parenago 2388
209	8410779-6416		2MASX 05362586-0624587
210	8410886-6134	05362611-0608038	V2679 Ori

Table 2.2 (cont'd)

Num.	IRS name	2MASS name	other names selected
211	8411618-6426	05362788-0625360	[FHM2008] F31-ap209
212	8412592-6712	05363023-0642460	V2687 Ori
213	8413152-6141	05363158-0608271	V1183 Ori, Parenago 2409
214	8413399-5287	05363213-0517135	V367 Ori, [FHM2008] S2-ap161, Parenago 2403
215	8413704-6739	05363288-0644208	
216	8414490-7187	05363476-0711133	
217	8415394-6556	05363692-0633241	V585 Ori
218	8416389-6503	05363933-0630111	[FHM2008] F31-ap207
219	8416834-6225	05364039-0613334	[FHM2008] F31-ap190
220	8416914-6175	05364058-0610332	V2702 Ori
221	8416978-6185	05364075-0611082	V2703 Ori
222	8421949-6718	05365269-0643083	V2713 Ori
223	8424570-6484	05365897-0629049	V2720 Ori
224	8424689-6154	05365925-0609164	V586 Ori, HD 37258, HBC 485, Parenago 2473
225	8425038-6557	05370010-0633273	BE Ori, HBC 168, Parenago 2479
226	8430527-6583	05371326-0635005	BF Ori, HBC 169, Parenago 2510
227	8440418-7404	05373700-0724167	V875 Ori
228	8443530-6843	05374448-0650366	V589 Ori
229	8444779-6608	05374746-0636298	
230	8445558-6860	05374934-0651373	
231	8447398-6788	05375376-0647170	
232	8448350-6815	05375602-0648549	
233	8450343-7265	05380082-0715541	V593 Ori
234	8452061-7269	05380496-0716107	V878 Ori, Parenago 2588
235	8453876-6821	05380931-0649166	V1787 Ori, Parenago 2649
236	8455602-7112	05381345-0706433	
237	8457266-7161	05381743-0709395	
238	8461533-6914	05382767-0654537	V594 Ori, Parenago 2682
239	8464666-7838	05383519-0750197	HBC 174
240	8465247-7776	05383660-0746344	

Table 2.2 (cont'd)

Num.	IRS name	2MASS name	other names selected
241	8466711-6987	05384011-0659148	
242	8468002-6969	05384322-0658089	
243	8468729-6970	05384495-0658146	
244	8469891-7104	05384773-0706148	
245	8472719-7464	05385451-0727520	
246	8476732-7058	05390415-0703299	
247	8477229-7184	05390536-0711052	
248	8486920-7342	05392860-0720314	
249	8488472-7373	05393231-0722241	V892 Ori
250	8492690-7387	05394244-0723165	
251	8494096-7377	05394582-0722373	
252	8495155-7404	05394838-0724147	
253	8497290-7502	05395350-0730095	
254	8497797-7462	05395474-0727443	
255	8499151-7482	05395796-0728576	
256	8499541-7426	05395891-0725335	
257	8502614-7795	05400626-0747445	
258	8504327-7460	05401036-0727384	
259	8508083-8237	05401940-0814163	
260	8508501-7431	05402040-0725540	
261	8508648-7916	05402073-0755000	
262	8510403-8125	05402496-0807332	V1304 Ori, HBC 179
263	8511308-8126	05402714-0807365	
264	8511602-7926	05402783-0755365	
265	8514861-7663	05403566-0739468	
266	8515568-8067	05403736-0804030	V1791 Ori
267	8516031-7796	05403847-0747470	
268	8518798-7373	05404511-0722250	V902 Ori
269	8519260-8090	05404622-0805243	UU Ori, CoKu DL Ori G4, HBC 495
270	8519428-8120	05404661-0807128	CoKu DL Ori G3(?), HBC 497 (?)

Table 2.2 (cont'd)

Num.	IRS name	2MASS name	other names selected
271	8520557-7775	05404931-0746327	
272	8520580-7960	05404939-0757379	
273	8530851-8132	05411403-0807573	
274	8534457-7821	05412269-0749160	
275	8535781-7830	05412586-0749506	
276	8536129-8706	05412670-0842245	
277	8537742-8080	05413058-0804482	
278	8538844-7917	05413322-0755022	
279	8538911-7999	05413338-0759562	
280	8542681-8618	05414245-0837075	
281	8543224-7972	05414373-0758223	
282	8545724-8008	05414973-0800322	V1305 Ori, HBC 182
283	8547523-7831	05415405-0749534	
284	8547770-7986	05415466-0759124	
285	8552157-8190	05420517-0811266	
286	8552280-8641	05420547-0838284	
287	8556074-7982	05421459-0758579	
288	8560743-8147	05422578-0808501	
289	8561044-7980	05422649-0758508	
290	8562845-8151	05423081-0809055	
291	8564835-8250	05423560-0815020	
292	8567003-8669	05424081-0840086	
293	8567545-8254	05424210-0815152	
294	8567670-8803	05424242-0848140	
295	8569204-8666	05424609-0840007	
296	8570200-8276	05424848-0816347	V2775 Ori
297	8570949-8577	05425027-0834378	
298	8571439-8650	05425142-0839020	
299	8574645-8156	05425913-0809236	
300	8576640-8652	05430392-0839094	

Table 2.2 (cont'd)

Num.	IRS name	2MASS name	other names selected
301	8576836-8303	05430440-0818105	
302	8579480-8565		
303	8580634-8516	05431353-0831004	

Note. — The sources of selected objects names: Parenago (1954) for Parenago XXX; Fűrész et al. (2008) for [FHM2008]XXX-XXXX; V* indicate the General Catalogue of Variable Stars (GCVS) (Kukarkin et al., 1971); HBC XXX indicate Herbig+Bell Catalog (Herbig & Bell, 1988).

2.2 SpeX/IRTF

2.2.1 Observations and Data Reduction

We observed 120 of our 241 IRS targets observed in both SL and LL modules in Orion A, at Near-IR (0.8-2.4 μm) wavelengths with the medium resolution spectrograph SpeX (Rayner et al., 2003), on the NASA Infrared Telescope Facility (IRTF) on Mauna Kea during the 2010A, 2011A , and 2011B semesters.

We observed all of the SpeX targets with the Short-wavelength Cross-dispersed mode (SXD). We obtained spectra with various slit widths of 0.3", 0.5" and 0.8" for observations during the 2010A semester depending on the seeing conditions of each night. We used only the 0.8" slit width for the observations 2011 February because the weather and seeing were generally poor. The spectra of 8 objects observed during the 2010A semester were used for spectral type determination as well as accretion rate determination. Among the 8 objects, OriA-34 was only observed with the 0.3" slit to get the highest resolution (R = 2000) available at SpeX in order to determine the spectral type as well as measure the mass accretion rate under good conditions (seeing $\sim$ 0.3"). The spectra of the other 7 objects were obtained with the 0.8" slit (R $\sim$ 800-1200), sufficient to narrow the spectral type range down to 2-3 subtypes by comparing absorption features of the Na I, Al I, Mg I, Ca I and CO to those of template spectra (Rayner et al., 2009; Cushing et al., 2005). The details on spectral type determination are described in Chapter 3.

During the SpeX observation, we discovered some of IRS targets are binary systems. Among the SpeX targets with a companion close by, the companions

of four objects, OriA-38, OriA-173, OriA-208, and OriA-290 were observed separately from the primary targets. For targets with very close neighbors, OriA-4, OriA-26, OriA-47, OriA-098, OriA-280, we oriented the slit so as to observe both simultaneously and extracted the spectra of primary and secondary separately during data reduction process. We also found that OriA-22, OriA-125, OriA-154, OriA-213, and OriA-233 could be a binary system because they appeared as a elongated and peanut shape through K-band guider image. The components of the systems were not able to be observed by separately nor extracted separately, so we present the SpeX spectra of them as a spectrum contributed from a primary and secondary of a binary system.

We observed an A0V star, HD 37887, every 30–60 minutes for the flux calibration and telluric absorption correction (Vacca et al., 2003). In case we changes the slit orientation to avoid entering nearby sources, we also observed the calibrator source with same position angle of the slit. The SpeX/IRTF observation log is given in Table 2.3. We reduced our spectra with the Spextool package (Cushing et al., 2004), and the flux calibration and telluric absorption correction (Vacca et al., 2003) were done with a spectrum of HD 37887, observed near in time and close in air mass to each object. In case we cannot take a spectrum of HD 37887 observed with same position angle as that observed for a target because of unexpected issues such as flux reduction by thick cloud or a fast changes of air mass between the observations of a target and a calibrator when airmass greater than 2, we used a telluric spectrum taken the next available in time and did light loss correction to correct a target spectrum for slit losses relative to the flux calibrator, HD 37887.

Table 2.3. Observation log of SpeX spectra

Num.	TD/FD	Obs. semester	Obs. Date (UT)	Slit Width (")	Total Int. Time (sec)	PA (°)	note
(1)	(2)	(3)	(4)	(5)	(6)	(7)	(8)
1	TD	2011B	2011 Nov 06	0.5	480		
2	FD	2011A	2011 Feb 28	0.8	480	-10.73	
3	FD	2011B	2011 Nov 07	0.8	120		
4	FD	2011A	2011 Feb 28	0.8	320	-30	b
5	TD	2011A	2011 Feb 28	0.8	400	-10.73	
11	TD	2010A	2010 Feb 18	0.8	480		
13	TD	2010A	2010 Feb 17	0.8	480		
16	TD	2010A	2010 Feb 18	0.8	240		
19	TD	2010A	2010 Feb 17	0.8	720		
20	FD	2011B	2011 Nov 07	0.8	720		
21	FD	2011A	2011 Feb 26	0.8	960	60.12	
22	FD	2011B	2011 Nov 10	0.8	400		c
23	TD	2011B	2011 Nov 07	0.8	240		
24	TD	2011A	2011 Feb 27	0.8	240		
25	TD	2010A	2010 Feb 16	0.5	480		
26	TD	2011B	2011 Nov 10	0.8	480	-27	b
28	FD	2011B	2011 Nov 07	0.8	200		
29	TD	2010A	2010 Feb 18	0.8	480		
32	FD	2011A	2011 Feb 26	0.8	960		
33	FD	2011B	2011 Nov 06	0.5	480		
34	TD	2010A	2010 Feb 16	0.3	2520		
36	FD	2011B	2011 Nov 10	0.8	240		
37	FD	2011A	2011 Feb 27	0.8	240	62.31	
38a	TD	2010A	2010 Feb 18	0.8	240		a
38b	TD	2010A	2010 Feb 18	0.8	240		a
39	TD	2011B	2011 Nov 06	0.5	480		
42	TD	2011B	2011 Nov 06	0.5	720		
44	TD	2010A	2010 Feb 16	0.5	240		

Table 2.3 (cont'd)

Num.	TD/FD	Obs. semester	Obs. Date (UT)	Slit Width (")	Total Int. Time (sec)	PA (°)	note
(1)	(2)	(3)	(4)	(5)	(6)	(7)	(8)
45	FD	2011A	2011 Feb 26	0.8	120		
47	TD	2011B	2011 Nov 07	0.8	480		b
48	FD	2011B	2011 Nov 07	0.8	480		
50	FD	2011B	2011 Nov 07	0.8	480		
51	FD	2011A	2011 Feb 28	0.8	400	53.01	
52	FD	2011A	2011 Feb 26	0.8	480		
58	FD	2011B	2011 Nov 07	0.8	480		
59	TD	2010A	2010 Feb 17	0.8	480		
66	TD	2010A	2010 Feb 16	0.5	960		
86	FD	2011A	2011 Feb 28	0.8	480	-10.73	
88	TD	2011A	2011 Feb 26	0.8	120		
97	FD	2011A	2011 Feb 26	0.8	960		
98	FD	2011B	2011 Nov 07	0.8	240	-55	b
108	TD	2010A	2010 Feb 16	0.5	240		
112	FD	2011B	2011 Nov 07	0.8	120		
117	FD	2011B	2011 Nov 07	0.8	480		
123	FD	2010A	2010 Feb 18	0.8	720		
125	FD	2011A	2011 Feb 27	0.8	240	62.31	c
134	FD	2011B	2011 Nov 07	0.8	480		
135	FD	2011A	2011 Feb 27	0.8	480	62.31	
141	FD	2011A	2011 Feb 27	0.8	120		
144	FD	2011B	2011 Nov 10	0.8	480		
154	TD	2011A	2011 Feb 28	0.8	320	53.01	c
159	FD	2011B	2011 Nov 07	0.8	480		
161	FD	2011A	2011 Feb 28	0.8	480	-10.73	
168	FD	2011A	2011 Feb 26	0.8	480	63.33	
169	TD	2010A	2010 Feb 17	0.8	480		
170	FD	2011A	2011 Feb 27	0.8	120		

Table 2.3 (cont'd)

Num.	TD/FD	Obs. semester	Obs. Date (UT)	Slit Width (")	Total Int. Time (sec)	PA (°)	note
(1)	(2)	(3)	(4)	(5)	(6)	(7)	(8)
172	TD	2010A	2010 Feb 17	0.8	480		
173a	FD	2011A	2011 Feb 28	0.8	120	45	a
173b	FD	2011A	2011 Feb 28	0.8	120	45	a
176	TD	2011B	2011 Nov 10	0.8	240		
177	TD	2010A	2010 Feb 16	0.5	240		
179	FD	2011B	2011 Nov 10	0.8	400		
182	FD	2011A	2011 Feb 28	0.8	240	60.97	
183	FD	2011A	2011 Feb 28	0.8	200	60.97	
184	TD	2011B	2011 Nov 10	0.8	400		
185	TD	2010A	2010 Feb 16	0.5	240		
186	FD	2010A	2010 Feb 16	0.5	240		
187	FD	2011B	2011 Nov 07	0.8	240		
190	FD	2011B	2011 Nov 10	0.8	720		
191	FD	2011A	2011 Feb 27	0.8	80	62.31	
196	FD	2011A	2011 Feb 28	0.8	240	60.97	
197	FD	2011B	2011 Nov 10	0.8	240		
198	TD	2011A	2011 Feb 28	0.8	240	60.97	
200	FD	2011B	2011 Nov 07	0.8	200		
204	TD	2011A	2011 Feb 28	0.8	960	-10.73	
206	FD	2011A	2011 Feb 27	0.8	240	62.31	
208a	FD	2011B	2011 Nov 10	0.8	120		a
208b	FD	2011B	2011 Nov 10	0.8	120		a
210	FD	2011A	2011 Feb 28	0.8	200	60.97	
211	TD	2011B	2011 Nov 10	0.8	240		
213	FD	2011A	2011 Feb 28	0.8	240	60.97	c
214	FD	2011A	2011 Feb 26	0.8	480		
217	FD	2011B	2011 Nov 06	0.5	400		
218	TD	2010A	2010 Feb 16	0.5	480		

Table 2.3 (cont'd)

Num.	TD/FD	Obs. semester	Obs. Date (UT)	Slit Width (")	Total Int. Time (sec)	PA (°)	note
(1)	(2)	(3)	(4)	(5)	(6)	(7)	(8)
219	TD	2010A	2010 Feb 17	0.8	480		
220	FD	2011A	2011 Feb 28	0.8	240	60.97	
223	TD	2011A	2011 Feb 26	0.8	960		
225	FD	2011A	2011 Feb 26	0.8	720	65.64	
226	FD	2011A	2011 Feb 28	0.8	120		
227	TD	2011A	2011 Feb 28	0.8	360	-10.73	
229	TD	2010A	2010 Feb 16	0.5	240		
230	TD	2010A	2010 Feb 18	0.8	720		
233	FD	2011A	2011 Feb 26	0.8	480		c
234	FD	2011A	2011 Feb 28	0.8	400	60.97	
235	FD	2011B	2011 Nov 07	0.8	240		
237	TD	2010A	2010 Feb 17	0.8	480		
239	TD	2010A	2010 Feb 18	0.8	240		
245	FD	2011A	2011 Feb 28	0.8	200	60.97	
246	FD	2011B	2011 Nov 06	0.5	480		
247	FD	2011B	2011 Nov 07	0.8	480		
249	FD	2011A	2011 Feb 26	0.8	1440	90	
257	TD	2010A	2010 Feb 17	0.8	480		
260	TD	2010A	2010 Feb 17	0.8	240		
262	FD	2011B	2011 Nov 06	0.5	200		
266	FD	2011B	2011 Nov 06	0.5	120		
269	FD	2011A	2011 Feb 27	0.8	120	62.31	
270	TD	2010A	2010 Feb 18	0.8	240		
271	TD	2010A	2010 Feb 18	0.8	960		
273	FD	2011A	2011 Feb 28	0.8	400	53.01	
275	TD	2010A	2010 Feb 17	0.8	240		
279	TD	2010A	2010 Feb 17	0.8	960		
280	FD	2011B	2011 Nov 10	0.8	360	-42	b

Table 2.3 (cont'd)

Num.	TD/FD	Obs. semester	Obs. Date (UT)	Slit Width (")	Total Int. Time (sec)	PA (^{o})	note
(1)	(2)	(3)	(4)	(5)	(6)	(7)	(8)
281	FD	2011A	2011 Feb 28	0.8	400	-10.73	
283	TD	2010A	2010 Feb 17	0.8	240		
286	FD	2011A	2011 Feb 28	0.8	400	53.01	
287	FD	2011B	2011 Nov 10	0.8	240		
288	FD	2011B	2011 Nov 10	0.8	200		
290a	TD	2011A	2011 Feb 28	0.8	480	-20	a
290b	TD	2011A	2011 Feb 28	0.8	480	-20	a
291	TD	2010A	2010 Feb 17	0.8	480		
294	TD	2010A	2010 Feb 18	0.8	240		
301	TD	2011A	2011 Feb 28	0.8	480	-10.73	
302	TD	2010A	2010 Feb 18	0.8	240		
303	TD	2010A	2010 Feb 18	0.8	960		

Note. — Column (1): Num. The number assigned in Table 2.1. Column (2): TD/FD. The indicator if a target is selected as a transitional disk in Chapter 4. Column (7): PA. The slit positional angle for observation of a target. Column (8): Note for observation of binary systems: a indicates for the system which its primary and secondary were observed separately; b indicates for the system which it primary and secondary were observed simultaneously and extracted their spectra separately; c indicates for the system which is suspicious to have a secondary, but the spectrum of each component were not resolved, and the spectrum is the composite spectrum of a primary and a secondary.

3 Properties of Protoplanetary Disks in Orion A

3.1 Basic Characteristics

In this chapter, we describe the stellar and disk properties of protoplanetary disks in Orion A. The purposes of this chapter are (1) to introduce how we measure and estimate various kinds of stellar and disk properties and (2) to compare distributions of properties of sub-samples separated by three broad sections of Orion A, Trapezium, ONC, and L1641, as well as to that of disks in Taurus. Because several sub-regions of Orion A offer a range of star-forming environments and median ages spanning from <1 Myr to ∼5 Myr, they offer an interesting view of disk evolution

3.1.1 The Young Stars of Orion A

Spectral Types

We list in Table 3.1 the spectral type of the host star of each of our targets. Most of our spectral-type information is gathered from the literature (Hillen-

brand, 1997; Rebull et al., 2000; Allen, 1995; da Rio et al., 2010; Fang et al., 2009; Parihar et al., 2009a), or from unpublished results kindly provided by Lori Allen, John Tobin and Jesús Hernández. In addition, we determined several new or improved spectral types from our IRTF SpeX spectra. In Figure 3.1, we show the SpeX spectra of these objects and illustrate our spectral-typing procedure. We used Mg I, Al I, Na I, Ca I, and CO features in the H and K band as the SpeX sensitivity is best in those bands, and as those absorption features are very sensitive to spectral types in the G-M range.

Most of our SpeX spectra were taken at R $\sim$ 800-1200. Only OriA-34 was observed with seeing good enough to obtain R $\sim$ 2000. Even though some lines are blended due to the modest spectral resolution, we were able to narrow down spectral types to +/− 2-3 subtypes. We adopt the spectral type of the first five objects from top of Figure 3.1 from the spectral typing using our SpeX spectra. The S/N on OriA-302 is not good enough to determine a subclass of its spectral type, but OriA-302 is thought to be an M-type star based on the broad spectral features attributable to Mg I, Na I, and CO overtone bands. We found that the uncertain spectral type from HECTOSPEC data (Lori Allen, private communication) of OriA-230, OriA-271, and OriA-294 are in agreement with those from our spectra.

The spectral type distribution of objects with available spectral types is shown in Figure 3.2. The total number of objects with known spectral type is 222: 48 samples in Trapezium with partial IRS spectra, and 174 objects for which we have the full range of IRS spectra in ONC and L1641. The fraction of our IRS targets for which we have accurate spectral types is 77 %, 69 % and

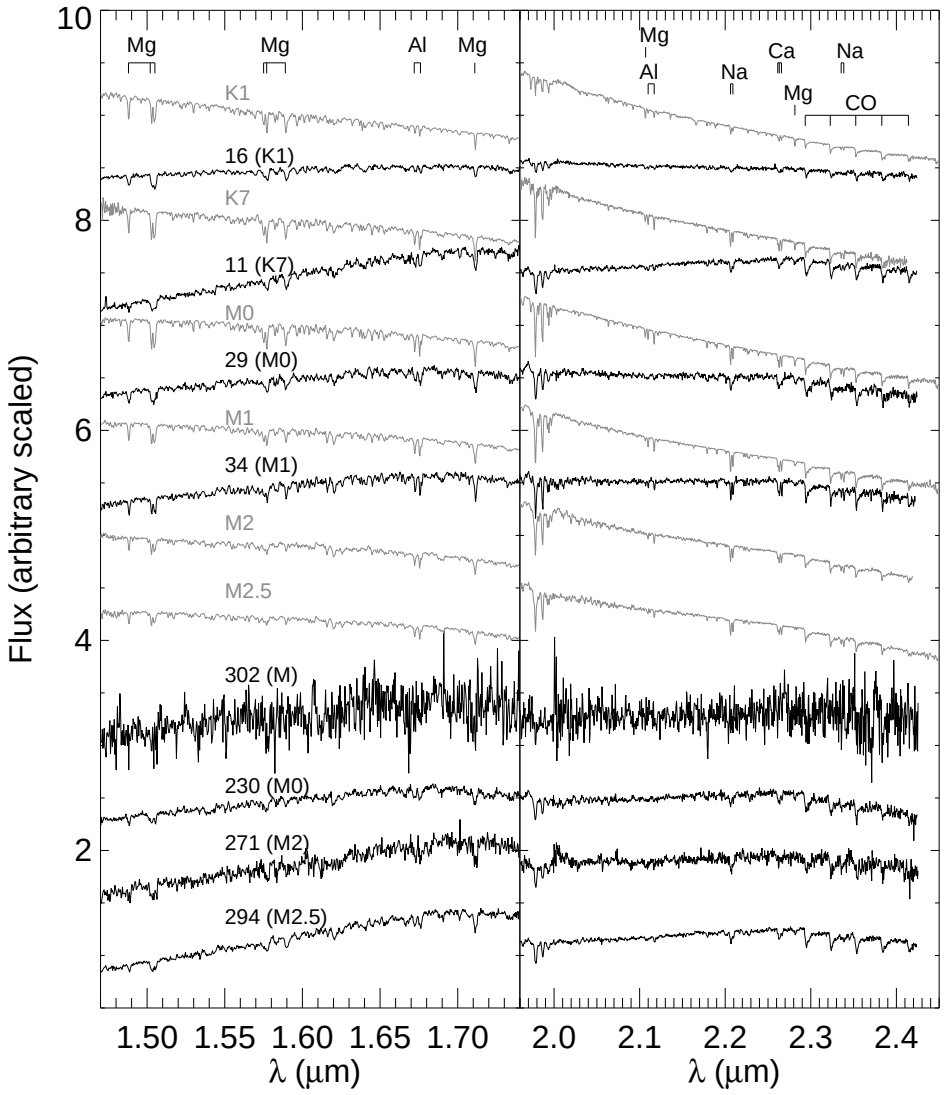


Figure 3.1 Spectral typing from SpeX spectra. The gray spectra with spectral type are the standard spectra of the spectral types (Rayner et al., 2009). The black spectra with number and spectra type are the SpeX spectra of the objects with the ID number. We estimated their spectral type as the spectral type next to the object's number.

76 % respectively for the Trapezium, ONC and L1641. The median spectral type of Class II objects in Orion A is M0: M1 for objects in Trapezium; M0 for objects in ONC; M1 for objects in L1641 (See Figure 3.2).

Extinction Correction

Improperly-corrected extinction toward protoplanetary disks can lead to misclassification of evolutionary stages and misinterpretation of disk spectra. To minimize the effects of extinction toward our targets, we de-reddened our data based on the estimates of visual extinction (A_V) obtained using the following relationship between A_V and the color excess $E(\lambda_1 - \lambda_2) = ([\lambda_1] - [\lambda_2])_{obs} - ([\lambda_1] - [\lambda_2])_{int}$:

$$A_V = \frac{\frac{A_V}{A_{\lambda_2}}}{\frac{A_{\lambda_1}}{A_{\lambda_2}} - 1} \times E(\lambda_1 - \lambda_2) \tag{3.1}$$

To get a color from two wavelengths, λ_1 and λ_2, we used 2MASS JHK photometry for most of the sample and DENIS IJH photometry for the rest, when available. We measured A_V from several combinations of color for each object. We used either $(J-H)_{2MASS}$, $(H-K)_{2MASS}$, or $(I-J)_{DENIS}$ as an observed color $([\lambda_1]-[\lambda_2])_{obs}$. For an intrinsic color, $([\lambda_1]-[\lambda_2])_{int}$, we prepared $I-J$, $J-H$, and $H-K$ photospheric colors from Kenyon & Hartmann (1995) if there is a known spectral type. If no spectral type information is available for an object, we adopt an intrinsic color from $J-H$ and $H-K$ of the Classical T Tauri Star (CTTS) locus of colors from Meyer et al. (1997) with assumption that all of the extinction toward an object is foreground extinction.

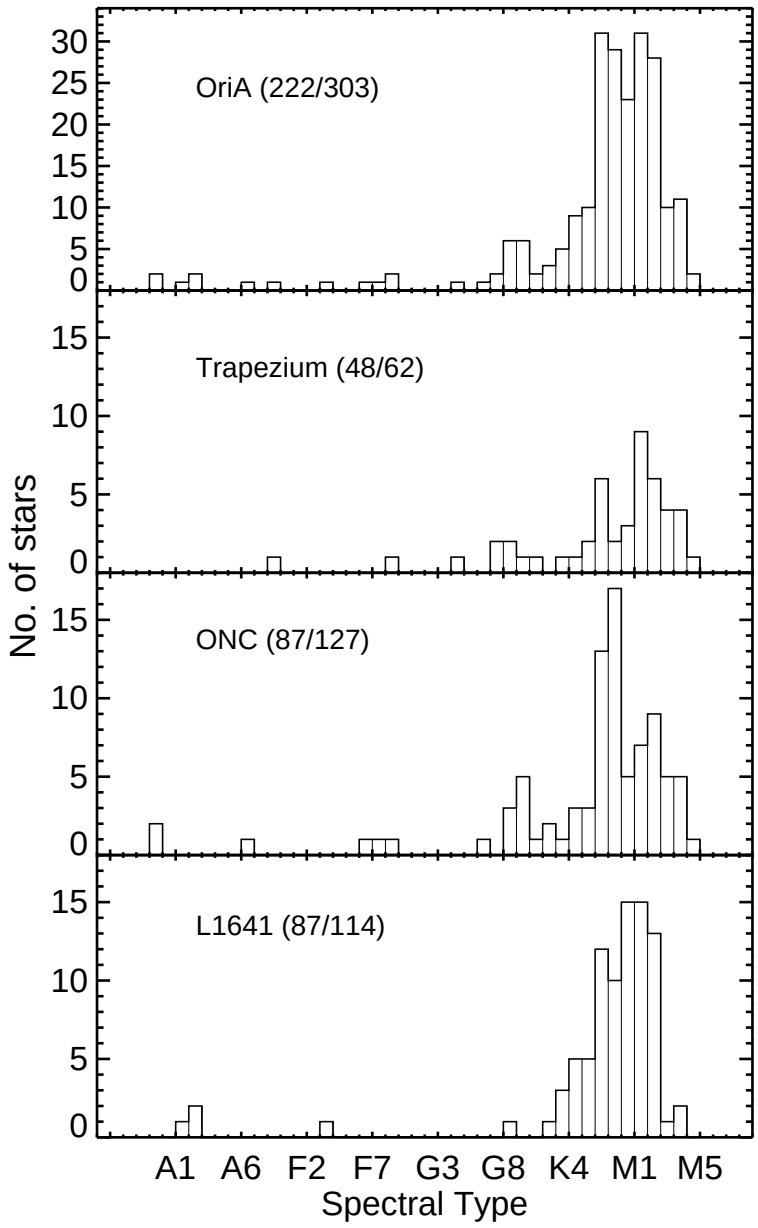


Figure 3.2 Spectral type distribution of Class II objects in Orion A that have available spectral types and which we observed with IRS.

The CTTS locus is indicated over the color-color diagram of our sample using 2MASS photometry in Figure 3.3.

To get A_λ for each set of λ_1 and λ_2, we used the Mathis (1990) extinction curve for $R_V = 5.0$ if the resulting $A_V < 3$. In case of $A_V > 3$, we followed the empirical extinction curves of McClure (2009): two composite extinction curves, one for $3 < A_V < 8$ and one for $A_V > 8$. After calculation of extinction corrections with each intrinsic color choice, we examined the extinction-corrected SEDs and selected a final result based on freedom from artifacts of the correction (e.g. artificial CO_2 ice features or structure in the silicate features) and good agreement with the photospheric spectrum of the star's type, at short wavelengths. (<1 μm). In Table 3.1, we list the A_V method selected for each object: $I - J$, $J - H$, and $H - K$.

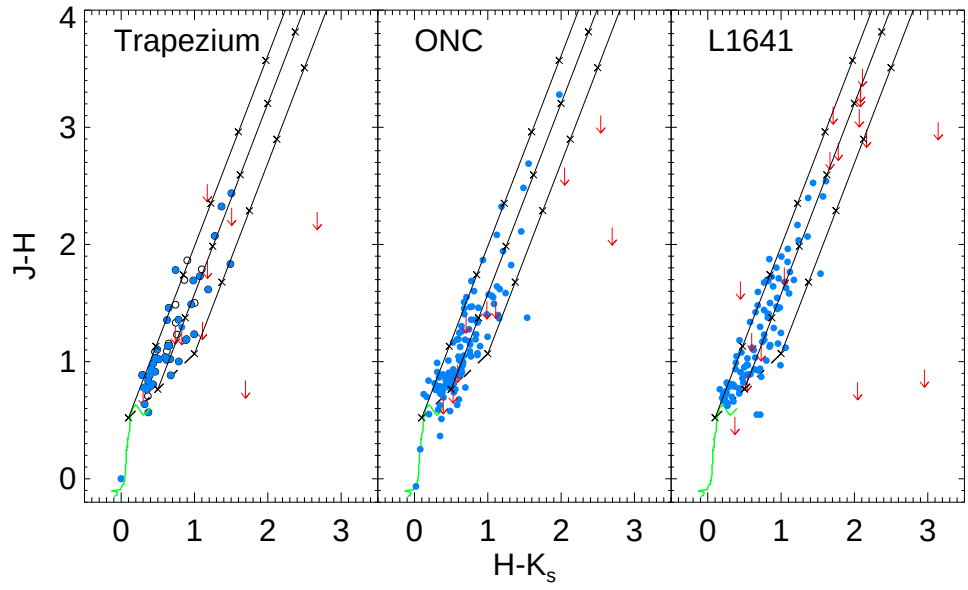


Figure 3.3 $J-H$ versus $H-K$ color-color diagram of Class II objets observed with IRS in the sub-regions of Orion A: Trapezium (the left panel), ONC (the middle panel), and L1641 (the right panel). The CTTS locus is indicated with the dashed line. The colors of main-sequence giants and dwarf (Bessell & Brett 1998) are also plotted with green solid line. The solid lines started from the CTTS locus indicate the increasing extinction. The increments of A_V are denoted by crosses by the interval of A_V=5. The downward arrows are used for objects which their 2MASS photometry have any bad flags.

Table 3.1. Spectral Type and Extinction

Num. (1)	IRS name (2)	Spectral types (3)	Spectral type adopted(4)	A_V (5)	A_V method (6)
1	8336884-5290	M0.0(8)	M0.0	0.61	I-J
2	8339347-5238	M3.0(8)	M3.0	0.82	CTTS J-H
3	8343858-5513	K1(3)	K1.0	4.73	J-H
4	8343917-6073	M1.5(1)	M1.5	0.09	CTTS J-H

Note. — The full table is Table A.1 in Appendix A. Column 3 is for spectral types and the references. The adopted spectral type is in coulumn 4.

[1]Allen & Mosby (2008), private communication; spectral types are measured from HECTOSPEC spectra

[3]Rebull et al. (2000)

[8]Hernandez & Tobin (2009), private communication; spectral types are measured from HECTOSPEC spectra or FAST spectra

Note. — Column (6) A_V method: the method which derived A_V in the column (5). See the text for details.

The distributions of the visual extinctions by the sub-regions of Orion A are shown in Figure 3.4. The median value of A_V increases from Trapezium to L1641 especially in case of including all objects whether a spectral type is available or not: 2.04, 2.25, and 3.65 for Trapezium, ONC, and L1641, respectively. When taking only objects with known spectral types, the median A_V of L1641 (2.5) is higher than that of Trapezium (2.04) or ONC (1.78). We performed Kolmogorov-Smirnov (K-S) tests on the distributions of A_V of pairs of sub-regions and list the results in Table 3.2. From the K-S test, where D is the maximum deviation between the cumulative distribution of two groups and p indicates the probability that there is no significant difference between the distributions, we confirm that the difference of A_V distributions by sub-regions is real and significant. This is possibly due to the strong UV from OB stars which has blown out small dust grains from Trapezium and ONC.

Table 3.2 K-S test for the visual extinction distribution

Regions compared	All objects		available spectral types	
	D	p	D	p
Trape. vs. ONC	0.30	0.0009	0.25	0.03
Trape. vs. L1641	0.30	0.0011	0.25	0.03
ONC vs. L1641	0.17	0.048	0.20	0.06

D is the maximum deviation between the cumulative distribution of two groups. p indicates the probability that there is no significant difference between the distributions

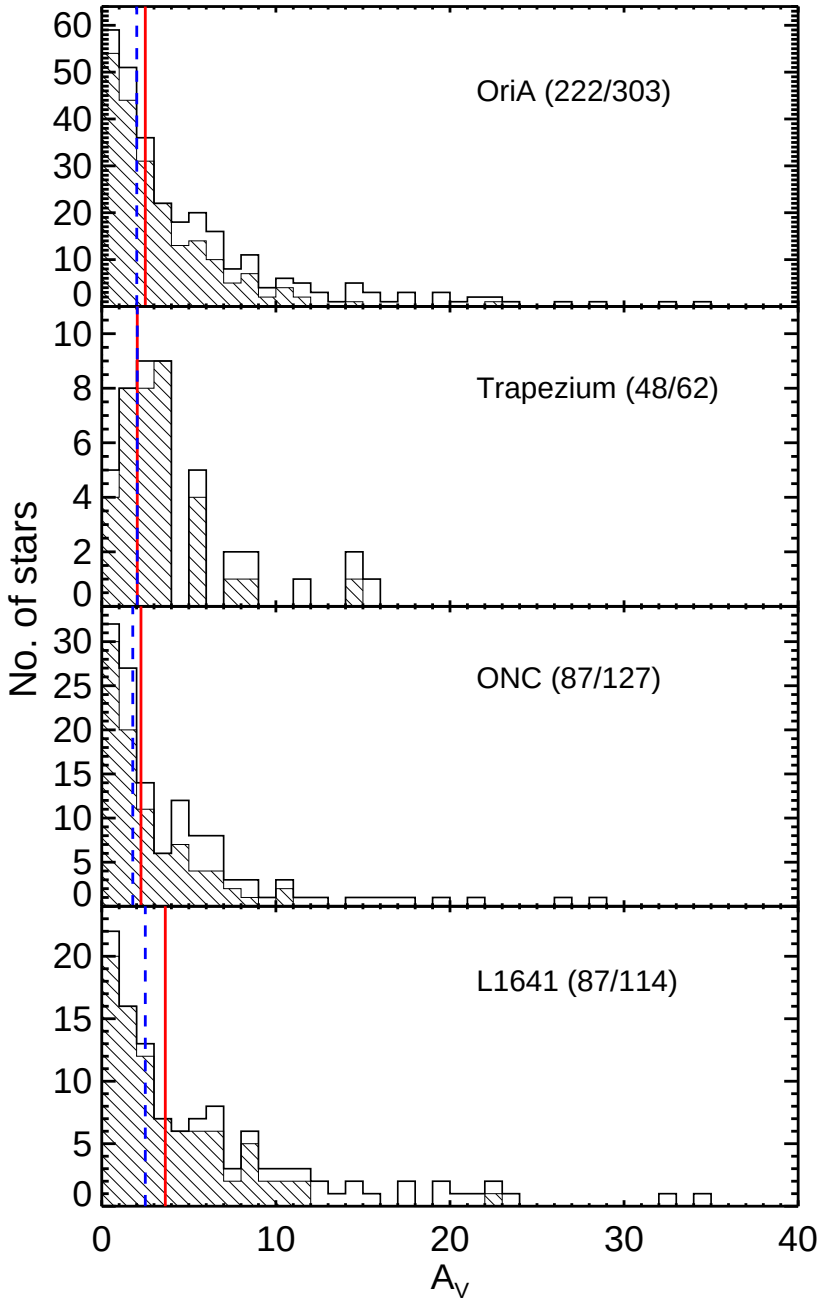


Figure 3.4 Distribution of visual extinction, A_V, for 303 Class II disks in Orion A observed as the IRS PID 30706. Hash lines indicate the A_V distribution of the objects with known spectral type information. The red solid lines indicate the median A_V of all objects. The blue dashed lines are for the median A_V of the objects with available spectra types.

3.1.2 Photometry and Spectral Energy Distributions

Ancillary Photometry

We also compiled broadband photometry from ultraviolet to mid-infrared wavelengths from the literature. From the Naval Observatory Merged Astrometric Dataset (NOMAD) catalog (Zacharias et al., 2005) we collect B (0.44 μm), V(0.55 μm), and R (0.64 μm). There is a rather recent photometry data set for ONC objects from da Rio et al. (2010). From their tables, we gathered optical photometry at U (0.347 μm), B (0.454 μm), V (0.538 μm), TiO (0.6217 μm), and I (0.862 μm). More optical and near-IR photometry at u (0.31 μm), g (0.48 μm), r (0.62 μm), i (0.76 μm), and z (0.91 μm) is added from the Sloan Digital Sky Survey (SDSS) photometric catalog (release 8, Adelman-McCarthy & et al. (2011)). Photometry from one more optical band (I at 0.8 μm) was taken from the DENIS database as well as two near-IR bands, J (1.25 μm) and K (2.16 μm). Most of our targets (except OriA-302) have 2MASS photometry in the J (1.25 μm), H (1.65 μm), and K (2.17 μm) bands. We collected 2MASS information from Skrutskie et al. (2006). The photometry in the JHK bands for OriA-302 in Figure 2 are the averaged fluxes from our SpeX spectra.

Additional photometry at Z (0.88 μm), Y (1.03 μm), J (1.25 μm), H (1.63 μm), and K (2.20 μm) bands came from the UKIRT Infrared Deep Sky Survy (UKIDSS DR8, Ukidss (2012)).

All of our targets were observed with IRAC (3.6, 4.5, 5.8, and 8.0 μm) and MIPS (24 μm) prior to the IRS observations (Megeath et al., 2012).

We also include near- to mid-IR observations at 3.4, 4.6, 12, and 22 μm from the Wide-field Infrared Survey Explorer (WISE) all-sky data release (Cutri & et al., 2012) if a corresponding observation has a "ex" tag value of zero, i.e., not an extended source, to avoid including neighboring objects because WISE has relatively coarse resolution. In case there are multiple (mostly two or three) sets of UKIDSS and SDSS for an object within the distance of 3 arcsec from our target position, we include the multiple sets in the corresponding SED as well as a combined photometric points for them; we cannot ignore the possibility of multiple system. However, we do not discuss multiplicity further here because the multiplicity information is quite incomplete.

Spectral Energy Distributions

We constructed SEDs of our sample with the broad band photometry that we assembled and SpeX and IRS spectra in Figure 3.5 and Figure 3.6. Figure 3.5 includes SEDs of 241 Class II objects observed in full IRS wavelength coverage from 5.2–35 μm. As we described in Chapter 2, there are 18 objects which cannot be reduced due to pixel saturation during IRS observation for the objects in Trapezium. Therefore we only present SEDs of 44 of these objects observed with partial IRS wavelength coverage of 5.2–14 μm in Figure 3.6.

Among 241 objects observed in full IRS wavelength coverage, four objects (OriA-7, OriA-136, OriA-148, and OriA-88) have incomplete spectra. OriA-247, 261, and 296 vary substantially over time. OriA-216 is a galaxy with Z=0.35. The SED of OriA-208 includes interesting information: the system is revealed as a binary from SpeX observation, and SDSS and UKIDSS photom-

etry agree with our SpeX spectra of the fainter object. It was not possible to distinguish two souces from IRS because the separation is about 1–2 arcsec. OriA-95 is not a galaxy, but it has very uncertain extinction correction. We do not include these 10 objects for the analysis in the present work, except OriA-88 in the analysis of transitional disks in Chapter 4.

There are many interesting individual objects in our survey, but the detailed description and discussion of individual objects is beyond the scope of this thesis.

3.1.3 Stellar Properties

In this section, we describe how we measure stellar properties like stellar luminosity ($L_\star$), stellar mass ($M_\star$), and mass accretion rate from disk to host-star ($\dot{M}$). We also present the compiled X-ray luminosity (L_X) from the 2XMM-Newton survey.

T_{eff} and $L_\star$

The effective temperatures, T_{eff}, are adopted from Kenyon & Hartmann (1995), corresponding to the spectral type of each object. For the objects of unknown spectral types, we used 3850K, the mean T_{eff} of Class II sources with known SpT in Orion A. The stellar luminosity ($L_\star$) of each object was derived from the stellar effective temperature and the stellar radius ($R_\star$). $R_\star$ was calculated from the scaling factor ($(R_\star/d)^2$) applied to the photosphere model, where $d = 414$ pc was assumed to be the distance to Orion A. The photosphere was derived from the intrinsic colors from Kenyon & Hartmann (1995) at temper-

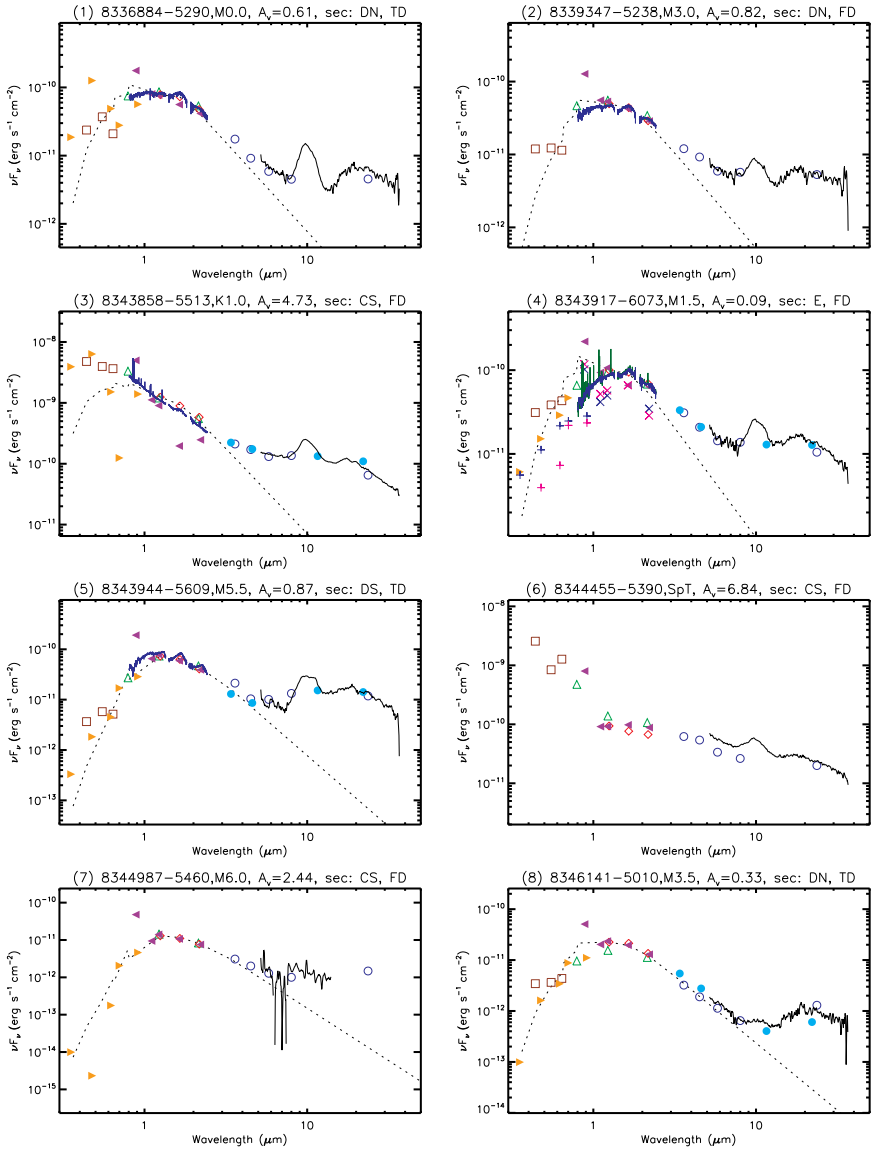


Figure 3.5 De-reddened SEDs of our samples in ONC and L1641, which were observed with IRS SL and LL moduels. The SEDs are composed of the following components: IRS (black line in the wavelength range of 5.2-35 (or 14) μm); SpeX (solid line in the wavelength range of 0.8-2.4 μm); IRAC and MIPS (open circles); 2MASS JHK (open diamonds); DENIS IJH(upward open triangles); UBVRI from da Rio et al. (2010) (downward open triangle); BVR from NOMAD (open squares); UKIDSS ($\times$ for multiple components; leftward filled triangle for the composite); SDSS (cross for multiple components; rightward filled triangle for the composite); WISE (solid circle); photosphere (black short dashed line). The SEDs of the remaining objects observed in SLLL mode are in Figure A.1 in Appendix A.

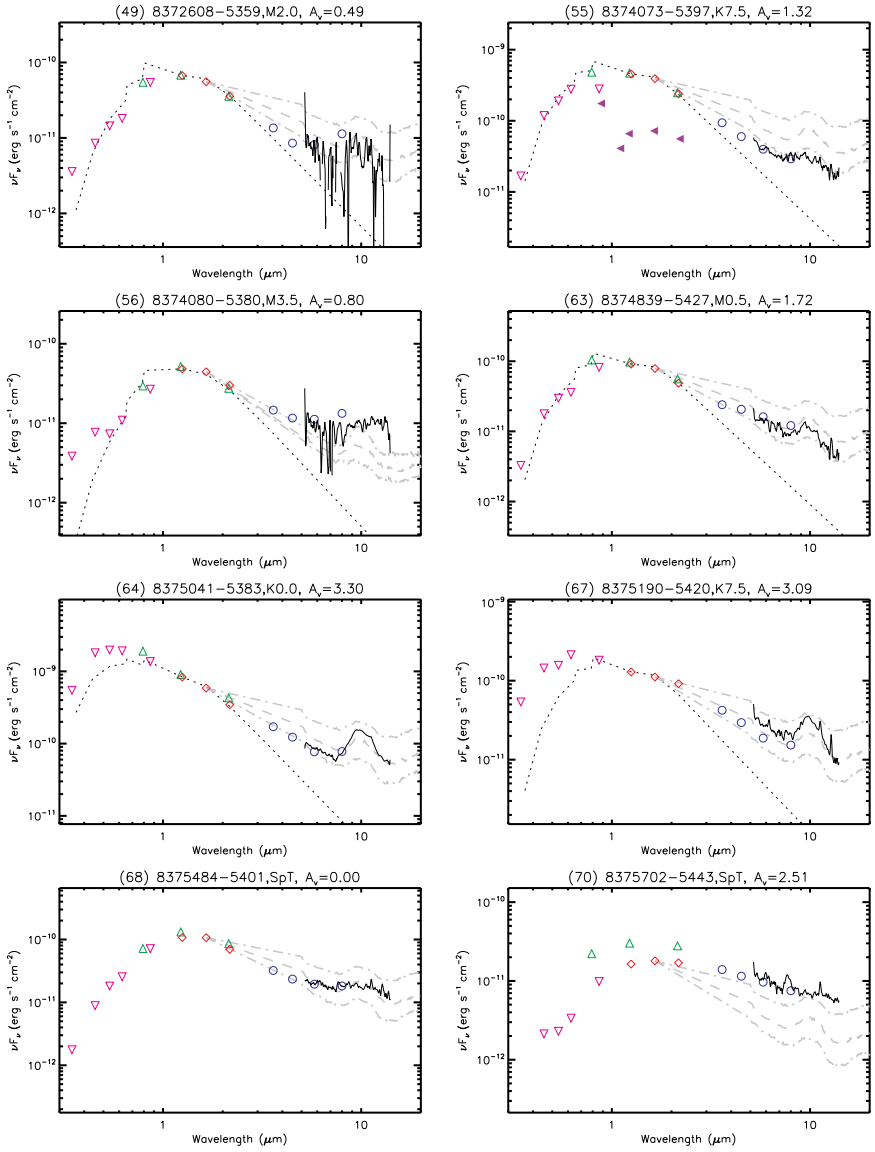


Figure 3.6 De-reddened SEDs of the reduced samples in Trapezium, which were observed with IRS SL module only. The meanings of symbols are same as in Figure 3.5 except the additional median (gray long dashed line) and the upper and lower quartile (dash-dot line) spectra of protoplanetary disks in Taurus. The SEDs of the remaining objects observed in SL mode are in Figure A.2 in Appendix A.

ature T_{eff}, scaled to match the de-reddened the 2MASS J band photometry (see SEDs in Figure 3.5 and 3.6). The adopted T_{eff} and estimated $L_\star$ are listed in Table 3.3.

We display the distribution of $L_\star$ of 231 objects from the samples in ONC and L1641 which have full IRS spectra in Figure 3.7. From the comparison of $L_\star$ distributions of ONC and L1641 and a K-S test, we observe no big difference in $L_\star$ distribution.

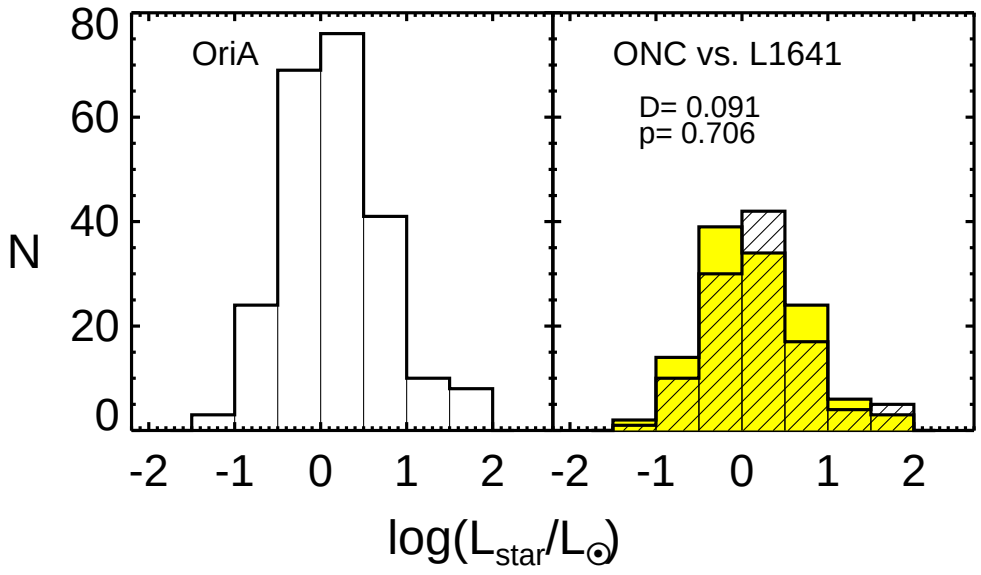


Figure 3.7 Distribution of $L_\star$ of the objects in Orion A (N=231; left panel). The right panel shows distribution of $L_\star$ of objects in ONC (N=122; yellow bars) and L1641 (N=109; hashed bars).

Evolutionary Tracks and $M_\star$

We inferred the mass of each star ($M_\star$) from the Siess PMS evolutionary tracks (Siess et al., 2000) using the derived luminosities and effective temper-

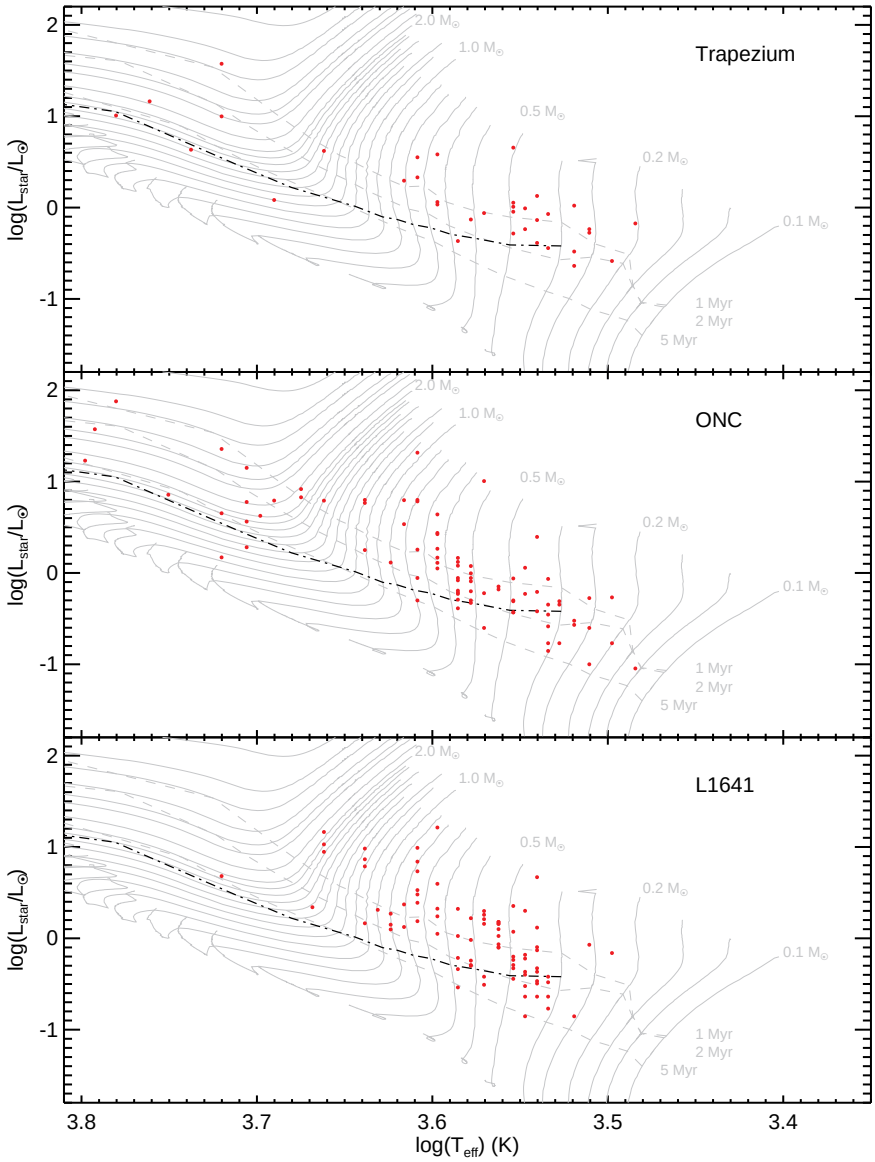


Figure 3.8 H-R diagrams for host stars of Class II disks. Evolutionary tracks and isochrones are from Siess et al. (2000) (Z=0.02). Isochrone ages of systems of Class II disks in Orion A range from < 1 Myr to ~ 5 Myr. The average disk life time in Tau-Aur (Bertout et al., 2007) is also shown as a dash-dotted line for reference.

atures. The objects with known spectral types in Orion A are shown on an H-R diagram along with the solar-metallicity (Z=0.02) evolutionary tracks in Figure 3.8.

We compared $M_\star$ distribution for the Class II disks in ONC and L1641 in Figure 3.9. There is no significant difference in the mass distribution.

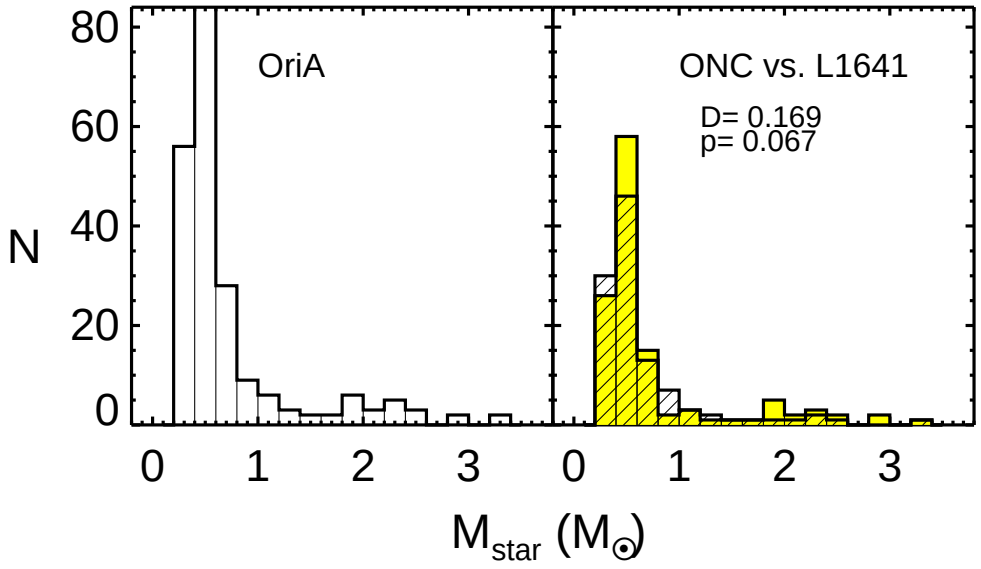


Figure 3.9 Distribution of $M_\star$ of the objects in Orion A (N=231; left panel). The right panel shows distribution of $M_\star$ of objects in ONC (N=122; yellow bars) and L1641 (N=109; hashed bars).

3.1.4 Mass Accretion Rates: $\dot{M}$

We observed 120 Class II disks with SpeX/IRTF in SXD mode from 0.8-2.4 μm to measure mass accretion rates from their hydrogen recombination lines: Paγ (1.094 μm), Paβ (1.282 μm), and Brγ (2.166 μm). From the dereddened SpeX spectra with the A_V determined as described in Section 3.1.1,

we obtained mass accretion rates of 113 objects except OriA-21, 45, 52, 88, 135, 170, and 266 which are mostly earlier spectral type objects with strong Hydrogen absorption lines. We also analyzed SpeX spectra of companions of nine objects, OriA-4, 26, 38, 47, 98, 173, 208, 280, and 290. Among them, six objects yielded mass accretion rates and three companions showed absorption lines. We do not include the mass accretion rates of companions, nor the mass accretion rate of OriA-208 and OriA-247 (two of "Ten") in the following analysis. Therefore, we use mass accretion rates of 111 objects in ONC and L1641 for any analysis related to disk-stellar mass accretion properties in this thesis.

The method of mass accretion rate measurement is as follows. We fit each hydrogen recombination line with a gaussian function plus a local continuum. We measure the line luminosity of each line from the fit. Then we use the following relations to convert line luminosity to accretion luminosity L_{acc} (Muzerolle et al., 1998; Gatti et al., 2008):

$$log(L_{acc}/L_{\odot}) = 1.36 \times log(L_{Pa\gamma}/L_{\odot}) + 4.1 \tag{3.2}$$

$$log(L_{acc}/L_{\odot}) = 1.14 \times log(L_{Pa\beta}/L_{\odot}) + 3.15 \tag{3.3}$$

$$log(L_{acc}/L_{\odot}) = 1.26 \times log(L_{Br\gamma}/L_{\odot}) + 4.43 \tag{3.4}$$

whence we obtain the disk-star accretion rate:

$$\dot{M} = \frac{L_{acc} R_{\star}}{G M_{\star}} \tag{3.5}$$

In Figure 3.10 we show as an example the results for OriA-59.

In general, the three recombination lines in our spectra yield similar results for accretion rate within a factor of 2–3, so we report the average in Table 3.3. When fewer than three lines were detected we adopt the resulting average $\dot{M}$ as an upper limit and indicate them as such in Table 3.3.

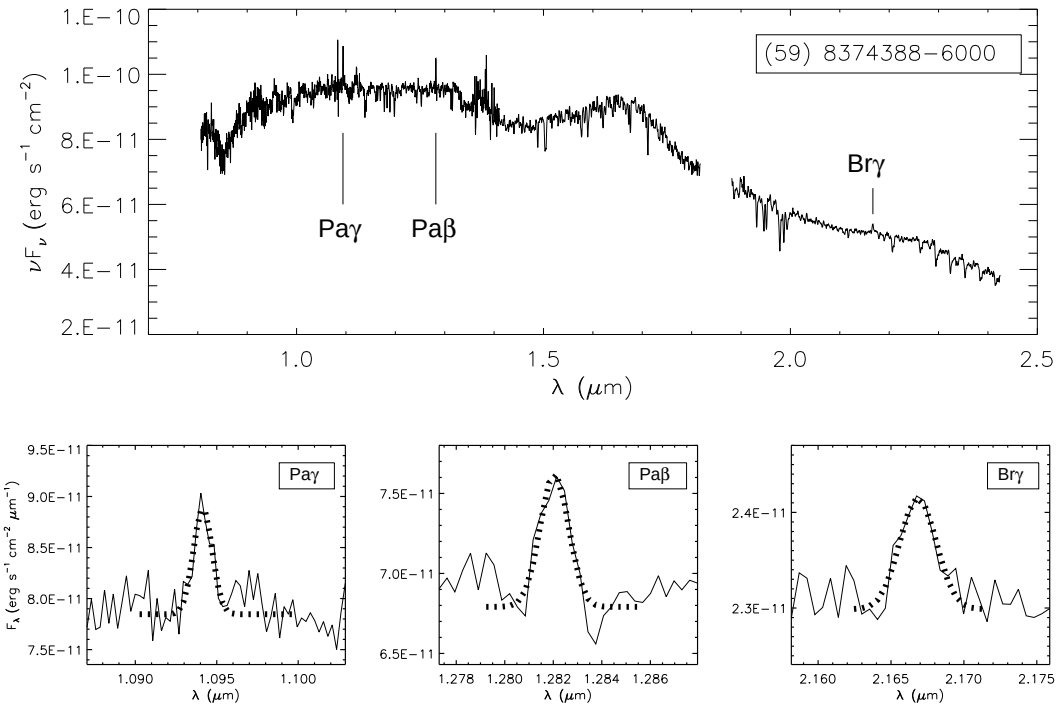


Figure 3.10 Example of mass accretion rate measurement from hydrogen recombination lines.

We find that the distributions of mass accretion rates of objects in ONC and L1641 are not very different, either by visual inspection or by the K-S test (Figure 3.11).

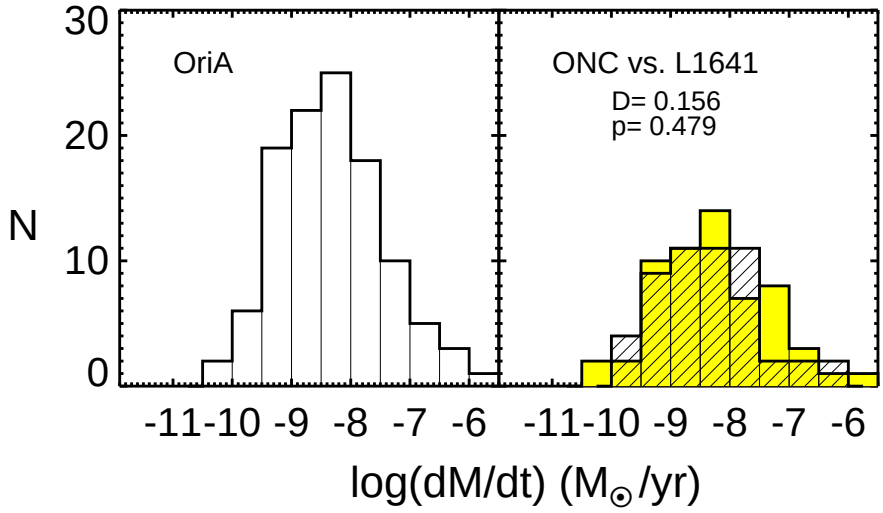


Figure 3.11 Distribution of $\dot{M}$ of the objects in Orion A (N=111; left panel). The right panel shows distribution of $\dot{M}$ of objects in ONC (N=59; yellow bars) and L1641 (N=52; hashed bars).

X-ray Luminosity: L_X

In this subsection, we present X-ray data from the Second XMM-Newton Serendipitous Source Catalog (Watson et al., 2009b). We compiled the 6 energy bands available from XMM-Newton catalog. The ranges of photon energy of each band are: 0.2–0.5 keV for band 1; 0.5–1.0 keV for band 2; 1.0–2.0 keV for band 3; 2.0–4.5 keV for band 4; 4.5–12 keV for band 5; 0.2–keV for band 8 of total energy band. As informed by the histogram distribution of L_X in Figure 3.12 and the median values of L_X by energy bands and subregions in Table 3.4, L_Xs of objects in ONC tend toward higher values than in L1641. This tendency is significant at band 3 (1.0–2.0 keV) and band 4 (2.0–4.5 keV) based on a K-S test. The gathered L_X information of each object is in Table 3.5.

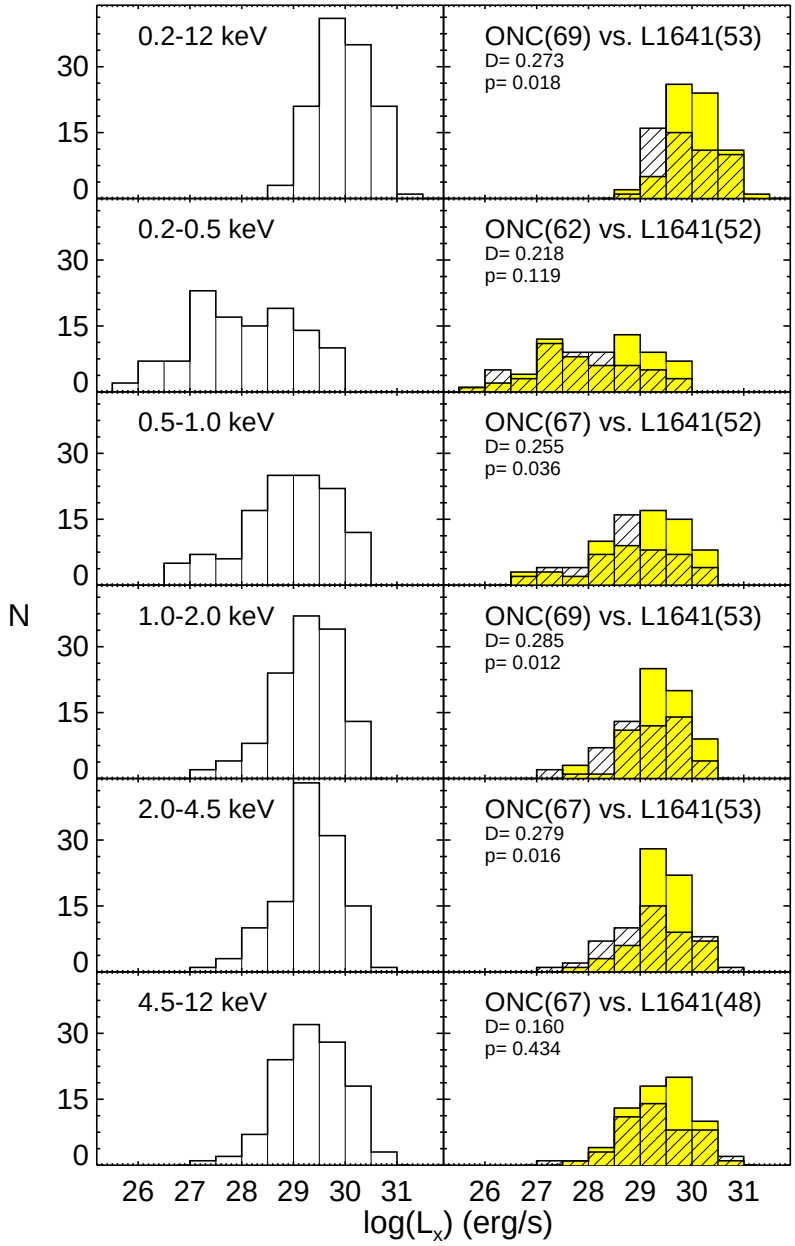


Figure 3.12 Histograms of L_X. L_X of the band 3 (1.0–2.0 keV) and band 4 (2.0–4.5) in ONC (yellow bars) is greater than in L1641 (hashed bars) based on K-S tests.

Table 3.3. Basic Stellar Properties I

Num. (1)	IRS name (2)	T_{eff} (3)	$L_\star$ adopted(4)	$M_\star$ (5)	e$M_\star$ (6)	$\dot{M}$ (7)
1	8336884-5290	3850	0.64	0.55	0.08	5.86E-10 ± 1.07E-10
2	8339347-5238	3470	0.38	0.33	0.06	9.19E-10 ± 6.54E-10
3	8343858-5513	5080	14.14	2.93	0.1	2.42E-07 ± 1.41E-07
4	8343917-6073	3650	0.79	0.42	0.06	2.75E-09 ± 4.29E-10
5	8343944-5609	3145	0.54	0.22	0.04	$<$ 1.00E-08

Note. — The full table is Table A.2 in Appendix A

Table 3.4 Median of $\log L_X$

Band	Energy Range(keV)	Ori A	ONC	L1641
8	0.2-12	30.0	30.1	29.8
1	0.2-0.5	28.0	28.4	27.9
2	0.5-1.0	29.0	29.1	28.7
3	1.0-2.0	29.3	29.4	29.1
4	2.0-4.5	29.3	29.4	29.2
5	4.5-12	29.3	29.4	29.2

Table 3.5. Basic Stellar Properties II

Num.	2XMM ID	L_X (10^{28} erg/s)					
		0.2–12 keV	0.2–0.5 keV	0.5–1.0 keV	1.0–2.0 keV	2.0–4.5 keV	4.5–12 keV
11	2XMMi J053354.4-053158	34.32 ± 19.99	0.00 ± 0.21	1.78 ± 0.86	9.90 ± 1.52	15.36 ± 3.53	6.88 ± 19.60
13	2XMM J053400.2-053542	130.00 ± 84.97	5.16 ± 3.30	18.34 ± 5.38	3.24 ± 3.38	2.06 ± 4.90	92.46 ± 84.13
14	2XMMi J053402.2-053618	96.06 ± 11.78	1.07 ± 0.56	3.71 ± 0.77	24.35 ± 1.57	47.48 ± 3.65	18.37 ± 10.70
17	2XMMi J053407.9-053612	18.15 ± 12.00	0.08 ± 0.31	1.64 ± 0.57	0.94 ± 0.58	1.67 ± 1.19	11.33 ± 11.85
19	2XMM J053412.7-052849	212.22 ± 95.77	3.88 ± 3.03	35.22 ± 7.71	24.91 ± 6.44	4.57 ± 5.48	127.08 ± 94.47

Note. — XMM-Newton X-ray data. The full table is Table A.3 in Appendix A.

3.2 Disk Properties

In this section, we describe the definition of spectral indices and introduce the distribution and characteristics of spectral indices measured from Class II disks in Orion A.

3.2.1 Spectral Index

The continuum spectral indices are defined as

$$n_{\lambda_1-\lambda_2} = \frac{\log(\lambda_2 F_{\lambda_2}) - \log(\lambda_1 F_{\lambda_1})}{\log(\lambda_2) - \log(\lambda_1)} \quad . \tag{3.6}$$

The wavelengths, λ_1 and λ_2, are selected to avoid emission features, and thus to represent the spectral shape of the optically-thick disk continuum emission. This in turn reveals disk structure, both radial (central clearings and gaps) and vertical (degree of flaring). We use n_{5-12}, n_{12-20}, n_{K-25}, n_{K-6}, n_{6-13}, n_{13-31}, and n_{20-31} to infer radial and vertical distribution of dust and so disk structure. The anchor positions have been selected to be useful in comparison of radial properties of disks from various previous studies (Furlan et al. 2006; McClure et al. 2010, Manoj P. et al 2011).

The wavelength interval of each anchor is summarized in Table 3.6. Spectral indices measured with any combinations of two wavelengths are listed in Table 3.7, except n_{20-31}, which is used as an index of outer disk truncation/evaporation in Chapter 6.

Table 3.6 Wavelength Ranges of Anchors for Spectral Indices

$\lambda_i(\mu\mathrm{m})$	wavelength ranges (μm)
K	2.17 (2MASS K band)
5	5.2–5.4
6	5.4–6.0
12	12.7–13.1
13	12.8–14.0
20	19.7–19.95
25	24.5–25.5
31	30.3–32.0

Table 3.7. Spectral Indices

Num.	module	n_{K-6}	$\sigma_{n_{K-6}}$	n_{6-13}	$\sigma_{n_{6-13}}$	n_{13-31}	$\sigma_{n_{13-31}}$	n_{5-12}	$\sigma_{n_{5-12}}$	n_{12-20}	$\sigma_{n_{12-20}}$	n_{K-25}	$\sigma_{n_{K-25}}$
1	SLLL	-2.06	0.1	-0.89	0.13	0.29	0.23	-1.02	0.1	0.95	0.15	-1.01	0.04
2	SLLL	-1.67	0.08	-0.53	0.11	0.06	0.16	-0.65	0.13	-0.18	0.18	-0.88	0.03
3	SLLL	-1.54	0.03	-0.28	0.03	-1.12	0.06	-0.33	0.04	-0.76	0.04	-1.03	0.01
4	SLLL	-1.62	0.11	-0.13	0.13	-0.66	0.06	-0.49	0.07	-0.17	0.24	-0.87	0.02
5	SLLL	-1.81	0.16	0.71	0.2	-0.81	0.11	0.35	0.1	-0.23	0.09	-0.67	0.04

Note. — Spectral indices. The full table is Table A.4 in Appendix A.

3.2.2 "Classic" Disk Classification

A venerable assessment of the evolutionary state of a young stellar object (YSO) comes from the slope of its SED (Lada, 1987). Two wavelengths at near- and at mid-IR, typically K ($\sim$2 μm) and 25 μm, have been used for YSO classification. n_{K-25} is used to define the SED classes: Class I for n_{K-25} greater than 0.3; Flat Spectrum if n_{K-25} is between -0.3 and 0.3; Class II if n_{K-25} is between -1.6 and -0.3; Class III for n_{K-25} less than -1.6. As is well known, SED class can give a misleading impression of evolutionary state for objects viewed close to face-on or edge-on (Robitaille et al., 2006; Crapsi et al., 2008; McClure et al., 2010). Therefore, McClure et al. (2010) made good use of the "extinction-free" indices, $n_{5.3-12.9}$ and $n_{12.9-19.8}$, which are independent of extinction in the McClure (2009) extinction curves. These are useful for classifying evolutionary stages: photospheres if n_{5-12} is less than -2.25; disks if n_{5-12} is between -2.25 and -0.2; envelope if n_{5-12} is greater than -0.2. Figure 3.13 compare the two classification scheme from n_{K-25} and n_{5-12}. We confirm that our samples indeed include only Class II disks.

The second extinction-free index, n_{12-20}, includes not only continuum but also 20 μm silicate feature. This index is used to divide roughly by how much the disk is cleared. We plot our samples over the two extinction-free indices in Figure 3.14. Our samples is mostly located in the area of "disks". Some objects are placed in the area for envelope, but it turns out that half of them are transitional disks, and others also do not show strong evidence for envelopes, such as silicate absorption at 10 μm, CO_2 ice absorption at 15 μm or steeply increasing flux after 20 μm.

We describe the selection criteria for transitional disks in Chapter 4.

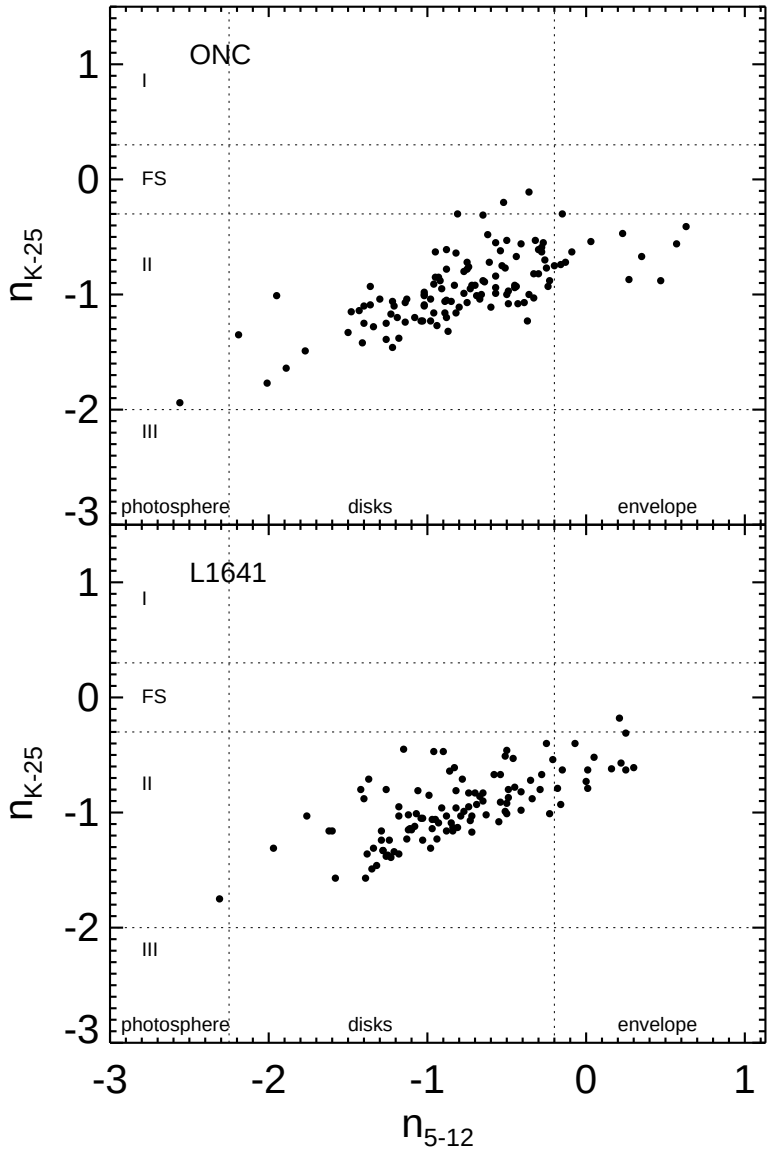


Figure 3.13 n_{5-12} versus n_{K-25}.

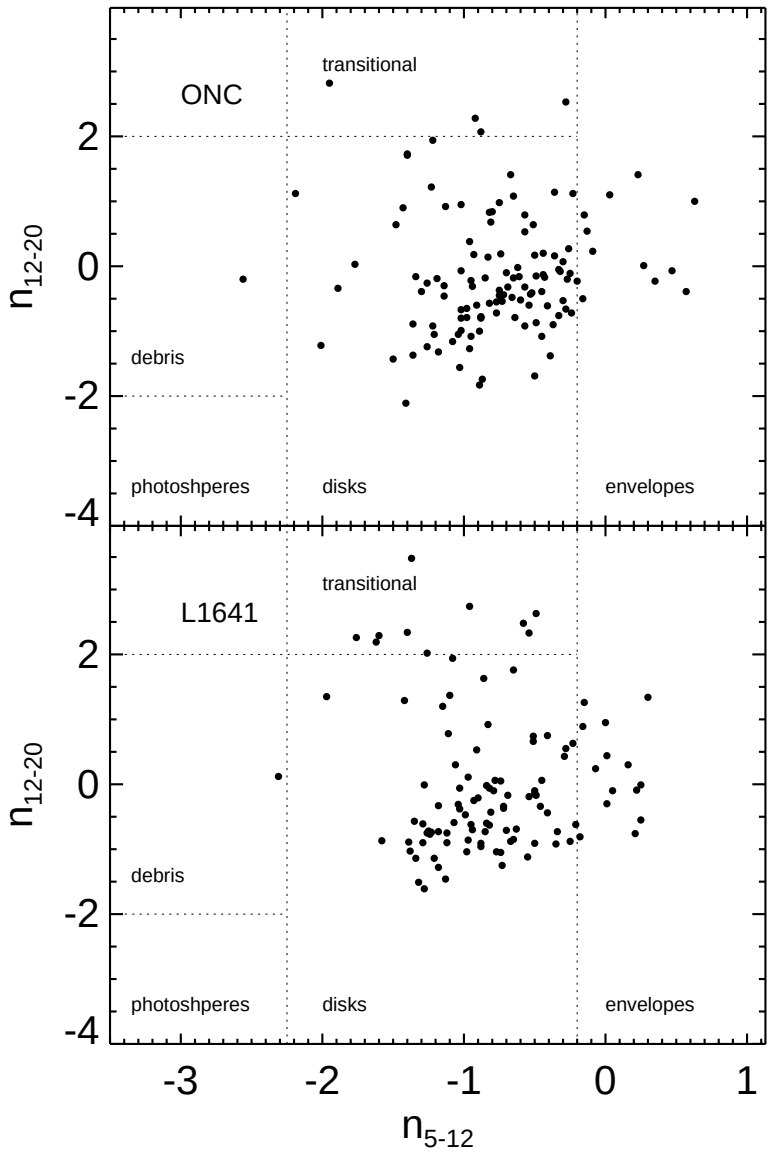


Figure 3.14 n_{5-12} versus n_{12-20}.

3.3 The Degree of Dust Processing

The continuum spectral indices are sensitive to the structure of the dust distribution structure. For clues of how much small dust grains are processed, we can utilize some parameters which can be extracted from silicate features at 10, 20, and/or 33 μm.

A parameter commonly used for understanding a strength of absorption or emission features is equivalent width. Equivalent width for the silicate emission features is a measure of optically thin emission per unit area of underlying optically thick continuum:

$$EW(\lambda) = \int_{\lambda_1}^{\lambda_2} \frac{F_\lambda - F_{\lambda,con}}{F_{\lambda,con}} \, d\lambda \quad , \tag{3.7}$$

In the limit of small silicate-feature optical depth, the equivalent width is proportional to the optical depth itself, or similarly the column density of dust in the inner disk (Watson et al., 2009a). We compute EW10, EW20, and EW33 for silicate emission features around 10 μm, 20 μm, and olivine feature at 33 μm. The wavelength ranges for integrating are 8–13 μm, 16–28 μm, and 32–35 μm for 10, 20, and 33 μm features, respectively.

Another useful parameter is an integrated flux of a feature, F_λ.

$$F_\lambda = \int_{\lambda_1}^{\lambda_2} F_\lambda - F_{\lambda,con} \, d\lambda \quad , \tag{3.8}$$

F_λ, the integrated flux after continuum subtraction, is a probe of the mass of dust lies in the uppermost optical depth of the disk, while EW(λ) indicate

the relative strength of the optically thin emission feature to its continuum of optically thick dust in the disk. We calculate F_{10} and F_{20} in the same wavelength limits used for the measurement of EW10 and EW20.

A parameter generally adopted as an index of the degree of dust processing is the ratio of flux, with continuum subtracted and normalized, at 11.3 μm and 9.8 μm. This index, $F_{11.3}/F_{9.8}$, has been used to probe the degree of grain growth and crystallinity in the inner (1–2 AU) parts of disks (Przygodda et al., 2003; van Boekel et al., 2005; Kessler-Silacci et al., 2006; Honda et al., 2006; Bouwman et al., 2008; Olofsson et al., 2009). Interstellar grains show narrow silicate profiles indicative of submicron, amorphous grains; protoplanetary-disk grains instead have profile with narrow substructure –owing to crystallization– and long-wavelength extension, due to grain growth. Both forms of processing are captured in the $F_{11.3}/F_{9.8}$ ("shape") index, although in disks of Taurus' age and younger, the change in shape is mostly due to crystallization (Watson et al., 2009a; Sargent et al., 2009).

We list the parameters related to dust processing in Table 3.8.

Table 3.8. Grain Properties

Num.	mod	EW10	σ_{EW10}	EW20	σ_{EW20}	EW33	σ_{EW33}	$F_{11.3}$	$\sigma_{F_{11.3}}$	$F_{9.8}$	$\sigma_{F_{9.8}}$	F10	σ_{F10}	F20	σ_{F20}
1	SLLL	8.02	0.16	3.22	0.33	0.02	0.07	1.38	0.04	3.04	0.07	2.67E-12	2.18E-14	7.53E-13	2.09E-02
2	SLLL	2.74	0.09	2.37	0.31	0.56	0.09	0.54	0.02	1.01	0.03	1.10E-12	2.23E-14	5.45E-13	1.29E-02
3	SLLL	2.57	0.09	2.49	0.31	0.08	0.07	0.39	0.02	0.96	0.03	3.08E-11	6.43E-13	1.01E-11	1.24E-02
4	SLLL	2.60	0.09	2.53	0.31	0.08	0.07	0.44	0.02	1.00	0.03	3.22E-12	7.47E-14	1.47E-12	1.27E-02
5	SLLL	5.41	0.12	2.56	0.31	0.24	0.08	0.89	0.03	1.77	0.04	5.51E-12	6.18E-14	1.53E-12	1.63E-02

Note. — The full table is in Table A.5 in Appendix A

3.4 Comparison of Disk and Dust Features by Sub-Regions to Taurus

In this section, we compare the distribution of spectral indices of the Orion A Class II samples to that of the Class II disk sample in Taurus. We also compare the distributions in ONC and L1641 to each other.

3.4.1 Index from 5-14 μm spectrum: Trapezium, ONC, L1641 to Taurus

As we described in Chapter 2, Class II objects in the Trapezium could only be observed with the SL module (5–14 μm). We display the distribution of n_{K-6}, n_{6-13}, EW10, and $F_{11.3}/F_{9.8}$ which are available from IRS SL spectra of objects in three sub-regions of Orion A and Taurus from Figure 3.15 to Figure 3.18.

The distributions of n_{K-6} from the disks in the three sub-regions of Orion A in Figure 3.15 show that n_{K-6} of ONC and L1641 is biased toward higher values than Taurus. Even though this difference is not statistically significant, it is interesting to compare this to the distribution comparison of other regions done in Fig. 17 of Arnold et al. (2012), in which n_{K-6} of disks in NGC 1333 is biased to lower values than that from Taurus and Ophiuchus. The median age of NGC 1333 is less than 1 Myr, similar to the median age of Trapezium. The distribution of n_{K-6} of Trapezium does not differ much from that of Taurus.

Figure 3.16 shows that the distribution of n_{6-13} in ONC is shifted to higher values of n_{6-13} compared to Taurus. A K-S test result for ONC versus Taurus

shows that this displacement is statically highly significant. The n_{6-13} distribution of L1641 also tends to higher values than that of Taurus, but the displacement is not noticeably large. The comparison of n_{6-13} among star-forming regions from Arnold et al. (2012) found no differences in n_{6-13} among Tau, Cha I, Oph, and NGC 1333.

The distributions of EW10 of the three sub-regions of Orion A in Figure 3.17 are all statistically significantly different than that of Taurus: all three are skewed toward larger EW10. The $F_{11.3}/F_{9.8}$ distributions of Orion A disks in Figure 3.18 show different distributions by subregion of Orion A. Comparing $F_{11.3}/F_{9.8}$ of Trapezium, ONC, and L1641 to that of Taurus, the D values from K-S tests decrease and the p values increase from Trapezium through ONC to L1641 in Figure 3.18. The $F_{11.3}/F_{9.8}$ distribution of ONC is concentrated around smaller values than that of Taurus. Considering the median age differences of ONC, L1641, and Taurus, we may infer that the $F_{11.3}/F_{9.8}$ distribution difference between ONC and Taurus, and the smaller — probably insignificant — difference between L1641 and Taurus, indicate increased processing of dust as time goes on.

On the other hand, the Trapezium is the youngest region among ONC, L1641, and Taurus, but its $F_{11.3}/F_{9.8}$ distribution is broad and skewed toward higher values than that of Taurus. This large shape difference between Trapezium and Taurus which goes in the direction of larger degrees of dust processing is possibly a disk-evolutionary difference rather than a dust-evolutionary difference: less-processed material at somewhat larger radii, which is still warm enough to contribute significantly to the 10 μm silicate feature, may have

been selectively removed from the systems, by radiation from the Trapezium stars. We discuss the outer disk evolution in Trapezium in detail in Chapter 6. We also compare subdivisions of $F_{11.3}/F_{9.8}$ distribution separated by the disk radial structures in Chapter 5.

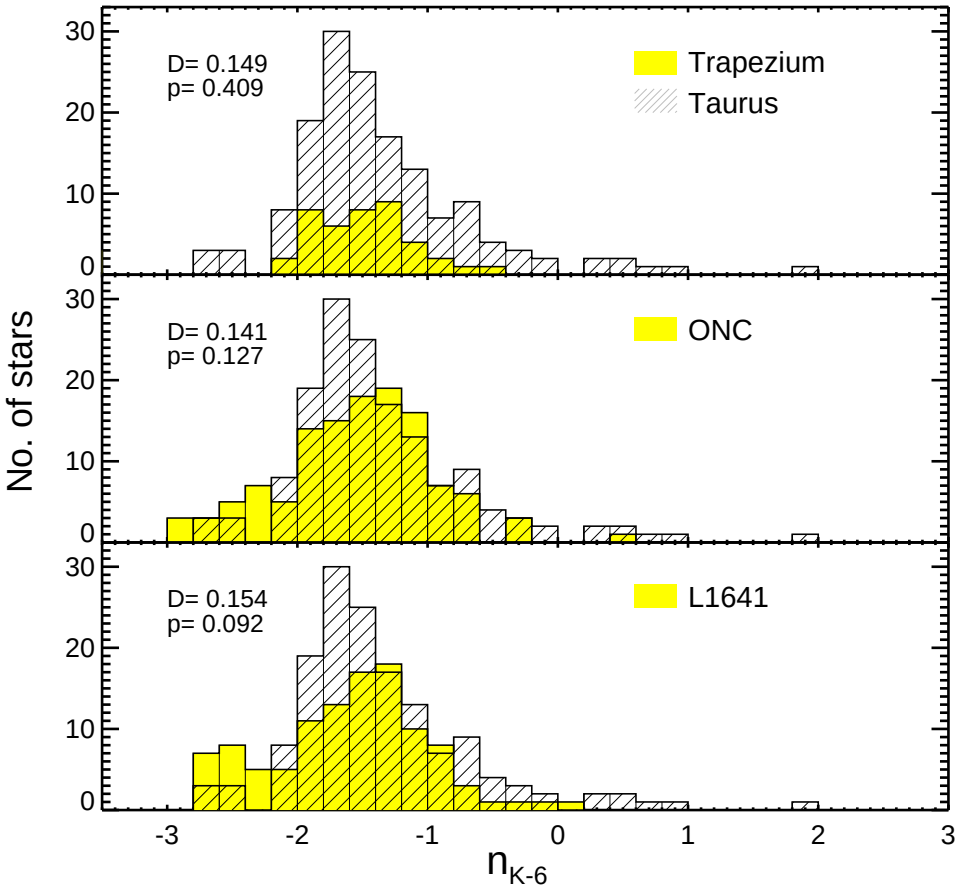


Figure 3.15 Distribution of n_{K-6} of Class II disks in three sub-regions of Orion A and their comparison to that of Taurus.

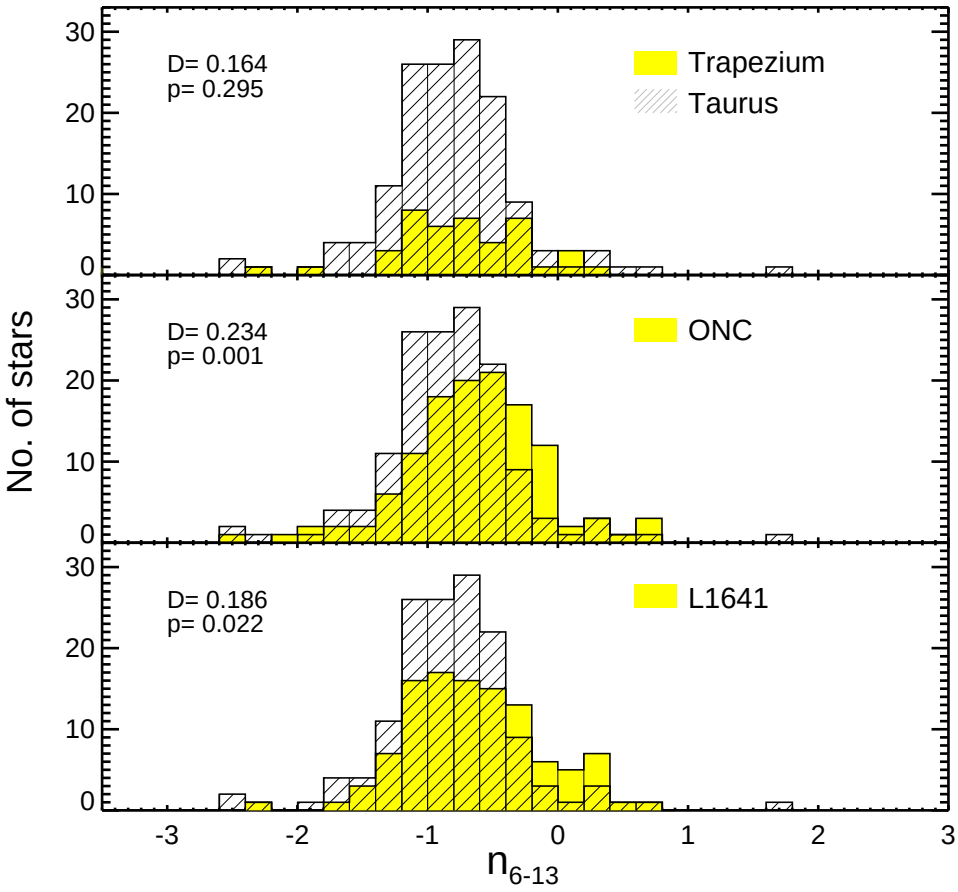


Figure 3.16 Distribution of n_{6-13} of Class II disks in three sub-regions of Orion A and their comparison to that of Taurus.

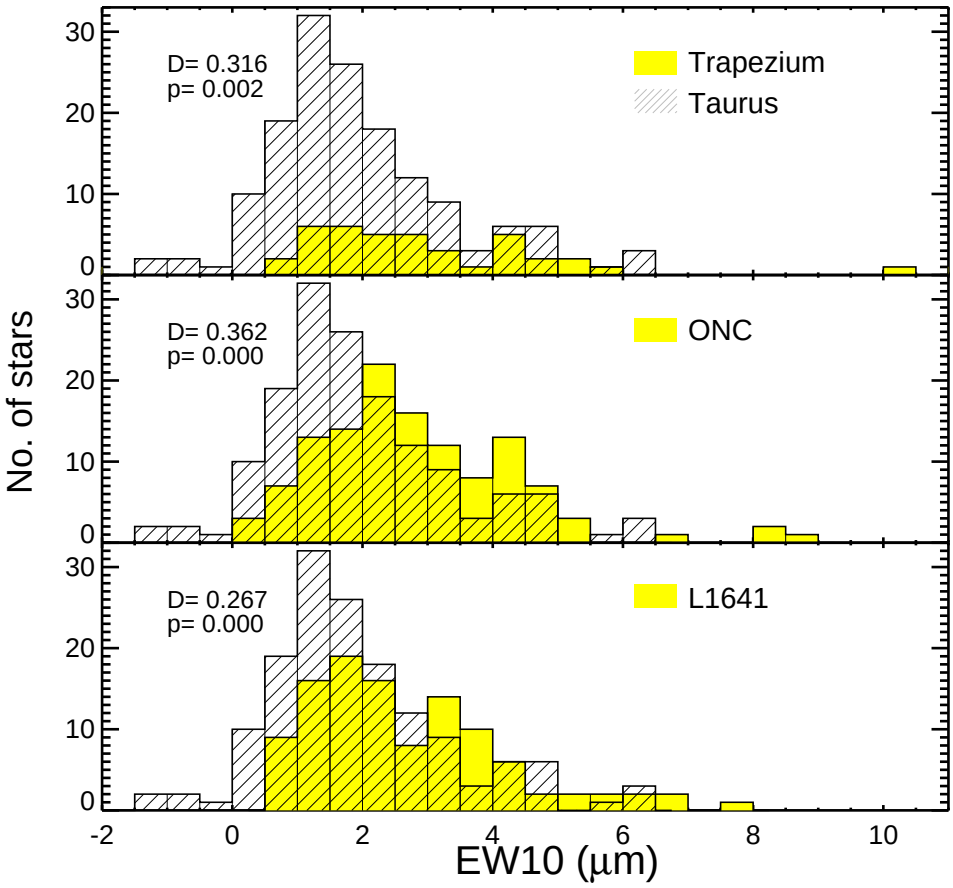


Figure 3.17 Distribution of EW10 of Class II disks in three sub-regions of Orion A and their comparison to that of Taurus.

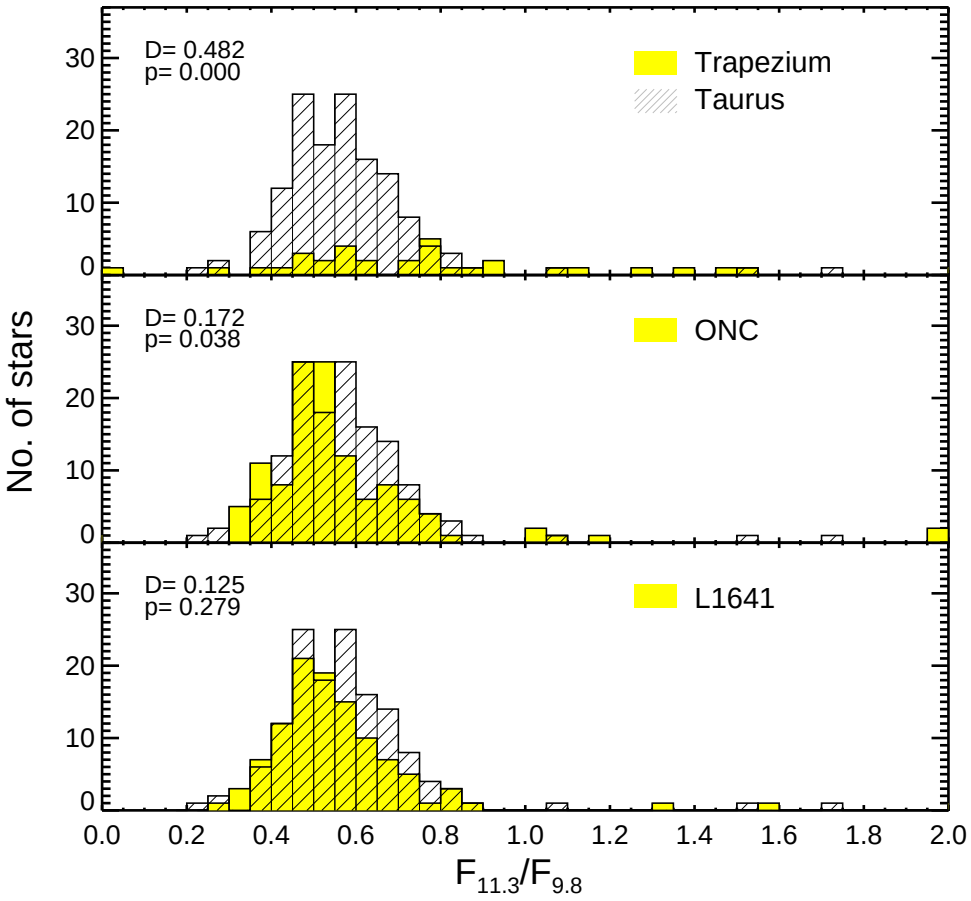


Figure 3.18 Distribution of $F_{11.3}/F_{9.8}$ of Class II disks in three sub-regions of Orion A and their comparison to that of Taurus.

3.4.2 Disk and Dust Processing Indicators from Full IRS Spectra: ONC, L1641 and Taurus

Now, we consider the properties of Class II samples in ONC and L1641 observed with full IRS spectrum, 5–37 μm. In contrast to the previous comparison of the inner disk indicators, the comparisons of the distribution of n_{13-31} of ONC, L1641, and Taurus do not show significant differences (Figure 3.19). This index is sensitive to the degree of sedimentation in the outer disk (e.g. Furlan et al., 2006); thus we find no difference in the settling of dust to mid-plane among these three regions.

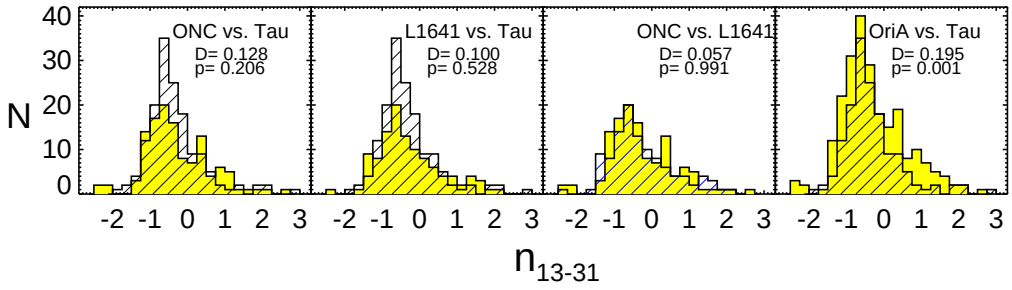


Figure 3.19 Histograms for comparison of n_{13-31} distribution by region: yellow vs. hatched.

Figure 3.20, Figure 3.21, and Figure 3.22 show the distribution of EW20 and EW33, $F_{9.8}$ and $F_{11.3}$, and F_{10}, F_{20}, and F_{20}/F_{10}, respectively. No significant differences exist between those properties in ONC and L1641, except EW33. IRS sensitivity degrades rapidly as wavelength increases past that of the 33.6 μm feature, and it is difficult to determine the continuum under the feature in many cases.

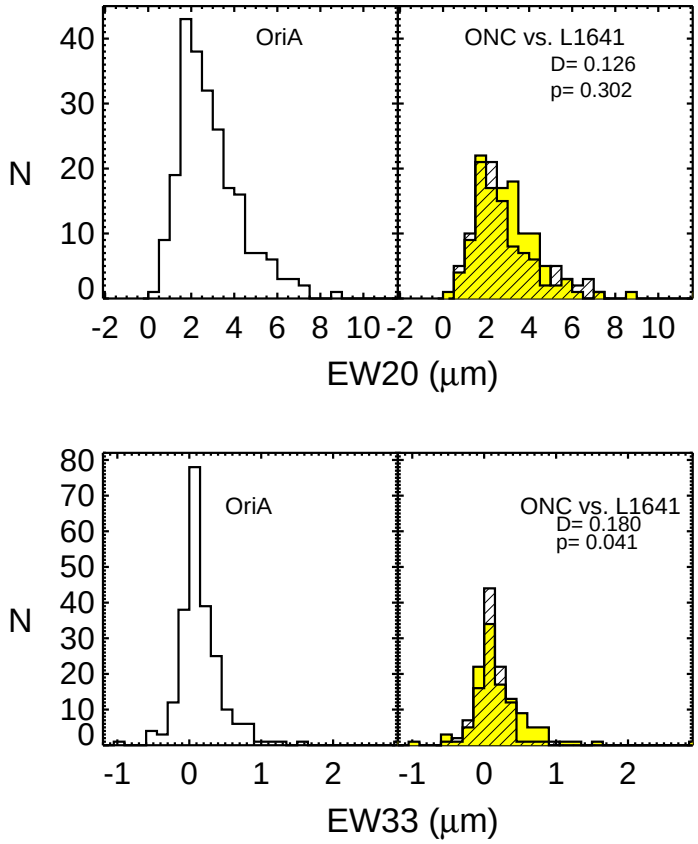


Figure 3.20 Histograms of the 20 and 33.6 μm silicate-feature equivalent widths: yellow vs. hatched.

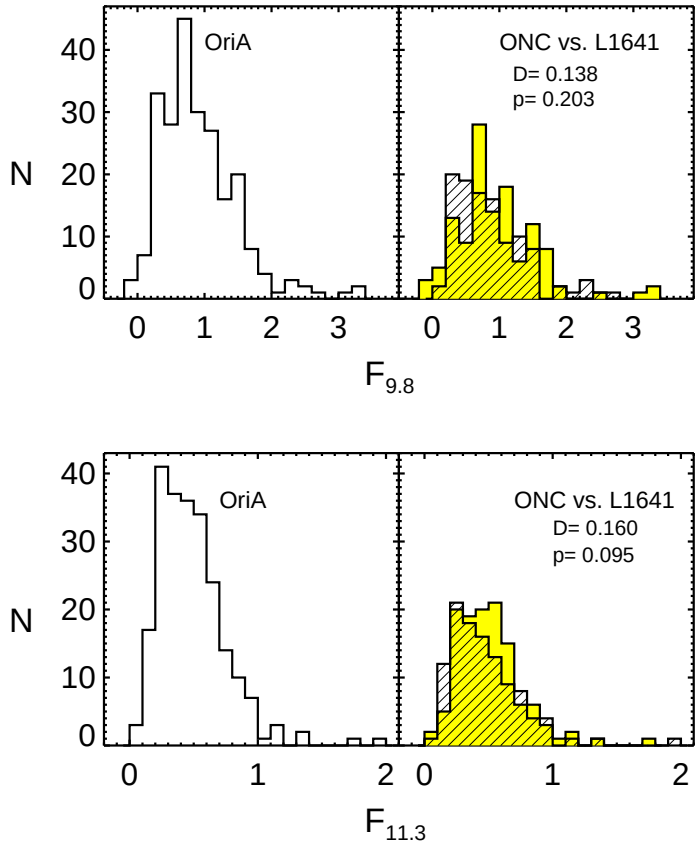


Figure 3.21 Histograms of $F_{9.8}$ and $F_{11.3}$: yellow vs. hatched.

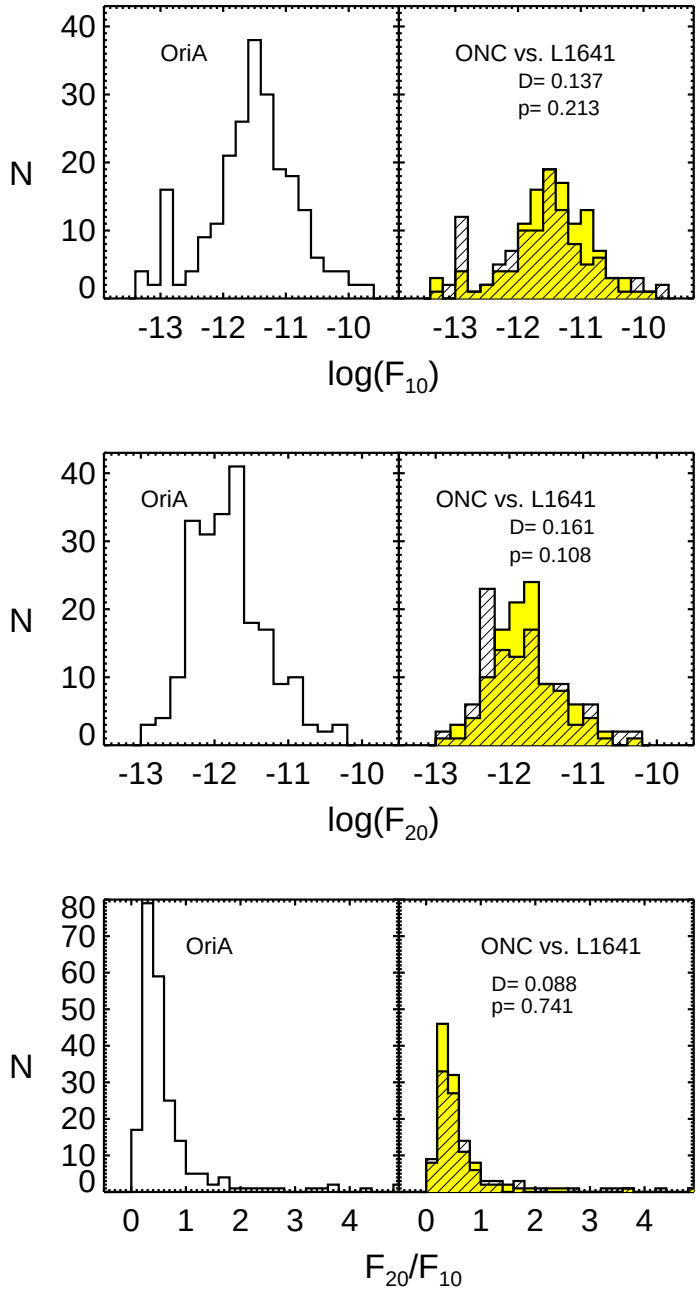


Figure 3.22 Histogram of F_{10}, F_{20}, and F_{20}/F_{10}: yellow vs. hatched

3.5 Median Spectra

We generated the median spectra of Class II disks in ONC and L1641, and compared them to the median spectrum of Class II disks in Taurus. To do so, we first selected the spectra of disks that do not show evidence of time variability or evidence for radial gap/central hole. Then, we gathered the spectra in similar ranges of spectral types: A0–K4, K5–M2, and M3–M6. We did not include the spectra without host-star spectral type information in the median spectra. We normalized the H-band flux of each spectrum in each category to the median H-band flux of the corresponding group to remove the effect of different stellar luminosity. Then the displayed median spectra in Figure 3.23 was normalized to the corresponding median H-band flux of Taurus disks in each panel for the comparison to the median spectrum of Taurus.

The median of A0–K4 group is noticeably different in ONC and L1641, from the median spectrum of Taurus. The A0–K4 group's median spectrum of ONC has very similar flux levels of disk emission to the K5–M2 median spectrum of Taurus over the wavelength range of SL coverage, but the ONC median spectrum shows steeply decreasing fluxes beyond 13 μm with prominent crystalline-silicate features. In contrast to the A0–K4 median of ONC, the median spectrum of A0-K4 group in L1641 has high fluxes compared to the K5–M2 median of Taurus over the wavelengths of IRS spectrum coverage. As we will discuss further in Chapter 6, this may indicate ablation of the outer disks in ONC, relative to those in L1641 and Taurus.

We compare the median spectra of K5-M2 group of ONC, L1641, and

Taurus in the panels in the second rows from the bottom of Figure 3.23. In the case of ONC versus Taurus, the median spectrum from ONC disks has more excess through 5-20 micron which indicate less evolution of inner disk than that of Taurus. In the other hand, the K5-M2 median spectra of L1641 and Taurus are generally similar. Even though some details like grain properties may show somewhat different characteristics, the general degree of disk evolution between Class II disks with K5-M2 spectral types in L1641 and Taurus appear to be similar.

The last row in Figure 3.23 contains the comparison of the M3-M5 median spectra. Due to the small numbers in the group, we included the spectra of M3 through M6 to compare the M3-M5 median of Taurus. In the both L1641 and ONC, the M3-M6 median spectra appear to have higher excess emission than Taurus. A possible explanation of this higher emission of disks around host-star with M3 or later spectral type in Orion A is the younger ages of the systems with M3-M6 spectral types in Orion A resulting less time for disk evolution than the systems in Taurus. Alternatively, the M3-M6 systems in Orion could have had large initial disk masses than systems with later spectral type in Taurus.

More discussion related to the median spectra will appear in Chapter 6.

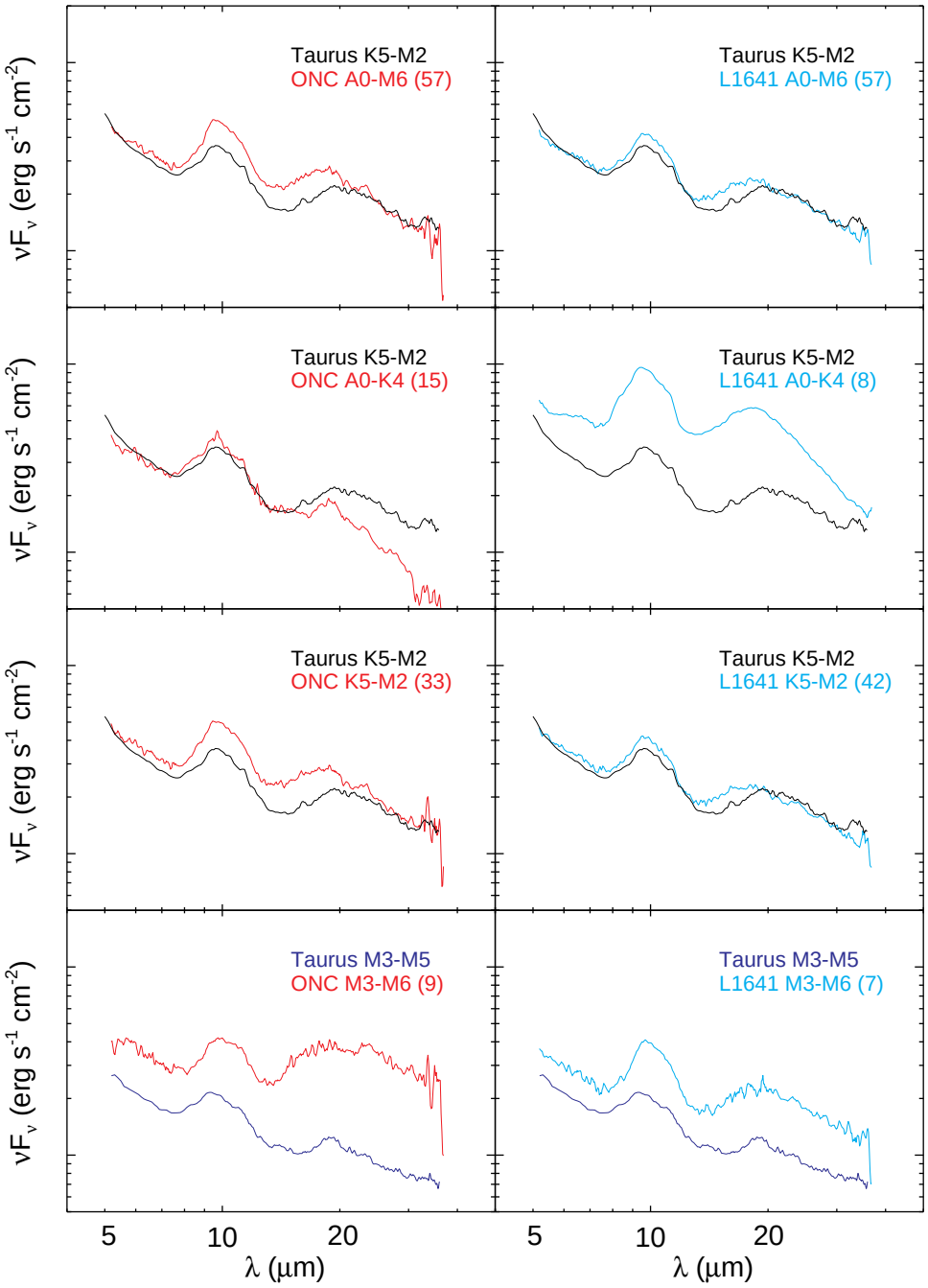


Figure 3.23 Median spectra compared to Taurus median.

3.6 Summary

In this chapter, we described the definition of various parameters which have been used to probe disk and dust characteristics. We compared the parameters measured from Class II disk samples from Orion A including Trapezium, ONC, and L1641 to them from Class II disks in Taurus when the comparison is possible. We found that the degree of dust processing for inner disks of ONC is smaller than that in Taurus based on statistically-significantly (1) larger EW10 and (2) smaller $F_{11.3}/F_{9.8}$, compared to Taurus. In particular, the comparisons of the distribution of $F_{11.3}/F_{9.8}$ of ONC, L1641, and Taurus indicate increased processing of dust as time goes on in the 1-2 Myr age range.

On the other hand, we infer that the higher values and large difference of $F_{11.3}/F_{9.8}$ distribution of the Trapezium region compared to that of Taurus, in spite of the younger median age of the Trapezium, is possibly due to a disk-evolutionary difference: less-processed small grains at somewhat larger radii may have been blown away or destroyed by radiation from the Trapezium stars.

Unlike the indicators of different properties of small dust grains, EW10 and $F_{11.3}/F_{9.8}$, we found no significant differences in the "sedimentation index" n_{13-31} among ONC, L1641, and Taurus.

4 Transitional Disks and their Origin

4.1 Introduction

Transitional disks (TDs) are protoplanetary disks around young stars which are optically thick and gas-rich, but which have AU-scale radial gaps or central clearings in their dust distribution. Usually the gap, which is depleted of small dust grains, is revealed as a deficit in the host T Tau star's infrared excess, with respect to its siblings. Such disks are thought to represent an evolutionary stage between Class II and Class III young stellar objects (YSOs).[1] Strom et al. (1989) first discussed the implications of young stars with little or no short wavelength excess, switching to large and strong excess at longer wavelengths.

After the distinctive spectrum of CoKu Tau/4 was discovered by Forrest et al. (2004), several TDs in the Taurus star-forming region were studied in detail with self-consistent disk modeling by D'Alessio et al. (2005) (CoKu Tau/4), Calvet et al. (2005) (DM Tau and GM Aur) and Espaillat et al. (2007a,b, 2008) (LkCa 15 and UX Tau A). Calvet et al. (2005) and D'Alessio

[1] See Chapter 1.

et al. (2005) suggested that DM Tau and CoKu Tau/4, respectively, can be explained with an empty central cavity in the disk surrounding the central star, but GM Aur requires a disk structure with a gap separating an inner optically thin disk and an outer optically thick disk to match the observed SED (Calvet et al., 2005). Espaillat et al. (2008, 2010) confirmed that LkCa 15 and UX Tau A have gaps between optically thick inner and outer disks. We will refer in the following to these three types of disks as classical transitional disks (CTDs; e.g. DM Tau), weak-excess transitional disks (WTDs; e.g., GM Aur) and pre-transitional disks (PTDs; e.g., LkCa 15), respectively.

There is generally good agreement with the gap sizes inferred from SED modeling, and direct observations of the outer edges of the gaps. Gaps in some 15 TDs have been confirmed by submillimeter interferometry (Piétu et al., 2006; Hughes et al., 2007, 2009; Andrews et al., 2009, 2011), and one of these, LkCa 15, also in near-infrared light scattered by the outer disk (Thalmann et al., 2010). The resolved inner disk of a PTD, T Cha, also confirms its gapped structure (Olofsson et al., 2011).

The definition and selection criteria of TDs have been far from homogeneous considering all objects called 'transition' or 'transitional' objects from other works. Many authors define TDs rather loosely, with diverse nomenclatures[2]. Circumstellar disks with a deficit of dust emission from the inner disk and large 30/13 μm flux ratio indicating an optically thick outer disk have been designated "cold disks" by Brown et al. (2007) and Merín et al. (2010). A more relaxed definition includes disks with a much smaller excess

[2]The definition of diverse nomenclatures is summarized in Evans et al. (2009)

for wavelengths beyond >13 μm representing a depleted or settled outer disk compared to our definition of TDs. Those disks are named "anemic disks" (Lada et al., 2006), "homologously depleted disks" (Currie et al., 2009), or "weak-excess disks"[3] (Muzerolle et al., 2010). Such SEDs can result from dust settling to the disk midplane (Luhman et al., 2010; Espaillat et al., 2012), or outward truncation of a disk by gravitational interaction with a companion (McClure et al., 2008). Therefore, it is important to clarify by which definition and selection criteria the sample of transitional/transition disks are selected, especially if the sample is to be used for searching for any trends to understand the properties of transitional disks and their origin.

Several physical mechanisms have been suggested to explain inside-out disk dispersal: photoevaporation (Clarke et al., 2001; Alexander et al., 2006a,b; Gorti et al., 2009; Owen et al., 2012); grain growth/coagulation/settling (Dullemond & Dominik, 2005; Ciesla, 2007); inside-out clearing by Magneto-Rotational Instability (MRI) (Chiang & Murray-Clay, 2007; Suzuki et al., 2010; Perez-Becker & Chiang, 2011); dynamical effects by stellar/substellar companions (Lubow & D'Angelo, 2006); giant planet formation (Marsh & Mahoney, 1992; Rice et al., 2003; Quillen et al., 2004; Varnière et al., 2006; Lubow & D'Angelo, 2006; Zhu et al., 2011, 2012). To distinguish and understand which mechanisms are dominant for the origin of transitional disks, not only flux density information at all wavelengths for a specific target but also empirical trends from observational data in a large sample are indispensable.

There have been several efforts to use statistical trends among several prop-

[3]The definition of WTDs in this work and in Muzerolle et al. (2010) are different.

erties of transitional disks and their host stars to constrain models of the origins of these objects. Kim et al. (2009) analyzed IRS spectra of 13 transitional disks in Taurus and Chamaeleon (1–3 Myr) and found a strong correlation between stellar mass and outer gap radius, R_{wall}. Merín et al. (2010) collected broad-band SEDs of some 15 "cold" disks from several young associations. Including some objects reported in the literature (Brown et al., 2007; Kim et al., 2009, e.g.) to improve the sample size, they found the gap radius to scale linearly with $M_\star$, and to be significantly correlated with disk mass, with more massive disks tending to have larger holes. In the somewhat older (4–12 Myr) clusters, Tr 37 and NGC 7160, Sicilia-Aguilar et al. (2010) found the median accretion rates in the TD systems to be about an order of magnitude smaller than the median mass accretion rate of normal Class IIs in Taurus and Chamaeleon, but similar to these associations' normal Class II YSOs, in contrast to Najita et al. (2007) who found that accretion rates for TDs in the Taurus-Aurigae association are systematically a factor of 10 smaller than the normal Class IIs in Taurus.

In this chapter, we present IRS spectra of 62 newly selected TDs in the Orion A star-forming region and near-IR spectra of 52 of them from SpeX/IRTF follow-up observation.

We consider 105 TDs not only of Orion A including ONC and L1641, but also of Taurus (henceforth Tau; Furlan et al., 2011), Chameleon I (henceforth Cha I; Manoj et al., 2011), Ophiuchus (henceforth Oph; McClure et al., 2010), and NGC 1333 (henceforth N1333; Arnold et al., 2012). From this very large sample of TDs selected homogeneously from disk properties measured with IRS

spectra, and comprehensive information on mass accretion rates from SpeX spectra and X-ray luminosity, we are now able to search for trends between stellar parameters and disk parameters with robust statistics. We anticipate this work to help in understanding mechanisms responsible for the origins of TDs.

In this chapter, we describe the selection criteria of transitional disks and subclassification of TDs in Section 4.2. We describe the extraction of the outer gap radius, R_{wall} in Section 4.3. We discuss the fraction of transitional disks and age trends in Section 4.4. In Section 4.5, we explore correlations and trends of the transitional disks properties and compare them to those of radially continuous disks where possible. Then, we review and discuss what these findings mean and how they can be used to help our understanding of the origin of transitional disks in Section 4.6. Summary and conclusions drawn from our finding follows in Section 4.7.

4.2 Transitional Disks: Selection Criteria and their Variety

4.2.1 Empirical Selection Criteria of TDs

Several spectral indices derived from IRS spectra of Class II YSOs have been used as a first step to separate transitional disks from the radially continuous bulk of the population (Furlan et al., 2009; Watson et al., 2009a; Manoj et al., 2011; McClure et al., 2010; Arnold et al., 2012), which we also use to identify

the TDs in Orion A. As we discussed in Chapter 3, the continuum spectral indices between two wavelengths selected to avoid emission features can be used to infer the disk structure. Especially, the continuum index between K-band ($\sim$2 μm) and 6 μm is useful to infer inner disk structure and the continuum index between 13 μm and 31 μm is a good indicator of vertical structure as well as radial structure. The equivalent width of the 10 μm silicate emission feature, EW10 (see, Equation 3.7), is a measure of the amount of optically thin dust per unit area of optically thick disk. Thus, a large EW10 is a sign of a large amount of optically thin dust and/or an indication of a reduction in disk continuum due to the absence of optically thick disk in the region where the 10 μm emission feature is formed. Here we use the continuum spectral indices along with EW10 to identify disks with central clearing or radial gap. The principles are that small values of n_{K-6} — down to the color of photospheres — and large values of n_{13-31} indicate the spectral "transition" that signifies a gap with outer gap radius in the few to few tens of AU range; and that large values of EW10 connote warm optically thin dust in gaps.

In our analysis EW10 does not depend much on temperature and composition. As is evident in the ubiquity of 10 μm excesses and silicate emission features, disks around young stars or brown dwarfs always have a distribution of temperatures which exceed that required for efficient excitation of 10 μm continuum ($T > 300$ K), and therefore are well above that required for the silicate features, which are dominated by emission from cooler material at larger radii. We also know from the shape of the silicate emission profiles that essentially all the dust grains we see are optically thin (internally, that is),

and composed of amorphous and crystalline silicates (see, e.g., Sargent et al. (2009)). In this case EW10 does not depend upon mass fractions of amorphous and crystalline material. One way to see this is to note that a grain with a given number N of silicate monomers has a fixed number of oscillators, with possibly a small range of oscillation frequency, in any given vibrational mode. Absorption or emission integrated over that mode is, to first order, proportional to N. (This is essentially the Thomas–Kuhn sum rule.) Thus two grains with the same N but different mineral fractions have the same equivalent width in the same vibrational mode — such as that which produces the 10 μm silicate feature — though the one with larger mineral fraction will have a larger number of oscillators at a small set of fixed frequencies, and identifiable sub-structure to the silicate feature.

To find break points for TDs among the Class II YSOs distribution in these observed parameter spaces, we utilized all (∼600) IRS spectra of Class II YSOs observed in Orion A, Tau, Cha I, Oph, and N1333. Using the properties of TDs already well identified in Tau (Furlan et al., 2011), Cha I (Manoj et al., 2011), Oph (McClure et al., 2010), and N1333 (Arnold et al., 2012) as a guide, we found that the breaks occur at

1. $n_{K-6} \leq$ -2.1 (the lowest octile for the distribution of n_{K-6}),
2. $n_{13-31} \geq 0.5$ (the highest octile for the distribution of n_{13-31}), and
3. EW10 $\geq$ 4.3 (the highest octile for the distribution of $EW(10\mu\text{m})$).

In Figure 4.1, we plot n_{13-31} versus n_{K-6} and n_{13-31} versus EW10 for objects in Orion A. We also added objects in Tau (Furlan et al., 2011) in the plots for comparison.

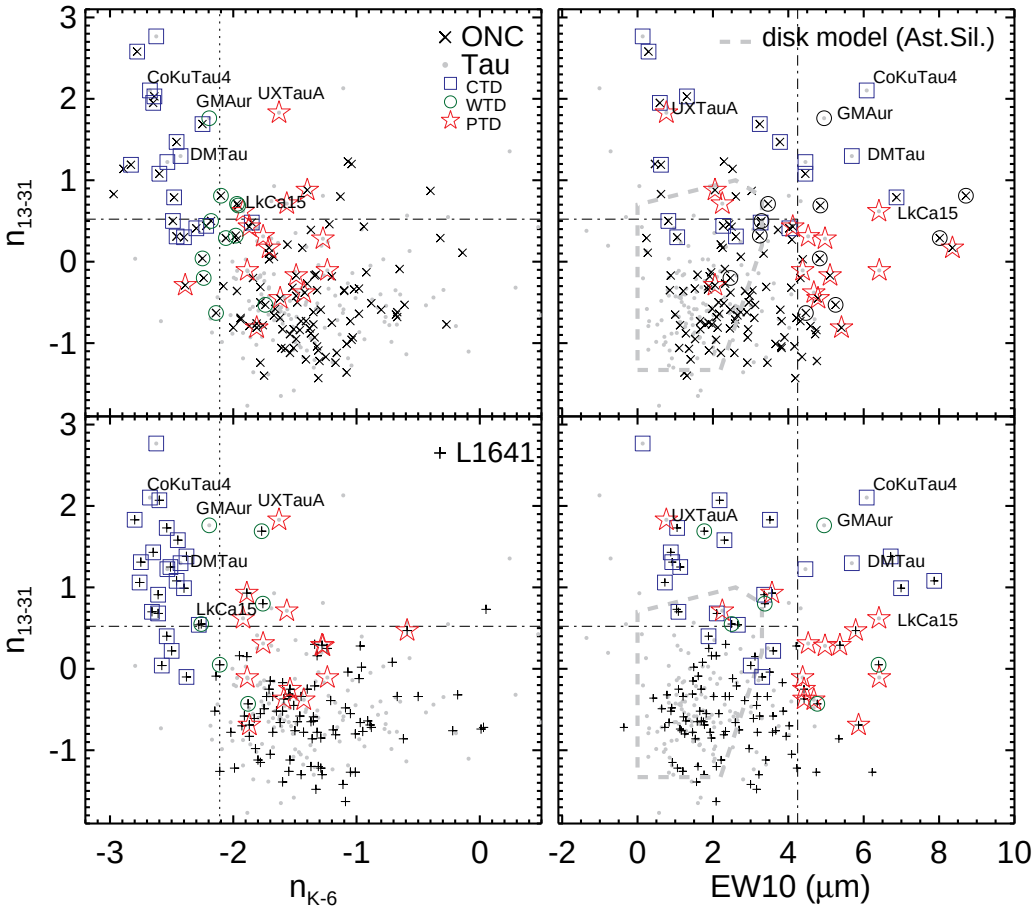


Figure 4.1 Selection of OriA TDs by n_{13-31} vs. n_{K-6} (the left panels) and n_{13-31} vs. EW10 (the right panels). In the right panels, the polygon with thick dashed line indicates the coverage area by a typical accretion disks model (D'Alessio et al., 2006). The upper panels are for the TD selection in ONC, and the lower panels are for the TD selection in L1641. In each plot, samples in Tau (Furlan et al., 2011) are also included for comparison. The dash-dotted lines indicate the upper octile; the dotted lines indicate the lower octile.

To identify TDs in Orion A, we first selected objects satisfying one of the above conditions as possible candidates. Second, we rejected objects with spectral types earlier than G because they have significantly higher masses ($>2M_{\odot}$) and their circumstellar disks evolve much faster by possibly different disk clearing mechanisms than the case of TDs around the low-mass T Tauri stars. However, we keep objects with unknown spectral type as all appear to lie in the same luminosity range as the low-mass T Tauri stars. Third, we examined the detailed shape of the SEDs, and selected objects with deficits of infrared excess in the 2–8 μm range, compared to the appropriate median IRS spectrum of Class II disks in Tau (Furlan et al., 2011). We used the median of Taurus K5–M2 for objects with the spectral type earlier than M3, and the median of Taurus M3–M5 for objects with the spectral type of M3 or later. We adopt the Taurus median spectra instead of Orion A median because transitional disks in Tau and the median CTTS SED of Tau have been well studied and used widely for comparison in studies of other star-forming regions. As shown in Figure 4.2, the previously characterized TDs in Tau, Cha I, Oph, and N1333 pass these filters clearly.

In Table 4.1, we indicate how the TDs in this paper were selected based on the selection criteria. Three objects, OriA-44, OriA-88, and OriA-172, are classified as TDs based upon examination of their SEDs which are indicative of gap/central hole, despite the fact that they do not pass any of the three criteria. The spectra of 62 transitional disks in Orion A appear in Figure 4.3. We use these 62 TDs in Orion A and 43 TDs from Tau (13), Cha I (11), Oph (10), and NGC 1333 (9) to unveil properties of transitional disks in the

following.

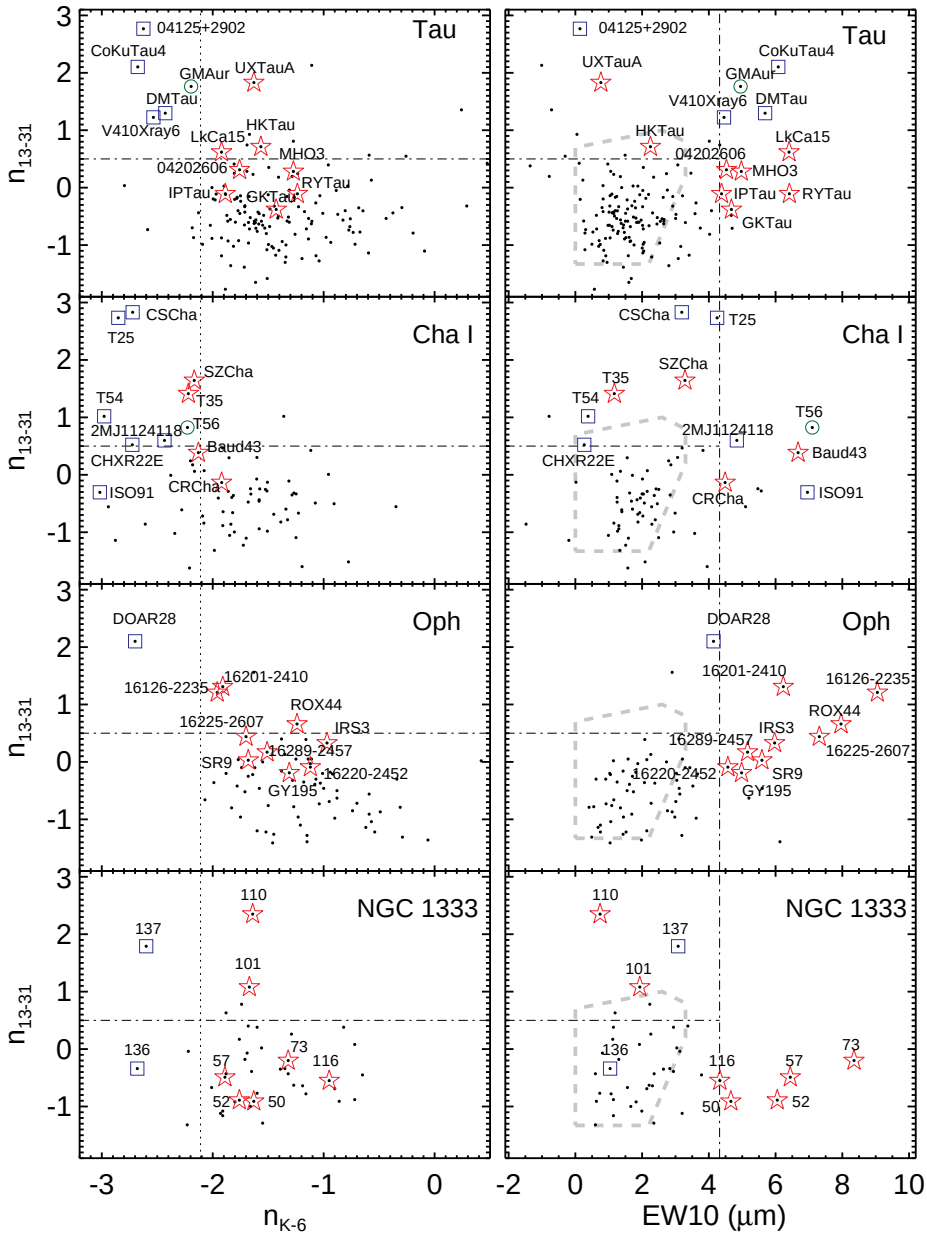
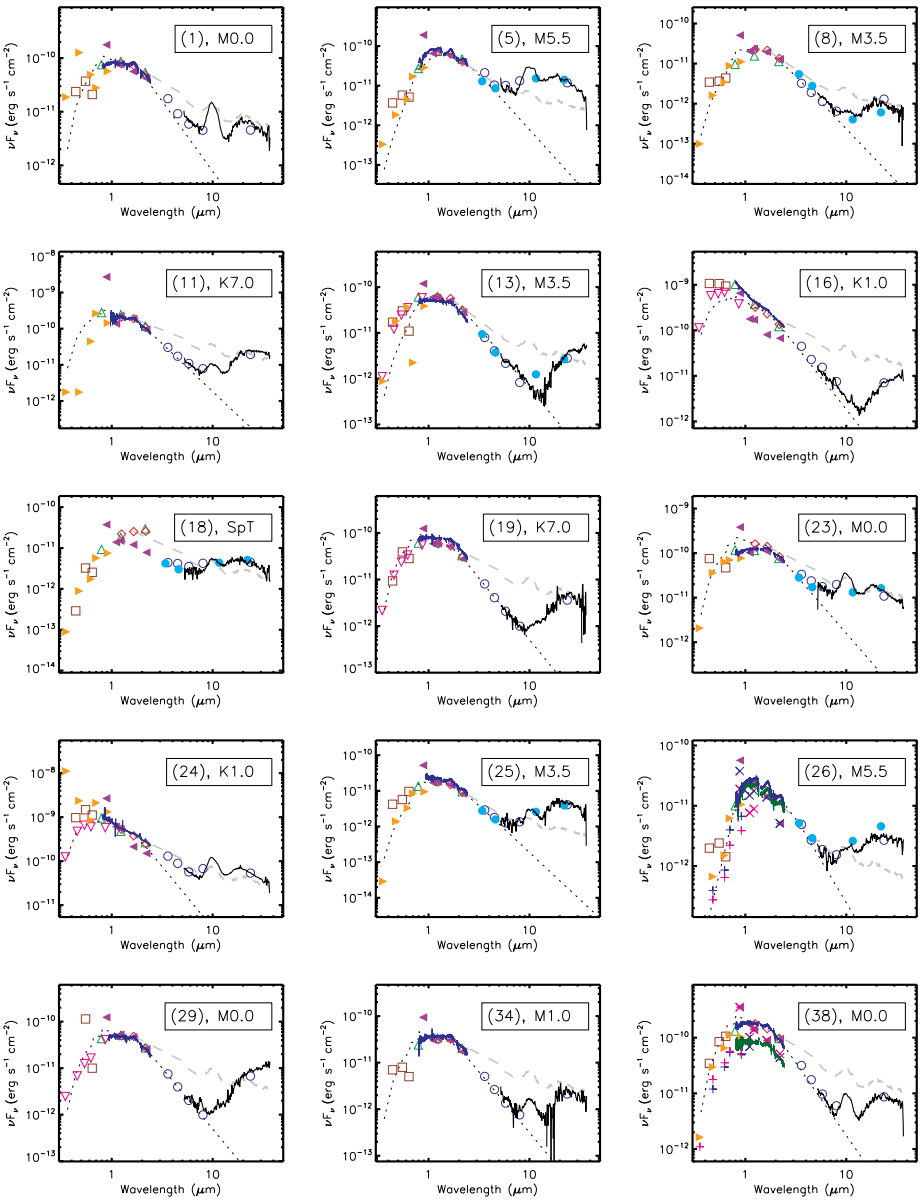
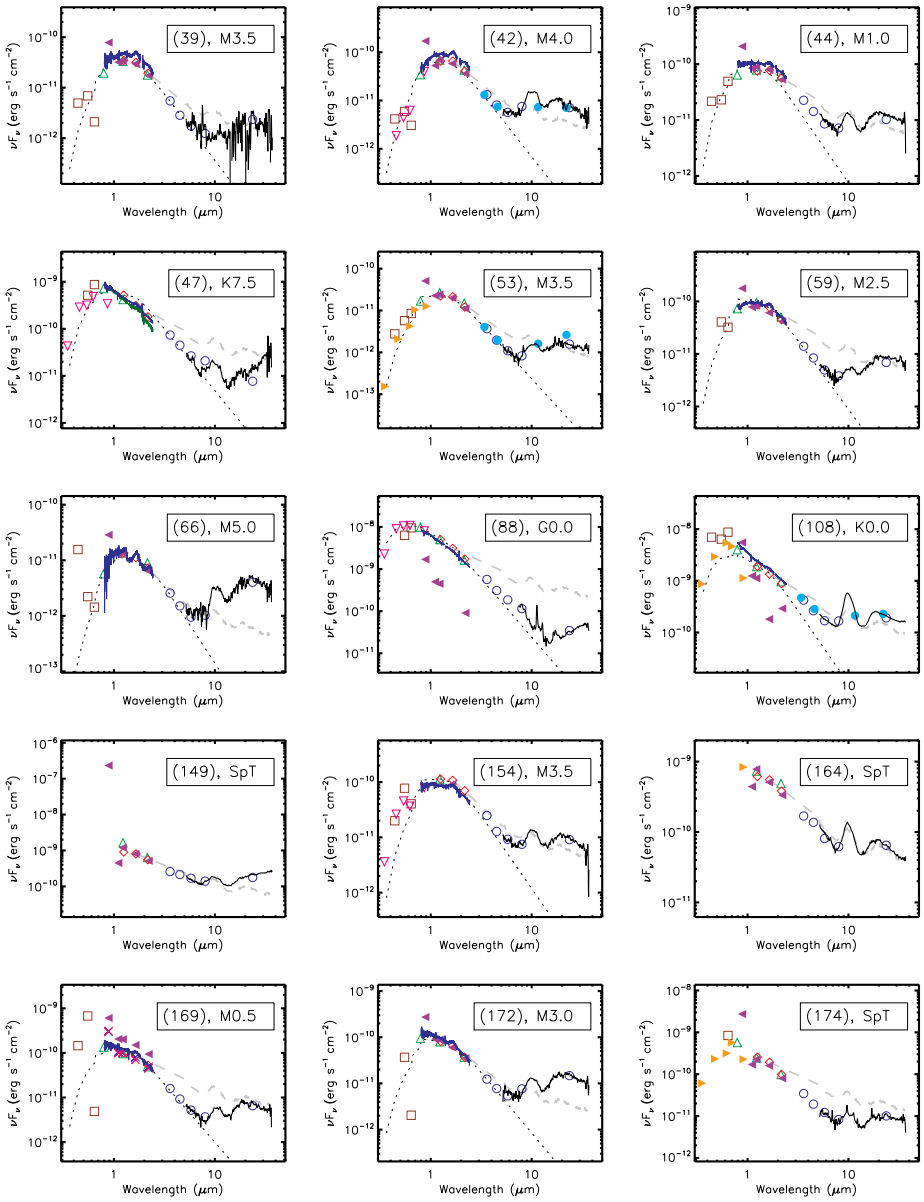


Figure 4.2 Selection of TDs in other star-forming regions, Tau, Cha I, Oph, and NGC 1333, by the criteria in n_{13-31} vs. n_{K-6} (the left panels) and n_{13-31} vs. EW10 (the right panels). The meanings of different symbols and lines are same as Figure 4.1.



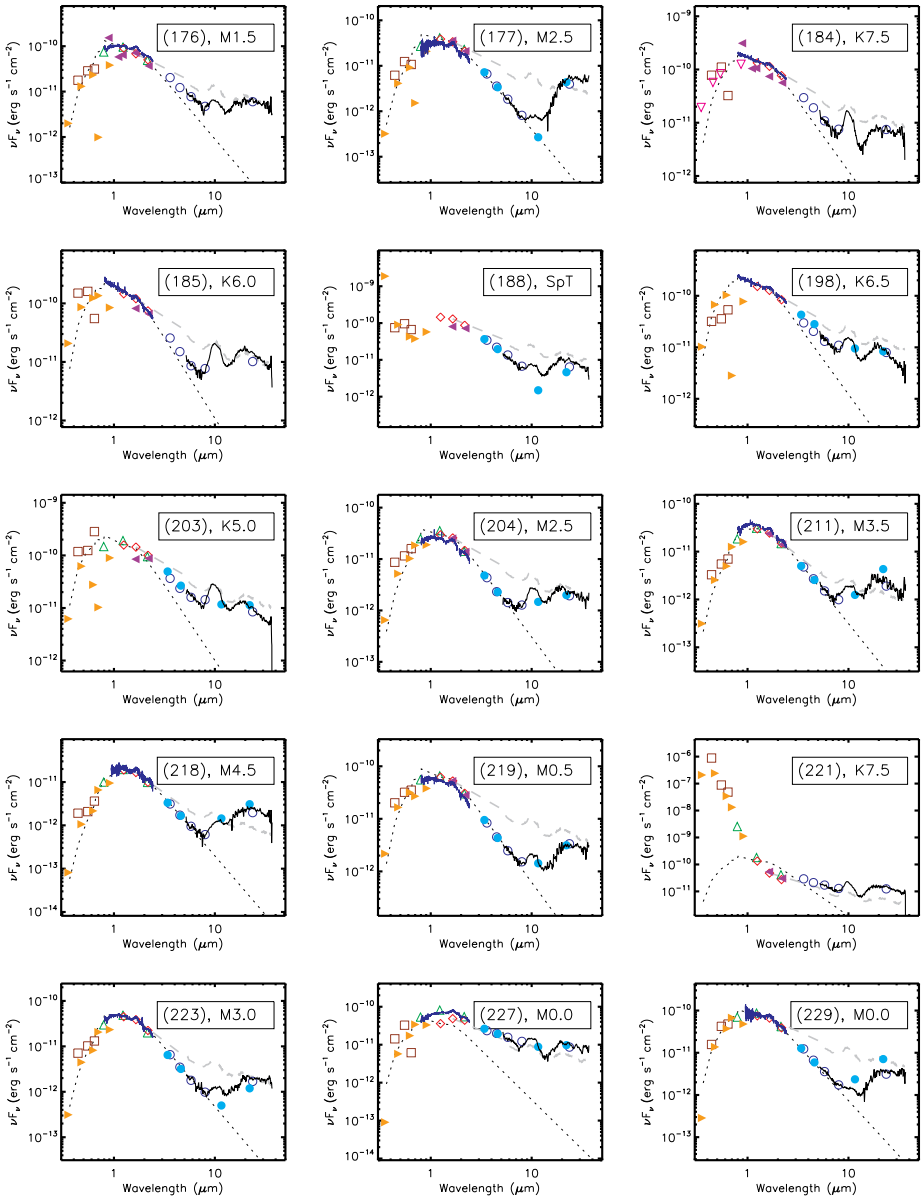
(a)

Figure 4.3 De-reddened SEDs of TDs in Orion A. The meanings of symbols are same as in Figure 3.5 except the median spectrum of protoplanetary disks in Taurus region (gray long dashed line).



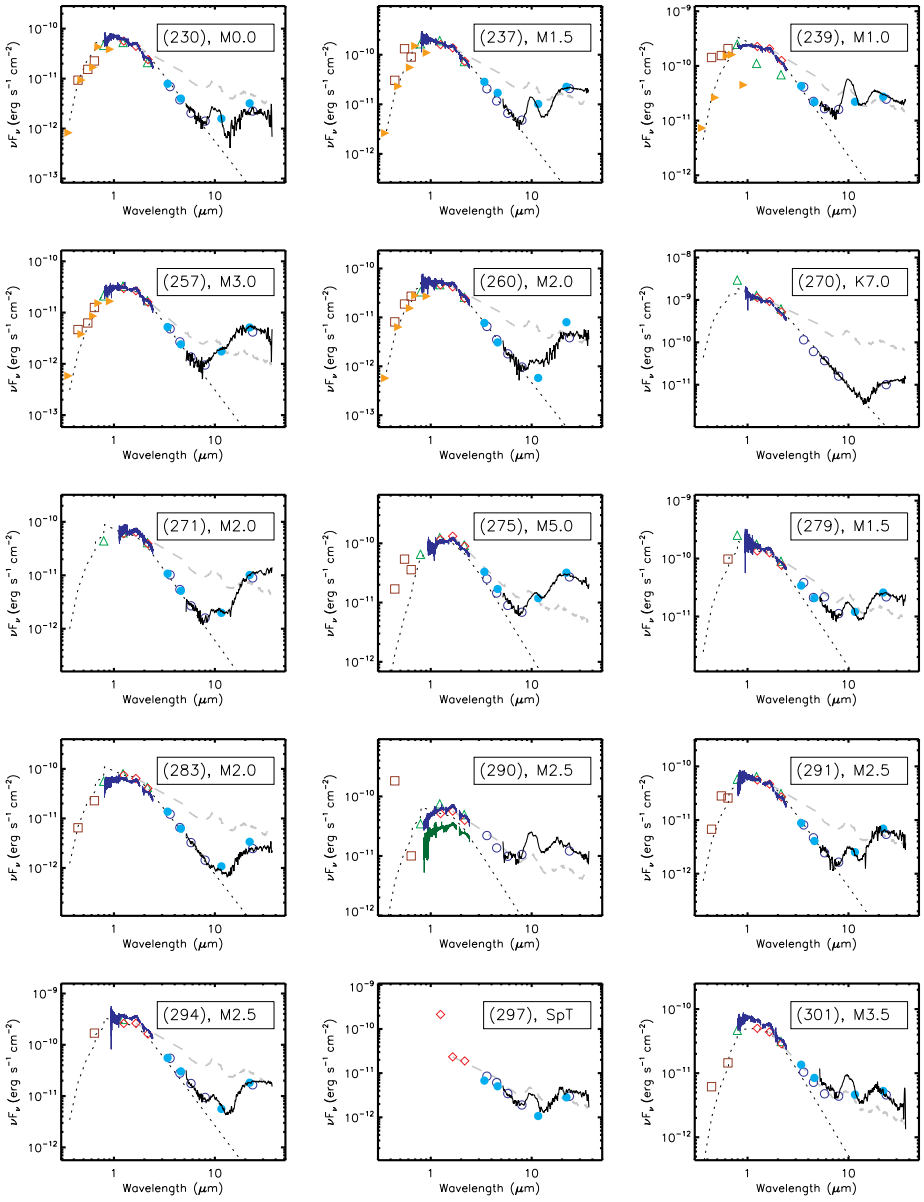
(b)

Figure 4.3 (Continued)



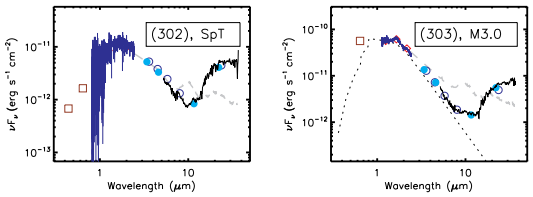
(c)

Figure 4.3 (Continued)



(d)

Figure 4.3 (Continued)



(e)

Figure 4.3 (Continued)

4.2.2 Subclassification of Transitional Disks: CTD, WTD, and PTD

The mid-infrared spectrum of a CTD like DM Tau or CoKu Tau/4, having a few-AU to few-tens of AU central clearing, is distinctive compared to a radially continuous Class II disk: it shows very little continuum excess over the photosphere from near-IR (1–2 μm) to wavelengths in the mid-infrared (around 8-13 μm), at which point the excess increases exponentially with increasing wavelength until it matches or exceeds the median spectrum. The other two types of TDs have excesses from near-IR to the shorter mid-infrared wavelengths ($\sim$5–8 μm) that are smaller than or similar to the median. In some, like LkCa 15 and UX Tau A, veiling in the near-IR spectra points to an underlying optically thick inner disk (Espaillat et al., 2007b, 2008), and their distinctive spectrum corresponds to optically thick inner and outer disks separated by a gap. These are PTDs. Intermediate between CTDs and PTDs are WTDs, in which the weaker near- and mid-infrared excess is best explained by an optically thin inner disk separated by a gap from an optically thick outer disk, as in GM Aur (Calvet et al., 2005; Espaillat et al., 2010). Therefore, the distinction between CTDs, WTDs, and PTDs is whether an (optically thick/thin)

inner disk exists or not.

It is useful to define the inner disk excess fraction (IDEF) to characterize the near-infrared and shorter-wavelength mid-infrared excess fraction relative to the K5–M2 median spectrum of Class II sources in Tau. Since our sample is complete in H band data from the 2MASS catalog and we have IRS spectra starting at $\sim$5.2 μm, we interpolate H band to 6 μm to acquire the assumed spectrum covering 1.65–6 μm:

$$IDEF = \frac{\int_{1.65\mu\mathrm{m}}^{6\mu\mathrm{m}} F_{\lambda,obj} - F_{\lambda,photosphere}\, d\lambda}{\int_{1.65\mu\mathrm{m}}^{6\mu\mathrm{m}} F_{\lambda,median} - F_{\lambda,photosphere}\, d\lambda} \tag{4.1}$$

In the case of OriA-88 for which we do not have an SL2 spectrum, the flux at IRAC channel 3 (5.8 μm) is used instead of IRS fluxes.

By taking the already well studied Taurus TDs as references, we adopt a set of infrared-excess ranges to subclassify TDs:

CTD: IDEF < 0.25

WTD: $0.25 \leq$ IDEF < 0.5

PTD: IDEF ≥ 0.5

The IDEF values for the TD subclassification criteria are derived by adopting the K5–M2 median spectrum. The M3–M5 median spectrum is fainter than the K5-M2 median spectrum due to an effect of lower stellar luminosity and lower disk emission (Furlan et al., 2011). Therefore the excess emission over photosphere at 2–8 μm is weaker. It may lead to misclassification to compare objects of M3 or later spectral type to the K5–M2 median spectrum: an IDEF value of an object with M3 or later spectral type derived from the K5–M2 me-

dian spectrum is generally lower than that derived from the M3–M5 median spectrum. Furthermore, there are no WTDs and few PTDs with M3 or later spectral type among the already well studied TDs in Tau, Cha I, and Oph. Thus, for M3–M5 types, we rely on confirmation by other TD selection criteria. Considering the additional contributions such as the disk inclination and scattered light to the degeneracy of the interpretation of the excess emission in the near-infrared, we consider the subclassification of TDs based on IDEF to preliminary until the existence and characteristics of an inner disk can be resolved by additional observations. We note the subclassification based on IDEF values and some cases of exceptions of using this criteria in Table 4.1.

With these criteria we obtain 34 CTDs, 15 WTDs and 13 PTDs in Orion A. Adding the four other nearby associations of Tau, Cha I, Oph, and N1333 brings the totals to 47 CTDs, 17 WTDs and 41 PTDs. Spectral indices of these objects are plotted in Figures 4.1 and 4.2.

Most CTDs are placed below the lower octile of n_{K-6}, which reflect their negligible short-wavelength infrared excess from the inner disk, while PTDs are distributed over the whole range greater than the lower octile of n_{K-6}. The WTDs are mostly located between the distribution of CTDs and PTDs in n_{K-6}.

In the plot of n_{13-31} versus EW10 in Figure 4.1 and 4.2, we also indicate the ranges occupied by radially continuous disk models with a range of inclination angles, stellar masses, degrees of dust settling, and mass accretion rates (D'Alessio et al., 2006; Watson et al., 2009a; Espaillat, 2009). Most of TDs in Orion A lie outside the model polygon. However, in contrast to the positions

of TDs in other star-forming regions, some of CTDs, WTDs, and PTDs in Orion A are located inside the polygon, indicating that they could be modeled as radially continuous disks, with respect *only* to these two parameters. With the exception of IRS-18 (PTD) and IRS-154 (WTD) in ONC, the TDs inside of the polygon are located in the region for vertically well-mixed disks (the area toward the upper right side in the polygon). Few objects lie in the domain of well-mixed disks for Tau, Cha I, Oph, and N1333. Furlan et al. (2009) concluded from this that substantial disk structural evolution, especially settling of dust to the disk midplane, has occurred in 1–2 Myr. Arnold et al. (2012) showed that the disks in N1333 are statistically indistinguishable from those in Tau, Cha I and Oph in this regard.

In the ternary plot of Figure 4.4, we see that the distribution of TDs is separated from the radially continuous disks in the three dimensional parameter spaces of n_{K-6}, n_{13-31}, and EW10: especially CTDs and WTDs are nicely located in the different region from the region occupied by the radially continuous disks.

We plot n_{13-31} and EW10 of disks in Orion A along IDEF in Figure 4.5, as well as TDs in Tau as the references of criteria along IDEF. We find that n_{13-31} of TDs decreases as IDEF increase, i.e., CTDs tend to have larger n_{13-31} than PTDs. We note that CTDs with low IDEF span through the ranges of EW10, whereas most PTDs have high values (>4) of EW10.

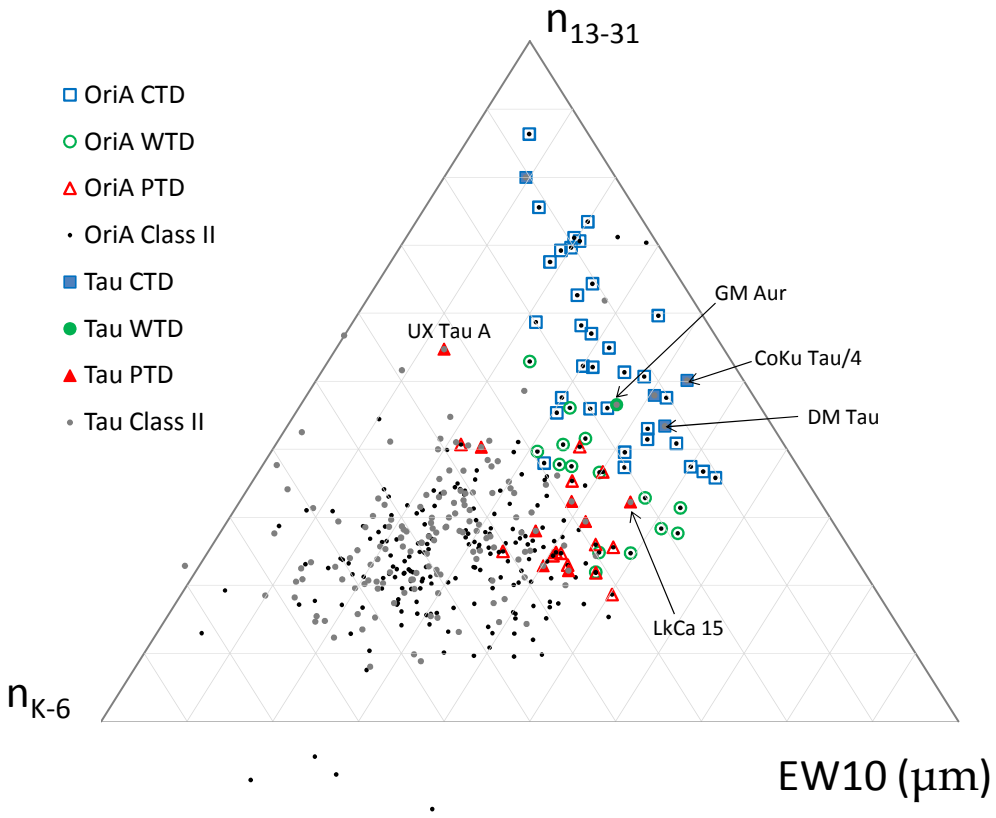


Figure 4.4 Disks samples of Orion A (black dots) and Tau (gray dots) are plotted in the spaces of three parameters. TDs are indicated by subtypes: CTDs (squares), WTDs (circles), and PTDs (triangles). Orion A TDs are open symbols and Tau TDs are filled symbols. The center of this plot is corresponding to the projected origin of the three axes. The three axes values are from 0 to 100, which are linearly transformed from their original values of [-3, 0] for n_{K-6}, [-2, 3] for n_{13-31}, and [-1, 9] for EW10.

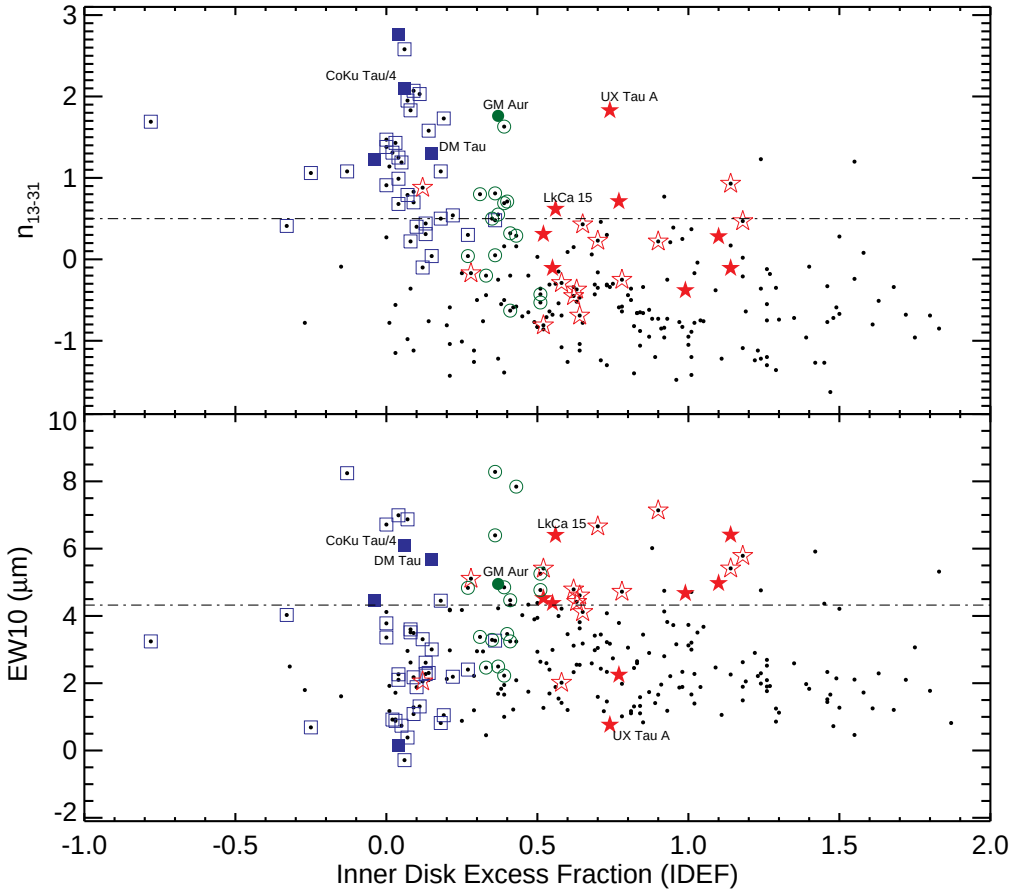


Figure 4.5 n_{13-31} and EW10 plotted against IDEF (Inner Disk Excess Fraction). TDs of Orion A and Tau are indicated in open and filled symbols: CTDs (squares), WTDs (circles) and PTDs (stars). The dots indicate radially-continuous disks of Orion A.

4.2.3 TD Selection Criteria in the Literature

We have compared our selection criteria for TDs to other selection criteria used in the literature. We plot TDs as well as Class II sources in OriA on the color-color diagrams used for the selection criteria by Merín et al. (2010) (left panel), Cieza et al. (2010) (middle panel), and Muzerolle et al. (2010) (right panel) in Figure 4.6. These authors used *Spitzer* IRAC and MIPS broadband photometry, not IRS spectra, for their selection criteria.

Merín et al. (2010) identified and characterized disks with inner holes from the *Spitzer* c2d Legacy program. They used [3.6]-[8.0] vs. [8.0]-[24] color–color diagram to identify TDs that fell in two separate regions:

Region A: $0.0 <$ [3.6]-[8.0] < 1.1 and $3.2 <$ [8.0]-[24] < 5.3
Region B: $1.1 <$ [3.6]-[8.0] < 1.8 and $3.2 <$ [8.0]-[24] < 5.3

Region A selects TDs with central clearings like CTDs in our sample. Region B corresponds to the disks with some excess flux in the IRAC bands like WTDs and PTDs in our sample. Their selection criteria of region A agrees with our criteria for CTDs in L1641, but some number of CTDs in Orion A fall in Region B or outside the Region A and B (the left panel of Figure 4.6).

Cieza et al. (2010) set selection criteria based on the [3.6]-[24] vs. [3.6]-[4.5] color–color diagram, in which TDs are located in the region where [3.6]-[4.5] < 0.25 and [3.6]-[24] > 2. We see that most of our CTDs fall in that region, but PTDs have [3.6]-[4.5] > 0.25 (the middle panel of Figure 4.6).

Muzerolle et al. (2010) used spectral slopes (i.e. spectral indices) at two different wavelength intervals, 3.6–5.8 μm and 8–24 μm. The criteria for the

classical transitional disks with central holes based on a red α_{8-24} in Muzerolle et al. (2010) agrees with our criteria for CTDs. However, similar to Cieza et al. (2010), most of our WTDs and all of our PTDs will be missed by this criterion (the right panel of Figure 4.6).

From the comparisons of selection criteria for TDs, we find that (1) CTDs can be commonly identified by a variety of criteria; (2) a criterion utilizing the largest wavelength interval in the IRAC channels (between ch1(3.6 μm) and ch4(8 μm) in Merín et al. (2010)) can select WTDs and PTDs, but a color (i.e., the spectral slope) based on other broadband channels, such as [3.6]-[4.5] in Cieza et al. (2010) or 3.6–5.8 μm in Muzerolle et al. (2010), cannot find PTDs.

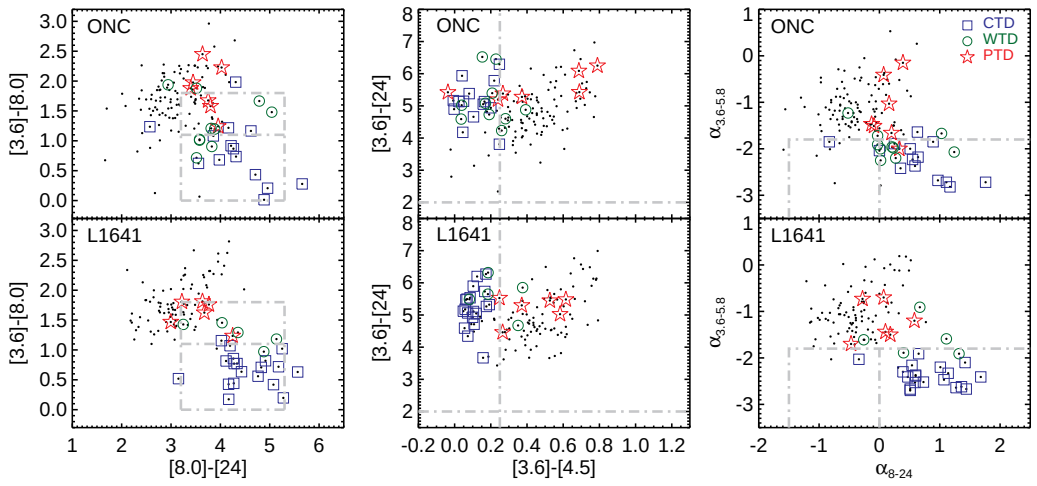


Figure 4.6 TDs of Orion A under other selection criteria. In each panel, the data points are our Orion A samples: the upper panels for ONC and the lower panels for L1641. Each selection criteria is indicated with the dot-dash lines. The left panel is for the selection criteria from Merín et al. (2010). The middle panel shows the selection criteria of Cieza et al. (2010). The right panel is the selection criteria from Muzerolle et al. (2010).

Table 4.1. Subclassification of TDs

ID (1)	name (2)	region (3)	n_{K-6} (4)	n_{13-31} (5)	EW10 (6)	subtype (7)	*IDEF* (8)
1	8336884-5290	ONC	N	N	Y	WTD	0.43
5	8343944-5609	ONC	N	N	Y	PTD	0.52[f]
8	8346141-5010	ONC	Y	Y	N	CTD	0.27[c]
11	8347711-5533	ONC	Y	Y	N	CTD	0.00
13	8350150-5595	ONC	Y	Y	N	CTD	0.06
16	8353051-5229	ONC	Y	Y	N	CTD	0.07
18	8355083-4835	ONC	Y	N	N	PTD	0.58
19	8355371-5480	ONC	Y	Y	N	CTD	0.05
23	8357031-5072	ONC	N	N	Y	WTD	0.51[d]
24	8358147-5505	ONC	N	N	Y	PTD	0.62
25	8358862-4842	ONC	N	Y	Y	WTD	0.39
26	8359203-5026	ONC	Y	N	N	CTD	0.13
29	8361167-5475	ONC	Y	Y	N	CTD	0.11
34	8365722-4816	ONC	Y	Y	Y	CTD	0.18
38	8367284-5798	ONC	Y	Y	Y	CTD	0.07
39	8368137-4860	ONC	Y	N	N	CTD	0.18
42	8369106-5686	ONC	Y	N	Y	WTD	0.41
44	8369980-5081	ONC	N	N	N	PTD[a]	0.65
47	8371984-5465	ONC	Y	Y	N	CTD	-0.78
53	8373930-6325	L1641	Y	N	N	CTD	0.15
59	8374388-6000	L1641	Y	Y	N	CTD	0.22
66	8375158-5162	ONC	N	Y	N	WTD	0.40
88	8377167-5247	ONC	n/a	Y	n/a	CTD[b]	0.22
108	8379312-5776	ONC	N	N	Y	PTD	0.90
149	8385365-5106	ONC	N	Y	N	PTD	0.12[e1]
154	8386523-5715	ONC	Y	N	N	WTD	0.33
164	8387753-4993	ONC	N	N	Y	PTD	0.28[e1]
169	8389033-4773	ONC	Y	N	N	CTD	0.13
172	8389673-4794	ONC	N	N	N	CTD	0.36[c]
174	8390073-5082	ONC	Y	N	N	CTD	-0.33
176	8390285-5070	ONC	N	N	N	WTD[a]	0.41
177	8390554-6390	L1641	Y	Y	N	CTD	0.09
184	8394216-5181	ONC	Y	Y	N	WTD	0.36
185	8394454-5823	ONC	Y	N	Y	WTD	0.27
188	8396035-5861	ONC	Y	N	N	WTD	0.35
198	8399269-6612	L1641	N	N	Y	WTD	0.51[d]
203	8406280-6293	L1641	N	N	Y	PTD	0.64
204	8406609-6247	L1641	Y	N	N	CTD	0.08
211	8411618-6426	L1641	Y	N	N	CTD	0.12
218	8416389-6503	L1641	Y	N	N	CTD	0.10

Table 4.1 (cont'd)

ID (1)	name (2)	region (3)	n_{K-6} (4)	n_{13-31} (5)	EW10 (6)	subtype (7)	*IDEF* (8)
219	8416834-6225	L1641	Y	Y	N	CTD	0.00
221	8416978-6185	L1641	N	N	Y	PTD	1.18
223	8424570-6484	L1641	Y	Y	N	CTD	0.04
227	8440418-7404	L1641	N	N	Y	PTD	0.70
229	8444779-6608	L1641	Y	Y	N	CTD	0.04
230	8445558-6860	L1641	Y	Y	Y	CTD	-0.13
237	8457266-7161	L1641	Y	Y	Y	CTD	0.00
239	8464666-7838	L1641	Y	N	Y	WTD	0.36
257	8502614-7795	L1641	Y	Y	N	CTD	0.09
260	8508501-7431	L1641	Y	Y	N	CTD	0.02
270	8519428-8120	L1641	Y	Y	N	CTD	-0.25
271	8520557-7775	L1641	Y	Y	N	CTD	0.08
275	8535781-7830	L1641	Y	Y	N	WTD	0.37
279	8538911-7999	L1641	N	Y	N	WTD	0.31
283	8547523-7831	L1641	Y	Y	N	CTD	0.03
290	8562845-8151	L1641	N	N	Y	PTD	0.78
291	8564835-8250	L1641	Y	Y	N	CTD	0.04
294	8567670-8803	L1641	Y	Y	N	CTD	0.14
297	8570949-8577	L1641	N	Y	Y	PTD	1.14
301	8576836-8303	L1641	N	N	Y	PTD	0.63[f]
302	8579480-8565	L1641	N	Y	N	WTD	0.39
303	8580634-8516	L1641	Y	Y	N	CTD	0.19
.	04202606	Tau	N	N	Y	PTD	0.52[f]
.	04125+2902	Tau	Y	Y	N	CTD	0.04
.	CoKuTau 4	Tau	Y	Y	Y	CTD	0.06
.	DMTau	Tau	Y	Y	Y	CTD	0.15
.	GKTau	Tau	N	N	Y	PTD	0.99
.	GMAur	Tau	Y	Y	Y	WTD	0.37
.	HKTau	Tau	N	Y	N	PTD	0.77
.	IPTau	Tau	N	N	Y	PTD	0.55
.	LkCa15	Tau	N	Y	Y	PTD	0.56
.	MHO3	Tau	N	N	Y	PTD	1.10
.	RYTau	Tau	N	N	Y	PTD	1.14
.	UXTauA	Tau	N	Y	N	PTD	0.74
.	V410 Xray6	Tau	Y	Y	Y	CTD	-0.04
.	2MJ1124118	Cha I	Y	Y	Y	CTD	-0.50
.	Baud43	Cha I	N	N	Y	PTD	0.45[e3]
T54	CHX22	Cha I	Y	Y	N	CTD	-0.03
.	CHXR22E	Cha I	Y	Y	N	CTD	0.18
.	CRCha	Cha I	N	N	Y	PTD	0.71

Table 4.1 (cont'd)

ID (1)	name (2)	region (3)	n_{K-6} (4)	n_{13-31} (5)	EW10 (6)	subtype (7)	*IDEF* (8)
T11	CSCha	Cha I	Y	Y	N	CTD	0.15
.	ISO91	Cha I	Y	N	Y	CTD	-0.22
T25	Sz18	Cha I	Y	Y	N	CTD	0.06
T35	Sz27	Cha I	Y	Y	N	PTD	0.44[e2]
T56	Sz45	Cha I	Y	Y	Y	WTD	0.35
T6	SZCha	Cha I	Y	Y	N	PTD	0.61
.	16126-2235	Oph	N	Y	Y	PTD	0.49[e3]
.	16201-2410	Oph	N	Y	Y	PTD	0.54
.	16220-2452	Oph	N	N	Y	PTD	1.10
.	16225-2607	Oph	N	N	Y	PTD	0.47[e2]
.	16289-2457	Oph	N	N	Y	PTD	0.63
.	DOAR28	Oph	Y	Y	N	CTD	0.07
.	GY195	Oph	N	N	Y	PTD	0.65[f]
.	IRS3	Oph	N	N	Y	PTD	1.38
.	Rox44	Oph	N	Y	Y	PTD	0.90
.	SR9	Oph	N	N	Y	PTD	0.53
spID 50	LAL 106	N1333	N	N	Y	PTD	0.80[f]
spID 52	LAL 110	N1333	N	N	Y	PTD	0.55
spID 57	LAL 129	N1333	N	N	Y	PTD	0.57
spID 73	LAL 171	N1333	N	N	Y	PTD	0.72
spID 101	LAL 245	N1333	N	Y	N	PTD	0.75[f]
spID 110	LAL 279	N1333	N	Y	N	PTD	0.81
spID 116	LAL 300	N1333	N	N	Y	PTD	1.71
spID 136	LAL 321	N1333	Y	N	N	CTD	0.03
spID 137	LAL 331	N1333	Y	Y	N	CTD	0.22

Note. — Column (4) indicates whether an object passes the criteria of n_{K-6}; Column (5) indicates whether an object passes the criteria of n_{13-31}; Column (6) indicates whether an object passes the criteria of EW10; Column (7): subtype of TDs based on the values of *IDEF* in column (8). See Section 4.1.1 for a detailed explanation of *IDEF* and the subtype separation points of *IDEF*.; Column (8): *IDEF* is the inner disk excess fraction.

[a]OriA-44 and OriA-176 do not pass n_{K-6}, n_{13-31}, and EW10, but their SEDs resemble a TD's SED.

[b]we did not calculate its n_{K-6} because its IRS spectrum is not complete, but its SED resemble a TD's SED.

[c]OriA-8 and OriA-172 are selected as CTD, but $IDEF > 0.25$. The spectral type of the objects is M3 or later. When measuring IDEF using the median spectrum of objects with M3-M5 in Tau, the *IDEF* values are 0.45 and 0.65, respectively.

[d]OriA-23 and OriA-198 are selected as WTD with $IDEF = 0.51$. The spectral type of objects is M0 and K6.5 respectively.

[e1]OriA-149 and OriA-164 have $IDEF<0.5$, but they are selected as PTD because we do not know their spectral types, but the fluxes at wavelength ranges of 2-6 μmare comparable to that of the median spectrum.

[e2]T35 (Sz 27) and 16126-2607 are PTDs, but their *IDEF* are slightly less than 0.5. Their spectral types are M0 and K7, respectively.

[e3]Baud 43 and 16126-2235 are PTDs , but their *IDEF* are less than 0.5. Their spectral types are M3.25 and M3.0, respectively. When measuring *IDEF* using the median spectrum of objects with M3-M5 in Tau, the *IDEF* values are 0.72 and 0.71, respectively.

[f]OriA-5, OriA-301, 04202606, GY 195, LAL 106, and LAL 245 have spectral types of M3 or later. Their *IDEF* estimated with K5-M2 median spectrum are higher than 0.5 and they are classified as PTDs. The *IDEF* estimated with M3-M5 median spectrum are much higher than the *IDEF* listed in this table: 0.94, 1.07, 0.87, 1.0, 1.5, and 1.14, respectively.

4.3 Radial Properties of Transitional Disks: R_{wall}

One of the most important properties of a TD is how large the gap or hole is; that is, the radius at which the inner wall of the optically thick outer disk lies. Bearing in mind the limitations of inference of structure from the SED, we derive the radius, R_{wall}, from the shape of the spectrum at the transition from small to large infrared excess within the IRS spectrum. Figure 4.7 is a diagram of the assumed structure of a transitional disk, which we adopt in the simple model described below. We model the inner edge of the outer disk as an optically thick insulating wall, with dust temperature T. As illustrated in Figure 4.8, we first subtract a power-law fit to the IRS spectrum in the 5–8 μm region to remove the flux from the photosphere and/or an excess from the inner disk. To the residuals, we fit a model with two components tightly constrained at 13–16 μm and 30–33 μm. One component is emission from optically-thin astronomical-silicate dust (Draine & Lee, 1984) with 0.1 μm radius, to represent the inner disk and the bulk of the optically thin atmosphere of the outer disk. The other component is a single-temperature (T) blackbody that represents the insulated inner edge of the optically thick outer disk. As we described in Kim et al. (2009), we do not aim to fit the details of the spectrum perfectly, but merely to separate the optically-thick continuum — for which the SED shape is the signature of the wall — from the silicate emission features centered at 10 and 20 μm. With the temperature T, we calculate R_{wall} using

radiative equilibrium at the inner wall:

$$R_{wall} = \sqrt{\frac{L_\star(1-A_\star)}{4\pi\sigma T^4 \epsilon_{IR}}} \left(\equiv \sqrt{\frac{L_\star}{4\pi\sigma T^4}} \right), \tag{4.2}$$

where $A_\star$ is the effective albedo at stellar wavelengths and ϵ_{IR} is the effective emissivity at mid-IR wavelengths. We adopt $(1 - A_\star)/\epsilon_{IR} = 1$: a perfectly black wall.

We compared the resulting R_{wall} of several TDs in Tau (CoKu Tau/4; DM Tau; GM Aur; LkCa 15; UX TauA), Cha I (CR Cha; SZ Cha; T11; T25; T35; T56), and Oph (Rox 44, 16126–2235AB) with the same quantity determined from detailed self-consistent models (Espaillat et al., 2010, 2011). We found the derived R_{wall} from Equation 4.2 are within about 33% of those obtained from detailed models. We also compared our R_{wall} estimates to the cavity radius (R_{cav}) derived from the Submillimeter Array (SMA) observation for DM Tau, GM Aur, LkCa 15, UX Tau A, and ROX 44 (Andrews et al., 2011), and these results lie within 34% of each other. Comparison of R_{wall} from the detailed model and the R_{cav} observed by SMA also gives a similar range of difference, about 34%. Therefore, we adopt 33% as the uncertainty of R_{wall} estimated from Equation 4.2. The R_{wall} results are listed in Table 4.2.

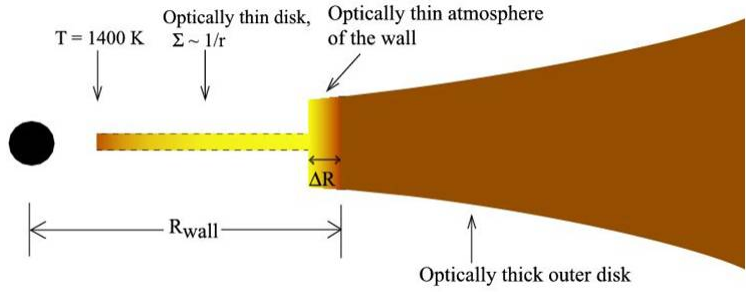


Figure 4.7 Schematic for the transitional disk structure used in the simple models.

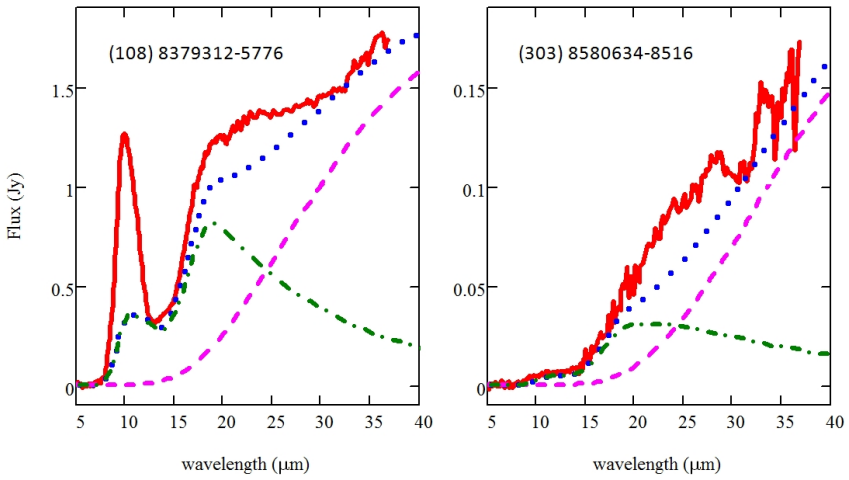


Figure 4.8 Example of fits using the simple model to estimate R_{wall} of transitional disks in Orion A and other star-forming regions included in this work. The thick solid line: a residuum of IRS spectra after subtracting a power-law fitted to 5-8 μm of IRS spectra, representing emission from the photosphere or a part of the inner disk. The dash-dotted line: astronomical silicate model to account for some contribution of emission from small dust grains in the atmosphere of wall and disk upper layers. The dashed line: a single blackbody profile with the wall temperature T. The dotted line: the continuum fit as the combination of the dash-dotted line and the dashed line.

Table 4.2. Stellar and Disk Properties

Num	IRS name	T_{eff} (K)	$L_\star$ ($L_\odot$)	$M_\star$ ($M_\odot$)	R_{wall} (AU)	TD type	$\dot{M}$ ($M_\odot/yr$)	$err_{\dot{M}}$ ($M_\odot/yr$)	L_X (erg/s)	err_{L_X} (erg/s)	region
1	8336884-5290	3850	0.64	0.55	13.7	WTD	5.9E-10	1.1E-10	···		ONC
5	8343944-5609	3145	0.54	0.22	3	PTD	< 1.0E-08		···		ONC
8	8346141-5010	3420	0.17	0.31	6.38	CTD	···		···		ONC
11	8347711-5533	4060	1.8	0.7	13.29	CTD	< 4.5E-10		3.4E+29	2.0E+29	ONC
13	8350150-5595	3420	0.45	0.31	20.03	CTD	3.4E-10	1.4E-10	1.3E+30	8.5E+29	ONC
16	8353051-5229	5080	3.65	1.88	52.56	CTD	2.8E-09	1.1E-09	···		ONC
18	8355083-4835	3850	0.18	0.58	3.04	PTD	···		···		ONC
19	8355371-5480	4060	0.5	0.77	6.58	CTD	1.7E-09	4.2E-10	2.1E+30	9.6E+29	ONC
23	8357031-5072	3850	1.32	0.54	21.47	WTD	< 7.6E-10		···		ONC
24	8358147-5505	5080	5.98	2.23	26.72	PTD	7.3E-08	2.4E-08	2.1E+30	5.1E+29	ONC
25	8358862-4842	3420	0.14	0.3	4.87	WTD	< 2.9E-10		···		ONC
26	8359203-5026	3145	0.17	0.21	6.64	CTD	9.2E-10	1.9E-10	···		ONC
29	8361167-5475	3850	0.41	0.56	10.32	CTD	1.0E-09	4.7E-11	1.2E+30	4.4E+29	ONC
34	8365722-4816	3720	0.25	0.47	7.59	CTD	< 8.9E-11		2.0E+29	2.5E+29	ONC
38	8367284-5798	3850	1.46	0.53	17.97	CTD	2.3E-09	6.6E-10	4.0E+30	7.3E+29	ONC
39	8368137-4860	3420	0.26	0.31	8.74	CTD	5.8E-10	5.6E-10	···		ONC
42	8369106-5686	3370	0.49	0.3	10.83	WTD	1.7E-09	7.4E-10	4.7E+29	3.0E+29	ONC
44	8369980-5081	3720	0.6	0.46	5.86	PTD	4.5E-09	1.8E-09	1.5E+30	2.5E+29	ONC
47	8371984-5465	3955	4.37	0.63	50.6	CTD	< 7.4E-10		2.5E+30	4.1E+29	ONC
53	8373930-6325	3420	0.17	0.31	7.07	CTD	···		···		L1641
59	8374388-6000	3525	0.66	0.36	13.36	CTD	5.4E-09	5.7E-10	1.8E+30	2.4E+29	L1641
66	8375158-5162	3240	0.1	0.23	2.9	WTD	< 7.9E-11		···		ONC
88	8377167-5247	6030	75.64	3.74	152.3	CTD	···		1.0E+31	6.5E+29	ONC
108	8379312-5776	5250	22.75	3.2	85.34	PTD	2.9E-08	1.7E-08	2.5E+30	8.1E+29	ONC
149	8385365-5106	3850	7.4	0.6	61.15	PTD	···		···		ONC
154	8386523-5715	3420	0.86	0.32	14.07	WTD	3.7E-09	2.4E-09	1.1E+30	2.6E+29	ONC

Table 4.2 (cont'd)

Num	IRS name	T_{eff} (K)	$L_\star$ ($L_\odot$)	$M_\star$ ($M_\odot$)	R_{wall} (AU)	TD type	$\dot{M}$ ($M_\odot/yr$)	$err_{\dot{M}}$ ($M_\odot/yr$)	L_X (erg/s)	err_{L_X} (erg/s)	region
164	8387753-4993	3850	5.02	0.56	18.47	PTD	···		3.3E+29	1.4E+29	ONC
169	8389033-4773	3785	0.81	0.5	7.87	CTD	2.9E-09	1.8E-09	3.3E+29	2.0E+29	ONC
172	8389673-4794	3470	0.62	0.34	7.21	CTD	< 9.3E-10		3.7E+30	3.0E+29	ONC
174	8390073-5082	3850	2.11	0.53	11.47	CTD	···		···		ONC
176	8390285-5070	3650	0.71	0.42	8.91	WTD	3.3E-09	4.0E-10	7.9E+29	1.2E+29	ONC
177	8390554-6390	3525	0.3	0.36	9.8	CTD	< 1.3E-09		1.3E+30	1.4E+29	L1641
184	8394216-5181	3955	1.12	0.62	16.71	WTD	7.5E-09	8.0E-10	6.8E+29	1.9E+29	ONC
185	8394454-5823	4205	1.3	0.87	11.66	WTD	5.9E-09	4.3E-09	1.3E+30	1.6E+29	ONC
188	8396035-5861	3850	1.19	0.54	9.26	WTD	···		2.3E+30	1.1E+29	ONC
198	8399269-6612	4132	1.33	0.78	19.37	WTD	4.8E-09	1.6E-09	···		L1641
203	8406280-6293	4350	1.46	1.07	25	PTD	···		3.3E+30	1.2E+29	L1641
204	8406609-6247	3525	0.23	0.36	5.24	CTD	1.5E-09	8.5E-10	8.3E+28	4.2E+28	L1641
211	8411618-6426	3420	0.23	0.31	7.28	CTD	3.6E-10	3.5E-10	2.0E+29	5.1E+28	L1641
218	8416389-6503	3305	0.14	0.26	3.32	CTD	< 4.9E-10		···		L1641
219	8416834-6225	3785	0.5	0.5	11.39	CTD	< 1.8E-10		8.6E+29	6.6E+28	L1641
221	8416978-6185	3955	1.12	0.62	17.77	PTD	···		···		L1641
223	8424570-6484	3470	0.34	0.34	9.59	CTD	5.3E-10	1.4E-10	···		L1641
227	8440418-7404	3850	0.29	0.57	6.76	PTD	2.5E-10	1.4E-10	···		L1641
229	8444779-6608	3850	0.61	0.55	13.68	CTD	1.8E-09	1.4E-09	···		L1641
230	8445558-6860	3850	0.46	0.56	8.67	CTD	2.7E-10	1.2E-10	2.6E+29	8.8E+28	L1641
237	8457266-7161	3650	1.26	0.41	18.09	CTD	< 2.6E-09		···		L1641
239	8464666-7838	3720	1.81	0.45	25.7	WTD	1.0E-08	4.8E-09	···		L1641
257	8502614-7795	3470	0.23	0.33	4.07	CTD	1.7E-09	1.1E-09	2.0E+29	2.0E+29	L1641
260	8508501-7431	3580	0.36	0.38	9.1	CTD	2.5E-09	1.4E-09	1.5E+29	1.4E+29	L1641
270	8519428-8120	4060	9.78	0.84	59.78	CTD	···		4.0E+30	4.8E+29	L1641
271	8520557-7775	3580	0.47	0.38	18.86	CTD	< 3.4E-10		1.5E+29	8.6E+28	L1641

Table 4.2 (cont'd)

Num	IRS name	T_{eff} (K)	$L_\star$ ($L_\odot$)	$M_\star$ ($M_\odot$)	R_{wall} (AU)	TD type	$\dot{M}$ ($M_\odot/yr$)	$err_{\dot{M}}$ ($M_\odot/yr$)	L_X (erg/s)	err_{L_X} (erg/s)	region
275	8535781-7830	3240	0.85	0.25	9.59	WTD	< 3.6E-09		2.5E+30	1.7E+29	L1641
279	8538911-7999	3650	1.06	0.41	15.93	WTD	< 7.8E-10		···		L1641
283	8547523-7831	3580	0.58	0.38	13.06	CTD	8.7E-10	7.6E-10	6.5E+30	2.1E+29	L1641
290	8562845-8151	3525	0.4	0.36	4.07	PTD	3.9E-09	1.9E-09	···		L1641
291	8564835-8250	3525	0.43	0.36	8.24	CTD	1.1E-09	7.1E-10	1.8E+29	5.7E+28	L1641
294	8567670-8803	3525	2	0.35	23.26	CTD	< 4.6E-09		4.5E+29	3.6E+29	L1641
297	8570949-8577	3850	1.75	0.53	22.68	PTD	···		···		L1641
301	8576836-8303	3420	0.38	0.31	14.19	PTD	7.3E-10	2.4E-10	3.5E+29	9.9E+28	L1641
302	8579480-8565	3850	0.2	0.58	6.65	WTD	6.1E-10	3.5E-10	···		L1641
303	8580634-8516	3470	0.43	0.33	10.35	CTD	6.9E-09	2.5E-09	1.7E+29	8.1E+28	L1641
.	4202606	3420	0.19	0.31	12.3	PTD	···		···		Tau
.	04125+2902	3685	0.36	0.44375	17	CTD	···		···		Tau
.	CoKu Tau/4	3650	0.6	0.44	12.74	CTD	< 1.0E-10[a]		···		Tau
.	DM Tau	3720	0.2	0.44	5.26	CTD	3.1E-09[b]	1.1E-09	···		Tau
.	GK Tau	4060	1.37	0.7075	9.7	PTD	6.0E-09[c]	2.0E-09	8.8E+29	2.0E+28	Tau
.	GM Aur	4350	1	1.25	25.18	WTD	4.7E-09[b]	1.6E-09	···		Tau
.	HK Tau	3785	0.65	0.49625	16.1	PTD	2.2E-08[c]	7.5E-09	6.1E+28	2.1E+28	Tau
.	IP Tau	3850	0.69	0.545	12.6	PTD	4.2E-10[b]	1.4E-10	···		Tau
.	LkCa 15	4350	1	1.08	34.81	PTD	3.3E-09[b]	1.1E-09	···		Tau
.	MHO 3	4060	0.87	0.72625	6.9	PTD	···		1.5E+29	1.4E+28	Tau
.	RY Tau	5945	19.75	2.3625	27.6	PTD	9.1E-08[b]	3.1E-08	3.0E+30	7.3E+28	Tau
.	UX Tau A	4900	2.2	1.63	39.56	PTD	1.1E-08[b]	3.8E-09	···		Tau
.	V410 Xray 6	3145	0.46	0.22	7.9	CTD	···		7.8E+28	1.6E+28	Tau
.	2MJ1124118	3240	0.06	0.2025	2.9	CTD	···		···		ChaI
.	Baud 43	3445	0.25	0.3225	6.5	PTD	···		5.6E+28	3.3E+28	ChaI
T54	CHX 22	5520	4.1	1.66	37.1	CTD	···		···		ChaI

Table 4.2 (cont'd)

Num	IRS name	T_{eff} (K)	$L_\star$ ($L_\odot$)	$M_\star$ ($M_\odot$)	R_{wall} (AU)	TD type	$\dot{M}$ ($M_\odot/yr$)	$err_{\dot{M}}$ ($M_\odot/yr$)	L_X (erg/s)	err_{L_X} (erg/s)	region
.	CHXR 22E	3420	0.2	0.31	7.4	CTD	···		2.6E+29	3.0E+28	ChaI
.	CR Cha	4900	2.54	1.7025	16.9	PTD	8.8E-09[b]	3.0E-09	1.5E+30	4.2E+28	ChaI
T11	CS Cha	4205	1	0.87	41.1	CTD	1.2E-08[b]	4.1E-09	2.8E+30	4.6E+28	ChaI
.	ISO 91	3470	0.3	0.3325	2.2	CTD	···		2.8E+28	1.0E+28	ChaI
T25	Sz 18	3470	0.2	0.33	8.1	CTD	9.7E-10[b]	3.3E-10	···		ChaI
T35	Sz 27	3850	0.4	0.56	15.3	PTD	1.2E-09[b]	4.1E-10	5.8E+29	5.8E+29	ChaI
T56	Sz 45	3785	0.3	0.52	18.3	WTD	1.5E-09[b]	5.1E-10	···		ChaI
T6	SZ Cha	5250	2.4	1.55	29.5	PTD	2.4E-09[b]	8.2E-10	1.2E+30	1.3E+29	ChaI
.	16126-2235	3470	0.8	0.34	12.2	PTD	···		1.9E+30	1.1E+28	Oph
.	16201-2410	6030	4.9	1.41	29.2	PTD	···		···		Oph
.	16220-2452	3470	0.28	0.33325	8.7	PTD	···		···		Oph
.	16225-2607	4060	1.37	0.7075	14.2	PTD	···		···		Oph
.	16289-2457	5770	4.61	1.5275	24.7	PTD	···		···		Oph
.	DOAR 28	4350	1	1.08	15	CTD	···		···		Oph
.	GY 195	3470	0.38	0.33575	6.6	PTD	1.0E-09[d]	3.4E-10	···		Oph
.	IRS 3	3580	0.39	0.38	13.4	PTD	1.2E-08[d]	4.1E-09	5.0E+28	1.2E+28	Oph
.	Rox 44	4900	3	1.77	26.7	PTD	9.0E-09[b]	3.1E-09	6.1E+29	3.2E+28	Oph
.	SR 9	4350	2.03	1.0575	14.6	PTD	1.2E-08[d]	4.1E-09	···		Oph
spID 50	LAL 50	3309	1.63	0.26625	45.4	PTD	···		1.2E+29	2.6E+28	N1333
spID 52	LAL 52	4060	1.01	0.7125	18	PTD	···		2.2E+30	1.0E+29	N1333
spID 57	LAL 57	4060	0.92	0.72125	23.2	PTD	···		3.7E+28	1.6E+28	N1333
spID 73	LAL 73	4900	8.38	2.4525	32.2	PTD	···		8.3E+30	1.5E+29	N1333
spID 101	LAL 101	3370	0.07	0.26	8.4	PTD	···		···		N1333
spID 110	LAL 110	3525	0.02	0.30625	3.7	PTD	···		···		N1333
spID 116	LAL 116	4205	1.17	0.8725	5	PTD	···		···		N1333
spID 136	LAL 136	3955	0.83	0.625	12.3	CTD	···		1.7E+30	1.3E+29	N1333

Table 4.2 (cont'd)

Num	IRS name	T_{eff} (K)	$L_\star$ ($L_\odot$)	$M_\star$ ($M_\odot$)	R_{wall} (AU)	TD type	$\dot{M}$ ($M_\odot/yr$)	$err\dot{M}$ ($M_\odot/yr$)	L_X (erg/s)	$err L_X$ (erg/s)	region
spID 137	LAL 137	3955	0.23	0.6575	6.6	CTD	...		1.3E+29	2.5E+28	N1333

Note. — The calculation of R_{wall} is explained in Section 4.3, and the values listed in the column have an uncertainty of about 33 %. $\dot{M}$ of ONC and L1641 is from this work. $\dot{M}$ for other regions are from the literatures. L_X are all from XMM-Newton Serendipitous Source Catalog (Watson et al., 2009b). The energy band is the total energy band of XMM-Newton (0.2-12 keV).

[a] Najita et al. (2007)

[b] Espaillat et al. (2011)

[c] Güdel et al. (2007)

[d] Natta et al. (2006)

4.4 Frequency

Most previous studies of TDs (e.g. Kim et al., 2009; Muzerolle et al., 2010; Merín et al., 2010; Currie & Sicilia-Aguilar, 2011) and protoplanetary disks (Furlan et al., 2009; Luhman et al., 2010; Manoj, 2010) have estimated the fractions of TDs to infer when the transition typically occurs and how long the transition stage persists. We take the fraction of CTDs+WTDs to compare to the Muzerolle's CTDs because the qualitative definition of the classical transitional disks in Muzerolle et al. (2010) is most nearly equivalent to the definition of the combined set of CTDs and WTDs in our sample. We note that the quantitative selection criteria used by Muzerolle et al. (2010) missed some WTDs as discussed in Section 4.2.3

The fraction of TDs in this work is defined as n(TD type)/n(disks) using the number of TDs and number of Class II sources identified from the IRS survey of each region (see, Table 4.3). We exclude samples in Ophiuchus for the frequency and age trend search even though it is listed in Table 4.3 because the selected TDs are from several sub-regions of Ophiuchus with differing estimated ages, and the sample sizes are too small to separate by subregion with high statistical significance.

The TD fraction is plotted as a function of age in Figure 4.9. We note that (1) the fraction of CTDs+WTDs can be high over the broad age ranges (1–10 Myr) and (2) the fraction of TDs varies from region to region at young ages (<3 Myr), with some having a fraction of only a few % while others have fractions of >20% even at age ≤1 Myr.

Also shown in Figure 4.9 are the fractions of TDs of each type from this

work only: CTD (square), WTD (circle), PTD (star), and the total of them (cross). If we consider the fraction of TDs including all CTD, WTD, and PTD, the fractions of all TDs in each region are significantly high even at very young ages of less than 1 Myr: 17±6% for N1333, 25±4% for ONC, and 26±5% for L1641 versus the TD fractions for the 2–3 Myr old associations: 8±2% for Tau and 16±5% for Cha I.

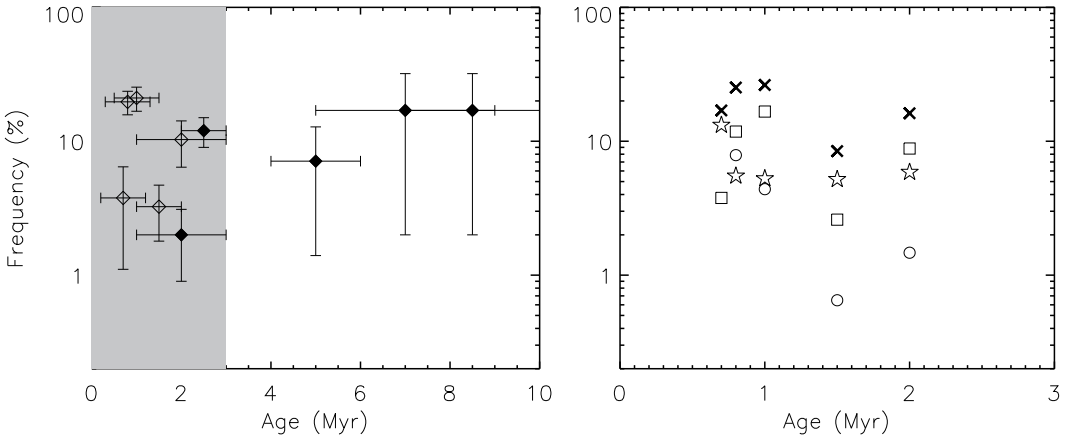


Figure 4.9 The fraction of transitional disks plotted against the estimated median age of the association. The solid diamonds in the left panel are from the fraction of classical transitional disks defined by Muzerolle et al. (2010). The empty diamonds in the left panel are the fraction of CTD plus WTD from this work. The right panel is for the shaded region covering ages of 0–3 Myr in the left panel, and it shows fractions of TD (=CTDs+WTDs+PTDs) types in N1333, ONC, L1641, Tau, and ChaI from younger ages to older ages of star-forming regions. The symbols in the right panel indicate the TD fraction (cross), the CTD fraction (square), the WTD fraction (circle), and the PTD fraction (star).

Table 4.3. number of transitional disks and age trend

region	Age (Myr)	CTD	WTD	PTD	total TD	disks
NGC 1333	< 1	2	0	7	9	53[a]
ONC	< 1	15	10	7	32	127[b]
L1641	1	19	5	6	30	114[b]
Tau	1.5	4	1	8	13	154[c]
ChaI	2	6	1	4	11	68[d]
Oph	0.3-2.1	1	0	9	10	90[e]

Note. — Number of transitional disks and the median age of each star-forming region. The median age of each star-forming region is taken from the literature listed below and references therein. The last column: n(disks) is the number of objects in our sample, which is complete for Class II objects and transitional disks with host stars of type M4 or earlier (see Chapter 2).

[a]We keep 53 objects after taking 4 Class I objects out from the 57 disk dominant objects reported in Arnold et al. (2012).

[b]from this work.

[c]This number comes from IRS survey of Taurus by Furlan et al. (2011).

[d]This number comes from IRS survey of Chamaeleon I by Manoj et al. (2011).

[e]This number is the number of disk dominant objects identified from IRS survey of Ophiuchus by McClure et al. (2010).

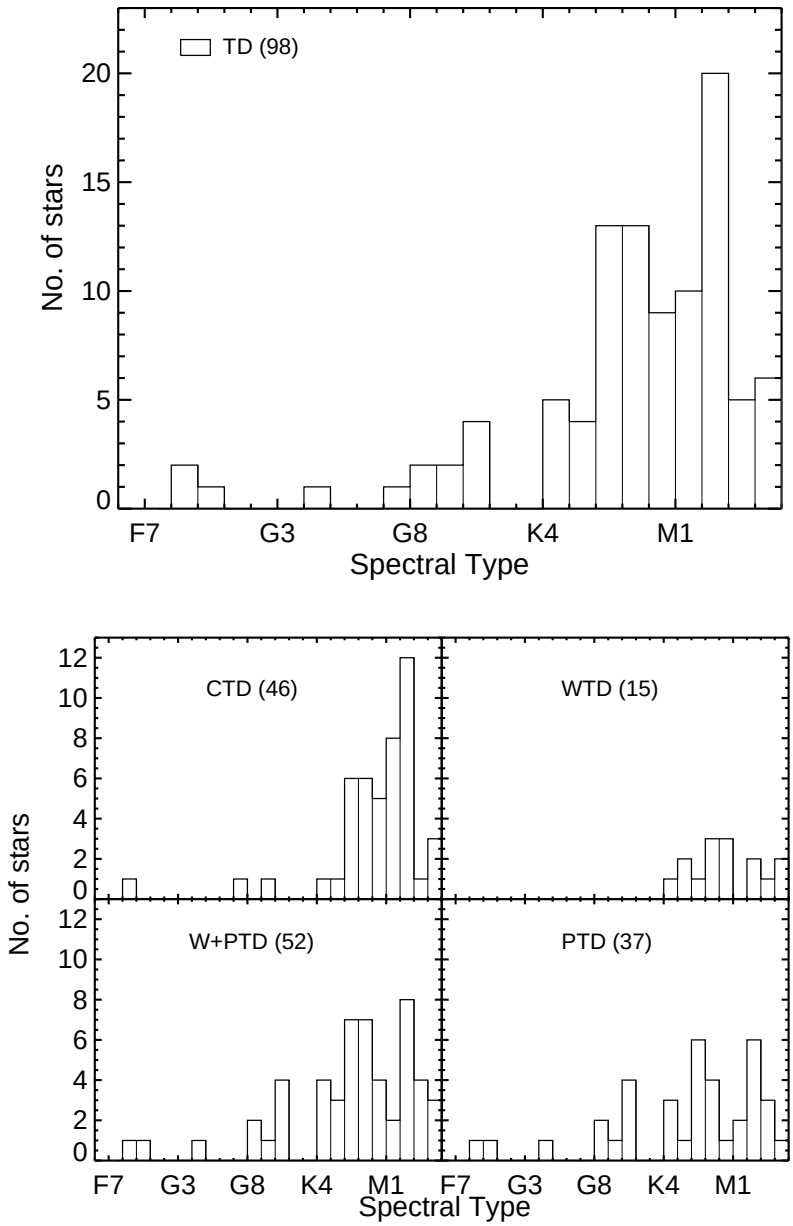


Figure 4.10 spectral type distribution of transitional disks. The upper bigger panel shows the spectral distribution of all TDs with known spectral types. The lower multiple panels show the spectral type distributions divided by TD subtypes. The results from K-S tests: (1) CTD vs. WTD: $D = 0.20$, $p = 0.69$; (2) WTD vs. PTD: $D = 0.32$, $p = 0.17$; (3) CTD vs. PTD: $D = 0.31$, $p = 0.04$; (4) CTD vs. WTD+PTD: $D = 0.24$, $p = 0.10$.

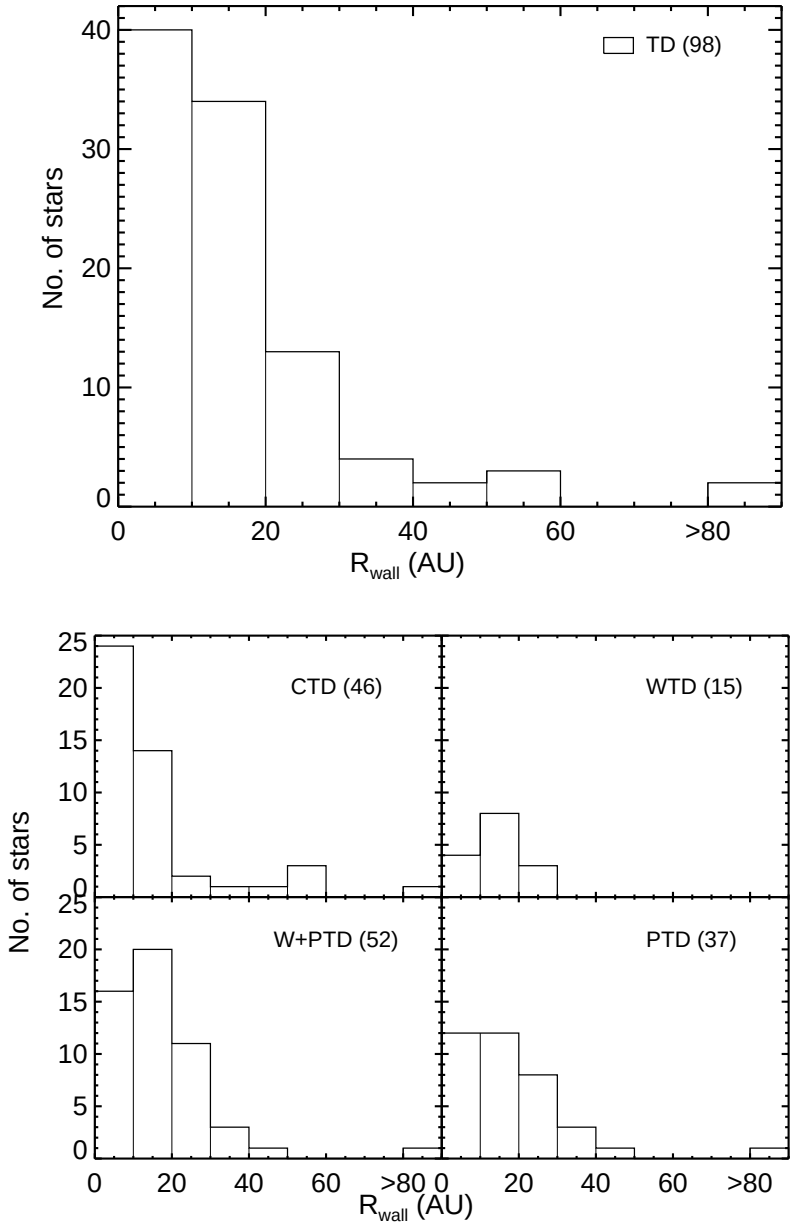


Figure 4.11 R_{wall} distribution of transitional disks. The upper bigger panel shows the R_{wall} distribution of all TDs with known spectral types. The lower multiple panels show the R_{wall} distributions divided by TD subtypes. The results from K-S tests: (1) CTD vs. WTD: $D = 0.32$, $p = 0.15$; (2) WTD vs. PTD: $D = 0.27$, $p = 0.36$; (3) CTD vs. PTD: $D = 0.29$, $p = 0.05$; (4) CTD vs. WTD+PTD: $D = 0.29$, $p = 0.02$.

4.5 Distribution and Trends among Properties

4.5.1 TD Subtypes versus Spectral Type, R_{wall}, and $\dot{M}$

In this section, we examine how the distributions of host-star spectral types, R_{wall}, and $\dot{M}$ compare for TDs with different inner disk structures: CTD, WTD, and PTD types. In this analysis we exclude the TDs for which we do not have reliable host-star spectral types.

In Figure 4.10, we show the spectral-type distribution for all TDs and for each subtype. The median spectral type differs slightly among the TD subtypes: M2 for CTDs; M1 for WTDs; K7 for PTDs; M0 for WTD+PTD; M1 for TDs. The spectral type distributions of CTDs and PTDs differ noticeably, even if we consider the general spectral-type uncertainty of one to two subtypes. However, a K-S test shows that the spectral type difference between CTDs and PTDs is of marginal statistical significance: for CTDs versus PTDs, $D = 0.31$ and $p = 0.04$.

In Figure 4.11, we show the frequency distribution of R_{wall} for each TD subtype. For almost 90% of TDs R_{wall} is less than 30 AU. This pattern is similar whether the inner disk exists or there is an empty inner cavity. However, we see that the median R_{wall} is smaller for CTDs than WTDs and PTDs. Most CTDs have $R_{wall} < 10$ AU (about 52%), whereas 71% of WTDs and PTDs with inner disks have $R_{wall} > 10$ AU. A K-S test that compares the R_{wall} distributions of CTDs and PTDs yields values similar to those for the comparison of the spectral type distributions: $D = 0.29$ and $p = 0.05$, which is

not very significant. The p value decreases to 0.02 when comparing CTDs and WTDs+PTDs. The difference in the R_{wall} distributions of the TD subtypes could also be due to the impossibility of distinguishing PTDs with very small gaps from radially continuous disks based on the IR spectrum alone. Overall, Figure 4.11 shows that the IRS spectra are most sensitive to disk holes with $R_{wall} < 30$ AU.

In Figure 4.12, we plot the $\dot{M}$ distribution for all TDs and broken down by subtype. TDs with central clearings (CTDs) and gapped disks (WTDs and PTDs) differ significantly in $\dot{M}$. Both groups also have $\dot{M}$ substantially smaller than the typical $\dot{M}$ of radially continuous disks. The median $\dot{M}$ of the gapped disks is $10^{-8.41} M_{\odot}/yr$ and that of CTDs is $10^{-8.98}$ $M_{\odot}/yr$. This visible difference is confirmed by statistical analysis with the K-S tests. When we include the upper limits, the K-S test results $D = 0.51$ and $p = 0.0002$. Even when we do not include the upper limits, the statistically significant difference between the two groups is still valid with $D = 0.55$ and $p = 0.0005$. Thus we confirm that the $\dot{M}$s of CTDs are smaller on average than those of WTDs and PTDs[4].

For fair comparison of the $\dot{M}$ of radially continuous disks and TDs, we need to be sure that these two groups have similar ages and stellar masses because $\dot{M}$ decreases with age (Hartmann et al., 1998) and increases with $M_{\odot}$ (Muzerolle et al., 2003; Calvet et al., 2004). Because systematic differences of stellar masses and ages can arise from a choice of different evolutionary tracks (e.g. Simon et al., 2000; Najita et al., 2007), the best would be to have

[4]The median $\dot{M}$ of the gapped disks is $10^{-8.77} M_{\odot}/yr$ and that of CTDs is $10^{-8.33}$ $M_{\odot}/yr$ when the upper limits are not included.

$\dot{M}$ estimated with the same method and assumptions used for $\dot{M}$ estimation of TDs. However, there is currently no such $\dot{M}$ survey of low-mass T Tauri stars through the star-forming regions of our TDs. A comparison between $\dot{M}$ of Orion A TDs and other radially continuous Class II disks in Orion A measured in an homogeneous method will be discussed Chapter 5.

Therefore, for the next best comparison, we use the $\dot{M}$ measurements of T Tauri stars in Taurus by Gullbring et al. (1998) for the following reasons. Gullbring et al. (1998) adopted the evolutionary tracks of D'Antona & Mazzitelli (1997), which tends to result in younger stellar ages and lower stellar masses. Simon et al. (2000) found both the Baraffe et al. (1998) model and Siess et al. (2000) model agree with dynamical masses in the 0.7-1 $M_{\odot}$ range, while D'Antona & Mazzitelli (1997) do not agree as precisely. Even though White & Ghez (2001) measured $\dot{M}$ of T Tauri stars in Taurus as adopting an evolutionary track combined Baraffe et al. (1998) and Palla & Stahler (1999), the samples are binary systems and $\dot{M}$ of binary system is not comparable to $\dot{M}$ of TDs. Hence, we adopt the median $\dot{M}$ from Gullbring et al. (1998) as the median $\dot{M}$ of radially-continuous disks in Taurus, $\dot{M} = 10^{-7.8} M_{\odot}/yr$.[5] While bearing in mind the possible uncertainties ($\sim$30%) of stellar masses between two different evolutionary tracks, we confirm that the ages and stellar masses of the Gullbring et al. (1998) sample are similar to those of TDs studied in this work. Thus our results confirm that TDs in general have substantially smaller $\dot{M}$ than radially-continuous disks, in accord with the findings by Najita et al.

[5]We excluded three TDs, GK Tau, GM Aur, and IP Tau, in the sample of Gullbring et al. (1998) to measure the median $\dot{M}$ of radially-continuous disks in Taurus. If we include those three TDs, the median $\dot{M}$ decreases to $\dot{M} = 10^{8} M_{\odot}/yr$.

(2007), Kim et al. (2009), and Espaillat et al. (2012).

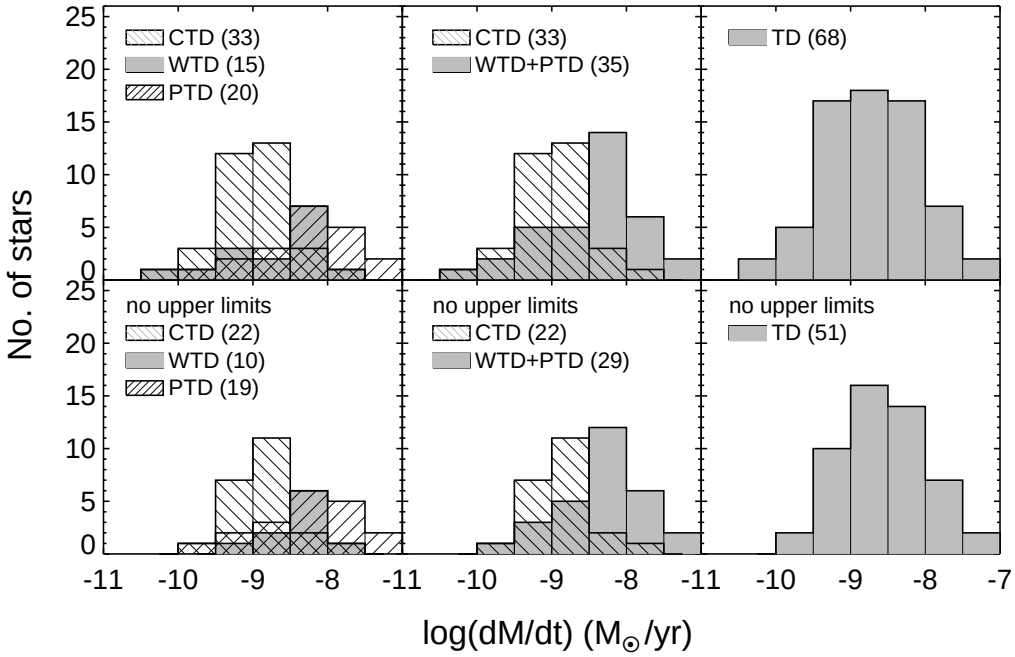


Figure 4.12 $\dot{M}$ distributions. The upper panels include upper limits of $\dot{M}$; the lower panels do not include upper limits of $\dot{M}$. The left panels show $\dot{M}$ distributions separated by three different TD types; the middle panels compare the $\dot{M}$ distribution of disks with central clearings (CTD) and to those with gaps (WTD and PTD); the right panels result from adding all types of TDs. The results of K-S tests of $\dot{M}$ distributions between CTD and WTD+PTD in the middle panels: $D = 0.51$, $p = 0.0002$ (upper middle); $D = 0.55$, $p = 0.0005$ (lower middle).

4.5.2 Trends among TD Properties

Understanding the correlations between disk and stellar properties of TDs is an essential and important key to understand how protoplanetary disks evolve from radially continuous optically thick disks to a final planetary system. We have gathered the largest sample of TDs which are identified by homogeneous criteria. From this large sample, we are able to find not only trends of TDs in general but also detailed trends of the three different types of TDs.

Except for $\dot{M}$, we estimate the stellar/disk properties of TDs in Tau, Cha I, Oph and N1333 in the same ways as for Orion A TDs. The $\dot{M}$ of TDs of other star-forming regions are from literature or personal communication. Adopting $\dot{M}$ measured by different techniques from that for the TDs of OriA should not affect significantly these trends, based on the demonstration of the tight correlation between the luminosities of IR hydrogen recombination lines and L_{acc} measured from the blue excess spectrometry and/or U-band photometry by Muzerolle et al. (1998). Therefore, we expect that any discrepancies in luminosity between the two (IR and UV) data sets on average will be small (Muzerolle et al., 1998). These stellar/disk properties and other properties obtained from the literature are also listed in Table 4.2.

Among trends from many possible combinations of properties, we present the trends of interesting pairs of properties showing somewhat different behaviors from non-transitional disks in Figure 4.13–4.18. The correlation parameters are calculated by using *linmix_err.pro* which was developed for the Bayesian approach to linear regression with errors in both X and Y, by Kelly (2007), and the trends line in each plot can be read in the manner

of $\log_{10}(Y) = (\alpha \pm e_\alpha) + (\beta \pm e_\beta)\log_{10}(X)$. We indicate the correlation parameters (*corr*) and probabilities (P) of pairs of properties in Table 4.4 for TDs without separation by subtype and in Table 4.5 for two subgroups of TDs separated by their radial disk structures, i.e., CTDs and WTPs+PTDs. In general, a 5% or lower P value is considered to be statistically significant. Sometimes $P \leq 2\%$ is considered as a conservative threshold of statistical significance. Therefore, we interpret a correlation to be a statistically significant with $P \leq 2\%$ and to be a marginally significant if P is 2%–5%.

Trends of TDs

Our search for trends related to $\dot{M}$ utilized weighted linear regression to account properly for upper limits of $\dot{M}$ in our samples. The resulting trend for $\dot{M}$–$M_\star$ in Figure 4.13(a) is $\dot{M} \propto {M_\star}^{1.8\pm0.3}$. To compare this to the $\dot{M}$–$M_\star$ relations from the previous studies ($\dot{M} \propto {M_\star}^{1.95}$, Calvet et al. (2004); $\dot{M} \propto {M_\star}^{2.0}$, Muzerolle et al. (2003); $\dot{M} \propto {M_\star}^{2.1}$, Muzerolle et al. (2005)), we include in Figure 4.13(a) a plot of the result, $\log \dot{M} \approx 2 \log M_\star - 7.5$ (Muzerolle et al., 2003; Telleschi et al., 2007). The slope of the $\dot{M}$–$M_\star$ relation of TD host stars is roughly consistent with previous studies among T Tauri stars, but the trend line for $\dot{M}$ is shifted downward by factor of about 10 with respect to the thick dashed line representing T Tauri stars in Taurus, consistent with the results discussed in Section 4.5.1.

In Figure 4.13(b), we plot L_X as a function of $M_\star$. Compared to the results in Taurus, $\log L_X = 1.69 \log M_\star + 30.33$ (Telleschi et al., 2007), the regression of our TD data is $\log L_X = 1.1 \log M_\star + 30.1$: a slightly smaller slope than

that of T Tauri stars with radially continuous disks.

Figure 4.13(c) shows $\dot{M}$ as a function of L_X compared to the Taurus results derived from Taurus's $\dot{M}$–$M_\star$ and L_X–$M_\star$, $\dot{M}$–L_X relation for T Tauri stars $\log \dot{M} = 1.2 \log L_X - 43$. The $\dot{M}$–L_X trend line for our TD sample, $\log \dot{M} = 0.2 \log L_X - 14.2$. This shows that TDs' $\dot{M}$ is not related to L_X, again unlike CTTSs with radially continuous disks.

The most interesting relations are the correlation of R_{wall} to stellar properties. In Figure 4.14(a), we find a very strong correlation between $M_\star$ and R_{wall}. For both cases of $\dot{M}$ and L_X, we also see the increasing trends of $\dot{M}$–R_{wall} in Figure 4.14(b) and L_X–R_{wall} in Figure 4.14(c). However, we should recall that there is a tight correlation of $M_\star$–R_{wall} and a statistically significant correlation of $\dot{M}$–$M_\star$. Therefore, the correlation showing in the plots of $\dot{M}$–R_{wall} may merely reflect the combination of correlations between $M_\star$–R_{wall} and $\dot{M}$–$M_\star$. To test this hypothesis, we looked for a trend between $\dot{M}$ and R_{wall} in smaller mass bins (e.g., 0.2-0.4 $M_\odot$, 0.4-0.7 $M_\odot$, and 0.7-2.3 $M_\odot$) and did not find significant trends. Similarly, the increasing trend of L_X–R_{wall} may be the result of combination of the correlations between L_X–$M_\star$ and $M_\star$–R_{wall}.

For further examination of the difference between $\dot{M}$–R_{wall} relationship of TDs and that of CTTSs under the strong dependence on $M_\star$, we derived an expected $\dot{M}(M_\star)$–R_{wall} of CTTSs by combining the $\dot{M}$–$M_\star$ of CTTSs ($\log \dot{M} = 2 \log M_\star - 7.5$) and a strong $M_\star$-R_{wall} correlation of TDs ($\log M_\star = 0.7 \log R_{wall} - 1.0$): $\log \dot{M}(M_\star) = 1.4 \log R_{wall} - 9.5$ (Figure 4.14(b)). The expected $L_X(M_\star)$-R_{wall} of CTTSs considering the $M_\star$ dependence is also derived by combining L_X–$M_\star$ of CTTSs and $M_\star$–R_{wall}: $\log L_X(M_\star) = 1.2 \log R_{wall} -$

28.6 (Figure 4.14(c)). We find that the trends of TDs in $\dot{M}$–R_{wall} and L_X–R_{wall} generally agree with the derived trends of CTTSs.

Several other interesting correlations for TDs are listed in Table 4.4. The very strong correlation of $L_\star \sim {M_\star}^{1.6}$ which is similar to that ($L_\star \sim {M_\star}^{1.5}$) found from T Tauri stars in Tau by Telleschi et al. (2007) supports that the basic stellar properties, $M_\star$ and $L_\star$, of TDs are not very different from the stars hosting radially continuous flared disks and/or homologously evolved disks.

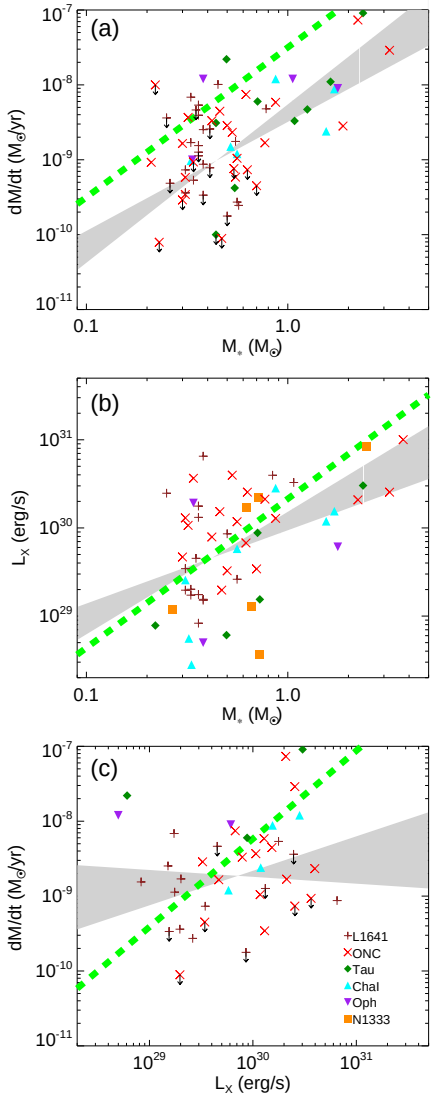


Figure 4.13 Trends among $M_\star$, $\dot{M}$ and L_X. In each plot, different symbols indicate TDs in different star-forming regions (plus: L1641; cross: ONC; solid diamond: Tau; solid triangle: ChaI; solid inverse-triangle: Oph; solid square: N1333). In each plot, the shaded area indicates the 1σ uncertainty of the linear regression (of the logarithms). If a shaded area is narrow with high slope (e.g., $\dot{M}$-$M_\star$), one can tell two properties in a panel is tightly correlated. If a shaded area is broad with very low slope (e.g., $\dot{M}$-L_X), two properties in a panel is not correlated. The thick dashed line indicates a correlation expected/observed among T Tau disks in Tau: $\dot{M} \propto {M_\star}^2$ from Muzerolle et al. (2003) in the upper panel; $L_X \propto {M_\star}^{1.69}$ from Telleschi et al. (2007) in the middle panel; $\dot{M} \propto {L_X}^{1.2}$ in the lower panel from above two relations. The down arrows indicate $\dot{M}$ upper limits.

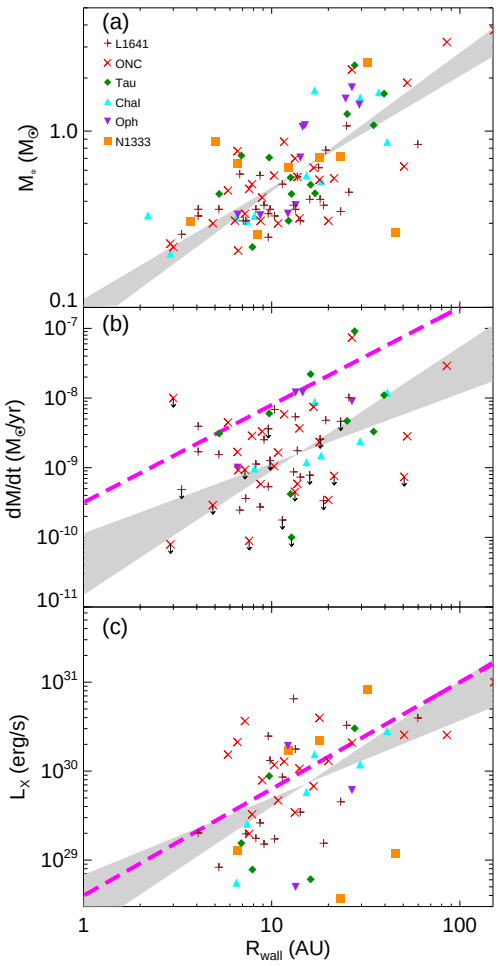


Figure 4.14 Trends related to R_{wall} with other stellar properties. Lines, shadow, and symbols have same meaning in Figure 4.13. The thick long-dashed line indicates an expected trend derived from the relationship of a property in y-axis with $M_\star$ shown in Figure 4.13 and the strong $M_\star$-R_{wall} correlation shown in the panel (a): $\dot{M} \propto {R_{wall}}^{1.4}$ in the panel (b); $L_X \propto {R_{wall}}^{1.2}$ the panel (c).

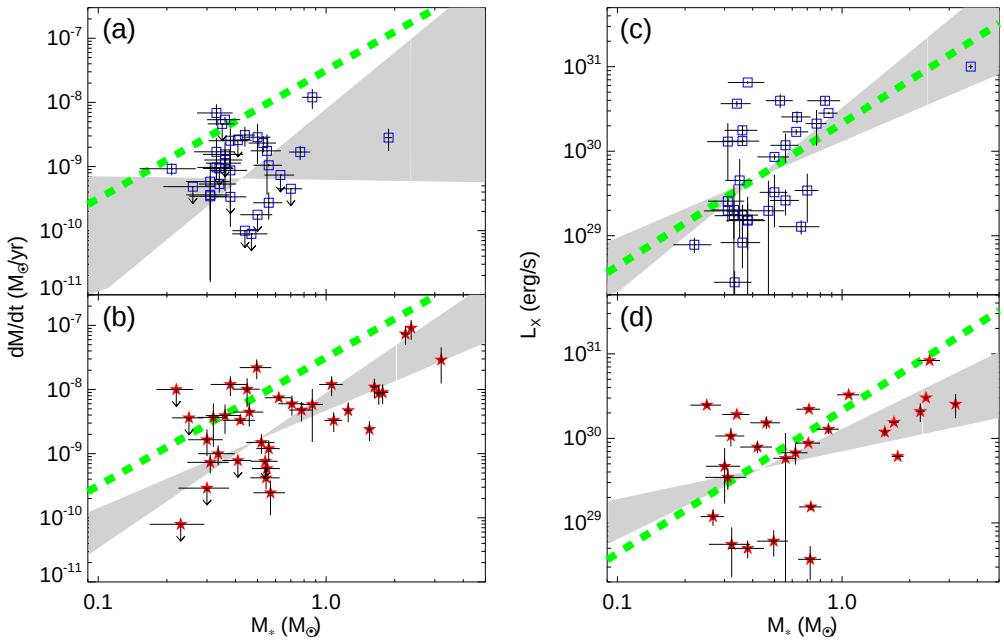


Figure 4.15 Detailed Trends of $\dot{M}$–$M_\star$ (the left panels) and L_X–$M_\star$ (the right panels) separated by subtypes of TDs. The upper panels (a and c) show the correlation of CTDs (open square). The lower panels (b and d) show the correlation of WTDs+PTDs (solid star). The lines and shade are defined in the caption of Figure 4.13.

Trends of $\dot{M}$ and L_X for Transitional Disk Subtypes

In this section we explore characteristics of $\dot{M}$ and L_X, which are sensitive to the different inner disk structures and to the different disk evolution mechanisms, by searching for detailed trends of sub-samples grouped by different TD types. The correlation parameters of the detailed trend analysis for the case of inner clearings (CTDs) and the case of radial gaps (WTDs+PTDs) are listed in Table 4.5.

It is clear that the trend between $\dot{M}$ and $M_\star$ of CTDs is different from that of WTDs+PTDs from the left panels ((a) and (b)) of Figure 4.15. When the inner disk is essentially empty as for the CTDs, no correlation exists between $\dot{M}$ and $M_\star$. However, for the case of WTDs+PTDs, $\dot{M}$ and $M_\star$ are significantly correlated each other, and the relation ($\dot{M} \propto {M_\star}^{2.0\pm0.5}$) is very close to that of CTTS ($\dot{M} \propto {M_\star}^2$). Therefore, the increasing tendency shown in Figure 4.13 probably leads to a strong effect from the significant correlation of $\dot{M}$ and $M_\star$ for WTDs+PTDs which still have an inner disk in their disk. In contrast to $\dot{M}$, we find no significant difference between the two sub-groups of TDs for the L_X–$M_\star$ correlation (the right panels ((c) and (d)) of Figure 4.15).

Similar to the left panels of Figure 4.15, in the left panels of Figure 4.16, we also see no correlation of $\dot{M}$–R_{wall} for CTDs but a significant and strong correlation for WTDs+PTDs. To find the genuine behavior of TDs between $\dot{M}$ and R_{wall} which is different from $\dot{M}$ of CTTSs, we divided $\dot{M}$ of our sample by the $\dot{M}(M_\star)$ (the thick long-dashed lines). The right panels of Figure 4.16 show the residual relation between $\dot{M}$ and R_{wall} of CTDs ((c); anti-correlation) and WTDs+PTDs ((d); no correlation) after taking the dominant effect of $M_\star$

out. This supports the ideas that (1) the mass accretion behaves similarly to the case of radially-continuous disks while an inner disk exists in a TD, and (2) the mass accretion rate decreases as the size of inner cavity increases.

In the left panels of Figure 4.17, CTDs have a very strong and significant correlation between L_X and R_{wall}, while WTDs+PTDs have a weak relationship with large uncertainty in the trend of L_X and R_{wall} comparing to that for all TDs combined. Therefore, we infer that the general increasing tendency of L_X along R_{wall} in Figure 4.14 is due to the dominant effect of the strong correlation for CTDs. After removing the underlying contribution from $M_\star$ to L_X–R_{wall} relation by dividing L_X–R_{wall} by $L_X(M_\star)$–R_{wall}, we see no correlation for CTDs and insignificant anti-correlation with large uncertainty for WTDs+PTDs from the right panel of Figure 4.17.

From Figure 4.18, we confirm that $\dot{M}$ and L_X are not correlated with each other regardless of subtypes of TDs not like the strong correlation between them in the case of T Tauri stars (the thick dashed line in the panels (a) and (b)). The residual $\dot{M}$ after removing the strong $\dot{M}$–L_X correlation of T Tauri stars in the right panels are anti-correlated to L_X for both CTDs and WTDs+PTDs. We note that this is similar to the trend found for CTTSs by Telleschi et al. (2007). Drake et al. (2009) also shows the similar result that the objects with higher L_X have lower $\dot{M}$ and find a strong anti-correlation between L_X normalized to $M_\star$ and $\dot{M}$ with CTTS/WTTS in ONC. Therefore, the anti-correlation shown in the right panels of Figure 4.18 for both CTDs (panel (c)) and WTDs+PTDs (panel (d)) may be a common characteristic of protoplanetary disks, not a unique characteristic of TDs.

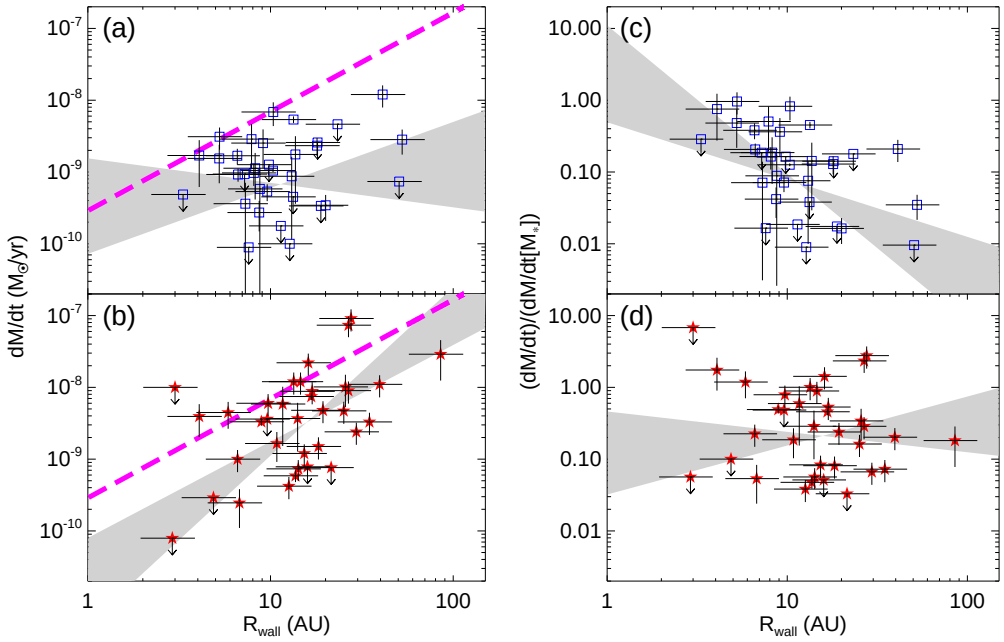


Figure 4.16 Detailed trends of $\dot{M}$-R_{wall}: correlations separated in two subgroups, CTDs (open square) and WTDs+PTDs (solid star). The symbol in each panel is same as Figure 4.15. The thick long-dashed line in the panel (a) and (b) is same in Figure 4.14 (b). The right panels show the trend at no $M_\star$ dependence by presenting the deviation of $\dot{M}$ from the thick long-dashed line of $\dot{M}(M_\star)$-R_{wall}.

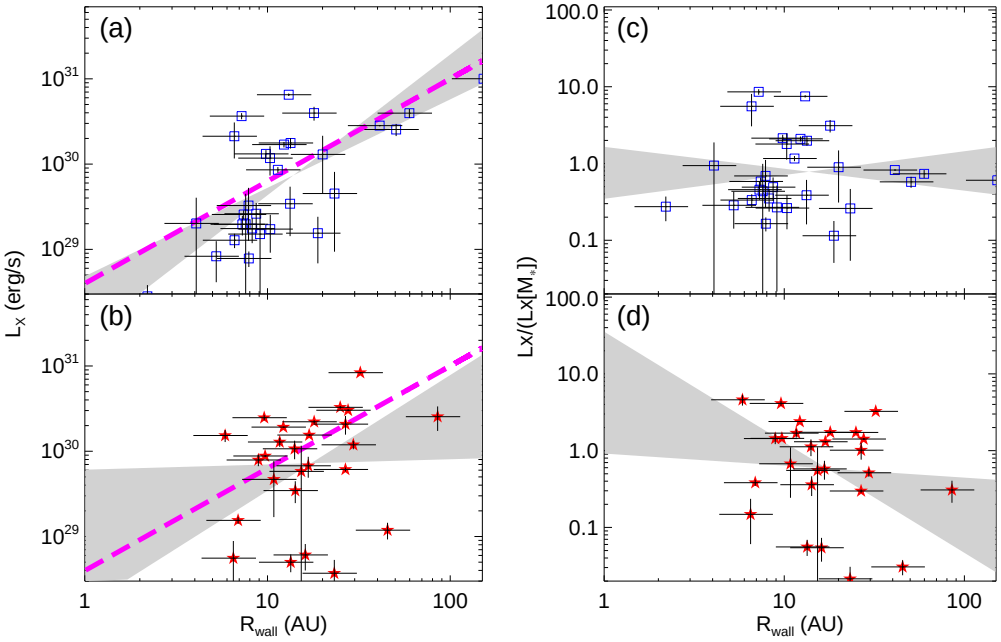


Figure 4.17 Detailed trends of L_X-R_{wall}: correlations separated in two subgroups, CTDs (open square) and WTDs+PTDs (solid star). The symbol in each panel is same as Figure 4.15. The thick long-dashed line in the panel (a) and (b) is same in Figure 4.14 (c). The right panels show the trend at no $M_\star$ dependence by presenting the deviation of L_X from the thick long-dashed line of $L_X(M_\star)$-R_{wall}.

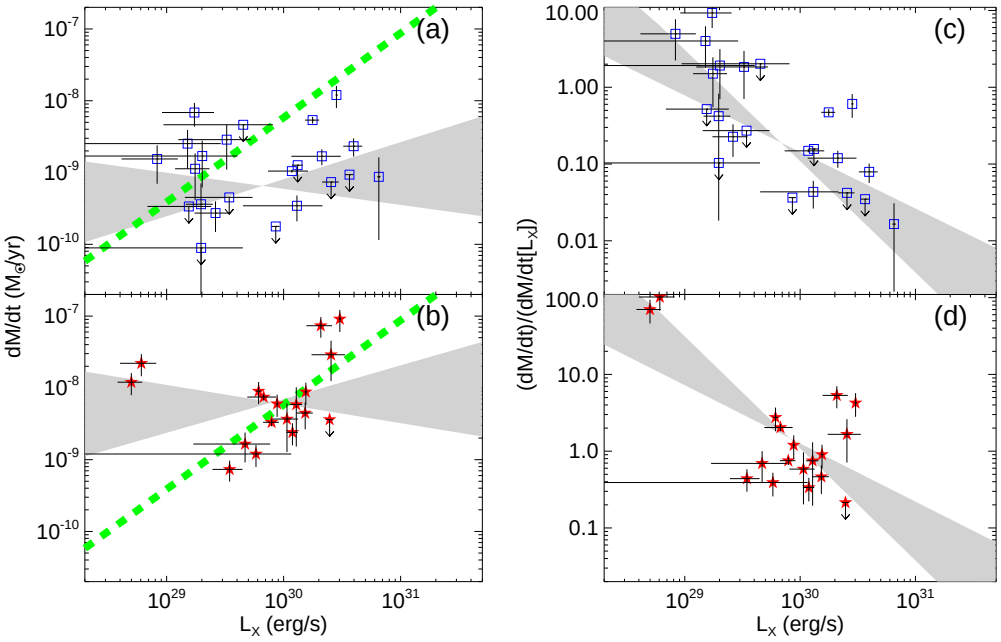


Figure 4.18 Detailed trends of $\dot{M}$-L_X: correlations separated in two sub-groups, CTDs (open square) and WTDs+PTDs (solid star). The symbol in each panel is same as Figure 4.15. The thick dashed line represent $\dot{M}$-L_X relation of T Tauri star in Tau as explained in Figure 4.13(c).

4.5.3 Summary of Significant Trends

Here, we summarize the correlations and trends of TD properties we find to help our insights on the origin of TDs, which will be discussed through the next section.

$L_\star$ and $M_\star$ are independent of the subtypes of TDs. The significantly strong correlation between $M_\star$ and R_{wall} is consistent regardless of the subtype of TDs as $M_\star \propto R_{wall}$.

$\dot{M}$ and L_X vary/evolve with time. We have seen that some trends differ by subtypes of TDs and some trends are comparable to those of the larger T Tauri star population overall. The residual (or normalized) properties after removing the underlying effect of $M_\star$ which is a parameter correlated with $\dot{M}$ and L_X may show the effect of the transition process from a radially continuous disk to a TD.

Some properties have very different trends according to whether the inner disk exists (WTD/PTD) or not (CTD).

(1) Trends related to $\dot{M}$ show a strong correlation with WTDs+PTDs, but no correlation with CTDs:

• $\dot{M}$ versus $M_\star$: WTDs+PTDs show a very similar correlation to that of T Tauri stars with $\dot{M} \propto {M_\star}^{2.0}$. In stark contrast, no correlation shows for CTDs.

• $\dot{M}$ versus R_{wall}: WTDs+PTDs show a very tight correlation between the two properties, $\dot{M} \propto {R_{wall}}^{1.8}$, but the two properties are not correlated for CTDs.

(2) Trends of some properties are strongly correlated for CTDs, but not

for WTDs+PTDs:

• L_X versus $M_\star$: The trend of CTDs ($L_X \propto {M_\star}^{1.7\pm0.5}$) alone is very close to the trend of T Tauri stars ($L_X \propto {M_\star}^{1.7}$), but the slope ($\beta$) of the trends of WTDs+PTDs is smaller by about a factor of two ($L_X \propto M_\star$).

• L_X versus R_{wall}: A significant correlation between L_X and R_{wall} for CTDs, but the trend for WTDs+PTDs is very uncertain.

• *residual* $\dot{M}$ versus R_{wall}: The residual trend of $\dot{M}$ and R_{wall} is opposite to the trend before removing $M_\star$ effect from $\dot{M}$ versus R_{wall}: CTDs show an anti-correlation, but WTDs+PTDs do not show any correlation.

On the other hand, $\dot{M}$ versus L_X show no correlations from any subtype of TDs, in contrast to the strong correlation for T Tauri stars with full disks.

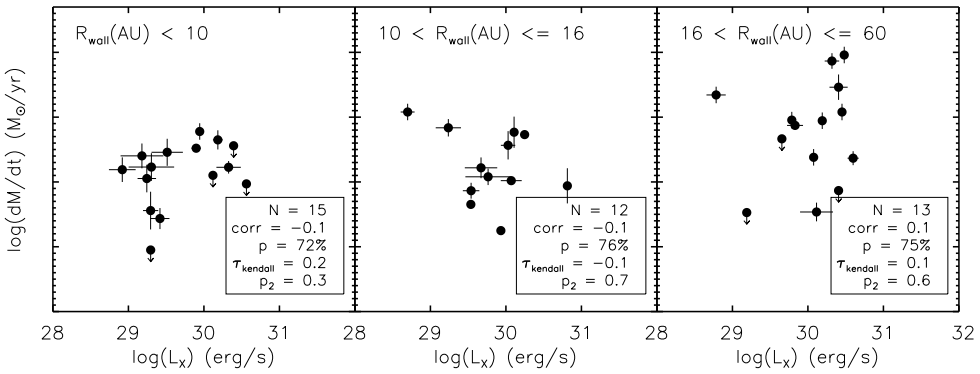


Figure 4.19 The tests to find the relationship between $\dot{M}$ and R_{wall} under a constant R_{wall} condition. We present the sub-groups separated by three R_{wall} bins. The coverage of R_{wall} of each bin is indicated on each panel with the number of sub-sample (N), a linear correlation coefficient (corr) between $log\dot{M}$ and $logL_X$, and a probability (p) of getting corr from random distribution. $\tau_{kentall}$ is Kendall's tau which indicates the degree of correlation between two variables; closer to 1, tighter correlation. p_2 indicate the two-sided p value of $\tau_{kentall}$; if p_2=1, the probability of no correlation is 100%.

Table 4.4. Correlation summary I

Correlation	N	α	β	$corr$[a]	P[b](%)	P_{range}[c](%)
$\dot{M}$ vs. $M_\star/M_\odot$	68	-8.4 ± 0.1	1.8 ± 0.3	0.6 ± 0.1	$\ll$ 0.001	$\ll$ 0.001
L_X vs. $M_\star/M_\odot$	54	30.1 ± 0.1	1.1 ± 0.3	0.5 ± 0.1	0.01	$\ll$ 0.001 - 0.3
$\dot{M}$ vs. L_X	41	-14.2 ± 8.2	0.2 ± 0.3	0.1 ± 0.2	54	5.7-100
$M_\star/M_\odot$ vs. R_{wall}	98	-1.0 ± 0.1	0.7 ± 0.1	0.8 ± 0.1	$\ll$ 0.001	$\ll$ 0.001
$\dot{M}$ vs. R_{wall}	68	-10.4 ± 0.4	1.4 ± 0.4	0.5 ± 0.1	0.001	$\ll$ 0.001-0.07
L_X vs. R_{wall}	56	28.5 ± 0.3	1.1 ± 0.3	0.6 ± 0.1	$\ll$ 0.001	$\ll$ 0.001-0.2
$\dot{M}/\dot{M}[M_\star, R_w]$ vs. R_{wall}	68	-0.1 ± 0.3	-0.6 ± 0.3	-0.3 ± 0.1	1.3	0.07-42
$L_X/L_X[M_\star, R_w]$ vs. R_{wall}	56	0.1 ± 0.3	-0.2 ± 0.3	-0.1 ± 0.2	14	2.5-100
$\dot{M}/\dot{M}[L_X]$ vs. L_X	41	30.1 ± 6.6	-1.0 ± 0.2	-0.6 ± 0.1	0.003	$\ll$ 0.001-0.09
$L_\star$ vs. $M_\star$	98	0.3 ± 0.0	1.6 ± 0.1	0.8 ± 0.0	$\ll$ 0.001	$\ll$ 0.001
$L_\star/L_\odot$ vs. R_{wall}	98	-1.9 ± 0.1	1.6 ± 0.1	0.9 ± 0.0	$\ll$ 0.001	$\ll$ 0.001
L_X vs. $L_\star/L_\odot$	56	29.8 ± 0.1	0.7 ± 0.1	0.6 ± 0.1	$\ll$ 0.001	$\ll$ 0.001-0.01
$L_X/L_\star$ vs. $M_\star/M_\odot$	54	-3.8 ± 0.1	-0.5 ± 0.3	-0.2 ± 0.1	15	0.3-47
$\dot{M}$ vs. $L_\star/L_\odot$	68	-8.7 ± 0.1	1.0 ± 0.2	0.6 ± 0.1	$\ll$ 0.001	$\ll$ 0.001-0.001
$\dot{M}$ vs. $L_X/L_\star$	39	-11.5 ± 1.0	-0.8 ± 0.3	-0.5 ± 0.2	0.1	$\ll$ 0.001-6.4

Note. — Summary of the results from the Bayesian linear regression between X and Y: Y vs. X; $logY = \alpha + \beta logX$. Objects has a known spectral type are only included for the correlations.

[a] $corr$ is the linear correlation coefficient between $logY$ and $logX$.

[b] P is the probability of getting $corr$ in random distribution.

[c] P_{range} is the range of P to get $corr$ in 1σ uncertainty.

Table 4.5. Correlation summary II: details by subtypes of TDs

Correlation	TD type	N	α	β	$corr$[a]	P[b](%)	P_{range}[c](%)	MRI[d]	XPE[e]	GPF[f]
$\dot{M}$ vs. $M_\star/M_\odot$	CTD	33	-8.7 ± 0.6	1.4 ± 1.5	0.3 ± 0.3	0.9	0.3-100			Y
	WTD+PTD	35	-8.2 ± 0.1	2.0 ± 0.5	0.7 ± 0.1	$\ll$ 0.001	$\ll$ 0.001-0.01			Y
L_X vs. $M_\star/M_\odot$	CTD	30	30.3 ± 0.2	1.7 ± 0.5	0.6 ± 0.2	0.05	$\ll$ 0.001-2.6			Y
	WTD+PTD	26	30.0 ± 0.1	0.9 ± 0.4	0.5 ± 0.2	0.9	0.007-14			Y
$\dot{M}$ vs. R_{wall}	CTD	33	-9.5 ± 0.7	0.3 ± 0.6	0.1 ± 0.2	56	2.1-100	N	Y?	Y
	WTD+PTD	35	-10.7 ± 0.6	1.8 ± 0.5	0.7 ± 0.1	$\ll$ 0.001	$\ll$ 0.001-0.2	Y	Y?	Y
$\dot{M}/\dot{M}(M_\star)$ vs. R_{wall}	CTD	33	0.4 ± 0.7	-1.4 ± 0.6	-0.5 ± 0.2	0.3	$\ll$ 0.001-9	N	Y?	Y
	WTD+PTD	35	-0.9 ± 0.6	0.2 ± 0.5	0.1 ± 0.2	25	7.9-100	N	N	Y
L_X vs. R_{wall}	CTD	30	28.3 ± 0.3	1.3 ± 0.3	0.7 ± 0.1	0.002	$\ll$ 0.001-0.05		Y?	Y
	WTD+PTD	26	29.0 ± 0.8	0.7 ± 0.6	0.3 ± 0.3	14	0.9-100		Y?	Y
$L_X/L_X(M_\star)$ vs. R_{wall}	CTD	30	-0.1 ± 0.3	0.0 ± 0.3	0.0 ± 0.2	96	29-100	N	N	Y
	WTD+PTD	26	0.8 ± 0.8	-0.8 ± 0.6	-0.3 ± 0.2	14	0.1-63	N	N	Y
$\dot{M}$ vs. L_X	CTD	23	-13.5 ± 11.0	0.1 ± 0.4	0.1 ± 0.3	65	5.9-100	N	N?	Y
	WTD+PTD	18	-11.2 ± 11.0	0.1 ± 0.4	0.1 ± 0.3	62	10-100	N		Y
$\dot{M}/\dot{M}(L_X)$ vs. L_X	CTD	23	31.9 ± 10.7	-1.1 ± 0.4	-0.6 ± 0.2	0.2	$\ll$ 0.001-1.5	N	Y?	Y
	WTD+PTD	18	33.3 ± 10.5	-1.1 ± 0.4	-0.7 ± 0.2	0.1	$\ll$ 0.001-3.5	N	Y?	Y
$M_\star/M_\odot$ vs. R_{wall}	CTD	46	-1.0 ± 0.1	0.6 ± 0.1	0.8 ± 0.1	$\ll$ 0.001	$\ll$ 0.001		Y	
	WTD+PTD	52	-1.1 ± 0.2	0.8 ± 0.1	0.7 ± 0.1	$\ll$ 0.001	$\ll$ 0.001		Y	
$\dot{M}$ vs. $L_\star/L_\odot$	CTD	33	-9.1 ± 0.2	0.1 ± 0.5	0.1 ± 0.2	58	9-100			Y

Table 4.5 (cont'd)

Correlation	TD type	N	α	β	$corr$[a]	P[b](%)	P_{range}[c](%)	MRI[d]	XPE[e]	GPF[f]
L_X vs. $L_\star/L_\odot$	WTD+PTD	35	-8.5 ± 0.1	1.2 ± 0.2	0.8 ± 0.1	$\ll$ 0.001	$\ll$ 0.001			Y
	CTD	30	29.9 ± 0.1	0.8 ± 0.2	0.6 ± 0.2	0.05	$\ll$ 0.001-2.9	Y		Y
	WTD+PTD	26	29.7 ± 0.1	0.8 ± 0.2	0.6 ± 0.2	0.1	$\ll$ 0.001-4.3	Y		Y

Note. — Summary of the results from the Bayesian linear regression between X and Y: Y vs. X; $logY = \alpha + \beta logX$. The index [a,b,] and [c] have the same meanings as in Table 4.4.

[d] *MRI*: The inside-out disk evolution driven by Magneto Rotational Instability.

[e] *XPE*: The disk dispersion by photoevaporation, specially X-ray photoevaporation

[f] *GPF*: Dynamical effects by infant giant planet formation.

Note. — N or Y checks indicate if a mechanism in the last three columns can explain the corresponding trends in a row.

4.6 Mechanisms for the Origins of Transitional Disks and Constraints

In this section, we briefly review proposed mechanisms for disk dispersal and compare how our findings are consistent, or not, with these predictions from the mechanisms: dust coagulation and settling; photoevaporation; inside-out disk clearing by MRI; gravitational effects of one or more low-mass companions.

Grain growth and settling. Dust grains should grow and settle to the disk midplane during the protoplanetary disk evolution process. As grains grow larger, the opacity of the grains becomes smaller, leading to weaker continuum emission in IR range. On this basis, it has been proposed that the flux deficit shown in SEDs of TDs may be due to the existence of an opacity hole caused by grain growth and settling in the inner disk rather than a real material deficit in the inner disk (e.g. Dullemond & Dominik, 2005). Tanaka et al. (2005) suggested that the SEDs of TDs could be due to differing opacity as a function of radius; e.g., smaller disk optical depth in the inner disk than in the outer disk at 10 μm. Some authors (Garaud, 2007; Brauer et al., 2007, 2008) have demonstrated the short time scale of grain growth and settling. However, considering grain growth/settling only as the main mechanism of TDs cannot explain the sharp transition represented by the sharp edge of the inner wall of the outer disk which is implied from the distinctive characterstic of TD's SEDs and is supported by many resolved submillimeter images of TDs (Hughes et al., 2009; Andrews et al., 2011). In any case, grain coagulation and settling

is a process that takes monotonically longer at increasing radius within the disk, so it cannot possibly explain the gaps in WTDs and PTDs.

MRI. A mechanism important in the large-scale mixing and turbulence in a disk is the MRI. Chiang & Murray-Clay (2007) showed how MRI accelerates mass accretion and leads to inside-out disk clearing. Perez-Becker & Chiang (2011) considered the ionization, necessary for the MRI mechanism, by stellar FUV radiation and demonstrated that the surface layer accretion driven by this could reproduce the trend of increasing accretion rate with increasing hole size seen in TDs. Suzuki et al. (2010), using MHD simulations with X-rays as the ionization source, showed the disk winds driven by MRI leads to a decrease in surface density in the manner of inside-out dispersal irrespective of the existence of a dead zone.

These models based on the inside-out disk clearing by MRI draining predict correlations between R_{wall}, $\dot{M}$, and L_X: (1) a positive correlation between $\dot{M}$ and R_{wall} at a given $M_\star$ because a larger ionized area leads to more mass accretion; (2) a positive correlation between $\dot{M}$ and L_X at a constant R_{wall} because more ionization of disk surface as exposed by stronger energy sources leads to more mass accretion. However, our findings on the trends of $\dot{M}$, L_X, and R_{wall} do not support these predicted correlations between R_{wall}, $\dot{M}$, and L_X. First, a strong correlation of $\dot{M}$ with R_{wall} is shown only for the case of TDs with radial gaps (WTDs+PTDs) not for the TDs with inner cavities (CTDs). Furthermore, that correlation disappears when differing stellar masses are accounted for. Second, we found no correlation between $\dot{M}$ and L_X for TDs regardless of their subtypes. To test for correlation between $\dot{M}$

and L_X at a given R_{wall}, we examine trends for several different R_{wall} ranges in Figure 4.19. We find no correlation between $\dot{M}$ and L_X for any ranges of R_{wall}.

Photoevaporation. Photoevaporation has long been thought to be an important and major disk dispersal mechanism (Shu et al., 1994; Hollenbach et al., 1994; Clarke et al., 2001; Font et al., 2004; Alexander et al., 2006a,b). High energy radiation from the central star ionizes and heats the disk surface, which can be unbound and leaves as a wind beyond a certain radius. A gap can be opened when the accretion rate is small enough that material from the outer disk beyond the photoevaporation radius cannot replenish the inner disk. The inner disk, decoupled from the outer disk, drains on to the central star while the outer disk is evaporated into space. These models encounter contradictions when only the EUV ionizing radiation is considered: (1) the mass accretion rates of TDs is higher than the photoevaporation rate (or mass-loss rate), (2) the ages of many TDs are less than the dispersal timescale of photoevaporation, and (3) the existence of the large radial gaps of PTDs. Recently, the photoevaporation model has been modified to address those issues by taking much higher energy radiation sources (FUV and X-ray) as sources (Ercolano et al., 2009; Gorti & Hollenbach, 2009; Owen et al., 2010, 2011a,b, 2012): (1) much higher mass-loss rate can be driven by X-rays (Ercolano et al., 2009) and (2) 1–10 AU gap creation at relatively early epochs (3–4 Myr; Gorti et al. (2009)) . Considering disk dispersal by photoevaporation through EUV, FUV, and X-ray radiation, Owen et al. (2012) concluded that the stars' intrinsic X-ray luminosity should have a decisive role in disk's life times and evolution.

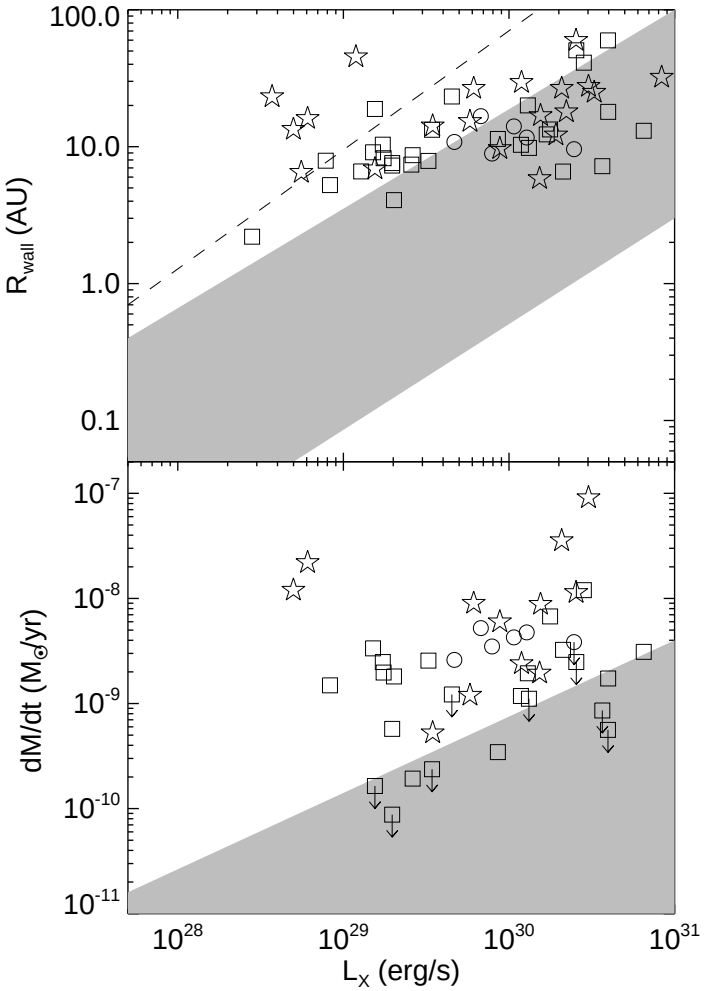


Figure 4.20 Comparison of the predictions by X-ray photoevaporation (Owen et al. (2012), Fig 18 in their paper) to the properties of observed TDs. The gray shadows are the domains in which X-ray photoevaporation is dominant. The dashed line adopted from Fig 18. in Owen et al. (2012) represents the maximum radius a TD may reach before thermal sweeping sets in and a disk dissipates beyond TD stage. The model domains are derived with $R_g \propto M_\star$ and the positive correlation between $M_\star$ and L_X (Owen et al., 2012), similar to our finding, so the photoevaporation prediction and the observed TDs properties generally show positive correlations.

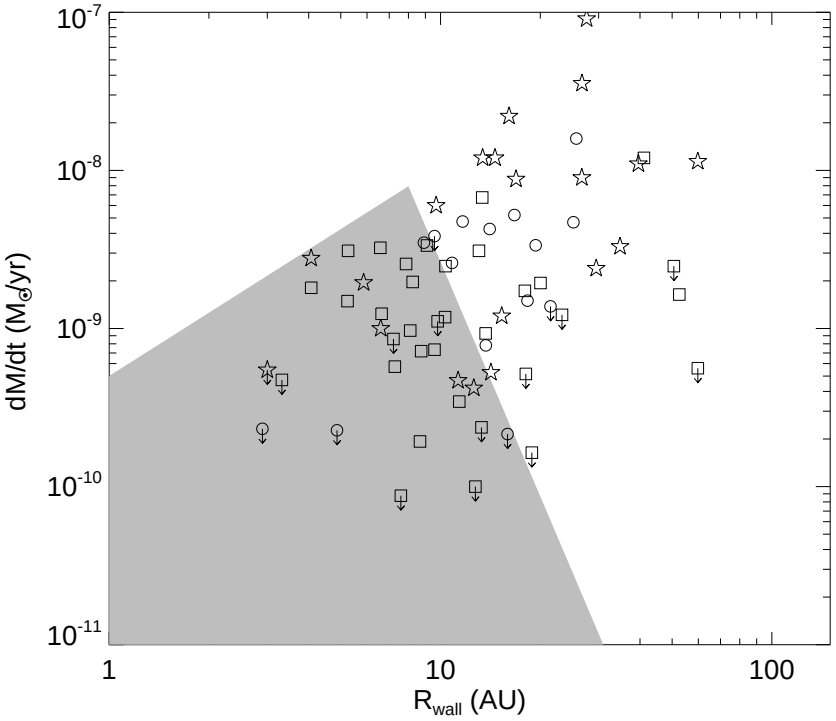


Figure 4.21 Comparison of $\dot{M}$ vs. R_{wall} to the predictions by X-ray photoevaporation (gray shadow region: Owen et al. (2012)). Each symbol indicate different subtype of TDs: square (CTD); circle (WTD); star (PTD).

We compare our data to the theoretical predictions from the X-ray photoevaporation (XPE) model by Owen et al. (2012). Both the TD data and the XPE model have tendencies of increasing R_{wall} and $\dot{M}$ as L_X and $M_\star$ increase. However, most TDs of all three types in our sample do not fall into the model domains, as indicated in Figures 4.20[6] and 4.21. In particular, the XPE model fails to explain the objects with either large R_{wall} or the large $\dot{M}$. More than half of all TDs fall outside the region allowed by the XPE in Figure 4.21. Therefore, we conclude that XPE is not the dominant mechanism for creating TDs in this work.

Morishima (2012) developed a gas disk model taking into account layered accretion driven by MRI and XPE winds. With a central star of 1 $M_\odot$ and an initial disk mass of 0.1 $M_\odot$, they found their gas dispersal model can open a gap at large radii while the mass accretion rate is still similar to that of CTTS when dead zones are considered. They show that their model with a dead zone can reconstruct the distribution of the observed TDs with high $\dot{M}$ and large R_{wall}, which is the range XPE cannot reconstruct.

Gravitational effects of companions. The average disk mass of Class II objects measured by observations of the submm-mm continuum of disks (Andrews & Williams (2005); Andrews & Williams (2007)) in Tau and Oph is about 5 M_J. This is much less than the minimum mass solar nebular (MMSN) and the requirement of disk mass to form giant gas planets or multiple planets which are observationally confirmed. It seems likely that submillimeter con-

[6]Owen et al. (2012) note the difficulty of determining a correlation between any two of the three properties because L_X, R_{wall}, and $M_\star$ are interdependent. Therefore, the predictions in the figures are the results from numerical simulation.

tinuum observations systematically underestimate disk masses (e.g. D'Alessio et al. (2001), Hartmann et al. (2006)). Alternatively, systems could have more substantial disk mass at the Class 0/I stage (Greaves & Rice, 2010).

As in our previous work (Kim et al., 2009), truncation by a companion is seems more promising than the other gap formation mechanisms. If the disks start with larger masses, photoevaporative gas dispersal models may encounter another challenge to deplete disk material because more massive disks require stronger energy sources to evaporate disk material. On the other hand, for a more massive disk, the more favorable mechanism to open and clear a gap in a protoplanetary disk is giant planet formation by gravitational instability. Recent theoretical results on planet formation by gravitational instability suggest the possibility of gas giant planet formation at even much closer distances to the central star (10 AU by Inutsuka et al. (2010); $R < 25$ AU by Meru & Bate (2010)). Even giant planet formation *via* core accretion model, which requires longer time scales, is possible in $\sim$1 Myr with disks substantially larger than the MMSN (Greaves & Rice, 2010).

Giant planet formation in protoplanetary disks has been proposed as the origin of gaps/holes of TDs and debris disks (e.g. Holland et al., 1998; Jura & Turner, 1998; Zuckerman & Song, 2004). Several hydrodynamical simulations show the companion's presence can reproduce the sharp inner disk truncation and gap formation in a short time scale (Quillen et al., 2004; Rice et al., 2006; Varnière et al., 2006; Zhu et al., 2011, 2012).

Whether the companion is a planetary object or a sub-stellar companion, the observational features can be explained by the dynamical effects of

the companion on the central star. The distribution of $\dot{M}$ shown in Figure 4.12 strongly supports for the idea of gap opening and disk dispersal by planet/companion formation. The displacements of $\dot{M}$ of the gapped disks and the CTDs from the median $\dot{M}$ of CTTS is almost a factor of 10, which is consistent with the estimated decrements of the mass flow across a gap created by a low-mass companion (Lubow & D'Angelo, 2006). As we discussed in Kim et al. (2009), the strong correlation between $L_\star$ or $M_\star$ versus R_{wall} is reminiscent of the observed dependence between binary separation and the system's stellar mass. While this similarity might be taken to suggest that the stellar mass versus separation dependence is imprinted when stars form, this argument has an important caveat. The strong trend of $M_\star$–R_{wall} of TDs is possibly driven by strong correlations of $L_\star$–$M_\star$ and $L_\star$–R_{wall}. More detailed studies are needed to investigate this possibility.

Giant planet formation can also explain the trends shown in $\dot{M}/\dot{M}(M_\star)$–R_{wall} (Figure 4.16). Assuming (1) $M_{disk} \propto M_\star$ at a given age which implies (2) normalization by $M_\star$ is the same as normalization by M_{disk}, the mass accretion rates of WTDs+PTDs may not be strongly related to R_{wall} since material accreting from an inner disk may not be dependent on a planet formation location or R_{wall} and the mass accretion from an inner disk may be dominant than mass accretion through a gap from an outer disk. In the case of CTDs when the inner disk is depleted, however, the outer disk mass will decrease as the size of an inner cavity increases. That will result less material to accrete through the larger inner hole, therefore the anti-correlation between $\dot{M}/\dot{M}(M_\star)$ and R_{wall} of CTDs is naturally explained.

The disk-clearing companion can be a stellar companion, as in the case of CoKu Tau 4 (Ireland & Kraus, 2008), because a large fraction of stars form in multiple systems. If stellar companions are the dominant origin of TDs, they should be of lower mass than the primary to explain the strong correlations in $\dot{M}$-$M_\star$ of WTD+PTD. Sensitive searches have made for 10 AU scale binaries in Taurus (Pott et al. (2010); Kraus et al. (2011)), but only one (CoKu Tau/4; Ireland & Kraus (2008)) of the nine TD systems so studied has a stellar companion detected with binary separation similar to the gap radius. The limits on companion luminosity for the other eight rule out stars. In addition, Kraus & Ireland (2012) have tentatively detected an infant giant planet in the gap of the LkCa 15 disk. Therefore, planet formation could be chiefly responsible for the origin of TDs.

Currently it is not clear that how different paths of disk evolution are followed, and which mechanisms dominate on a track of evolution given different initial conditions. Mechanisms such as grain growth, MRI action in the inner disk, and photoevaporation must be important to the dispersal of dusts. In other types of evolved disks, such as the anemic, homologously depleted, and weak excess disks, which are not covered in this study, grain growth and photoevaporation could be dominant mechanisms. However, the trends we find indicate that giant planet formation is the dominant mechanism in gap formation for our sample of TDs.

4.7 Summary and Conclusions

We presented the SEDs of 62 new TDs identified from IRS spectra in the Orion A star-forming region and discussed selection criteria for TDs. Utilizing the TDs already identified in Taurus, Chamaeleon I, Ophiuchus, and NGC 1333, in a manner similar to TDs in Orion A, we explored statistically robust trends with the largest and most homogeneous set of TDs to date.

We presented a set of TD selection criteria and a quantitative empirical method to classify three subtypes of TDs: CTD, WTD, and PTD.

We found the TD fraction of Class II YSOs is very high ($\sim$20%) even at the youngest ages ($\leq$ 1 Myr, Orion A and NGC 1333). This could indicate early disk evolution even in the Class 0/I stages, most likely due to giant planet formation (Lubow & D'Angelo, 2006).

We have examined various mechanisms of disk clearing utilizing our observation of TDs. We confirm that disk clearing mechanisms including MRI action and photoevaporation generated by X-ray/FUV photons are consistent with some of the observations, but not all. In particular, there are several observational trends which cannot be explained by these mechanisms, especially those related to $\dot{M}$ and L_X:

(1) The observed mass accretion rate suppression of CTDs ($10^{-8.8}$ $M_\odot/yr$) and PTDs ($10^{-8.4}$ $M_\odot/yr$) compared to the radially continuous disks ($10^{-7.8}$ $M_\odot/yr$).

(2) The lack (or negative) of correlation between $\dot{M}$ and R_{wall} after accounting for $M_\star$'s effects.

(3) No correlation of L_X and R_{wall} after correcting for $M_\star$'s effects.

(4) No correlation of L_X and $\dot{M}$ at constant R_{wall}.

However, these properties/trends are naturally explained by substellar companions, formed within the disks in the early stages of disk evolution. Infant Jovian-mass planets would nicely explain the size and structure observed for the gaps (Quillen et al. (2004); Edgar et al. (2007)).

Based on our results from the largest sample of TDs to date, as summarized above, we conclude that giant planet formation plays the dominant role in opening gaps and creating TDs.

5 Disk Evolution

In this chapter, we examine the characteristics of the properties of Class II disks observed in IRS SLLL mode in ONC and L1641 measured from Chapter 3. Our main goal is to compare the parameters of radially continuous (full) disks (FD) to those of transitional disks (TD). By "parameters" we mean the collections of stellar properties, spectral indices, and spectral-feature strength with which we have searched for trends in Chapter 3 and 4. We hope thereby to find trends that will illuminate the role of transitional disks in the evolution of protoplanetary disks, at least through the time during which the disks are gas-rich, optically thick, and, as we saw in Chapter 4, forming gas-giant planets.

5.1 Comparisons of the distribution of properties between FD and TD

To measure the quantitative difference between the distributions of a given parameters among FDs and TDs, we take a K-S test of the difference D between

the two cumultative distributions, and measure the median of the property for each group. The output from the statistical tests are listed in Table 5.1. We plot histograms of the properties from Figure 5.1–5.7 visually to display the difference of distribution of a property of FDs and that of TDs. We consider a K-S difference D between two groups to be significant if p, the probability that the K-S difference D could be formed in two random selections from the same distribution, is less than 0.05. If p is less than 0.01, we take the deviation to be a strongly significant.

With small p, the value of D indicates a significant maximum difference between the cumulative distributions. In our data D varies all the way from nearly unity to about 0.1–0.2. The largest values indicate completely distinct, non-overlapping distributions; the smallest values indicate largely overlapping distributions with maximum differences consistent with Poisson statistics and the total numbers in our samples. D and p for all pairs appear along with the histograms in Figure 5.1–5.12.

We can, therefore, rank the significant differences as large ($D > 0.5$), medium (D=0.25–0.5), and small ($D < 0.25$). Small is consistent with zero difference.

Table 5.1 Distribution of Properties: FD versus TD

	Ori A				ONC				L1641			
	median		K-S test		median		K-S test		median		K-S test	
parameters	FD	TD	D	p	FD	TD	D	p	FD	TD	D	p
$\log M_\star$	0.54	0.45	0.30	$\ll 0.001$	0.54	0.53	0.23	0.14	0.54	0.38	0.44	$\ll 0.001$
$\log L_\star$	0.23	-0.22	0.36	$\ll 0.001$	0.16	-0.15	0.25	0.10	0.27	-0.33	0.52	$\ll 0.001$
n_{K-6}	-1.36	-2.28	0.69	$\ll 0.001$	-1.35	-2.20	0.72	$\ll 0.001$	-1.37	-2.40	0.68	$\ll 0.001$
n_{6-13}	-0.67	-0.53	0.20	0.04	-0.65	-0.44	0.27	0.06	-0.68	-0.62	0.17	0.54
n_{13-31}	-0.66	0.54	0.67	$\ll 0.001$	-0.66	0.44	0.62	$\ll 0.001$	-0.66	0.80	0.75	$\ll 0.001$
EW (10μm)	2.33	3.36	0.36	$\ll 0.001$	2.46	3.46	0.39	0.00	2.09	3.36	0.33	0.01
EW (20μm)	2.22	3.73	0.55	$\ll 0.001$	2.29	3.48	0.51	$\ll 0.001$	2.18	4.19	0.65	$\ll 0.001$
EW (33μm)	0.10	0.07	0.12	0.48	0.13	0.05	0.21	0.24	0.07	0.17	0.35	0.01
$\log F_{10}$	-11.35	-12.01	0.47	$\ll 0.001$	-11.33	-11.72	0.39	0.00	-11.40	-12.30	0.59	$\ll 0.001$
$\log F_{20}$	-11.77	-12.05	0.25	0.01	-11.78	-11.93	0.26	0.08	-11.77	-12.13	0.34	0.01
F_{20}/F_{10}	0.39	0.96	0.54	$\ll 0.001$	0.38	0.76	0.50	$\ll 0.001$	0.39	1.21	0.68	$\ll 0.001$
$F_{9.8}$	0.74	1.07	0.30	$\ll 0.001$	0.78	1.28	0.37	0.00	0.69	0.96	0.31	0.03
$F_{11.3}$	0.39	0.68	0.48	$\ll 0.001$	0.42	0.68	0.56	$\ll 0.001$	0.35	0.63	0.44	$\ll 0.001$
$F_{11.3}/F_{9.8}$	0.52	0.58	0.25	0.01	0.52	0.53	0.11	0.94	0.52	0.64	0.43	$\ll 0.001$
$\log \dot{M}$	-7.90	-8.81	0.56	$\ll 0.001$	-7.82	-8.78	0.54	$\ll 0.001$	-7.90	-8.81	0.62	$\ll 0.001$
$\log L_X$ 8	29.96	30.03	0.16	0.47	29.98	30.11	0.15	0.88	29.89	29.54	0.33	0.13
$\log L_X$ 1	27.94	28.59	0.21	0.22	27.94	28.71	0.36	0.07	27.89	27.77	0.21	0.65
$\log L_X$ 2	28.88	29.26	0.26	0.06	29.07	29.45	0.34	0.07	28.81	28.96	0.21	0.61
$\log L_X$ 3	29.25	29.32	0.09	0.99	29.36	29.40	0.18	0.71	29.21	28.96	0.14	0.96
$\log L_X$ 4	29.40	29.19	0.25	0.09	29.46	29.32	0.24	0.41	29.29	28.99	0.34	0.11
$\log L_X$ 5	29.43	29.01	0.31	0.02	29.44	29.03	0.33	0.09	29.29	28.98	0.38	0.08

Note. — D is the maximum deviation between the cumulative distribution of two groups. p indicates the probability that there is no significant difference between the distributions

Some of the differences are already discussed above, in Chapter 4. Large or medium values of D are obtained between TDs and FDs for n_{K-6} and n_{13-31} (see, Figure 5.2). The fluxes, equivalent widths of silicate features, and the silicate feature 20/10 μm flux ratio are also large to medium D values (Figure 5.3 and Figure 5.4). These differences have been employed to distinguish between TDs and FDs. The large values of D between TDs and FDs for $\dot{M}$, and the small values for n_{6-13}, are also discussed above (see also Figure 5.6 for the comparison of $\dot{M}$, measured by our SpeX observation, between TDs and FDs in Orion A).

Other cumulative-distribution differences of note are following:

• With large or medium differences in D, TDs are more likely than FDs to be found around low-mass and low-luminosity stars in Orion A, especially in L1641 (Figure 5.1). The number of TDs in Taurus is too small to yield a significant measure of this difference.

• TDs in Orion are more likely to have large 10 and 20 μm silicate equivalent widths than FDs, but FDs are more likely to have large fluxes in the silicate features (see, Figure 5.3 and Figure 5.4). Thus the large EWs in TDs comes from reduction of continuum emission from the inner disk, owing to the gap, as discussed in Chapter 4. The same conclusion was expressed in our previous work, including for example Kim et al. (2009) and Calvet et al. (2005).

• The X-ray luminosity and spectrum of the Orion A FDs and TDs differ insignificantly. A medium-size difference between FDs and TDs for the full sample at 4.5-12 keV is not corroborated separately in the ONC or L1641 sample (Figure 5.7).

• The FD populations in Orion A and Taurus must have similar typical radial and vertical structure, as the differences in their continuum indices are small or insignificant. (Figure 5.8, 5.9, and 5.10).

• We have found the difference of the degree of processing of dust grains between Orion A and Taurus, inferred from $F_{11.3}/F_{9.8}$ distributions (Figure 5.12) is statistically significant for FDs.[1] The small dust grains in ONC FDs are closer to pristine on the average, and the small dust grains in the Taurus FDs must have much larger crystalline and >1 μm mass fractions than those in ONC, based on the $F_{11.3}/F_{9.8}$. Combining $F_{11.3}/F_{9.8}$ of disks in NGC 1333 (Arnold et al., 2012) and Cha I (Manoj et al., 2011), the median $F_{11.3}/F_{9.8}$ increases as the average age increases: 0.5 (NGC1333) < 0.52 (ONC) < 0.56 (Tau) < 0.59 (Cha I). Recalling that no significant differences in n_{13-31} between Orion A and Taurus, this indicates that the time scales for dust processing must exceed those of sedimentation.

• The TDs of L1641 are more likely to have significant concentrations of processed grains than the FDs (Figure 5.12), again judging by $F_{11.3}/F_{9.8}$. In contrast, there is no significant difference between the ONC's TDs and FDs in the degree of dust processing (Figure 5.5). The dust grains in TDs of Taurus are much closer to pristine than TDs of ONC. Therefore the dust processing in TDs must be much complicated than that in FDs.

[1]This cannot be due to the only substantial, relevant systematic difference between Orion and Taurus disks: the typical extinction toward the YSOs. Overcorrection for the larger Orion extinction in the lower range of the McClure (2009) curves could potentially produce artificially pristine silicate profiles. However, this would produce other artifacts for which we have searched unsuccessfully in the results, as described in Chapters 3–4. It would also lead to a large anti-correlation between $F_{11.3}/F_{9.8}$ and A_V, but we see no significant correlation between these quantities.

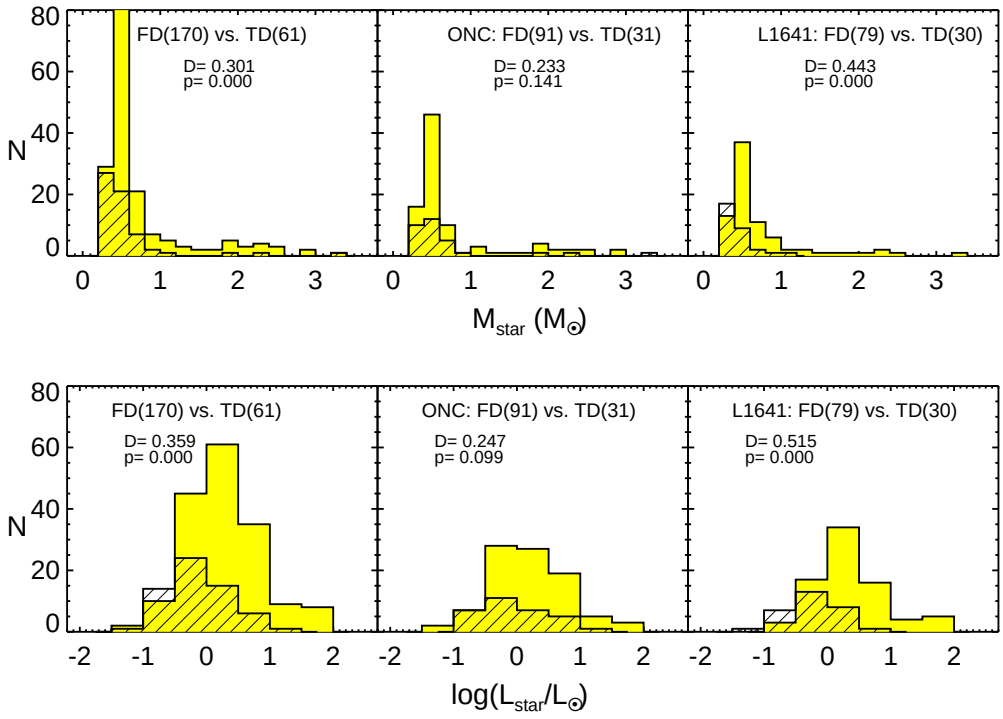


Figure 5.1 Distribution of $M_\star$ and $L_\star$ separated by FDs (yellow solid) and TDs (hatched) and OriA/ONC/L1641 (left/middle/right).

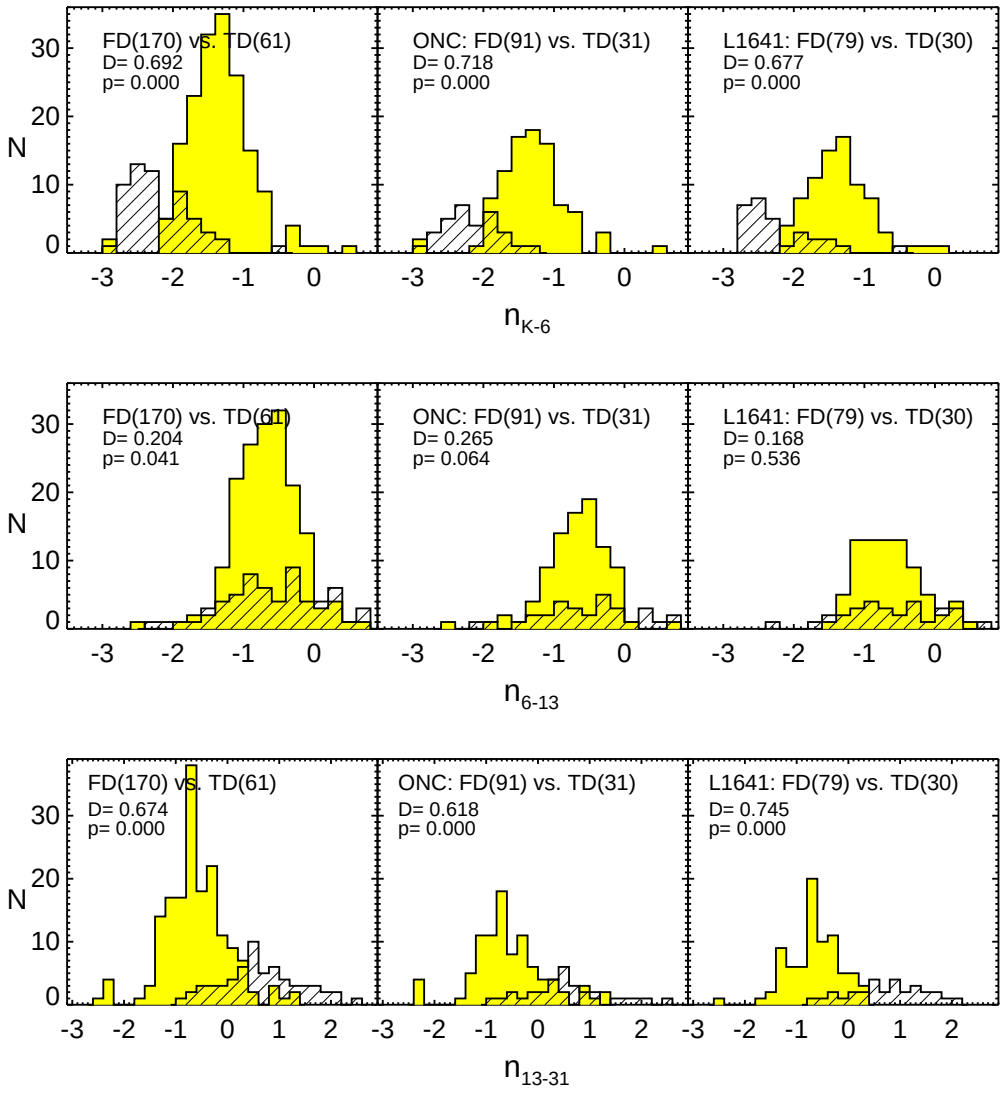


Figure 5.2 Distribution of n_{K-6}, n_{6-13}, and n_{13-31} separated by FDs (yellow solid) and TDs (hatched) and OriA/ONC/L1641 (left/middle/right).

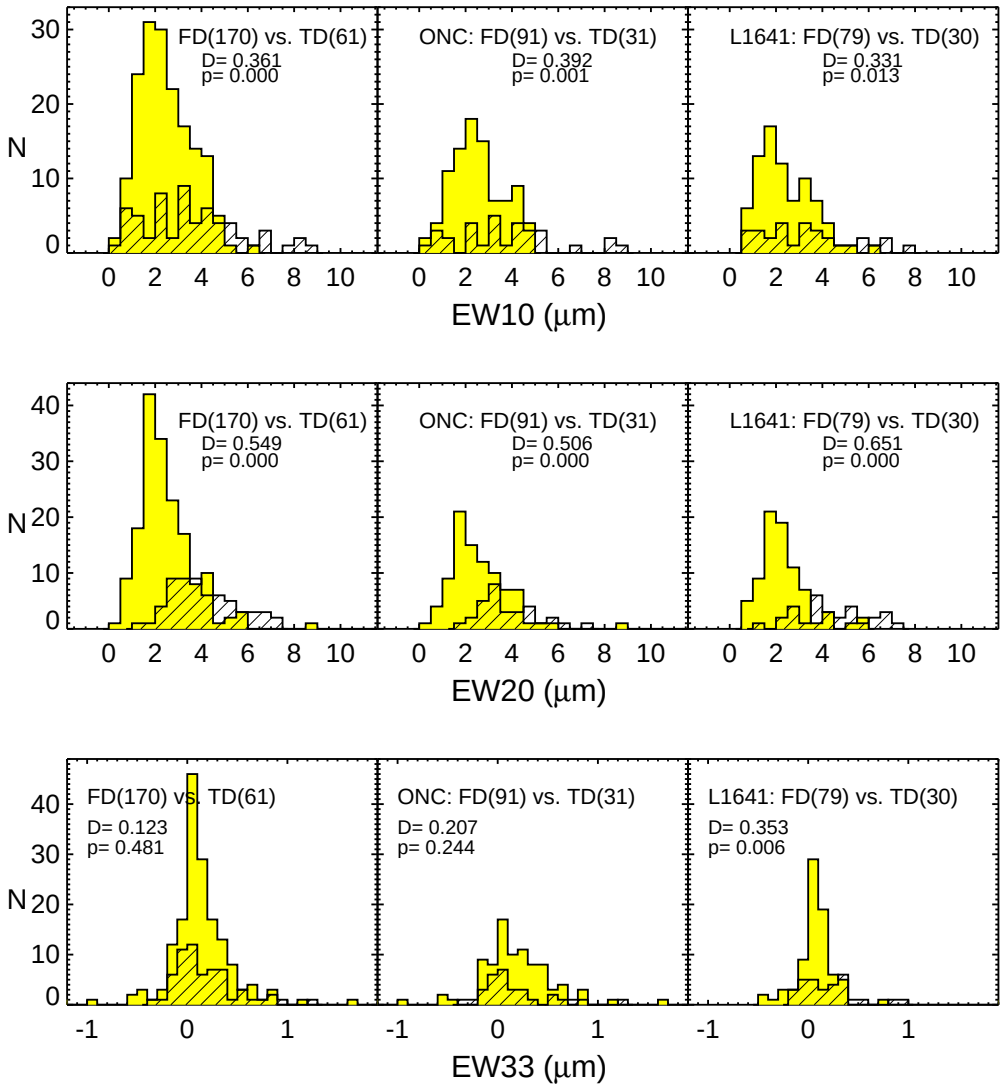


Figure 5.3 Distribution of EW10, EW20, and EW33 separated by FDs (yellow solid) and TDs (hatched) and OriA/ONC/L1641 (left/middle/right).

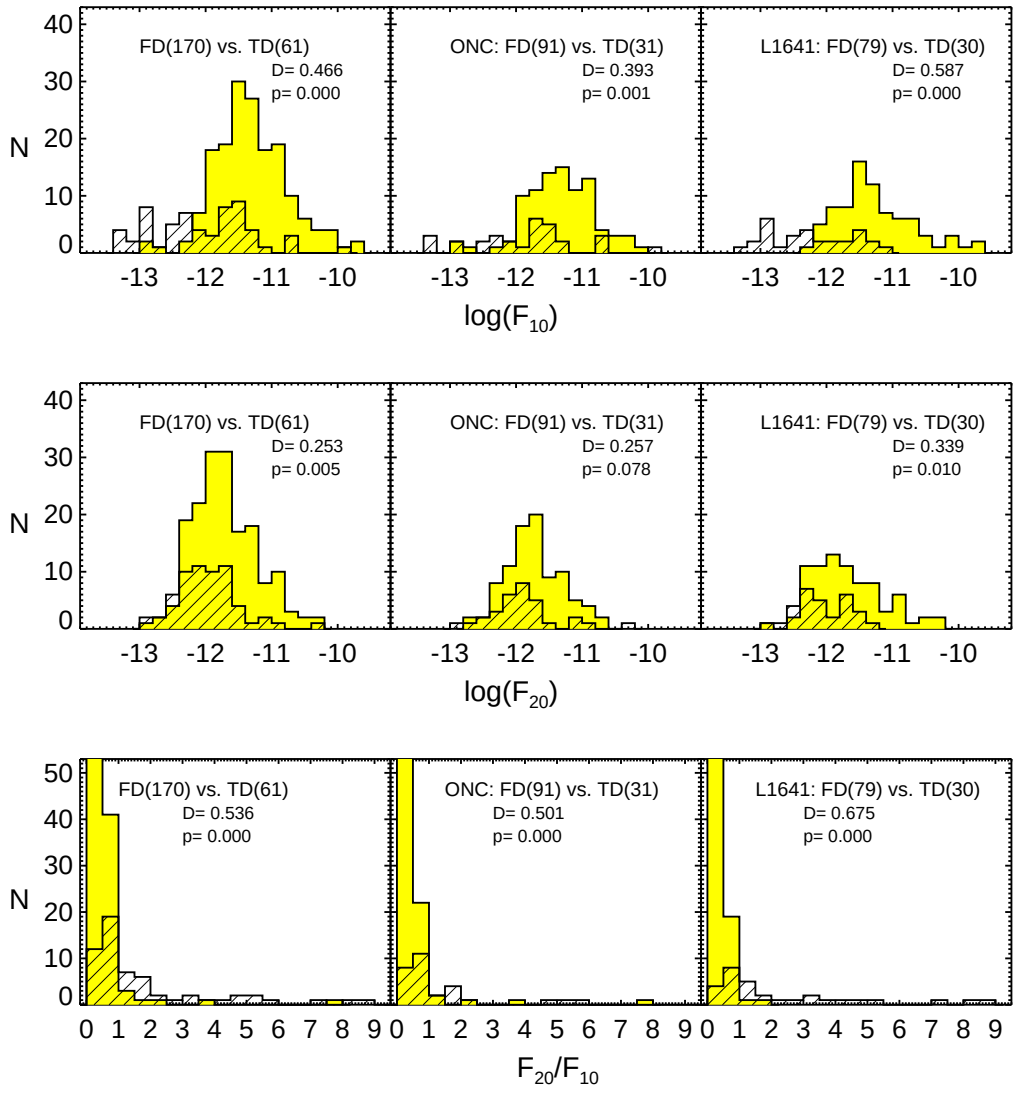


Figure 5.4 Distribution of F_{10}, F_{20}, and F_{20}/F_{10} separated by FDs (yellow solid) and TDs (hatched) and OriA/ONC/L1641 (left/middle/right).

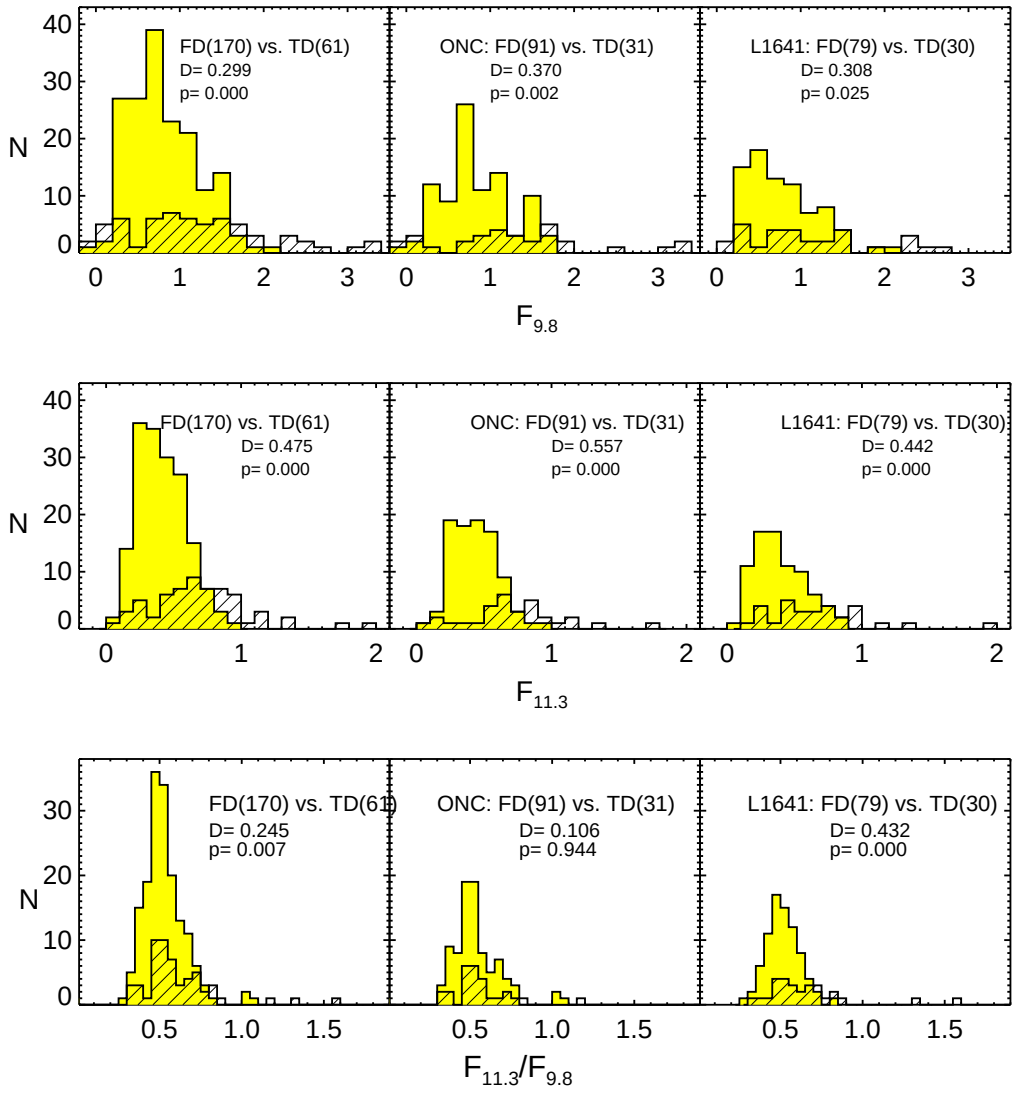


Figure 5.5 Distribution of $F_{9.8}$, $F_{11.3}$, and $F_{11.3}/F_{9.8}$ separated by FDs (yellow solid) and TDs (hatched) and OriA/ONC/L1641 (left/middle/right).

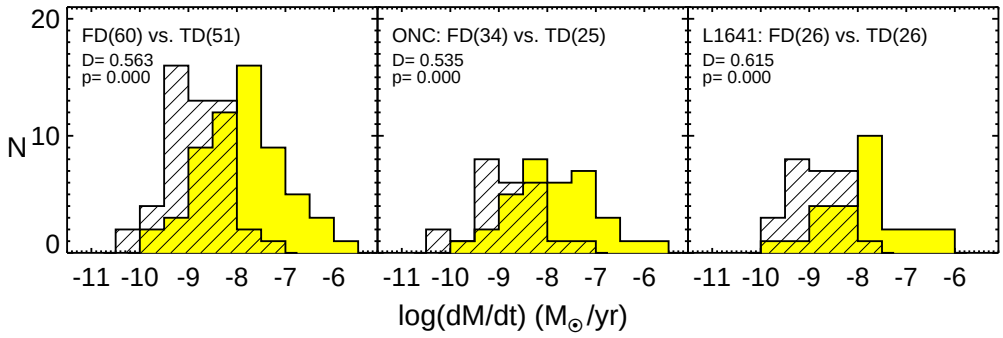


Figure 5.6 Distribution of $\dot{M}$ separated by FDs (yellow solid) and TDs (hatched) and OriA/ONC/L1641 (left/middle/right).

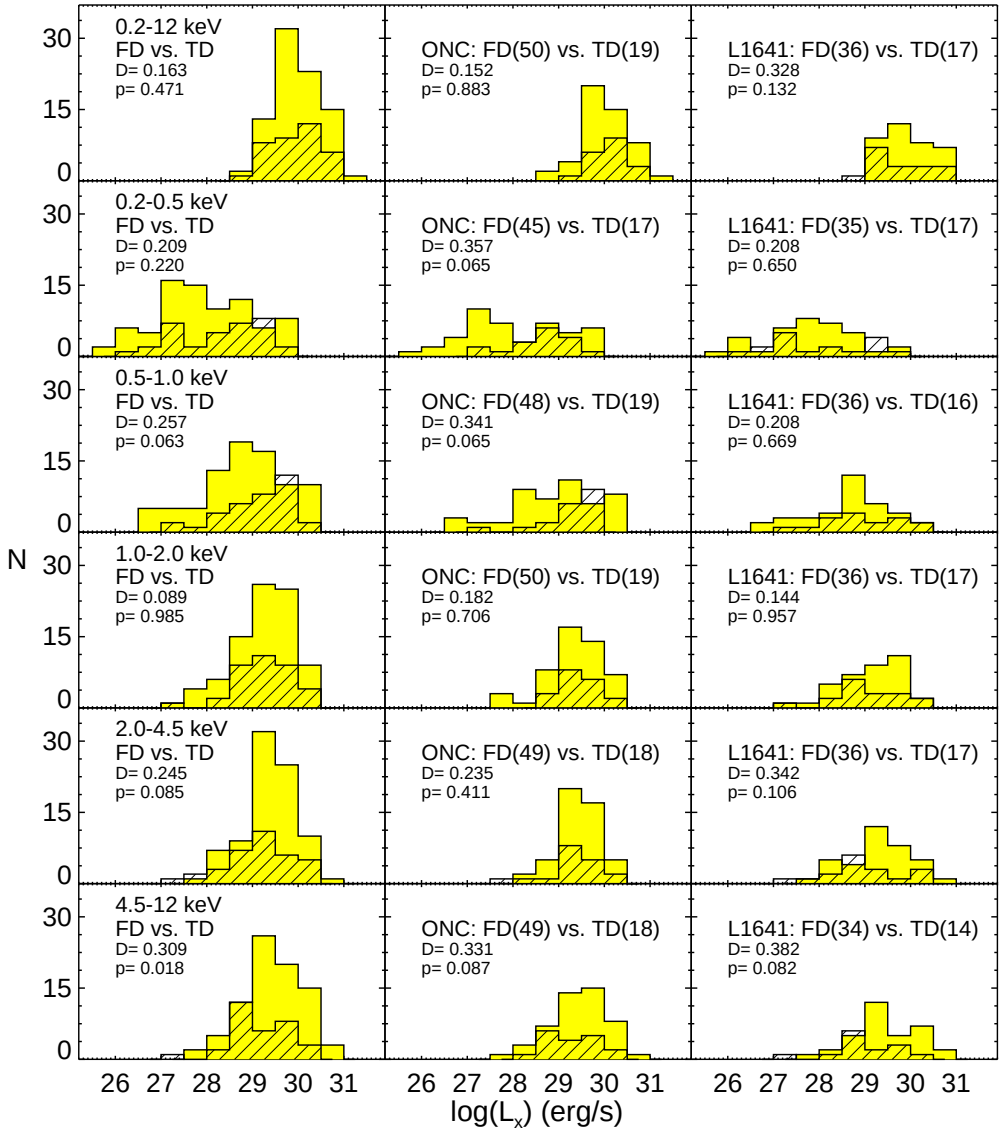


Figure 5.7 Distribution of several L_X by energy bands separated by FDs (yellow solid) and TDs (hatched) and OriA/ONC/L1641 (left/middle/right).

Table 5.2 Distribution of Properties Comparison to Taurus:FD and TD

			K-S test					
		Taurus	Ori A		ONC		L1641	
	parameter	Median	D	p	D	p	D	p
FD	n_{K-6}	-1.49	0.13	0.14	0.16	0.11	0.13	0.36
	n_{6-13}	-0.87	0.20	<0.01	0.23	<0.01	0.18	0.06
	n_{13-31}	-0.54	0.15	0.05	0.16	0.12	0.17	0.10
	EW(10μm)	1.56	0.32	<0.01	0.38	<0.01	0.26	<0.01
	$F_{11.3}/F_{9.8}$	0.56	0.22	<0.01	0.21	0.02	0.24	<0.01
TD	n_{K-6}	-1.89	0.34	0.14	0.36	0.15	0.36	0.15
	n_{6-13}	-0.75	0.17	0.90	0.21	0.77	0.13	1.00
	n_{13-31}	0.71	0.23	0.55	0.30	0.32	0.24	0.60
	EW(10μm)	4.67	0.41	0.04	0.38	0.10	0.44	0.04
	$F_{11.3}/F_{9.8}$	0.50	0.27	0.35	0.19	0.84	0.38	0.11

Note. — D is the maximum deviation between the cumulative distribution of two groups. p indicates the probability that there is no significant difference between the distributions

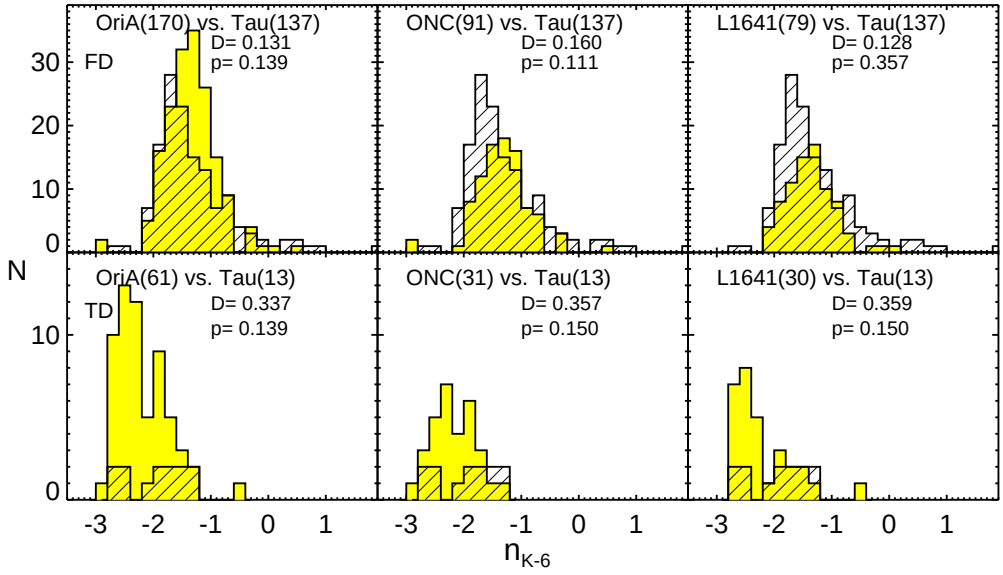


Figure 5.8 Comparison of n_{K-6} between Orion A (yellow solid) and Taurus (hatched). Sub-samples are separated by FDs/TDs (upper panels/lower panels) and OriA/ONC/L1641 (left/middle/right).

5.2 Correlations

Here we search for significant correlations from any combinations of two properties from all available parameters we have: $M_\star$, $L_\star$, n_{K-6}, n_{6-13}, n_{13-31}, F_{10}, F_{20}, F_{20}/F_{10}, $F_{11.3}$, $F_{9.8}$, $F_{11.3}/F_{9.8}$, EW10, EW20, EW33, $\dot{M}$, L_X total, L_X band 1, L_X band 2, L_X band 3, L_X band 4, and L_X band 5. We have subdivided the search into the several sub-groups of our sample, separated by disk structure (All, TDs, or FDs) and by sub-regions (OriA, ONC, or L1641) among objects having spectral type information, and among objects regardless of the availability of spectral type information. The exhaustive results are

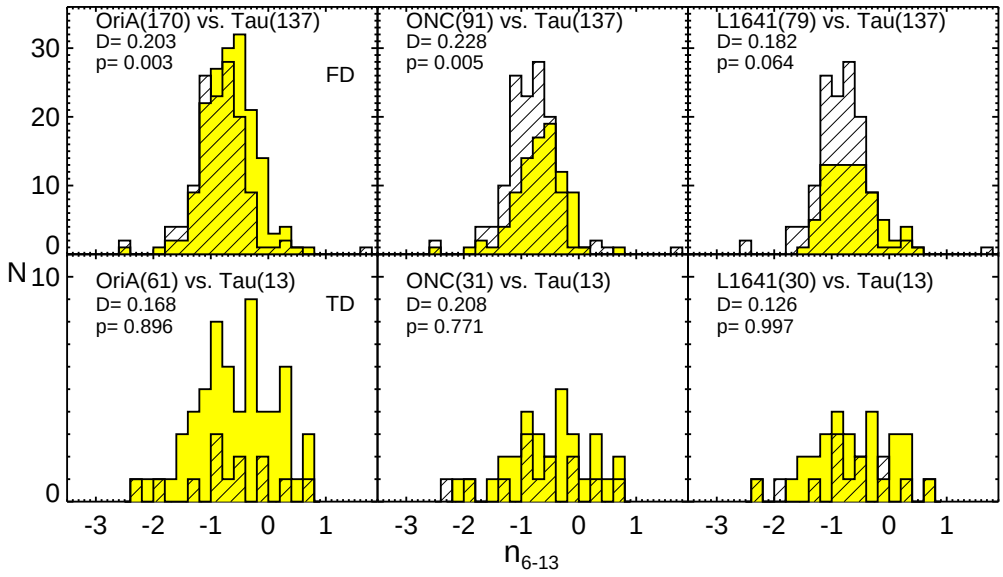


Figure 5.9 Comparison of n_{6-13} between Orion A (yellow solid) and Taurus (hatched). Sub-samples are separated by FDs/TDs (upper panels/lower panels) and OriA/ONC/L1641 (left/middle/right).

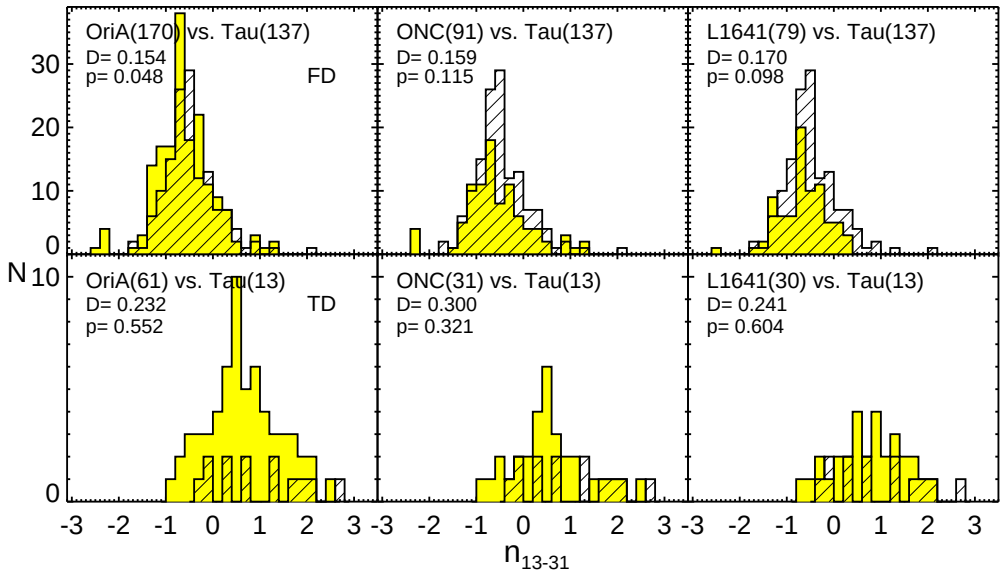


Figure 5.10 Comparison of n_{13-31} between Orion A (yellow solid) and Taurus (hatched). Sub-samples are separated by FDs/TDs (upper panels/lower panels) and OriA/ONC/L1641 (left/middle/right).

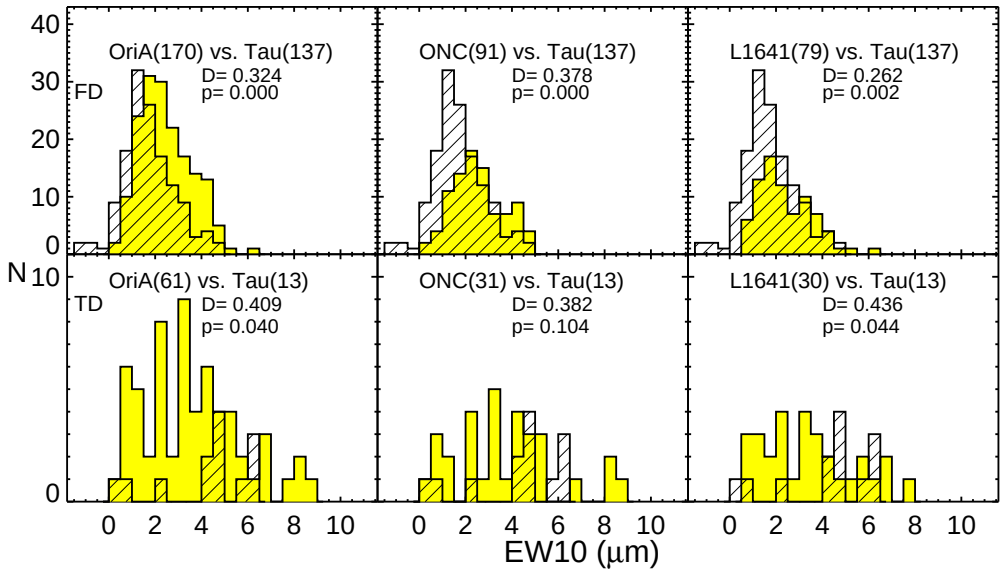


Figure 5.11 Comparison of EW10 between Orion A (yellow solid) and Taurus (hatched). Sub-samples are separated by FDs/TDs (upper panels/lower panels) and OriA/ONC/L1641 (left/middle/right).

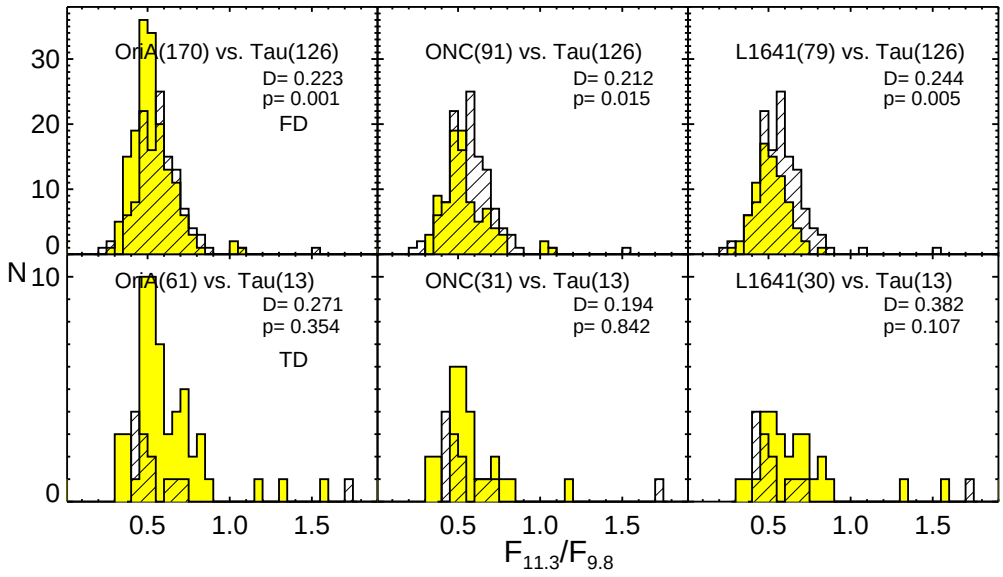


Figure 5.12 Comparison of $F_{11.3}/F_{9.8}$ between Orion A (yellow solid) and Taurus (hatched). Sub-samples are separated by FDs/TDs (upper panels/lower panels) and OriA/ONC/L1641 (left/middle/right).

attached in Appendix C.

In this work, we discuss only the strongest and most significant correlations, in the interest of priority of the discussion.

5.2.1 Categories of significance of correlation

As seen in the tables of each combination of properties in Appendix C, we take three statistical tests to find the strength of correlation between any two properties. We use two methods for rank correlation, Spearman's ρ and Kendall's τ since the properties are not always normally distributed. In addition, we also compute Pearsons's linear correlation coefficient, r. To select definitive trends of importance to disk evolution, we tagged their significance of correlation in 3 (or 7) categories. The rules are following:

• First of all, the correlations are statistically significant, i.e., the corresponding p should be less than 0.05.

• We tagged "5" if all of ρ, τ, and r are greater than 0.5; we tagged "-5" if they indicate anti-correlation with -0.5.

• We tagged "3" if two among ρ, τ, and r are greater than 0.5 and one of them is between 0.5 and 0.3; we tagged "-3" if they indicate anti-correlation.

• We tagged "1" if one among ρ, τ, and r is greater than 0.5 or all of ρ, τ, and r are between 0.5 and 0.3; we tagged "-1" if they indicate anti-correlation.

• We did not tag pairs which do not satisfy any of conditions described above.

We indicate the tags for every pairs from the properties measured from objects with known spectral types in Table 5.3 for ONC disks and Table 5.4 for L1641. The results from all data are in Table C.391 and Table C.392 in

Appendix C. In the Table 5.3 and 5.4, the entries above diagonal indicate correlations from FDs and the area below diagonal is for TDs. This is useful in finding evolution-related (TD vs. FD or ONC vs. L1641) difference in correlation: simply compare corresponding entries above and below.

According to strength and significance of correlation, it is also useful to sort pairs of properties into these evolution-related groups:

• Group A. Pair of properties which are always appeared correlated with each other, tightly and statistically significantly, i.e., tagged as 5 or 3 for samples of TD, FD, ONC, and L1641.

• Group B. Pair of properties in Group B is tagged with 5 or 3 for both TD and FD, but for only one region, ONC or L1641.

• Group C. Pairs in Group C have differences in correlation between FDs and TDs, with the difference from one tag to the other greater than 2. Differences are observed in both ONC and L1641.

• Group D. Pairs differ between FDs and TDs like Group C, but this difference is only observed in one region, ONC or L1641.

Table 5.3 Significance of correlations I: disks in ONC with known spectral types

ONC	P01	P02	P03	P04	P05	P06	P07	P08	P09	P10	P11	P12	P13	P14	P15	p16	P17	P18	P19	P20	P21	P22	P23
P01	···	5		-1	-1								5	1			5	3		1	3	3	
P02	5	···			-1								1	1			1	3		3	1	1	
P03			···																				
P04			3	···																		-1	
P05			-3	-3	···					1					-3								
P06			3			···			-1	1	5	5											
P07							···																
P08								···															
P09									···		-3												
P10			-5		1	-5				···					-3			-1			-1		
P11			3			5				-5	···	5											
P12						5				-3	5	···											
P13	3				-3								···			5	5						
P14	5	1												···			5						
P15			5			5				-5	5	3			···		5						
p16			3			3					3		5			···	5						
P17	3				-1								1	1	3	1	···						
P18																		···					
P19																			···				
P20																				···			
P21																					···		
P22															3	3						···	
P23																							···

Properties measured from Class II disks around host-stars with known spectral types in ONC. Above diagonal is for FD's. Below diagonal is for TD's.
P1: $\log L_\star$; P2: $log M_\star$; P3: n_{K-6}; P4: n_{6-13}; P5: n_{13-31}; P6: EW10; P7: EW20; P8: EW33; P9: $F_{11.3}/F_{9.8}$; P10: F_{20}/F_{10}; P11: $F_{9.8}$; P12: $F_{11.3}$; P13: F_{10}; P14: F_{20}; P15: $\log F_{10}$; P16: $\log F_{20}$; P17: $\log \dot{M}$; P18: $\log L_X(0.2-12keV)$; P19: $\log L_X(0.2-0.5keV)$; P20: $\log L_X(0.5-1.0keV)$; P21: $\log L_X(1.0-2.0keV)$; P22: $\log L_X(2.0-4.5keV)$; P23: $\log L_X(4.5-12keV)$
Positive numbers indicate positive correlation; negative numbers indicate negative correlation.
5 or -5: Spearman's ρ, Kendall's τ, and Pearson's r are all greater than 0.5 and the probabilities that these correlations are generated from a random distribution are all less than 0.05.
3 or -3: Two among ρ, τ, and r are greater than 0.5 and the probabilities are all less than 0.05.
1 or -1: ρ, τ, and r are greater than 0.3 and the probabilities are all less than 0.05, but they cannot meet above two conditions.

Table 5.4 Significance of correlations II: disks in L1641 with known spectral types

L1641	P01	P02	P03	P04	P05	P06	P07	P08	P09	P10	P11	P12	P13	P14	P15	p16	P17	P18	P19	P20	P21	P22	P23
P01		5											5	5			5	1			3		1
P02	3												5	3			5	3			1		3
P03															3	3							
P04		-3																					
P05			-3							3													
P06			3								5	5											
P07										3	1	1											
P08																					1		
P09											-1												
P10			-5		5	-5																	
P11			3			5				-5		5											
P12						5				-5	5												
P13	1															5							
P14	3																						
P15			5		-3	5				-5	5	5					1	1					1
p16			1										3				1						
P17	1													1		1							
P18	5																						
P19																							
P20																							
P21	5			-1																			
P22	5			-3																			
P23																							

Properties measured from Class II disks around host-stars with known spectral types in L1641. Above diagonal is for FD's. Below diagonal is for TD's.
P1: $\log L_\star$; P2: $log M_\star$; P3: n_{K-6}; P4: n_{6-13}; P5: n_{13-31}; P6: EW10; P7: EW20; P8: EW33; P9: $F_{11.3}/F_{9.8}$; P10: F_{20}/F_{10}; P11: $F_{9.8}$; P12: $F_{11.3}$; P13: F_{10}; P14: F_{20}; P15: $\log F_{10}$; P16: $\log F_{20}$; P17: $\log \dot{M}$; P18: $\log L_X(0.2-12keV)$; P19: $\log L_X(0.2-0.5keV)$; P20: $\log L_X(0.5-1.0keV)$; P21: $\log L_X(1.0-2.0keV)$; P22: $\log L_X(2.0-4.5keV)$; P23: $\log L_X(4.5-12keV)$
Positive numbers indicate positive correlation; negative numbers indicate negative correlation.
5 or -5: Spearman's ρ, Kendall's τ, and Pearson's r are all greater than 0.5 and the probabilities that these correlations are generated from a random distribution are all less than 0.05.
3 or -3: Two among ρ, τ, and r are greater than 0.5 and the probabilities are all less than 0.05.
1 or -1: ρ, τ, and r are greater than 0.3 and the probabilities are all less than 0.05, but they cannot meet above two conditions.

Group A.

This group has the pairs of properties tagged with 5 or 3 in all cases whether the sample is TD or FD and whether the sample is in ONC or L1641. Table 5.5 lists the pairs in Group A, and Figure 5.13 shows each of the pairs is strongly correlated in any cases of sample groupings. The first pair of properties in Group A is $M_\star$ and $L_\star$, which are tightly correlated by the intrinsic characteristic of Class II objects: this can be considered a "sanity check". The other pairs of properties are all those related to the indicators of grain properties. However, we notice that EW10, $F_{9.8}$, and $F_{11.3}$ which are measured after continuum subtraction and then normalization to the continuum are tightly correlated each other, but they are not correlated to other parameters of dust properties, F_{10} or F_{20}, though the K-S D is large for both sets.

Table 5.5 Group A. Properties with Significant Correlation in Any Case (Known Spectral types only)

properties	ONC (FD, TD)	L1641 (FD, TD)
$\log M_\star$–$\log L_\star$	(5, 5)	(5, 3)
EW10–$F_{9.8}$	(5, 5)	(5, 5)
EW10–$F_{11.3}$	(5, 5)	(5, 5)
$F_{9.8}$–$F_{11.3}$	(5, 5)	(5, 5)
F_{10}–$\log F_{20}$	(5, 5)	(5, 3)

Note. — Two properties in the first column show a very strong and significant correlations regardless of subset by FD/TD or L1641/ONC.

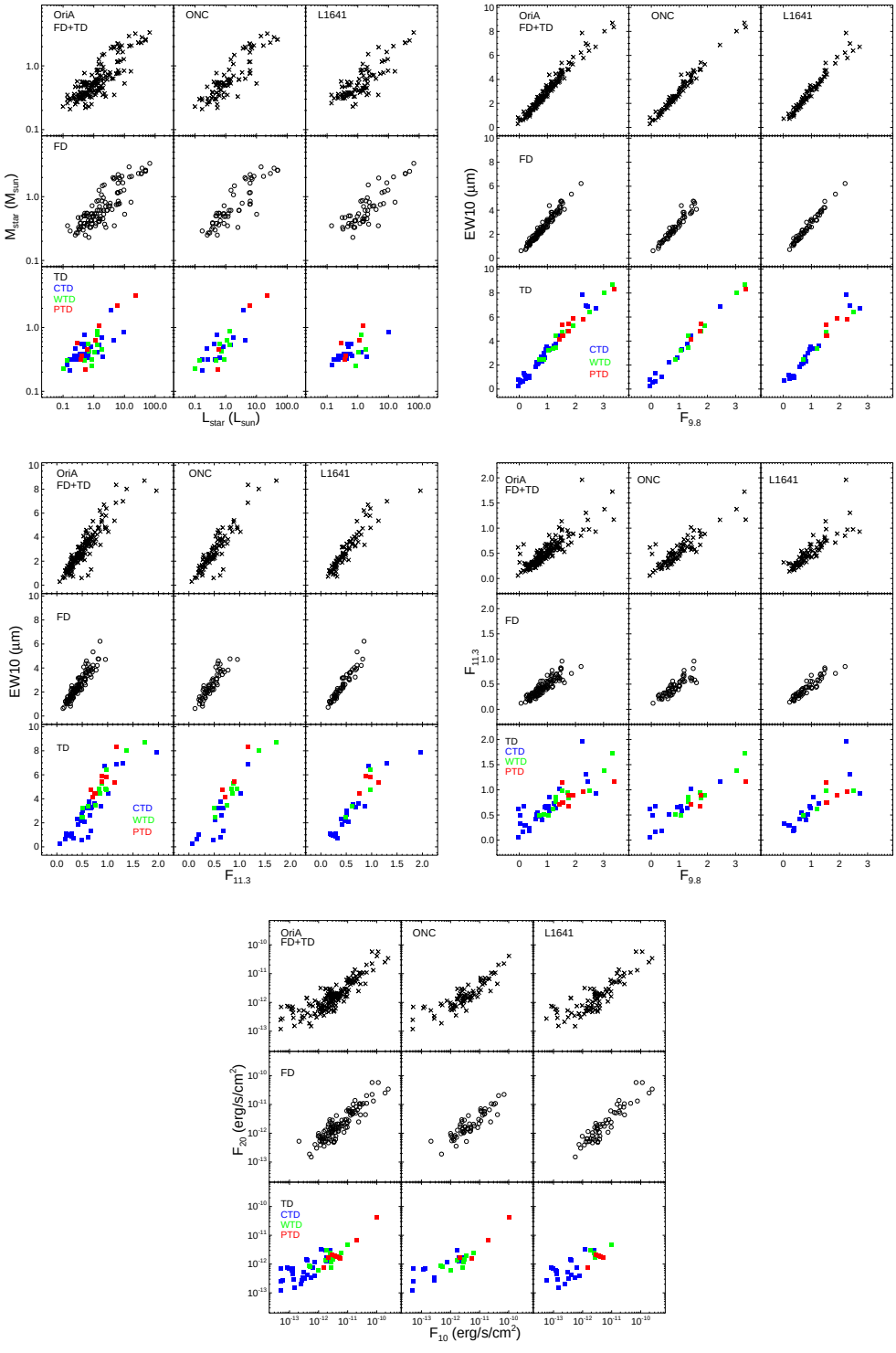


Figure 5.13 Properties in Group A and their correlations.

Group B.

In this group, we gathered the pair of properties with strong correlation in both FD and TD, but the tags for the strong correlation indication appear only for the disks in a subregion of Orion A. Table 5.6 is for the list of the properties in Group B and the dominant region for each of the pairs is also indicated in the table. In this case we must be wary of poor corrrelation which is dominated by a small number of outliers. For instance, from the inspection of the data over the range of each pair of Group B in Figure 5.14, we find the possibility of weak correlation between $L_\star$ and F_{10} of TD in L1641, which is tagged "1", is lack of data points with larger value of F_{10}. In the other way, the tag with "1" to $L_\star$-F_{20} of FDs in ONC could be due to the outliers located in the area for larger $L_\star$ and smaller F_{20}.

Table 5.6 Group B. Properties with Significant Correlation in both TD and FD dominantly in one of L1641 or ONC (Known Spectral types only)

properties	Significance (FD, TD)	Dominant Region
F_{10}–$\log L_\star$	(5, 3)	ONC
F_{20}–$\log L_\star$	(5, 3)	L1641
$\log \dot{M}$–$\log L_\star$	(5, 3)	ONC
$\log \dot{M}$–$\log F_{10}$	(5, 3)	ONC
$\log L_X 3$–$\log L_\star$	(3, 5)	L1641
F_{20}/F_{10}–n_{13-31}	(3, 5)	L1641

Note. — Two properties in the first column show a strong and significant correlations for both FD and TD, dominantly in one of L1641 or ONC.

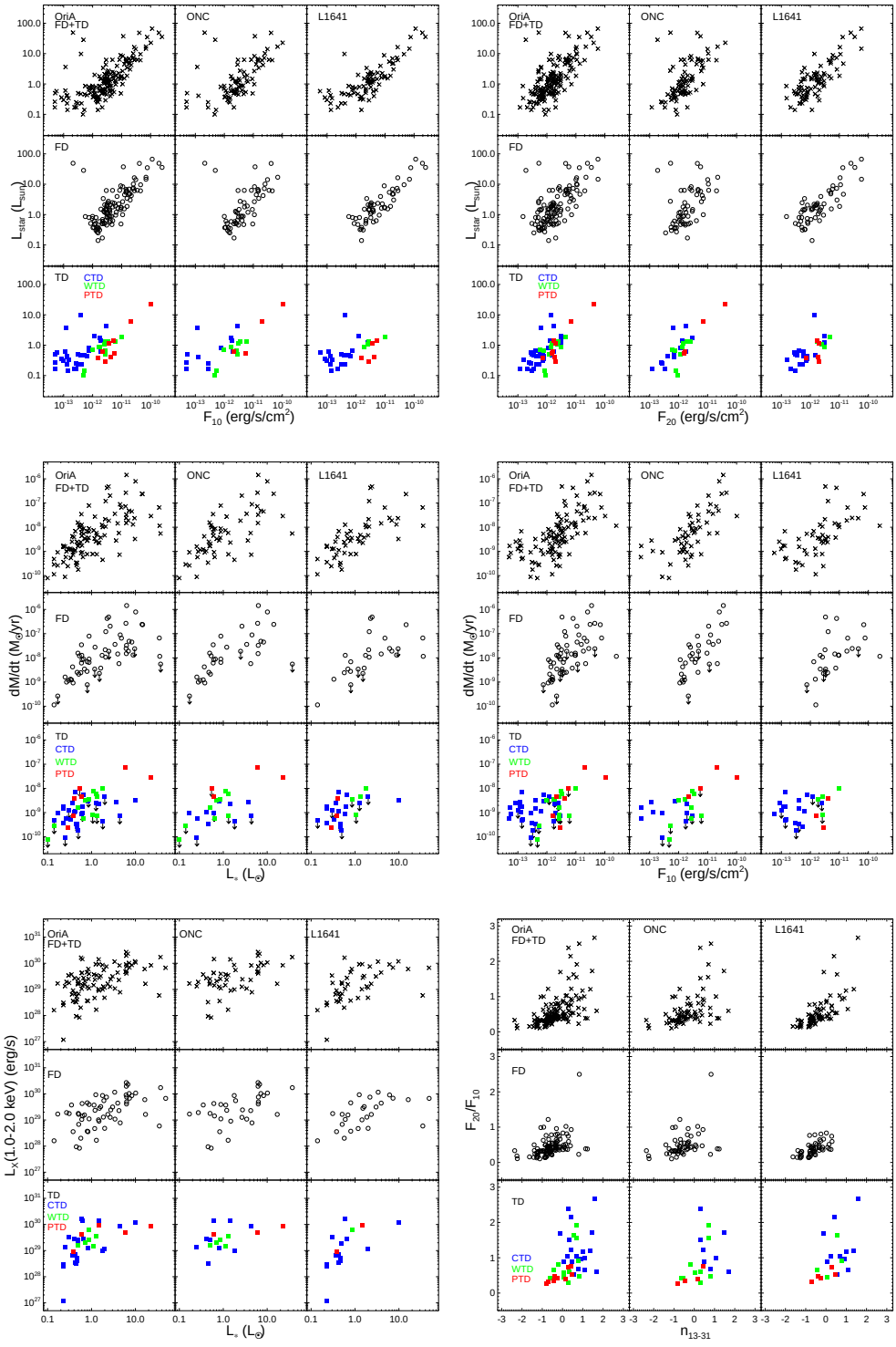


Figure 5.14 Properties in Group B and their correlations.

Group C.

The combination of properties in this group show differences in the correlations of TDs and FDs. The discrepancies appear in both from ONC and L1641. Most pairs of properties in Table 5.7 have correlation differences from FD to TD for ONC and L1641 as indicated by the sets of tag values of FD and TDs. Few pairs show opposite differences between ONC and L1641.

A pair of properties in this group is mostly comprised of a property normalized to a continuum and a property not normalized to continuum, in contrast to Group A. The correlations are plotted in Figure 5.15.

Table 5.7 Group C. Properties observed Correlation Changes between FD and TD in both L1641 and ONC (Known Spectral types only)

properties	ONC (FD, TD)	L1641 (FD, TD)
n_{6-13}–n_{13-31}	(0, -3)	(0, -3)
F_{20}/F_{10}–EW10	(0, -5)	(0, -5)
F_{20}/F_{10}-$F_{9.8}$	(0, -5)	(0, -5)
F_{20}/F_{10}-$F_{11.3}$	(0, -3)	(0, -5)
$\log F_{10}$–EW10	(0, 5)	(0, 5)
$\log F_{10}$–n_{13-31}	(-3, 0)	(0, -3)
$\log F_{10}$–$F_{9.8}$	(0, 5)	(0, 5)
$\log F_{10}$–$F_{11.3}$	(0, 3)	(0, 5)
$\log F_{10}$–F_{20}/F_{10}	(0, -5)	(0, -5)
$\log L_X 8$–$\log M_\star$	(3, 0)	(3, 0)
$\log L_X 8$–$\log L_\star$	(5, 0)	(1, 5)
$\log L_X 4$–$\log L_\star$	(3, 0)	(0, 5)

Note. — Two properties in the first column are observed changes of correlations between FD and TD in both of L1641 or ONC.

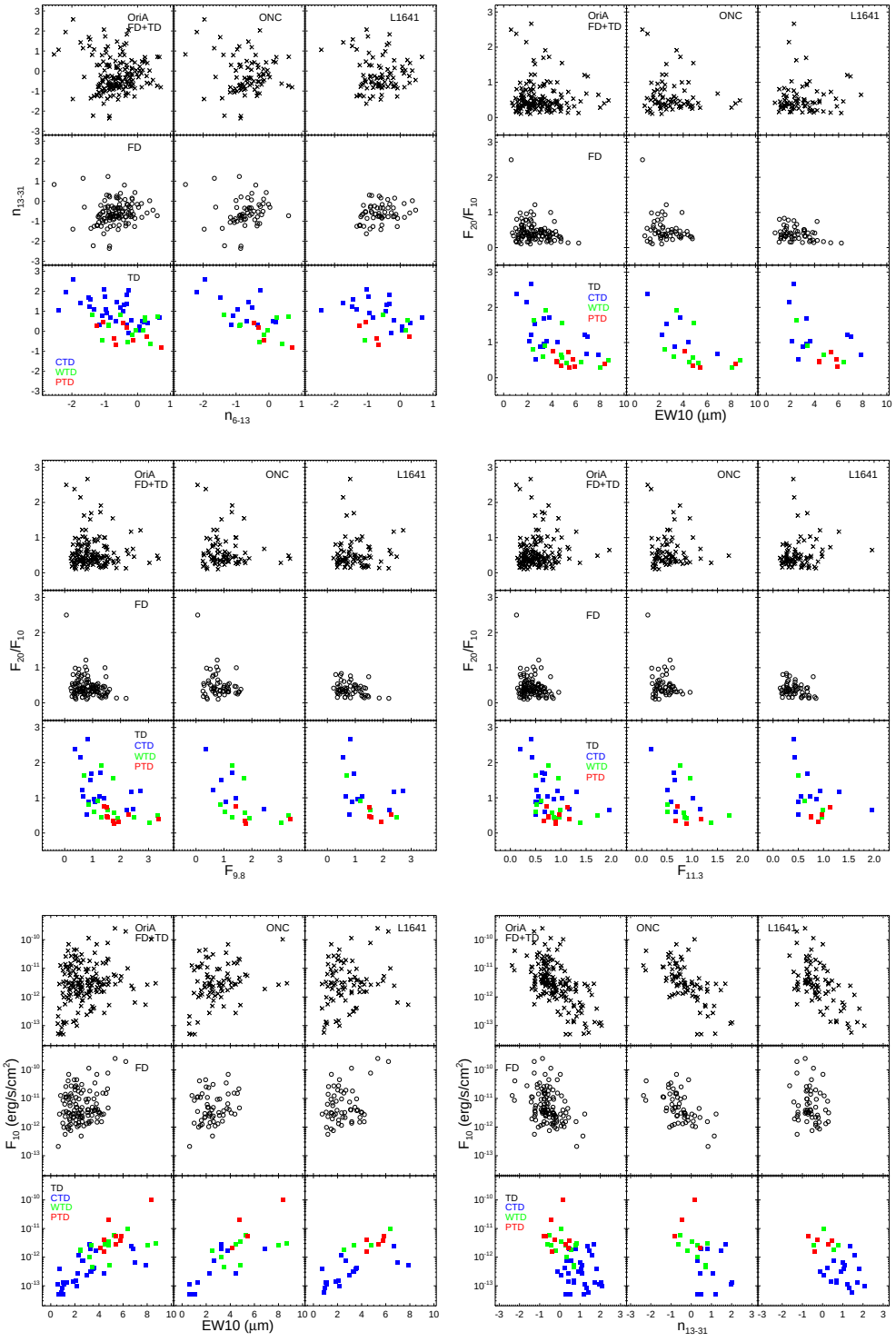


Figure 5.15 Properties in Group C and their correlations.

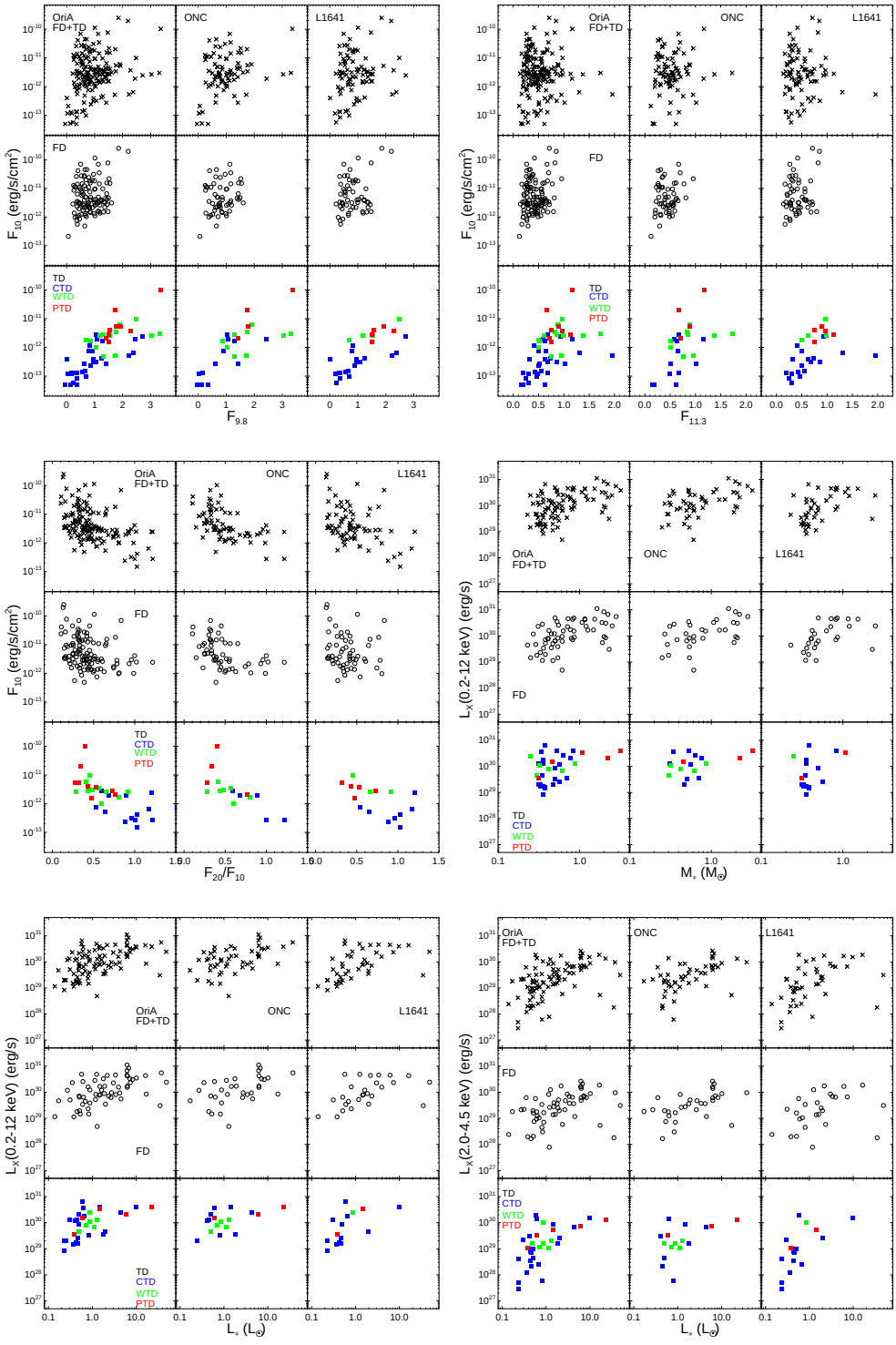


Figure 5.15 (Continued.)

Group D.

This group is the collection of combinations of properties that have tag difference greater than 2 between TD and FD only from one of L1641 and ONC. The list of property pairs are in Table 5.8, and Figure 5.16 show the correlations. As we see from the tag values in the column to indicate significance in Table 5.8, most pair in this group show no correlation for FDs. The difference of tags between FDs and TDs are mostly 3 rather than 5. However, this difference between no correlation and marginal correlation could still be an important clue to understand the mechanisms of disk evolution. Therefore, we keep the list of Group D for more investigation in the future.

Table 5.8 Group D. Properties observed Correlation Changes between FD and TD dominantly one of L1641 and ONC (Known Spectral types only)

properties	Significance (FD, TD)	Dominent Region
n_{K-6}–n_{6-13}	(0, 3)	ONC
n_{K-6}–n_{13-31}	(0, -3)	ONC
n_{K-6}–EW10	(0, 3)	ONC
n_{K-6}–F_{20}/F_{10}	(0, -5)	ONC
n_{K-6}–log F_{10}	(0, 5)	ONC
n_{K-6}–log F_{20}	(0, 3)	ONC
log $\dot{M}$–log F_{20}	(5, 1)	ONC
log $M_\star$–n_{6-13}	(0, -3)	L1641
log $M_\star$–F_{10}	(5, 0)	L1641
log $\dot{M}$–log $M_\star$	(5, 0)	L1641
$F_{9.8}$–$F_{11.3}/F_{9.8}$	(0, -3)	ONC
$F_{9.8}$–F_{20}	(0, 3)	ONC
log F_{10}–EW10	(0, 5)	ONC
log L_X2–log $M_\star$	(3, 0)	ONC
log L_X5–log $M_\star$	(3, 0)	L1641
log L_X4–n_{6-13}	(0, -3)	L1641
F_{20}/F_{10}–EW20	(3, 0)	L1641

Two properties in the first column are observed changes of correlations between FD and TD dominantly in one of L1641 or ONC.

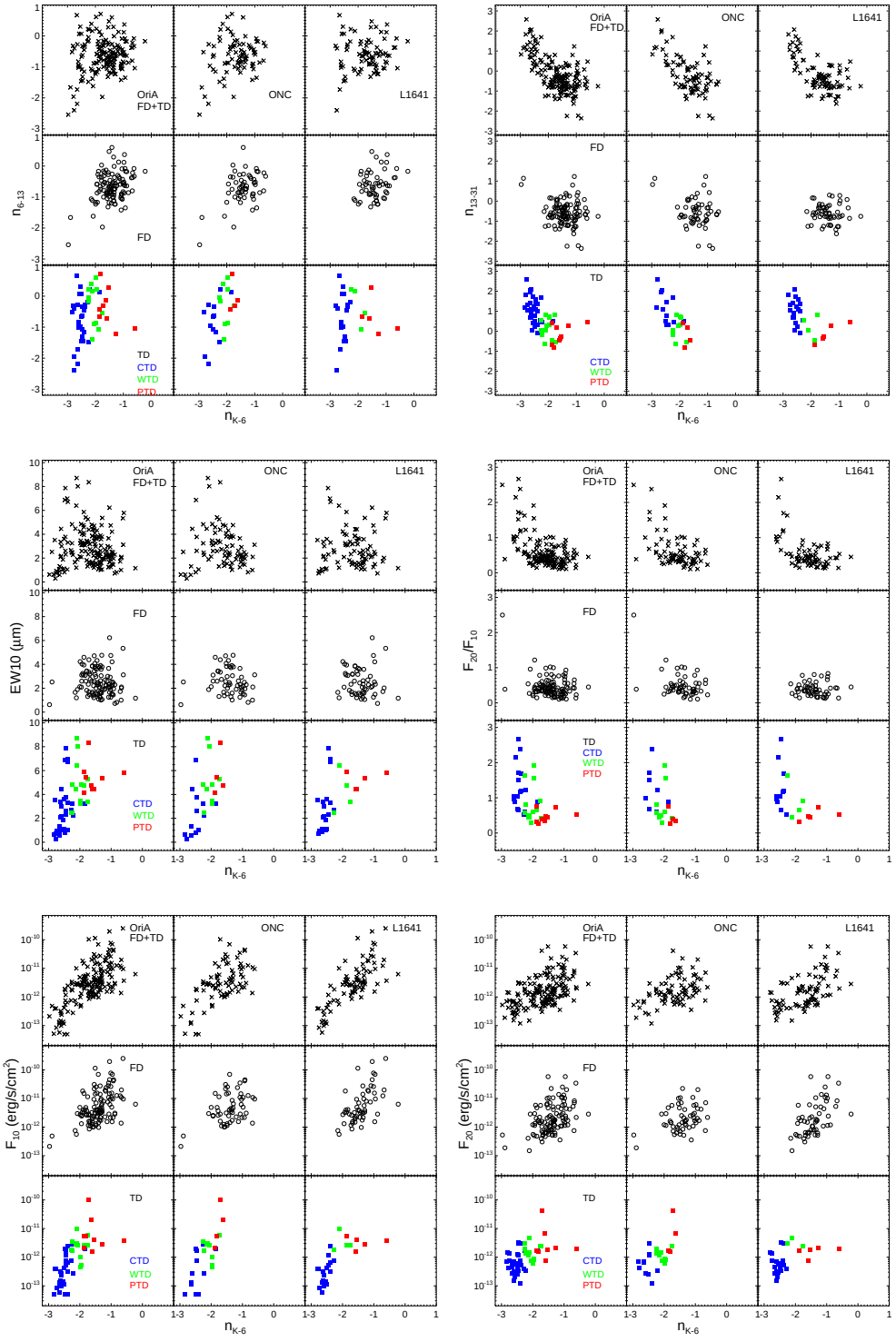


Figure 5.16 Properties in Group D and their correlations.

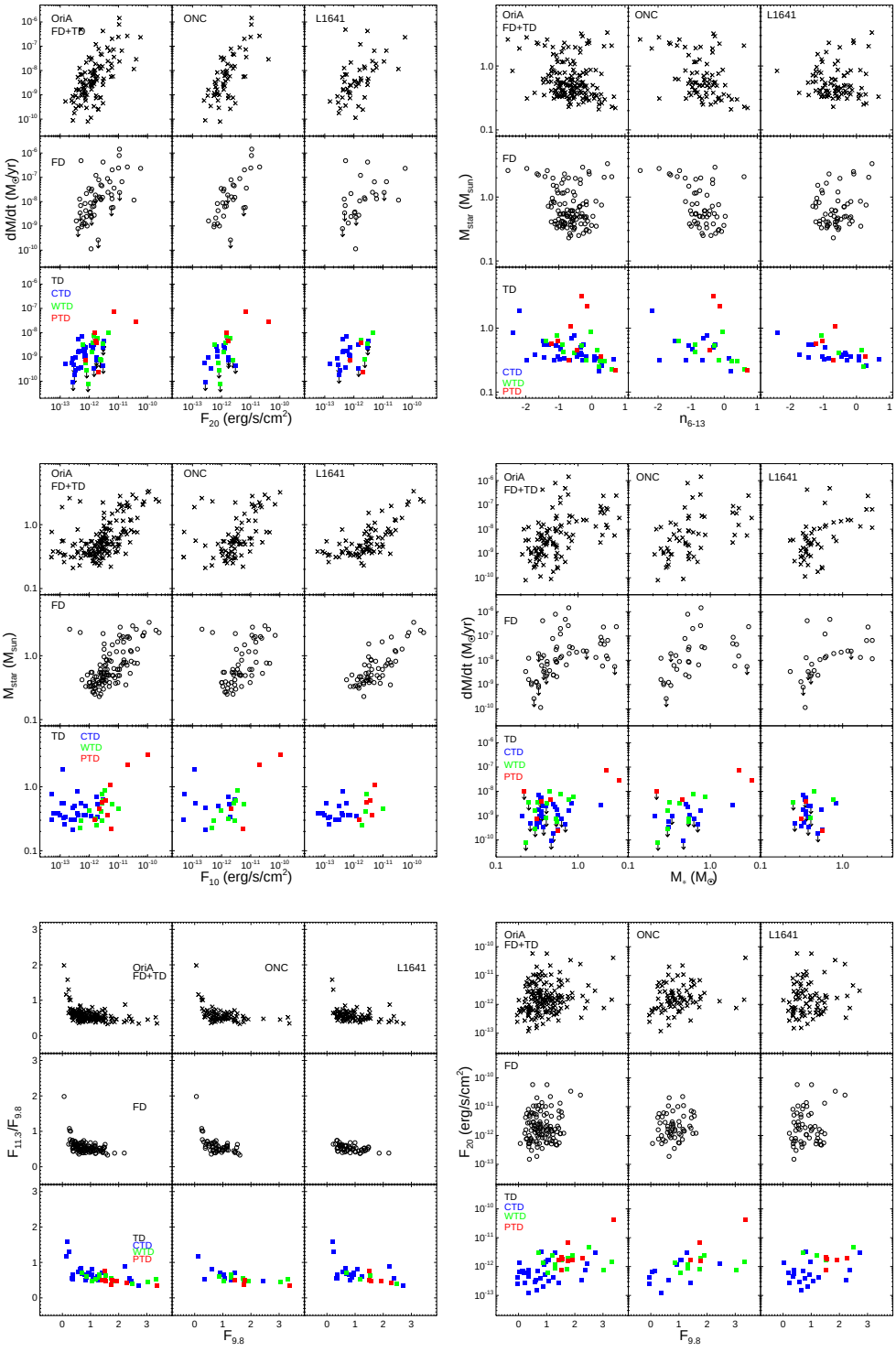


Figure 5.16 (Continued.)

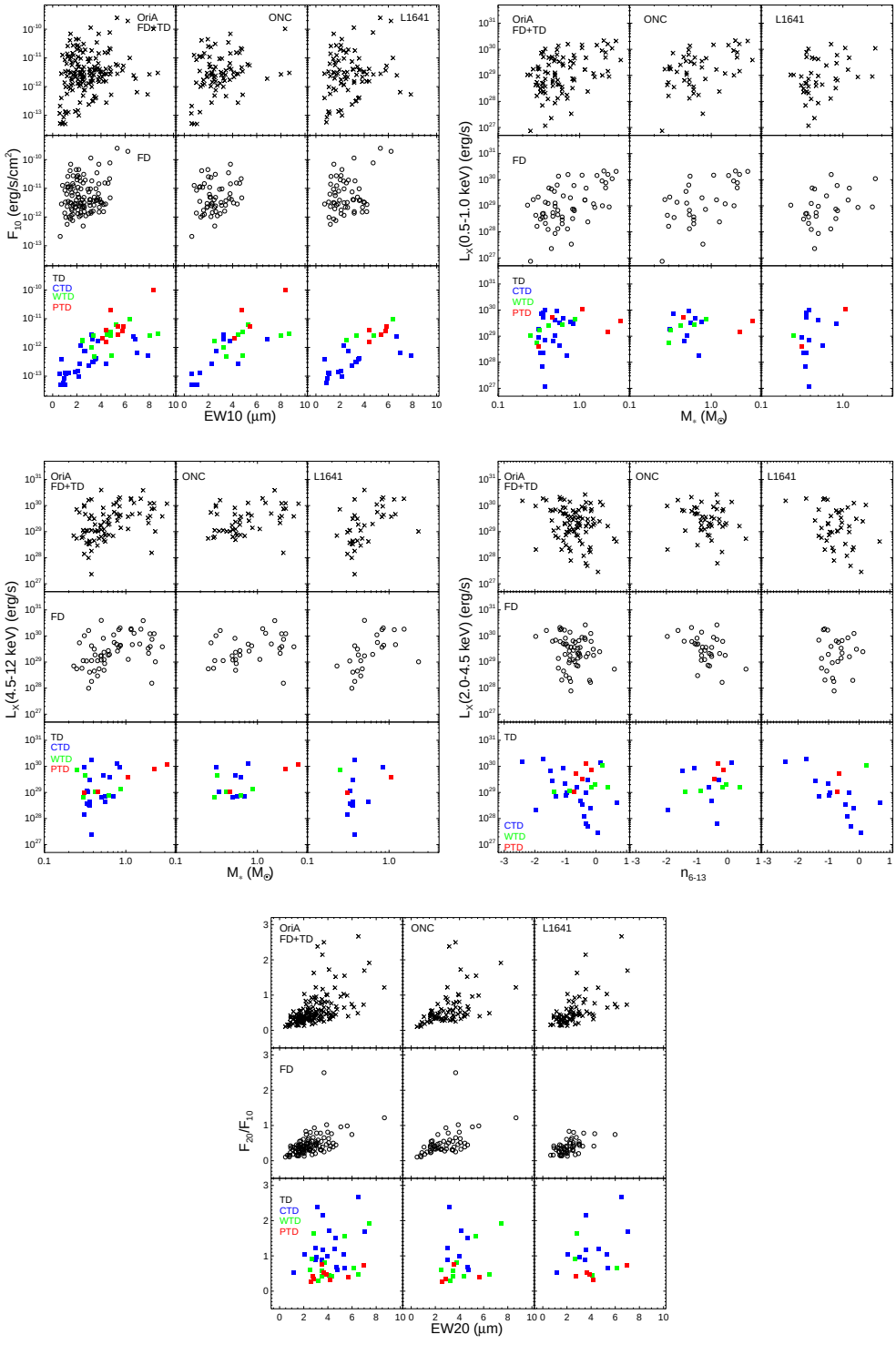


Figure 5.16 (Continued.)

5.3 Summary

We have examined characteristics of disk evolution from FDs to TDs by comparing the distribution of each properties between FDs and TDs. We also compared Orion A disks to Taurus disks in the manner of Orion A FD versus Taurus FD and Orion A TD versus Taurus TD. We confirmed that n_{K-6} and n_{13-31}, and EW10 are good parameters to separate TDs and FDs, and EW20, F_{10}, F_{20}, F_{20}/F_{10} are also the parameters having different distributions for FDs and TDs.

We note that substantially decrease of F_{10}, and increase of EW10, is associated with the TD phase of disk evolution, in Orion as in other YSO associations. This is a reflection of the formation of the gap in the optically-thick dust disk. The decrease of continuum is larger than the decrease in silicate-feature emission.

We have observed a statistically significant difference of $F_{11.3}/F_{9.8}$ distribution between ONC and Taurus for FDs. We conclude that the time scales for dust processing – crystallization and elimination of submicron sized grains by growth – must exceed those of sedimentation based on (1) the median $F_{11.3}/F_{9.8}$ increment with the average age: 0.5 (NGC1333) $<$ 0.52 (ONC) $<$ 0.56 (Tau) $<$ 0.59 (Cha I) and (2) no significant differences in n_{13-31} between Orion A and Taurus.

We found no significant difference between TDs and FDs in ONC, in which small grains are closer to pristine and less processed compared to FDs in L1641 and Taurus. However, the TDs of L1641 indicate more processed grains compared to the FDs in L1641 and even compared to the FDs in Taurus. The

dust grains in TDs of Taurus are much closer to pristine than TDs of ONC. Therefore the dust processing in TDs must be much complicated than that in FDs.

We examined the relations between properties and searched for some trends falling in four categories: Group A for the properties always correlated with high significance; Group B for the properties with strong correlations in both TDs and FDs in one region; Group C for the properties having a correlation difference between FDs and TDs; Group D for the properties having a correlation change between FDs and TDs but only in one region. Even though we do not infer or conclude from the list of property pairs falling in Group A, B, C, and D in this thesis, this is useful for the future investigation to understand disk evolution and the related characteristics.

6 The Evolution of Protoplanetary Disks in an OB Association

6.1 Introduction

The Orion A star-forming region is a much richer environment than Taurus and Chamaeleon I, in which the stellar density is small throughout, and the UV radiation field is not much larger than the interstellar field. However, most stars form in denser clusters containing high mass stars (Lada & Lada, 2003), like Orion. Not only the high stellar density in Orion but also the strong ionizing radiation from OB associations affect the evolution of protoplanetary disks. The evidence of action of photoevaporative winds from Trapezium cluster over the outer disks of protoplanetary disks within or near the Orion Nebula —"proplyds"— were observed by the *Hubble Space Telescope* (HST): comet-shaped ionized gas clouds surrounding each disk, and smaller-than-usual disk sizes measured directly from the disk silhouette. In this section, we will discuss the effects of star-forming environment particulary within the huge UV field

variation along Orion A to the evolution of protoplanetary disks. A similar study of variation of disk properties with stellar or molecular-cloud density would be interesting as well, but in the interest of finity we place those topics beyond the scope of this dissertation.

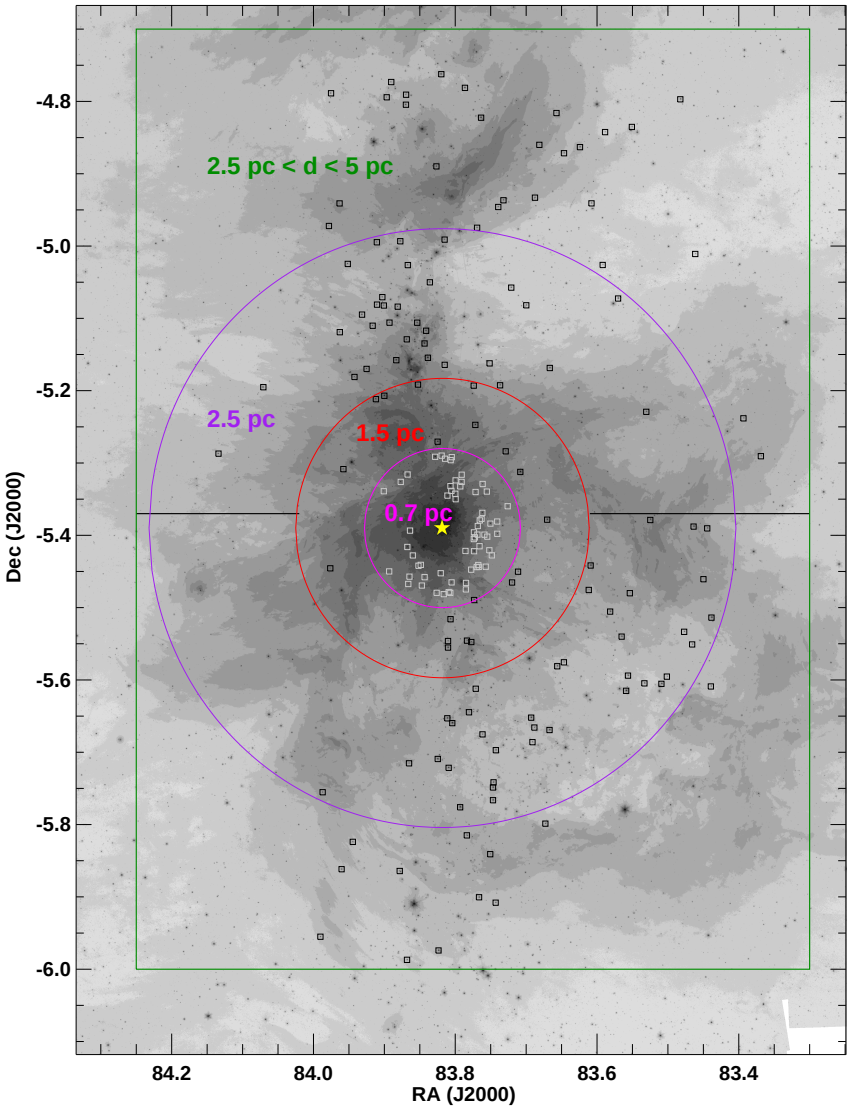


Figure 6.1 IRS targets in the subsections of ONC. This image is revisiting Figure 2.1 with indication of distance range of each section from θ^1 Ori C.

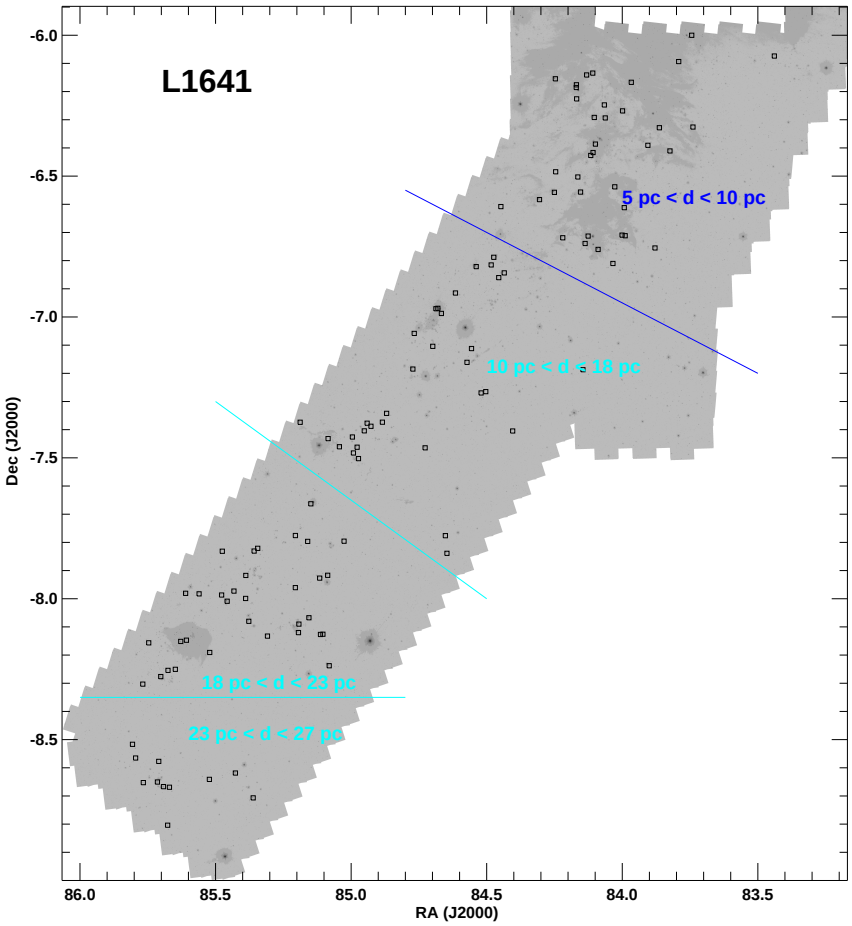


Figure 6.2 IRS targets in the subsections of L1641. This image is revisiting Figure 2.2 with indication of distance range of each section from θ^1 Ori C.

6.2 Disks in Subsections

6.2.1 Median Spectra

As we described in Chapter 2, we assembled the targets belonging to ONC and L1641 into regions with a range of center distance from θ^1 Ori C. We plot the subsections and targets over the images of ONC and L1641 in Figure 6.1

and 6.2. Then we grouped the targets in each subsection by spectral types: A0–K4, K5–M2, and M3–M6. Then, we generated a median spectrum of each spectral-type group of each subsection as the manner we generated the median spectra of ONC and L1641 in Chapter 3. Each spectrum is normalized to a median H-band of each subgroup for median calculation. TDs of all three types are omitted. For a fair comparison of each median as well as a comparison to the Taurus median spectrum, we plot the grid of median spectra of subsection by subregion in Figure 6.3 after normalizing H-band flux of each median spectrum to that of Taurus median. In Figure 6.4, we re-plot the median spectra of A0–K4 and K5–M2 with histograms of spectral types in each subsection for better visual comparison of spectral type distribution which might affect difference of median spectra of each subsection. We do not plot the M3-M6 in Figure 6.4 because the number of objects in each subsection of M3-M6 is very small except in the Trapezium region.

A noticeable feature of the median spectra displayed in Figure 6.3 and Figure 6.4 is the steeply decreasing flux beyond 20 μm of the spectra of targets lying in subsection B, CN, and CS: those closest to θ^1 Ori C. This is consistent with outward truncation of the disks, which would happen more readily the closer disks are to the major UV sources in the Trapezium, as is also the case for the proplyds.

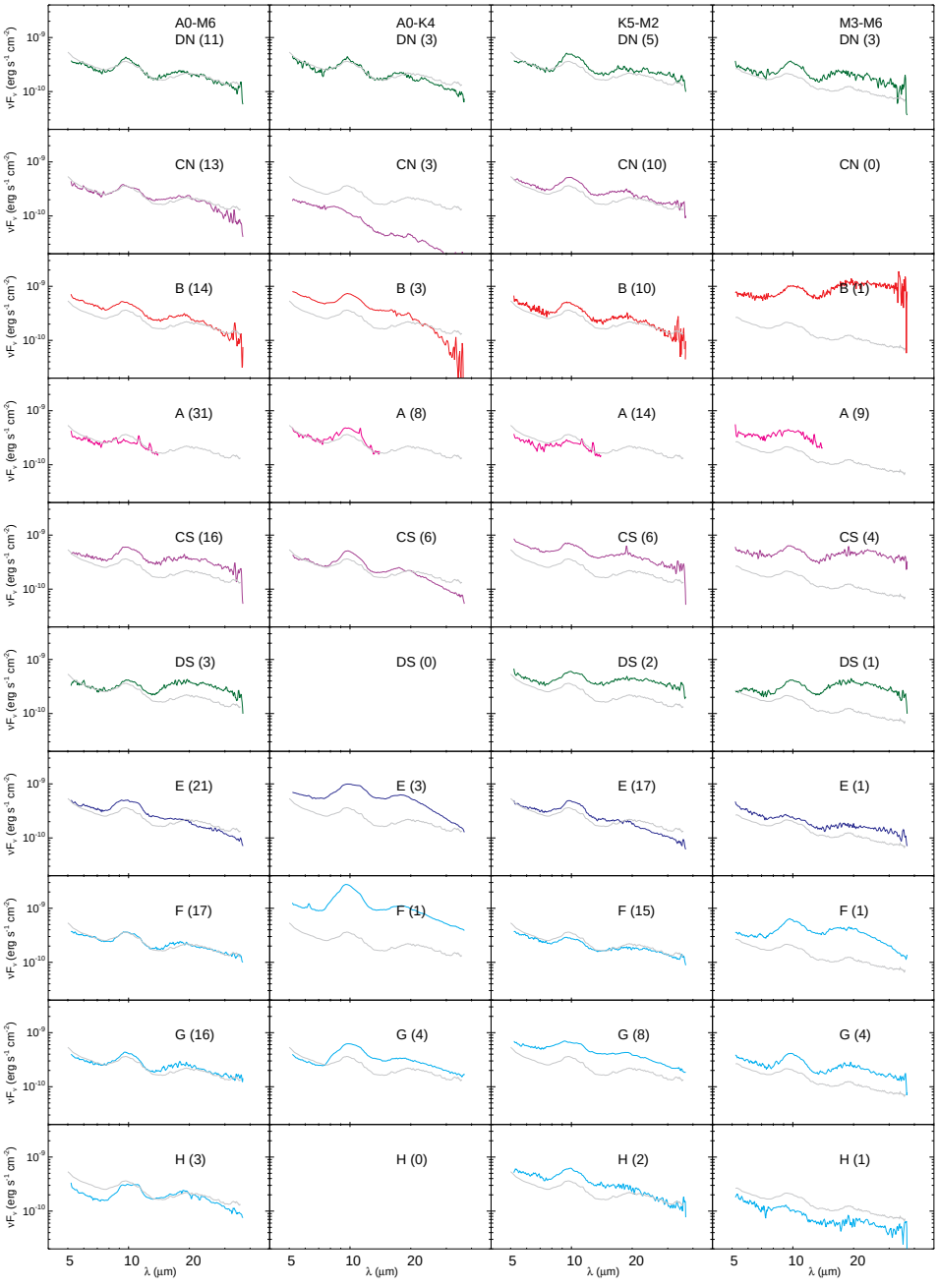


Figure 6.3 Grid of median spectra separated by subsection and ranges of spectral types.

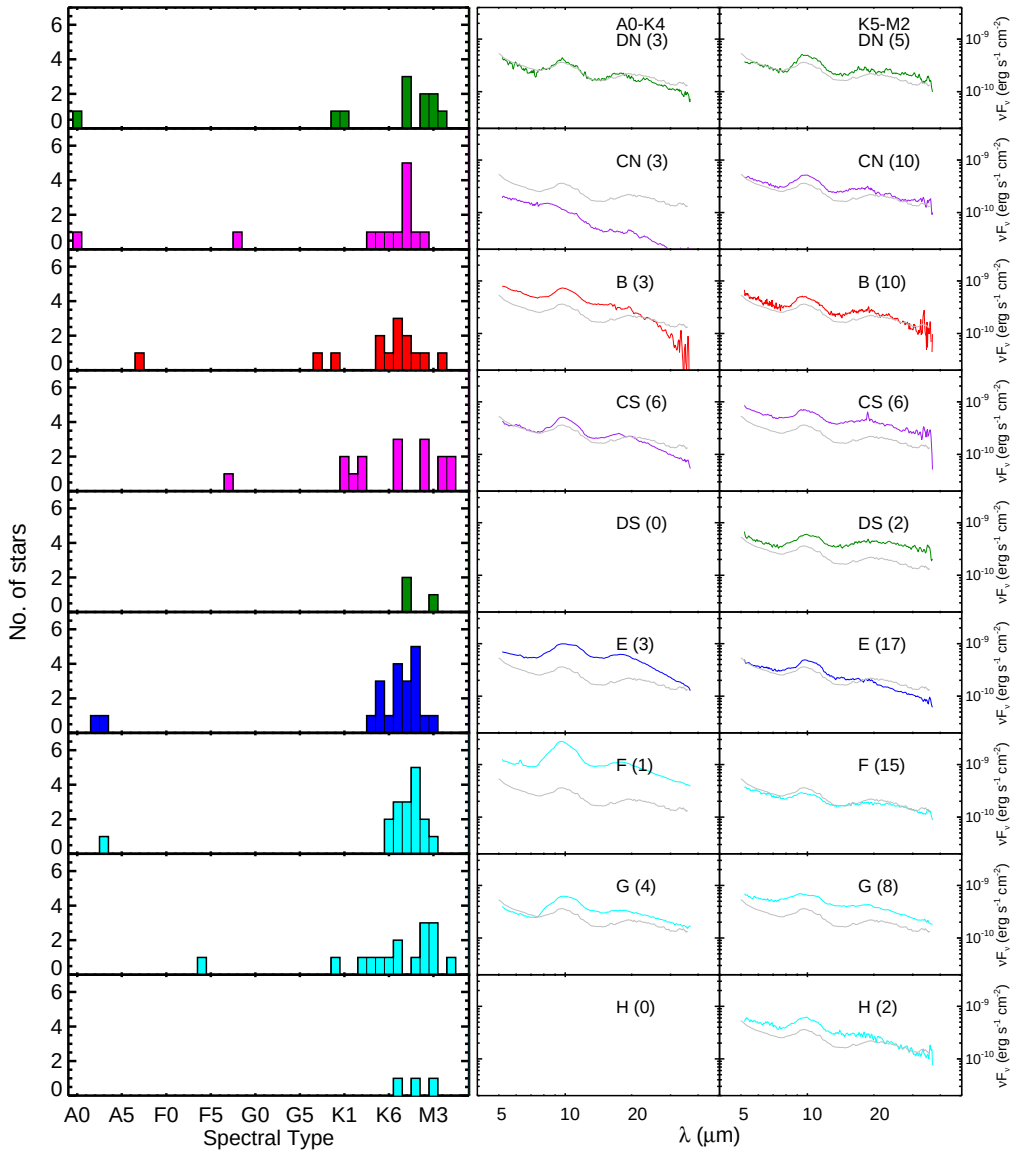


Figure 6.4 Distribution of spectral types of full disks and median spectra by subsections.

6.2.2 Evolutionary Features of Outer Disks by Distance from θ^1 Ori C

Behavior of n_{20-31} and n_{13-31}

To test this hypothesis of outer disk ablation by UV radiation from the Trapezium, we construct a spectral index sensitive to the optically thick continuum of outer disk (r > 5 AU from 5-37 μm coverage of IRS) and the optically thin small dust grain in the surface of the outer disk, n_{20-31}. The anchor points for 20 μm and 31 μm are same as indicated in Table 3.6. The measured n_{20-31} and the projected distances of objects from θ^1 Ori C are listed in Table 6.1.

In Figure 6.5, we compare the distribution of n_{20-31} by subsection and spectral types. We notice the broad distribution pattern of n_{20-31} through the stacked subsections appears curved with a turning point at section B[1], except in M3-M6.

We present the variation of n_{20-31} in finer scale of distance by plotting n_{20-31} and the projected distance of each target from θ^1 Ori C in Figure 6.6. In Figure 6.6 which shows n_{20-31} of FDs, we see that n_{20-31} of FDs in section B increases as distance, d, increases. At greater distance, we do not see the steep variation pattern of n_{20-31} as seen in section B, through section C to L1641.

The spectral index n_{13-31}, implying the outer disk (r > 5 AU) continuum structure, show a distribution with similarly curved pattern Figure 6.7. The distribution of n_{13-31} via distance is in Figure 6.8. The remarkable declining

[1]IRS Spectra of objects in section A do not have LL spectra covering 15–37 μm. So, it is impossible to measure n_{20-31} for section A.

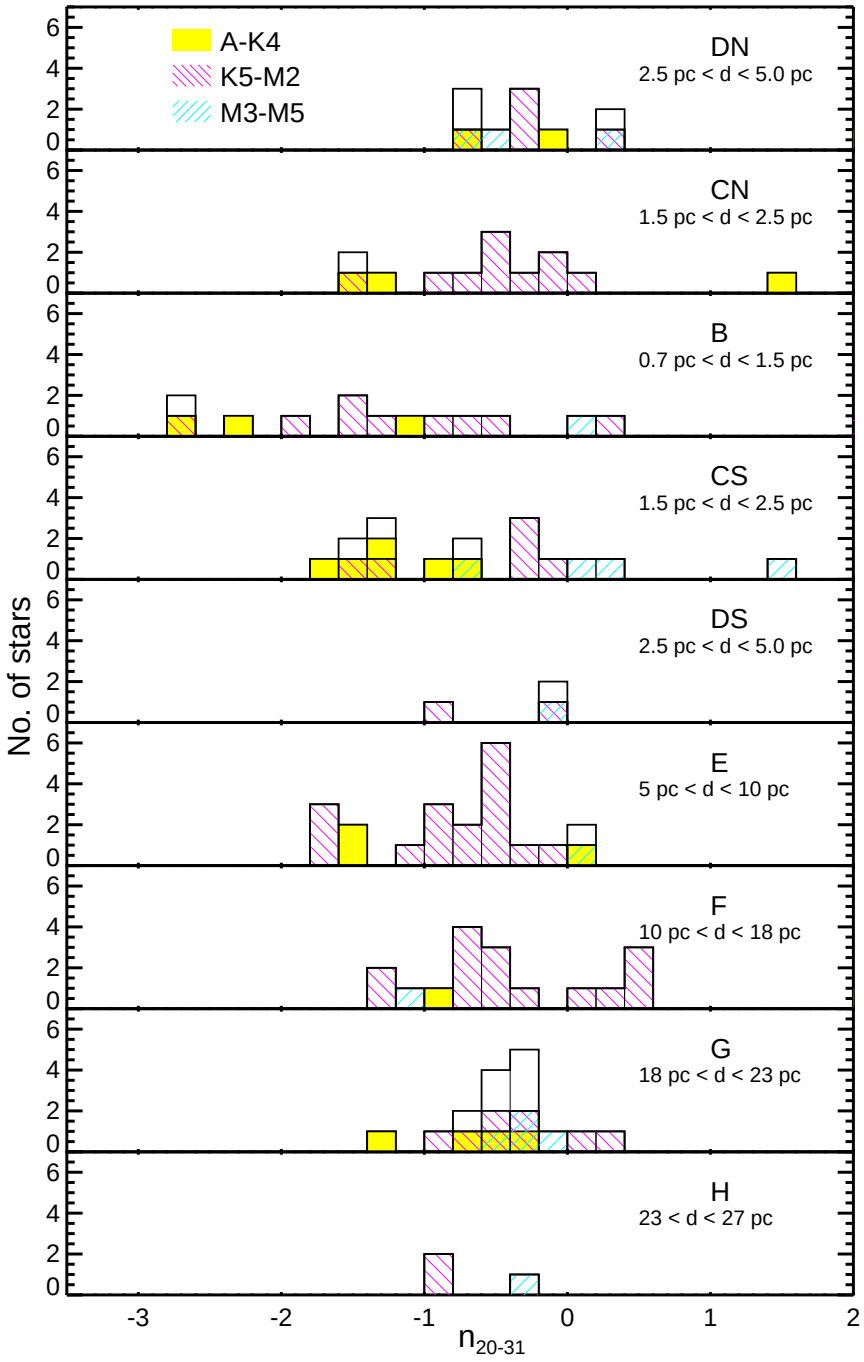


Figure 6.5 Distribution of n_{20-31} of each section separated by spectral types.

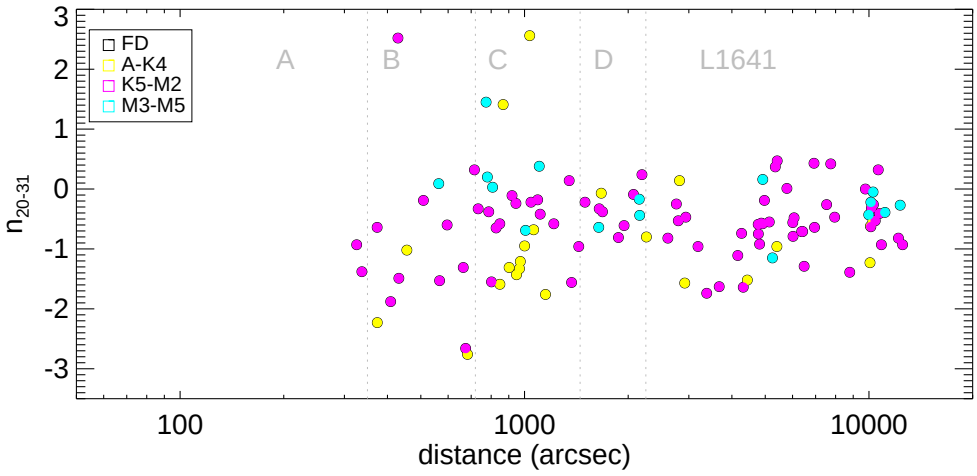


Figure 6.6 Variation of n_{20-31} via distance from θ^1 Ori C.

pattern of spectral index closer to θ^1 Ori C shown for n_{20-31} is also observed for n_{13-31}, but little bit weaker declining tendency compared to n_{20-31}.

EW20 and F_{20}

Figure 6.9 shows the stack of histograms of EW20, and we find a weak but shifted distribution toward smaller EW20 in the subsection B comparing to the subsections in ONC (CN, CS, DN, and DS). The declining pattern of EW20 in ONC is recognized better in Figure 6.10. On the other hand, the distribution of F_{20} in Figure 6.11 and Figure 6.12 displays the opposite pattern of n_{20-31}, n_{13-31}, and EW20.

Evolution of the outer (r > 5 AU) disk

It seems that the effect of UV illumination by the Trapezium stars is largest within 1.5 pc of θ^1 Ori C, based on the observed variation patterns of n_{20-31},

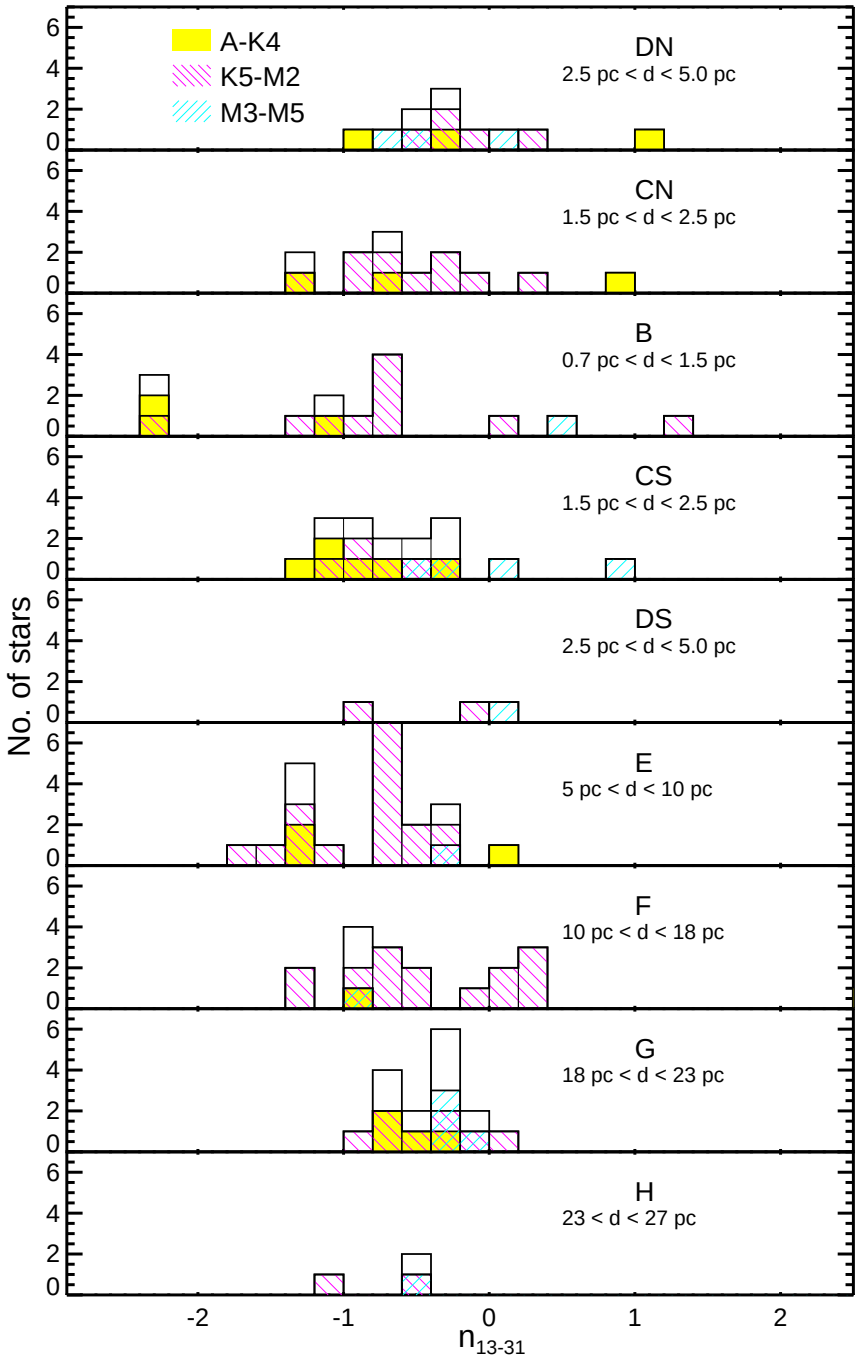


Figure 6.7 Distribution of n_{13-31} of each section separated by spectral types.

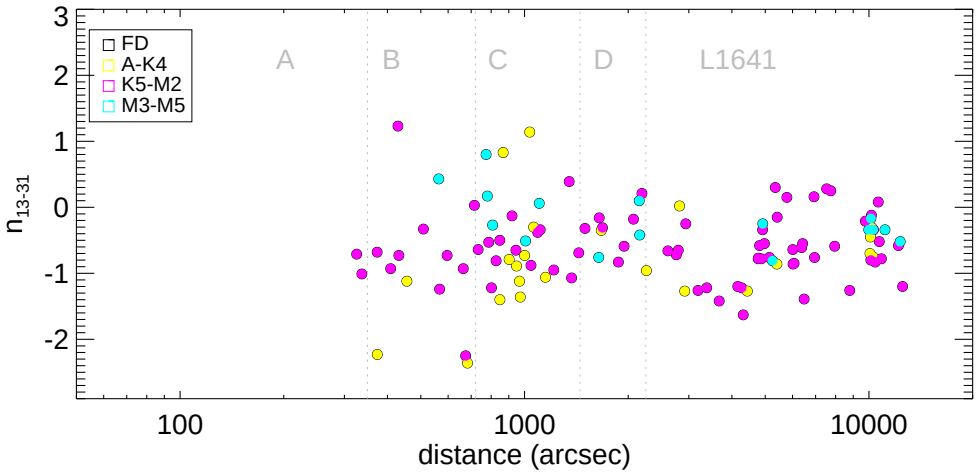


Figure 6.8 Variation of n_{13-31} via distance from θ^1 Ori C.

n_{13-31}, EW20, and F_{20}. Combining the clues acquired from the distribution of n_{20-31}, n_{13-31}, EW20, and F_{20} along the projected distance, we suggest a solution explaining our observation. Considering that n_{20-31} is the index combining optically thin small grains and the optically thick continuum and that n_{13-31} is more representing continuum variation, we infer that evaporation of small particles and gases on surface of the outer disk may be dominant and faster than the outward truncation of the optically-thick disk itself. This conjecture is supported if we take the facts that EW20 is smaller for the closer targets while F_{20} is larger or similar for the closer objects to the O-type star. EW20 tracks the column density of small silicate grains per unit area of optically thick disk continuum while F_{20} is simply proportional to silicate grain column density. That EW20 is decreasing faster than F_{20} can be considered a reflection of the depletion of optically thin surface material: that is, either growth and sedimentation of grains, or blowing out small grains by radiative

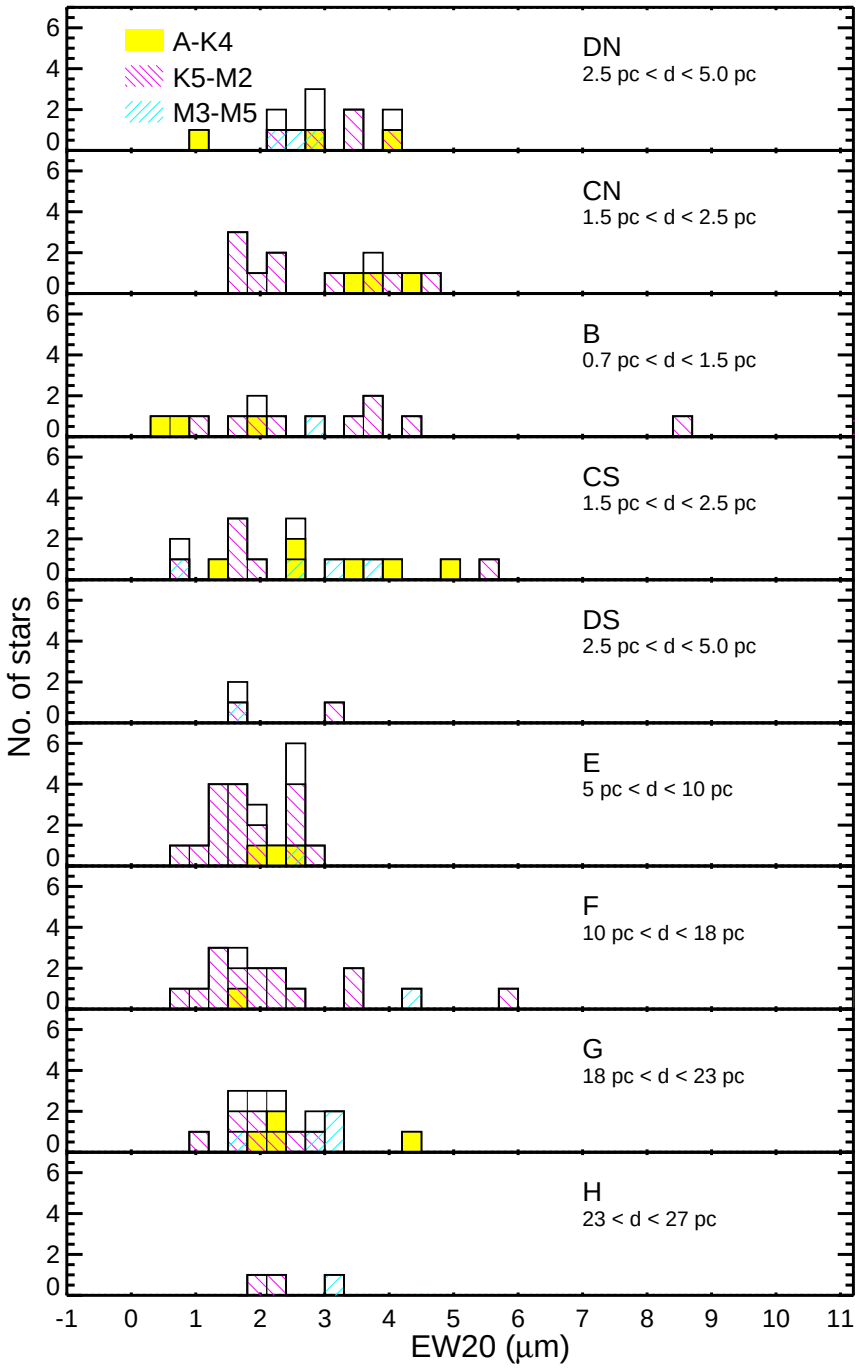


Figure 6.9 Distribution of EW20 of each section separated by spectral types.

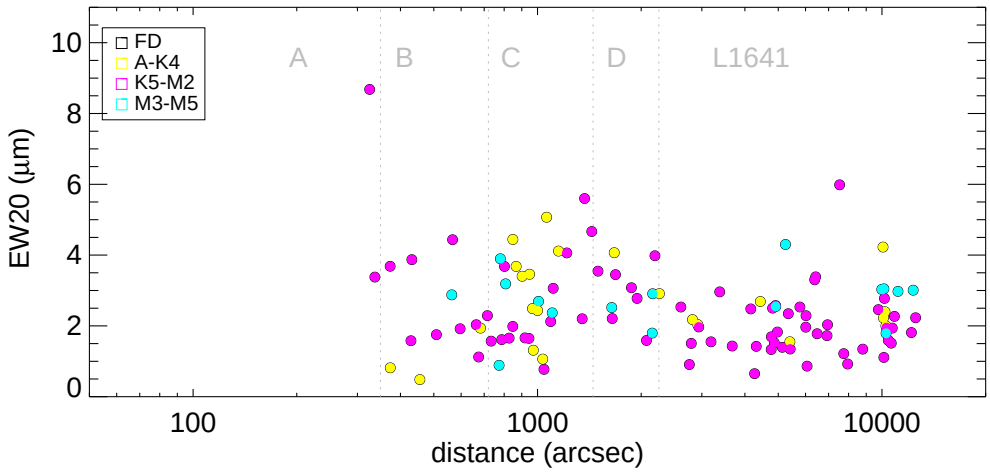


Figure 6.10 Variation of EW20 via distance from θ^1 Ori C.

pressure.

We examine the parameters useful to infer the evolutionary status of inner disks (r $<$ 1 AU), n_{K-6}, EW10, F_{10}, and $F_{11.3}/F_{9.8}$ via distance from θ^1 Ori C. However, we do not see any prominent dependence of the parameters to a target's separation from θ^1 Ori C. Therefore, we do not make any detail inference about the environmental effect to the inner disk evolution based on our observations of n_{K-6}, EW10, F_{10}, and $F_{11.3}/F_{9.8}$. The histograms of the parameters by subsections and scattered plots by distance are in Appendix D.

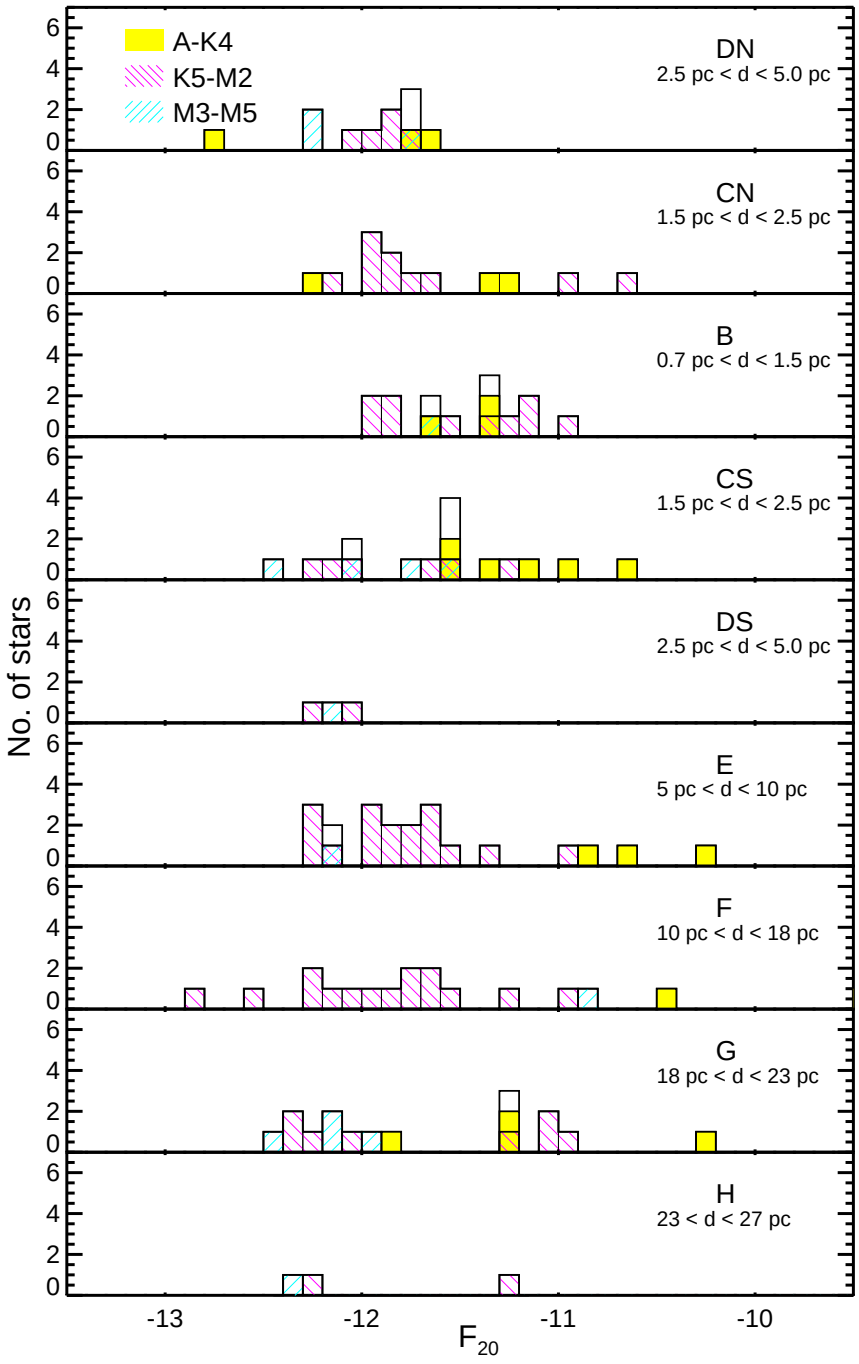


Figure 6.11 Distribution of F_{20} of each section separated by spectral types.

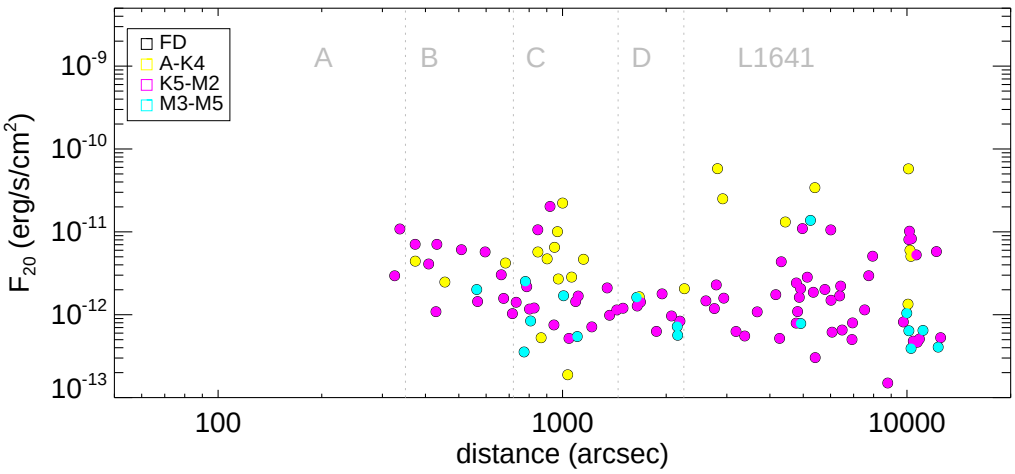


Figure 6.12 Variation of F_{20} via distance from θ^1 Ori C.

Table 6.1. n_{20-31} and d from θ^1 Ori C

ID	IRS modules	n_{20-31}	$\sigma_{n_{20-31}}$	d (arcsec)	d (pc)	Section	TD/FD
1	SLLL	-0.31	0.43	1075.8	2.2	DN	TD
2	SLLL	0.38	0.3	1103.5	2.2	DN	FD
3	SLLL	-1.33	0.1	966.8	1.9	CS	FD
4	SLLL	-0.82	0.21	2607.3	5.2	E	FD
5	SLLL	-1.13	0.17	1164.1	2.3	DS	TD
6	SLLL	-0.65	0.18	844	1.7	CS	FD
8	SLLL	-0.86	0.42	1584	3.2	DN	TD
9	SLLL	-0.61	0.1	800.6	1.6	CS	FD
10	SLLL	0.05	0.36	985.1	2.0	CS	FD
11	SLLL	0.91	0.15	928.1	1.9	CS	TD
12	SLLL	-0.48	0.19	2264.5	4.6	DN	FD
13	SLLL	1.8	0.34	1029.6	2.1	CS	TD
14	SLLL	-0.22	0.22	1044.2	2.1	CS	FD
15	SLLL	-1.31	0.36	664	1.3	CS	FD
16	SLLL	2.43	0.2	869.9	1.8	CN	TD
17	SLLL	-0.69	0.32	1006.9	2.0	CS	FD
18	SLLL	-0.23	0.46	2085.4	4.2	DN	TD
19	SLLL	0.43	0.71	680.5	1.4	CS	TD
20	SLLL	-0.24	0.27	944.1	1.9	CS	FD
21	SLLL	-0.95	0.07	1000.5	2.0	CS	FD
22	SLLL	-0.38	0.17	787.2	1.6	CS	FD
23	SLLL	-1.12	0.16	1272	2.6	CN	TD
24	SLLL	-0.71	0.18	678.2	1.4	CS	TD
25	SLLL	0.1	0.6	2037.6	4.1	DN	TD
26	SLLL	0.8	0.3	1405.2	2.8	DN	TD
27	SLLL	-0.38	0.24	1684.3	3.4	DN	FD
28	SLLL	-0.19	0.1	508.7	1.0	CS	FD
29	SLLL	1.47	0.22	559.9	1.1	CS	TD
30	SLLL	-0.61	0.17	1945.7	3.9	DN	FD

Table 6.1 (cont'd)

ID	IRS modules	n_{20-31}	$\sigma_{n_{20-31}}$	d (arcsec)	d (pc)	Section	TD/FD
31	SLLL	0.66	0.06	1905.2	3.8	DN	FD
32	SLLL	1.45	0.37	773.4	1.6	CS	FD
33	SLLL	0.2	0.13	780.2	1.6	CS	FD
34	SLLL	0.17	1.25	2097.1	4.2	DN	TD
35	SLLL	1.41	0.85	866.8	1.7	CN	FD
36	SLLL	-0.68	0.23	1062.7	2.1	CS	FD
37	SLLL	-1.38	0.24	337.1	0.7	B	FD
38	SLLL	0.41	0.29	1508.7	3.0	DS	TD
39	SLLL	-0.26	1.44	1931.8	3.9	DN	TD
40	SLLL	-0.07	0.25	1670.3	3.4	DN	FD
41	SLLL	0.08	0.28	1036.5	2.1	CS	FD
42	SLLL	-1.15	0.47	1104.8	2.2	CS	TD
43	SLLL	-0.59	0.09	986.3	2.0	CS	FD
44	SLLL	0.05	0.22	1140.2	2.3	CN	TD
45	SLLL	-2.23	0.11	373.7	0.8	B	FD
46	SLLL	-0.93	1.26	325.6	0.7	B	FD
47	SLLL	2.17	0.37	351.5	0.7	B	TD
48	SLLL	-0.58	0.63	1216.2	2.4	CN	FD
49	SL	-999	-999	235	0.5	A	Trap
50	SLLL	-1.49	0.7	431.7	0.9	B	FD
51	SLLL	-0.64	0.21	1642.6	3.3	DN	FD
52	SLLL	-0.33	0.19	733.6	1.5	CN	FD
53	SLLL	-0.28	0.27	3374.7	6.8	E	TD
54	SLLL	-1.84	0.67	1607.4	3.2	DN	FD
55	SL	-999	-999	178.2	0.4	A	Trap
56	SL	-999	-999	178.5	0.4	A	Trap
57	SLLL	-0.25	0.21	1119.8	2.3	CS	FD
58	SLLL	-0.81	0.43	1873.5	3.8	DS	FD
59	SLLL	0.53	0.21	2203.8	4.4	E	TD

Table 6.1 (cont'd)

ID	IRS modules	n_{20-31}	$\sigma_{n_{20-31}}$	d (arcsec)	d (pc)	Section	TD/FD
60	SLLL	0.21	0.34	1277.3	2.6	CS	FD
61	SLLL	-0.43	0.2	1302.4	2.6	CS	FD
62	SLLL	-1.25	0.26	1365.3	2.7	CS	FD
63	SL	-999	-999	209.3	0.4	A	Trap
64	SL	-999	-999	155.4	0.3	A	Trap
65	SLLL	-0.13	0.47	1631.5	3.3	DS	FD
66	SLLL	0.5	0.42	833	1.7	CN	TD
67	SL	-999	-999	187.2	0.4	A	Trap
68	SL	-999	-999	150.4	0.3	A	Trap
70	SL	-999	-999	238	0.5	A	Trap
71	SL	-999	-999	139	0.3	A	Trap
73	SLLL	-0.24	0.76	1035.8	2.1	CS	FD
74	SL	-999	-999	148.6	0.3	A	Trap
75	SL	-999	-999	133.7	0.3	A	Trap
76	SLLL	-1.15	0.19	2045.9	4.1	DN	FD
77	SL	-999	-999	125.7	0.3	A	Trap
78	SL	-999	-999	150.3	0.3	A	Trap
79	SLLL	-0.41	0.17	1842.5	3.7	DS	FD
80	SL	-999	-999	226.5	0.5	A	Trap
81	SL	-999	-999	217.8	0.4	A	Trap
82	SL	-999	-999	114.2	0.2	A	Trap
83	SL	-999	-999	117.5	0.2	A	Trap
84	SLLL	-0.22	0.38	1498.3	3.0	DN	FD
85	SL	-999	-999	223.9	0.5	A	Trap
86	SLLL	0.03	0.32	807.8	1.6	CS	FD
88	SLLL	2.08	0.11	523.7	1.1	B	TD
89	SL	-999	-999	114.6	0.2	A	Trap
90	SLLL	-0.64	0.26	373.4	0.8	B	FD
91	SL	-999	-999	154.5	0.3	A	Trap

Table 6.1 (cont'd)

ID	IRS modules	n_{20-31}	$\sigma_{n_{20-31}}$	d (arcsec)	d (pc)	Section	TD/FD
92	SL	-999	-999	104	0.2	A	Trap
93	SL	-999	-999	115.3	0.2	A	Trap
94	SLLL	0.32	0.37	715.3	1.4	B	FD
95	SLLL	0.13	0.13	575.9	1.2	B	FD
96	SL	-999	-999	227.6	0.5	A	Trap
97	SLLL	0.98	0.2	921.9	1.9	CS	FD
98	SLLL	-1.53	0.72	566.8	1.1	B	FD
99	SLLL	-0.34	0.49	1532.7	3.1	DS	FD
100	SL	-999	-999	284.3	0.6	A	Trap
101	SL	-999	-999	315.6	0.6	A	Trap
102	SL	-999	-999	136.9	0.3	A	Trap
103	SLLL	-1.38	0.19	2191.8	4.4	DN	FD
106	SLLL	-0.89	0.23	2534	5.1	E	FD
108	SLLL	-0.22	0.04	1391.9	2.8	CS	TD
112	SLLL	-1.21	0.13	972.4	2.0	CS	FD
114	SL	-999	-999	272.9	0.5	A	Trap
117	SLLL	-1.02	0.24	455.4	0.9	B	FD
119	SL	-999	-999	324.2	0.7	A	Trap
120	SL	-999	-999	320.8	0.6	A	Trap
121	SLLL	-0.81	0.22	1194.7	2.4	CS	FD
122	SLLL	-0.6	0.12	596.1	1.2	B	FD
123	SLLL	0.09	0.33	563.6	1.1	B	FD
125	SLLL	-1.43	0.14	948	1.9	CS	FD
127	SLLL	1.76	0.3	811.9	1.6	CN	FD
128	SLLL	1.08	0.19	1435.2	2.9	CN	FD
129	SL	-999	-999	329.9	0.7	A	Trap
131	SLLL	-0.8	0.1	2258.6	4.5	DN	FD
132	SL	-999	-999	225.7	0.5	A	Trap
133	SLLL	-0.62	0.15	2103.7	4.2	DS	FD

Table 6.1 (cont'd)

ID	IRS modules	n_{20-31}	$\sigma_{n_{20-31}}$	d (arcsec)	d (pc)	Section	TD/FD
134	SLLL	-1.63	0.28	3675.3	7.4	E	FD
135	SLLL	-1.76	0.18	1150.5	2.3	CS	FD
137	SL	-999	-999	323.7	0.7	A	Trap
138	SLLL	-0.59	0.18	1799.7	3.6	DN	FD
139	SL	-999	-999	354.6	0.7	A	Trap
140	SLLL	-1.96	0.2	1223.1	2.5	CN	FD
141	SLLL	-1.59	0.17	848.1	1.7	CN	FD
142	SLLL	-1.33	0.43	982.7	2.0	CN	FD
143	SL	-999	-999	251.6	0.5	A	Trap
144	SLLL	-0.11	0.05	919.8	1.9	CN	FD
145	SL	-999	-999	294.1	0.6	A	Trap
146	SL	-999	-999	196	0.4	A	Trap
147	SL	-999	-999	202.8	0.4	A	Trap
149	SLLL	1.19	0.03	1024.6	2.1	CN	TD
150	SL	-999	-999	165.6	0.3	A	Trap
151	SLLL	-1.74	0.36	3380.3	6.8	E	FD
152	SL	-999	-999	102.9	0.2	A	Trap
153	SL	-999	-999	264	0.5	A	Trap
154	SLLL	-0.39	0.29	1176.7	2.4	CS	TD
155	SL	-999	-999	299.1	0.6	A	Trap
156	SLLL	-1.22	0.34	1312.8	2.6	CN	FD
158	SL	-999	-999	145.7	0.3	A	Trap
159	SLLL	-0.17	0.34	2153.2	4.3	DS	FD
160	SLLL	-3.12	0.84	945.4	1.9	CN	FD
161	SLLL	-0.44	0.54	2159.5	4.3	DN	FD
162	SLLL	-1.5	0.16	2109.9	4.2	DN	FD
163	SL	-999	-999	264.1	0.5	A	Trap
164	SLLL	-0.56	0.11	1433.3	2.9	CN	TD
165	SLLL	-0.78	0.33	1713.4	3.4	DS	FD

Table 6.1 (cont'd)

ID	IRS modules	n_{20-31}	$\sigma_{n_{20-31}}$	d (arcsec)	d (pc)	Section	TD/FD
166	SLLL	0.16	0.35	4917	9.9	E	FD
167	SLLL	-0.42	0.21	1110.4	2.2	CN	FD
168	SLLL	-0.58	0.06	847.6	1.7	CN	FD
169	SLLL	-0.02	0.29	2225.5	4.5	DN	TD
170	SLLL	2.56	0.41	1035.3	2.1	DN	FD
172	SLLL	0.08	0.21	2150.8	4.3	DN	TD
173	SLLL	-2.76	0.66	683	1.4	B	FD
174	SLLL	-0.07	0.19	1122.5	2.3	CN	TD
175	SL	-999	-999	260.2	0.5	A	Trap
176	SLLL	-0.02	0.52	1164.2	2.3	CN	TD
177	SLLL	0.91	0.38	3608.5	7.3	E	TD
178	SLLL	-1.35	0.36	1130.6	2.3	CN	FD
179	SLLL	-0.96	0.53	1437.1	2.9	CN	FD
180	SLLL	-2.66	0.63	674.6	1.4	B	FD
181	SLLL	-0.4	0.61	1030.3	2.1	CN	FD
182	SLLL	-0.65	0.35	827.1	1.7	CN	FD
183	SLLL	-0.18	0.23	1091.9	2.2	CN	FD
184	SLLL	0.53	0.41	801.4	1.6	CN	TD
185	SLLL	-0.84	0.22	1588.6	3.2	DS	TD
186	SLLL	0.14	0.12	1348	2.7	CN	FD
187	SLLL	2.52	0.07	429.1	0.9	B	FD
188	SLLL	-0.57	0.27	1729	3.5	DS	TD
189	SLLL	-1.12	0.25	1027.2	2.1	CN	FD
190	SLLL	-0.33	0.22	1648	3.3	DN	FD
191	SLLL	0.14	0.02	2818.4	5.7	E	FD
192	SLLL	0.24	0.39	2192.3	4.4	DN	FD
193	SLLL	-1.88	1.91	408.7	0.8	B	FD
194	SLLL	1.11	0.54	1545.5	3.1	DN	FD
195	SLLL	-1.56	1.4	1369.8	2.8	CS	FD

Table 6.1 (cont'd)

ID	IRS modules	n_{20-31}	$\sigma_{n_{20-31}}$	d (arcsec)	d (pc)	Section	TD/FD
196	SLLL	-0.75	0.13	4774.4	9.6	E	FD
197	SLLL	-0.09	0.27	2071.8	4.2	DS	FD
198	SLLL	-1.49	0.32	4417.6	8.9	E	TD
199	SLLL	-0.96	0.28	3189.6	6.4	E	FD
200	SLLL	-0.59	0.24	4768.6	9.6	E	FD
201	SLLL	-1.11	0.16	4160.9	8.4	E	FD
202	SLLL	-0.55	0.14	5136.4	10.3	E	FD
203	SLLL	-1.07	0.24	3300	6.6	E	TD
204	SLLL	-0.35	0.44	3137.6	6.3	E	TD
205	SLLL	-1.31	0.16	902.3	1.8	CN	FD
206	SLLL	-0.19	0.04	4971.4	10.0	E	FD
207	SLLL	-0.32	0.17	3643.4	7.3	E	FD
208	SLLL	-0.24	0.07	3310.3	6.7	E	FD
209	SLLL	-0.54	0.11	3752.9	7.6	E	FD
210	SLLL	-0.25	0.07	2759.6	5.6	E	FD
211	SLLL	-0.74	0.9	3792.7	7.6	E	TD
212	SLLL	-0.92	0.31	4813.3	9.7	E	FD
213	SLLL	-0.53	0.03	2795.3	5.6	E	FD
214	SLLL	-1.55	0.72	801.8	1.6	CN	FD
215	SLLL	-0.58	0.17	4910.7	9.9	E	FD
216	SLLL	1.23	0.22	6512.3	13.1	F	FD
217	SLLL	-0.74	0.24	4268.4	8.6	E	FD
218	SLLL	0.03	0.28	4083.2	8.2	E	TD
219	SLLL	-0.02	0.42	3111.9	6.3	E	TD
220	SLLL	-0.47	0.2	2938.7	5.9	E	FD
221	SLLL	-0.12	0.29	2972.6	6.0	E	TD
222	SLLL	-0.57	0.22	4869.8	9.8	E	FD
223	SLLL	0.28	0.34	4057.8	8.2	E	TD
224	SLLL	-1.57	0.1	2918.1	5.9	E	FD

Table 6.1 (cont'd)

ID	IRS modules	n_{20-31}	$\sigma_{n_{20-31}}$	d (arcsec)	d (pc)	Section	TD/FD
225	SLLL	-1.64	0.2	4315.7	8.7	E	FD
226	SLLL	-1.52	0.1	4435.3	8.9	E	FD
227	SLLL	-0.63	0.31	7372.8	14.8	F	TD
228	SLLL	0.47	0.2	5415.3	10.9	F	FD
229	SLLL	0.36	0.41	4610.5	9.3	E	TD
230	SLLL	0.15	0.28	5485.8	11.0	F	TD
231	SLLL	-1.15	0.17	5246.8	10.6	F	FD
232	SLLL	0.37	0.12	5346.8	10.8	F	FD
233	SLLL	0.43	0.15	6925.5	13.9	F	FD
234	SLLL	-0.64	0.19	6950.3	14.0	F	FD
235	SLLL	-0.96	0.07	5403.4	10.9	F	FD
236	SLLL	-0.71	0.22	6419.7	12.9	F	FD
237	SLLL	0.53	0.06	6599.7	13.3	F	TD
238	SLLL	0.01	0.12	5777.3	11.6	F	FD
239	SLLL	-0.24	0.09	9012.4	18.1	F	TD
240	SLLL	-1.39	0.48	8794.9	17.7	F	FD
241	SLLL	-0.48	0.28	6061.9	12.2	F	FD
242	SLLL	-0.56	0.11	6008.9	12.1	F	FD
243	SLLL	-0.79	0.25	6019.5	12.1	F	FD
244	SLLL	-1.29	0.22	6483.6	13.1	F	FD
245	SLLL	0.42	0.05	7745	15.6	F	FD
246	SLLL	-0.71	0.34	6376.8	12.8	F	FD
247	SLLL	-0.25	0.05	6811	13.7	F	FD
248	SLLL	-0.15	0.12	7417.2	14.9	F	FD
249	SLLL	-0.26	0.5	7535.5	15.2	F	FD
250	SLLL	-1.35	0.32	7615.6	15.3	F	FD
251	SLLL	-1.31	0.27	7589	15.3	F	FD
252	SLLL	-0.15	0.17	7689.1	15.5	F	FD
253	SLLL	-3.86	0.99	8039.8	16.2	F	FD

Table 6.1 (cont'd)

ID	IRS modules	n_{20-31}	$\sigma_{n_{20-31}}$	d (arcsec)	d (pc)	Section	TD/FD
254	SLLL	-1.67	0.2	7906.2	15.9	F	FD
255	SLLL	-0.53	0.43	7985.7	16.1	F	FD
256	SLLL	-0.31	0.11	7796.6	15.7	F	FD
257	SLLL	0.38	0.28	9079.9	18.3	G	TD
258	SLLL	-0.47	0.09	7950.6	16.0	F	FD
259	SLLL	0.32	0.03	10641.3	21.4	G	FD
260	SLLL	0.83	0.25	7886.8	15.9	F	TD
261	SLLL	-0.09	0.08	9536.3	19.2	G	FD
262	SLLL	-0.54	0.09	10268.3	20.7	G	FD
263	SLLL	-0.05	0.47	10277.1	20.7	G	FD
264	SLLL	-0.94	0.51	9591.2	19.3	G	FD
265	SLLL	-0.91	0.57	8716.7	17.5	G	FD
266	SLLL	-0.62	0.06	10100.7	20.3	G	FD
267	SLLL	-1.22	0.16	9177.7	18.5	G	FD
268	SLLL	-0.66	0.08	7781.6	15.7	F	FD
269	SLLL	-0.25	0.05	10203.6	20.5	G	FD
270	SLLL	1.47	0.1	10308.1	20.7	G	TD
271	SLLL	1.23	0.24	9141.7	18.4	G	TD
272	SLLL	-0.55	0.53	9770	19.7	G	FD
273	SLLL	-0.53	0.54	10430.8	21.0	G	FD
274	SLLL	-0.6	0.23	9405.8	18.9	G	FD
275	SLLL	0.05	0.14	9449.1	19.0	G	TD
276	SLLL	-0.68	0.08	12438.3	25.0	H	FD
277	SLLL	-0.26	0.04	10303.9	20.7	G	FD
278	SLLL	0	0.28	9764.3	19.7	G	FD
279	SLLL	0.1	0.15	10039.5	20.2	G	TD
280	SLLL	-0.82	0.08	12177.2	24.5	H	FD
281	SLLL	-0.43	0.35	9986.5	20.1	G	FD
282	SLLL	-0.63	0.07	10127.9	20.4	G	FD

Table 6.1 (cont'd)

ID	IRS modules	n_{20-31}	$\sigma_{n_{20-31}}$	d (arcsec)	d (pc)	Section	TD/FD
283	SLLL	1.4	0.22	9551.8	19.2	G	TD
284	SLLL	-1.23	0.54	10070.9	20.3	G	FD
285	SLLL	-1.18	0.35	10790.7	21.7	G	FD
286	SLLL	-0.27	0.58	12320.6	24.8	H	FD
287	SLLL	-0.22	0.29	10128.5	20.4	G	FD
288	SLLL	-0.41	0.51	10716	21.6	G	FD
289	SLLL	-0.32	0.09	10166	20.5	G	FD
290	SLLL	-0.6	0.24	10748.3	21.6	G	TD
291	SLLL	-0.41	0.34	11095.4	22.3	G	TD
292	SLLL	-0.93	0.34	12522.7	25.2	H	FD
293	SLLL	-0.39	0.53	11130.7	22.4	G	FD
294	SLLL	0.99	0.13	12986	26.1	H	TD
295	SLLL	-1.91	0.07	12531.9	25.2	H	FD
296	SLLL	0.35	0.04	11226.9	22.6	G	FD
297	SLLL	-0.04	0.33	12242.4	24.6	H	TD
298	SLLL	-1.52	0.28	12493.9	25.1	H	FD
299	SLLL	-0.93	0.31	10869	21.9	G	FD
300	SLLL	-0.08	0.2	12541.5	25.2	H	FD
301	SLLL	-1.06	0.28	11373.1	22.9	G	TD
302	SLLL	0.86	0.34	12270.9	24.7	H	TD
303	SLLL	1.24	0.2	12117.4	24.4	H	TD

6.3 Summary

We have searched for trends among disk parameters and strength of the UV illumination which the disks experiece. From the examination of median spectra in subsections of Orion A, we found the median spectra in the subsections of ONC are quite blue at long wavelengths beyond 20 μm, which is consistent with outward truncation of the disks due to UV radiation field from the Trapezium, as in the case for the proplyds. We checked out the distributions of spectral indices, equivalent widths, and integrated fluxes by the variation of the distance of objects from θ^1 Ori C. We observed a remarkable decline of n_{20-31} toward to the center of Trapezium. The distribution of n_{13-31} shows that similar declining pattern. We also verified EW20 is smaller in subsection closer to the Trapezium. On the other hand, F_{20} increases steeply as the distance decreases. These declining trend of n_{20-31}, n_{13-31}, and EW20 and the inclining trend of F_{20} are dominantly observed within 1.5 pc from θ^1 Ori C. Considering the definitions and the implications of the parameters, we suggest a depletion of optically thin surface material of the outer parts (r $>$ 5) of disks in close proximity to the Trapezium stars.

7 Polycyclic Aromatic Hydrocarbon (PAH) Molecules in the Disks around Low Mass Stars

7.1 Introduction

Polycyclic Aromatic Hydrocarbon (PAH) molecules are generally considered as the carriers (Leger & Puget, 1984; Allamandola et al., 1985) of the unidentified infrared (UIR) emission features (Gillett et al., 1973) at 3.3, 6.2, 7.7, 8.6, and 11.3 μm. PAH features in these bands are found in a wide variety of astrophysical objects; post-AGB stars, PNe, the local diffuse interstellar medium, reflection nebulae, PDR/star formation regions in our own galaxy, other nearby normal galaxies, distant starburst galaxies, ultraluminous infrared galaxies (ULIRGs), and Be hypergiant stars (e.g. Kastner et al., 2006). Those observational sources have common characteristics: they are exposed to substantial ultraviolet (UV) illumination. The UV radiation drives the

molecules into excited electronic and vibrational states, which subsequently decay to lower electronic states through fluorescence and IR emission.

Unlike high-mass stars or HAeBe stars which are commonly ($\sim 50\%$) observed to have strong PAH emission, there are not many PAH detections from disks around lower-mass T Tauri stars. It is thought because that sources with spectral type later than G have stellar UV fields weaker by many orders of magnitude than those of HAeBe stars. Geers et al. (2006) found some T Tauri stars that show mid-IR PAH emission features from protoplanetary disks, but still most of the sources are earlier spectral type (A-G) stars.

There are several reasons why PAHs in protoplanetary disks are important, and that we can learn much from PAHs in disks around low mass stars. First, the existence and concentration of PAHs in very young (~ 1 Myr) protoplanetary disks may tell us about the origin of organic molecules in the Earth and meteorites (e.g. Sephton et al., 2003; Scmitt-Kopplin et al., 2010). Second, in comparison to the ISM, protoplanetary disks supply a very dense environment for gas molecules. Therefore, PAH species in disks may be different in sizes, molecular structure, vibrational modes, etc than that in diffuse ISM. We may also expect to detect size variation from the surface layers of disks to the midplane, which will help to understand dust evolution through grain growth and dust settling. Third, because M type stars cannot supply enough high energy UV photons to trigger PAH emission features in disks, UV sources of PAHs in disks around later type stars (K-M) must be outside of the system. With uniform external illumination, it would be simpler to deduce the PAH molecules concentration in the upper disk than it would be, for example,

in an Ae star. Finally, the detection of PAHs in disks around low mass T Tauri stars allow us to examine various environment parameters (density, UV strength, disk structure) depending on the uniqueness or similarity of features or classifications to those for PAHs in ISM and HAeBe disk. For example, Sloan et al. (2005) found feature shifts for PAHs of HAeBe stars. Keller et al. (2008) found that and PAHs in disks around HAeBe star are fall in a narrow range of PAH spectral classifications (Meeus et al., 2001; Peeters et al., 2002). These tell us that PAHs in HAeBe disks are different than PAHs in the ISM. Keller et al. (2008) also found no correlation between PAH features and radial disk structures. PAH features from disks around low mass stars will help us to understand the evolution of organic molecules from the ISM to planets.

We have detected strong PAH features in several of the disks around M and K stars in our ONC and Trapezium samples. This marks the first detection of complex organic molecules in the protoplnaetary disks of solar-analogue and lower-mass stars.

7.2 The Objects with PAHs

Among our 44 IRS targets nearest to the Trapezium which were not lost in the bright and variable nebular background (see Section 3.1.2) , we find that 14 objects have PAH features and they are not confused by low signal-to-noise ratio or background-subtraction issues. We indicate the 14 objects in a sky chart of ONC in Figure 7.1. The spectral type and the projected distance from θ^1 Ori C to the objects marked in Figure 7.1 is in Table 7.1.

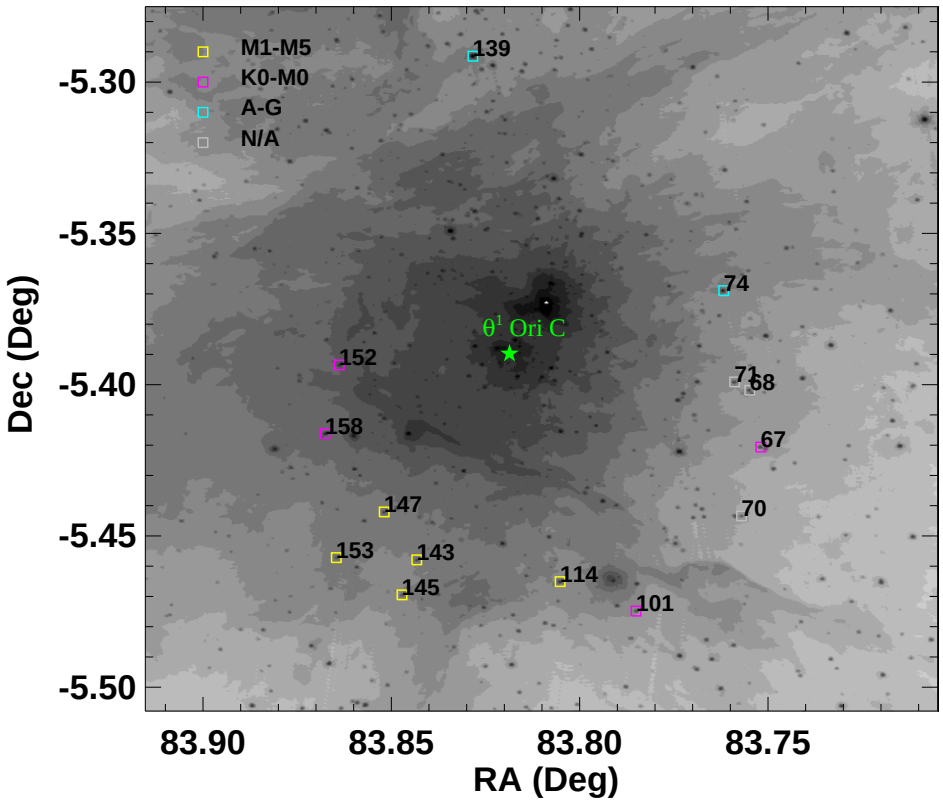


Figure 7.1 The objects with PAHs emissions from their protoplanetary disks.

7.3 Analysis

7.3.1 Extraction of the PAH Features

To extract the PAH features and to measure the integrated flux and center positions of the features, we use a two step continuum subtraction as presented in Sloan et al. (2007) and Keller et at. (2008). We first fit broad polynomial interpolations to the continuum contribution from star, disk, and silicate dust grains (Fig 7.2). After removing the broad continuum, we fit a local continuum

Table 7.1. List of Objects

ID	IRS Name	Common Name	Spectral Type	T_{eff} (K)	d (arcsec)	d (parsec)
67	8375190-5420	V2012 Ori	K7.5	3955	187.2	0.4
74	8376176-5368	V2125 Ori	G0.0	6030	148.6	0.3
101	8378503-5474	V1397 Ori	K2.0	4900	315.6	0.6
114	8380518-5465	V2237 Ori	M2.0	3580	272.9	0.5
139	8382835-5291	V2338 Ori	A9.0	7390	354.6	0.7
143	8384325-5457	V1340 Ori	M5.0	3240	251.6	0.5
145	8384717-5469	V1530 Ori	M3.5	3420	294.1	0.6
147	8385190-5442	V1283 Ori	M4.5	3305	202.8	0.4
152	8386383-5393	V2463 Ori	K4.0	4590	102.9	0.2
153	8386462-5457	V1287 Ori	M2.0	3580	264.0	0.5
158	8386759-5416	V420 Ori	K7.0	4060	145.7	0.3
68	8375484-5401	Parenago 1694	SpT	3850	150.4	0.3
70	8375702-5443	V2114 Ori	SpT	3850	238.0	0.5
71	8375886-5399	V2121 Ori	SpT	3850	139.0	0.3

Note. — The list of objects with PAHs emissions from externally illuminated disks around θ^1 Ori C.

around the each PAH feature with a linear interpolation between two anchors adjacent to the features (Figure 7.3). From this step, we can correct the asymmetric continuum levels on the right and left side of the feature which could be caused by the broad continuum fit. We measure the integrated flux after subtracting the local continuum. For the blended PAH feature of 7-9 μm, we subtract a underlying line segment of the broad feature including 7.7 μm feature and 8.6 μm feature. To measure the integrated flux of a PAH feature of 7.7 μm and a PAH of 8.6 μm separate, we split the broad feature at 8.2 μm which is the apparent dip position between 7.7 and 8.6 μm PAH features. The wavelength ranges used for integrating flux densities of PAH features are indicated in Figure 7.4. The measured fluxes of PAH features are listed in Table 7.2.

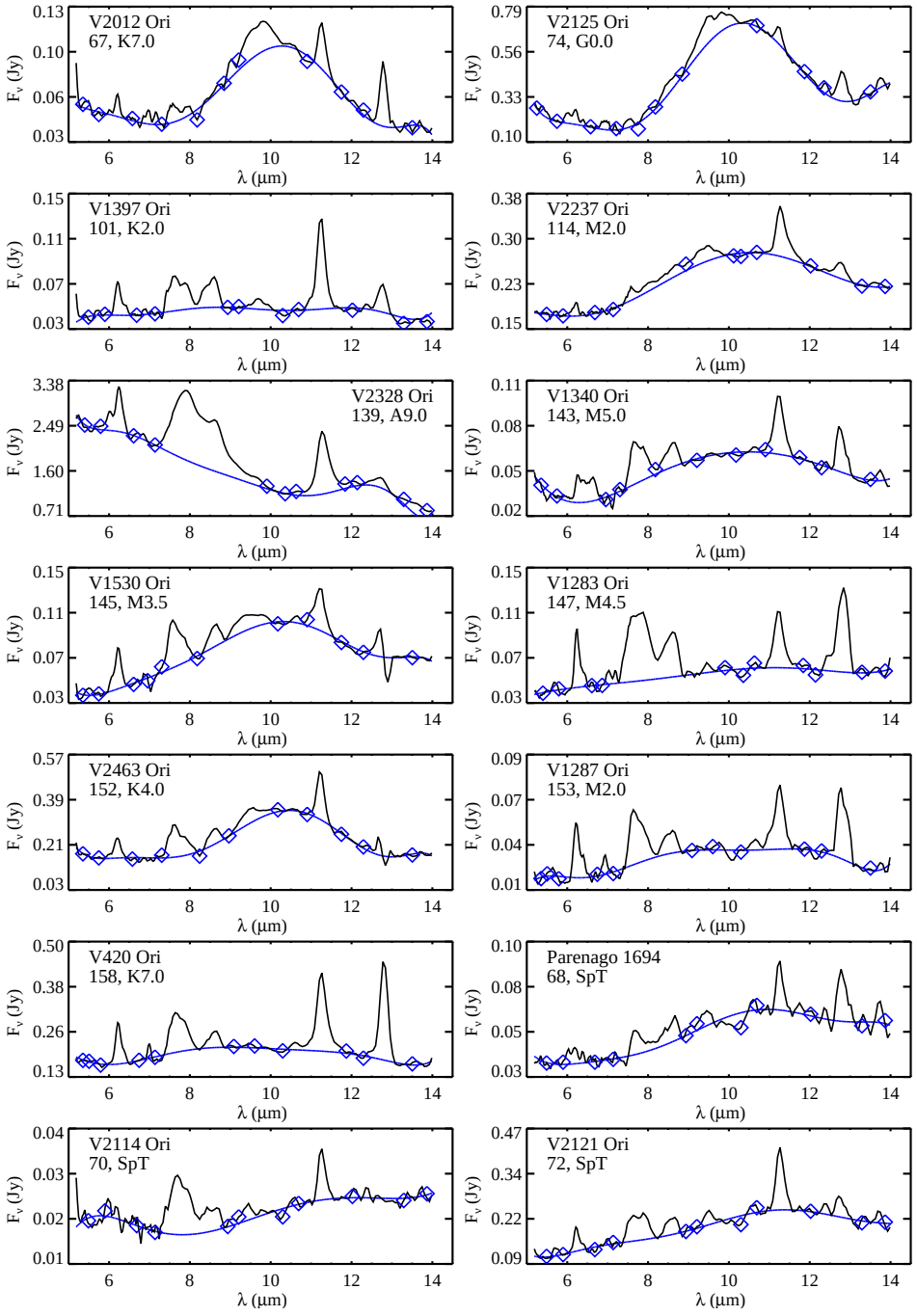


Figure 7.2 PAH extraction step 1: broad continuum fitting.

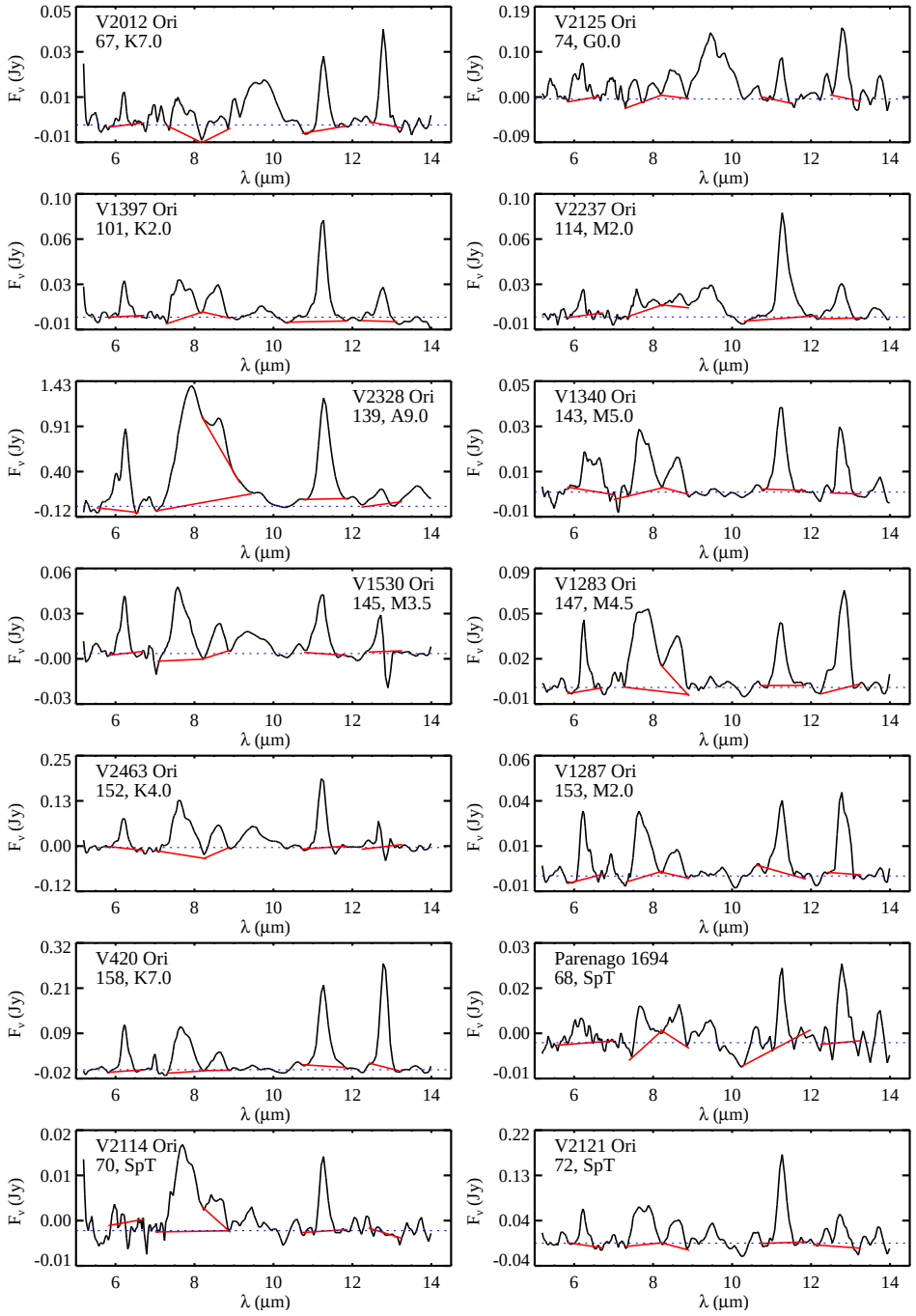


Figure 7.3 PAH extraction step 2: local continuum fitting.

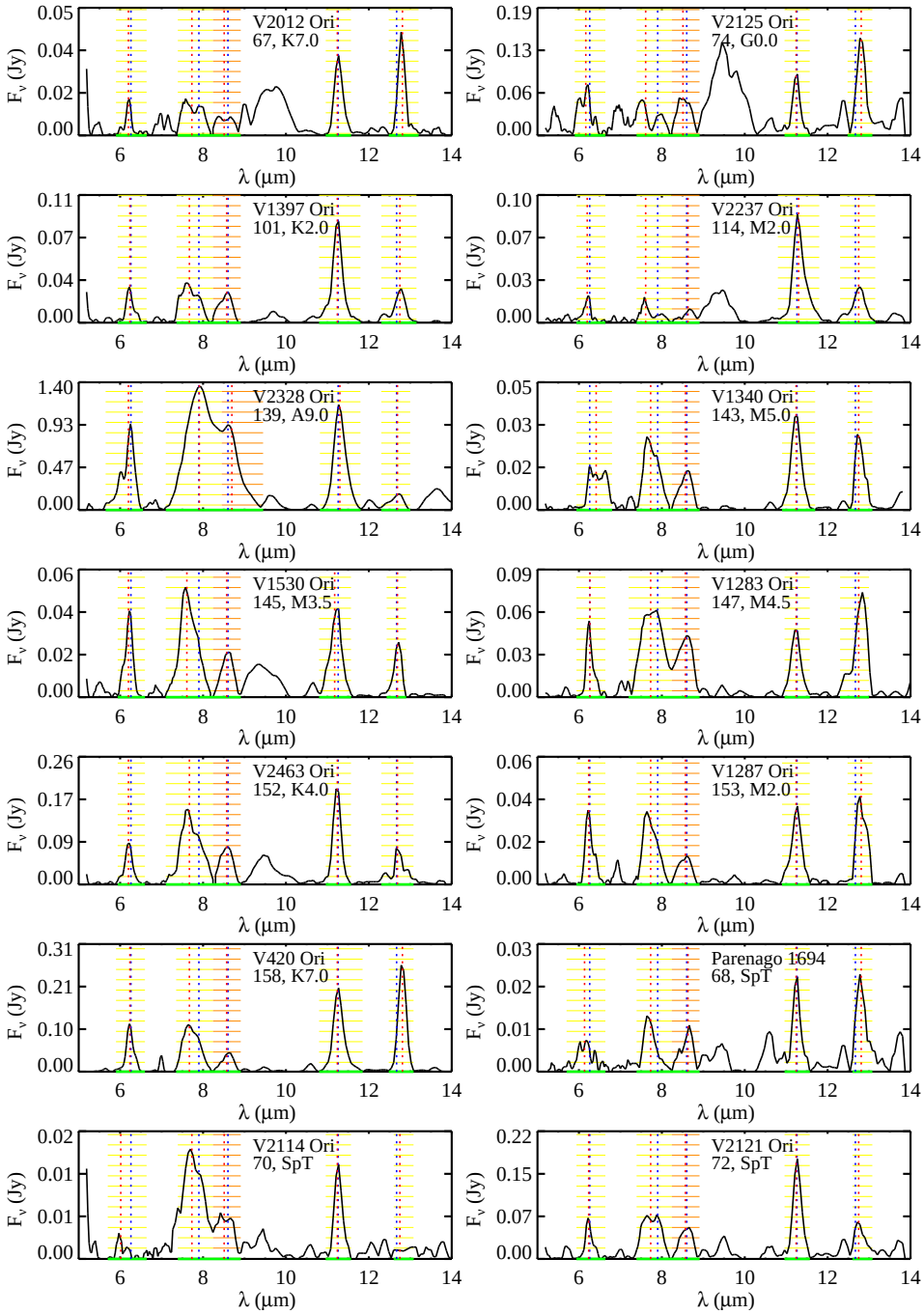


Figure 7.4 PAH emission features after subtracting continuum.

Table 7.2. Integrated Fluxes

	$F(10^{-16}W/m^2)$				
ID	6.2 μm	7.7-8.2 μm	8.6 μm	11.2 μm	12.7 μm
67	2.32 ± 0.39	4.11 ± 0.43	1.70 ± 0.24	2.04 ± 0.12	1.76 ± 0.84
74	19.70 ± 3.00	11.60 ± 4.69	9.83 ± 1.97	5.16 ± 1.90	7.24 ± 2.10
101	4.94 ± 0.36	8.38 ± 0.84	3.82 ± 0.36	6.09 ± 0.39	1.67 ± 0.32
114	3.42 ± 0.53	2.89 ± 1.10	1.40 ± 1.00	6.55 ± 0.26	1.87 ± 0.45
139	233.00 ± 2.89	515.00 ± 7.09	163.00 ± 2.72	95.80 ± 0.84	12.20 ± 1.23
143	5.78 ± 0.65	6.14 ± 0.55	2.27 ± 0.47	2.73 ± 0.59	1.43 ± 1.35
145	6.75 ± 0.22	12.40 ± 0.81	2.96 ± 0.28	3.29 ± 0.34	1.05 ± 0.66
147	7.97 ± 0.63	20.00 ± 1.18	7.88 ± 0.37	3.32 ± 0.27	4.53 ± 1.41
152	15.20 ± 2.25	41.80 ± 2.14	11.80 ± 2.47	11.30 ± 1.88	4.30 ± 4.19
153	5.97 ± 0.41	6.83 ± 0.86	2.03 ± 0.34	2.50 ± 0.27	2.23 ± 0.67
158	19.30 ± 0.91	28.30 ± 2.02	6.42 ± 0.67	15.00 ± 1.80	11.60 ± 1.41
68	2.85 ± 0.42	2.51 ± 0.25	1.54 ± 0.40	1.43 ± 0.43	1.30 ± 0.60
70	0.60 ± 0.39	3.72 ± 0.26	1.08 ± 0.13	0.66 ± 0.15	0.09 ± 0.29
71	11.20 ± 1.46	21.30 ± 2.50	8.38 ± 2.04	10.50 ± 1.44	3.56 ± 1.64

7.3.2 Morphological Characteristics

Classes of PAH Features

There are three categories of PAH profiles (Peeters et al., 2002): A, B, and C. As demonstrated in van Diedenhoven et al. (2004) and Tielens (2008) (see Figure 7.5), the center positions and feature profiles vary depending on the source type. Class A type shows the PAH emission at 6.2 μm and 7.7 μm, and often appear for the sources of reflection nebular, HII region, and general interstellar medium. Class B type features have shifts of center positions to longer wavelengths compared to Class A type. The sources with Class B consist of circumstellar disks around HAeBe stars, PNe, and post-AGB objects. Class C type also shows center position shift to longer wavelengths and distinctive and much broad emission profile at 7-9 μm. Some carbon-rich post-AGB objects are known as sources with Class C PAH features. Therefore, the

central position and emission profile of PAH features are important parameters for classification of PAH features.

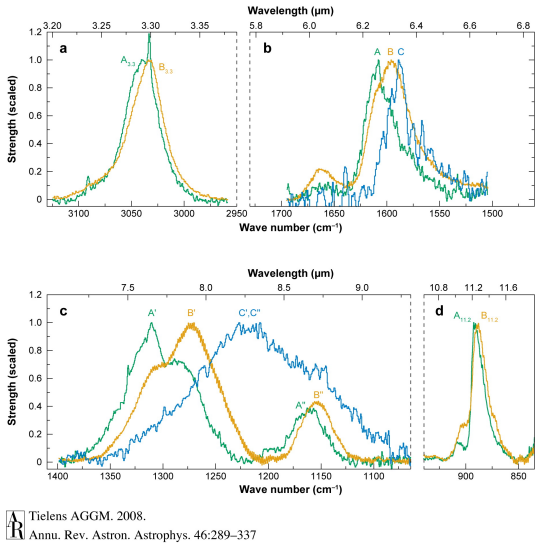


Figure 7.5 Center position variation by source classification. class A (green) peaks at the shortest wavelengths, and class B (orange) peaks at longer wavelengths. Figure 4 in Tielens (2008).

Central Wavelengths of PAH Features, λ_c

To find central wavelengths of PAH features, we measured $\lambda_{c,red}$ and $\lambda_{c,blue}$ which are the wavelengths which divide each feature into two equal-flux halves, integrating respectively from the long-wavelength and short-wavelength sides of the feature. (These wavelengths would of course be identical in noiseless spectra.) Then the center position is the mean of the two positions. The measured central positions are listed in Table 7.3. We also indicate each feature's central wavelengths of each objects in Figure 7.4 with the central positions (6.26, 7.9, and 11.26 μm) of Class B type features for comparison.

Table 7.3. Center Positions of PAH features

	$\lambda_C(\mu$m)				
ID	6.2 μm PAH	7.7-8.2 μm PAH	8.6 μm PAH	11.2 μm PAH	12.7μm
67	6.20 ± 0.02	7.73 ± 0.03	8.51 ± 0.03	11.24 ± 0.03	12.81 ± 0.03
74	6.16 ± 0.03	7.61 ± 0.15	8.51 ± 0.03	11.24 ± 0.03	12.81 ± 0.03
101	6.23 ± 0.02	7.67 ± 0.03	8.57 ± 0.03	11.24 ± 0.03	12.75 ± 0.03
114	6.20 ± 0.02	7.61 ± 0.09	8.63 ± 0.15	11.30 ± 0.03	12.75 ± 0.03
139	6.20 ± 0.02	7.91 ± 0.03	8.69 ± 0.03	11.30 ± 0.03	12.69 ± 0.03
143	6.41 ± 0.03	7.73 ± 0.03	8.57 ± 0.03	11.24 ± 0.03	12.75 ± 0.15
145	6.20 ± 0.02	7.61 ± 0.03	8.57 ± 0.03	11.18 ± 0.03	12.69 ± 0.03
147	6.27 ± 0.02	7.73 ± 0.03	8.57 ± 0.03	11.24 ± 0.03	12.75 ± 0.03
152	6.20 ± 0.02	7.67 ± 0.03	8.57 ± 0.03	11.24 ± 0.03	12.69 ± 0.88
153	6.23 ± 0.02	7.73 ± 0.03	8.57 ± 0.03	11.24 ± 0.03	12.81 ± 0.03
158	6.23 ± 0.02	7.67 ± 0.03	8.57 ± 0.03	11.24 ± 0.03	12.81 ± 0.03
68	6.14 ± 0.02	7.73 ± 0.03	8.63 ± 0.03	11.24 ± 0.03	12.81 ± 0.03
70	6.02 ± 0.12	7.73 ± 0.03	8.51 ± 0.03	11.24 ± 0.03	12.75 ± 1.48
71	6.23 ± 0.02	7.73 ± 0.03	8.57 ± 0.03	11.24 ± 0.03	12.75 ± 0.06

Distinctive PAH features from an Externarally Illuminated Disk

One target, the A type star OriA-139 (V2328 Ori, A9.0), has the central positions and emission profiles of PAH features conforming to Class B. The PAH features of most objects with K-M type host stars appear to belong neither to Class A nor Class B. To illustrate how the PAH features from the externally-illuminated protoplanetary disks around K-M type host stars differs from PAH features from background nebular and/or protoplanetary disks illuminated by photons from K-M type host star, we compare the spectrum of background around OriA-147 (V1283 Ori; M4.5) and a spectrum of UX Tau A (K2; a PTD in Taurus) to that of OriA-147. The continuum fittings for the background around OriA-147 and UX Tau A are presented in Fig 7.6. We compared the absolute strength of PAH features (feature/continuum ratio) in Figure 7.7. UX Tau A has much weaker PAH features compared to that of OriA-147 in spite of much earlier spectral type and higher T_{eff} of the host star. We scaled

the PAH features normalized to the continuum of OriA-147 and UX Tau A to that of the background in the bottom plot of Figure 7.7 to compare the profiles of PAH features of them. We found that the PAH features from OriA-147 are not only different from the PAH features from background sky around OriA-147 but also different from the PAH emission from the protoplanetary disk around UX Tau A.

From these comparisons, we can confirm that (1) the UV radiation from θ^1 Ori C is strong enough that the PAH excitation it produces is much larger than that by the central stars, in disks 0.7 pc away; (2) based on their different profiles, the PAHs in each sources probably have somewhat different size, mass, degree of ionization, and vibrational modes.

7.4 Discussion

7.4.1 Dependence of the PAH emission on T_{eff} and Distance

The fluxes of the PAH features (I_{PAH}) from disks around B-G type stars increase with T_{eff} of the host star (Geers et al., 2006). Sloan et al. (2005) and Keller et al. (2008) found the center position of PAH features (of mostly HAe/Be objects) to depend on T_{eff}. These dependence of the properties of PAH features is because UV and optical radiation incident on the disk surface is the main source to excite PAHs and the earlier type stars illuminate their circumstellar disk with stronger UV/optical radiation than the later type stars.

However, the trend of dependance on T_{eff} and PAH-feature are not strongly

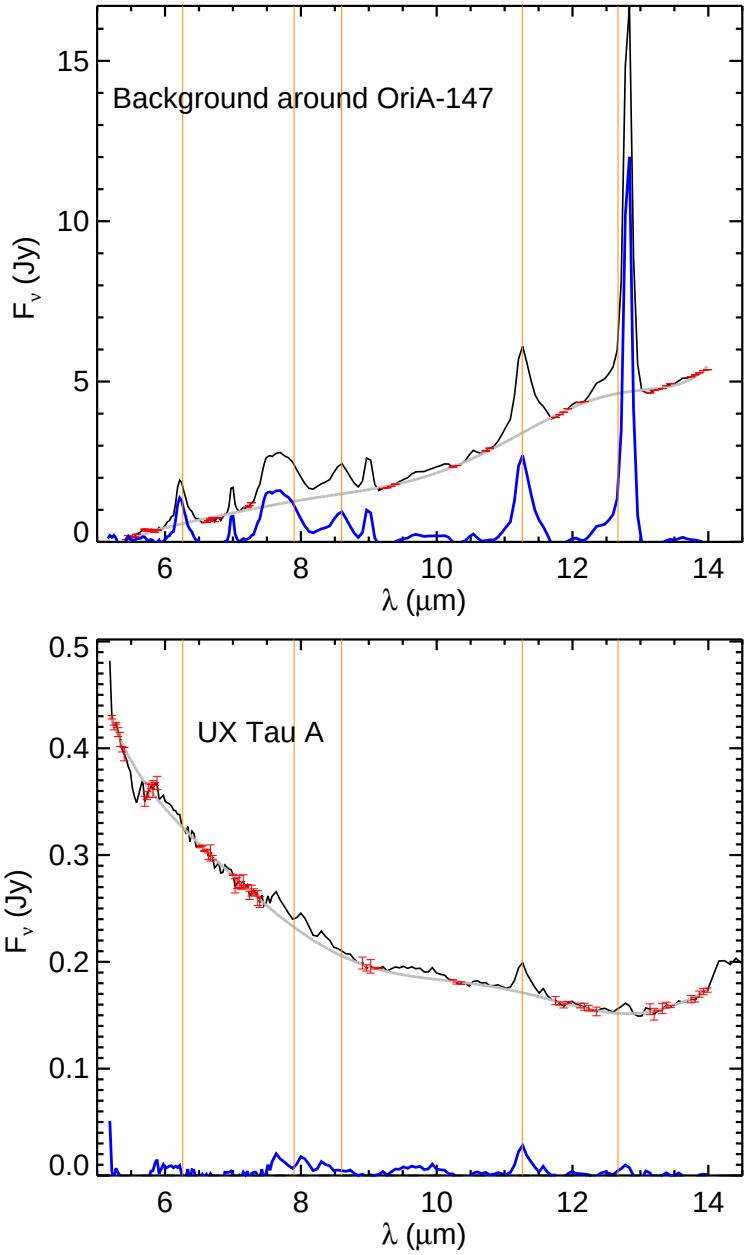


Figure 7.6 Background emission around OriA-147, PAHs in UX Tau A

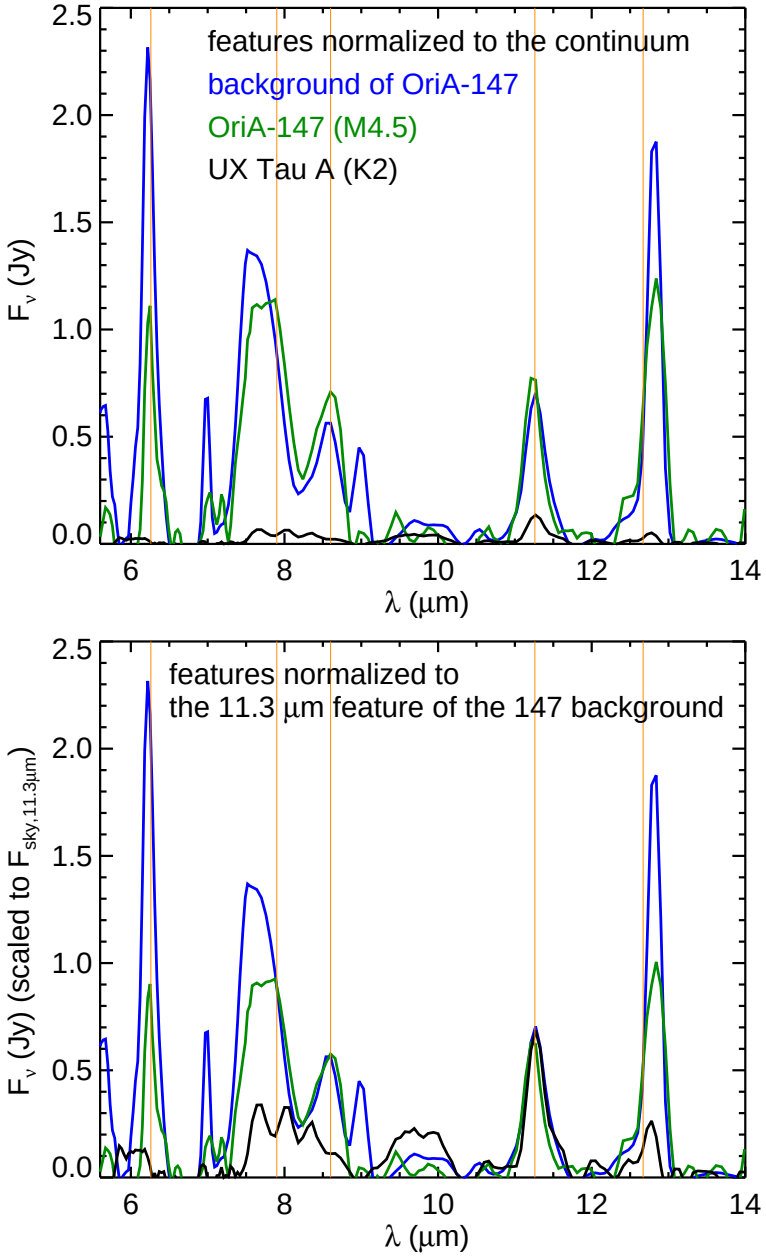


Figure 7.7 Continuum subtracted and normalized flux

correlated for the disks around K-M type stars in this study[1]. T_{eff} spans the range of 3000-8000K (Figure 7.8). We see the PAH strengths increase with T_{eff} for the earlier type stars with G0 and A9, which is similar to the previous studies, but we see no correlation between I_{PAH} and T_{eff} for $T_{eff} \leq 4000$ K. On the other hand, we find a relation between I_{PAH} and the projected distance (d) from θ_1 Ori C in Figure 7.9: $I_{PAH} \propto d^{-4/3}$ without including the two disks around G0 and A9 type star. This is the evidence that the UV photons incident from θ_1 Ori C are the major source of the PAH excitation mechanism from the disks around M-K type stars rather than the UV photons from their host star.

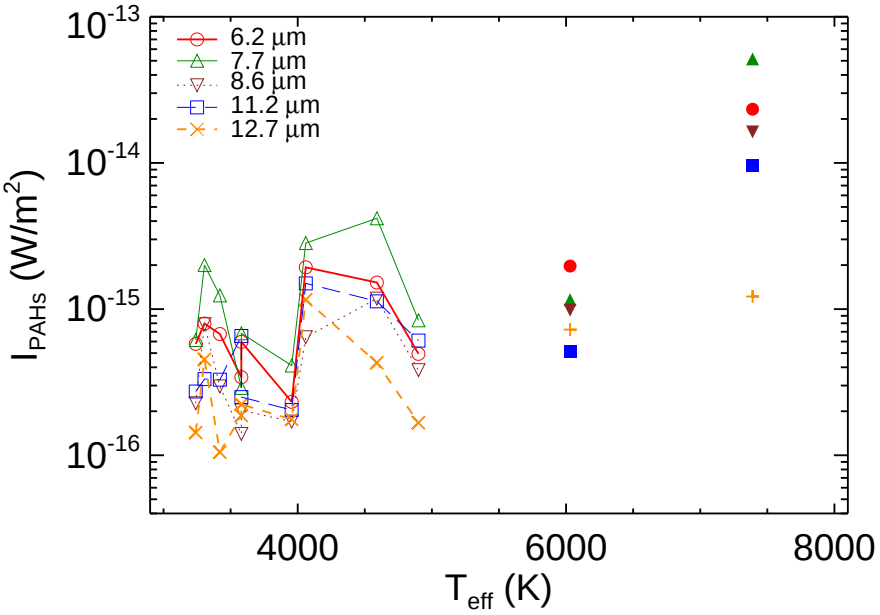


Figure 7.8 PAH intensity versus T_{eff}

[1]We take 11 of 14 objects into our analysis because remaining three objects do not have their stellar spectral types determineded.

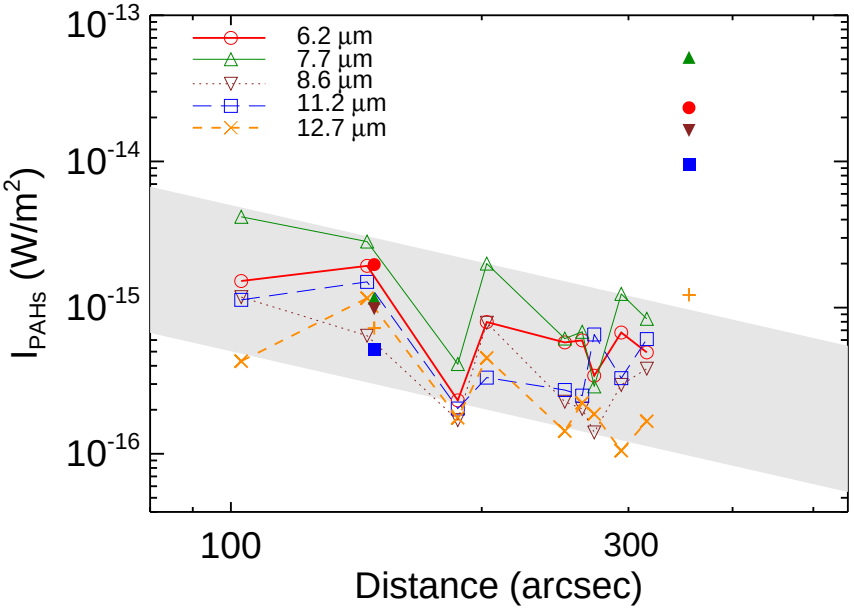


Figure 7.9 PAH intensity along distance from θ^1 Ori C.

We find no correlation between the cental position (λ_C) of the PAH features and T_{eff} or d in Figure 7.10. Considering that (1) λ_C of the PAH features of the sources in this study do not agree to the λ_C for the type of known classification and (2) there is no strong correlation of λ_C to T_{eff} or d, the PAHs in the externally illuminated disks around low mass T-Tauri stars could have different properties than the PAHs in the disks illuminated by the central star.

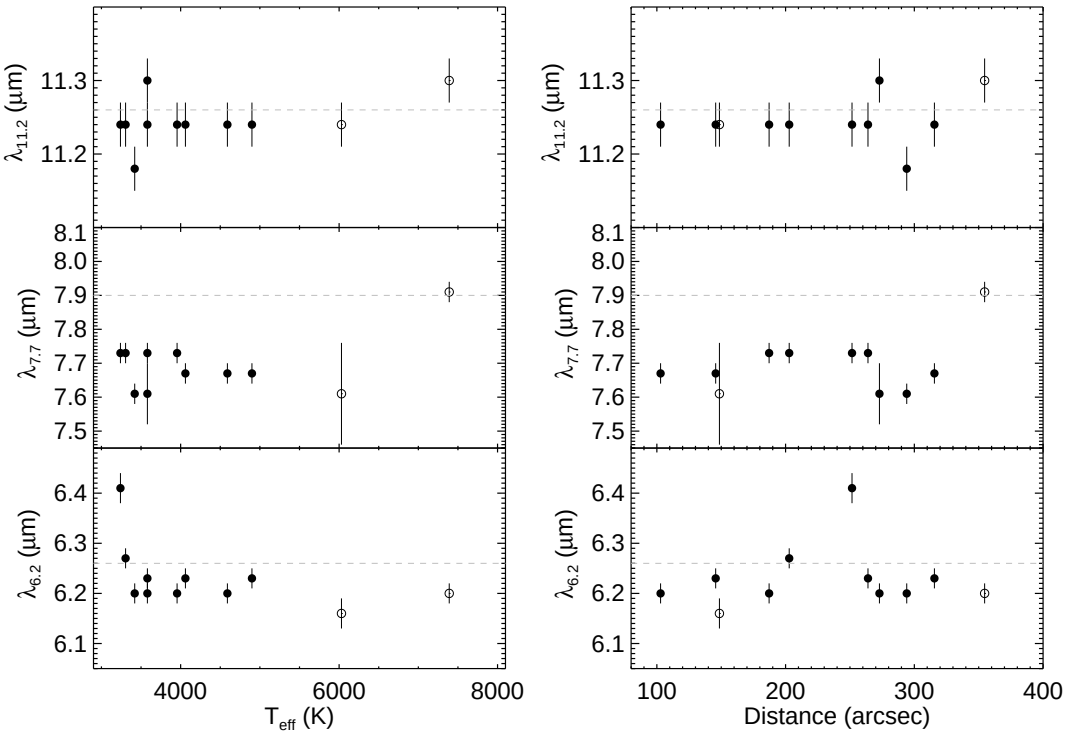


Figure 7.10 PAH Center position along T_{eff} and distance from θ^1 Ori C. The dashed lines indicate λ_C of PAHs features of Class B type as a reference.

7.4.2 PAH Relative Flux Ratio

The PAH features at $\lambda = 6.2$ and 7.7 μm originate from a C-C stretching mode, and they get stronger relative to other PAH features in ionized PAHs. The PAH features at $\lambda = 11.2$ and 12.7 μm are from C-H out-of-plane bending modes, and the features are stronger in neutral PAHs. Therefore, the flux ratio between the 6.2 μm feature and the 11.2 μm feature, $F_{6.2}/F_{11.2}$, has been used as an indicator of the degree of ionization in the PAHs. We plot two relative flux ratios, $F_{6.2}/F_{11.2}$ and $F_{7.7}/F_{11.2}$ in the upper panel of Figure 7.11. Because both 6.2 and 7.7 μm bands come from ionized PAHs, the relative flux ratio of them to the 11.2 μm band are tightly correlated in the upper panel of Figure 7.11. The results of rank correlations and a linear correlation test show that the strong correlation is statistically very significant. In the lower panel of Figure 7.11 we plot $F_{12.7}/F_{11.2}$ to $F_{7.7}/F_{11.2}$. Even though the 11.2 μm and 12.7 μm features decrease for charged PAHs, Hony et al. (2001) found that the relative strength of the trio mode (three adjacent hydrogen) of the 12.7 μm band to the solo mode (single adjacent hydrogen) of the 11.2 μm is correlated to the ionization ratio of PAHs. Our data also show an increasing trend of $F_{12.7}/F_{11.2}$ along $F_{7.7}/F_{11.2}$, but in much scattered manner. The rank correlation and linear correlation also indicate the trend of $F_{12.7}/F_{11.2}$ is not statistically significant.

Figure 7.12 show the variation of the ionization ratios, $F_{6.2}/F_{11.2}$, $F_{7.7}/F_{11.2}$, and $F_{12.7}/F_{11.2}$ to the effective temperature of the host-stars and to the distance from θ^1 Ori C. We find no significant correlation between any ionization ratio and distance. The "ionization" ratio, $F_{6.2}/F_{11.2}$, and T_{eff} look to have an

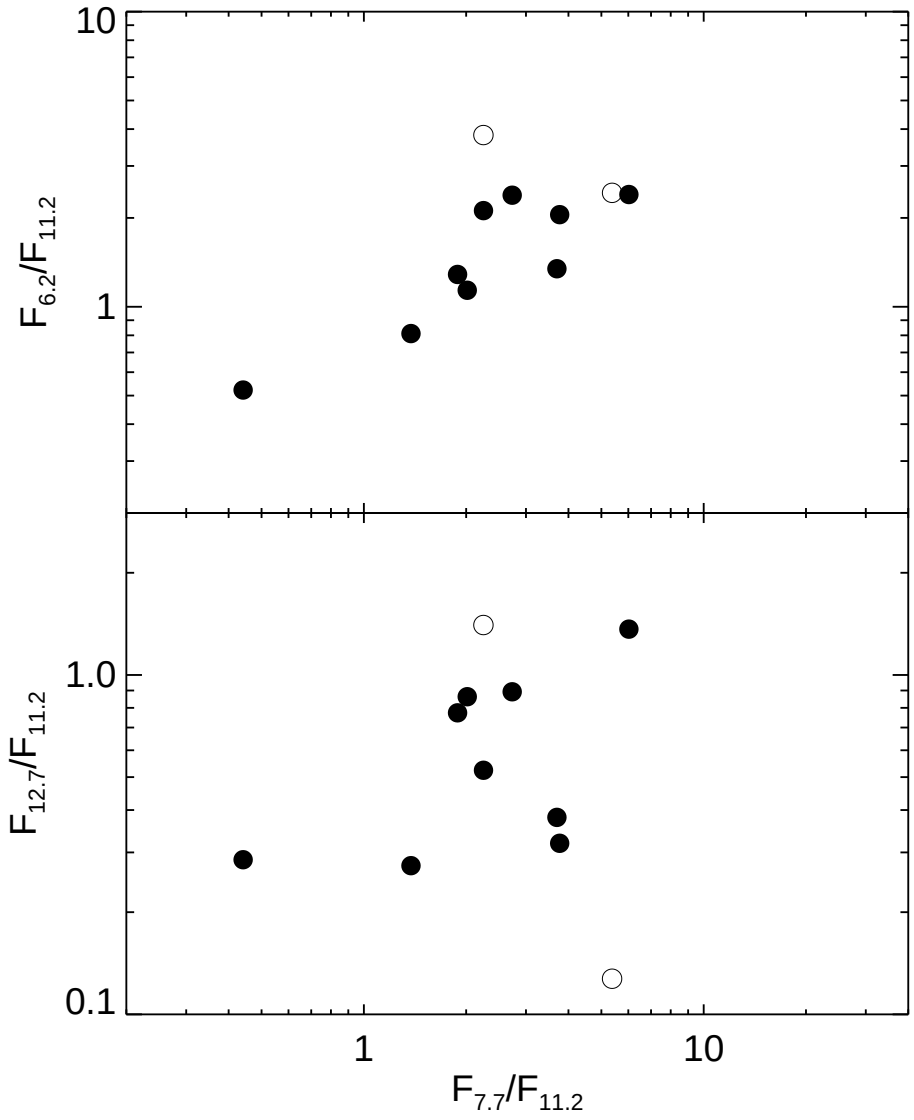


Figure 7.11 Flux ratio between different features. The statistical test between $F_{6.2}/F_{11.2}$ and $F_{7.7}/F_{11.2}$: Spearman's ρ=0.85, Kendall's τ=0.72, and Pearson's r=0.74 for N=9 of the objects with black solid dots. The probability of the each correlation could be occur by a random distribution: P_ρ=0.004, P_τ=0.007, and P_r=0.02. The statistical test result of bottom panel for $F_{12.7}/F_{11.2}$ and $F_{7.7}/F_{11.2}$: ρ=0.52, tau=0.33, and r=0.6 for N=9 of the objects with black solid dots. The probability of the each correlation could be occur by a random distribution: P_ρ=0.15, P_τ=0.21, and P_r=0.09.

anti-correlation, but statistical tests say the correlation is neither tight nor significant. If the ionization ratio and T_{eff} were anti-correlated, it would be an opposite result to the previous finding with disks around host-stars with T_{eff} greater than 5000 K which probably the UV photons from the host star is the main source to excite PAH molecules, allowing more ionization with more stronger energy.

Other relative flux ratios from all possible combinations of any two PAHs features are displayed in Appendix E.

7.5 Summary

In this chapter, we reported the detection of emission from PAHs in protoplanetary disks around low-mass T Tauri stars with later type of spectral types (K-M). The PAHs in the disks are thought to be excited by external illumination from strong UV photons from the nearby OB association, notably θ^1 Ori C. We found that the PAH profiles do not agree to the current classification of PAHs features. We find the PAH flux is not related to the effective temperature of the host star. However, the strength of PAH bands are depend on the distance from θ^1 Ori C: $I_{PAH} \propto d^{-4/3}$.

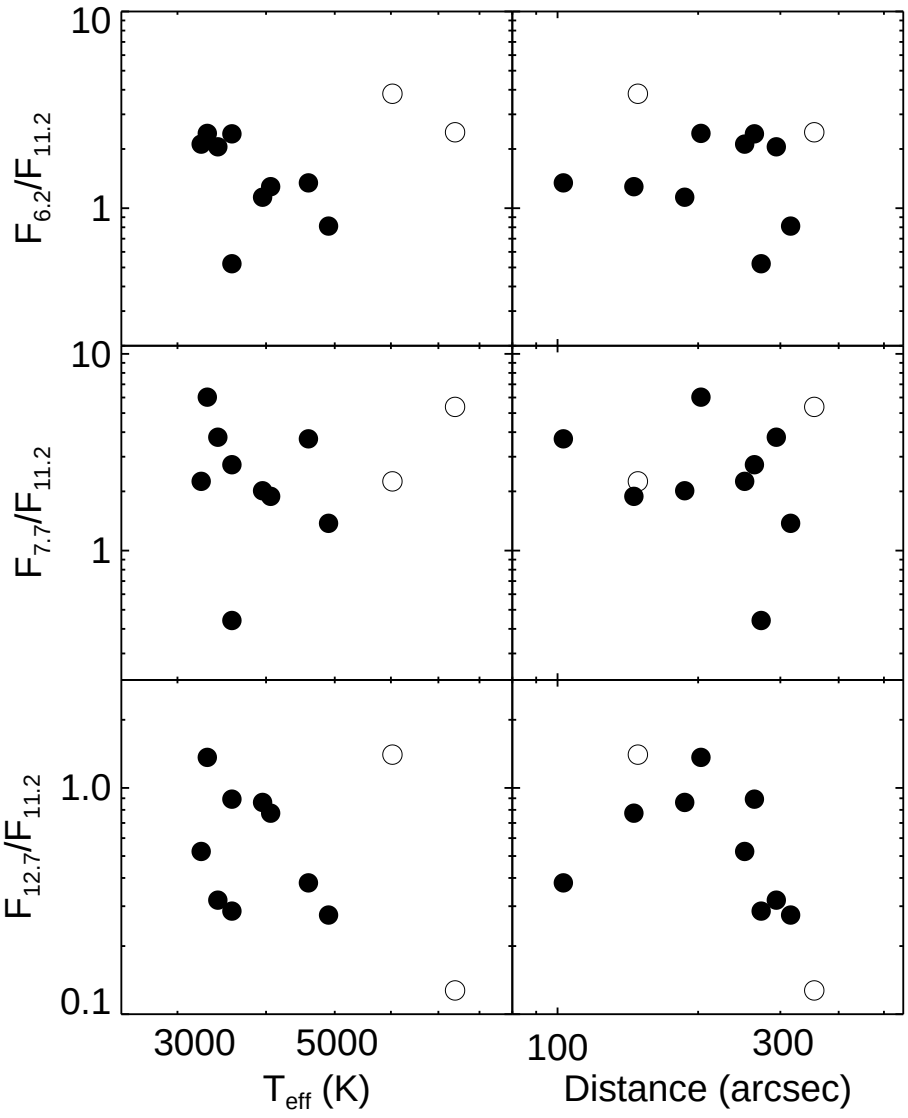


Figure 7.12 The relative flux ratio along T_{eff} and distance from θ^1 Ori C.

References

Adelman-McCarthy, J. K. & et al. 2011, VizieR Online Data Catalog, 2306, 0

Alexander, R. D., Clarke, C. J., & Pringle, J. E. 2006a, MNRAS, 369, 216

—. 2006b, MNRAS, 369, 229

Allamandola, L. J., Tielens, A. G. G. M., & Barker, J. R. 1985, ApJ, 290, L25

Allen, L. & Mosby, G. 2008, personal communication

Allen, L. E. 1995, PhD thesis, School of Physics, University of New South Wales, Sydney, NSW 2052, Australia ¡EMAIL¿lea@newt.phys.unsw.edu.au¡/EMAIL¿

Andre, P., Ward-Thompson, D., & Barsony, M. 1993, ApJ, 406, 122

Andrews, S. M. & Williams, J. P. 2005, ApJ, 631, 1134

—. 2007, ApJ, 671, 1800

Andrews, S. M., Wilner, D. J., Espaillat, C., Hughes, A. M., Dullemond, C. P., McClure, M. K., Qi, C., & Brown, J. M. 2011, ApJ, 732, 42

Andrews, S. M., Wilner, D. J., Hughes, A. M., Qi, C., & Dullemond, C. P. 2009, ApJ, 700, 1502

Arnold, L. A., Watson, D. M., Kim, K. H., Manoj, P., Remming, I., Sheehan, P., Adame, L., et al. 2012, ApJS, 201, 12

Baraffe, I., Chabrier, G., Allard, F., & Hauschildt, P. H. 1998, A&A, 337, 403

Bertout, C., Siess, L., & Cabrit, S. 2007, A&A, 473, L21

Bouwman, J., Henning, T., Hillenbrand, L. A., Meyer, M. R., Pascucci, I., Carpenter, J., Hines, D., et al. 2008, ApJ, 683, 479

Brauer, F., Dullemond, C. P., & Henning, T. 2008, A&A, 480, 859

Brauer, F., Dullemond, C. P., Johansen, A., Henning, T., Klahr, H., & Natta, A. 2007, A&A, 469, 1169

Brown, J. M., Blake, G. A., Dullemond, C. P., Merín, B., Augereau, J. C., Boogert, A. C. A., Evans, II, N. J., et al. 2007, ApJ, 664, L107

Calvet, N., D'Alessio, P., Watson, D. M., Franco-Hernández, R., Furlan, E., Green, J., Sutter, P. M., et al. 2005, ApJ, 630, L185

Calvet, N., Muzerolle, J., Briceño, C., Hernández, J., Hartmann, L., Saucedo, J. L., & Gordon, K. D. 2004, AJ, 128, 1294

Caratti O Garatti, A., Garcia Lopez, R., Antoniucci, S., Nisini, B., Giannini, T., Eislöffel, J., Ray, T. P., Lorenzetti, D., & Cabrit, S. 2012, A&A, 538, A64

Chiang, E. & Murray-Clay, R. 2007, Nature Physics, 3, 604

Ciesla, F. J. 2007, ApJ, 654, L159

Cieza, L. A., Schreiber, M. R., Romero, G. A., Mora, M. D., Merin, B., Swift, J. J., Orellana, M., et al. 2010, ApJ, 712, 925

Clarke, C. J., Gendrin, A., & Sotomayor, M. 2001, MNRAS, 328, 485

Crapsi, A., van Dishoeck, E. F., Hogerheijde, M. R., Pontoppidan, K. M., & Dullemond, C. P. 2008, A&A, 486, 245

Currie, T., Lada, C. J., Plavchan, P., Robitaille, T. P., Irwin, J., & Kenyon, S. J. 2009, ApJ, 698, 1

Currie, T. & Sicilia-Aguilar, A. 2011, ApJ, 732, 24

Cushing, M. C., Rayner, J. T., & Vacca, W. D. 2005, ApJ, 623, 1115

Cushing, M. C., Vacca, W. D., & Rayner, J. T. 2004, PASP, 116, 362

Cutri, R. M. & et al. 2012, VizieR Online Data Catalog, 2311, 0

da Rio, N., Robberto, M., Soderblom, D. R., Panagia, N., Hillenbrand, L. A., Palla, F., & Stassun, K. 2010, VizieR Online Data Catalog, 218, 30261

Daemgen, S., Correia, S., & Petr-Gotzens, M. G. 2012, A&A, 540, A46

D'Alessio, P., Calvet, N., & Hartmann, L. 2001, ApJ, 553, 321

D'Alessio, P., Calvet, N., Hartmann, L., Franco-Hernández, R., & Servín, H. 2006, ApJ, 638, 314

D'Alessio, P., Hartmann, L., Calvet, N., Franco-Hernández, R., Forrest, W. J., Sargent, B., Furlan, E., et al. 2005, ApJ, 621, 461

D'Antona, F. & Mazzitelli, I. 1997, Mem. Soc. Astron. Italiana, 68, 807

Draine, B. T. & Lee, H. M. 1984, ApJ, 285, 89

Drake, J. J., Ercolano, B., Flaccomio, E., & Micela, G. 2009, ApJ, 699, L35

Dullemond, C. P. & Dominik, C. 2005, A&A, 434, 971

Edgar, R. G., Quillen, A. C., & Park, J. 2007, MNRAS, 381, 1280

Ercolano, B., Clarke, C. J., & Drake, J. J. 2009, ApJ, 699, 1639

Espaillat, C. 2009, PhD thesis, University of Michigan

Espaillat, C., Calvet, N., D'Alessio, P., Bergin, E., Hartmann, L., Watson, D., Furlan, E., et al. 2007a, ApJ, 664, L111

Espaillat, C., Calvet, N., D'Alessio, P., Hernández, J., Qi, C., Hartmann, L., Furlan, E., & Watson, D. M. 2007b, ApJ, 670, L135

Espaillat, C., Calvet, N., Luhman, K. L., Muzerolle, J., & D'Alessio, P. 2008, ApJ, 682, L125

Espaillat, C., D'Alessio, P., Hernández, J., Nagel, E., Luhman, K. L., Watson, D. M., Calvet, N., Muzerolle, J., & McClure, M. 2010, ApJ, 717, 441

Espaillat, C., Furlan, E., D'Alessio, P., Sargent, B., Nagel, E., Calvet, N., Watson, D. M., & Muzerolle, J. 2011, ApJ, 728, 49

Espaillat, C., Ingleby, L., Hernández, J., Furlan, E., D'Alessio, P., Calvet, N., Andrews, S., et al. 2012, ApJ, 747, 103

Evans, N., Calvet, N., Cieza, L., Forbrich, J., Hillenbrand, L., Lada, C., Merín, B., Strom, S., & Watson, D. 2009, ArXiv e-prints

Fang, M., van Boekel, R., Wang, W., Carmona, A., Sicilia-Aguilar, A., & Henning, T. 2009, A&A, 504, 461

Fűrész, G., Hartmann, L. W., Megeath, S. T., Szentgyorgyi, A. H., & Hamden, E. T. 2008, ApJ, 676, 1109

Font, A. S., McCarthy, I. G., Johnstone, D., & Ballantyne, D. R. 2004, ApJ, 607, 890

Forrest, W. J., Sargent, B., Furlan, E., D'Alessio, P., Calvet, N., Hartmann, L., Uchida, K. I., et al. 2004, ApJS, 154, 443

Furlan, E., Hartmann, L., Calvet, N., D'Alessio, P., Franco-Hernández, R., Forrest, W. J., Watson, D. M., et al. 2006, ApJS, 165, 568

Furlan, E., Luhman, K. L., Espaillat, C., D'Alessio, P., Adame, L., Manoj, P., Kim, K. H., et al. 2011, ApJS, 195, 3

Furlan, E., Sargent, B., Calvet, N., Forrest, W. J., D'Alessio, P., Hartmann, L., Watson, D. M., et al. 2007, ApJ, 664, 1176

Furlan, E., Watson, D. M., McClure, M. K., Manoj, P., Espaillat, C., D'Alessio, P., Calvet, N., et al. 2009, ApJ, 703, 1964

Gâlfalk, M. & Olofsson, G. 2008, A&A, 489, 1409

Garaud, P. 2007, ApJ, 671, 2091

Gatti, T., Natta, A., Randich, S., Testi, L., & Sacco, G. 2008, A&A, 481, 423

Geers, V. C., Augereau, J.-C., Pontoppidan, K. M., Dullemond, C. P., Visser, R., Kessler-Silacci, J. E., Evans, II, N. J., et al. 2006, A&A, 459, 545

Gillett, F. C., Forrest, W. J., & Merrill, K. M. 1973, ApJ, 183, 87

Glebocki, R. & Gnacinski, P. 2005, VizieR Online Data Catalog, 3244, 0

Gorti, U., Dullemond, C. P., & Hollenbach, D. 2009, ApJ, 705, 1237

Gorti, U. & Hollenbach, D. 2009, ApJ, 690, 1539

Grankin, K. N., Melnikov, S. Y., Bouvier, J., Herbst, W., & Shevchenko, V. S. 2007, A&A, 461, 183

Greaves, J. S. & Rice, W. K. M. 2010, MNRAS, 407, 1981

Greene, T. P., Wilking, B. A., Andre, P., Young, E. T., & Lada, C. J. 1994, ApJ, 434, 614

Güdel, M., Briggs, K. R., Arzner, K., Audard, M., Bouvier, J., Feigelson, E. D., Franciosini, E., et al. 2007, A&A, 468, 353

Gullbring, E., Hartmann, L., Briceno, C., & Calvet, N. 1998, ApJ, 492, 323

Hartmann, L., Calvet, N., Gullbring, E., & D'Alessio, P. 1998, ApJ, 495, 385

Hartmann, L., D'Alessio, P., Calvet, N., & Muzerolle, J. 2006, ApJ, 648, 484

Herbig, G. H. & Bell, K. R. 1988, Third Catalog of Emission-Line Stars of the Orion Population : 3 : 1988

Hernandez, J. 2008, personal communication

Hernandez, J. & Tobin, J. 2009, personal communication

Higdon, S. J. U., Devost, D., Higdon, J. L., Brandl, B. R., Houck, J. R., Hall, P., Barry, D., et al. 2004, PASP, 116, 975

Hillenbrand, L. A. 1997, AJ, 113, 1733

Hillenbrand, L. A. & Carpenter, J. M. 2000, ApJ, 540, 236

Holland, W. S., Greaves, J. S., Zuckerman, B., Webb, R. A., McCarthy, C., Coulson, I. M., Walther, D. M., et al. 1998, Nature, 392, 788

Hollenbach, D., Johnstone, D., Lizano, S., & Shu, F. 1994, ApJ, 428, 654

Honda, M., Kataza, H., Okamoto, Y. K., Yamashita, T., Min, M., Miyata, T., Sako, S., et al. 2006, ApJ, 646, 1024

Houk, N. & Swift, C. 2000, VizieR Online Data Catalog, 3214, 0

Hughes, A. M., Andrews, S. M., Espaillat, C., Wilner, D. J., Calvet, N., D'Alessio, P., Qi, C., Williams, J. P., & Hogerheijde, M. R. 2009, ApJ, 698, 131

Hughes, A. M., Wilner, D. J., Calvet, N., D'Alessio, P., Claussen, M. J., & Hogerheijde, M. R. 2007, ApJ, 664, 536

Inutsuka, S.-i., Machida, M. N., & Matsumoto, T. 2010, ApJ, 718, L58

Ireland, M. J. & Kraus, A. L. 2008, ApJ, 678, L59

Jura, M. & Turner, J. 1998, Nature, 395, 144

Kastner, J. H., Buchanan, C. L., Sargent, B., & Forrest, W. J. 2006, ApJ, 638, L29

Keller, L. D., Sloan, G. C., Forrest, W. J., Ayala, S., D'Alessio, P., Shah, S., Calvet, N., et al. 2008, ApJ, 684, 411

Kelly, B. C. 2007, ApJ, 665, 1489

Kenyon, S. J. & Hartmann, L. 1995, ApJS, 101, 117

Kessler-Silacci, J., Augereau, J.-C., Dullemond, C. P., Geers, V., Lahuis, F., Evans, II, N. J., van Dishoeck, E. F., et al. 2006, ApJ, 639, 275

Kim, K. H., Watson, D. M., Manoj, P., Furlan, E., Najita, J., Forrest, W. J., Sargent, B., et al. 2009, ApJ, 700, 1017

Kraus, A. L. & Ireland, M. J. 2012, ApJ, 745, 5

Kraus, A. L., Ireland, M. J., Martinache, F., & Hillenbrand, L. A. 2011, ApJ, 731, 8

Kukarkin, B. V., Kholopov, P. N., Pskovsky, Y. P., Efremov, Y. N., Kukarkina, N. P., Kurochkin, N. E., & Medvedeva, G. I. 1971, in General Catalogue of Variable Stars, 3rd ed. (1971), 0–+

Lada, C. J. 1987, in IAU Symposium, Vol. 115, Star Forming Regions, ed. M. Peimbert & J. Jugaku, 1–17

Lada, C. J. & Lada, E. A. 2003, ARA&A, 41, 57

Lada, C. J., Muench, A. A., Luhman, K. L., Allen, L., Hartmann, L., Megeath, T., Myers, P., et al. 2006, AJ, 131, 1574

Lebouteiller, V., Bernard-Salas, J., Sloan, G. C., & Barry, D. J. 2010, PASP, 122, 231

Leger, A. & Puget, J. L. 1984, A&A, 137, L5

Lubow, S. H. & D'Angelo, G. 2006, ApJ, 641, 526

Luhman, K. L., Allen, P. R., Espaillat, C., Hartmann, L., & Calvet, N. 2010, ApJS, 186, 111

Manoj, P. 2010, in Astronomical Society of the Pacific Conference Series, Vol. 432, New Horizons in Astronomy: Frank N. Bash Symposium 2009, ed. L. M. Stanford, J. D. Green, L. Hao, & Y. Mao, 49

Manoj, P., Bhatt, H. C., Maheswar, G., & Muneer, S. 2006, ApJ, 653, 657

Manoj, P., Kim, K. H., Furlan, E., McClure, M. K., Luhman, K. L., Watson, D. M., Espaillat, C., et al. 2011, ApJS, 193, 11

Marsh, K. A. & Mahoney, M. J. 1992, ApJ, 395, L115

Mathis, J. S. 1990, ARA&A, 28, 37

McClure, M. 2009, ApJ, 693, L81

McClure, M. K., Forrest, W. J., Sargent, B. A., Watson, D. M., Furlan, E., Manoj, P., Luhman, K. L., et al. 2008, ApJ, 683, L187

McClure, M. K., Furlan, E., Manoj, P., Luhman, K. L., Watson, D. M., Forrest, W. J., Espaillat, C., et al. 2010, ApJS, 188, 75

Meeus, G., Waters, L. B. F. M., Bouwman, J., van den Ancker, M. E., Waelkens, C., & Malfait, K. 2001, A&A, 365, 476

Megeath, S. T., Gutermuth, R., Muzerolle, J., Kryukova, E., Flaherty, K., Hora, J. L., Allen, L. E., et al. 2012, AJ, 144, 192

Menten, K. M., Reid, M. J., Forbrich, J., & Brunthaler, A. 2007, A&A, 474, 515

Merín, B., Brown, J. M., Oliveira, I., Herczeg, G. J., van Dishoeck, E. F., Bottinelli, S., Evans, II, N. J., et al. 2010, ApJ, 718, 1200

Meru, F. & Bate, M. R. 2010, MNRAS, 406, 2279

Meyer, M. R., Calvet, N., & Hillenbrand, L. A. 1997, AJ, 114, 288

Morishima, R. 2012, MNRAS, 420, 2851

Muzerolle, J., Allen, L. E., Megeath, S. T., Hernández, J., & Gutermuth, R. A. 2010, ApJ, 708, 1107

Muzerolle, J., Hartmann, L., & Calvet, N. 1998, AJ, 116, 2965

Muzerolle, J., Hillenbrand, L., Calvet, N., Briceño, C., & Hartmann, L. 2003, ApJ, 592, 266

Muzerolle, J., Luhman, K. L., Briceño, C., Hartmann, L., & Calvet, N. 2005, ApJ, 625, 906

Najita, J. R., Strom, S. E., & Muzerolle, J. 2007, MNRAS, 378, 369

Natta, A., Testi, L., & Randich, S. 2006, A&A, 452, 245

Ochsenbein, F. 1980, Bulletin d'Information du Centre de Donnees Stellaires, 19, 74

Ochsenbein, F., Bauer, P., & Marcout, J. 2000, A&AS, 143, 23

Olofsson, J., Augereau, J.-C., van Dishoeck, E. F., Merín, B., Lahuis, F., Kessler-Silacci, J., Dullemond, C. P., et al. 2009, A&A, 507, 327

Olofsson, J., Benisty, M., Augereau, J.-C., Pinte, C., Ménard, F., Tatulli, E., Berger, J.-P., et al. 2011, A&A, 528, L6

Owen, J. E., Clarke, C. J., & Ercolano, B. 2012, MNRAS, 422, 1880

Owen, J. E., Ercolano, B., & Clarke, C. J. 2011a, MNRAS, 412, 13

—. 2011b, MNRAS, 411, 1104

Owen, J. E., Ercolano, B., Clarke, C. J., & Alexander, R. D. 2010, MNRAS, 401, 1415

Palla, F. & Stahler, S. W. 1999, ApJ, 525, 772

Parenago, P. P. 1954, Trudy Gosudarstvennogo Astronomicheskogo Instituta, 25, 1

Parihar, P., Messina, S., Distefano, E., Shantikumar, N. S., & Medhi, B. J. 2009a, MNRAS, 400, 603

—. 2009b, MNRAS, 400, 603

Peeters, E., Hony, S., Van Kerckhoven, C., Tielens, A. G. G. M., Allamandola, L. J., Hudgins, D. M., & Bauschlicher, C. W. 2002, A&A, 390, 1089

Perez-Becker, D. & Chiang, E. 2011, ApJ, 735, 8

Piétu, V., Dutrey, A., Guilloteau, S., Chapillon, E., & Pety, J. 2006, A&A, 460, L43

Pott, J.-U., Perrin, M. D., Furlan, E., Ghez, A. M., Herbst, T. M., & Metchev, S. 2010, ApJ, 710, 265

Przygodda, F., van Boekel, R., Àbrahàm, P., Melnikov, S. Y., Waters, L. B. F. M., & Leinert, C. 2003, A&A, 412, L43

Quillen, A. C., Blackman, E. G., Frank, A., & Varnière, P. 2004, ApJ, 612, L137

Rayner, J. T., Cushing, M. C., & Vacca, W. D. 2009, ApJS, 185, 289

Rayner, J. T., Toomey, D. W., Onaka, P. M., Denault, A. J., Stahlberger, W. E., Vacca, W. D., Cushing, M. C., & Wang, S. 2003, PASP, 115, 362

Rebull, L. M. 2001, AJ, 121, 1676

Rebull, L. M., Hillenbrand, L. A., Strom, S. E., Duncan, D. K., Patten, B. M., Pavlovsky, C. M., Makidon, R., & Adams, M. T. 2000, AJ, 119, 3026

Riaz, B., Gizis, J. E., & Harvin, J. 2006, AJ, 132, 866

Rice, W. K. M., Armitage, P. J., Wood, K., & Lodato, G. 2006, MNRAS, 373, 1619

Rice, W. K. M., Wood, K., Armitage, P. J., Whitney, B. A., & Bjorkman, J. E. 2003, MNRAS, 342, 79

Robitaille, T. P., Whitney, B. A., Indebetouw, R., Wood, K., & Denzmore, P. 2006, ApJS, 167, 256

Sargent, B. A., Forrest, W. J., Tayrien, C., McClure, M. K., Watson, D. M., Sloan, G. C., Li, A., et al. 2009, ApJS, 182, 477

Scmitt-Kopplin, P., Cabelica, Z., Gougeon, R. D., Fekete, A., Kanawati, B., Harir, M., Gebefuegi, I., Eckel, G., & Hertkorn, N. 2010, Proceedings of the National Academy of Science, 107, 2763

Sephton, M. A., Love, G. D., Watson, J. S., Verchovsky, A. B., Wright, I. P., Snape, C. E., & Gilmour, I. 2003, in Lunar and Planetary Inst. Technical Report, Vol. 34, Lunar and Planetary Institute Science Conference Abstracts, ed. S. Mackwell & E. Stansbery, 1619

Shu, F., Najita, J., Ostriker, E., Wilkin, F., Ruden, S., & Lizano, S. 1994, ApJ, 429, 781

Sicilia-Aguilar, A., Henning, T., & Hartmann, L. W. 2010, ApJ, 710, 597

Siess, L., Dufour, E., & Forestini, M. 2000, A&A, 358, 593

Simon, M., Dutrey, A., & Guilloteau, S. 2000, ApJ, 545, 1034

Skrutskie, M. F., Cutri, R. M., Stiening, R., Weinberg, M. D., Schneider, S., Carpenter, J. M., Beichman, C., et al. 2006, AJ, 131, 1163

Sloan, G. C., Keller, L. D., Forrest, W. J., Leibensperger, E., Sargent, B., Li, A., Najita, J., et al. 2005, ApJ, 632, 956

Strom, K. M., Strom, S. E., Edwards, S., Cabrit, S., & Skrutskie, M. F. 1989, AJ, 97, 1451

Suzuki, T. K., Muto, T., & Inutsuka, S.-i. 2010, ApJ, 718, 1289

Tanaka, H., Himeno, Y., & Ida, S. 2005, ApJ, 625, 414

Tayrien, C. & Forrest, W. J. 2013, in preparation

Telleschi, A., Güdel, M., Briggs, K. R., Audard, M., & Palla, F. 2007, A&A, 468, 425

Thalmann, C., Grady, C. A., Goto, M., Wisniewski, J. P., Janson, M., Henning, T., Fukagawa, M., et al. 2010, ApJ, 718, L87

Tielens, A. G. G. M. 2008, ARA&A, 46, 289

Ukidss, C. 2012, VizieR Online Data Catalog, 2314, 0

Vacca, W. D., Cushing, M. C., & Rayner, J. T. 2003, PASP, 115, 389

van Boekel, R., Min, M., Waters, L. B. F. M., de Koter, A., Dominik, C., van den Ancker, M. E., & Bouwman, J. 2005, A&A, 437, 189

van Diedenhoven, B., Peeters, E., Van Kerckhoven, C., Hony, S., Hudgins, D. M., Allamandola, L. J., & Tielens, A. G. G. M. 2004, ApJ, 611, 928

Varnière, P., Bjorkman, J. E., Frank, A., Quillen, A. C., Carciofi, A. C., Whitney, B. A., & Wood, K. 2006, ApJ, 637, L125

Watson, D. M., Leisenring, J. M., Furlan, E., Bohac, C. J., Sargent, B., Forrest, W. J., Calvet, N., et al. 2009a, ApJS, 180, 84

Watson, M. G., Schröder, A. C., Fyfe, D., Page, C. G., Lamer, G., Mateos, S., Pye, J., et al. 2009b, A&A, 493, 339

White, R. J. & Ghez, A. M. 2001, ApJ, 556, 265

Wolff, S. C., Strom, S. E., & Hillenbrand, L. A. 2004, ApJ, 601, 979

Wouterloot, J. G. A. & Brand, J. 1992, A&A, 265, 144

Zacharias, N., Monet, D. G., Levine, S. E., Urban, S. E., Gaume, R., & Wycoff, G. L. 2005, VizieR Online Data Catalog, 1297, 0

Zhu, Z., Nelson, R. P., Dong, R., Espaillat, C., & Hartmann, L. 2012, ApJ, 755, 6

Zhu, Z., Nelson, R. P., Hartmann, L., Espaillat, C., & Calvet, N. 2011, ApJ, 729, 47

Zuckerman, B. & Song, I. 2004, ApJ, 603, 738

A Appendix to Chapter 3

A.1 SEDs of Class II disks in Orion A: observed in full IRS wavelength range, 5-35 μm

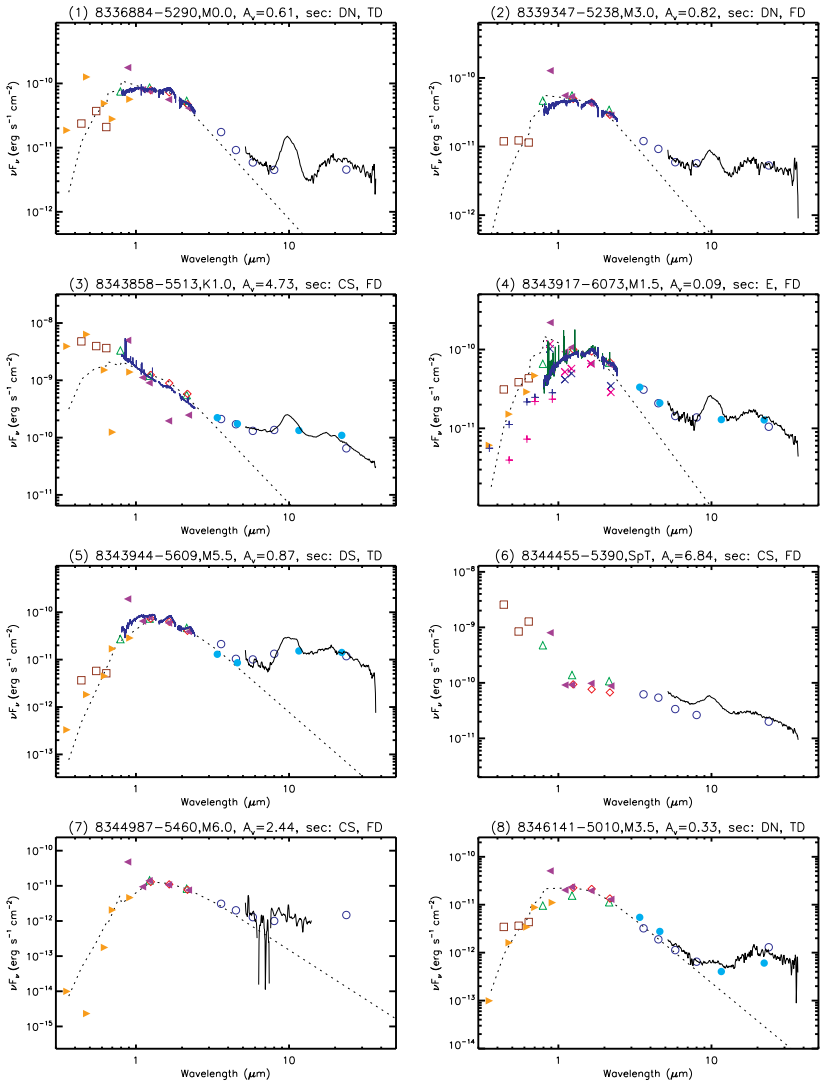


Figure A.1 De-reddened SEDs of our samples in ONC and L1641, which were observed with IRS SL and LL modules. The SEDs are composed of the following components: IRS (black line in the wavelength range of 5.2-35 μm); SpeX (black line in the wavelength range of 0.8-2.4 μm); IRAC and MIPS (open circles); 2MASS JHK (open diamonds); DENIS IJH(upward open triangles); UBVRI from da Rio et al. (2010) (downward open triangle); BVR from NOMAD (open squares); UKIDSS ($\times$ for multiple components; leftward filled triangle for the composite); SDSS (cross for multiple components; rightward filled triangle for the composite); WISE (filled circle);photosphere (black short dashed line).

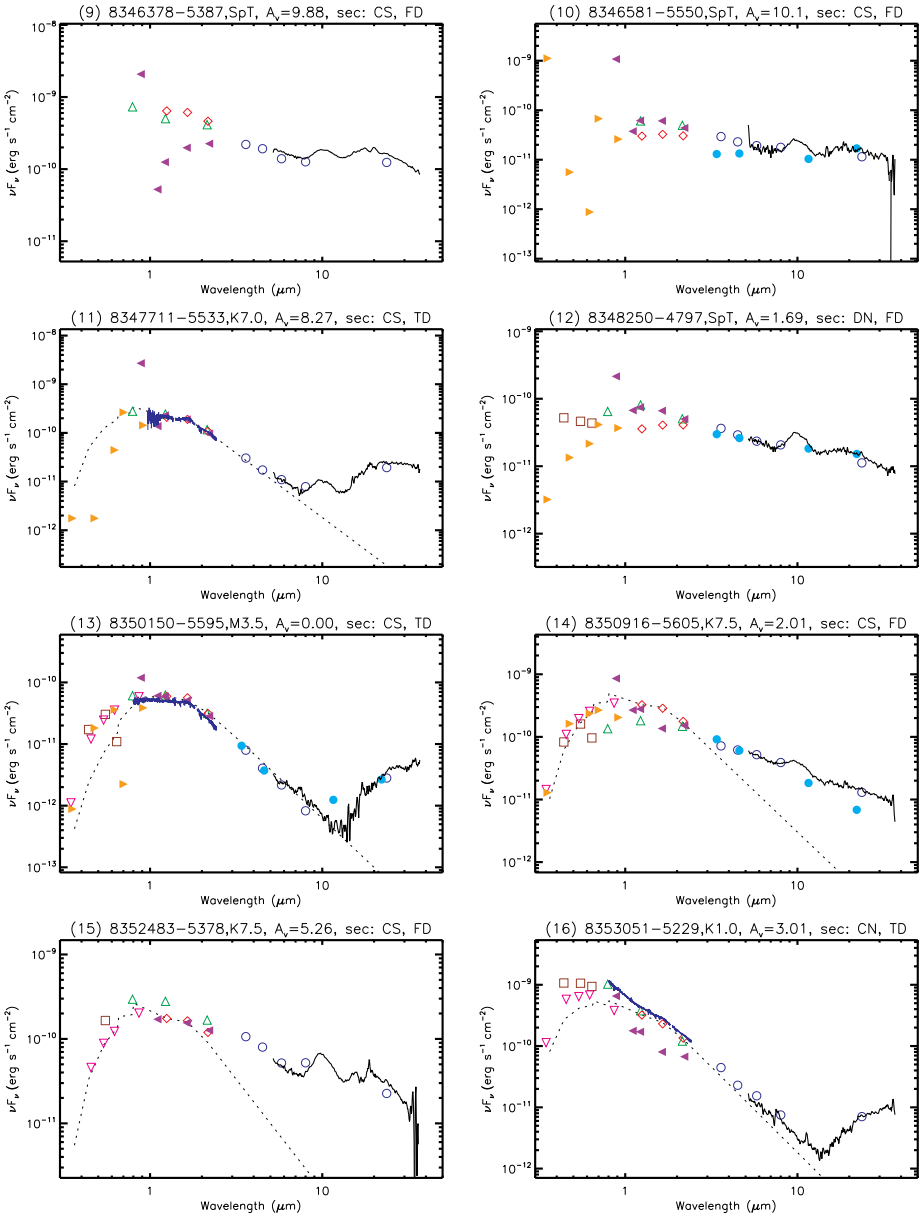


Figure A.1 continued.

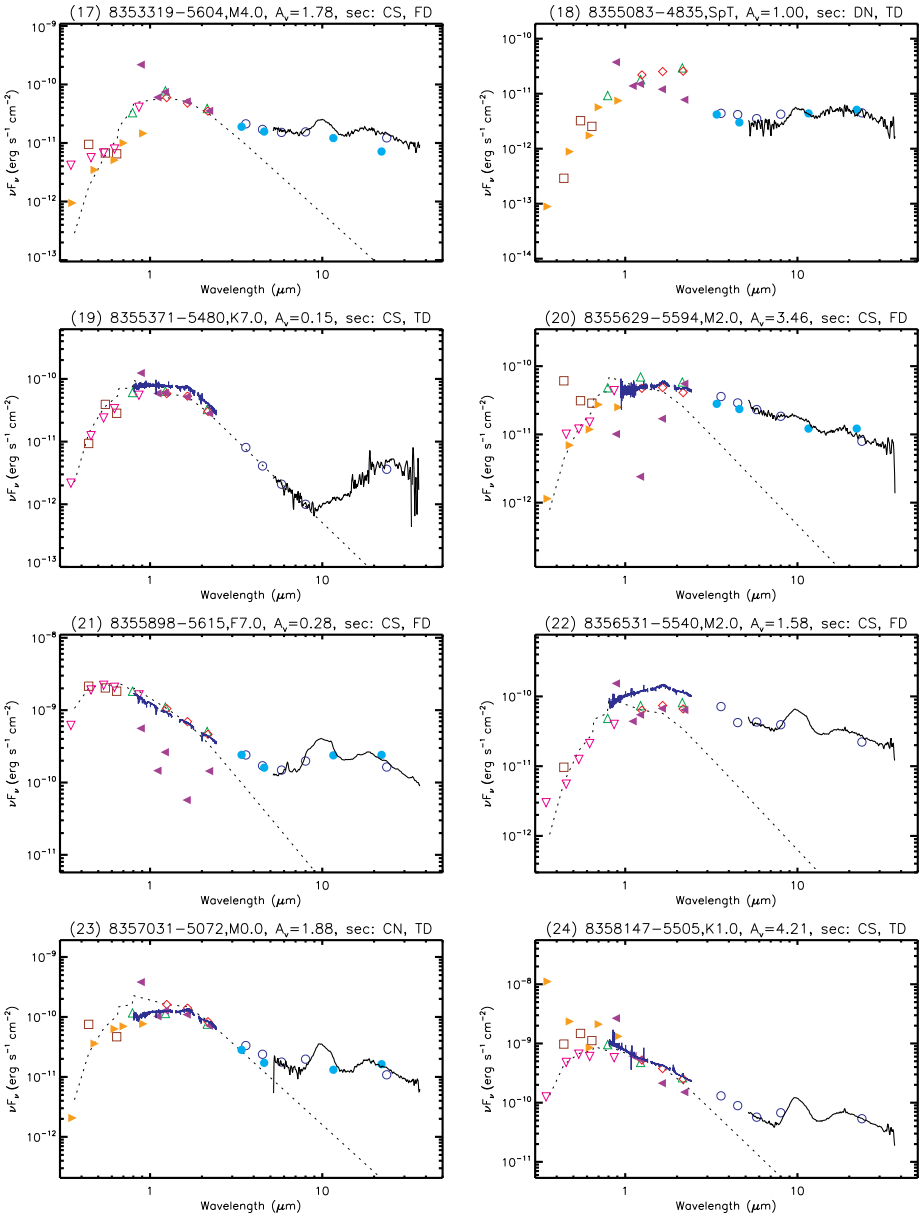


Figure A.1 continued

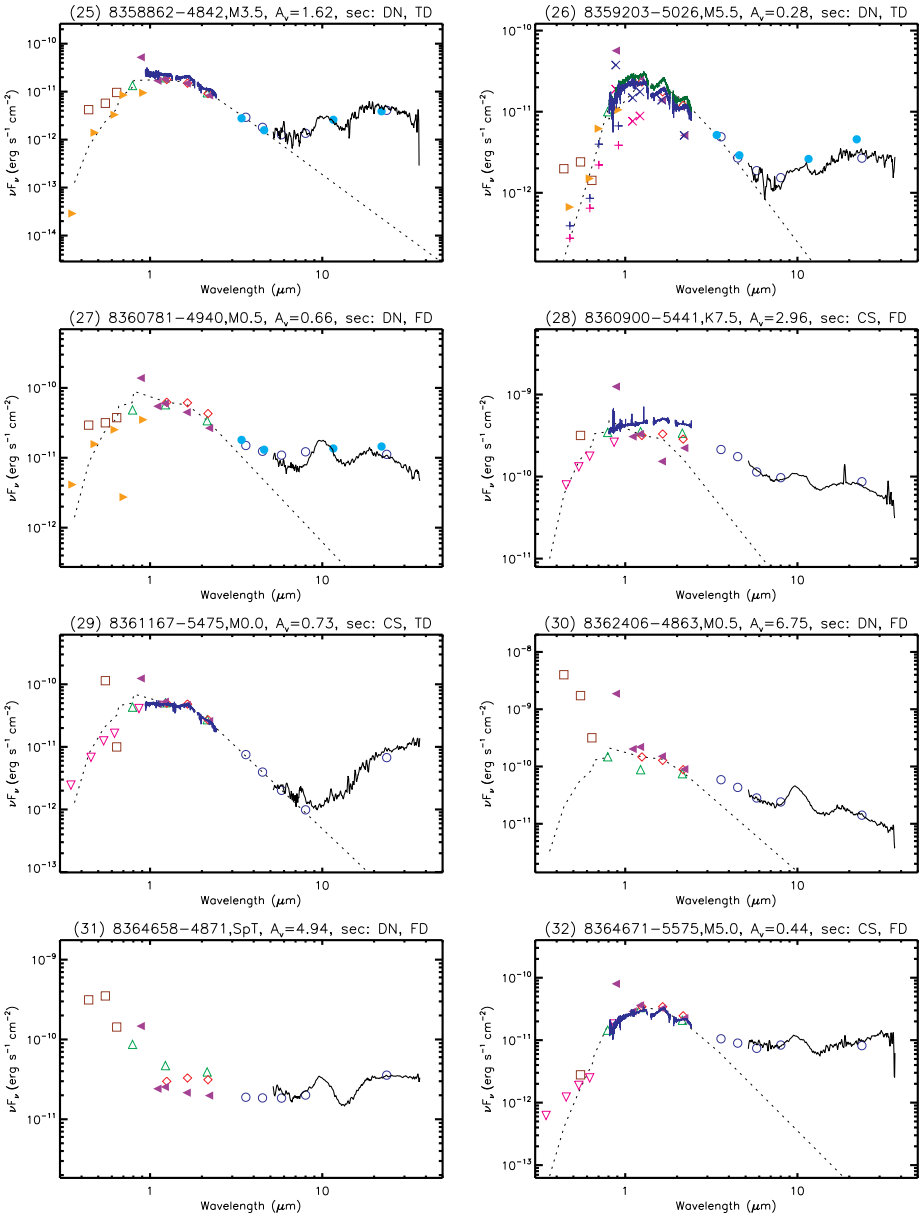


Figure A.1 continued

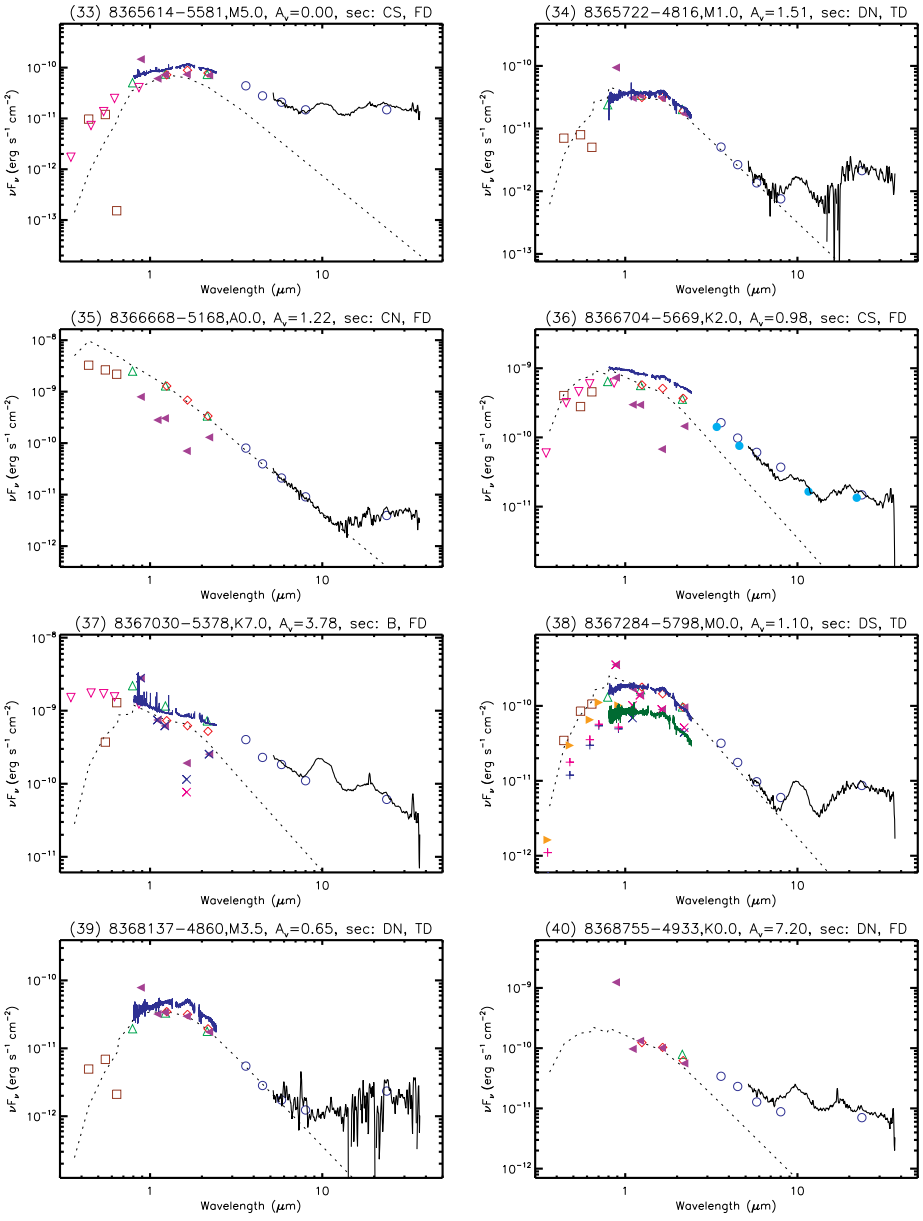


Figure A.1 continued

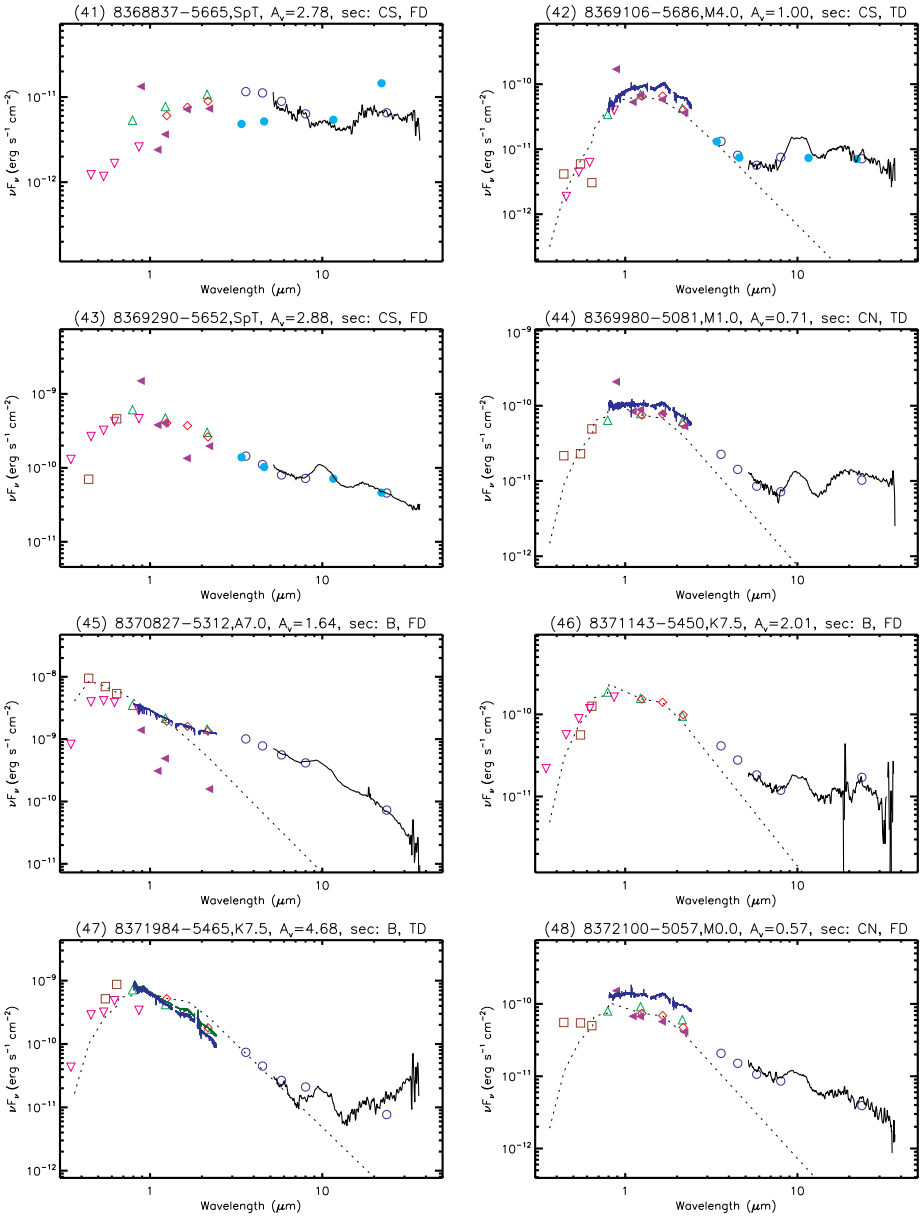


Figure A.1 continued

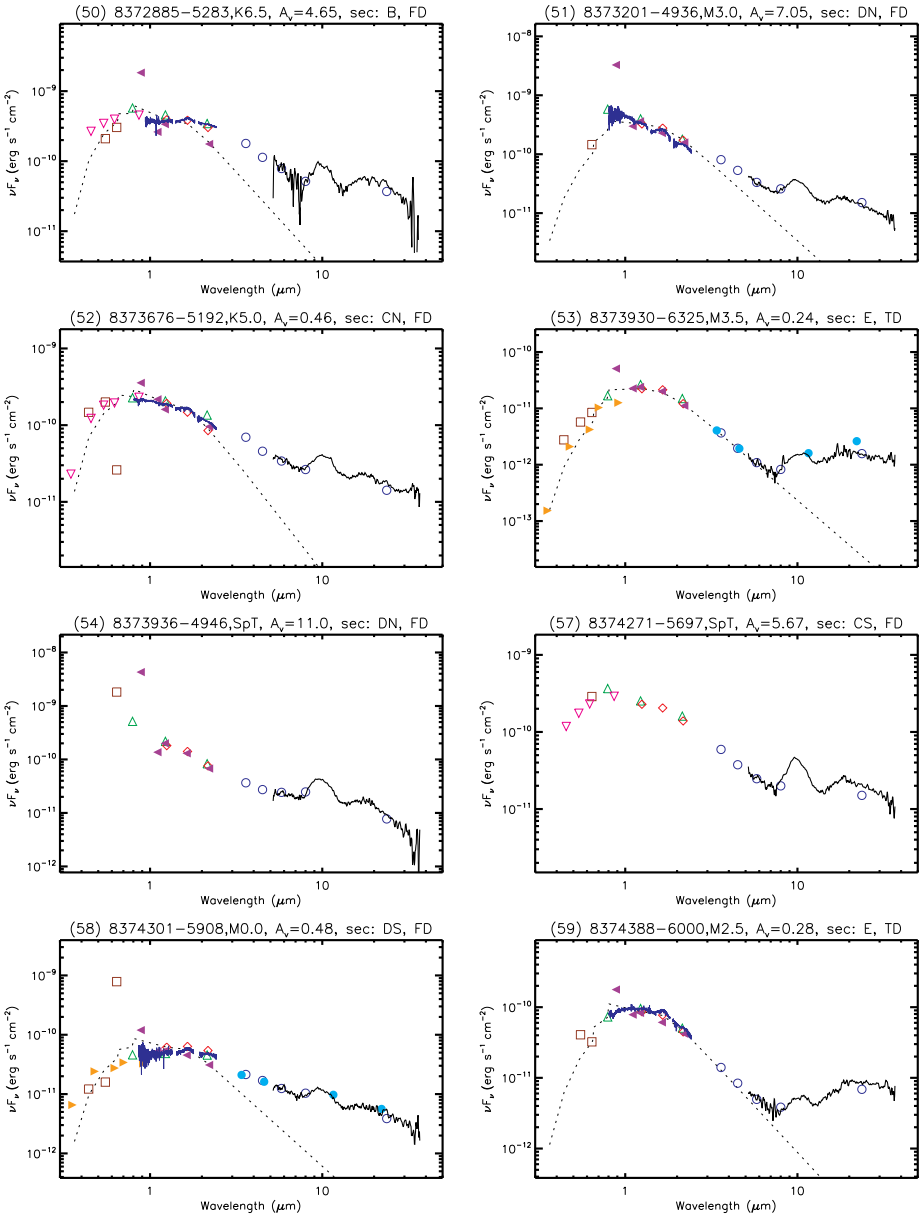


Figure A.1 continued

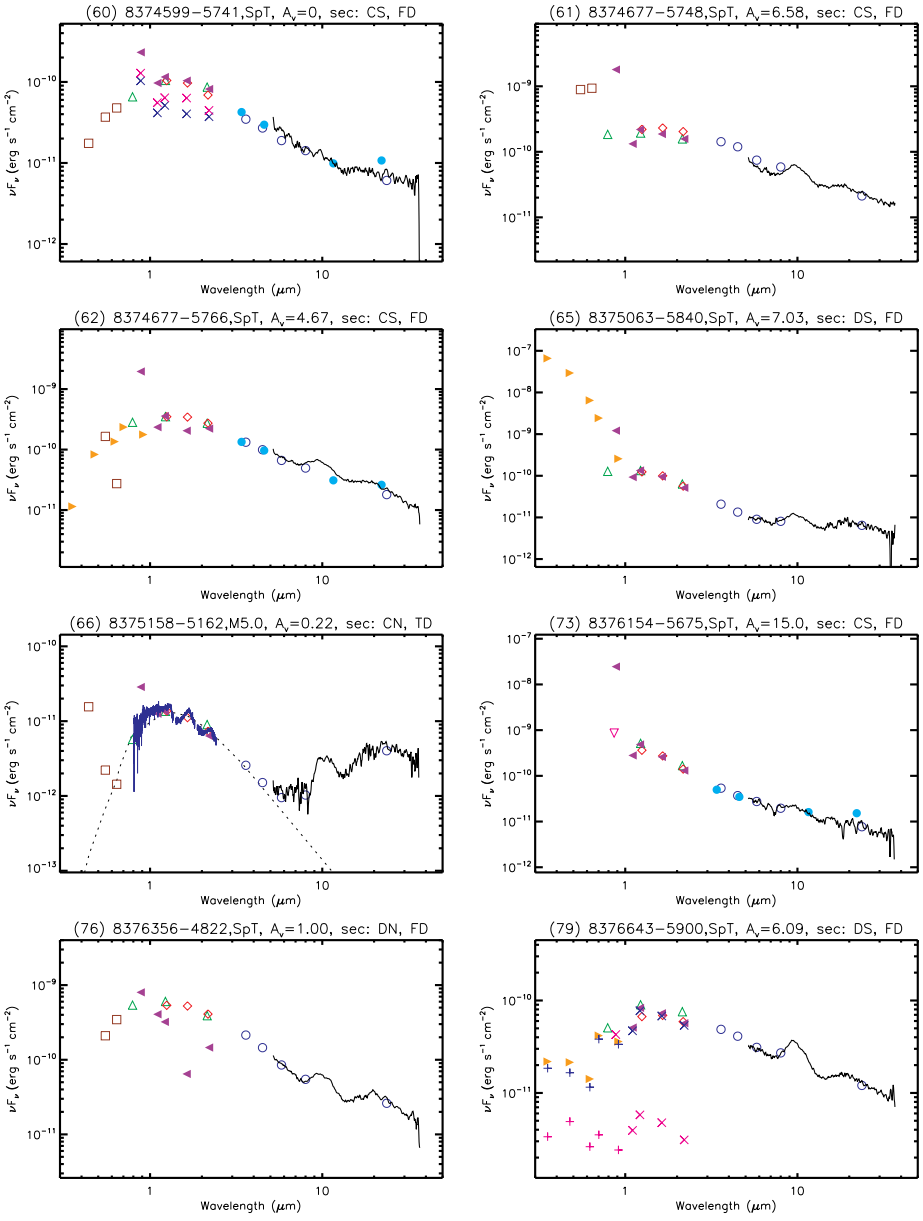


Figure A.1 continued

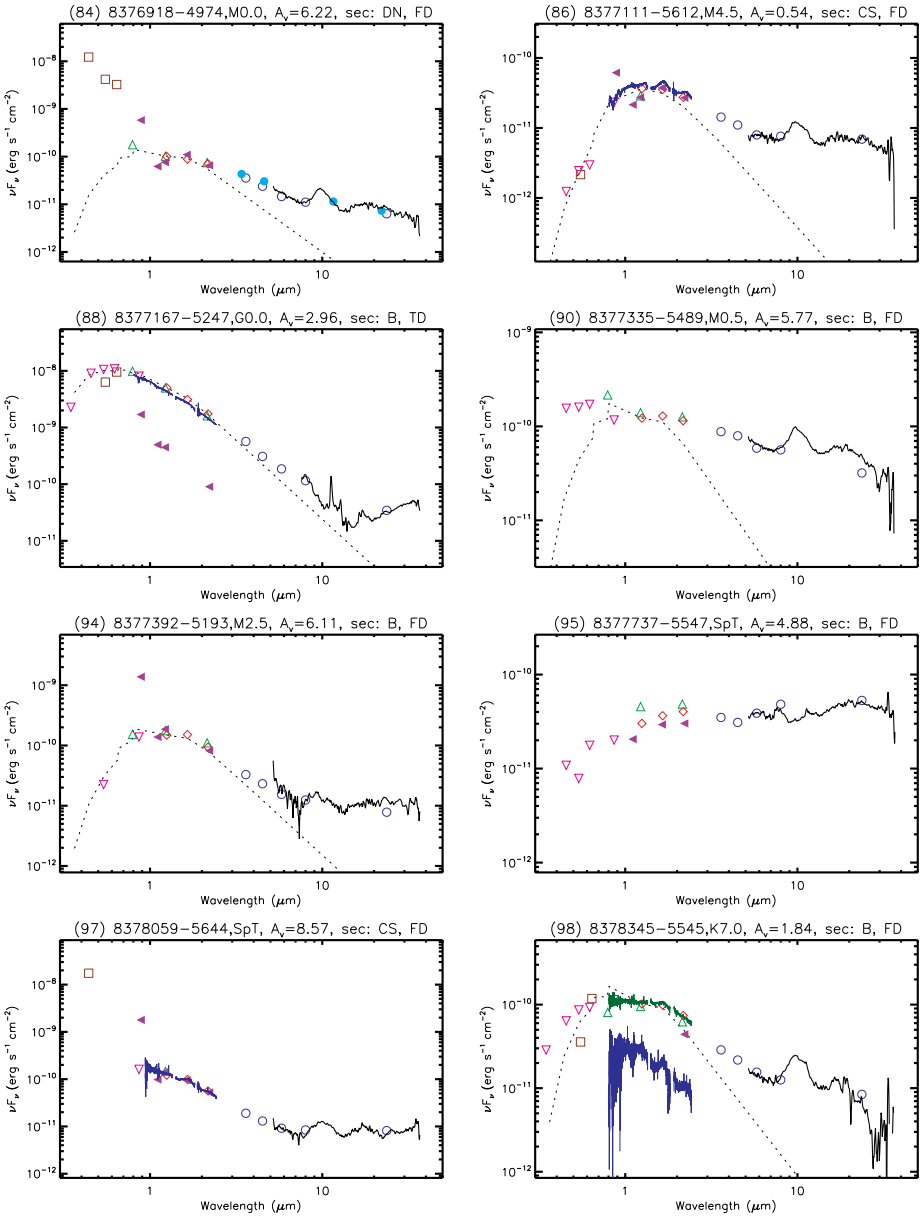


Figure A.1 continued

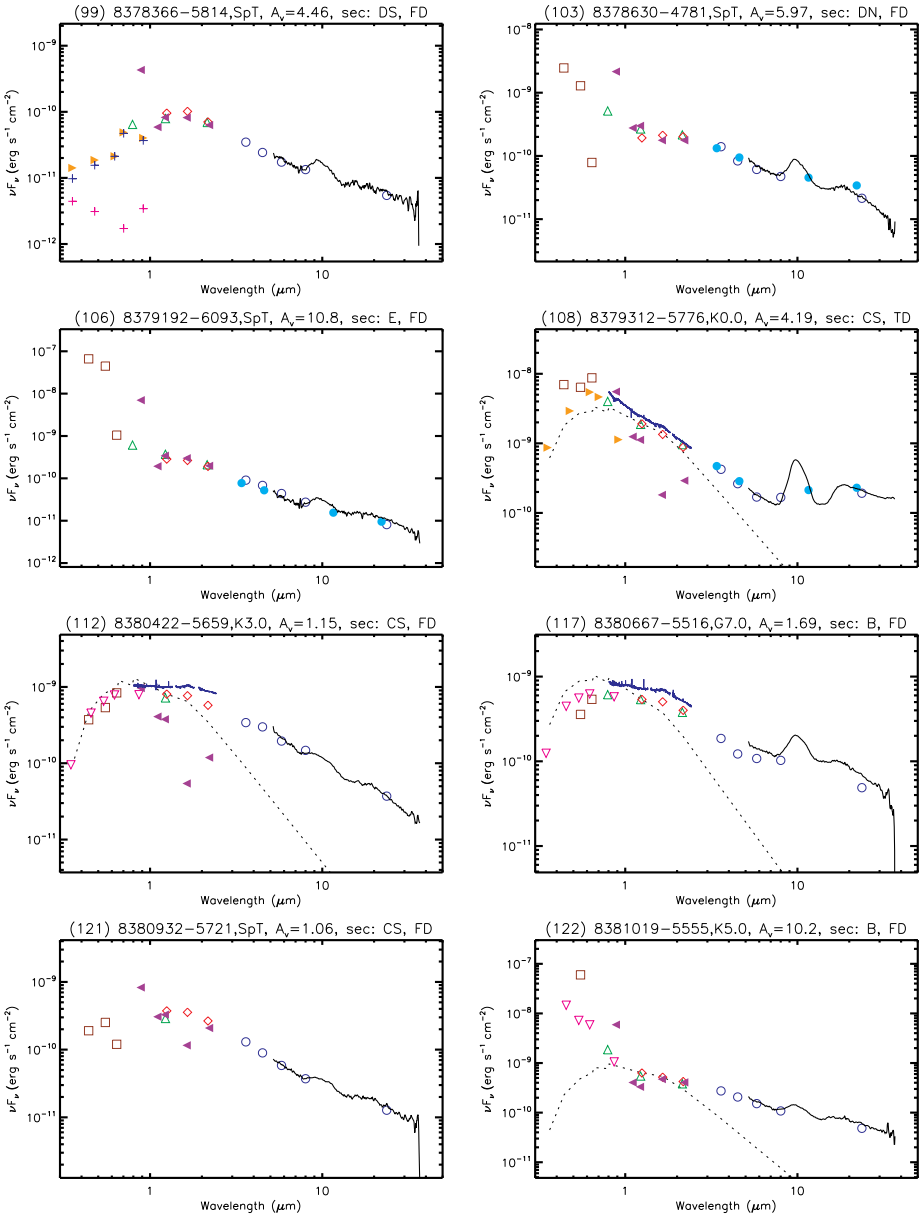


Figure A.1 continued

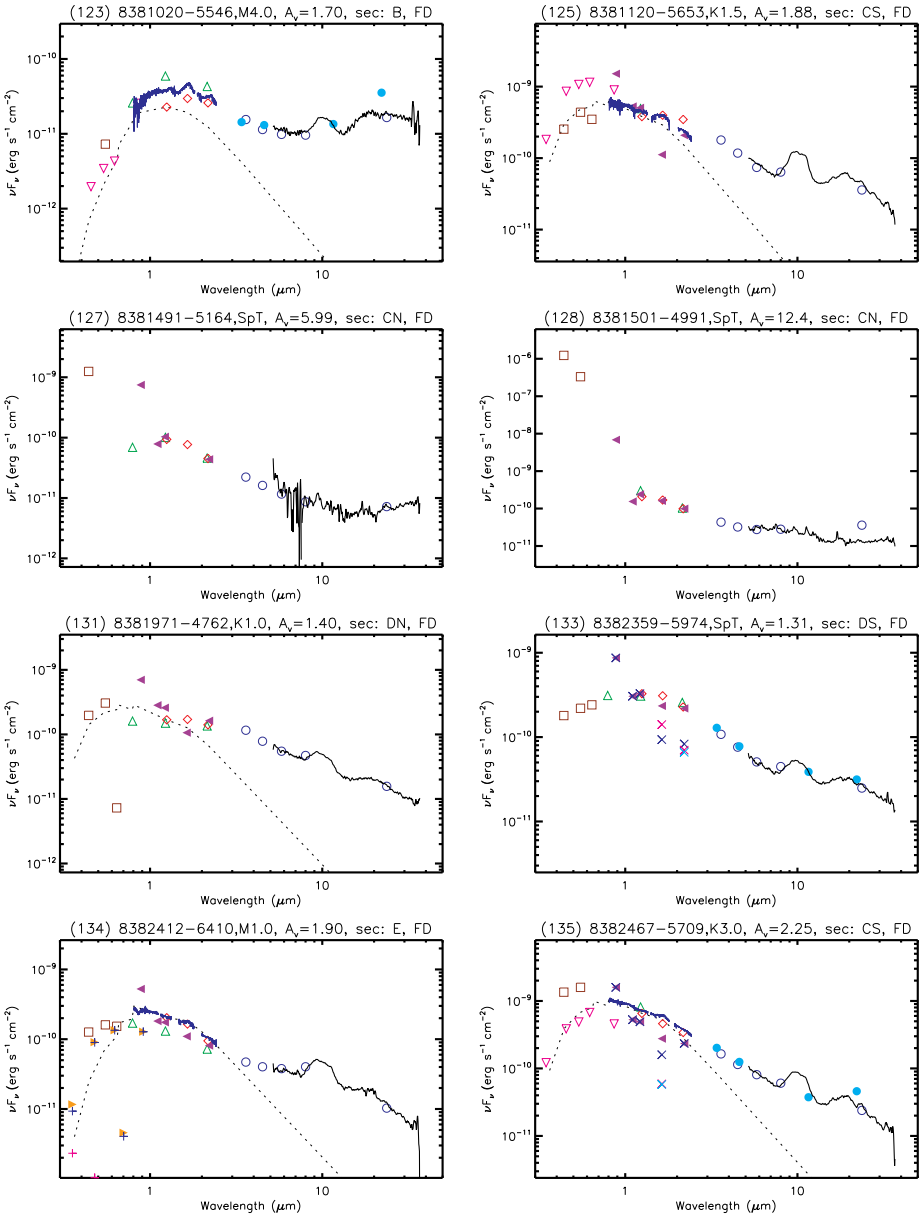


Figure A.1 continued

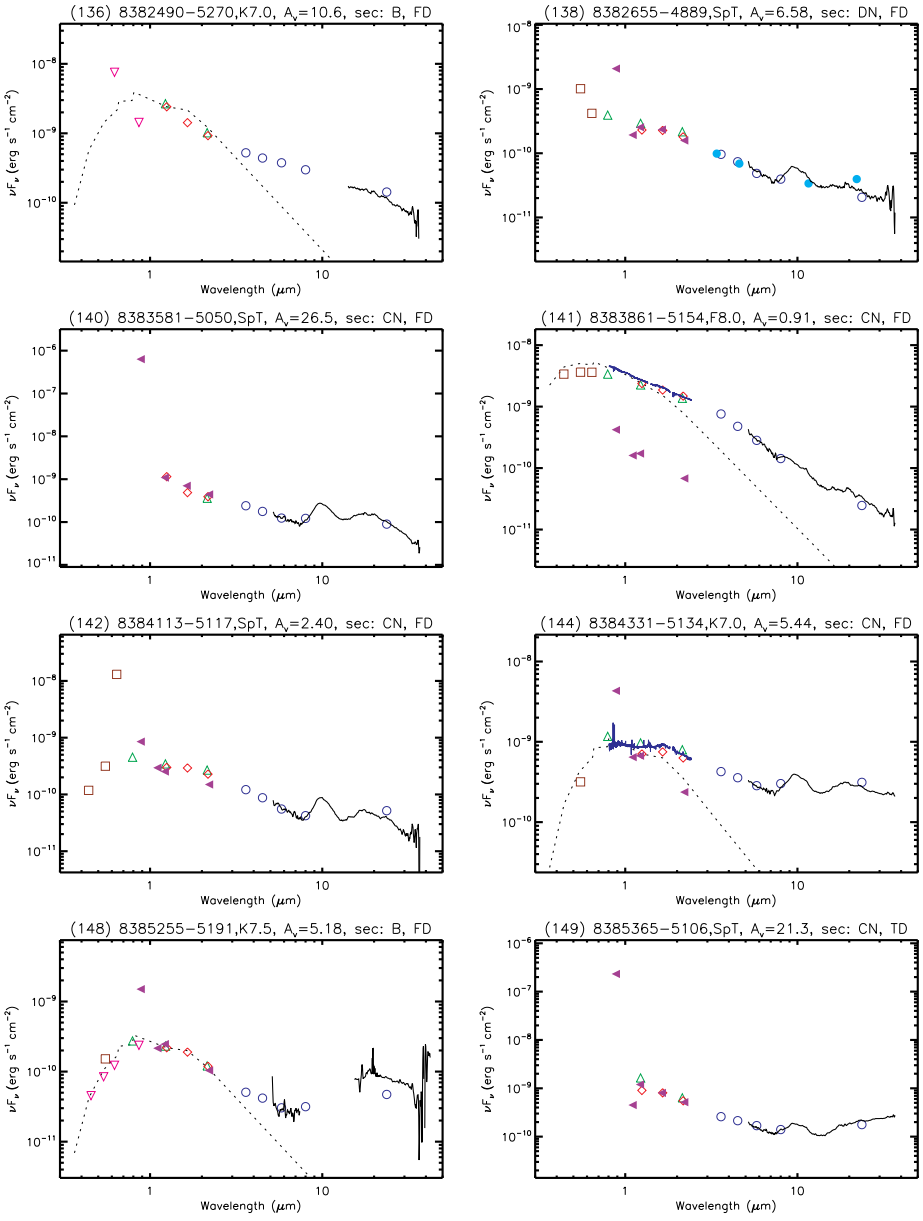


Figure A.1 continued

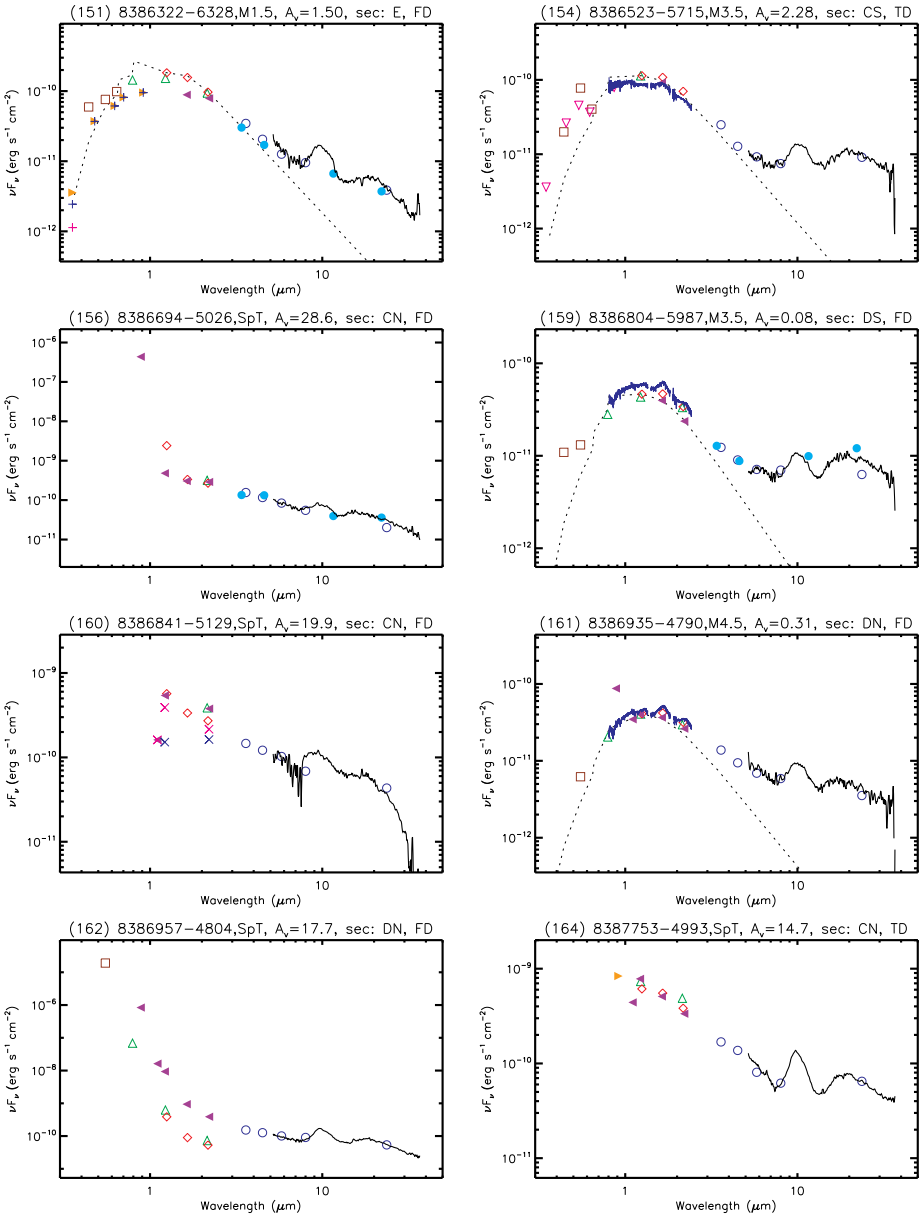


Figure A.1 continued

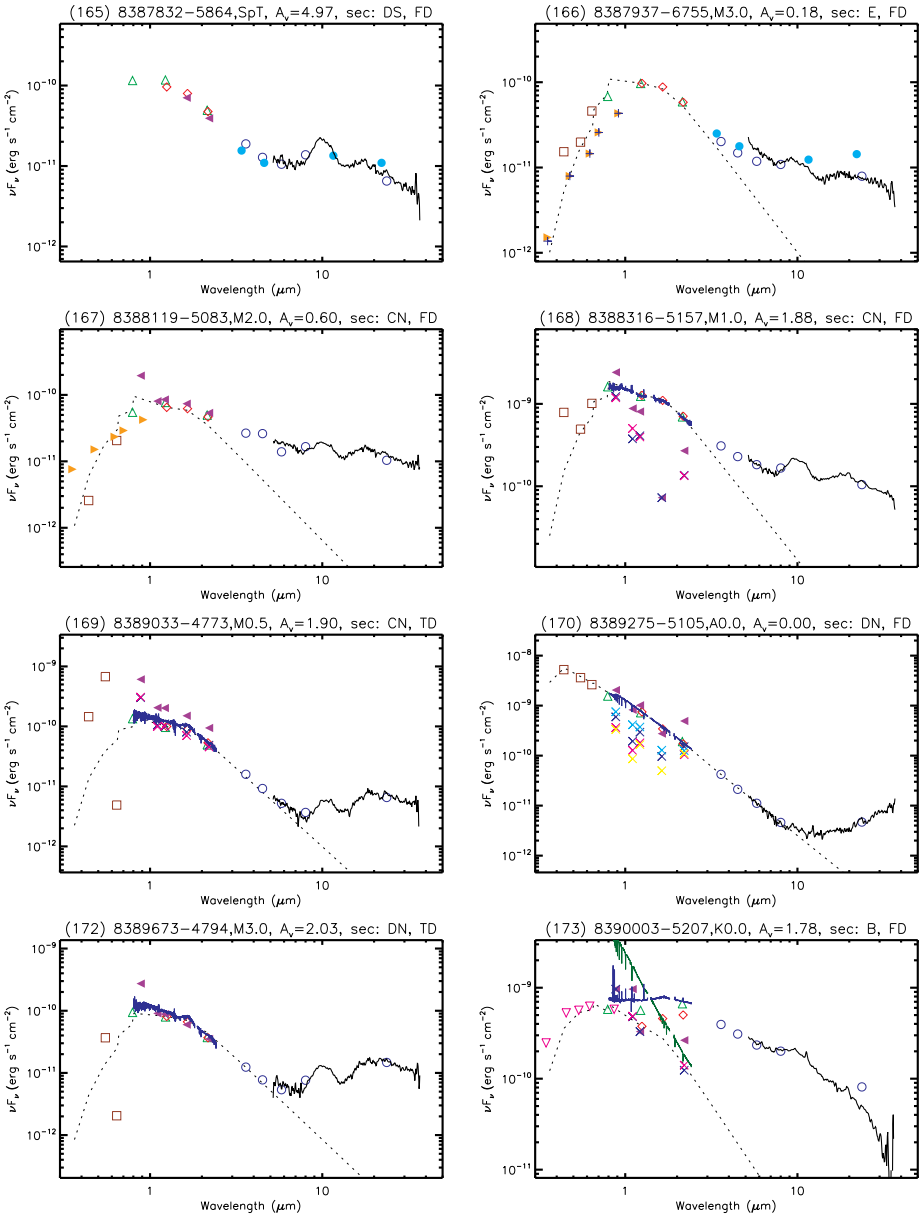


Figure A.1 continued

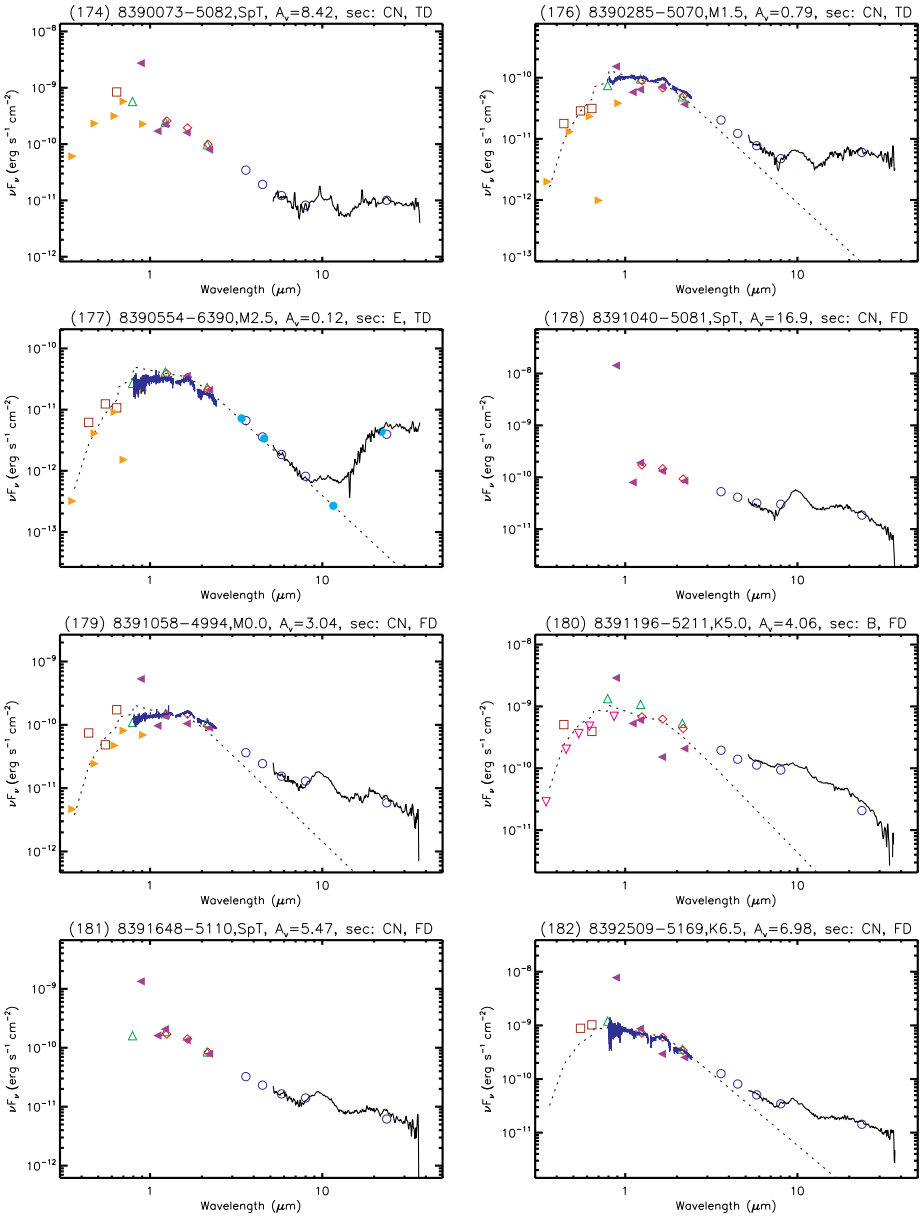


Figure A.1 continued

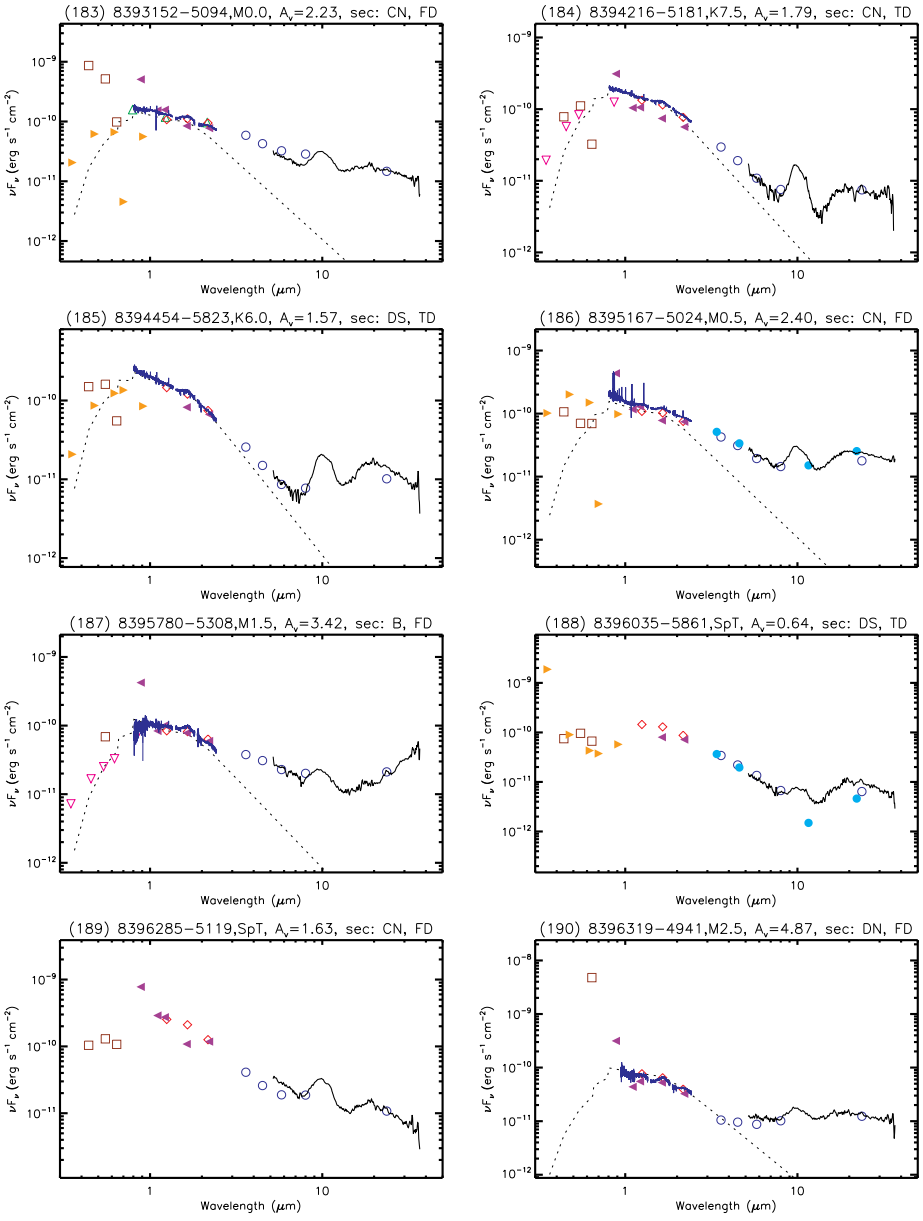


Figure A.1 continued

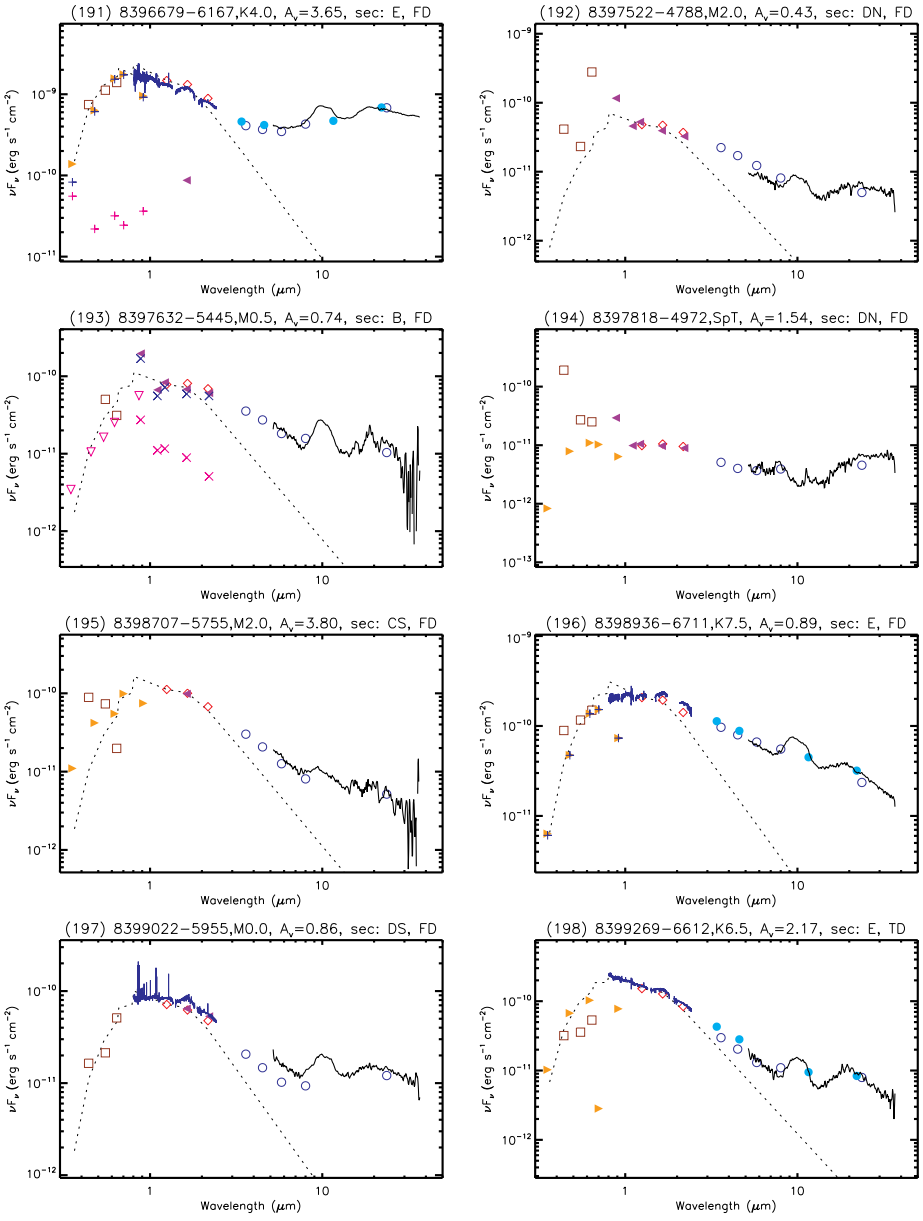


Figure A.1 continued

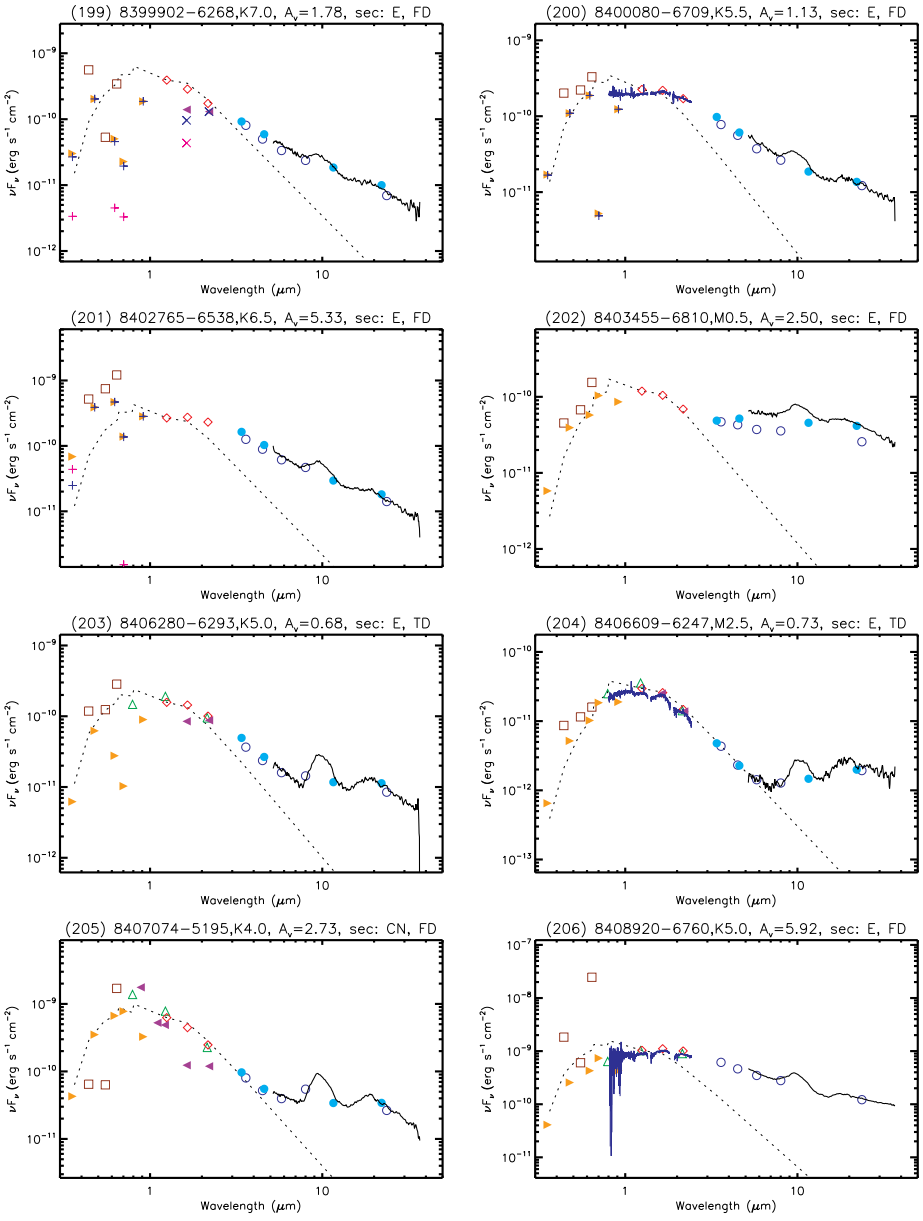


Figure A.1 continued

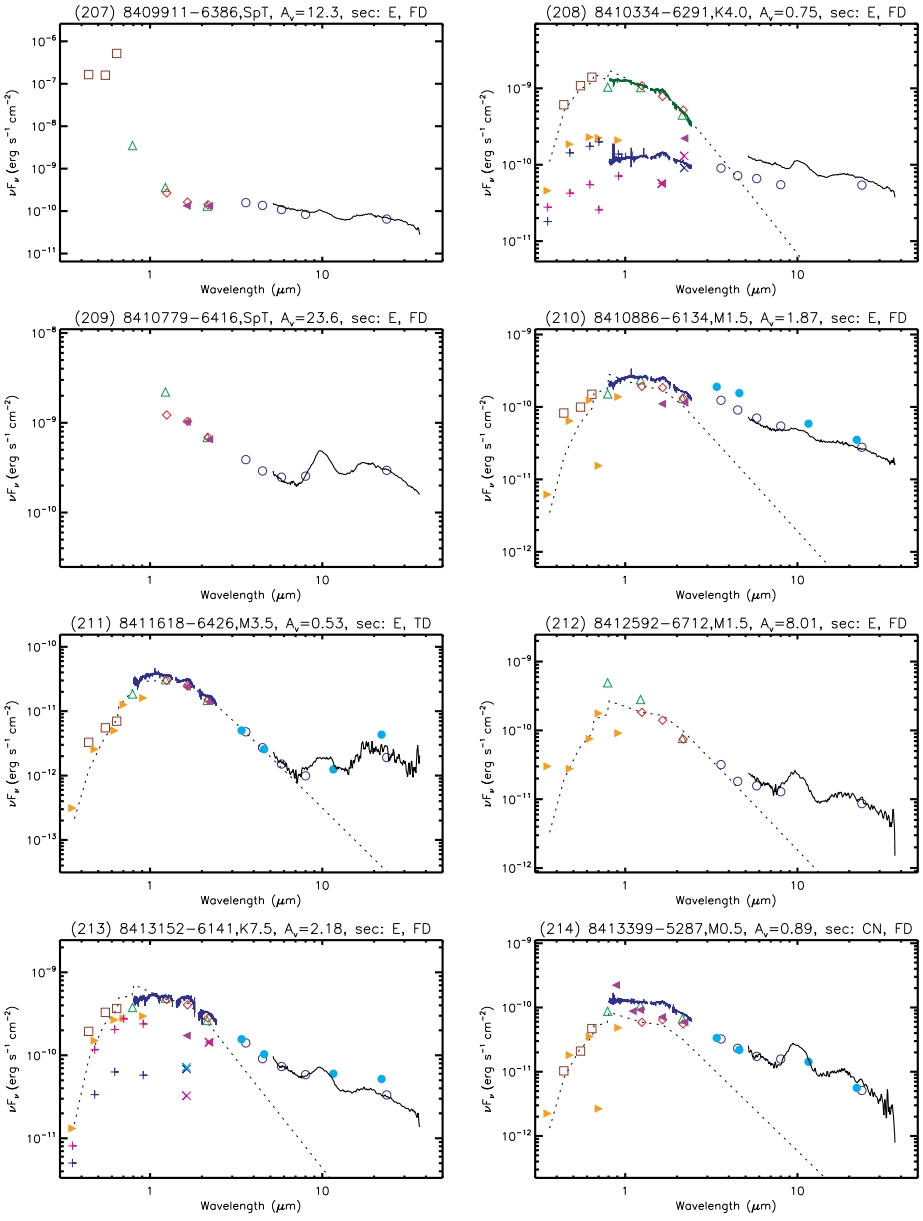


Figure A.1 continued

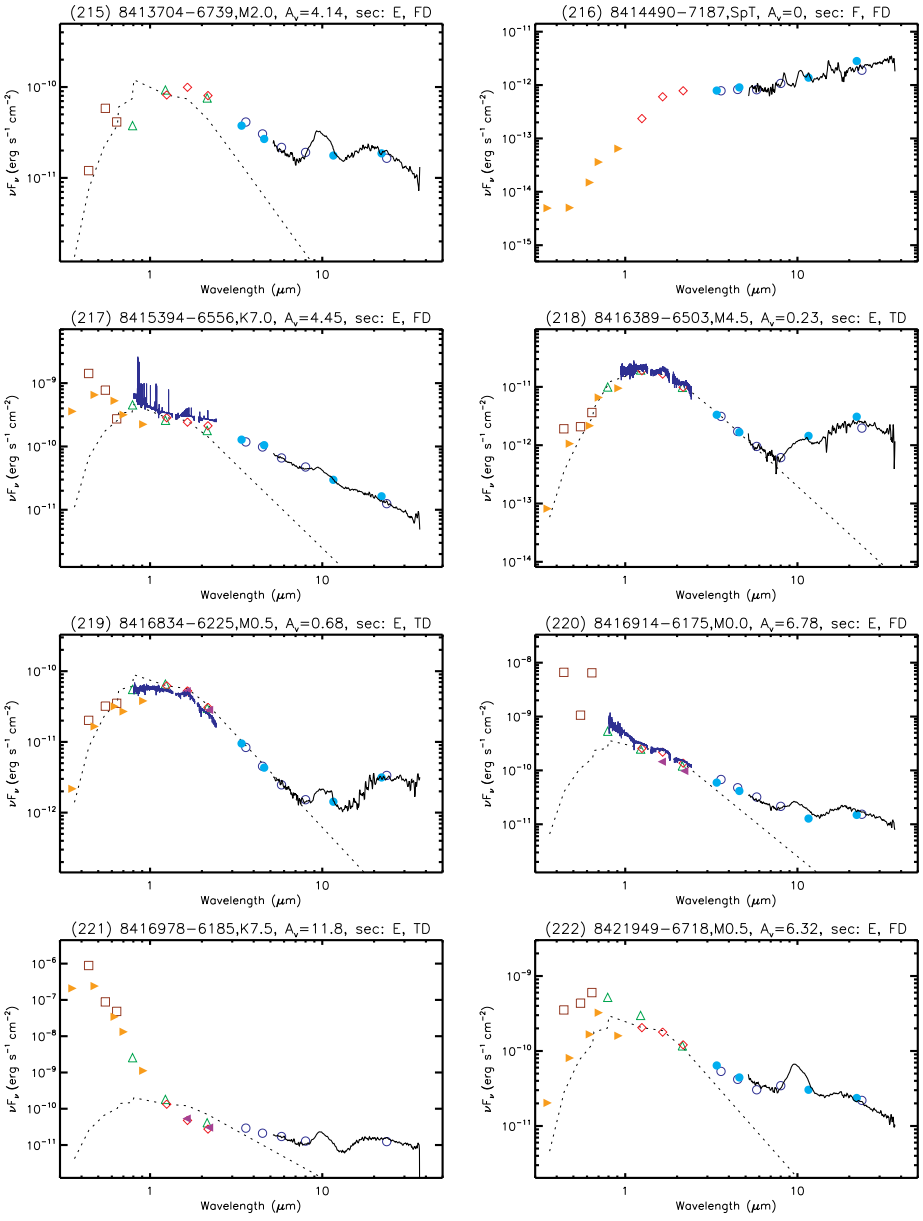


Figure A.1 continued

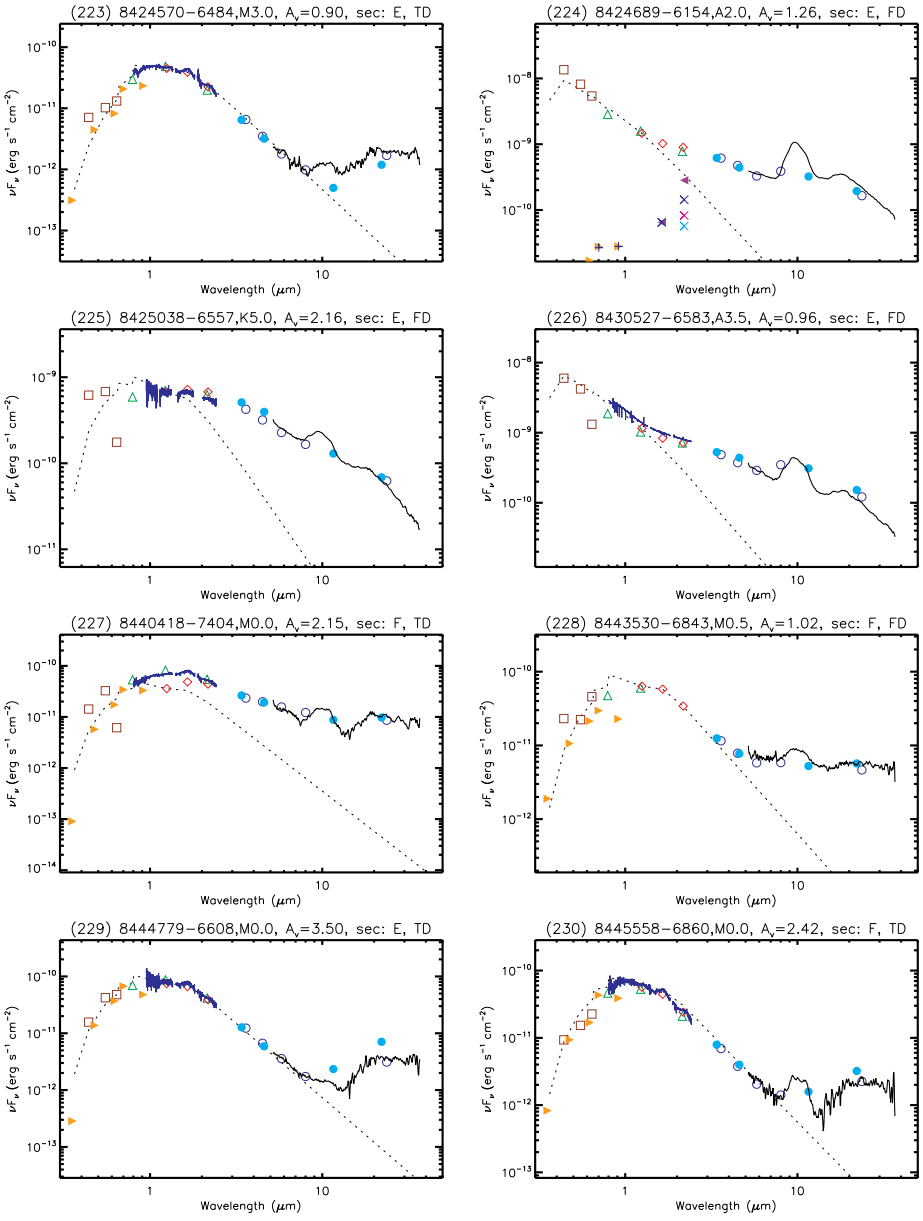


Figure A.1 continued

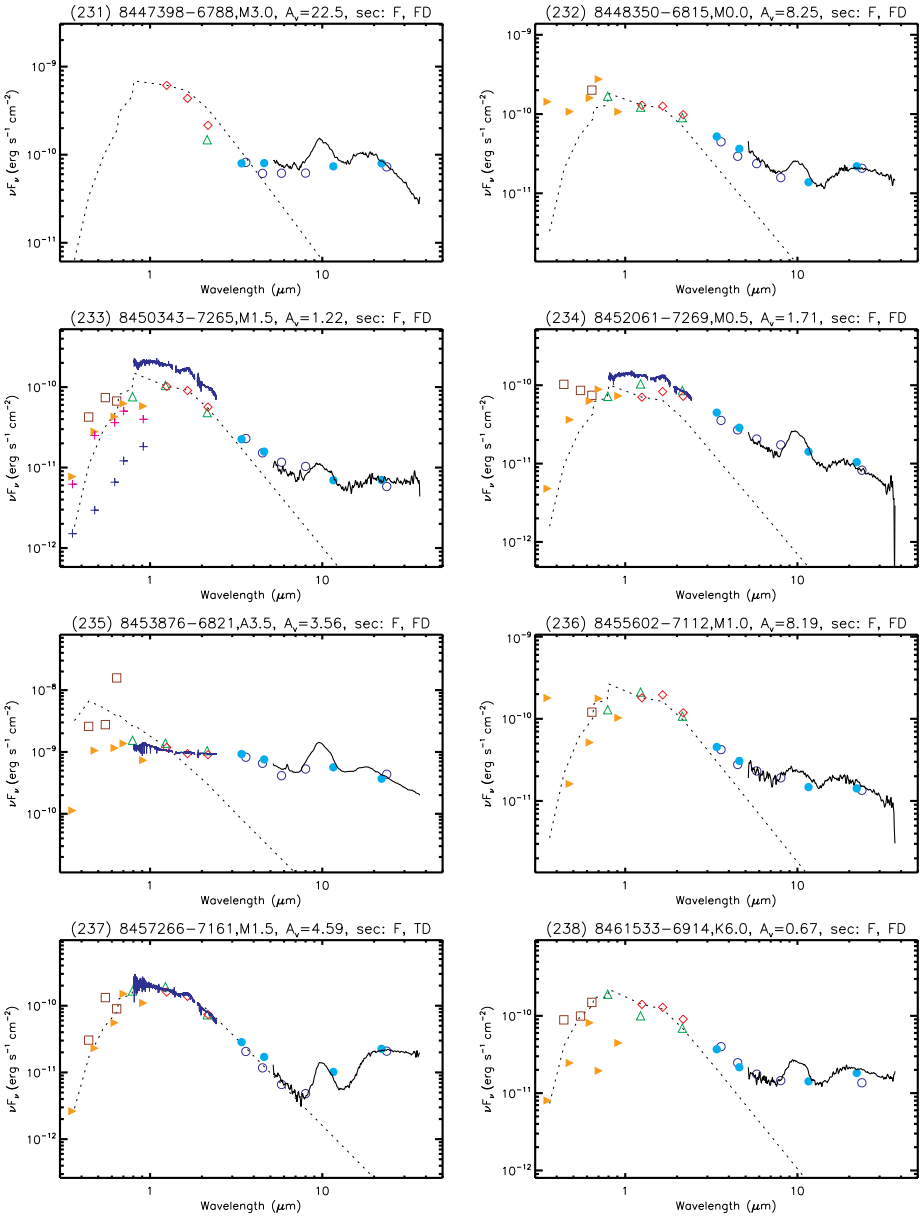


Figure A.1 continued

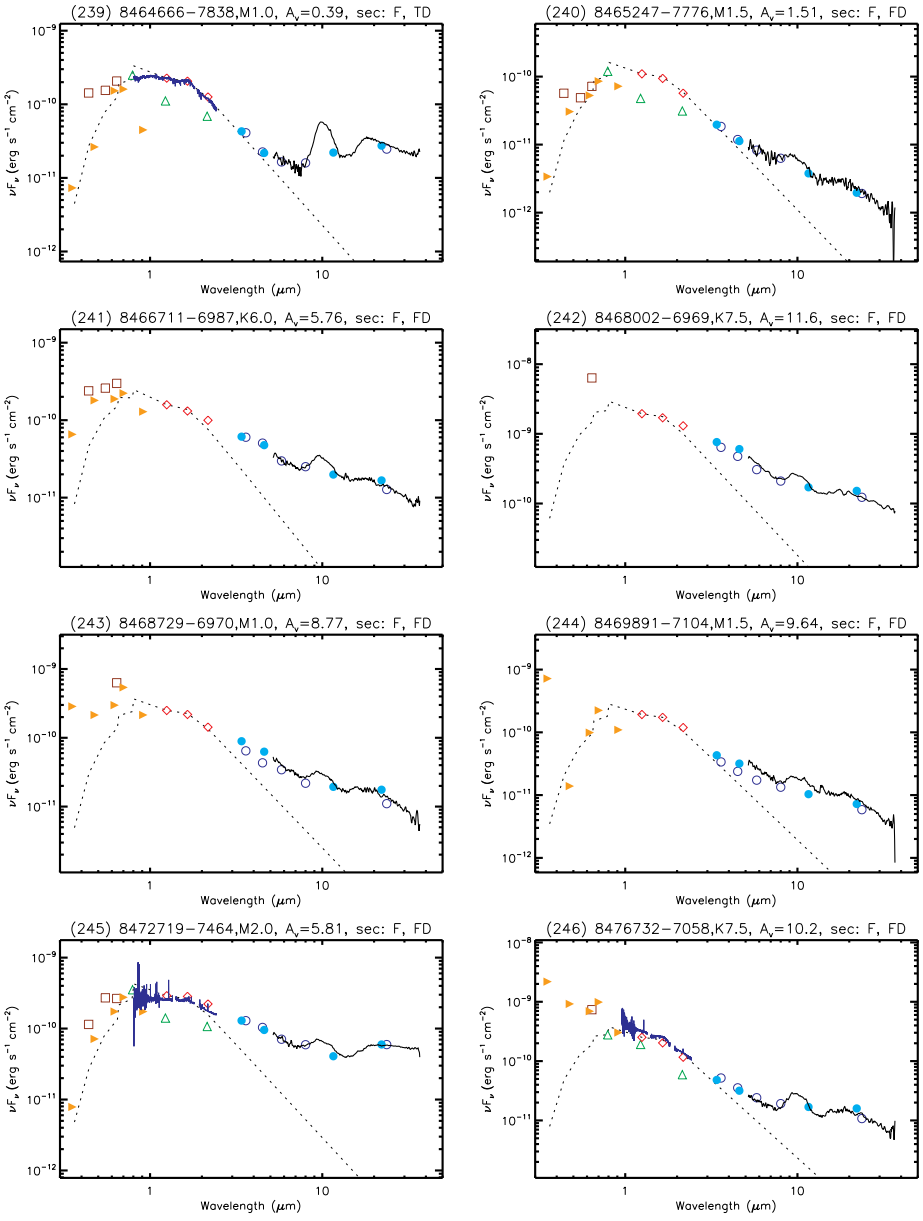


Figure A.1 continued

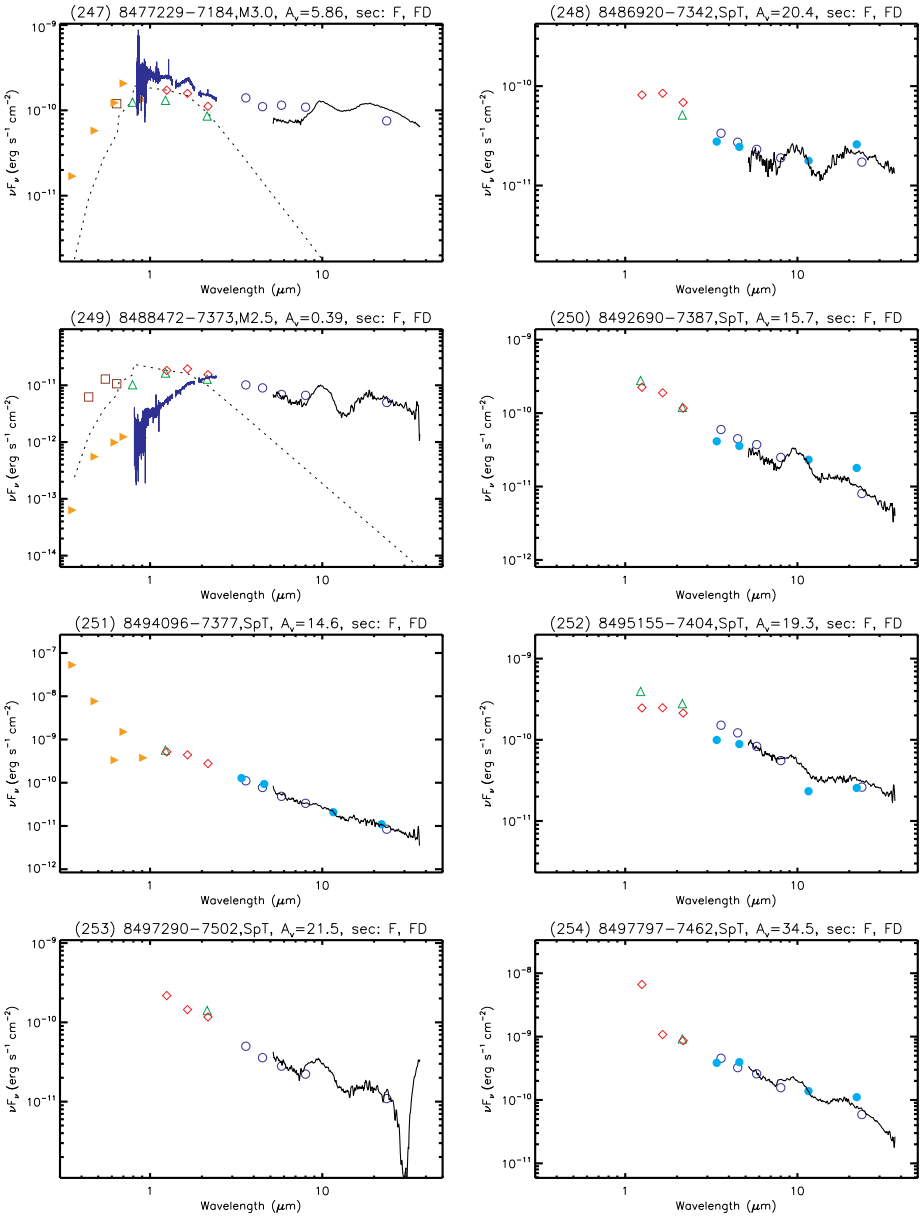


Figure A.1 continued

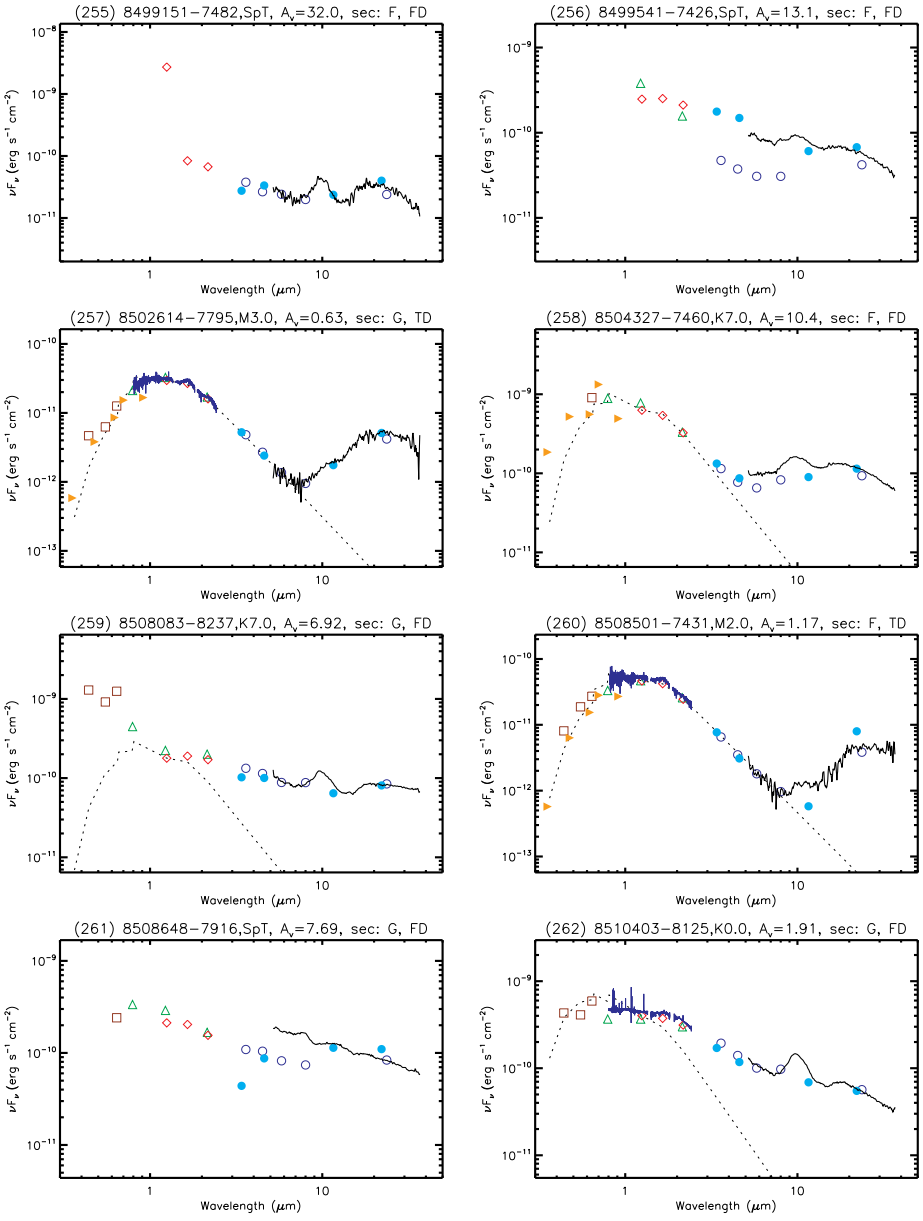


Figure A.1 continued

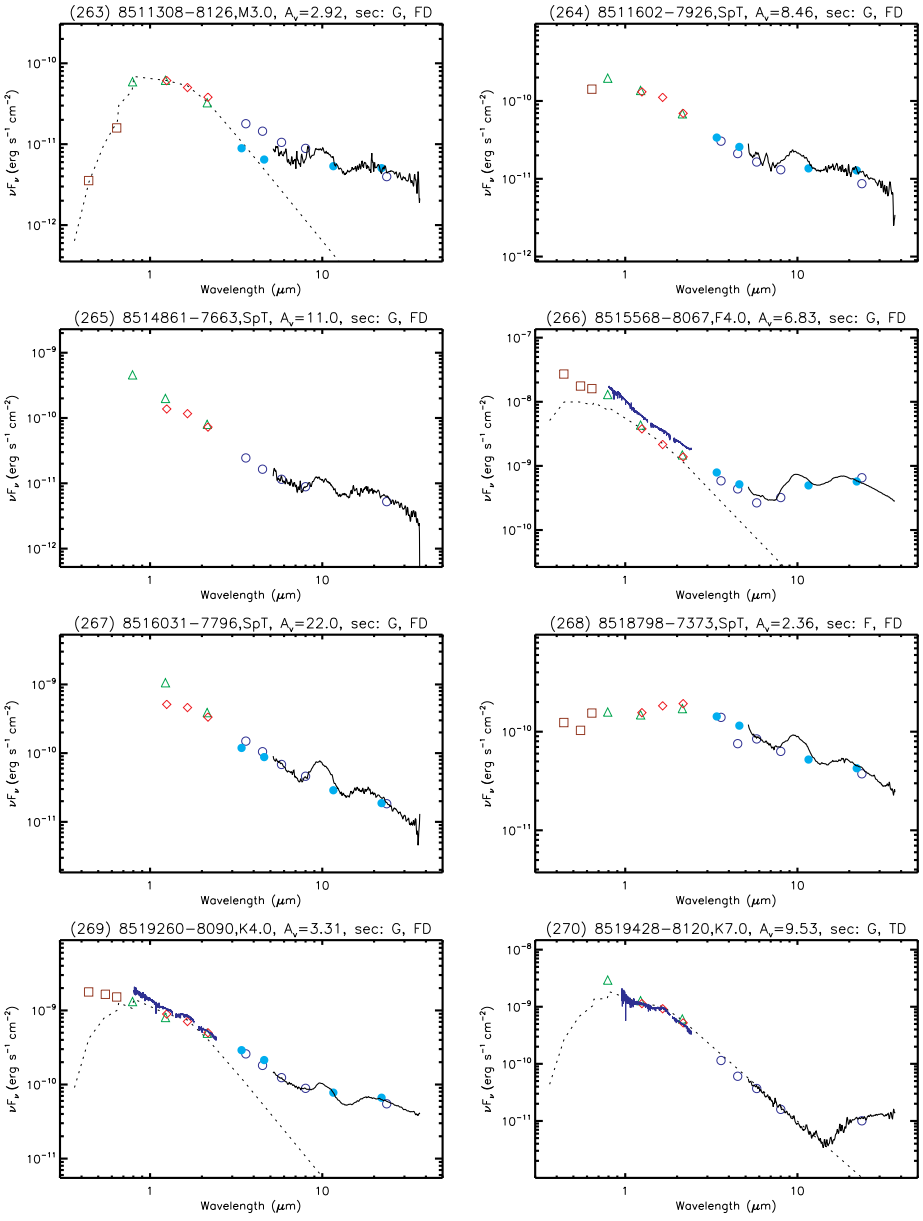


Figure A.1 continued

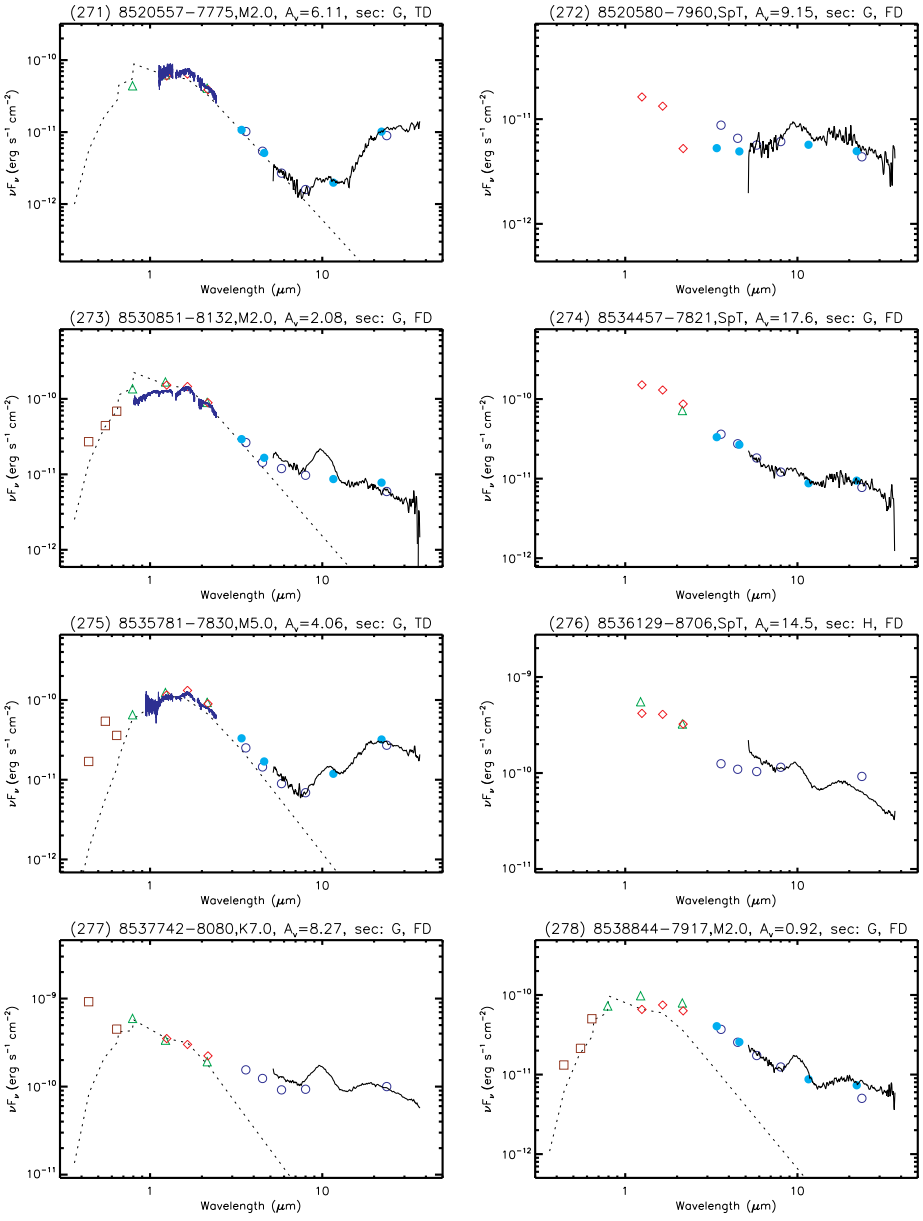


Figure A.1 continued

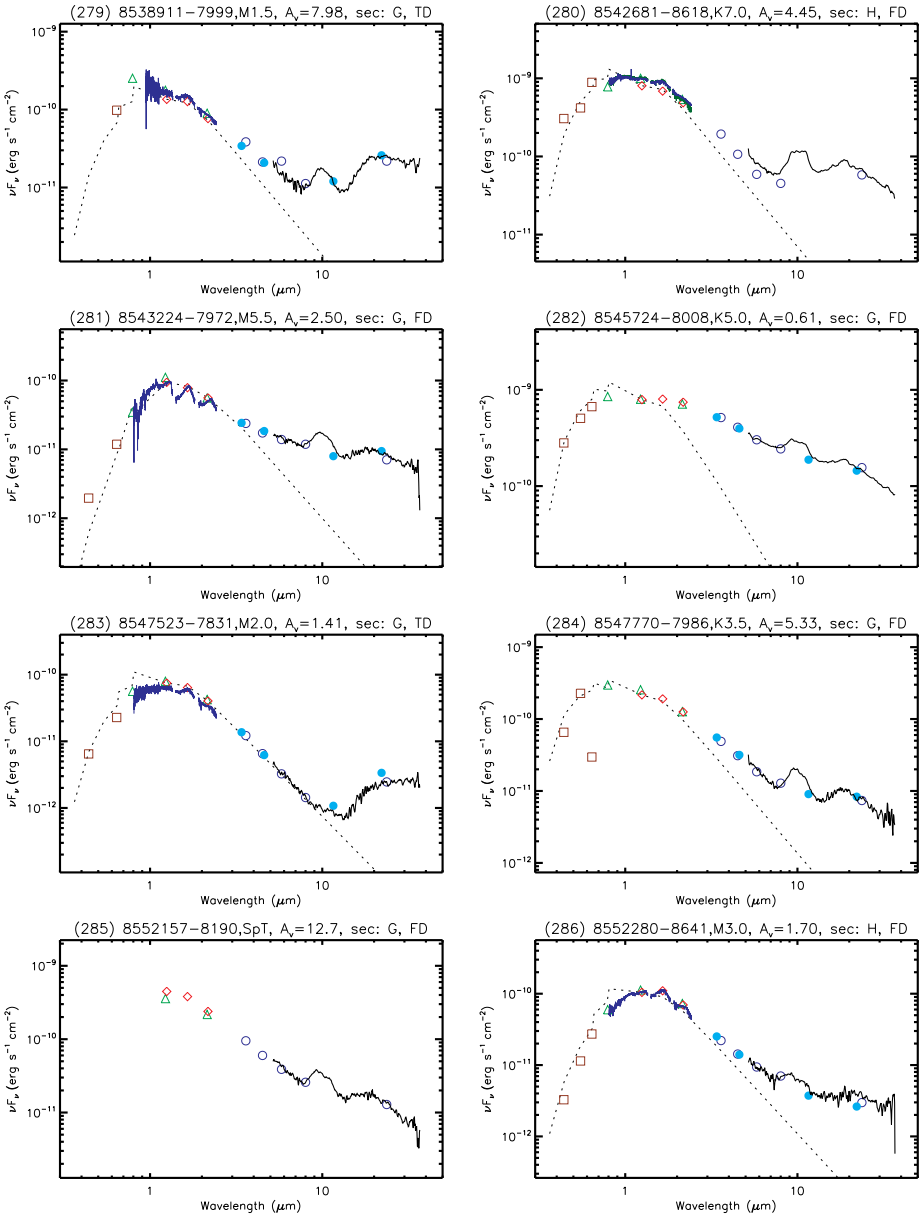


Figure A.1 continued

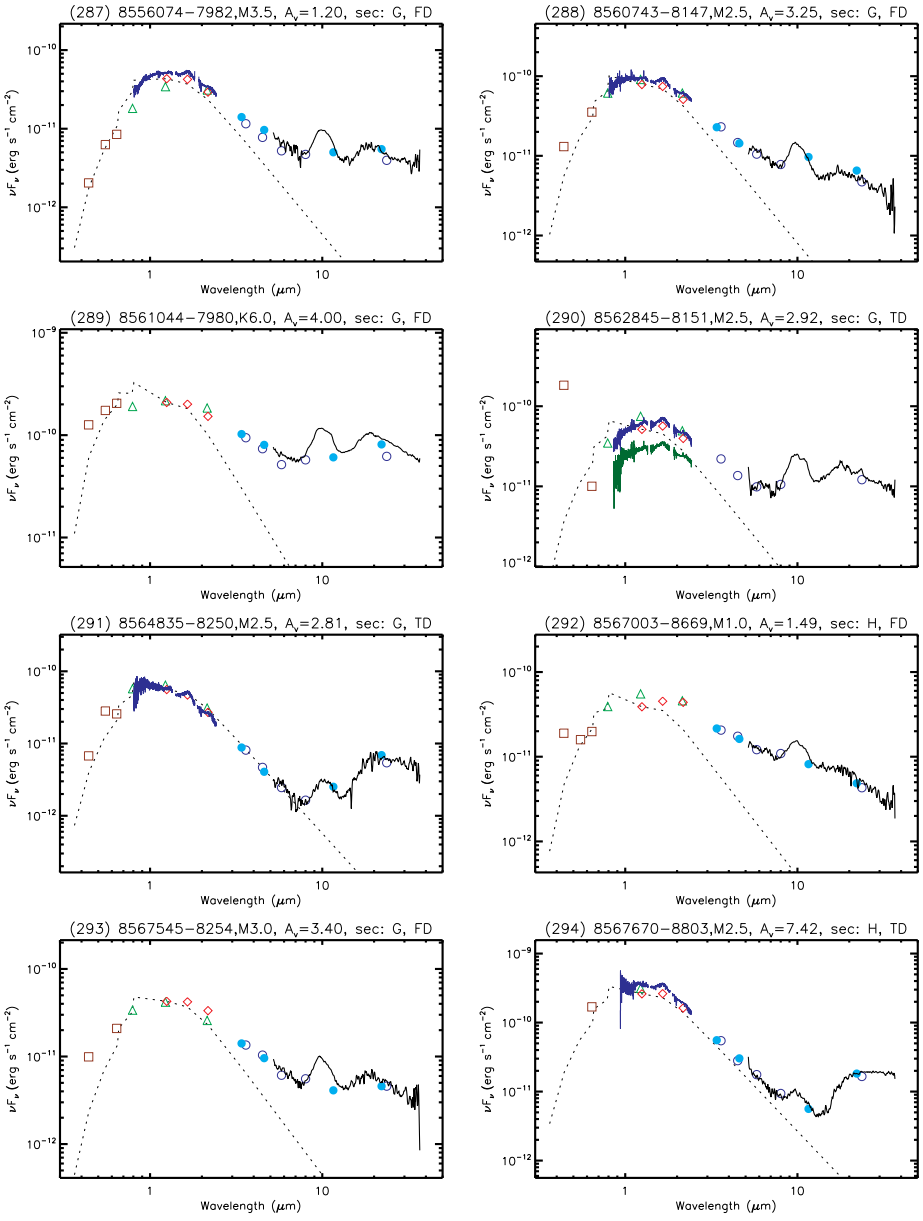


Figure A.1 continued

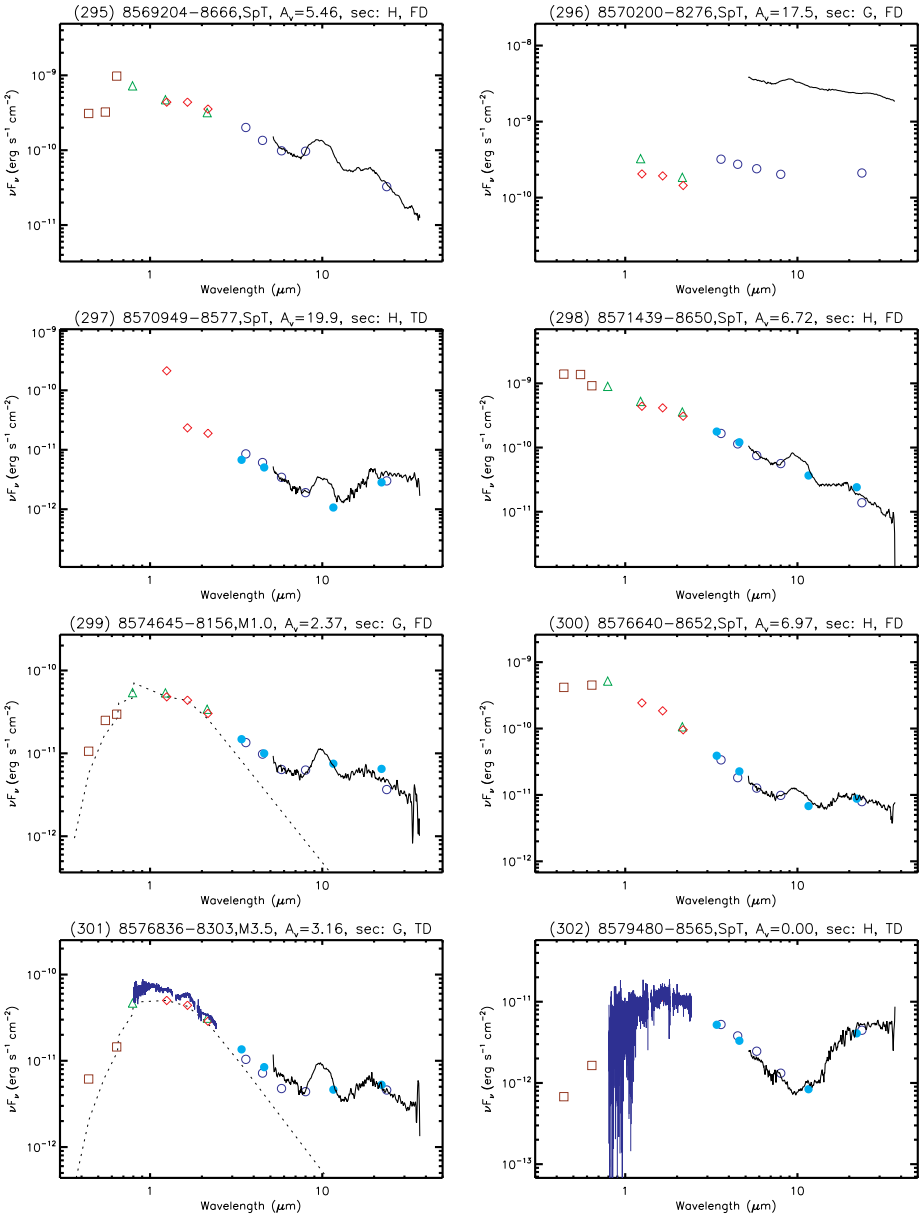


Figure A.1 continued

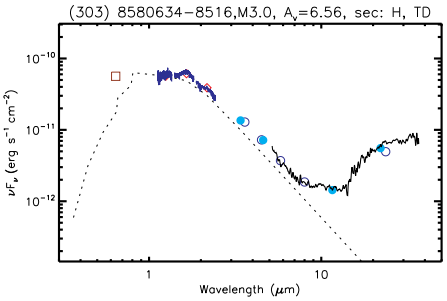


Figure A.1 continued

A.2 SEDs of Class II disks in Orion A: observed in partial IRS wavelength coverage, 5-14 μm

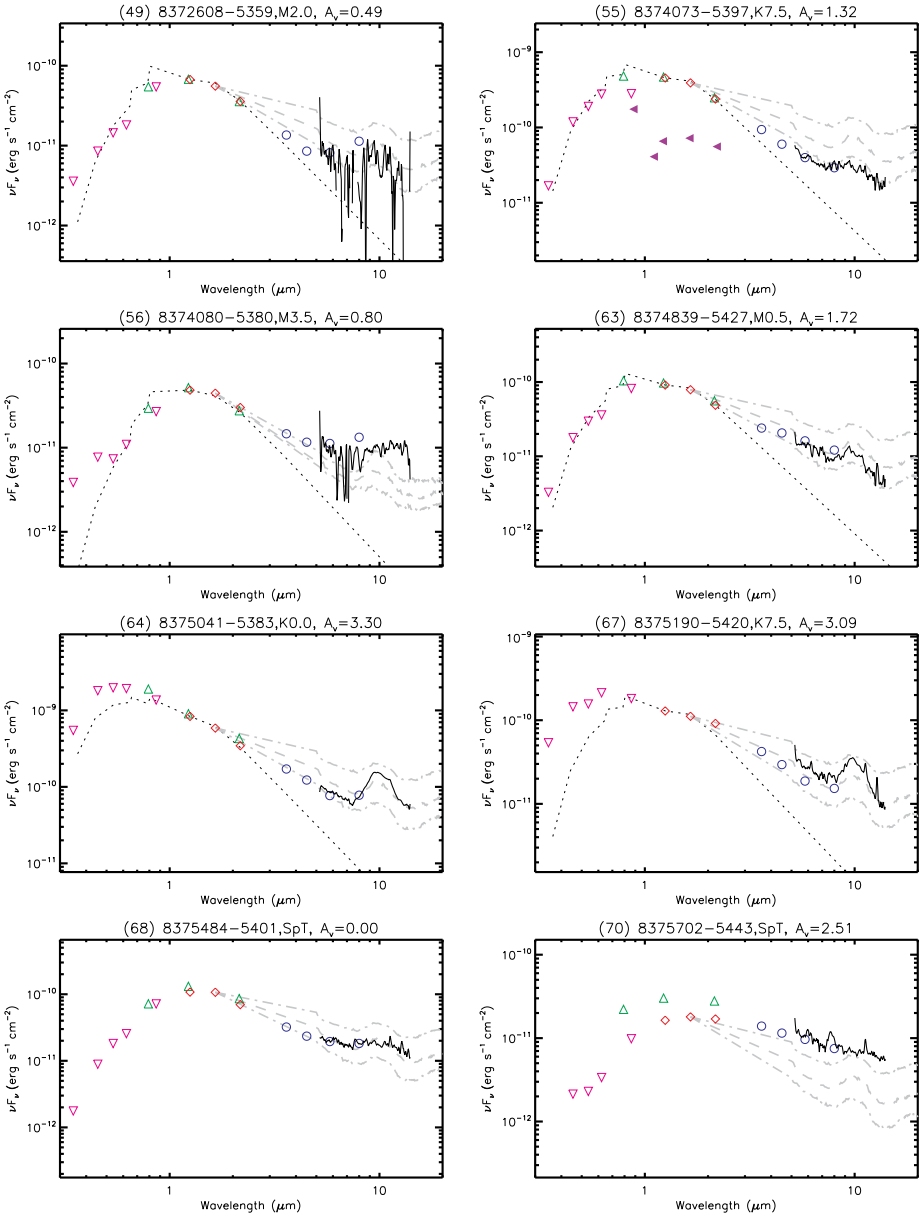


Figure A.2 De-reddened SEDs of our Trapezium sample, which were observed with IRS SL module only. De-reddened SEDs of the reduced our samples in Trapezium, which were observed with IRS SL module only. The meanings of symbols are same as in Figure A.1 except the additional median (gray long dashed line) and the upper and lower quartile (dash-dot line) spectra of protoplanetary disks in Taurus.

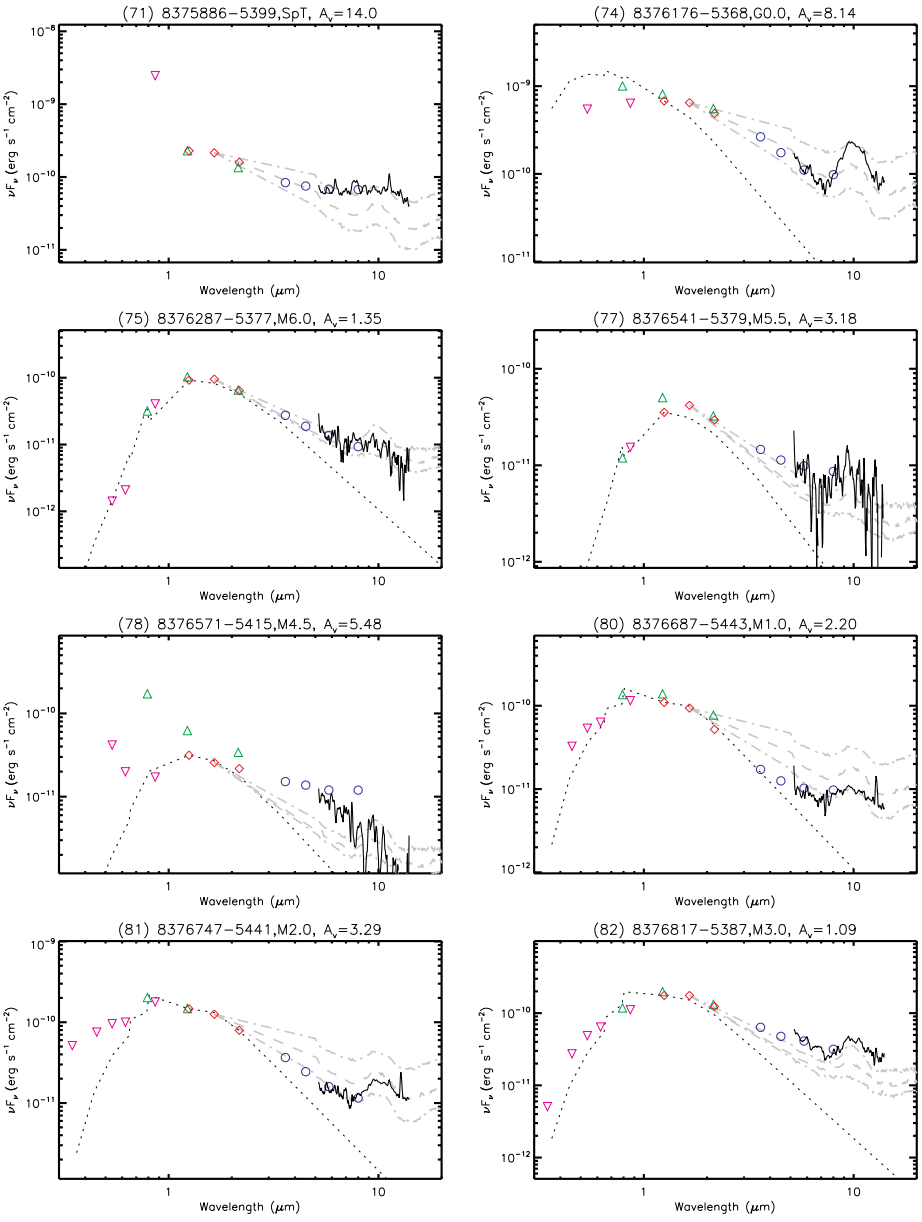


Figure A.2 continued

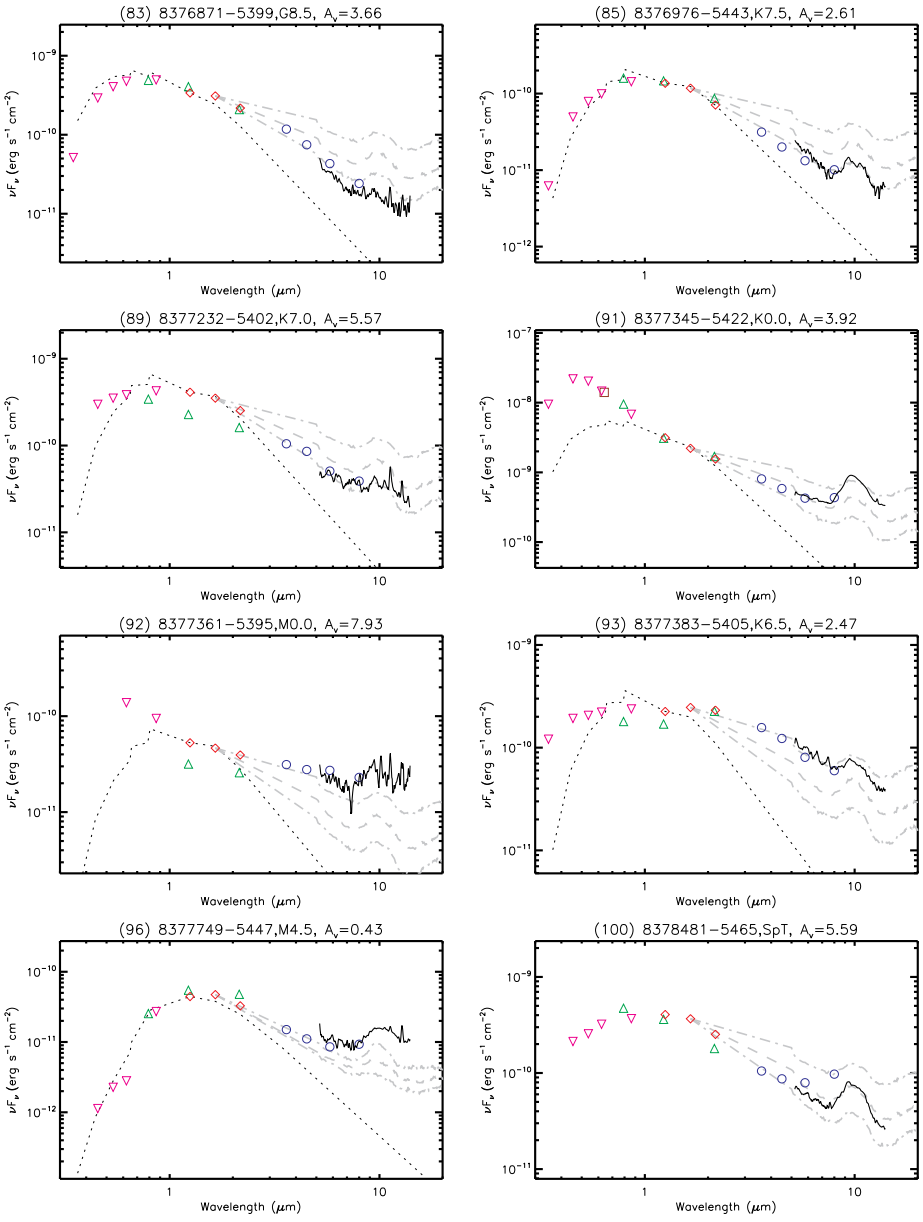


Figure A.2 continued

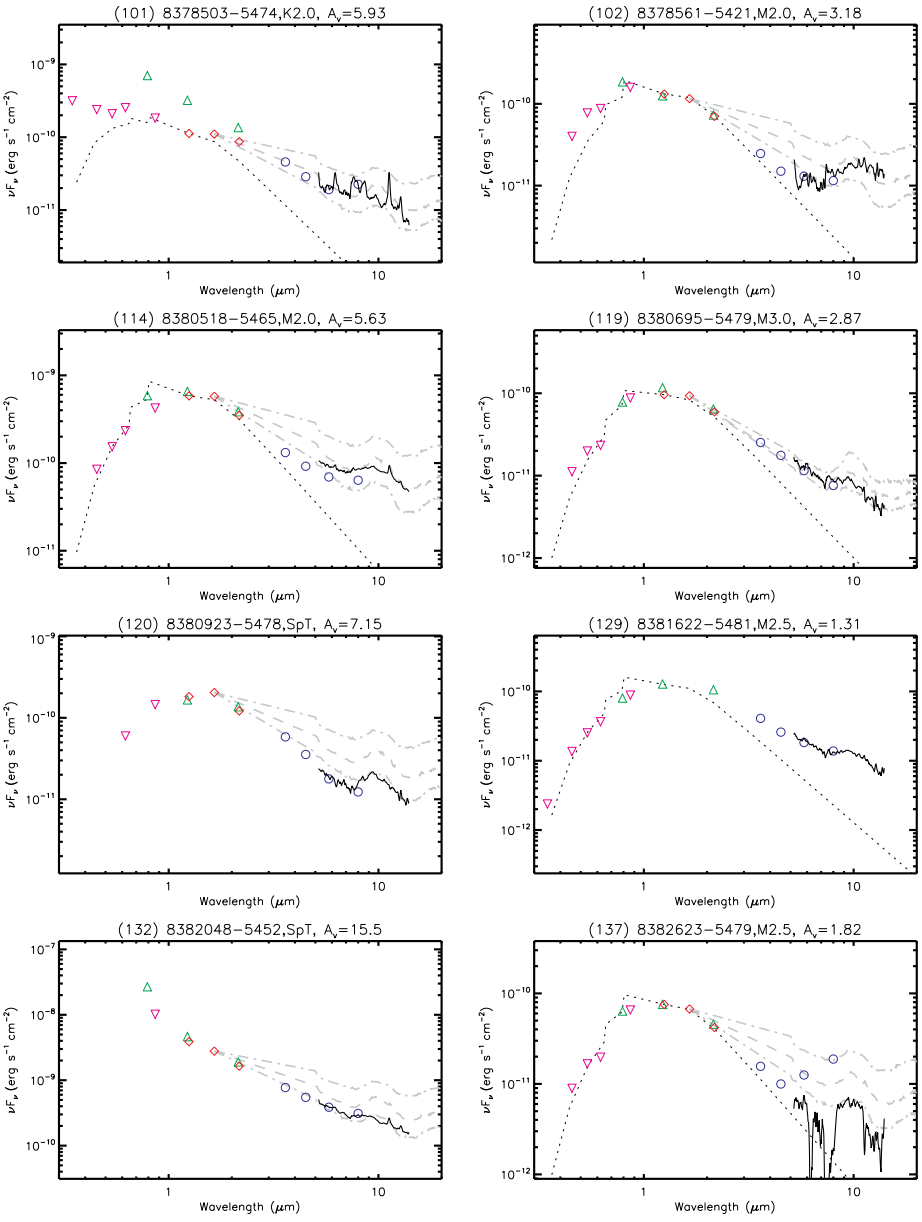


Figure A.2 continued

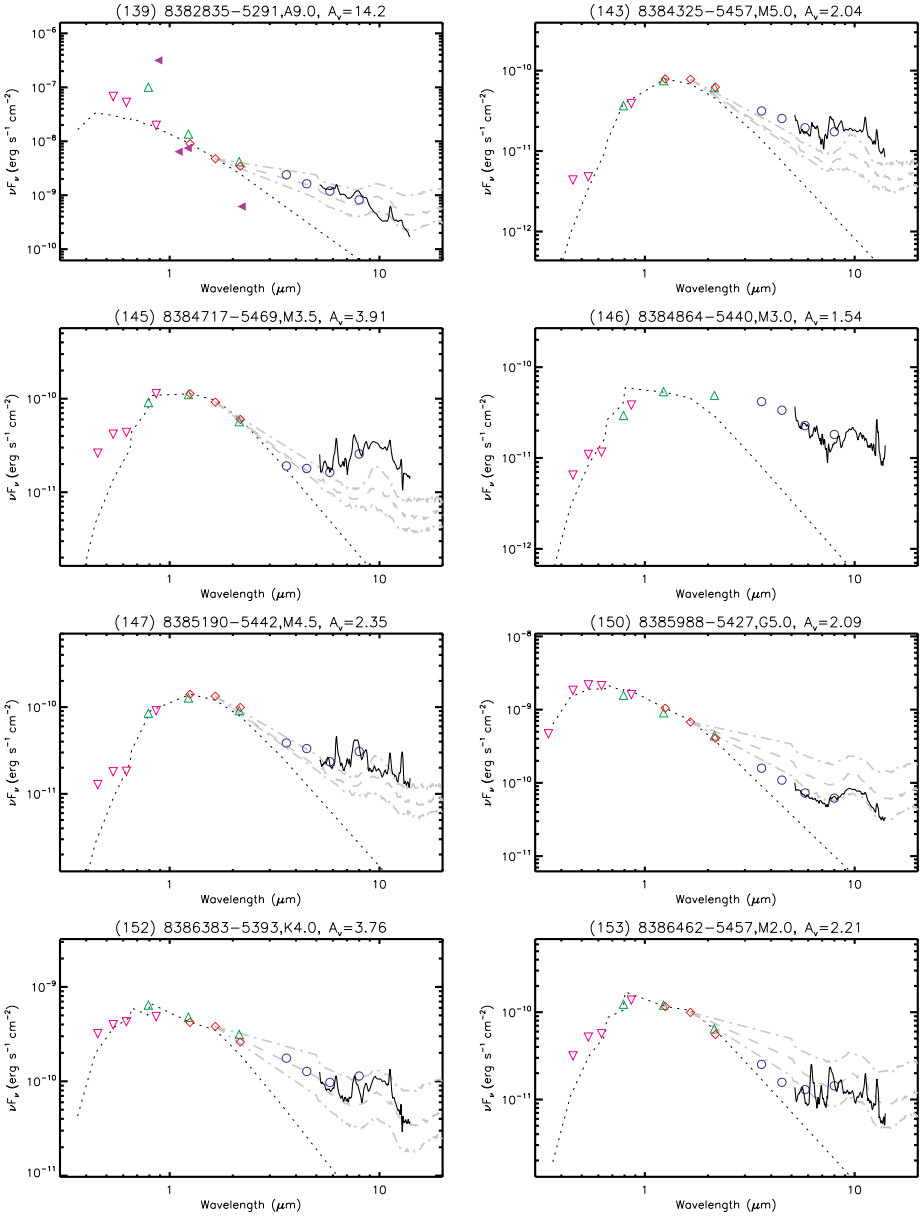


Figure A.2 continued

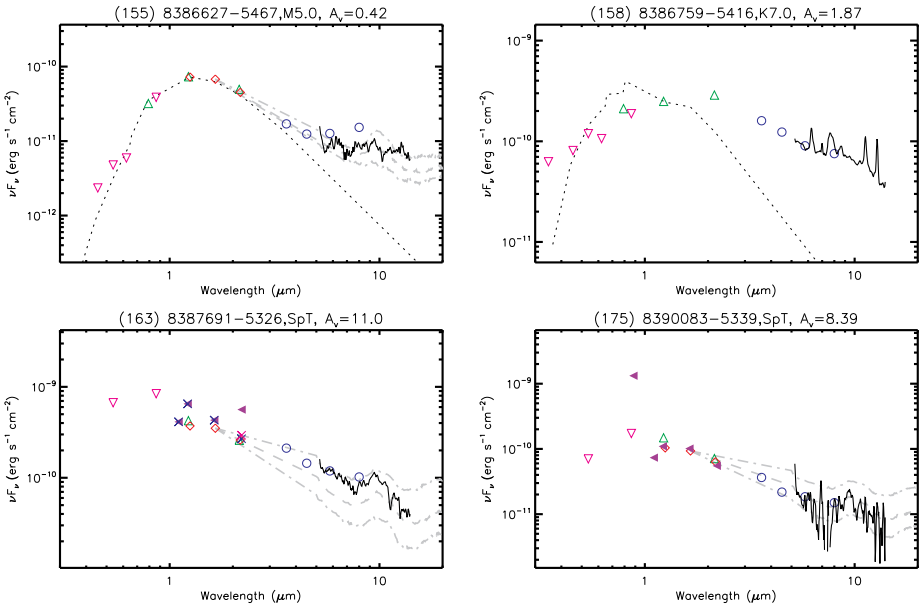


Figure A.2 continued

A.3 Tables

Table A.1. Spectral Type and Extinction

Num. (1)	IRS name (2)	Spectral types (3)	Spectral type adopted(4)	A_V (5)	A_V method (6)
1	8336884-5290	M0.0(8)	M0.0	0.61	I-J
2	8339347-5238	M3.0(8)	M3.0	0.82	CTTS J-H
3	8343858-5513	K1(3)	K1.0	4.73	J-H
4	8343917-6073	M1.5(1)	M1.5	0.09	CTTS J-H
5	8343944-5609	M5.5(3); M5.5(8)	M5.5	0.87	I-J
6	8344455-5390	...	...	6.84	J-H
7	8344987-5460	M6(3)	M6.0	2.44	J-H
8	8346141-5010	M2(3); M3.5(8)	M3.5	0.33	I-J
9	8346378-5387	...	...	9.88	CTTS J-H
10	8346581-5550	...	...	10.1	CTTS J-H
11	8347711-5533	SpeX	K7.0	8.27	H-K
12	8348250-4797	...	...	1.69	CTTS J-H
13	8350150-5595	M3.5(3)	M3.5	0	I-J
14	8350916-5605	K7.5(8); K7(11)	K7.5	2.01	I-J
15	8352483-5378	K7.5(8)	K7.5	5.26	CTTS J-H
16	8353051-5229	SpeX	K1.0	3.01	J-H
17	8353319-5604	M4.0(8); M3.5(9)	M4.0	1.78	J-H
18	8355083-4835	...	...	1	CTTS J-H
19	8355371-5480	K7.0(H)(2)	K7.0	0.15	H-K
20	8355629-5594	M1.9(9)	M2.0	3.46	CTTS J-H
21	8355898-5615	F6(5); F7.0(8); F8(12)	F7.0	0.28	I-J
22	8356531-5540	M2.0(8); K8e(3)	M2.0	1.58	I-J
23	8357031-5072	K7(3); M0.0(8)	M0.0	1.88	J-H
24	8358147-5505	K5(H)(2); K1e(3)	K1.0	4.21	J-H
25	8358862-4842	M3.0(7); M3.5(8)	M3.5	1.62	CTTS J-H
26	8359203-5026	M5.5(8)	M5.5	0.28	I-J
27	8360781-4940	M0.5(8)	M0.5	0.66	I-J
28	8360900-5441	K2-K3e(H)(2); K7.5(8); K2.5e(11)	K7.5	2.96	CTTS J-H
29	8361167-5475	SpeX	M0.0	0.73	I-J
30	8362406-4863	M0.5(8); K7(11)	M0.5	6.75	J-H
31	8364658-4871	...	...	4.94	CTTS J-H
32	8364671-5575	M4(H)(2); M5.0(8)	M5.0	0.44	I-J
33	8365614-5581	K2-K5e(H)(2); M5.0(8); K3.5(11)	M5.0	0	I-J
34	8365722-4816	SpeX	M1.0	1.51	I-J
35	8366668-5168	B8(WSH)A0(Par)B8V(Her)B8V(vA)(2); B8(5); A0(11)	A0.0	1.22	I-J
36	8366704-5669	K2(5); K0e(11)	K2.0	0.98	I-J
37	8367030-5378	K1e(H)G-Ke(Par)K7.3(P)(2); K7(5); G:e(11)	K7.0	3.78	J-H
38	8367284-5798	M0(3)	M0.0	1.1	I-J
39	8368137-4860	M3.5(8)	M3.5	0.65	I-J
40	8368755-4933	K0(3)	K0.0	7.2	CTTS J-H

Table A.1 (cont'd)

Num. (1)	IRS name (2)	Spectral types (3)	Spectral type adopted(4)	A_V (5)	A_V method (6)
41	8368837-5665	···	···	2.78	CTTS H-K
42	8369106-5686	M3.5(3); M4.0(8); M3.0e(9)	M4.0	1	I-J
43	8369290-5652	···	···	2.88	CTTS J-H
44	8369980-5081	K7(3); M1.0(8)	M1.0	0.71	I-J
45	8370827-5312	A3(WSH)A3:(H)A2(Par)A2Vp(LA)A5V:(vA) A6-7V(J)Am(M)A2(T)(2); A3, A2(5);	A7.0	1.64	I-J
46	8371143-5450	M0e(H)(2); K7.5(8); M0(13)	K7.5	2.01	CTTS J-H
47	8371984-5465	K7.5(8)	K7.5	4.68	H-K
48	8372100-5057	K5 (herbig+1988); M0.0(8); G:e(11)	M0.0	0.57	I-J
49	8372608-5359	M2(H)(2)	M2.0	0.49	I-J
50	8372885-5283	K4-K6e(H)(2),K6.5(8); K4.7:e(15)	K6.5	4.65	CTTS J-H
51	8373201-4936	M3.0(8)	M3.0	7.05	CTTS J-H
52	8373676-5192	K5(H)K6(CK)(2); K5(11)	K5.0	0.46	I-J
53	8373930-6325	M3.5(1)	M3.5	0.24	I-J
54	8373936-4946	···	···	11	CTTS J-H
55	8374073-5397	K8(H)(2)	K7.5	1.32	J-H
56	8374080-5380	M3(H)(2); M3.5(8)	M3.5	0.8	I-J
57	8374271-5697	···	···	5.67	CTTS J-H
58	8374301-5908	M0.0(8)	M0.0	0.48	CTTS J-H
59	8374388-6000	K5(3); M2.5(8)	M2.5	0.28	I-J
60	8374599-5741	···	···	0	0
61	8374677-5748	···	···	6.58	CTTS J-H
62	8374677-5766	···	···	4.67	CTTS J-H
63	8374839-5427	M2(H)(2); M0.5(8)	M0.5	1.72	J-H
64	8375041-5383	K0-K2e(H)K0e(Par)K6(CK)K0e(J)(2)	K0.0	3.3	J-H
65	8375063-5840	···	···	7.03	CTTS J-H
66	8375158-5162	M5.5(H)(2); M5.0(8)	M5.0	0.22	J-H
67	8375190-5420	K6e(H)(2); K7.5(8)	K7.5	3.09	J-H
68	8375484-5401	···	···	0	CTTS J-H
70	8375702-5443	···	···	2.51	CTTS J-H
71	8375886-5399	···	···	14	CTTS J-H
73	8376154-5675	···	···	15	CTTS J-H
74	8376176-5368	G:(H)(2)	G0.0	8.14	CTTS J-H
75	8376287-5377	M6(H)(2)	M6.0	1.35	I-J
76	8376356-4822	···	···	1	CTTS J-H
77	8376541-5379	M5.5e(H)(2)	M5.5	3.18	I-J
78	8376571-5415	M4.3(9)	M4.5	5.48	J-H
79	8376643-5900	···	···	6.09	CTTS J-H
80	8376687-5443	M2(H)(2); M1.0(8)	M1.0	2.2	J-H
81	8376747-5441	M2e(H)(2)	M2.0	3.29	J-H

Table A.1 (cont'd)

Num. (1)	IRS name (2)	Spectral types (3)	Spectral type adopted(4)	A_V (5)	A_V method (6)
82	8376817-5387	M0.5-M2e(H)M1.2(P)M3(Eetal)K4-M0(Sam)(2)	M3.0	1.09	I-J
83	8376871-5399	K2(H)M0; M4(Sam)(2); G8.5(8)	G8.5	3.66	CTTS J-H
84	8376918-4974	M0.0(8)	M0.0	6.22	J-H
85	8376976-5443	M0.5(H)(2); K7.5(8)	K7.5	2.61	J-H
86	8377111-5612	M4.5(H)(2); M4.5(8)	M4.5	0.54	CTTS J-H
88	8377167-5247	F8(WSH)G5(S)(2); F8; G2(5); G0+F7 (16)	G0.0	2.96	J-H
89	8377232-5402	M0(H)(2); K7.0(8)	K7.0	5.57	J-H
90	8377335-5489	M0.5(H)(2)	M0.5	5.77	CTTS J-H
91	8377345-5422	K0(WSH)K0-K3e(H)A0V+K1V(?)A0V(vA)K0:e(J) K4eIV(W)K3(CK)(2); K0; K2(5)	K0.0	3.92	J-H
92	8377361-5395	¡M0e(H)(2)	M0.0	7.93	J-H
93	8377383-5405	K2-K7e(H)(2); K6.5(8)	K6.5	2.47	CTTS J-H
94	8377392-5193	M2.5(8)	M2.5	6.11	H-K
95	8377737-5547	···	···	4.88	CTTS J-H
96	8377749-5447	M4.5e(H)(2)	M4.5	0.43	CTTS J-H
97	8378059-5644	···	···	8.57	CTTS J-H
98	8378345-5545	K7.0(8); M0(13)	K7.0	1.84	I-J
99	8378366-5814	···	···	4.46	CTTS J-H
100	8378481-5465	···	···	5.59	CTTS J-H
101	8378503-5474	K2(H)(2)	K2.0	5.93	CTTS J-H
102	8378561-5421	M2(H)(2)	M2.0	3.18	H-K
103	8378630-4781	···	···	5.97	CTTS J-H
106	8379192-6093	S(1)	···	10.8	CTTS J-H
108	8379312-5776	K4(14), K0.0(7); Ke(17)	K0.0	4.19	J-H
112	8380422-5659	K3(5)	K3.0	1.15	CTTS J-H
114	8380518-5465	M2.0 (11)	M2.0	5.63	H-K
117	8380667-5516	K5e(H)F8-G0III-IV(?)(2); G7:e(13)	G7.0	1.69	I-J
119	8380695-5479	M2.8(9)	M3.0	2.87	H-K
120	8380923-5478	···	···	7.15	H-K
121	8380932-5721	···	···	1.06	CTTS J-H
122	8381019-5555	K5(P)K4-M0:(H) (2)	K5.0	10.2	J-H
123	8381020-5546	M4(13)	M4.0	1.7	I-J
125	8381120-5653	K0-K3(P)(2)	K1.5	1.88	CTTS J-H
127	8381491-5164	···	···	5.99	CTTS J-H
128	8381501-4991	···	···	12.4	CTTS J-H
129	8381622-5481	M2.5 (11)	M2.5	1.31	I-J
131	8381971-4762	K1e(14)	K1.0	1.4	I-J
132	8382048-5452	···	···	15.5	H-K
133	8382359-5974	···	···	1.31	CTTS J-H
134	8382412-6410	M0.5(1); M2(4); M1(10)	M1.0	1.9	CTTS J-H

Table A.1 (cont'd)

Num. (1)	IRS name (2)	Spectral types (3)	Spectral type adopted(4)	A_V (5)	A_V method (6)
135	8382467-5709	K3(5)	K3.0	2.25	H-K
136	8382490-5270	K7+M1.5(16)	K7.0	10.6	H-K
137	8382623-5479	M2.5(9)	M2.5	1.82	H-K
138	8382655-4889	···	···	6.58	CTTS J-H
139	8382835-5291	A8-F0(H)(2)	A9.0	14.2	J-H
140	8383581-5050	···	···	26.5	CTTS H-K
141	8383861-5154	G1(WSH)G0(Par)F9IV(vA)K2Ve(D)F8-G0III-IV, V(LDW,J,M)G0III(W)(2); G1, G0(5); F8.0(8)	F8.0	0.91	I-J
142	8384113-5117	···	···	2.4	CTTS J-H
143	8384325-5457	M4.5e(H)(2); M5.0(8)	M5.0	2.04	CTTS J-H
144	8384331-5134	K7.0(8)	K7.0	5.44	CTTS J-H
145	8384717-5469	M3.5(H)(2)	M3.5	3.91	J-H
146	8384864-5440	M3.0(11)	M3.0	1.54	I-J
147	8385190-5442	M4-M4.5e(H)M5.3(P)M4(Eetal)(2)	M4.5	2.35	CTTS J-H
148	8385255-5191	K6e(H)(2); K7.5(8)	K7.5	5.18	J-H
149	8385365-5106	···	···	21.3	CTTS J-H
150	8385988-5427	G5(Par)G0III(HB)G-K:(GS)K1; M3(Sam)(2)	G5.0	2.09	J-H
151	8386322-6328	M2.0(1); M2.5(4); M1.5(10)	M1.5	1.5	J-H
152	8386383-5393	K4(Sam)(2)	K4.0	3.76	CTTS J-H
153	8386462-5457	M3(H)M3.2(P)(2); M2.0(8)	M2.0	2.21	J-H
154	8386523-5715	M3.6(9)	M3.5	2.28	H-K
155	8386627-5467	M5(H)(2)	M5.0	0.42	I-J
156	8386694-5026	···	···	28.6	CTTS H-K
158	8386759-5416	K7.0(11)	K7.0	1.87	I-J
159	8386804-5987	M3.5(8)	M3.5	0.08	I-J
160	8386841-5129	···	···	19.9	CTTS H-K
161	8386935-4790	K1(3); M4.5(8)	M4.5	0.31	I-J
162	8386957-4804	···	···	17.7	H-K
163	8387691-5326	···	···	11	CTTS J-H
164	8387753-4993	···	···	14.7	CTTS J-H
165	8387832-5864	···	···	4.97	CTTS J-H
166	8387937-6755	M3(4); M3(10)	M3.0	0.18	I-J
167	8388119-5083	M2.0(8)	M2.0	0.6	CTTS J-H
168	8388316-5157	K3(WSH)K6(CK)K4-M0eIV(W)(2); K4(5); M0.5+M1.5(16)	M1.0	1.88	CTTS J-H
169	8389033-4773	K4(3); M0.5(8)	M0.5	1.9	H-K
170	8389275-5105	A0(5)	A0.0	0	J-H
172	8389673-4794	M1.0(7); M3.0(8)	M3.0	2.03	J-H
173	8390003-5207	G6-K2e(H)(2)	K0.0	1.78	I-J
174	8390073-5082	···	···	8.42	CTTS J-H
175	8390083-5339	···	···	8.39	CTTS J-H

Table A.1 (cont'd)

Num. (1)	IRS name (2)	Spectral types (3)	Spectral type adopted(4)	A_V (5)	A_V method (6)
176	8390285-5070	M1.5(8)	M1.5	0.79	I-J
177	8390554-6390	M2.5(1)	M2.5	0.12	H-K
178	8391040-5081	···	···	16.9	CTTS J-H
179	8391058-4994	M0.0(8)	M0.0	3.04	J-H
180	8391196-5211	K2(H)(2); K5.0(8)	K5.0	4.06	CTTS J-H
181	8391648-5110	···	···	5.47	CTTS J-H
182	8392509-5169	K6-K8(H)(2); K6.5(8)	K6.5	6.98	J-H
183	8393152-5094	M0.0(8)	M0.0	2.23	CTTS J-H
184	8394216-5181	K7e(H)(2); K7.5(8)	K7.5	1.79	J-H
185	8394454-5823	K6.0(7)	K6.0	1.57	J-H
186	8395167-5024	M0.5(8); K5e(14)	M0.5	2.4	CTTS J-H
187	8395780-5308	M1.5(8)	M1.5	3.42	CTTS J-H
188	8396035-5861	···	···	0.64	CTTS J-H
189	8396285-5119	···	···	1.63	CTTS J-H
190	8396319-4941	M2.5(8)	M2.5	4.87	J-H
191	8396679-6167	K4.0(1)	K4.0	3.65	CTTS J-H
192	8397522-4788	M2.0(8)	M2.0	0.43	CTTS J-H
193	8397632-5445	M0.5e(H)(2); M0.5(8)	M0.5	0.74	CTTS J-H
194	8397818-4972	···	···	1.54	CTTS J-H
195	8398707-5755	M2(3)	M2.0	3.8	CTTS J-H
196	8398936-6711	K7.5(1); M0(4); K4(10)	K7.5	0.89	CTTS J-H
197	8399022-5955	K7.5(1); M0.0(8); M0e(3); K7,M0 (14)	M0.0	0.86	J-H
198	8399269-6612	K6.5(1); M0(4); M0(10)	K6.5	2.17	J-H
199	8399902-6268	M2.5(1); M0(4); K4.5(10); K7(18)	K7.0	1.78	J-H
200	8400080-6709	K5.5(1); K5(4); K5(10)	K5.5	1.13	CTTS J-H
201	8402765-6538	K6.5(1); K5(4); K5(10)	K6.5	5.33	CTTS J-H
202	8403455-6810	M0.5(1); M2(4); M0.5(10)	M0.5	2.5	CTTS J-H
203	8406280-6293	K5(4); K3(10)	K5.0	0.68	CTTS J-H
204	8406609-6247	M2.5(4); M2.5(8); M2.5(10)	M2.5	0.73	I-J
205	8407074-5195	K6(19); K4IV-Ve(Parenago)	K4.0	2.73	H-K
206	8408920-6760	K5.0(1); Cs(11); G8 (Cohen & Schwartz 1979, CS)	K5.0	5.92	CTTS J-H
207	8409911-6386	E(4)	···	12.3	J-H
208	8410334-6291	K4e (11)	K4.0	0.75	I-J
209	8410779-6416	···	···	23.6	CTTS H-K
210	8410886-6134	M1.5(1)	M1.5	1.87	I-J
211	8411618-6426	M3.5(1); M3.5(8); M3(10)	M3.5	0.53	I-J
212	8412592-6712	M1.5(1); M2(4); M1.5(10)	M1.5	8.01	CTTS J-H
213	8413152-6141	K7.5(1)	K7.5	2.18	J-H
214	8413399-5287	M0.5(8); K8e (3)	M0.5	0.89	I-J
215	8413704-6739	M2.0(1); M2(4); M1.0(10)	M2.0	4.14	I-J

Table A.1 (cont'd)

Num. (1)	IRS name (2)	Spectral types (3)	Spectral type adopted(4)	A_V (5)	A_V method (6)
216	8414490-7187	···	···	0	0
217	8415394-6556	K7.0(1); K8(4); K8(10)	K7.0	4.45	J-H
218	8416389-6503	M4.5(1); M4.5(8)	M4.5	0.23	I-J
219	8416834-6225	M0.5(7); M0.5(8)	M0.5	0.68	I-J
220	8416914-6175	M0.0(1)	M0.0	6.78	CTTS J-H
221	8416978-6185	K7.5(1)	K7.5	11.8	H-K
222	8421949-6718	M0.5(1)	M0.5	6.32	J-H
223	8424570-6484	M3.0(7)	M3.0	0.9	I-J
224	8424689-6154	A0.0 (12); A2/3 (20); A2V (21)	A2.0	1.26	I-J
225	8425038-6557	K5.0(1); K0 (14)	K5.0	2.16	CTTS J-H
226	8430527-6583	A3.5(1); A5II-IIIev (14)	A3.5	0.96	I-J
227	8440418-7404	M0.0(1)	M0.0	2.15	I-J
228	8443530-6843	M0.5(1); M0e (22)	M0.5	1.02	I-J
229	8444779-6608	S(1); ¿M0.0(7)	M0.0	3.5	H-K
230	8445558-6860	S(1); SpeX	M0.0	2.42	CTTS J-H
231	8447398-6788	M3.0(7)	M3.0	22.5	CTTS H-K
232	8448350-6815	M0.0(1)	M0.0	8.25	CTTS J-H
233	8450343-7265	M1.5(1); K7(22)	M1.5	1.22	I-J
234	8452061-7269	M0.5(1)	M0.5	1.71	I-J
235	8453876-6821	A3.5(1); A5e(23)	A3.5	3.56	I-J
236	8455602-7112	M1.0(1); K4.5(10)	M1.0	8.19	H-K
237	8457266-7161	S(1); M1.5(7)	M1.5	4.59	J-H
238	8461533-6914	K6.0(1)	K6.0	0.67	CTTS J-H
239	8464666-7838	M1.0(1); K5e(14)	M1.0	0.39	H-K
240	8465247-7776	M1.5(1)	M1.5	1.51	J-H
241	8466711-6987	K6.0(1)	K6.0	5.76	J-H
242	8468002-6969	S?(1); K7.5(10)	K7.5	11.6	J-H
243	8468729-6970	S(1); M1.0(10)	M1.0	8.77	CTTS J-H
244	8469891-7104	M1.5(1); M1.0(10)	M1.5	9.64	CTTS J-H
245	8472719-7464	M2.0(1)	M2.0	5.81	CTTS J-H
246	8476732-7058	K7.5(1)	K7.5	10.2	CTTS J-H
247	8477229-7184	M3.0(1)	M3.0	5.86	CTTS J-H
248	8486920-7342	···	···	20.4	CTTS H-K
249	8488472-7373	SpeX	M2.5	0.39	CTTS J-H
250	8492690-7387	···	···	15.7	CTTS J-H
251	8494096-7377	···	···	14.6	CTTS J-H
252	8495155-7404	···	···	20.2	CTTS H-K
253	8497290-7502	···	···	21.5	CTTS H-K
254	8497797-7462	···	···	34.5	CTTS H-K
255	8499151-7482	···	···	32	CTTS H-K

Table A.1 (cont'd)

Num. (1)	IRS name (2)	Spectral types (3)	Spectral type adopted(4)	A_V (5)	A_V method (6)
256	8499541-7426	···	···	13.1	CTTS J-H
257	8502614-7795	M3.0(1)	M3.0	0.63	I-J
258	8504327-7460	K7.0(1)	K7.0	10.4	J-H
259	8508083-8237	S(1); K7e(4); K7.0(10)	K7.0	6.92	CTTS J-H
260	8508501-7431	M2.0(1)	M2.0	1.17	I-J
261	8508648-7916	S(1)	···	7.69	CTTS J-H
262	8510403-8125	S?(1-as4?); K0e(4); K0(10)	K0.0	1.91	I-J
263	8511308-8126	M3e(4); M3(10)	M3.0	2.92	J-H
264	8511602-7926	S(1)	···	8.46	CTTS J-H
265	8514861-7663	···	···	11	CTTS J-H
266	8515568-8067	F0-G0e(4); F(10)	F4.0	6.83	J-H
267	8516031-7796	···	···	22	CTTS H-K
268	8518798-7373	···	···	2.36	CTTS J-H
269	8519260-8090	K4.0(1); K1e(4); K1(10)	K4.0	3.31	J-H
270	8519428-8120	S(1); K7(4); K7(10)	K7.0	9.53	H-K
271	8520557-7775	S(1); SpeX	M2.0	6.11	H-K
272	8520580-7960	···	···	9.15	J-H
273	8530851-8132	M2(1); M2(4); M2(10)	M2.0	2.08	H-K
274	8534457-7821	···	···	17.6	CTTS H-K
275	8535781-7830	S(1); ¡M5.0(7)	M5.0	4.06	H-K
276	8536129-8706	···	···	14.5	CTTS J-H
277	8537742-8080	K7e(4); K7(10)	K7.0	8.27	J-H
278	8538844-7917	M2(11)	M2.0	0.92	I-J
279	8538911-7999	S(1); M1.5(10)	M1.5	7.98	H-K
280	8542681-8618	K7.0(1)	K7.0	4.45	J-H
281	8543224-7972	S(1); M5.5(10)	M5.5	2.5	J-H
282	8545724-8008	K5(4); K5(10)	K5.0	0.61	I-J
283	8547523-7831	M2.0(7)	M2.0	1.41	J-H
284	8547770-7986	S(1); K8(4); K3.5(10)	K3.5	5.33	CTTS J-H
285	8552157-8190	···	···	12.7	CTTS J-H
286	8552280-8641	M3.0(1)	M3.0	1.7	I-J
287	8556074-7982	M3.5(10)	M3.5	1.2	I-J
288	8560743-8147	S(1); M2.5(10)	M2.5	3.25	J-H
289	8561044-7980	K6.0(10)	K6.0	4	CTTS J-H
290	8562845-8151	M2.5(1)	M2.5	2.92	I-J
291	8564835-8250	M2.5(1)	M2.5	2.81	J-H
292	8567003-8669	M1.0(1)	M1.0	1.49	I-J
293	8567545-8254	M3.0(1); M1(4); M1.0(10)	M3.0	3.4	CTTS J-H
294	8567670-8803	S(1); SpeX	M2.5	7.42	H-K
295	8569204-8666	S(1)	···	5.46	CTTS J-H

Table A.1 (cont'd)

Num. (1)	IRS name (2)	Spectral types (3)	Spectral type adopted(4)	A_V (5)	A_V method (6)
296	8570200-8276	···	···	17.5	CTTS J-H
297	8570949-8577	···	···	19.9	CTTS H-K
298	8571439-8650	···	···	6.72	CTTS J-H
299	8574645-8156	M1.0(1); M1(4); M1.0(10)	M1.0	2.37	CTTS J-H
300	8576640-8652	···	···	6.97	CTTS J-H
301	8576836-8303	M3.5(1)	M3.5	3.16	CTTS J-H
302	8579480-8565	SpeX	M	3.41	CTTS J-H
303	8580634-8516	S(1); M3.0(7)	M3.0	6.56	4

Note. — The methods or literature of spectral type is indicated with parentheses, and the meaning of the numbers in parentheses is listed in the next page.

Note. — Column (6) A_V method: the method which derived A_V in the column (5). See the text for details.

• Table note for the literature of spectral type information in column 3 of Table A.1

(1) Allen & Mosby (2008), private communication; spectral types are measured from HECTOSPEC spectra

(2) Hillenbrand (1997)

(3) Rebull et al. (2000)

(4) Allen (1995)

(5) Wolff et al. (2004)

(6) Hillenbrand & Carpenter (2000)

(7) Hernandez (2008), private communication; spectral types measured from MDM spectroscopic data

(8) Hernandez & Tobin (2009), private communication; spectral types are measured from HECTOSPEC spectra or FAST spectra

(9) da Rio et al. (2010)

(10) Fang et al. (2009)

(11) Parihar et al. (2009a)

(12) Manoj et al. (2006)

(13) Parihar et al. (2009b)

(14) Herbig & Bell (1988)

(15) Glebocki & Gnacinski (2005)

(16) Daemgen et al. (2012)

(17) Grankin et al. (2007)

(18) Riaz et al. (2006)

(19) Rebull (2001)

(20) Houk & Swift (2000)

(21) Ochsenbein (1980)

(22) Wouterloot & Brand (1992)

(23) Caratti O Garatti et al. (2012)

(SpeX) Spectral typing with SpeX spectra in this work

Table A.2. Basic Stellar Properties

Num. (1)	IRS name (2)	T_{eff} (3)	$L_\star$ adopted(4)	$M_\star$ (5)	eM_{star} (6)	$\dot{M}$ (7)
1	8336884-5290	3850	0.64	0.55	0.08	5.86E-10 ± 1.07E-10
2	8339347-5238	3470	0.38	0.33	0.06	9.19E-10 ± 6.54E-10
3	8343858-5513	5080	14.14	2.93	0.1	2.42E-07 ± 1.41E-07
4	8343917-6073	3650	0.79	0.42	0.06	2.75E-09 ± 4.29E-10
5	8343944-5609	3145	0.54	0.22	0.04	< 1.00E-08
6	8344455-5390	3850	0.77	0.55	0.07	···
7	8344987-5460	3050	0.09	0.15	0.05	···
8	8346141-5010	3420	0.17	0.31	0.07	···
9	8346378-5387	3850	5.26	0.57	0.08	···
10	8346581-5550	3850	0.25	0.57	0.09	···
11	8347711-5533	4060	1.8	0.7	0.09	< 4.50E-10
12	8348250-4797	3850	0.29	0.57	0.09	···
13	8350150-5595	3420	0.45	0.31	0.06	3.44E-10 ± 1.35E-10
14	8350916-5605	3955	2.74	0.61	0.09	···
15	8352483-5378	3955	1.47	0.61	0.09	···
16	8353051-5229	5080	3.65	1.88	0.07	2.82E-09 ± 1.08E-09
17	8353319-5604	3370	0.45	0.3	0.06	···
18	8355083-4835	3850	0.18	0.58	0.09	···
19	8355371-5480	4060	0.5	0.77	0.08	1.68E-09 ± 4.21E-10
20	8355629-5594	3580	0.37	0.39	0.07	4.23E-09 ± 1.29E-09
21	8355898-5615	6280	16.97	2.08	0.04	···
22	8356531-5540	3580	0.49	0.38	0.07	1.56E-08 ± 7.46E-09
23	8357031-5072	3850	1.32	0.54	0.07	< 7.62E-10
24	8358147-5505	5080	5.98	2.23	0.1	7.34E-08 ± 2.35E-08
25	8358862-4842	3420	0.14	0.3	0.07	< 2.91E-10
26	8359203-5026	3145	0.17	0.21	0.06	9.23E-10 ± 1.91E-10
27	8360781-4940	3785	0.5	0.5	0.08	···
28	8360900-5441	3955	2.66	0.61	0.09	2.03E-07 ± 2.21E-08
29	8361167-5475	3850	0.41	0.56	0.08	1.05E-09 ± 4.74E-11
30	8362406-4863	3785	1.19	0.49	0.07	···
31	8364658-4871	3850	0.24	0.57	0.09	···
32	8364671-5575	3240	0.25	0.25	0.05	1.61E-09 ± 7.91E-10
33	8365614-5581	3240	0.53	0.25	0.04	1.21E-08 ± 4.13E-09
34	8365722-4816	3720	0.25	0.47	0.08	< 8.91E-11
35	8366668-5168	9520	49.07	2.6	0.19	···
36	8366704-5669	4900	6.2	2.22	0.2	1.50E-08 ± 4.77E-09
37	8367030-5378	4060	6.3	0.77	0.12	1.45E-06 ± 6.96E-07
38	8367284-5798	3850	1.46	0.53	0.07	2.33E-09 ± 6.56E-10
39	8368137-4860	3420	0.26	0.31	0.07	5.81E-10 ± 5.64E-10
40	8368755-4933	5250	1.48	1.26	0.03	···

Table A.2 (cont'd)

Num. (1)	IRS name (2)	T_{eff} (3)	$L_\star$ adopted(4)	$M_\star$ (5)	eM_{star} (6)	$\dot{M}$ (7)
41	8368837-5665	3850	0.05	0.5	0.05	···
42	8369106-5686	3370	0.49	0.3	0.05	1.65E-09 ± 7.37E-10
43	8369290-5652	3850	3.32	0.54	0.07	···
44	8369980-5081	3720	0.6	0.46	0.07	4.46E-09 ± 1.81E-09
45	8370827-5312	7850	48.34	2.59	0.09	···
46	8371143-5450	3955	1.29	0.61	0.08	···
47	8371984-5465	3955	4.37	0.63	0.09	< 7.36E-10
48	8372100-5057	3850	0.61	0.55	0.08	8.33E-09 ± 1.24E-09
49	8372608-5359	3580	0.52	0.38	0.07	···
50	8372885-5283	4132	3.42	0.79	0.11	3.60E-08 ± 1.01E-08
51	8373201-4936	3470	2.48	0.33	0.04	< 1.86E-08
52	8373676-5192	4350	1.78	1.07	0.12	···
53	8373930-6325	3420	0.17	0.31	0.07	···
54	8373936-4946	3850	1.49	0.53	0.07	···
55	8374073-5397	3955	3.82	0.63	0.09	···
56	8374080-5380	3420	0.36	0.31	0.06	···
57	8374271-5697	3850	1.87	0.53	0.07	···
58	8374301-5908	3850	0.51	0.55	0.08	2.12E-09 ± 1.13E-09
59	8374388-6000	3525	0.66	0.36	0.06	5.37E-09 ± 5.67E-10
60	8374599-5741	3850	0.85	0.54	0.08	···
61	8374677-5748	3850	1.8	0.53	0.07	···
62	8374677-5766	3850	2.86	0.53	0.07	···
63	8374839-5427	3785	0.74	0.49	0.08	···
64	8375041-5383	5250	9.96	2.5	0.04	···
65	8375063-5840	3850	1.02	0.54	0.07	···
66	8375158-5162	3240	0.1	0.23	0.06	< 7.92E-11
67	8375190-5420	3955	1.08	0.62	0.08	···
68	8375484-5401	3850	0.88	0.54	0.07	···
70	8375702-5443	3850	0.13	0.57	0.09	···
71	8375886-5399	3850	1.87	0.53	0.08	···
73	8376154-5675	3850	2.98	0.54	0.08	···
74	8376176-5368	6030	10.18	1.87	0.07	···
75	8376287-5377	3050	0.67	0.19	0.03	···
76	8376356-4822	3850	4.4	0.56	0.08	···
77	8376541-5379	3145	0.26	0.22	0.05	···
78	8376571-5415	3305	0.23	0.27	0.06	···
79	8376643-5900	3850	0.55	0.55	0.08	···
80	8376687-5443	3720	0.87	0.45	0.06	···
81	8376747-5441	3580	1.13	0.38	0.05	···
82	8376817-5387	3470	1.34	0.33	0.04	···

Table A.2 (cont'd)

Num. (1)	IRS name (2)	T_{eff} (3)	$L_\star$ adopted(4)	$M_\star$ (5)	eM_{star} (6)	$\dot{M}$ (7)
83	8376871-5399	5465	4.3	1.7	0.01	···
84	8376918-4974	3850	0.83	0.54	0.08	···
85	8376976-5443	3955	1.15	0.62	0.08	···
86	8377111-5612	3305	0.27	0.27	0.06	9.96E-10 ± 7.47E-10
88	8377167-5247	6030	75.64	3.74	0.09	···
89	8377232-5402	4060	3.55	0.71	0.1	···
90	8377335-5489	3785	0.99	0.49	0.07	···
91	8377345-5422	5250	37.51	3.68	0.06	···
92	8377361-5395	3850	0.43	0.56	0.08	···
93	8377383-5405	4132	1.97	0.8	0.11	···
94	8377392-5193	3525	1.14	0.35	0.05	···
95	8377737-5547	3850	0.25	0.57	0.09	···
96	8377749-5447	3305	0.33	0.27	0.05	···
97	8378059-5644	3850	1	0.54	0.07	2.87E-08 ± 6.04E-09
98	8378345-5545	4060	0.88	0.72	0.09	6.49E-09 ± 3.13E-09
99	8378366-5814	3850	0.78	0.54	0.08	···
100	8378481-5465	3850	3.33	0.54	0.08	···
101	8378503-5474	4900	1.21	1.3	0.05	···
102	8378561-5421	3580	1.02	0.38	0.06	···
103	8378630-4781	3850	1.58	0.53	0.07	···
106	8379192-6093	3850	2.33	0.53	0.07	···
108	8379312-5776	5250	22.75	3.2	0.08	2.90E-08 ± 1.65E-08
112	8380422-5659	4730	8.28	2.09	0.29	4.49E-08 ± 1.34E-08
114	8380518-5465	3580	4.53	0.39	0.06	···
117	8380667-5516	5630	7.18	1.88	0.01	4.85E-08 ± 2.32E-09
119	8380695-5479	3470	0.73	0.33	0.05	···
120	8380923-5478	3850	1.49	0.53	0.07	···
121	8380932-5721	3850	3.06	0.54	0.07	···
122	8381019-5555	4350	5.84	1.15	0.17	···
123	8381020-5546	3370	0.17	0.29	0.07	< 2.63E-10
125	8381120-5653	4990	4.22	1.99	0.1	5.76E-09 ± 3.13E-09
127	8381491-5164	3850	0.77	0.54	0.08	···
128	8381501-4991	3850	1.7	0.53	0.07	···
129	8381622-5481	3525	0.98	0.35	0.05	···
131	8381971-4762	5080	1.91	1.48	0.05	···
132	8382048-5452	3850	31.81	0.96	0.31	···
133	8382359-5974	3850	2.68	0.54	0.07	···
134	8382412-6410	3720	1.62	0.45	0.06	3.76E-09 ± 6.63E-10
135	8382467-5709	4730	6.73	1.98	0.25	···
136	8382490-5270	4060	20.73	1.03	0.17	···

Table A.2 (cont'd)

Num. (1)	IRS name (2)	T_{eff} (3)	$L_\star$ adopted(4)	$M_\star$ (5)	eM_{star} (6)	$\dot{M}$ (7)
137	8382623-5479	3525	0.58	0.36	0.06	···
138	8382655-4889	3850	1.89	0.53	0.07	···
139	8382835-5291	7390	199.29	3.47	2	···
140	8383581-5050	3850	9.4	0.63	0.09	···
141	8383861-5154	6200	37.42	2.8	0.07	< 5.51E-09
142	8384113-5117	3850	2.45	0.53	0.07	···
143	8384325-5457	3240	0.58	0.25	0.04	···
144	8384331-5134	4060	6.07	0.76	0.12	2.68E-07 ± 1.12E-07
145	8384717-5469	3420	0.85	0.31	0.04	···
146	8384864-5440	3470	0.41	0.34	0.06	···
147	8385190-5442	3305	1.05	0.27	0.03	···
148	8385255-5191	3955	1.84	0.61	0.08	···
149	8385365-5106	3850	7.4	0.6	0.09	···
150	8385988-5427	5770	14.55	2.24	0.04	···
151	8386322-6328	3650	1.44	0.41	0.06	···
152	8386383-5393	4590	4.17	1.54	0.2	···
153	8386462-5457	3580	0.9	0.38	0.06	···
154	8386523-5715	3420	0.86	0.32	0.05	3.68E-09 ± 2.40E-09
155	8386627-5467	3240	0.53	0.25	0.04	···
156	8386694-5026	3850	19.8	0.75	0.14	···
158	8386759-5416	4060	2.14	0.7	0.09	···
159	8386804-5987	3420	0.35	0.31	0.06	1.23E-09 ± 5.00E-10
160	8386841-5129	3850	4.66	0.56	0.08	···
161	8386935-4790	3305	0.3	0.27	0.06	1.16E-09 ± 7.74E-10
162	8386957-4804	3850	3.17	0.54	0.08	···
163	8387691-5326	3850	3.05	0.54	0.08	···
164	8387753-4993	3850	5.02	0.56	0.08	···
165	8387832-5864	3850	0.79	0.54	0.08	···
166	8387937-6755	3470	0.74	0.33	0.05	···
167	8388119-5083	3580	0.5	0.38	0.07	···
168	8388316-5157	3720	10.13	0.53	0.09	7.89E-07 ± 2.86E-07
169	8389033-4773	3785	0.81	0.5	0.07	2.87E-09 ± 1.77E-09
170	8389275-5105	9520	28.53	2.31	0.12	···
172	8389673-4794	3470	0.62	0.34	0.05	< 9.33E-10
173	8390003-5207	5250	4.5	1.9	0.05	8.87E-08 ± 1.45E-08
174	8390073-5082	3850	2.11	0.53	0.07	···
175	8390083-5339	3850	0.85	0.54	0.08	···
176	8390285-5070	3650	0.71	0.42	0.07	3.31E-09 ± 4.03E-10
177	8390554-6390	3525	0.3	0.36	0.07	< 1.26E-09
178	8391040-5081	3850	1.41	0.53	0.07	···

Table A.2 (cont'd)

Num. (1)	IRS name (2)	T_{eff} (3)	$L_\star$ adopted(4)	$M_\star$ (5)	eM_{star} (6)	$\dot{M}$ (7)
179	8391058-4994	3850	1.2	0.54	0.07	2.75E-08 ± 1.51E-09
180	8391196-5211	4350	6.3	1.16	0.17	···
181	8391648-5110	3850	1.4	0.53	0.07	···
182	8392509-5169	4132	6.26	0.85	0.13	3.28E-08 ± 6.16E-09
183	8393152-5094	3850	0.88	0.54	0.08	8.87E-09 ± 2.44E-09
184	8394216-5181	3955	1.12	0.62	0.08	7.45E-09 ± 7.96E-10
185	8394454-5823	4205	1.3	0.87	0.1	5.85E-09 ± 4.33E-09
186	8395167-5024	3785	0.88	0.49	0.07	7.89E-08 ± 2.03E-08
187	8395780-5308	3650	0.66	0.42	0.07	8.87E-09 ± 3.91E-09
188	8396035-5861	3850	1.19	0.54	0.07	···
189	8396285-5119	3850	2.08	0.53	0.07	···
190	8396319-4941	3525	0.59	0.36	0.06	6.12E-09 ± 3.41E-10
191	8396679-6167	4590	14.59	2.04	0.33	2.34E-07 ± 4.87E-08
192	8397522-4788	3580	0.37	0.38	0.08	···
193	8397632-5445	3785	0.63	0.5	0.08	···
194	8397818-4972	3850	0.08	0.56	0.08	···
195	8398707-5755	3580	0.87	0.38	0.06	···
196	8398936-6711	3955	1.74	0.61	0.09	1.27E-08 ± 7.46E-09
197	8399022-5955	3850	0.59	0.55	0.08	3.47E-08 ± 2.15E-09
198	8399269-6612	4132	1.33	0.78	0.09	4.79E-09 ± 1.62E-09
199	8399902-6268	4060	3.37	0.72	0.1	···
200	8400080-6709	4277	2.05	0.96	0.12	2.15E-08 ± 3.63E-09
201	8402765-6538	4132	2.35	0.82	0.18	···
202	8403455-6810	3785	0.96	0.49	0.07	···
203	8406280-6293	4350	1.46	1.07	0.12	···
204	8406609-6247	3525	0.23	0.36	0.07	1.54E-09 ± 8.49E-10
205	8407074-5195	4590	6.19	1.63	0.23	···
206	8408920-6760	4350	9.6	1.27	0.2	< 2.37E-08
207	8409911-6386	3850	2.2	0.53	0.07	···
208	8410334-6291	4590	10.67	1.86	0.29	1.01E-08 ± 1.84E-09
209	8410779-6416	3850	10.01	0.63	0.1	···
210	8410886-6134	3650	1.51	0.41	0.06	< 2.27E-09
211	8411618-6426	3420	0.23	0.31	0.07	3.61E-10 ± 3.46E-10
212	8412592-6712	3650	1.44	0.41	0.06	···
213	8413152-6141	3955	3.95	0.63	0.09	1.45E-08 ± 7.23E-09
214	8413399-5287	3785	0.47	0.5	0.08	2.52E-09 ± 1.41E-10
215	8413704-6739	3580	0.63	0.38	0.06	···
216	8414490-7187	3850	0	-999	-999	···
217	8415394-6556	4060	2.45	0.7	0.09	4.85E-07 ± 1.86E-07
218	8416389-6503	3305	0.14	0.26	0.07	< 4.86E-10

Table A.2 (cont'd)

Num. (1)	IRS name (2)	T_{eff} (3)	$L_\star$ adopted(4)	$M_\star$ (5)	eM_{star} (6)	$\dot{M}$ (7)
219	8416834-6225	3785	0.5	0.5	0.08	< 1.77E-10
220	8416914-6175	3850	2.1	0.53	0.07	1.07E-08 ± 1.05E-08
221	8416978-6185	3955	1.12	0.62	0.08	···
222	8421949-6718	3785	1.66	0.49	0.07	···
223	8424570-6484	3470	0.34	0.34	0.06	5.33E-10 ± 1.41E-10
224	8424689-6154	8970	48.87	2.5	0.08	···
225	8425038-6557	4350	6.13	1.16	0.17	2.43E-08 ± 1.16E-08
226	8430527-6583	8590	35.03	2.3	0.12	6.59E-08 ± 2.81E-08
227	8440418-7404	3850	0.29	0.57	0.09	2.46E-10 ± 1.36E-10
228	8443530-6843	3785	0.51	0.5	0.08	···
229	8444779-6608	3850	0.61	0.55	0.08	1.76E-09 ± 1.40E-09
230	8445558-6860	3850	0.46	0.56	0.08	2.72E-10 ± 1.24E-10
231	8447398-6788	3470	4.67	0.35	0.05	···
232	8448350-6815	3850	1.06	0.54	0.07	···
233	8450343-7265	3650	0.8	0.42	0.06	6.88E-09 ± 1.23E-09
234	8452061-7269	3785	0.57	0.5	0.08	2.42E-09 ± 1.49E-09
235	8453876-6821	8590	35.79	2.3	0.12	1.16E-08 ± 4.88E-09
236	8455602-7112	3720	1.44	0.45	0.06	···
237	8457266-7161	3650	1.26	0.41	0.06	< 2.58E-09
238	8461533-6914	4205	1.25	0.85	0.11	···
239	8464666-7838	3720	1.81	0.45	0.06	1.01E-08 ± 4.83E-09
240	8465247-7776	3650	0.86	0.42	0.06	···
241	8466711-6987	4205	1.41	0.87	0.1	···
242	8468002-6969	3955	16.33	0.82	0.16	···
243	8468729-6970	3720	1.99	0.45	0.06	···
244	8469891-7104	3650	1.51	0.41	0.06	···
245	8472719-7464	3580	2.26	0.37	0.05	4.25E-07 ± 5.58E-08
246	8476732-7058	3955	2.11	0.61	0.08	1.21E-07 ± 8.58E-08
247	8477229-7184	3470	1.31	0.33	0.04	1.86E-07 ± 1.53E-08
248	8486920-7342	3850	0.67	0.55	0.08	···
249	8488472-7373	3525	0.14	0.35	0.08	1.14E-10 ± 6.42E-11
250	8492690-7387	3850	1.84	0.53	0.07	···
251	8494096-7377	3850	4.24	0.55	0.08	···
252	8495155-7404	3850	2.03	0.53	0.07	···
253	8497290-7502	3850	1.78	0.54	0.07	···
254	8497797-7462	3850	54.54	1.1	0.16	···
255	8499151-7482	3850	22.23	0.78	0.13	···
256	8499541-7426	3850	2.03	0.53	0.07	···
257	8502614-7795	3470	0.23	0.33	0.07	1.70E-09 ± 1.08E-09
258	8504327-7460	4060	5.41	0.75	0.12	···

Table A.2 (cont'd)

Num. (1)	IRS name (2)	T_{eff} (3)	$L_\star$ adopted(4)	$M_\star$ (5)	eM_{star} (6)	$\dot{M}$ (7)
259	8508083-8237	4060	1.54	0.7	0.09	···
260	8508501-7431	3580	0.36	0.38	0.08	2.53E-09 ± 1.40E-09
261	8508648-7916	3850	1.74	0.55	0.09	···
262	8510403-8125	5250	4.8	1.96	0.04	6.51E-08 ± 8.24E-09
263	8511308-8126	3470	0.47	0.34	0.06	···
264	8511602-7926	3850	1.07	0.54	0.07	···
265	8514861-7663	3850	1.13	0.54	0.07	···
266	8515568-8067	6590	66.74	3.33	0.05	···
267	8516031-7796	3850	4.2	0.55	0.07	···
268	8518798-7373	3850	1.28	0.54	0.07	···
269	8519260-8090	4590	8.84	1.65	0.3	1.31E-08 ± 1.39E-08
270	8519428-8120	4060	9.78	0.84	0.14	ndt
271	8520557-7775	3580	0.47	0.38	0.07	< 3.37E-10
272	8520580-7960	3850	0.13	0.57	0.08	···
273	8530851-8132	3580	1.18	0.38	0.05	< 3.41E-09
274	8534457-7821	3850	1.24	0.54	0.07	···
275	8535781-7830	3240	0.85	0.25	0.04	< 3.62E-09
276	8536129-8706	3850	3.43	0.54	0.08	···
277	8537742-8080	4060	3.02	0.71	0.09	···
278	8538844-7917	3580	0.51	0.38	0.07	···
279	8538911-7999	3650	1.06	0.41	0.06	< 7.82E-10
280	8542681-8618	4060	6.91	0.78	0.12	1.90E-08 ± 1.06E-08
281	8543224-7972	3145	0.69	0.23	0.04	3.44E-09 ± 4.02E-09
282	8545724-8008	4350	7.33	1.2	0.18	···
283	8547523-7831	3580	0.58	0.38	0.07	8.71E-10 ± 7.56E-10
284	8547770-7986	4660	2.19	1.53	0.12	···
285	8552157-8190	3850	3.66	0.54	0.08	···
286	8552280-8641	3470	0.8	0.33	0.05	< 7.73E-10
287	8556074-7982	3420	0.33	0.31	0.06	1.31E-09 ± 1.13E-09
288	8560743-8147	3525	0.6	0.36	0.06	1.27E-08 ± 1.55E-09
289	8561044-7980	4205	1.86	0.86	0.11	···
290	8562845-8151	3525	0.4	0.36	0.06	3.93E-09 ± 1.90E-09
291	8564835-8250	3525	0.43	0.36	0.06	1.13E-09 ± 7.15E-10
292	8567003-8669	3720	0.31	0.47	0.08	···
293	8567545-8254	3470	0.32	0.33	0.07	···
294	8567670-8803	3525	2	0.35	0.05	< 4.62E-09
295	8569204-8666	3850	3.59	0.54	0.08	···
296	8570200-8276	3850	1.68	0.54	0.07	···
297	8570949-8577	3850	1.75	0.53	0.07	···
298	8571439-8650	3850	3.61	0.54	0.08	···

Table A.2 (cont'd)

Num. (1)	IRS name (2)	T_{eff} (3)	$L_\star$ adopted(4)	$M_\star$ (5)	eM_{star} (6)	$\dot{M}$ (7)
299	8574645-8156	3720	0.38	0.47	0.08	···
300	8576640-8652	3850	2	0.53	0.07	···
301	8576836-8303	3420	0.38	0.31	0.06	7.32E-10 ± 2.38E-10
302	8579480-8565	3850	0.07	0.58	0.09	6.13E-10 ± 3.46E-10
303	8580634-8516	3470	0.43	0.33	0.06	6.85E-09 ± 2.49E-09
companions observed by SpeX						
4	8343917-6073					7.60E-08 ± 1.77E-08
26	8359203-5026					5.33E-10 ± 3.30E-10
38	8367284-5798					< 4.72E-10
47	8371984-5465					1.07E-08 ± 4.69E-09
98	8378345-5545					< 4.00E-10
173	8390003-5207					···
208	8410334-6291					···
280	8542681-8618					···
290	8562845-8151					1.85E-09 ± 4.10E-10

Table A.3. Basic Stellar Properties

Num.	2XMM ID	L_X (10^{28} erg/s)					
		0.2-12 keV	0.2-0.5 keV	0.5-1.0 keV	1.0-2.0 keV	2.0-4.5 keV	4.5-12 keV
11	2XMMi J053354.4-053158	34.32 ± 19.99	0.00 ± 0.21	1.78 ± 0.86	9.90 ± 1.52	15.36 ± 3.53	6.88 ± 19.60
13	2XMM J053400.2-053542	130.00 ± 84.97	5.16 ± 3.30	18.34 ± 5.38	3.24 ± 3.38	2.06 ± 4.90	92.46 ± 84.13
14	2XMMi J053402.2-053618	96.06 ± 11.78	1.07 ± 0.56	3.71 ± 0.77	24.35 ± 1.57	47.48 ± 3.65	18.37 ± 10.70
17	2XMMi J053407.9-053612	18.15 ± 12.00	0.08 ± 0.31	1.64 ± 0.57	0.94 ± 0.58	1.67 ± 1.19	11.33 ± 11.85
19	2XMM J053412.7-052849	212.22 ± 95.77	3.88 ± 3.03	35.22 ± 7.71	24.91 ± 6.44	4.57 ± 5.48	127.08 ± 94.47
21	2XMM J053414.1-053654	85.24 ± 31.65	7.71 ± 3.71	48.80 ± 7.20	16.38 ± 4.34	5.35 ± 5.90	1.55 ± 29.18
24	2XMM J053419.6-053020	208.00 ± 51.39	1.06 ± 1.67	14.55 ± 3.95	47.40 ± 6.80	72.02 ± 14.13	76.38 ± 47.11
28	2XMMi J053426.1-052629	62.70 ± 11.74	0.05 ± 0.26	2.04 ± 0.61	12.66 ± 1.06	21.38 ± 2.53	27.31 ± 11.37
29	2XMM J053427.1-052831	117.62 ± 44.16	12.90 ± 5.33	33.50 ± 5.29	27.02 ± 3.29	30.30 ± 9.87	7.14 ± 41.81
33	2XMMi J053437.4-053453	14.68 ± 4.53	0.04 ± 0.13	0.07 ± 0.20	0.84 ± 0.32	7.55 ± 1.31	5.51 ± 4.30
34	2XMM J053437.8-044859	19.72 ± 25.12	0.00 ± 0.68	6.42 ± 3.49	13.30 ± 4.68	0.00 ± 4.54	0.00 ± 24.00
36	2XMM J053440.0-054009	672.75 ± 78.47	31.53 ± 6.20	159.53 ± 12.53	195.96 ± 15.53	162.15 ± 26.11	122.11 ± 70.49
37	2XMM J053440.9-052243	174.59 ± 70.89	0.21 ± 1.80	20.19 ± 5.58	49.26 ± 8.56	49.09 ± 14.71	48.74 ± 67.29
38	2XMM J053441.4-054756	396.72 ± 73.29	14.80 ± 6.64	94.91 ± 12.68	140.94 ± 14.76	85.59 ± 20.31	46.14 ± 64.30
40	2XMM J053444.8-045601	167.02 ± 65.91	0.42 ± 0.75	2.41 ± 1.61	9.03 ± 3.16	28.09 ± 10.29	127.07 ± 65.00
42	2XMM J053445.9-054109	46.82 ± 29.92	0.50 ± 1.34	5.40 ± 2.33	15.93 ± 4.46	16.29 ± 9.92	6.37 ± 27.49
43	2XMM J053446.1-053909	127.73 ± 34.49	0.11 ± 1.06	13.54 ± 3.36	41.02 ± 5.65	42.97 ± 9.77	26.81 ± 32.29
44	2XMM J053448.3-050458	148.27 ± 24.64	11.02 ± 2.07	51.08 ± 3.94	42.70 ± 3.80	31.83 ± 6.45	10.23 ± 22.37
46	2XMMi J053450.5-052701	4.88 ± 5.24	0.02 ± 0.18	2.89 ± 0.64	1.67 ± 0.62	0.00 ± 0.84	0.00 ± 5.05
47	2XMM J053452.8-052752	254.70 ± 41.47	2.38 ± 2.14	48.45 ± 6.95	83.14 ± 8.18	67.29 ± 13.41	37.66 ± 35.82
48	2XMM J053453.0-050327	257.25 ± 19.00	49.97 ± 3.64	136.43 ± 5.85	42.67 ± 3.47	17.71 ± 4.56	8.76 ± 16.20
49	2XMM J053454.1-052135	69.12 ± 55.81	6.44 ± 2.43	15.49 ± 3.52	23.39 ± 5.39	15.17 ± 10.28	8.04 ± 54.33
50	2XMM J053455.0-051702	81.60 ± 44.41	0.17 ± 1.10	0.34 ± 1.47	10.82 ± 3.47	37.49 ± 11.07	26.35 ± 42.43
52	2XMM J053456.8-051133	328.60 ± 46.00	50.36 ± 6.42	148.66 ± 9.62	86.39 ± 7.51	36.30 ± 9.46	12.65 ± 41.69
54	2XMM J053457.4-045646	95.68 ± 19.50	0.21 ± 0.41	0.06 ± 0.30	10.28 ± 1.24	24.82 ± 3.43	58.71 ± 19.09
55	2XMM J053457.7-052351	390.92 ± 97.15	10.19 ± 4.91	90.03 ± 13.07	113.81 ± 14.55	84.32 ± 22.90	84.24 ± 89.94

Table A.3 (cont'd)

Num.	2XMM ID	L_X (10^{28} erg/s)					
		0.2-12 keV	0.2-0.5 keV	0.5-1.0 keV	1.0-2.0 keV	2.0-4.5 keV	4.5-12 keV
56	2XMMi J053457.7-052250	41.33 ± 11.10	0.24 ± 0.47	13.72 ± 1.50	13.70 ± 1.74	14.07 ± 3.51	0.00 ± 10.13
57	2XMMi J053458.3-054149	25.96 ± 8.88	0.00 ± 0.22	0.18 ± 0.40	4.15 ± 0.97	13.40 ± 2.65	8.65 ± 8.29
59	2XMM J053458.5-060000	176.91 ± 24.47	28.15 ± 3.53	77.30 ± 4.95	27.58 ± 3.13	2.49 ± 2.56	31.12 ± 22.80
60	2XMM J053458.9-054431	75.78 ± 39.80	4.41 ± 3.39	15.85 ± 4.61	20.48 ± 5.03	19.28 ± 10.01	1.80 ± 36.20
61	2XMM J053459.2-054455	81.97 ± 41.70	0.27 ± 1.34	0.64 ± 1.27	10.46 ± 3.39	25.17 ± 8.27	43.87 ± 40.62
62	2XMM J053459.1-054558	73.70 ± 43.17	0.04 ± 0.85	1.93 ± 1.29	9.91 ± 2.55	11.82 ± 4.34	47.00 ± 42.78
63	2XMM J053459.7-052540	83.87 ± 24.30	3.86 ± 1.49	17.93 ± 2.64	23.82 ± 3.58	29.65 ± 8.96	7.77 ± 22.03
64	2XMM J053500.0-052301	258.90 ± 61.76	5.53 ± 2.84	61.18 ± 9.44	89.75 ± 12.26	60.35 ± 20.03	36.56 ± 55.39
67	2XMM J053500.3-052515	187.94 ± 76.98	4.44 ± 2.98	43.25 ± 7.50	58.23 ± 8.50	33.79 ± 13.56	37.22 ± 74.27
68	2XMM J053501.0-052408	252.60 ± 80.68	8.06 ± 3.10	60.23 ± 8.08	67.74 ± 8.69	46.58 ± 14.12	57.49 ± 77.51
69	2XMMi J053501.3-052022	110.95 ± 39.78	2.24 ± 1.00	12.37 ± 2.03	23.74 ± 3.23	34.34 ± 8.14	38.26 ± 38.74
74	2XMMi J053502.8-052208	5980.08 ± 115.28	3.39 ± 0.98	36.85 ± 2.48	526.22 ± 8.87	1707.58 ± 27.67	3733.07 ± 111.33
80	2XMM J053504.3-052637	288.10 ± 72.60	6.52 ± 2.81	54.25 ± 7.19	70.17 ± 9.71	58.74 ± 17.58	98.41 ± 69.34
82	2XMM J053504.4-052312	160.40 ± 117.96	1.68 ± 3.11	15.24 ± 6.58	21.94 ± 7.75	48.68 ± 20.97	39.29 ± 113.86
83	2XMMi J053504.6-052357	71.10 ± 9.62	1.74 ± 0.74	8.34 ± 1.40	24.04 ± 2.17	30.16 ± 4.49	0.00 ± 7.66
84	2XMM J053504.5-045828	14.60 ± 8.20	0.11 ± 0.21	1.32 ± 0.46	3.57 ± 0.75	3.02 ± 1.68	4.84 ± 7.76
85	2XMM J053504.3-052637	542.17 ± 76.75	4.89 ± 3.80	100.76 ± 11.00	175.11 ± 14.14	138.51 ± 22.30	111.27 ± 68.46
86	2XMM J053505.1-053643	118.70 ± 65.75	4.32 ± 2.82	17.21 ± 4.98	19.21 ± 4.52	21.23 ± 10.62	54.56 ± 64.08
88	2XMM J053505.2-051449	1002.73 ± 64.60	6.32 ± 2.01	132.39 ± 7.49	322.43 ± 11.48	281.31 ± 18.56	253.98 ± 59.97
91	2XMM J053505.6-052517	437.25 ± 107.29	8.11 ± 3.03	82.98 ± 9.92	102.94 ± 11.87	95.31 ± 22.34	145.67 ± 103.57
94	2XMM J053505.8-051135	284.49 ± 62.45	0.00 ± 0.67	3.55 ± 1.94	37.24 ± 5.27	82.15 ± 13.61	161.22 ± 60.68
95	2XMMi J053506.6-053253	70.46 ± 13.07	0.00 ± 0.10	0.00 ± 0.27	1.95 ± 0.69	21.46 ± 3.06	46.01 ± 12.66
100	2XMM J053508.2-052755	236.53 ± 73.86	2.40 ± 2.10	5.54 ± 3.12	44.47 ± 7.05	87.34 ± 17.65	96.74 ± 70.17
105	2XMM J053509.7-051930	57.53 ± 66.25	0.46 ± 1.75	5.83 ± 4.09	21.73 ± 6.73	9.48 ± 9.95	4.87 ± 64.42
108	2XMM J053510.3-054634	382.56 ± 81.23	4.00 ± 4.30	38.62 ± 9.30	83.92 ± 10.98	132.74 ± 26.86	118.49 ± 73.93
109	2XMMi J053511.9-052103	540.10 ± 61.87	0.00 ± 0.26	0.00 ± 1.54	41.99 ± 4.88	176.48 ± 15.43	321.63 ± 59.69

Table A.3 (cont'd)

Num.	2XMM ID	L_X (10^{28} erg/s)					
		0.2-12 keV	0.2-0.5 keV	0.5-1.0 keV	1.0-2.0 keV	2.0-4.5 keV	4.5-12 keV
110	2XMM J053512.0-051926	1141.37 ± 155.76	10.66 ± 4.32	74.92 ± 8.31	240.49 ± 14.30	334.17 ± 31.64	457.47 ± 151.06
111	2XMM J053512.1-052035	797.25 ± 136.24	3.07 ± 3.41	19.98 ± 4.14	154.44 ± 15.52	315.72 ± 39.75	304.04 ± 129.27
112	2XMM J053512.9-053934	308.18 ± 77.54	16.39 ± 5.58	76.04 ± 10.22	85.93 ± 10.99	62.93 ± 17.72	74.41 ± 73.55
114	2XMMi J053513.1-052753	20.09 ± 9.83	0.00 ± 0.30	1.94 ± 0.65	1.49 ± 0.80	9.26 ± 2.55	5.76 ± 9.33
117	2XMM J053513.6-053056	327.08 ± 55.21	18.47 ± 4.71	89.57 ± 9.31	102.91 ± 10.03	73.45 ± 14.66	33.55 ± 47.64
118	2XMM J053513.7-051954	1401.52 ± 184.54	19.18 ± 6.03	99.36 ± 11.30	269.18 ± 17.60	442.70 ± 41.02	562.56 ± 177.55
119	2XMM J053513.7-052846	253.10 ± 89.36	0.15 ± 1.52	18.69 ± 6.56	71.71 ± 11.50	66.31 ± 18.87	102.46 ± 85.77
121	2XMM J053513.9-054317	291.39 ± 68.54	12.84 ± 4.43	73.85 ± 7.64	81.60 ± 9.30	45.44 ± 11.78	79.94 ± 65.79
123	2XMMi J053514.4-053245	47.18 ± 7.54	0.00 ± 0.08	4.32 ± 0.68	16.91 ± 1.26	18.08 ± 2.50	5.78 ± 6.77
125	2XMMi J053514.7-053909	94.43 ± 16.74	0.00 ± 0.19	0.00 ± 0.40	22.92 ± 2.46	36.47 ± 4.72	39.23 ± 15.81
128	2XMM J053515.5-045928	70.00 ± 22.75	0.02 ± 0.35	1.00 ± 0.77	10.08 ± 1.82	19.25 ± 3.71	34.45 ± 21.58
129	2XMM J053515.9-052852	105.90 ± 53.95	0.94 ± 1.79	15.35 ± 5.35	43.08 ± 8.49	20.94 ± 10.20	13.17 ± 50.39
131	2XMM J053516.7-044543	170.35 ± 38.24	0.52 ± 1.11	11.86 ± 2.62	55.09 ± 4.93	50.92 ± 8.40	49.44 ± 36.83
133	2XMM J053517.7-055826	284.92 ± 18.62	25.59 ± 4.38	138.92 ± 8.49	80.60 ± 6.47	31.17 ± 7.53	0.79 ± 11.16
134	2XMMi J053517.7-062437	120.44 ± 10.02	17.51 ± 1.15	43.99 ± 1.71	32.56 ± 1.67	14.10 ± 2.32	11.22 ± 9.35
135	2XMM J053517.7-054234	844.14 ± 99.11	36.25 ± 7.10	214.78 ± 15.38	232.08 ± 16.65	210.09 ± 29.49	121.23 ± 89.30
136	2XMM J053517.8-051612	139.85 ± 36.25	0.04 ± 0.66	0.00 ± 0.82	28.22 ± 6.36	72.69 ± 14.68	33.49 ± 30.16
137	2XMM J053518.3-052846	75.82 ± 36.66	2.07 ± 1.46	18.79 ± 3.59	19.90 ± 4.84	34.07 ± 10.94	1.31 ± 34.28
138	2XMM J053518.2-045323	249.13 ± 77.14	0.89 ± 1.49	9.21 ± 2.56	32.71 ± 5.27	82.15 ± 13.94	114.16 ± 75.43
140	2XMM J053520.6-050301	8.65 ± 3.39	0.00 ± 0.14	0.00 ± 0.08	0.64 ± 0.33	5.19 ± 1.28	1.03 ± 2.85
141	2XMM J053521.3-050915	555.43 ± 34.52	33.12 ± 4.16	207.84 ± 9.11	172.94 ± 8.43	96.21 ± 11.17	38.52 ± 28.49
142	2XMM J053521.8-050702	90.64 ± 13.27	0.30 ± 0.37	12.52 ± 1.59	25.13 ± 2.24	29.71 ± 4.68	19.73 ± 11.79
145	2XMMi J053523.2-052811	51.36 ± 8.66	1.59 ± 0.64	11.76 ± 1.46	28.46 ± 2.40	13.66 ± 4.81	0.00 ± 5.90
146	2XMMi J053523.7-052626	60.12 ± 15.64	0.41 ± 0.51	6.11 ± 1.46	18.98 ± 2.20	32.60 ± 4.95	3.13 ± 14.22
150	2XMM J053526.4-052542	1740.51 ± 314.44	14.81 ± 4.98	160.30 ± 11.40	388.01 ± 27.30	332.95 ± 28.63	807.53 ± 309.71
151	2XMM J053527.2-061939	77.20 ± 32.12	5.28 ± 1.46	12.27 ± 2.12	10.13 ± 2.06	13.73 ± 4.60	31.35 ± 31.57

Table A.3 (cont'd)

Num.	2XMM ID	L_X (10^{28} erg/s)					
		0.2-12 keV	0.2-0.5 keV	0.5-1.0 keV	1.0-2.0 keV	2.0-4.5 keV	4.5-12 keV
152	2XMMi J053527.2-052336	1104.29 ± 82.72	4.09 ± 1.59	38.48 ± 4.18	218.28 ± 10.40	380.65 ± 24.58	462.78 ± 78.16
154	2XMM J053527.6-054255	106.85 ± 26.24	1.07 ± 0.94	17.20 ± 2.04	25.13 ± 2.52	15.61 ± 3.98	46.62 ± 25.64
156	2XMM J053528.0-050135	154.48 ± 23.55	0.14 ± 0.36	0.09 ± 0.39	4.39 ± 1.17	42.04 ± 5.32	106.58 ± 22.84
157	2XMM J053528.1-051857	176.49 ± 55.76	0.55 ± 1.13	1.50 ± 1.58	16.24 ± 4.16	61.54 ± 11.77	90.83 ± 53.88
158	2XMMi J053528.3-052502	153.78 ± 32.52	4.26 ± 1.22	23.54 ± 2.72	39.80 ± 3.80	52.86 ± 7.75	28.49 ± 31.13
159	2XMM J053528.3-055913	234.06 ± 25.94	4.01 ± 1.44	21.61 ± 2.57	37.54 ± 3.38	62.11 ± 7.28	102.31 ± 24.24
160	2XMM J053528.4-050746	36.03 ± 9.79	0.01 ± 0.25	0.21 ± 0.59	4.50 ± 1.14	16.22 ± 3.58	10.81 ± 8.34
162	2XMM J053528.4-044817	53.75 ± 33.09	0.87 ± 2.19	1.19 ± 1.68	7.51 ± 2.76	29.06 ± 8.09	8.82 ± 31.46
164	2XMM J053530.6-045936	32.66 ± 14.38	0.14 ± 0.38	0.22 ± 0.39	8.41 ± 1.58	16.50 ± 4.12	5.04 ± 13.29
167	2XMM J053531.4-050501	71.77 ± 11.69	3.04 ± 0.90	13.64 ± 1.70	17.83 ± 1.99	19.64 ± 3.94	11.34 ± 10.21
168	2XMM J053531.9-050927	352.19 ± 42.57	5.47 ± 1.60	62.38 ± 5.11	107.62 ± 6.39	88.75 ± 9.18	81.34 ± 39.97
169	2XMM J053533.7-044623	32.63 ± 20.04	0.31 ± 0.92	10.71 ± 2.48	12.63 ± 2.75	0.61 ± 2.26	6.37 ± 18.89
172	2XMM J053535.2-044739	365.61 ± 30.16	6.19 ± 2.35	71.84 ± 5.78	144.19 ± 8.03	138.35 ± 13.54	10.60 ± 23.01
173	2XMM J053535.9-051225	55.72 ± 19.77	0.87 ± 0.75	10.01 ± 1.88	7.79 ± 1.48	11.72 ± 3.86	21.63 ± 18.96
176	2XMM J053536.6-050413	78.97 ± 12.19	6.77 ± 1.52	25.22 ± 2.70	20.82 ± 2.48	11.45 ± 3.50	10.31 ± 10.57
177	2XMM J053537.3-062326	131.72 ± 14.10	21.47 ± 1.90	50.61 ± 2.85	34.02 ± 2.50	21.18 ± 3.77	4.43 ± 12.46
179	2XMM J053538.5-045941	82.70 ± 19.76	0.34 ± 0.49	6.66 ± 1.53	23.50 ± 2.81	26.43 ± 5.50	23.73 ± 18.45
180	2XMM J053538.8-051242	422.52 ± 49.75	0.60 ± 1.02	16.83 ± 2.99	75.45 ± 5.73	139.84 ± 13.12	189.49 ± 47.38
181	2XMM J053539.9-050636	38.15 ± 10.19	0.18 ± 0.56	1.54 ± 1.04	14.88 ± 2.29	9.23 ± 3.31	3.59 ± 8.26
182	2XMM J053542.0-051011	153.94 ± 18.55	0.30 ± 0.50	7.25 ± 1.56	41.11 ± 3.11	61.12 ± 6.59	41.89 ± 16.69
183	2XMM J053543.5-050540	38.91 ± 12.59	1.15 ± 0.71	4.54 ± 1.17	11.06 ± 1.75	7.09 ± 2.79	12.47 ± 11.93
184	2XMM J053546.0-051052	67.55 ± 18.61	6.10 ± 1.73	28.02 ± 3.10	14.54 ± 2.32	10.97 ± 3.89	7.53 ± 17.42
185	2XMM J053546.6-054926	128.32 ± 15.78	10.42 ± 1.99	45.32 ± 3.45	35.12 ± 3.19	20.87 ± 4.68	14.01 ± 14.00
186	2XMMi J053548.5-050132	122.19 ± 12.16	9.07 ± 1.39	35.47 ± 2.45	39.26 ± 2.78	16.44 ± 3.43	17.35 ± 10.81
188	2XMM J053550.4-055142	233.06 ± 11.36	32.94 ± 3.00	91.81 ± 4.19	59.84 ± 3.50	39.06 ± 5.03	1.81 ± 5.40
189	2XMM J053551.0-050709	536.76 ± 24.23	60.39 ± 3.51	154.13 ± 5.41	138.62 ± 5.25	100.89 ± 7.69	78.25 ± 20.62

Table A.3 (cont'd)

Num.	2XMM ID	L_X (10^{28} erg/s)					
		0.2-12 keV	0.2-0.5 keV	0.5-1.0 keV	1.0-2.0 keV	2.0-4.5 keV	4.5-12 keV
193	2XMM J053554.2-052643	64.68 ± 46.50	3.55 ± 3.38	12.60 ± 5.02	14.27 ± 4.76	12.41 ± 8.37	11.98 ± 44.58
199	2XMM J053559.7-061605	460.05 ± 17.56	60.93 ± 2.48	157.71 ± 4.12	116.03 ± 3.80	69.27 ± 5.25	56.34 ± 15.53
201	2XMM J053606.6-063216	71.55 ± 16.74	0.44 ± 0.32	7.45 ± 0.95	16.34 ± 1.48	5.83 ± 1.98	37.01 ± 16.46
203	2XMM J053615.0-061737	327.49 ± 11.81	32.16 ± 1.40	111.59 ± 2.61	92.73 ± 2.60	52.98 ± 3.64	37.74 ± 10.47
204	2XMM J053615.7-061450	8.30 ± 4.18	0.01 ± 0.10	2.38 ± 0.60	3.06 ± 0.70	0.29 ± 0.59	0.00 ± 3.78
205	2XMM J053616.9-051142	1115.98 ± 110.82	46.81 ± 6.27	144.55 ± 10.41	270.07 ± 14.02	265.60 ± 24.29	387.20 ± 106.14
207	2XMM J053623.6-062313	21.37 ± 7.00	0.01 ± 0.07	0.07 ± 0.16	0.12 ± 0.22	2.58 ± 1.13	15.51 ± 6.81
208	2XMM J053624.9-061732	1574.33 ± 21.37	132.43 ± 2.74	481.28 ± 5.31	460.81 ± 5.64	298.47 ± 8.09	199.11 ± 17.77
211	2XMM J053627.8-062535	19.68 ± 5.15	4.11 ± 0.52	9.06 ± 0.79	2.50 ± 0.58	0.49 ± 0.67	1.40 ± 4.82
213	2XMM J053631.5-060831	157.01 ± 52.36	2.71 ± 1.99	23.99 ± 4.72	44.28 ± 6.22	64.48 ± 13.52	19.66 ± 49.90
219	2XMM J053640.3-061333	85.70 ± 6.64	12.15 ± 1.14	42.04 ± 2.09	18.35 ± 1.61	9.70 ± 2.65	0.00 ± 4.57
224	2XMM J053659.3-060916	243.64 ± 17.70	36.11 ± 3.21	109.28 ± 5.72	67.28 ± 5.49	30.98 ± 8.27	0.00 ± 13.11
225	2XMM J053700.1-063326	450.24 ± 43.52	1.77 ± 0.75	16.52 ± 1.84	90.75 ± 4.23	167.53 ± 10.67	173.76 ± 41.75
226	2XMMi J053713.4-063457	30.72 ± 10.59	3.36 ± 0.72	9.03 ± 1.12	5.89 ± 1.14	1.80 ± 1.76	10.21 ± 10.24
228	2XMMi J053744.5-065036	64.60 ± 17.07	0.15 ± 0.35	9.53 ± 1.36	16.49 ± 1.83	16.04 ± 3.45	17.22 ± 16.49
230	2XMMi J053749.3-065136	26.18 ± 8.82	0.08 ± 0.23	4.42 ± 0.78	5.36 ± 1.01	6.86 ± 2.08	4.22 ± 7.71
233	2XMM J053801.0-071553	161.22 ± 97.23	4.67 ± 4.81	48.01 ± 11.70	45.46 ± 11.99	33.96 ± 22.52	18.77 ± 92.32
234	2XMM J053804.9-071610	489.77 ± 213.14	1.24 ± 3.40	0.87 ± 3.10	2.01 ± 4.69	57.23 ± 28.41	395.76 ± 210.63
238	2XMM J053827.6-065453	487.55 ± 63.16	6.93 ± 2.41	59.73 ± 6.32	92.59 ± 7.07	124.97 ± 14.85	202.63 ± 59.78
242	2XMM J053843.2-065810	434.69 ± 81.32	0.63 ± 1.32	3.22 ± 2.40	60.03 ± 8.31	186.54 ± 24.54	174.90 ± 75.52
243	2XMM J053845.1-065812	35.20 ± 19.60	0.77 ± 1.18	0.23 ± 0.87	4.80 ± 2.24	19.65 ± 7.64	2.95 ± 17.04
244	2XMM J053847.6-070615	80.87 ± 32.38	0.03 ± 0.82	1.24 ± 1.52	28.12 ± 5.25	39.68 ± 9.18	4.52 ± 28.33
247	2XMMi J053905.2-071104	68.78 ± 28.59	0.03 ± 0.20	0.11 ± 0.45	4.90 ± 1.37	8.80 ± 3.84	47.24 ± 28.20
249	2XMMi J053932.2-072222	11.57 ± 4.84	1.19 ± 0.36	4.93 ± 0.63	1.60 ± 0.46	2.41 ± 1.27	0.99 ± 4.50
250	2XMMi J053942.3-072317	48.80 ± 9.88	0.09 ± 0.14	0.13 ± 0.19	1.68 ± 0.51	15.54 ± 2.24	31.08 ± 9.60
251	2XMMi J053945.9-072236	21.59 ± 6.77	0.00 ± 0.12	0.17 ± 0.28	3.21 ± 0.63	9.32 ± 1.81	8.22 ± 6.43

Table A.3 (cont'd)

Num.	2XMM ID	L_X (10^{28} erg/s)					
		0.2-12 keV	0.2-0.5 keV	0.5-1.0 keV	1.0-2.0 keV	2.0-4.5 keV	4.5-12 keV
254	2XMMi J053954.7-072746	29.55 ± 16.09	0.02 ± 0.12	0.36 ± 0.29	0.58 ± 0.48	14.28 ± 2.76	12.53 ± 15.83
257	2XMMi J054006.2-074743	20.16 ± 20.21	0.59 ± 0.56	2.29 ± 0.68	0.12 ± 0.45	4.18 ± 2.47	11.40 ± 20.01
260	2XMMi J054020.4-072552	15.11 ± 13.90	0.17 ± 0.64	7.25 ± 2.49	6.50 ± 2.66	1.19 ± 3.22	0.00 ± 13.00
265	2XMMi J054035.5-073947	30.91 ± 10.03	0.16 ± 0.27	0.05 ± 0.20	2.68 ± 0.70	12.48 ± 2.48	15.17 ± 9.68
267	2XMMi J054038.4-074745	32.04 ± 12.70	0.02 ± 0.18	0.74 ± 0.38	1.63 ± 0.64	16.20 ± 2.72	10.27 ± 12.28
270	2XMMi J054046.5-080711	395.77 ± 47.78	1.64 ± 0.88	29.34 ± 2.74	118.81 ± 6.18	152.33 ± 13.34	93.66 ± 45.37
271	2XMMi J054049.2-074633	15.48 ± 8.62	0.19 ± 0.35	0.12 ± 0.38	4.08 ± 1.09	9.72 ± 2.88	0.23 ± 7.90
273	2XMMi J054114.1-080757	52.71 ± 27.07	0.28 ± 0.35	2.11 ± 0.68	4.71 ± 1.16	0.78 ± 1.74	41.95 ± 26.94
275	2XMMi J054125.9-074951	247.36 ± 17.41	0.27 ± 0.26	10.44 ± 0.98	60.19 ± 2.45	105.15 ± 5.77	71.84 ± 16.19
277	2XMMi J054130.5-080446	227.50 ± 19.25	0.01 ± 0.11	1.30 ± 0.40	31.42 ± 1.69	84.92 ± 4.83	110.27 ± 18.52
278	2XMMi J054133.2-075503	19.48 ± 5.15	0.12 ± 0.26	3.74 ± 0.68	6.80 ± 0.99	2.04 ± 1.27	1.81 ± 4.39
281	2XMMi J054143.7-075821	44.51 ± 5.50	1.89 ± 0.38	10.54 ± 0.74	15.57 ± 1.00	10.45 ± 1.68	7.06 ± 5.04
282	2XMMi J054149.7-080032	233.96 ± 9.74	6.13 ± 0.58	47.26 ± 1.47	68.39 ± 1.93	66.31 ± 3.42	46.50 ± 8.71
283	2XMMi J054154.0-074954	651.31 ± 21.34	21.22 ± 1.27	103.17 ± 2.66	163.93 ± 3.72	186.42 ± 7.07	172.59 ± 19.39
284	2XMMi J054154.6-075912	440.85 ± 14.68	0.73 ± 0.28	8.66 ± 0.67	75.16 ± 1.97	173.84 ± 5.17	182.47 ± 13.52
286	2XMMi J054205.3-083827	23.27 ± 32.30	0.27 ± 0.71	3.08 ± 1.17	3.73 ± 1.57	4.52 ± 3.02	11.00 ± 32.09
288	2XMMi J054225.7-080849	34.22 ± 12.63	0.92 ± 0.56	5.09 ± 1.13	10.53 ± 1.66	9.42 ± 3.24	4.10 ± 11.90
289	2XMMi J054226.3-075854	89.04 ± 16.61	0.71 ± 0.41	6.48 ± 0.84	12.89 ± 1.26	24.89 ± 3.12	44.00 ± 16.22
291	2XMMi J054235.6-081501	17.53 ± 5.72	0.04 ± 0.15	2.30 ± 0.54	7.14 ± 0.99	3.38 ± 1.62	3.29 ± 5.06
292	2XMMi J054240.8-084008	50.90 ± 8.28	0.10 ± 0.17	3.97 ± 0.67	17.61 ± 1.39	22.19 ± 2.86	5.48 ± 7.45
294	2XMMi J054242.4-084813	45.17 ± 35.79	2.59 ± 1.66	0.70 ± 0.98	11.65 ± 3.11	26.77 ± 7.95	3.46 ± 34.70
295	2XMMi J054246.0-084000	295.00 ± 18.11	1.65 ± 0.47	16.59 ± 1.28	67.93 ± 2.68	100.37 ± 5.62	107.72 ± 16.84
298	2XMMi J054251.4-083901	946.26 ± 24.61	1.69 ± 0.41	16.34 ± 1.07	140.66 ± 3.23	339.42 ± 8.48	449.27 ± 22.77
299	2XMMi J054259.0-080923	11.38 ± 5.46	0.41 ± 0.32	5.41 ± 0.89	3.58 ± 0.93	1.98 ± 1.77	0.00 ± 4.88
300	2XMMi J054303.8-083909	264.44 ± 17.10	0.90 ± 0.37	7.50 ± 0.86	49.85 ± 2.21	99.01 ± 5.42	107.88 ± 16.00
301	2XMMi J054304.3-081810	34.57 ± 9.93	0.11 ± 0.26	4.13 ± 0.85	9.09 ± 1.27	10.81 ± 2.65	9.53 ± 9.24

Table A.3 (cont'd)

Num.	2XMM ID	L_X (10^{28} erg/s) 0.2-12 keV	0.2-0.5 keV	0.5-1.0 keV	1.0-2.0 keV	2.0-4.5 keV	4.5-12 keV
303	2XMMi J054313.6-083102	17.28 ± 8.14	0.11 ± 0.27	0.00 ± 0.22	3.39 ± 0.74	7.42 ± 2.01	3.75 ± 7.67

Note. — XMM-Newton X-ray data

Table A.4. Basic Stellar Properties

Num.	module	n_{K-6}	$\sigma_{n_{K-6}}$	n_{6-13}	$\sigma_{n_{6-13}}$	n_{13-31}	$\sigma_{n_{13-31}}$	n_{5-12}	$\sigma_{n_{5-12}}$	n_{12-20}	$\sigma_{n_{12-20}}$	n_{K-25}	$\sigma_{n_{K-25}}$
1	SLLL	-2.06	0.1	-0.89	0.13	0.29	0.23	-1.02	0.1	0.95	0.15	-1.01	0.04
2	SLLL	-1.67	0.08	-0.53	0.11	0.06	0.16	-0.65	0.13	-0.18	0.18	-0.88	0.03
3	SLLL	-1.54	0.03	-0.28	0.03	-1.12	0.06	-0.33	0.04	-0.76	0.04	-1.03	0.01
4	SLLL	-1.62	0.11	-0.13	0.13	-0.66	0.06	-0.49	0.07	-0.17	0.24	-0.87	0.02
5	SLLL	-1.81	0.16	0.71	0.2	-0.81	0.11	0.35	0.1	-0.23	0.09	-0.67	0.04
6	SLLL	-0.27	0.05	-0.74	0.07	-0.77	0.11	-0.88	0.06	-0.78	0.07	-0.61	0.02
7	SLLL	...	...	...	...	...	...	...	...	...	...	...	...
8	SLLL	-2.4	0.07	-1.15	0.11	0.3	0.16	-1.4	0.08	1.71	0.37	-1.25	0.04
9	SLLL	-1.1	0.03	-0.17	0.03	-0.36	0.06	-0.3	0.03	0.07	0.03	-0.61	0.01
10	SLLL	-0.65	0.15	-0.31	0.18	-0.09	0.09	-0.62	0.45	-0.02	0.36	-0.48	0.02
11	SLLL	-2.46	0.08	-0.62	0.11	1.47	0.09	-0.88	0.15	2.07	0.17	-0.78	0.02
12	SLLL	-0.67	0.1	-0.43	0.12	-0.62	0.11	-0.54	0.1	-0.6	0.16	-0.62	0.01
13	SLLL	-2.78	0.07	-1.96	0.41	2.58	0.43	-1.95	0.45	2.82	0.91	-1.01	0.03
14	SLLL	-1.37	0.04	-1.02	0.07	-0.88	0.11	-1.03	0.07	-1.56	0.17	-1.23	0.02
15	SLLL	-1.03	0.05	-0.43	0.06	-0.93	0.19	-0.53	0.05	-0.43	0.12	-0.75	0.02
16	SLLL	-2.65	0.09	-2.19	0.27	1.95	0.26	-2.19	0.23	1.12	0.47	-1.35	0.01
17	SLLL	-0.88	0.08	-0.18	0.11	-0.51	0.17	-0.27	0.09	-0.2	0.11	-0.55	0.02
18	SLLL	-2.39	0.18	0.45	0.22	-0.29	0.26	0.47	0.49	-0.07	0.19	-0.88	0.04
19	SLLL	-2.83	0.14	-0.52	0.19	1.19	0.37	-0.92	0.11	2.28	0.27	-0.88	0.04

Table A.4 (cont'd)

Num.	module	n_{K-6}	$\sigma_{n_{K-6}}$	n_{6-13}	$\sigma_{n_{6-13}}$	n_{13-31}	$\sigma_{n_{13-31}}$	n_{5-12}	$\sigma_{n_{5-12}}$	n_{12-20}	$\sigma_{n_{12-20}}$	n_{K-25}	$\sigma_{n_{K-25}}$
20	SLLL	-0.68	0.08	-0.8	0.11	-0.65	0.15	-0.95	0.15	-1.08	0.17	-0.85	0.04
21	SLLL	-1.41	0.05	0.6	0.05	-0.73	0.04	0.57	0.04	-0.39	0.08	-0.56	0.02
22	SLLL	-0.61	0.05	-0.33	0.05	-0.53	0.09	-0.41	0.07	-0.61	0.06	-0.56	0.02
23	SLLL	-1.74	0.15	-0.3	0.18	-0.53	0.11	-0.44	0.42	0.2	0.09	-0.93	0.02
24	SLLL	-1.62	0.07	-0.14	0.07	-0.45	0.1	-0.33	0.04	-0.05	0.07	-0.82	0.01
25	SLLL	-1.96	0.32	0.23	0.39	0.69	0.25	0.23	0.33	1.41	0.56	-0.47	0.06
26	SLLL	-2.22	0.17	0.21	0.19	0.44	0.13	-0.26	0.04	0.27	0.24	-0.7	0.05
27	SLLL	-1.78	0.15	0.03	0.18	-0.31	0.15	-0.2	0.19	-0.23	0.19	-0.75	0.02
28	SLLL	-0.98	0.05	-0.6	0.06	-0.33	0.06	-0.75	0.07	-0.37	0.09	-0.72	0.01
29	SLLL	-2.64	0.11	-0.27	0.18	2.03	0.18	-0.28	0.16	2.53	0.24	-0.63	0.02
30	SLLL	-1.29	0.06	-0.65	0.08	-0.59	0.1	-0.73	0.11	-0.54	0.11	-0.95	0.02
31	SLLL	-0.4	0.11	-0.44	0.12	0.87	0.05	-0.36	0.11	1.14	0.06	-0.11	0.01
32	SLLL	-1.13	0.09	-0.4	0.13	0.8	0.16	-0.5	0.11	0.17	0.32	-0.53	0.02
33	SLLL	-1.44	0.07	-0.64	0.09	0.17	0.07	-0.74	0.1	0.19	0.14	-0.76	0.02
34	SLLL	-2.6	0.16	-0.96	0.27	1.08	0.31	-1.22	0.24	1.94	1.27	-1.06	0.05
35	SLLL	-2.97	0.11	-2.54	0.38	0.83	0.38	-2.56	0.16	-0.2	0.91	-1.94	0.04
36	SLLL	-2.08	0.13	-1.62	0.18	-0.3	0.16	-1.77	0.08	0.03	0.13	-1.49	0.02
37	SLLL	-1.08	0.06	-0.97	0.09	-1.01	0.14	-0.98	0.09	-0.65	0.15	-1.04	0.02
38	SLLL	-2.48	0.07	-1.08	0.11	0.79	0.18	-1.23	0.13	1.22	0.15	-1.17	0.02

Table A.4 (cont'd)

Num.	module	n_{K-6}	$\sigma_{n_{K-6}}$	n_{6-13}	$\sigma_{n_{6-13}}$	n_{13-31}	$\sigma_{n_{13-31}}$	n_{5-12}	$\sigma_{n_{5-12}}$	n_{12-20}	$\sigma_{n_{12-20}}$	n_{K-25}	$\sigma_{n_{K-25}}$
39	SLLL	-2.49	0.26	-0.67	0.51	0.5	0.7	-0.67	0.47	1.41	1.24	-1.04	0.11
40	SLLL	-1.32	0.13	-0.74	0.16	-0.35	0.11	-0.91	0.09	-0.6	0.21	-0.95	0.02
41	SLLL	-0.32	0.08	-0.58	0.1	0.29	0.14	-0.81	0.14	0.68	0.17	-0.3	0.02
42	SLLL	-2.14	0.1	0.39	0.12	-0.63	0.2	0.27	0.14	0.01	0.31	-0.87	0.04
43	SLLL	-1.2	0.05	-0.49	0.06	-0.75	0.06	-0.64	0.06	-0.79	0.05	-0.89	0.01
44	SLLL	-1.87	0.1	-0.44	0.14	0.43	0.11	-0.75	0.06	0.98	0.21	-0.78	0.02
45	SLLL	-0.93	0.06	-1.35	0.09	-2.23	0.08	-1.41	0.04	-2.11	0.09	-1.42	0.01
46	SLLL	-1.94	0.08	-0.58	0.14	-0.71	0.68	-0.66	0.12	-0.48	0.19	-1	0.05
47	SLLL	-2.25	0.09	-1.48	0.25	1.69	0.24	-1.48	0.21	0.64	0.55	-1.15	0.07
48	SLLL	-1.49	0.08	-0.85	0.11	-0.95	0.35	-0.96	0.1	-1.27	0.13	-1.16	0.05
49	SL	-1.71	0.33	-999	3.55	...	...	-1.52	2.09	...	...	...	...
50	SLLL	-1.45	0.13	-0.82	0.25	-0.73	0.43	-1.02	0.28	-0.07	0.23	-0.98	0.03
51	SLLL	-1.81	0.11	-0.75	0.14	-0.76	0.12	-0.98	0.09	-0.79	0.19	-1.23	0.01
52	SLLL	-0.98	0.07	-0.52	0.09	-0.64	0.08	-0.57	0.1	-0.92	0.18	-0.84	0.03
53	SLLL	-2.58	0.11	0.07	0.14	0.04	0.13	-0.23	0.14	0.63	0.18	-1.01	0.01
54	SLLL	-1.31	0.09	-0.47	0.12	-1.43	0.35	-0.49	0.24	-0.87	0.26	-1.08	0.02
55	SL	-1.93	0.07	-0.95	0.29	...	...	-1.03	0.18	...	...	...	...
56	SL	-1.3	0.2	0.04	0.38	...	...	-0.1	0.87	...	...	...	...
57	SLLL	-1.84	0.07	-0.43	0.09	-0.2	0.12	-0.49	0.09	-0.15	0.11	-0.97	0.02

Table A.4 (cont'd)

Num.	module	n_{K-6}	$\sigma_{n_{K-6}}$	n_{6-13}	$\sigma_{n_{6-13}}$	n_{13-31}	$\sigma_{n_{13-31}}$	n_{5-12}	$\sigma_{n_{5-12}}$	n_{12-20}	$\sigma_{n_{12-20}}$	n_{K-25}	$\sigma_{n_{K-25}}$
58	SLLL	-1.6	0.1	-0.86	0.14	-0.83	0.2	-0.88	0.12	-0.8	0.32	-1.2	0.04
59	SLLL	-2.28	0.09	-0.18	0.13	0.54	0.1	-0.41	0.13	0.75	0.21	-0.82	0.02
60	SLLL	-1.1	0.07	-1.36	0.12	-0.35	0.21	-1.36	0.16	-0.89	0.2	-1.09	0.03
61	SLLL	-1.35	0.07	-0.73	0.09	-0.77	0.12	-0.89	0.05	-1	0.04	-1.06	0.03
62	SLLL	-1.41	0.05	-0.97	0.07	-1.2	0.14	-1.04	0.06	-1.05	0.1	-1.23	0.02
63	SL	-1.36	0.07	-1.21	0.33	···	···	-0.85	0.33	···	···	···	···
64	SL	-1.51	0.06	-0.45	0.1	···	···	-0.57	0.08	···	···	···	···
65	SLLL	-1.97	0.08	-0.52	0.1	-0.36	0.23	-0.6	0.11	-0.52	0.31	-1.11	0.06
66	SLLL	-1.97	0.18	0.61	0.25	0.71	0.2	0.63	0.37	1	0.4	-0.41	0.03
67	SL	-1.31	0.1	-1.16	0.34	···	···	-0.89	0.41	···	···	···	···
68	SL	-1.4	0.09	-0.38	0.23	···	···	-0.3	0.18	···	···	···	···
70	SL	-0.56	0.09	-0.71	0.15	···	···	-1.34	0.2	···	···	···	···
71	SL	-1.05	0.1	-0.25	0.21	···	···	-0.13	0.2	···	···	···	···
73	SLLL	-1.76	0.09	-1.11	0.15	-0.78	0.36	-1.18	0.1	-1.32	0.47	-1.38	0.02
74	SL	-1.59	0.13	-0.37	0.26	···	···	-0.58	0.21	···	···	···	···
75	SL	-1.78	0.21	-1.07	0.9	···	···	-1.26	0.44	···	···	···	···
76	SLLL	-1.67	0.06	-1.29	0.09	-0.66	0.11	-1.34	0.08	-0.16	0.14	-1.28	0.02
77	SL	-1.35	0.26	-2.24	3.9	···	···	-0.53	0.89	···	···	···	···
78	SL	-1.01	0.18	-3.86	5	···	···	-5.1	1.46	···	···	···	···

Table A.4 (cont'd)

Num.	module	n_{K-6}	$\sigma_{n_{K-6}}$	n_{6-13}	$\sigma_{n_{6-13}}$	n_{13-31}	$\sigma_{n_{13-31}}$	n_{5-12}	$\sigma_{n_{5-12}}$	n_{12-20}	$\sigma_{n_{12-20}}$	n_{K-25}	$\sigma_{n_{K-25}}$
79	SLLL	-0.8	0.06	-0.74	0.08	-0.59	0.1	-0.77	0.07	-0.72	0.08	-0.8	0.01
80	SL	-1.92	0.14	-0.24	0.42	···	···	0.19	0.39	···	···	···	···
81	SL	-1.85	0.15	-0.15	0.33	···	···	0.28	0.4	···	···	···	···
82	SL	-1.18	0.08	-0.61	0.23	···	···	-0.73	0.21	···	···	···	···
83	SL	-2.02	0.06	-1.12	0.29	···	···	-1.53	0.29	···	···	···	···
84	SLLL	-1.52	0.07	-0.98	0.11	-0.32	0.22	-1.14	0.09	-0.3	0.08	-1.07	0.04
85	SL	-1.5	0.08	-1.32	0.21	···	···	-2.31	0.28	···	···	···	···
86	SLLL	-1.4	0.06	-0.26	0.09	-0.27	0.18	-0.16	0.13	-0.5	0.13	-0.74	0.03
88	SLLL	···	···	···	···	0.71	0.49	-999	-999	-1.94	0.75	-0.38	0.02
89	SL	-1.83	0.08	-0.73	0.28	···	···	-0.37	0.28	···	···	···	···
90	SLLL	-0.67	0.05	-0.22	0.06	-0.68	0.14	-0.28	0.06	-0.66	0.09	-0.59	0.01
91	SL	-1.35	0.03	-0.28	0.08	···	···	-0.3	0.11	···	···	···	···
92	SL	-0.69	0.12	0.1	0.45	···	···	0.22	0.38	···	···	···	···
93	SL	-0.98	0.03	-1.02	0.08	···	···	-1.38	0.13	···	···	···	···
94	SLLL	-1.71	0.2	-1	0.29	0.03	0.26	-1.3	0.29	-0.39	0.36	-1.04	0.03
95	SLLL	-0.14	0.04	0.01	0.05	0.11	0.07	0.09	0.07	0.11	0.11	-0.09	0.01
96	SL	-1.23	0.1	0.05	0.24	···	···	0.17	0.27	···	···	···	···
97	SLLL	-1.97	0.1	-0.4	0.14	0.27	0.13	-0.45	0.23	-0.39	0.2	-0.94	0.02
98	SLLL	-1.78	0.07	-0.36	0.09	-1.24	0.38	-0.37	0.1	-0.9	0.19	-1.23	0.06

Table A.4 (cont'd)

Num.	module	n_{K-6}	$\sigma_{n_{K-6}}$	n_{6-13}	$\sigma_{n_{6-13}}$	n_{13-31}	$\sigma_{n_{13-31}}$	n_{5-12}	$\sigma_{n_{5-12}}$	n_{12-20}	$\sigma_{n_{12-20}}$	n_{K-25}	$\sigma_{n_{K-25}}$
99	SLLL	-1.38	0.05	-1.05	0.09	-0.82	0.26	-1.08	0.11	-1.16	0.19	-1.2	0.03
100	SL	-1.56	0.05	-0.86	0.08	···	···	-0.95	0.07	···	···	···	···
101	SL	-1.63	0.1	-1.05	0.32	···	···	-0.65	0.33	···	···	···	···
102	SL	-1.96	0.19	0.36	0.35	···	···	-0.21	0.59	···	···	···	···
103	SLLL	-1.17	0.08	-0.89	0.1	-1.24	0.11	-1.02	0.07	-0.99	0.05	-1.1	0.01
106	SLLL	-1.8	0.1	-0.97	0.16	-1.12	0.16	-1.18	0.12	-1.28	0.15	-1.36	0.02
108	SLLL	-1.71	0.06	-0.32	0.06	0.17	0.02	-0.51	0.04	0.64	0.06	-0.77	0.01
112	SLLL	-1.08	0.08	-1.42	0.08	-1.36	0.08	-1.5	0.06	-1.43	0.08	-1.33	0.02
114	SL	-1.47	0.05	-0.64	0.09	···	···	-0.63	0.09	···	···	···	···
117	SLLL	-1.16	0.04	-0.35	0.05	-1.12	0.13	-0.45	0.06	-1.08	0.07	-0.92	0.02
119	SL	-1.69	0.1	-1.29	0.18	···	···	-1.31	0.24	···	···	···	···
120	SL	-1.99	0.09	-0.76	0.16	···	···	-0.77	0.15	···	···	···	···
121	SLLL	-1.61	0.06	-1.2	0.08	-1.06	0.12	-1.26	0.05	-1.24	0.13	-1.39	0.01
122	SLLL	-1.05	0.04	-0.9	0.05	-0.73	0.07	-1.02	0.06	-0.8	0.06	-1	0.01
123	SLLL	-0.94	0.05	-0.08	0.08	0.43	0.13	-0.15	0.11	0.79	0.31	-0.3	0.01
125	SLLL	-1.54	0.06	-0.71	0.07	-0.89	0.07	-0.85	0.03	-0.18	0.07	-1.06	0.02
127	SLLL	-1.22	0.35	-1.21	0.52	0.46	0.35	-1.36	0.42	-1.37	0.54	-0.93	0.03
128	SLLL	-1.34	0.11	-0.71	0.21	-0.17	0.2	-0.5	0.18	-1.69	0.32	-1	0.02
129	SL	-999	-999	-1.18	0.15	···	···	-1.2	0.17	···	···	···	···

Table A.4 (cont'd)

Num.	module	n_{K-6}	$\sigma_{n_{K-6}}$	n_{6-13}	$\sigma_{n_{6-13}}$	n_{13-31}	$\sigma_{n_{13-31}}$	n_{5-12}	$\sigma_{n_{5-12}}$	n_{12-20}	$\sigma_{n_{12-20}}$	n_{K-25}	$\sigma_{n_{K-25}}$
131	SLLL	-1.04	0.07	-1.07	0.09	-0.96	0.07	-1.21	0.06	-1.05	0.1	-1.1	0.01
132	SL	-1.57	0.04	-0.98	0.1	···	···	-0.95	0.11	···	···	···	···
133	SLLL	-1.66	0.08	-0.61	0.09	-0.58	0.08	-0.75	0.05	-0.45	0.09	-1.07	0.01
134	SLLL	-1.11	0.07	-0.59	0.1	-1.42	0.1	-0.55	0.1	-1.12	0.28	-1.08	0.02
135	SLLL	-1.51	0.05	-1.18	0.06	-1.06	0.1	-1.26	0.08	-0.26	0.12	-1.25	0.02
136	SLLL	···	···	···	···	···	···	···	···	···	···	···	···
137	SL	-2.09	0.16	-1.11	0.49	···	···	-1	0.35	···	···	···	···
138	SLLL	-1.35	0.06	-0.61	0.07	-0.62	0.1	-0.77	0.08	-0.55	0.08	-0.99	0.02
139	SL	-1.11	0.03	-1.99	0.21	···	···	-1.79	0.16	···	···	···	···
140	SLLL	-1.25	0.07	-0.07	0.07	-1.17	0.11	-0.25	0.11	-0.11	0.06	-0.77	0.02
141	SLLL	-1.75	0.09	-1.97	0.13	-1.4	0.12	-2.01	0.08	-1.22	0.14	-1.77	0.01
142	SLLL	-1.46	0.12	-0.58	0.14	-0.84	0.23	-0.7	0.08	-0.1	0.05	-0.92	0.02
143	SL	-1.43	0.08	-0.53	0.25	···	···	-0.53	0.38	···	···	···	···
144	SLLL	-0.92	0.06	-0.17	0.06	-0.13	0.03	-0.32	0.02	-0.08	0.05	-0.53	0.02
145	SL	-1.32	0.11	-0.22	0.23	···	···	-0.16	0.48	···	···	···	···
146	SL	-999	-999	-0.75	0.48	···	···	-0.25	0.57	···	···	···	···
147	SL	-1.63	0.11	-0.42	0.47	···	···	0.15	0.39	···	···	···	···
148	SLLL	···	···	···	···	···	···	···	···	···	···	···	···
149	SLLL	-1.4	0.05	-0.4	0.06	0.88	0.03	-0.57	0.07	0.53	0.09	-0.55	0.01

Table A.4 (cont'd)

Num.	module	n_{K-6}	$\sigma_{n_{K-6}}$	n_{6-13}	$\sigma_{n_{6-13}}$	n_{13-31}	$\sigma_{n_{13-31}}$	n_{5-12}	$\sigma_{n_{5-12}}$	n_{12-20}	$\sigma_{n_{12-20}}$	n_{K-25}	$\sigma_{n_{K-25}}$
150	SL	-1.92	0.08	-0.76	0.2	···	···	-0.61	0.24	···	···	···	···
151	SLLL	-1.99	0.16	-1.23	0.19	-1.22	0.2	-1.35	0.12	-0.57	0.14	-1.49	0.02
152	SL	-1.29	0.07	-0.86	0.3	···	···	-1.08	0.66	···	···	···	···
153	SL	-1.77	0.19	-0.51	0.6	···	···	0.31	0.55	···	···	···	···
154	SLLL	-2.24	0.08	-0.16	0.1	-0.2	0.14	-0.36	0.12	0.16	0.16	-1	0.02
155	SL	-1.81	0.19	-0.23	0.3	···	···	-0.28	0.35	···	···	···	···
156	SLLL	-1.31	0.08	-0.76	0.13	-1.09	0.2	-1.02	0.1	-0.67	0.18	-1.09	0.02
158	SL	-999	-999	-0.82	0.5	···	···	-0.29	0.48	···	···	···	···
159	SLLL	-1.71	0.07	-0.16	0.1	0.1	0.17	-0.13	0.09	0.54	0.2	-0.72	0.02
160	SLLL	-1.1	0.16	-0.51	0.2	-2.34	0.46	-0.39	0.21	-1.38	0.11	-1.07	0.02
161	SLLL	-1.49	0.09	-0.67	0.16	-0.42	0.3	-0.69	0.16	-0.32	0.24	-1.01	0.03
162	SLLL	0.52	0.05	-0.39	0.07	-1.04	0.08	-0.52	0.09	-0.41	0.1	-0.2	0.01
163	SL	-0.9	0.05	-1.16	0.17	···	···	-1.19	0.13	···	···	···	···
164	SLLL	-1.49	0.06	-0.79	0.1	-0.17	0.1	-0.96	0.05	0.38	0.04	-0.91	0.01
165	SLLL	-1.51	0.12	-0.15	0.13	-0.83	0.16	-0.24	0.1	-0.72	0.18	-0.93	0.01
166	SLLL	-1.4	0.05	-0.9	0.08	-0.25	0.14	-1.07	0.07	-0.59	0.27	-1.01	0.02
167	SLLL	-1.02	0.06	-0.54	0.09	-0.34	0.12	-0.61	0.1	-0.16	0.14	-0.72	0.02
168	SLLL	-1.48	0.05	-0.46	0.07	-0.5	0.05	-0.57	0.08	-0.32	0.09	-0.94	0.01
169	SLLL	-2.46	0.14	-0.33	0.17	0.31	0.18	-0.57	0.14	0.79	0.15	-0.99	0.03

Table A.4 (cont'd)

Num.	module	n_{K-6}	$\sigma_{n_{K-6}}$	n_{6-13}	$\sigma_{n_{6-13}}$	n_{13-31}	$\sigma_{n_{13-31}}$	n_{5-12}	$\sigma_{n_{5-12}}$	n_{12-20}	$\sigma_{n_{12-20}}$	n_{K-25}	$\sigma_{n_{K-25}}$
170	SLLL	-2.89	0.1	-1.66	0.21	1.14	0.2	-1.89	0.15	-0.34	0.49	-1.64	0.04
172	SLLL	-1.85	0.17	0.14	0.21	0.48	0.13	0.03	0.2	1.1	0.16	-0.54	0.03
173	SLLL	-0.82	0.06	-0.86	0.1	-2.36	0.36	-0.89	0.06	-1.83	0.14	-1.16	0.02
174	SLLL	-2.3	0.14	-0.85	0.18	0.41	0.11	-0.8	0.14	0.84	0.22	-1.11	0.02
175	SL	-1.54	0.28	-0.86	1.14	...	...	-0.7	0.48	...	...	...	...
176	SLLL	-1.98	0.06	-0.87	0.12	0.32	0.24	-1.13	0.14	0.92	0.37	-1.04	0.02
177	SLLL	-2.6	0.06	-1.02	0.12	2.07	0.13	-1.37	0.08	3.48	0.4	-0.71	0.03
178	SLLL	-1.32	0.07	-0.14	0.09	-1.04	0.15	-0.3	0.11	-0.53	0.28	-0.82	0.02
179	SLLL	-1.94	0.07	-0.87	0.09	-0.69	0.28	-0.94	0.13	-0.31	0.2	-1.27	0.03
180	SLLL	-1.33	0.03	-0.85	0.07	-2.25	0.34	-0.87	0.07	-1.74	0.14	-1.32	0.03
181	SLLL	-1.78	0.05	-0.78	0.09	-0.5	0.3	-0.82	0.14	-0.57	0.29	-1.16	0.04
182	SLLL	-2	0.05	-1.17	0.09	-0.81	0.19	-1.22	0.05	-0.92	0.15	-1.46	0.02
183	SLLL	-1.42	0.07	-0.59	0.08	-0.38	0.08	-0.72	0.05	-0.44	0.2	-0.92	0.01
184	SLLL	-2.1	0.09	-1.38	0.26	0.81	0.28	-1.43	0.27	0.9	0.57	-1.14	0.04
185	SLLL	-2.25	0.1	-0.04	0.12	0.04	0.12	-0.23	0.11	1.12	0.14	-0.88	0.02
186	SLLL	-1.37	0.1	-0.52	0.12	0.39	0.08	-0.82	0.12	0.83	0.07	-0.64	0.01
187	SLLL	-1.07	0.04	-0.9	0.09	1.23	0.09	-0.95	0.09	-0.22	0.1	-0.63	0.03
188	SLLL	-2.18	0.1	-1.23	0.13	0.5	0.14	-1.4	0.11	1.73	0.23	-1.1	0.02
189	SLLL	-1.62	0.06	-1.04	0.09	-0.69	0.15	-1.19	0.06	-0.19	0.12	-1.2	0.02

Table A.4 (cont'd)

Num.	module	n_{K-6}	$\sigma_{n_{K-6}}$	n_{6-13}	$\sigma_{n_{6-13}}$	n_{13-31}	$\sigma_{n_{13-31}}$	n_{5-12}	$\sigma_{n_{5-12}}$	n_{12-20}	$\sigma_{n_{12-20}}$	n_{K-25}	$\sigma_{n_{K-25}}$
190	SLLL	-1.33	0.08	-0.01	0.11	-0.16	0.12	-0.09	0.07	0.23	0.09	-0.63	0.02
191	SLLL	-0.96	0.03	0.37	0.03	0.02	0.02	0.25	0.02	-0.01	0.03	-0.31	0.01
192	SLLL	-1.56	0.05	-0.85	0.11	0.21	0.15	-0.83	0.12	0.14	0.41	-0.92	0.02
193	SLLL	-1.34	0.05	-0.75	0.09	-0.93	1.02	-0.93	0.09	0.18	0.21	-0.85	0.04
194	SLLL	-1.04	0.17	-0.55	0.21	1.2	0.15	-0.65	0.21	1.08	0.58	-0.31	0.02
195	SLLL	-1.58	0.08	-1.05	0.11	-1.07	0.74	-1.14	0.08	-0.46	0.23	-1.24	0.05
196	SLLL	-0.95	0.05	-0.63	0.06	-0.77	0.07	-0.7	0.04	-0.71	0.09	-0.83	0.01
197	SLLL	-1.2	0.09	-0.3	0.11	-0.18	0.16	-0.44	0.07	-0.13	0.05	-0.67	0.02
198	SLLL	-1.88	0.14	-1.07	0.18	-0.43	0.19	-1.11	0.18	0.78	0.1	-1.14	0.03
199	SLLL	-1.55	0.07	-1.32	0.1	-1.26	0.15	-1.32	0.06	-1.51	0.15	-1.46	0.01
200	SLLL	-1.43	0.09	-1.2	0.11	-0.78	0.12	-1.29	0.07	-0.9	0.17	-1.24	0.02
201	SLLL	-1.31	0.07	-1.23	0.08	-1.2	0.09	-1.34	0.06	-1.14	0.07	-1.31	0.01
202	SLLL	-0.22	0.05	-0.17	0.06	-0.76	0.08	-0.25	0.03	-0.88	0.05	-0.4	0.01
203	SLLL	-1.87	0.08	-0.65	0.14	-0.69	0.15	-0.72	0.1	-0.37	0.17	-1.17	0.02
204	SLLL	-2.5	0.12	0.07	0.14	0.22	0.24	-0.16	0.1	0.89	0.09	-0.93	0.02
205	SLLL	-1.87	0.04	-0.35	0.06	-0.79	0.08	-0.43	0.05	-0.17	0.11	-1.08	0.02
206	SLLL	-1.05	0.06	-1.05	0.07	-0.55	0.04	-1.12	0.04	-0.9	0.07	-1.02	0.01
207	SLLL	-0.18	0.05	-0.8	0.05	-0.32	0.09	-0.9	0.04	-0.21	0.07	-0.47	0.02
208	SLLL	-1.65	0.03	-0.49	0.04	-0.52	0.04	-0.57	0.03	-0.71	0.05	-1.02	0.01

Table A.4 (cont'd)

Num.	module	n_{K-6}	$\sigma_{n_{K-6}}$	n_{6-13}	$\sigma_{n_{6-13}}$	n_{13-31}	$\sigma_{n_{13-31}}$	n_{5-12}	$\sigma_{n_{5-12}}$	n_{12-20}	$\sigma_{n_{12-20}}$	n_{K-25}	$\sigma_{n_{K-25}}$
209	SLLL	-1.21	0.07	0.21	0.07	-0.39	0.05	0.05	0.03	-0.1	0.06	-0.52	0.01
210	SLLL	-0.88	0.06	-0.64	0.07	-0.72	0.05	-0.74	0.04	-1.05	0.06	-0.83	0.01
211	SLLL	-2.38	0.1	-0.28	0.13	-0.1	0.36	-0.51	0.13	0.66	0.65	-0.99	0.05
212	SLLL	-1.46	0.1	-0.86	0.12	-0.58	0.17	-1.03	0.05	-0.06	0.1	-1.05	0.02
213	SLLL	-1.48	0.06	-0.75	0.06	-0.65	0.03	-0.95	0.05	-0.62	0.03	-1.06	0.01
214	SLLL	-1.3	0.07	-0.73	0.09	-1.22	0.38	-0.88	0.1	-0.78	0.23	-1.05	0.03
215	SLLL	-1.54	0.06	-0.21	0.09	-0.34	0.1	-0.45	0.1	0.06	0.1	-0.78	0.02
216	SLLL	0.05	0.21	0.54	0.2	0.73	0.14	0.5	0.3	0.3	0.07	0.3	0.05
217	SLLL	-1.29	0.05	-1.23	0.06	-1.22	0.13	-1.28	0.05	-1.61	0.06	-1.33	0.03
218	SLLL	-2.54	0.1	0.3	0.13	0.4	0.12	0	0.14	0.95	0.23	-0.73	0.04
219	SLLL	-2.61	0.1	-0.95	0.14	0.91	0.16	-1.08	0.1	1.94	0.38	-1.12	0.03
220	SLLL	-1.71	0.08	-0.78	0.11	-0.25	0.09	-0.97	0.08	0.11	0.2	-1.06	0.02
221	SLLL	-0.59	0.07	-1.04	0.12	0.47	0.14	-1.15	0.11	1.2	0.3	-0.45	0.03
222	SLLL	-1.32	0.06	-0.37	0.07	-0.78	0.12	-0.5	0.07	-0.91	0.08	-0.92	0.02
223	SLLL	-2.61	0.08	-0.83	0.18	0.68	0.21	-1.1	0.12	1.37	0.25	-1.15	0.03
224	SLLL	-1.05	0.05	-0.09	0.04	-1.27	0.06	-0.18	0.03	-0.81	0.07	-0.79	0.02
225	SLLL	-1.09	0.05	-1.03	0.06	-1.63	0.11	-1.13	0.04	-1.46	0.08	-1.23	0.02
226	SLLL	-1.01	0.06	-0.83	0.07	-1.27	0.06	-0.88	0.05	-0.91	0.1	-1.03	0.02
227	SLLL	-1.28	0.06	-1.23	0.13	0.29	0.19	-1.42	0.14	1.29	0.26	-0.8	0.03

Table A.4 (cont'd)

Num.	module	n_{K-6}	$\sigma_{n_{K-6}}$	n_{6-13}	$\sigma_{n_{6-13}}$	n_{13-31}	$\sigma_{n_{13-31}}$	n_{5-12}	$\sigma_{n_{5-12}}$	n_{12-20}	$\sigma_{n_{12-20}}$	n_{K-25}	$\sigma_{n_{K-25}}$
228	SLLL	-1.7	0.12	-0.32	0.14	-0.15	0.12	-0.34	0.12	-0.73	0.08	-0.88	0.02
229	SLLL	-2.51	0.07	-1.46	0.11	1.25	0.18	-1.62	0.11	2.19	0.36	-1.16	0.03
230	SLLL	-2.46	0.13	-1.32	0.23	1.08	0.23	-1.6	0.16	2.29	0.16	-1.16	0.05
231	SLLL	-1.17	0.07	0.13	0.09	-0.81	0.1	0.01	0.05	-0.3	0.05	-0.63	0.01
232	SLLL	-1.34	0.1	-0.94	0.12	0.3	0.07	-1.06	0.08	0.3	0.14	-0.81	0.02
233	SLLL	-1.95	0.1	-0.59	0.13	0.16	0.1	-0.79	0.09	-0.1	0.13	-1.03	0.03
234	SLLL	-1.5	0.07	-0.68	0.1	-0.76	0.12	-0.85	0.11	-0.73	0.1	-1.09	0.01
235	SLLL	-0.62	0.05	-0.08	0.05	-0.86	0.04	-0.21	0.03	-0.62	0.07	-0.54	0.01
236	SLLL	-1.78	0.1	-0.47	0.12	-0.55	0.1	-0.72	0.12	-0.34	0.2	-1.03	0.01
237	SLLL	-2.38	0.16	-0.34	0.19	1.38	0.07	-0.54	0.15	2.33	0.07	-0.67	0.01
238	SLLL	-1.89	0.14	-0.17	0.17	0.15	0.08	-0.29	0.15	0.43	0.14	-0.8	0.01
239	SLLL	-2.11	0.15	0.16	0.17	0.05	0.06	0.01	0.14	0.44	0.11	-0.79	0.01
240	SLLL	-2.11	0.17	-1.11	0.27	-1.26	0.32	-1.39	0.27	-0.89	0.31	-1.57	0.07
241	SLLL	-1.29	0.07	-0.56	0.11	-0.85	0.15	-0.77	0.06	-1.04	0.18	-0.99	0.02
242	SLLL	-1.35	0.06	-1.13	0.07	-0.64	0.07	-1.29	0.05	-0.61	0.07	-1.16	0.01
243	SLLL	-1.36	0.09	-1.01	0.12	-0.86	0.14	-1.12	0.1	-0.75	0.17	-1.15	0.03
244	SLLL	-1.6	0.1	-0.92	0.18	-1.39	0.18	-1.21	0.08	-1.14	0.15	-1.34	0.04
245	SLLL	-1.24	0.06	-0.64	0.07	0.25	0.04	-0.78	0.05	0.06	0.05	-0.71	0.01
246	SLLL	-1.83	0.06	-0.65	0.09	-0.61	0.15	-0.81	0.09	-0.43	0.25	-1.13	0.03

Table A.4 (cont'd)

Num.	module	n_{K-6}	$\sigma_{n_{K-6}}$	n_{6-13}	$\sigma_{n_{6-13}}$	n_{13-31}	$\sigma_{n_{13-31}}$	n_{5-12}	$\sigma_{n_{5-12}}$	n_{12-20}	$\sigma_{n_{12-20}}$	n_{K-25}	$\sigma_{n_{K-25}}$
247	SLLL	-0.5	0.04	0.37	0.04	-0.34	0.03	0.23	0.03	-0.25	0.02	-0.2	0.01
248	SLLL	-1.32	0.13	-0.53	0.18	0.16	0.12	-0.28	0.25	0.55	0.13	-0.67	0.02
249	SLLL	-0.97	0.13	-0.87	0.18	0.28	0.24	-0.83	0.19	0.92	0.44	-0.61	0.03
250	SLLL	-1.54	0.1	-0.88	0.17	-1.12	0.21	-0.94	0.16	-0.7	0.17	-1.23	0.04
251	SLLL	-1.78	0.04	-1.48	0.12	-1.15	0.18	-1.58	0.15	-0.87	0.18	-1.57	0.04
252	SLLL	-1.09	0.07	-1.03	0.1	-0.48	0.11	-1.18	0.09	-0.73	0.16	-0.95	0.02
253	SLLL	-1.42	0.1	-0.97	0.13	-2.5	0.5	-0.97	0.13	-0.86	0.43	-1.14	0.06
254	SLLL	-1.28	0.07	-1.13	0.09	-1.3	0.09	-1.24	0.07	-0.77	0.17	-1.24	0.02
255	SLLL	-1.07	0.19	-0.34	0.19	-0.04	0.2	-0.51	0.11	0.74	0.28	-0.51	0.04
256	SLLL	-0.97	0.07	-0.31	0.08	-0.66	0.06	-0.35	0.07	-0.92	0.05	-0.72	0.01
257	SLLL	-2.66	0.23	0.67	0.27	0.7	0.18	0.3	0.31	1.34	0.11	-0.61	0.02
258	SLLL	-1.35	0.05	0.29	0.05	-0.59	0.05	0.25	0.04	-0.55	0.04	-0.63	0.01
259	SLLL	-0.71	0.07	-0.38	0.08	0.08	0.02	-0.5	0.04	-0.1	0.04	-0.46	0.01
260	SLLL	-2.75	0.16	-0.4	0.24	1.31	0.2	-0.65	0.23	1.76	0.23	-0.83	0.01
261	SLLL	0.03	0.05	-0.45	0.06	-0.72	0.05	-0.51	0.04	-1.31	0.09	-0.43	0.01
262	SLLL	-1.19	0.04	-0.5	0.04	-0.75	0.05	-0.65	0.04	-0.85	0.04	-0.9	0.01
263	SLLL	-1.73	0.12	-0.6	0.15	-0.34	0.1	-0.63	0.14	-0.69	0.49	-1.02	0.01
264	SLLL	-1.37	0.07	-0.49	0.08	-0.65	0.22	-0.54	0.08	-0.19	0.34	-0.91	0.03
265	SLLL	-2.02	0.1	-0.56	0.13	-0.78	0.28	-1.03	0.13	-0.38	0.32	-1.24	0.04

Table A.4 (cont'd)

Num.	module	n_{K-6}	$\sigma_{n_{K-6}}$	n_{6-13}	$\sigma_{n_{6-13}}$	n_{13-31}	$\sigma_{n_{13-31}}$	n_{5-12}	$\sigma_{n_{5-12}}$	n_{12-20}	$\sigma_{n_{12-20}}$	n_{K-25}	$\sigma_{n_{K-25}}$
266	SLLL	-1.51	0.06	0.47	0.04	-0.45	0.04	0.22	0.06	-0.09	0.03	-0.57	0.02
267	SLLL	-1.7	0.08	-1.19	0.12	-1.05	0.12	-1.26	0.11	-0.75	0.18	-1.38	0.04
268	SLLL	-0.89	0.05	-0.67	0.05	-0.69	0.05	-0.82	0.06	-0.63	0.03	-0.81	0.01
269	SLLL	-1.55	0.05	-0.91	0.06	-0.31	0.04	-1.04	0.05	-0.31	0.06	-1.05	0.01
270	SLLL	-2.76	0.06	-2.4	0.2	1.06	0.2	-2.31	0.14	0.12	0.28	-1.75	0.03
271	SLLL	-2.8	0.11	-0.32	0.14	1.83	0.09	-0.58	0.13	2.48	0.24	-0.67	0.02
272	SLLL	0.01	0.18	0.2	0.19	-0.74	0.25	0.21	0.18	-0.76	0.31	-0.18	0.05
273	SLLL	-1.87	0.08	-0.82	0.1	-0.83	0.24	-0.98	0.05	-1.04	0.36	-1.31	0.04
274	SLLL	-1.75	0.08	-0.8	0.11	-0.49	0.14	-0.93	0.11	-0.25	0.13	-1.09	0.04
275	SLLL	-2.26	0.12	0.22	0.15	0.55	0.1	-0.15	0.11	1.26	0.06	-0.63	0.01
276	SLLL	-0.91	0.05	-0.85	0.05	-0.64	0.05	-0.99	0.06	-0.47	0.05	-0.85	0.01
277	SLLL	-0.67	0.04	-0.37	0.04	-0.34	0.03	-0.46	0.04	-0.34	0.03	-0.53	0.01
278	SLLL	-1.34	0.08	-1.12	0.1	-0.21	0.14	-1.18	0.11	-0.33	0.2	-1.03	0.02
279	SLLL	-1.76	0.1	-0.53	0.12	0.8	0.09	-0.86	0.1	1.63	0.09	-0.64	0.02
280	SLLL	-1.91	0.07	-0.27	0.08	-0.58	0.04	-0.5	0.05	-0.15	0.06	-1.01	0.02
281	SLLL	-1.45	0.05	-0.7	0.09	-0.34	0.12	-0.82	0.07	-0.06	0.33	-0.96	0.02
282	SLLL	-1.01	0.03	-0.56	0.03	-0.8	0.04	-0.67	0.05	-0.88	0.06	-0.86	0.01
283	SLLL	-2.65	0.1	-1.73	0.17	1.43	0.16	-1.97	0.12	1.35	0.2	-1.31	0.03
284	SLLL	-1.93	0.08	-1.17	0.11	-0.7	0.29	-1.28	0.09	-0.01	0.14	-1.33	0.01

Table A.4 (cont'd)

Num.	module	n_{K-6}	$\sigma_{n_{K-6}}$	n_{6-13}	$\sigma_{n_{6-13}}$	n_{13-31}	$\sigma_{n_{13-31}}$	n_{5-12}	$\sigma_{n_{5-12}}$	n_{12-20}	$\sigma_{n_{12-20}}$	n_{K-25}	$\sigma_{n_{K-25}}$
285	SLLL	-1.82	0.07	-1.18	0.16	-0.98	0.22	-1.23	0.09	-0.74	0.2	-1.39	0.04
286	SLLL	-2.15	0.12	-1.06	0.17	-0.52	0.24	-1.25	0.11	-0.72	0.45	-1.37	0.03
287	SLLL	-1.6	0.11	-0.55	0.14	-0.17	0.14	-0.74	0.09	0.05	0.23	-0.95	0.03
288	SLLL	-1.6	0.08	-0.88	0.11	-0.52	0.21	-0.84	0.11	-0.6	0.38	-1.13	0.03
289	SLLL	-0.98	0.05	0.12	0.05	-0.12	0.05	-0.07	0.05	0.24	0.05	-0.4	0.02
290	SLLL	-1.54	0.13	0.28	0.15	-0.25	0.13	0.16	0.34	0.3	0.13	-0.62	0.02
291	SLLL	-2.4	0.12	-0.45	0.17	0.99	0.2	-0.49	0.2	2.63	0.2	-0.8	0.04
292	SLLL	-1.37	0.06	-0.56	0.09	-1.2	0.17	-0.73	0.09	-1.25	0.2	-1.07	0.02
293	SLLL	-1.68	0.06	-0.53	0.09	-0.34	0.28	-0.69	0.1	-0.17	0.16	-0.93	0.03
294	SLLL	-2.45	0.09	-1.44	0.14	1.58	0.11	-1.76	0.09	2.26	0.17	-1.03	0.01
295	SLLL	-1.33	0.07	-0.73	0.09	-1.48	0.07	-0.88	0.07	-0.96	0.1	-1.16	0.02
296	SLLL	3.22	0.03	-0.25	0.03	-0.36	0.03	-0.34	0.02	-1.02	0.02	0.98	0.01
297	SLLL	-1.89	0.13	-0.97	0.16	0.93	0.16	-1.26	0.11	2.02	0.26	-0.8	0.04
298	SLLL	-1.45	0.07	-1.28	0.1	-1.3	0.14	-1.38	0.07	-1.03	0.18	-1.36	0.02
299	SLLL	-1.68	0.1	-0.21	0.13	-0.78	0.18	-0.41	0.1	-0.44	0.13	-0.98	0.02
300	SLLL	-2.14	0.11	-0.72	0.15	-0.09	0.11	-0.84	0.05	-0.02	0.16	-1.16	0.03
301	SLLL	-1.59	0.09	-0.71	0.13	-0.37	0.13	-0.91	0.14	0.53	0.28	-0.96	0.04
302	SLLL	-1.77	0.07	-0.62	0.2	1.69	0.24	-0.96	0.09	2.74	0.2	-0.47	0.04
303	SLLL	-2.54	0.17	-0.98	0.22	1.73	0.13	-1.4	0.08	2.34	0.16	-0.88	0.02

Table A.5. Basic Stellar Properties

Num.	module	EW10	σ_{EW10}	EW20	σ_{EW20}	EW33	σ_{EW33}	$F_{11.3}$	$\sigma_{F_{11.3}}$	$F_{9.8}$	$\sigma_{F_{9.8}}$	F10	σ_{F10}	F20	σ_{F20}
id	module	EW10	erew10	EW20	erew20	EW33	erew33	F11.3	erF11.2	F9.8	erF9.8	F10	erF10	F20	erF20
1	SLLL	8.02	0.16	3.22	0.33	0.02	0.07	1.38	0.04	3.04	0.07	2.67E-12	2.18E-14	7.53E-13	2.09E-02
2	SLLL	2.74	0.09	2.37	0.31	0.56	0.09	0.54	0.02	1.01	0.03	1.10E-12	2.23E-14	5.45E-13	1.29E-02
3	SLLL	2.57	0.09	2.49	0.31	0.08	0.07	0.39	0.02	0.96	0.03	3.08E-11	6.43E-13	1.01E-11	1.24E-02
4	SLLL	2.60	0.09	2.53	0.31	0.08	0.07	0.44	0.02	1.00	0.03	3.22E-12	7.47E-14	1.47E-12	1.27E-02
5	SLLL	5.41	0.12	2.56	0.31	0.24	0.08	0.89	0.03	1.77	0.04	5.51E-12	6.18E-14	1.53E-12	1.63E-02
6	SLLL	1.80	0.08	1.88	0.30	0.11	0.07	0.26	0.02	0.64	0.03	6.01E-12	1.83E-13	2.06E-12	1.08E-02
7	SLLL	...	...	...	...	...	...	...	...	...	...	...	...	...	...
8	SLLL	1.05	0.07	3.16	0.32	-0.07	0.07	0.19	0.02	0.36	0.02	5.00E-14	3.39E-15	1.19E-13	1.05E-02
9	SLLL	1.21	0.07	1.21	0.28	0.10	0.07	0.21	0.02	0.39	0.02	1.57E-11	7.28E-13	9.29E-12	1.07E-02
10	SLLL	2.32	0.08	2.51	0.31	-0.92	0.08	0.42	0.02	0.78	0.03	3.02E-12	7.87E-14	1.64E-12	1.23E-02
11	SLLL	3.78	0.10	4.10	0.34	-0.01	0.07	0.63	0.03	1.28	0.04	1.73E-12	2.84E-14	2.98E-12	1.39E-02
12	SLLL	2.74	0.09	1.76	0.29	0.06	0.07	0.48	0.02	0.93	0.03	4.22E-12	9.22E-14	1.18E-12	1.25E-02
13	SLLL	0.29	0.06	4.72	0.36	0.53	0.08	0.06	0.02	-0.05	0.01	-8.65E-15	9.46E-15	4.23E-13	6.20E-03
14	SLLL	1.28	0.07	0.77	0.28	0.14	0.08	0.22	0.02	0.39	0.02	3.51E-12	1.53E-13	5.18E-13	1.09E-02
15	SLLL	2.92	0.09	2.03	0.30	2.87	0.19	0.45	0.02	1.00	0.03	9.24E-12	1.76E-13	3.03E-12	1.28E-02
16	SLLL	0.59	0.06	3.30	0.33	0.06	0.07	0.49	0.02	0.03	0.02	1.17E-13	2.93E-14	6.42E-13	1.29E-02
17	SLLL	2.29	0.08	2.69	0.31	0.22	0.08	0.39	0.02	0.77	0.03	3.06E-12	7.84E-14	1.69E-12	1.19E-02
18	SLLL	2.05	0.08	2.47	0.31	-0.36	0.07	0.28	0.02	0.84	0.03	6.03E-13	1.88E-14	4.68E-13	1.11E-02
19	SLLL	0.62	0.06	5.54	0.38	1.27	0.14	0.16	0.02	0.14	0.02	5.18E-14	1.03E-14	7.00E-13	1.14E-02
20	SLLL	1.00	0.07	1.65	0.29	0.65	0.09	0.21	0.02	0.27	0.02	1.37E-12	8.35E-14	7.53E-13	1.05E-02
21	SLLL	3.82	0.10	2.44	0.31	0.15	0.07	0.67	0.03	1.13	0.03	6.93E-11	9.75E-13	2.23E-11	1.45E-02
22	SLLL	3.12	0.09	1.61	0.29	0.24	0.08	0.55	0.02	1.02	0.03	9.52E-12	1.70E-13	2.18E-12	1.36E-02
23	SLLL	5.26	0.12	4.37	0.34	0.10	0.07	0.88	0.03	1.91	0.05	6.00E-12	7.58E-14	2.47E-12	1.65E-02
24	SLLL	4.79	0.11	2.83	0.31	0.33	0.08	0.67	0.03	1.75	0.04	2.01E-11	2.35E-13	6.85E-12	1.48E-02
25	SLLL	4.85	0.11	5.39	0.37	-0.02	0.07	0.96	0.03	1.72	0.04	5.21E-13	1.08E-14	8.07E-13	1.75E-02
26	SLLL	2.27	0.08	3.01	0.32	0.54	0.08	0.51	0.02	0.63	0.03	2.77E-13	1.10E-14	3.38E-13	1.26E-02

Table A.5 (cont'd)

Num.	module	EW10	σ_{EW10}	EW20	σ_{EW20}	EW33	σ_{EW33}	$F_{11.3}$	$\sigma_{F_{11.3}}$	$F_{9.8}$	$\sigma_{F_{9.8}}$	F10	σ_{F10}	F20	σ_{F20}
27	SLLL	3.41	0.10	3.45	0.33	-0.14	0.07	0.56	0.02	1.19	0.03	2.59E-12	5.04E-14	1.42E-12	1.42E-02
28	SLLL	1.52	0.07	1.75	0.29	0.46	0.08	0.33	0.02	0.46	0.02	1.08E-11	3.92E-13	6.09E-12	1.15E-02
29	SLLL	1.31	0.07	2.67	0.32	-0.03	0.07	0.68	0.03	0.16	0.02	1.29E-13	9.47E-15	7.12E-13	1.29E-02
30	SLLL	3.79	0.10	2.78	0.31	0.08	0.07	0.57	0.02	1.43	0.04	6.50E-12	9.59E-14	1.79E-12	1.43E-02
31	SLLL	3.03	0.09	1.88	0.30	-0.02	0.07	0.53	0.02	1.02	0.03	4.77E-12	9.08E-14	2.48E-12	1.38E-02
32	SLLL	2.61	0.09	0.89	0.28	0.31	0.08	0.48	0.02	0.84	0.03	1.55E-12	3.63E-14	3.55E-13	1.32E-02
33	SLLL	2.26	0.08	3.90	0.34	0.32	0.08	0.45	0.02	0.74	0.03	2.47E-12	6.42E-14	2.52E-12	1.30E-02
34	SLLL	4.45	0.11	3.96	0.37	0.62	0.09	1.02	0.03	1.42	0.04	2.75E-13	1.37E-14	2.76E-13	1.74E-02
35	SLLL	0.62	0.06	3.68	0.35	0.53	0.09	0.12	0.02	0.06	0.02	2.11E-13	3.60E-14	5.27E-13	9.70E-03
36	SLLL	1.89	0.08	5.07	0.36	1.17	0.10	0.33	0.02	0.51	0.02	2.96E-12	1.27E-13	2.84E-12	1.24E-02
37	SLLL	3.66	0.10	3.38	0.33	0.84	0.10	0.70	0.03	1.16	0.03	3.48E-11	5.30E-13	1.08E-11	1.48E-02
38	SLLL	6.87	0.14	4.69	0.36	0.07	0.07	1.17	0.04	2.45	0.06	1.90E-12	1.95E-14	1.29E-12	1.92E-02
39	SLLL	0.82	0.07	4.44	0.40	0.26	0.09	0.62	0.03	-0.04	0.01	5.01E-14	1.69E-14	2.50E-13	1.17E-02
40	SLLL	3.05	0.09	4.07	0.34	-0.12	0.07	0.55	0.02	1.14	0.03	3.21E-12	7.57E-14	1.65E-12	1.32E-02
41	SLLL	0.24	0.06	3.20	0.32	0.45	0.08	0.03	0.01	0.09	0.02	1.02E-13	2.94E-14	7.98E-13	9.38E-03
42	SLLL	4.47	0.11	3.48	0.33	0.84	0.10	0.86	0.03	1.30	0.04	2.74E-12	3.81E-14	1.19E-12	1.65E-02
43	SLLL	1.89	0.08	1.91	0.30	-0.08	0.07	0.31	0.02	0.66	0.03	1.19E-11	3.43E-13	4.35E-12	1.16E-02
44	SLLL	4.12	0.10	3.51	0.33	-0.02	0.07	0.71	0.03	1.42	0.04	2.16E-12	3.43E-14	1.65E-12	1.53E-02
45	SLLL	1.44	0.07	0.82	0.27	1.60	0.13	0.27	0.02	0.41	0.02	4.11E-11	1.56E-12	4.43E-12	1.13E-02
46	SLLL	2.60	0.09	8.68	0.48	0.44	0.17	0.56	0.02	0.76	0.03	2.42E-12	6.18E-14	2.95E-12	1.37E-02
47	SLLL	3.24	0.09	4.76	0.35	0.23	0.09	0.68	0.03	1.04	0.03	2.88E-12	4.75E-14	1.72E-12	1.33E-02
48	SLLL	1.53	0.07	4.06	0.35	0.34	0.08	0.32	0.02	0.44	0.02	1.14E-12	4.38E-14	7.13E-13	1.09E-02
49	SL	-13.03	0.12	...	...	...	...	-2.07	0.03	-2.70	0.03	4.30E-12	2.32E-13	...	...
50	SLLL	4.32	0.11	3.87	0.34	0.58	0.13	0.62	0.03	1.44	0.04	1.54E-11	3.14E-13	7.07E-12	1.29E-02
51	SLLL	2.59	0.09	2.52	0.31	0.01	0.07	0.41	0.02	0.86	0.03	4.83E-12	1.06E-13	1.62E-12	1.27E-02
52	SLLL	2.17	0.08	1.57	0.29	0.45	0.08	0.47	0.02	0.68	0.03	4.95E-12	1.30E-13	1.41E-12	1.23E-02
53	SLLL	3.00	0.09	3.51	0.33	0.31	0.08	0.51	0.02	0.87	0.03	2.39E-13	1.02E-14	2.10E-13	1.36E-02

Table A.5 (cont'd)

Num.	module	EW10	σ_{EW10}	EW20	σ_{EW20}	EW33	σ_{EW33}	$F_{11.3}$	$\sigma_{F_{11.3}}$	$F_{9.8}$	$\sigma_{F_{9.8}}$	F10	σ_{F10}	F20	σ_{F20}
54	SLLL	4.19	0.11	2.69	0.31	-0.50	0.07	0.61	0.03	1.33	0.04	7.25E-12	9.58E-14	1.52E-12	1.37E-02
55	SL	2.10	0.08	···	···	···	···	0.44	0.02	0.48	0.02	3.98E-12	2.31E-13	···	···
56	SL	4.50	0.11	···	···	···	···	0.84	0.03	1.29	0.04	2.13E-12	7.56E-14	···	···
57	SLLL	4.32	0.11	2.44	0.31	-0.18	0.07	0.63	0.03	1.52	0.04	7.41E-12	9.90E-14	2.17E-12	1.45E-02
58	SLLL	1.67	0.07	3.08	0.32	-0.51	0.06	0.31	0.02	0.52	0.02	1.25E-12	4.32E-14	6.29E-13	1.05E-02
59	SLLL	2.66	0.09	1.15	0.28	0.41	0.08	0.50	0.02	0.78	0.03	7.56E-13	2.26E-14	4.04E-13	1.36E-02
60	SLLL	0.86	0.06	2.01	0.30	0.03	0.07	0.19	0.02	0.37	0.02	8.71E-13	6.62E-14	6.22E-13	1.01E-02
61	SLLL	1.98	0.08	1.69	0.29	0.10	0.07	0.31	0.02	0.66	0.03	6.98E-12	1.97E-13	1.96E-12	1.18E-02
62	SLLL	1.41	0.07	2.03	0.30	0.12	0.07	0.22	0.02	0.43	0.02	6.14E-12	2.33E-13	2.13E-12	1.07E-02
63	SL	2.24	0.08	···	···	···	···	0.18	0.02	0.69	0.03	1.39E-12	6.56E-14	···	···
64	SL	5.57	0.12	···	···	···	···	1.00	0.03	1.80	0.04	2.89E-11	3.04E-13	···	···
65	SLLL	2.85	0.09	2.62	0.31	-0.60	0.07	0.41	0.02	0.86	0.03	1.68E-12	3.51E-14	7.34E-13	1.28E-02
66	SLLL	3.46	0.10	7.43	0.43	-0.01	0.08	0.76	0.03	1.30	0.04	4.67E-13	1.58E-14	8.94E-13	1.52E-02
67	SL	4.91	0.11	···	···	···	···	1.22	0.04	1.62	0.04	5.82E-12	1.02E-13	···	···
68	SL	1.37	0.07	···	···	···	···	0.46	0.02	0.22	0.02	1.84E-12	1.25E-13	···	···
70	SL	1.03	0.07	···	···	···	···	0.46	0.02	0.17	0.02	5.77E-13	4.25E-14	···	···
71	SL	0.94	0.07	···	···	···	···	0.61	0.03	0.10	0.02	4.85E-12	3.39E-13	···	···
73	SLLL	1.13	0.07	2.19	0.32	0.01	0.08	0.23	0.02	0.39	0.02	1.69E-12	8.32E-14	7.38E-13	1.01E-02
74	SL	10.36	0.18	···	···	···	···	1.67	0.04	3.46	0.07	5.16E-11	3.78E-13	···	···
75	SL	5.22	0.13	···	···	···	···	1.09	0.04	1.32	0.04	2.16E-12	2.25E-13	···	···
76	SLLL	2.69	0.09	2.90	0.32	0.26	0.08	0.54	0.02	0.78	0.03	8.92E-12	1.96E-13	3.42E-12	1.35E-02
77	SL	39.87	10.50	···	···	···	···	-17.60	0.45	219.16	1.97	3.44E-12	2.86E-13	···	···
78	SL	-30.62	4.74	···	···	···	···	-3.01	0.07	1.81	0.05	5.42E-13	6.45E-14	···	···
79	SLLL	2.46	0.08	2.23	0.30	0.08	0.07	0.38	0.02	0.79	0.03	4.63E-12	1.03E-13	1.30E-12	1.21E-02
80	SL	3.07	0.09	···	···	···	···	0.42	0.02	0.79	0.03	1.70E-12	5.73E-14	···	···
81	SL	3.33	0.09	···	···	···	···	0.68	0.03	0.93	0.03	3.11E-12	8.49E-14	···	···
82	SL	4.43	0.11	···	···	···	···	0.53	0.02	1.36	0.04	7.90E-12	2.47E-13	···	···

Table A.5 (cont'd)

Num.	module	EW10	σ_{EW10}	EW20	σ_{EW20}	EW33	σ_{EW33}	$F_{11.3}$	$\sigma_{F_{11.3}}$	$F_{9.8}$	$\sigma_{F_{9.8}}$	F10	σ_{F10}	F20	σ_{F20}
83	SL	2.86	0.09	···	···	···	···	0.87	0.03	0.82	0.03	2.77E-12	5.72E-14	···	···
84	SLLL	4.08	0.11	3.55	0.33	0.08	0.08	0.53	0.02	1.61	0.04	3.10E-12	4.60E-14	1.20E-12	1.40E-02
85	SL	5.30	0.12	···	···	···	···	1.01	0.03	1.62	0.04	2.47E-12	4.63E-14	···	···
86	SLLL	2.33	0.08	3.19	0.33	-0.12	0.07	0.42	0.02	0.85	0.03	1.43E-12	3.94E-14	8.40E-13	1.27E-02
88	SLLL	-999.00	-999.00	···	···	···	···	···	···	···	···	···	···	···	···
89	SL	1.48	0.07	···	···	···	···	0.77	0.03	0.31	0.02	3.58E-12	1.80E-13	···	···
90	SLLL	2.10	0.08	3.68	0.33	0.41	0.09	0.35	0.02	0.78	0.03	1.09E-11	2.84E-13	7.08E-12	1.18E-02
91	SL	4.37	0.11	···	···	···	···	0.64	0.03	1.54	0.04	1.46E-10	1.86E-12	···	···
92	SL	2.75	0.09	···	···	···	···	0.77	0.03	0.50	0.02	4.35E-12	2.39E-13	···	···
93	SL	1.23	0.07	···	···	···	···	0.24	0.02	0.42	0.02	5.89E-12	3.02E-13	···	···
94	SLLL	4.39	0.11	2.29	0.31	0.88	0.09	0.57	0.02	1.07	0.03	2.84E-12	5.57E-14	1.03E-12	1.31E-02
95	SLLL	0.27	0.06	-0.02	0.26	0.46	0.08	0.17	0.02	-0.01	0.02	8.52E-13	1.85E-13	-1.16E-14	9.85E-03
96	SL	2.68	0.09	···	···	···	···	0.57	0.02	0.74	0.03	2.31E-12	7.14E-14	···	···
97	SLLL	4.10	0.10	4.21	0.34	0.18	0.08	0.69	0.03	1.31	0.04	2.12E-12	3.11E-14	1.24E-12	1.51E-02
98	SLLL	3.45	0.10	4.44	0.35	-19.47	0.90	0.66	0.03	1.16	0.03	3.69E-12	6.27E-14	1.44E-12	1.40E-02
99	SLLL	2.43	0.08	1.08	0.28	0.04	0.08	0.38	0.02	0.76	0.03	2.32E-12	5.70E-14	3.24E-13	1.17E-02
100	SL	4.05	0.10	···	···	···	···	0.68	0.03	1.20	0.03	1.29E-11	1.81E-13	···	···
101	SL	1.69	0.08	···	···	···	···	1.27	0.04	0.23	0.02	1.79E-12	9.14E-14	···	···
102	SL	1.94	0.08	···	···	···	···	0.50	0.02	0.57	0.02	2.23E-12	1.09E-13	···	···
103	SLLL	2.92	0.09	1.33	0.28	0.29	0.08	0.44	0.02	1.10	0.03	1.14E-11	2.17E-13	1.67E-12	1.26E-02
106	SLLL	2.22	0.08	1.54	0.29	0.03	0.07	0.35	0.02	0.71	0.03	4.03E-12	1.07E-13	8.25E-13	1.27E-02
108	SLLL	8.35	0.16	5.68	0.37	0.00	0.07	1.17	0.04	3.37	0.07	1.03E-10	6.69E-13	4.11E-11	1.95E-02
112	SLLL	1.25	0.07	1.31	0.28	0.39	0.08	0.23	0.02	0.32	0.02	1.10E-11	4.91E-13	2.70E-12	1.08E-02
114	SL	1.66	0.07	···	···	···	···	0.47	0.02	0.37	0.02	9.71E-12	3.39E-13	···	···
117	SLLL	2.21	0.08	0.48	0.27	0.34	0.08	0.34	0.02	0.79	0.03	2.39E-11	5.79E-13	2.48E-12	1.18E-02
119	SL	2.09	0.08	···	···	···	···	0.29	0.02	0.62	0.03	1.07E-12	3.95E-14	···	···
120	SL	2.74	0.09	···	···	···	···	0.36	0.02	0.76	0.03	2.88E-12	6.64E-14	···	···

Table A.5 (cont'd)

Num.	module	EW10	σ_{EW10}	EW20	σ_{EW20}	EW33	σ_{EW33}	$F_{11.3}$	$\sigma_{F_{11.3}}$	$F_{9.8}$	$\sigma_{F_{9.8}}$	F10	σ_{F10}	F20	σ_{F20}
121	SLLL	1.11	0.07	1.40	0.29	0.33	0.08	0.23	0.02	0.31	0.02	2.96E-12	1.54E-13	1.06E-12	1.10E-02
122	SLLL	1.66	0.07	1.92	0.30	0.34	0.08	0.26	0.02	0.56	0.02	1.46E-11	4.75E-13	5.73E-12	1.10E-02
123	SLLL	2.50	0.08	2.88	0.31	0.64	0.09	0.49	0.02	0.79	0.03	2.16E-12	5.06E-14	2.01E-12	1.31E-02
125	SLLL	4.71	0.11	3.46	0.33	0.27	0.08	0.96	0.03	1.52	0.04	2.16E-11	2.54E-13	6.51E-12	1.69E-02
127	SLLL	2.43	0.08	0.64	0.27	-0.18	0.07	0.49	0.02	0.63	0.03	1.25E-12	6.90E-14	1.91E-13	1.01E-02
128	SLLL	0.88	0.07	1.92	0.29	0.00	0.07	0.47	0.02	0.24	0.02	1.50E-12	1.46E-13	1.15E-12	1.25E-02
129	SL	1.88	0.08	···	···	···	···	0.39	0.02	0.51	0.02	1.56E-12	5.88E-14	···	···
131	SLLL	2.08	0.08	2.91	0.32	-0.09	0.07	0.39	0.02	0.60	0.03	6.15E-12	1.75E-13	2.06E-12	1.21E-02
132	SL	1.31	0.07	···	···	···	···	0.38	0.02	0.28	0.02	2.45E-11	1.05E-12	···	···
133	SLLL	1.98	0.08	2.13	0.30	0.17	0.08	0.34	0.02	0.63	0.03	6.15E-12	1.68E-13	2.58E-12	1.19E-02
134	SLLL	3.00	0.09	1.43	0.28	0.40	0.08	0.56	0.02	0.83	0.03	7.50E-12	1.43E-13	1.08E-12	1.37E-02
135	SLLL	3.82	0.10	4.11	0.34	0.30	0.08	0.77	0.03	1.17	0.03	1.43E-11	2.16E-13	4.67E-12	1.56E-02
136	SLLL	···	···	···	···	···	···	···	···	···	···	···	···	···	···
137	SL	709.38	70.82	···	···	···	···	5.91	0.17	-23.28	0.36	2.13E-12	6.09E-14	···	···
138	SLLL	2.90	0.09	1.25	0.28	0.84	0.10	0.44	0.02	0.89	0.03	8.74E-12	1.71E-13	1.65E-12	1.26E-02
139	SL	1.64	0.08	···	···	···	···	0.78	0.03	0.05	0.02	6.44E-11	2.23E-12	···	···
140	SLLL	4.37	0.11	2.97	0.31	-0.04	0.07	0.54	0.02	1.67	0.04	4.28E-11	5.30E-13	1.55E-11	1.38E-02
141	SLLL	1.31	0.07	4.44	0.35	0.31	0.08	0.29	0.02	0.29	0.02	1.15E-11	5.04E-13	5.72E-12	1.10E-02
142	SLLL	4.75	0.11	3.33	0.33	0.46	0.09	0.71	0.03	1.77	0.04	1.43E-11	1.77E-13	5.40E-12	1.54E-02
143	SL	4.07	0.10	···	···	···	···	1.19	0.04	0.81	0.03	3.93E-12	1.54E-13	···	···
144	SLLL	1.95	0.08	1.66	0.29	0.08	0.07	0.31	0.02	0.65	0.03	4.48E-11	1.26E-12	2.03E-11	1.15E-02
145	SL	2.42	0.08	···	···	···	···	0.64	0.03	0.67	0.03	4.55E-12	1.23E-13	···	···
146	SL	3.49	0.10	···	···	···	···	0.57	0.02	1.05	0.03	3.26E-12	1.74E-13	···	···
147	SL	0.78	0.07	···	···	···	···	0.43	0.02	0.02	0.02	1.32E-12	1.64E-13	···	···
148	SLLL	···	···	···	···	···	···	···	···	···	···	···	···	···	···
149	SLLL	2.05	0.08	1.93	0.30	0.04	0.07	0.35	0.02	0.65	0.03	2.20E-11	5.74E-13	1.48E-11	1.14E-02
150	SL	3.92	0.10	···	···	···	···	0.82	0.03	1.07	0.03	1.43E-11	2.73E-13	···	···

Table A.5 (cont'd)

Num.	module	EW10	σ_{EW10}	EW20	σ_{EW20}	EW33	σ_{EW33}	$F_{11.3}$	$\sigma_{F_{11.3}}$	$F_{9.8}$	$\sigma_{F_{9.8}}$	F10	σ_{F10}	F20	σ_{F20}
151	SLLL	4.23	0.11	2.96	0.32	-0.03	0.07	0.71	0.03	1.45	0.04	2.72E-12	5.21E-14	5.54E-13	1.60E-02
152	SL	4.39	0.11	···	···	···	···	1.41	0.04	1.23	0.04	1.90E-11	4.66E-13	···	···
153	SL	2.66	0.09	···	···	···	···	1.05	0.03	0.39	0.02	1.98E-12	9.27E-14	···	···
154	SLLL	2.46	0.08	3.74	0.34	-0.24	0.07	0.51	0.02	0.86	0.03	1.70E-12	4.29E-14	1.36E-12	1.29E-02
155	SL	1.55	0.07	···	···	···	···	0.24	0.02	0.31	0.02	9.32E-13	9.92E-14	···	···
156	SLLL	1.90	0.08	2.15	0.30	0.22	0.08	0.29	0.02	0.61	0.03	8.68E-12	2.46E-13	3.54E-12	1.13E-02
158	SL	1.29	0.07	···	···	···	···	0.75	0.03	0.11	0.02	6.20E-12	3.83E-13	···	···
159	SLLL	3.35	0.09	1.80	0.29	-0.11	0.07	0.59	0.02	1.12	0.03	1.61E-12	3.41E-14	7.21E-13	1.51E-02
160	SLLL	2.47	0.08	1.90	0.30	8.67	0.37	0.25	0.02	0.68	0.03	1.59E-11	3.37E-13	3.77E-12	1.07E-02
161	SLLL	2.97	0.09	2.91	0.32	-0.19	0.07	0.48	0.02	0.98	0.03	1.30E-12	3.10E-14	5.65E-13	1.29E-02
162	SLLL	3.81	0.10	3.33	0.32	0.23	0.08	0.55	0.02	1.49	0.04	2.42E-11	3.45E-13	8.79E-12	1.35E-02
163	SL	2.28	0.08	···	···	···	···	0.02	0.01	0.78	0.03	1.24E-11	3.48E-13	···	···
164	SLLL	5.11	0.12	3.00	0.32	0.04	0.07	0.75	0.03	1.95	0.05	2.21E-11	2.41E-13	8.09E-12	1.55E-02
165	SLLL	2.94	0.09	1.40	0.28	0.41	0.08	0.52	0.02	1.03	0.03	3.01E-12	5.89E-14	6.09E-13	1.34E-02
166	SLLL	1.09	0.07	2.55	0.31	-0.14	0.07	0.19	0.02	0.30	0.02	9.73E-13	5.24E-14	7.83E-13	1.08E-02
167	SLLL	1.87	0.08	3.06	0.32	0.12	0.07	0.41	0.02	0.62	0.03	2.14E-12	7.76E-14	1.68E-12	1.19E-02
168	SLLL	2.00	0.08	1.99	0.30	0.04	0.07	0.36	0.02	0.63	0.03	2.53E-11	7.06E-13	1.06E-11	1.16E-02
169	SLLL	2.61	0.09	4.64	0.35	0.05	0.07	0.65	0.03	0.92	0.03	7.53E-13	1.98E-14	1.14E-12	1.40E-02
170	SLLL	2.52	0.08	1.06	0.28	0.42	0.08	0.29	0.02	0.65	0.03	4.87E-13	2.23E-14	1.89E-13	1.25E-02
172	SLLL	3.27	0.09	3.00	0.32	-0.10	0.07	0.59	0.03	1.07	0.03	1.94E-12	3.86E-14	1.73E-12	1.41E-02
173	SLLL	0.82	0.06	1.94	0.30	0.21	0.12	0.27	0.02	0.25	0.02	1.26E-11	8.72E-13	4.21E-12	1.05E-02
174	SLLL	4.03	0.10	3.17	0.32	0.13	0.07	0.96	0.03	1.65	0.05	2.05E-12	3.38E-14	1.17E-12	1.55E-02
175	SL	13.72	0.24	···	···	···	···	2.37	0.06	4.27	0.09	4.53E-12	1.23E-13	···	···
176	SLLL	3.24	0.09	2.49	0.31	0.18	0.08	0.50	0.02	1.04	0.03	9.88E-13	2.31E-14	5.94E-13	1.38E-02
177	SLLL	2.18	0.08	5.21	0.37	0.25	0.08	0.47	0.02	0.70	0.03	9.90E-14	3.70E-15	7.12E-13	1.24E-02
178	SLLL	4.17	0.11	1.94	0.30	0.06	0.07	0.53	0.02	1.57	0.04	8.73E-12	1.15E-13	2.00E-12	1.29E-02
179	SLLL	3.10	0.09	4.67	0.36	0.06	0.08	0.47	0.02	1.01	0.03	2.55E-12	4.94E-14	1.14E-12	1.30E-02

Table A.5 (cont'd)

Num.	module	EW10	σ_{EW10}	EW20	σ_{EW20}	EW33	σ_{EW33}	$F_{11.3}$	$\sigma_{F_{11.3}}$	$F_{9.8}$	$\sigma_{F_{9.8}}$	F10	σ_{F10}	F20	σ_{F20}
180	SLLL	1.02	0.07	1.12	0.28	0.04	0.21	0.27	0.02	0.26	0.02	8.57E-12	4.64E-13	1.57E-12	1.06E-02
181	SLLL	2.95	0.09	2.74	0.32	-0.17	0.07	0.52	0.02	0.88	0.03	2.53E-12	5.08E-14	8.65E-13	1.29E-02
182	SLLL	2.13	0.08	1.65	0.29	-0.07	0.07	0.28	0.02	0.70	0.03	4.86E-12	1.30E-13	1.21E-12	1.15E-02
183	SLLL	2.47	0.08	2.12	0.30	-0.10	0.07	0.39	0.02	0.86	0.03	3.99E-12	9.19E-14	1.44E-12	1.24E-02
184	SLLL	8.71	0.17	6.49	0.39	0.80	0.09	1.73	0.05	3.32	0.07	3.01E-12	3.80E-14	1.46E-12	2.13E-02
185	SLLL	4.83	0.11	3.48	0.33	-0.12	0.07	0.83	0.03	1.76	0.04	3.40E-12	4.27E-14	1.92E-12	1.59E-02
186	SLLL	3.73	0.10	2.20	0.30	-0.06	0.07	0.63	0.03	1.39	0.04	4.47E-12	7.10E-14	2.11E-12	1.39E-02
187	SLLL	2.30	0.08	1.58	0.29	-0.05	0.07	0.29	0.02	0.74	0.03	2.85E-12	8.47E-14	1.09E-12	1.19E-02
188	SLLL	3.29	0.09	3.19	0.32	-0.10	0.07	0.82	0.03	1.05	0.03	1.13E-12	2.97E-14	1.12E-12	1.52E-02
189	SLLL	4.22	0.11	4.43	0.35	0.23	0.08	0.75	0.03	1.41	0.04	5.36E-12	7.78E-14	1.92E-12	1.50E-02
190	SLLL	1.60	0.07	2.21	0.30	0.10	0.07	0.21	0.02	0.59	0.03	1.71E-12	5.99E-14	1.27E-12	1.05E-02
191	SLLL	1.49	0.07	2.18	0.30	0.05	0.07	0.27	0.02	0.50	0.02	6.94E-11	2.53E-12	5.79E-11	1.10E-02
192	SLLL	2.21	0.08	3.98	0.34	-0.07	0.07	0.49	0.02	0.71	0.03	1.03E-12	2.96E-14	8.36E-13	1.30E-02
193	SLLL	3.90	0.10	13.43	0.56	-1.83	0.14	0.61	0.03	1.44	0.04	4.10E-12	6.84E-14	4.09E-12	1.39E-02
194	SLLL	0.46	0.06	1.81	0.30	0.02	0.07	0.47	0.02	-0.10	0.01	1.11E-13	1.82E-14	4.00E-13	1.07E-02
195	SLLL	1.37	0.07	5.60	0.39	0.66	0.11	0.20	0.02	0.38	0.02	9.97E-13	4.22E-14	9.85E-13	1.13E-02
196	SLLL	2.33	0.08	1.69	0.29	-0.02	0.07	0.41	0.02	0.69	0.03	9.58E-12	2.22E-13	2.42E-12	1.28E-02
197	SLLL	1.92	0.08	1.59	0.29	0.13	0.07	0.37	0.02	0.67	0.03	2.27E-12	6.67E-14	9.66E-13	1.18E-02
198	SLLL	4.77	0.11	6.17	0.39	0.04	0.07	0.98	0.03	1.53	0.04	2.66E-12	4.78E-14	1.75E-12	1.73E-02
199	SLLL	1.20	0.07	1.55	0.29	0.16	0.08	0.20	0.02	0.38	0.02	2.32E-12	1.20E-13	6.28E-13	1.02E-02
200	SLLL	1.46	0.07	1.33	0.29	0.09	0.07	0.27	0.02	0.44	0.02	3.19E-12	1.43E-13	7.92E-13	1.13E-02
201	SLLL	1.60	0.07	2.48	0.31	0.18	0.08	0.22	0.02	0.55	0.02	5.60E-12	2.00E-13	1.75E-12	1.07E-02
202	SLLL	1.16	0.07	1.40	0.29	0.14	0.07	0.21	0.02	0.38	0.02	6.28E-12	3.00E-13	2.84E-12	1.08E-02
203	SLLL	5.86	0.13	4.19	0.34	-0.06	0.07	0.89	0.03	1.92	0.05	5.29E-12	4.86E-14	1.68E-12	1.68E-02
204	SLLL	3.60	0.10	5.32	0.37	-0.16	0.07	0.74	0.03	1.25	0.04	4.16E-13	7.41E-15	4.28E-13	1.54E-02
205	SLLL	4.59	0.11	3.40	0.32	0.21	0.08	0.58	0.02	1.55	0.04	1.50E-11	1.81E-13	4.73E-12	1.41E-02
206	SLLL	2.16	0.08	1.83	0.29	0.05	0.07	0.33	0.02	0.72	0.03	4.51E-11	1.13E-12	1.10E-11	1.20E-02

Table A.5 (cont'd)

Num.	module	EW10	σ_{EW10}	EW20	σ_{EW20}	EW33	σ_{EW33}	$F_{11.3}$	$\sigma_{F_{11.3}}$	$F_{9.8}$	$\sigma_{F_{9.8}}$	F10	σ_{F10}	F20	σ_{F20}
207	SLLL	0.78	0.06	1.09	0.28	0.12	0.07	0.14	0.02	0.32	0.02	5.84E-12	4.16E-13	3.93E-12	9.74E-03
208	SLLL	0.89	0.07	1.15	0.28	0.12	0.07	0.21	0.02	0.32	0.02	6.73E-12	4.46E-13	3.58E-12	1.06E-02
209	SLLL	2.84	0.09	2.36	0.30	0.01	0.07	0.35	0.02	1.04	0.03	6.57E-11	1.23E-12	3.14E-11	1.18E-02
210	SLLL	0.72	0.06	0.91	0.28	-0.02	0.07	0.14	0.02	0.22	0.02	2.83E-12	2.18E-13	1.19E-12	1.01E-02
211	SLLL	3.31	0.09	7.02	0.41	0.06	0.08	0.68	0.03	0.95	0.03	3.09E-13	6.21E-15	5.23E-13	1.46E-02
212	SLLL	3.59	0.10	2.50	0.31	0.24	0.08	0.58	0.02	1.22	0.04	3.76E-12	5.94E-14	1.09E-12	1.46E-02
213	SLLL	1.58	0.07	1.51	0.29	0.13	0.07	0.27	0.02	0.55	0.02	6.96E-12	2.45E-13	2.29E-12	1.12E-02
214	SLLL	4.76	0.11	3.68	0.33	0.62	0.10	0.81	0.03	1.49	0.04	4.66E-12	6.45E-14	1.17E-12	1.58E-02
215	SLLL	3.44	0.10	2.58	0.31	0.03	0.07	0.51	0.02	1.14	0.03	4.94E-12	8.20E-14	2.06E-12	1.35E-02
216	SLLL	1.04	0.07	-0.92	0.24	0.08	0.07	0.17	0.02	0.05	0.02	1.12E-13	6.67E-15	-9.50E-14	1.11E-02
217	SLLL	1.06	0.07	0.65	0.27	-0.21	0.07	0.19	0.02	0.36	0.02	3.32E-12	1.73E-13	5.18E-13	1.01E-02
218	SLLL	1.88	0.08	3.55	0.34	-0.07	0.07	0.42	0.02	0.57	0.02	1.37E-13	4.91E-15	2.93E-13	1.26E-02
219	SLLL	3.36	0.10	3.03	0.33	-0.11	0.07	0.86	0.03	1.07	0.03	3.21E-13	8.87E-15	3.07E-13	1.61E-02
220	SLLL	1.69	0.07	1.97	0.29	-0.03	0.07	0.28	0.02	0.60	0.03	2.61E-12	8.73E-14	1.58E-12	1.12E-02
221	SLLL	5.79	0.13	3.64	0.33	-0.10	0.07	0.97	0.03	2.29	0.05	3.69E-12	4.01E-14	1.97E-12	1.74E-02
222	SLLL	3.58	0.10	1.52	0.29	0.06	0.07	0.56	0.02	1.29	0.04	9.65E-12	1.55E-13	1.62E-12	1.40E-02
223	SLLL	2.10	0.08	2.05	0.31	0.24	0.08	0.55	0.02	0.65	0.03	1.49E-13	5.58E-15	1.53E-13	1.37E-02
224	SLLL	6.23	0.13	2.04	0.30	0.09	0.07	0.85	0.03	2.20	0.05	1.95E-10	1.66E-12	2.51E-11	1.65E-02
225	SLLL	2.09	0.08	1.42	0.29	0.11	0.07	0.38	0.02	0.63	0.03	2.77E-11	7.24E-13	4.36E-12	1.23E-02
226	SLLL	4.74	0.11	2.69	0.31	0.13	0.07	0.82	0.03	1.48	0.04	7.69E-11	9.33E-13	1.32E-11	1.62E-02
227	SLLL	5.37	0.12	6.97	0.40	0.94	0.09	1.14	0.04	1.51	0.04	2.80E-12	3.82E-14	2.04E-12	1.82E-02
228	SLLL	1.47	0.07	1.35	0.29	0.02	0.07	0.27	0.02	0.46	0.02	8.55E-13	3.55E-14	3.04E-13	1.11E-02
229	SLLL	1.13	0.07	5.71	0.38	0.81	0.09	0.30	0.02	0.19	0.02	1.16E-13	7.61E-15	5.97E-13	1.17E-02
230	SLLL	7.87	0.15	5.36	0.38	0.10	0.08	1.96	0.05	2.23	0.05	5.34E-13	7.83E-15	3.45E-13	2.72E-02
231	SLLL	2.29	0.08	4.30	0.34	0.01	0.07	0.33	0.02	0.83	0.03	1.80E-11	4.18E-13	1.38E-11	1.17E-02
232	SLLL	2.34	0.08	2.35	0.30	0.10	0.07	0.44	0.02	0.79	0.03	3.14E-12	7.68E-14	1.87E-12	1.29E-02
233	SLLL	2.09	0.08	1.73	0.29	0.18	0.08	0.38	0.02	0.66	0.03	1.31E-12	3.88E-14	5.02E-13	1.21E-02

Table A.5 (cont'd)

Num.	module	EW10	σ_{EW10}	EW20	σ_{EW20}	EW33	σ_{EW33}	$F_{11.3}$	$\sigma_{F_{11.3}}$	$F_{9.8}$	$\sigma_{F_{9.8}}$	F10	σ_{F10}	F20	σ_{F20}
234	SLLL	3.67	0.10	2.03	0.30	0.03	0.07	0.59	0.02	1.23	0.04	3.94E-12	6.80E-14	7.97E-13	1.43E-02
235	SLLL	5.34	0.12	1.55	0.29	0.07	0.07	0.71	0.03	1.86	0.05	2.49E-10	2.58E-12	3.41E-11	1.51E-02
236	SLLL	1.82	0.08	3.39	0.33	0.20	0.08	0.27	0.02	0.47	0.02	2.83E-12	9.09E-14	2.22E-12	1.19E-02
237	SLLL	6.72	0.14	4.59	0.35	0.01	0.07	0.93	0.03	2.72	0.06	2.47E-12	2.39E-14	2.98E-12	1.75E-02
238	SLLL	3.12	0.09	2.53	0.31	0.06	0.07	0.56	0.02	0.97	0.03	3.94E-12	7.97E-14	2.02E-12	1.39E-02
239	SLLL	6.40	0.14	4.14	0.34	0.00	0.07	0.98	0.03	2.49	0.06	9.96E-12	1.03E-13	4.55E-12	1.72E-02
240	SLLL	1.20	0.07	1.34	0.29	0.33	0.09	0.17	0.02	0.39	0.02	5.59E-13	3.25E-14	1.50E-13	1.04E-02
241	SLLL	1.96	0.08	0.86	0.27	0.03	0.07	0.31	0.02	0.63	0.03	3.85E-12	1.09E-13	6.16E-13	1.18E-02
242	SLLL	1.69	0.07	1.96	0.30	0.17	0.07	0.31	0.02	0.53	0.02	2.74E-11	8.98E-13	1.06E-11	1.17E-02
243	SLLL	1.53	0.07	2.29	0.30	-0.43	0.06	0.27	0.02	0.45	0.02	3.05E-12	1.13E-13	1.49E-12	1.14E-02
244	SLLL	1.57	0.07	1.78	0.30	0.10	0.07	0.30	0.02	0.44	0.02	1.93E-12	7.18E-14	6.53E-13	1.14E-02
245	SLLL	1.89	0.08	1.22	0.28	-0.03	0.07	0.34	0.02	0.54	0.02	8.01E-12	2.34E-13	2.96E-12	1.17E-02
246	SLLL	3.07	0.09	3.30	0.33	-0.31	0.06	0.55	0.02	1.03	0.03	4.09E-12	7.29E-14	1.69E-12	1.32E-02
247	SLLL	1.21	0.07	1.22	0.28	-0.03	0.07	0.16	0.02	0.44	0.02	1.05E-11	4.64E-13	6.02E-12	1.01E-02
248	SLLL	1.96	0.08	2.23	0.31	0.29	0.08	0.32	0.02	0.66	0.03	2.81E-12	7.78E-14	1.82E-12	1.17E-02
249	SLLL	4.21	0.11	5.99	0.38	-0.27	0.07	0.80	0.03	1.48	0.04	1.54E-12	2.57E-14	1.14E-12	1.54E-02
250	SLLL	3.40	0.10	2.22	0.30	0.00	0.07	0.56	0.02	1.09	0.03	4.80E-12	8.16E-14	1.03E-12	1.34E-02
251	SLLL	0.92	0.07	1.82	0.30	0.19	0.08	0.20	0.02	0.25	0.02	2.04E-12	1.23E-13	8.34E-13	1.08E-02
252	SLLL	0.91	0.07	2.13	0.31	0.04	0.07	0.12	0.02	0.32	0.02	4.02E-12	2.32E-13	2.67E-12	9.17E-03
253	SLLL	2.50	0.08	5.85	0.39	5.28	0.21	0.40	0.02	0.72	0.03	4.46E-12	9.53E-14	2.52E-12	1.26E-02
254	SLLL	1.77	0.08	3.47	0.33	0.07	0.07	0.28	0.02	0.52	0.02	2.36E-11	7.10E-13	1.09E-11	1.09E-02
255	SLLL	3.51	0.10	4.46	0.35	-0.19	0.07	0.41	0.02	1.38	0.04	6.07E-12	9.35E-14	5.05E-12	1.25E-02
256	SLLL	0.84	0.06	0.93	0.28	0.02	0.07	0.13	0.02	0.28	0.02	5.91E-12	3.81E-13	2.61E-12	9.88E-03
257	SLLL	1.08	0.07	2.24	0.31	-0.16	0.07	0.19	0.02	0.35	0.02	1.33E-13	9.60E-15	4.37E-13	1.02E-02
258	SLLL	1.22	0.07	0.92	0.28	0.03	0.07	0.17	0.02	0.39	0.02	1.40E-11	6.06E-13	5.08E-12	1.01E-02
259	SLLL	1.72	0.08	1.51	0.29	-0.01	0.07	0.26	0.02	0.63	0.03	1.23E-11	3.82E-13	5.27E-12	1.10E-02
260	SLLL	0.92	0.07	6.26	0.40	0.56	0.09	0.24	0.02	0.37	0.02	8.50E-14	7.33E-15	7.50E-13	1.05E-02

Table A.5 (cont'd)

Num.	module	EW10	σ_{EW10}	EW20	σ_{EW20}	EW33	σ_{EW33}	$F_{11.3}$	$\sigma_{F_{11.3}}$	$F_{9.8}$	$\sigma_{F_{9.8}}$	F10	σ_{F10}	F20	σ_{F20}
261	SLLL	-0.36	0.05	1.49	0.29	0.10	0.07	-0.04	0.01	-0.12	0.01	-5.56E-12	7.64E-13	5.44E-12	8.36E-03
262	SLLL	2.69	0.09	2.00	0.30	0.07	0.07	0.44	0.02	0.91	0.03	1.93E-11	3.93E-13	5.06E-12	1.27E-02
263	SLLL	2.33	0.08	1.79	0.29	0.14	0.08	0.39	0.02	0.67	0.03	1.15E-12	4.38E-14	3.92E-13	1.29E-02
264	SLLL	1.75	0.08	1.82	0.30	0.13	0.08	0.28	0.02	0.57	0.02	2.42E-12	7.62E-14	9.61E-13	1.08E-02
265	SLLL	1.93	0.08	2.29	0.30	0.18	0.08	0.30	0.02	0.58	0.02	1.36E-12	4.00E-14	6.58E-13	1.16E-02
266	SLLL	3.16	0.09	2.22	0.30	0.00	0.07	0.42	0.02	1.01	0.03	1.14E-10	1.97E-12	5.76E-11	1.26E-02
267	SLLL	4.09	0.10	3.95	0.34	0.22	0.08	0.62	0.03	1.43	0.04	1.20E-11	1.61E-13	3.57E-12	1.47E-02
268	SLLL	1.77	0.08	1.64	0.29	0.21	0.08	0.31	0.02	0.54	0.02	9.95E-12	3.07E-13	3.27E-12	1.17E-02
269	SLLL	1.46	0.07	2.40	0.31	0.04	0.07	0.31	0.02	0.49	0.02	9.33E-12	3.67E-13	6.00E-12	1.15E-02
270	SLLL	0.73	0.06	4.42	0.35	-0.06	0.07	0.32	0.02	0.02	0.02	4.00E-13	5.88E-14	1.39E-12	1.15E-02
271	SLLL	3.51	0.10	4.97	0.37	0.32	0.08	0.63	0.03	0.96	0.03	3.92E-13	8.15E-15	1.45E-12	1.44E-02
272	SLLL	1.13	0.07	2.16	0.30	-0.02	0.07	0.18	0.02	0.33	0.02	7.20E-13	3.52E-14	5.73E-13	9.99E-03
273	SLLL	3.94	0.10	1.59	0.29	0.15	0.08	0.70	0.03	1.33	0.04	3.34E-12	5.10E-14	4.80E-13	1.59E-02
274	SLLL	0.64	0.06	3.23	0.33	-0.48	0.06	0.09	0.02	0.27	0.02	6.53E-13	5.54E-14	1.16E-12	9.59E-03
275	SLLL	2.50	0.08	2.85	0.32	0.35	0.08	0.49	0.02	0.70	0.03	1.83E-12	4.39E-14	2.99E-12	1.36E-02
276	SLLL	1.28	0.07	2.68	0.31	0.05	0.07	0.20	0.02	0.47	0.02	1.05E-11	4.49E-13	7.62E-12	1.04E-02
277	SLLL	2.02	0.08	1.95	0.30	0.10	0.07	0.30	0.02	0.69	0.03	1.97E-11	5.20E-13	8.26E-12	1.15E-02
278	SLLL	2.63	0.09	2.46	0.31	0.01	0.07	0.48	0.02	0.93	0.03	2.15E-12	5.28E-14	8.18E-13	1.33E-02
279	SLLL	3.38	0.10	2.65	0.31	0.34	0.08	0.62	0.03	1.19	0.03	2.58E-12	4.94E-14	2.37E-12	1.40E-02
280	SLLL	3.24	0.09	1.81	0.29	0.16	0.07	0.68	0.03	1.00	0.03	1.82E-11	3.06E-13	5.78E-12	1.44E-02
281	SLLL	2.44	0.08	3.03	0.32	0.06	0.07	0.44	0.02	0.82	0.03	2.19E-12	5.29E-14	1.05E-12	1.29E-02
282	SLLL	1.25	0.07	1.11	0.28	0.13	0.07	0.26	0.02	0.35	0.02	2.60E-11	1.13E-12	8.06E-12	1.10E-02
283	SLLL	0.88	0.07	3.61	0.33	0.29	0.08	0.29	0.02	0.23	0.02	5.72E-14	5.97E-15	2.75E-13	1.21E-02
284	SLLL	4.02	0.10	4.23	0.34	0.33	0.08	0.66	0.03	1.37	0.04	3.24E-12	4.84E-14	1.34E-12	1.45E-02
285	SLLL	2.96	0.09	2.30	0.30	0.74	0.09	0.51	0.02	0.92	0.03	5.24E-12	9.95E-14	1.46E-12	1.34E-02
286	SLLL	1.65	0.07	3.01	0.33	0.39	0.08	0.27	0.02	0.37	0.02	7.52E-13	2.96E-14	4.06E-13	1.12E-02
287	SLLL	3.84	0.10	3.05	0.32	-0.20	0.07	0.68	0.03	1.32	0.04	1.48E-12	2.88E-14	6.41E-13	1.52E-02

Table A.5 (cont'd)

Num.	module	EW10	σ_{EW10}	EW20	σ_{EW20}	EW33	σ_{EW33}	$F_{11.3}$	$\sigma_{F_{11.3}}$	$F_{9.8}$	$\sigma_{F_{9.8}}$	F10	σ_{F10}	F20	σ_{F20}
288	SLLL	3.86	0.10	1.94	0.30	-0.28	0.07	0.62	0.03	1.36	0.04	2.18E-12	3.73E-14	4.65E-13	1.54E-02
289	SLLL	2.52	0.08	2.78	0.31	0.05	0.07	0.44	0.02	0.84	0.03	1.54E-11	3.31E-13	1.02E-11	1.26E-02
290	SLLL	4.42	0.11	2.76	0.31	-0.03	0.07	0.75	0.03	1.55	0.04	4.14E-12	6.33E-14	1.80E-12	1.49E-02
291	SLLL	6.99	0.14	3.57	0.34	0.17	0.08	1.31	0.04	2.38	0.05	6.41E-13	9.51E-15	7.50E-13	2.11E-02
292	SLLL	2.09	0.08	2.23	0.31	0.17	0.08	0.36	0.02	0.74	0.03	1.75E-12	5.11E-14	5.29E-13	1.20E-02
293	SLLL	3.17	0.09	2.98	0.32	0.18	0.08	0.46	0.02	1.19	0.04	1.37E-12	2.60E-14	6.46E-13	1.26E-02
294	SLLL	2.31	0.08	6.54	0.39	0.06	0.07	0.40	0.02	0.82	0.03	1.18E-12	3.67E-14	3.16E-12	1.25E-02
295	SLLL	3.16	0.09	2.34	0.30	0.27	0.08	0.53	0.02	0.91	0.03	2.13E-11	3.64E-13	4.42E-12	1.35E-02
296	SLLL	0.42	0.06	0.19	0.26	-0.02	0.07	0.03	0.01	0.11	0.02	1.33E-10	1.58E-11	2.12E-11	8.88E-03
297	SLLL	3.57	0.10	5.16	0.37	0.15	0.07	0.72	0.03	1.22	0.04	4.98E-13	8.32E-15	6.24E-13	1.45E-02
298	SLLL	3.22	0.09	2.73	0.31	0.37	0.08	0.62	0.03	0.92	0.03	1.16E-11	2.07E-13	2.40E-12	1.54E-02
299	SLLL	3.18	0.09	2.27	0.30	0.00	0.08	0.44	0.02	1.17	0.03	1.55E-12	3.10E-14	5.10E-13	1.31E-02
300	SLLL	1.61	0.07	5.04	0.37	0.04	0.07	0.25	0.02	0.54	0.02	1.25E-12	4.36E-14	1.52E-12	1.06E-02
301	SLLL	4.42	0.11	3.87	0.33	0.32	0.08	0.75	0.03	1.51	0.04	1.55E-12	2.29E-14	7.39E-13	1.56E-02
302	SLLL	1.77	0.08	6.86	0.41	0.28	0.08	0.59	0.02	0.23	0.02	1.06E-13	6.22E-15	8.81E-13	1.53E-02
303	SLLL	1.05	0.07	2.78	0.32	0.30	0.08	0.20	0.02	0.37	0.02	1.32E-13	8.03E-15	5.66E-13	1.04E-02

B Appendix to Chapter 4

B.1 Consideration of $\dot{M}$ and $\dot{M}_W$ from XPE

To ponder the mass dissipation through $\dot{M}$ and/or the expected mass loss rate ($\dot{M}_W$), we overlay ($\dot{M}_W$) by XPE (Owen et al., 2012) on the observed mass accretion rate of TDs in Figure B.1. The plus and cross data points in Figure B.1 are the estimated $\dot{M}_W$ of each TD with its $M_\star$ and L_X as the input condition of $\dot{M}_W$. The estimated $\dot{M}_W$ have higher values than the mass accretion rates for most targets with high L_X and high $\dot{M}$. However, $\dot{M}_W$ is weaker comparing $\dot{M}$ of CTTS indicated as the gray dashed line. From this, we may raise the question of when $\dot{M}_W$ overcomes $\dot{M}$ to create a gap/hole like in TDs. The $\dot{M}$ of TDs is not the $\dot{M}$ when $\dot{M}_W$ is able to open a gap. However, the estimated $\dot{M}_W$ are not very different whether for radially continuous disks (plus sign) or disks with a large inner hole (cross sign). If we assume that each TD should have followed the gray dashed line for their initial $\dot{M}$–L_X relation before they became TDs, their initial $\dot{M}$ must have been greater than the theoretical $\dot{M}_W$. And the current $\dot{M}$ of TDs are much lower than the theoretical $\dot{M}_W$

of TDs. Some possible scenarios might explain these inconsistencies: (1) the TDs in our sample have already evolved much after gap opening, and they have lost much inner material to accrete to the central star; (2) there could be some other contribution (e.g. planets) to make the mass accretion rate decrease quickly, such as intercepting disk material on the way to the central star while $\dot{M}_W$ forces material to drift away outward.

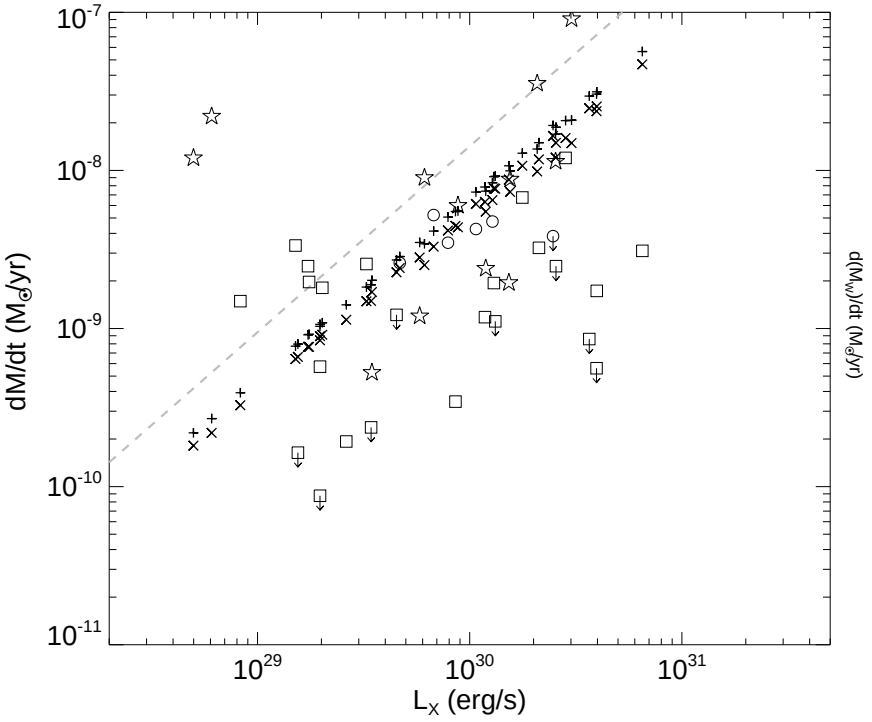


Figure B.1 Comparison of $\dot{M}$ vs. L_X of transitional disks to M_W vs. L_X expected by the X-ray photoevaporation model (Owen et al., 2012). The plus signs are for the expected X-ray photoevaporation wind rates in case of a radially continuous primordial disk with TDs $M_\star$ and L_X, and the cross signs are for that in case of transitional disks with inner hole. The squares, circles, and stars are CTDs, WTDs, and PTDs of our sample. The gray dashed line indicate the expected $\dot{M}$-L_X of CTTS, which is derived from $\dot{M}$-$M_\star$ and $L_\star$-$M_\star$ of CTTS in Figure 4.13. Detail discussion is in Appendix B.

B.2 Trends of TDs in Orion A

We examine trends for the sample of TDs in Orion A and the linear correlations of any two properties in $\log - \log$ scale are listed in Tables B.1 and Table B.2. Comparing trends in Table B.1 and Table 4.4 before separating by subtypes of TDs, the trends of TDs in Orion A generally agree within 1σ uncertainties with the trends of the full sample of TDs not only from Orion A but also from Tau, ChaI, Oph, and N1333, despite L_X and $M_\star$ of TDs in Orion A tend to distribute toward lower values than that of other region. The trends of subtypes of TDs of Orion A in Table B.2 are also not very different from that of full samples in Table 4.5, even though uncertainties of the results from linear regression are larger due to smaller sample sizes for some correlations. We will discuss difference/similarity of properties of TDs and Class II objects in Orion A from that in other star-forming regions in Chapter 5.

Table B.1. Correlation summary III: TDs in Orion A

Correlation	N	α	β	$corr$[a]	P[b](%)	P_{range}[c](%)
$\dot{M}$ vs. $M_\star/M_\odot$	49	-8.5 ± 0.2	1.7 ± 0.5	0.5 ± 0.1	0.03	$\ll$ 0.001-0.4
L_X vs. $M_\star/M_\odot$	33	30.2 ± 0.1	1.0 ± 0.3	0.5 ± 0.2	0.3	0.02-9
$\dot{M}$ vs. L_X	32	-19.0 ± 10.6	0.3 ± 0.4	0.2 ± 0.2	27	0.4-100
$M_\star/M_\odot$ vs. R_{wall}	55	-1.1 ± 0.1	0.7 ± 0.1	0.8 ± 0.1	$\ll$ 0.001	$\ll$ 0.001
$\dot{M}$ vs. R_{wall}	49	-10.2 ± 0.5	1.1 ± 0.5	0.4 ± 0.2	0.4	$\ll$ 0.001-17
L_X vs. R_{wall}	35	28.8 ± 0.3	1.0 ± 0.3	0.6 ± 0.1	0.01	$\ll$ 0.001-1.7
$\dot{M}/\dot{M}[M_\star, R_w]$ vs. R_{wall}	49	0.1 ± 0.4	-0.8 ± 0.3	-0.4 ± 0.2	0.4	$\ll$ 0.001-17
$L_X/L_X[M_\star, R_w]$ vs. R_{wall}	35	0.3 ± 0.3	-0.3 ± 0.3	-0.2 ± 0.2	25	1.8-100
$\dot{M}/\dot{M}[L_X]$ vs. L_X	32	25.9 ± 7.4	-0.9 ± 0.2	-0.6 ± 0.1	0.03	$\ll$ 0.001-0.44
$L_\star$ vs. $M_\star$	55	0.4 ± 0.1	1.8 ± 0.2	0.9 ± 0.1	$\ll$ 0.001	$\ll$ 0.001
$L_\star/L_\odot$ vs. R_{wall}	55	-1.9 ± 0.1	1.6 ± 0.1	1.0 ± 0.0	$\ll$ 0.001	$\ll$ 0.001
L_X vs. $L_\star/L_\odot$	35	30.0 ± 0.1	0.6 ± 0.1	0.6 ± 0.1	0.01	$\ll$ 0.001-0.2
$L_X/L_\star$ vs. $M_\star/M_\odot$	33	-3.8 ± 0.1	-0.8 ± 0.3	-0.5 ± 0.2	0.3	0.02-9
$\dot{M}$ vs. $L_\star/L_\odot$	49	-8.8 ± 0.1	1.0 ± 0.2	0.6 ± 0.1	$\ll$ 0.001	$\ll$ 0.001-0.03
$\dot{M}$ vs. $L_X/L_\star$	30	-10.9 ± 1.4	-0.5 ± 0.4	-0.3 ± 0.2	11	0.05-60

Note. — Summary of the results from the Bayesian linear regression between X and Y: Y vs. X; $logY = \alpha + \beta logX$. Objects has a known spectral type and in Orion A are only included for the correlations.
The index [a,b,] and [c] have the same meanings in Table **??**.

Table B.2. Correlation summary IV: details by subtypes of TDs in Orion A

Correlation	TD type	N	α	β	$corr$[a]	P[b](%)	P_{range}[c](%)
$\dot{M}$ vs. $M_\star/M_\odot$	CTD	29	-8.9 ± 0.5	1.0 ± 1.3	0.2 ± 0.3	25	0.6-100
	WTD+PTD	20	-8.1 ± 0.3	2.5 ± 0.7	0.7 ± 0.2	0.002	$\ll$ 0.001-0.06
L_X vs. $M_\star/M_\odot$	CTD	24	30.3 ± 0.2	1.4 ± 0.6	0.5 ± 0.2	1.3	0.01-15
	WTD+PTD	11	30.2 ± 0.1	0.5 ± 0.3	0.5 ± 0.3	12	0.02-56
$\dot{M}$ vs. R_{wall}	CTD	29	-9.2 ± 0.7	0.0 ± 0.7	0.0 ± 0.3	92	14-100
	WTD+PTD	20	-10.9 ± 0.8	1.9 ± 0.7	0.7 ± 0.2	0.06	$\ll$ 0.001-2.5
$\dot{M}/\dot{M}(M_\star)$ vs. R_{wall}	CTD	29	0.7 ± 0.7	-1.7 ± 0.7	-0.6 ± 0.2	0.06	$\ll$ 0.001-3.2
	WTD+PTD	20	-1.0 ± 0.8	0.2 ± 0.7	0.1 ± 0.3	67	8 - 100
L_X vs. R_{wall}	CTD	24	28.6 ± 0.4	1.1 ± 0.4	0.6 ± 0.2	0.2	$\ll$ 0.001-5.3
	WTD+PTD	11	29.6 ± 0.5	0.4 ± 0.4	0.4 ± 0.4	22	0.3-100
$L_X/L_X(M_\star)$ vs. R_{wall}	CTD	24	0.2 ± 0.4	-0.2 ± 0.4	-0.1 ± 0.2	64	5.1 - 100
	WTD+PTD	11	1.2 ± 0.6	-0.9 ± 0.5	-0.7 ± 0.3	1.6	0.02-22
$\dot{M}$ vs. L_X	CTD	22	-6.8 ± 10.9	-0.1 ± 0.4	0.0 ± 0.3	83	17-100
	WTD+PTD	10	-46.5 ± 31.1	1.3 ± 1.0	0.6 ± 0.4	6.7	0.04-58
$\dot{M}/\dot{M}(L_X)$ vs. L_X	CTD	22	36.0 ± 9.8	-1.2 ± 0.3	-0.7 ± 0.2	0.03	$\ll$ 0.001-0.3
	WTD+PTD	10	-0.9 ± 29.0	0.0 ± 1.0	0.0 ± 0.5	91	14-100
$M_\star/M_\odot$ vs. R_{wall}	CTD	33	-1.0 ± 0.1	0.6 ± 0.1	0.8 ± 0.1	$\ll$ 0.001	$\ll$ 0.001
	WTD+PTD	22	-1.1 ± 0.2	0.8 ± 0.2	0.8 ± 0.1	$\ll$ 0.001	$\ll$ 0.001-0.03
$\dot{M}$ vs. $L_\star/L_\odot$	CTD	29	-9.1 ± 0.2	0.1 ± 0.4	0.1 ± 0.3	61	11.4 - 100
	WTD+PTD	20	-8.7 ± 0.2	1.4 ± 0.3	0.8 ± 0.1	0.002	$\ll$ 0.001-0.06
L_X vs. $L_\star/L_\odot$	CTD	24	30.0 ± 0.1	0.6 ± 0.2	0.6 ± 0.2	0.2	$\ll$ 0.001-5.3
	WTD+PTD	11	30.1 ± 0.1	0.4 ± 0.2	0.6 ± 0.3	5.1	0.3-37

Note. — Summary of the results from the Bayesian linear regression between X and Y: Y vs. X; $logY = \alpha + \beta logX$. Objects has a known spectral type and in Orion A are only included for the correlations. The index ^{a,b,} and ^{d} have the same meanings in Table **??**.

C Appendix to Chapter 5

C.1 Trends

To each figure corresponds a table on the following page. Tables with indication of (I) are for correlations measured with data from all objects regardless the availability of their spectral type information. Tables with indication of (II) are for correlations measured with data from the objects having reliable spectral type information.

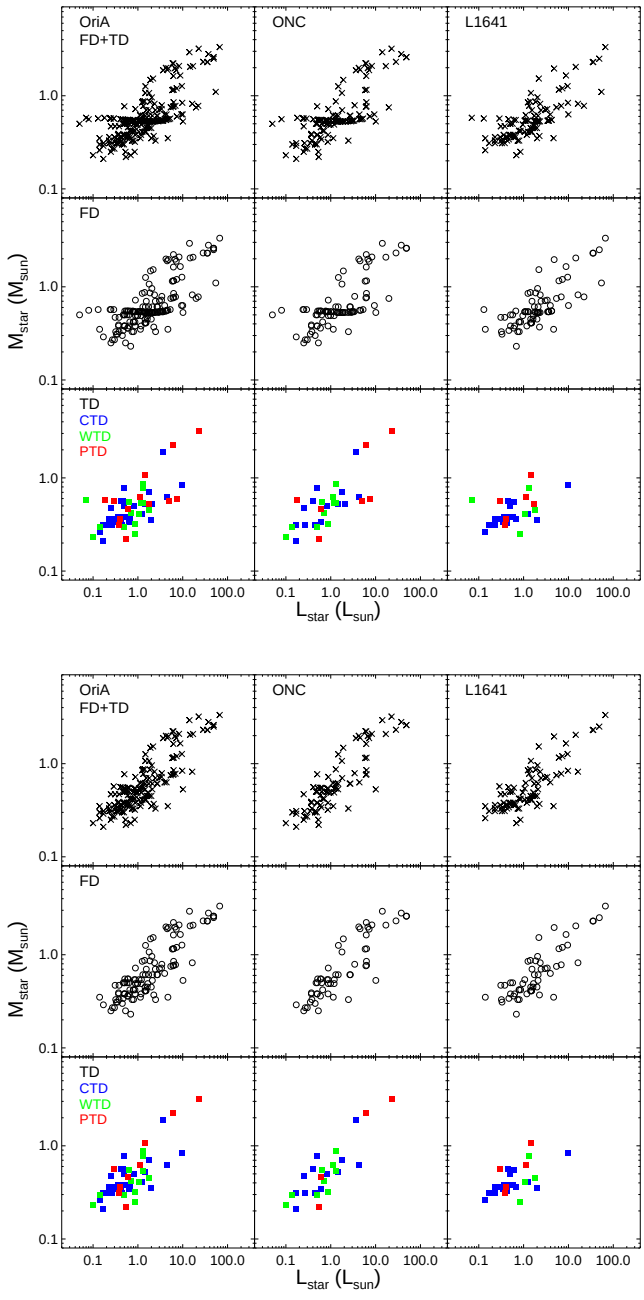


Figure C.1 $M_\star$ vs. $L_\star$. Upper panel: all available objects; Lower panel: objects with available spectral types only

Table C.1 $M_\star$ vs. $L_\star$ (I)

	Ori A				ONC				L1641			
	N	ρ	τ	r	N	ρ	τ	r	N	ρ	τ	r
TDFD	231	0.692	0.524	0.750	122	0.699	0.528	0.756	109	0.697	0.536	0.757
		0.000	0.000	0.000		0.000	0.000	0.000		0.000	0.000	0.000
FD	170	0.697	0.530	0.746	91	0.684	0.519	0.746	79	0.723	0.558	0.767
		0.000	0.000	0.000		0.000	0.000	0.000		0.000	0.000	0.000
TD	61	0.617	0.461	0.690	31	0.711	0.536	0.764	30	0.484	0.384	0.489
		0.000	0.000	0.000		0.000	0.000	0.000		0.007	0.003	0.006

ρ: Spearsman's ρ
τ: Kendall's τ
r: Pearson's r

Table C.2 $M_\star$ vs. $L_\star$ (II)

	Ori A				ONC				L1641			
	N	ρ	τ	r	N	ρ	τ	r	N	ρ	τ	r
TDFD	168	0.799	0.619	0.847	83	0.857	0.683	0.874	85	0.745	0.577	0.828
		0.000	0.000	0.000		0.000	0.000	0.000		0.000	0.000	0.000
FD	114	0.820	0.646	0.852	57	0.870	0.704	0.874	57	0.769	0.608	0.841
		0.000	0.000	0.000		0.000	0.000	0.000		0.000	0.000	0.000
TD	54	0.684	0.522	0.779	26	0.778	0.608	0.856	28	0.590	0.469	0.609
		0.000	0.000	0.000		0.000	0.000	0.000		0.001	0.000	0.001

ρ: Spearsman's ρ
τ: Kendall's τ
r: Pearson's r

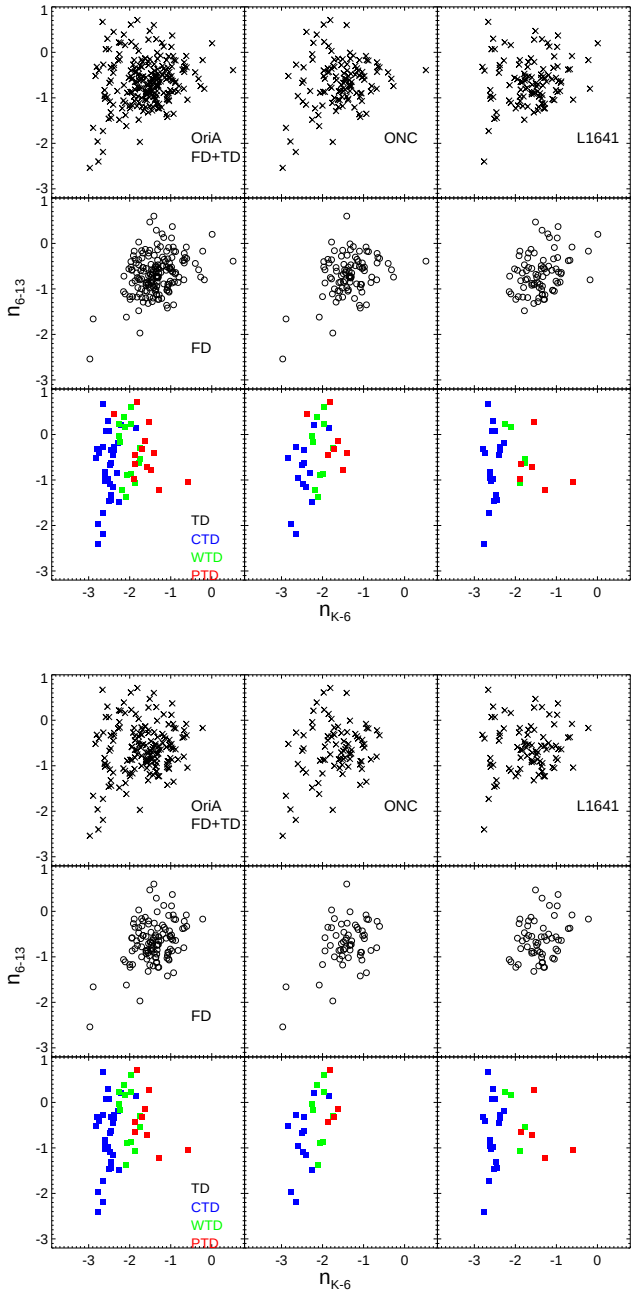


Figure C.2 n_{K-6} vs. n_{6-13}. Upper panel: all available objects; Lower panel: objects with available spectral types only

Table C.3 n_{K-6} vs. n_{6-13} (I)

	Ori A				ONC				L1641			
	N	ρ	τ	r	N	ρ	τ	r	N	ρ	τ	r
TDFD	231	0.111	0.080	0.166	122	0.118	0.086	0.197	109	0.101	0.071	0.131
		0.091	0.069	0.012		0.196	0.161	0.030		0.298	0.272	0.175
FD	170	0.266	0.181	0.353	91	0.247	0.172	0.380	79	0.274	0.184	0.323
		0.000	0.000	0.000		0.018	0.016	0.000		0.014	0.017	0.004
TD	61	0.200	0.145	0.167	31	0.406	0.265	0.393	30	0.035	0.030	-0.013
		0.122	0.099	0.198		0.023	0.036	0.029		0.855	0.816	0.946

ρ: Spearsman's ρ
τ: Kendall's τ
r: Pearson's r

Table C.4 n_{K-6} vs. n_{6-13} (II)

	Ori A				ONC				L1641			
	N	ρ	τ	r	N	ρ	τ	r	N	ρ	τ	r
TDFD	168	0.089	0.063	0.172	83	0.128	0.092	0.241	85	0.060	0.038	0.103
		0.251	0.226	0.026		0.249	0.216	0.028		0.586	0.604	0.348
FD	114	0.240	0.165	0.385	57	0.272	0.200	0.467	57	0.217	0.137	0.275
		0.010	0.009	0.000		0.040	0.028	0.000		0.105	0.133	0.038
TD	54	0.261	0.194	0.205	26	0.545	0.380	0.532	28	0.068	0.053	-0.002
		0.057	0.039	0.137		0.004	0.007	0.005		0.729	0.691	0.992

ρ: Spearsman's ρ
τ: Kendall's τ
r: Pearson's r

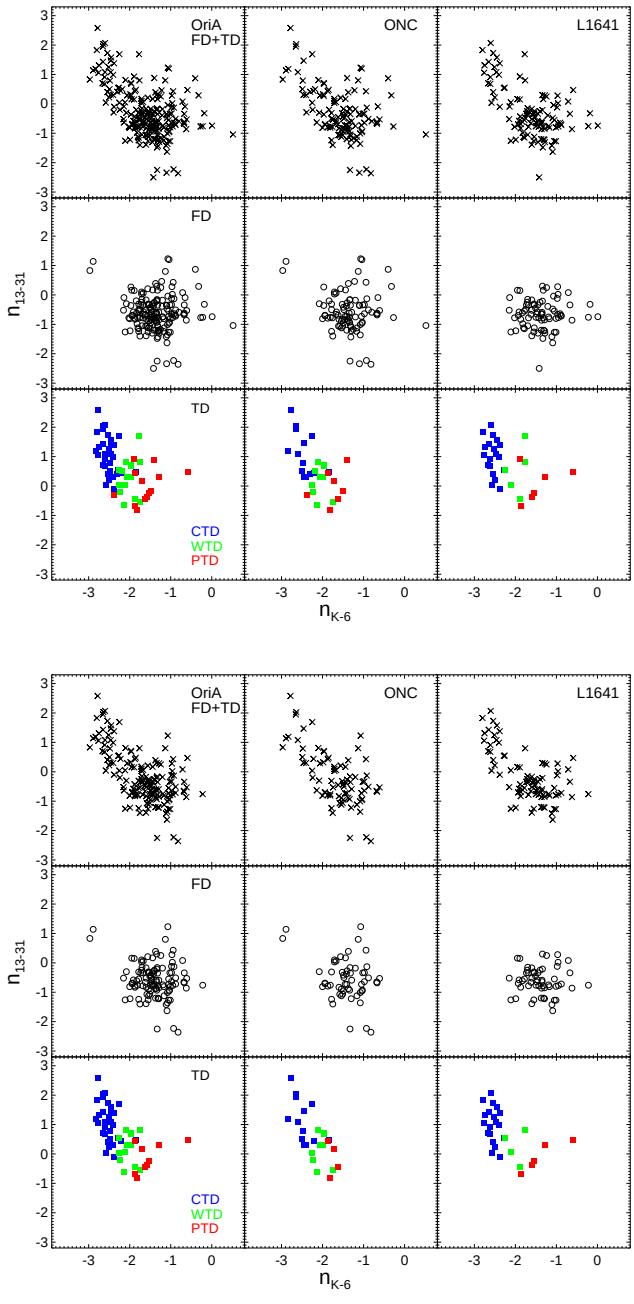


Figure C.3 n_{K-6} vs. n_{13-31}. Upper panel: all available objects; Lower panel: objects with available spectral types only

Table C.5 n_{K-6} vs. n_{13-31} (I)

	Ori A				ONC				L1641			
	N	ρ	τ	r	N	ρ	τ	r	N	ρ	τ	r
TDFD	231	-0.444	-0.311	-0.528	122	-0.424	-0.311	-0.503	109	-0.461	-0.318	-0.559
		0.000	0.000	0.000		0.000	0.000	0.000		0.000	0.000	0.000
FD	170	-0.013	-0.013	-0.076	91	-0.035	-0.037	-0.143	79	0.003	0.001	0.035
		0.863	0.802	0.325		0.740	0.605	0.176		0.977	0.990	0.759
TD	61	-0.577	-0.390	-0.504	31	-0.548	-0.384	-0.585	30	-0.512	-0.360	-0.449
		0.000	0.000	0.000		0.001	0.002	0.001		0.004	0.005	0.013

ρ: Spearsman's ρ
τ: Kendall's τ
r: Pearson's r

Table C.6 n_{K-6} vs. n_{13-31} (II)

	Ori A				ONC				L1641			
	N	ρ	τ	r	N	ρ	τ	r	N	ρ	τ	r
TDFD	168	-0.552	-0.391	-0.637	83	-0.543	-0.393	-0.634	85	-0.560	-0.399	-0.645
		0.000	0.000	0.000		0.000	0.000	0.000		0.000	0.000	0.000
FD	114	-0.090	-0.059	-0.201	57	-0.089	-0.063	-0.297	57	-0.102	-0.073	-0.032
		0.343	0.349	0.032		0.511	0.489	0.025		0.450	0.424	0.813
TD	54	-0.668	-0.461	-0.582	26	-0.677	-0.497	-0.705	28	-0.610	-0.428	-0.528
		0.000	0.000	0.000		0.000	0.000	0.000		0.001	0.001	0.004

ρ: Spearsman's ρ
τ: Kendall's τ
r: Pearson's r

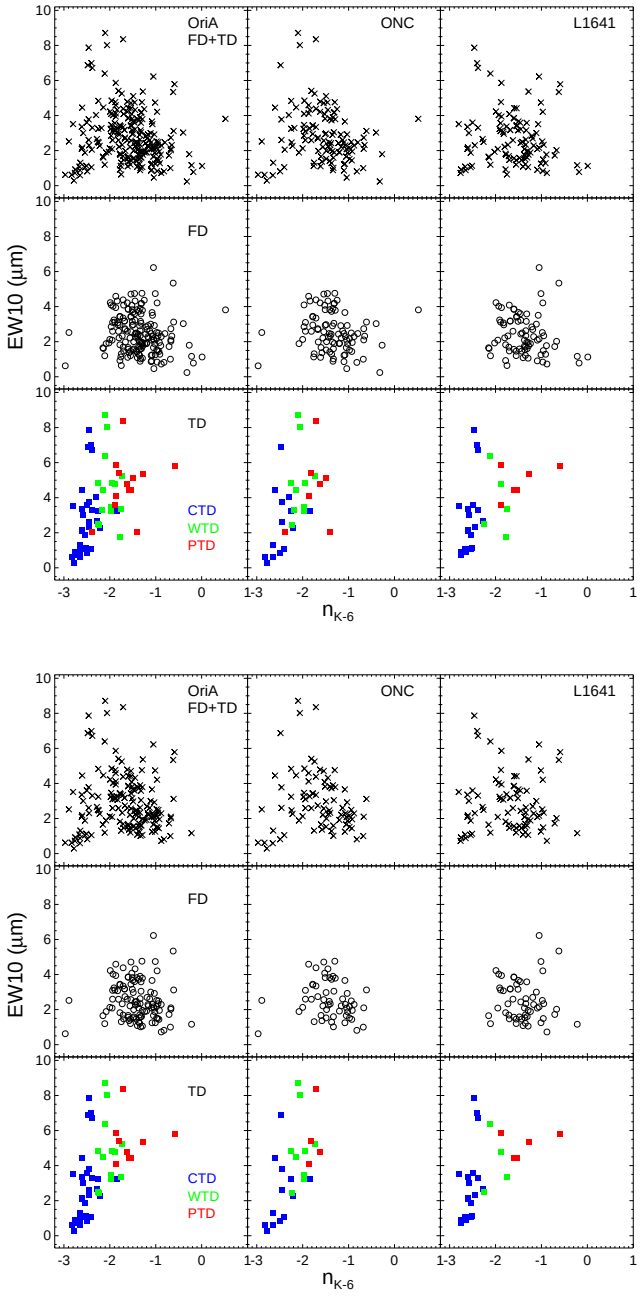


Figure C.4 n_{K-6} vs. EW10μm. Upper panel: all available objects; Lower panel: objects with available spectral types only

Table C.7 n_{K-6} vs. EW10μm (I)

	Ori A				ONC				L1641			
	N	ρ	τ	r	N	ρ	τ	r	N	ρ	τ	r
TDFD	231	-0.158	-0.116	-0.134	122	-0.225	-0.158	-0.154	109	-0.112	-0.087	-0.119
		0.016	0.008	0.042		0.013	0.010	0.090		0.245	0.182	0.218
FD	170	-0.199	-0.136	-0.131	91	-0.243	-0.158	-0.131	79	-0.176	-0.129	-0.139
		0.009	0.008	0.089		0.020	0.027	0.216		0.120	0.092	0.222
TD	61	0.582	0.425	0.469	31	0.572	0.430	0.492	30	0.601	0.420	0.463
		0.000	0.000	0.000		0.001	0.001	0.005		0.000	0.001	0.010

ρ: Spearsmans ρ
τ: Kendalls τ
r: Pearsons r

Table C.8 n_{K-6} vs. EW10μm (II)

	Ori A				ONC				L1641			
	N	ρ	τ	r	N	ρ	τ	r	N	ρ	τ	r
TDFD	168	-0.088	-0.073	-0.073	83	-0.167	-0.134	-0.112	85	-0.022	-0.024	-0.037
		0.258	0.160	0.347		0.130	0.073	0.313		0.843	0.749	0.737
FD	114	-0.180	-0.124	-0.081	57	-0.245	-0.166	-0.111	57	-0.125	-0.096	-0.050
		0.055	0.051	0.392		0.066	0.068	0.411		0.354	0.294	0.712
TD	54	0.656	0.474	0.529	26	0.647	0.482	0.602	28	0.661	0.459	0.507
		0.000	0.000	0.000		0.000	0.001	0.001		0.000	0.001	0.006

ρ: Spearsman's ρ
τ: Kendall's τ
r: Pearson's r

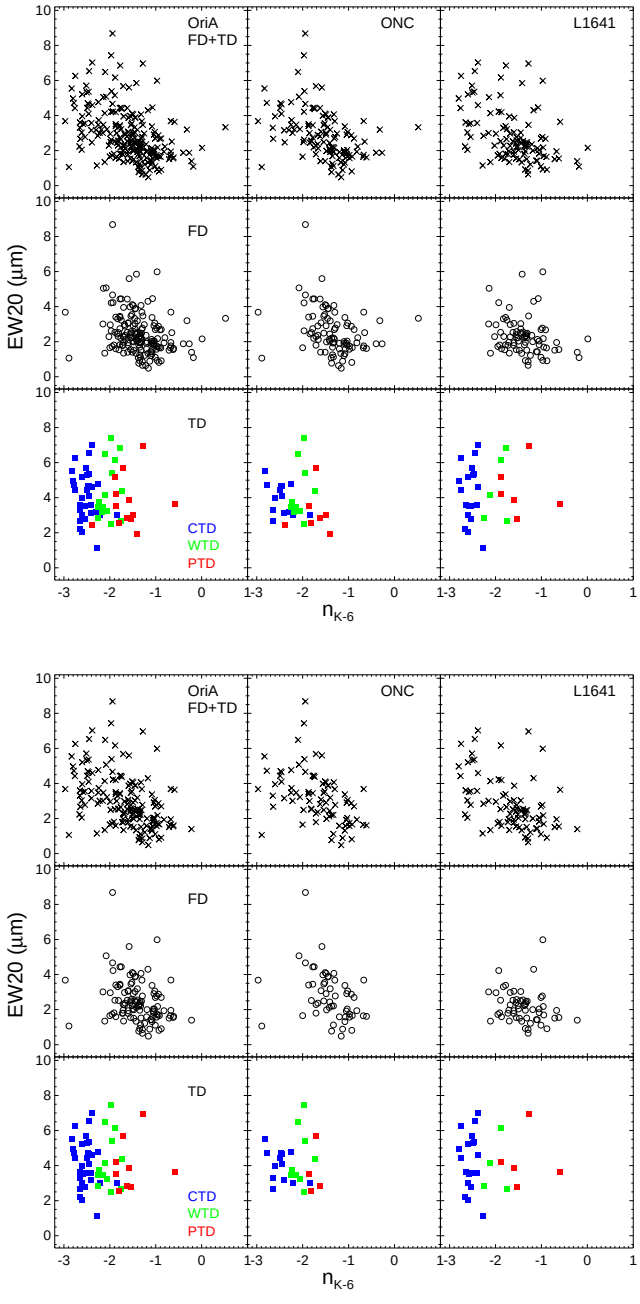


Figure C.5 n_{K-6} vs. $EW20(\mu\mathrm{m})$.Upper panel: all available objects; Lower panel: objects with available spectral types only

Table C.9 n_{K-6} vs. $EW20(\mu\text{m})$ (I)

	Ori A				ONC				L1641			
	N	ρ	τ	r	N	ρ	τ	r	N	ρ	τ	r
TDFD	231	-0.496	-0.346	-0.393	122	-0.534	-0.368	-0.346	109	-0.467	-0.328	-0.457
		0.000	0.000	0.000		0.000	0.000	0.000		0.000	0.000	0.000
FD	170	-0.308	-0.210	-0.205	91	-0.377	-0.255	-0.211	79	-0.271	-0.185	-0.225
		0.000	0.000	0.007		0.000	0.000	0.045		0.016	0.016	0.046
TD	61	-0.082	-0.056	-0.038	31	-0.250	-0.183	-0.182	30	0.098	0.078	0.066
		0.528	0.520	0.771		0.175	0.148	0.327		0.606	0.543	0.729

ρ: Spearsman's ρ
τ: Kendall's τ
r: Pearson's r

Table C.10 n_{K-6} vs. $EW20(\mu\text{m})$ (II)

	Ori A				ONC				L1641			
	N	ρ	τ	r	N	ρ	τ	r	N	ρ	τ	r
TDFD	168	-0.507	-0.356	-0.396	83	-0.528	-0.368	-0.331	85	-0.501	-0.358	-0.491
		0.000	0.000	0.000		0.000	0.000	0.002		0.000	0.000	0.000
FD	114	-0.328	-0.220	-0.209	57	-0.445	-0.306	-0.233	57	-0.282	-0.194	-0.187
		0.000	0.001	0.026		0.001	0.001	0.081		0.033	0.033	0.164
TD	54	-0.064	-0.045	-0.021	26	-0.152	-0.127	-0.058	28	0.030	0.029	0.001
		0.643	0.632	0.880		0.458	0.365	0.778		0.881	0.827	0.996

ρ: Spearsman's ρ
τ: Kendall's τ
r: Pearson's r

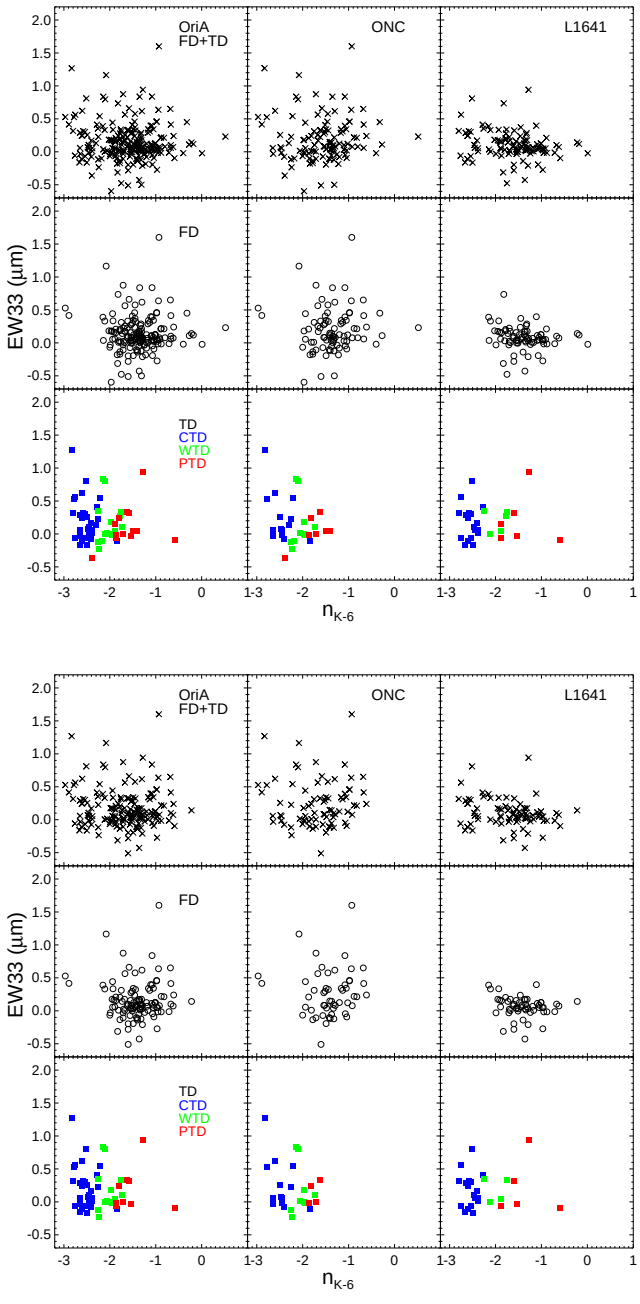


Figure C.6 n_{K-6} vs. $EW33(\mu\mathrm{m})$. Zoomed in. Upper panel: all available objects; Lower panel: objects with available spectral types only

Table C.11 n_{K-6} vs. $EW33(\mu\text{m})$ (I)

	Ori A				ONC				L1641			
	N	ρ	τ	r	N	ρ	τ	r	N	ρ	τ	r
TDFD	231	-0.022	-0.014	0.032	122	0.101	0.070	0.059	109	-0.208	-0.142	-0.053
		0.744	0.754	0.628		0.270	0.256	0.519		0.030	0.028	0.584
FD	170	0.009	0.009	0.075	91	0.122	0.084	0.111	79	-0.185	-0.120	-0.053
		0.902	0.855	0.331		0.249	0.237	0.295		0.102	0.119	0.643
TD	61	-0.102	-0.075	-0.110	31	-0.144	-0.104	-0.270	30	0.047	0.002	0.041
		0.433	0.392	0.399		0.438	0.413	0.142		0.804	0.986	0.830

ρ: Spearsman's ρ
τ: Kendall's τ
r: Pearson's r

Table C.12 n_{K-6} vs. $EW33(\mu\text{m})$ (II)

	Ori A				ONC				L1641			
	N	ρ	τ	r	N	ρ	τ	r	N	ρ	τ	r
TDFD	168	-0.023	-0.014	0.007	83	0.112	0.079	0.034	85	-0.214	-0.149	-0.231
		0.771	0.785	0.928		0.314	0.289	0.760		0.049	0.043	0.033
FD	114	0.059	0.044	0.089	57	0.187	0.138	0.125	57	-0.185	-0.121	-0.150
		0.536	0.488	0.346		0.163	0.131	0.354		0.168	0.184	0.265
TD	54	-0.110	-0.091	-0.107	26	-0.173	-0.148	-0.303	28	0.044	-0.016	0.034
		0.430	0.330	0.441		0.397	0.288	0.132		0.823	0.905	0.864

ρ: Spearsman's ρ
τ: Kendall's τ
r: Pearson's r

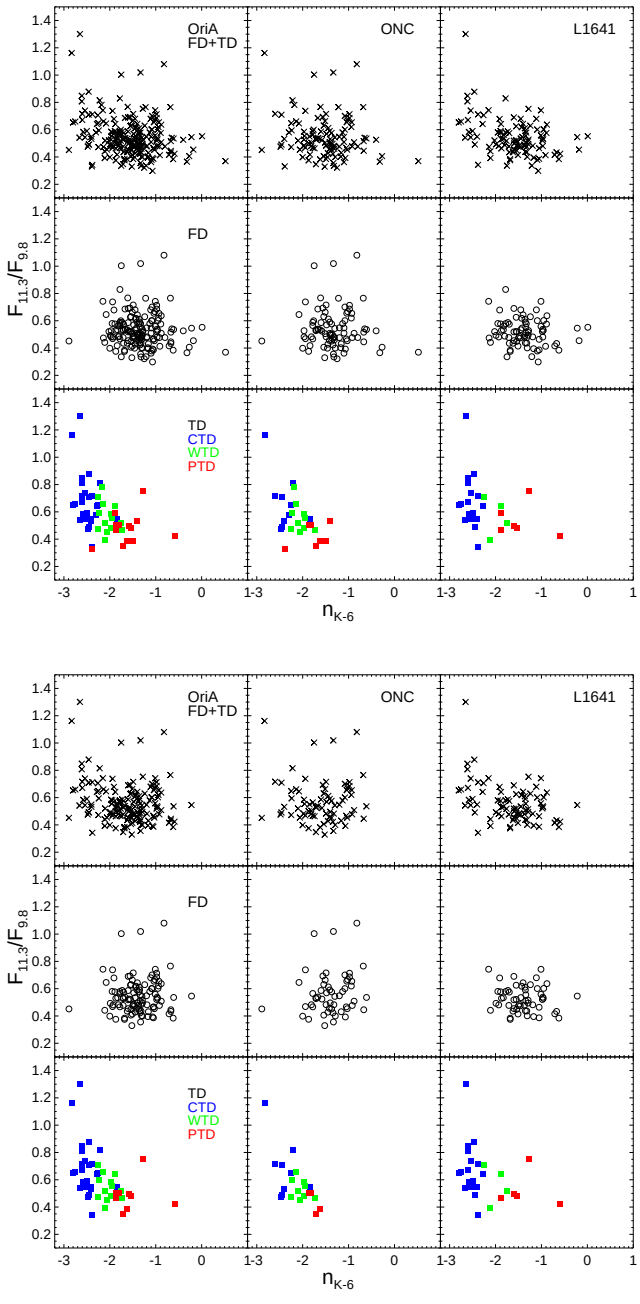


Figure C.7 n_{K-6} vs. $F_{11.3}/F_{9.8}$. Zoomed in. Upper panel: all available objects; Lower panel: objects with available spectral types only

Table C.13 n_{K-6} vs. $F_{11.3}/F_{9.8}$ (I)

	Ori A				ONC				L1641			
	N	ρ	τ	r	N	ρ	τ	r	N	ρ	τ	r
TDFD	231	-0.241	-0.168	-0.144	122	-0.133	-0.092	-0.072	109	-0.369	-0.250	-0.221
		0.000	0.000	0.029		0.145	0.131	0.431		0.000	0.000	0.021
FD	170	-0.096	-0.066	-0.132	91	-0.088	-0.060	-0.156	79	-0.114	-0.071	-0.132
		0.215	0.202	0.086		0.405	0.398	0.140		0.315	0.357	0.246
TD	61	-0.437	-0.316	-0.156	31	-0.321	-0.256	-0.091	30	-0.430	-0.305	-0.200
		0.000	0.000	0.230		0.078	0.043	0.626		0.018	0.018	0.289

ρ: Spearsman's ρ
τ: Kendall's τ
r: Pearson's r

Table C.14 n_{K-6} vs. $F_{11.3}/F_{9.8}$ (II)

	Ori A				ONC				L1641			
	N	ρ	τ	r	N	ρ	τ	r	N	ρ	τ	r
TDFD	168	-0.199	-0.138	-0.145	83	-0.031	-0.015	-0.058	85	-0.375	-0.259	-0.229
		0.010	0.008	0.061		0.779	0.838	0.602		0.000	0.000	0.035
FD	114	0.024	0.016	-0.209	57	0.097	0.077	-0.260	57	-0.066	-0.044	-0.108
		0.799	0.800	0.026		0.471	0.396	0.051		0.628	0.629	0.424
TD	54	-0.502	-0.372	-0.165	26	-0.372	-0.312	-0.102	28	-0.524	-0.369	-0.210
		0.000	0.000	0.233		0.061	0.026	0.620		0.004	0.006	0.283

ρ: Spearsman's ρ
τ: Kendall's τ
r: Pearson's r

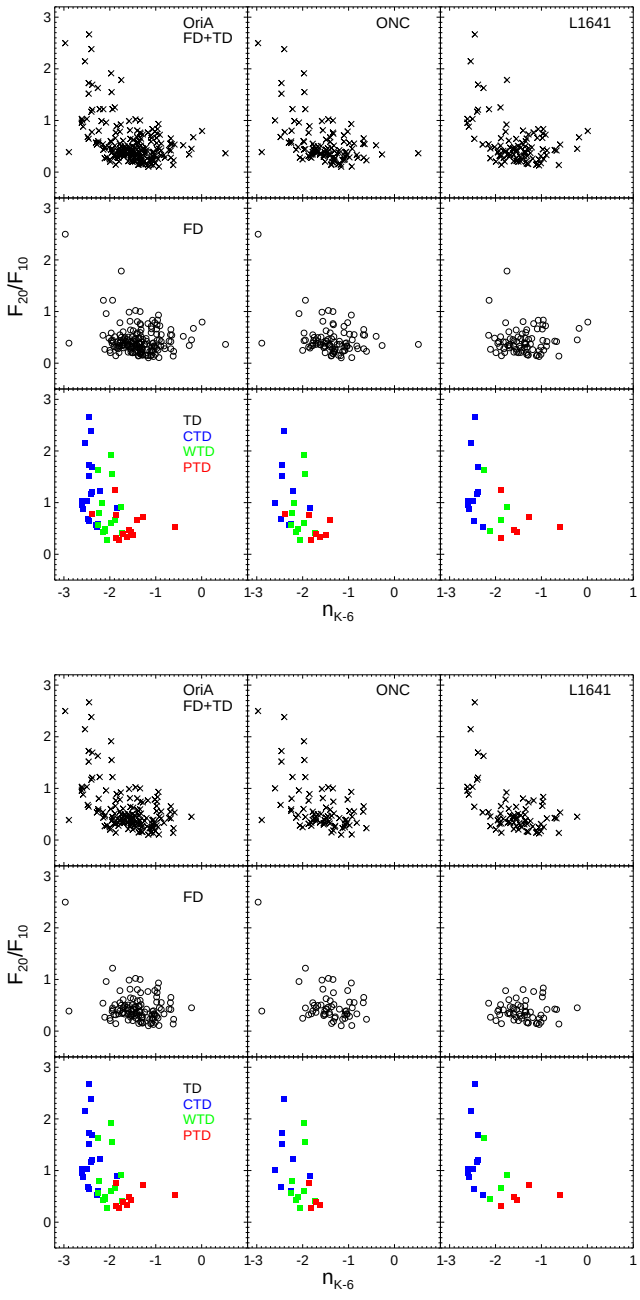


Figure C.8 n_{K-6} vs. F_{20}/F_{10}. Upper panel: all available objects; Lower panel: objects with available spectral types only

Table C.15 n_{K-6} vs. F_{20}/F_{10} (I)

	Ori A				ONC				L1641			
	N	ρ	τ	r	N	ρ	τ	r	N	ρ	τ	r
TDFD	230	-0.416	-0.295	-0.395	121	-0.406	-0.291	-0.302	109	-0.440	-0.302	-0.498
		0.000	0.000	0.000		0.000	0.000	0.001		0.000	0.000	0.000
FD	170	-0.035	-0.030	0.082	91	-0.111	-0.078	0.102	79	0.037	0.019	0.018
		0.650	0.564	0.288		0.296	0.274	0.336		0.749	0.802	0.875
TD	60	-0.693	-0.505	-0.465	30	-0.678	-0.509	-0.591	30	-0.625	-0.452	-0.376
		0.000	0.000	0.000		0.000	0.000	0.001		0.000	0.000	0.041

ρ: Spearsman's ρ
τ: Kendall's τ
r: Pearson's r

Table C.16 n_{K-6} vs. F_{20}/F_{10} (II)

	Ori A				ONC				L1641			
	N	ρ	τ	r	N	ρ	τ	r	N	ρ	τ	r
TDFD	167	-0.539	-0.388	-0.541	82	-0.497	-0.352	-0.494	85	-0.580	-0.418	-0.595
		0.000	0.000	0.000		0.000	0.000	0.000		0.000	0.000	0.000
FD	114	-0.140	-0.100	-0.294	57	-0.196	-0.128	-0.428	57	-0.104	-0.082	-0.023
		0.138	0.116	0.001		0.143	0.161	0.001		0.442	0.369	0.865
TD	53	-0.764	-0.553	-0.543	25	-0.700	-0.535	-0.652	28	-0.747	-0.539	-0.519
		0.000	0.000	0.000		0.000	0.000	0.000		0.000	0.000	0.005

ρ: Spearsman's ρ
τ: Kendall's τ
r: Pearson's r

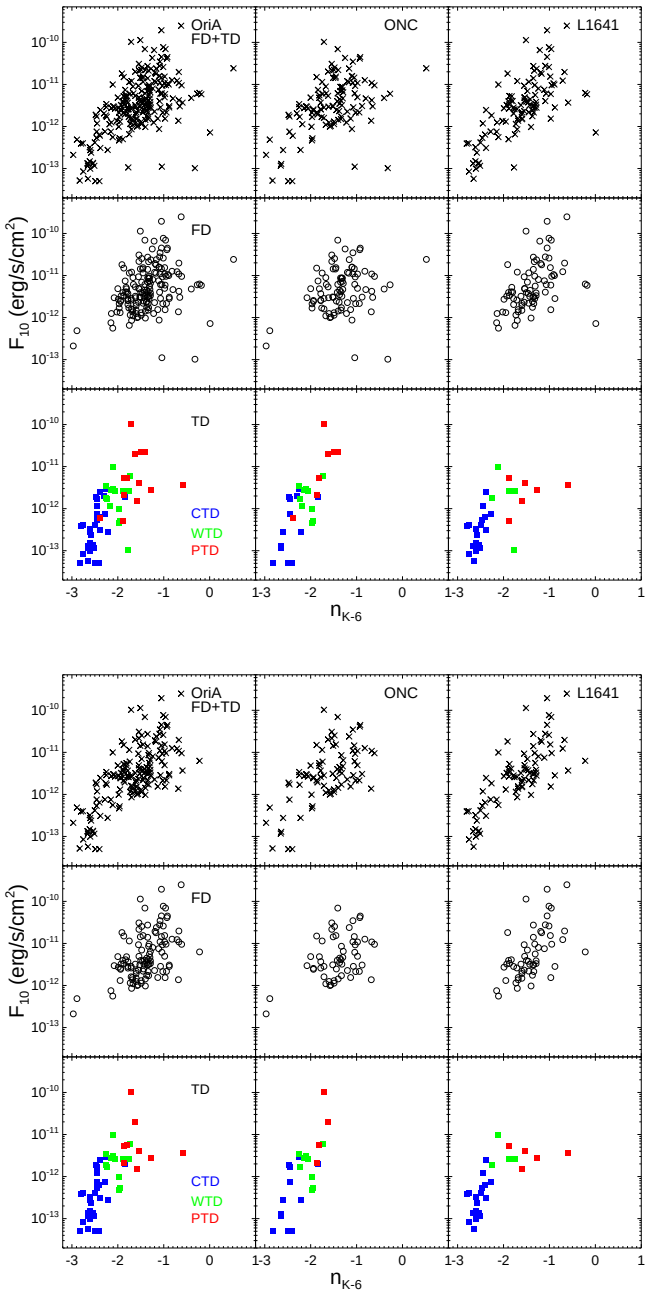


Figure C.9 n_{K-6} vs. $\log F_{10}$. Upper panel: all available objects; Lower panel: objects with available spectral types only

Table C.17 n_{K-6} vs. $\log F_{10}$ (I)

	Ori A				ONC				L1641			
	N	ρ	τ	r	N	ρ	τ	r	N	ρ	τ	r
TDFD	230	0.593	0.428	0.594	121	0.468	0.330	0.491	109	0.715	0.534	0.693
		0.000	0.000	0.000		0.000	0.000	0.000		0.000	0.000	0.000
FD	170	0.389	0.268	0.323	91	0.250	0.171	0.249	79	0.541	0.386	0.427
		0.000	0.000	0.000		0.017	0.016	0.017		0.000	0.000	0.000
TD	60	0.764	0.565	0.686	30	0.750	0.560	0.795	30	0.729	0.549	0.650
		0.000	0.000	0.000		0.000	0.000	0.000		0.000	0.000	0.000

ρ: Spearsman's ρ
τ: Kendall's τ
r: Pearson's r

Table C.18 n_{K-6} vs. $\log F_{10}$ (II)

	Ori A				ONC				L1641			
	N	ρ	τ	r	N	ρ	τ	r	N	ρ	τ	r
TDFD	167	0.671	0.487	0.713	82	0.553	0.392	0.630	85	0.769	0.583	0.779
		0.000	0.000	0.000		0.000	0.000	0.000		0.000	0.000	0.000
FD	114	0.464	0.323	0.503	57	0.325	0.228	0.444	57	0.597	0.430	0.574
		0.000	0.000	0.000		0.014	0.012	0.001		0.000	0.000	0.000
TD	53	0.803	0.589	0.699	25	0.715	0.522	0.755	28	0.829	0.629	0.727
		0.000	0.000	0.000		0.000	0.000	0.000		0.000	0.000	0.000

ρ: Spearsman's ρ
τ: Kendall's τ
r: Pearson's r

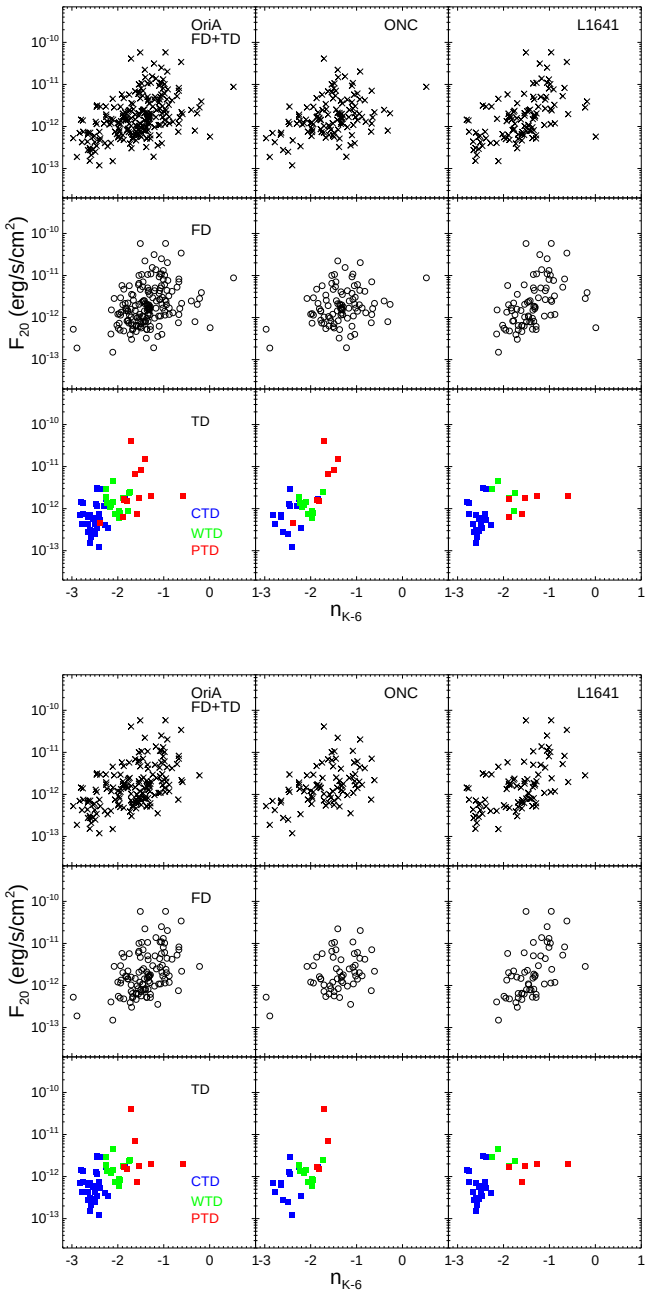


Figure C.10 n_{K-6} vs. $\log F_{20}$. Upper panel: all available objects; Lower panel: objects with available spectral types only

Table C.19 n_{K-6} vs. $\log F_{20}$ (I)

	Ori A				ONC				L1641			
	N	ρ	τ	r	N	ρ	τ	r	N	ρ	τ	r
TDFD	231	0.481	0.332	0.460	122	0.375	0.255	0.384	109	0.591	0.420	0.534
		0.000	0.000	0.000		0.000	0.000	0.000		0.000	0.000	0.000
FD	170	0.389	0.262	0.356	91	0.230	0.149	0.271	79	0.555	0.387	0.461
		0.000	0.000	0.000		0.028	0.037	0.009		0.000	0.000	0.000
TD	61	0.608	0.416	0.552	31	0.658	0.481	0.691	30	0.529	0.341	0.459
		0.000	0.000	0.000		0.000	0.000	0.000		0.003	0.008	0.011

ρ: Spearsman's ρ
τ: Kendall's τ
r: Pearson's r

Table C.20 n_{K-6} vs. $\log F_{20}$ (II)

	Ori A				ONC				L1641			
	N	ρ	τ	r	N	ρ	τ	r	N	ρ	τ	r
TDFD	168	0.520	0.361	0.519	83	0.453	0.309	0.463	85	0.587	0.415	0.563
		0.000	0.000	0.000		0.000	0.000	0.000		0.000	0.000	0.000
FD	114	0.444	0.310	0.449	57	0.286	0.194	0.347	57	0.588	0.421	0.558
		0.000	0.000	0.000		0.031	0.033	0.008		0.000	0.000	0.000
TD	54	0.590	0.393	0.504	26	0.598	0.423	0.583	28	0.547	0.337	0.479
		0.000	0.000	0.000		0.001	0.002	0.002		0.003	0.012	0.010

ρ: Spearsman's ρ
τ: Kendall's τ
r: Pearson's r

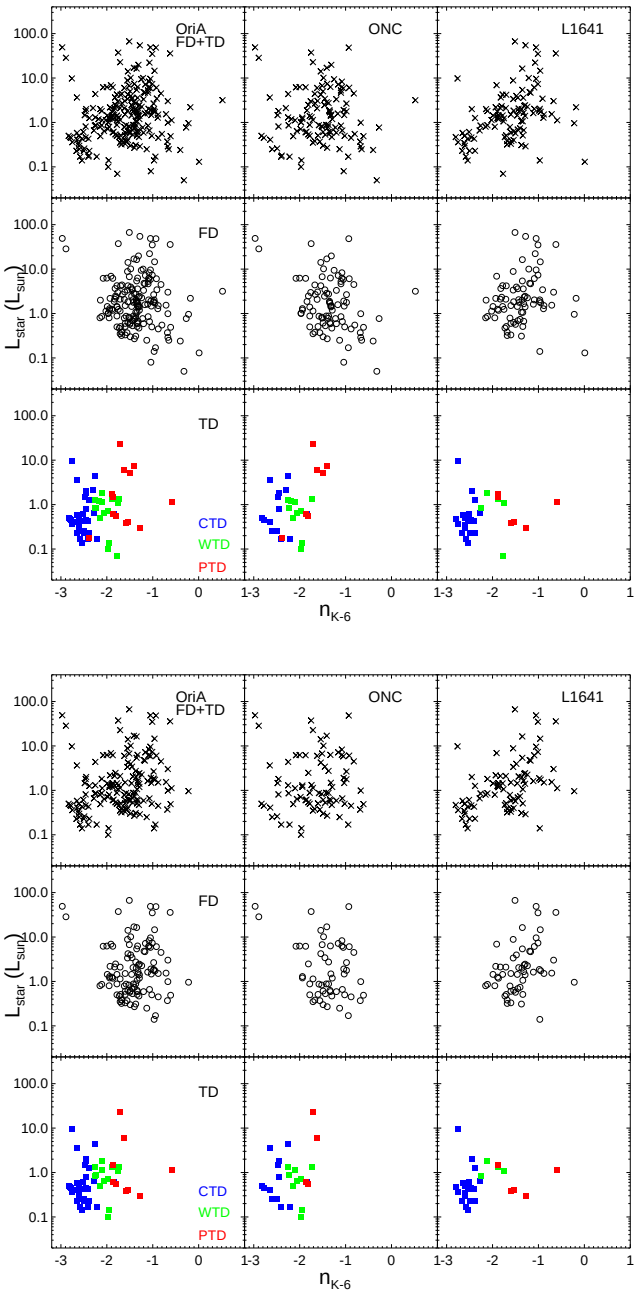


Figure C.11 n_{K-6} vs. $\log L_\star$. Upper panel: all available objects; Lower panel: objects with available spectral types only

Table C.21 n_{K-6} vs. $\log L_\star$ (I)

	Ori A				ONC				L1641			
	N	ρ	τ	r	N	ρ	τ	r	N	ρ	τ	r
TDFD	231	0.219	0.156	0.159	122	0.024	0.015	-0.031	109	0.432	0.305	0.377
		0.001	0.000	0.016		0.791	0.810	0.735		0.000	0.000	0.000
FD	170	-0.020	-0.011	-0.142	91	-0.242	-0.170	-0.344	79	0.261	0.173	0.148
		0.799	0.837	0.065		0.021	0.017	0.001		0.020	0.024	0.193
TD	61	0.264	0.165	0.240	31	0.315	0.173	0.405	30	0.177	0.116	0.079
		0.040	0.060	0.062		0.085	0.173	0.024		0.350	0.368	0.678

ρ: Spearsman's ρ
τ: Kendall's τ
r: Pearson's r

Table C.22 n_{K-6} vs. $\log L_\star$ (II)

	Ori A				ONC				L1641			
	N	ρ	τ	r	N	ρ	τ	r	N	ρ	τ	r
TDFD	168	0.301	0.207	0.255	83	0.099	0.058	0.044	85	0.496	0.353	0.466
		0.000	0.000	0.001		0.373	0.441	0.693		0.000	0.000	0.000
FD	114	0.082	0.053	-0.042	57	-0.168	-0.127	-0.323	57	0.378	0.253	0.314
		0.387	0.401	0.657		0.212	0.162	0.014		0.004	0.005	0.017
TD	54	0.234	0.143	0.180	26	0.189	0.087	0.244	28	0.248	0.163	0.137
		0.089	0.127	0.193		0.356	0.535	0.230		0.203	0.224	0.487

ρ: Spearsman's ρ
τ: Kendall's τ
r: Pearson's r

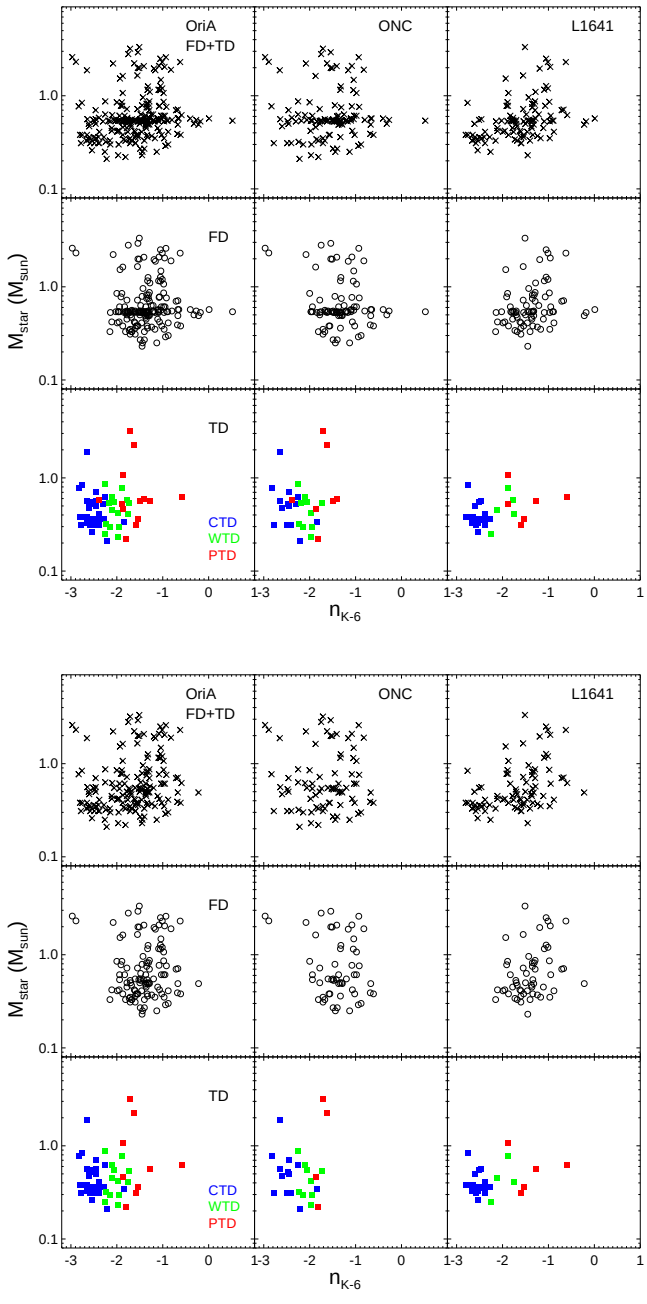


Figure C.12 n_{K-6} vs. $\log M_\star$. Upper panel: all available objects; Lower panel: objects with available spectral types only

Table C.23 n_{K-6} vs. $M_\star$ (I)

	Ori A				ONC				L1641			
	N	ρ	τ	r	N	ρ	τ	r	N	ρ	τ	r
TDFD	231	0.256	0.177	0.161	122	0.068	0.049	-0.022	109	0.445	0.308	0.394
		0.000	0.000	0.014		0.459	0.425	0.810		0.000	0.000	0.000
FD	170	0.129	0.089	-0.028	91	-0.027	-0.021	-0.217	79	0.305	0.206	0.243
		0.093	0.085	0.717		0.801	0.767	0.039		0.006	0.007	0.031
TD	61	0.152	0.100	0.189	31	-0.025	-0.026	0.094	30	0.243	0.170	0.339
		0.243	0.256	0.145		0.893	0.837	0.615		0.195	0.188	0.067

ρ: Spearsman's ρ
τ: Kendall's τ
r: Pearson's r

Table C.24 n_{K-6} vs. $M_\star$ (II)

	Ori A				ONC				L1641			
	N	ρ	τ	r	N	ρ	τ	r	N	ρ	τ	r
TDFD	168	0.252	0.172	0.206	83	0.037	0.023	0.012	85	0.461	0.317	0.436
		0.001	0.001	0.007		0.739	0.760	0.914		0.000	0.000	0.000
FD	114	0.098	0.072	-0.014	57	-0.139	-0.095	-0.252	57	0.341	0.232	0.318
		0.299	0.258	0.882		0.304	0.296	0.059		0.009	0.011	0.016
TD	54	0.056	0.028	0.170	26	-0.100	-0.096	0.087	28	0.164	0.112	0.307
		0.685	0.762	0.219		0.627	0.490	0.673		0.406	0.405	0.112

ρ: Spearsman's ρ
τ: Kendall's τ
r: Pearson's r

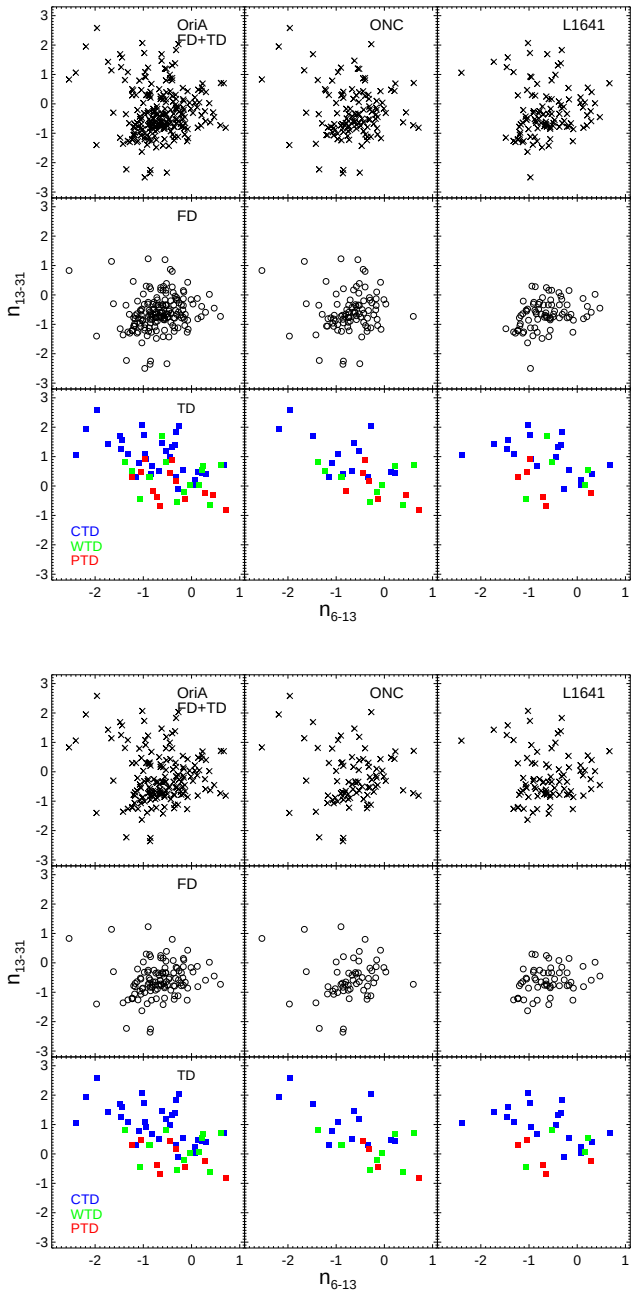


Figure C.13 n_{6-13} vs. n_{13-31}. Upper panel: all available objects; Lower panel: objects with available spectral types only

Table C.25 n_{6-13} vs. n_{13-31} (I)

	Ori A				ONC				L1641			
	N	ρ	τ	r	N	ρ	τ	r	N	ρ	τ	r
TDFD	231	0.115	0.087	-0.041	122	0.068	0.056	-0.096	109	0.161	0.113	0.025
		0.081	0.050	0.535		0.456	0.361	0.293		0.095	0.081	0.796
FD	170	0.268	0.186	0.144	91	0.185	0.141	0.033	79	0.352	0.228	0.343
		0.000	0.000	0.061		0.078	0.048	0.756		0.001	0.003	0.002
TD	61	-0.472	-0.322	-0.503	31	-0.527	-0.383	-0.624	30	-0.369	-0.235	-0.352
		0.000	0.000	0.000		0.002	0.002	0.000		0.045	0.068	0.056

ρ: Spearsman's ρ
τ: Kendall's τ
r: Pearson's r

Table C.26 n_{6-13} vs. n_{13-31} (II)

	Ori A				ONC				L1641			
	N	ρ	τ	r	N	ρ	τ	r	N	ρ	τ	r
TDFD	168	0.064	0.059	-0.089	83	0.068	0.069	-0.115	85	0.057	0.046	-0.060
		0.406	0.254	0.251		0.541	0.358	0.301		0.602	0.531	0.585
FD	114	0.259	0.185	0.119	57	0.265	0.208	0.044	57	0.230	0.149	0.274
		0.005	0.003	0.207		0.046	0.022	0.745		0.086	0.102	0.039
TD	54	-0.490	-0.326	-0.517	26	-0.554	-0.403	-0.654	28	-0.382	-0.230	-0.361
		0.000	0.000	0.000		0.003	0.004	0.000		0.045	0.085	0.059

ρ: Spearsman's ρ
τ: Kendall's τ
r: Pearson's r

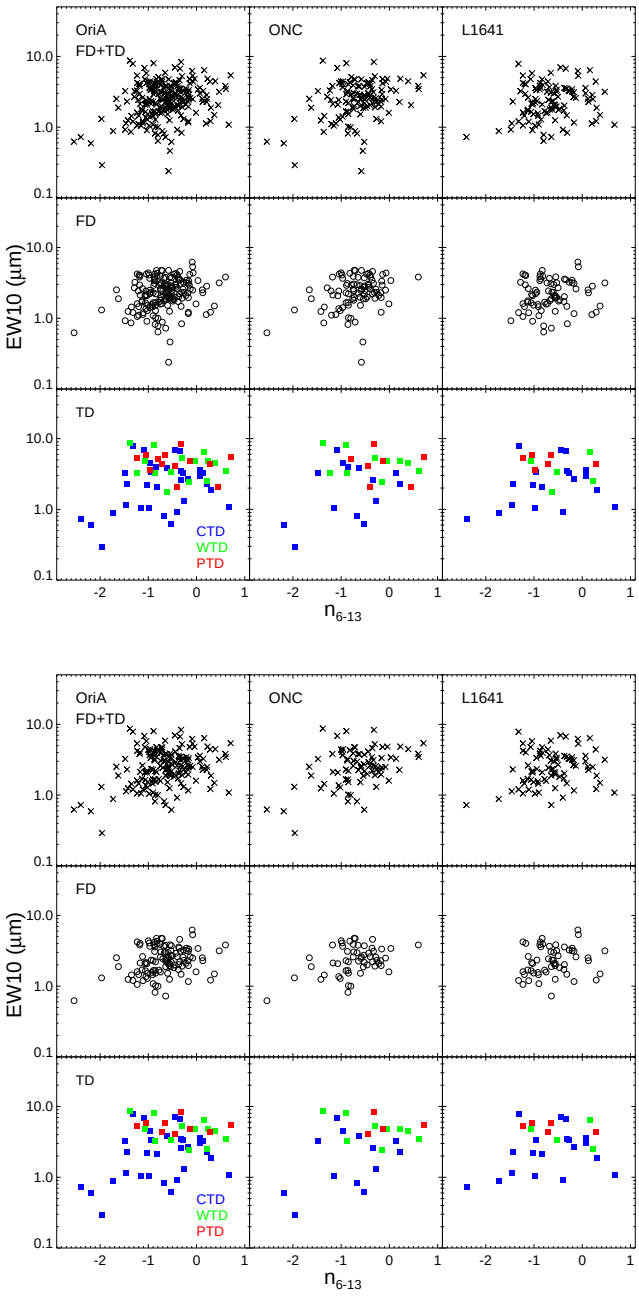


Figure C.14 n_{6-13} vs. EW10(μm). Upper panel: all available objects; Lower panel: objects with available spectral types only

Table C.27 n_{6-13} vs. EW10 (μm) (I)

	Ori A				ONC				L1641			
	N	ρ	τ	r	N	ρ	τ	r	N	ρ	τ	r
TDFD	231	0.216	0.149	0.188	122	0.273	0.187	0.251	109	0.140	0.093	0.114
		0.001	0.001	0.004		0.002	0.002	0.005		0.146	0.152	0.238
FD	170	0.230	0.157	0.227	91	0.308	0.207	0.324	79	0.126	0.083	0.122
		0.003	0.002	0.003		0.003	0.004	0.002		0.269	0.279	0.284
TD	61	0.121	0.070	0.122	31	0.156	0.106	0.123	30	0.105	0.051	0.111
		0.352	0.428	0.349		0.401	0.404	0.510		0.580	0.694	0.559

ρ: Spearsman's ρ
τ: Kendall's τ
r: Pearson's r

Table C.28 n_{6-13} vs. EW10 (μm) (II)

	Ori A				ONC				L1641			
	N	ρ	τ	r	N	ρ	τ	r	N	ρ	τ	r
TDFD	168	0.238	0.161	0.200	83	0.300	0.202	0.267	85	0.173	0.110	0.127
		0.002	0.002	0.009		0.006	0.007	0.015		0.113	0.136	0.247
FD	114	0.241	0.158	0.239	57	0.281	0.174	0.319	57	0.199	0.125	0.166
		0.010	0.013	0.010		0.034	0.056	0.016		0.138	0.169	0.217
TD	54	0.163	0.094	0.152	26	0.249	0.173	0.178	28	0.109	0.056	0.114
		0.238	0.317	0.273		0.221	0.216	0.384		0.582	0.678	0.564

ρ: Spearsman's ρ
τ: Kendall's τ
r: Pearson's r

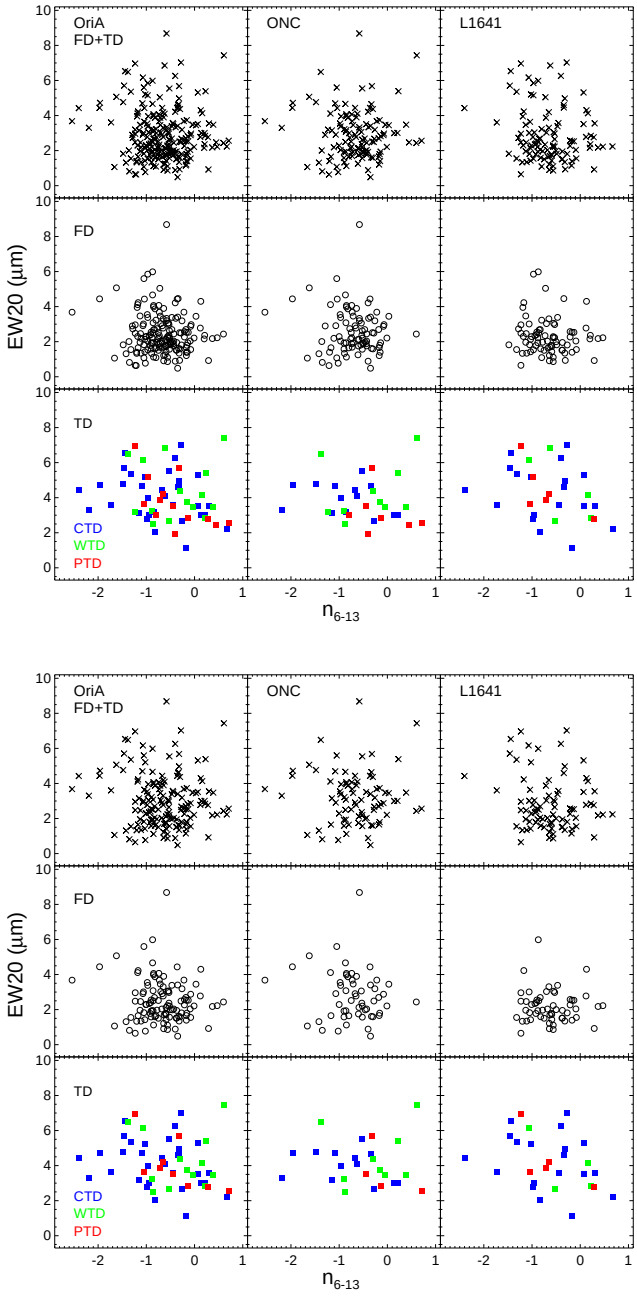


Figure C.15 n_{6-13} vs. EW10 (μm). Upper panel: all available objects; Lower panel: objects with available spectral types only

Table C.29 n_{6-13} vs. EW20 (μm) (I)

	Ori A				ONC				L1641			
	N	ρ	τ	r	N	ρ	τ	r	N	ρ	τ	r
TDFD	231	-0.055	-0.033	-0.079	122	-0.025	-0.014	-0.023	109	-0.121	-0.080	-0.152
		0.406	0.461	0.232		0.782	0.824	0.801		0.211	0.217	0.115
FD	170	-0.037	-0.023	-0.083	91	-0.035	-0.027	-0.077	79	-0.091	-0.056	-0.085
		0.629	0.652	0.282		0.745	0.705	0.468		0.427	0.468	0.456
TD	61	-0.292	-0.200	-0.218	31	-0.202	-0.148	-0.067	30	-0.393	-0.267	-0.332
		0.022	0.023	0.091		0.277	0.241	0.720		0.032	0.038	0.073

ρ: Spearsman's ρ
τ: Kendall's τ
r: Pearson's r

Table C.30 n_{6-13} vs. EW20 (μm) (II)

	Ori A				ONC				L1641			
	N	ρ	τ	r	N	ρ	τ	r	N	ρ	τ	r
TDFD	168	-0.072	-0.042	-0.091	83	-0.079	-0.048	-0.031	85	-0.100	-0.064	-0.162
		0.354	0.423	0.241		0.479	0.523	0.781		0.364	0.390	0.139
FD	114	-0.046	-0.027	-0.097	57	-0.122	-0.088	-0.099	57	0.004	0.010	-0.018
		0.626	0.671	0.305		0.366	0.334	0.464		0.975	0.912	0.894
TD	54	-0.300	-0.199	-0.216	26	-0.206	-0.151	-0.051	28	-0.411	-0.273	-0.343
		0.027	0.033	0.117		0.312	0.280	0.805		0.030	0.042	0.074

ρ: Spearsman's ρ
τ: Kendall's τ
r: Pearson's r

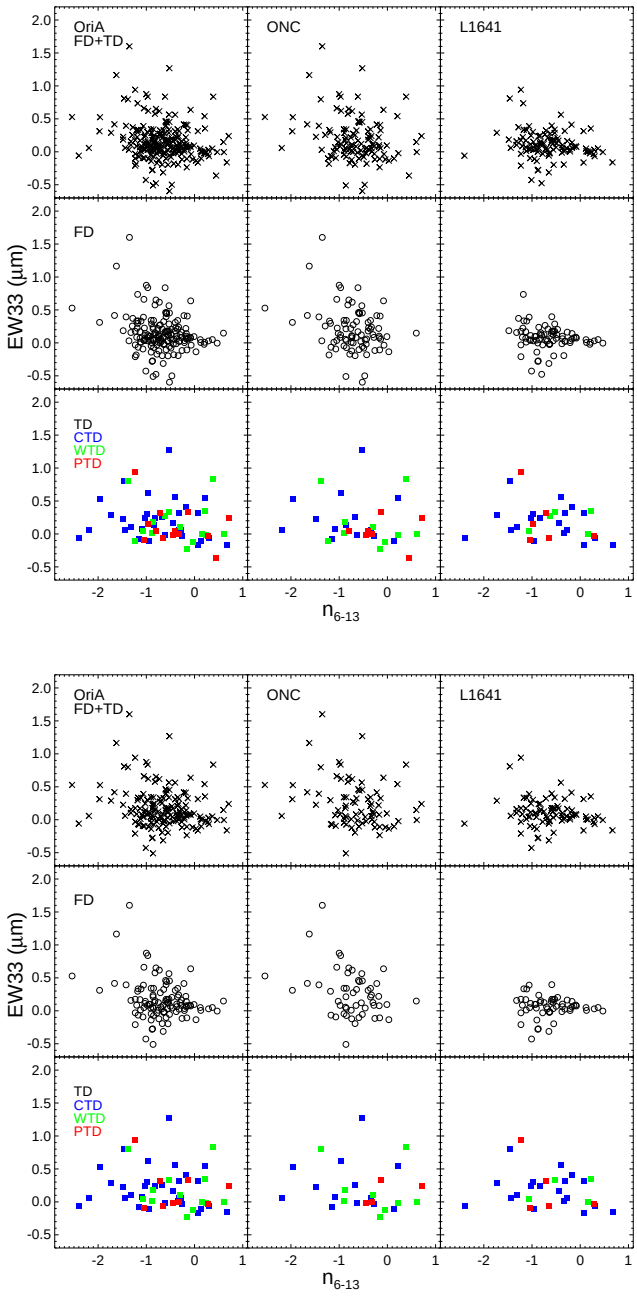


Figure C.16 n_{6-13} vs. EW33 (μm). Zoomed in; Upper panel: all available objects; Lower panel: objects with available spectral types only

Table C.31 n_{6-13} vs. EW33 (μm) (I)

	Ori A				ONC				L1641			
	N	ρ	τ	r	N	ρ	τ	r	N	ρ	τ	r
TDFD	231	-0.187	-0.128	-0.071	122	-0.191	-0.128	-0.070	109	-0.197	-0.138	-0.126
		0.004	0.004	0.283		0.035	0.037	0.444		0.040	0.033	0.192
FD	170	-0.178	-0.121	-0.083	91	-0.168	-0.116	-0.088	79	-0.216	-0.147	-0.125
		0.020	0.019	0.282		0.111	0.104	0.407		0.056	0.055	0.272
TD	61	-0.226	-0.152	-0.177	31	-0.233	-0.168	-0.143	30	-0.174	-0.108	-0.223
		0.080	0.084	0.172		0.207	0.184	0.443		0.359	0.401	0.236

ρ: Spearsman's ρ
τ: Kendall's τ
r: Pearson's r

Table C.32 n_{6-13} vs. EW33 (μm) (II)

	Ori A				ONC				L1641			
	N	ρ	τ	r	N	ρ	τ	r	N	ρ	τ	r
TDFD	168	-0.174	-0.120	-0.071	83	-0.230	-0.158	-0.086	85	-0.126	-0.091	-0.142
		0.024	0.021	0.360		0.037	0.034	0.439		0.250	0.217	0.195
FD	114	-0.152	-0.104	-0.092	57	-0.234	-0.166	-0.124	57	-0.086	-0.059	-0.033
		0.108	0.102	0.330		0.080	0.068	0.358		0.523	0.520	0.807
TD	54	-0.221	-0.149	-0.161	26	-0.201	-0.142	-0.117	28	-0.198	-0.133	-0.227
		0.108	0.112	0.245		0.324	0.310	0.569		0.313	0.322	0.245

ρ: Spearsman's ρ
τ: Kendall's τ
r: Pearson's r

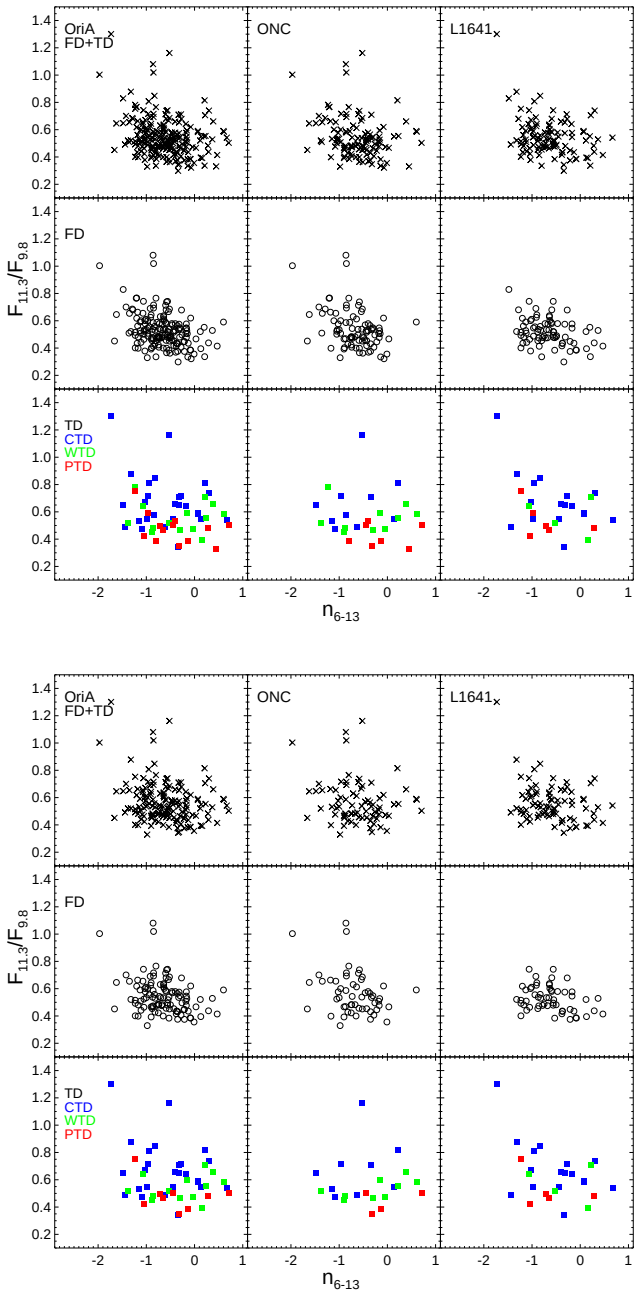


Figure C.17 n_{6-13} vs. $F_{11.3}/F_{9.8}$. Zoomed in, Upper panel: all available objects; Lower panel: objects with available spectral types only

Table C.33 n_{6-13} vs. $F_{11.3}/F_{9.8}$ (I)

	Ori A				ONC				L1641			
	N	ρ	τ	r	N	ρ	τ	r	N	ρ	τ	r
TDFD	231	-0.247	-0.169	-0.264	122	-0.225	-0.149	-0.188	109	-0.256	-0.177	-0.354
		0.000	0.000	0.000		0.013	0.015	0.038		0.007	0.006	0.000
FD	170	-0.326	-0.220	-0.197	91	-0.343	-0.232	-0.221	79	-0.291	-0.196	-0.333
		0.000	0.000	0.010		0.001	0.001	0.035		0.009	0.010	0.003
TD	61	-0.184	-0.129	-0.369	31	-0.021	-0.015	-0.235	30	-0.360	-0.249	-0.509
		0.157	0.143	0.003		0.913	0.905	0.203		0.051	0.054	0.004

ρ: Spearsman's ρ
τ: Kendall's τ
r: Pearson's r

Table C.34 n_{6-13} vs. $F_{11.3}/F_{9.8}$ (II)

	Ori A				ONC				L1641			
	N	ρ	τ	r	N	ρ	τ	r	N	ρ	τ	r
TDFD	168	-0.208	-0.142	-0.285	83	-0.131	-0.082	-0.198	85	-0.276	-0.190	-0.389
		0.007	0.006	0.000		0.239	0.273	0.073		0.011	0.010	0.000
FD	114	-0.301	-0.206	-0.473	57	-0.286	-0.198	-0.553	57	-0.316	-0.208	-0.306
		0.001	0.001	0.000		0.031	0.029	0.000		0.017	0.022	0.021
TD	54	-0.136	-0.096	-0.380	26	0.103	0.071	-0.244	28	-0.392	-0.273	-0.516
		0.325	0.306	0.005		0.617	0.612	0.230		0.039	0.042	0.005

ρ: Spearsman's ρ
τ: Kendall's τ
r: Pearson's r

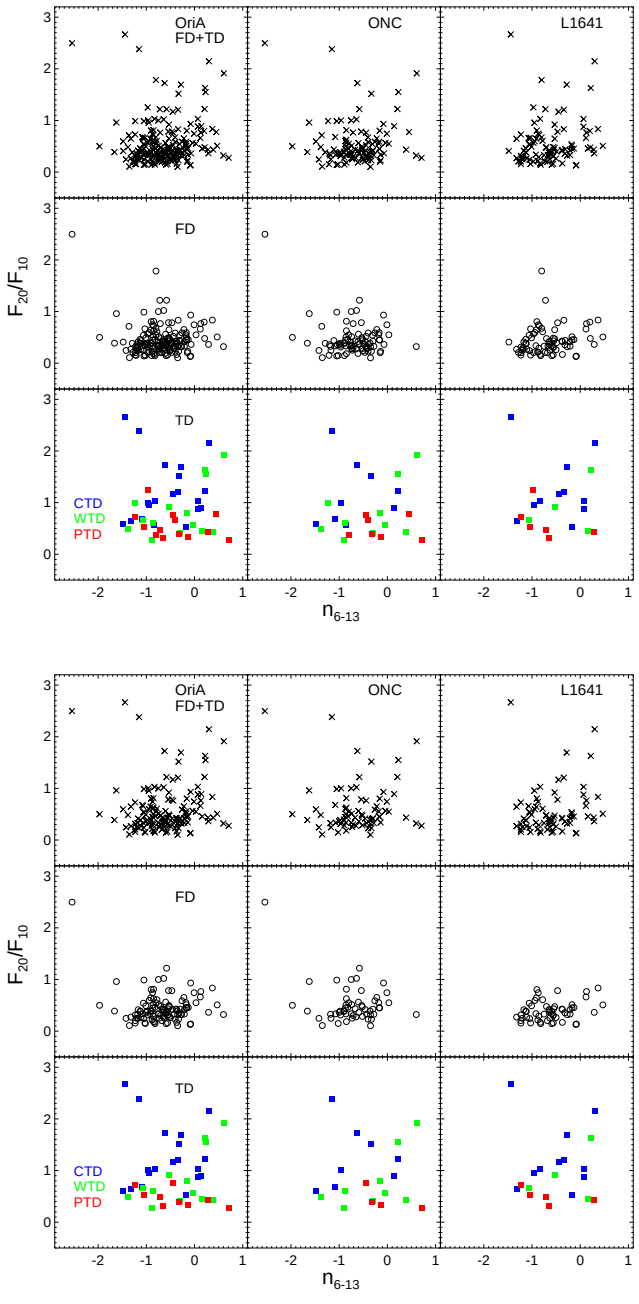


Figure C.18 n_{6-13} vs. F_{20}/F_{10}. Upper panel: all available objects; Lower panel: objects with available spectral types only

Table C.35 n_{6-13} vs. F_{20}/F_{10} (I)

	Ori A				ONC				L1641			
	N	ρ	τ	r	N	ρ	τ	r	N	ρ	τ	r
TDFD	230	0.109	0.078	-0.063	121	0.089	0.066	-0.044	109	0.121	0.092	-0.085
		0.099	0.077	0.342		0.333	0.285	0.632		0.208	0.157	0.380
FD	170	0.156	0.108	-0.017	91	0.078	0.058	-0.060	79	0.239	0.171	0.178
		0.042	0.036	0.826		0.464	0.419	0.572		0.034	0.026	0.117
TD	60	-0.152	-0.091	-0.186	30	-0.094	-0.053	-0.152	30	-0.174	-0.106	-0.198
		0.245	0.304	0.155		0.621	0.682	0.423		0.358	0.411	0.294

ρ: Spearsman's ρ
τ: Kendall's τ
r: Pearson's r

Table C.36 n_{6-13} vs. F_{20}/F_{10} (II)

	Ori A				ONC				L1641			
	N	ρ	τ	r	N	ρ	τ	r	N	ρ	τ	r
TDFD	167	0.093	0.069	-0.097	82	0.100	0.077	-0.067	85	0.084	0.063	-0.133
		0.232	0.183	0.212		0.372	0.304	0.550		0.446	0.390	0.225
FD	114	0.154	0.109	-0.159	57	0.100	0.078	-0.322	57	0.216	0.154	0.269
		0.101	0.086	0.091		0.460	0.392	0.015		0.107	0.091	0.043
TD	53	-0.183	-0.100	-0.206	25	-0.165	-0.087	-0.177	28	-0.193	-0.109	-0.235
		0.190	0.289	0.139		0.429	0.544	0.397		0.325	0.417	0.229

ρ: Spearsman's ρ
τ: Kendall's τ
r: Pearson's r

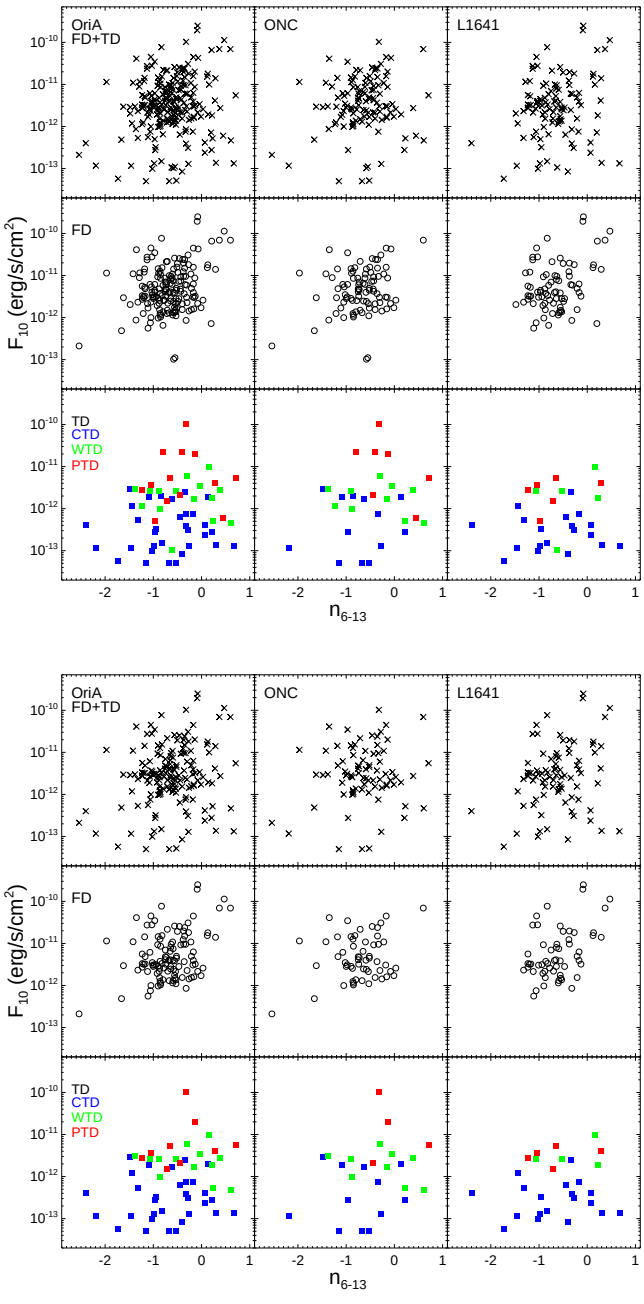


Figure C.19 n_{6-13} vs. $\log F_{10}$. Upper panel: all available objects; Lower panel: objects with available spectral types only

Table C.37 n_{6-13} vs. $\log F_{10}$ (I)

	Ori A				ONC				L1641			
	N	ρ	τ	r	N	ρ	τ	r	N	ρ	τ	r
TDFD	230	0.119	0.087	0.166	121	0.098	0.073	0.137	109	0.143	0.103	0.195
		0.071	0.049	0.012		0.287	0.235	0.134		0.138	0.114	0.042
FD	170	0.189	0.134	0.295	91	0.164	0.116	0.255	79	0.214	0.149	0.336
		0.013	0.010	0.000		0.121	0.104	0.015		0.058	0.052	0.002
TD	60	0.156	0.098	0.176	30	0.121	0.071	0.165	30	0.110	0.069	0.140
		0.235	0.269	0.179		0.523	0.580	0.384		0.563	0.592	0.461

ρ: Spearsman's ρ
τ: Kendall's τ
r: Pearson's r

Table C.38 n_{6-13} vs. $\log F_{10}$ (II)

	Ori A				ONC				L1641			
	N	ρ	τ	r	N	ρ	τ	r	N	ρ	τ	r
TDFD	167	0.127	0.091	0.191	82	0.028	0.024	0.135	85	0.219	0.156	0.246
		0.102	0.081	0.013		0.802	0.754	0.227		0.044	0.034	0.023
FD	114	0.213	0.151	0.352	57	0.065	0.049	0.257	57	0.358	0.250	0.446
		0.023	0.017	0.000		0.631	0.590	0.054		0.006	0.006	0.001
TD	53	0.193	0.123	0.210	25	0.237	0.147	0.243	28	0.119	0.077	0.143
		0.165	0.192	0.131		0.254	0.304	0.242		0.548	0.566	0.468

ρ: Spearsman's ρ
τ: Kendall's τ
r: Pearson's r

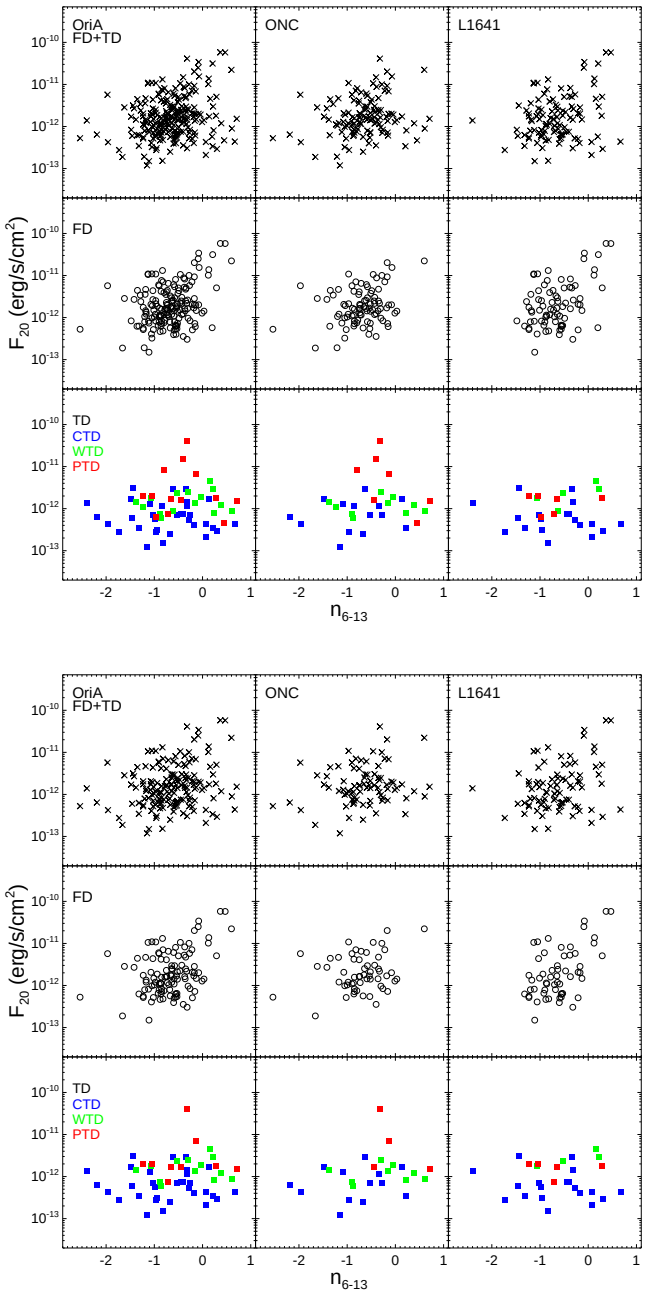


Figure C.20 n_{6-13} vs. $\log F_{20}$. Upper panel: all available objects; Lower panel: objects with available spectral types only

Table C.39 n_{6-13} vs. $\log F_{20}$ (I)

	Ori A				ONC				L1641			
	N	ρ	τ	r	N	ρ	τ	r	N	ρ	τ	r
TDFD	231	0.194	0.136	0.238	122	0.190	0.130	0.209	109	0.186	0.131	0.269
		0.003	0.002	0.000		0.036	0.034	0.021		0.053	0.043	0.005
FD	170	0.260	0.183	0.364	91	0.216	0.154	0.286	79	0.296	0.208	0.442
		0.001	0.000	0.000		0.040	0.031	0.006		0.008	0.007	0.000
TD	61	0.107	0.069	0.106	31	0.210	0.127	0.166	30	-0.015	-0.014	-0.008
		0.413	0.429	0.416		0.257	0.316	0.372		0.936	0.915	0.967

ρ: Spearsman's ρ
τ: Kendall's τ
r: Pearson's r

Table C.40 n_{6-13} vs. $\log F_{20}$ (II)

	Ori A				ONC				L1641			
	N	ρ	τ	r	N	ρ	τ	r	N	ρ	τ	r
TDFD	168	0.212	0.148	0.249	83	0.161	0.104	0.194	85	0.244	0.175	0.305
		0.006	0.005	0.001		0.145	0.165	0.079		0.025	0.018	0.005
FD	114	0.297	0.208	0.388	57	0.158	0.108	0.241	57	0.413	0.296	0.542
		0.001	0.001	0.000		0.241	0.235	0.071		0.001	0.001	0.000
TD	54	0.137	0.090	0.139	26	0.318	0.200	0.256	28	-0.016	-0.019	-0.014
		0.324	0.336	0.316		0.113	0.152	0.207		0.934	0.890	0.944

ρ: Spearsman's ρ
τ: Kendall's τ
r: Pearson's r

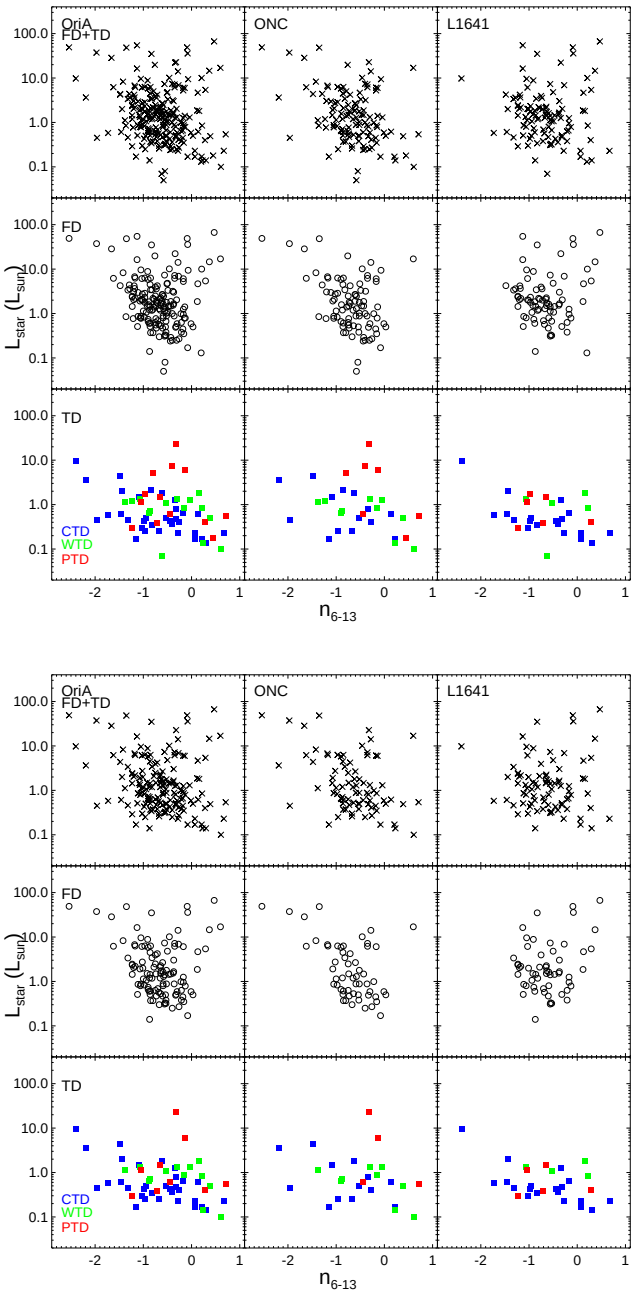


Figure C.21 n_{6-13} vs. $\log L_\star$. Upper panel: all available objects; Lower panel: objects with available spectral types only

Table C.41 n_{6-13} vs. $\log L_\star$ (I)

	Ori A				ONC				L1641			
	N	ρ	τ	r	N	ρ	τ	r	N	ρ	τ	r
TDFD	231	-0.232	-0.169	-0.239	122	-0.302	-0.218	-0.372	109	-0.156	-0.118	-0.080
		0.000	0.000	0.000		0.001	0.000	0.000		0.106	0.070	0.408
FD	170	-0.196	-0.149	-0.174	91	-0.305	-0.222	-0.389	79	-0.080	-0.074	0.088
		0.010	0.004	0.023		0.003	0.002	0.000		0.486	0.337	0.441
TD	61	-0.329	-0.224	-0.358	31	-0.321	-0.211	-0.319	30	-0.392	-0.282	-0.479
		0.010	0.011	0.005		0.078	0.095	0.080		0.032	0.029	0.007

ρ: Spearsman's ρ
τ: Kendall's τ
r: Pearson's r

Table C.42 n_{6-13} vs. $\log L_\star$ (II)

	Ori A				ONC				L1641			
	N	ρ	τ	r	N	ρ	τ	r	N	ρ	τ	r
TDFD	168	-0.225	-0.163	-0.239	83	-0.365	-0.270	-0.429	85	-0.083	-0.059	-0.017
		0.003	0.002	0.002		0.001	0.000	0.000		0.452	0.423	0.877
FD	114	-0.189	-0.142	-0.168	57	-0.425	-0.320	-0.493	57	0.051	0.025	0.239
		0.044	0.026	0.074		0.001	0.000	0.000		0.708	0.787	0.073
TD	54	-0.313	-0.218	-0.367	26	-0.284	-0.191	-0.286	28	-0.407	-0.296	-0.515
		0.021	0.020	0.006		0.160	0.171	0.157		0.032	0.027	0.005

ρ: Spearsman's ρ
τ: Kendall's τ
r: Pearson's r

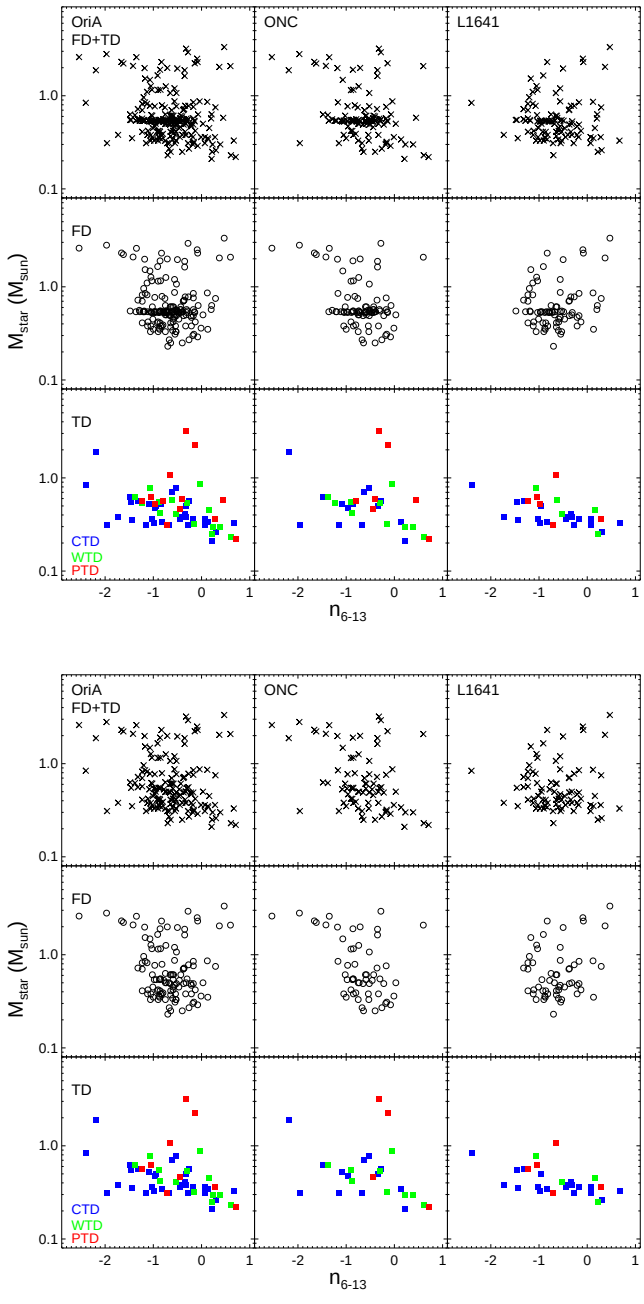


Figure C.22 n_{6-13} vs. $\log M_\star$. Upper panel: all available objects; Lower panel: objects with available spectral types only

Table C.43 n_{6-13} vs. $\log M_\star$ (I)

	Ori A				ONC				L1641			
	N	ρ	τ	r	N	ρ	τ	r	N	ρ	τ	r
TDFD	231	-0.195	-0.142	-0.212	122	-0.253	-0.181	-0.369	109	-0.133	-0.096	0.001
		0.003	0.001	0.001		0.005	0.003	0.000		0.169	0.138	0.992
FD	170	-0.103	-0.073	-0.135	91	-0.263	-0.184	-0.395	79	0.071	0.054	0.219
		0.181	0.160	0.079		0.012	0.010	0.000		0.535	0.479	0.052
TD	61	-0.414	-0.305	-0.349	31	-0.300	-0.204	-0.301	30	-0.551	-0.409	-0.555
		0.001	0.001	0.006		0.101	0.107	0.100		0.002	0.002	0.001

ρ: Spearsman's ρ
τ: Kendall's τ
r: Pearson's r

Table C.44 n_{6-13} vs. $\log M_\star$ (II)

	Ori A				ONC				L1641			
	N	ρ	τ	r	N	ρ	τ	r	N	ρ	τ	r
TDFD	168	-0.250	-0.180	-0.239	83	-0.373	-0.270	-0.411	85	-0.117	-0.081	0.000
		0.001	0.001	0.002		0.001	0.000	0.000		0.287	0.271	1.000
FD	114	-0.152	-0.108	-0.166	57	-0.415	-0.300	-0.447	57	0.136	0.105	0.244
		0.108	0.088	0.078		0.001	0.001	0.000		0.312	0.250	0.067
TD	54	-0.472	-0.345	-0.365	26	-0.395	-0.269	-0.325	28	-0.559	-0.404	-0.559
		0.000	0.000	0.007		0.046	0.054	0.105		0.002	0.003	0.002

ρ: Spearsman's ρ
τ: Kendall's τ
r: Pearson's r

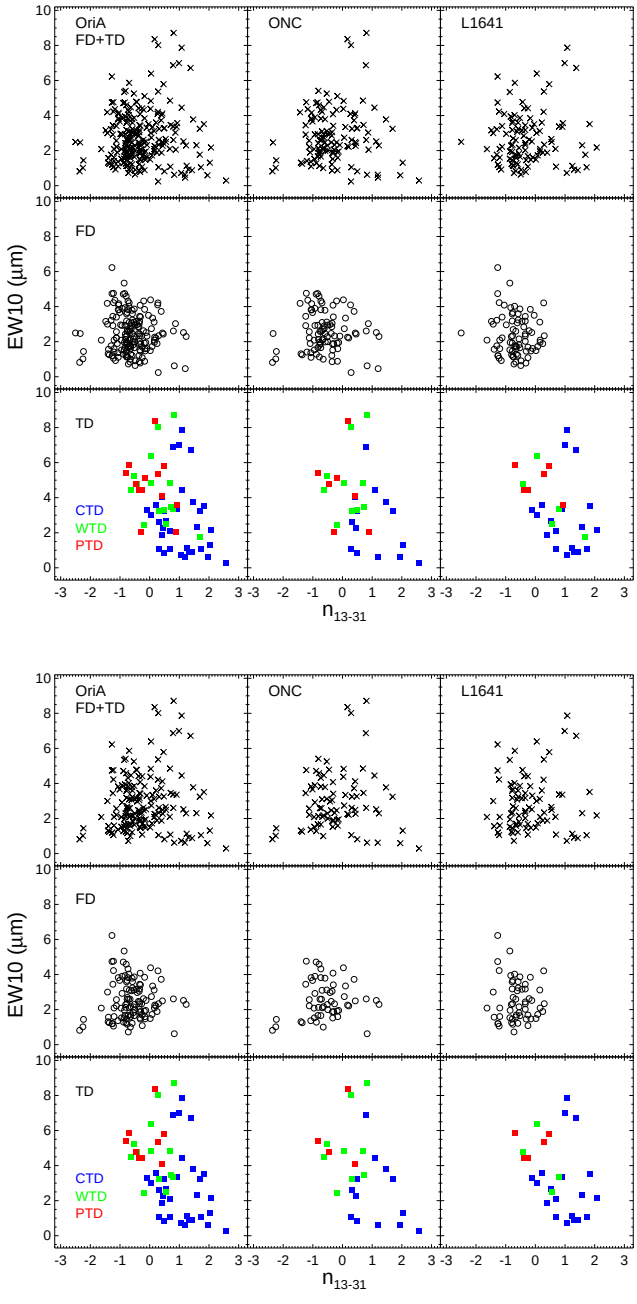


Figure C.23 n_{13-31} vs. EW10 (μm). Upper panel: all available objects; Lower panel: objects with available spectral types only

Table C.45 n_{13-31} vs. EW10 (μm) (I)

	Ori A				ONC				L1641			
	N	ρ	τ	r	N	ρ	τ	r	N	ρ	τ	r
TDFD	231	0.036	0.030	0.062	122	0.030	0.031	0.041	109	0.043	0.033	0.088
		0.588	0.490	0.348		0.744	0.613	0.654		0.659	0.614	0.363
FD	170	-0.039	-0.025	-0.047	91	-0.023	-0.010	-0.029	79	-0.070	-0.047	-0.093
		0.616	0.629	0.543		0.826	0.891	0.785		0.539	0.543	0.415
TD	61	-0.443	-0.305	-0.403	31	-0.437	-0.293	-0.409	30	-0.434	-0.306	-0.385
		0.000	0.001	0.001		0.014	0.020	0.022		0.017	0.018	0.036

ρ: Spearsman's ρ
τ: Kendall's τ
r: Pearson's r

Table C.46 n_{13-31} vs. EW10 (μm) (II)

	Ori A				ONC				L1641			
	N	ρ	τ	r	N	ρ	τ	r	N	ρ	τ	r
TDFD	168	0.055	0.046	0.070	83	0.069	0.060	0.071	85	0.034	0.031	0.070
		0.482	0.374	0.367		0.536	0.422	0.524		0.755	0.672	0.524
FD	114	0.071	0.045	0.039	57	0.110	0.077	0.116	57	0.008	0.003	-0.066
		0.454	0.481	0.680		0.414	0.400	0.390		0.952	0.972	0.626
TD	54	-0.440	-0.307	-0.406	26	-0.459	-0.314	-0.436	28	-0.407	-0.302	-0.363
		0.001	0.001	0.002		0.018	0.024	0.026		0.031	0.024	0.058

ρ: Spearsman's ρ
τ: Kendall's τ
r: Pearson's r

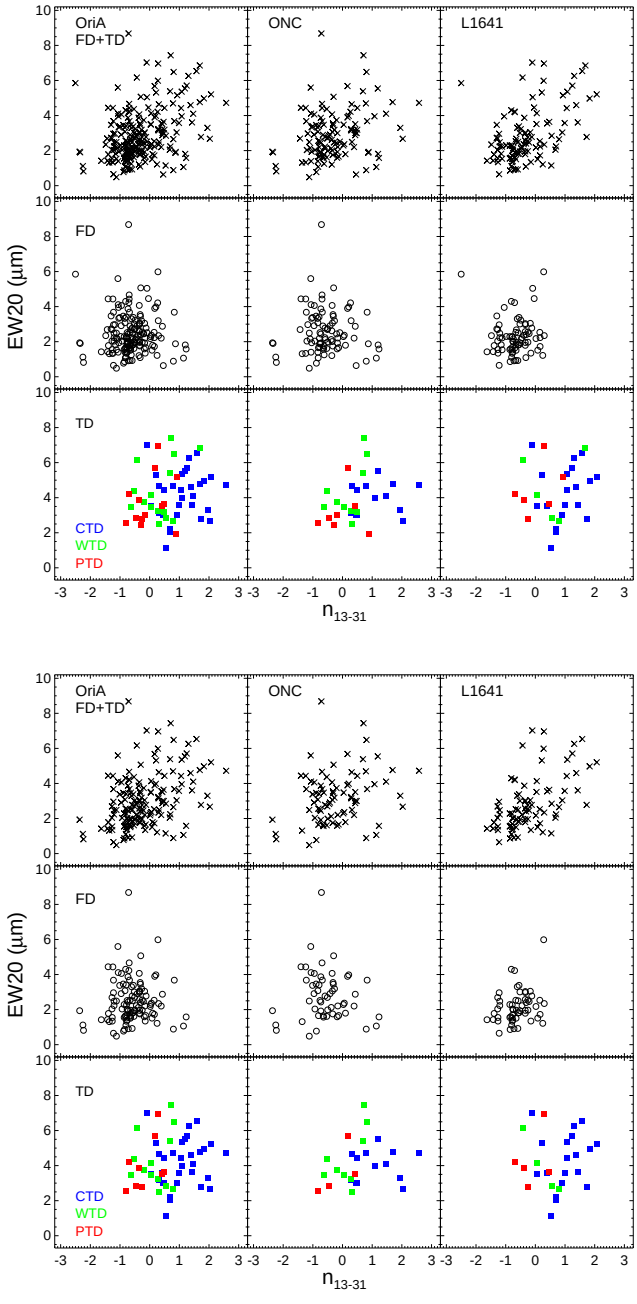


Figure C.24 n_{13-31} vs. EW20 (μm). Upper panel: all available objects; Lower panel: objects with available spectral types only

Table C.47 n_{13-31} vs. EW20 (μm) (I)

	Ori A				ONC				L1641			
	N	ρ	τ	r	N	ρ	τ	r	N	ρ	τ	r
TDFD	231	0.351	0.246	0.319	122	0.223	0.161	0.184	109	0.474	0.333	0.492
		0.000	0.000	0.000		0.014	0.008	0.042		0.000	0.000	0.000
FD	170	0.066	0.047	-0.019	91	-0.028	-0.018	-0.054	79	0.162	0.113	0.031
		0.390	0.363	0.806		0.789	0.805	0.611		0.153	0.142	0.786
TD	61	0.222	0.142	0.201	31	0.340	0.233	0.245	30	0.152	0.131	0.135
		0.086	0.107	0.120		0.061	0.066	0.184		0.421	0.309	0.477

ρ: Spearsman's ρ
τ: Kendall's τ
r: Pearson's r

Table C.48 n_{13-31} vs. EW20 (μm) (II)

	Ori A				ONC				L1641			
	N	ρ	τ	r	N	ρ	τ	r	N	ρ	τ	r
TDFD	168	0.384	0.269	0.325	83	0.213	0.151	0.160	85	0.555	0.391	0.557
		0.000	0.000	0.000		0.053	0.044	0.148		0.000	0.000	0.000
FD	114	0.090	0.059	0.013	57	-0.098	-0.077	-0.081	57	0.289	0.192	0.277
		0.341	0.349	0.891		0.469	0.396	0.549		0.029	0.035	0.037
TD	54	0.167	0.104	0.135	26	0.346	0.218	0.221	28	0.078	0.079	0.060
		0.227	0.269	0.330		0.084	0.118	0.278		0.692	0.553	0.762

ρ: Spearsman's ρ
τ: Kendall's τ
r: Pearson's r

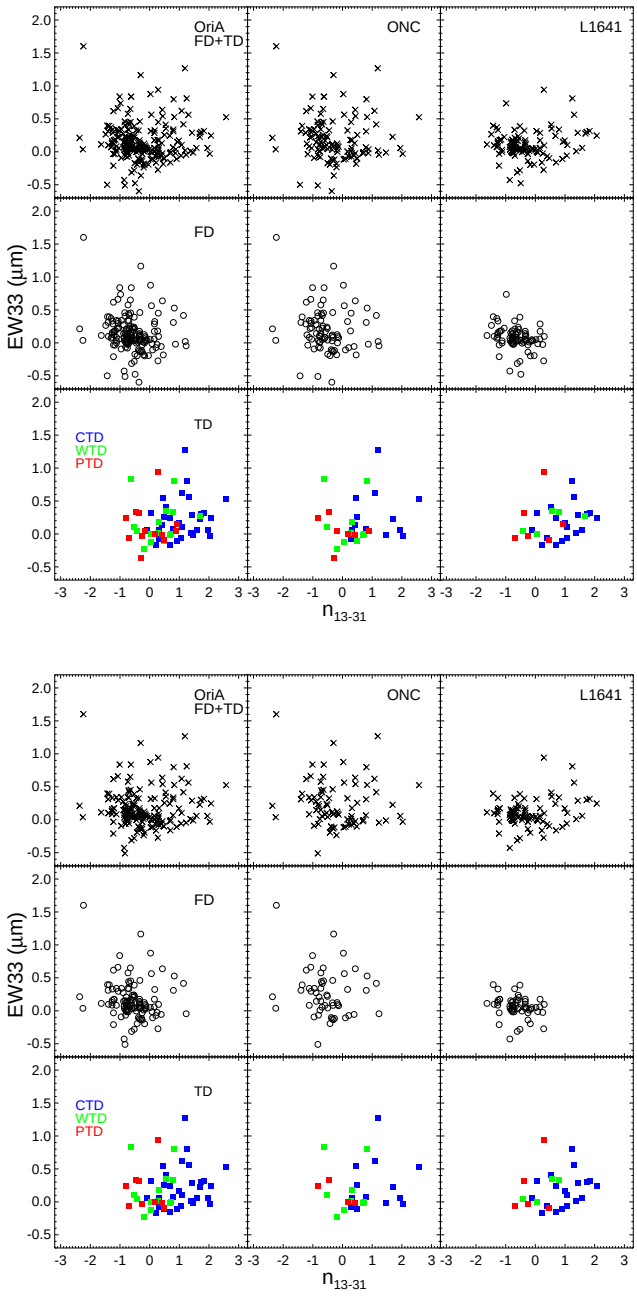


Figure C.25 n_{13-31} vs. EW33 (μm). Zoomed in, Upper panel: all available objects; Lower panel: objects with available spectral types only

Table C.49 n_{13-31} vs. EW33 (μm) (I)

	Ori A				ONC				L1641			
	N	ρ	τ	r	N	ρ	τ	r	N	ρ	τ	r
TDFD	231	-0.108	-0.077	-0.034	122	-0.158	-0.105	-0.007	109	-0.023	-0.029	-0.172
		0.102	0.080	0.607		0.082	0.086	0.939		0.810	0.655	0.074
FD	170	-0.233	-0.162	-0.094	91	-0.169	-0.118	-0.037	79	-0.335	-0.226	-0.473
		0.002	0.002	0.223		0.109	0.097	0.728		0.003	0.003	0.000
TD	61	0.247	0.166	0.194	31	0.147	0.127	0.166	30	0.267	0.170	0.233
		0.055	0.059	0.134		0.431	0.315	0.372		0.154	0.186	0.215

ρ: Spearsman's ρ
τ: Kendall's τ
r: Pearson's r

Table C.50 n_{13-31} vs. EW33 (μm) (II)

	Ori A				ONC				L1641			
	N	ρ	τ	r	N	ρ	τ	r	N	ρ	τ	r
TDFD	168	-0.037	-0.030	0.092	83	-0.102	-0.063	0.104	85	0.064	0.027	0.227
		0.635	0.559	0.236		0.357	0.397	0.349		0.559	0.711	0.037
FD	114	-0.157	-0.106	0.076	57	-0.086	-0.055	0.102	57	-0.261	-0.174	-0.243
		0.095	0.093	0.422		0.527	0.549	0.450		0.049	0.056	0.069
TD	54	0.209	0.134	0.154	26	0.119	0.105	0.108	28	0.251	0.156	0.227
		0.130	0.151	0.266		0.564	0.453	0.599		0.198	0.243	0.245

ρ: Spearsman's ρ
τ: Kendall's τ
r: Pearson's r

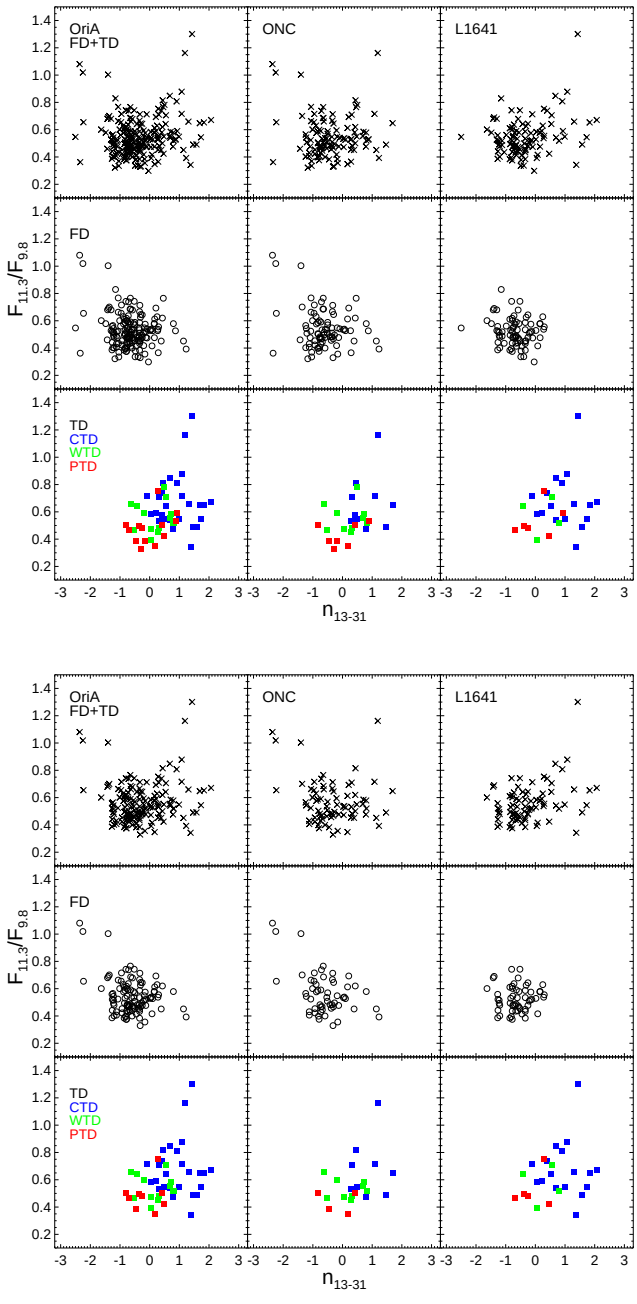


Figure C.26 n_{13-31} vs. $F_{11.3}/F_{9.8}$. Zoomed in, Upper panel: all available objects; Lower panel: objects with available spectral types only

Table C.51 n_{13-31} vs. $F_{11.3}/F_{9.8}$ (I)

	Ori A				ONC				L1641			
	N	ρ	τ	r	N	ρ	τ	r	N	ρ	τ	r
TDFD	231	0.146	0.102	0.141	122	0.071	0.052	0.092	109	0.235	0.162	0.200
		0.026	0.021	0.032		0.437	0.396	0.314		0.014	0.013	0.037
FD	170	-0.051	-0.032	-0.198	91	-0.006	0.001	-0.227	79	-0.126	-0.084	-0.145
		0.507	0.535	0.010		0.952	0.992	0.030		0.270	0.274	0.202
TD	61	0.386	0.277	0.209	31	0.370	0.284	0.262	30	0.313	0.232	0.123
		0.002	0.002	0.106		0.041	0.025	0.154		0.092	0.072	0.517

ρ: Spearsman's ρ
τ: Kendall's τ
r: Pearson's r

Table C.52 n_{13-31} vs. $F_{11.3}/F_{9.8}$ (II)

	Ori A				ONC				L1641			
	N	ρ	τ	r	N	ρ	τ	r	N	ρ	τ	r
TDFD	168	0.142	0.102	0.164	83	-0.034	-0.024	0.138	85	0.337	0.240	0.193
		0.066	0.049	0.034		0.763	0.753	0.213		0.002	0.001	0.077
FD	114	-0.070	-0.039	-0.049	57	-0.194	-0.130	-0.082	57	0.071	0.050	0.034
		0.461	0.539	0.605		0.149	0.154	0.544		0.598	0.584	0.802
TD	54	0.333	0.236	0.203	26	0.321	0.255	0.268	28	0.273	0.206	0.115
		0.014	0.012	0.141		0.110	0.067	0.186		0.161	0.123	0.560

ρ: Spearsman's ρ
τ: Kendall's τ
r: Pearson's r

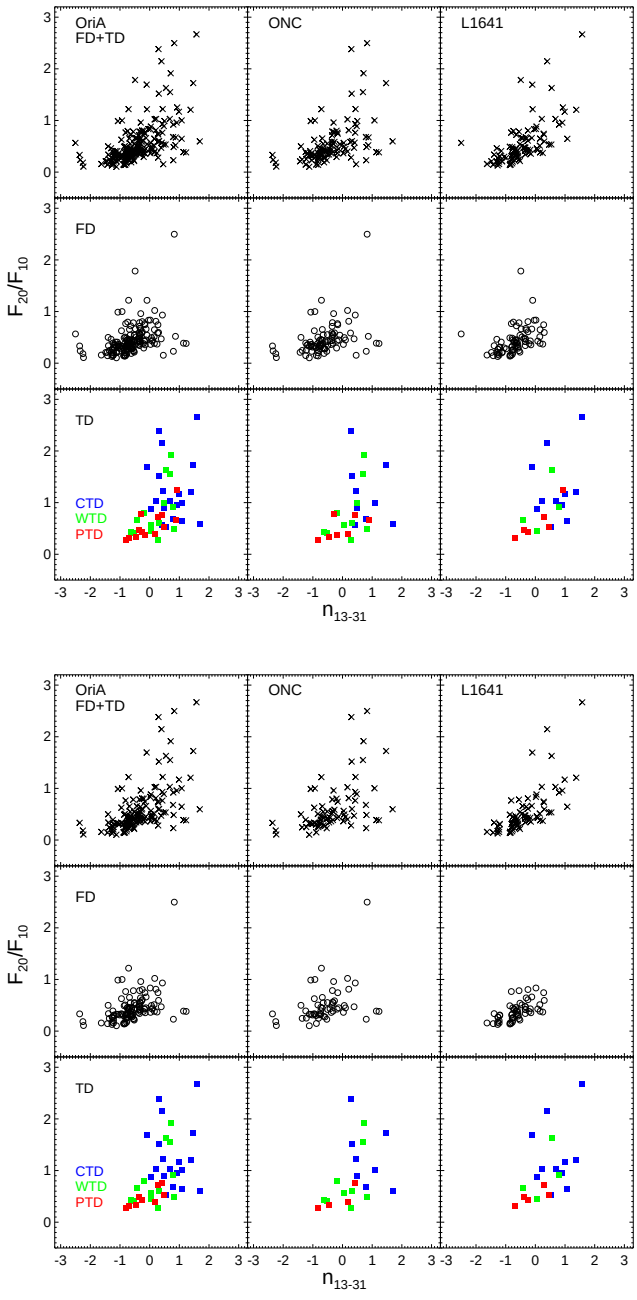


Figure C.27 n_{13-31} vs. F_{20}/F_{10}. Upper panel: all available objects; Lower panel: objects with available spectral types only

Table C.53 n_{13-31} vs. F_{20}/F_{10} (I)

	Ori A				ONC				L1641			
	N	ρ	τ	r	N	ρ	τ	r	N	ρ	τ	r
TDFD	230	0.716	0.538	0.569	121	0.637	0.473	0.454	109	0.793	0.602	0.699
		0.000	0.000	0.000		0.000	0.000	0.000		0.000	0.000	0.000
FD	170	0.566	0.405	0.340	91	0.508	0.367	0.339	79	0.624	0.436	0.431
		0.000	0.000	0.000		0.000	0.000	0.001		0.000	0.000	0.000
TD	60	0.713	0.528	0.586	30	0.648	0.470	0.476	30	0.771	0.577	0.691
		0.000	0.000	0.000		0.000	0.000	0.008		0.000	0.000	0.000

ρ: Spearsman's ρ
τ: Kendall's τ
r: Pearson's r

Table C.54 n_{13-31} vs. F_{20}/F_{10} (II)

	Ori A				ONC				L1641			
	N	ρ	τ	r	N	ρ	τ	r	N	ρ	τ	r
TDFD	167	0.732	0.557	0.583	82	0.609	0.457	0.465	85	0.844	0.657	0.721
		0.000	0.000	0.000		0.000	0.000	0.000		0.000	0.000	0.000
FD	114	0.558	0.398	0.431	57	0.442	0.314	0.376	57	0.683	0.488	0.613
		0.000	0.000	0.000		0.001	0.001	0.004		0.000	0.000	0.000
TD	53	0.711	0.530	0.566	25	0.677	0.487	0.477	28	0.760	0.571	0.681
		0.000	0.000	0.000		0.000	0.001	0.016		0.000	0.000	0.000

ρ: Spearsman's ρ
τ: Kendall's τ
r: Pearson's r

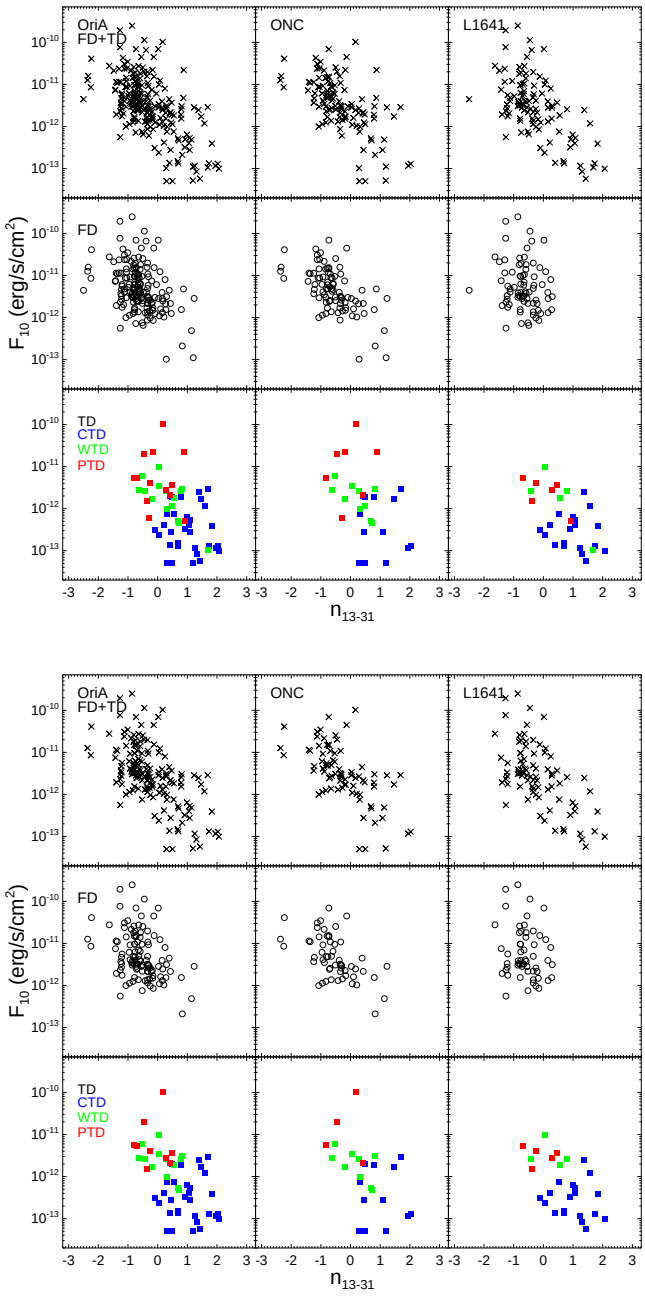


Figure C.28 n_{13-31} vs. $\log F_{10}$. Upper panel: all available objects; Lower panel: objects with available spectral types only

Table C.55 n_{13-31} vs. $\log F_{10}$ (I)

	Ori A				ONC				L1641			
	N	ρ	τ	r	N	ρ	τ	r	N	ρ	τ	r
TDFD	230	-0.582	-0.412	-0.610	121	-0.611	-0.438	-0.610	109	-0.554	-0.390	-0.612
		0.000	0.000	0.000		0.000	0.000	0.000		0.000	0.000	0.000
FD	170	-0.394	-0.272	-0.412	91	-0.565	-0.402	-0.591	79	-0.197	-0.124	-0.157
		0.000	0.000	0.000		0.000	0.000	0.000		0.082	0.105	0.167
TD	60	-0.537	-0.379	-0.519	30	-0.456	-0.313	-0.447	30	-0.579	-0.416	-0.574
		0.000	0.000	0.000		0.011	0.015	0.013		0.001	0.001	0.001

ρ: Spearsman's ρ
τ: Kendall's τ
r: Pearson's r

Table C.56 n_{13-31} vs. $\log F_{10}$ (II)

	Ori A				ONC				L1641			
	N	ρ	τ	r	N	ρ	τ	r	N	ρ	τ	r
TDFD	167	-0.613	-0.437	-0.624	82	-0.652	-0.471	-0.631	85	-0.581	-0.415	-0.621
		0.000	0.000	0.000		0.000	0.000	0.000		0.000	0.000	0.000
FD	114	-0.364	-0.254	-0.370	57	-0.542	-0.390	-0.551	57	-0.190	-0.123	-0.159
		0.000	0.000	0.000		0.000	0.000	0.000		0.157	0.176	0.237
TD	53	-0.549	-0.390	-0.530	25	-0.548	-0.387	-0.503	28	-0.557	-0.407	-0.549
		0.000	0.000	0.000		0.005	0.007	0.010		0.002	0.002	0.002

ρ: Spearsman's ρ
τ: Kendall's τ
r: Pearson's r

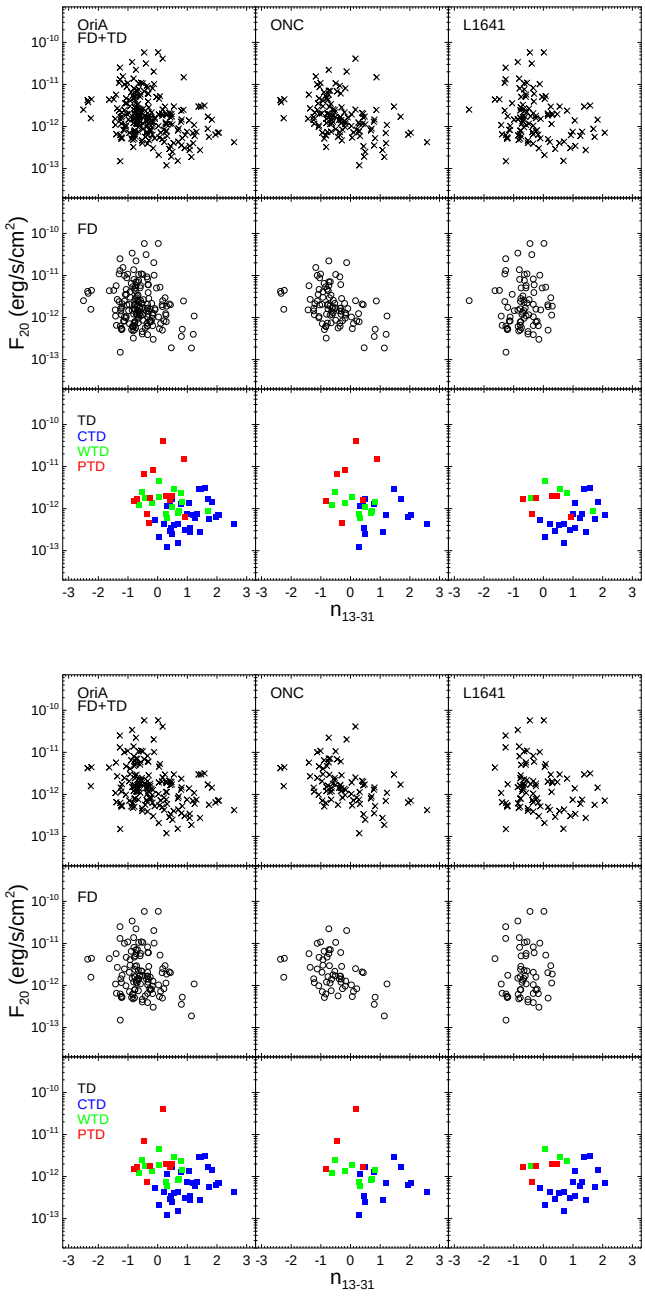


Figure C.29 n_{13-31} vs. $\log F_{20}$. Upper panel: all available objects; Lower panel: objects with available spectral types only

Table C.57 n_{13-31} vs. $\log F_{20}$ (I)

	Ori A				ONC				L1641			
	N	ρ	τ	r	N	ρ	τ	r	N	ρ	τ	r
TDFD	231	-0.301	-0.201	-0.305	122	-0.417	-0.285	-0.386	109	-0.198	-0.126	-0.228
		0.000	0.000	0.000		0.000	0.000	0.000		0.039	0.053	0.017
FD	170	-0.157	-0.105	-0.198	91	-0.382	-0.264	-0.413	79	0.067	0.051	0.059
		0.040	0.042	0.010		0.000	0.000	0.000		0.554	0.504	0.606
TD	61	-0.207	-0.129	-0.194	31	-0.279	-0.177	-0.240	30	-0.032	0.007	-0.081
		0.110	0.143	0.134		0.128	0.163	0.193		0.866	0.957	0.670

ρ: Spearsman's ρ
τ: Kendall's τ
r: Pearson's r

Table C.58 n_{13-31} vs. $\log F_{20}$ (II)

	Ori A				ONC				L1641			
	N	ρ	τ	r	N	ρ	τ	r	N	ρ	τ	r
TDFD	168	-0.315	-0.212	-0.317	83	-0.480	-0.328	-0.439	85	-0.186	-0.125	-0.213
		0.000	0.000	0.000		0.000	0.000	0.000		0.089	0.092	0.050
FD	114	-0.135	-0.092	-0.173	57	-0.389	-0.267	-0.413	57	0.066	0.042	0.075
		0.153	0.146	0.066		0.003	0.003	0.001		0.625	0.642	0.579
TD	54	-0.213	-0.132	-0.208	26	-0.361	-0.231	-0.295	28	-0.042	-0.005	-0.081
		0.121	0.160	0.131		0.070	0.098	0.143		0.834	0.968	0.682

ρ: Spearsman's ρ
τ: Kendall's τ
r: Pearson's r

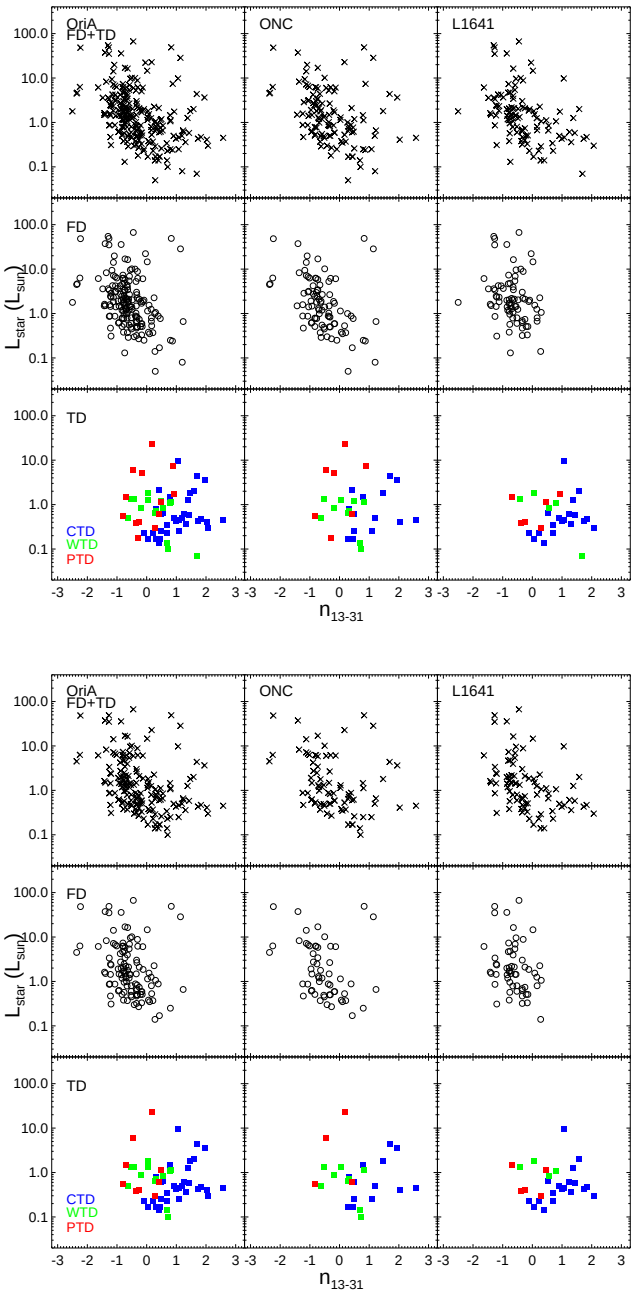


Figure C.30 n_{13-31} vs. $\log L_\star$. Upper panel: all available objects; Lower panel: objects with available spectral types only

Table C.59 n_{13-31} vs. $L_\star$ (I)

	Ori A				ONC				L1641			
	N	ρ	τ	r	N	ρ	τ	r	N	ρ	τ	r
TDFD	231	-0.462	-0.324	-0.399	122	-0.437	-0.318	-0.369	109	-0.494	-0.343	-0.434
		0.000	0.000	0.000		0.000	0.000	0.000		0.000	0.000	0.000
FD	170	-0.401	-0.286	-0.361	91	-0.497	-0.370	-0.431	79	-0.277	-0.190	-0.236
		0.000	0.000	0.000		0.000	0.000	0.000		0.013	0.013	0.036
TD	61	-0.032	-0.024	-0.044	31	-0.069	-0.050	-0.012	30	0.051	0.021	-0.033
		0.804	0.783	0.736		0.714	0.695	0.949		0.790	0.872	0.863

ρ: Spearsman's ρ
τ: Kendall's τ
r: Pearson's r

Table C.60 n_{13-31} vs. $\log L_\star$ (II)

	Ori A				ONC				L1641			
	N	ρ	τ	r	N	ρ	τ	r	N	ρ	τ	r
TDFD	168	-0.455	-0.318	-0.378	83	-0.419	-0.310	-0.344	85	-0.497	-0.343	-0.418
		0.000	0.000	0.000		0.000	0.000	0.001		0.000	0.000	0.000
FD	114	-0.371	-0.265	-0.306	57	-0.439	-0.343	-0.327	57	-0.295	-0.200	-0.279
		0.000	0.000	0.001		0.001	0.000	0.013		0.026	0.028	0.036
TD	54	-0.014	-0.013	-0.001	26	-0.129	-0.092	-0.031	28	0.127	0.064	0.062
		0.922	0.887	0.994		0.530	0.508	0.881		0.521	0.634	0.754

ρ: Spearsman's ρ
τ: Kendall's τ
r: Pearson's r

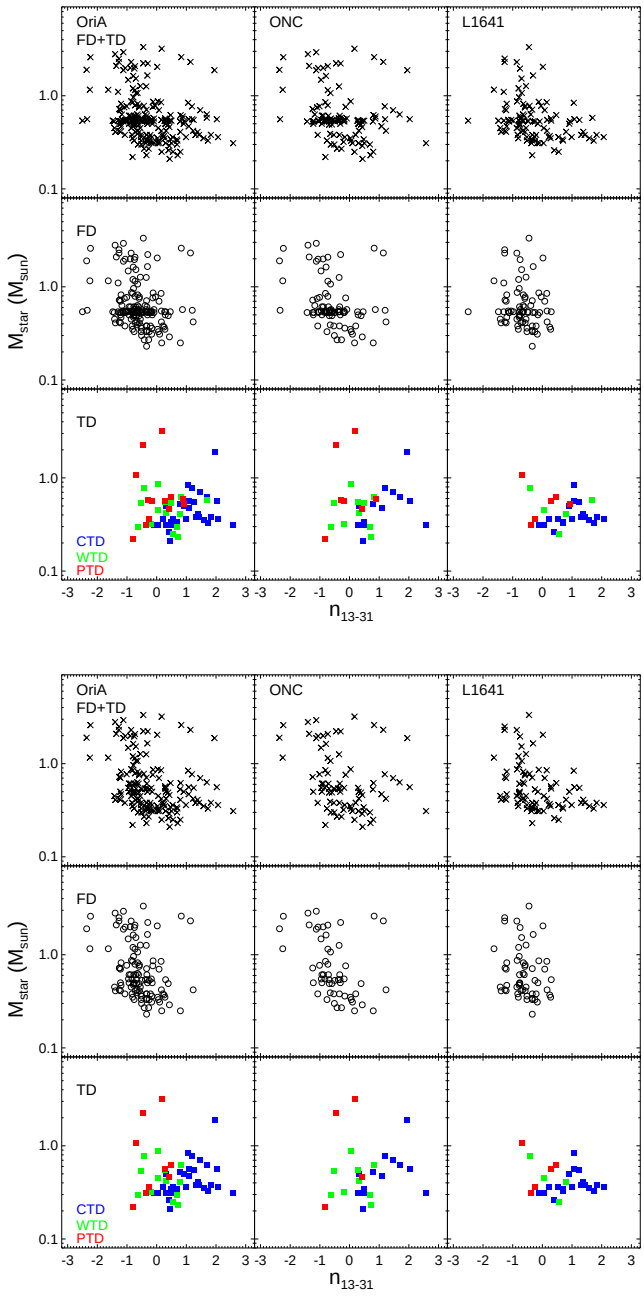


Figure C.31 n_{13-31} vs. $\log M_\star$. Upper panel: all available objects; Lower panel: objects with available spectral types only

Table C.61 n_{13-31} vs. $\log M_\star$ (I)

	Ori A				ONC				L1641			
	N	ρ	τ	r	N	ρ	τ	r	N	ρ	τ	r
TDFD	231	-0.314	-0.219	-0.278	122	-0.279	-0.203	-0.250	109	-0.364	-0.241	-0.320
		0.000	0.000	0.000		0.002	0.001	0.005		0.000	0.000	0.001
FD	170	-0.283	-0.201	-0.246	91	-0.379	-0.278	-0.318	79	-0.171	-0.114	-0.132
		0.000	0.000	0.001		0.000	0.000	0.002		0.132	0.136	0.246
TD	61	0.074	0.044	-0.011	31	0.150	0.102	0.090	30	0.066	0.035	-0.144
		0.572	0.614	0.933		0.420	0.420	0.630		0.729	0.785	0.448

ρ: Spearsman's ρ
τ: Kendall's τ
r: Pearson's r

Table C.62 n_{13-31} vs. $\log M_\star$ (II)

	Ori A				ONC				L1641			
	N	ρ	τ	r	N	ρ	τ	r	N	ρ	τ	r
TDFD	168	-0.377	-0.262	-0.329	83	-0.356	-0.261	-0.306	85	-0.416	-0.276	-0.365
		0.000	0.000	0.000		0.001	0.000	0.005		0.000	0.000	0.001
FD	114	-0.383	-0.275	-0.319	57	-0.508	-0.389	-0.401	57	-0.231	-0.156	-0.192
		0.000	0.000	0.001		0.000	0.000	0.002		0.084	0.087	0.152
TD	54	0.099	0.064	-0.008	26	0.173	0.121	0.102	28	0.021	-0.011	-0.204
		0.474	0.496	0.954		0.397	0.387	0.620		0.916	0.935	0.298

ρ: Spearsman's ρ
τ: Kendall's τ
r: Pearson's r

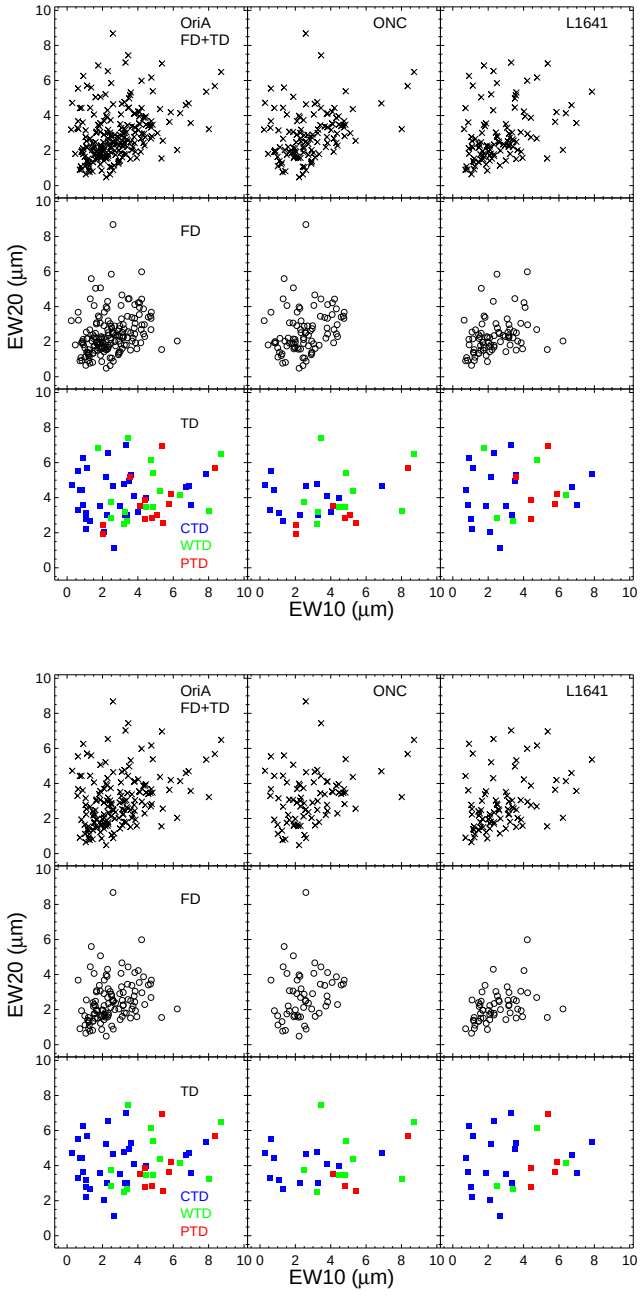


Figure C.32 EW10 vs. EW20. Upper panel: all available objects; Lower panel: objects with available spectral types only

Table C.63 EW10 vs. EW20 (I)

	Ori A				ONC				L1641			
	N	ρ	τ	r	N	ρ	τ	r	N	ρ	τ	r
TDFD	231	0.372	0.264	0.334	122	0.357	0.248	0.320	109	0.385	0.274	0.349
		0.000	0.000	0.000		0.000	0.000	0.000		0.000	0.000	0.000
FD	170	0.382	0.261	0.292	91	0.349	0.234	0.280	79	0.406	0.281	0.321
		0.000	0.000	0.000		0.001	0.001	0.007		0.000	0.000	0.004
TD	61	0.146	0.109	0.153	31	0.176	0.123	0.248	30	0.120	0.085	0.094
		0.263	0.213	0.239		0.344	0.332	0.179		0.528	0.509	0.621

ρ: Spearsman's ρ
τ: Kendall's τ
r: Pearson's r

Table C.64 EW10 vs. EW20 (II)

	Ori A				ONC				L1641			
	N	ρ	τ	r	N	ρ	τ	r	N	ρ	τ	r
TDFD	168	0.351	0.255	0.324	83	0.293	0.203	0.284	85	0.396	0.286	0.373
		0.000	0.000	0.000		0.007	0.007	0.009		0.000	0.000	0.000
FD	114	0.396	0.275	0.281	57	0.304	0.207	0.270	57	0.478	0.332	0.388
		0.000	0.000	0.002		0.021	0.023	0.042		0.000	0.000	0.003
TD	54	0.153	0.109	0.174	26	0.129	0.074	0.216	28	0.179	0.122	0.150
		0.270	0.244	0.208		0.530	0.596	0.289		0.362	0.363	0.446

ρ: Spearsman's ρ
τ: Kendall's τ
r: Pearson's r

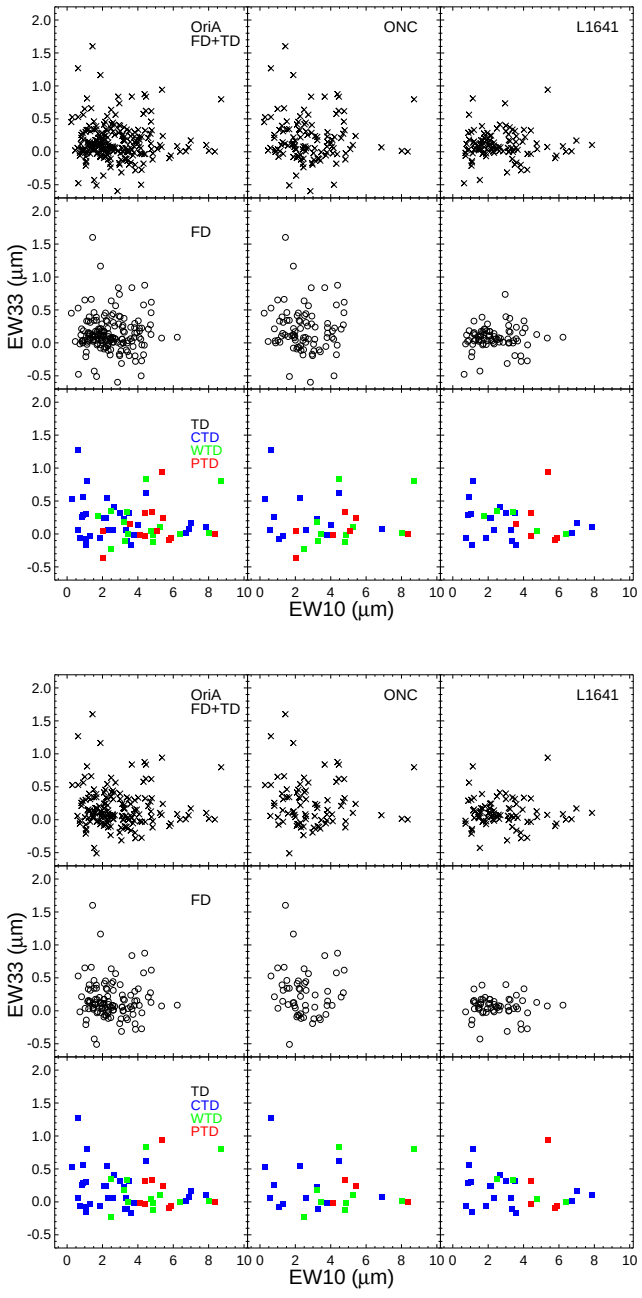


Figure C.33 EW10 vs. EW33. Zoomed in, Upper panel: all available objects; Lower panel: objects with available spectral types only

Table C.65 EW10 vs. EW33 (I)

	Ori A				ONC				L1641			
	N	ρ	τ	r	N	ρ	τ	r	N	ρ	τ	r
TDFD	231	-0.063	-0.043	-0.040	122	-0.098	-0.067	-0.052	109	-0.014	-0.008	-0.007
		0.341	0.331	0.545		0.283	0.276	0.569		0.887	0.900	0.942
FD	170	-0.027	-0.022	-0.064	91	-0.100	-0.071	-0.096	79	0.063	0.037	0.027
		0.731	0.676	0.407		0.347	0.317	0.365		0.579	0.626	0.813
TD	61	-0.097	-0.065	-0.094	31	0.047	0.039	-0.015	30	-0.210	-0.138	-0.206
		0.456	0.462	0.471		0.803	0.759	0.936		0.265	0.284	0.275

ρ: Spearsman's ρ
τ: Kendall's τ
r: Pearson's r

Table C.66 EW10 vs. EW33 (II)

	Ori A				ONC				L1641			
	N	ρ	τ	r	N	ρ	τ	r	N	ρ	τ	r
TDFD	168	-0.103	-0.072	-0.040	83	-0.133	-0.094	-0.051	85	-0.071	-0.045	-0.040
		0.182	0.168	0.607		0.230	0.211	0.647		0.521	0.538	0.716
FD	114	-0.091	-0.066	-0.090	57	-0.153	-0.112	-0.131	57	-0.015	-0.010	-0.043
		0.335	0.300	0.341		0.254	0.218	0.331		0.911	0.912	0.751
TD	54	-0.117	-0.076	-0.121	26	-0.011	-0.015	-0.070	28	-0.177	-0.103	-0.199
		0.399	0.420	0.383		0.956	0.912	0.734		0.367	0.440	0.310

ρ: Spearsmans ρ
τ: Kendalls τ
r: Pearsons r

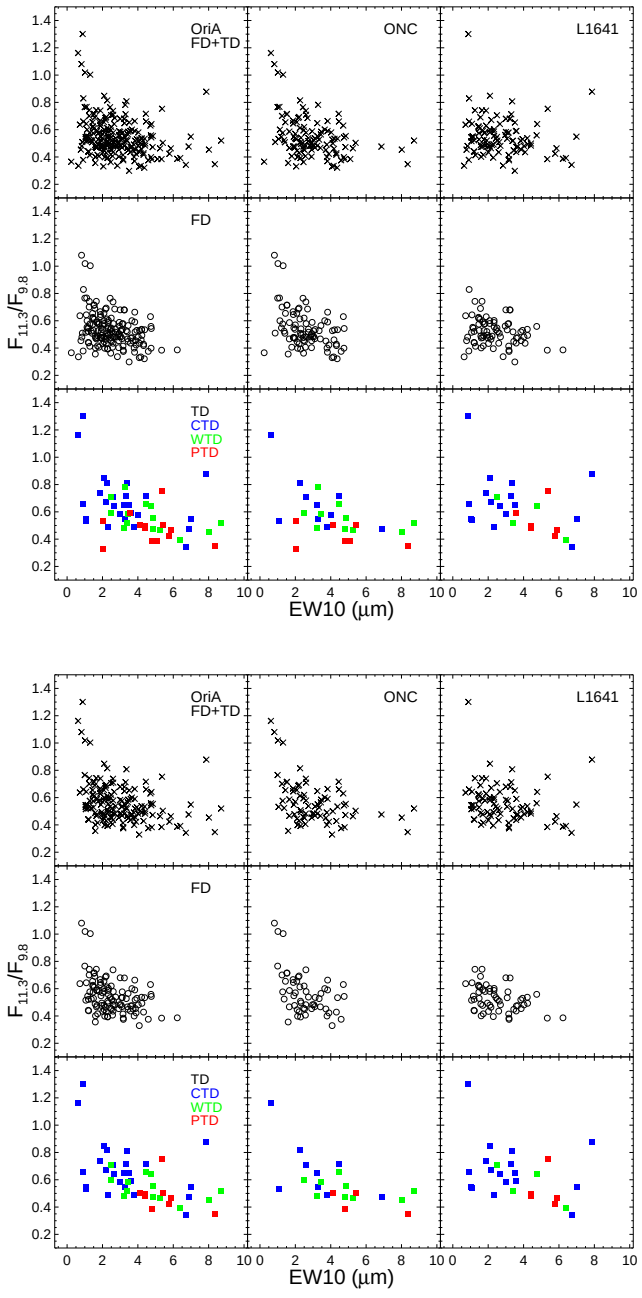


Figure C.34 EW10 vs. $F_{11.3}/F_{9.8}$. Zoomed in, Upper panel: all available objects; Lower panel: objects with available spectral types only

Table C.67 EW10 vs. $F_{11.3}/F_{9.8}$ (I)

	Ori A				ONC				L1641			
	N	ρ	τ	r	N	ρ	τ	r	N	ρ	τ	r
TDFD	231	-0.254	-0.181	-0.080	122	-0.291	-0.213	-0.022	109	-0.187	-0.131	-0.143
		0.000	0.000	0.226		0.001	0.001	0.810		0.051	0.043	0.138
FD	170	-0.290	-0.208	-0.028	91	-0.364	-0.266	-0.001	79	-0.201	-0.143	-0.248
		0.000	0.000	0.717		0.000	0.000	0.992		0.076	0.062	0.028
TD	61	-0.433	-0.341	-0.163	31	-0.321	-0.265	-0.044	30	-0.515	-0.402	-0.294
		0.000	0.000	0.209		0.078	0.036	0.814		0.004	0.002	0.115

ρ: Spearsman's ρ
τ: Kendall's τ
r: Pearson's r

Table C.68 EW10 vs. $F_{11.3}/F_{9.8}$ (II)

	Ori A				ONC				L1641			
	N	ρ	τ	r	N	ρ	τ	r	N	ρ	τ	r
TDFD	168	-0.347	-0.245	-0.106	83	-0.374	-0.270	-0.052	85	-0.308	-0.215	-0.163
		0.000	0.000	0.171		0.000	0.000	0.641		0.004	0.004	0.136
FD	114	-0.410	-0.287	-0.398	57	-0.476	-0.339	-0.490	57	-0.371	-0.254	-0.386
		0.000	0.000	0.000		0.000	0.000	0.000		0.004	0.005	0.003
TD	54	-0.461	-0.365	-0.163	26	-0.390	-0.333	-0.046	28	-0.489	-0.386	-0.289
		0.000	0.000	0.239		0.049	0.017	0.823		0.008	0.004	0.136

ρ: Spearsman's ρ
τ: Kendall's τ
r: Pearson's r

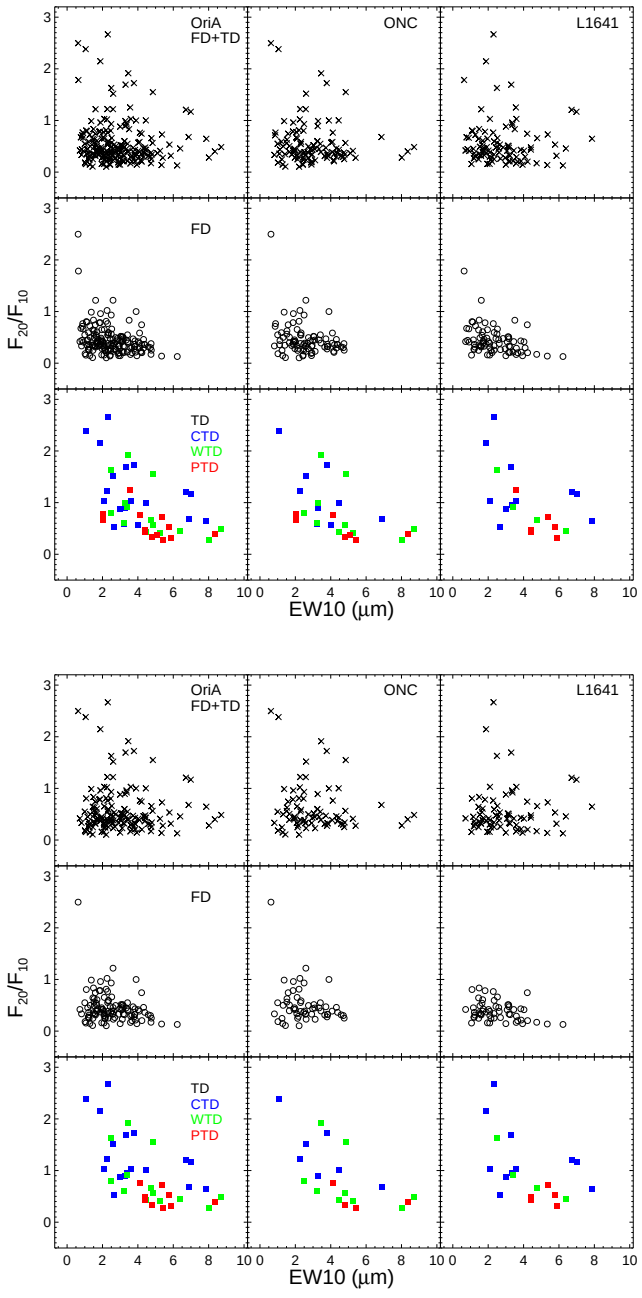


Figure C.35 EW10 vs. F_{20}/F_{10}. Upper panel: all available objects; Lower panel: objects with available spectral types only

Table C.69 EW10 vs. F_{20}/F_{10} (I)

	Ori A				ONC				L1641			
	N	ρ	τ	r	N	ρ	τ	r	N	ρ	τ	r
TDFD	230	-0.212	-0.143	-0.270	121	-0.222	-0.146	-0.311	109	-0.195	-0.137	-0.218
		0.001	0.001	0.000		0.014	0.017	0.001		0.042	0.035	0.023
FD	170	-0.324	-0.228	-0.307	91	-0.287	-0.197	-0.354	79	-0.379	-0.273	-0.386
		0.000	0.000	0.000		0.006	0.006	0.001		0.001	0.000	0.000
TD	60	-0.753	-0.551	-0.601	30	-0.755	-0.555	-0.562	30	-0.753	-0.554	-0.638
		0.000	0.000	0.000		0.000	0.000	0.001		0.000	0.000	0.000

ρ: Spearsman's ρ
τ: Kendall's τ
r: Pearson's r

Table C.70 EW10 vs. F_{20}/F_{10} (II)

	Ori A				ONC				L1641			
	N	ρ	τ	r	N	ρ	τ	r	N	ρ	τ	r
TDFD	167	-0.151	-0.103	-0.271	82	-0.193	-0.137	-0.292	85	-0.130	-0.089	-0.246
		0.051	0.048	0.000		0.083	0.068	0.008		0.235	0.230	0.023
FD	114	-0.185	-0.139	-0.253	57	-0.185	-0.145	-0.266	57	-0.257	-0.184	-0.310
		0.048	0.028	0.007		0.167	0.112	0.046		0.054	0.043	0.019
TD	53	-0.775	-0.576	-0.624	25	-0.794	-0.604	-0.607	28	-0.733	-0.540	-0.649
		0.000	0.000	0.000		0.000	0.000	0.001		0.000	0.000	0.000

ρ: Spearsman's ρ
τ: Kendall's τ
r: Pearson's r

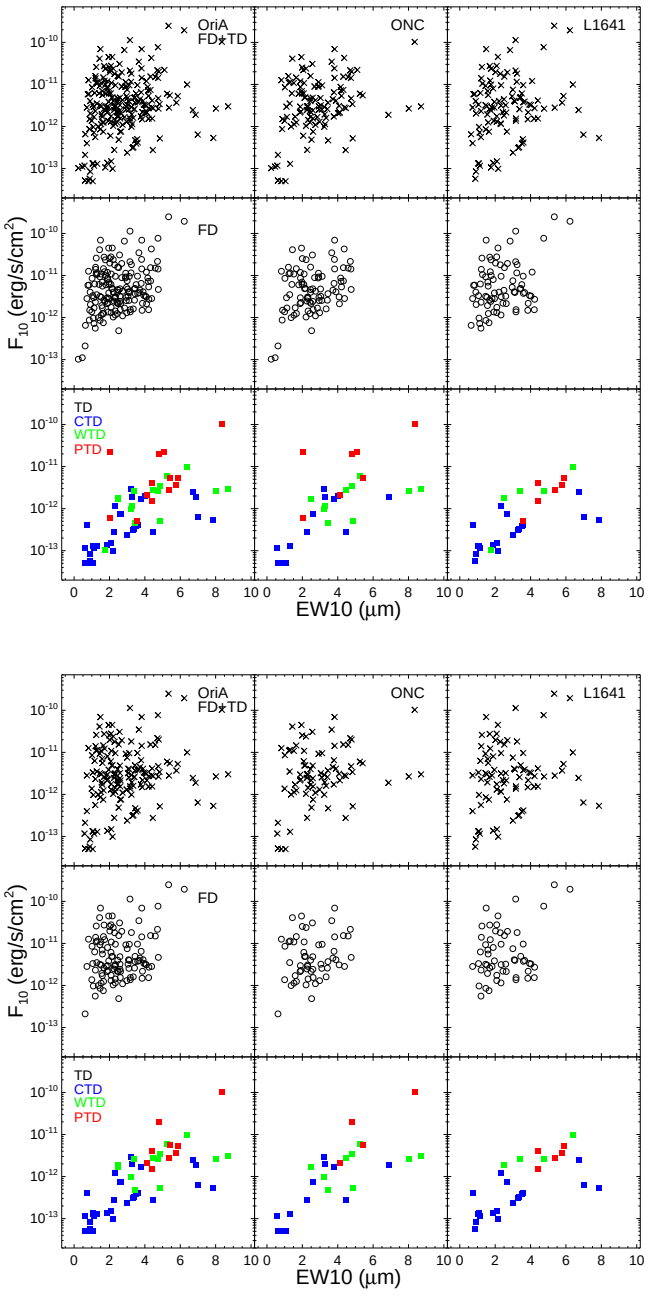


Figure C.36 EW10 vs. $\log F_{10}$. Upper panel: all available objects; Lower panel: objects with available spectral types only

Table C.71 EW10 vs. $\log F_{10}$ (I)

	Ori A				ONC				L1641			
	N	ρ	τ	r	N	ρ	τ	r	N	ρ	τ	r
TDFD	230	0.201	0.138	0.252	121	0.239	0.163	0.321	109	0.142	0.100	0.179
		0.002	0.002	0.000		0.008	0.008	0.000		0.142	0.125	0.063
FD	170	0.241	0.167	0.352	91	0.257	0.179	0.368	79	0.220	0.146	0.353
		0.002	0.001	0.000		0.014	0.012	0.000		0.051	0.057	0.001
TD	60	0.741	0.565	0.689	30	0.695	0.537	0.676	30	0.776	0.605	0.717
		0.000	0.000	0.000		0.000	0.000	0.000		0.000	0.000	0.000

ρ: Spearsman's ρ
τ: Kendall's τ
r: Pearson's r

Table C.72 EW10 vs. $\log F_{10}$ (II)

	Ori A				ONC				L1641			
	N	ρ	τ	r	N	ρ	τ	r	N	ρ	τ	r
TDFD	167	0.180	0.124	0.233	82	0.209	0.145	0.282	85	0.151	0.107	0.188
		0.020	0.017	0.002		0.060	0.054	0.010		0.166	0.146	0.085
FD	114	0.141	0.097	0.265	57	0.150	0.112	0.211	57	0.146	0.090	0.312
		0.135	0.126	0.004		0.267	0.218	0.115		0.278	0.322	0.018
TD	53	0.785	0.600	0.745	25	0.786	0.598	0.772	28	0.760	0.598	0.708
		0.000	0.000	0.000		0.000	0.000	0.000		0.000	0.000	0.000

ρ: Spearsman's ρ
τ: Kendall's τ
r: Pearson's r

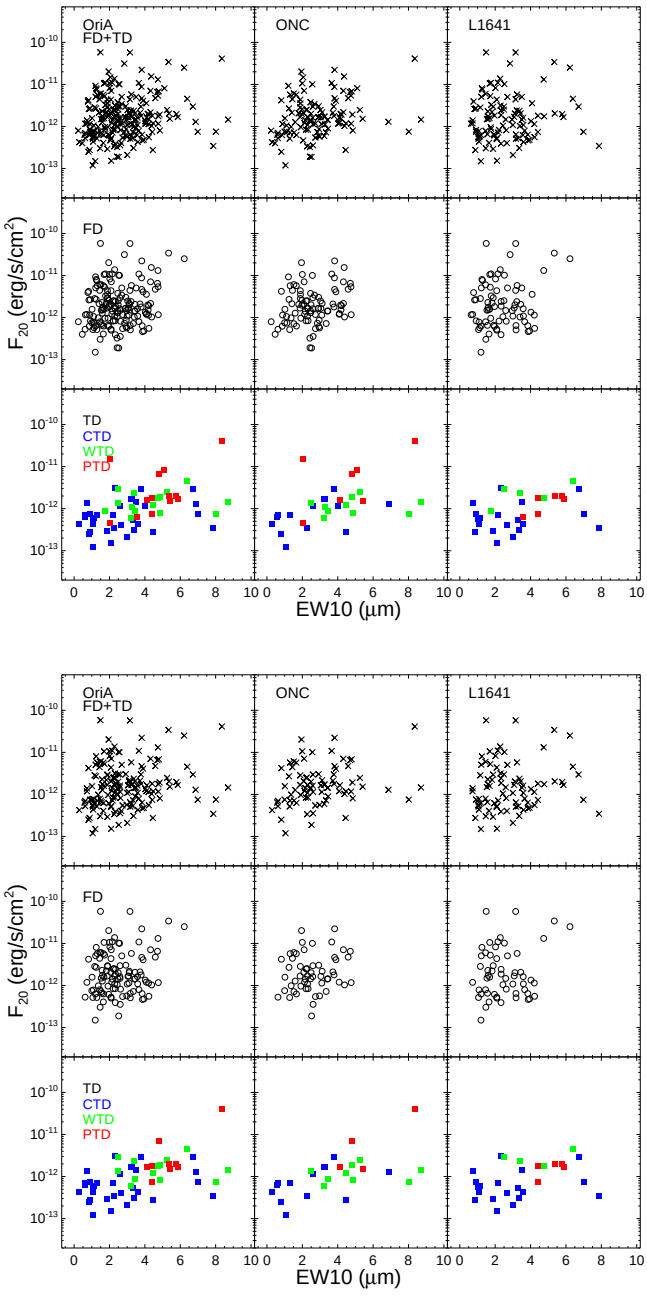


Figure C.37 EW10 vs. $\log F_{20}$. Upper panel: all available objects; Lower panel: objects with available spectral types only

Table C.73 EW10 vs. $\log F_{20}$ (I)

	Ori A				ONC				L1641			
	N	ρ	τ	r	N	ρ	τ	r	N	ρ	τ	r
TDFD	231	0.165	0.110	0.174	122	0.237	0.160	0.260	109	0.063	0.043	0.090
		0.012	0.013	0.008		0.008	0.009	0.004		0.516	0.504	0.352
FD	170	0.129	0.085	0.198	91	0.189	0.126	0.238	79	0.058	0.039	0.174
		0.093	0.098	0.010		0.073	0.078	0.023		0.612	0.614	0.125
TD	61	0.490	0.334	0.440	31	0.555	0.386	0.486	30	0.367	0.246	0.364
		0.000	0.000	0.000		0.001	0.002	0.006		0.046	0.056	0.048

ρ: Spearsman's ρ
τ: Kendall's τ
r: Pearson's r

Table C.74 EW10 vs. $\log F_{20}$ (II)

	Ori A				ONC				L1641			
	N	ρ	τ	r	N	ρ	τ	r	N	ρ	τ	r
TDFD	168	0.169	0.113	0.173	83	0.225	0.158	0.241	85	0.108	0.071	0.115
		0.029	0.029	0.025		0.041	0.035	0.028		0.325	0.335	0.295
FD	114	0.083	0.055	0.174	57	0.127	0.093	0.167	57	0.061	0.033	0.179
		0.378	0.386	0.064		0.346	0.305	0.214		0.654	0.720	0.183
TD	54	0.516	0.345	0.493	26	0.599	0.413	0.582	28	0.385	0.249	0.371
		0.000	0.000	0.000		0.001	0.003	0.002		0.043	0.063	0.052

ρ: Spearsman's ρ
τ: Kendall's τ
r: Pearson's r

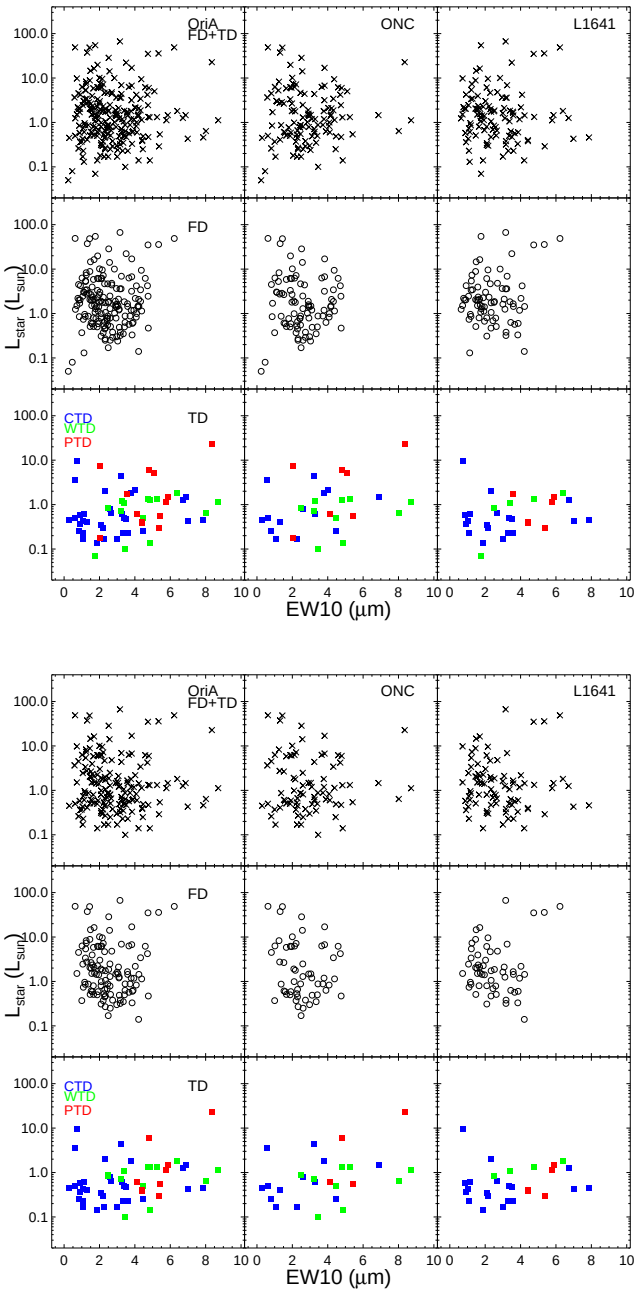


Figure C.38 EW10 vs. $\log L_\star$. Upper panel: all available objects; Lower panel: objects with available spectral types only

Table C.75 EW10 vs. $\log L_\star$ (I)

	Ori A				ONC				L1641			
	N	ρ	τ	r	N	ρ	τ	r	N	ρ	τ	r
TDFD	231	-0.054	-0.035	0.010	122	0.002	0.008	0.034	109	-0.122	-0.082	-0.016
		0.416	0.428	0.880		0.979	0.898	0.710		0.205	0.207	0.869
FD	170	-0.064	-0.041	0.055	91	-0.072	-0.041	-0.021	79	-0.020	-0.016	0.165
		0.410	0.428	0.476		0.498	0.562	0.843		0.861	0.839	0.146
TD	61	0.282	0.184	0.269	31	0.307	0.194	0.332	30	0.231	0.164	0.156
		0.028	0.036	0.036		0.093	0.125	0.068		0.220	0.203	0.410

ρ: Spearsman's ρ
τ: Kendall's τ
r: Pearson's r

Table C.76 EW10 vs. $\log L_\star$ (II)

	Ori A				ONC				L1641			
	N	ρ	τ	r	N	ρ	τ	r	N	ρ	τ	r
TDFD	168	-0.102	-0.071	-0.038	83	-0.043	-0.029	-0.039	85	-0.168	-0.115	-0.039
		0.188	0.174	0.625		0.701	0.699	0.726		0.124	0.121	0.723
FD	114	-0.164	-0.113	-0.028	57	-0.186	-0.128	-0.187	57	-0.131	-0.095	0.130
		0.082	0.075	0.767		0.167	0.159	0.164		0.332	0.294	0.335
TD	54	0.270	0.175	0.268	26	0.330	0.207	0.372	28	0.189	0.133	0.104
		0.049	0.062	0.050		0.099	0.139	0.061		0.335	0.321	0.598

ρ: Spearsman's ρ
τ: Kendall's τ
r: Pearson's r

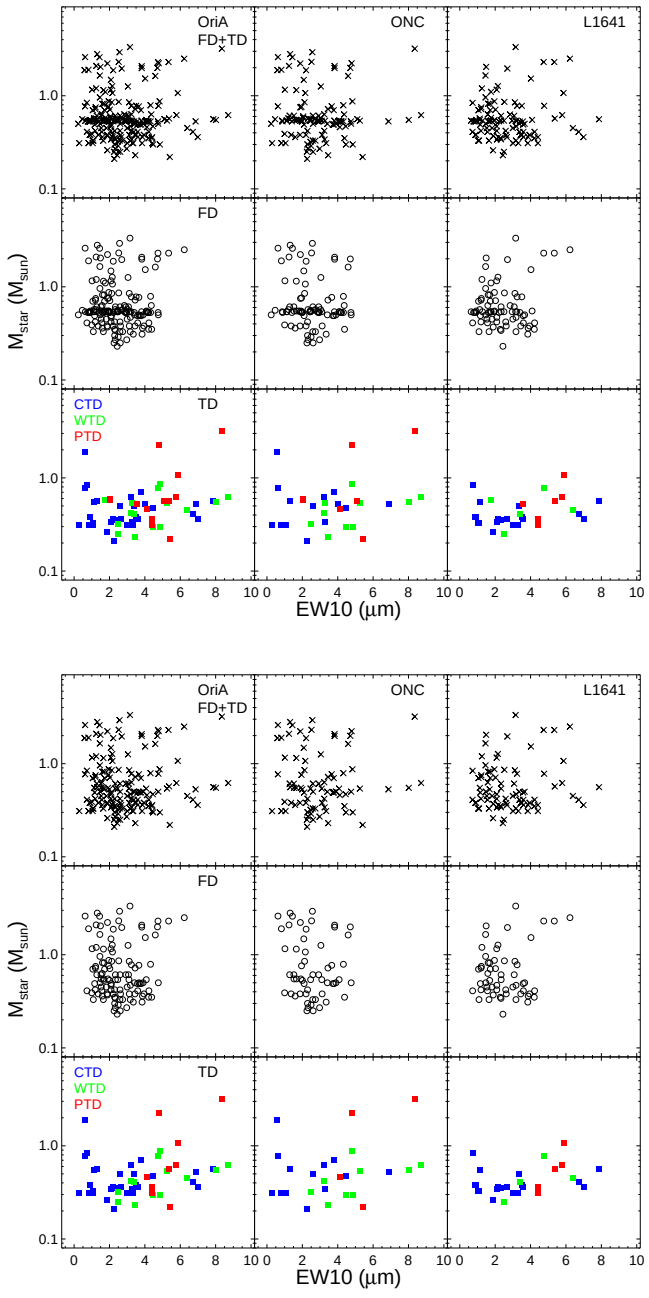


Figure C.39 EW10 vs. log $M_\star$. Upper panel: all available objects; Lower panel: objects with available spectral types only

Table C.77 EW10 vs. $M_\star$ (I)

	Ori A				ONC				L1641			
	N	ρ	τ	r	N	ρ	τ	r	N	ρ	τ	r
TDFD	231	-0.056	-0.038	0.035	122	-0.095	-0.062	-0.005	109	-0.058	-0.041	0.079
		0.393	0.384	0.597		0.297	0.309	0.956		0.550	0.524	0.414
FD	170	-0.080	-0.052	0.043	91	-0.148	-0.098	-0.086	79	-0.037	-0.022	0.199
		0.302	0.313	0.578		0.161	0.170	0.418		0.747	0.770	0.079
TD	61	0.220	0.158	0.261	31	0.114	0.091	0.248	30	0.282	0.195	0.287
		0.088	0.073	0.042		0.541	0.471	0.179		0.131	0.130	0.124

ρ: Spearsman's ρ
τ: Kendall's τ
r: Pearson's r

Table C.78 EW10 vs. $M_\star$ (II)

	Ori A				ONC				L1641			
	N	ρ	τ	r	N	ρ	τ	r	N	ρ	τ	r
TDFD	168	-0.033	-0.021	0.031	83	-0.082	-0.049	-0.017	85	-0.023	-0.017	0.086
		0.669	0.682	0.690		0.459	0.516	0.879		0.832	0.818	0.434
FD	114	-0.088	-0.059	0.037	57	-0.178	-0.114	-0.121	57	-0.040	-0.027	0.203
		0.351	0.352	0.696		0.185	0.211	0.370		0.769	0.771	0.130
TD	54	0.281	0.197	0.283	26	0.175	0.143	0.264	28	0.344	0.228	0.324
		0.040	0.036	0.038		0.393	0.307	0.193		0.073	0.089	0.093

ρ: Spearsman's ρ
τ: Kendall's τ
r: Pearson's r

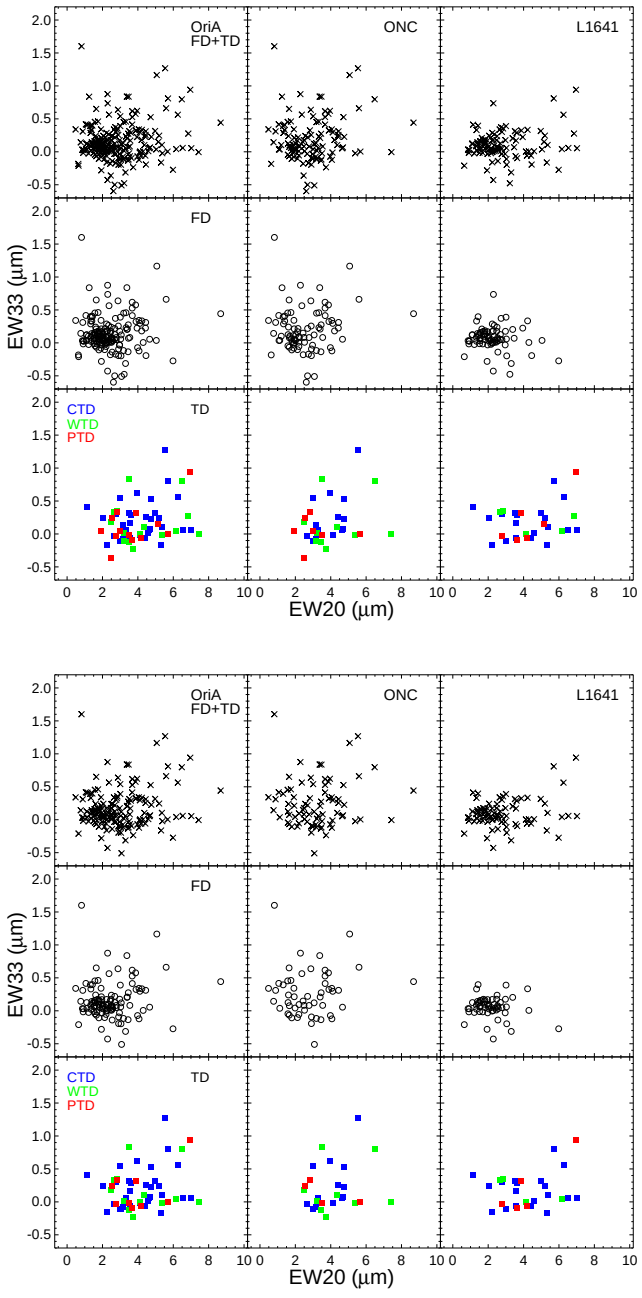


Figure C.40 EW20 vs. EW33. Zoomed in, Upper panel: all available objects; Lower panel: objects with available spectral types only

Table C.79 EW20 vs. EW33 (I)

	Ori A				ONC				L1641			
	N	ρ	τ	r	N	ρ	τ	r	N	ρ	τ	r
TDFD	231	0.022	0.013	-0.060	122	-0.002	-0.003	-0.133	109	0.064	0.049	0.243
		0.744	0.765	0.364		0.983	0.961	0.144		0.511	0.447	0.011
FD	170	-0.008	-0.010	-0.107	91	-0.027	-0.025	-0.172	79	-0.002	0.007	0.334
		0.918	0.846	0.165		0.801	0.721	0.103		0.989	0.929	0.003
TD	61	0.186	0.133	0.255	31	0.238	0.164	0.303	30	0.082	0.064	0.218
		0.151	0.129	0.047		0.197	0.196	0.098		0.667	0.617	0.247

ρ: Spearsman's ρ
τ: Kendall's τ
r: Pearson's r

Table C.80 EW20 vs. EW33 (II)

	Ori A				ONC				L1641			
	N	ρ	τ	r	N	ρ	τ	r	N	ρ	τ	r
TDFD	168	0.012	0.010	-0.086	83	-0.042	-0.034	-0.126	85	0.039	0.035	0.231
		0.875	0.844	0.268		0.708	0.654	0.256		0.725	0.632	0.033
FD	114	-0.012	-0.011	-0.162	57	-0.070	-0.056	-0.171	57	-0.037	-0.022	-0.141
		0.898	0.858	0.085		0.604	0.536	0.203		0.783	0.809	0.295
TD	54	0.132	0.099	0.206	26	0.173	0.123	0.216	28	0.081	0.061	0.212
		0.342	0.293	0.135		0.397	0.377	0.289		0.683	0.649	0.279

ρ: Spearsman's ρ
τ: Kendall's τ
r: Pearson's r

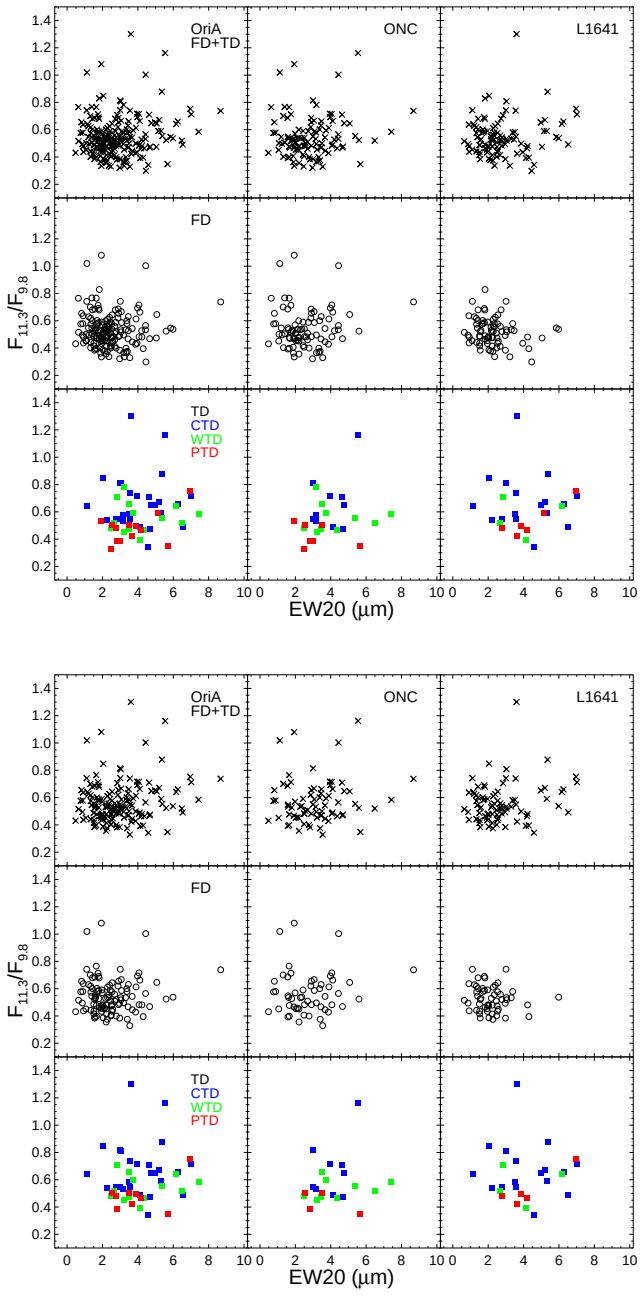


Figure C.41 EW20 vs $F_{11.3}/F_{9.8}$. Zoomed in, Upper panel: all available objects; Lower panel: objects with available spectral types only

Table C.81 EW20 vs $F_{11.3}/F_{9.8}$ (I)

	Ori A				ONC				L1641			
	N	ρ	τ	r	N	ρ	τ	r	N	ρ	τ	r
TDFD	231	0.080	0.052	0.042	122	0.044	0.031	-0.034	109	0.127	0.079	0.142
		0.224	0.236	0.525		0.627	0.608	0.710		0.188	0.221	0.141
FD	170	-0.069	-0.043	0.029	91	0.006	0.010	0.050	79	-0.171	-0.119	-0.183
		0.370	0.407	0.707		0.956	0.885	0.638		0.133	0.120	0.106
TD	61	0.149	0.094	-0.025	31	0.039	0.032	-0.145	30	0.240	0.163	0.046
		0.252	0.284	0.848		0.835	0.799	0.436		0.200	0.205	0.809

ρ: Spearsman's ρ
τ: Kendall's τ
r: Pearson's r

Table C.82 EW20 vs $F_{11.3}/F_{9.8}$ (II)

	Ori A				ONC				L1641			
	N	ρ	τ	r	N	ρ	τ	r	N	ρ	τ	r
TDFD	168	0.097	0.062	0.021	83	0.026	0.020	-0.057	85	0.154	0.098	0.136
		0.211	0.235	0.787		0.815	0.786	0.609		0.159	0.186	0.215
FD	114	-0.020	-0.012	0.039	57	0.049	0.040	0.016	57	-0.156	-0.106	-0.136
		0.836	0.852	0.680		0.717	0.660	0.906		0.247	0.245	0.313
TD	54	0.057	0.026	-0.051	26	-0.062	-0.046	-0.167	28	0.160	0.101	0.035
		0.681	0.783	0.714		0.764	0.741	0.415		0.417	0.453	0.860

ρ: Spearsman's ρ
τ: Kendall's τ
r: Pearson's r

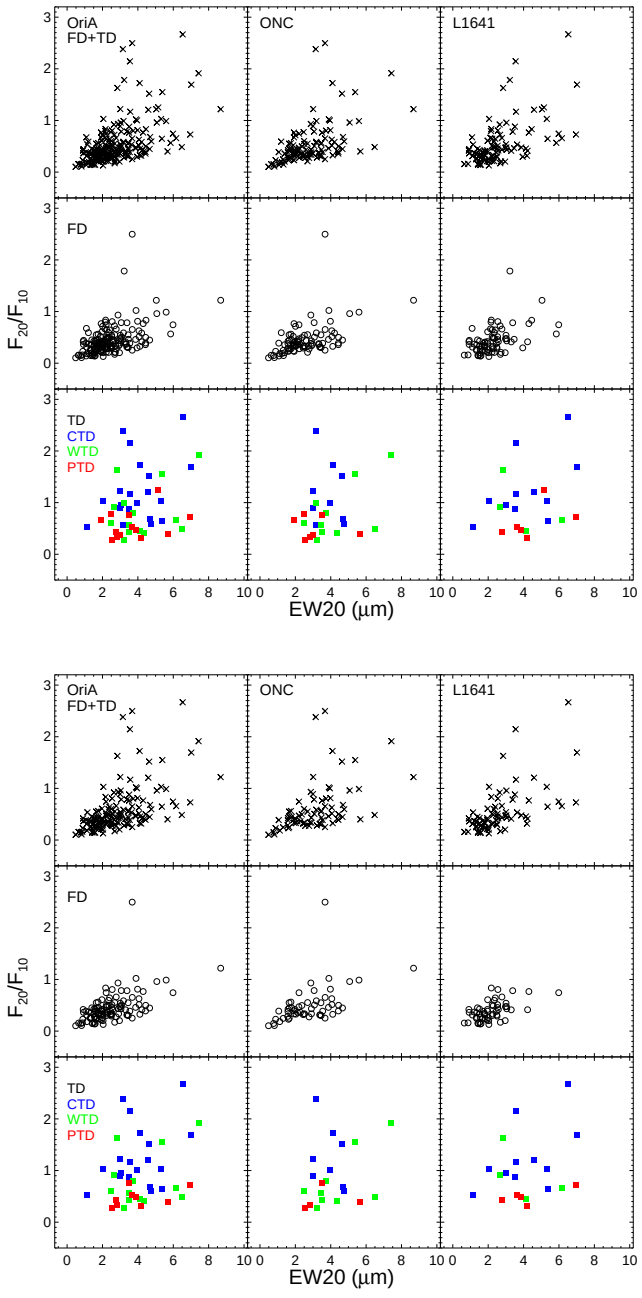


Figure C.42 EW20 vs. F_{20}/F_{10}. Upper panel: all available objects; Lower panel: objects with available spectral types only

Table C.83 EW20 vs. F_{20}/F_{10} (I)

	Ori A				ONC				L1641			
	N	ρ	τ	r	N	ρ	τ	r	N	ρ	τ	r
TDFD	230	0.600	0.424	0.365	121	0.556	0.399	0.234	109	0.641	0.446	0.538
		0.000	0.000	0.000		0.000	0.000	0.010		0.000	0.000	0.000
FD	170	0.508	0.358	0.222	91	0.517	0.373	0.177	79	0.478	0.319	0.482
		0.000	0.000	0.004		0.000	0.000	0.093		0.000	0.000	0.000
TD	60	0.261	0.180	0.298	30	0.201	0.149	0.210	30	0.283	0.186	0.355
		0.044	0.043	0.021		0.286	0.246	0.265		0.130	0.148	0.054

ρ: Spearsman's ρ
τ: Kendall's τ
r: Pearson's r

Table C.84 EW20 vs. F_{20}/F_{10} (II)

	Ori A				ONC				L1641			
	N	ρ	τ	r	N	ρ	τ	r	N	ρ	τ	r
TDFD	167	0.646	0.456	0.347	82	0.586	0.413	0.232	85	0.688	0.480	0.515
		0.000	0.000	0.000		0.000	0.000	0.036		0.000	0.000	0.000
FD	114	0.590	0.416	0.524	57	0.591	0.422	0.484	57	0.530	0.348	0.559
		0.000	0.000	0.000		0.000	0.000	0.000		0.000	0.000	0.000
TD	53	0.186	0.126	0.209	25	0.152	0.120	0.157	28	0.215	0.138	0.266
		0.183	0.182	0.133		0.467	0.400	0.454		0.273	0.304	0.171

ρ: Spearsman's ρ
τ: Kendall's τ
r: Pearson's r

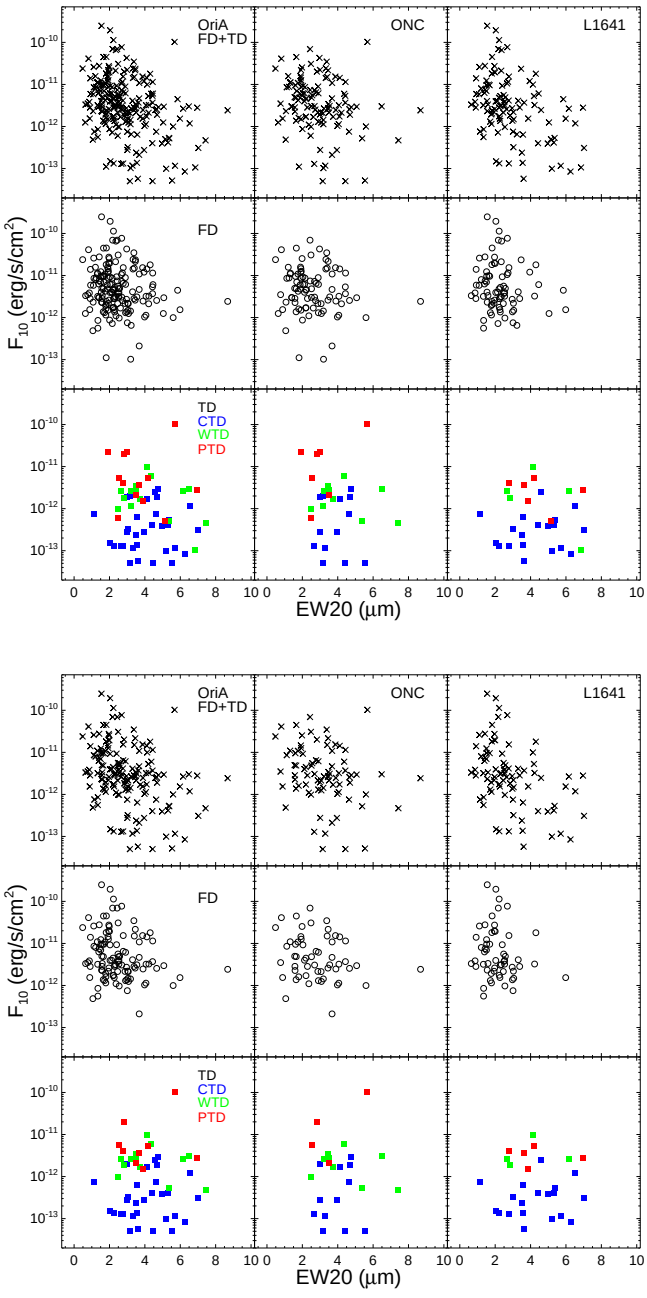


Figure C.43 EW20 vs. $\log F_{10}$. Upper panel: all available objects; Lower panel: objects with available spectral types only

Table C.85 EW20 vs. $\log F_{10}$ (I)

	Ori A				ONC				L1641			
	N	ρ	τ	r	N	ρ	τ	r	N	ρ	τ	r
TDFD	230	-0.323	-0.215	-0.298	121	-0.244	-0.163	-0.187	109	-0.400	-0.264	-0.426
		0.000	0.000	0.000		0.007	0.008	0.040		0.000	0.000	0.000
FD	170	-0.121	-0.081	-0.114	91	-0.110	-0.079	-0.098	79	-0.126	-0.070	-0.126
		0.116	0.117	0.139		0.298	0.267	0.355		0.270	0.363	0.269
TD	60	-0.128	-0.081	-0.108	30	-0.103	-0.067	-0.090	30	-0.068	-0.044	-0.051
		0.329	0.358	0.411		0.590	0.605	0.636		0.722	0.735	0.789

ρ: Spearsman's ρ
τ: Kendall's τ
r: Pearson's r

Table C.86 EW20 vs. $\log F_{10}$ (II)

	Ori A				ONC				L1641			
	N	ρ	τ	r	N	ρ	τ	r	N	ρ	τ	r
TDFD	167	-0.365	-0.243	-0.301	82	-0.273	-0.185	-0.199	85	-0.447	-0.295	-0.432
		0.000	0.000	0.000		0.013	0.014	0.073		0.000	0.000	0.000
FD	114	-0.190	-0.125	-0.160	57	-0.188	-0.134	-0.160	57	-0.180	-0.105	-0.157
		0.043	0.049	0.089		0.162	0.141	0.234		0.181	0.250	0.243
TD	53	-0.017	-0.012	0.015	25	0.008	-0.007	0.031	28	0.013	0.005	0.019
		0.903	0.902	0.915		0.971	0.963	0.883		0.949	0.968	0.924

ρ: Spearsman's ρ
τ: Kendall's τ
r: Pearson's r

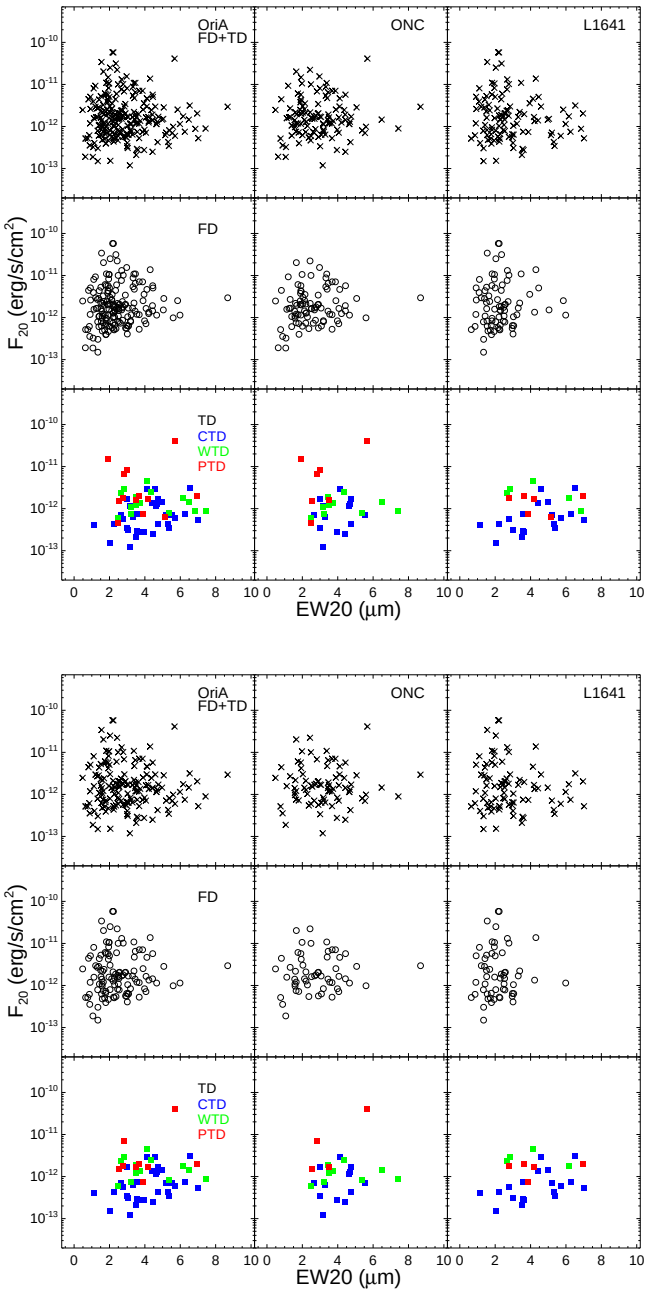


Figure C.44 EW20 vs. $\log F_{20}$. Upper panel: all available objects; Lower panel: objects with available spectral types only

Table C.87 EW20 vs. $\log F_{20}$ (I)

	Ori A				ONC				L1641			
	N	ρ	τ	r	N	ρ	τ	r	N	ρ	τ	r
TDFD	231	-0.022	-0.016	-0.014	122	0.022	0.010	0.074	109	-0.076	-0.047	-0.109
		0.737	0.721	0.832		0.808	0.870	0.418		0.433	0.471	0.259
FD	170	0.140	0.093	0.119	91	0.176	0.113	0.177	79	0.096	0.075	0.074
		0.068	0.072	0.122		0.094	0.112	0.093		0.398	0.328	0.517
TD	61	0.080	0.054	0.085	31	-0.001	0.002	0.009	30	0.257	0.159	0.243
		0.538	0.542	0.515		0.995	0.986	0.962		0.171	0.218	0.196

ρ: Spearsman's ρ
τ: Kendall's τ
r: Pearson's r

Table C.88 EW20 vs. $\log F_{20}$ (II)

	Ori A				ONC				L1641			
	N	ρ	τ	r	N	ρ	τ	r	N	ρ	τ	r
TDFD	168	-0.047	-0.032	-0.025	83	-0.014	-0.017	0.057	85	-0.092	-0.059	-0.122
		0.545	0.538	0.748		0.900	0.817	0.609		0.401	0.425	0.266
FD	114	0.098	0.065	0.080	57	0.125	0.068	0.135	57	0.058	0.046	0.028
		0.302	0.308	0.397		0.352	0.457	0.317		0.670	0.615	0.836
TD	54	0.164	0.107	0.208	26	0.102	0.071	0.173	28	0.275	0.175	0.262
		0.235	0.254	0.131		0.619	0.612	0.398		0.156	0.192	0.178

ρ: Spearsman's ρ
τ: Kendall's τ
r: Pearson's r

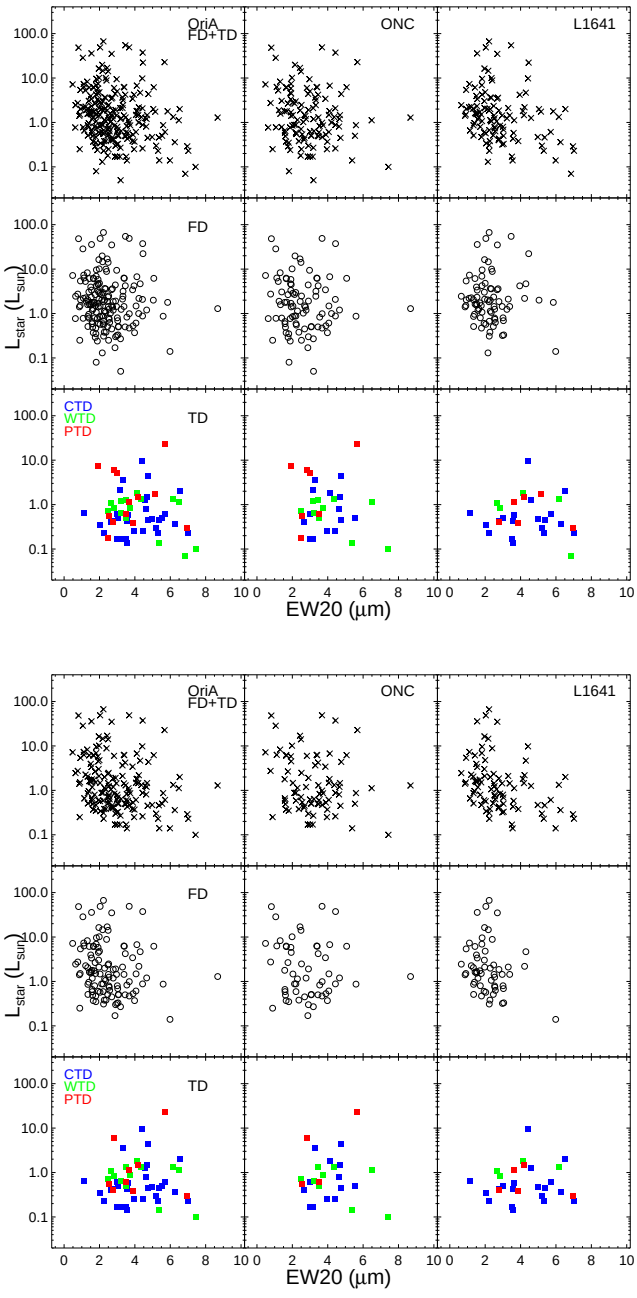


Figure C.45 EW20 vs. logL$_\star$. Upper panel: all available objects; Lower panel: objects with available spectral types only y

Table C.89 EW20 vs. $\log L_\star$ (I)

	Ori A				ONC				L1641			
	N	ρ	τ	r	N	ρ	τ	r	N	ρ	τ	r
TDFD	231	-0.245	-0.163	-0.224	122	-0.154	-0.109	-0.153	109	-0.325	-0.215	-0.311
		0.000	0.000	0.001		0.089	0.076	0.092		0.001	0.001	0.001
FD	170	-0.108	-0.073	-0.093	91	-0.084	-0.065	-0.093	79	-0.079	-0.048	-0.060
		0.160	0.157	0.228		0.430	0.363	0.381		0.488	0.530	0.599
TD	61	-0.065	-0.043	-0.118	31	-0.071	-0.056	-0.124	30	-0.012	0.007	-0.058
		0.617	0.622	0.365		0.705	0.658	0.506		0.948	0.957	0.761

ρ: Spearsman's ρ
τ: Kendall's τ
r: Pearson's r

Table C.90 EW20 vs. $\log L_\star$ (II)

	Ori A				ONC				L1641			
	N	ρ	τ	r	N	ρ	τ	r	N	ρ	τ	r
TDFD	168	-0.314	-0.213	-0.268	83	-0.162	-0.114	-0.198	85	-0.428	-0.284	-0.372
		0.000	0.000	0.000		0.144	0.128	0.073		0.000	0.000	0.000
FD	114	-0.225	-0.151	-0.178	57	-0.124	-0.091	-0.156	57	-0.240	-0.149	-0.245
		0.016	0.018	0.058		0.356	0.317	0.247		0.073	0.102	0.066
TD	54	0.019	0.015	0.005	26	0.034	0.031	-0.024	28	0.069	0.053	0.047
		0.890	0.869	0.971		0.868	0.825	0.907		0.728	0.691	0.812

ρ: Spearsman's ρ
τ: Kendall's τ
r: Pearson's r

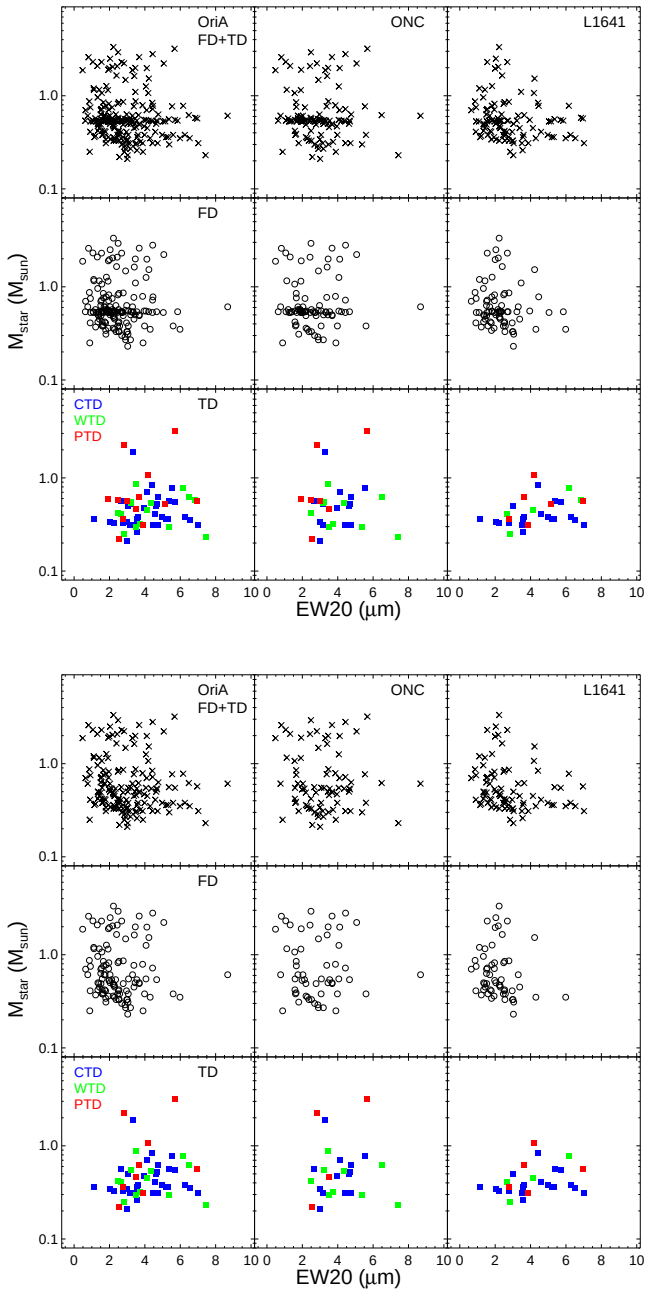


Figure C.46 EW20 vs. logM$_\star$. Upper panel: all available objects; Lower panel: objects with available spectral types only

Table C.91 EW20 vs. $\log M_\star$ (I)

	Ori A				ONC				L1641			
	N	ρ	τ	r	N	ρ	τ	r	N	ρ	τ	r
TDFD	231	-0.152	-0.108	-0.109	122	-0.100	-0.082	-0.058	109	-0.228	-0.153	-0.194
		0.021	0.014	0.098		0.271	0.178	0.526		0.017	0.019	0.043
FD	170	-0.094	-0.072	-0.043	91	-0.075	-0.068	-0.018	79	-0.134	-0.090	-0.115
		0.221	0.164	0.578		0.482	0.343	0.866		0.238	0.238	0.313
TD	61	0.136	0.087	0.091	31	0.018	-0.013	0.013	30	0.392	0.256	0.323
		0.296	0.323	0.486		0.922	0.918	0.945		0.032	0.047	0.082

ρ: Spearsman's ρ
τ: Kendall's τ
r: Pearson's r

Table C.92 EW20 vs. $\log M_\star$ (II)

	Ori A				ONC				L1641			
	N	ρ	τ	r	N	ρ	τ	r	N	ρ	τ	r
TDFD	168	-0.174	-0.120	-0.137	83	-0.063	-0.053	-0.101	85	-0.330	-0.219	-0.238
		0.024	0.021	0.077		0.573	0.476	0.364		0.002	0.003	0.028
FD	114	-0.126	-0.094	-0.069	57	-0.033	-0.041	-0.070	57	-0.260	-0.174	-0.167
		0.181	0.139	0.466		0.806	0.652	0.605		0.051	0.056	0.214
TD	54	0.194	0.127	0.116	26	0.122	0.077	0.043	28	0.349	0.217	0.280
		0.160	0.176	0.404		0.551	0.579	0.835		0.068	0.105	0.149

ρ: Spearsman's ρ
τ: Kendall's τ
r: Pearson's r

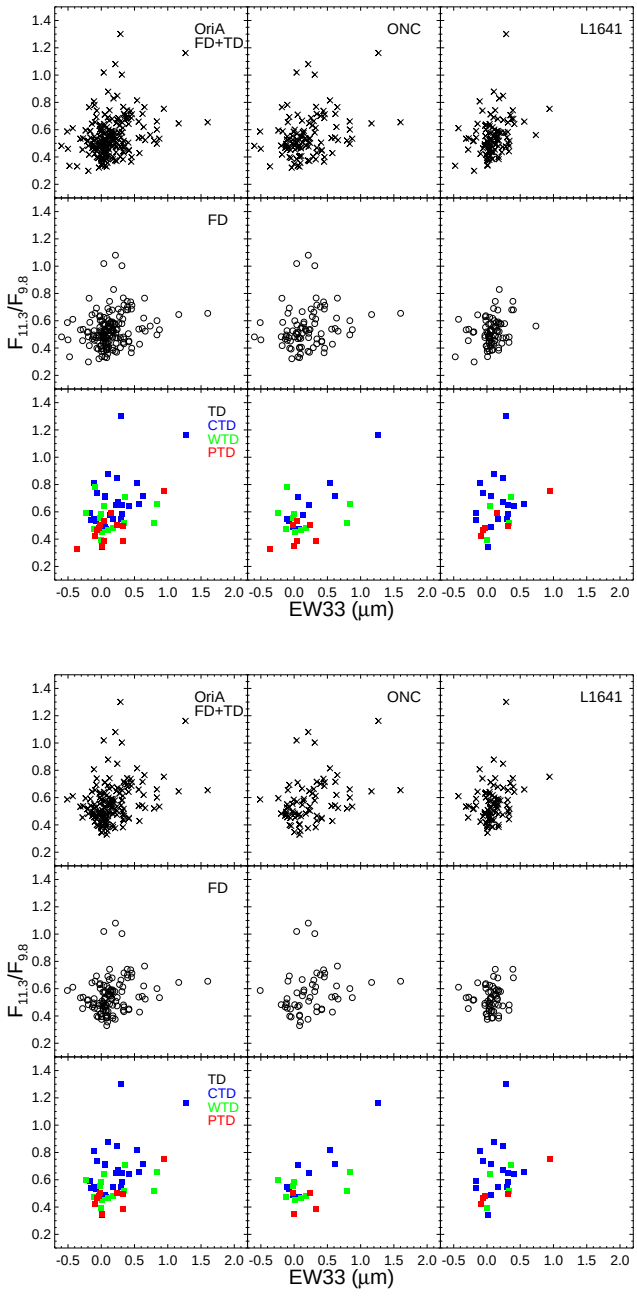


Figure C.47 EW33 vs. $F_{11.3}/F_{9.8}$. Zoomed in, Upper panel: all available objects; Lower panel: objects with available spectral types only

Table C.93 EW33 vs. $F_{11.3}/F_{9.8}$ (I)

	Ori A				ONC				L1641			
	N	ρ	τ	r	N	ρ	τ	r	N	ρ	τ	r
TDFD	231	0.218	0.146	-0.008	122	0.158	0.107	-0.007	109	0.318	0.217	-0.021
		0.001	0.001	0.904		0.081	0.081	0.939		0.001	0.001	0.828
FD	170	0.212	0.140	0.001	91	0.184	0.125	-0.003	79	0.225	0.149	0.107
		0.005	0.007	0.990		0.080	0.080	0.977		0.046	0.052	0.348
TD	61	0.223	0.156	-0.100	31	0.077	0.047	-0.081	30	0.261	0.184	-0.135
		0.084	0.075	0.443		0.682	0.708	0.665		0.164	0.153	0.477

ρ: Spearsman's ρ
τ: Kendall's τ
r: Pearson's r

Table C.94 EW33 vs. $F_{11.3}/F_{9.8}$ (II)

	Ori A				ONC				L1641			
	N	ρ	τ	r	N	ρ	τ	r	N	ρ	τ	r
TDFD	168	0.242	0.156	-0.005	83	0.243	0.158	-0.004	85	0.250	0.167	-0.048
		0.002	0.003	0.949		0.027	0.035	0.971		0.021	0.024	0.663
FD	114	0.263	0.166	0.033	57	0.305	0.199	0.040	57	0.081	0.048	0.098
		0.005	0.009	0.727		0.021	0.029	0.768		0.548	0.600	0.468
TD	54	0.202	0.139	-0.116	26	0.053	0.025	-0.092	28	0.259	0.188	-0.140
		0.142	0.137	0.404		0.798	0.860	0.655		0.183	0.160	0.477

ρ: Spearsman's ρ
τ: Kendall's τ
r: Pearson's r

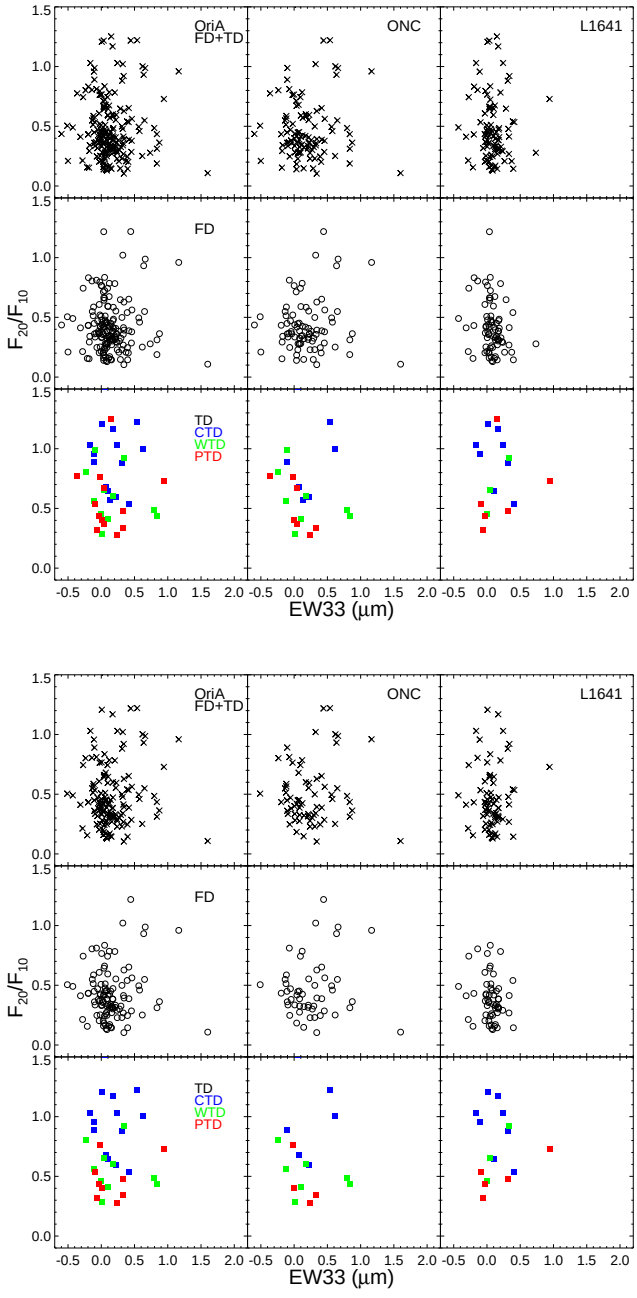


Figure C.48 EW33 vs. F_{20}/F_{10}. Zoomed in, Upper panel: all available objects; Lower panel: objects with available spectral types only

Table C.95 EW33 vs. F_{20}/F_{10} (I)

	Ori A				ONC				L1641			
	N	ρ	τ	r	N	ρ	τ	r	N	ρ	τ	r
TDFD	230	-0.055	-0.043	0.045	121	-0.103	-0.073	0.042	109	0.028	0.010	0.083
		0.402	0.330	0.497		0.261	0.237	0.647		0.772	0.873	0.391
FD	170	-0.112	-0.081	0.004	91	-0.044	-0.031	0.010	79	-0.216	-0.154	-0.051
		0.144	0.117	0.959		0.679	0.663	0.925		0.055	0.044	0.655
TD	60	0.100	0.059	0.403	30	-0.174	-0.115	0.457	30	0.238	0.161	0.321
		0.448	0.507	0.001		0.357	0.372	0.011		0.206	0.211	0.084

ρ: Spearsman's ρ
τ: Kendall's τ
r: Pearson's r

Table C.96 EW33 vs. F_{20}/F_{10} (II)

	Ori A				ONC				L1641			
	N	ρ	τ	r	N	ρ	τ	r	N	ρ	τ	r
TDFD	167	-0.009	-0.013	0.069	82	-0.101	-0.075	0.062	85	0.097	0.059	0.349
		0.905	0.808	0.376		0.365	0.320	0.580		0.380	0.420	0.001
FD	114	-0.057	-0.047	0.016	57	-0.020	-0.028	0.031	57	-0.175	-0.118	-0.172
		0.546	0.459	0.866		0.883	0.762	0.819		0.192	0.195	0.201
TD	53	0.070	0.035	0.398	25	-0.172	-0.130	0.446	28	0.217	0.151	0.329
		0.620	0.713	0.003		0.410	0.362	0.025		0.267	0.259	0.087

ρ: Spearsman's ρ
τ: Kendall's τ
r: Pearson's r

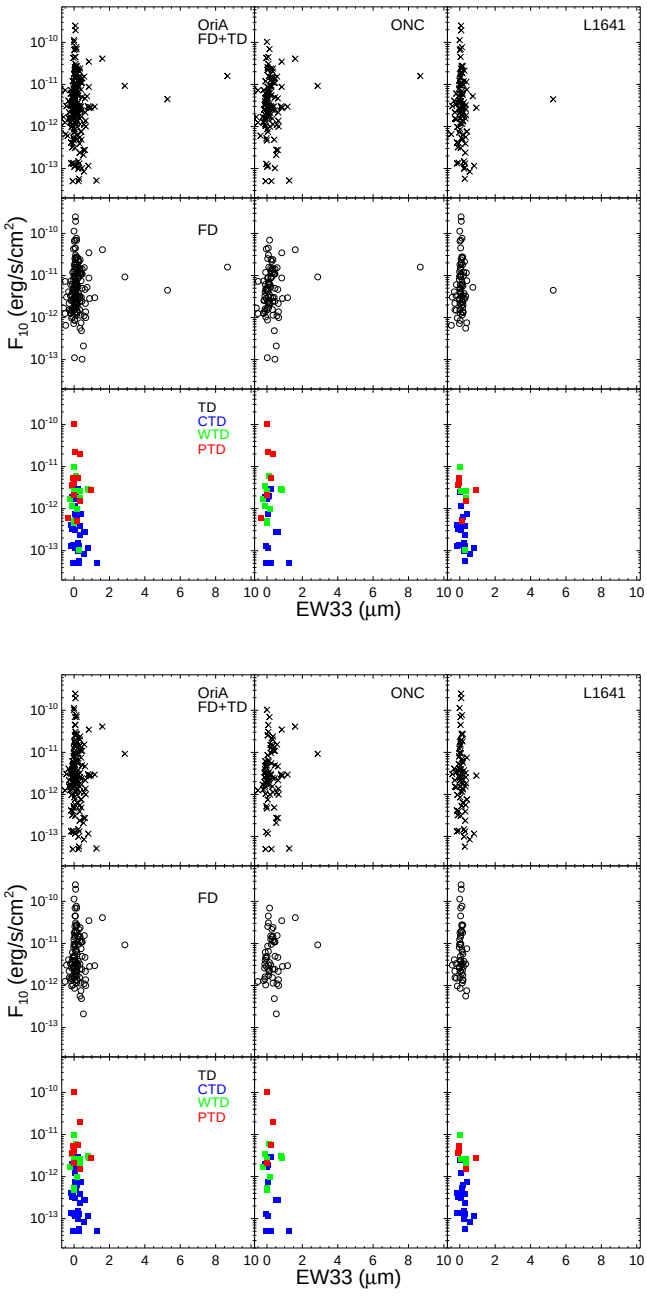


Figure C.49 EW33 vs. $\log F_{10}$. Upper panel: all available objects; Lower panel: objects with available spectral types only

Table C.97 EW33 vs. $\log F_{10}$ (I)

	Ori A				ONC				L1641			
	N	ρ	τ	r	N	ρ	τ	r	N	ρ	τ	r
TDFD	230	0.057	0.041	0.022	121	0.171	0.119	0.044	109	-0.116	-0.068	-0.038
		0.386	0.358	0.740		0.061	0.053	0.632		0.229	0.294	0.695
FD	170	0.146	0.098	0.062	91	0.191	0.137	0.086	79	0.079	0.056	0.012
		0.057	0.058	0.422		0.070	0.054	0.418		0.489	0.463	0.916
TD	60	-0.154	-0.096	-0.191	30	0.047	0.032	-0.185	30	-0.196	-0.129	-0.185
		0.241	0.278	0.144		0.804	0.803	0.328		0.300	0.317	0.328

ρ: Spearsman's ρ
τ: Kendall's τ
r: Pearson's r

Table C.98 EW33 vs. $\log F_{10}$ (II)

	Ori A				ONC				L1641			
	N	ρ	τ	r	N	ρ	τ	r	N	ρ	τ	r
TDFD	167	0.003	0.006	-0.016	82	0.122	0.083	0.001	85	-0.178	-0.105	-0.216
		0.970	0.912	0.837		0.276	0.272	0.993		0.103	0.156	0.047
FD	114	0.075	0.053	0.041	57	0.098	0.073	0.056	57	0.019	0.024	0.039
		0.429	0.405	0.665		0.466	0.425	0.679		0.891	0.793	0.773
TD	53	-0.131	-0.080	-0.177	25	0.039	0.030	-0.190	28	-0.176	-0.114	-0.176
		0.350	0.398	0.205		0.854	0.833	0.363		0.371	0.395	0.370

ρ: Spearsman's ρ
τ: Kendall's τ
r: Pearson's r

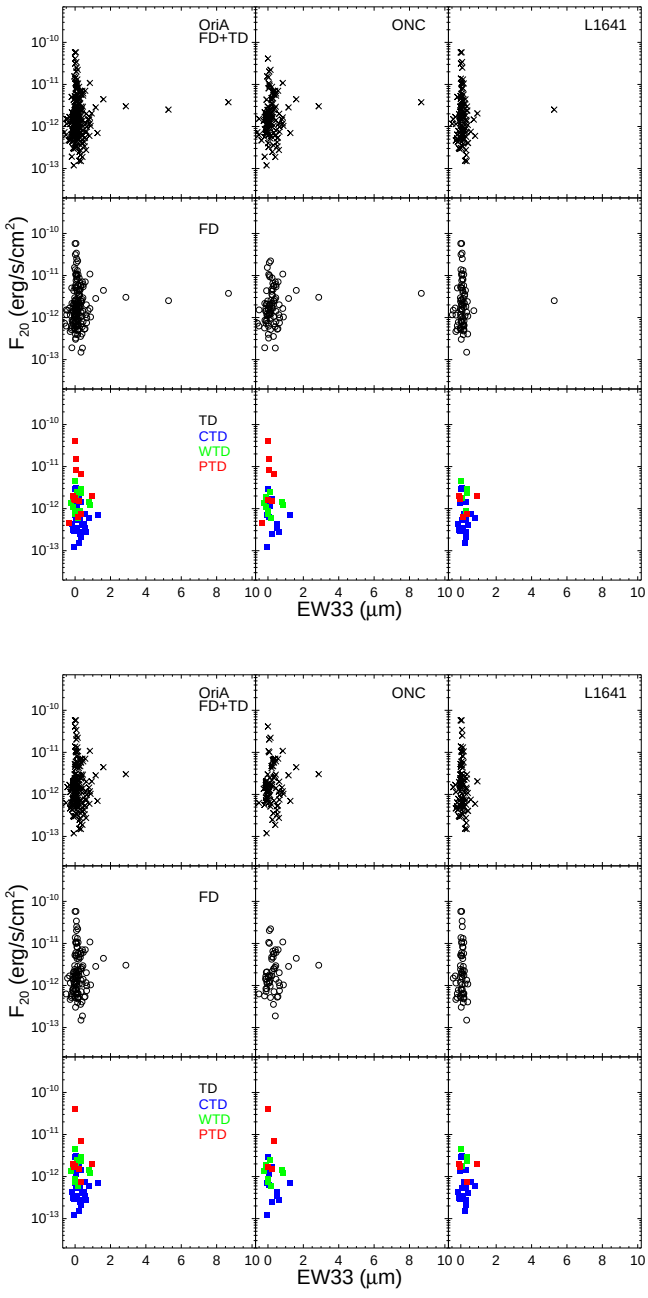


Figure C.50 EW33 vs. $\log F_{20}$. Upper panel: all available objects; Lower panel: objects with available spectral types only

Table C.99 EW33 vs. $\log F_{20}$ (I)

	Ori A				ONC				L1641			
	N	ρ	τ	r	N	ρ	τ	r	N	ρ	τ	r
TDFD	231	0.052	0.037	0.033	122	0.131	0.096	0.052	109	-0.070	-0.039	-0.004
		0.429	0.404	0.618		0.149	0.119	0.569		0.472	0.545	0.967
FD	170	0.134	0.088	0.053	91	0.220	0.156	0.079	79	0.007	0.008	0.013
		0.080	0.088	0.492		0.036	0.028	0.457		0.949	0.916	0.909
TD	61	-0.124	-0.087	-0.115	31	-0.167	-0.116	-0.167	30	0.051	0.037	-0.014
		0.342	0.319	0.377		0.369	0.358	0.369		0.789	0.775	0.941

ρ: Spearsman's ρ
τ: Kendall's τ
r: Pearson's r

Table C.100 EW33 vs. $\log F_{20}$ (II)

	Ori A				ONC				L1641			
	N	ρ	τ	r	N	ρ	τ	r	N	ρ	τ	r
TDFD	168	0.017	0.017	0.005	83	0.082	0.067	0.022	85	-0.095	-0.054	-0.100
		0.832	0.740	0.949		0.463	0.370	0.844		0.389	0.466	0.363
FD	114	0.100	0.071	0.035	57	0.172	0.134	0.061	57	-0.041	-0.023	-0.016
		0.288	0.262	0.712		0.202	0.141	0.652		0.762	0.804	0.906
TD	54	-0.125	-0.087	-0.114	26	-0.255	-0.173	-0.192	28	0.070	0.045	-0.016
		0.368	0.351	0.412		0.208	0.216	0.347		0.725	0.737	0.936

ρ: Spearsman's ρ
τ: Kendall's τ
r: Pearson's r

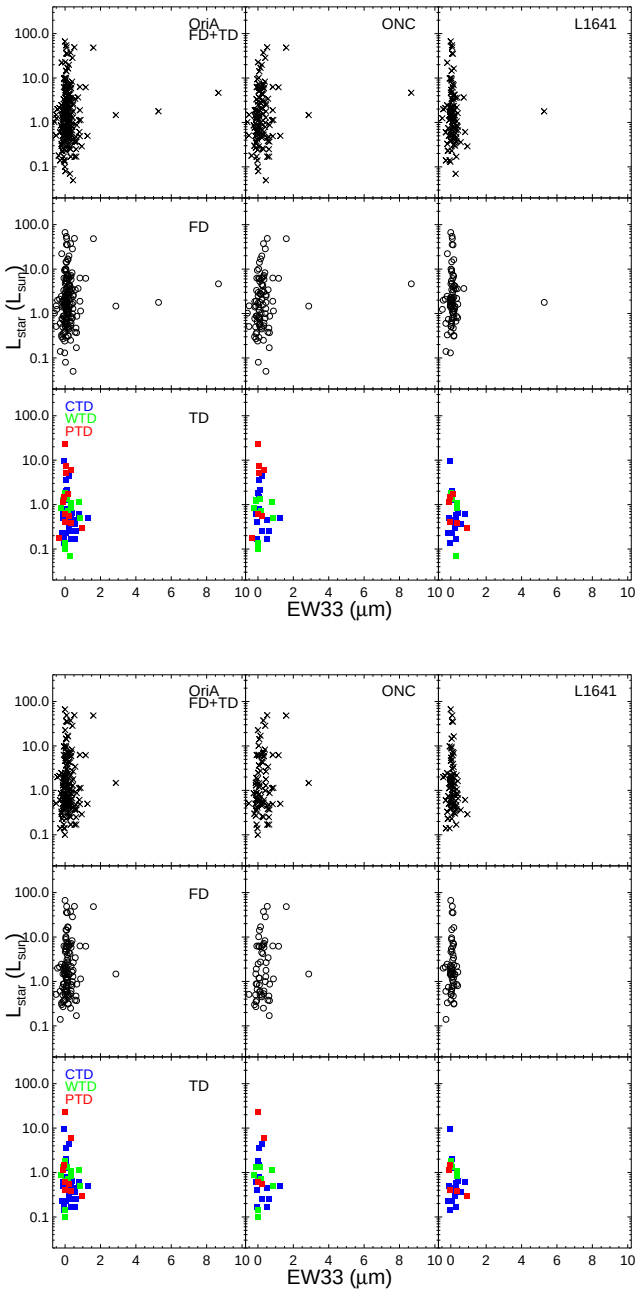


Figure C.51 EW33 vs. $\log L_\star$. Upper panel: all available objects; Lower panel: objects with available spectral types only

Table C.101 EW33 vs. $\log L_\star$ (I)

	Ori A				ONC				L1641			
	N	ρ	τ	r	N	ρ	τ	r	N	ρ	τ	r
TDFD	231	0.084	0.059	0.064	122	0.179	0.125	0.097	109	-0.082	-0.054	-0.029
		0.201	0.180	0.333		0.048	0.042	0.288		0.394	0.408	0.765
FD	170	0.186	0.130	0.092	91	0.252	0.176	0.122	79	0.077	0.058	0.011
		0.015	0.012	0.233		0.016	0.013	0.249		0.501	0.450	0.923
TD	61	-0.095	-0.072	-0.137	31	0.008	-0.015	-0.097	30	-0.093	-0.074	-0.200
		0.467	0.413	0.292		0.966	0.905	0.604		0.623	0.566	0.289

ρ: Spearsman's ρ
τ: Kendall's τ
r: Pearson's r

Table C.102 EW33 vs. $\log L_\star$ (II)

	Ori A				ONC				L1641			
	N	ρ	τ	r	N	ρ	τ	r	N	ρ	τ	r
TDFD	168	0.055	0.041	0.044	83	0.146	0.100	0.072	85	-0.106	-0.067	-0.123
		0.480	0.436	0.571		0.188	0.181	0.518		0.335	0.361	0.262
FD	114	0.173	0.126	0.089	57	0.231	0.163	0.113	57	0.073	0.060	0.115
		0.065	0.047	0.346		0.084	0.074	0.403		0.591	0.507	0.394
TD	54	-0.091	-0.072	-0.142	26	-0.057	-0.046	-0.124	28	-0.055	-0.051	-0.191
		0.511	0.445	0.306		0.782	0.740	0.546		0.783	0.706	0.330

ρ: Spearsman's ρ
τ: Kendall's τ
r: Pearson's r

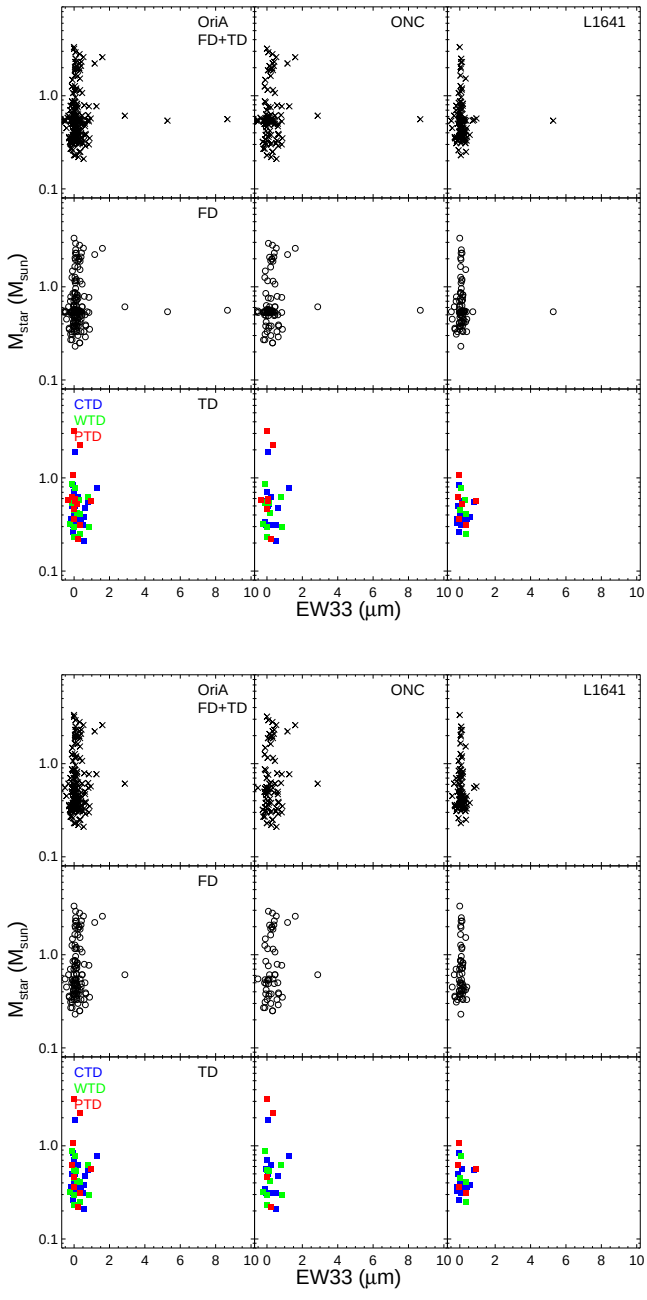


Figure C.52 EW33 vs. $\log M_\star$. Upper panel: all available objects; Lower panel: objects with available spectral types only

Table C.103 EW33 vs. $\log M_\star$ (I)

	Ori A				ONC				L1641			
	N	ρ	τ	r	N	ρ	τ	r	N	ρ	τ	r
TDFD	231	0.041	0.030	-0.002	122	0.100	0.067	0.006	109	-0.054	-0.030	-0.030
		0.531	0.500	0.976		0.272	0.273	0.948		0.580	0.642	0.757
FD	170	0.123	0.087	0.007	91	0.149	0.104	0.013	79	0.093	0.066	-0.012
		0.109	0.091	0.928		0.158	0.143	0.903		0.413	0.387	0.916
TD	61	-0.122	-0.092	-0.062	31	-0.078	-0.072	-0.048	30	-0.131	-0.094	-0.082
		0.349	0.293	0.635		0.677	0.572	0.798		0.489	0.466	0.667

ρ: Spearsman's ρ
τ: Kendall's τ
r: Pearson's r

Table C.104 EW33 vs. $\log M_\star$ (II)

	Ori A				ONC				L1641			
	N	ρ	τ	r	N	ρ	τ	r	N	ρ	τ	r
TDFD	168	0.063	0.046	0.004	83	0.134	0.094	0.014	85	-0.070	-0.041	-0.060
		0.415	0.381	0.959		0.227	0.209	0.900		0.523	0.574	0.585
FD	114	0.165	0.118	0.027	57	0.185	0.130	0.033	57	0.120	0.086	0.114
		0.080	0.064	0.776		0.169	0.155	0.807		0.374	0.344	0.398
TD	54	-0.082	-0.062	-0.041	26	-0.043	-0.037	-0.034	28	-0.131	-0.090	-0.092
		0.556	0.511	0.768		0.835	0.790	0.869		0.506	0.504	0.641

ρ: Spearsman's ρ
τ: Kendall's τ
r: Pearson's r

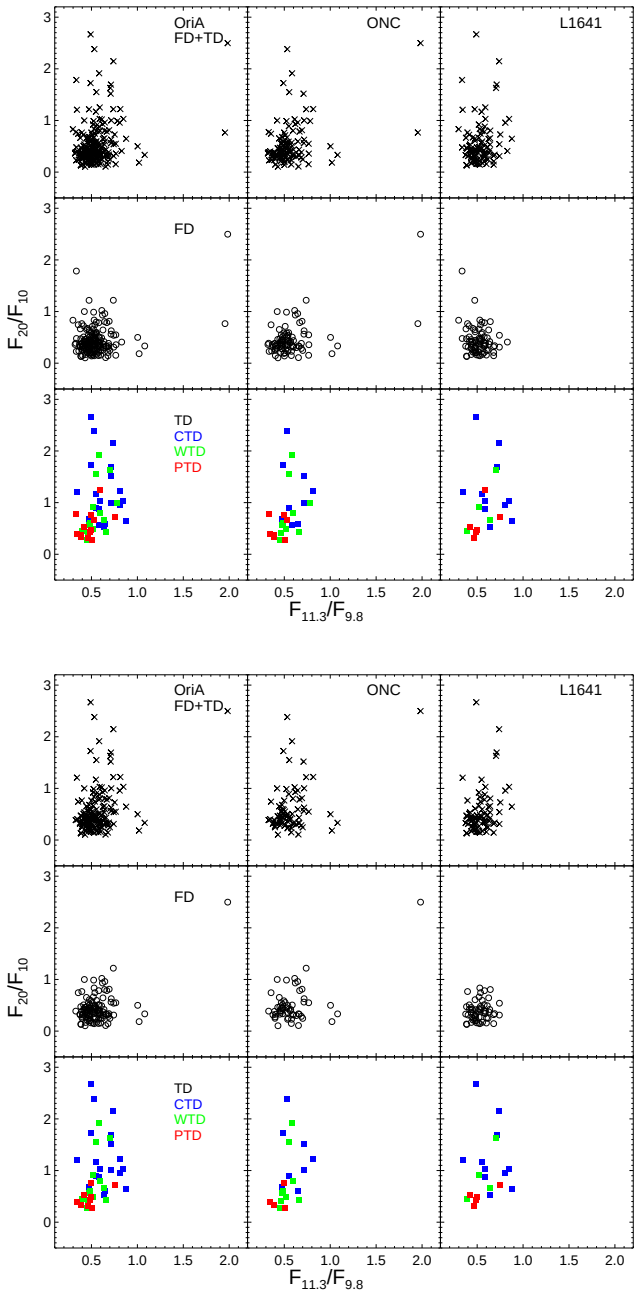


Figure C.53 $F_{11.3}/F_{9.8}$ vs. F_{20}/F_{10}. Upper panel: all available objects; Lower panel: objects with available spectral types only

Table C.105 $F_{11.3}/F_{9.8}$ vs. F_{20}/F_{10} (I)

	Ori A				ONC				L1641			
	N	ρ	τ	r	N	ρ	τ	r	N	ρ	τ	r
TDFD	230	0.244	0.168	0.139	121	0.225	0.166	0.056	109	0.266	0.175	0.234
		0.000	0.000	0.035		0.013	0.007	0.542		0.005	0.007	0.014
FD	170	0.030	0.018	-0.275	91	0.114	0.083	-0.282	79	-0.092	-0.070	-0.201
		0.700	0.730	0.000		0.280	0.242	0.007		0.419	0.363	0.076
TD	60	0.565	0.397	0.134	30	0.547	0.398	0.099	30	0.499	0.343	0.154
		0.000	0.000	0.307		0.002	0.002	0.603		0.005	0.008	0.416

ρ: Spearsman's ρ
τ: Kendall's τ
r: Pearson's r

Table C.106 $F_{11.3}/F_{9.8}$ vs. F_{20}/F_{10} (II)

	Ori A				ONC				L1641			
	N	ρ	τ	r	N	ρ	τ	r	N	ρ	τ	r
TDFD	167	0.328	0.224	0.158	82	0.250	0.181	0.106	85	0.410	0.273	0.218
		0.000	0.000	0.041		0.023	0.016	0.343		0.000	0.000	0.045
FD	114	0.122	0.077	0.534	57	0.105	0.066	0.596	57	0.135	0.075	0.121
		0.196	0.227	0.000		0.437	0.466	0.000		0.316	0.409	0.370
TD	53	0.544	0.380	0.119	25	0.559	0.413	0.096	28	0.459	0.307	0.141
		0.000	0.000	0.396		0.004	0.004	0.648		0.014	0.022	0.474

ρ: Spearsman's ρ
τ: Kendall's τ
r: Pearson's r

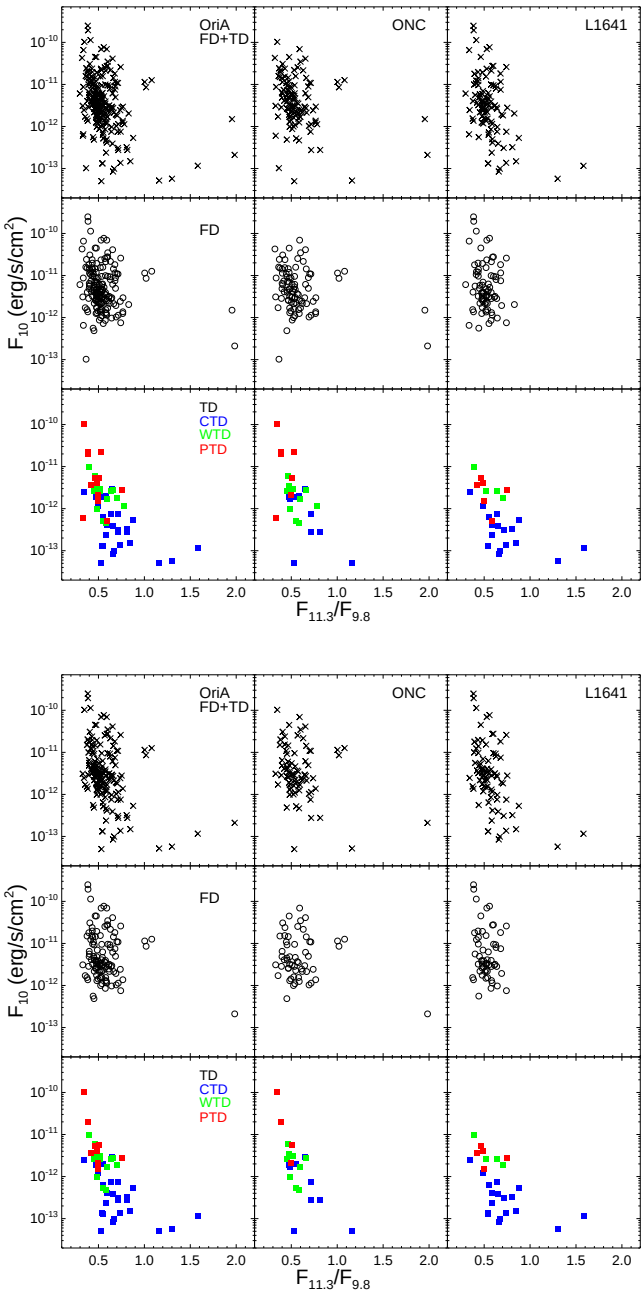


Figure C.54 $F_{11.3}/F_{9.8}$ vs. $\log F_{10}$. Upper panel: all available objects; Lower panel: objects with available spectral types only

Table C.107 $F_{11.3}/F_{9.8}$ vs. $\log F_{10}$ (I)

	Ori A				ONC				L1641			
	N	ρ	τ	r	N	ρ	τ	r	N	ρ	τ	r
TDFD	230	-0.339	-0.252	-0.078	121	-0.279	-0.215	0.017	109	-0.420	-0.304	-0.170
		0.000	0.000	0.239		0.002	0.000	0.853		0.000	0.000	0.077
FD	170	-0.154	-0.118	0.116	91	-0.178	-0.135	0.191	79	-0.124	-0.094	-0.159
		0.046	0.022	0.132		0.091	0.058	0.070		0.278	0.221	0.162
TD	60	-0.602	-0.445	-0.069	30	-0.491	-0.398	-0.007	30	-0.611	-0.439	-0.104
		0.000	0.000	0.600		0.006	0.002	0.971		0.000	0.001	0.584

ρ: Spearsman's ρ
τ: Kendall's τ
r: Pearson's r

Table C.108 $F_{11.3}/F_{9.8}$ vs. $\log F_{10}$ (II)

	Ori A				ONC				L1641			
	N	ρ	τ	r	N	ρ	τ	r	N	ρ	τ	r
TDFD	167	-0.356	-0.264	-0.095	82	-0.262	-0.200	-0.024	85	-0.461	-0.339	-0.159
		0.000	0.000	0.222		0.017	0.008	0.831		0.000	0.000	0.146
FD	114	-0.130	-0.103	-0.201	57	-0.096	-0.074	-0.223	57	-0.165	-0.132	-0.204
		0.167	0.104	0.032		0.478	0.417	0.095		0.219	0.148	0.128
TD	53	-0.603	-0.454	-0.056	25	-0.542	-0.460	-0.001	28	-0.591	-0.418	-0.095
		0.000	0.000	0.690		0.005	0.001	0.996		0.001	0.002	0.631

ρ: Spearsman's ρ
τ: Kendall's τ
r: Pearson's r

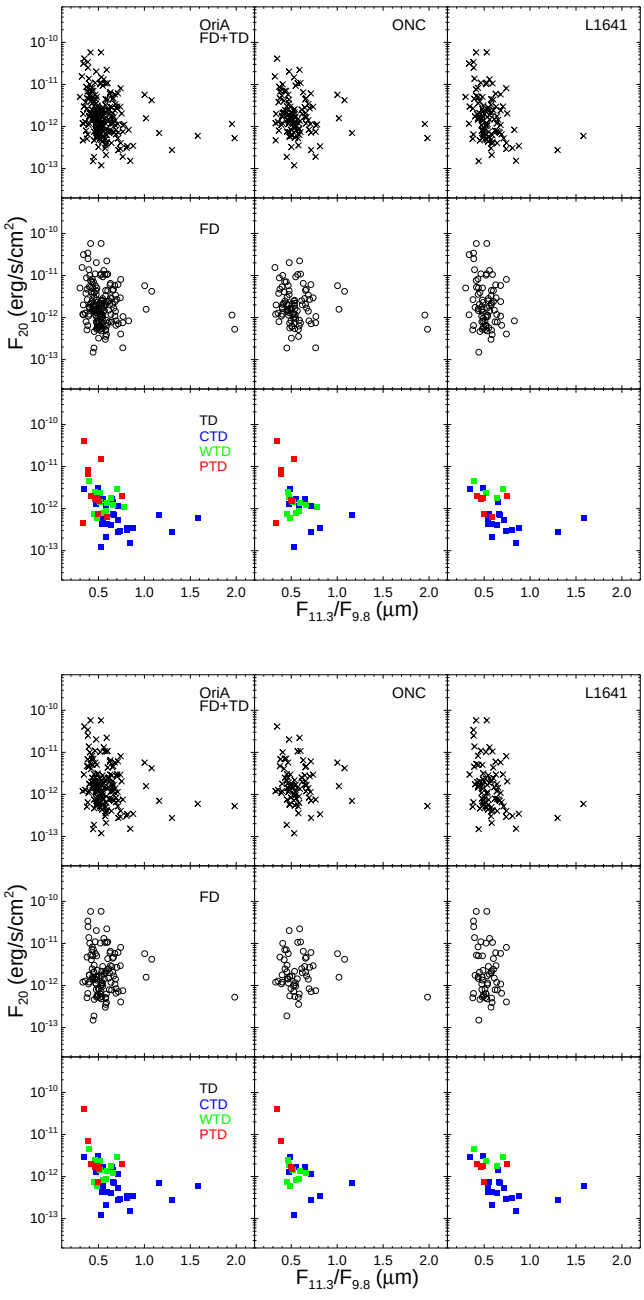


Figure C.55 $F_{11.3}/F_{9.8}$ vs. $\log F_{20}$. Upper panel: all available objects; Lower panel: objects with available spectral types only

Table C.109 $F_{11.3}/F_{9.8}$ vs. $\log F_{20}$ (I)

	Ori A				ONC				L1641			
	N	ρ	τ	r	N	ρ	τ	r	N	ρ	τ	r
TDFD	231	-0.254	-0.178	0.005	122	-0.171	-0.124	0.059	109	-0.357	-0.252	-0.046
		0.000	0.000	0.940		0.059	0.043	0.519		0.000	0.000	0.635
FD	170	-0.134	-0.091	0.033	91	-0.101	-0.069	0.093	79	-0.182	-0.127	-0.220
		0.081	0.079	0.669		0.341	0.335	0.381		0.108	0.098	0.051
TD	61	-0.411	-0.299	0.057	31	-0.258	-0.234	0.081	30	-0.487	-0.347	0.073
		0.001	0.001	0.663		0.161	0.064	0.665		0.006	0.007	0.701

ρ: Spearsman's ρ
τ: Kendall's τ
r: Pearson's r

Table C.110 $F_{11.3}/F_{9.8}$ vs. $\log F_{20}$ (II)

	Ori A				ONC				L1641			
	N	ρ	τ	r	N	ρ	τ	r	N	ρ	τ	r
TDFD	168	-0.225	-0.158	0.003	83	-0.135	-0.103	0.048	85	-0.332	-0.237	-0.032
		0.003	0.002	0.969		0.223	0.170	0.667		0.002	0.001	0.771
FD	114	-0.063	-0.041	-0.090	57	-0.018	-0.023	-0.083	57	-0.121	-0.084	-0.161
		0.504	0.520	0.341		0.894	0.804	0.539		0.370	0.356	0.232
TD	54	-0.448	-0.328	0.073	26	-0.314	-0.274	0.098	28	-0.544	-0.397	0.070
		0.001	0.000	0.600		0.118	0.050	0.634		0.003	0.003	0.723

ρ: Spearsman's ρ
τ: Kendall's τ
r: Pearson's r

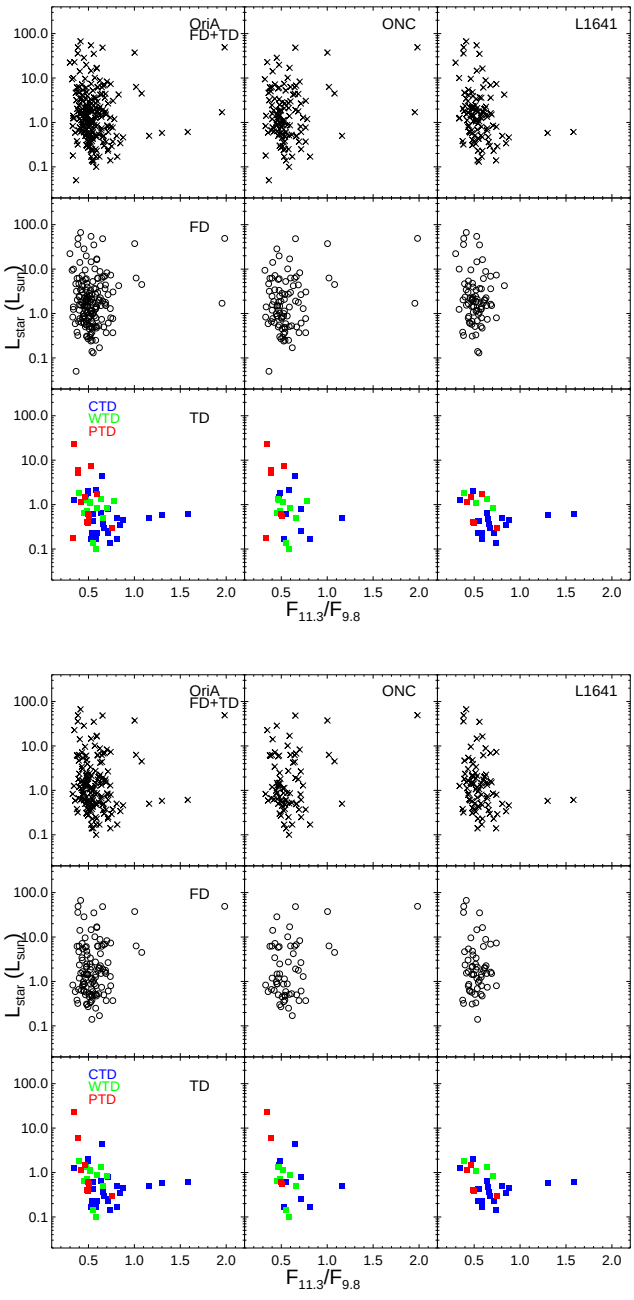


Figure C.56 $F_{11.3}/F_{9.8}$ vs. $\log L_{\star}$. Upper panel: all available objects; Lower panel: objects with available spectral types only

Table C.111 $F_{11.3}/F_{9.8}$ vs. $logL_\star$ (I)

	Ori A				ONC				L1641			
	N	ρ	τ	r	N	ρ	τ	r	N	ρ	τ	r
TDFD	231	-0.117	-0.087	0.135	122	-0.009	-0.014	0.170	109	-0.268	-0.190	0.093
		0.075	0.049	0.040		0.922	0.816	0.061		0.005	0.003	0.336
FD	170	0.025	0.012	0.223	91	0.075	0.047	0.313	79	-0.055	-0.040	-0.087
		0.745	0.818	0.003		0.479	0.506	0.003		0.630	0.599	0.446
TD	61	-0.274	-0.195	0.317	31	-0.194	-0.151	0.237	30	-0.304	-0.215	0.505
		0.033	0.027	0.013		0.295	0.234	0.199		0.102	0.096	0.004

ρ: Spearsman's ρ
τ: Kendall's τ
r: Pearson's r

Table C.112 $F_{11.3}/F_{9.8}$ vs. $logL_\star$ (II)

	Ori A				ONC				L1641			
	N	ρ	τ	r	N	ρ	τ	r	N	ρ	τ	r
TDFD	168	-0.127	-0.094	0.147	83	-0.045	-0.041	0.151	85	-0.244	-0.175	0.145
		0.101	0.072	0.057		0.687	0.581	0.173		0.024	0.018	0.185
FD	114	0.058	0.032	0.227	57	0.098	0.061	0.363	57	-0.004	-0.011	-0.054
		0.538	0.615	0.015		0.469	0.503	0.006		0.979	0.901	0.690
TD	54	-0.298	-0.206	0.390	26	-0.287	-0.222	0.272	28	-0.242	-0.160	0.602
		0.029	0.028	0.004		0.155	0.112	0.179		0.215	0.233	0.001

ρ: Spearsman's ρ
τ: Kendall's τ
r: Pearson's r

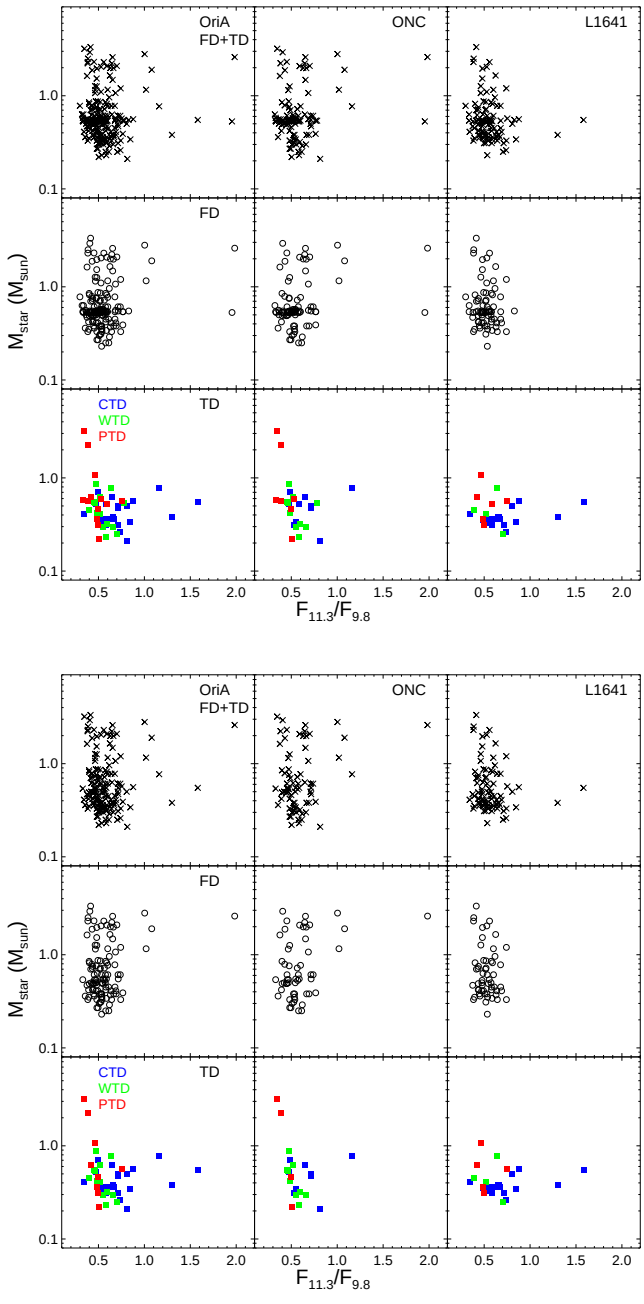


Figure C.57 $F_{11.3}/F_{9.8}$ vs. $\log M_\star$. Upper panel: all available objects; Lower panel: objects with available spectral types only

Table C.113 $F_{11.3}/F_{9.8}$ vs. $\log M_\star$ (I)

	Ori A				ONC				L1641			
	N	ρ	τ	r	N	ρ	τ	r	N	ρ	τ	r
TDFD	231	-0.046	-0.033	0.141	122	0.056	0.032	0.210	109	-0.167	-0.114	0.062
		0.487	0.450	0.032		0.542	0.597	0.020		0.082	0.080	0.522
FD	170	0.048	0.035	0.095	91	0.163	0.112	0.140	79	-0.085	-0.056	-0.116
		0.535	0.503	0.218		0.123	0.114	0.186		0.459	0.465	0.309
TD	61	-0.042	-0.032	0.335	31	-0.122	-0.104	0.371	30	0.112	0.087	0.389
		0.747	0.720	0.008		0.512	0.411	0.040		0.556	0.500	0.034

ρ: Spearsman's ρ
τ: Kendall's τ
r: Pearson's r

Table C.114 $F_{11.3}/F_{9.8}$ vs. $\log M_\star$ (II)

	Ori A				ONC				L1641			
	N	ρ	τ	r	N	ρ	τ	r	N	ρ	τ	r
TDFD	168	-0.048	-0.035	0.143	83	0.076	0.043	0.214	85	-0.196	-0.134	0.065
		0.535	0.495	0.064		0.496	0.563	0.052		0.073	0.069	0.555
FD	114	0.046	0.033	0.231	57	0.201	0.142	0.355	57	-0.115	-0.081	-0.146
		0.627	0.604	0.013		0.134	0.118	0.007		0.395	0.374	0.279
TD	54	-0.036	-0.032	0.340	26	-0.108	-0.102	0.373	28	0.045	0.033	0.394
		0.794	0.734	0.012		0.600	0.464	0.061		0.822	0.808	0.038

ρ: Spearsman's ρ
τ: Kendall's τ
r: Pearson's r

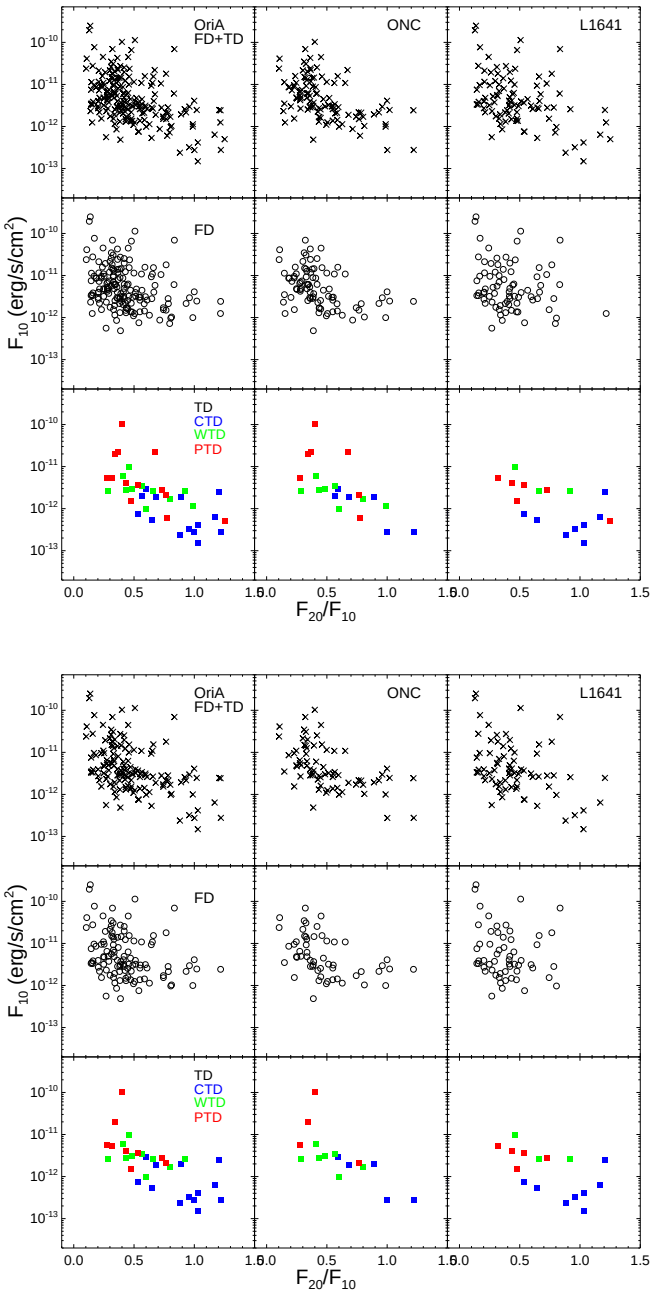


Figure C.58 F_{20}/F_{10} vs. $\log F_{10}$. Upper panel: all available objects; Lower panel: objects with available spectral types only

Table C.115 F_{20}/F_{10} vs. $\log F_{10}$ (I)

	Ori A				ONC				L1641			
	N	ρ	τ	r	N	ρ	τ	r	N	ρ	τ	r
TDFD	230	-0.615	-0.445	-0.618	121	-0.643	-0.464	-0.621	109	-0.593	-0.429	-0.617
		0.000	0.000	0.000		0.000	0.000	0.000		0.000	0.000	0.000
FD	170	-0.382	-0.261	-0.434	91	-0.497	-0.347	-0.554	79	-0.250	-0.167	-0.284
		0.000	0.000	0.000		0.000	0.000	0.000		0.026	0.030	0.011
TD	60	-0.865	-0.678	-0.669	30	-0.890	-0.697	-0.643	30	-0.826	-0.664	-0.699
		0.000	0.000	0.000		0.000	0.000	0.000		0.000	0.000	0.000

ρ: Spearsman's ρ
τ: Kendall's τ
r: Pearson's r

Table C.116 F_{20}/F_{10} vs. $\log F_{10}$ (II)

	Ori A				ONC				L1641			
	N	ρ	τ	r	N	ρ	τ	r	N	ρ	τ	r
TDFD	167	-0.655	-0.482	-0.609	82	-0.715	-0.525	-0.611	85	-0.617	-0.458	-0.616
		0.000	0.000	0.000		0.000	0.000	0.000		0.000	0.000	0.000
FD	114	-0.383	-0.263	-0.379	57	-0.563	-0.393	-0.542	57	-0.222	-0.157	-0.161
		0.000	0.000	0.000		0.000	0.000	0.000		0.097	0.085	0.232
TD	53	-0.866	-0.682	-0.673	25	-0.908	-0.713	-0.662	28	-0.815	-0.656	-0.696
		0.000	0.000	0.000		0.000	0.000	0.000		0.000	0.000	0.000

ρ: Spearsman's ρ
τ: Kendall's τ
r: Pearson's r

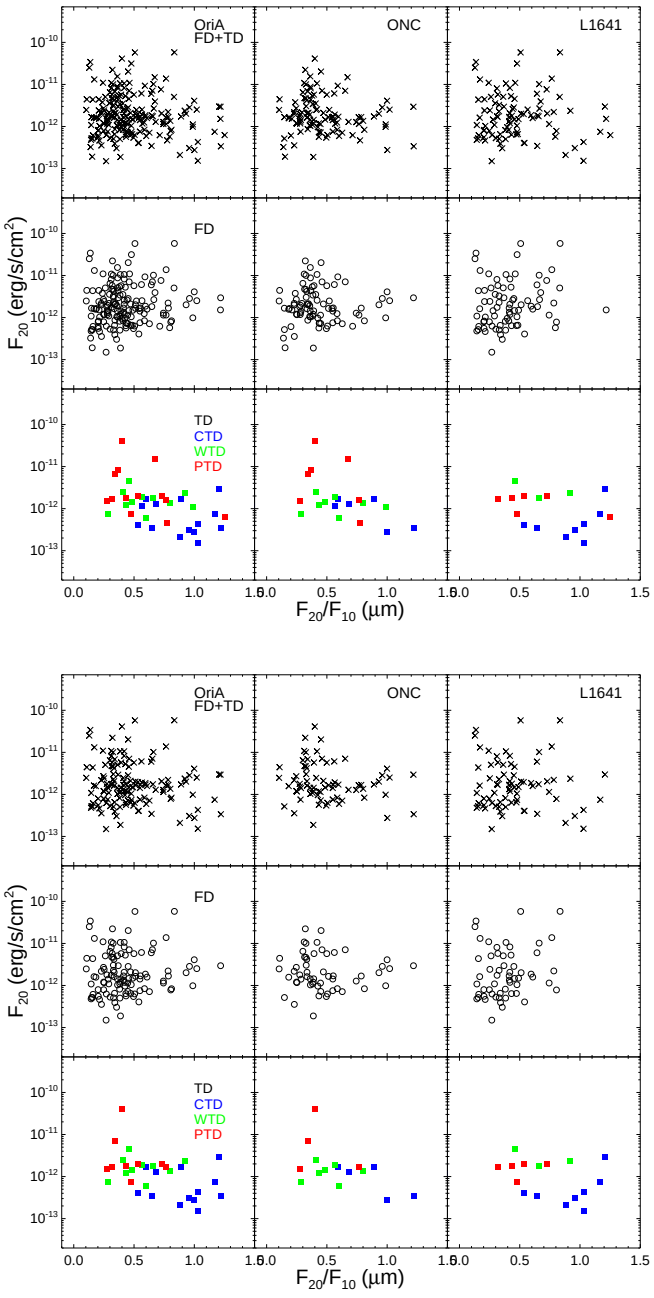


Figure C.59 F_{20}/F_{10} vs. $\log F_{20}$. Upper panel: all available objects; Lower panel: objects with available spectral types only

Table C.117 F_{20}/F_{10} vs. $\log F_{20}$ (I)

	Ori A				ONC				L1641			
	N	ρ	τ	r	N	ρ	τ	r	N	ρ	τ	r
TDFD	230	-0.185	-0.122	-0.231	121	-0.253	-0.170	-0.255	109	-0.144	-0.086	-0.209
		0.005	0.006	0.000		0.005	0.006	0.005		0.136	0.187	0.029
FD	170	0.054	0.037	-0.088	91	-0.074	-0.053	-0.166	79	0.169	0.121	0.095
		0.484	0.476	0.254		0.483	0.461	0.116		0.137	0.114	0.405
TD	60	-0.441	-0.280	-0.254	30	-0.600	-0.430	-0.311	30	-0.179	-0.076	-0.129
		0.000	0.002	0.050		0.000	0.001	0.094		0.344	0.556	0.497

ρ: Spearsman's ρ
τ: Kendall's τ
r: Pearson's r

Table C.118 F_{20}/F_{10} vs. $\log F_{20}$ (II)

	Ori A				ONC				L1641			
	N	ρ	τ	r	N	ρ	τ	r	N	ρ	τ	r
TDFD	167	-0.213	-0.141	-0.236	82	-0.319	-0.212	-0.274	85	-0.157	-0.096	-0.207
		0.006	0.007	0.002		0.004	0.005	0.013		0.151	0.192	0.057
FD	114	0.054	0.037	-0.010	57	-0.116	-0.081	-0.148	57	0.167	0.114	0.186
		0.569	0.562	0.916		0.389	0.371	0.272		0.216	0.210	0.166
TD	53	-0.422	-0.261	-0.250	25	-0.588	-0.413	-0.309	28	-0.200	-0.085	-0.156
		0.002	0.006	0.071		0.002	0.004	0.133		0.307	0.527	0.428

ρ: Spearsman's ρ
τ: Kendall's τ
r: Pearson's r

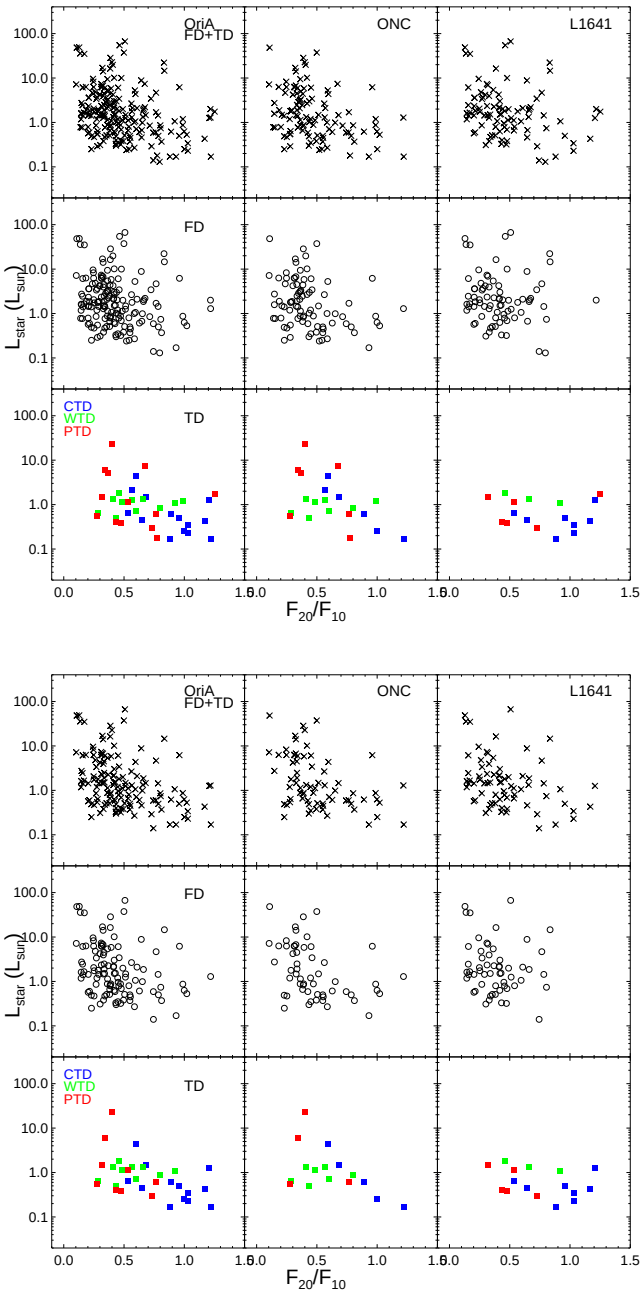


Figure C.60 F_{20}/F_{10} vs. $\log L_\star$. Upper panel: all available objects; Lower panel: objects with available spectral types only

Table C.119 F_{20}/F_{10} vs. $\log L_\star$ (I)

	Ori A				ONC				L1641			
	N	ρ	τ	r	N	ρ	τ	r	N	ρ	τ	r
TDFD	230	-0.405	-0.278	-0.305	121	-0.395	-0.272	-0.269	109	-0.420	-0.284	-0.350
		0.000	0.000	0.000		0.000	0.000	0.003		0.000	0.000	0.000
FD	170	-0.246	-0.167	-0.264	91	-0.325	-0.217	-0.324	79	-0.149	-0.096	-0.120
		0.001	0.001	0.001		0.002	0.002	0.002		0.191	0.210	0.292
TD	60	-0.403	-0.270	-0.246	30	-0.489	-0.327	-0.195	30	-0.241	-0.169	-0.276
		0.001	0.002	0.058		0.006	0.011	0.302		0.200	0.191	0.140

ρ: Spearsman's ρ
τ: Kendall's τ
r: Pearson's r

Table C.120 F_{20}/F_{10} vs. $\log L_\star$ (II)

	Ori A				ONC				L1641			
	N	ρ	τ	r	N	ρ	τ	r	N	ρ	τ	r
TDFD	167	-0.452	-0.317	-0.230	82	-0.442	-0.315	-0.180	85	-0.463	-0.318	-0.290
		0.000	0.000	0.003		0.000	0.000	0.106		0.000	0.000	0.007
FD	114	-0.303	-0.213	-0.071	57	-0.374	-0.271	-0.026	57	-0.187	-0.128	-0.155
		0.001	0.001	0.453		0.004	0.003	0.848		0.164	0.159	0.250
TD	53	-0.359	-0.244	-0.146	25	-0.454	-0.304	-0.169	28	-0.189	-0.138	-0.094
		0.008	0.010	0.297		0.023	0.033	0.419		0.335	0.302	0.634

ρ: Spearsman's ρ
τ: Kendall's τ
r: Pearson's r

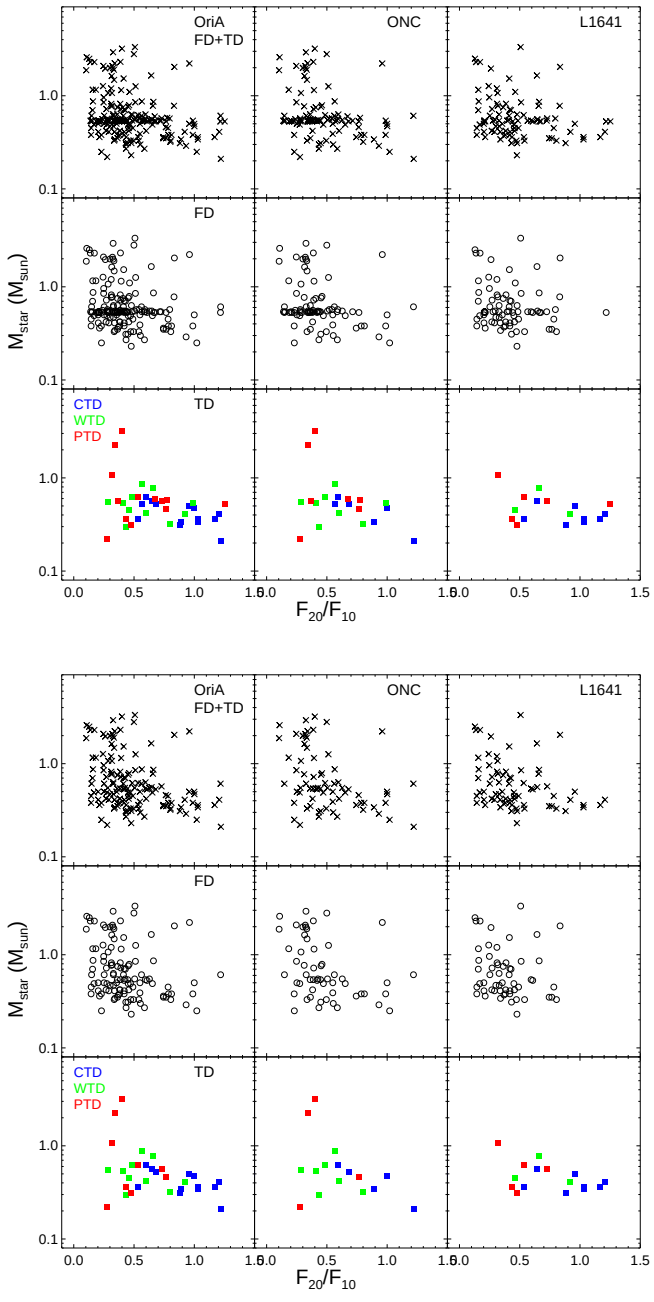


Figure C.61 F_{20}/F_{10} vs. $\log M_\star$. Upper panel: all available objects; Lower panel: objects with available spectral types only

Table C.121 F_{20}/F_{10} vs. $\log M_\star$ (I)

	Ori A				ONC				L1641			
	N	ρ	τ	r	N	ρ	τ	r	N	ρ	τ	r
TDFD	230	-0.294	-0.204	-0.103	121	-0.246	-0.173	-0.019	109	-0.350	-0.238	-0.213
		0.000	0.000	0.119		0.006	0.005	0.836		0.000	0.000	0.026
FD	170	-0.186	-0.130	-0.054	91	-0.224	-0.156	-0.051	79	-0.141	-0.099	-0.125
		0.015	0.012	0.484		0.033	0.028	0.631		0.217	0.197	0.272
TD	60	-0.210	-0.153	0.024	30	-0.163	-0.143	0.109	30	-0.156	-0.101	-0.057
		0.107	0.084	0.856		0.388	0.266	0.566		0.410	0.433	0.765

ρ: Spearsman's ρ
τ: Kendall's τ
r: Pearson's r

Table C.122 F_{20}/F_{10} vs. $\log M_\star$ (II)

	Ori A				ONC				L1641			
	N	ρ	τ	r	N	ρ	τ	r	N	ρ	τ	r
TDFD	167	-0.378	-0.263	-0.120	82	-0.332	-0.239	-0.027	85	-0.457	-0.316	-0.248
		0.000	0.000	0.122		0.002	0.002	0.810		0.000	0.000	0.022
FD	114	-0.287	-0.203	-0.071	57	-0.338	-0.247	-0.060	57	-0.260	-0.188	-0.169
		0.002	0.001	0.453		0.010	0.007	0.658		0.051	0.039	0.209
TD	53	-0.197	-0.142	0.026	25	-0.114	-0.100	0.118	28	-0.235	-0.163	-0.148
		0.158	0.134	0.853		0.587	0.482	0.574		0.228	0.224	0.452

ρ: Spearsman's ρ
τ: Kendall's τ
r: Pearson's r

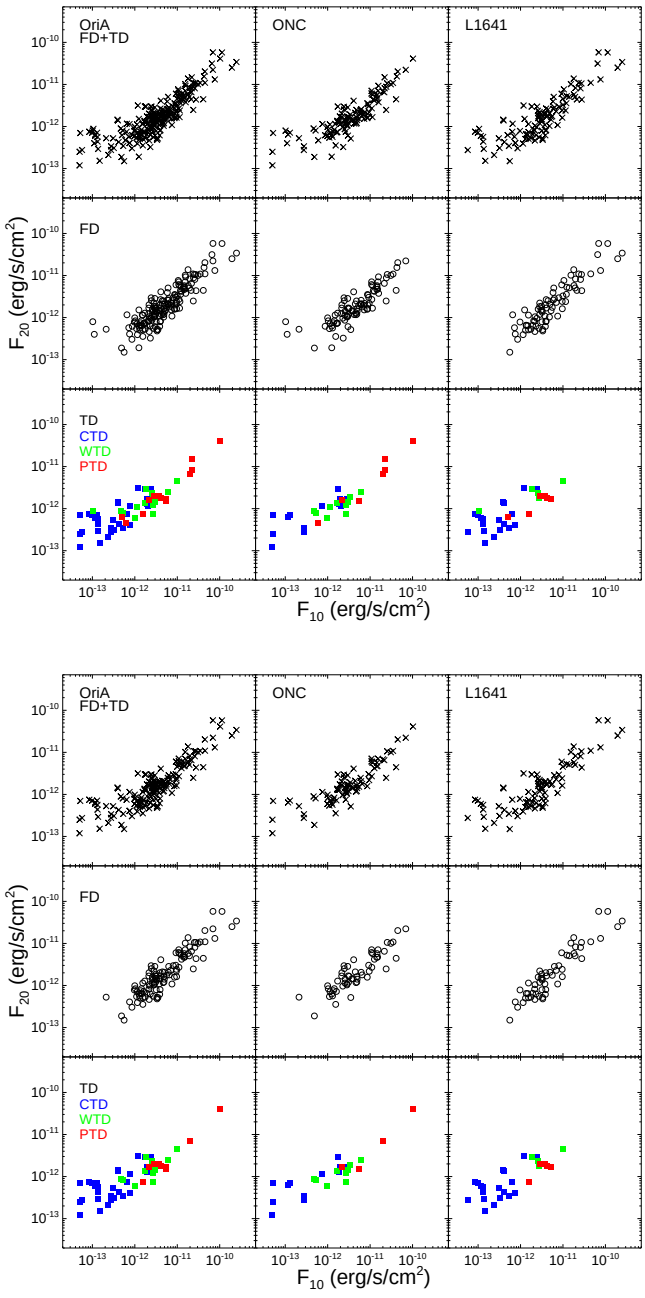


Figure C.62 $\log F_{10}$ vs. $\log F_{20}$. Upper panel: all available objects; Lower panel: objects with available spectral types only

Table C.123 $\log F_{10}$ vs. $\log F_{20}$ (I)

	Ori A				ONC				L1641			
	N	ρ	τ	r	N	ρ	τ	r	N	ρ	τ	r
TDFD	230	0.857	0.677	0.622	121	0.877	0.706	0.747	109	0.841	0.657	0.626
		0.000	0.000	0.000		0.000	0.000	0.000		0.000	0.000	0.000
FD	170	0.879	0.702	0.626	91	0.876	0.706	0.773	79	0.885	0.712	0.650
		0.000	0.000	0.000		0.000	0.000	0.000		0.000	0.000	0.000
TD	60	0.814	0.602	0.643	30	0.886	0.733	0.734	30	0.666	0.411	0.675
		0.000	0.000	0.000		0.000	0.000	0.000		0.000	0.001	0.000

ρ: Spearsman's ρ
τ: Kendall's τ
r: Pearson's r

Table C.124 $\log F_{10}$ vs. $\log F_{20}$ (II)

	Ori A				ONC				L1641			
	N	ρ	τ	r	N	ρ	τ	r	N	ρ	τ	r
TDFD	167	0.840	0.659	0.630	82	0.862	0.687	0.746	85	0.825	0.638	0.638
		0.000	0.000	0.000		0.000	0.000	0.000		0.000	0.000	0.000
FD	114	0.874	0.700	0.639	57	0.860	0.688	0.773	57	0.894	0.729	0.670
		0.000	0.000	0.000		0.000	0.000	0.000		0.000	0.000	0.000
TD	53	0.805	0.579	0.616	25	0.859	0.700	0.743	28	0.701	0.429	0.679
		0.000	0.000	0.000		0.000	0.000	0.000		0.000	0.001	0.000

ρ: Spearsman's ρ
τ: Kendall's τ
r: Pearson's r

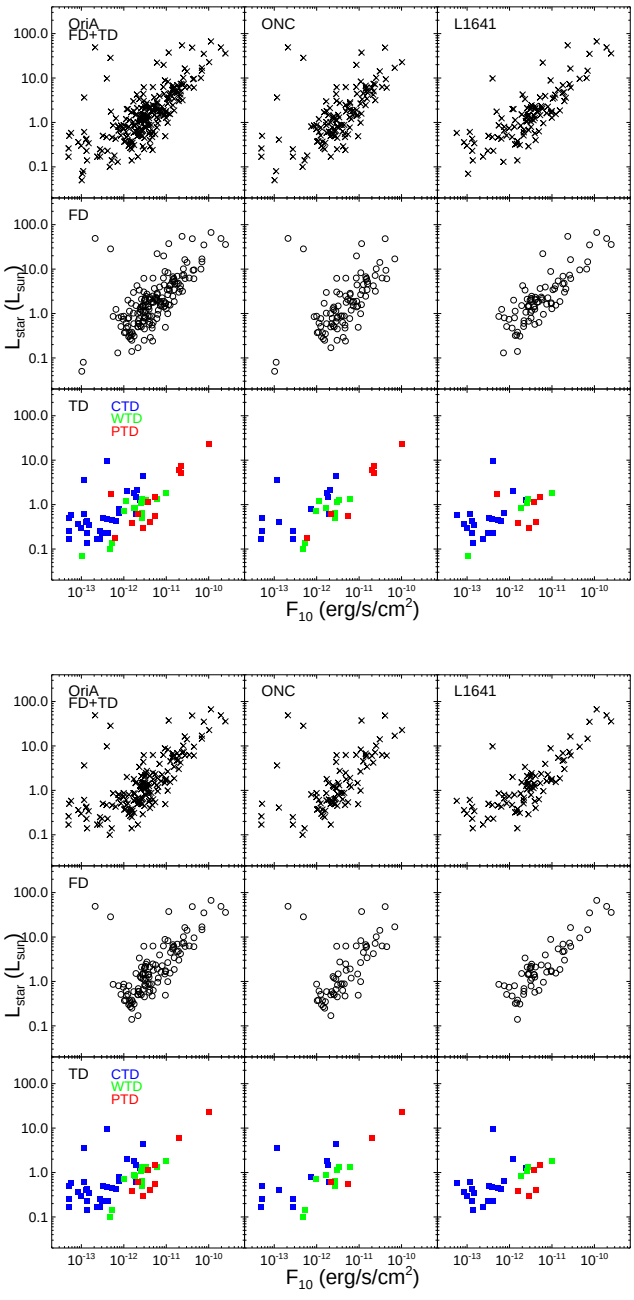


Figure C.63 logF_{10} vs. log$L_\star$. Upper panel: all available objects; Lower panel: objects with available spectral types only

Table C.125 $\log F_{10}$ vs. $\log L_\star$ (I)

	Ori A				ONC				L1641			
	N	ρ	τ	r	N	ρ	τ	r	N	ρ	τ	r
TDFD	230	0.732	0.563	0.543	121	0.683	0.522	0.573	109	0.787	0.612	0.602
		0.000	0.000	0.000		0.000	0.000	0.000		0.000	0.000	0.000
FD	170	0.718	0.547	0.538	91	0.660	0.501	0.575	79	0.796	0.610	0.639
		0.000	0.000	0.000		0.000	0.000	0.000		0.000	0.000	0.000
TD	60	0.621	0.444	0.549	30	0.686	0.502	0.633	30	0.525	0.367	0.393
		0.000	0.000	0.000		0.000	0.000	0.000		0.003	0.004	0.032

ρ: Spearsman's ρ
τ: Kendall's τ
r: Pearson's r

Table C.126 $\log F_{10}$ vs. $\log L_\star$ (II)

	Ori A				ONC				L1641			
	N	ρ	τ	r	N	ρ	τ	r	N	ρ	τ	r
TDFD	167	0.737	0.572	0.578	82	0.678	0.527	0.578	85	0.790	0.619	0.665
		0.000	0.000	0.000		0.000	0.000	0.000		0.000	0.000	0.000
FD	114	0.738	0.574	0.579	57	0.645	0.513	0.582	57	0.829	0.639	0.710
		0.000	0.000	0.000		0.000	0.000	0.000		0.000	0.000	0.000
TD	53	0.588	0.415	0.543	25	0.619	0.431	0.638	28	0.505	0.356	0.413
		0.000	0.000	0.000		0.001	0.003	0.001		0.006	0.008	0.029

ρ: Spearsman's ρ
τ: Kendall's τ
r: Pearson's r

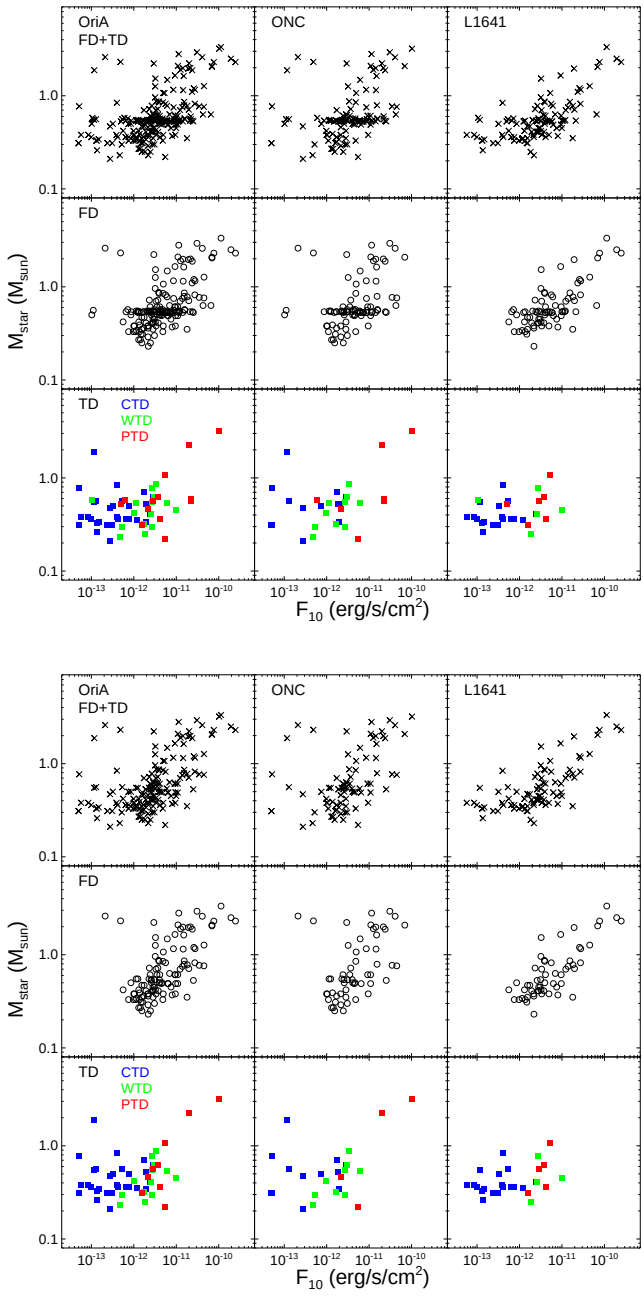


Figure C.64 logF_{10} vs. log$M_\star$. Upper panel: all available objects; Lower panel: objects with available spectral types only

Table C.127 $\log F_{10}$ vs. $\log M_\star$ (I)

	Ori A				ONC				L1641			
	N	ρ	τ	r	N	ρ	τ	r	N	ρ	τ	r
TDFD	230	0.537	0.388	0.510	121	0.455	0.327	0.494	109	0.624	0.457	0.640
		0.000	0.000	0.000		0.000	0.000	0.000		0.000	0.000	0.000
FD	170	0.540	0.391	0.498	91	0.449	0.320	0.447	79	0.641	0.476	0.662
		0.000	0.000	0.000		0.000	0.000	0.000		0.000	0.000	0.000
TD	60	0.330	0.234	0.563	30	0.345	0.259	0.604	30	0.287	0.185	0.310
		0.010	0.008	0.000		0.062	0.044	0.000		0.124	0.150	0.095

ρ: Spearsman's ρ
τ: Kendall's τ
r: Pearson's r

Table C.128 $\log F_{10}$ vs. $\log M_\star$ (II)

	Ori A				ONC				L1641			
	N	ρ	τ	r	N	ρ	τ	r	N	ρ	τ	r
TDFD	167	0.605	0.445	0.516	82	0.529	0.388	0.521	85	0.687	0.507	0.651
		0.000	0.000	0.000		0.000	0.000	0.000		0.000	0.000	0.000
FD	114	0.638	0.472	0.497	57	0.541	0.394	0.480	57	0.728	0.551	0.669
		0.000	0.000	0.000		0.000	0.000	0.000		0.000	0.000	0.000
TD	53	0.325	0.234	0.574	25	0.313	0.247	0.615	28	0.370	0.239	0.353
		0.018	0.013	0.000		0.127	0.083	0.001		0.052	0.075	0.065

ρ: Spearsman's ρ
τ: Kendall's τ
r: Pearson's r

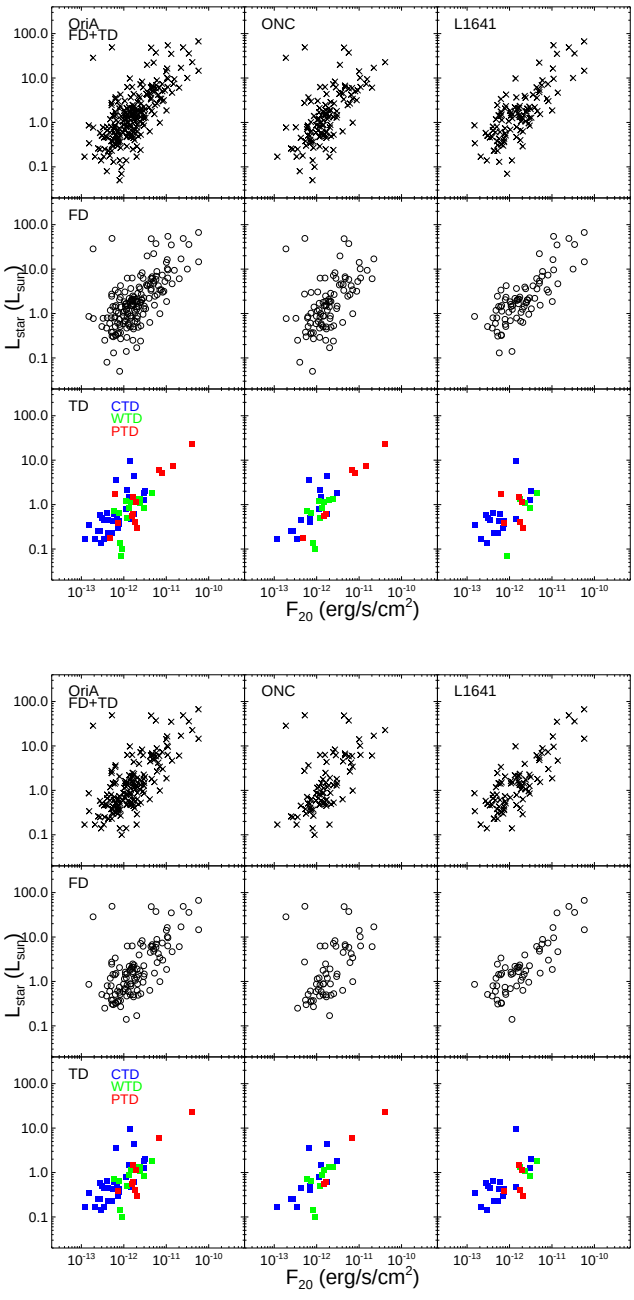


Figure C.65 logF_{20} vs. log$L_\star$. Upper panel: all available objects; Lower panel: objects with available spectral types only

Table C.129 $\log F_{20}$ vs. $\log L_\star$ (I)

	Ori A				ONC				L1641			
	N	ρ	τ	r	N	ρ	τ	r	N	ρ	τ	r
TDFD	231	0.676	0.502	0.549	122	0.625	0.471	0.505	109	0.729	0.538	0.616
		0.000	0.000	0.000		0.000	0.000	0.000		0.000	0.000	0.000
FD	170	0.650	0.479	0.538	91	0.560	0.414	0.487	79	0.756	0.569	0.647
		0.000	0.000	0.000		0.000	0.000	0.000		0.000	0.000	0.000
TD	61	0.673	0.486	0.581	31	0.748	0.577	0.656	30	0.537	0.358	0.534
		0.000	0.000	0.000		0.000	0.000	0.000		0.002	0.005	0.002

ρ: Spearsman's ρ
τ: Kendall's τ
r: Pearson's r

Table C.130 $\log F_{20}$ vs. $\log L_\star$ (II)

	Ori A				ONC				L1641			
	N	ρ	τ	r	N	ρ	τ	r	N	ρ	τ	r
TDFD	168	0.670	0.503	0.570	83	0.620	0.478	0.494	85	0.720	0.536	0.663
		0.000	0.000	0.000		0.000	0.000	0.000		0.000	0.000	0.000
FD	114	0.636	0.473	0.562	57	0.529	0.401	0.469	57	0.765	0.583	0.700
		0.000	0.000	0.000		0.000	0.000	0.000		0.000	0.000	0.000
TD	54	0.682	0.495	0.567	26	0.702	0.549	0.641	28	0.609	0.420	0.600
		0.000	0.000	0.000		0.000	0.000	0.000		0.001	0.002	0.001

ρ: Spearsman's ρ
τ: Kendall's τ
r: Pearson's r

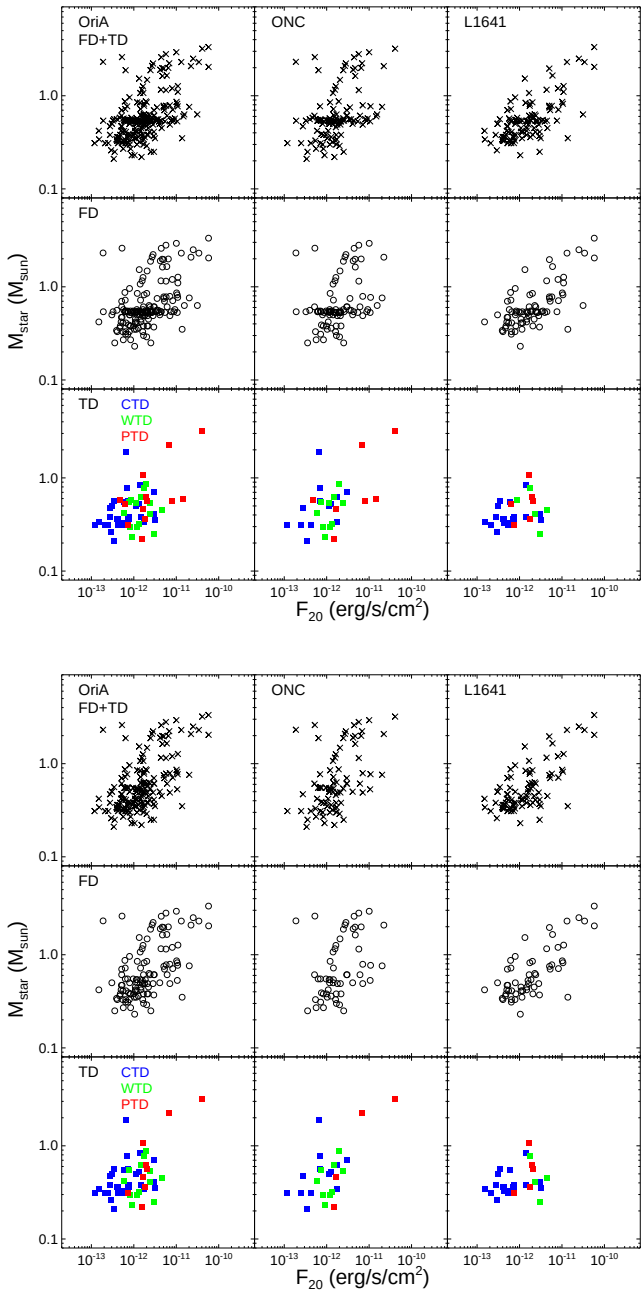


Figure C.66 logF_{20} vs. log$M_\star$. Upper panel: all available objects; Lower panel: objects with available spectral types only

Table C.131 $\log F_{20}$ vs. $\log M_\star$ (I)

	Ori A				ONC				L1641			
	N	ρ	τ	r	N	ρ	τ	r	N	ρ	τ	r
TDFD	231	0.492	0.351	0.492	122	0.416	0.293	0.409	109	0.565	0.413	0.630
		0.000	0.000	0.000		0.000	0.000	0.000		0.000	0.000	0.000
FD	170	0.487	0.350	0.470	91	0.369	0.260	0.326	79	0.609	0.460	0.652
		0.000	0.000	0.000		0.000	0.000	0.002		0.000	0.000	0.000
TD	61	0.408	0.283	0.545	31	0.455	0.312	0.595	30	0.322	0.223	0.145
		0.001	0.001	0.000		0.010	0.014	0.000		0.083	0.083	0.445

ρ: Spearsman's ρ
τ: Kendall's τ
r: Pearson's r

Table C.132 $\log F_{20}$ vs. $\log M_\star$ (II)

	Ori A				ONC				L1641			
	N	ρ	τ	r	N	ρ	τ	r	N	ρ	τ	r
TDFD	168	0.532	0.383	0.511	83	0.483	0.345	0.436	85	0.561	0.414	0.653
		0.000	0.000	0.000		0.000	0.000	0.000		0.000	0.000	0.000
FD	114	0.538	0.387	0.482	57	0.430	0.309	0.345	57	0.623	0.478	0.674
		0.000	0.000	0.000		0.001	0.001	0.009		0.000	0.000	0.000
TD	54	0.399	0.278	0.563	26	0.464	0.337	0.616	28	0.318	0.217	0.174
		0.003	0.003	0.000		0.017	0.016	0.001		0.099	0.105	0.376

ρ: Spearsman's ρ
τ: Kendall's τ
r: Pearson's r

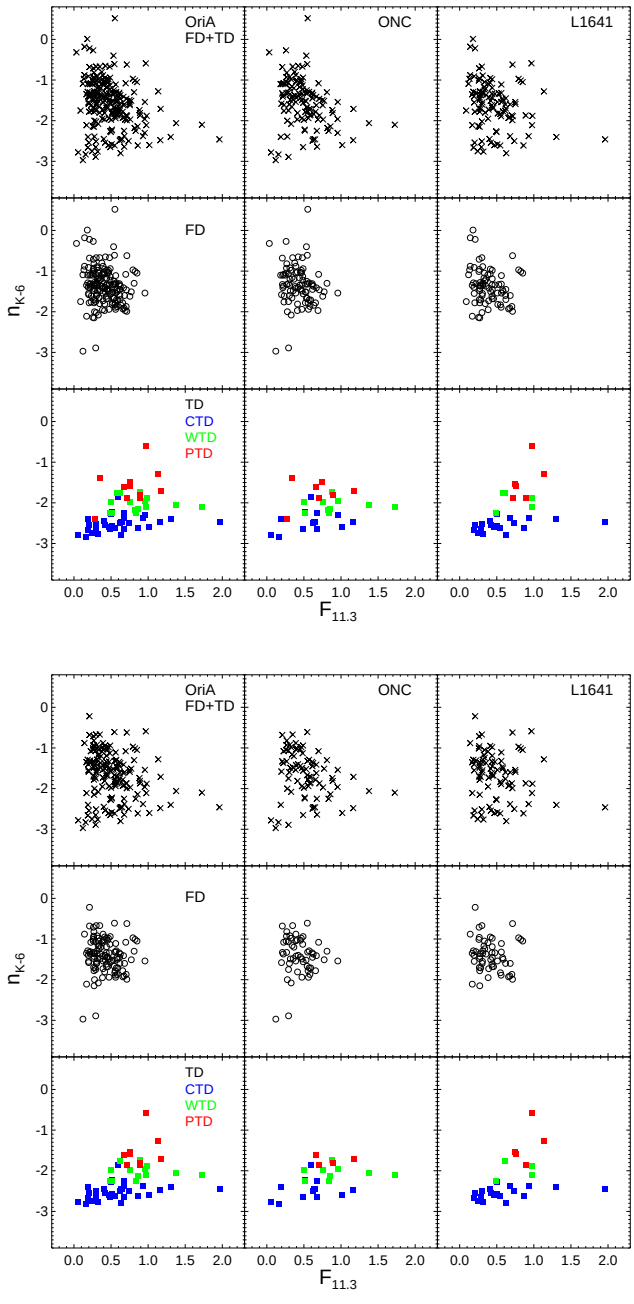


Figure C.67 $F_{11.3}$ vs. n_{K-6}. Upper panel: all available objects; Lower panel: objects with available spectral types only

Table C.133 $F_{11.3}$ vs. n_{K-6} (I)

	Ori A				ONC				L1641			
	N	ρ	τ	r	N	ρ	τ	r	N	ρ	τ	r
TDFD	231	-0.279	-0.200	-0.261	122	-0.346	-0.245	-0.282	109	-0.244	-0.177	-0.248
		0.000	0.000	0.000		0.000	0.000	0.002		0.010	0.006	0.009
FD	170	-0.187	-0.130	-0.132	91	-0.206	-0.138	-0.099	79	-0.195	-0.142	-0.185
		0.015	0.012	0.086		0.050	0.053	0.350		0.086	0.064	0.103
TD	61	0.476	0.330	0.331	31	0.315	0.211	0.275	30	0.593	0.401	0.370
		0.000	0.000	0.009		0.084	0.095	0.134		0.001	0.002	0.044

ρ: Spearsmans ρ
τ: Kendalls τ
r: Pearsons r

Table C.134 $F_{11.3}$ vs. n_{K-6} (II)

	Ori A				ONC				L1641			
	N	ρ	τ	r	N	ρ	τ	r	N	ρ	τ	r
TDFD	168	-0.220	-0.160	-0.202	83	-0.308	-0.224	-0.233	85	-0.158	-0.120	-0.177
		0.004	0.002	0.009		0.005	0.003	0.034		0.149	0.103	0.105
FD	114	-0.144	-0.100	-0.051	57	-0.163	-0.105	-0.005	57	-0.135	-0.104	-0.098
		0.127	0.113	0.590		0.226	0.248	0.971		0.317	0.251	0.468
TD	54	0.555	0.390	0.394	26	0.432	0.299	0.415	28	0.612	0.406	0.385
		0.000	0.000	0.003		0.028	0.032	0.035		0.001	0.002	0.043

ρ: Spearsmans ρ
τ: Kendalls τ
r: Pearsons r

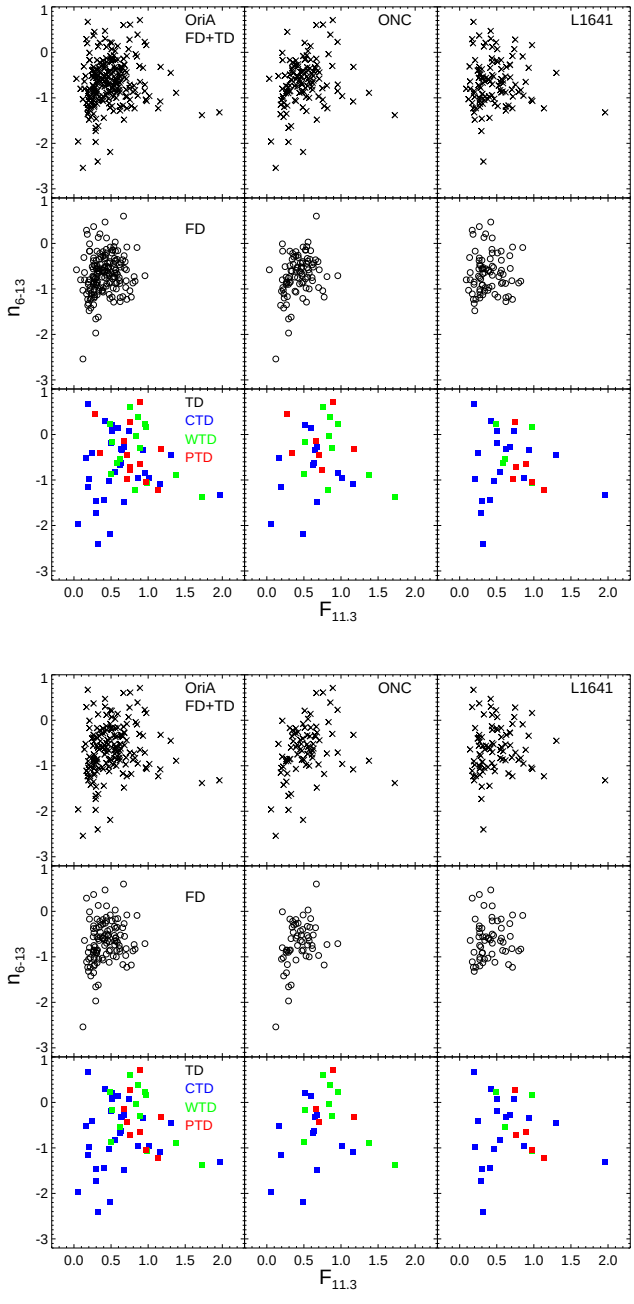


Figure C.68 $F_{11.3}$ vs. n_{6-13}. Upper panel: all available objects; Lower panel: objects with available spectral types only

Table C.135 $F_{11.3}$ vs. n_{6-13} (I)

	Ori A				ONC				L1641			
	N	ρ	τ	r	N	ρ	τ	r	N	ρ	τ	r
TDFD	231	0.167	0.116	0.095	122	0.259	0.185	0.198	109	0.055	0.031	-0.016
		0.011	0.009	0.150		0.004	0.002	0.029		0.571	0.636	0.869
FD	170	0.184	0.126	0.165	91	0.308	0.210	0.310	79	0.049	0.029	0.018
		0.016	0.015	0.032		0.003	0.003	0.003		0.671	0.702	0.875
TD	61	0.007	-0.015	-0.020	31	0.042	0.017	0.010	30	-0.020	-0.041	-0.061
		0.960	0.866	0.878		0.824	0.892	0.957		0.918	0.748	0.749

ρ: Spearsmans ρ
τ: Kendalls τ
r: Pearsons r

Table C.136 $F_{11.3}$ vs. n_{6-13} (II)

	Ori A				ONC				L1641			
	N	ρ	τ	r	N	ρ	τ	r	N	ρ	τ	r
TDFD	168	0.211	0.146	0.119	83	0.328	0.236	0.250	85	0.087	0.049	-0.013
		0.006	0.005	0.124		0.002	0.002	0.023		0.428	0.508	0.906
FD	114	0.223	0.147	0.205	57	0.336	0.219	0.345	57	0.123	0.077	0.072
		0.017	0.021	0.029		0.011	0.016	0.009		0.361	0.395	0.595
TD	54	0.075	0.033	0.025	26	0.182	0.132	0.105	28	-0.023	-0.050	-0.060
		0.589	0.726	0.858		0.373	0.343	0.610		0.909	0.707	0.762

ρ: Spearsmans ρ
τ: Kendalls τ
r: Pearsons r

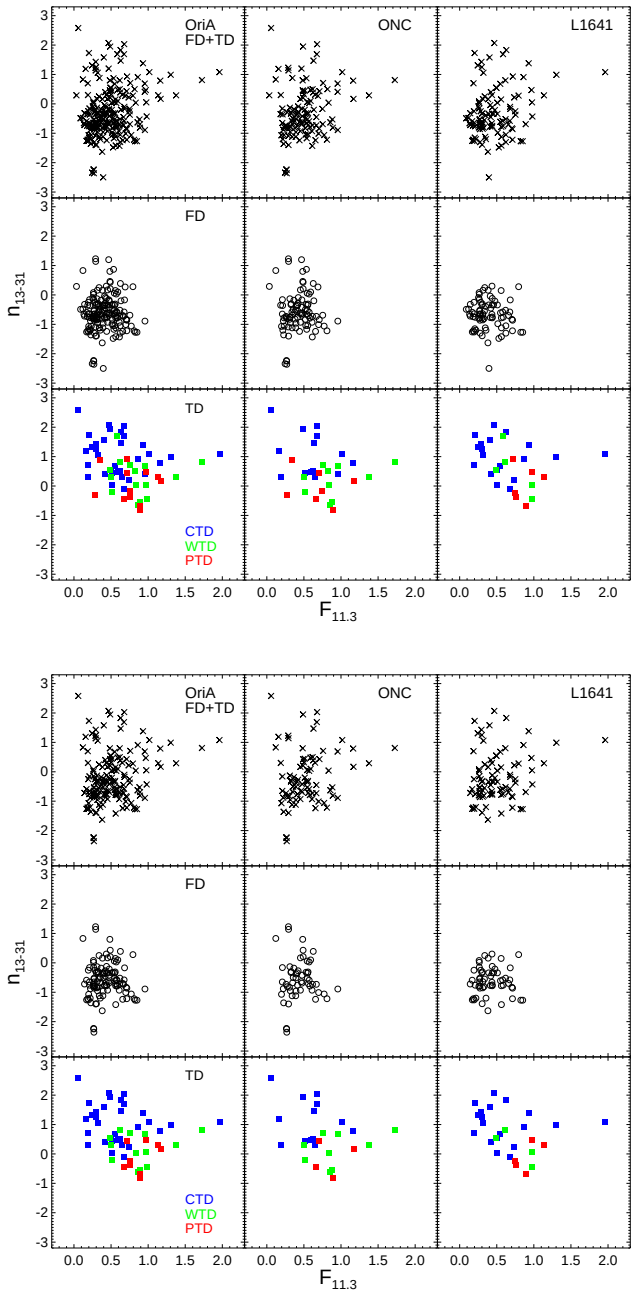


Figure C.69 $F_{11.3}$ vs. n_{13-31}. Upper panel: all available objects; Lower panel: objects with available spectral types only

Table C.137 $F_{11.3}$ vs. n_{13-31} (I)

	Ori A				ONC				L1641			
	N	ρ	τ	r	N	ρ	τ	r	N	ρ	τ	r
TDFD	231	0.197	0.137	0.226	122	0.224	0.162	0.219	109	0.169	0.113	0.235
		0.003	0.002	0.001		0.013	0.008	0.015		0.079	0.081	0.014
FD	170	0.011	0.008	0.006	91	0.082	0.056	0.048	79	-0.094	-0.065	-0.081
		0.885	0.881	0.938		0.438	0.429	0.651		0.409	0.399	0.478
TD	61	-0.341	-0.230	-0.259	31	-0.216	-0.131	-0.234	30	-0.439	-0.297	-0.276
		0.007	0.009	0.044		0.242	0.299	0.205		0.015	0.021	0.140

ρ: Spearsmans ρ
τ: Kendalls τ
r: Pearsons r

Table C.138 $F_{11.3}$ vs. n_{13-31} (II)

	Ori A				ONC				L1641			
	N	ρ	τ	r	N	ρ	τ	r	N	ρ	τ	r
TDFD	168	0.186	0.132	0.200	83	0.208	0.153	0.192	85	0.171	0.120	0.211
		0.016	0.011	0.009		0.060	0.040	0.082		0.117	0.105	0.053
FD	114	0.047	0.025	0.004	57	0.068	0.032	0.010	57	0.010	0.003	-0.011
		0.622	0.692	0.966		0.616	0.725	0.941		0.939	0.972	0.935
TD	54	-0.370	-0.249	-0.283	26	-0.264	-0.163	-0.286	28	-0.451	-0.312	-0.275
		0.006	0.008	0.038		0.192	0.243	0.157		0.016	0.020	0.157

ρ: Spearsmans ρ
τ: Kendalls τ
r: Pearsons r

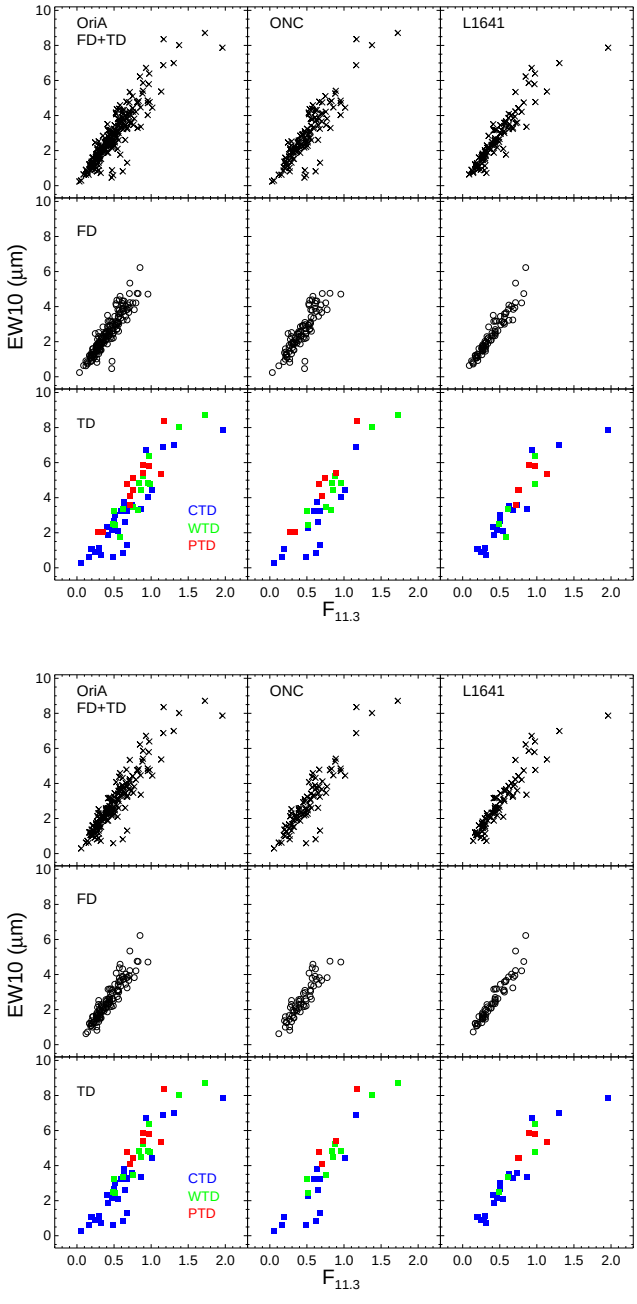


Figure C.70 $F_{11.3}$ vs. EW10. Upper panel: all available objects; Lower panel: objects with available spectral types only

Table C.139 $F_{11.3}$ vs. EW10 (I)

	Ori A				ONC				L1641			
	N	ρ	τ	r	N	ρ	τ	r	N	ρ	τ	r
TDFD	231	0.900	0.759	0.910	122	0.862	0.713	0.892	109	0.947	0.814	0.931
		0.000	0.000	0.000		0.000	0.000	0.000		0.000	0.000	0.000
FD	170	0.922	0.779	0.914	91	0.887	0.721	0.872	79	0.969	0.854	0.958
		0.000	0.000	0.000		0.000	0.000	0.000		0.000	0.000	0.000
TD	61	0.916	0.756	0.904	31	0.888	0.734	0.896	30	0.943	0.798	0.917
		0.000	0.000	0.000		0.000	0.000	0.000		0.000	0.000	0.000

ρ: Spearsmans ρ
τ: Kendalls τ
r: Pearsons r

Table C.140 $F_{11.3}$ vs. EW10 (II)

	Ori A				ONC				L1641			
	N	ρ	τ	r	N	ρ	τ	r	N	ρ	τ	r
TDFD	168	0.912	0.774	0.920	83	0.865	0.725	0.911	85	0.955	0.824	0.932
		0.000	0.000	0.000		0.000	0.000	0.000		0.000	0.000	0.000
FD	114	0.947	0.797	0.933	57	0.916	0.744	0.904	57	0.969	0.858	0.959
		0.000	0.000	0.000		0.000	0.000	0.000		0.000	0.000	0.000
TD	54	0.925	0.775	0.911	26	0.908	0.764	0.908	28	0.949	0.810	0.922
		0.000	0.000	0.000		0.000	0.000	0.000		0.000	0.000	0.000

ρ: Spearsmans ρ
τ: Kendalls τ
r: Pearsons r

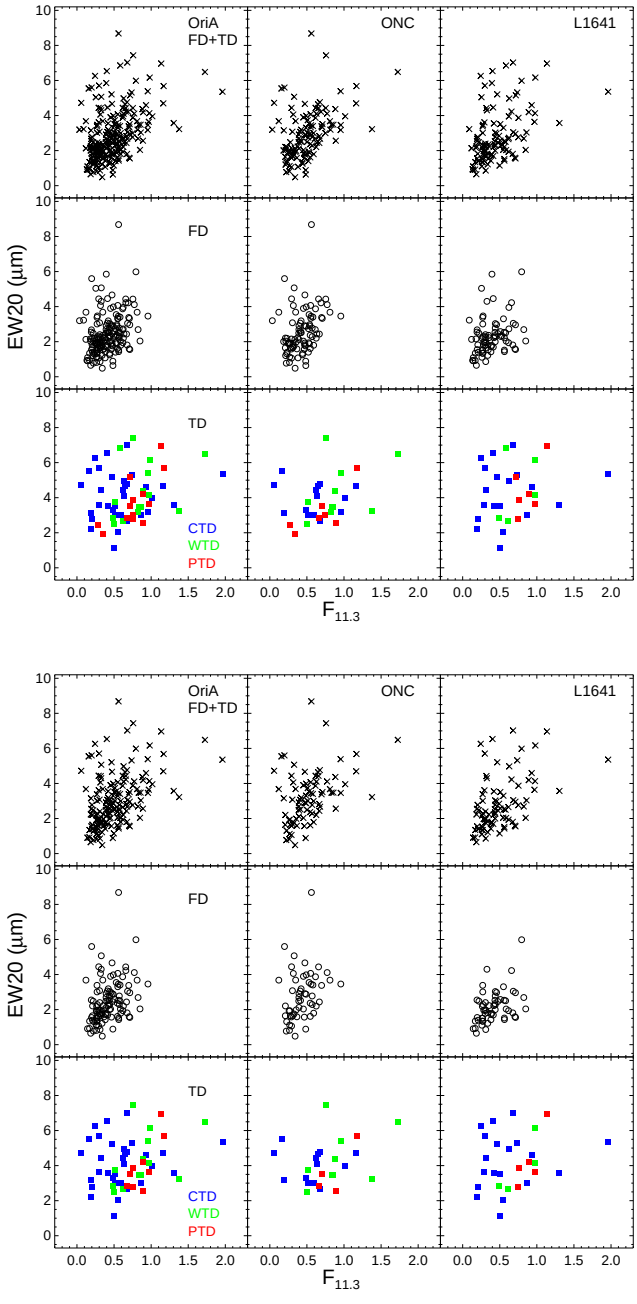


Figure C.71 $F_{11.3}$ vs. EW20. Upper panel: all available objects; Lower panel: objects with available spectral types only

Table C.141 $F_{11.3}$ vs. EW20 (I)

	Ori A				ONC				L1641			
	N	ρ	τ	r	N	ρ	τ	r	N	ρ	τ	r
TDFD	231	0.465	0.331	0.417	122	0.479	0.344	0.387	109	0.461	0.327	0.450
		0.000	0.000	0.000		0.000	0.000	0.000		0.000	0.000	0.000
FD	170	0.383	0.269	0.314	91	0.414	0.287	0.318	79	0.353	0.250	0.307
		0.000	0.000	0.000		0.000	0.000	0.002		0.001	0.001	0.006
TD	61	0.233	0.172	0.234	31	0.301	0.228	0.322	30	0.202	0.140	0.191
		0.071	0.051	0.070		0.100	0.071	0.077		0.285	0.276	0.312

ρ: Spearsmans ρ
τ: Kendalls τ
r: Pearsons r

Table C.142 $F_{11.3}$ vs. EW20 (II)

	Ori A				ONC				L1641			
	N	ρ	τ	r	N	ρ	τ	r	N	ρ	τ	r
TDFD	168	0.466	0.338	0.406	83	0.420	0.310	0.346	85	0.493	0.352	0.476
		0.000	0.000	0.000		0.000	0.000	0.001		0.000	0.000	0.000
FD	114	0.431	0.306	0.326	57	0.394	0.282	0.306	57	0.453	0.319	0.431
		0.000	0.000	0.000		0.002	0.002	0.021		0.000	0.000	0.001
TD	54	0.218	0.156	0.233	26	0.247	0.175	0.271	28	0.215	0.153	0.215
		0.113	0.096	0.090		0.223	0.209	0.181		0.272	0.252	0.272

ρ: Spearsmans ρ
τ: Kendalls τ
r: Pearsons r

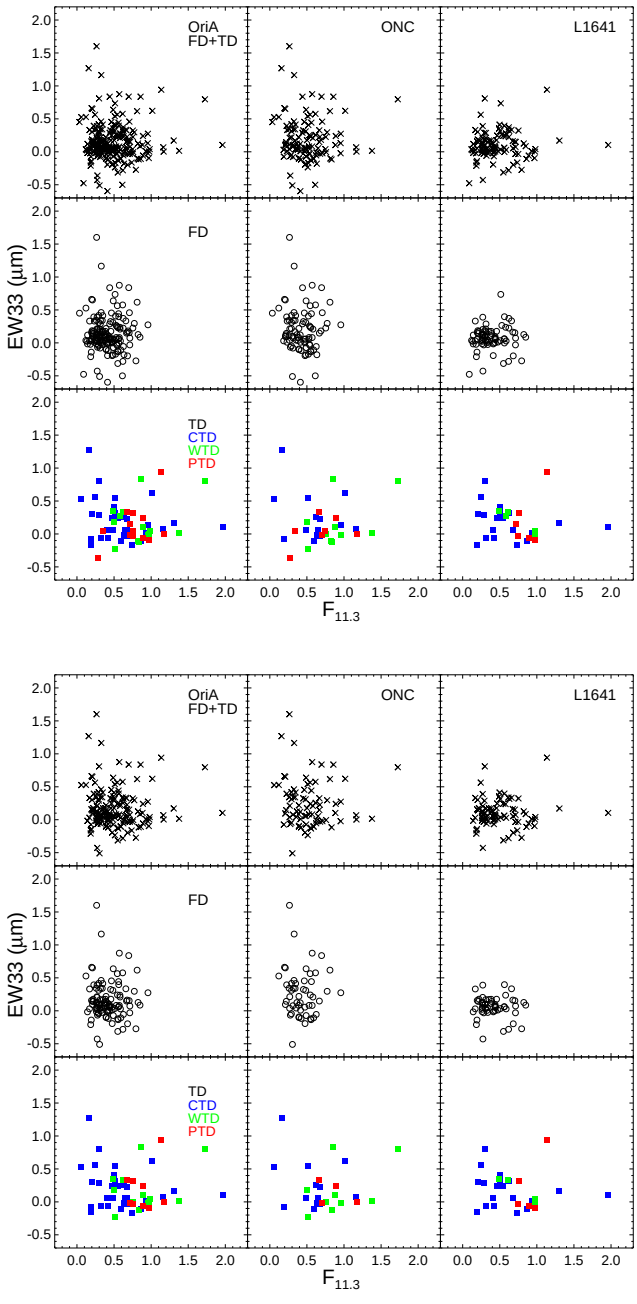


Figure C.72 $F_{11.3}$ vs. EW33. Zoomed in. Upper panel: all available objects; Lower panel: objects with available spectral types only

Table C.143 $F_{11.3}$ vs. EW33 (I)

	Ori A				ONC				L1641			
	N	ρ	τ	r	N	ρ	τ	r	N	ρ	τ	r
TDFD	231	-0.051	-0.036	-0.062	122	-0.128	-0.087	-0.091	109	0.043	0.031	0.008
		0.443	0.422	0.348		0.160	0.154	0.319		0.657	0.633	0.934
FD	170	-0.019	-0.021	-0.125	91	-0.137	-0.106	-0.187	79	0.099	0.064	0.026
		0.806	0.690	0.104		0.196	0.138	0.076		0.385	0.406	0.820
TD	61	-0.105	-0.074	-0.039	31	0.085	0.067	0.042	30	-0.224	-0.157	-0.139
		0.419	0.397	0.765		0.650	0.597	0.822		0.233	0.225	0.464

ρ: Spearsmans ρ
τ: Kendalls τ
r: Pearsons r

Table C.144 $F_{11.3}$ vs. EW33 (II)

	Ori A				ONC				L1641			
	N	ρ	τ	r	N	ρ	τ	r	N	ρ	τ	r
TDFD	168	-0.093	-0.063	-0.044	83	-0.154	-0.104	-0.064	85	-0.044	-0.027	0.025
		0.231	0.224	0.571		0.164	0.163	0.565		0.687	0.715	0.820
FD	114	-0.062	-0.048	-0.131	57	-0.147	-0.114	-0.186	57	-0.017	-0.013	-0.066
		0.514	0.448	0.165		0.275	0.210	0.166		0.901	0.890	0.626
TD	54	-0.135	-0.090	-0.077	26	0.020	0.025	-0.035	28	-0.188	-0.125	-0.136
		0.331	0.336	0.580		0.922	0.860	0.865		0.338	0.352	0.490

ρ: Spearsmans ρ
τ: Kendalls τ
r: Pearsons r

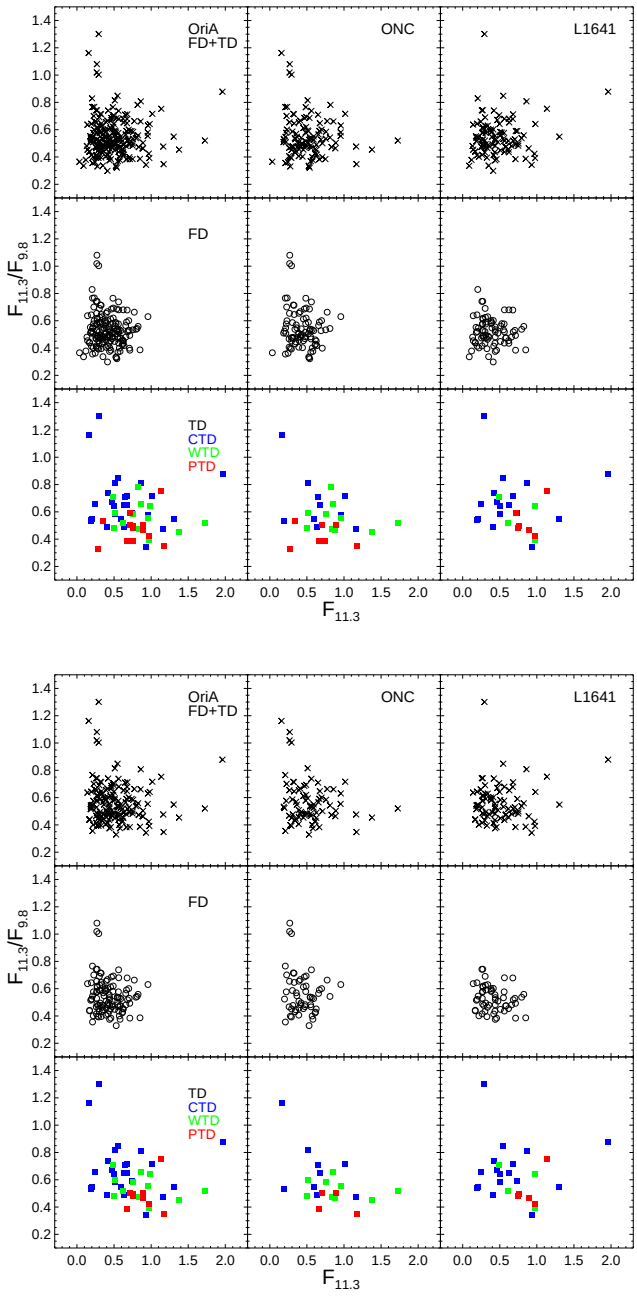


Figure C.73 $F_{11.3}$ vs. $F_{11.3}/F_{9.8}$. Zoomed in. Upper panel: all available objects; Lower panel: objects with available spectral types only

Table C.145 $F_{11.3}$ vs. $F_{11.3}/F_{9.8}$ (I)

	Ori A				ONC				L1641			
	N	ρ	τ	r	N	ρ	τ	r	N	ρ	τ	r
TDFD	231	0.000	0.001	-0.035	122	-0.032	-0.016	-0.022	109	0.054	0.037	-0.041
		1.000	0.976	0.597		0.730	0.797	0.810		0.576	0.570	0.672
FD	170	-0.055	-0.037	-0.067	91	-0.099	-0.055	-0.090	79	-0.021	-0.019	-0.041
		0.473	0.472	0.385		0.352	0.442	0.396		0.855	0.799	0.720
TD	61	-0.230	-0.164	-0.119	31	-0.089	-0.065	-0.034	30	-0.285	-0.209	-0.196
		0.075	0.062	0.361		0.634	0.610	0.856		0.126	0.104	0.299

ρ: Spearsmans ρ
τ: Kendalls τ
r: Pearsons r

Table C.146 $F_{11.3}$ vs. $F_{11.3}/F_{9.8}$ (II)

	Ori A				ONC				L1641			
	N	ρ	τ	r	N	ρ	τ	r	N	ρ	τ	r
TDFD	168	-0.102	-0.066	-0.053	83	-0.112	-0.076	-0.035	85	-0.080	-0.048	-0.067
		0.190	0.202	0.495		0.313	0.308	0.753		0.465	0.514	0.542
FD	114	-0.160	-0.104	-0.229	57	-0.168	-0.105	-0.304	57	-0.195	-0.127	-0.195
		0.089	0.101	0.014		0.211	0.247	0.022		0.146	0.164	0.146
TD	54	-0.296	-0.212	-0.124	26	-0.218	-0.157	-0.040	28	-0.273	-0.206	-0.194
		0.030	0.024	0.372		0.284	0.261	0.846		0.160	0.123	0.323

ρ: Spearsmans ρ
τ: Kendalls τ
r: Pearsons r

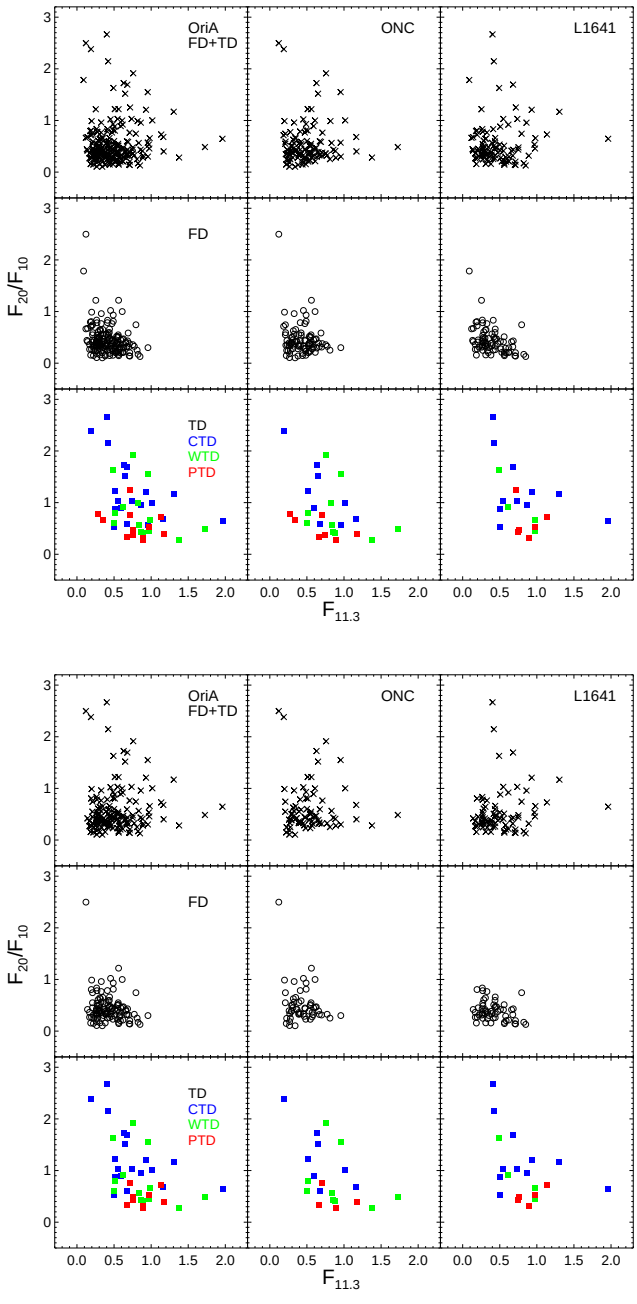


Figure C.74 $F_{11.3}$ vs. F_{20}/F_{10}. Upper panel: all available objects; Lower panel: objects with available spectral types only

Table C.147 $F_{11.3}$ vs. F_{20}/F_{10} (I)

	Ori A				ONC				L1641			
	N	ρ	τ	r	N	ρ	τ	r	N	ρ	τ	r
TDFD	230	-0.030	-0.022	-0.111	121	0.031	0.024	-0.139	109	-0.078	-0.061	-0.077
		0.652	0.616	0.093		0.732	0.695	0.128		0.420	0.347	0.426
FD	170	-0.265	-0.181	-0.247	91	-0.124	-0.079	-0.272	79	-0.426	-0.304	-0.415
		0.000	0.000	0.001		0.242	0.266	0.009		0.000	0.000	0.000
TD	60	-0.621	-0.430	-0.490	30	-0.533	-0.373	-0.437	30	-0.718	-0.508	-0.536
		0.000	0.000	0.000		0.002	0.004	0.016		0.000	0.000	0.002

ρ: Spearsmans ρ
τ: Kendalls τ
r: Pearsons r

Table C.148 $F_{11.3}$ vs. F_{20}/F_{10} (II)

	Ori A				ONC				L1641			
	N	ρ	τ	r	N	ρ	τ	r	N	ρ	τ	r
TDFD	167	0.029	0.019	-0.126	82	0.040	0.032	-0.118	85	0.009	0.003	-0.134
		0.707	0.708	0.105		0.720	0.674	0.291		0.933	0.970	0.221
FD	114	-0.149	-0.105	-0.207	57	-0.089	-0.060	-0.220	57	-0.265	-0.184	-0.278
		0.114	0.097	0.027		0.509	0.508	0.100		0.046	0.043	0.036
TD	53	-0.670	-0.473	-0.535	25	-0.603	-0.447	-0.507	28	-0.733	-0.519	-0.583
		0.000	0.000	0.000		0.001	0.002	0.010		0.000	0.000	0.001

ρ: Spearsmans ρ
τ: Kendalls τ
r: Pearsons r

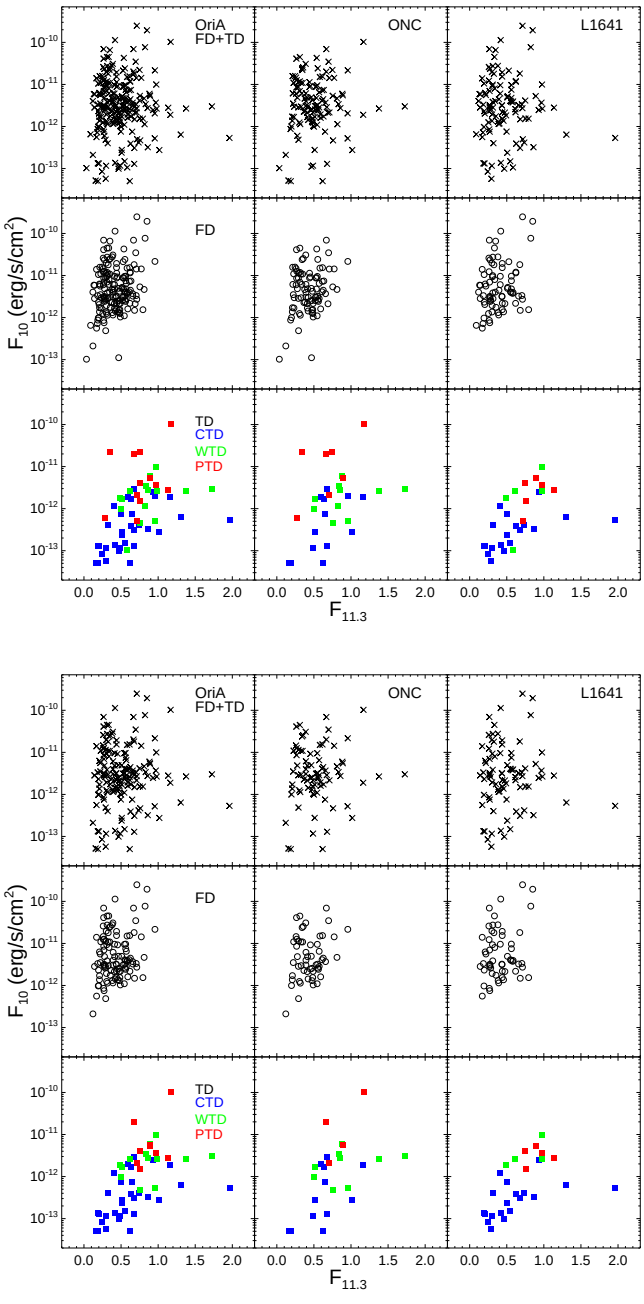


Figure C.75 $F_{11.3}$ vs. $\log F_{10}$. Upper panel: all available objects; Lower panel: objects with available spectral types only

Table C.149 $F_{11.3}$ vs. $\log F_{10}$ (I)

	Ori A				ONC				L1641			
	N	ρ	τ	r	N	ρ	τ	r	N	ρ	τ	r
TDFD	230	0.018	0.014	0.030	121	0.030	0.018	0.078	109	-0.005	0.000	-0.019
		0.783	0.757	0.651		0.744	0.776	0.395		0.959	0.996	0.845
FD	170	0.166	0.116	0.252	91	0.148	0.103	0.251	79	0.200	0.136	0.276
		0.031	0.025	0.001		0.161	0.148	0.016		0.077	0.075	0.014
TD	60	0.581	0.413	0.458	30	0.450	0.327	0.410	30	0.705	0.503	0.514
		0.000	0.000	0.000		0.013	0.011	0.024		0.000	0.000	0.004

ρ: Spearsmans ρ
τ: Kendalls τ
r: Pearsons r

Table C.150 $F_{11.3}$ vs. $\log F_{10}$ (II)

	Ori A				ONC				L1641			
	N	ρ	τ	r	N	ρ	τ	r	N	ρ	τ	r
TDFD	167	0.020	0.014	0.035	82	0.033	0.019	0.074	85	0.011	0.007	0.000
		0.801	0.789	0.653		0.771	0.801	0.509		0.922	0.924	1.000
FD	114	0.128	0.090	0.224	57	0.151	0.109	0.235	57	0.121	0.078	0.227
		0.175	0.156	0.017		0.262	0.230	0.078		0.368	0.393	0.089
TD	53	0.648	0.469	0.527	25	0.579	0.427	0.535	28	0.715	0.513	0.518
		0.000	0.000	0.000		0.002	0.003	0.006		0.000	0.000	0.005

ρ: Spearsmans ρ
τ: Kendalls τ
r: Pearsons r

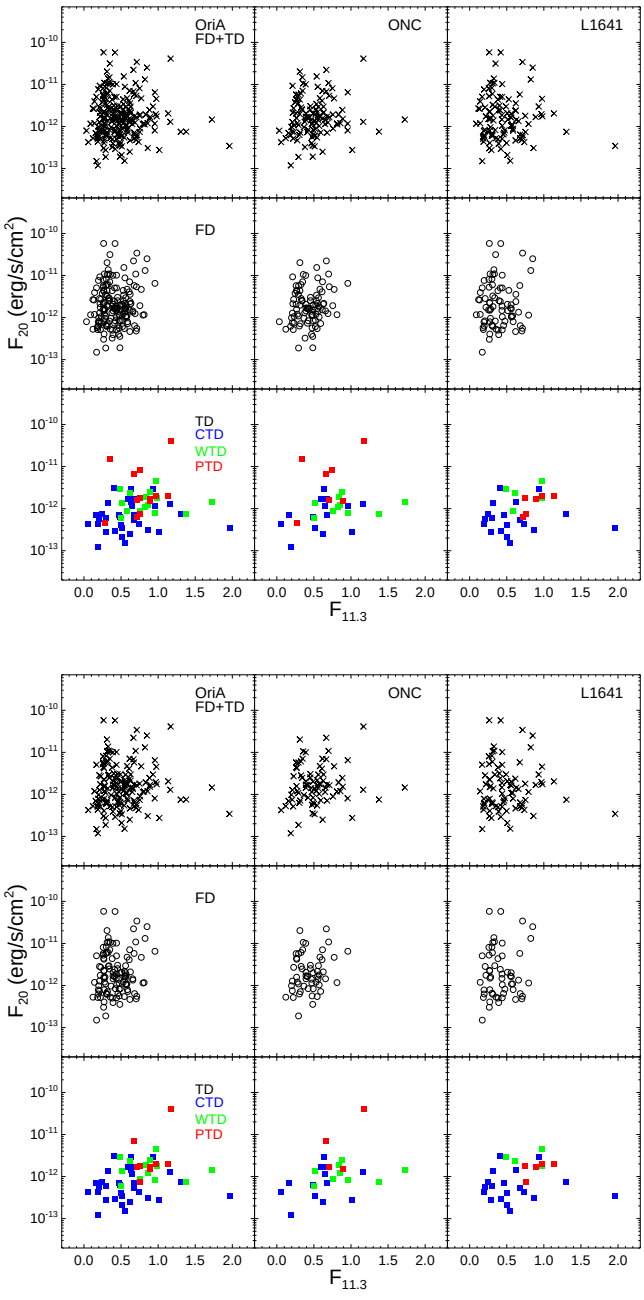


Figure C.76 $F_{11.3}$-log F_{20}. Upper panel: all available objects; Lower panel: objects with available spectral types only

Table C.151 $F_{11.3}$ vs. $\log F_{20}$ (I)

	Ori A				ONC				L1641			
	N	ρ	τ	r	N	ρ	τ	r	N	ρ	τ	r
TDFD	231	0.045	0.029	0.016	122	0.118	0.074	0.104	109	-0.036	-0.025	-0.065
		0.500	0.511	0.809		0.195	0.225	0.254		0.710	0.704	0.502
FD	170	0.078	0.052	0.124	91	0.160	0.105	0.185	79	0.021	0.013	0.087
		0.309	0.314	0.107		0.129	0.140	0.079		0.852	0.865	0.446
TD	61	0.345	0.234	0.225	31	0.328	0.207	0.268	30	0.297	0.209	0.161
		0.006	0.008	0.081		0.071	0.102	0.145		0.111	0.104	0.395

ρ: Spearsmans ρ
τ: Kendalls τ
r: Pearsons r

Table C.152 $F_{11.3}$ vs. $\log F_{20}$ (II)

	Ori A				ONC				L1641			
	N	ρ	τ	r	N	ρ	τ	r	N	ρ	τ	r
TDFD	168	0.074	0.047	0.034	83	0.131	0.083	0.115	85	0.017	0.008	-0.033
		0.342	0.363	0.662		0.238	0.265	0.301		0.875	0.909	0.764
FD	114	0.096	0.058	0.153	57	0.195	0.125	0.223	57	0.034	0.014	0.107
		0.311	0.357	0.104		0.146	0.168	0.095		0.800	0.879	0.428
TD	54	0.372	0.249	0.280	26	0.405	0.255	0.380	28	0.286	0.196	0.163
		0.006	0.008	0.040		0.040	0.067	0.056		0.141	0.144	0.407

ρ: Spearsmans ρ
τ: Kendalls τ
r: Pearsons r

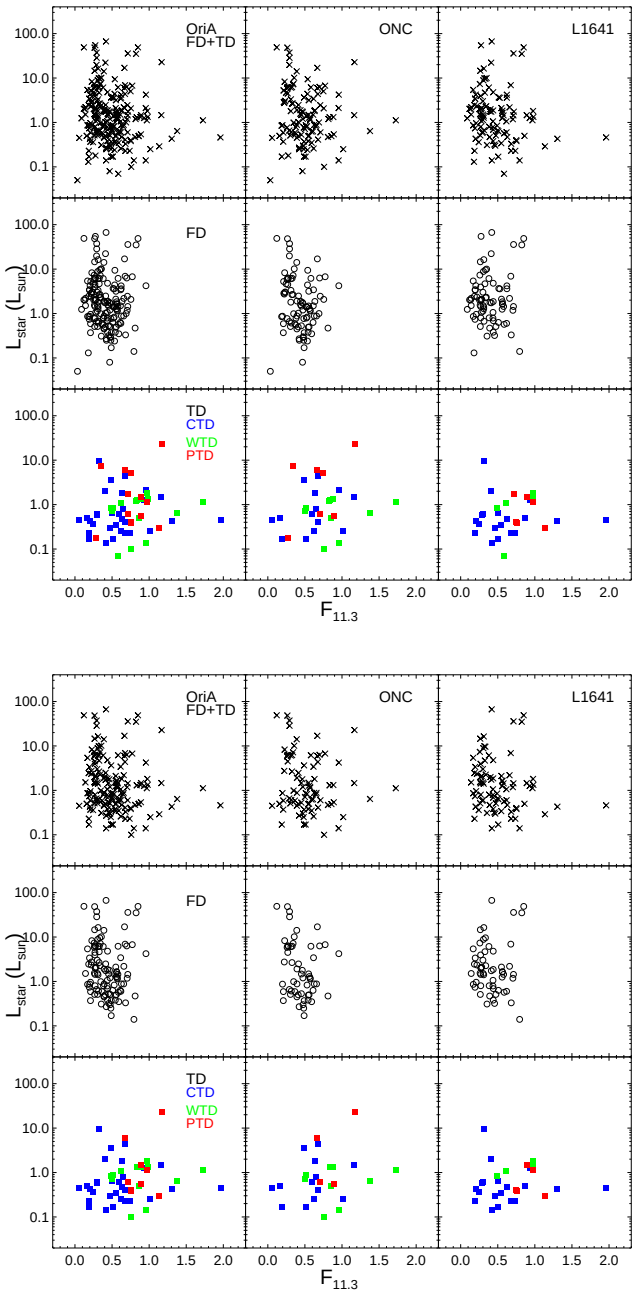


Figure C.77 $F_{11.3}$ vs. $\log L_\star$. Upper panel: all available objects; Lower panel: objects with available spectral types only

Table C.153 $F_{11.3}$ vs. $\log L_\star$ (I)

	Ori A				ONC				L1641			
	N	ρ	τ	r	N	ρ	τ	r	N	ρ	τ	r
TDFD	231	-0.167	-0.109	-0.128	122	-0.116	-0.074	-0.097	109	-0.214	-0.139	-0.159
		0.011	0.014	0.052		0.204	0.226	0.288		0.026	0.032	0.099
FD	170	-0.135	-0.086	-0.045	91	-0.171	-0.112	-0.130	79	-0.037	-0.024	0.076
		0.080	0.094	0.560		0.105	0.116	0.219		0.744	0.750	0.506
TD	61	0.204	0.140	0.140	31	0.173	0.119	0.193	30	0.167	0.136	0.053
		0.116	0.111	0.282		0.351	0.349	0.298		0.377	0.290	0.781

ρ: Spearsmans ρ
τ: Kendalls τ
r: Pearsons r

Table C.154 $F_{11.3}$ vs. $\log L_\star$ (II)

	Ori A				ONC				L1641			
	N	ρ	τ	r	N	ρ	τ	r	N	ρ	τ	r
TDFD	168	-0.199	-0.133	-0.156	83	-0.157	-0.107	-0.157	85	-0.242	-0.161	-0.158
		0.010	0.010	0.043		0.157	0.153	0.156		0.026	0.029	0.149
FD	114	-0.191	-0.129	-0.092	57	-0.241	-0.165	-0.227	57	-0.131	-0.088	0.049
		0.042	0.043	0.330		0.071	0.069	0.089		0.332	0.334	0.717
TD	54	0.178	0.130	0.144	26	0.157	0.111	0.224	28	0.163	0.144	0.035
		0.199	0.164	0.299		0.445	0.427	0.271		0.407	0.283	0.860

ρ: Spearsmans ρ
τ: Kendalls τ
r: Pearsons r

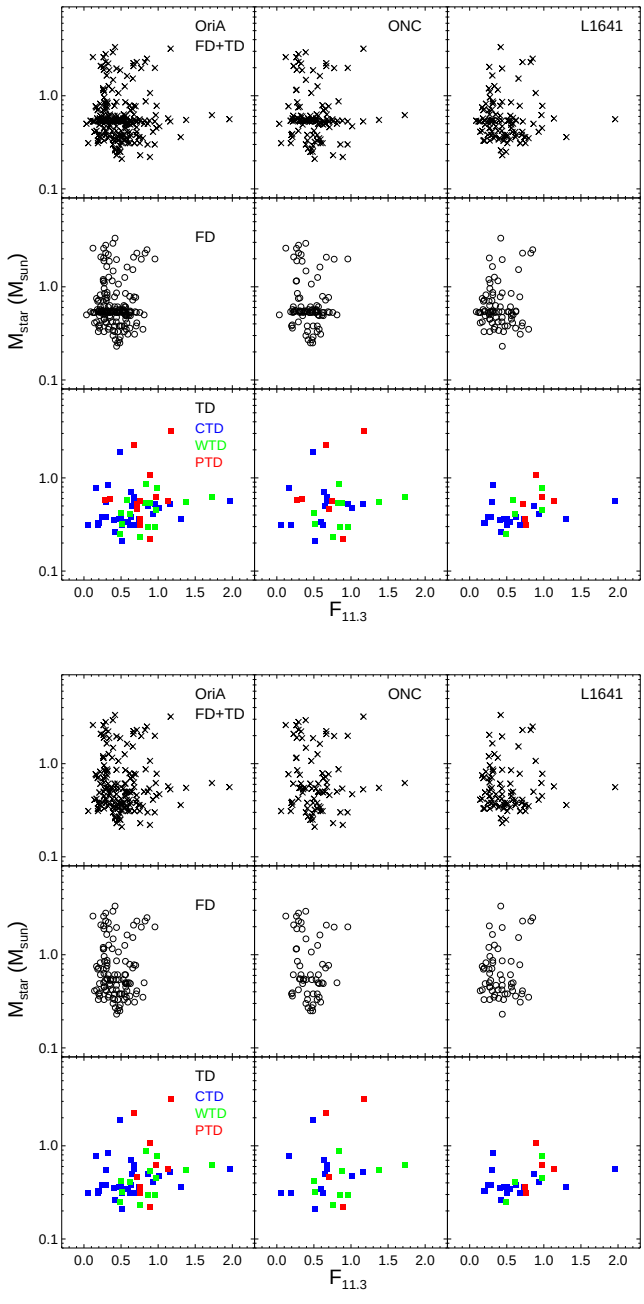


Figure C.78 $F_{11.3}$ vs. $\log M_\star$. Upper panel: all available objects; Lower panel: objects with available spectral types only

Table C.155 $F_{11.3}$ vs. $\log M_\star$ (I)

	Ori A				ONC				L1641			
	N	ρ	τ	r	N	ρ	τ	r	N	ρ	τ	r
TDFD	231	-0.098	-0.065	-0.026	122	-0.125	-0.086	-0.054	109	-0.101	-0.065	-0.005
		0.139	0.144	0.694		0.170	0.160	0.555		0.294	0.315	0.959
FD	170	-0.095	-0.062	0.024	91	-0.151	-0.099	-0.071	79	-0.052	-0.032	0.127
		0.220	0.231	0.756		0.152	0.165	0.504		0.648	0.676	0.265
TD	61	0.241	0.171	0.219	31	0.044	0.037	0.155	30	0.412	0.289	0.341
		0.061	0.052	0.090		0.815	0.771	0.405		0.024	0.025	0.065

ρ: Spearsmans ρ
τ: Kendalls τ
r: Pearsons r

Table C.156 $F_{11.3}$ vs. $\log M_\star$ (II)

	Ori A				ONC				L1641			
	N	ρ	τ	r	N	ρ	τ	r	N	ρ	τ	r
TDFD	168	-0.081	-0.051	-0.035	83	-0.112	-0.073	-0.078	85	-0.077	-0.048	0.001
		0.294	0.328	0.652		0.314	0.329	0.483		0.486	0.519	0.993
FD	114	-0.099	-0.065	0.013	57	-0.184	-0.118	-0.100	57	-0.053	-0.037	0.127
		0.294	0.307	0.891		0.170	0.194	0.459		0.693	0.687	0.346
TD	54	0.302	0.210	0.241	26	0.127	0.102	0.180	28	0.422	0.304	0.355
		0.026	0.025	0.079		0.538	0.464	0.379		0.025	0.023	0.064

ρ: Spearsmans ρ
τ: Kendalls τ
r: Pearsons r

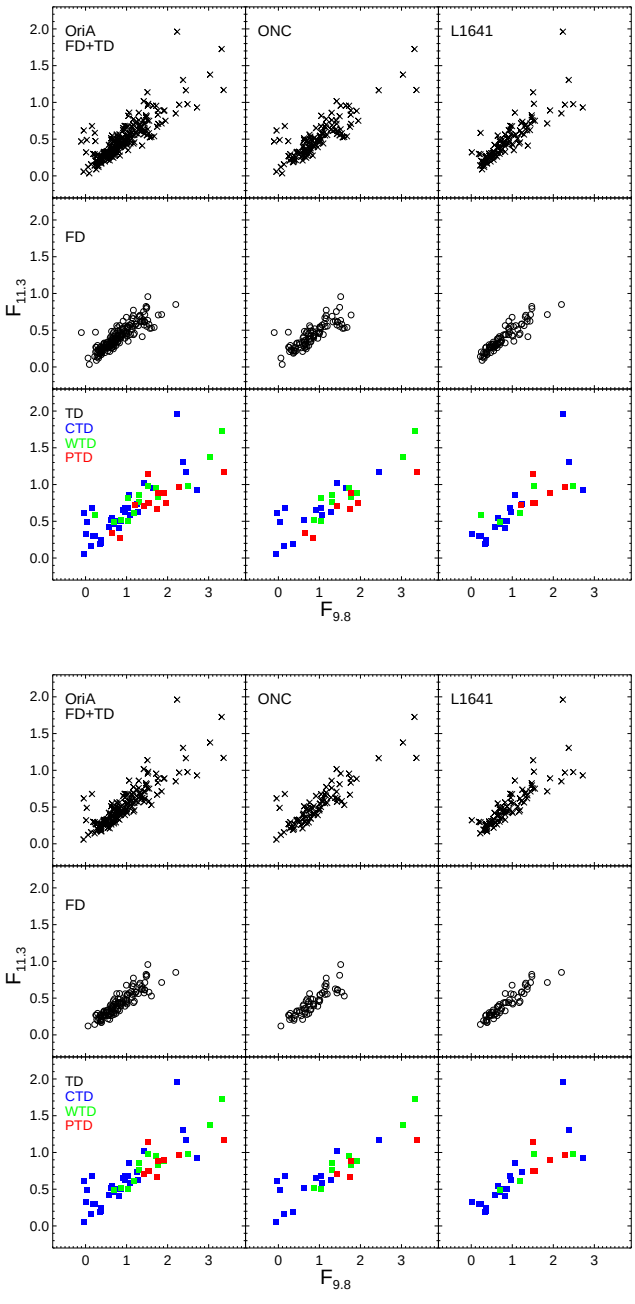


Figure C.79 $F_{9.8}$ vs. $F_{11.3}$. Upper panel: all available objects; Lower panel: objects with available spectral types only

Table C.157 $F_{9.8}$ vs. $F_{11.3}$ (I)

	Ori A				ONC				L1641			
	N	ρ	τ	r	N	ρ	τ	r	N	ρ	τ	r
TDFD	231	0.860	0.702	0.856	122	0.830	0.666	0.859	109	0.900	0.746	0.859
		0.000	0.000	0.000		0.000	0.000	0.000		0.000	0.000	0.000
FD	170	0.891	0.723	0.866	91	0.859	0.673	0.819	79	0.938	0.790	0.920
		0.000	0.000	0.000		0.000	0.000	0.000		0.000	0.000	0.000
TD	61	0.884	0.704	0.837	31	0.866	0.689	0.866	30	0.905	0.723	0.817
		0.000	0.000	0.000		0.000	0.000	0.000		0.000	0.000	0.000

ρ: Spearsmans ρ
τ: Kendalls τ
r: Pearsons r

Table C.158 $F_{9.8}$ vs. $F_{11.3}$ (II)

	Ori A				ONC				L1641			
	N	ρ	τ	r	N	ρ	τ	r	N	ρ	τ	r
TDFD	168	0.883	0.724	0.871	83	0.838	0.692	0.882	85	0.931	0.767	0.865
		0.000	0.000	0.000		0.000	0.000	0.000		0.000	0.000	0.000
FD	114	0.921	0.748	0.901	57	0.898	0.711	0.867	57	0.944	0.801	0.933
		0.000	0.000	0.000		0.000	0.000	0.000		0.000	0.000	0.000
TD	54	0.896	0.727	0.848	26	0.889	0.729	0.882	28	0.920	0.739	0.828
		0.000	0.000	0.000		0.000	0.000	0.000		0.000	0.000	0.000

ρ: Spearsmans ρ
τ: Kendalls τ
r: Pearsons r

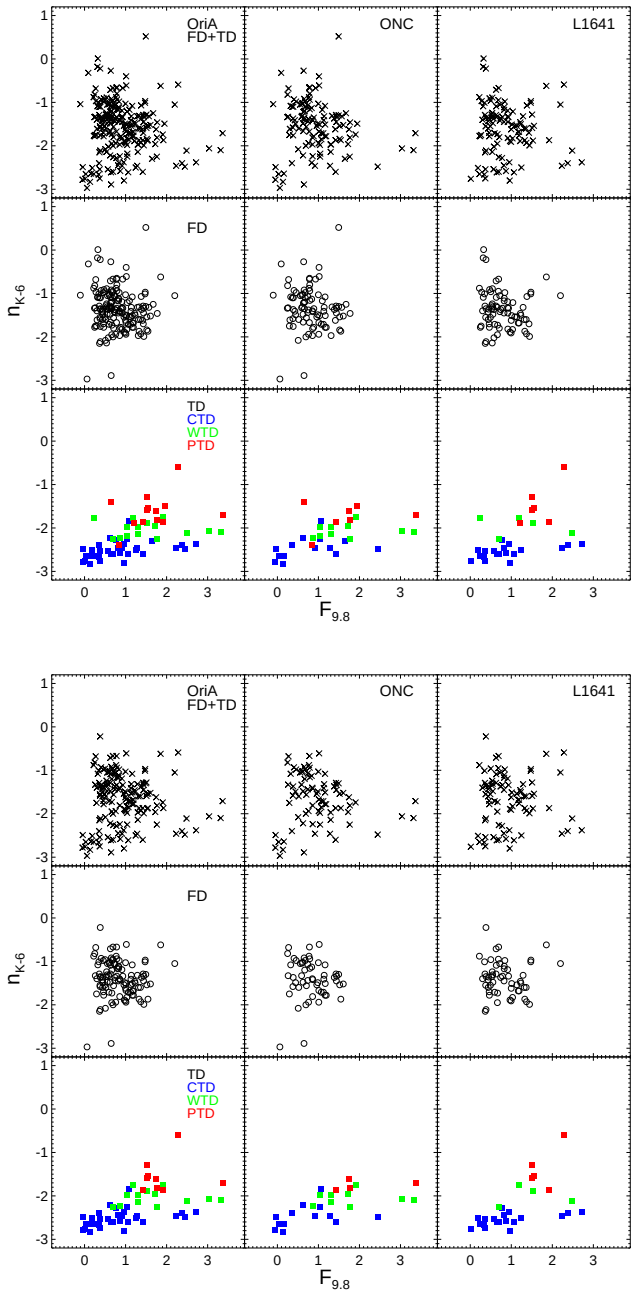


Figure C.80 $F_{9.8}$ vs. n_{K-6}. Upper panel: all available objects; Lower panel: objects with available spectral types only

Table C.159 $F_{9.8}$ vs. n_{K-6} (I)

	Ori A				ONC				L1641			
	N	ρ	τ	r	N	ρ	τ	r	N	ρ	τ	r
TDFD	231	-0.113	-0.082	-0.086	122	-0.180	-0.126	-0.107	109	-0.066	-0.052	-0.068
		0.087	0.064	0.193		0.048	0.040	0.241		0.494	0.423	0.482
FD	170	-0.144	-0.097	-0.070	91	-0.171	-0.108	-0.048	79	-0.139	-0.105	-0.104
		0.060	0.062	0.364		0.104	0.129	0.651		0.222	0.170	0.362
TD	61	0.598	0.433	0.476	31	0.576	0.442	0.501	30	0.593	0.418	0.476
		0.000	0.000	0.000		0.001	0.000	0.004		0.001	0.001	0.008

ρ: Spearsmans ρ
τ: Kendalls τ
r: Pearsons r

Table C.160 $F_{9.8}$ vs. n_{K-6} (II)

	Ori A				ONC				L1641			
	N	ρ	τ	r	N	ρ	τ	r	N	ρ	τ	r
TDFD	168	-0.044	-0.040	-0.029	83	-0.117	-0.100	-0.068	85	0.015	0.008	0.010
		0.572	0.440	0.709		0.293	0.179	0.541		0.893	0.915	0.928
FD	114	-0.131	-0.087	-0.031	57	-0.178	-0.117	-0.037	57	-0.085	-0.064	-0.025
		0.164	0.171	0.743		0.186	0.197	0.785		0.528	0.481	0.854
TD	54	0.684	0.489	0.542	26	0.653	0.491	0.607	28	0.681	0.473	0.538
		0.000	0.000	0.000		0.000	0.000	0.001		0.000	0.000	0.003

ρ: Spearsmans ρ
τ: Kendalls τ
r: Pearsons r

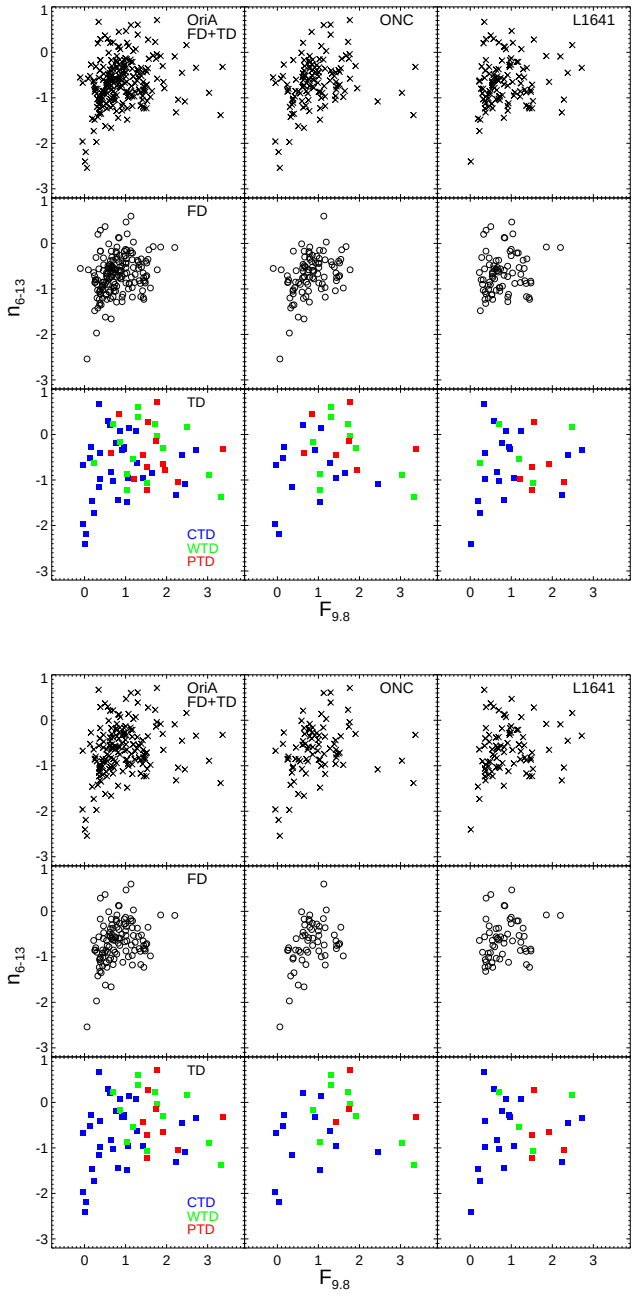


Figure C.81 $F_{9.8}$ vs. n_{6-13}. Upper panel: all available objects; Lower panel: objects with available spectral types only

Table C.161 $F_{9.8}$ vs. n_{6-13} (I)

	Ori A				ONC				L1641			
	N	ρ	τ	r	N	ρ	τ	r	N	ρ	τ	r
TDFD	231	0.249	0.174	0.219	122	0.319	0.220	0.265	109	0.162	0.112	0.159
		0.000	0.000	0.001		0.000	0.000	0.003		0.092	0.083	0.099
FD	170	0.294	0.204	0.279	91	0.394	0.264	0.386	79	0.165	0.114	0.157
		0.000	0.000	0.000		0.000	0.000	0.000		0.145	0.138	0.167
TD	61	0.128	0.078	0.143	31	0.127	0.080	0.111	30	0.146	0.081	0.167
		0.326	0.376	0.272		0.497	0.529	0.552		0.442	0.531	0.378

ρ: Spearsmans ρ
τ: Kendalls τ
r: Pearsons r

Table C.162 $F_{9.8}$ vs. n_{6-13} (II)

	Ori A				ONC				L1641			
	N	ρ	τ	r	N	ρ	τ	r	N	ρ	τ	r
TDFD	168	0.260	0.179	0.226	83	0.327	0.224	0.274	85	0.189	0.127	0.169
		0.001	0.001	0.003		0.003	0.003	0.012		0.084	0.085	0.122
FD	114	0.296	0.199	0.289	57	0.365	0.232	0.399	57	0.224	0.146	0.182
		0.001	0.002	0.002		0.005	0.011	0.002		0.094	0.108	0.175
TD	54	0.165	0.099	0.170	26	0.220	0.145	0.157	28	0.148	0.085	0.175
		0.232	0.289	0.219		0.281	0.300	0.444		0.451	0.526	0.373

ρ: Spearsmans ρ
τ: Kendalls τ
r: Pearsons r

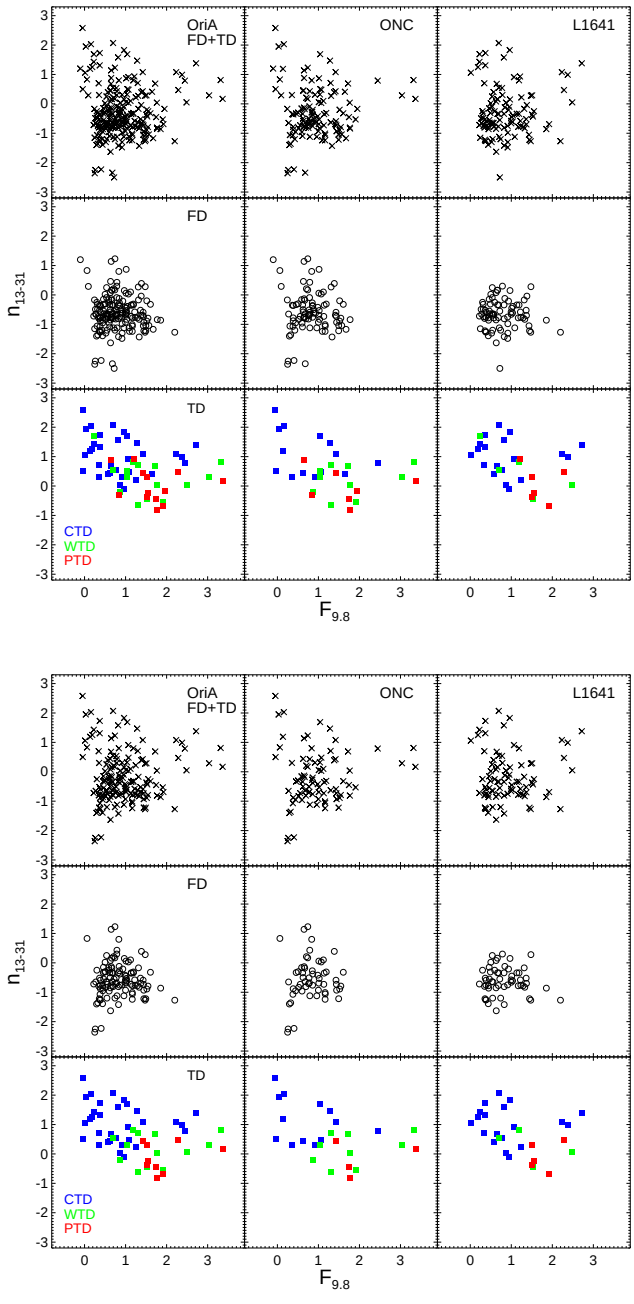


Figure C.82 $F_{9.8}$ vs. n_{13-31}. Upper panel: all available objects; Lower panel: objects with available spectral types only

Table C.163 $F_{9.8}$ vs. n_{13-31} (I)

	Ori A				ONC				L1641			
	N	ρ	τ	r	N	ρ	τ	r	N	ρ	τ	r
TDFD	231	0.026	0.025	0.045	122	0.010	0.018	0.023	109	0.032	0.024	0.075
		0.691	0.571	0.496		0.912	0.768	0.801		0.743	0.713	0.438
FD	170	-0.016	-0.011	-0.040	91	-0.039	-0.023	-0.054	79	-0.020	-0.020	-0.033
		0.834	0.835	0.605		0.716	0.747	0.611		0.862	0.798	0.773
TD	61	-0.461	-0.313	-0.404	31	-0.440	-0.293	-0.411	30	-0.443	-0.299	-0.376
		0.000	0.000	0.001		0.013	0.021	0.022		0.014	0.020	0.041

ρ: Spearsmans ρ
τ: Kendalls τ
r: Pearsons r

Table C.164 $F_{9.8}$ vs. n_{13-31} (II)

	Ori A				ONC				L1641			
	N	ρ	τ	r	N	ρ	τ	r	N	ρ	τ	r
TDFD	168	0.039	0.035	0.056	83	0.045	0.049	0.057	85	0.022	0.016	0.055
		0.613	0.502	0.471		0.685	0.516	0.609		0.839	0.828	0.617
FD	114	0.074	0.045	0.043	57	0.093	0.067	0.110	57	0.019	-0.003	-0.048
		0.435	0.479	0.650		0.493	0.461	0.415		0.888	0.972	0.723
TD	54	-0.449	-0.313	-0.391	26	-0.462	-0.311	-0.423	28	-0.409	-0.289	-0.341
		0.001	0.001	0.003		0.018	0.026	0.031		0.030	0.031	0.076

ρ: Spearsmans ρ
τ: Kendalls τ
r: Pearsons r

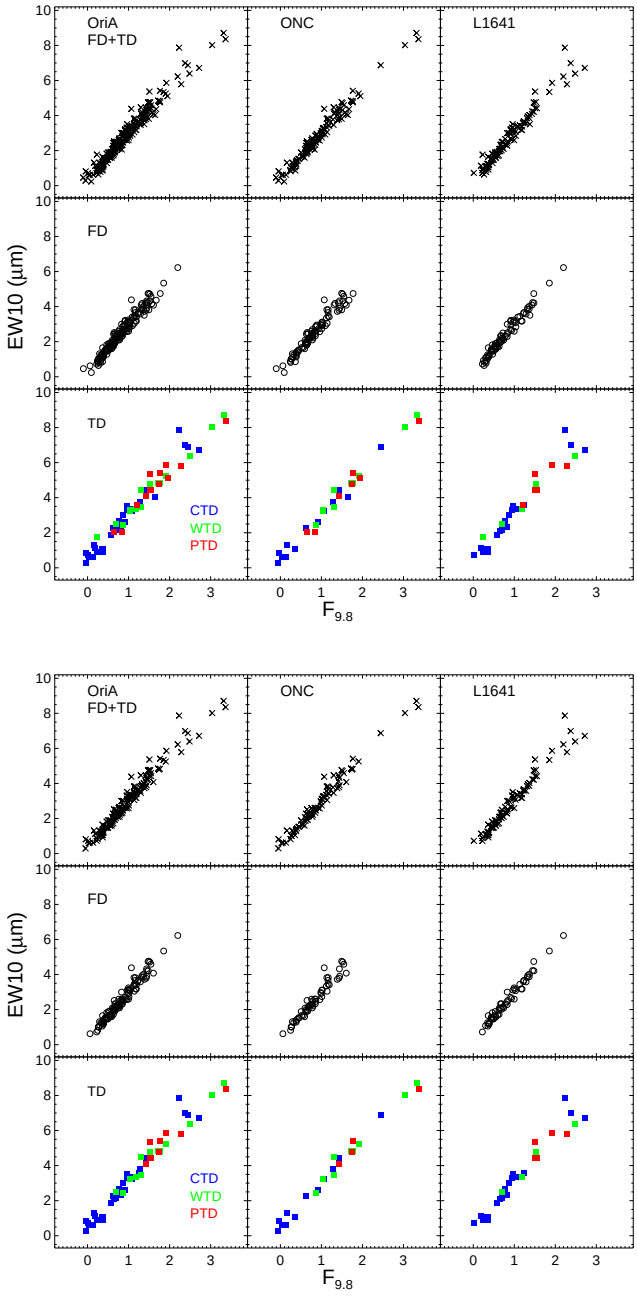


Figure C.83 $F_{9.8}$ vs. EW10. Upper panel: all available objects; Lower panel: objects with available spectral types only

Table C.165 $F_{9.8}$ vs. EW10 (I)

	Ori A				ONC				L1641			
	N	ρ	τ	r	N	ρ	τ	r	N	ρ	τ	r
TDFD	231	0.983	0.893	0.981	122	0.980	0.889	0.984	109	0.981	0.894	0.978
		0.000	0.000	0.000		0.000	0.000	0.000		0.000	0.000	0.000
FD	170	0.981	0.884	0.978	91	0.975	0.873	0.972	79	0.982	0.893	0.985
		0.000	0.000	0.000		0.000	0.000	0.000		0.000	0.000	0.000
TD	61	0.984	0.893	0.981	31	0.989	0.920	0.991	30	0.977	0.888	0.971
		0.000	0.000	0.000		0.000	0.000	0.000		0.000	0.000	0.000

ρ: Spearsmans ρ
τ: Kendalls τ
r: Pearsons r

Table C.166 $F_{9.8}$ vs. EW10 (II)

	Ori A				ONC				L1641			
	N	ρ	τ	r	N	ρ	τ	r	N	ρ	τ	r
TDFD	168	0.986	0.903	0.982	83	0.985	0.907	0.986	85	0.986	0.905	0.979
		0.000	0.000	0.000		0.000	0.000	0.000		0.000	0.000	0.000
FD	114	0.981	0.886	0.979	57	0.974	0.876	0.967	57	0.981	0.897	0.988
		0.000	0.000	0.000		0.000	0.000	0.000		0.000	0.000	0.000
TD	54	0.986	0.901	0.983	26	0.991	0.937	0.993	28	0.977	0.887	0.972
		0.000	0.000	0.000		0.000	0.000	0.000		0.000	0.000	0.000

ρ: Spearsmans ρ
τ: Kendalls τ
r: Pearsons r

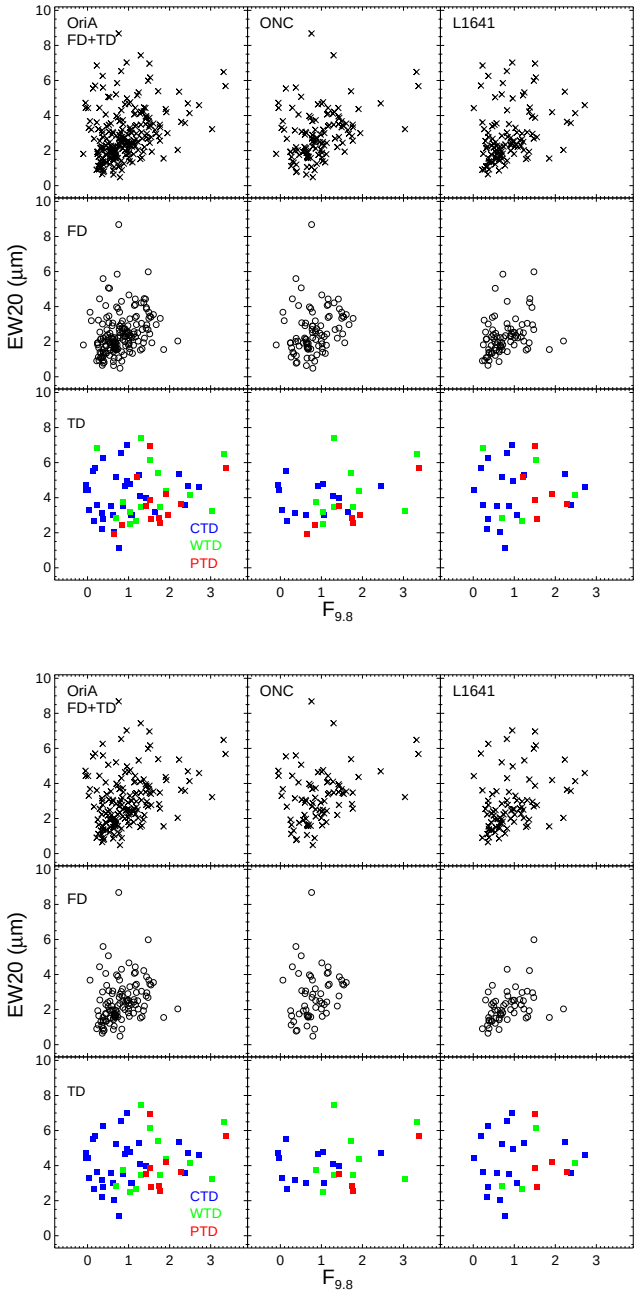


Figure C.84 $F_{9.8}$ vs. EW20.Upper panel: all available objects; Lower panel: objects with available spectral types only

Table C.167 $F_{9.8}$ vs. EW20 (I)

	Ori A				ONC				L1641			
	N	ρ	τ	r	N	ρ	τ	r	N	ρ	τ	r
TDFD	231	0.354	0.251	0.313	122	0.350	0.235	0.321	109	0.355	0.260	0.298
		0.000	0.000	0.000		0.000	0.000	0.000		0.000	0.000	0.002
FD	170	0.380	0.261	0.295	91	0.341	0.221	0.281	79	0.407	0.296	0.329
		0.000	0.000	0.000		0.001	0.002	0.007		0.000	0.000	0.003
TD	61	0.105	0.078	0.123	31	0.161	0.110	0.270	30	0.056	0.037	0.021
		0.419	0.373	0.345		0.386	0.386	0.142		0.769	0.775	0.912

ρ: Spearsmans ρ
τ: Kendalls τ
r: Pearsons r

Table C.168 $F_{9.8}$ vs. EW20 (II)

	Ori A				ONC				L1641			
	N	ρ	τ	r	N	ρ	τ	r	N	ρ	τ	r
TDFD	168	0.343	0.249	0.309	83	0.294	0.206	0.292	85	0.389	0.284	0.328
		0.000	0.000	0.000		0.007	0.006	0.007		0.000	0.000	0.002
FD	114	0.394	0.281	0.284	57	0.302	0.207	0.281	57	0.474	0.350	0.394
		0.000	0.000	0.002		0.022	0.023	0.034		0.000	0.000	0.002
TD	54	0.135	0.092	0.167	26	0.136	0.089	0.264	28	0.132	0.082	0.093
		0.331	0.325	0.227		0.509	0.523	0.193		0.502	0.540	0.638

ρ: Spearsmans ρ
τ: Kendalls τ
r: Pearsons r

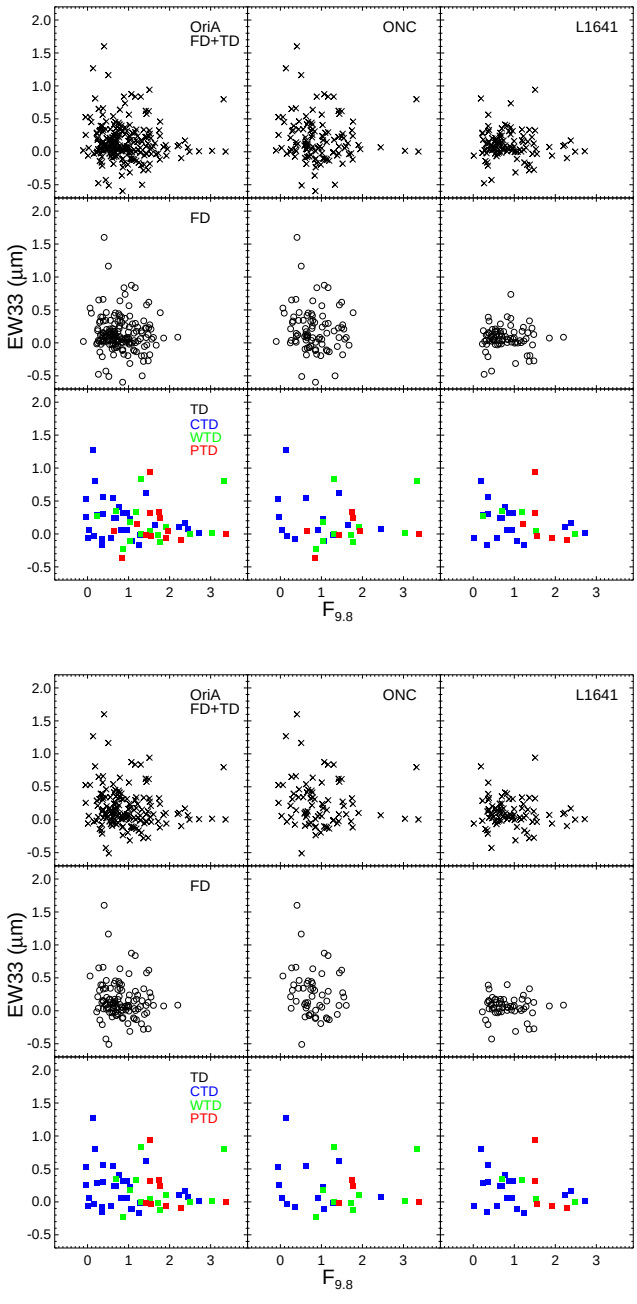


Figure C.85 $F_{9.8}$ vs. EW33. Zoomed in. Upper panel: all available objects; Lower panel: objects with available spectral types only

Table C.169 $F_{9.8}$ vs. EW33 (I)

	Ori A				ONC				L1641			
	N	ρ	τ	r	N	ρ	τ	r	N	ρ	τ	r
TDFD	231	-0.117	-0.079	-0.057	122	-0.147	-0.098	-0.064	109	-0.079	-0.054	-0.053
		0.076	0.074	0.389		0.105	0.110	0.484		0.417	0.409	0.584
FD	170	-0.078	-0.056	-0.088	91	-0.144	-0.100	-0.117	79	0.000	-0.002	-0.021
		0.314	0.282	0.254		0.173	0.162	0.269		1.000	0.976	0.854
TD	61	-0.160	-0.114	-0.144	31	0.007	-0.004	-0.056	30	-0.275	-0.196	-0.280
		0.217	0.193	0.268		0.970	0.973	0.765		0.141	0.129	0.134

ρ: Spearsmans ρ
τ: Kendalls τ
r: Pearsons r

Table C.170 $F_{9.8}$ vs. EW33 (II)

	Ori A				ONC				L1641			
	N	ρ	τ	r	N	ρ	τ	r	N	ρ	τ	r
TDFD	168	-0.155	-0.109	-0.051	83	-0.194	-0.135	-0.058	85	-0.115	-0.084	-0.109
		0.045	0.036	0.511		0.078	0.071	0.602		0.295	0.257	0.321
FD	114	-0.149	-0.107	-0.104	57	-0.227	-0.160	-0.151	57	-0.065	-0.050	-0.085
		0.113	0.092	0.271		0.089	0.078	0.262		0.631	0.581	0.530
TD	54	-0.162	-0.118	-0.162	26	-0.030	-0.037	-0.097	28	-0.248	-0.175	-0.272
		0.243	0.210	0.242		0.885	0.791	0.637		0.203	0.191	0.161

ρ: Spearsmans ρ
τ: Kendalls τ
r: Pearsons r

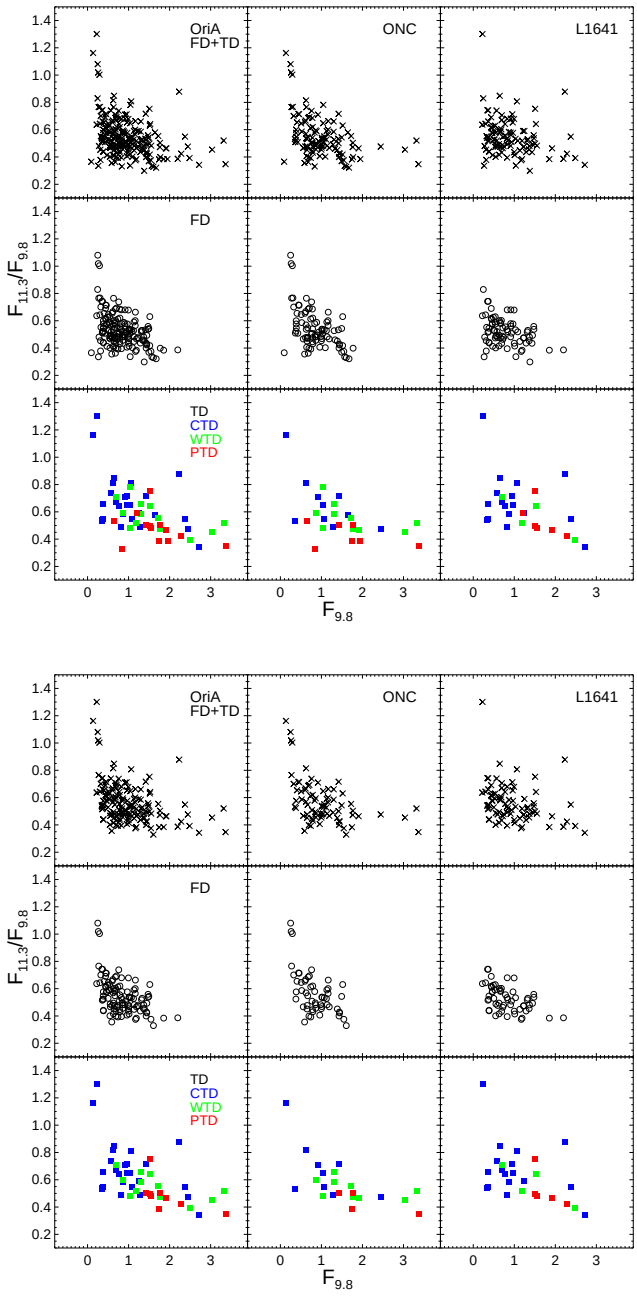


Figure C.86 $F_{9.8}$ vs. $F_{11.3}/F_{9.8}$. Zoomed in. Upper panel: all available objects; Lower panel: objects with available spectral types only

Table C.171 $F_{9.8}$ vs. $F_{11.3}/F_{9.8}$ (I)

	Ori A				ONC				L1641			
	N	ρ	τ	r	N	ρ	τ	r	N	ρ	τ	r
TDFD	231	-0.349	-0.253	-0.090	122	-0.364	-0.271	-0.009	109	-0.309	-0.218	-0.186
		0.000	0.000	0.173		0.000	0.000	0.922		0.001	0.001	0.053
FD	170	-0.394	-0.285	-0.027	91	-0.448	-0.333	0.016	79	-0.325	-0.231	-0.371
		0.000	0.000	0.727		0.000	0.000	0.880		0.003	0.003	0.001
TD	61	-0.505	-0.408	-0.167	31	-0.344	-0.299	-0.028	30	-0.633	-0.488	-0.328
		0.000	0.000	0.198		0.058	0.018	0.881		0.000	0.000	0.077

ρ: Spearsmans ρ
τ: Kendalls τ
r: Pearsons r

Table C.172 $F_{9.8}$ vs. $F_{11.3}/F_{9.8}$ (II)

	Ori A				ONC				L1641			
	N	ρ	τ	r	N	ρ	τ	r	N	ρ	τ	r
TDFD	168	-0.429	-0.309	-0.115	83	-0.429	-0.318	-0.041	85	-0.408	-0.282	-0.201
		0.000	0.000	0.138		0.000	0.000	0.713		0.000	0.000	0.065
FD	114	-0.508	-0.357	-0.473	57	-0.545	-0.395	-0.563	57	-0.482	-0.327	-0.487
		0.000	0.000	0.000		0.000	0.000	0.000		0.000	0.000	0.000
TD	54	-0.521	-0.426	-0.163	26	-0.387	-0.342	-0.029	28	-0.602	-0.469	-0.324
		0.000	0.000	0.239		0.051	0.014	0.888		0.001	0.000	0.093

ρ: Spearsmans ρ
τ: Kendalls τ
r: Pearsons r

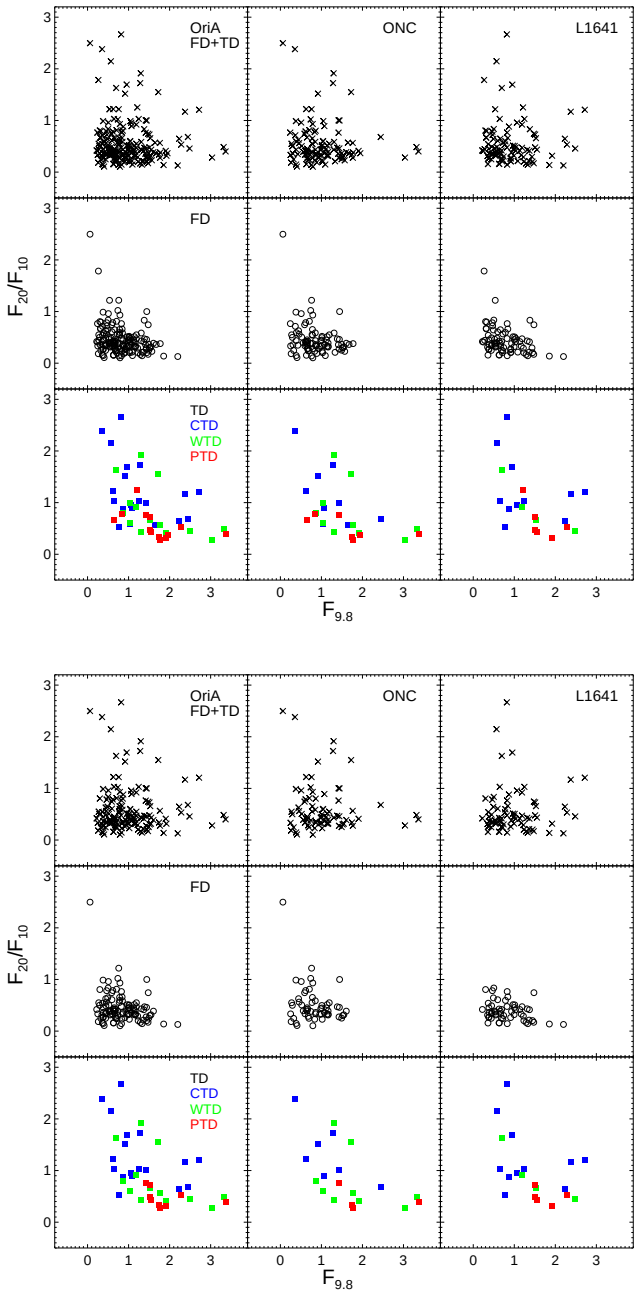


Figure C.87 $F_{9.8}$ vs. F_{20}/F_{10}. Upper panel: all available objects; Lower panel: objects with available spectral types only

Table C.173 $F_{9.8}$ vs. F_{20}/F_{10} (I)

	Ori A				ONC				L1641			
	N	ρ	τ	r	N	ρ	τ	r	N	ρ	τ	r
TDFD	230	-0.212	-0.142	-0.285	121	-0.212	-0.142	-0.312	109	-0.208	-0.145	-0.247
		0.001	0.001	0.000		0.020	0.021	0.000		0.030	0.026	0.010
FD	170	-0.293	-0.203	-0.295	91	-0.269	-0.187	-0.344	79	-0.339	-0.243	-0.333
		0.000	0.000	0.000		0.010	0.009	0.001		0.002	0.002	0.003
TD	60	-0.775	-0.575	-0.595	30	-0.769	-0.563	-0.553	30	-0.764	-0.575	-0.634
		0.000	0.000	0.000		0.000	0.000	0.002		0.000	0.000	0.000

ρ: Spearsmans ρ
τ: Kendalls τ
r: Pearsons r

Table C.174 $F_{9.8}$ vs. F_{20}/F_{10} (II)

	Ori A				ONC				L1641			
	N	ρ	τ	r	N	ρ	τ	r	N	ρ	τ	r
TDFD	167	-0.161	-0.109	-0.279	82	-0.194	-0.133	-0.299	85	-0.139	-0.096	-0.252
		0.038	0.037	0.000		0.080	0.077	0.006		0.203	0.192	0.020
FD	114	-0.172	-0.124	-0.255	57	-0.173	-0.125	-0.273	57	-0.238	-0.172	-0.293
		0.067	0.051	0.006		0.198	0.169	0.040		0.075	0.059	0.027
TD	53	-0.790	-0.592	-0.598	25	-0.799	-0.593	-0.584	28	-0.742	-0.559	-0.616
		0.000	0.000	0.000		0.000	0.000	0.002		0.000	0.000	0.000

ρ: Spearsmans ρ
τ: Kendalls τ
r: Pearsons r

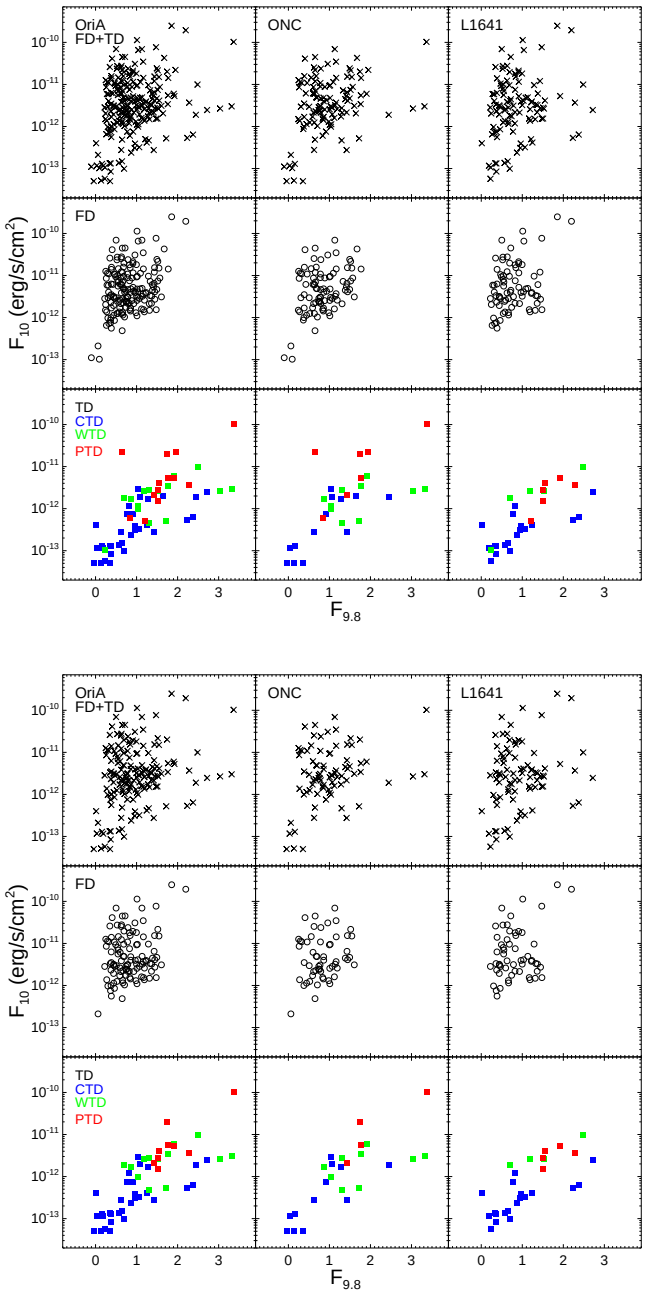


Figure C.88 $F_{9.8}$ vs. $\log F_{10}$. Upper panel: all available objects; Lower panel: objects with available spectral types only

Table C.175 $F_{9.8}$ vs. $\log F_{10}$ (I)

	Ori A				ONC				L1641			
	N	ρ	τ	r	N	ρ	τ	r	N	ρ	τ	r
TDFD	230	0.226	0.155	0.282	121	0.264	0.182	0.342	109	0.186	0.129	0.216
		0.001	0.000	0.000		0.003	0.003	0.000		0.053	0.046	0.024
FD	170	0.252	0.174	0.358	91	0.288	0.205	0.388	79	0.231	0.154	0.340
		0.001	0.001	0.000		0.006	0.004	0.000		0.041	0.045	0.002
TD	60	0.771	0.593	0.719	30	0.720	0.563	0.692	30	0.801	0.631	0.750
		0.000	0.000	0.000		0.000	0.000	0.000		0.000	0.000	0.000

ρ: Spearsmans ρ
τ: Kendalls τ
r: Pearsons r

Table C.176 $F_{9.8}$ vs. $\log F_{10}$ (II)

	Ori A				ONC				L1641			
	N	ρ	τ	r	N	ρ	τ	r	N	ρ	τ	r
TDFD	167	0.203	0.141	0.259	82	0.241	0.167	0.301	85	0.184	0.131	0.219
		0.008	0.007	0.001		0.029	0.026	0.006		0.092	0.076	0.044
FD	114	0.154	0.104	0.258	57	0.185	0.133	0.208	57	0.167	0.105	0.299
		0.102	0.100	0.006		0.168	0.144	0.121		0.215	0.247	0.024
TD	53	0.812	0.629	0.765	25	0.798	0.613	0.777	28	0.790	0.623	0.738
		0.000	0.000	0.000		0.000	0.000	0.000		0.000	0.000	0.000

ρ: Spearsmans ρ
τ: Kendalls τ
r: Pearsons r

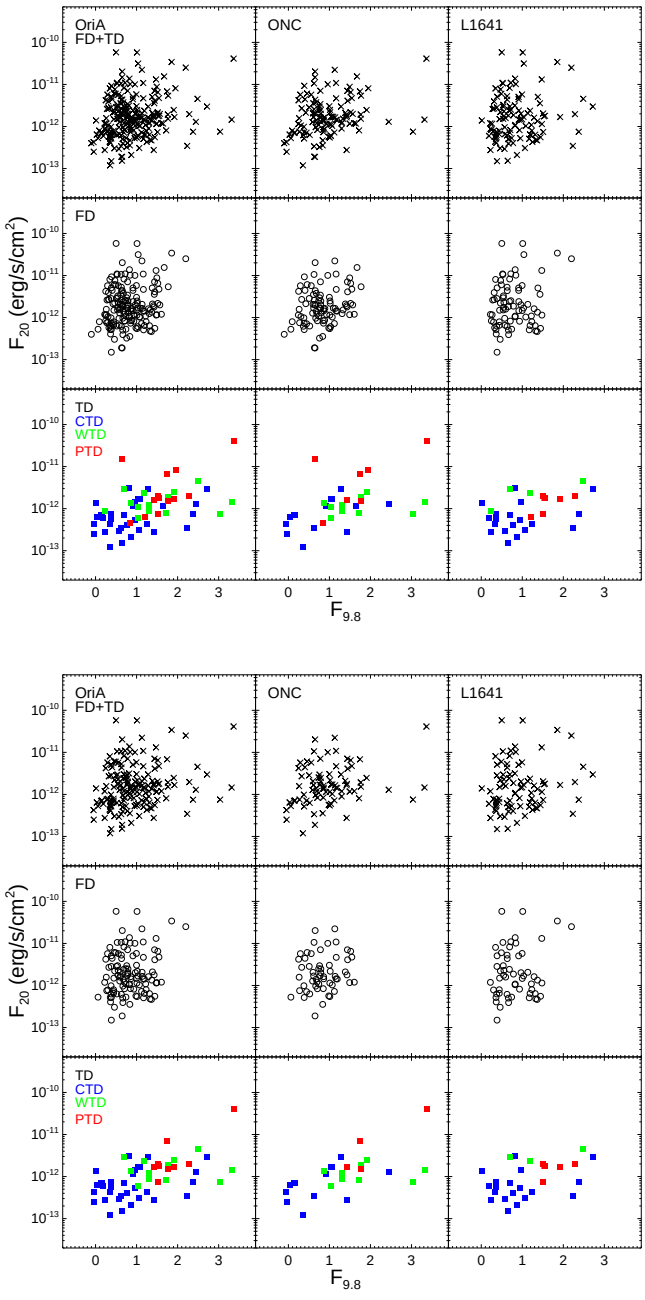


Figure C.89 $F_{9.8}$ vs. $\log F_{20}$. Upper panel: all available objects; Lower panel: objects with available spectral types only

Table C.177 $F_{9.8}$ vs. $\log F_{20}$ (I)

	Ori A				ONC				L1641			
	N	ρ	τ	r	N	ρ	τ	r	N	ρ	τ	r
TDFD	231	0.189	0.124	0.209	122	0.267	0.178	0.289	109	0.102	0.067	0.127
		0.004	0.005	0.001		0.003	0.004	0.001		0.290	0.300	0.188
FD	170	0.148	0.094	0.220	91	0.220	0.142	0.271	79	0.085	0.050	0.183
		0.053	0.068	0.004		0.036	0.046	0.009		0.455	0.512	0.106
TD	61	0.522	0.358	0.488	31	0.586	0.419	0.514	30	0.411	0.272	0.425
		0.000	0.000	0.000		0.001	0.001	0.003		0.024	0.035	0.019

ρ: Spearsmans ρ
τ: Kendalls τ
r: Pearsons r

Table C.178 $F_{9.8}$ vs. $\log F_{20}$ (II)

	Ori A				ONC				L1641			
	N	ρ	τ	r	N	ρ	τ	r	N	ρ	τ	r
TDFD	168	0.189	0.126	0.201	83	0.257	0.175	0.264	85	0.140	0.097	0.145
		0.014	0.016	0.009		0.019	0.019	0.016		0.200	0.189	0.185
FD	114	0.097	0.059	0.171	57	0.155	0.104	0.168	57	0.087	0.048	0.174
		0.306	0.348	0.069		0.249	0.253	0.212		0.518	0.601	0.196
TD	54	0.554	0.376	0.544	26	0.621	0.440	0.609	28	0.442	0.294	0.440
		0.000	0.000	0.000		0.001	0.002	0.001		0.019	0.028	0.019

ρ: Spearsmans ρ
τ: Kendalls τ
r: Pearsons r

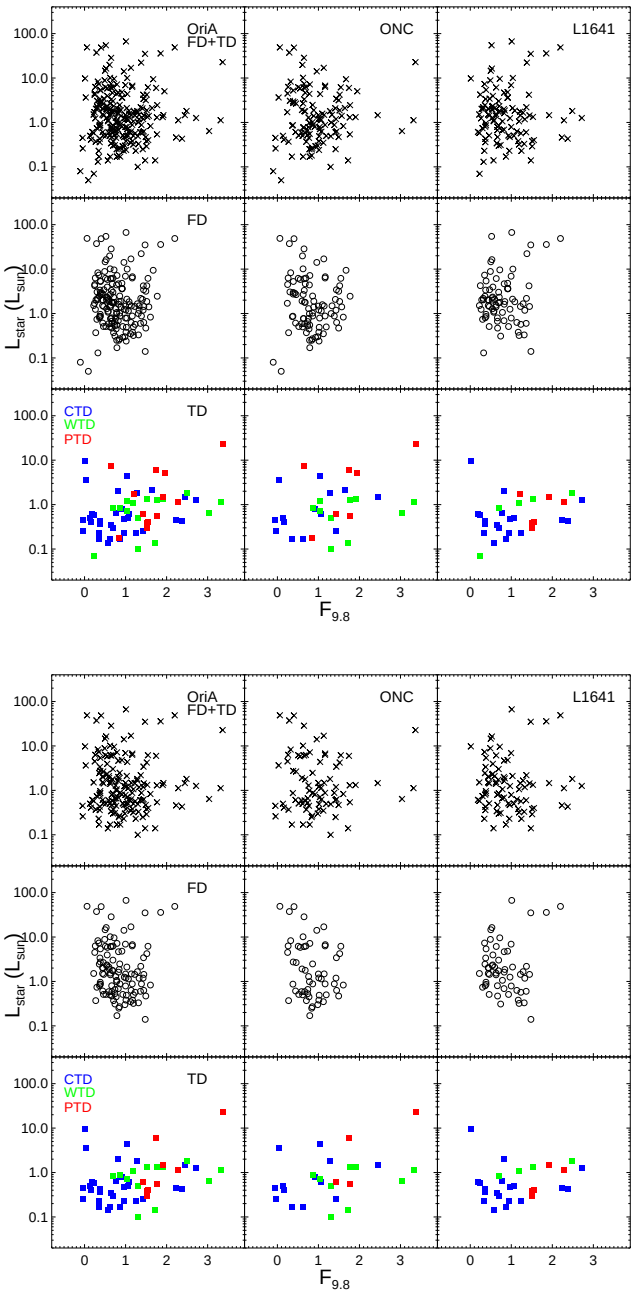


Figure C.90 $F_{9.8}$ vs. $\log L_\star$. Upper panel: all available objects; Lower panel: objects with available spectral types only

Table C.179 $F_{9.8}$ vs. $\log L_\star$ (I)

	Ori A				ONC				L1641			
	N	ρ	τ	r	N	ρ	τ	r	N	ρ	τ	r
TDFD	231	-0.051	-0.034	0.023	122	-0.007	0.000	0.033	109	-0.082	-0.050	0.013
		0.438	0.436	0.728		0.935	0.998	0.718		0.394	0.438	0.893
FD	170	-0.092	-0.062	0.031	91	-0.108	-0.067	-0.054	79	-0.010	-0.004	0.151
		0.233	0.230	0.688		0.309	0.345	0.611		0.930	0.959	0.184
TD	61	0.330	0.227	0.320	31	0.365	0.237	0.360	30	0.274	0.213	0.219
		0.009	0.010	0.012		0.043	0.061	0.047		0.143	0.099	0.245

ρ: Spearsmans ρ
τ: Kendalls τ
r: Pearsons r

Table C.180 $F_{9.8}$ vs. $\log L_\star$ (II)

	Ori A				ONC				L1641			
	N	ρ	τ	r	N	ρ	τ	r	N	ρ	τ	r
TDFD	168	-0.105	-0.071	-0.034	83	-0.045	-0.029	-0.042	85	-0.149	-0.095	-0.025
		0.175	0.171	0.662		0.688	0.696	0.706		0.173	0.199	0.820
FD	114	-0.195	-0.134	-0.078	57	-0.223	-0.153	-0.261	57	-0.119	-0.080	0.101
		0.038	0.035	0.409		0.096	0.094	0.050		0.380	0.377	0.455
TD	54	0.313	0.213	0.310	26	0.369	0.234	0.399	28	0.226	0.173	0.146
		0.021	0.023	0.023		0.063	0.093	0.043		0.247	0.196	0.458

ρ: Spearsmans ρ
τ: Kendalls τ
r: Pearsons r

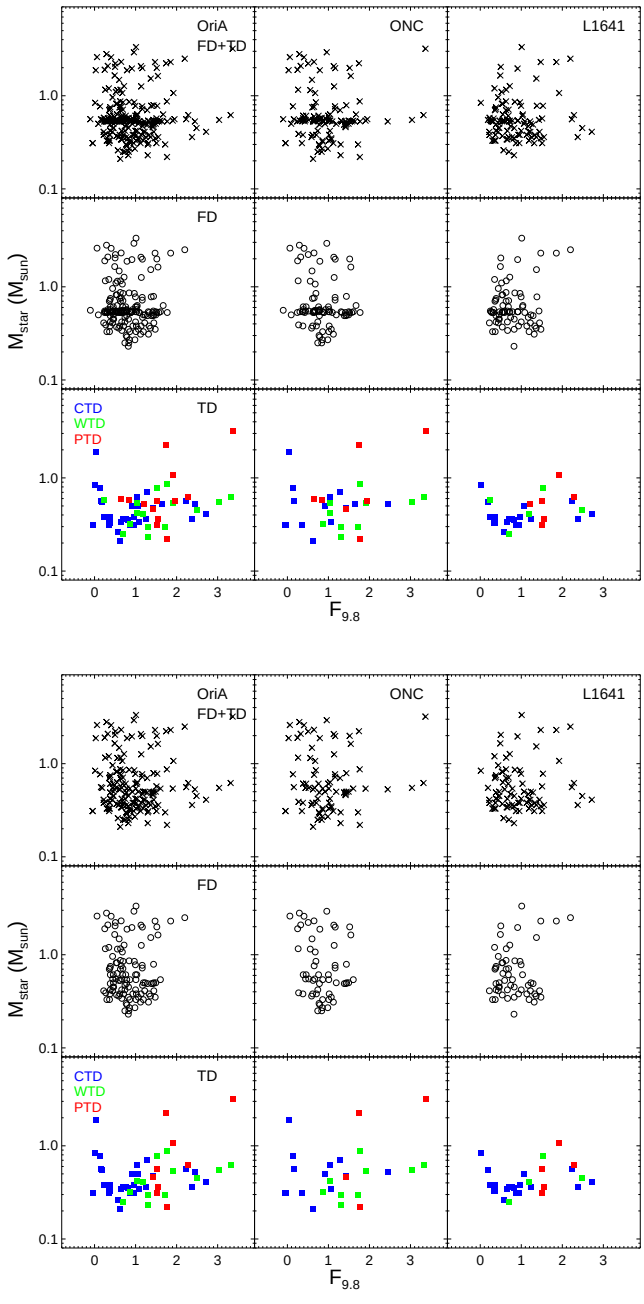


Figure C.91 $F_{9.8}$ vs. $\log M_\star$. Upper panel: all available objects; Lower panel: objects with available spectral types only

Table C.181 $F_{9.8}$ vs. $\log M_\star$ (I)

	Ori A				ONC				L1641			
	N	ρ	τ	r	N	ρ	τ	r	N	ρ	τ	r
TDFD	231	-0.059	-0.039	0.034	122	-0.100	-0.062	-0.001	109	-0.040	-0.030	0.073
		0.370	0.383	0.607		0.276	0.308	0.991		0.677	0.648	0.451
FD	170	-0.096	-0.061	0.013	91	-0.177	-0.116	-0.128	79	-0.009	-0.008	0.191
		0.213	0.235	0.866		0.092	0.103	0.227		0.938	0.914	0.092
TD	61	0.236	0.168	0.281	31	0.184	0.143	0.293	30	0.234	0.169	0.224
		0.067	0.056	0.028		0.321	0.258	0.110		0.214	0.189	0.234

ρ: Spearsmans ρ
τ: Kendalls τ
r: Pearsons r

Table C.182 $F_{9.8}$ vs. $\log M_\star$ (II)

	Ori A				ONC				L1641			
	N	ρ	τ	r	N	ρ	τ	r	N	ρ	τ	r
TDFD	168	-0.032	-0.018	0.031	83	-0.079	-0.044	-0.010	85	0.001	0.001	0.079
		0.682	0.729	0.690		0.480	0.555	0.929		0.992	0.994	0.472
FD	114	-0.101	-0.067	0.000	57	-0.202	-0.136	-0.177	57	-0.005	-0.008	0.188
		0.287	0.290	1.000		0.132	0.136	0.188		0.970	0.934	0.161
TD	54	0.288	0.201	0.302	26	0.232	0.183	0.307	28	0.316	0.214	0.273
		0.035	0.032	0.026		0.254	0.191	0.127		0.102	0.109	0.160

ρ: Spearsmans ρ
τ: Kendalls τ
r: Pearsons r

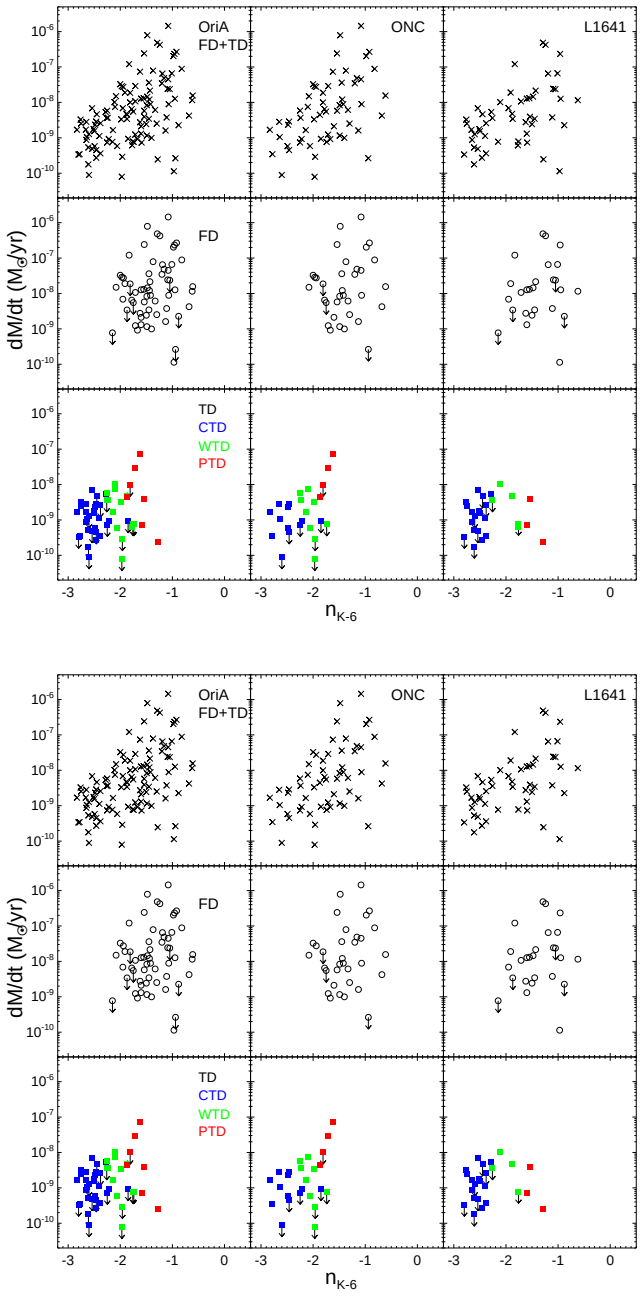


Figure C.92 n_{K-6} vs. $\log \dot{M}$. Upper panel: all available objects; Lower panel: objects with available spectral types only

Table C.183 n_{K-6} vs. $\log \dot{M}$ (I)

	Ori A				ONC				L1641			
	N	ρ	τ	r	N	ρ	τ	r	N	ρ	τ	r
TDFD	111	0.508	0.362	0.501	59	0.513	0.368	0.510	52	0.504	0.360	0.488
		0.000	0.000	0.000		0.000	0.000	0.000		0.000	0.000	0.000
FD	60	0.179	0.117	0.143	34	0.166	0.093	0.123	26	0.213	0.166	0.172
		0.171	0.186	0.276		0.348	0.440	0.488		0.295	0.233	0.401
TD	51	0.202	0.150	0.210	25	0.341	0.268	0.407	26	0.126	0.074	-0.014
		0.154	0.121	0.139		0.095	0.061	0.043		0.539	0.595	0.946

ρ: Spearsmans ρ
τ: Kendalls τ
r: Pearsons r

Table C.184 n_{K-6} vs. $\log \dot{M}$ (II)

	Ori A				ONC				L1641			
	N	ρ	τ	r	N	ρ	τ	r	N	ρ	τ	r
TDFD	109	0.519	0.370	0.508	58	0.525	0.378	0.520	51	0.516	0.368	0.495
		0.000	0.000	0.000		0.000	0.000	0.000		0.000	0.000	0.000
FD	59	0.199	0.134	0.157	33	0.192	0.116	0.145	26	0.213	0.166	0.172
		0.130	0.135	0.235		0.283	0.343	0.421		0.295	0.233	0.401
TD	50	0.228	0.166	0.231	25	0.341	0.268	0.407	25	0.179	0.104	0.024
		0.112	0.090	0.107		0.095	0.061	0.043		0.391	0.467	0.909

ρ: Spearsmans ρ
τ: Kendalls τ
r: Pearsons r

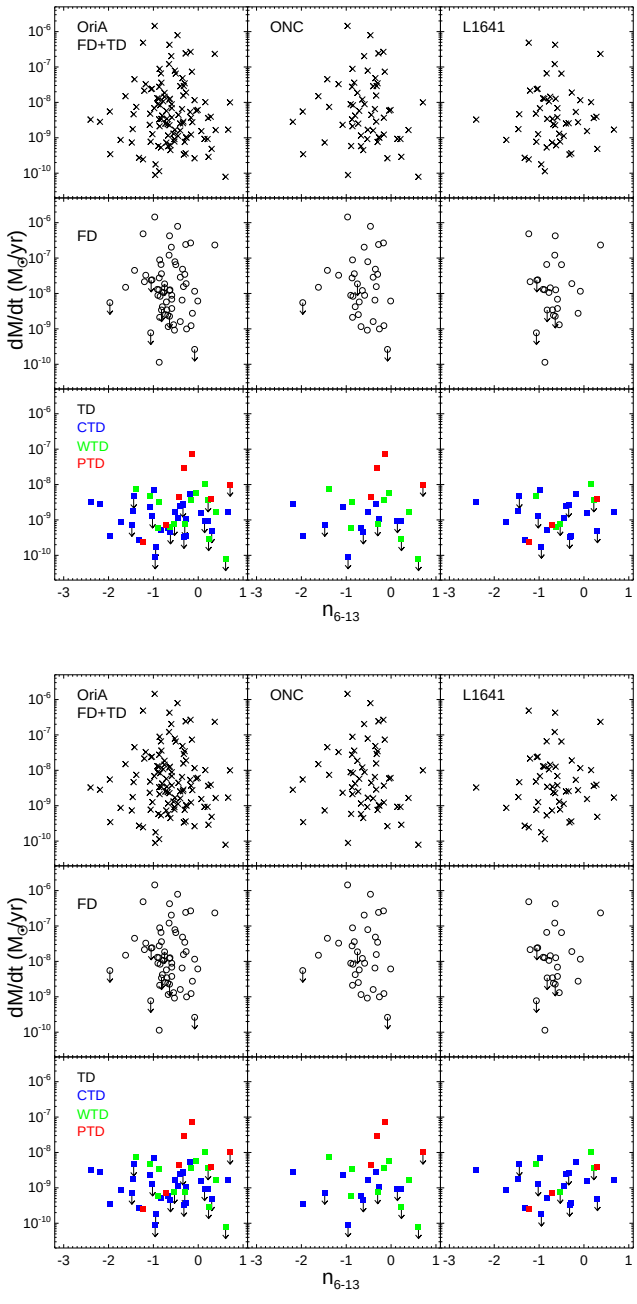


Figure C.93 n_{6-13} vs. $\log \dot{M}$. Upper panel: all available objects; Lower panel: objects with available spectral types only

Table C.185 n_{6-13} vs. $\log \dot{M}$ (I)

	Ori A				ONC				L1641			
	N	ρ	τ	r	N	ρ	τ	r	N	ρ	τ	r
TDFD	111	-0.038	-0.027	-0.024	59	-0.108	-0.071	-0.089	52	0.014	0.008	0.048
		0.695	0.679	0.803		0.417	0.428	0.503		0.920	0.937	0.735
FD	60	-0.075	-0.065	-0.031	34	-0.129	-0.088	-0.105	26	-0.090	-0.071	0.086
		0.568	0.466	0.814		0.469	0.467	0.555		0.662	0.611	0.676
TD	51	0.127	0.100	0.093	25	0.107	0.080	0.066	26	0.116	0.114	0.118
		0.376	0.302	0.516		0.611	0.575	0.754		0.573	0.415	0.566

ρ: Spearsmans ρ
τ: Kendalls τ
r: Pearsons r

Table C.186 n_{6-13} vs. $\log \dot{M}$ (II)

	Ori A				ONC				L1641			
	N	ρ	τ	r	N	ρ	τ	r	N	ρ	τ	r
TDFD	109	-0.044	-0.032	-0.027	58	-0.116	-0.078	-0.093	51	0.024	0.012	0.050
		0.652	0.625	0.780		0.387	0.390	0.487		0.869	0.903	0.728
FD	59	-0.090	-0.075	-0.036	33	-0.145	-0.100	-0.112	26	-0.090	-0.071	0.086
		0.496	0.401	0.787		0.420	0.411	0.535		0.662	0.611	0.676
TD	50	0.121	0.093	0.092	25	0.107	0.080	0.066	25	0.118	0.113	0.120
		0.402	0.340	0.525		0.611	0.575	0.754		0.575	0.427	0.568

ρ: Spearsmans ρ
τ: Kendalls τ
r: Pearsons r

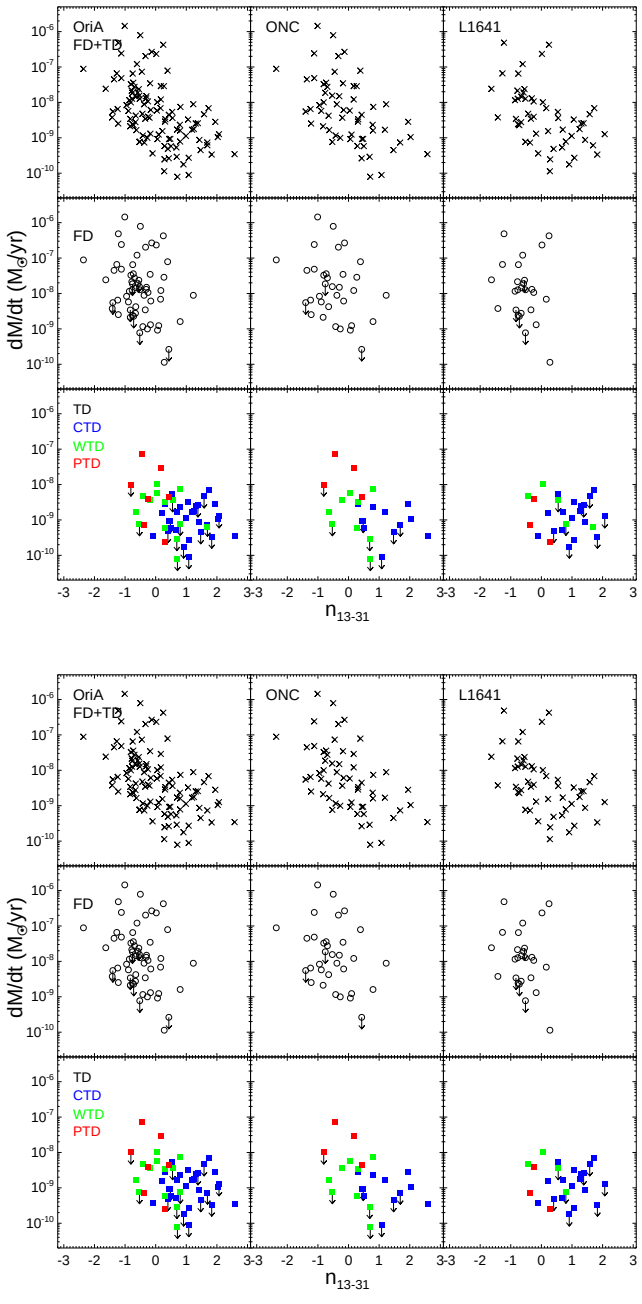


Figure C.94 n_{13-31} vs. $\log \dot{M}$. Upper panel: all available objects; Lower panel: objects with available spectral types only

Table C.187 n_{13-31} vs. $\log \dot{M}$ (I)

	Ori A				ONC				L1641			
	N	ρ	τ	r	N	ρ	τ	r	N	ρ	τ	r
TDFD	111	-0.567	-0.378	-0.525	59	-0.569	-0.392	-0.542	52	-0.559	-0.374	-0.497
		0.000	0.000	0.000		0.000	0.000	0.000		0.000	0.000	0.000
FD	60	-0.204	-0.141	-0.241	34	-0.249	-0.175	-0.291	26	-0.182	-0.136	-0.167
		0.118	0.110	0.064		0.155	0.146	0.095		0.373	0.331	0.415
TD	51	-0.277	-0.187	-0.305	25	-0.490	-0.347	-0.444	26	-0.054	-0.022	-0.064
		0.049	0.053	0.030		0.013	0.015	0.026		0.795	0.877	0.756

ρ: Spearsmans ρ
τ: Kendalls τ
r: Pearsons r

Table C.188 n_{13-31} vs. $\log \dot{M}$ (II)

	Ori A				ONC				L1641			
	N	ρ	τ	r	N	ρ	τ	r	N	ρ	τ	r
TDFD	109	-0.566	-0.378	-0.523	58	-0.579	-0.400	-0.550	51	-0.546	-0.363	-0.483
		0.000	0.000	0.000		0.000	0.000	0.000		0.000	0.000	0.000
FD	59	-0.224	-0.156	-0.254	33	-0.274	-0.195	-0.309	26	-0.182	-0.136	-0.167
		0.088	0.080	0.052		0.123	0.110	0.080		0.373	0.331	0.415
TD	50	-0.268	-0.181	-0.295	25	-0.490	-0.347	-0.444	25	-0.024	0.007	-0.030
		0.060	0.064	0.038		0.013	0.015	0.026		0.910	0.963	0.887

ρ: Spearsmans ρ
τ: Kendalls τ
r: Pearsons r

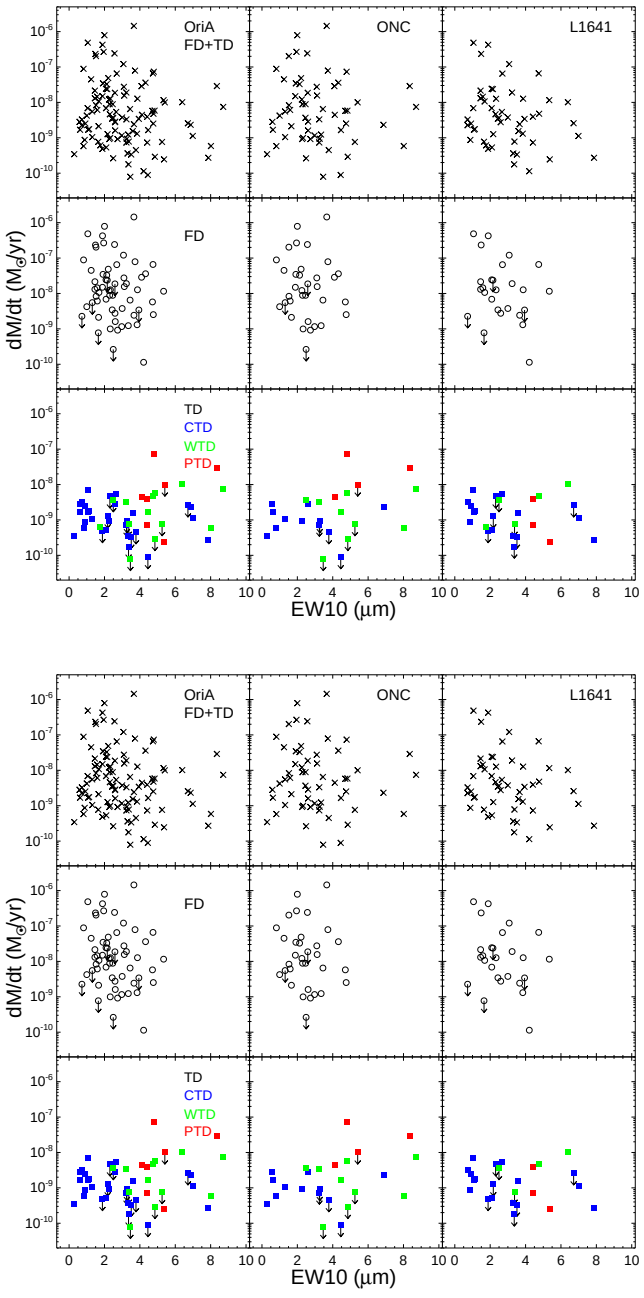


Figure C.95 EW10 vs. log $\dot{M}$. Upper panel: all available objects; Lower panel: objects with available spectral types only

Table C.189 EW10 vs. $\log \dot{M}$ (I)

	Ori A				ONC				L1641			
	N	ρ	τ	r	N	ρ	τ	r	N	ρ	τ	r
TDFD	111	-0.150	-0.100	-0.152	59	-0.124	-0.078	-0.088	52	-0.212	-0.146	-0.251
		0.116	0.120	0.111		0.350	0.380	0.507		0.130	0.126	0.073
FD	60	-0.176	-0.114	-0.170	34	-0.128	-0.077	-0.079	26	-0.253	-0.200	-0.273
		0.179	0.198	0.194		0.471	0.524	0.657		0.213	0.152	0.177
TD	51	0.090	0.055	0.151	25	0.284	0.197	0.320	26	-0.141	-0.108	-0.130
		0.531	0.570	0.290		0.169	0.168	0.119		0.494	0.440	0.527

ρ: Spearsmans ρ
τ: Kendalls τ
r: Pearsons r

Table C.190 EW10 vs. $\log \dot{M}$ (II)

	Ori A				ONC				L1641			
	N	ρ	τ	r	N	ρ	τ	r	N	ρ	τ	r
TDFD	109	-0.173	-0.115	-0.165	58	-0.138	-0.088	-0.096	51	-0.233	-0.158	-0.269
		0.073	0.077	0.086		0.302	0.327	0.473		0.100	0.103	0.056
FD	59	-0.196	-0.129	-0.182	33	-0.150	-0.095	-0.099	26	-0.253	-0.200	-0.273
		0.137	0.148	0.168		0.406	0.439	0.584		0.213	0.152	0.177
TD	50	0.083	0.051	0.142	25	0.284	0.197	0.320	25	-0.161	-0.113	-0.154
		0.567	0.604	0.325		0.169	0.168	0.119		0.443	0.427	0.462

ρ: Spearsmans ρ
τ: Kendalls τ
r: Pearsons r

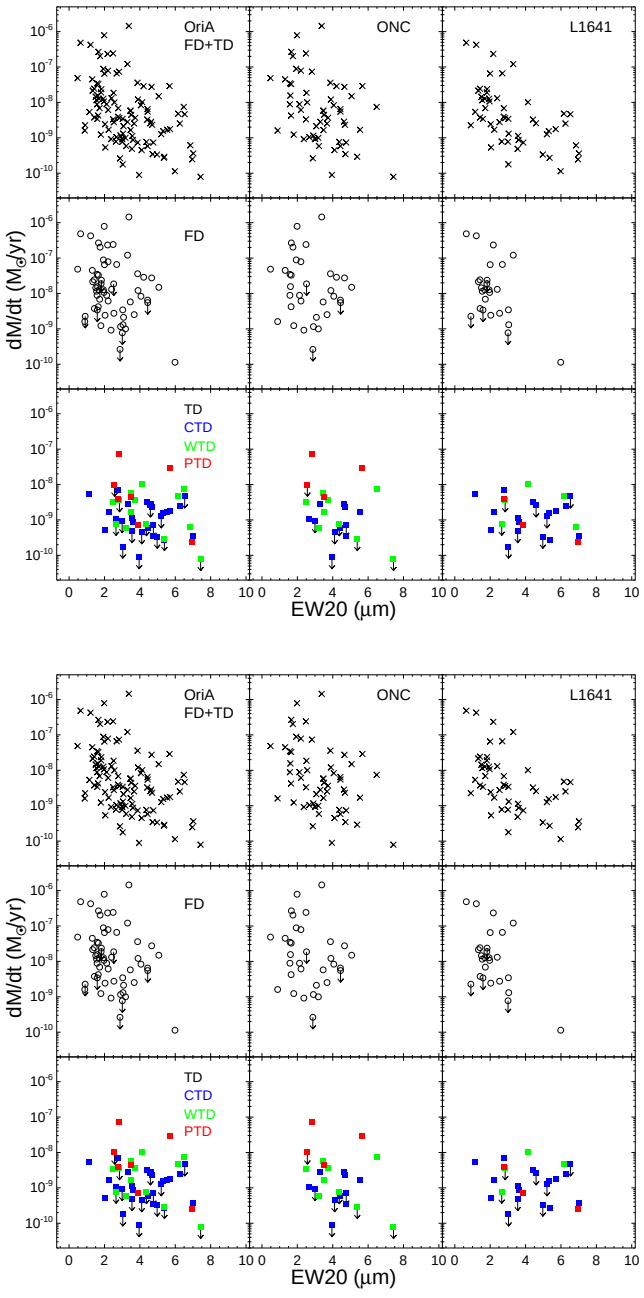


Figure C.96 EW20 vs. log $\dot{M}$. Upper panel: all available objects; Lower panel: objects with available spectral types only

Table C.191 EW20 vs. $\log \dot{M}$ (I)

	Ori A				ONC				L1641			
	N	ρ	τ	r	N	ρ	τ	r	N	ρ	τ	r
TDFD	111	-0.491	-0.341	-0.478	59	-0.402	-0.266	-0.405	52	-0.626	-0.437	-0.571
		0.000	0.000	0.000		0.002	0.003	0.001		0.000	0.000	0.000
FD	60	-0.225	-0.153	-0.271	34	-0.200	-0.112	-0.139	26	-0.314	-0.218	-0.530
		0.084	0.085	0.036		0.256	0.350	0.433		0.118	0.118	0.005
TD	51	-0.232	-0.170	-0.228	25	-0.283	-0.220	-0.274	26	-0.196	-0.126	-0.196
		0.102	0.078	0.108		0.170	0.123	0.185		0.338	0.366	0.337

ρ: Spearsmans ρ
τ: Kendalls τ
r: Pearsons r

Table C.192 EW20 vs. $\log \dot{M}$ (II)

	Ori A				ONC				L1641			
	N	ρ	τ	r	N	ρ	τ	r	N	ρ	τ	r
TDFD	109	-0.494	-0.342	-0.477	58	-0.419	-0.278	-0.417	51	-0.612	-0.424	-0.560
		0.000	0.000	0.000		0.001	0.002	0.001		0.000	0.000	0.000
FD	59	-0.246	-0.165	-0.287	33	-0.216	-0.121	-0.158	26	-0.314	-0.218	-0.530
		0.060	0.064	0.028		0.227	0.321	0.380		0.118	0.118	0.005
TD	50	-0.209	-0.154	-0.213	25	-0.283	-0.220	-0.274	25	-0.149	-0.087	-0.163
		0.145	0.114	0.138		0.170	0.123	0.185		0.476	0.544	0.436

ρ: Spearsmans ρ
τ: Kendalls τ
r: Pearsons r

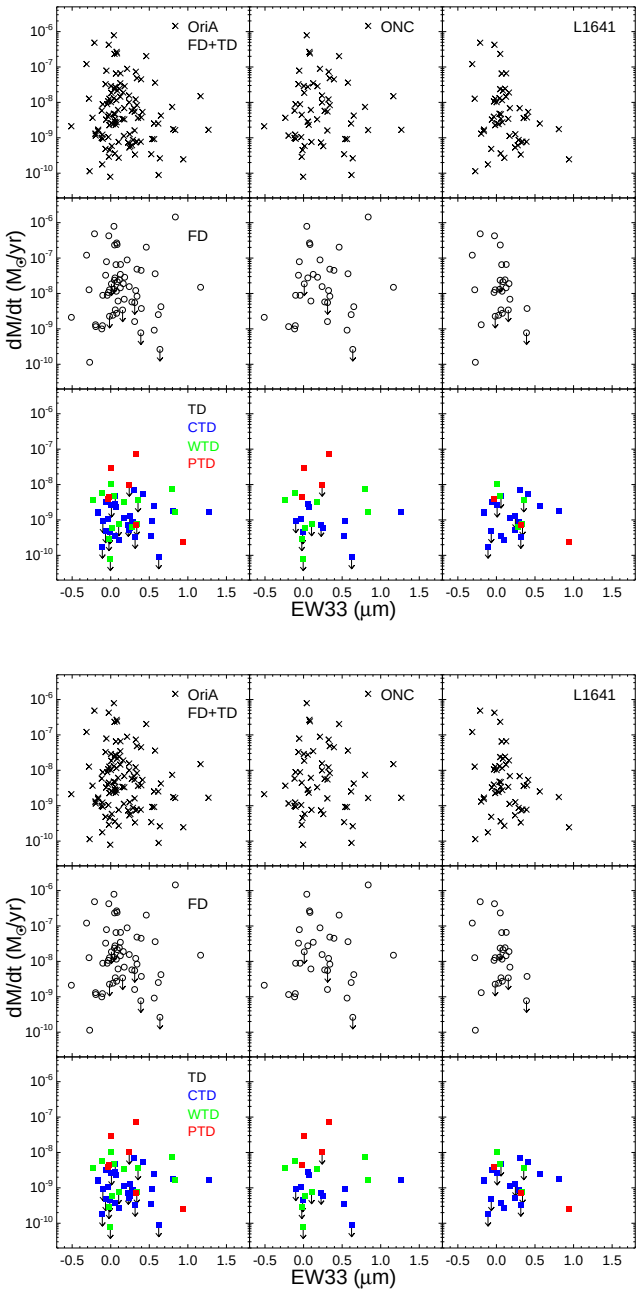


Figure C.97 EW33 vs. log $\dot{M}$. Upper panel: all available objects; Lower panel: objects with available spectral types only

Table C.193 EW33 vs. $\log \dot{M}$ (I)

	Ori A				ONC				L1641			
	N	ρ	τ	r	N	ρ	τ	r	N	ρ	τ	r
TDFD	111	-0.047	-0.030	-0.023	59	0.067	0.039	-0.002	52	-0.220	-0.137	-0.293
		0.623	0.646	0.811		0.615	0.666	0.988		0.118	0.153	0.035
FD	60	0.040	0.028	0.053	34	0.086	0.048	0.080	26	-0.102	-0.055	-0.138
		0.764	0.754	0.688		0.630	0.689	0.653		0.620	0.691	0.501
TD	51	-0.066	-0.042	-0.064	25	-0.041	-0.037	-0.033	26	-0.037	-0.009	-0.124
		0.643	0.661	0.655		0.845	0.797	0.876		0.859	0.947	0.546

ρ: Spearsmans ρ
τ: Kendalls τ
r: Pearsons r

Table C.194 EW33 vs. $\log \dot{M}$ (II)

	Ori A				ONC				L1641			
	N	ρ	τ	r	N	ρ	τ	r	N	ρ	τ	r
TDFD	109	-0.042	-0.028	-0.023	58	0.065	0.038	-0.003	51	-0.202	-0.127	-0.284
		0.664	0.669	0.812		0.628	0.677	0.982		0.155	0.188	0.043
FD	59	0.036	0.023	0.052	33	0.092	0.053	0.078	26	-0.102	-0.055	-0.138
		0.786	0.793	0.696		0.610	0.664	0.666		0.620	0.691	0.501
TD	50	-0.062	-0.041	-0.061	25	-0.041	-0.037	-0.033	25	-0.035	-0.013	-0.118
		0.670	0.676	0.674		0.845	0.797	0.876		0.870	0.926	0.574

ρ: Spearsmans ρ
τ: Kendalls τ
r: Pearsons r

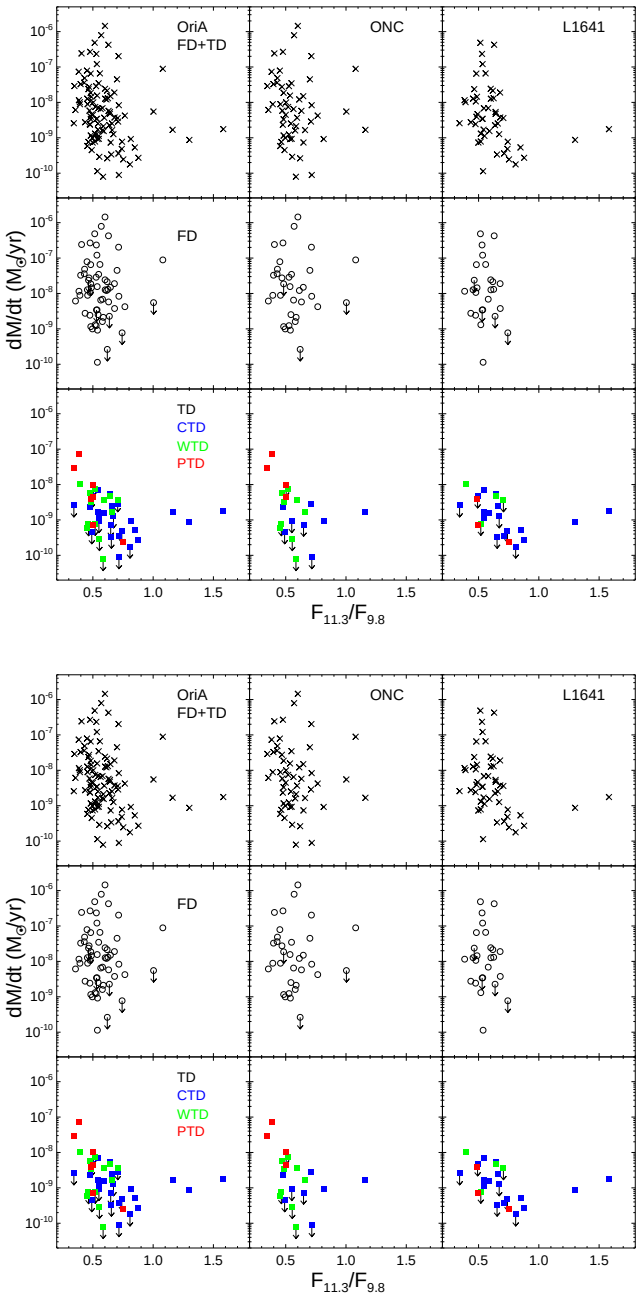


Figure C.98 $F_{11.3}/F_{9.8}$ vs. $\log \dot{M}$. Upper panel: all available objects; Lower panel: objects with available spectral types only

Table C.195 $F_{11.3}/F_{9.8}$ vs. $\log \dot{M}$ (I)

	Ori A				ONC				L1641			
	N	ρ	τ	r	N	ρ	τ	r	N	ρ	τ	r
TDFD	111	-0.286	-0.188	0.002	59	-0.163	-0.108	0.056	52	-0.451	-0.294	-0.050
		0.002	0.003	0.983		0.218	0.226	0.674		0.001	0.002	0.725
FD	60	-0.104	-0.058	-0.018	34	-0.129	-0.070	0.002	26	-0.042	-0.028	-0.083
		0.431	0.515	0.891		0.466	0.563	0.991		0.838	0.843	0.687
TD	51	-0.302	-0.197	0.122	25	-0.114	-0.080	0.134	26	-0.491	-0.311	0.128
		0.031	0.041	0.394		0.588	0.575	0.523		0.011	0.026	0.533

ρ: Spearsmans ρ
τ: Kendalls τ
r: Pearsons r

Table C.196 $F_{11.3}/F_{9.8}$ vs. $\log \dot{M}$ (II)

	Ori A				ONC				L1641			
	N	ρ	τ	r	N	ρ	τ	r	N	ρ	τ	r
TDFD	109	-0.271	-0.179	0.008	58	-0.158	-0.106	0.057	51	-0.428	-0.280	-0.041
		0.004	0.006	0.934		0.235	0.240	0.671		0.002	0.004	0.775
FD	59	-0.098	-0.054	-0.016	33	-0.120	-0.061	0.005	26	-0.042	-0.028	-0.083
		0.458	0.543	0.904		0.507	0.620	0.978		0.838	0.843	0.687
TD	50	-0.296	-0.192	0.127	25	-0.114	-0.080	0.134	25	-0.476	-0.307	0.136
		0.037	0.049	0.379		0.588	0.575	0.523		0.016	0.032	0.517

ρ: Spearsmans ρ
τ: Kendalls τ
r: Pearsons r

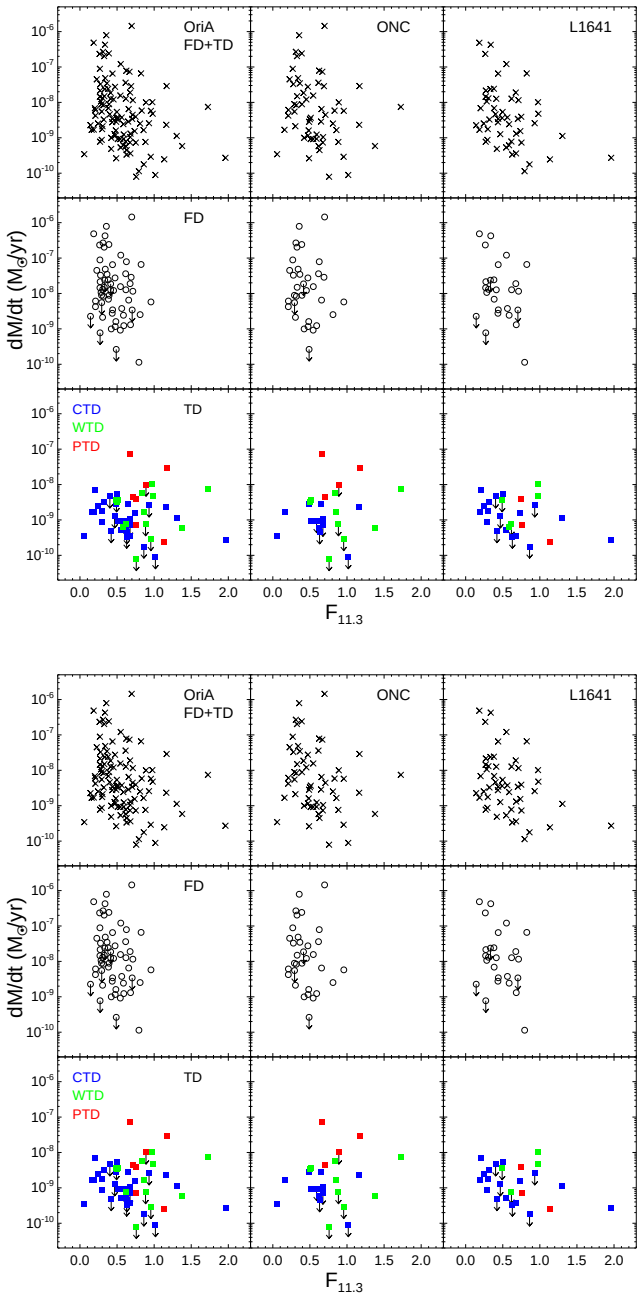


Figure C.99 $F_{11.3}$ vs. $\log \dot{M}$. Upper panel: all available objects; Lower panel: objects with available spectral types only

Table C.197 $F_{11.3}$ vs. $\log \dot{M}$ (I)

	Ori A				ONC				L1641			
	N	ρ	τ	r	N	ρ	τ	r	N	ρ	τ	r
TDFD	111	-0.325	-0.219	-0.310	59	-0.304	-0.200	-0.248	52	-0.365	-0.247	-0.395
		0.001	0.001	0.001		0.019	0.025	0.058		0.008	0.010	0.004
FD	60	-0.193	-0.127	-0.206	34	-0.154	-0.087	-0.120	26	-0.258	-0.194	-0.312
		0.140	0.151	0.114		0.386	0.468	0.499		0.203	0.165	0.121
TD	51	-0.080	-0.051	-0.057	25	0.085	0.073	0.150	26	-0.288	-0.188	-0.334
		0.577	0.598	0.691		0.685	0.607	0.474		0.153	0.179	0.095

ρ: Spearsmans ρ
τ: Kendalls τ
r: Pearsons r

Table C.198 $F_{11.3}$ vs. $\log \dot{M}$ (II)

	Ori A				ONC				L1641			
	N	ρ	τ	r	N	ρ	τ	r	N	ρ	τ	r
TDFD	109	-0.335	-0.226	-0.315	58	-0.322	-0.212	-0.254	51	-0.359	-0.244	-0.397
		0.000	0.000	0.001		0.014	0.019	0.054		0.010	0.012	0.004
FD	59	-0.213	-0.141	-0.218	33	-0.180	-0.106	-0.138	26	-0.258	-0.194	-0.312
		0.106	0.113	0.097		0.315	0.386	0.444		0.203	0.165	0.121
TD	50	-0.081	-0.051	-0.062	25	0.085	0.073	0.150	25	-0.284	-0.187	-0.343
		0.576	0.598	0.669		0.685	0.607	0.474		0.169	0.191	0.093

ρ: Spearsmans ρ
τ: Kendalls τ
r: Pearsons r

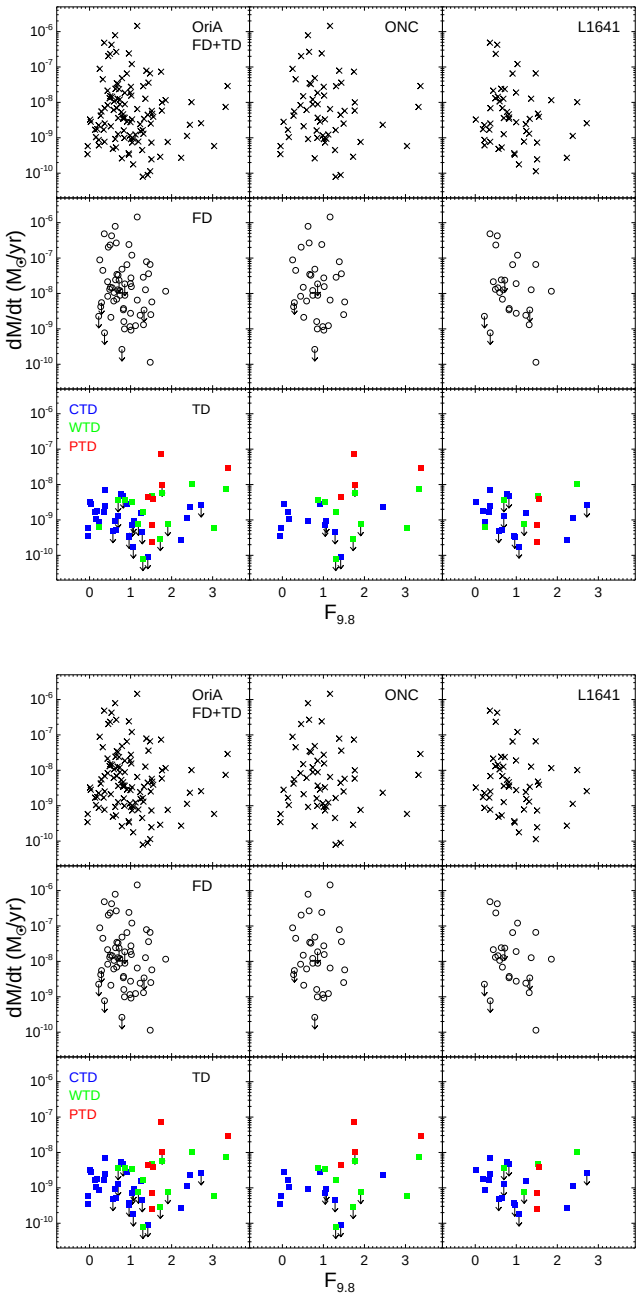


Figure C.100 $F_{9.8}$ vs. $\log \dot{M}$. Upper panel: all available objects; Lower panel: objects with available spectral types only

Table C.199 $F_{9.8}$ vs. $\log \dot{M}$ (I)

	Ori A				ONC				L1641			
	N	ρ	τ	r	N	ρ	τ	r	N	ρ	τ	r
TDFD	111	-0.108	-0.070	-0.101	59	-0.083	-0.054	-0.059	52	-0.148	-0.109	-0.182
		0.260	0.279	0.292		0.532	0.547	0.657		0.296	0.252	0.197
FD	60	-0.156	-0.099	-0.170	34	-0.101	-0.062	-0.073	26	-0.239	-0.194	-0.281
		0.235	0.262	0.194		0.569	0.604	0.682		0.240	0.165	0.164
TD	51	0.156	0.104	0.224	25	0.309	0.213	0.337	26	-0.023	-0.031	0.007
		0.275	0.283	0.114		0.133	0.135	0.099		0.913	0.825	0.973

ρ: Spearsmans ρ
τ: Kendalls τ
r: Pearsons r

Table C.200 $F_{9.8}$ vs. $\log \dot{M}$ (II)

	Ori A				ONC				L1641			
	N	ρ	τ	r	N	ρ	τ	r	N	ρ	τ	r
TDFD	109	-0.138	-0.089	-0.117	58	-0.098	-0.065	-0.064	51	-0.189	-0.135	-0.210
		0.154	0.170	0.226		0.463	0.469	0.633		0.183	0.162	0.139
FD	59	-0.172	-0.112	-0.181	33	-0.125	-0.083	-0.089	26	-0.239	-0.194	-0.281
		0.193	0.212	0.170		0.489	0.495	0.622		0.240	0.165	0.164
TD	50	0.145	0.096	0.213	25	0.309	0.213	0.337	25	-0.058	-0.050	-0.025
		0.315	0.323	0.138		0.133	0.135	0.099		0.781	0.726	0.906

ρ: Spearsmans ρ
τ: Kendalls τ
r: Pearsons r

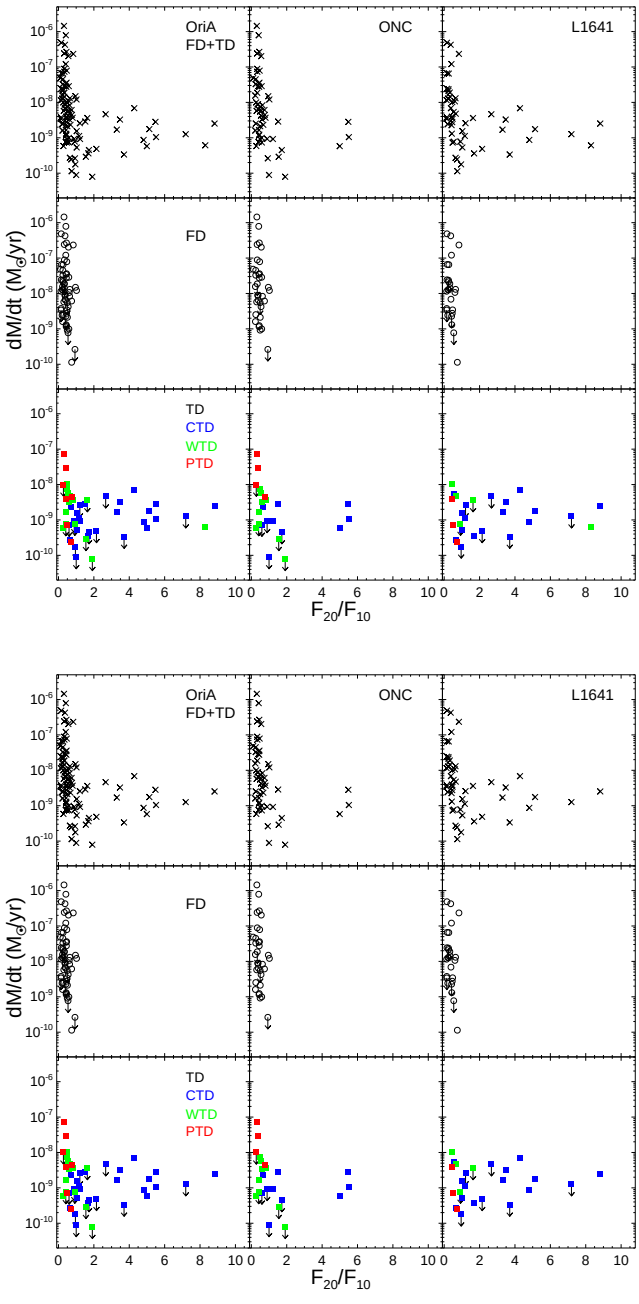


Figure C.101 F_{20}/F_{10} vs. $\log \dot{M}$. Upper panel: all available objects; Lower panel: objects with available spectral types only

Table C.201 F_{20}/F_{10} vs. $\log \dot{M}$ (I)

	Ori A				ONC				L1641			
	N	ρ	τ	r	N	ρ	τ	r	N	ρ	τ	r
TDFD	110	-0.568	-0.382	-0.289	58	-0.527	-0.371	-0.258	52	-0.598	-0.394	-0.312
		0.000	0.000	0.002		0.000	0.000	0.051		0.000	0.000	0.024
FD	60	-0.243	-0.167	-0.230	34	-0.290	-0.198	-0.272	26	-0.248	-0.182	-0.220
		0.061	0.059	0.077		0.096	0.100	0.120		0.222	0.193	0.280
TD	50	-0.277	-0.190	-0.082	24	-0.477	-0.348	-0.138	26	-0.041	-0.009	0.032
		0.052	0.051	0.571		0.019	0.017	0.520		0.844	0.947	0.877

ρ: Spearsmans ρ
τ: Kendalls τ
r: Pearsons r

Table C.202 F_{20}/F_{10} vs. $\log \dot{M}$ (II)

	Ori A				ONC				L1641			
	N	ρ	τ	r	N	ρ	τ	r	N	ρ	τ	r
TDFD	108	-0.566	-0.379	-0.271	57	-0.533	-0.375	-0.256	51	-0.586	-0.384	-0.282
		0.000	0.000	0.005		0.000	0.000	0.055		0.000	0.000	0.045
FD	59	-0.261	-0.177	-0.237	33	-0.305	-0.205	-0.281	26	-0.248	-0.182	-0.220
		0.046	0.048	0.071		0.084	0.094	0.113		0.222	0.193	0.280
TD	49	-0.264	-0.182	-0.054	24	-0.477	-0.348	-0.138	25	-0.005	0.020	0.111
		0.067	0.065	0.712		0.019	0.017	0.520		0.983	0.889	0.597

ρ: Spearsmans ρ
τ: Kendalls τ
r: Pearsons r

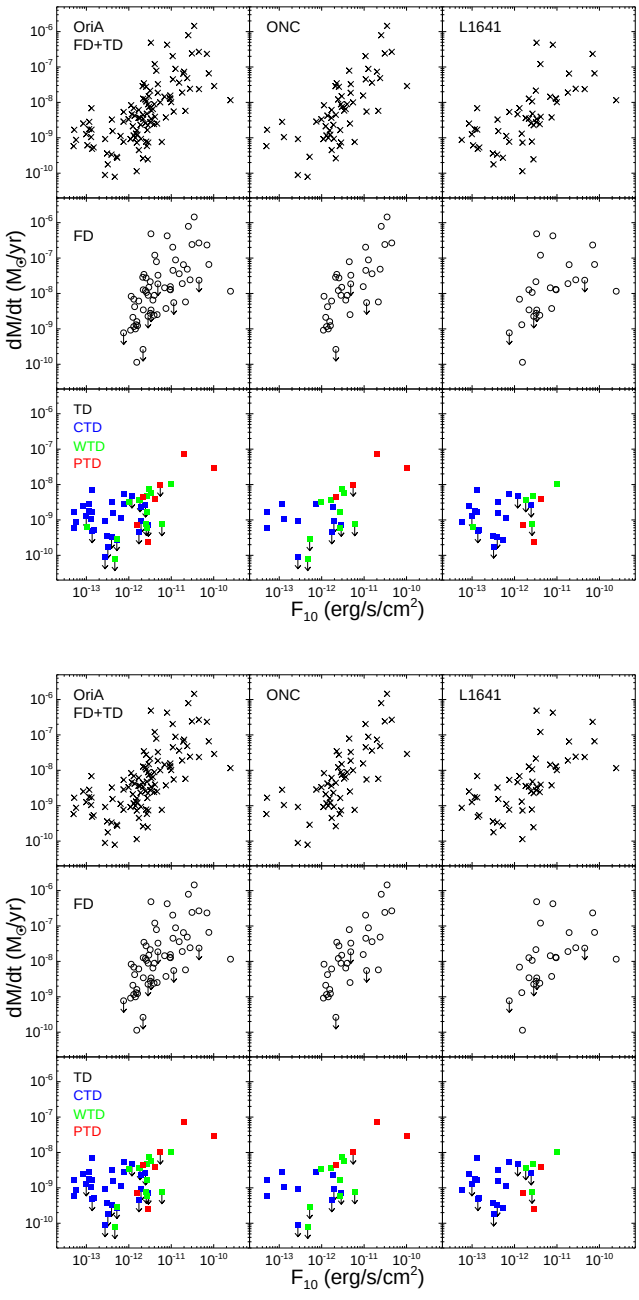


Figure C.102 $\log F_{10}$ vs. $\log \dot{M}$. Upper panel: all available objects; Lower panel: objects with available spectral types only

Table C.203 $\log F_{10}$ vs. $\log \dot{M}$ (I)

	Ori A				ONC				L1641			
	N	ρ	τ	r	N	ρ	τ	r	N	ρ	τ	r
TDFD	110	0.730	0.520	0.322	58	0.734	0.544	0.506	52	0.716	0.493	0.291
		0.000	0.000	0.001		0.000	0.000	0.000		0.000	0.000	0.036
FD	60	0.685	0.490	0.228	34	0.760	0.572	0.709	26	0.632	0.446	0.175
		0.000	0.000	0.080		0.000	0.000	0.000		0.001	0.001	0.393
TD	50	0.394	0.273	0.421	24	0.521	0.399	0.484	26	0.249	0.138	0.418
		0.005	0.005	0.002		0.009	0.006	0.017		0.221	0.321	0.034

ρ: Spearsmans ρ
τ: Kendalls τ
r: Pearsons r

Table C.204 $\log F_{10}$ vs. $\log \dot{M}$ (II)

	Ori A				ONC				L1641			
	N	ρ	τ	r	N	ρ	τ	r	N	ρ	τ	r
TDFD	108	0.733	0.523	0.323	57	0.743	0.553	0.514	51	0.711	0.490	0.288
		0.000	0.000	0.001		0.000	0.000	0.000		0.000	0.000	0.040
FD	59	0.703	0.506	0.231	33	0.777	0.591	0.722	26	0.632	0.446	0.175
		0.000	0.000	0.078		0.000	0.000	0.000		0.001	0.001	0.393
TD	49	0.387	0.270	0.419	24	0.521	0.399	0.484	25	0.231	0.133	0.408
		0.006	0.006	0.003		0.009	0.006	0.017		0.267	0.350	0.043

ρ: Spearsmans ρ
τ: Kendalls τ
r: Pearsons r

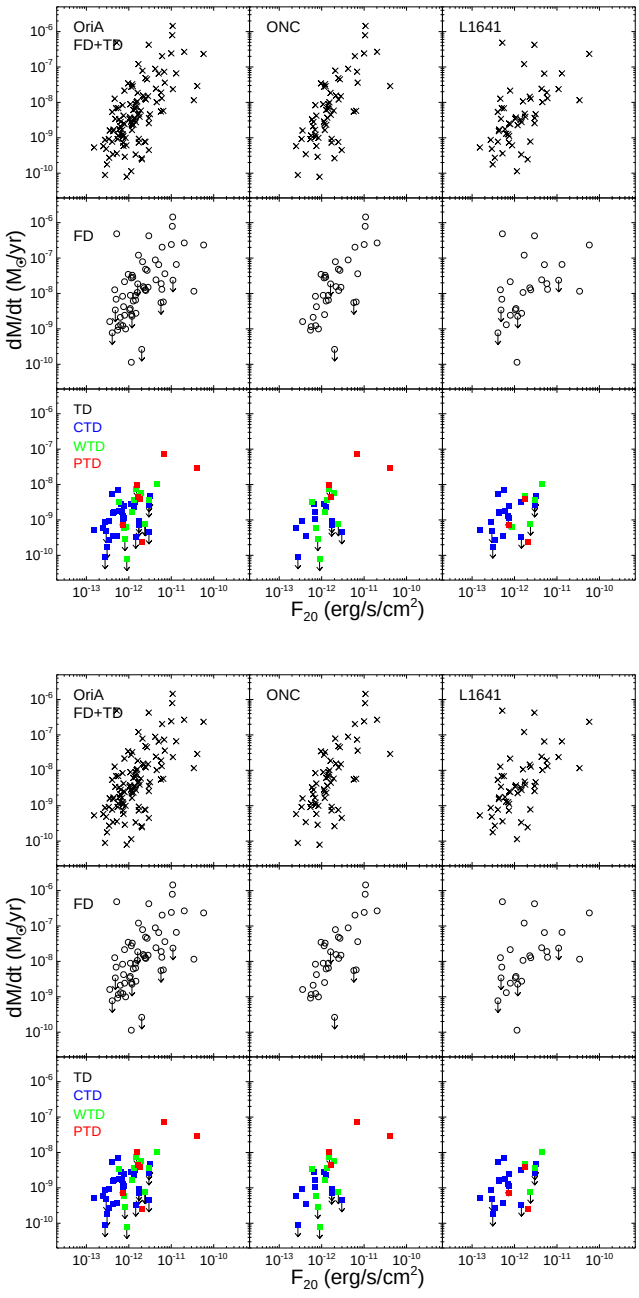


Figure C.103 $\log F_{20}$ vs. $\log \dot{M}$. Upper panel: all available objects; Lower panel: objects with available spectral types only

Table C.205 $\log F_{20}$ vs. $\log \dot{M}$ (I)

	Ori A				ONC				L1641			
	N	ρ	τ	r	N	ρ	τ	r	N	ρ	τ	r
TDFD	111	0.606	0.440	0.411	59	0.646	0.476	0.454	52	0.564	0.412	0.408
		0.000	0.000	0.000		0.000	0.000	0.000		0.000	0.000	0.003
FD	60	0.621	0.456	0.382	34	0.715	0.540	0.668	26	0.525	0.378	0.352
		0.000	0.000	0.003		0.000	0.000	0.000		0.006	0.007	0.078
TD	51	0.450	0.325	0.413	25	0.471	0.333	0.459	26	0.423	0.305	0.474
		0.001	0.001	0.003		0.018	0.020	0.021		0.031	0.029	0.014

ρ: Spearsmans ρ
τ: Kendalls τ
r: Pearsons r

Table C.206 $\log F_{20}$ vs. $\log \dot{M}$ (II)

	Ori A				ONC				L1641			
	N	ρ	τ	r	N	ρ	τ	r	N	ρ	τ	r
TDFD	109	0.610	0.446	0.414	58	0.653	0.485	0.461	51	0.572	0.421	0.407
		0.000	0.000	0.000		0.000	0.000	0.000		0.000	0.000	0.003
FD	59	0.628	0.463	0.385	33	0.729	0.557	0.677	26	0.525	0.378	0.352
		0.000	0.000	0.003		0.000	0.000	0.000		0.006	0.007	0.078
TD	50	0.453	0.329	0.412	25	0.471	0.333	0.459	25	0.441	0.327	0.471
		0.001	0.001	0.003		0.018	0.020	0.021		0.027	0.022	0.017

ρ: Spearsmans ρ
τ: Kendalls τ
r: Pearsons r

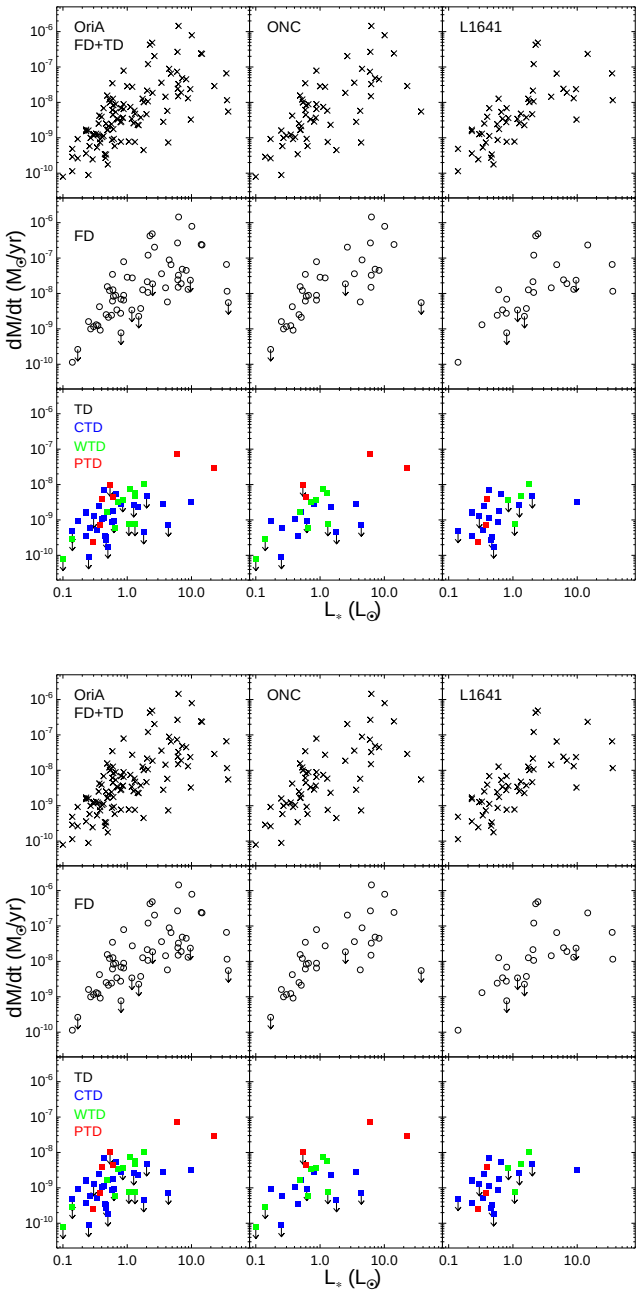


Figure C.104 $\log L_\star$ vs. $\log \dot{M}$. Upper panel: all available objects; Lower panel: objects with available spectral types only

Table C.207 $\log L_\star$ vs. $\log \dot{M}$ (I)

	Ori A				ONC				L1641			
	N	ρ	τ	r	N	ρ	τ	r	N	ρ	τ	r
TDFD	111	0.743	0.541	0.698	59	0.698	0.520	0.689	52	0.809	0.600	0.716
		0.000	0.000	0.000		0.000	0.000	0.000		0.000	0.000	0.000
FD	60	0.708	0.515	0.653	34	0.769	0.603	0.700	26	0.744	0.542	0.629
		0.000	0.000	0.000		0.000	0.000	0.000		0.000	0.000	0.001
TD	51	0.576	0.403	0.613	25	0.560	0.420	0.677	26	0.524	0.350	0.506
		0.000	0.000	0.000		0.004	0.003	0.000		0.006	0.012	0.008

ρ: Spearsmans ρ
τ: Kendalls τ
r: Pearsons r

Table C.208 $\log L_\star$ vs. $\log \dot{M}$ (II)

	Ori A				ONC				L1641			
	N	ρ	τ	r	N	ρ	τ	r	N	ρ	τ	r
TDFD	109	0.742	0.540	0.699	58	0.699	0.520	0.694	51	0.803	0.597	0.712
		0.000	0.000	0.000		0.000	0.000	0.000		0.000	0.000	0.000
FD	59	0.714	0.521	0.657	33	0.771	0.605	0.705	26	0.744	0.542	0.629
		0.000	0.000	0.000		0.000	0.000	0.000		0.000	0.000	0.001
TD	50	0.570	0.402	0.615	25	0.560	0.420	0.677	25	0.509	0.342	0.498
		0.000	0.000	0.000		0.004	0.003	0.000		0.009	0.016	0.011

ρ: Spearsmans ρ
τ: Kendalls τ
r: Pearsons r

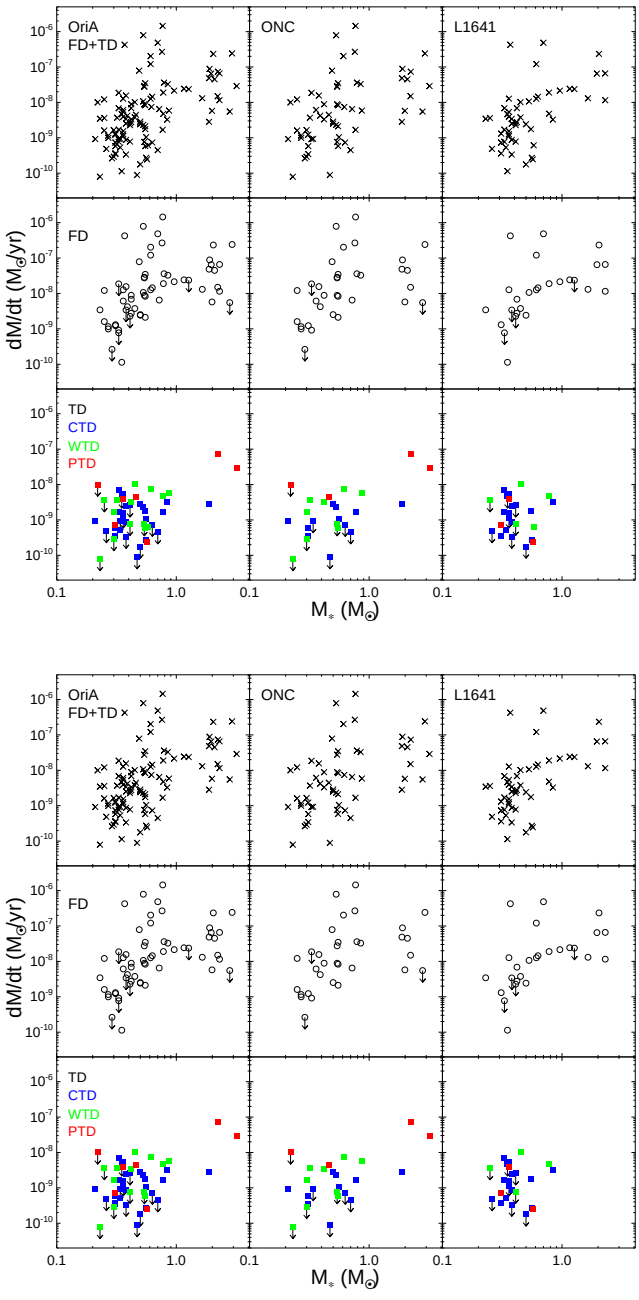


Figure C.105 $\log M_\star$ vs. $\log \dot{M}$. Upper panel: all available objects; Lower panel: objects with available spectral types only

Table C.209 $\log M_\star$ vs. $\log \dot{M}$ (I)

	Ori A				ONC				L1641			
	N	ρ	τ	r	N	ρ	τ	r	N	ρ	τ	r
TDFD	111	0.545	0.376	0.514	59	0.521	0.354	0.485	52	0.546	0.391	0.550
		0.000	0.000	0.000		0.000	0.000	0.000		0.000	0.000	0.000
FD	60	0.607	0.421	0.478	34	0.562	0.392	0.450	26	0.659	0.507	0.526
		0.000	0.000	0.000		0.001	0.001	0.008		0.000	0.000	0.006
TD	51	0.211	0.148	0.425	25	0.385	0.274	0.574	26	-0.066	-0.047	-0.017
		0.138	0.125	0.002		0.058	0.055	0.003		0.750	0.735	0.934

ρ: Spearsmans ρ
τ: Kendalls τ
r: Pearsons r

Table C.210 $\log M_\star$ vs. $\log \dot{M}$ (II)

	Ori A				ONC				L1641			
	N	ρ	τ	r	N	ρ	τ	r	N	ρ	τ	r
TDFD	109	0.555	0.383	0.519	58	0.521	0.352	0.489	51	0.569	0.411	0.560
		0.000	0.000	0.000		0.000	0.000	0.000		0.000	0.000	0.000
FD	59	0.610	0.422	0.481	33	0.563	0.387	0.453	26	0.659	0.507	0.526
		0.000	0.000	0.000		0.001	0.002	0.008		0.000	0.000	0.006
TD	50	0.225	0.159	0.433	25	0.385	0.274	0.574	25	-0.038	-0.027	0.018
		0.116	0.103	0.002		0.058	0.055	0.003		0.859	0.848	0.932

ρ: Spearsmans ρ
τ: Kendalls τ
r: Pearsons r

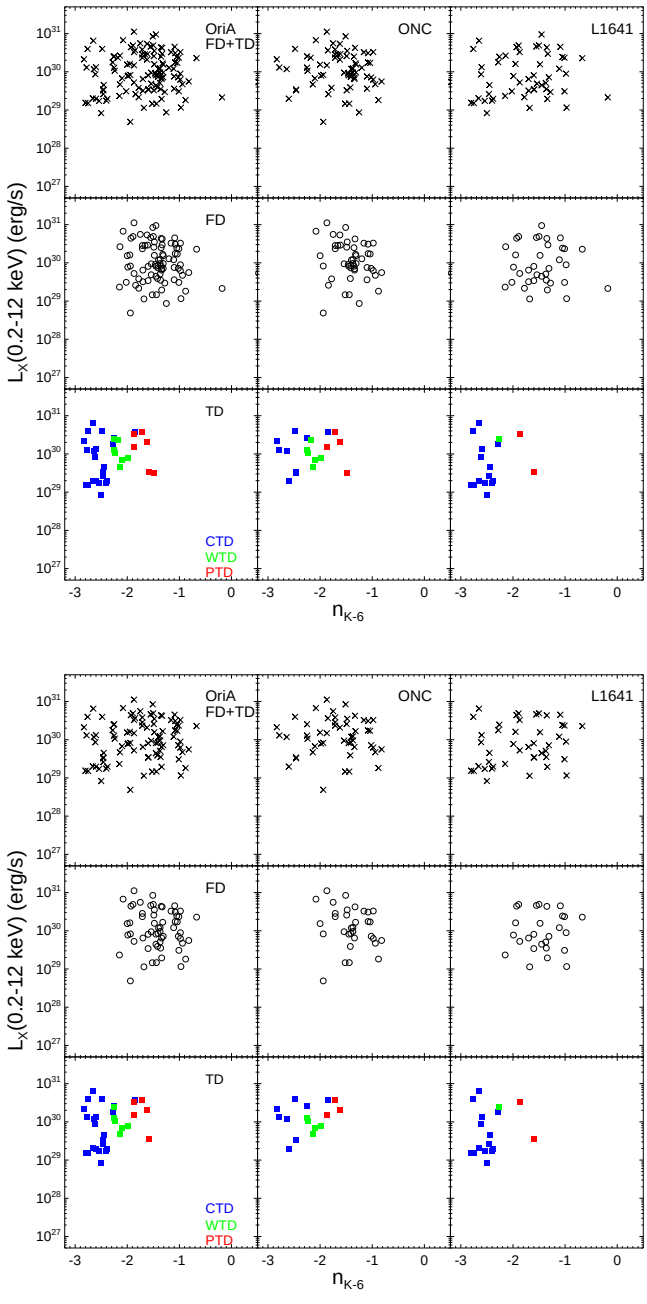


Figure C.106 n_{K-6} vs. $\log L_X 8$. Upper panel: all available objects; Lower panel: objects with available spectral types only

Table C.211 n_{K-6} vs. $\log L_X 8$ (I)

	Ori A				ONC				L1641			
	N	ρ	τ	r	N	ρ	τ	r	N	ρ	τ	r
TDFD	122	0.028	0.022	0.045	69	-0.128	-0.090	-0.091	53	0.164	0.123	0.139
		0.763	0.724	0.623		0.296	0.273	0.457		0.239	0.194	0.321
FD	86	-0.108	-0.072	-0.112	50	-0.234	-0.170	-0.187	36	-0.029	-0.016	-0.040
		0.324	0.326	0.305		0.101	0.082	0.193		0.866	0.891	0.817
TD	36	0.209	0.163	0.212	19	0.091	0.076	0.131	17	0.199	0.176	0.134
		0.222	0.163	0.215		0.710	0.647	0.593		0.445	0.323	0.608

ρ: Spearsmans ρ
τ: Kendalls τ
r: Pearsons r

Table C.212 n_{K-6} vs. $\log L_X 8$ (II)

	Ori A				ONC				L1641			
	N	ρ	τ	r	N	ρ	τ	r	N	ρ	τ	r
TDFD	94	0.085	0.059	0.132	50	-0.040	-0.032	-0.002	44	0.195	0.143	0.215
		0.414	0.402	0.205		0.783	0.743	0.989		0.205	0.171	0.161
FD	60	-0.126	-0.087	-0.071	33	-0.243	-0.169	-0.181	27	-0.002	-0.009	0.042
		0.336	0.327	0.590		0.173	0.166	0.313		0.994	0.950	0.835
TD	34	0.229	0.188	0.278	17	0.216	0.178	0.325	17	0.199	0.176	0.134
		0.192	0.118	0.111		0.405	0.319	0.203		0.445	0.323	0.608

ρ: Spearsmans ρ
τ: Kendalls τ
r: Pearsons r

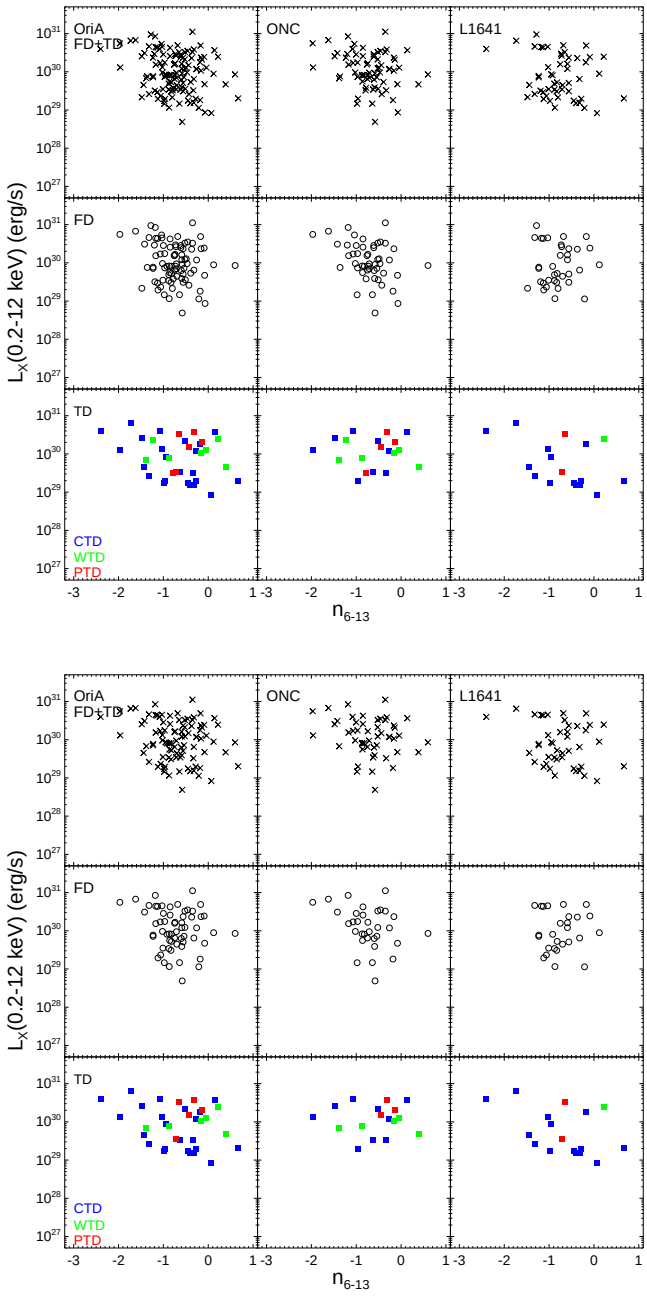


Figure C.107 n_{6-13} vs. $\log L_X 8$. Upper panel: all available objects; Lower panel: objects with available spectral types only

Table C.213 n_{6-13} vs. $\log L_X 8$ (I)

	Ori A				ONC				L1641			
	N	ρ	τ	r	N	ρ	τ	r	N	ρ	τ	r
TDFD	122	-0.166	-0.107	-0.217	69	-0.221	-0.148	-0.255	53	-0.161	-0.104	-0.210
		0.067	0.080	0.016		0.068	0.072	0.034		0.248	0.271	0.131
FD	86	-0.136	-0.090	-0.187	50	-0.329	-0.241	-0.369	36	0.080	0.059	0.059
		0.212	0.220	0.085		0.020	0.014	0.008		0.642	0.612	0.732
TD	36	-0.196	-0.138	-0.265	19	-0.025	-0.006	-0.015	17	-0.419	-0.294	-0.462
		0.251	0.236	0.118		0.920	0.972	0.951		0.094	0.099	0.062

ρ: Spearsmans ρ
τ: Kendalls τ
r: Pearsons r

Table C.214 n_{6-13} vs. $\log L_X 8$ (II)

	Ori A				ONC				L1641			
	N	ρ	τ	r	N	ρ	τ	r	N	ρ	τ	r
TDFD	94	-0.168	-0.108	-0.219	50	-0.176	-0.120	-0.206	44	-0.183	-0.118	-0.254
		0.106	0.122	0.034		0.221	0.221	0.151		0.233	0.260	0.096
FD	60	-0.142	-0.092	-0.182	33	-0.273	-0.207	-0.317	27	0.058	0.063	0.024
		0.281	0.300	0.164		0.125	0.090	0.072		0.774	0.645	0.905
TD	34	-0.179	-0.125	-0.255	17	0.007	0.015	0.008	17	-0.419	-0.294	-0.462
		0.311	0.299	0.146		0.978	0.934	0.976		0.094	0.099	0.062

ρ: Spearsmans ρ
τ: Kendalls τ
r: Pearsons r

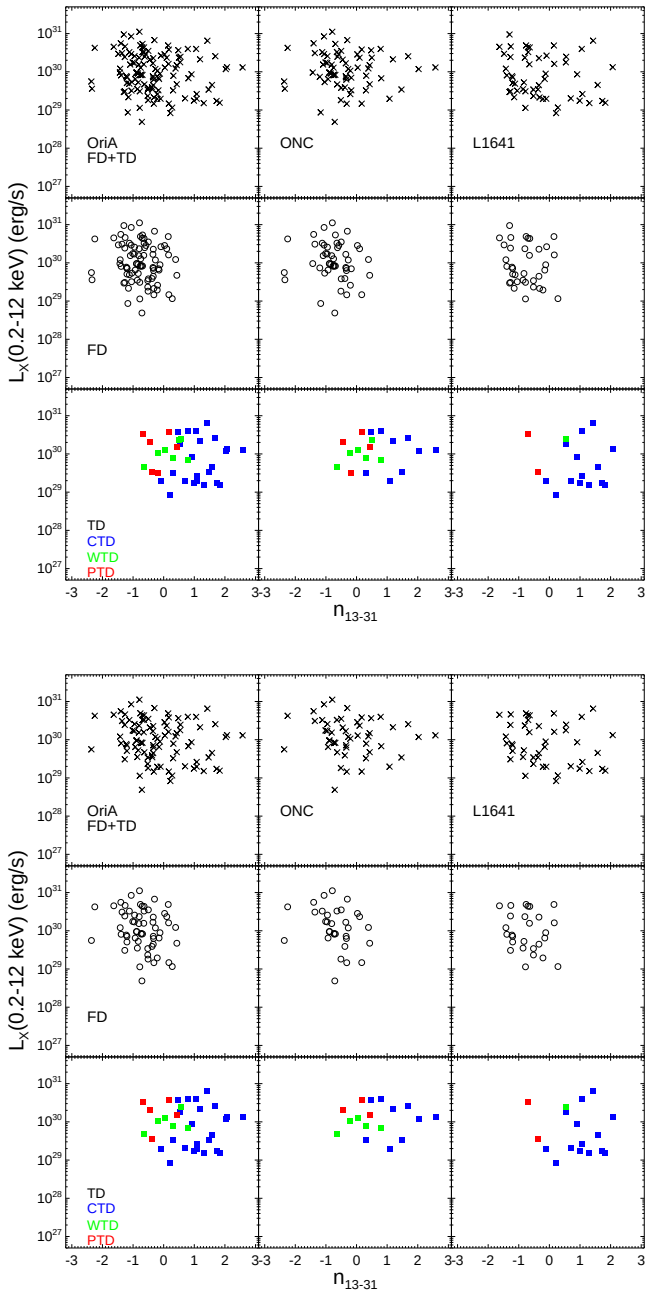


Figure C.108 n_{13-31} vs. $\log L_X 8$. Upper panel: all available objects; Lower panel: objects with available spectral types only

Table C.215 n_{13-31} vs. $\log L_X 8$ (I)

	Ori A				ONC				L1641			
	N	ρ	τ	r	N	ρ	τ	r	N	ρ	τ	r
TDFD	122	-0.148	-0.099	-0.130	69	-0.102	-0.076	-0.045	53	-0.253	-0.185	-0.204
		0.103	0.106	0.154		0.406	0.358	0.714		0.068	0.051	0.143
FD	86	-0.144	-0.097	-0.133	50	-0.199	-0.152	-0.129	36	-0.165	-0.134	-0.149
		0.186	0.184	0.222		0.165	0.119	0.372		0.337	0.250	0.386
TD	36	-0.079	-0.049	-0.045	19	0.132	0.088	0.064	17	-0.113	-0.088	-0.062
		0.646	0.673	0.794		0.591	0.600	0.795		0.667	0.621	0.813

ρ: Spearsmans ρ
τ: Kendalls τ
r: Pearsons r

Table C.216 n_{13-31} vs. $\log L_X 8$ (II)

	Ori A				ONC				L1641			
	N	ρ	τ	r	N	ρ	τ	r	N	ρ	τ	r
TDFD	94	-0.215	-0.142	-0.196	50	-0.197	-0.132	-0.140	44	-0.268	-0.193	-0.239
		0.037	0.043	0.058		0.171	0.175	0.332		0.079	0.065	0.118
FD	60	-0.228	-0.155	-0.227	33	-0.343	-0.252	-0.263	27	-0.162	-0.135	-0.186
		0.079	0.080	0.081		0.051	0.039	0.139		0.418	0.324	0.353
TD	34	-0.098	-0.057	-0.064	17	0.051	0.044	-0.001	17	-0.113	-0.088	-0.062
		0.582	0.635	0.719		0.844	0.805	0.997		0.667	0.621	0.813

ρ: Spearsmans ρ
τ: Kendalls τ
r: Pearsons r

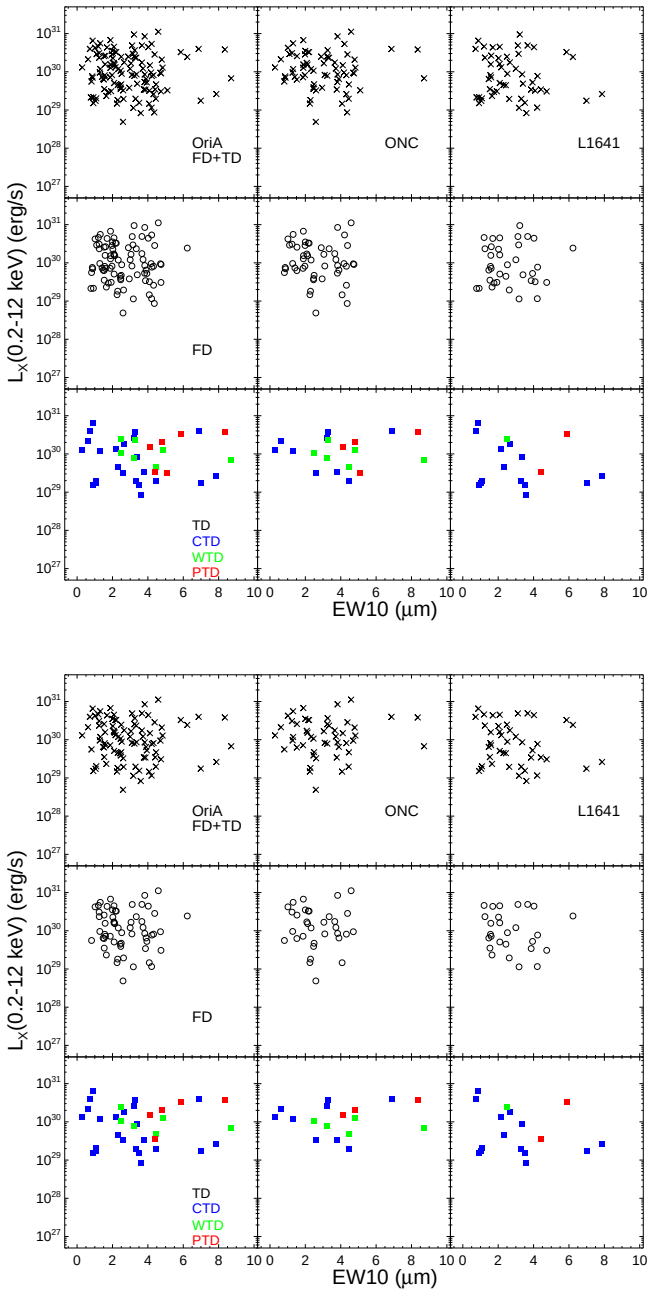


Figure C.109 EW10 vs. $\log L_X 8$. Upper panel: all available objects; Lower panel: objects with available spectral types only

Table C.217 EW10 vs. $\log L_X 8$ (I)

	Ori A				ONC				L1641			
	N	ρ	τ	r	N	ρ	τ	r	N	ρ	τ	r
TDFD	122	-0.089	-0.061	-0.057	69	-0.112	-0.073	-0.037	53	-0.086	-0.057	-0.109
		0.329	0.317	0.533		0.361	0.375	0.763		0.541	0.550	0.437
FD	86	-0.063	-0.044	-0.043	50	-0.134	-0.090	-0.103	36	0.021	0.022	0.029
		0.562	0.551	0.694		0.354	0.357	0.477		0.903	0.849	0.867
TD	36	-0.081	-0.037	-0.029	19	0.032	0.000	0.057	17	-0.250	-0.162	-0.218
		0.638	0.754	0.867		0.895	1.000	0.817		0.333	0.365	0.401

ρ: Spearsmans ρ
τ: Kendalls τ
r: Pearsons r

Table C.218 EW10 vs. $\log L_X 8$ (II)

	Ori A				ONC				L1641			
	N	ρ	τ	r	N	ρ	τ	r	N	ρ	τ	r
TDFD	94	-0.119	-0.084	-0.066	50	-0.074	-0.047	0.020	44	-0.184	-0.133	-0.188
		0.252	0.232	0.527		0.610	0.627	0.890		0.231	0.203	0.222
FD	60	-0.134	-0.098	-0.067	33	-0.131	-0.093	-0.024	27	-0.161	-0.117	-0.112
		0.306	0.270	0.611		0.469	0.447	0.895		0.422	0.393	0.578
TD	34	-0.063	-0.014	-0.011	17	0.110	0.066	0.117	17	-0.250	-0.162	-0.218
		0.724	0.906	0.951		0.673	0.710	0.655		0.333	0.365	0.401

ρ: Spearsmans ρ
τ: Kendalls τ
r: Pearsons r

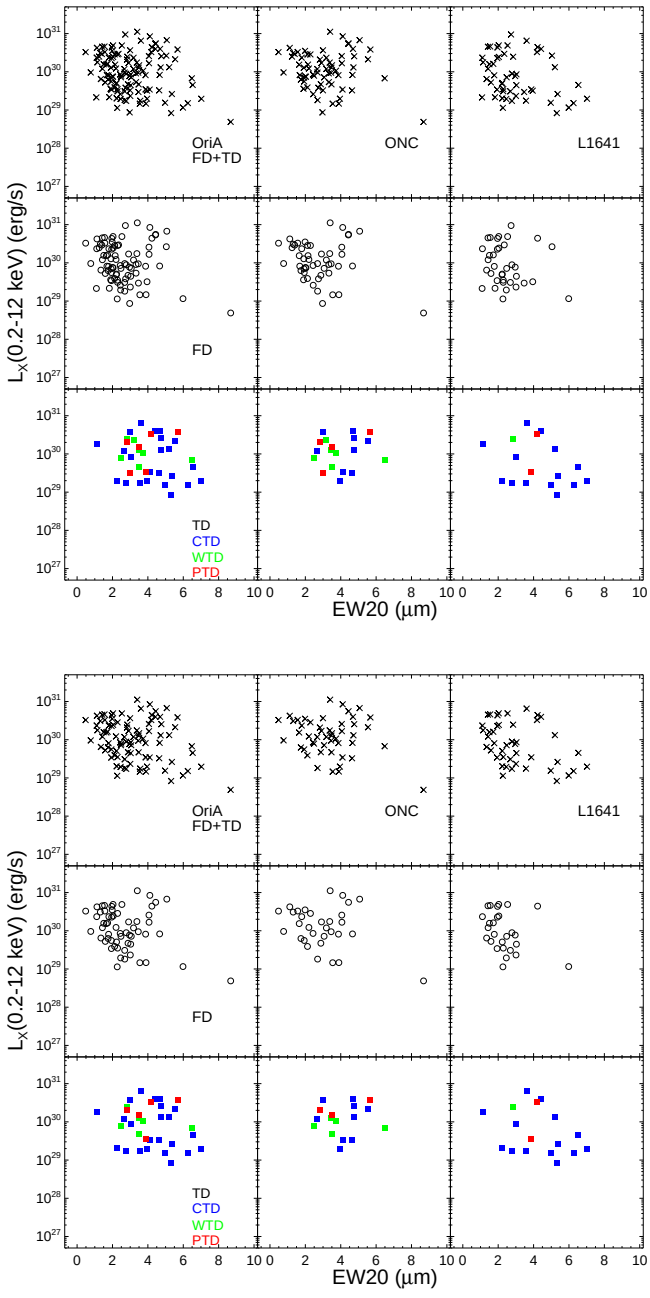


Figure C.110 EW20 vs. $\log L_X 8$. Upper panel: all available objects; Lower panel: objects with available spectral types only

Table C.219 EW20 vs. $\log L_X 8$ (I)

	Ori A				ONC				L1641			
	N	ρ	τ	r	N	ρ	τ	r	N	ρ	τ	r
TDFD	122	-0.147	-0.106	-0.192	69	-0.048	-0.049	-0.147	53	-0.275	-0.189	-0.296
		0.105	0.083	0.034		0.694	0.555	0.228		0.046	0.045	0.031
FD	86	-0.133	-0.102	-0.165	50	-0.117	-0.105	-0.197	36	-0.171	-0.117	-0.176
		0.223	0.164	0.129		0.419	0.281	0.170		0.319	0.313	0.305
TD	36	-0.131	-0.086	-0.201	19	0.170	0.099	0.110	17	-0.287	-0.191	-0.334
		0.445	0.462	0.240		0.486	0.552	0.654		0.264	0.284	0.190

ρ: Spearsmans ρ
τ: Kendalls τ
r: Pearsons r

Table C.220 EW20 vs. $\log L_X 8$ (II)

	Ori A				ONC				L1641			
	N	ρ	τ	r	N	ρ	τ	r	N	ρ	τ	r
TDFD	94	-0.207	-0.143	-0.258	50	-0.086	-0.074	-0.218	44	-0.388	-0.261	-0.399
		0.046	0.042	0.012		0.552	0.447	0.128		0.009	0.012	0.007
FD	60	-0.177	-0.128	-0.242	33	-0.137	-0.117	-0.272	27	-0.371	-0.242	-0.376
		0.176	0.149	0.062		0.447	0.337	0.126		0.057	0.076	0.053
TD	34	-0.147	-0.098	-0.209	17	0.172	0.103	0.081	17	-0.287	-0.191	-0.334
		0.408	0.415	0.236		0.510	0.564	0.757		0.264	0.284	0.190

ρ: Spearsmans ρ
τ: Kendalls τ
r: Pearsons r

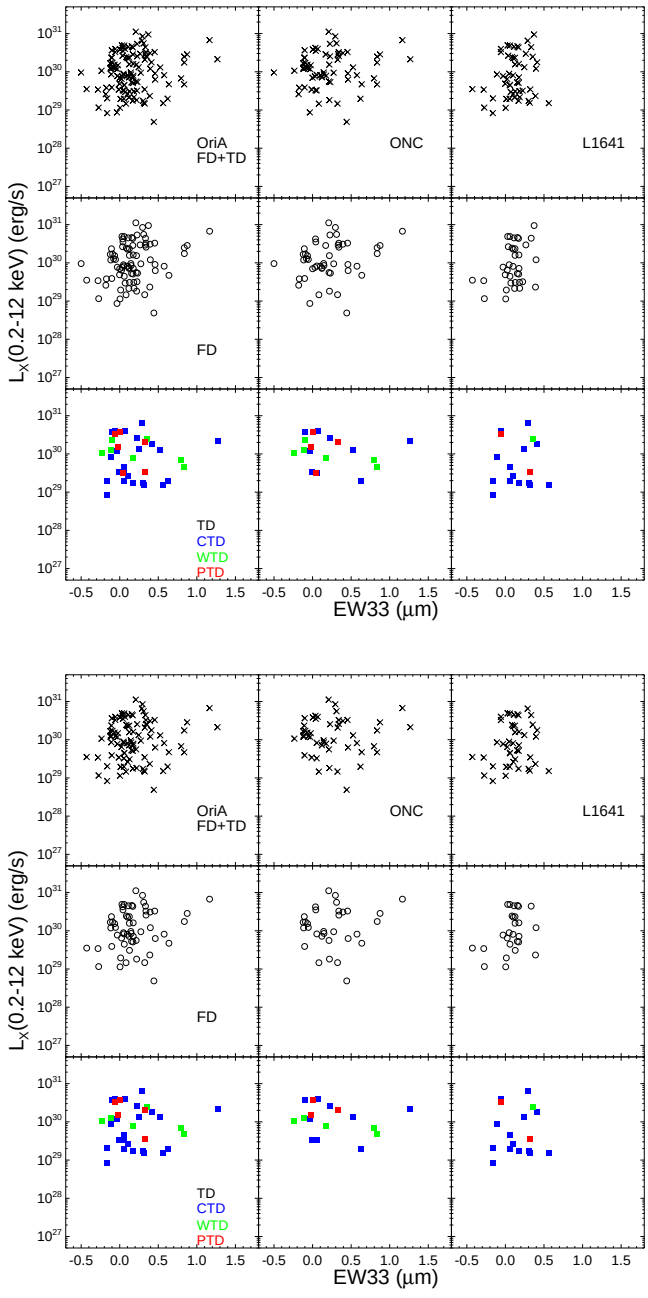


Figure C.111 EW33 vs. $\log L_X 8$. Upper panel: all available objects; Lower panel: objects with available spectral types only

Table C.221 EW33 vs. $\log L_X 8$ (I)

	Ori A				ONC				L1641			
	N	ρ	τ	r	N	ρ	τ	r	N	ρ	τ	r
TDFD	122	0.133	0.084	-0.007	69	0.089	0.052	-0.066	53	0.134	0.085	0.197
		0.145	0.169	0.939		0.467	0.527	0.590		0.339	0.369	0.157
FD	86	0.240	0.157	-0.005	50	0.191	0.120	-0.058	36	0.224	0.149	0.354
		0.026	0.033	0.964		0.184	0.219	0.689		0.188	0.200	0.034
TD	36	-0.080	-0.062	-0.042	19	-0.181	-0.135	-0.181	17	-0.006	-0.022	0.036
		0.644	0.595	0.808		0.459	0.421	0.458		0.981	0.901	0.891

ρ: Spearsmans ρ
τ: Kendalls τ
r: Pearsons r

Table C.222 EW33 vs. $\log L_X 8$ (II)

	Ori A				ONC				L1641			
	N	ρ	τ	r	N	ρ	τ	r	N	ρ	τ	r
TDFD	94	0.092	0.057	0.113	50	0.001	-0.010	0.063	44	0.149	0.092	0.172
		0.380	0.416	0.278		0.994	0.920	0.664		0.335	0.378	0.264
FD	60	0.199	0.121	0.202	33	0.101	0.042	0.151	27	0.315	0.197	0.380
		0.128	0.172	0.122		0.577	0.733	0.402		0.109	0.149	0.051
TD	34	-0.058	-0.046	-0.030	17	-0.145	-0.103	-0.201	17	-0.006	-0.022	0.036
		0.743	0.700	0.866		0.580	0.564	0.439		0.981	0.901	0.891

ρ: Spearsmans ρ
τ: Kendalls τ
r: Pearsons r

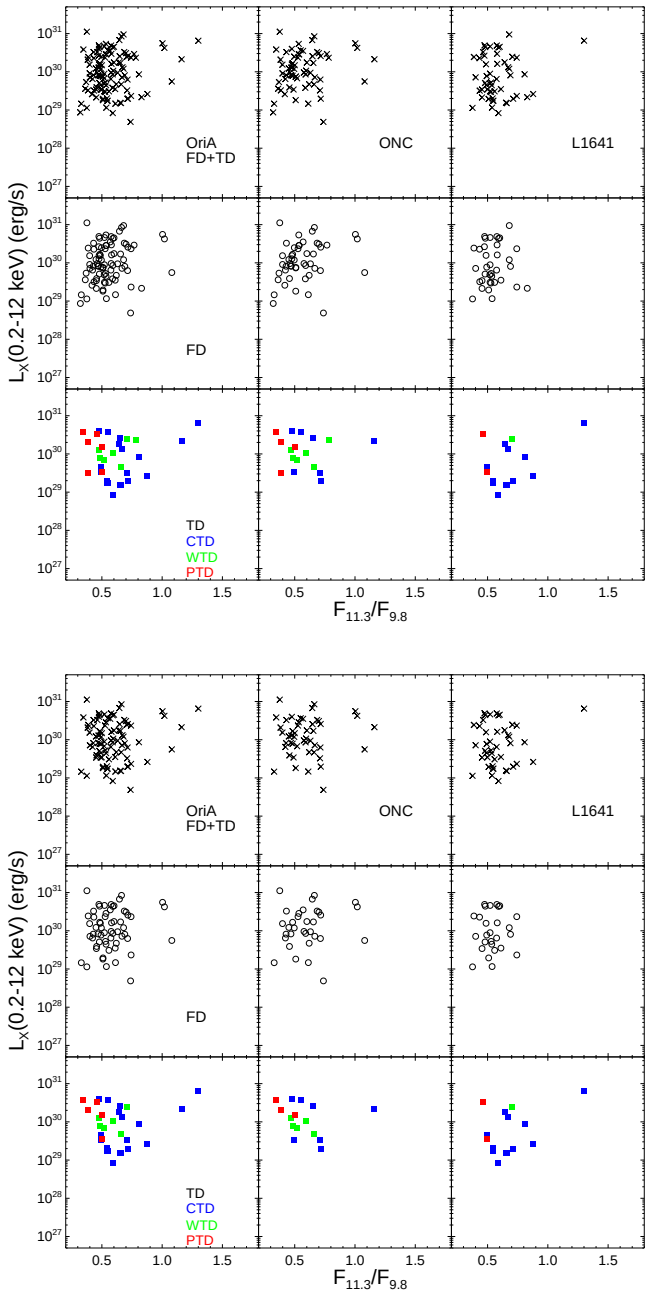


Figure C.112 $F_{11.3}/F_{9.8}$ vs. $\log L_X 8$. Upper panel: all available objects; Lower panel: objects with available spectral types only

Table C.223 $F_{11.3}/F_{9.8}$ vs. $\log L_X 8$ (I)

	Ori A				ONC				L1641			
	N	ρ	τ	r	N	ρ	τ	r	N	ρ	τ	r
TDFD	122	0.096	0.063	0.119	69	0.152	0.108	0.038	53	0.048	0.020	0.187
		0.292	0.306	0.192		0.212	0.188	0.757		0.735	0.830	0.180
FD	86	0.196	0.139	0.108	50	0.269	0.210	0.118	36	0.112	0.070	0.074
		0.070	0.059	0.322		0.059	0.032	0.414		0.514	0.549	0.668
TD	36	-0.023	-0.029	0.236	19	-0.182	-0.158	-0.011	17	0.287	0.147	0.386
		0.893	0.806	0.166		0.455	0.345	0.964		0.264	0.410	0.126

ρ: Spearsmans ρ
τ: Kendalls τ
r: Pearsons r

Table C.224 $F_{11.3}/F_{9.8}$ vs. $\log L_X 8$ (II)

	Ori A				ONC				L1641			
	N	ρ	τ	r	N	ρ	τ	r	N	ρ	τ	r
TDFD	94	0.016	0.006	0.125	50	-0.013	-0.016	0.006	44	0.024	0.004	0.205
		0.877	0.935	0.230		0.928	0.874	0.967		0.877	0.968	0.182
FD	60	0.111	0.075	0.122	33	0.138	0.102	0.129	27	0.040	0.014	0.052
		0.399	0.400	0.353		0.445	0.403	0.474		0.844	0.917	0.797
TD	34	-0.084	-0.073	0.240	17	-0.377	-0.294	-0.041	17	0.287	0.147	0.386
		0.635	0.543	0.172		0.135	0.099	0.876		0.264	0.410	0.126

ρ: Spearsmans ρ
τ: Kendalls τ
r: Pearsons r

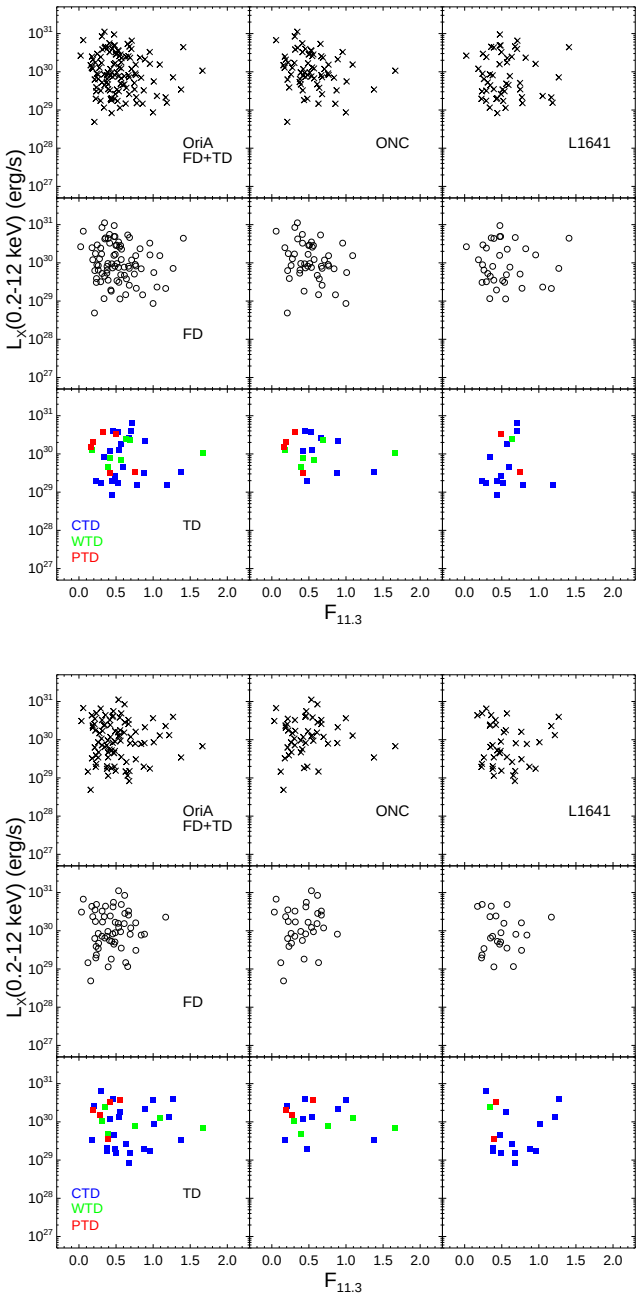


Figure C.113 $F_{11.3}$ vs. $\log L_X 8$. Upper panel: all available objects; Lower panel: objects with available spectral types only

Table C.225 $F_{11.3}$ vs. $\log L_X 8$ (I)

	Ori A				ONC				L1641			
	N	ρ	τ	r	N	ρ	τ	r	N	ρ	τ	r
TDFD	122	-0.046	-0.033	-0.081	69	-0.063	-0.044	-0.045	53	-0.026	-0.012	-0.133
		0.614	0.594	0.375		0.604	0.593	0.714		0.852	0.896	0.342
FD	86	0.002	-0.003	-0.013	50	-0.069	-0.048	-0.060	36	0.064	0.046	0.035
		0.986	0.964	0.905		0.633	0.621	0.679		0.711	0.692	0.839
TD	36	-0.051	-0.038	-0.100	19	0.014	-0.006	-0.064	17	-0.037	-0.059	-0.199
		0.766	0.744	0.562		0.955	0.972	0.795		0.889	0.742	0.444

ρ: Spearsmans ρ
τ: Kendalls τ
r: Pearsons r

Table C.226 $F_{11.3}$ vs. $\log L_X 8$ (II)

	Ori A				ONC				L1641			
	N	ρ	τ	r	N	ρ	τ	r	N	ρ	τ	r
TDFD	94	-0.121	-0.082	-0.136	50	-0.094	-0.058	-0.070	44	-0.133	-0.092	-0.218
		0.245	0.243	0.191		0.518	0.552	0.629		0.390	0.379	0.155
FD	60	-0.103	-0.075	-0.105	33	-0.104	-0.066	-0.072	27	-0.133	-0.097	-0.148
		0.435	0.396	0.425		0.564	0.587	0.690		0.508	0.478	0.461
TD	34	-0.071	-0.055	-0.108	17	0.012	-0.015	-0.077	17	-0.037	-0.059	-0.199
		0.688	0.646	0.543		0.963	0.934	0.769		0.889	0.742	0.444

ρ: Spearsmans ρ
τ: Kendalls τ
r: Pearsons r

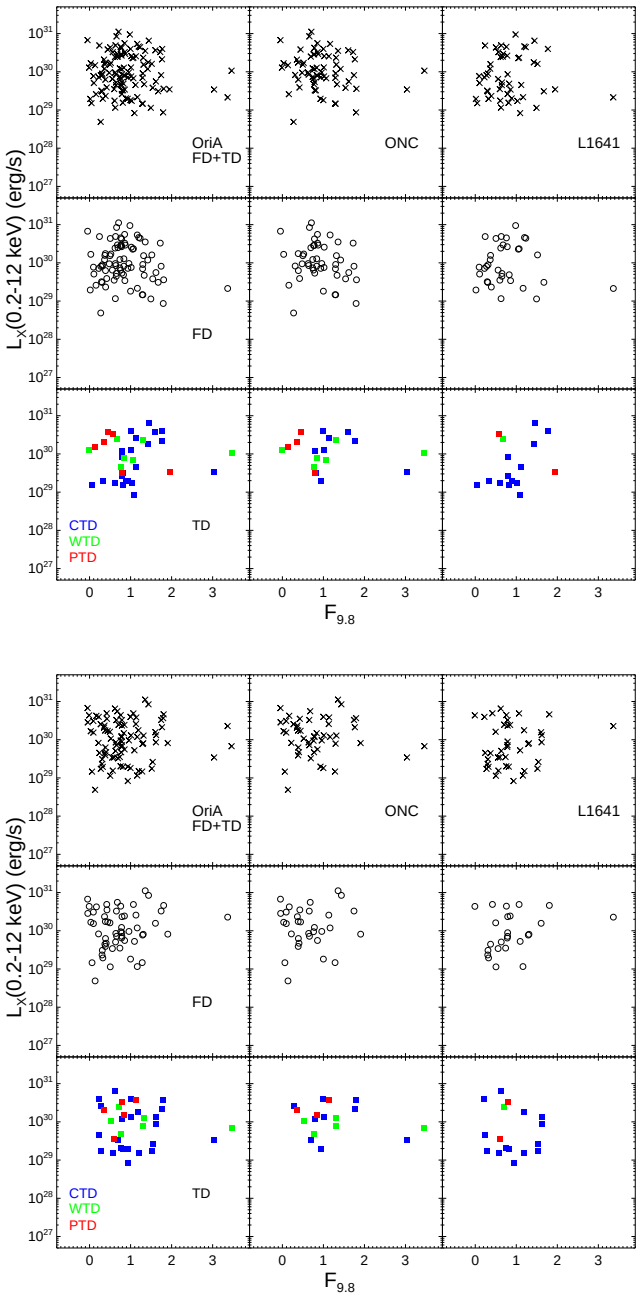


Figure C.114 $F_{9.8}$ vs. $\log L_X 8$. Upper panel: all available objects; Lower panel: objects with available spectral types only

Table C.227 $F_{9.8}$ vs. $\log L_X 8$ (I)

	Ori A				ONC				L1641			
	N	ρ	τ	r	N	ρ	τ	r	N	ρ	τ	r
TDFD	122	-0.121	-0.085	-0.078	69	-0.139	-0.101	-0.064	53	-0.108	-0.084	-0.141
		0.183	0.164	0.393		0.253	0.220	0.601		0.443	0.374	0.314
FD	86	-0.101	-0.073	-0.106	50	-0.187	-0.143	-0.180	36	0.019	0.013	-0.017
		0.354	0.317	0.331		0.195	0.143	0.211		0.913	0.913	0.922
TD	36	-0.038	-0.029	-0.006	19	0.070	0.029	0.083	17	-0.275	-0.221	-0.265
		0.825	0.806	0.972		0.775	0.861	0.736		0.286	0.217	0.304

ρ: Spearsmans ρ
τ: Kendalls τ
r: Pearsons r

Table C.228 $F_{9.8}$ vs. $\log L_X 8$ (II)

	Ori A				ONC				L1641			
	N	ρ	τ	r	N	ρ	τ	r	N	ρ	τ	r
TDFD	94	-0.143	-0.101	-0.072	50	-0.075	-0.051	0.004	44	-0.209	-0.165	-0.207
		0.170	0.151	0.490		0.607	0.604	0.978		0.174	0.115	0.178
FD	60	-0.156	-0.114	-0.120	33	-0.140	-0.110	-0.106	27	-0.152	-0.117	-0.129
		0.234	0.198	0.361		0.436	0.369	0.557		0.449	0.393	0.521
TD	34	-0.025	-0.012	0.019	17	0.157	0.088	0.158	17	-0.275	-0.221	-0.265
		0.890	0.917	0.915		0.548	0.621	0.545		0.286	0.217	0.304

ρ: Spearsmans ρ
τ: Kendalls τ
r: Pearsons r

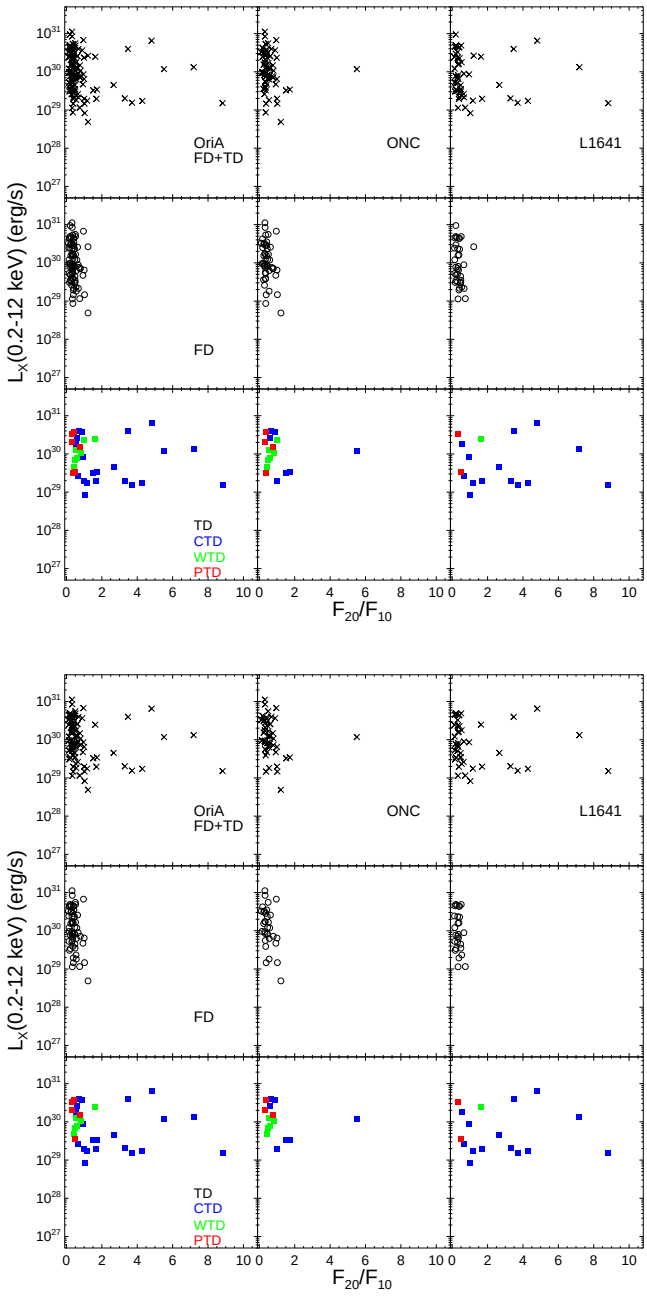


Figure C.115 F_{20}/F_{10} vs. $\log L_X 8$. Upper panel: all available objects; Lower panel: objects with available spectral types only

Table C.229 F_{20}/F_{10} vs. $\log L_X 8$ (I)

	Ori A				ONC				L1641			
	N	ρ	τ	r	N	ρ	τ	r	N	ρ	τ	r
TDFD	121	-0.246	-0.172	-0.073	68	-0.212	-0.150	0.014	53	-0.327	-0.235	-0.137
		0.007	0.005	0.426		0.083	0.070	0.910		0.017	0.013	0.328
FD	86	-0.238	-0.165	-0.256	50	-0.275	-0.202	-0.345	36	-0.303	-0.200	-0.170
		0.028	0.025	0.017		0.053	0.039	0.014		0.073	0.086	0.322
TD	35	-0.231	-0.160	-0.012	18	-0.115	-0.033	0.126	17	-0.162	-0.132	-0.030
		0.182	0.177	0.945		0.651	0.850	0.618		0.535	0.458	0.909

ρ: Spearsmans ρ
τ: Kendalls τ
r: Pearsons r

Table C.230 F_{20}/F_{10} vs. $\log L_X 8$ (II)

	Ori A				ONC				L1641			
	N	ρ	τ	r	N	ρ	τ	r	N	ρ	τ	r
TDFD	93	-0.299	-0.210	-0.097	49	-0.352	-0.243	-0.010	44	-0.302	-0.216	-0.158
		0.004	0.003	0.355		0.013	0.014	0.946		0.046	0.039	0.306
FD	60	-0.262	-0.186	-0.350	33	-0.428	-0.314	-0.479	27	-0.198	-0.128	-0.270
		0.043	0.035	0.006		0.013	0.010	0.005		0.323	0.348	0.173
TD	33	-0.258	-0.189	-0.015	16	-0.247	-0.117	0.111	17	-0.162	-0.132	-0.030
		0.147	0.121	0.934		0.356	0.528	0.682		0.535	0.458	0.909

ρ: Spearsmans ρ
τ: Kendalls τ
r: Pearsons r

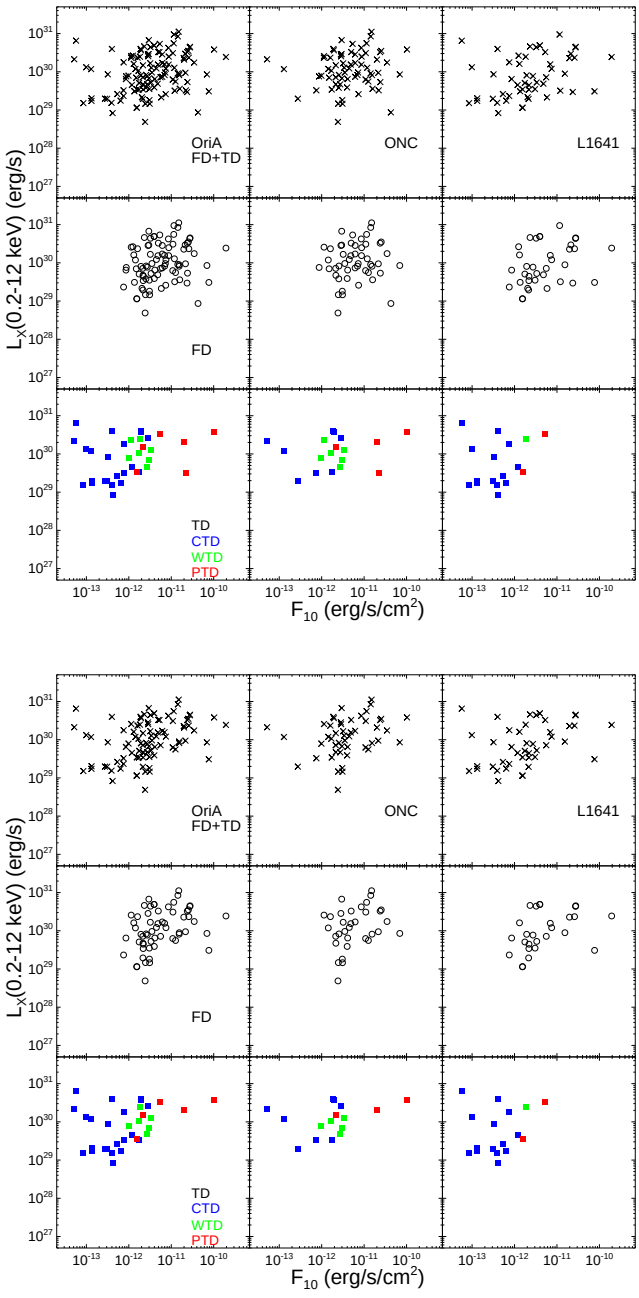


Figure C.116 $\log F_{10}$ vs. $\log L_X 8$. Upper panel: all available objects; Lower panel: objects with available spectral types only

Table C.231 $\log F_{10}$ vs. $\log L_X 8$ (I)

	Ori A				ONC				L1641			
	N	ρ	τ	r	N	ρ	τ	r	N	ρ	τ	r
TDFD	121	0.293	0.207	0.138	68	0.151	0.106	0.086	53	0.390	0.279	0.180
		0.001	0.001	0.131		0.220	0.200	0.486		0.004	0.003	0.197
FD	86	0.280	0.193	0.094	50	0.175	0.122	-0.016	36	0.360	0.263	0.177
		0.009	0.008	0.389		0.224	0.213	0.912		0.031	0.024	0.302
TD	35	0.341	0.257	0.245	18	0.218	0.150	0.295	17	0.228	0.191	0.366
		0.045	0.030	0.156		0.385	0.384	0.235		0.379	0.284	0.149

ρ: Spearsmans ρ
τ: Kendalls τ
r: Pearsons r

Table C.232 $\log F_{10}$ vs. $\log L_X 8$ (II)

	Ori A				ONC				L1641			
	N	ρ	τ	r	N	ρ	τ	r	N	ρ	τ	r
TDFD	93	0.409	0.288	0.193	49	0.309	0.218	0.228	44	0.451	0.331	0.189
		0.000	0.000	0.064		0.031	0.027	0.115		0.002	0.002	0.219
FD	60	0.416	0.284	0.144	33	0.339	0.246	0.162	27	0.523	0.385	0.187
		0.001	0.001	0.272		0.054	0.044	0.368		0.005	0.005	0.350
TD	33	0.375	0.292	0.281	16	0.371	0.267	0.382	17	0.228	0.191	0.366
		0.032	0.017	0.113		0.158	0.150	0.144		0.379	0.284	0.149

ρ: Spearsmans ρ
τ: Kendalls τ
r: Pearsons r

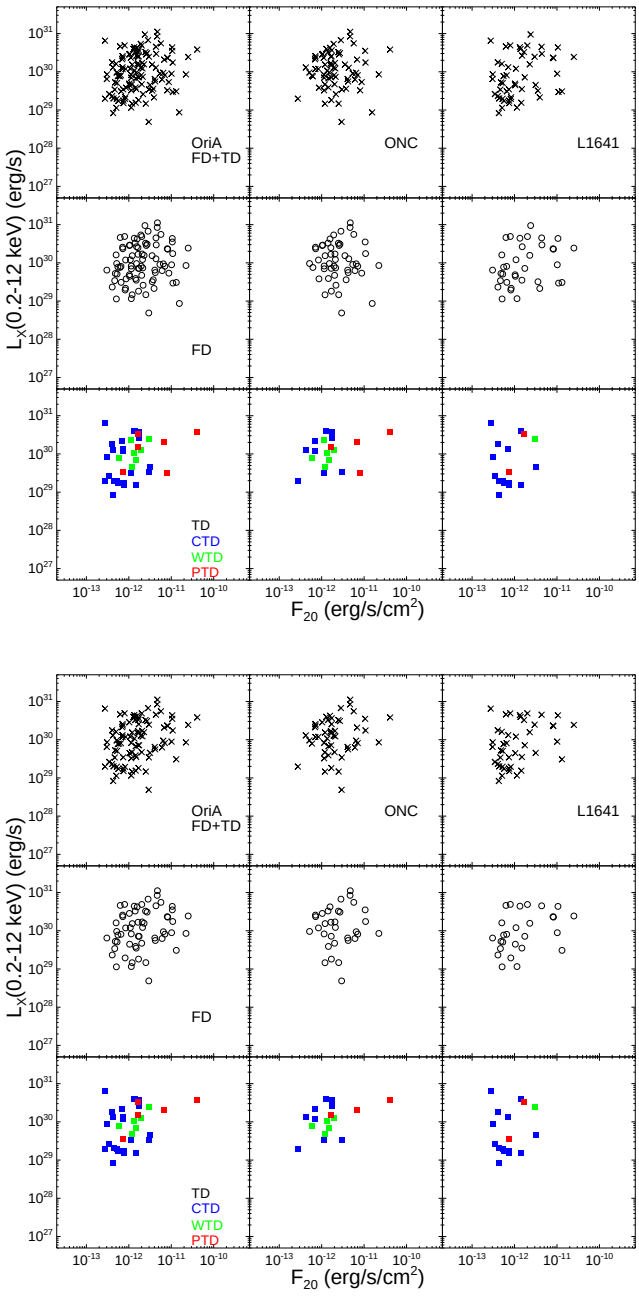


Figure C.117 $\log F_{20}$ vs. $\log L_X 8$. Upper panel: all available objects; Lower panel: objects with available spectral types only

Table C.233 $\log F_{20}$ vs. $\log L_X 8$ (I)

	Ori A				ONC				L1641			
	N	ρ	τ	r	N	ρ	τ	r	N	ρ	τ	r
TDFD	122	0.221	0.151	0.123	69	0.020	0.020	0.051	53	0.278	0.170	0.205
		0.014	0.014	0.177		0.872	0.812	0.677		0.044	0.073	0.141
FD	86	0.171	0.117	0.042	50	-0.023	-0.011	-0.098	36	0.257	0.165	0.188
		0.115	0.110	0.701		0.873	0.913	0.498		0.130	0.157	0.272
TD	36	0.288	0.187	0.241	19	0.223	0.170	0.293	17	0.012	-0.044	0.246
		0.088	0.108	0.157		0.359	0.310	0.223		0.963	0.805	0.341

ρ: Spearsmans ρ
τ: Kendalls τ
r: Pearsons r

Table C.234 $\log F_{20}$ vs. $\log L_X 8$ (II)

	Ori A				ONC				L1641			
	N	ρ	τ	r	N	ρ	τ	r	N	ρ	τ	r
TDFD	94	0.313	0.213	0.217	50	0.161	0.118	0.173	44	0.309	0.190	0.257
		0.002	0.002	0.036		0.265	0.225	0.230		0.041	0.069	0.092
FD	60	0.272	0.186	0.161	33	0.067	0.061	0.063	27	0.384	0.259	0.259
		0.035	0.035	0.219		0.713	0.620	0.728		0.048	0.058	0.192
TD	34	0.321	0.212	0.272	17	0.397	0.294	0.369	17	0.012	-0.044	0.246
		0.064	0.078	0.120		0.115	0.099	0.145		0.963	0.805	0.341

ρ: Spearsmans ρ
τ: Kendalls τ
r: Pearsons r

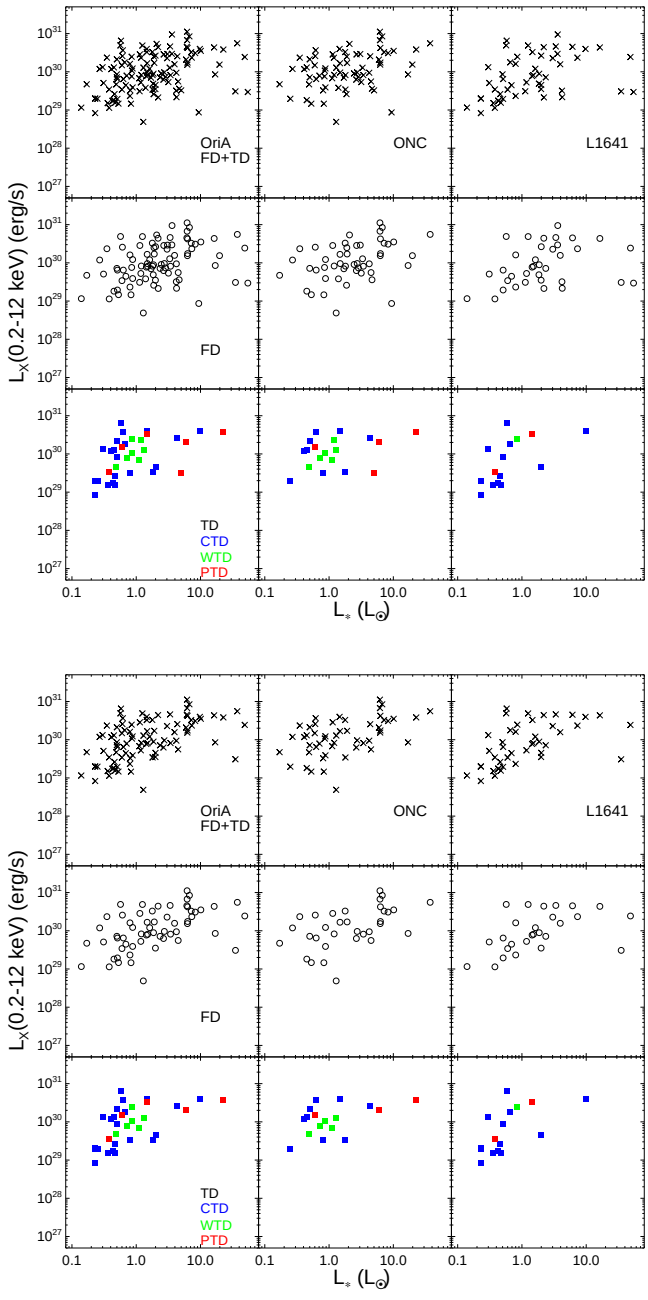


Figure C.118 $\log L_\star$ vs. $\log L_X 8$. Upper panel: all available objects; Lower panel: objects with available spectral types only

Table C.235 $\log L_\star$ vs. $\log L_X 8$ (I)

	Ori A				ONC				L1641			
	N	ρ	τ	r	N	ρ	τ	r	N	ρ	τ	r
TDFD	122	0.421	0.293	0.393	69	0.359	0.242	0.347	53	0.496	0.349	0.413
		0.000	0.000	0.000		0.002	0.003	0.003		0.000	0.000	0.002
FD	86	0.384	0.276	0.343	50	0.417	0.285	0.371	36	0.310	0.238	0.309
		0.000	0.000	0.001		0.003	0.003	0.008		0.065	0.041	0.067
TD	36	0.593	0.418	0.513	19	0.302	0.216	0.331	17	0.687	0.508	0.610
		0.000	0.000	0.001		0.209	0.196	0.166		0.002	0.004	0.009

ρ: Spearsmans ρ
τ: Kendalls τ
r: Pearsons r

Table C.236 $\log L_\star$ vs. $\log L_X 8$ (II)

	Ori A				ONC				L1641			
	N	ρ	τ	r	N	ρ	τ	r	N	ρ	τ	r
TDFD	94	0.554	0.392	0.536	50	0.506	0.351	0.502	44	0.626	0.451	0.545
		0.000	0.000	0.000		0.000	0.000	0.000		0.000	0.000	0.000
FD	60	0.538	0.383	0.510	33	0.567	0.380	0.521	27	0.523	0.403	0.491
		0.000	0.000	0.000		0.001	0.002	0.002		0.005	0.003	0.009
TD	34	0.632	0.450	0.574	17	0.387	0.279	0.485	17	0.687	0.508	0.610
		0.000	0.000	0.000		0.125	0.118	0.048		0.002	0.004	0.009

ρ: Spearsmans ρ
τ: Kendalls τ
r: Pearsons r

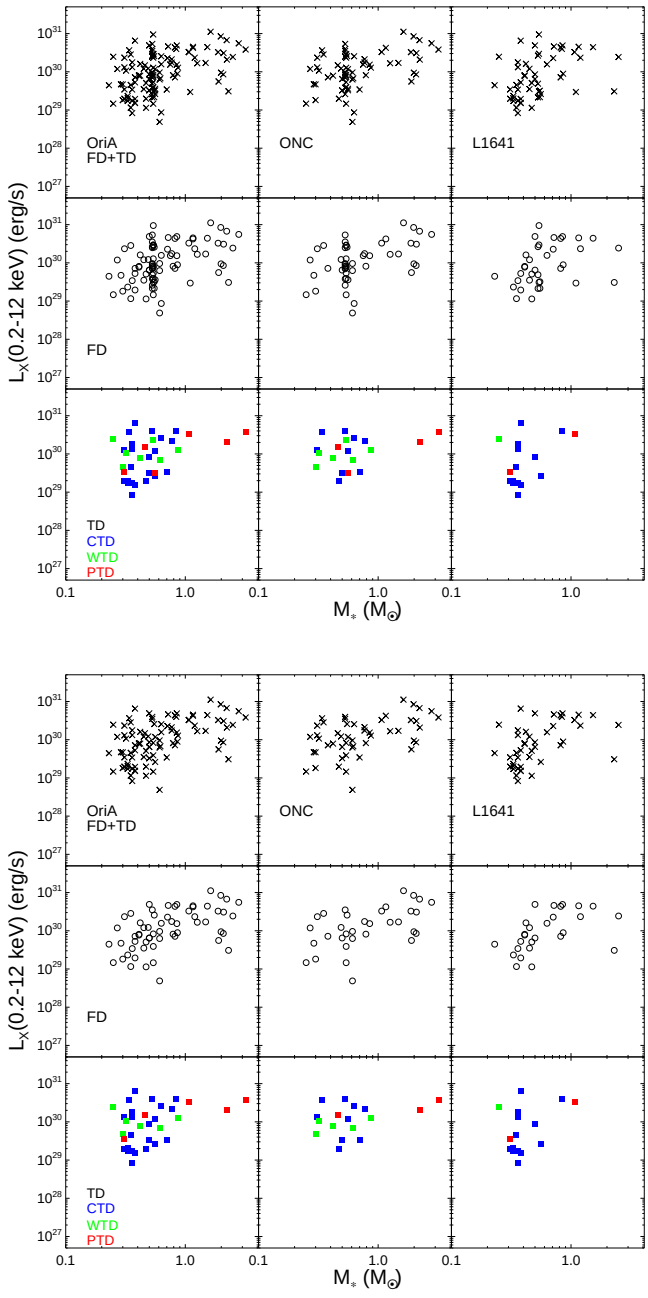


Figure C.119 $\log M_\star$ vs. $\log L_X 8$. Upper panel: all available objects; Lower panel: objects with available spectral types only

Table C.237 $\log M_\star$ vs. $\log L_X 8$ (I)

	Ori A				ONC				L1641			
	N	ρ	τ	r	N	ρ	τ	r	N	ρ	τ	r
TDFD	122	0.416	0.290	0.432	69	0.351	0.241	0.427	53	0.468	0.319	0.413
		0.000	0.000	0.000		0.003	0.003	0.000		0.000	0.001	0.002
FD	86	0.422	0.299	0.435	50	0.385	0.274	0.462	36	0.426	0.300	0.382
		0.000	0.000	0.000		0.006	0.005	0.001		0.010	0.010	0.022
TD	36	0.344	0.240	0.402	19	0.246	0.176	0.329	17	0.239	0.146	0.407
		0.040	0.040	0.015		0.311	0.293	0.169		0.356	0.414	0.105

ρ: Spearsmans ρ
τ: Kendalls τ
r: Pearsons r

Table C.238 $\log M_\star$ vs. $\log L_X 8$ (II)

	Ori A				ONC				L1641			
	N	ρ	τ	r	N	ρ	τ	r	N	ρ	τ	r
TDFD	94	0.503	0.350	0.497	50	0.454	0.312	0.477	44	0.547	0.379	0.490
		0.000	0.000	0.000		0.001	0.001	0.000		0.000	0.000	0.001
FD	60	0.549	0.390	0.521	33	0.500	0.350	0.523	27	0.608	0.445	0.501
		0.000	0.000	0.000		0.003	0.004	0.002		0.001	0.001	0.008
TD	34	0.354	0.242	0.411	17	0.301	0.206	0.354	17	0.239	0.146	0.407
		0.040	0.044	0.016		0.240	0.249	0.163		0.356	0.414	0.105

ρ: Spearsmans ρ
τ: Kendalls τ
r: Pearsons r

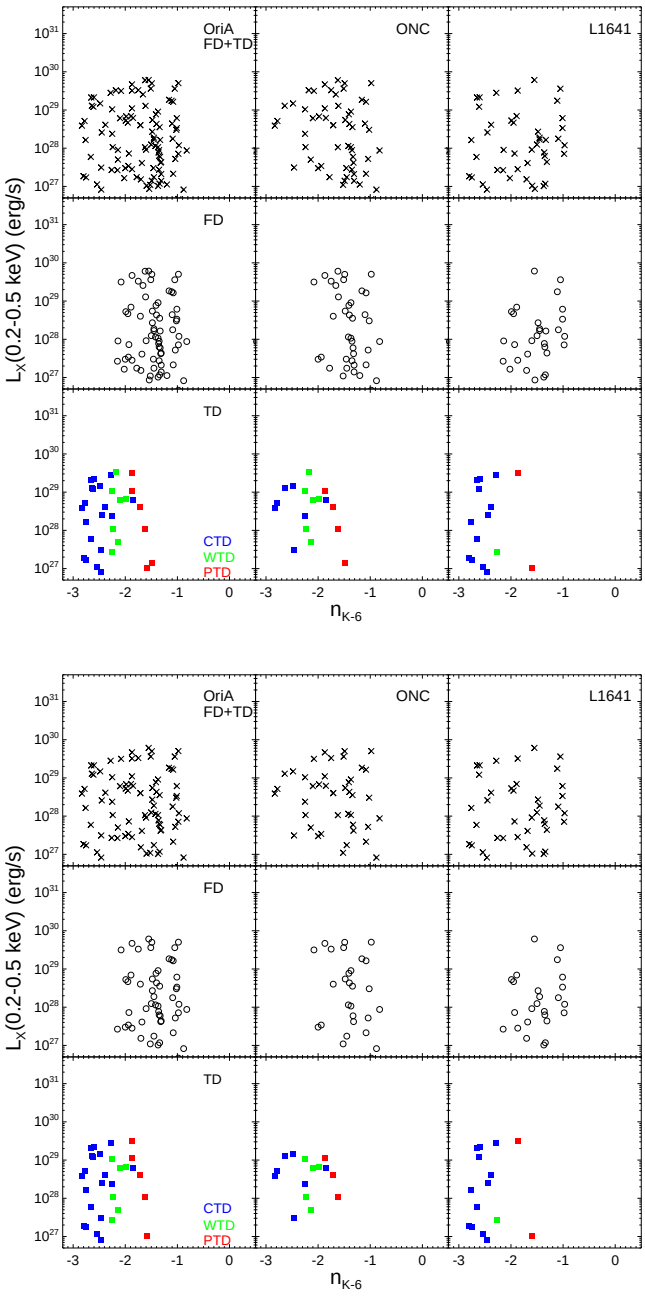


Figure C.120 n_{K-6} vs. $\log L_X 1$. Upper panel: all available objects; Lower panel: objects with available spectral types only

Table C.239 n_{K-6} vs. $\log L_X 1$ (I)

	Ori A				ONC				L1641			
	N	ρ	τ	r	N	ρ	τ	r	N	ρ	τ	r
TDFD	114	-0.154	-0.103	-0.163	62	-0.310	-0.209	-0.264	52	-0.029	-0.014	-0.121
		0.101	0.103	0.083		0.014	0.017	0.038		0.837	0.881	0.393
FD	80	-0.108	-0.078	-0.136	45	-0.211	-0.161	-0.145	35	0.010	0.005	-0.157
		0.342	0.305	0.229		0.164	0.118	0.342		0.957	0.966	0.368
TD	34	0.046	0.029	0.022	17	-0.234	-0.170	-0.302	17	0.051	0.059	0.029
		0.794	0.812	0.902		0.366	0.342	0.239		0.844	0.742	0.912

ρ: Spearsmans ρ
τ: Kendalls τ
r: Pearsons r

Table C.240 n_{K-6} vs. $\log L_X 1$ (II)

	Ori A				ONC				L1641			
	N	ρ	τ	r	N	ρ	τ	r	N	ρ	τ	r
TDFD	89	-0.046	-0.030	-0.045	45	-0.166	-0.117	-0.186	44	0.056	0.046	0.020
		0.672	0.675	0.675		0.277	0.259	0.221		0.720	0.663	0.897
FD	57	-0.043	-0.031	-0.060	30	-0.111	-0.090	-0.105	27	0.041	0.026	-0.023
		0.749	0.730	0.658		0.560	0.485	0.581		0.838	0.851	0.909
TD	32	0.079	0.051	0.097	15	-0.109	-0.077	-0.094	17	0.051	0.059	0.029
		0.667	0.684	0.597		0.699	0.691	0.739		0.844	0.742	0.912

ρ: Spearsmans ρ
τ: Kendalls τ
r: Pearsons r

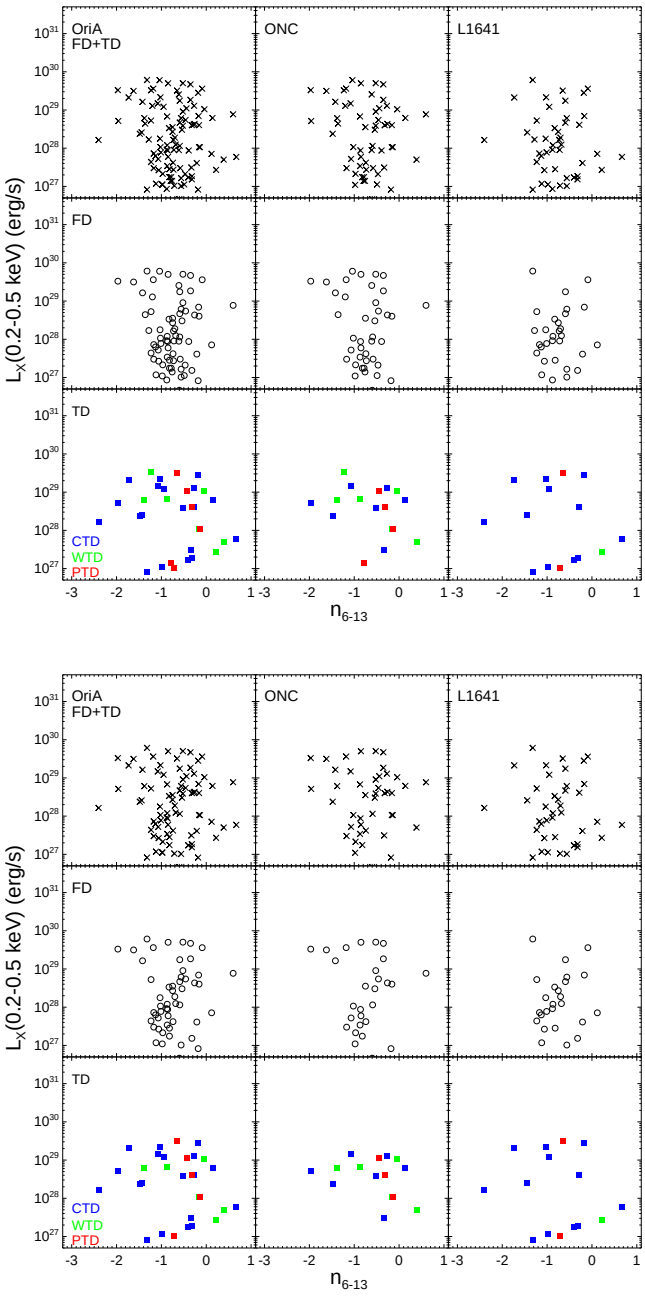


Figure C.121 n_{6-13} vs. $\log L_X 1$. Upper panel: all available objects; Lower panel: objects with available spectral types only

Table C.241 n_{6-13} vs. $\log L_X 1$ (I)

	Ori A				ONC				L1641			
	N	ρ	τ	r	N	ρ	τ	r	N	ρ	τ	r
TDFD	114	-0.081	-0.051	-0.113	62	-0.109	-0.065	-0.148	52	-0.055	-0.017	-0.093
		0.390	0.418	0.231		0.397	0.454	0.251		0.697	0.855	0.512
FD	80	-0.028	-0.015	-0.059	45	-0.118	-0.079	-0.163	35	0.095	0.101	0.102
		0.805	0.841	0.603		0.442	0.444	0.285		0.589	0.391	0.560
TD	34	-0.209	-0.114	-0.247	17	-0.211	-0.147	-0.280	17	-0.164	-0.059	-0.284
		0.236	0.342	0.159		0.417	0.410	0.276		0.529	0.742	0.269

ρ: Spearsmans ρ
τ: Kendalls τ
r: Pearsons r

Table C.242 n_{6-13} vs. $\log L_X 1$ (II)

	Ori A				ONC				L1641			
	N	ρ	τ	r	N	ρ	τ	r	N	ρ	τ	r
TDFD	89	-0.070	-0.044	-0.127	45	-0.030	-0.015	-0.105	44	-0.121	-0.060	-0.167
		0.517	0.541	0.236		0.846	0.883	0.492		0.434	0.563	0.279
FD	57	0.036	0.038	-0.055	30	0.035	0.032	-0.093	27	0.044	0.086	0.005
		0.789	0.678	0.684		0.854	0.802	0.625		0.826	0.530	0.980
TD	32	-0.197	-0.103	-0.234	15	-0.200	-0.143	-0.313	17	-0.164	-0.059	-0.284
		0.279	0.408	0.197		0.475	0.458	0.256		0.529	0.742	0.269

ρ: Spearsmans ρ
τ: Kendalls τ
r: Pearsons r

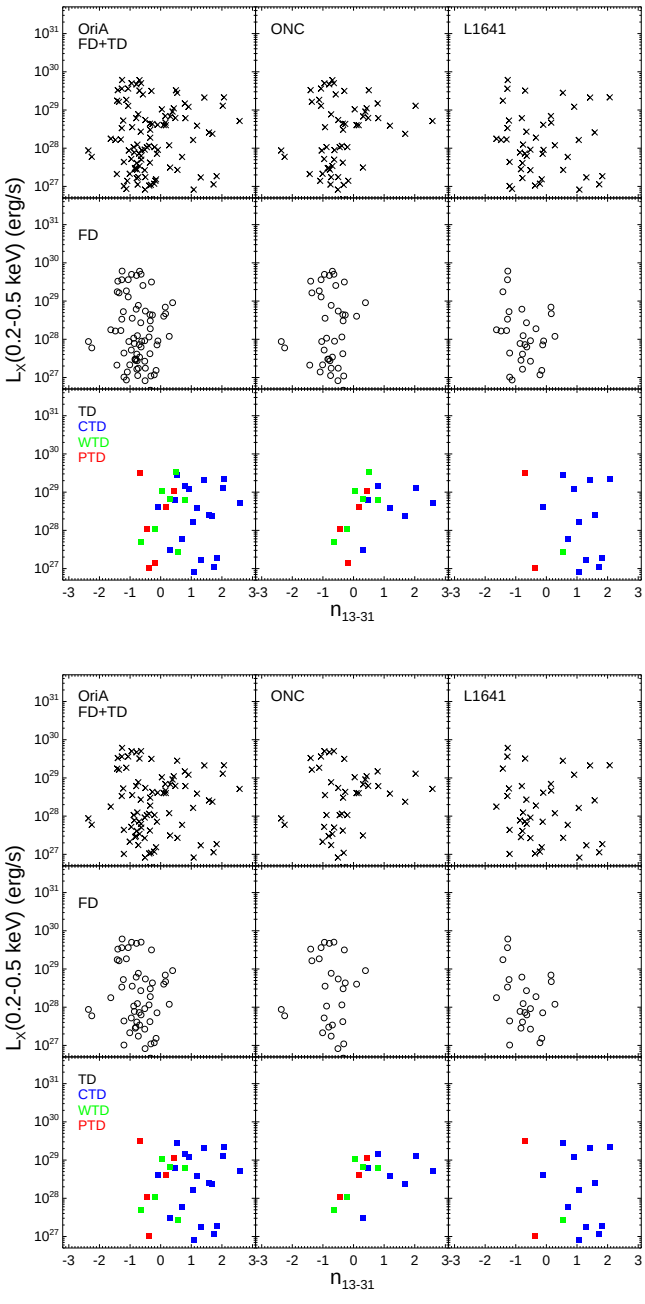


Figure C.122 n_{13-31} vs. $\log L_X 1$. Upper panel: all available objects; Lower panel: objects with available spectral types only

Table C.243 n_{13-31} vs. $\log L_X 1$ (I)

	Ori A				ONC				L1641			
	N	ρ	τ	r	N	ρ	τ	r	N	ρ	τ	r
TDFD	114	0.068	0.056	0.119	62	0.157	0.113	0.247	52	-0.047	-0.023	0.016
		0.470	0.376	0.207		0.222	0.193	0.053		0.742	0.812	0.910
FD	80	-0.052	-0.027	-0.002	45	-0.039	-0.033	0.065	35	-0.138	-0.073	-0.104
		0.647	0.720	0.986		0.801	0.746	0.671		0.430	0.539	0.552
TD	34	0.063	0.055	0.087	17	0.495	0.309	0.437	17	-0.039	0.000	-0.024
		0.724	0.646	0.625		0.043	0.084	0.079		0.881	1.000	0.927

ρ: Spearsmans ρ
τ: Kendalls τ
r: Pearsons r

Table C.244 n_{13-31} vs. $\log L_X 1$ (II)

	Ori A				ONC				L1641			
	N	ρ	τ	r	N	ρ	τ	r	N	ρ	τ	r
TDFD	89	-0.045	-0.015	0.003	45	0.049	0.049	0.131	44	-0.147	-0.091	-0.082
		0.673	0.831	0.978		0.750	0.638	0.391		0.341	0.383	0.597
FD	57	-0.191	-0.116	-0.149	30	-0.211	-0.138	-0.125	27	-0.215	-0.135	-0.185
		0.155	0.204	0.269		0.262	0.284	0.510		0.282	0.324	0.356
TD	32	0.038	0.040	0.065	15	0.436	0.276	0.448	17	-0.039	0.000	-0.024
		0.837	0.746	0.724		0.104	0.151	0.094		0.881	1.000	0.927

ρ: Spearsmans ρ
τ: Kendalls τ
r: Pearsons r

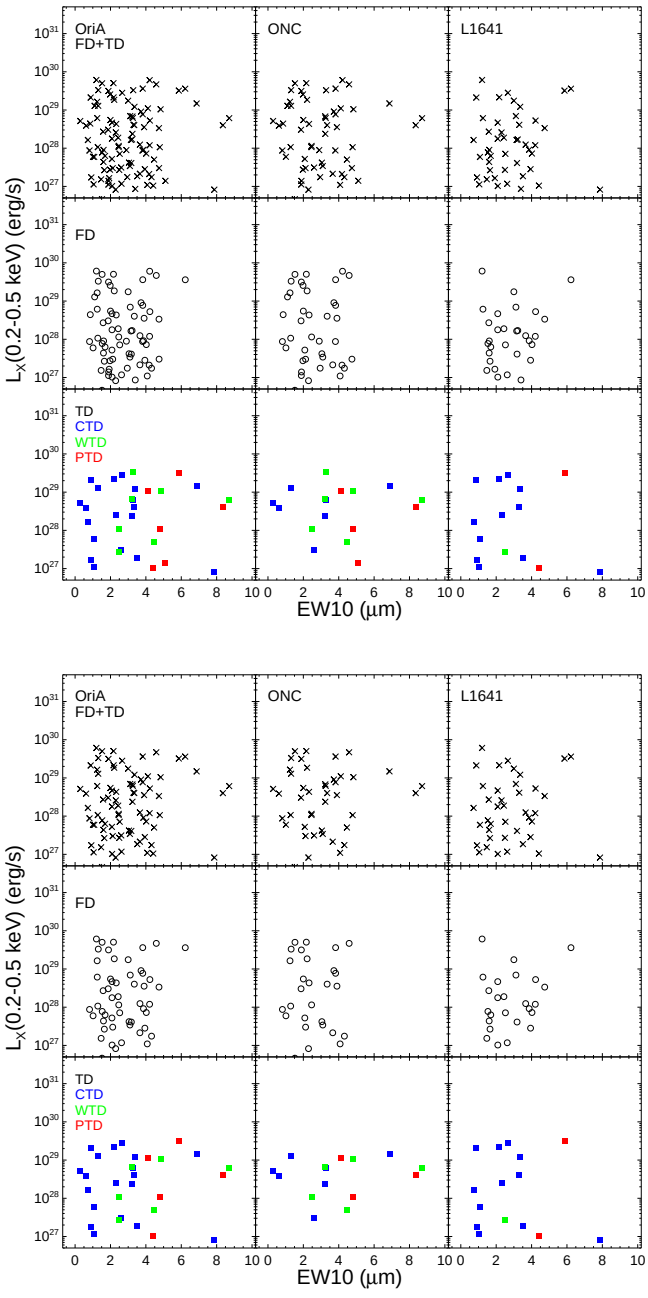


Figure C.123 EW10 vs. $\log L_X 1$. Upper panel: all available objects; Lower panel: objects with available spectral types only

Table C.245 EW10 vs. $\log L_X 1$ (I)

	Ori A				ONC				L1641			
	N	ρ	τ	r	N	ρ	τ	r	N	ρ	τ	r
TDFD	114	0.064	0.043	0.081	62	0.049	0.048	0.108	52	0.057	0.038	0.038
		0.500	0.502	0.392		0.707	0.584	0.403		0.687	0.693	0.789
FD	80	0.090	0.060	0.145	45	0.008	0.013	0.046	35	0.203	0.129	0.299
		0.429	0.432	0.199		0.959	0.899	0.764		0.241	0.274	0.081
TD	34	-0.087	-0.061	-0.078	17	0.052	0.022	0.011	17	-0.311	-0.191	-0.257
		0.624	0.614	0.661		0.844	0.901	0.967		0.224	0.284	0.319

ρ: Spearsmans ρ
τ: Kendalls τ
r: Pearsons r

Table C.246 EW10 vs. $\log L_X 1$ (II)

	Ori A				ONC				L1641			
	N	ρ	τ	r	N	ρ	τ	r	N	ρ	τ	r
TDFD	89	0.032	0.016	0.043	45	0.016	0.023	0.090	44	0.029	0.025	-0.018
		0.766	0.829	0.689		0.915	0.822	0.557		0.852	0.808	0.908
FD	57	0.038	0.021	0.123	30	-0.081	-0.060	-0.016	27	0.200	0.151	0.301
		0.777	0.820	0.362		0.671	0.642	0.933		0.318	0.269	0.127
TD	32	-0.049	-0.034	-0.051	15	0.175	0.115	0.137	17	-0.311	-0.191	-0.257
		0.788	0.783	0.782		0.532	0.551	0.626		0.224	0.284	0.319

ρ: Spearsmans ρ
τ: Kendalls τ
r: Pearsons r

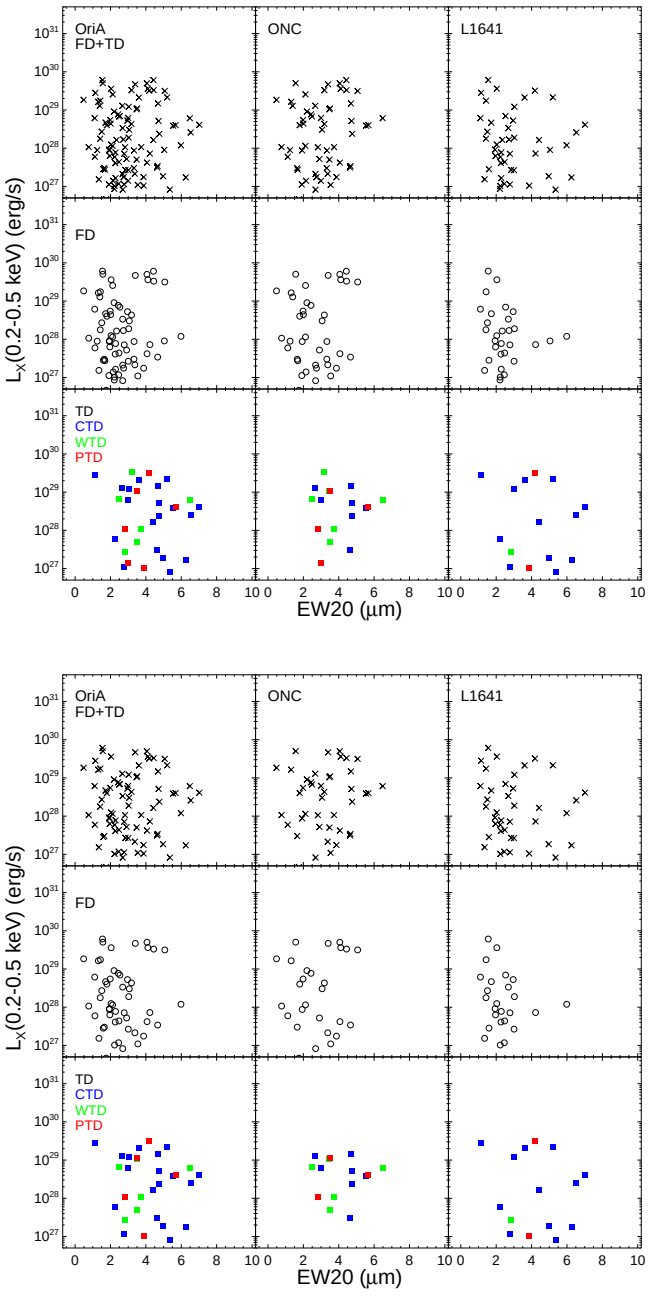


Figure C.124 EW20 vs. $\log L_X 1$. Upper panel: all available objects; Lower panel: objects with available spectral types only

Table C.247 EW20 vs. $\log L_X 1$ (I)

	Ori A				ONC				L1641			
	N	ρ	τ	r	N	ρ	τ	r	N	ρ	τ	r
TDFD	114	0.035	0.024	0.034	62	0.118	0.080	0.068	52	-0.073	-0.041	-0.045
		0.714	0.702	0.720		0.360	0.359	0.599		0.609	0.664	0.751
FD	80	-0.015	-0.010	0.014	45	0.048	0.020	0.019	35	-0.087	-0.035	-0.076
		0.893	0.894	0.902		0.752	0.845	0.901		0.621	0.766	0.664
TD	34	-0.143	-0.080	-0.114	17	-0.130	-0.044	0.032	17	-0.132	-0.074	-0.143
		0.420	0.505	0.521		0.619	0.805	0.903		0.613	0.680	0.584

ρ: Spearsmans ρ
τ: Kendalls τ
r: Pearsons r

Table C.248 EW20 vs. $\log L_X 1$ (II)

	Ori A				ONC				L1641			
	N	ρ	τ	r	N	ρ	τ	r	N	ρ	τ	r
TDFD	89	-0.053	-0.040	-0.049	45	-0.044	-0.034	-0.061	44	-0.132	-0.086	-0.101
		0.620	0.583	0.648		0.774	0.739	0.691		0.392	0.412	0.514
FD	57	-0.085	-0.066	-0.054	30	-0.079	-0.076	-0.100	27	-0.108	-0.054	-0.066
		0.530	0.466	0.690		0.678	0.556	0.599		0.592	0.692	0.744
TD	32	-0.163	-0.089	-0.124	15	-0.211	-0.086	-0.027	17	-0.132	-0.074	-0.143
		0.371	0.476	0.499		0.451	0.656	0.924		0.613	0.680	0.584

ρ: Spearsmans ρ
τ: Kendalls τ
r: Pearsons r

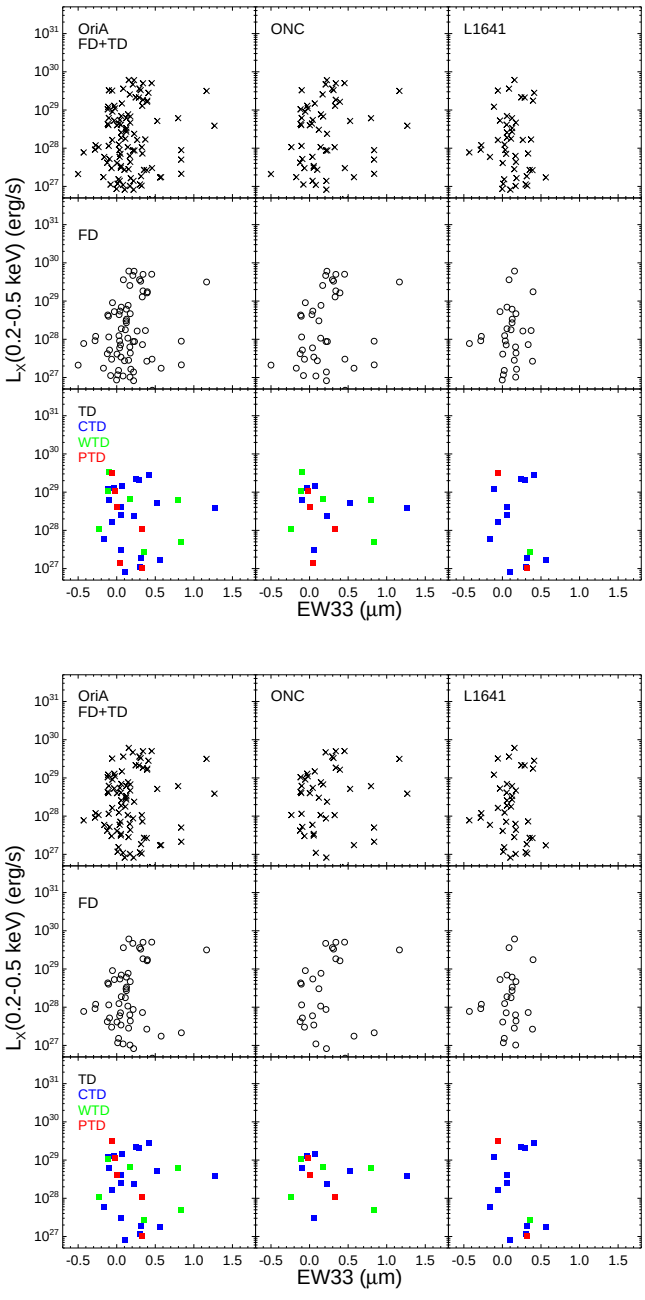


Figure C.125 EW33 vs. $\log L_X 1$. Upper panel: all available objects; Lower panel: objects with available spectral types only

Table C.249 EW33 vs. $\log L_X 1$ (I)

	Ori A				ONC				L1641			
	N	ρ	τ	r	N	ρ	τ	r	N	ρ	τ	r
TDFD	114	0.023	0.017	-0.161	62	0.027	0.023	-0.251	52	-0.016	0.005	0.007
		0.811	0.789	0.087		0.835	0.794	0.049		0.910	0.956	0.961
FD	80	0.088	0.061	-0.182	45	0.070	0.059	-0.257	35	0.052	0.042	0.036
		0.439	0.422	0.106		0.649	0.570	0.088		0.766	0.722	0.837
TD	34	-0.154	-0.089	-0.055	17	-0.355	-0.235	-0.144	17	-0.043	-0.007	-0.062
		0.385	0.458	0.757		0.162	0.187	0.581		0.870	0.967	0.813

ρ: Spearsmans ρ
τ: Kendalls τ
r: Pearsons r

Table C.250 EW33 vs. $\log L_X 1$ (II)

	Ori A				ONC				L1641			
	N	ρ	τ	r	N	ρ	τ	r	N	ρ	τ	r
TDFD	89	0.011	0.011	0.017	45	0.018	0.019	-0.009	44	-0.048	-0.005	0.002
		0.916	0.876	0.874		0.907	0.852	0.953		0.759	0.960	0.990
FD	57	0.070	0.050	0.033	30	0.039	0.039	0.008	27	0.054	0.066	0.072
		0.605	0.582	0.807		0.838	0.762	0.967		0.790	0.631	0.721
TD	32	-0.129	-0.067	-0.037	15	-0.354	-0.238	-0.179	17	-0.043	-0.007	-0.062
		0.483	0.592	0.841		0.196	0.216	0.523		0.870	0.967	0.813

ρ: Spearsmans ρ
τ: Kendalls τ
r: Pearsons r

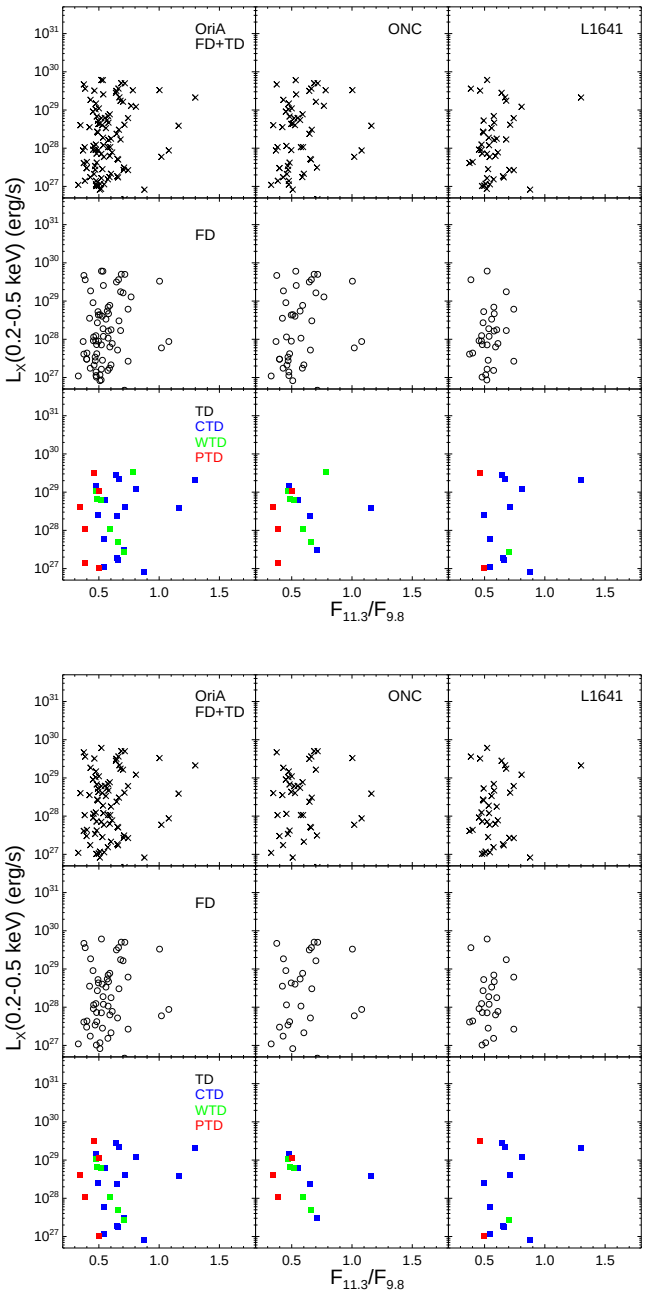


Figure C.126 $F_{11.3}/F_{9.8}$ vs. $\log L_X 1$. Upper panel: all available objects; Lower panel: objects with available spectral types only

Table C.251 $F_{11.3}/F_{9.8}$ vs. $\log L_X 1$ (I)

	Ori A				ONC				L1641			
	N	ρ	τ	r	N	ρ	τ	r	N	ρ	τ	r
TDFD	114	0.153	0.100	0.033	62	0.178	0.118	0.050	52	0.190	0.137	0.062
		0.104	0.113	0.727		0.165	0.176	0.700		0.177	0.151	0.662
FD	80	0.201	0.141	0.007	45	0.173	0.121	-0.059	35	0.273	0.200	0.187
		0.073	0.065	0.951		0.255	0.240	0.700		0.112	0.091	0.282
TD	34	0.032	0.005	0.022	17	0.091	0.015	0.184	17	0.105	0.059	0.069
		0.858	0.965	0.902		0.729	0.934	0.480		0.687	0.742	0.792

ρ: Spearsmans ρ
τ: Kendalls τ
r: Pearsons r

Table C.252 $F_{11.3}/F_{9.8}$ vs. $\log L_X 1$ (II)

	Ori A				ONC				L1641			
	N	ρ	τ	r	N	ρ	τ	r	N	ρ	τ	r
TDFD	89	0.036	0.020	0.024	45	0.033	0.014	0.088	44	0.065	0.053	0.043
		0.736	0.782	0.823		0.829	0.891	0.565		0.674	0.613	0.782
FD	57	0.100	0.080	0.094	30	0.100	0.080	0.083	27	0.126	0.111	0.052
		0.459	0.378	0.487		0.599	0.532	0.663		0.530	0.416	0.797
TD	32	-0.089	-0.069	0.020	15	-0.218	-0.181	0.181	17	0.105	0.059	0.069
		0.629	0.581	0.913		0.435	0.347	0.519		0.687	0.742	0.792

ρ: Spearsmans ρ
τ: Kendalls τ
r: Pearsons r

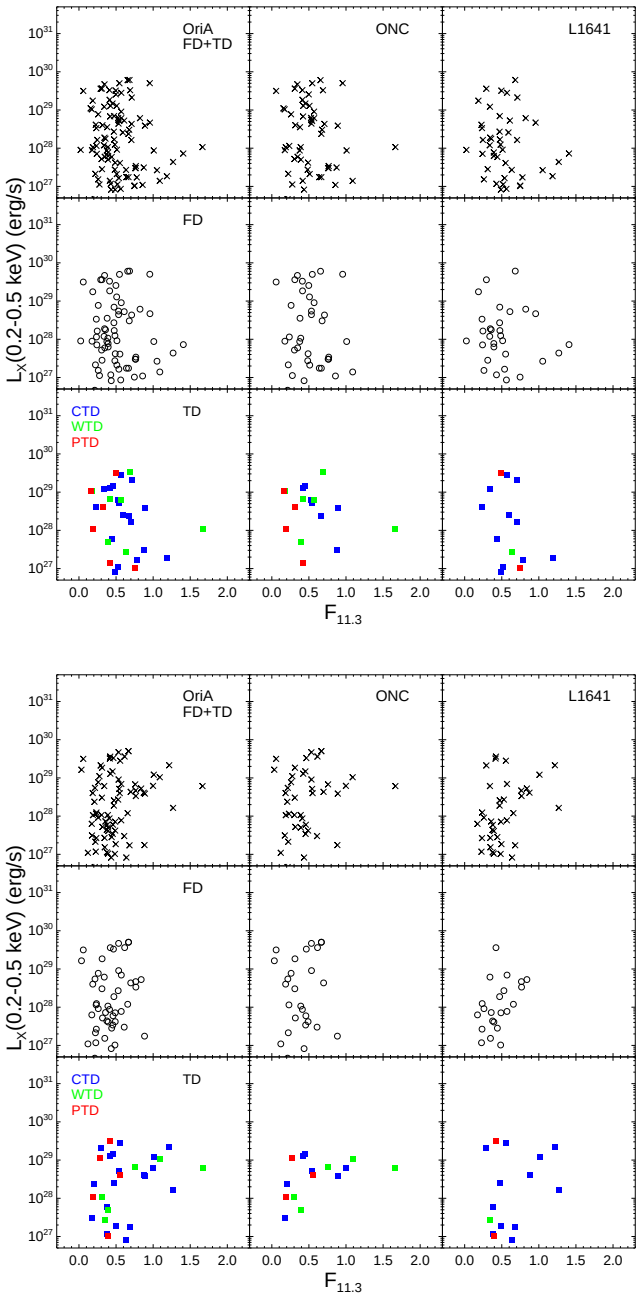


Figure C.127 $F_{11.3}$ vs. $\log L_X 1$. Upper panel: all available objects; Lower panel: objects with available spectral types only

Table C.253 $F_{11.3}$ vs. $\log L_X1$ (I)

	Ori A				ONC				L1641			
	N	ρ	τ	r	N	ρ	τ	r	N	ρ	τ	r
TDFD	114	0.150	0.100	0.096	62	0.151	0.094	0.173	52	0.142	0.108	0.016
		0.111	0.116	0.310		0.242	0.279	0.179		0.317	0.259	0.910
FD	80	0.154	0.097	0.185	45	0.068	0.032	0.085	35	0.261	0.185	0.324
		0.172	0.202	0.100		0.658	0.754	0.579		0.130	0.117	0.058
TD	34	0.016	0.012	-0.095	17	0.206	0.118	0.126	17	-0.169	-0.059	-0.271
		0.927	0.917	0.593		0.428	0.510	0.630		0.516	0.742	0.293

ρ: Spearsmans ρ
τ: Kendalls τ
r: Pearsons r

Table C.254 $F_{11.3}$ vs. $\log L_X1$ (II)

	Ori A				ONC				L1641			
	N	ρ	τ	r	N	ρ	τ	r	N	ρ	τ	r
TDFD	89	0.091	0.062	0.016	45	0.070	0.047	0.106	44	0.095	0.079	-0.067
		0.398	0.387	0.882		0.649	0.652	0.488		0.540	0.448	0.666
FD	57	0.103	0.061	0.129	30	-0.035	-0.032	-0.020	27	0.246	0.183	0.296
		0.444	0.504	0.339		0.853	0.803	0.916		0.217	0.182	0.134
TD	32	0.001	0.012	-0.108	15	0.236	0.143	0.148	17	-0.169	-0.059	-0.271
		0.995	0.922	0.556		0.398	0.458	0.599		0.516	0.742	0.293

ρ: Spearsmans ρ
τ: Kendalls τ
r: Pearsons r

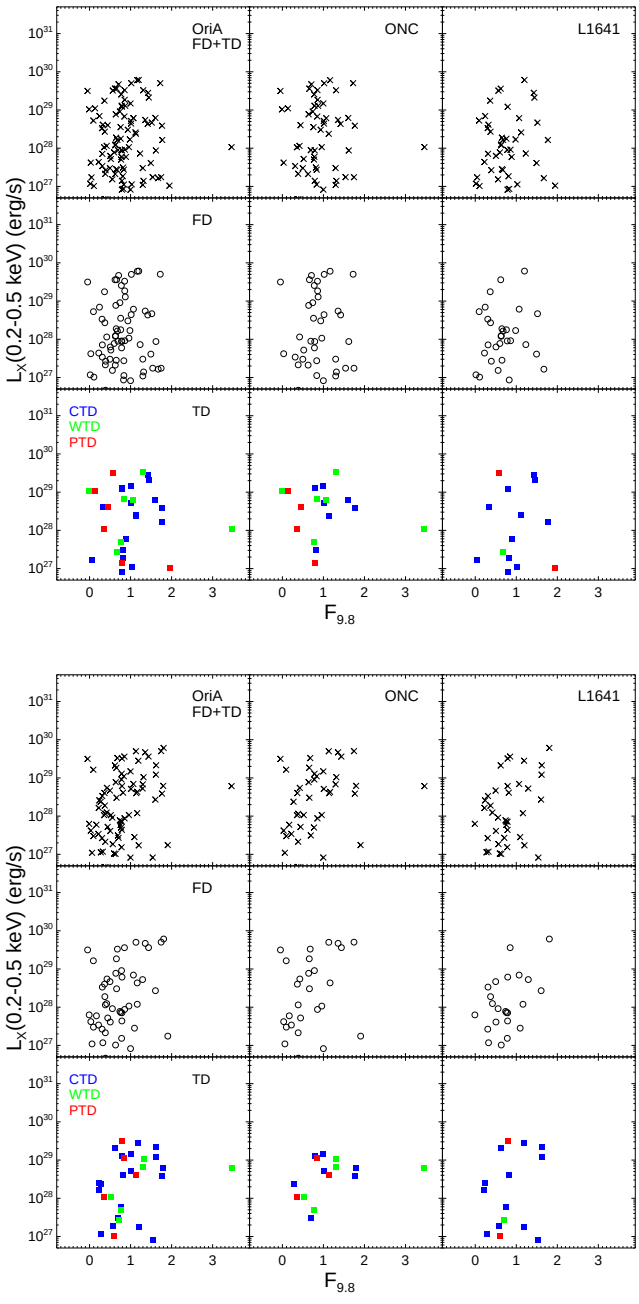


Figure C.128 $F_{9.8}$ vs. $\log L_X 1$. Upper panel: all available objects; Lower panel: objects with available spectral types only

Table C.255 $F_{9.8}$ vs. $\log L_X 1$ (I)

	Ori A				ONC				L1641			
	N	ρ	τ	r	N	ρ	τ	r	N	ρ	τ	r
TDFD	114	0.039	0.025	0.070	62	0.032	0.031	0.091	52	0.039	0.027	0.015
		0.682	0.690	0.459		0.806	0.725	0.482		0.785	0.776	0.916
FD	80	0.076	0.052	0.117	45	0.006	0.006	0.032	35	0.213	0.150	0.253
		0.500	0.498	0.301		0.971	0.953	0.835		0.220	0.206	0.143
TD	34	-0.086	-0.062	-0.060	17	0.051	0.000	-0.014	17	-0.321	-0.221	-0.279
		0.627	0.604	0.736		0.844	1.000	0.957		0.209	0.217	0.278

ρ: Spearsmans ρ
τ: Kendalls τ
r: Pearsons r

Table C.256 $F_{9.8}$ vs. $\log L_X 1$ (II)

	Ori A				ONC				L1641			
	N	ρ	τ	r	N	ρ	τ	r	N	ρ	τ	r
TDFD	89	0.004	0.001	0.037	45	-0.001	0.011	0.070	44	-0.001	0.002	-0.030
		0.968	0.992	0.731		0.995	0.914	0.648		0.993	0.984	0.847
FD	57	0.026	0.020	0.083	30	-0.083	-0.057	-0.055	27	0.194	0.151	0.263
		0.847	0.826	0.539		0.665	0.656	0.773		0.332	0.269	0.185
TD	32	-0.049	-0.036	-0.024	15	0.196	0.105	0.130	17	-0.321	-0.221	-0.279
		0.791	0.770	0.896		0.483	0.586	0.644		0.209	0.217	0.278

ρ: Spearsmans ρ
τ: Kendalls τ
r: Pearsons r

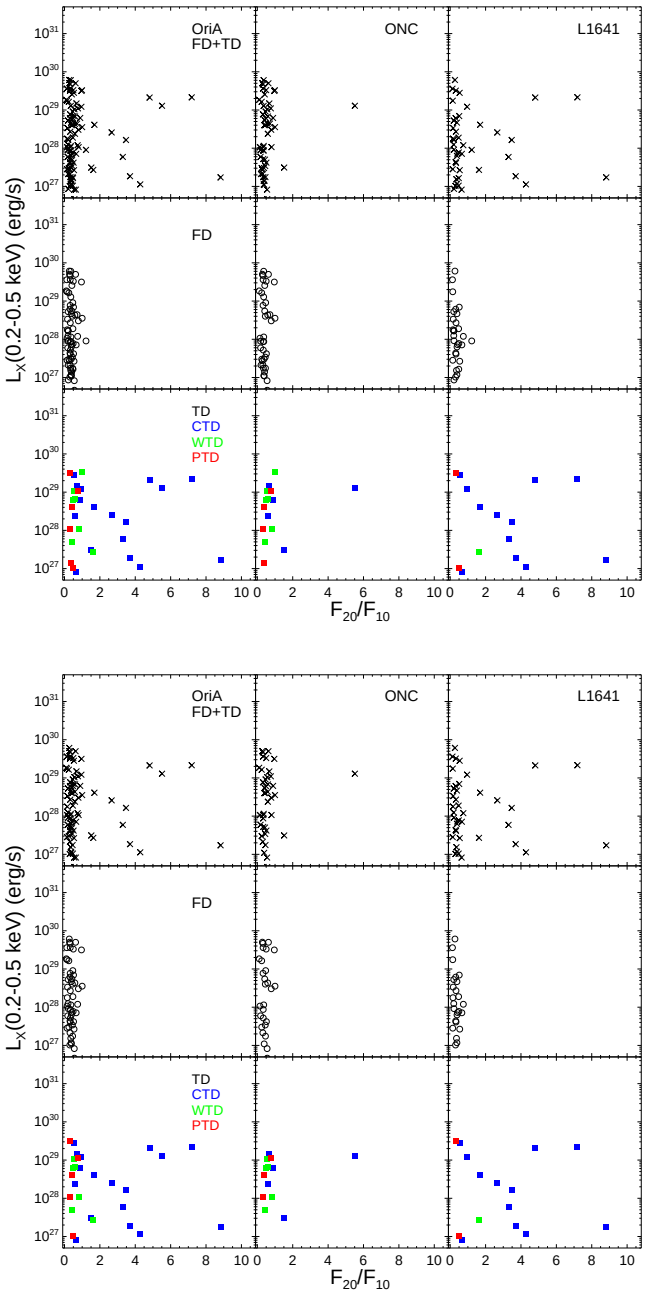


Figure C.129 F_{20}/F_{10} vs. $\log L_X 1$. Upper panel: all available objects; Lower panel: objects with available spectral types only

Table C.257 F_{20}/F_{10} vs. $\log L_X 1$ (I)

	Ori A				ONC				L1641			
	N	ρ	τ	r	N	ρ	τ	r	N	ρ	τ	r
TDFD	113	-0.036	-0.029	0.059	61	0.072	0.043	0.090	52	-0.165	-0.109	0.059
		0.704	0.652	0.535		0.582	0.627	0.490		0.243	0.256	0.678
FD	80	-0.157	-0.115	-0.144	45	-0.101	-0.091	-0.123	35	-0.359	-0.234	-0.240
		0.164	0.130	0.203		0.509	0.379	0.421		0.034	0.048	0.165
TD	33	-0.051	-0.030	0.028	16	0.385	0.300	0.118	17	0.017	-0.015	0.066
		0.776	0.804	0.877		0.141	0.105	0.663		0.948	0.934	0.801

ρ: Spearsmans ρ
τ: Kendalls τ
r: Pearsons r

Table C.258 F_{20}/F_{10} vs. $\log L_X 1$ (II)

	Ori A				ONC				L1641			
	N	ρ	τ	r	N	ρ	τ	r	N	ρ	τ	r
TDFD	88	-0.122	-0.080	0.018	44	-0.059	-0.040	0.059	44	-0.204	-0.137	0.008
		0.259	0.267	0.868		0.705	0.701	0.704		0.185	0.189	0.959
FD	57	-0.217	-0.154	-0.208	30	-0.239	-0.195	-0.256	27	-0.327	-0.214	-0.271
		0.104	0.090	0.121		0.204	0.129	0.172		0.096	0.118	0.172
TD	31	-0.109	-0.075	0.025	14	0.204	0.165	0.111	17	0.017	-0.015	0.066
		0.558	0.552	0.894		0.483	0.412	0.706		0.948	0.934	0.801

ρ: Spearsmans ρ
τ: Kendalls τ
r: Pearsons r

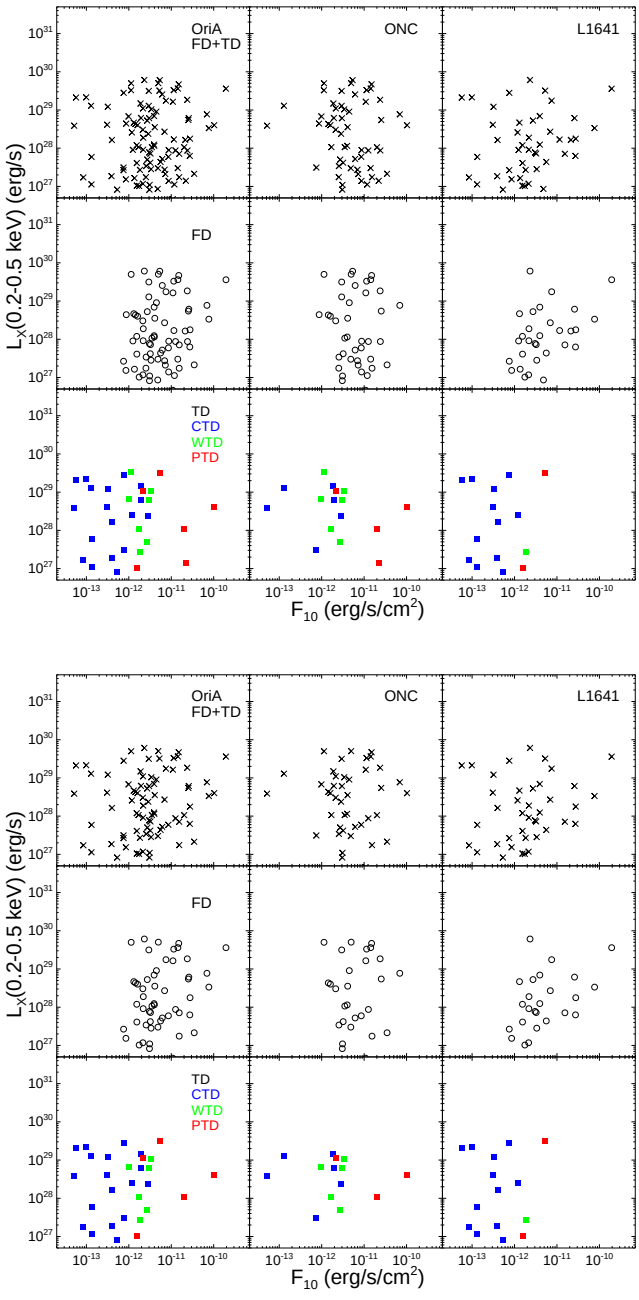


Figure C.130 $\log F_{10}$ vs. $\log L_X 1$. Upper panel: all available objects; Lower panel: objects with available spectral types only

Table C.259 $\log F_{10}$ vs. $\log L_X1$ (I)

	Ori A				ONC				L1641			
	N	ρ	τ	r	N	ρ	τ	r	N	ρ	τ	r
TDFD	113	0.007	0.010	0.143	61	-0.113	-0.067	0.032	52	0.072	0.055	0.233
		0.941	0.876	0.131		0.387	0.448	0.807		0.612	0.564	0.096
FD	80	0.080	0.059	0.197	45	0.052	0.044	0.098	35	0.190	0.129	0.323
		0.483	0.440	0.080		0.733	0.667	0.522		0.275	0.274	0.058
TD	33	0.051	0.034	0.038	16	-0.294	-0.217	-0.111	17	-0.064	-0.044	0.251
		0.776	0.780	0.834		0.269	0.242	0.682		0.808	0.805	0.331

ρ: Spearsmans ρ
τ: Kendalls τ
r: Pearsons r

Table C.260 $\log F_{10}$ vs. $\log L_X1$

	Ori A				ONC				L1641			
	N	ρ	τ	r	N	ρ	τ	r	N	ρ	τ	r
TDFD	88	0.146	0.104	0.191	44	0.015	0.017	0.086	44	0.206	0.149	0.264
		0.175	0.152	0.075		0.925	0.871	0.579		0.180	0.154	0.083
FD	57	0.219	0.155	0.243	30	0.181	0.140	0.159	27	0.376	0.254	0.368
		0.102	0.088	0.069		0.338	0.276	0.401		0.053	0.064	0.059
TD	31	0.106	0.075	0.087	14	-0.108	-0.077	-0.016	17	-0.064	-0.044	0.251
		0.570	0.552	0.642		0.714	0.702	0.957		0.808	0.805	0.331

ρ: Spearsmans ρ
τ: Kendalls τ
r: Pearsons r

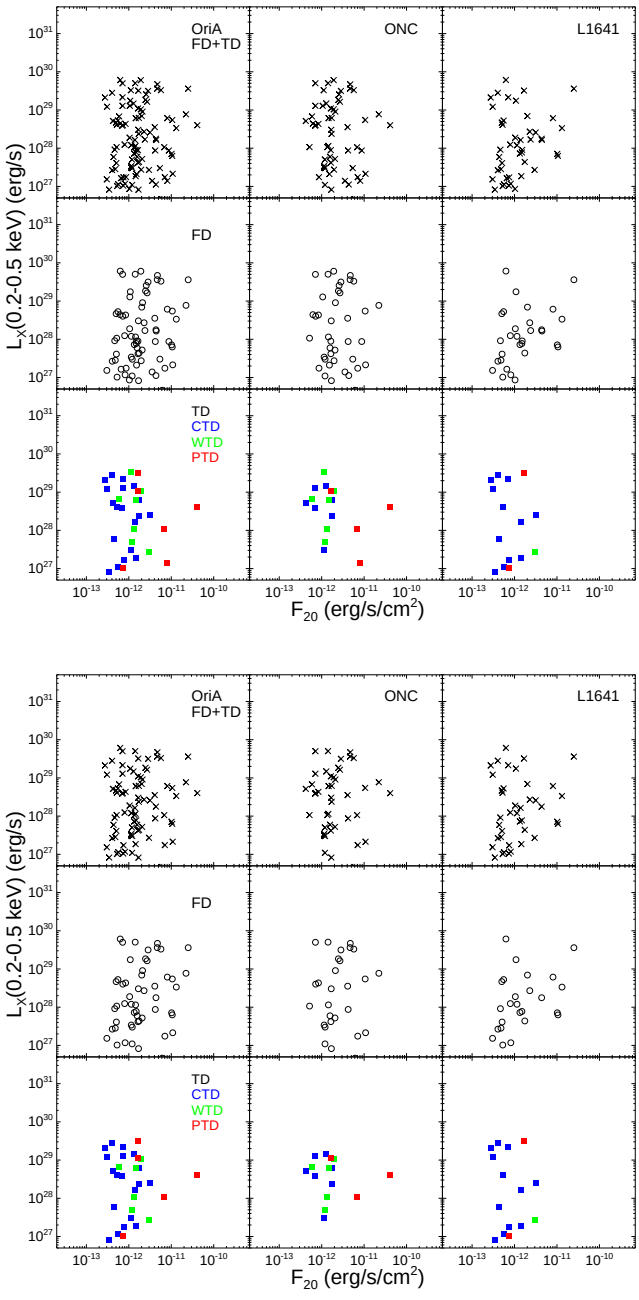


Figure C.131 $\log F_{20}$ vs. $\log L_X 1$. Upper panel: all available objects; Lower panel: objects with available spectral types only

Table C.261 $\log F_{20}$ vs. $\log L_X 1$ (I)

	Ori A				ONC				L1641			
	N	ρ	τ	r	N	ρ	τ	r	N	ρ	τ	r
TDFD	114	-0.015	-0.004	0.060	62	-0.138	-0.078	0.016	52	0.026	0.030	0.098
		0.873	0.947	0.526		0.286	0.372	0.902		0.856	0.752	0.489
FD	80	0.023	0.016	0.100	45	-0.047	-0.024	0.057	35	0.102	0.072	0.157
		0.842	0.829	0.377		0.758	0.814	0.710		0.559	0.541	0.368
TD	34	-0.052	-0.016	0.032	17	-0.267	-0.162	-0.092	17	-0.034	0.015	0.024
		0.770	0.894	0.857		0.300	0.365	0.725		0.896	0.934	0.927

ρ: Spearsmans ρ
τ: Kendalls τ
r: Pearsons r

Table C.262 $\log F_{20}$ vs. $\log L_X 1$ (II)

	Ori A				ONC				L1641			
	N	ρ	τ	r	N	ρ	τ	r	N	ρ	τ	r
TDFD	89	0.102	0.079	0.115	45	-0.022	0.002	0.036	44	0.137	0.108	0.186
		0.340	0.272	0.283		0.885	0.984	0.814		0.374	0.302	0.227
FD	57	0.148	0.108	0.162	30	0.002	0.021	0.070	27	0.289	0.197	0.261
		0.273	0.236	0.229		0.992	0.872	0.713		0.143	0.150	0.189
TD	32	-0.013	0.024	0.073	15	-0.046	-0.010	-0.011	17	-0.034	0.015	0.024
		0.943	0.846	0.691		0.869	0.961	0.969		0.896	0.934	0.927

ρ: Spearsmans ρ
τ: Kendalls τ
r: Pearsons r

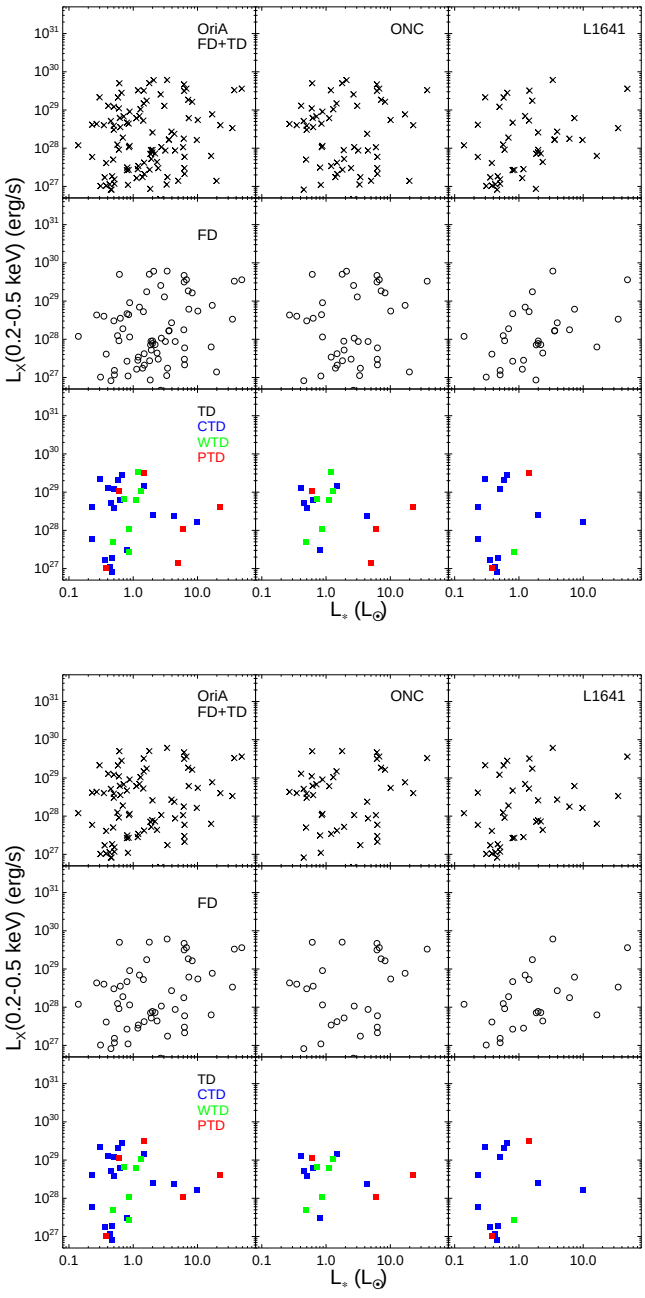


Figure C.132 $\log L_\star$ vs. $\log L_X 1$. Upper panel: all available objects; Lower panel: objects with available spectral types only

Table C.263 $\log L_\star$ vs. $\log L_X 1$ (I)

	Ori A				ONC				L1641			
	N	ρ	τ	r	N	ρ	τ	r	N	ρ	τ	r
TDFD	114	0.102	0.075	0.099	62	0.017	0.003	0.032	52	0.169	0.135	0.119
		0.282	0.239	0.295		0.896	0.976	0.805		0.231	0.159	0.401
FD	80	0.159	0.109	0.154	45	0.169	0.091	0.165	35	0.168	0.143	0.132
		0.160	0.153	0.173		0.268	0.378	0.279		0.335	0.227	0.450
TD	34	0.254	0.174	0.165	17	-0.186	-0.118	-0.246	17	0.400	0.299	0.280
		0.148	0.148	0.351		0.474	0.510	0.341		0.112	0.094	0.276

ρ: Spearsmans ρ
τ: Kendalls τ
r: Pearsons r

Table C.264 $\log L_\star$ vs. $\log L_X 1$ (II)

	Ori A				ONC				L1641			
	N	ρ	τ	r	N	ρ	τ	r	N	ρ	τ	r
TDFD	89	0.258	0.179	0.273	45	0.152	0.091	0.177	44	0.349	0.251	0.310
		0.015	0.013	0.010		0.317	0.378	0.245		0.020	0.016	0.041
FD	57	0.322	0.213	0.345	30	0.294	0.168	0.310	27	0.395	0.283	0.374
		0.015	0.019	0.009		0.114	0.192	0.095		0.042	0.038	0.055
TD	32	0.289	0.199	0.231	15	-0.143	-0.086	-0.104	17	0.400	0.299	0.280
		0.109	0.110	0.203		0.612	0.656	0.712		0.112	0.094	0.276

ρ: Spearsmans ρ
τ: Kendalls τ
r: Pearsons r

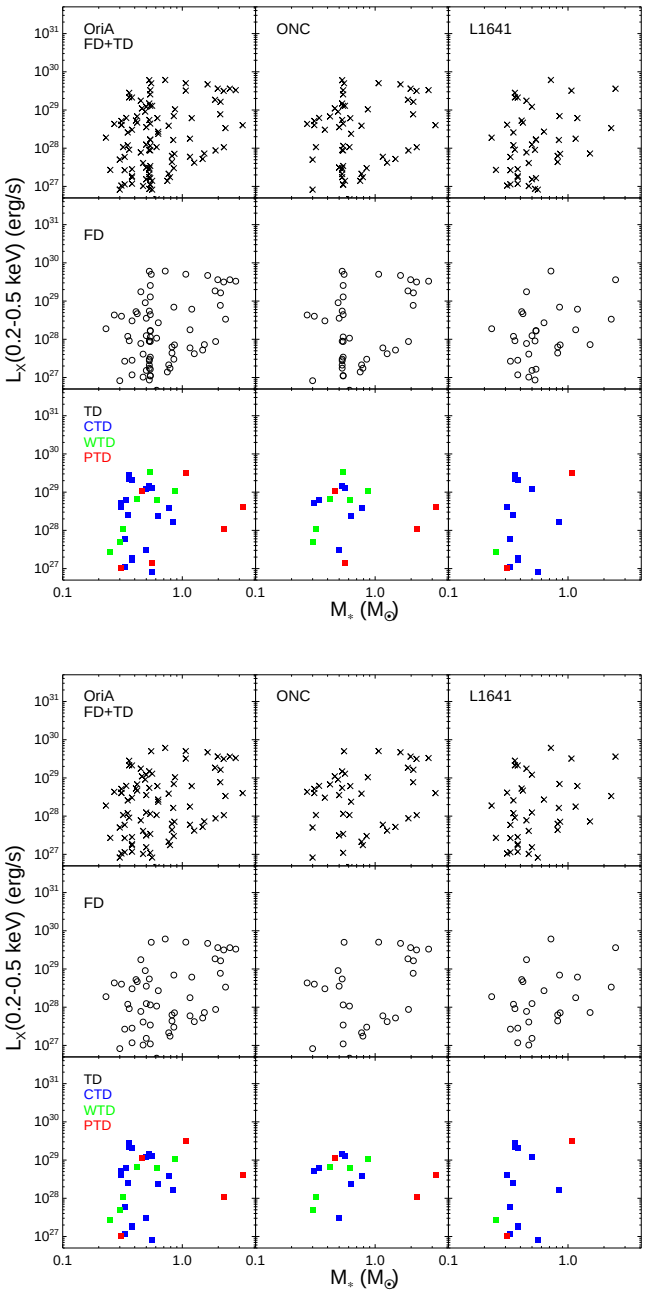


Figure C.133 $\log M_\star$ vs. $\log L_X 1$. Upper panel: all available objects; Lower panel: objects with available spectral types only

Table C.265 $\log M_\star$ vs. $\log L_X 1$ (I)

	Ori A				ONC				L1641			
	N	ρ	τ	r	N	ρ	τ	r	N	ρ	τ	r
TDFD	114	0.206	0.143	0.282	62	0.197	0.142	0.289	52	0.146	0.096	0.214
		0.028	0.024	0.002		0.125	0.103	0.023		0.303	0.313	0.128
FD	80	0.243	0.170	0.358	45	0.284	0.202	0.408	35	0.177	0.121	0.246
		0.030	0.026	0.001		0.059	0.051	0.005		0.310	0.308	0.154
TD	34	0.270	0.177	0.238	17	0.002	0.037	0.014	17	0.220	0.161	0.325
		0.123	0.140	0.175		0.993	0.836	0.957		0.396	0.367	0.203

ρ: Spearsmans ρ
τ: Kendalls τ
r: Pearsons r

Table C.266 $\log M_\star$ vs. $\log L_X 1$ (II)

	Ori A				ONC				L1641			
	N	ρ	τ	r	N	ρ	τ	r	N	ρ	τ	r
TDFD	89	0.304	0.209	0.341	45	0.259	0.186	0.320	44	0.275	0.185	0.301
		0.004	0.004	0.001		0.085	0.072	0.032		0.071	0.077	0.047
FD	57	0.360	0.248	0.426	30	0.392	0.257	0.463	27	0.304	0.210	0.335
		0.006	0.006	0.001		0.032	0.046	0.010		0.123	0.125	0.088
TD	32	0.299	0.190	0.253	15	0.057	0.067	0.020	17	0.220	0.161	0.325
		0.097	0.126	0.162		0.840	0.729	0.944		0.396	0.367	0.203

ρ: Spearsmans ρ
τ: Kendalls τ
r: Pearsons r

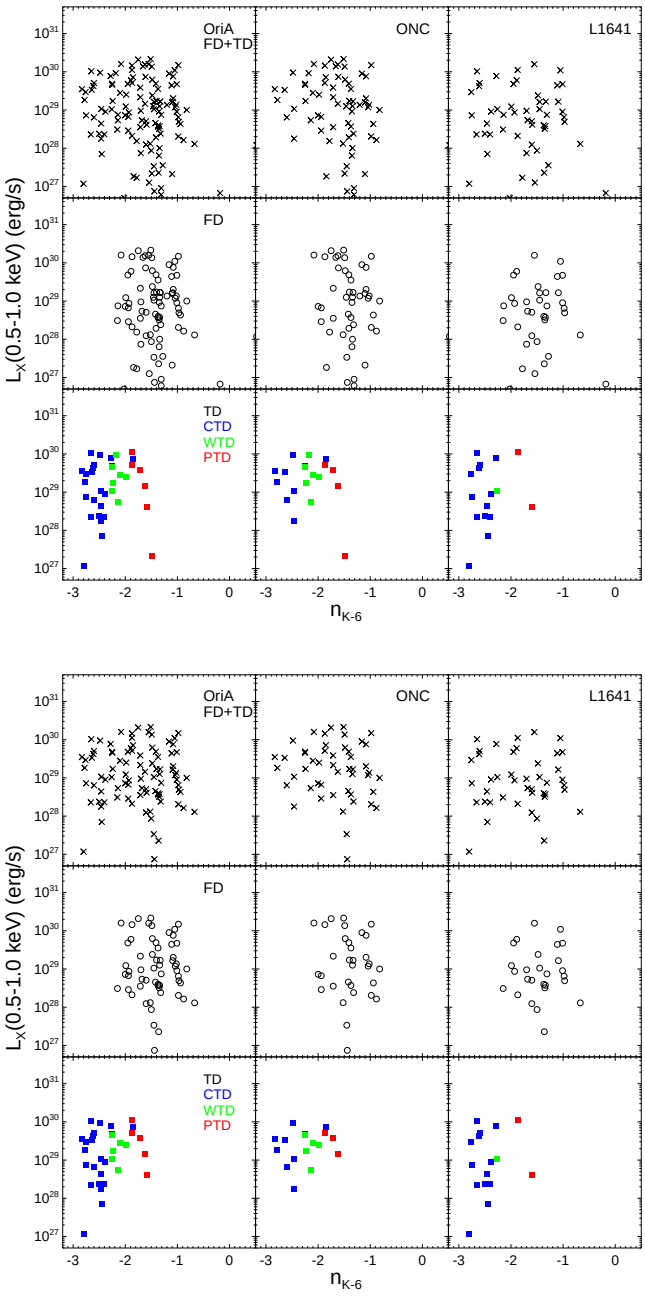


Figure C.134 n_{K-6} vs. $\log L_X 2$. Upper panel: all available objects; Lower panel: objects with available spectral types only

Table C.267 n_{K-6} vs. $\log L_X 2$ (I)

	Ori A				ONC				L1641			
	N	ρ	τ	r	N	ρ	τ	r	N	ρ	τ	r
TDFD	119	-0.161	-0.106	-0.171	67	-0.284	-0.186	-0.257	52	-0.048	-0.029	-0.117
		0.081	0.087	0.063		0.020	0.026	0.036		0.734	0.758	0.409
FD	84	-0.063	-0.054	-0.109	48	-0.192	-0.150	-0.173	36	0.049	0.032	-0.055
		0.566	0.466	0.324		0.191	0.134	0.240		0.775	0.785	0.750
TD	35	0.113	0.079	0.056	19	-0.028	-0.029	-0.203	16	0.218	0.167	0.182
		0.518	0.502	0.749		0.909	0.860	0.405		0.418	0.368	0.500

ρ: Spearsmans ρ
τ: Kendalls τ
r: Pearsons r

Table C.268 n_{K-6} vs. $\log L_X 2$ (II)

	Ori A				ONC				L1641			
	N	ρ	τ	r	N	ρ	τ	r	N	ρ	τ	r
TDFD	92	-0.076	-0.053	-0.042	49	-0.166	-0.118	-0.146	43	0.003	0.000	0.021
		0.469	0.451	0.691		0.253	0.232	0.317		0.985	1.000	0.894
FD	59	-0.071	-0.062	-0.066	32	-0.155	-0.136	-0.119	27	-0.028	-0.031	-0.016
		0.594	0.486	0.619		0.395	0.275	0.517		0.891	0.818	0.937
TD	33	0.180	0.126	0.245	17	0.142	0.089	0.198	16	0.218	0.167	0.182
		0.317	0.304	0.169		0.586	0.618	0.446		0.418	0.368	0.500

ρ: Spearsmans ρ
τ: Kendalls τ
r: Pearsons r

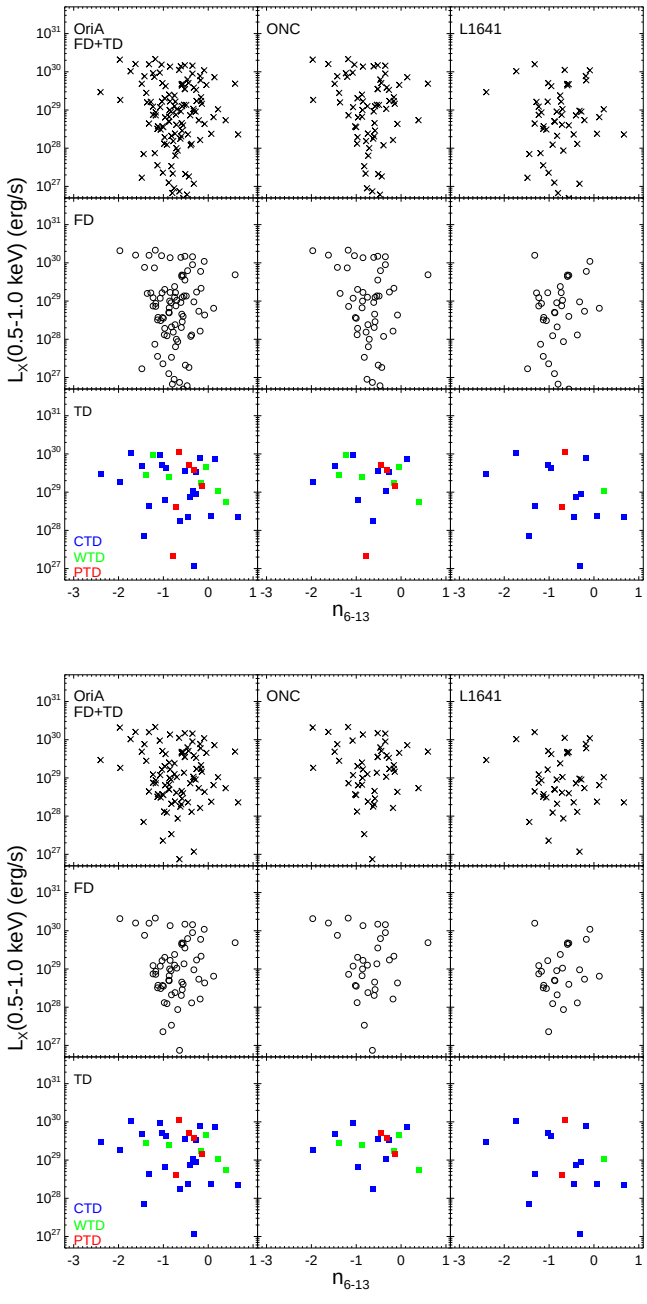


Figure C.135 n_{6-13} vs. $\log L_X 2$. Upper panel: all available objects; Lower panel: objects with available spectral types only

Table C.269 n_{6-13} vs. $\log L_X 2$ (I)

	Ori A				ONC				L1641			
	N	ρ	τ	r	N	ρ	τ	r	N	ρ	τ	r
TDFD	119	-0.040	-0.029	-0.067	67	-0.127	-0.080	-0.146	52	0.056	0.042	0.006
		0.663	0.639	0.469		0.305	0.337	0.238		0.693	0.663	0.966
FD	84	-0.014	-0.009	-0.037	48	-0.184	-0.126	-0.215	36	0.211	0.152	0.229
		0.901	0.907	0.738		0.212	0.206	0.142		0.216	0.193	0.179
TD	35	-0.200	-0.135	-0.189	19	-0.125	-0.053	-0.071	16	-0.262	-0.167	-0.297
		0.250	0.256	0.277		0.611	0.753	0.773		0.327	0.368	0.264

ρ: Spearsmans ρ
τ: Kendalls τ
r: Pearsons r

Table C.270 n_{6-13} vs. $\log L_X 2$ (II)

	Ori A				ONC				L1641			
	N	ρ	τ	r	N	ρ	τ	r	N	ρ	τ	r
TDFD	92	-0.036	-0.026	-0.095	49	-0.049	-0.030	-0.108	43	-0.018	-0.007	-0.100
		0.736	0.717	0.368		0.739	0.762	0.460		0.911	0.950	0.523
FD	59	0.028	0.028	-0.036	32	-0.076	-0.042	-0.154	27	0.173	0.137	0.181
		0.836	0.758	0.787		0.681	0.733	0.400		0.388	0.315	0.366
TD	33	-0.191	-0.131	-0.199	17	-0.071	-0.029	-0.100	16	-0.262	-0.167	-0.297
		0.288	0.285	0.267		0.786	0.869	0.703		0.327	0.368	0.264

ρ: Spearsmans ρ
τ: Kendalls τ
r: Pearsons r

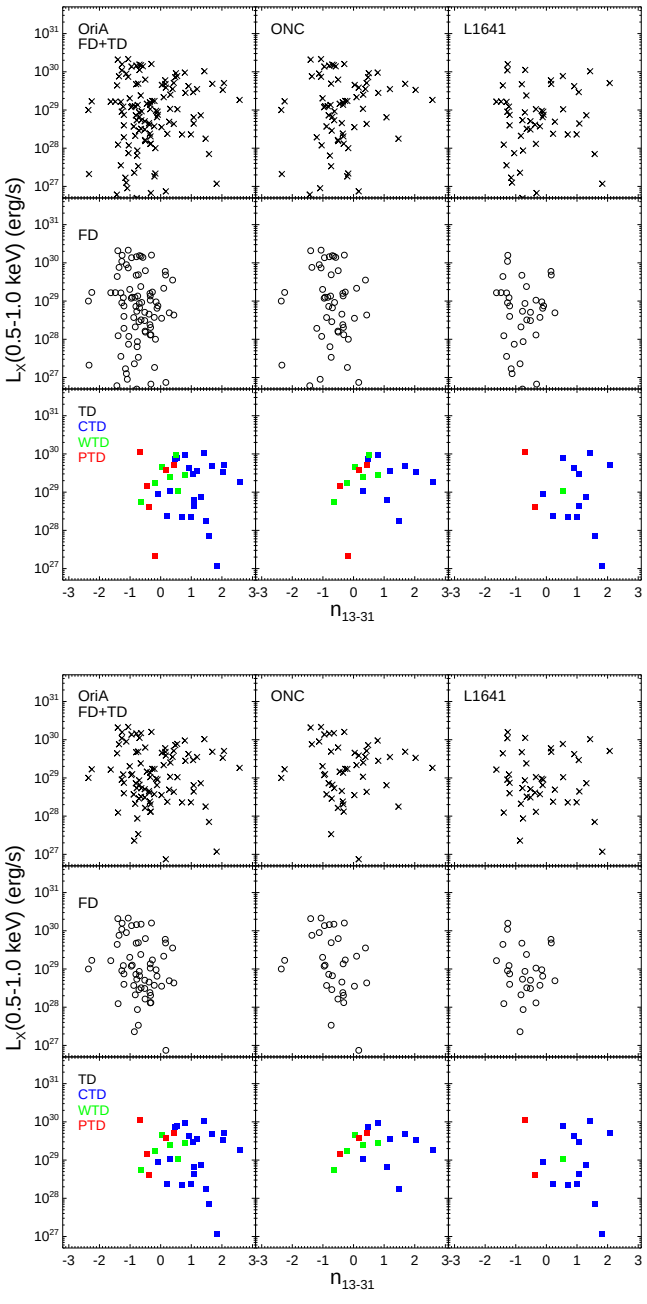


Figure C.136 n_{13-31} vs. $\log L_X 2$. Upper panel: all available objects; Lower panel: objects with available spectral types only

Table C.271 n_{13-31} vs. $\log L_X 2$ (I)

	Ori A				ONC				L1641			
	N	ρ	τ	r	N	ρ	τ	r	N	ρ	τ	r
TDFD	119	0.078	0.057	0.107	67	0.082	0.060	0.144	52	0.023	0.020	0.072
		0.399	0.362	0.247		0.509	0.474	0.245		0.871	0.837	0.612
FD	84	-0.067	-0.044	-0.011	48	-0.112	-0.084	-0.037	36	-0.084	-0.045	0.016
		0.546	0.551	0.921		0.449	0.397	0.803		0.628	0.702	0.926
TD	35	-0.032	-0.013	-0.050	19	0.242	0.181	0.180	16	-0.203	-0.150	-0.238
		0.854	0.909	0.775		0.318	0.278	0.461		0.451	0.418	0.375

ρ: Spearsmans ρ
τ: Kendalls τ
r: Pearsons r

Table C.272 n_{13-31} vs. $\log L_X 2$ (II)

	Ori A				ONC				L1641			
	N	ρ	τ	r	N	ρ	τ	r	N	ρ	τ	r
TDFD	92	-0.058	-0.034	-0.064	49	-0.065	-0.040	-0.039	43	-0.070	-0.046	-0.085
		0.581	0.627	0.544		0.658	0.685	0.790		0.655	0.667	0.588
FD	59	-0.245	-0.162	-0.218	32	-0.367	-0.252	-0.316	27	-0.104	-0.066	-0.066
		0.061	0.069	0.097		0.039	0.042	0.078		0.604	0.630	0.744
TD	33	-0.079	-0.047	-0.137	17	0.147	0.118	0.036	16	-0.203	-0.150	-0.238
		0.663	0.698	0.447		0.573	0.510	0.891		0.451	0.418	0.375

ρ: Spearsmans ρ
τ: Kendalls τ
r: Pearsons r

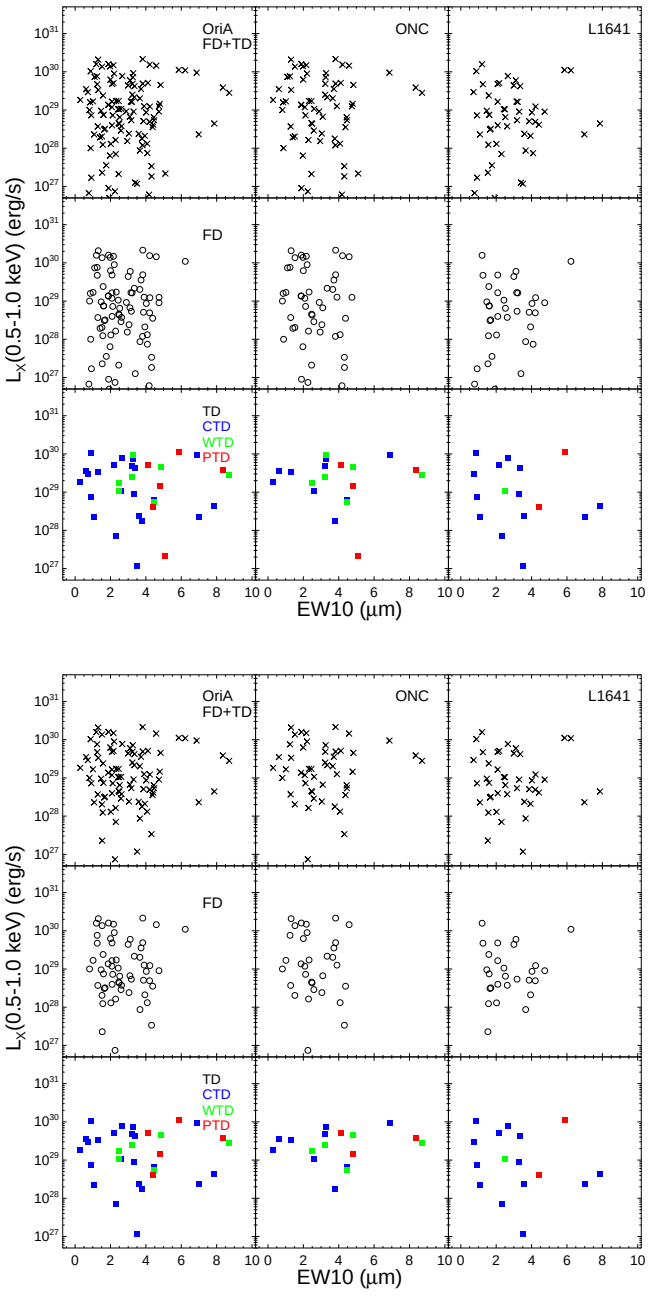


Figure C.137 EW10 vs. $\log L_X 2$. Upper panel: all available objects; Lower panel: objects with available spectral types only

Table C.273 EW10 vs. $\log L_X 2$ (I)

	Ori A				ONC				L1641			
	N	ρ	τ	r	N	ρ	τ	r	N	ρ	τ	r
TDFD	119	-0.005	-0.002	0.051	67	-0.040	-0.026	0.002	52	0.026	0.015	0.102
		0.958	0.974	0.582		0.748	0.753	0.987		0.852	0.875	0.472
FD	84	-0.018	-0.013	0.031	48	-0.134	-0.088	-0.125	36	0.141	0.098	0.249
		0.873	0.856	0.780		0.366	0.379	0.397		0.411	0.398	0.143
TD	35	-0.092	-0.057	-0.048	19	0.021	0.000	-0.015	16	-0.218	-0.150	-0.166
		0.597	0.629	0.784		0.932	1.000	0.951		0.418	0.418	0.539

ρ: Spearsmans ρ
τ: Kendalls τ
r: Pearsons r

Table C.274 EW10 vs. $\log L_X 2$ (II)

	Ori A				ONC				L1641			
	N	ρ	τ	r	N	ρ	τ	r	N	ρ	τ	r
TDFD	92	-0.048	-0.033	0.016	49	-0.021	-0.016	0.040	43	-0.074	-0.052	-0.032
		0.647	0.644	0.880		0.885	0.870	0.785		0.635	0.623	0.839
FD	59	-0.101	-0.069	-0.020	32	-0.161	-0.107	-0.119	27	0.023	0.037	0.124
		0.446	0.440	0.880		0.378	0.390	0.517		0.911	0.786	0.538
TD	33	-0.045	-0.028	0.005	17	0.147	0.081	0.136	16	-0.218	-0.150	-0.166
		0.802	0.816	0.978		0.573	0.649	0.603		0.418	0.418	0.539

ρ: Spearsmans ρ
τ: Kendalls τ
r: Pearsons r

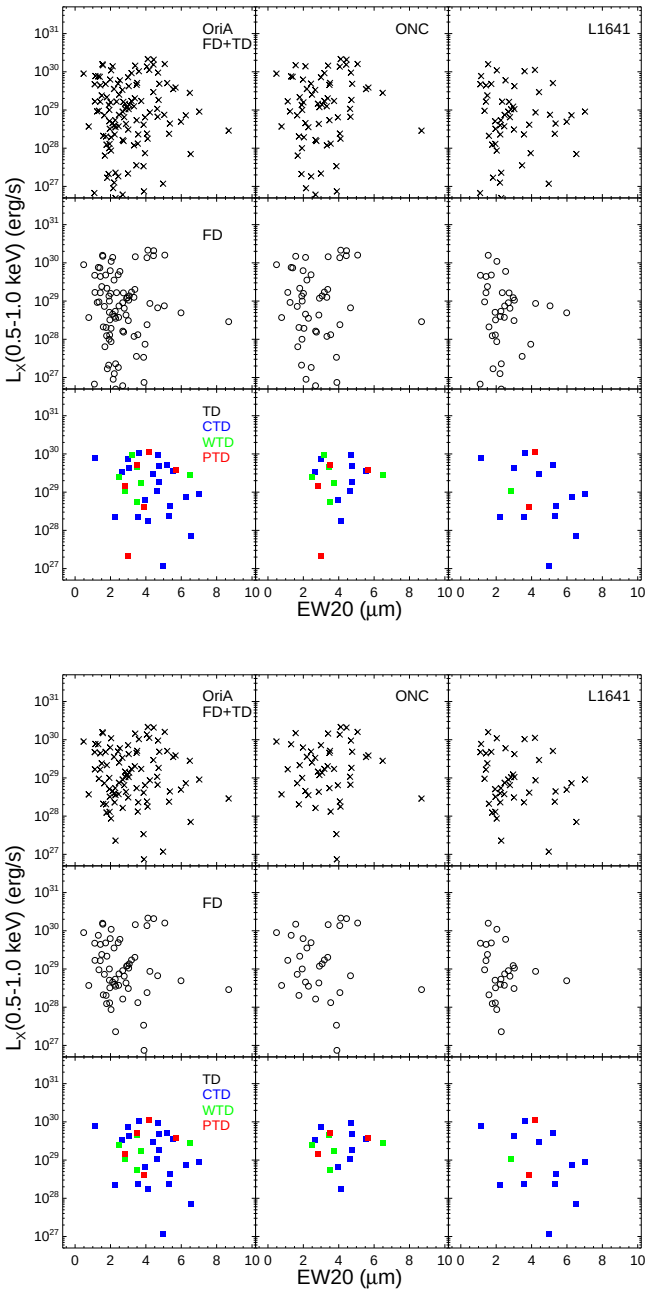


Figure C.138 EW20 vs. $\log L_X 2$. Upper panel: all available objects; Lower panel: objects with available spectral types only

Table C.275 EW20 vs. $\log L_X 2$ (I)

	Ori A				ONC				L1641			
	N	ρ	τ	r	N	ρ	τ	r	N	ρ	τ	r
TDFD	119	0.054	0.041	0.056	67	0.156	0.100	0.096	52	-0.056	-0.023	-0.036
		0.559	0.513	0.545		0.207	0.232	0.440		0.694	0.813	0.800
FD	84	-0.036	-0.022	0.033	48	0.041	0.023	0.035	36	-0.119	-0.067	-0.049
		0.746	0.769	0.766		0.780	0.817	0.813		0.491	0.567	0.777
TD	35	-0.146	-0.092	-0.170	19	0.121	0.076	0.172	16	-0.262	-0.133	-0.347
		0.403	0.435	0.329		0.622	0.649	0.481		0.327	0.471	0.188

ρ: Spearsmans ρ
τ: Kendalls τ
r: Pearsons r

Table C.276 EW20 vs. $\log L_X 2$ (II)

	Ori A				ONC				L1641			
	N	ρ	τ	r	N	ρ	τ	r	N	ρ	τ	r
TDFD	92	-0.039	-0.020	-0.068	49	0.041	0.019	-0.029	43	-0.165	-0.079	-0.198
		0.714	0.777	0.520		0.781	0.850	0.843		0.291	0.457	0.203
FD	59	-0.095	-0.059	-0.059	32	-0.038	-0.032	-0.079	27	-0.226	-0.111	-0.178
		0.476	0.509	0.657		0.834	0.795	0.667		0.256	0.416	0.374
TD	33	-0.189	-0.121	-0.238	17	0.103	0.059	0.087	16	-0.262	-0.133	-0.347
		0.293	0.321	0.182		0.694	0.742	0.740		0.327	0.471	0.188

ρ: Spearsmans ρ
τ: Kendalls τ
r: Pearsons r

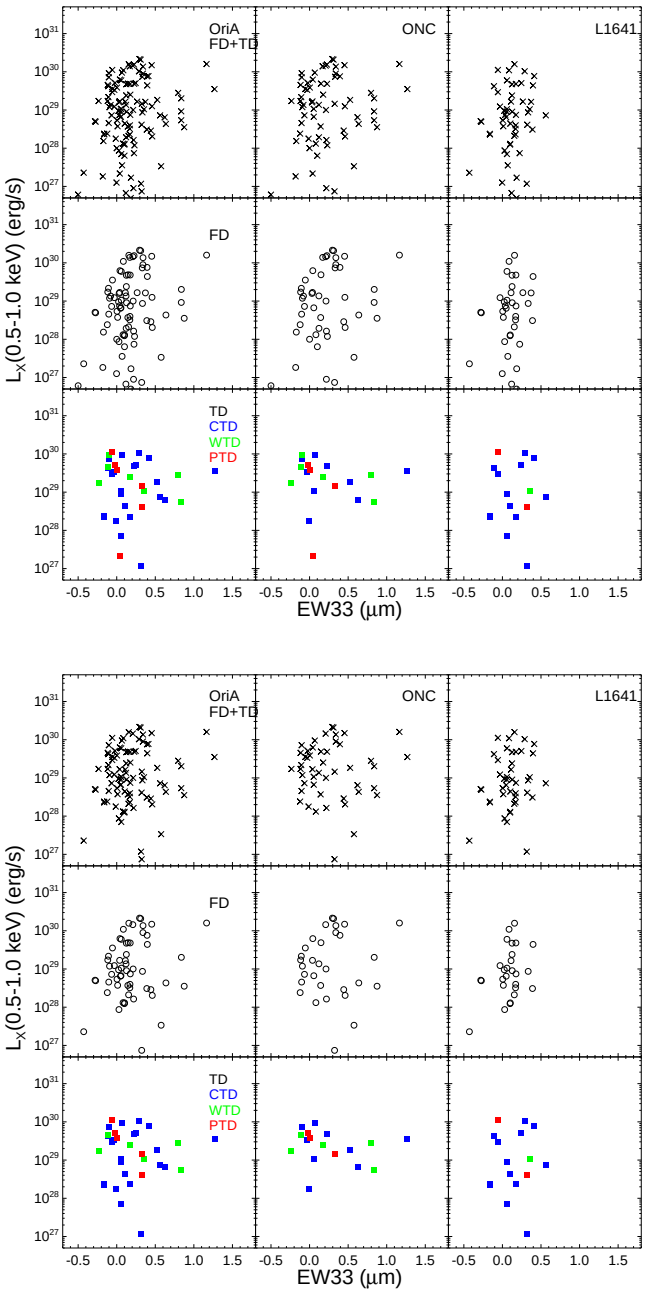


Figure C.139 EW33 vs. $\log L_X 2$. Upper panel: all available objects; Lower panel: objects with available spectral types only

Table C.277 EW33 vs. $\log L_X 2$ (I)

	Ori A				ONC				L1641			
	N	ρ	τ	r	N	ρ	τ	r	N	ρ	τ	r
TDFD	119	0.112	0.076	-0.091	67	0.089	0.067	-0.165	52	0.115	0.081	0.149
		0.224	0.219	0.325		0.473	0.420	0.182		0.418	0.398	0.292
FD	84	0.177	0.125	-0.099	48	0.162	0.122	-0.168	36	0.131	0.105	0.201
		0.108	0.091	0.370		0.272	0.220	0.254		0.445	0.368	0.240
TD	35	-0.115	-0.071	-0.014	19	-0.319	-0.205	-0.083	16	0.104	0.059	0.009
		0.510	0.551	0.936		0.183	0.221	0.736		0.700	0.752	0.974

ρ: Spearsmans ρ
τ: Kendalls τ
r: Pearsons r

Table C.278 EW33 vs. $\log L_X 2$ (II)

	Ori A				ONC				L1641			
	N	ρ	τ	r	N	ρ	τ	r	N	ρ	τ	r
TDFD	92	0.087	0.063	0.087	49	0.012	0.021	0.010	43	0.160	0.118	0.206
		0.407	0.373	0.410		0.937	0.829	0.946		0.306	0.266	0.185
FD	59	0.134	0.102	0.125	32	0.055	0.052	0.044	27	0.221	0.180	0.381
		0.312	0.252	0.346		0.767	0.673	0.811		0.267	0.188	0.050
TD	33	-0.094	-0.063	-0.021	17	-0.309	-0.206	-0.191	16	0.104	0.059	0.009
		0.604	0.609	0.908		0.228	0.249	0.463		0.700	0.752	0.974

ρ: Spearsmans ρ
τ: Kendalls τ
r: Pearsons r

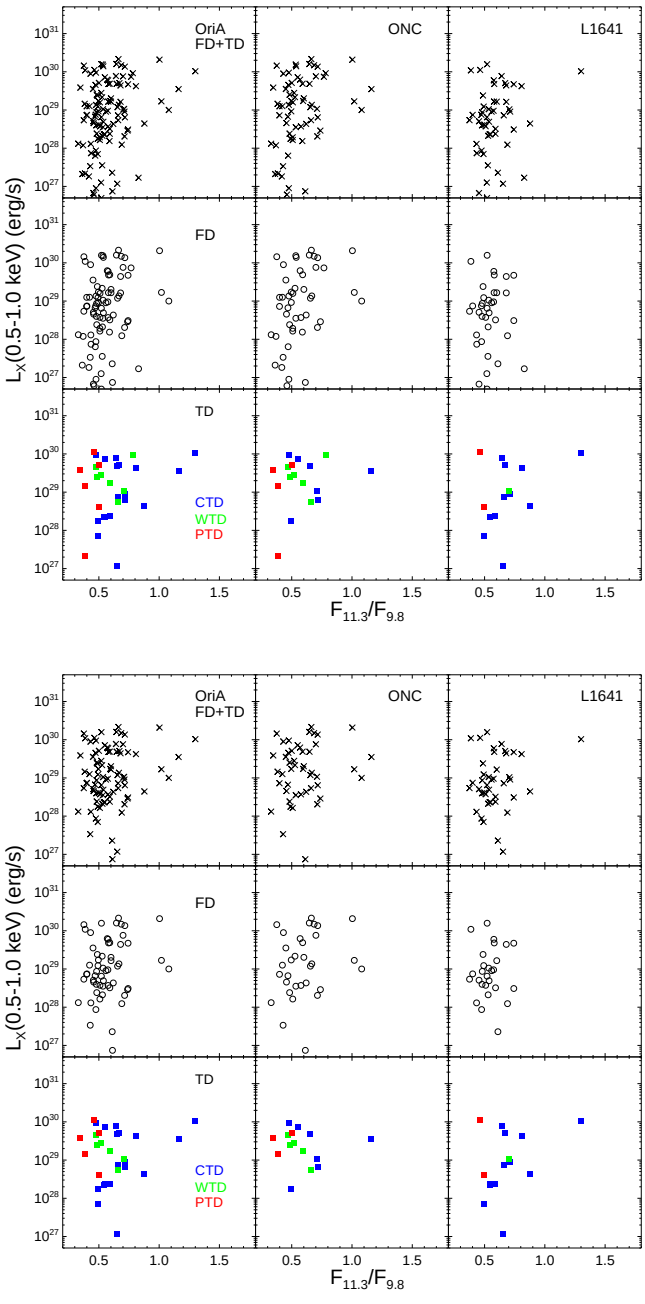


Figure C.140 $F_{11.3}/F_{9.8}$ vs. $\log L_X 2$. Upper panel: all available objects; Lower panel: objects with available spectral types only

Table C.279 $F_{11.3}/F_{9.8}$ vs. $\log L_X 2$ (I)

	Ori A				ONC				L1641			
	N	ρ	τ	r	N	ρ	τ	r	N	ρ	τ	r
TDFD	119	0.232	0.153	0.082	67	0.281	0.189	0.095	52	0.201	0.139	0.130
		0.011	0.014	0.375		0.021	0.024	0.444		0.153	0.147	0.358
FD	84	0.258	0.176	0.101	48	0.343	0.234	0.115	36	0.125	0.095	0.001
		0.018	0.018	0.361		0.017	0.019	0.436		0.469	0.414	0.995
TD	35	0.094	0.076	0.106	19	0.072	0.053	0.120	16	0.368	0.283	0.186
		0.591	0.523	0.544		0.770	0.753	0.625		0.161	0.126	0.490

ρ: Spearsmans ρ
τ: Kendalls τ
r: Pearsons r

Table C.280 $F_{11.3}/F_{9.8}$ vs. $\log L_X 2$ (II)

	Ori A				ONC				L1641			
	N	ρ	τ	r	N	ρ	τ	r	N	ρ	τ	r
TDFD	92	0.128	0.078	0.079	49	0.105	0.066	0.094	43	0.144	0.099	0.129
		0.223	0.272	0.454		0.473	0.501	0.521		0.358	0.352	0.410
FD	59	0.175	0.119	0.192	32	0.239	0.157	0.232	27	0.037	0.043	0.005
		0.186	0.184	0.145		0.188	0.206	0.201		0.856	0.755	0.980
TD	33	-0.017	0.000	0.104	17	-0.174	-0.103	0.096	16	0.368	0.283	0.186
		0.925	1.000	0.565		0.504	0.564	0.714		0.161	0.126	0.490

ρ: Spearsmans ρ
τ: Kendalls τ
r: Pearsons r

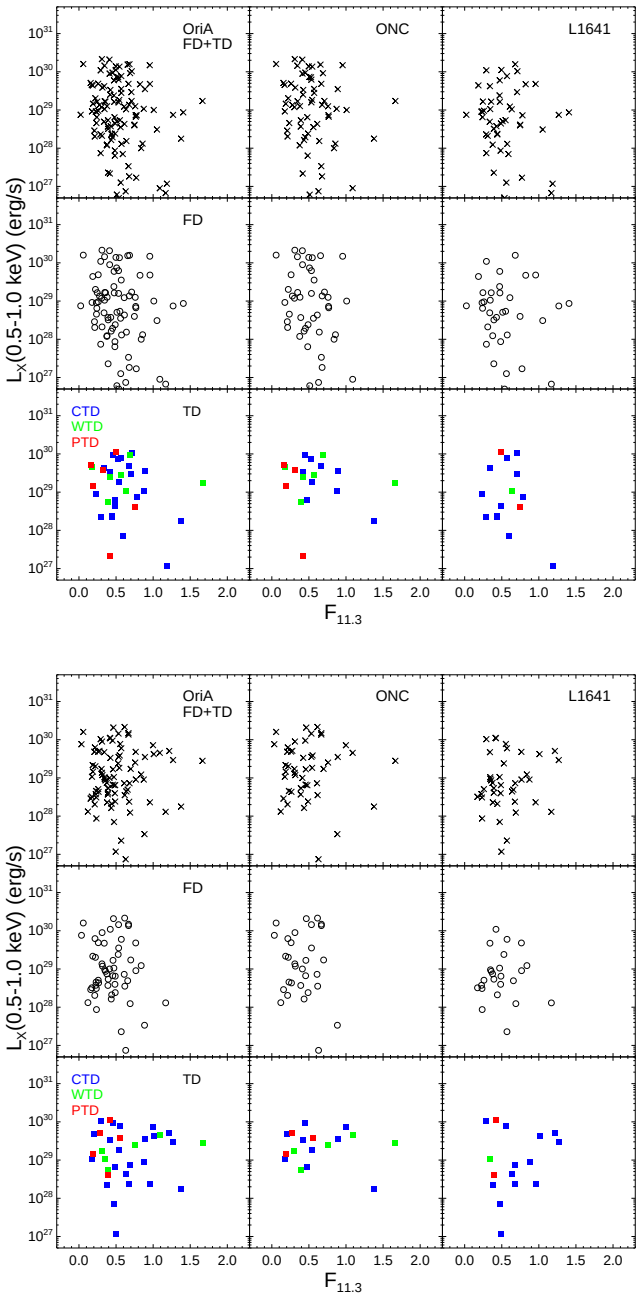


Figure C.141 $F_{11.3}$ vs. $\log L_X 2$. Upper panel: all available objects; Lower panel: objects with available spectral types only

Table C.281 $F_{11.3}$ vs. $\log L_X 2$ (I)

	Ori A				ONC				L1641			
	N	ρ	τ	r	N	ρ	τ	r	N	ρ	τ	r
TDFD	119	0.114	0.073	0.117	67	0.106	0.064	0.110	52	0.130	0.100	0.119
		0.218	0.238	0.205		0.394	0.442	0.376		0.357	0.293	0.401
FD	84	0.077	0.044	0.111	48	-0.003	-0.014	-0.010	36	0.164	0.135	0.263
		0.484	0.554	0.315		0.982	0.887	0.946		0.338	0.246	0.121
TD	35	0.026	0.008	-0.014	19	0.151	0.088	0.072	16	0.000	0.000	-0.120
		0.882	0.943	0.936		0.538	0.600	0.770		1.000	1.000	0.658

ρ: Spearsmans ρ
τ: Kendalls τ
r: Pearsons r

Table C.282 $F_{11.3}$ vs. $\log L_X 2$ (II)

	Ori A				ONC				L1641			
	N	ρ	τ	r	N	ρ	τ	r	N	ρ	τ	r
TDFD	92	0.034	0.018	0.031	49	0.076	0.048	0.080	43	0.014	0.020	-0.028
		0.747	0.798	0.769		0.603	0.629	0.585		0.928	0.850	0.859
FD	59	-0.016	-0.022	0.015	32	-0.033	-0.030	-0.052	27	0.014	0.034	0.100
		0.907	0.804	0.910		0.858	0.808	0.777		0.946	0.802	0.620
TD	33	0.012	-0.004	-0.018	17	0.169	0.088	0.098	16	0.000	0.000	-0.120
		0.947	0.975	0.921		0.516	0.621	0.708		1.000	1.000	0.658

ρ: Spearsmans ρ
τ: Kendalls τ
r: Pearsons r

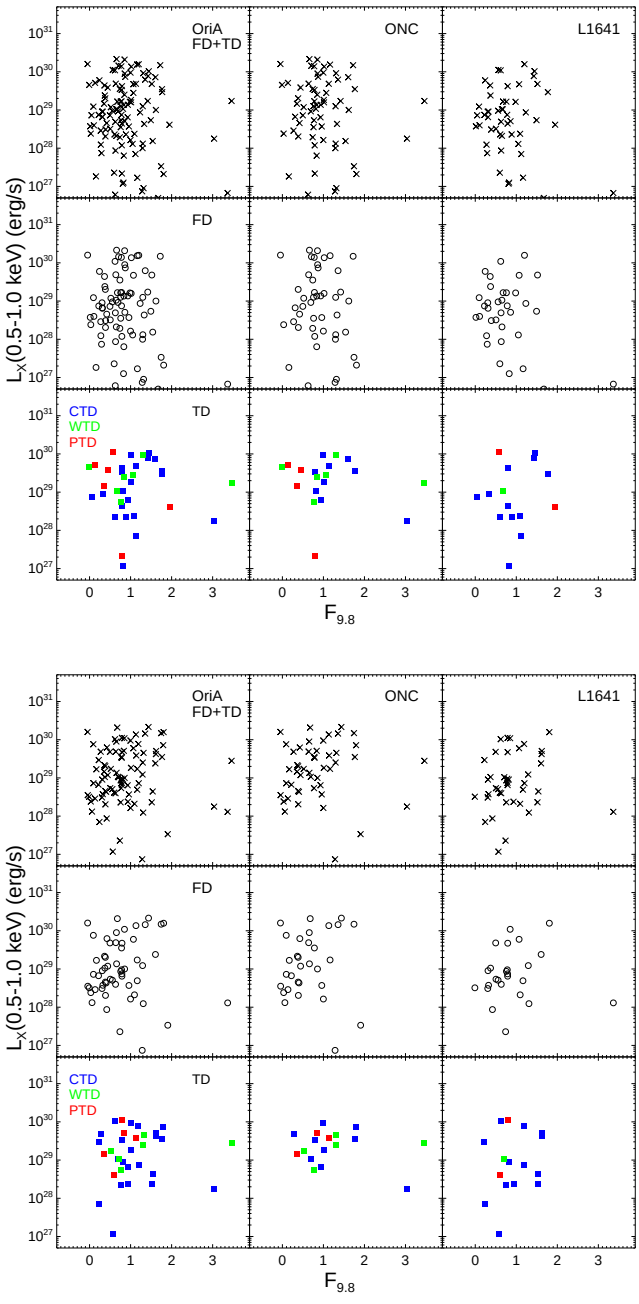


Figure C.142 $F_{9.8}$ vs. $\log L_X 2$. Upper panel: all available objects; Lower panel: objects with available spectral types only

Table C.283 $F_{9.8}$ vs. $\log L_X 2$ (I)

	Ori A				ONC				L1641			
	N	ρ	τ	r	N	ρ	τ	r	N	ρ	τ	r
TDFD	119	-0.021	-0.013	0.042	67	-0.052	-0.033	-0.006	52	0.031	0.021	0.089
		0.824	0.831	0.650		0.678	0.689	0.962		0.825	0.825	0.530
FD	84	-0.024	-0.016	0.011	48	-0.133	-0.087	-0.142	36	0.170	0.121	0.227
		0.827	0.826	0.921		0.368	0.384	0.336		0.321	0.301	0.183
TD	35	-0.050	-0.029	-0.031	19	0.054	0.029	-0.022	16	-0.238	-0.167	-0.174
		0.777	0.809	0.860		0.825	0.861	0.929		0.374	0.368	0.519

ρ: Spearsmans ρ
τ: Kendalls τ
r: Pearsons r

Table C.284 $F_{9.8}$ vs. $\log L_X 2$ (II)

	Ori A				ONC				L1641			
	N	ρ	τ	r	N	ρ	τ	r	N	ρ	τ	r
TDFD	92	-0.062	-0.040	0.017	49	-0.023	-0.013	0.033	43	-0.077	-0.056	-0.036
		0.556	0.569	0.872		0.877	0.897	0.822		0.623	0.594	0.819
FD	59	-0.099	-0.064	-0.052	32	-0.141	-0.093	-0.164	27	0.046	0.048	0.111
		0.455	0.476	0.696		0.442	0.456	0.370		0.818	0.723	0.582
TD	33	-0.002	0.004	0.043	17	0.196	0.132	0.161	16	-0.238	-0.167	-0.174
		0.993	0.975	0.812		0.451	0.458	0.537		0.374	0.368	0.519

ρ: Spearsmans ρ
τ: Kendalls τ
r: Pearsons r

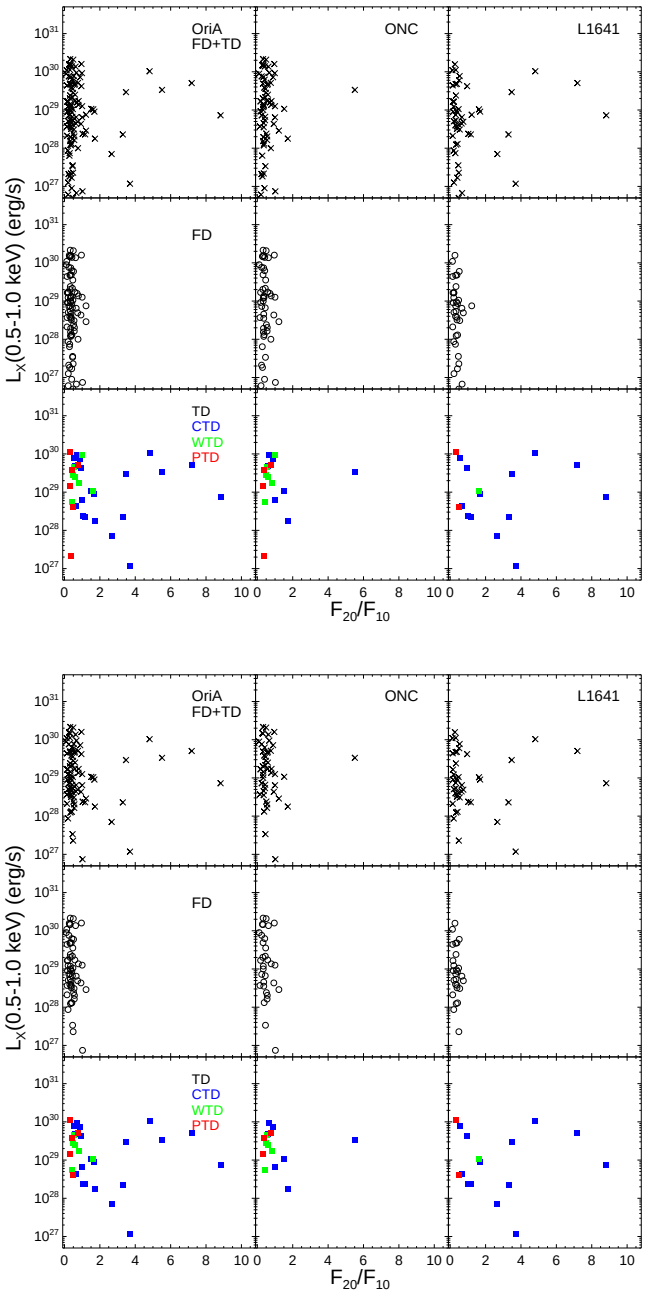


Figure C.143 F_{20}/F_{10} vs. $\log L_X 2$. Upper panel: all available objects; Lower panel: objects with available spectral types only

Table C.285 F_{20}/F_{10} vs. $\log L_X 2$ (I)

	Ori A				ONC				L1641			
	N	ρ	τ	r	N	ρ	τ	r	N	ρ	τ	r
TDFD	118	-0.006	-0.006	0.078	66	0.075	0.050	0.096	52	-0.127	-0.089	0.084
		0.949	0.924	0.401		0.547	0.554	0.443		0.370	0.352	0.554
FD	84	-0.128	-0.087	-0.096	48	-0.030	-0.025	-0.066	36	-0.335	-0.232	-0.218
		0.246	0.240	0.385		0.842	0.803	0.656		0.046	0.047	0.202
TD	34	-0.154	-0.119	0.030	18	0.102	0.111	0.119	16	-0.141	-0.150	0.019
		0.385	0.321	0.866		0.687	0.520	0.638		0.602	0.418	0.944

ρ: Spearsmans ρ
τ: Kendalls τ
r: Pearsons r

Table C.286 F_{20}/F_{10} vs. $\log L_X 2$ (II)

	Ori A				ONC				L1641			
	N	ρ	τ	r	N	ρ	τ	r	N	ρ	τ	r
TDFD	91	-0.124	-0.090	0.018	48	-0.143	-0.098	0.048	43	-0.148	-0.114	0.009
		0.240	0.208	0.866		0.332	0.328	0.746		0.345	0.281	0.954
FD	59	-0.223	-0.161	-0.216	32	-0.290	-0.206	-0.294	27	-0.258	-0.191	-0.232
		0.089	0.072	0.100		0.108	0.098	0.102		0.193	0.162	0.244
TD	32	-0.233	-0.185	-0.002	16	-0.082	-0.017	0.085	16	-0.141	-0.150	0.019
		0.200	0.136	0.991		0.762	0.928	0.754		0.602	0.418	0.944

ρ: Spearsmans ρ
τ: Kendalls τ
r: Pearsons r

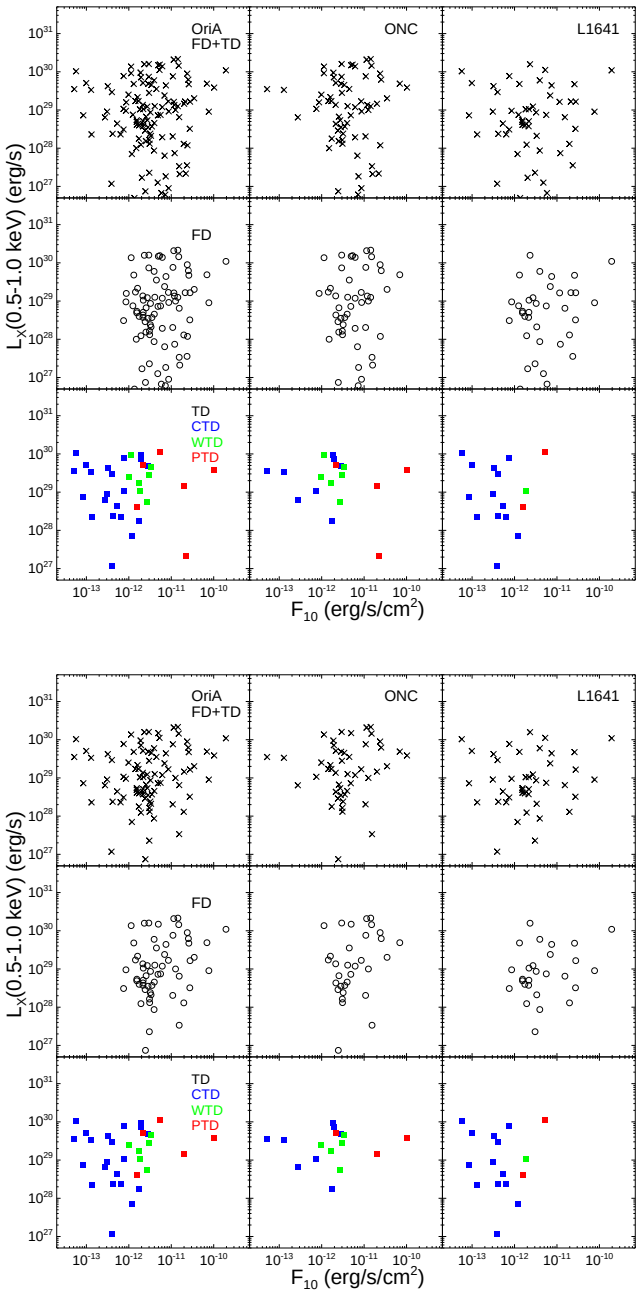


Figure C.144 $\log F_{10}$ vs. $\log L_X 2$. Upper panel: all available objects; Lower panel: objects with available spectral types only

Table C.287 $\log F_{10}$ vs. $\log L_X 2$ (I)

	Ori A				ONC				L1641			
	N	ρ	τ	r	N	ρ	τ	r	N	ρ	τ	r
TDFD	118	0.019	0.011	0.142	66	-0.037	-0.028	0.082	52	0.030	0.019	0.208
		0.838	0.863	0.125		0.766	0.744	0.513		0.835	0.844	0.139
FD	84	0.141	0.090	0.196	48	0.103	0.073	0.161	36	0.192	0.124	0.293
		0.201	0.225	0.074		0.488	0.466	0.274		0.262	0.288	0.083
TD	34	0.108	0.059	0.045	18	0.001	-0.072	-0.033	16	-0.056	-0.050	0.253
		0.543	0.625	0.800		0.997	0.677	0.897		0.837	0.787	0.344

ρ: Spearsmans ρ
τ: Kendalls τ
r: Pearsons r

Table C.288 $\log F_{10}$ vs. $\log L_X 2$ (II)

	Ori A				ONC				L1641			
	N	ρ	τ	r	N	ρ	τ	r	N	ρ	τ	r
TDFD	91	0.156	0.101	0.200	48	0.153	0.087	0.182	43	0.107	0.078	0.238
		0.141	0.158	0.057		0.298	0.384	0.216		0.494	0.464	0.124
FD	59	0.252	0.168	0.242	32	0.310	0.206	0.269	27	0.235	0.162	0.339
		0.054	0.061	0.065		0.084	0.098	0.137		0.238	0.235	0.084
TD	32	0.200	0.117	0.137	16	0.232	0.067	0.124	16	-0.056	-0.050	0.253
		0.272	0.347	0.455		0.387	0.719	0.647		0.837	0.787	0.344

ρ: Spearsmans ρ
τ: Kendalls τ
r: Pearsons r

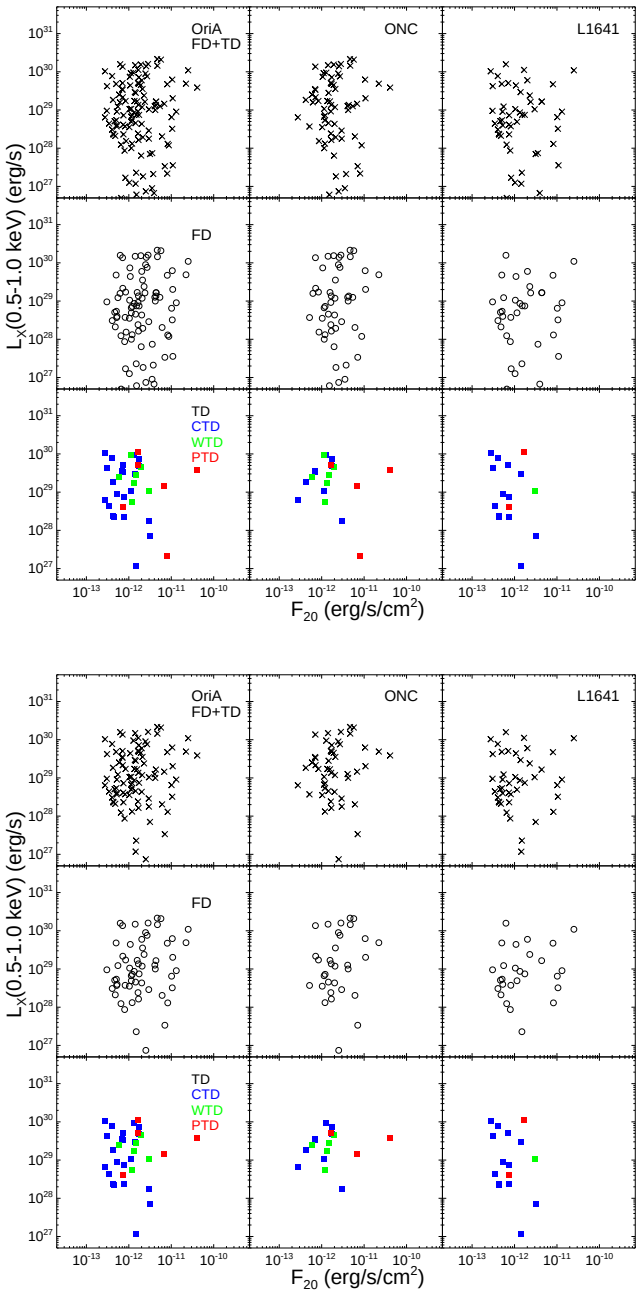


Figure C.145 $\log F_{20}$ vs. $\log L_X 2$. Upper panel: all available objects; Lower panel: objects with available spectral types only

Table C.289 $\log F_{20}$ vs. $\log L_X 2$ (I)

	Ori A				ONC				L1641			
	N	ρ	τ	r	N	ρ	τ	r	N	ρ	τ	r
TDFD	119	0.018	0.017	0.088	67	-0.021	-0.010	0.069	52	-0.043	-0.033	0.095
		0.844	0.785	0.341		0.863	0.901	0.579		0.764	0.728	0.503
FD	84	0.127	0.092	0.151	48	0.089	0.060	0.132	36	0.113	0.076	0.189
		0.250	0.216	0.170		0.547	0.546	0.371		0.511	0.513	0.270
TD	35	-0.060	-0.035	0.022	19	0.004	0.006	-0.019	16	-0.285	-0.217	-0.267
		0.731	0.766	0.900		0.989	0.972	0.938		0.284	0.242	0.317

ρ: Spearsmans ρ
τ: Kendalls τ
r: Pearsons r

Table C.290 $\log F_{20}$ vs. $\log L_X 2$ (II)

	Ori A				ONC				L1641			
	N	ρ	τ	r	N	ρ	τ	r	N	ρ	τ	r
TDFD	92	0.127	0.089	0.146	49	0.137	0.083	0.121	43	0.008	0.003	0.152
		0.229	0.210	0.165		0.348	0.398	0.408		0.957	0.975	0.331
FD	59	0.221	0.157	0.204	32	0.192	0.121	0.173	27	0.187	0.128	0.258
		0.093	0.079	0.121		0.293	0.331	0.344		0.349	0.348	0.194
TD	33	0.014	0.015	0.097	17	0.240	0.162	0.115	16	-0.285	-0.217	-0.267
		0.937	0.901	0.591		0.353	0.365	0.660		0.284	0.242	0.317

ρ: Spearsmans ρ
τ: Kendalls τ
r: Pearsons r

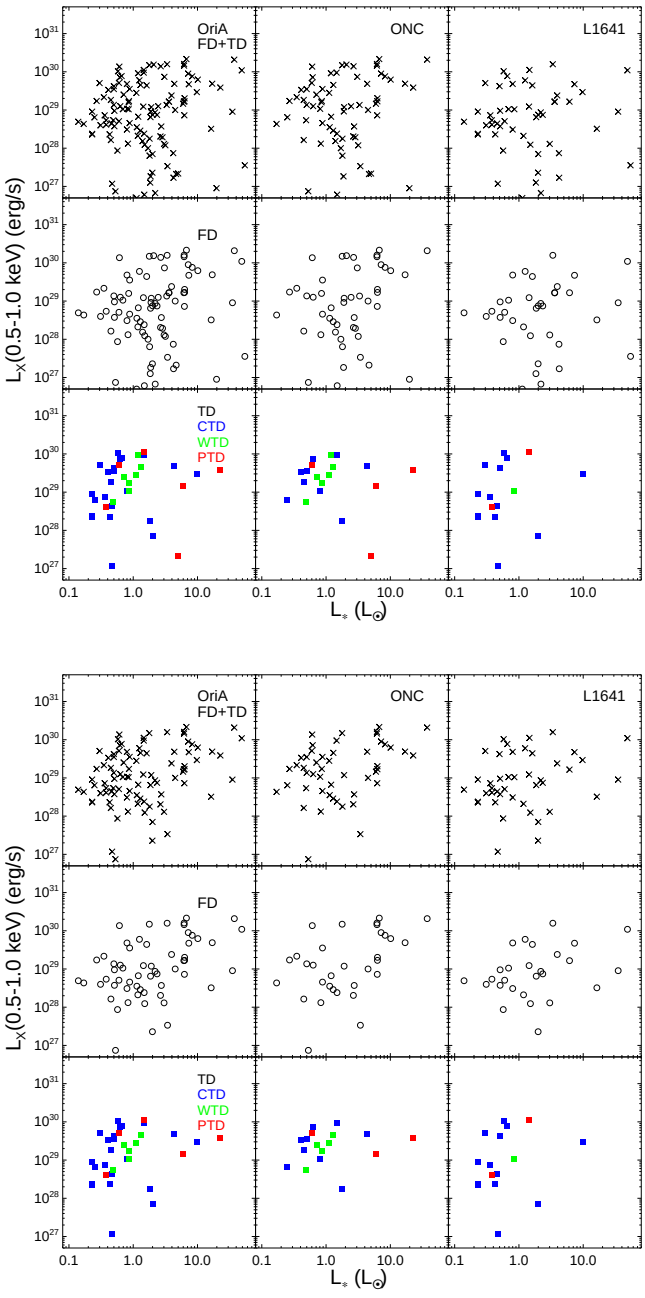


Figure C.146 $\log L_\star$ vs. $\log L_X 2$ Upper panel: all available objects; Lower panel: objects with available spectral types only

Table C.291 $\log L_\star$ vs. $\log L_X 2$ (I)

	Ori A				ONC				L1641			
	N	ρ	τ	r	N	ρ	τ	r	N	ρ	τ	r
TDFD	119	0.121	0.081	0.081	67	0.140	0.083	0.101	52	0.077	0.058	0.027
		0.190	0.193	0.381		0.259	0.319	0.416		0.587	0.542	0.849
FD	84	0.222	0.141	0.160	48	0.276	0.163	0.227	36	0.136	0.099	0.077
		0.042	0.057	0.146		0.057	0.102	0.121		0.429	0.398	0.655
TD	35	0.265	0.206	0.106	19	0.070	0.076	-0.129	16	0.330	0.228	0.210
		0.125	0.082	0.544		0.775	0.649	0.599		0.211	0.218	0.435

ρ: Spearsmans ρ
τ: Kendalls τ
r: Pearsons r

Table C.292 $\log L_\star$ vs. $\log L_X 2$ (II)

	Ori A				ONC				L1641			
	N	ρ	τ	r	N	ρ	τ	r	N	ρ	τ	r
TDFD	92	0.301	0.200	0.315	49	0.335	0.220	0.347	43	0.251	0.168	0.244
		0.004	0.005	0.002		0.019	0.026	0.015		0.104	0.113	0.115
FD	59	0.398	0.258	0.408	32	0.469	0.303	0.469	27	0.337	0.226	0.320
		0.002	0.004	0.001		0.007	0.015	0.007		0.086	0.099	0.104
TD	33	0.339	0.249	0.246	17	0.186	0.147	0.149	16	0.330	0.228	0.210
		0.053	0.041	0.168		0.474	0.410	0.568		0.211	0.218	0.435

ρ: Spearsmans ρ
τ: Kendalls τ
r: Pearsons r

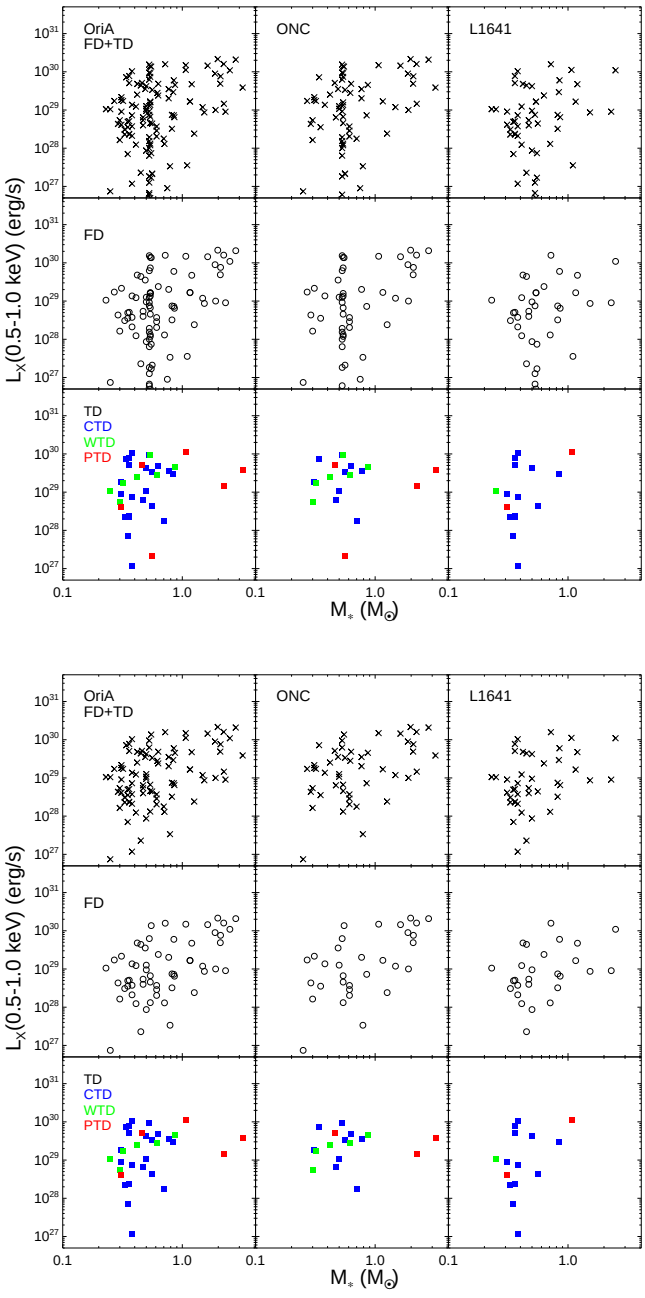


Figure C.147 $\log M_\star$ vs. $\log L_X 2$. Upper panel: all available objects; Lower panel: objects with available spectral types only

Table C.293 $\log M_\star$ vs. $\log L_X 2$ (I)

	Ori A				ONC				L1641			
	N	ρ	τ	r	N	ρ	τ	r	N	ρ	τ	r
TDFD	119	0.256	0.172	0.308	67	0.273	0.186	0.342	52	0.185	0.114	0.207
		0.005	0.006	0.001		0.026	0.026	0.005		0.189	0.233	0.141
FD	84	0.318	0.220	0.390	48	0.367	0.259	0.454	36	0.244	0.159	0.257
		0.003	0.003	0.000		0.010	0.009	0.001		0.152	0.173	0.130
TD	35	0.301	0.193	0.248	19	0.107	0.082	0.068	16	0.364	0.226	0.386
		0.079	0.104	0.151		0.663	0.623	0.782		0.165	0.221	0.140

ρ: Spearsmans ρ
τ: Kendalls τ
r: Pearsons r

Table C.294 $\log M_\star$ vs. $\log L_X 2$ (II)

	Ori A				ONC				L1641			
	N	ρ	τ	r	N	ρ	τ	r	N	ρ	τ	r
TDFD	92	0.382	0.257	0.416	49	0.375	0.255	0.431	43	0.327	0.211	0.337
		0.000	0.000	0.000		0.008	0.010	0.002		0.032	0.047	0.027
FD	59	0.470	0.327	0.519	32	0.507	0.353	0.574	27	0.403	0.273	0.387
		0.000	0.000	0.000		0.003	0.005	0.001		0.037	0.046	0.046
TD	33	0.347	0.223	0.289	17	0.172	0.132	0.091	16	0.364	0.226	0.386
		0.048	0.069	0.103		0.510	0.458	0.728		0.165	0.221	0.140

ρ: Spearsmans ρ
τ: Kendalls τ
r: Pearsons r

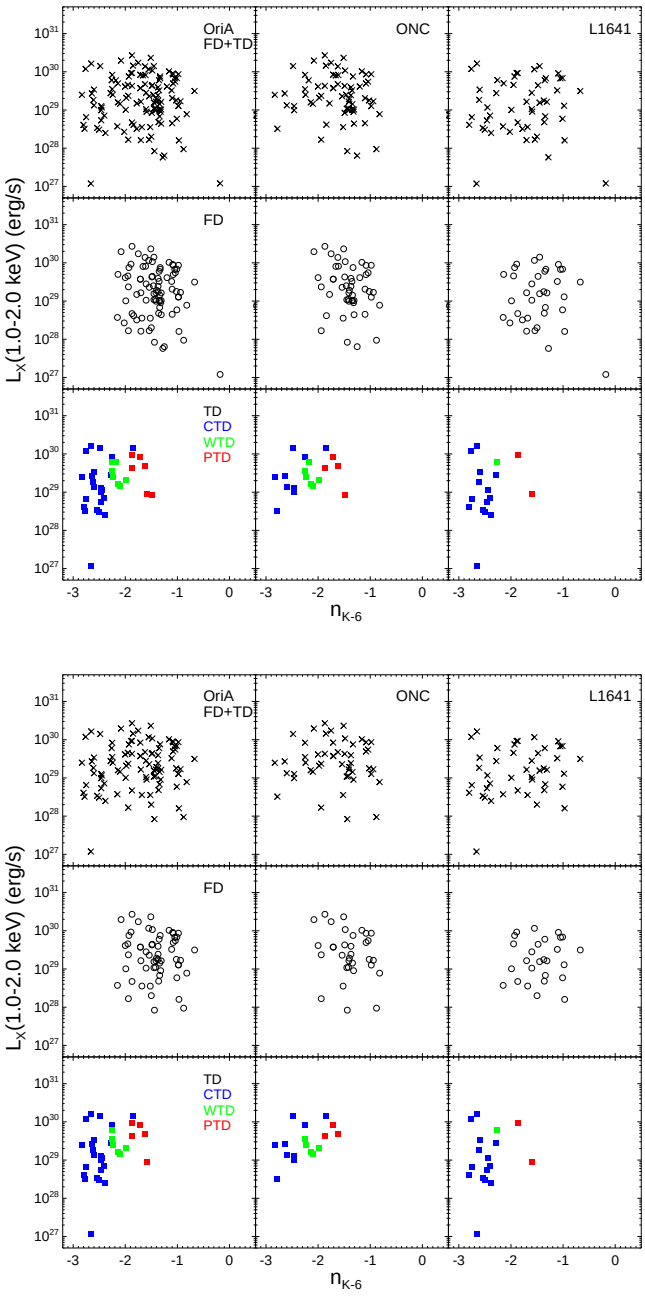


Figure C.148 n_{K-6} vs. $\log L_X 3$. Upper panel: all available objects; Lower panel: objects with available spectral types only

Table C.295 n_{K-6} vs. $\log L_X 3$ (I)

	Ori A				ONC				L1641			
	N	ρ	τ	r	N	ρ	τ	r	N	ρ	τ	r
TDFD	122	-0.036	-0.026	-0.056	69	-0.196	-0.132	-0.157	53	0.039	0.034	-0.026
		0.697	0.668	0.540		0.106	0.108	0.198		0.781	0.718	0.853
FD	86	-0.116	-0.084	-0.186	50	-0.265	-0.193	-0.238	36	0.000	0.013	-0.172
		0.288	0.255	0.086		0.063	0.048	0.096		0.998	0.913	0.316
TD	36	0.296	0.201	0.294	19	0.271	0.194	0.310	17	0.120	0.103	0.170
		0.080	0.085	0.082		0.261	0.246	0.196		0.646	0.564	0.514

ρ: Spearsmans ρ
τ: Kendalls τ
r: Pearsons r

Table C.296 n_{K-6} vs. $\log L_X 3$ (II)

	Ori A				ONC				L1641			
	N	ρ	τ	r	N	ρ	τ	r	N	ρ	τ	r
TDFD	94	0.066	0.047	0.103	50	-0.050	-0.025	-0.040	44	0.128	0.101	0.187
		0.527	0.504	0.323		0.733	0.795	0.783		0.409	0.336	0.224
FD	60	-0.097	-0.064	-0.085	33	-0.238	-0.162	-0.218	27	0.033	0.043	0.066
		0.460	0.469	0.518		0.183	0.186	0.223		0.870	0.754	0.744
TD	34	0.334	0.235	0.350	17	0.479	0.341	0.514	17	0.120	0.103	0.170
		0.054	0.051	0.042		0.052	0.056	0.035		0.646	0.564	0.514

ρ: Spearsmans ρ
τ: Kendalls τ
r: Pearsons r

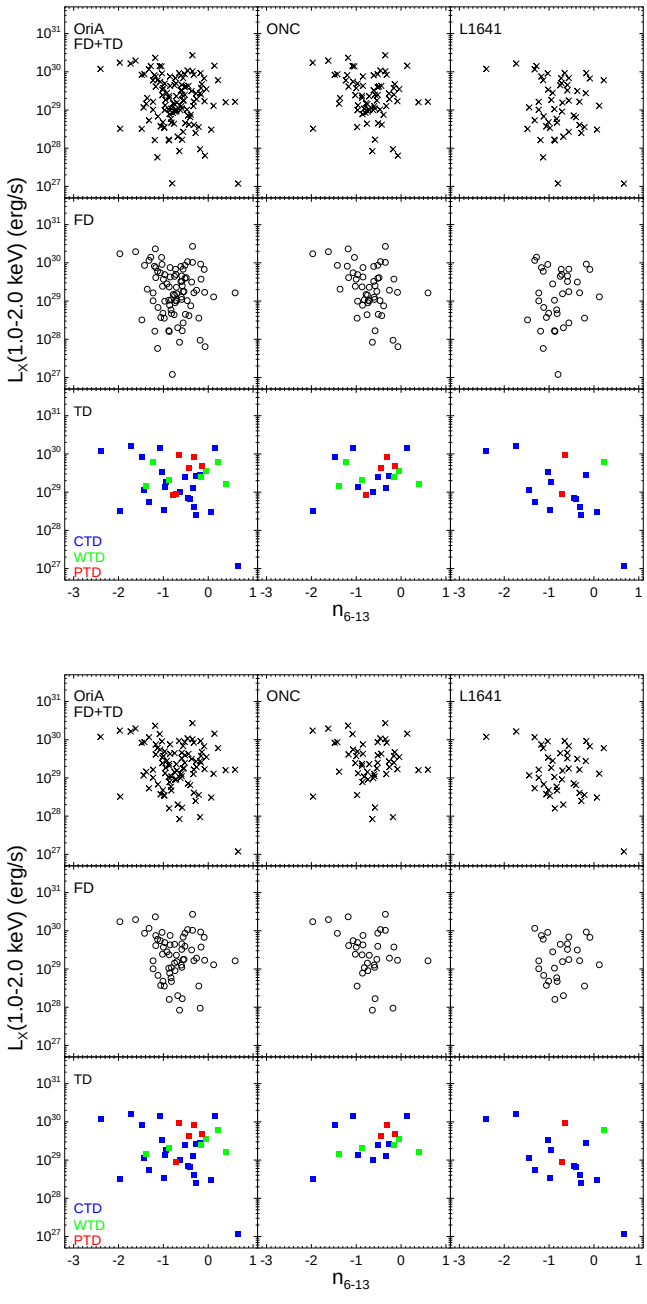


Figure C.149 n_{6-13} vs. $\log L_X 3$. Upper panel: all available objects; Lower panel: objects with available spectral types only

Table C.297 n_{6-13} vs. $\log L_X 3$ (I)

	Ori A				ONC				L1641			
	N	ρ	τ	r	N	ρ	τ	r	N	ρ	τ	r
TDFD	122	-0.120	-0.081	-0.192	69	-0.159	-0.112	-0.200	53	-0.116	-0.085	-0.225
		0.189	0.187	0.034		0.193	0.172	0.099		0.409	0.368	0.105
FD	86	-0.117	-0.080	-0.154	50	-0.326	-0.233	-0.397	36	0.084	0.049	0.122
		0.283	0.278	0.157		0.021	0.017	0.004		0.625	0.671	0.478
TD	36	-0.100	-0.065	-0.273	19	0.244	0.193	0.269	17	-0.498	-0.397	-0.598
		0.562	0.576	0.107		0.314	0.248	0.265		0.042	0.026	0.011

ρ: Spearsmans ρ
τ: Kendalls τ
r: Pearsons r

Table C.298 n_{6-13} vs. $\log L_X 3$ (II)

	Ori A				ONC				L1641			
	N	ρ	τ	r	N	ρ	τ	r	N	ρ	τ	r
TDFD	94	-0.124	-0.084	-0.230	50	-0.100	-0.072	-0.126	44	-0.203	-0.154	-0.359
		0.235	0.228	0.026		0.491	0.460	0.383		0.186	0.141	0.017
FD	60	-0.126	-0.091	-0.198	33	-0.280	-0.203	-0.342	27	0.027	0.006	0.046
		0.339	0.306	0.129		0.115	0.096	0.051		0.894	0.967	0.820
TD	34	-0.080	-0.046	-0.262	17	0.324	0.250	0.321	17	-0.498	-0.397	-0.598
		0.654	0.700	0.134		0.205	0.161	0.209		0.042	0.026	0.011

ρ: Spearsmans ρ
τ: Kendalls τ
r: Pearsons r

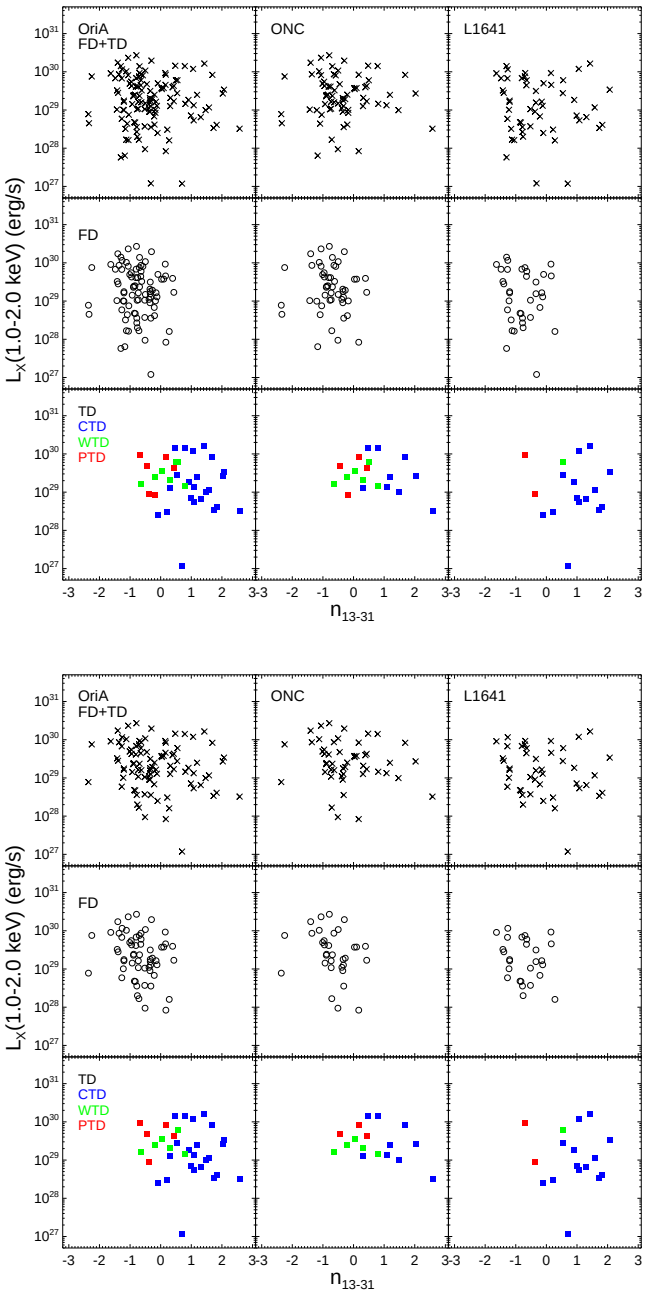


Figure C.150 n_{13-31} vs. $\log L_X 3$. Upper panel: all available objects; Lower panel: objects with available spectral types only

Table C.299 n_{13-31} vs. $\log L_X 3$ (I)

	Ori A				ONC				L1641			
	N	ρ	τ	r	N	ρ	τ	r	N	ρ	τ	r
TDFD	122	-0.058	-0.040	-0.052	69	-0.019	-0.016	-0.018	53	-0.092	-0.070	-0.063
		0.523	0.512	0.569		0.876	0.848	0.883		0.514	0.461	0.654
FD	86	-0.092	-0.060	-0.080	50	-0.111	-0.087	-0.071	36	-0.152	-0.105	-0.109
		0.400	0.413	0.464		0.443	0.374	0.624		0.376	0.366	0.527
TD	36	-0.152	-0.106	-0.129	19	-0.114	-0.064	-0.245	17	0.042	0.015	0.004
		0.376	0.361	0.453		0.642	0.700	0.312		0.874	0.934	0.988

ρ: Spearsmans ρ
τ: Kendalls τ
r: Pearsons r

Table C.300 n_{13-31} vs. $\log L_X 3$ (II)

	Ori A				ONC				L1641			
	N	ρ	τ	r	N	ρ	τ	r	N	ρ	τ	r
TDFD	94	-0.189	-0.128	-0.180	50	-0.205	-0.139	-0.172	44	-0.177	-0.136	-0.175
		0.068	0.067	0.083		0.154	0.155	0.232		0.250	0.195	0.256
FD	60	-0.248	-0.162	-0.234	33	-0.360	-0.248	-0.262	27	-0.182	-0.146	-0.207
		0.056	0.068	0.072		0.039	0.042	0.141		0.363	0.285	0.300
TD	34	-0.177	-0.125	-0.143	17	-0.248	-0.162	-0.330	17	0.042	0.015	0.004
		0.317	0.299	0.420		0.338	0.365	0.196		0.874	0.934	0.988

ρ: Spearsmans ρ
τ: Kendalls τ
r: Pearsons r

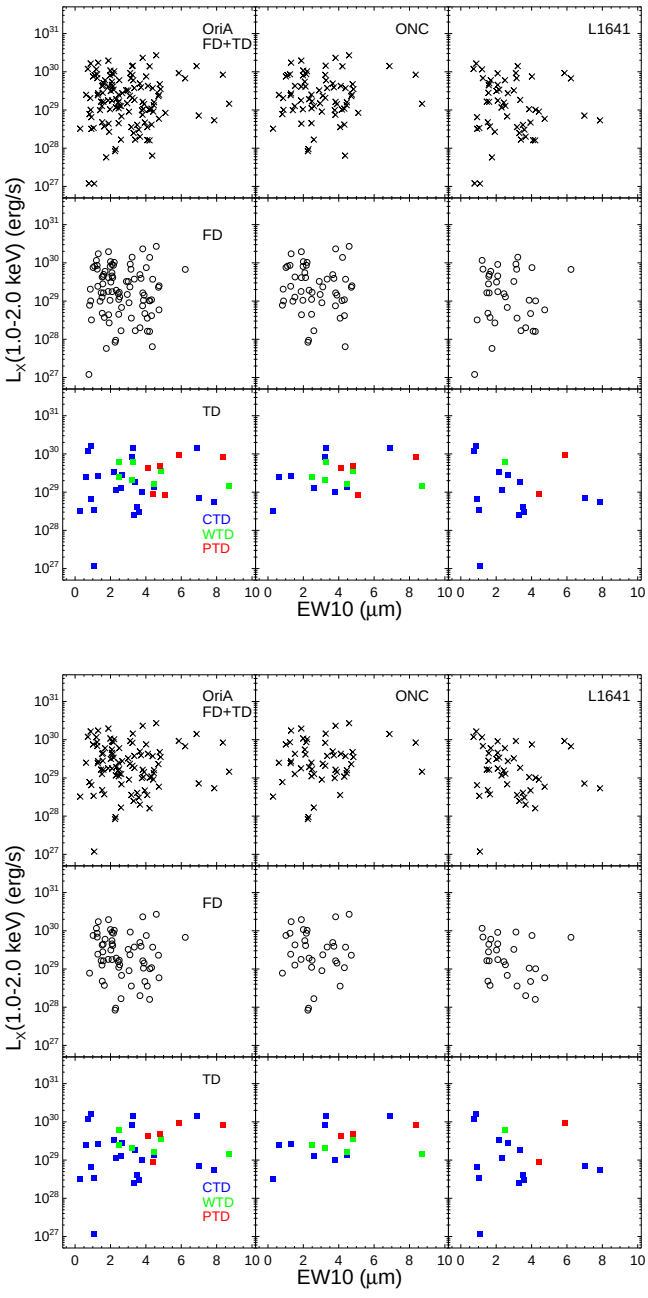


Figure C.151 EW10 vs. $\log L_X 3$. Upper panel: all available objects; Lower panel: objects with available spectral types only

Table C.301 EW10 vs. $\log L_X 3$ (I)

	Ori A				ONC				L1641			
	N	ρ	τ	r	N	ρ	τ	r	N	ρ	τ	r
TDFD	122	-0.040	-0.030	0.042	69	0.001	0.006	0.062	53	-0.116	-0.093	-0.009
		0.661	0.623	0.646		0.993	0.938	0.613		0.409	0.326	0.949
FD	86	-0.113	-0.078	-0.040	50	-0.136	-0.085	-0.102	36	-0.091	-0.076	0.022
		0.302	0.286	0.715		0.347	0.384	0.481		0.598	0.513	0.899
TD	36	0.046	0.037	0.154	19	0.198	0.129	0.313	17	-0.235	-0.176	-0.035
		0.791	0.754	0.370		0.416	0.440	0.192		0.363	0.323	0.894

ρ: Spearsmans ρ
τ: Kendalls τ
r: Pearsons r

Table C.302 EW10 vs. $\log L_X 3$ (II)

	Ori A				ONC				L1641			
	N	ρ	τ	r	N	ρ	τ	r	N	ρ	τ	r
TDFD	94	-0.089	-0.065	0.013	50	0.020	0.021	0.128	44	-0.249	-0.197	-0.138
		0.394	0.353	0.901		0.889	0.828	0.376		0.102	0.060	0.372
FD	60	-0.244	-0.168	-0.129	33	-0.170	-0.104	-0.031	27	-0.328	-0.259	-0.251
		0.060	0.058	0.326		0.345	0.394	0.864		0.094	0.058	0.207
TD	34	0.081	0.071	0.170	17	0.332	0.244	0.385	17	-0.235	-0.176	-0.035
		0.650	0.553	0.336		0.193	0.172	0.127		0.363	0.323	0.894

ρ: Spearsmans ρ
τ: Kendalls τ
r: Pearsons r

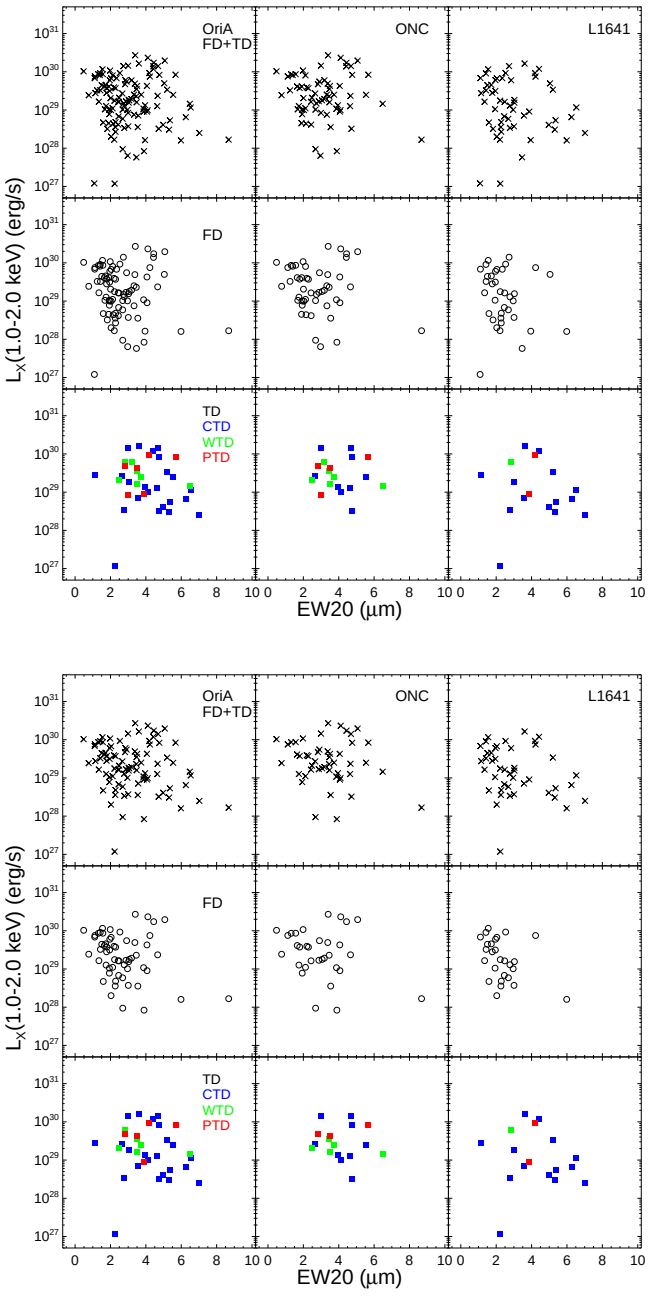


Figure C.152 EW20 vs. $\log L_X$3.Upper panel: all available objects; Lower panel: objects with available spectral types only

Table C.303 EW20 vs. $\log L_X 3$ (I)

	Ori A				ONC				L1641			
	N	ρ	τ	r	N	ρ	τ	r	N	ρ	τ	r
TDFD	122	-0.093	-0.064	-0.083	69	-0.031	-0.032	-0.097	53	-0.136	-0.089	-0.110
		0.309	0.294	0.363		0.801	0.694	0.428		0.333	0.345	0.433
FD	86	-0.146	-0.104	-0.098	50	-0.101	-0.084	-0.132	36	-0.194	-0.133	-0.148
		0.180	0.157	0.369		0.484	0.389	0.361		0.257	0.253	0.389
TD	36	-0.182	-0.127	-0.091	19	-0.068	-0.076	-0.067	17	-0.179	-0.118	-0.064
		0.287	0.276	0.598		0.781	0.649	0.785		0.492	0.510	0.807

ρ: Spearsmans ρ
τ: Kendalls τ
r: Pearsons r

Table C.304 EW20 vs. $\log L_X 3$ (II)

	Ori A				ONC				L1641			
	N	ρ	τ	r	N	ρ	τ	r	N	ρ	τ	r
TDFD	94	-0.194	-0.132	-0.184	50	-0.152	-0.117	-0.196	44	-0.287	-0.189	-0.259
		0.061	0.059	0.076		0.293	0.232	0.173		0.058	0.070	0.090
FD	60	-0.240	-0.168	-0.212	33	-0.168	-0.129	-0.225	27	-0.425	-0.282	-0.420
		0.064	0.057	0.104		0.349	0.292	0.208		0.027	0.039	0.029
TD	34	-0.211	-0.148	-0.090	17	-0.150	-0.132	-0.107	17	-0.179	-0.118	-0.064
		0.232	0.219	0.613		0.567	0.458	0.683		0.492	0.510	0.807

ρ: Spearsmans ρ
τ: Kendalls τ
r: Pearsons r

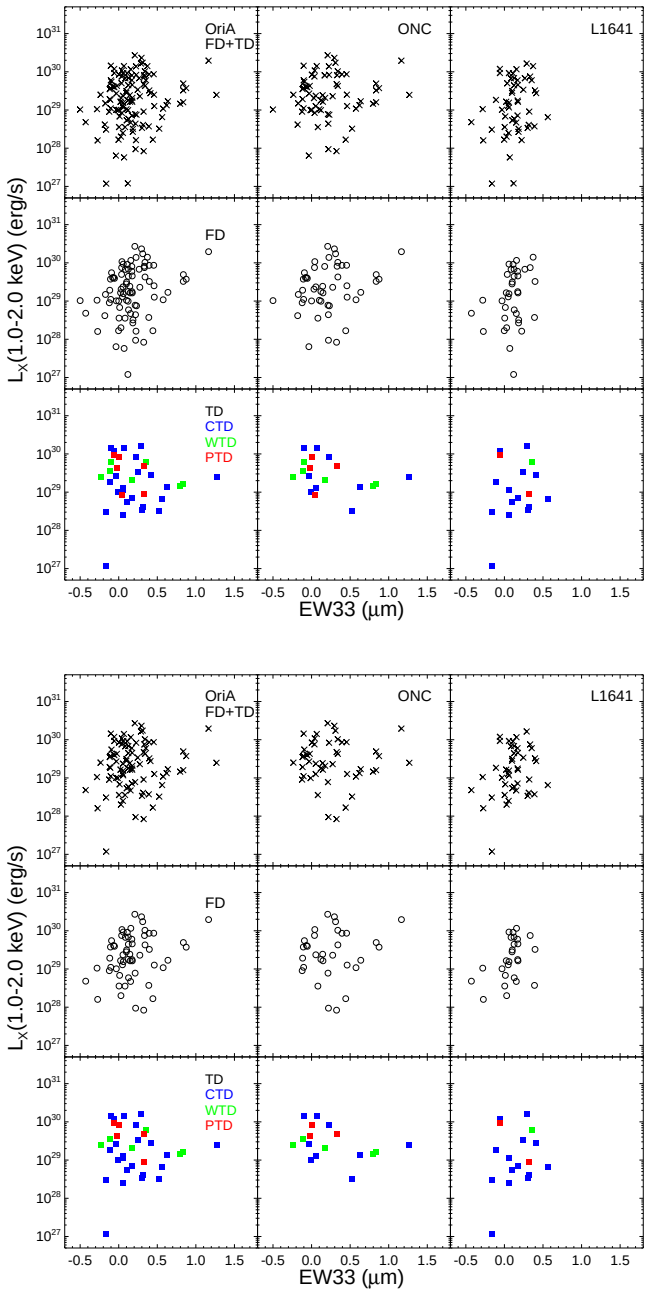


Figure C.153 EW33 vs. $\log L_X 3$. Upper panel: all available objects; Lower panel: objects with available spectral types only

Table C.305 EW33 vs. $\log L_X 3$ (I)

	Ori A				ONC				L1641			
	N	ρ	τ	r	N	ρ	τ	r	N	ρ	τ	r
TDFD	122	0.127	0.084	-0.016	69	0.059	0.046	-0.103	53	0.214	0.146	0.253
		0.164	0.168	0.861		0.632	0.576	0.400		0.123	0.122	0.068
FD	86	0.247	0.165	-0.014	50	0.201	0.135	-0.081	36	0.293	0.210	0.286
		0.022	0.024	0.898		0.161	0.168	0.576		0.083	0.072	0.091
TD	36	-0.125	-0.078	-0.033	19	-0.367	-0.193	-0.347	17	0.195	0.140	0.222
		0.466	0.504	0.848		0.123	0.248	0.146		0.453	0.432	0.392

ρ: Spearsmans ρ
τ: Kendalls τ
r: Pearsons r

Table C.306 EW33 vs. $\log L_X 3$ (II)

	Ori A				ONC				L1641			
	N	ρ	τ	r	N	ρ	τ	r	N	ρ	τ	r
TDFD	94	0.097	0.068	0.122	50	-0.022	0.003	0.027	44	0.232	0.154	0.279
		0.351	0.332	0.241		0.877	0.973	0.852		0.130	0.141	0.067
FD	60	0.243	0.164	0.210	33	0.129	0.083	0.145	27	0.440	0.306	0.421
		0.061	0.064	0.107		0.473	0.495	0.421		0.022	0.025	0.029
TD	34	-0.111	-0.068	-0.019	17	-0.377	-0.191	-0.376	17	0.195	0.140	0.222
		0.533	0.573	0.915		0.135	0.284	0.137		0.453	0.432	0.392

ρ: Spearsmans ρ
τ: Kendalls τ
r: Pearsons r

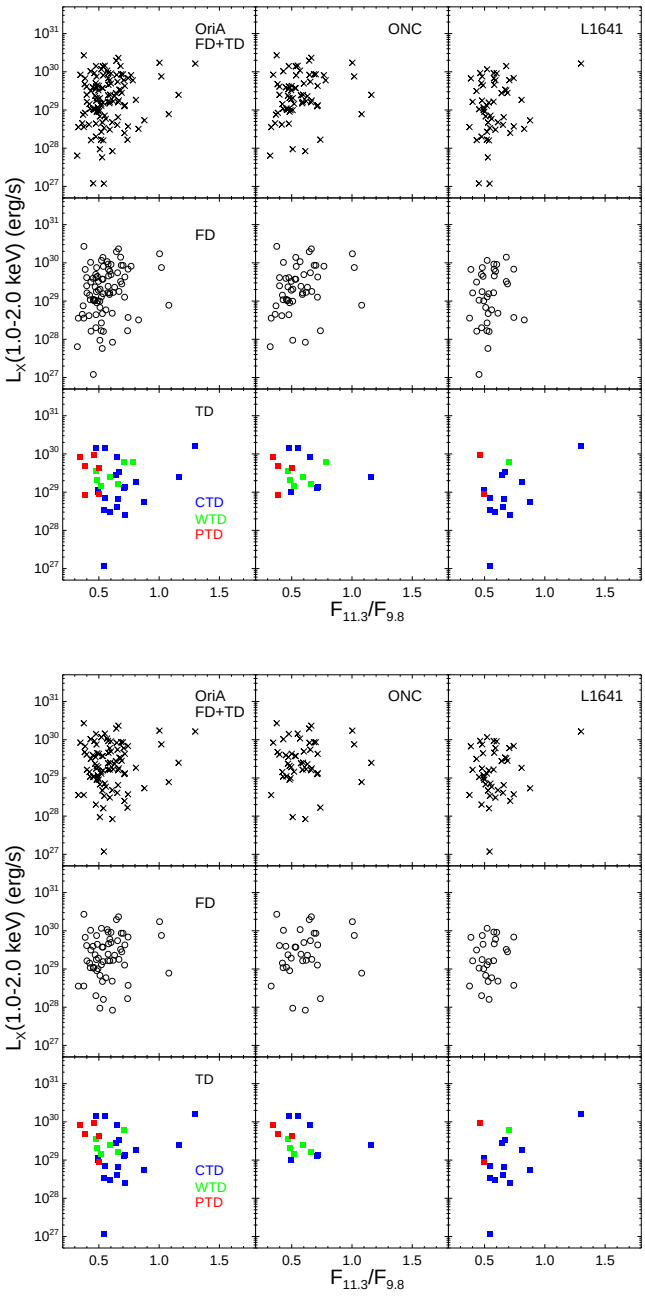


Figure C.154 $F_{11.3}/F_{9.8}$ vs. $\log L_X 3$. Upper panel: all available objects; Lower panel: objects with available spectral types only

Table C.307 $F_{11.3}/F_{9.8}$ vs. $\log L_X 3$ (I)

	Ori A				ONC				L1641			
	N	ρ	τ	r	N	ρ	τ	r	N	ρ	τ	r
TDFD	122	0.186	0.125	0.140	69	0.248	0.174	0.122	53	0.182	0.112	0.200
		0.040	0.042	0.124		0.040	0.035	0.318		0.193	0.237	0.151
FD	86	0.261	0.176	0.136	50	0.301	0.215	0.124	36	0.227	0.143	0.166
		0.015	0.016	0.212		0.034	0.028	0.391		0.184	0.220	0.333
TD	36	0.058	0.044	0.247	19	0.019	0.018	0.196	17	0.279	0.191	0.358
		0.735	0.703	0.146		0.937	0.916	0.421		0.277	0.284	0.158

ρ: Spearsmans ρ
τ: Kendalls τ
r: Pearsons r

Table C.308 $F_{11.3}/F_{9.8}$ vs. $\log L_X 3$ (II)

	Ori A				ONC				L1641			
	N	ρ	τ	r	N	ρ	τ	r	N	ρ	τ	r
TDFD	94	0.086	0.053	0.151	50	0.052	0.030	0.106	44	0.100	0.055	0.226
		0.408	0.451	0.146		0.722	0.757	0.464		0.516	0.599	0.140
FD	60	0.171	0.113	0.144	33	0.138	0.091	0.125	27	0.153	0.088	0.116
		0.192	0.202	0.272		0.445	0.457	0.488		0.445	0.518	0.564
TD	34	-0.006	-0.002	0.250	17	-0.174	-0.118	0.183	17	0.279	0.191	0.358
		0.972	0.988	0.154		0.504	0.510	0.482		0.277	0.284	0.158

ρ: Spearsmans ρ
τ: Kendalls τ
r: Pearsons r

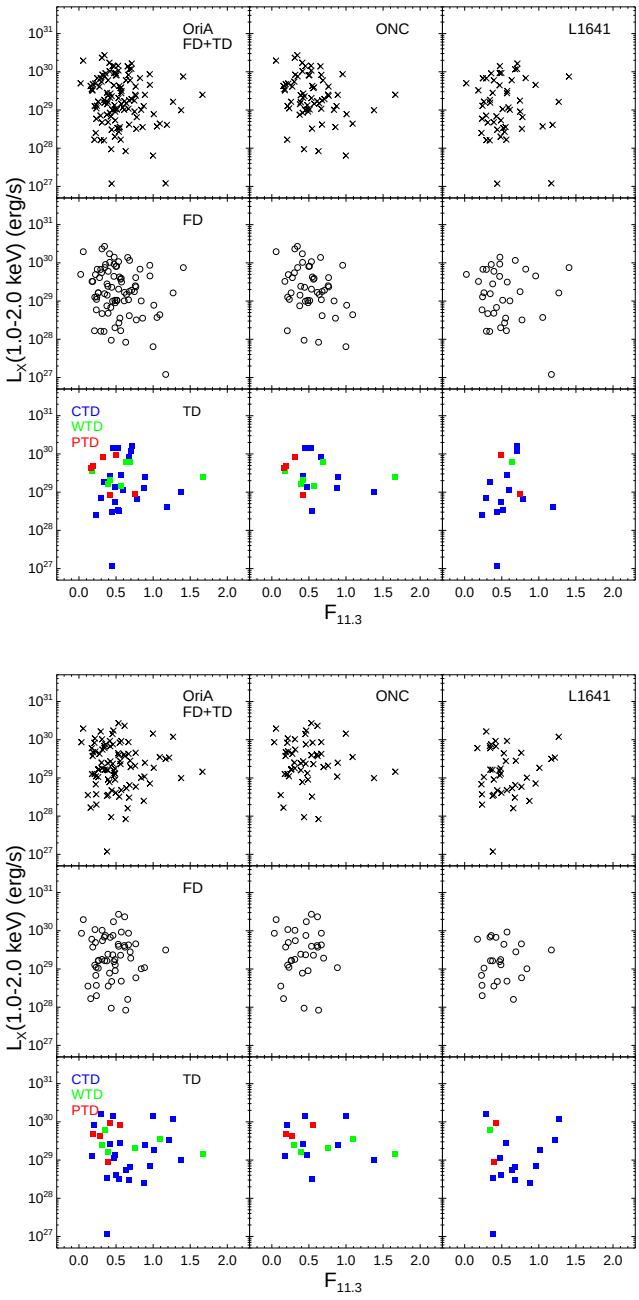


Figure C.155 $F_{11.3}$ vs. $\log L_X 3$. Upper panel: all available objects; Lower panel: objects with available spectral types only

Table C.309 $F_{11.3}$ vs. $\log L_X 3$ (I)

	Ori A				ONC				L1641			
	N	ρ	τ	r	N	ρ	τ	r	N	ρ	τ	r
TDFD	122	0.032	0.019	0.055	69	0.095	0.064	0.102	53	-0.006	-0.005	-0.004
		0.725	0.762	0.547		0.440	0.434	0.404		0.967	0.957	0.977
FD	86	-0.043	-0.035	0.010	50	-0.053	-0.033	-0.029	36	-0.033	-0.033	0.039
		0.695	0.638	0.927		0.714	0.731	0.842		0.848	0.774	0.821
TD	36	0.092	0.060	0.111	19	0.230	0.170	0.268	17	0.015	-0.015	-0.023
		0.595	0.605	0.519		0.344	0.310	0.267		0.955	0.934	0.930

ρ: Spearsmans ρ
τ: Kendalls τ
r: Pearsons r

Table C.310 $F_{11.3}$ vs. $\log L_X 3$ (II)

	Ori A				ONC				L1641			
	N	ρ	τ	r	N	ρ	τ	r	N	ρ	τ	r
TDFD	94	-0.069	-0.046	-0.029	50	0.035	0.033	0.079	44	-0.156	-0.113	-0.147
		0.512	0.516	0.781		0.810	0.731	0.586		0.310	0.279	0.341
FD	60	-0.212	-0.145	-0.161	33	-0.140	-0.078	-0.066	27	-0.297	-0.217	-0.291
		0.103	0.101	0.219		0.438	0.525	0.715		0.132	0.113	0.141
TD	34	0.084	0.052	0.107	17	0.265	0.191	0.277	17	0.015	-0.015	-0.023
		0.636	0.667	0.547		0.305	0.284	0.282		0.955	0.934	0.930

ρ: Spearsmans ρ
τ: Kendalls τ
r: Pearsons r

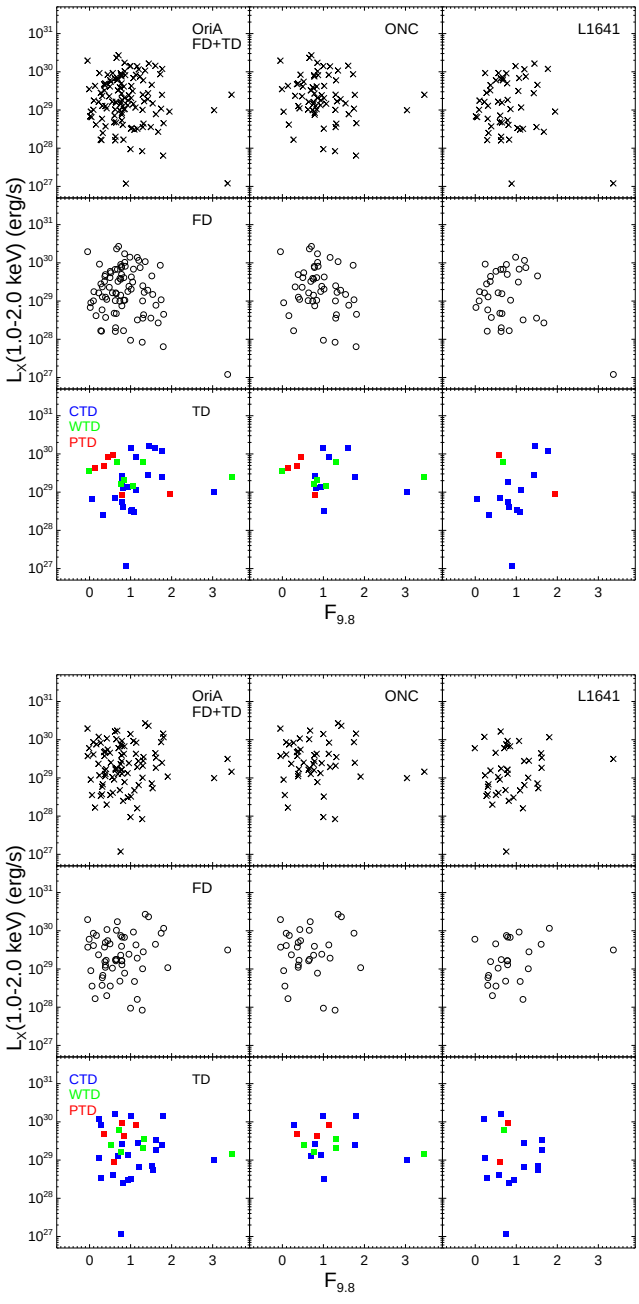


Figure C.156 $F_{9.8}$ vs. $\log L_X 3$. Upper panel: all available objects; Lower panel: objects with available spectral types only

Table C.311 $F_{9.8}$ vs. $\log L_X 3$ (I)

	Ori A				ONC				L1641			
	N	ρ	τ	r	N	ρ	τ	r	N	ρ	τ	r
TDFD	122	-0.071	-0.056	0.019	69	-0.033	-0.027	0.028	53	-0.114	-0.100	-0.040
		0.437	0.358	0.835		0.788	0.744	0.819		0.417	0.290	0.776
FD	86	-0.144	-0.105	-0.095	50	-0.177	-0.125	-0.173	36	-0.078	-0.079	-0.018
		0.187	0.154	0.384		0.219	0.201	0.230		0.652	0.496	0.917
TD	36	0.095	0.057	0.164	19	0.239	0.158	0.301	17	-0.208	-0.147	-0.064
		0.581	0.624	0.339		0.325	0.345	0.210		0.422	0.410	0.807

ρ: Spearsmans ρ
τ: Kendalls τ
r: Pearsons r

Table C.312 $F_{9.8}$ vs. $\log L_X 3$ (II)

	Ori A				ONC				L1641			
	N	ρ	τ	r	N	ρ	τ	r	N	ρ	τ	r
TDFD	94	-0.112	-0.086	0.006	50	0.010	0.011	0.102	44	-0.247	-0.203	-0.155
		0.281	0.222	0.954		0.947	0.907	0.481		0.106	0.052	0.315
FD	60	-0.263	-0.189	-0.176	33	-0.171	-0.114	-0.108	27	-0.310	-0.259	-0.255
		0.043	0.033	0.179		0.341	0.353	0.550		0.115	0.058	0.199
TD	34	0.126	0.087	0.185	17	0.375	0.265	0.385	17	-0.208	-0.147	-0.064
		0.479	0.468	0.295		0.138	0.138	0.127		0.422	0.410	0.807

ρ: Spearsmans ρ
τ: Kendalls τ
r: Pearsons r

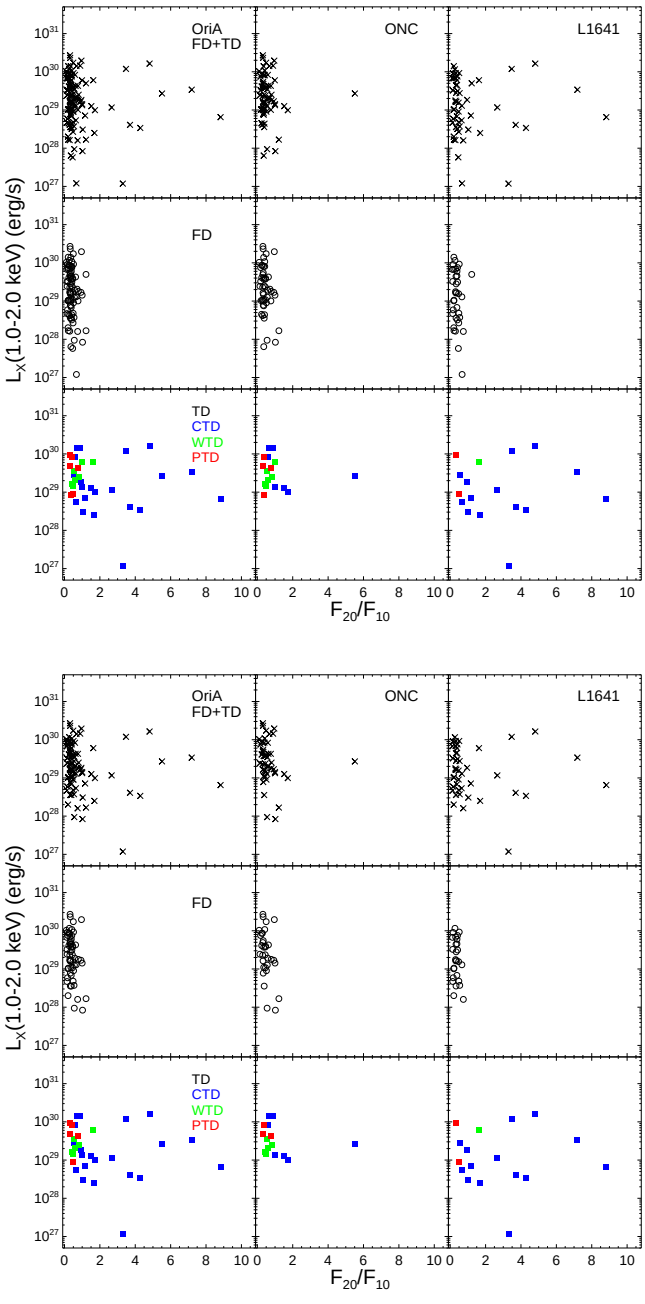


Figure C.157 F_{20}/F_{10} vs. $\log L_X 3$. Upper panel: all available objects; Lower panel: objects with available spectral types only

Table C.313 F_{20}/F_{10} vs. $\log L_X 3$ (I)

	Ori A				ONC				L1641			
	N	ρ	τ	r	N	ρ	τ	r	N	ρ	τ	r
TDFD	121	-0.150	-0.107	-0.048	68	-0.118	-0.082	-0.021	53	-0.163	-0.118	-0.034
		0.100	0.082	0.601		0.339	0.325	0.865		0.243	0.214	0.809
FD	86	-0.195	-0.134	-0.206	50	-0.226	-0.158	-0.283	36	-0.227	-0.152	-0.183
		0.071	0.068	0.057		0.115	0.106	0.046		0.184	0.191	0.285
TD	35	-0.238	-0.170	-0.097	18	-0.141	-0.098	-0.104	17	-0.047	-0.059	0.003
		0.169	0.151	0.579		0.576	0.570	0.681		0.859	0.742	0.991

ρ: Spearsmans ρ
τ: Kendalls τ
r: Pearsons r

Table C.314 F_{20}/F_{10} vs. $\log L_X 3$ (II)

	Ori A				ONC				L1641			
	N	ρ	τ	r	N	ρ	τ	r	N	ρ	τ	r
TDFD	93	-0.247	-0.179	-0.103	49	-0.329	-0.228	-0.070	44	-0.191	-0.140	-0.102
		0.017	0.011	0.326		0.021	0.021	0.633		0.214	0.182	0.510
FD	60	-0.262	-0.182	-0.314	33	-0.451	-0.311	-0.451	27	-0.116	-0.066	-0.212
		0.043	0.040	0.015		0.008	0.011	0.008		0.565	0.632	0.288
TD	33	-0.277	-0.208	-0.100	16	-0.344	-0.233	-0.146	17	-0.047	-0.059	0.003
		0.119	0.088	0.580		0.192	0.207	0.590		0.859	0.742	0.991

ρ: Spearsmans ρ
τ: Kendalls τ
r: Pearsons r

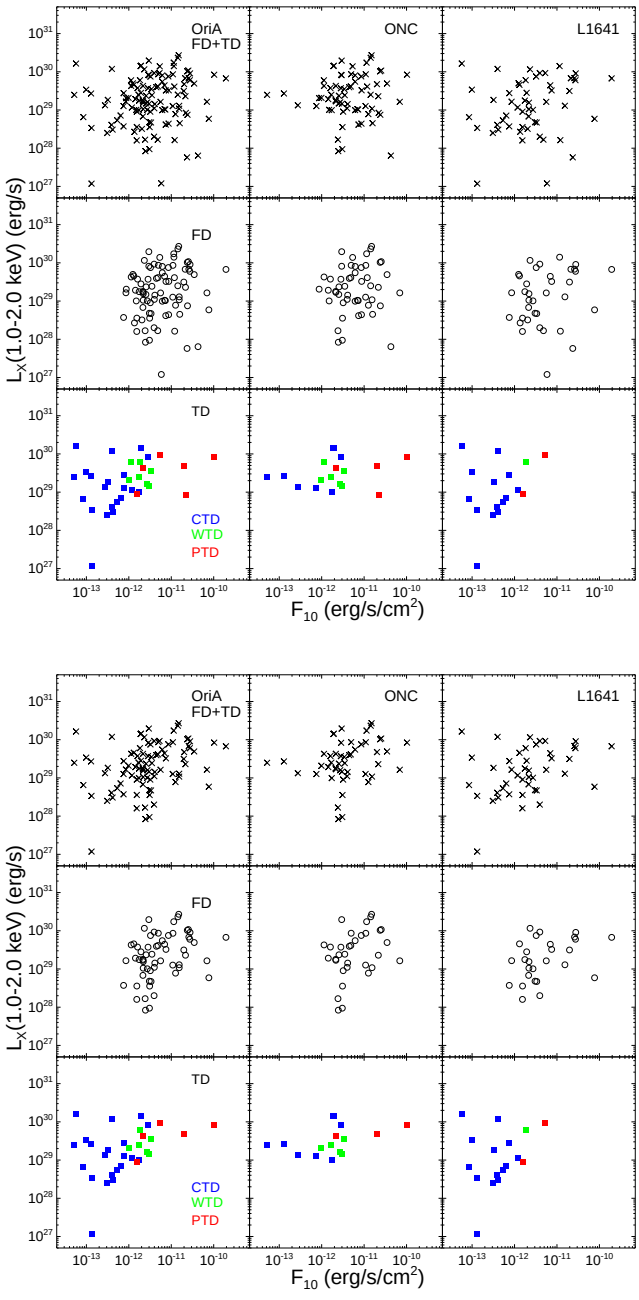


Figure C.158 $\log F_{10}$ vs. $\log L_X 3$. Upper panel: all available objects; Lower panel: objects with available spectral types only

Table C.315 $\log F_{10}$ vs. $\log L_X 3$ (I)

	Ori A				ONC				L1641			
	N	ρ	τ	r	N	ρ	τ	r	N	ρ	τ	r
TDFD	121	0.190	0.127	0.113	68	0.055	0.038	0.042	53	0.200	0.139	0.162
		0.037	0.039	0.217		0.655	0.649	0.734		0.150	0.143	0.246
FD	86	0.203	0.131	0.097	50	0.120	0.091	-0.025	36	0.240	0.146	0.188
		0.061	0.075	0.374		0.405	0.353	0.863		0.159	0.210	0.272
TD	35	0.361	0.267	0.199	18	0.218	0.137	0.235	17	0.218	0.206	0.369
		0.033	0.024	0.252		0.385	0.426	0.348		0.400	0.249	0.145

ρ: Spearsmans ρ
τ: Kendalls τ
r: Pearsons r

Table C.316 $\log F_{10}$ vs. $\log L_X 3$ (II)

	Ori A				ONC				L1641			
	N	ρ	τ	r	N	ρ	τ	r	N	ρ	τ	r
TDFD	93	0.349	0.240	0.184	49	0.275	0.192	0.198	44	0.338	0.242	0.194
		0.001	0.001	0.077		0.056	0.051	0.173		0.025	0.020	0.207
FD	60	0.373	0.247	0.167	33	0.348	0.265	0.184	27	0.401	0.265	0.234
		0.003	0.005	0.202		0.047	0.030	0.305		0.038	0.053	0.240
TD	33	0.413	0.311	0.227	16	0.447	0.283	0.328	17	0.218	0.206	0.369
		0.017	0.011	0.204		0.083	0.126	0.215		0.400	0.249	0.145

ρ: Spearsmans ρ
τ: Kendalls τ
r: Pearsons r

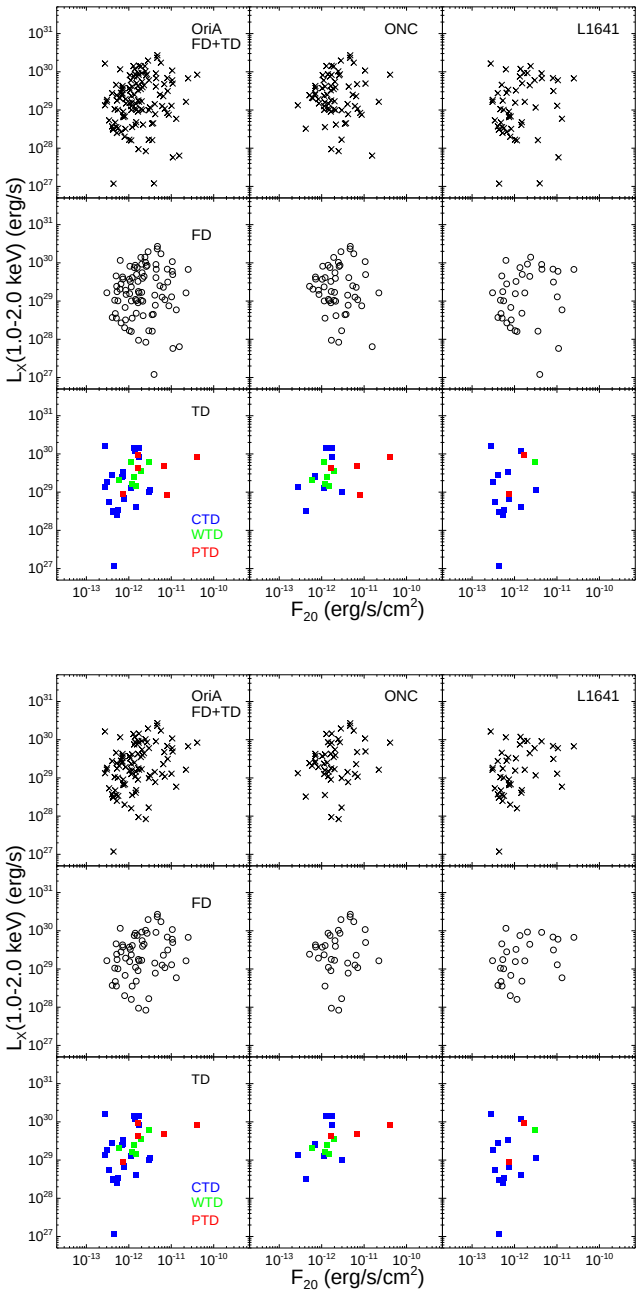


Figure C.159 $\log F_{20}$ vs. $\log L_X 3$. Upper panel: all available objects; Lower panel: objects with available spectral types only

Table C.317 $\log F_{20}$ vs. $\log L_X 3$ (I)

	Ori A				ONC				L1641			
	N	ρ	τ	r	N	ρ	τ	r	N	ρ	τ	r
TDFD	122	0.194	0.136	0.085	69	0.014	0.015	0.028	53	0.203	0.116	0.124
		0.032	0.026	0.352		0.906	0.852	0.819		0.145	0.220	0.376
FD	86	0.139	0.097	0.016	50	-0.027	-0.019	-0.101	36	0.202	0.111	0.124
		0.203	0.185	0.884		0.855	0.847	0.485		0.239	0.340	0.471
TD	36	0.367	0.260	0.211	19	0.314	0.251	0.253	17	0.174	0.118	0.298
		0.028	0.025	0.217		0.190	0.132	0.296		0.504	0.510	0.245

ρ: Spearsmans ρ
τ: Kendalls τ
r: Pearsons r

Table C.318 $\log F_{20}$ vs. $\log L_X 3$ (II)

	Ori A				ONC				L1641			
	N	ρ	τ	r	N	ρ	τ	r	N	ρ	τ	r
TDFD	94	0.334	0.230	0.206	50	0.197	0.144	0.158	44	0.317	0.195	0.245
		0.001	0.001	0.046		0.169	0.139	0.273		0.036	0.063	0.109
FD	60	0.275	0.189	0.174	33	0.088	0.064	0.085	27	0.366	0.231	0.280
		0.033	0.033	0.184		0.627	0.598	0.638		0.060	0.091	0.157
TD	34	0.416	0.298	0.233	17	0.537	0.412	0.317	17	0.174	0.118	0.298
		0.014	0.013	0.185		0.026	0.021	0.215		0.504	0.510	0.245

ρ: Spearsmans ρ
τ: Kendalls τ
r: Pearsons r

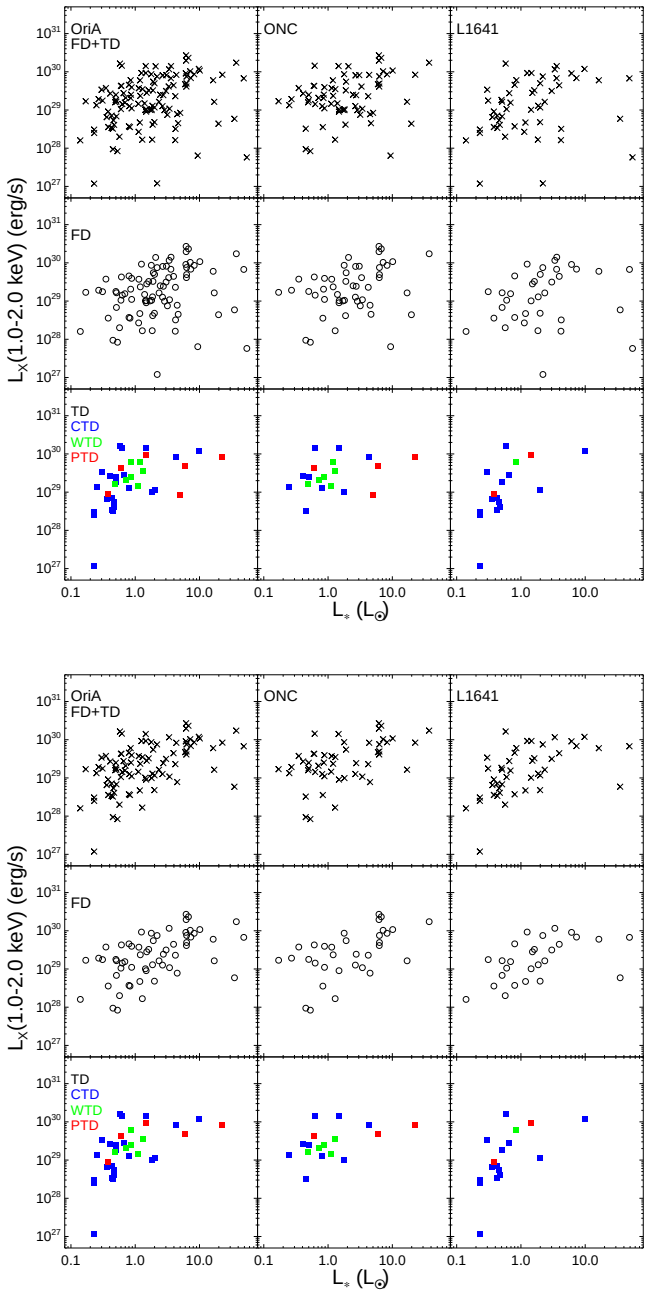


Figure C.160 $\log L_\star$ vs. $\log L_X 3$. Upper panel: all available objects; Lower panel: objects with available spectral types only

Table C.319 $\log L_\star$ vs. $\log L_X 3$ (I)

	Ori A				ONC				L1641			
	N	ρ	τ	r	N	ρ	τ	r	N	ρ	τ	r
TDFD	122	0.355	0.248	0.285	69	0.279	0.185	0.276	53	0.366	0.277	0.259
		0.000	0.000	0.001		0.020	0.025	0.022		0.007	0.003	0.061
FD	86	0.335	0.234	0.237	50	0.328	0.221	0.309	36	0.285	0.216	0.160
		0.002	0.001	0.028		0.020	0.023	0.029		0.092	0.064	0.351
TD	36	0.604	0.431	0.521	19	0.312	0.228	0.334	17	0.747	0.567	0.621
		0.000	0.000	0.001		0.193	0.172	0.162		0.001	0.001	0.008

ρ: Spearsmans ρ
τ: Kendalls τ
r: Pearsons r

Table C.320 $\log L_\star$ vs. $\log L_X 3$ (II)

	Ori A				ONC				L1641			
	N	ρ	τ	r	N	ρ	τ	r	N	ρ	τ	r
TDFD	94	0.554	0.389	0.535	50	0.495	0.338	0.503	44	0.612	0.449	0.538
		0.000	0.000	0.000		0.000	0.001	0.000		0.000	0.000	0.000
FD	60	0.561	0.388	0.539	33	0.561	0.383	0.549	27	0.575	0.420	0.525
		0.000	0.000	0.000		0.001	0.002	0.001		0.002	0.002	0.005
TD	34	0.651	0.468	0.568	17	0.426	0.309	0.469	17	0.747	0.567	0.621
		0.000	0.000	0.000		0.088	0.084	0.058		0.001	0.001	0.008

ρ: Spearsmans ρ
τ: Kendalls τ
r: Pearsons r

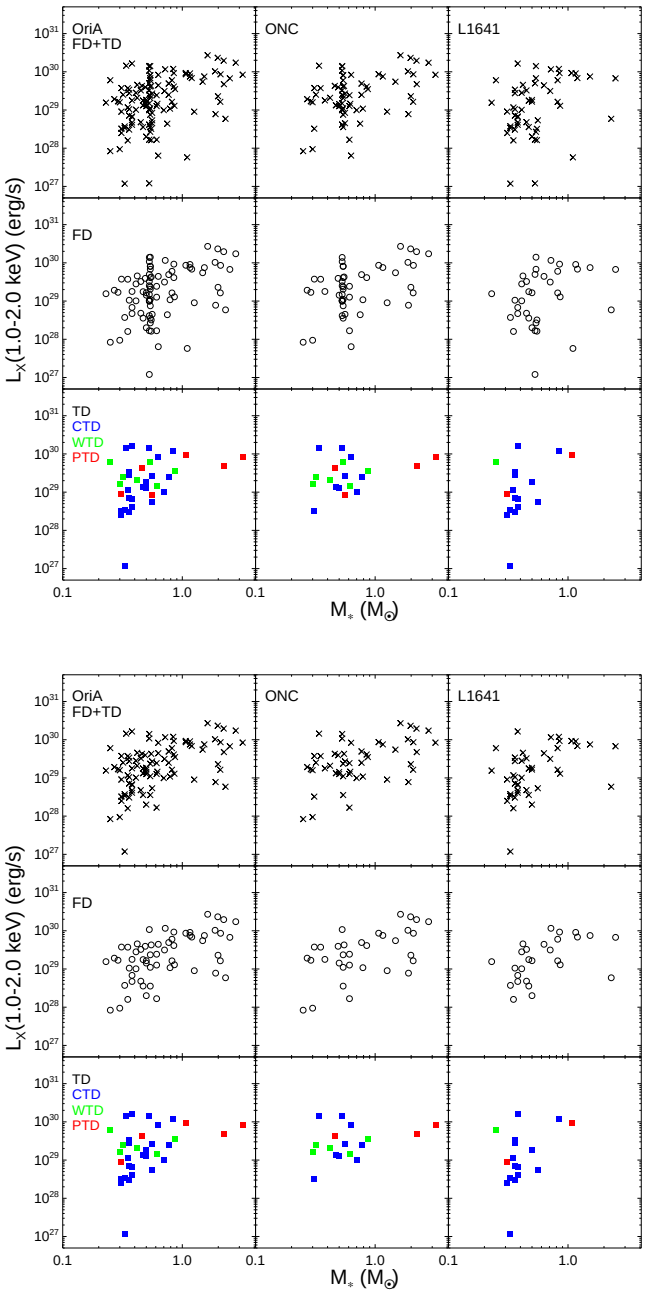


Figure C.161 $\log M_\star$ vs. $\log L_X 3$. Upper panel: all available objects; Lower panel: objects with available spectral types only

Table C.321 $\log M_\star$ vs. $\log L_X 3$ (I)

	Ori A				ONC				L1641			
	N	ρ	τ	r	N	ρ	τ	r	N	ρ	τ	r
TDFD	122	0.369	0.256	0.381	69	0.294	0.193	0.417	53	0.362	0.241	0.298
		0.000	0.000	0.000		0.014	0.019	0.000		0.008	0.011	0.030
FD	86	0.379	0.263	0.395	50	0.335	0.228	0.466	36	0.377	0.236	0.278
		0.000	0.000	0.000		0.018	0.019	0.001		0.024	0.043	0.101
TD	36	0.408	0.294	0.396	19	0.231	0.164	0.321	17	0.386	0.268	0.415
		0.013	0.012	0.017		0.342	0.326	0.180		0.126	0.133	0.098

ρ: Spearsmans ρ
τ: Kendalls τ
r: Pearsons r

Table C.322 $\log M_\star$ vs. $\log L_X 3$ (II)

	Ori A				ONC				L1641			
	N	ρ	τ	r	N	ρ	τ	r	N	ρ	τ	r
TDFD	94	0.489	0.346	0.488	50	0.414	0.280	0.482	44	0.524	0.363	0.452
		0.000	0.000	0.000		0.003	0.004	0.000		0.000	0.001	0.002
FD	60	0.526	0.377	0.539	33	0.473	0.339	0.549	27	0.582	0.394	0.491
		0.000	0.000	0.000		0.005	0.006	0.001		0.001	0.004	0.009
TD	34	0.429	0.307	0.401	17	0.289	0.206	0.341	17	0.386	0.268	0.415
		0.011	0.011	0.019		0.260	0.249	0.180		0.126	0.133	0.098

ρ: Spearsmans ρ
τ: Kendalls τ
r: Pearsons r

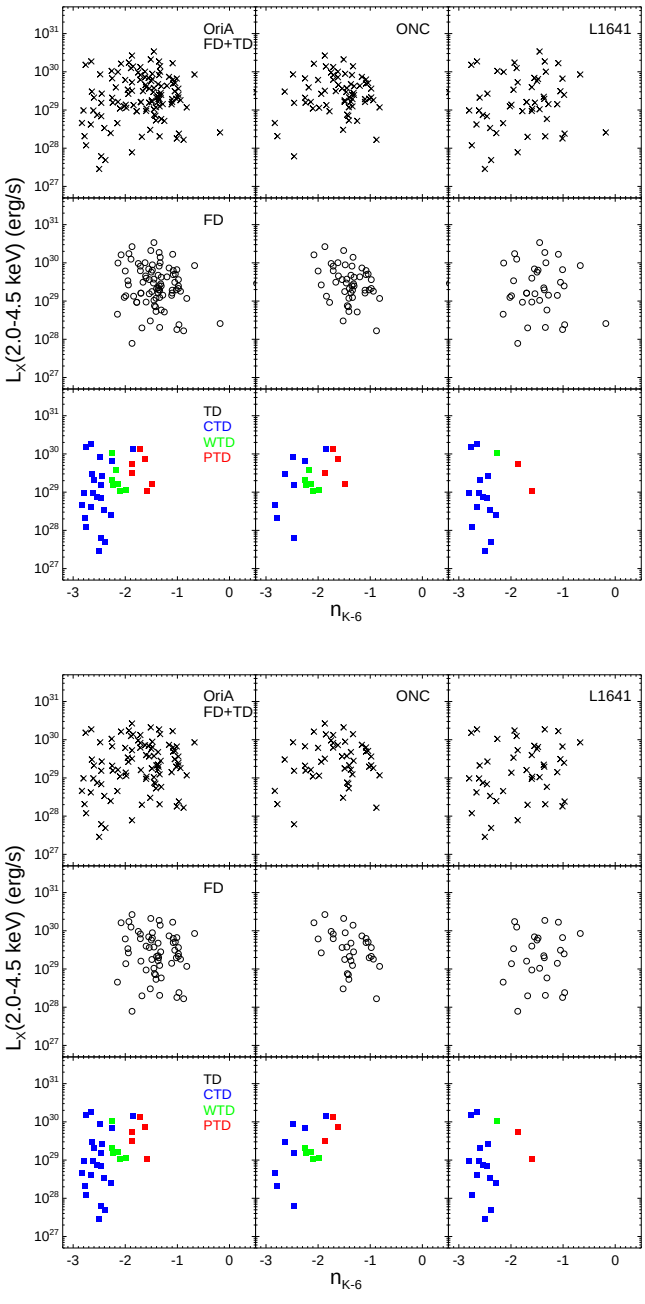


Figure C.162 n_{K-6} vs. $\log L_X 4$. Upper panel: all available objects; Lower panel: objects with available spectral types only

Table C.323 n_{K-6} vs. $\log L_X 4$ (I)

	Ori A				ONC				L1641			
	N	ρ	τ	r	N	ρ	τ	r	N	ρ	τ	r
TDFD	120	0.098	0.062	0.146	67	-0.022	-0.023	0.088	53	0.153	0.114	0.148
		0.288	0.317	0.112		0.858	0.782	0.479		0.276	0.228	0.290
FD	85	-0.125	-0.083	-0.139	49	-0.270	-0.182	-0.247	36	-0.011	0.013	-0.078
		0.256	0.262	0.205		0.060	0.065	0.087		0.950	0.913	0.651
TD	35	0.343	0.219	0.331	18	0.452	0.296	0.517	17	-0.037	-0.044	0.052
		0.044	0.064	0.052		0.059	0.086	0.028		0.889	0.805	0.843

ρ: Spearsmans ρ
τ: Kendalls τ
r: Pearsons r

Table C.324 n_{K-6} vs. $\log L_X 4$ (II)

	Ori A				ONC				L1641			
	N	ρ	τ	r	N	ρ	τ	r	N	ρ	τ	r
TDFD	92	0.136	0.081	0.198	48	0.021	0.001	0.125	44	0.177	0.126	0.211
		0.195	0.251	0.058		0.886	0.993	0.397		0.250	0.228	0.169
FD	59	-0.167	-0.121	-0.124	32	-0.397	-0.279	-0.412	27	0.044	0.043	0.079
		0.207	0.174	0.349		0.024	0.025	0.019		0.829	0.754	0.695
TD	33	0.335	0.215	0.346	16	0.530	0.353	0.597	17	-0.037	-0.044	0.052
		0.057	0.079	0.049		0.035	0.057	0.015		0.889	0.805	0.843

ρ: Spearsmans ρ
τ: Kendalls τ
r: Pearsons r

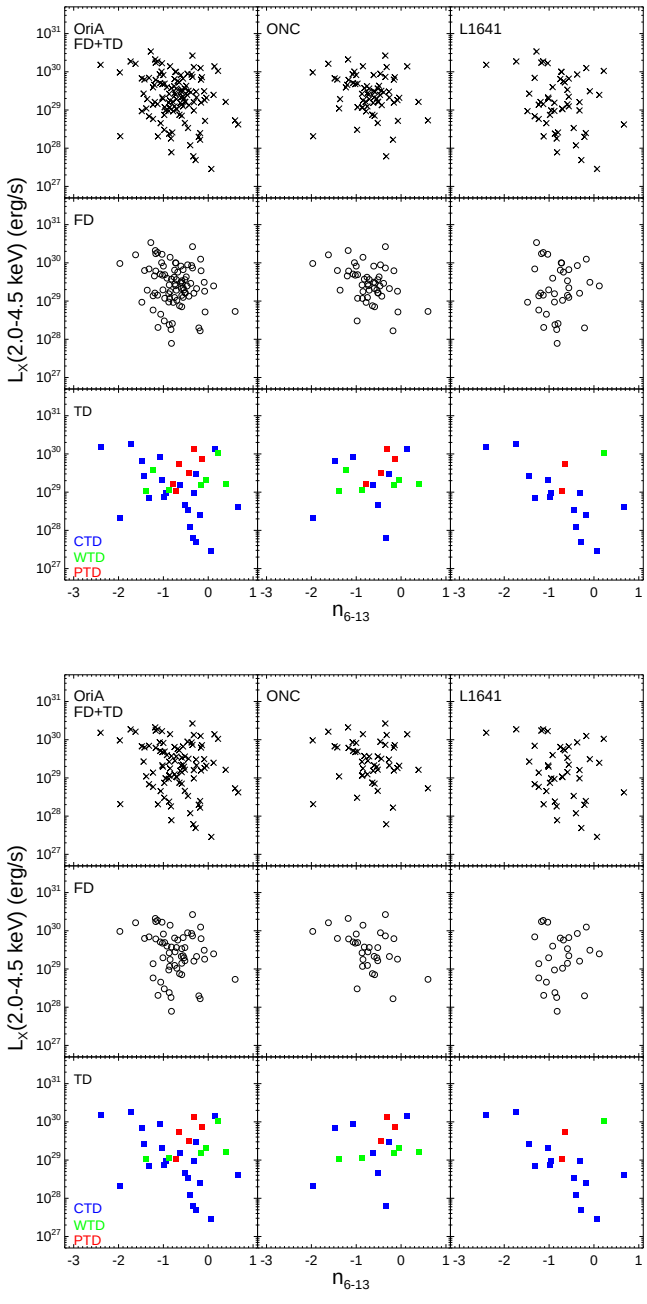


Figure C.163 n_{6-13} vs. $\log L_X 4$. Upper panel: all available objects; Lower panel: objects with available spectral types only

Table C.325 n_{6-13} vs. $\log L_X 4$ (I)

	Ori A				ONC				L1641			
	N	ρ	τ	r	N	ρ	τ	r	N	ρ	τ	r
TDFD	120	-0.168	-0.115	-0.226	67	-0.199	-0.145	-0.180	53	-0.217	-0.149	-0.301
		0.066	0.062	0.013		0.107	0.084	0.145		0.119	0.115	0.029
FD	85	-0.134	-0.095	-0.192	49	-0.351	-0.256	-0.420	36	0.034	0.014	0.010
		0.222	0.198	0.078		0.013	0.010	0.003		0.845	0.902	0.954
TD	35	-0.160	-0.131	-0.242	18	0.265	0.176	0.201	17	-0.571	-0.426	-0.567
		0.357	0.268	0.161		0.287	0.306	0.424		0.017	0.017	0.018

ρ: Spearsmans ρ
τ: Kendalls τ
r: Pearsons r

Table C.326 n_{6-13} vs. $\log L_X 4$ (II)

	Ori A				ONC				L1641			
	N	ρ	τ	r	N	ρ	τ	r	N	ρ	τ	r
TDFD	92	-0.191	-0.134	-0.227	48	-0.184	-0.149	-0.159	44	-0.236	-0.156	-0.310
		0.069	0.059	0.030		0.211	0.137	0.280		0.124	0.136	0.041
FD	59	-0.181	-0.128	-0.200	32	-0.388	-0.305	-0.436	27	0.024	0.023	0.048
		0.169	0.151	0.129		0.028	0.014	0.013		0.904	0.867	0.812
TD	33	-0.133	-0.112	-0.229	16	0.365	0.250	0.238	17	-0.571	-0.426	-0.567
		0.461	0.360	0.200		0.165	0.177	0.375		0.017	0.017	0.018

ρ: Spearsmans ρ
τ: Kendalls τ
r: Pearsons r

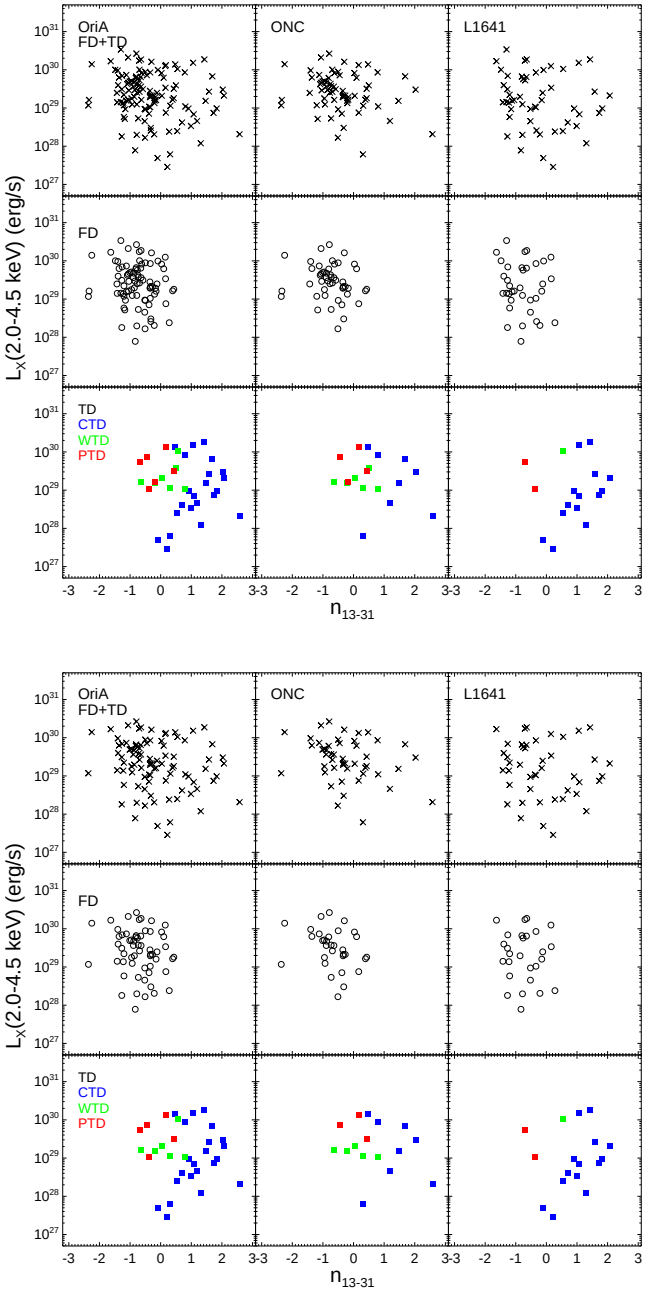


Figure C.164 n_{13-31} vs. $\log L_X 4$. Upper panel: all available objects; Lower panel: objects with available spectral types only

Table C.327 n_{13-31} vs. $\log L_X 4$ (I)

	Ori A				ONC				L1641			
	N	ρ	τ	r	N	ρ	τ	r	N	ρ	τ	r
TDFD	120	-0.193	-0.124	-0.199	67	-0.200	-0.146	-0.226	53	-0.201	-0.124	-0.164
		0.034	0.044	0.029		0.104	0.081	0.066		0.148	0.191	0.241
FD	85	-0.120	-0.079	-0.138	49	-0.198	-0.153	-0.163	36	-0.106	-0.067	-0.131
		0.276	0.283	0.208		0.172	0.122	0.263		0.538	0.565	0.446
TD	35	-0.069	-0.029	-0.027	18	-0.158	-0.085	-0.208	17	0.240	0.191	0.202
		0.694	0.809	0.878		0.531	0.622	0.408		0.353	0.284	0.437

ρ: Spearsmans ρ
τ: Kendalls τ
r: Pearsons r

Table C.328 n_{13-31} vs. $\log L_X 4$ (II)

	Ori A				ONC				L1641			
	N	ρ	τ	r	N	ρ	τ	r	N	ρ	τ	r
TDFD	92	-0.227	-0.150	-0.206	48	-0.293	-0.217	-0.292	44	-0.159	-0.089	-0.125
		0.030	0.034	0.049		0.044	0.029	0.044		0.302	0.395	0.419
FD	59	-0.171	-0.117	-0.162	32	-0.327	-0.256	-0.262	27	-0.028	-0.009	-0.080
		0.197	0.192	0.220		0.068	0.039	0.147		0.888	0.950	0.692
TD	33	-0.048	-0.019	-0.017	16	-0.203	-0.133	-0.217	17	0.240	0.191	0.202
		0.789	0.877	0.925		0.451	0.471	0.420		0.353	0.284	0.437

ρ: Spearsmans ρ
τ: Kendalls τ
r: Pearsons r

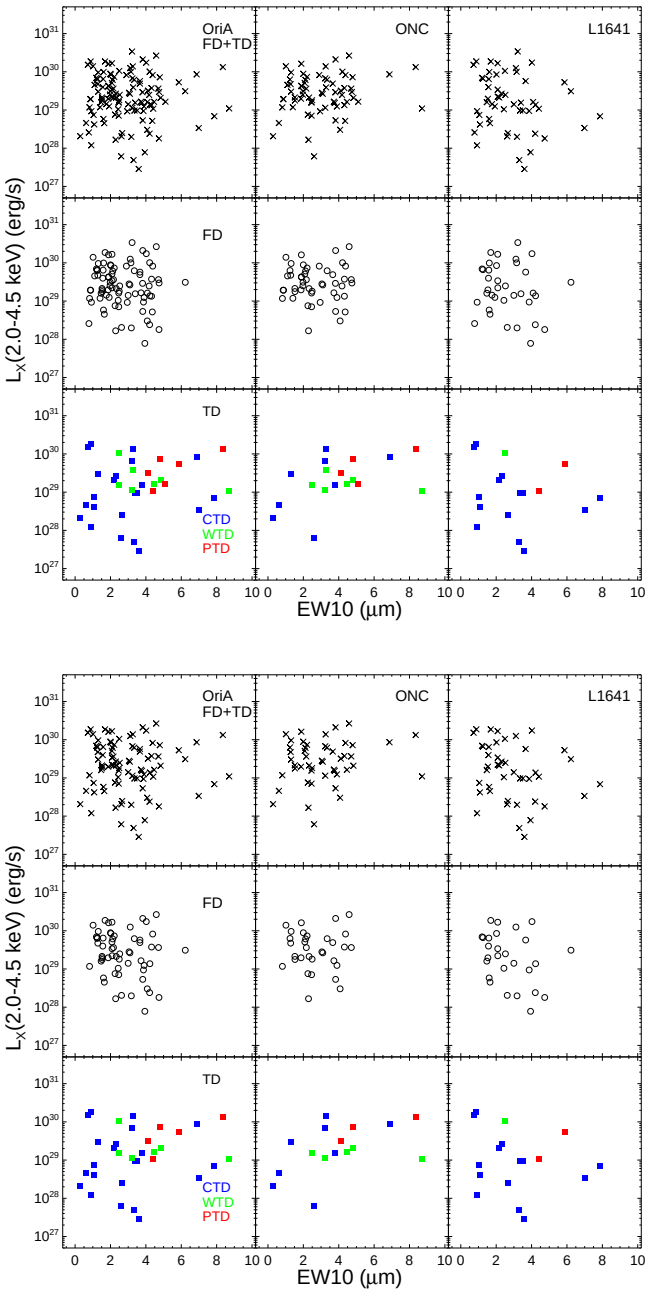


Figure C.165 EW10 vs. $\log L_X 4$. Upper panel: all available objects; Lower panel: objects with available spectral types only

Table C.329 EW10 vs. $\log L_X 4$ (I)

	Ori A				ONC				L1641			
	N	ρ	τ	r	N	ρ	τ	r	N	ρ	τ	r
TDFD	120	-0.044	-0.030	-0.019	67	0.062	0.043	0.137	53	-0.204	-0.136	-0.191
		0.633	0.629	0.837		0.618	0.603	0.269		0.144	0.149	0.171
FD	85	-0.083	-0.054	-0.087	49	-0.054	-0.035	-0.033	36	-0.134	-0.086	-0.146
		0.452	0.464	0.429		0.711	0.724	0.822		0.436	0.462	0.396
TD	35	0.100	0.084	0.151	18	0.432	0.315	0.461	17	-0.299	-0.176	-0.186
		0.568	0.477	0.387		0.074	0.068	0.054		0.244	0.323	0.475

ρ: Spearsmans ρ
τ: Kendalls τ
r: Pearsons r

Table C.330 EW10 vs. $\log L_X 4$ (II)

	Ori A				ONC				L1641			
	N	ρ	τ	r	N	ρ	τ	r	N	ρ	τ	r
TDFD	92	-0.091	-0.069	-0.037	48	0.092	0.054	0.175	44	-0.314	-0.222	-0.255
		0.386	0.330	0.726		0.534	0.587	0.234		0.038	0.034	0.095
FD	59	-0.210	-0.151	-0.179	32	-0.102	-0.087	-0.023	27	-0.358	-0.259	-0.306
		0.110	0.091	0.175		0.578	0.485	0.901		0.067	0.058	0.121
TD	33	0.103	0.089	0.153	16	0.481	0.377	0.481	17	-0.299	-0.176	-0.186
		0.570	0.466	0.395		0.059	0.042	0.059		0.244	0.323	0.475

ρ: Spearsmans ρ
τ: Kendalls τ
r: Pearsons r

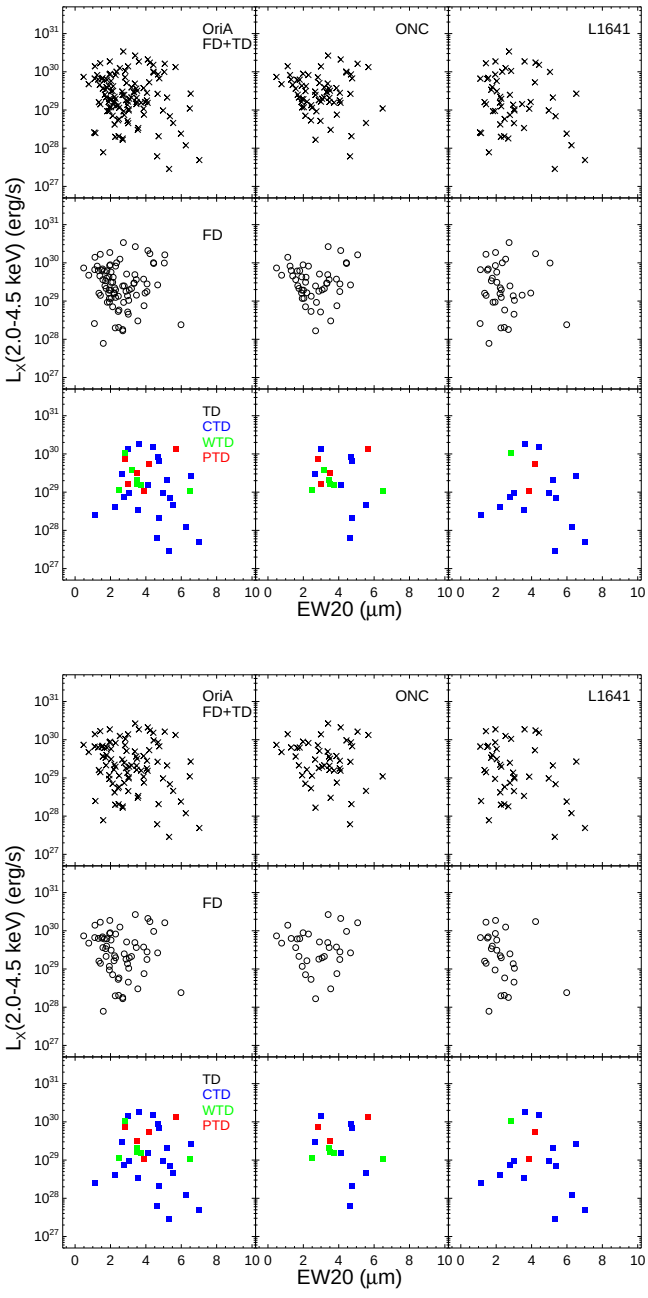


Figure C.166 EW20 vs. $\log L_X 4$. Upper panel: all available objects; Lower panel: objects with available spectral types only

Table C.331 EW20 vs. $\log L_X 4$ (I)

	Ori A				ONC				L1641			
	N	ρ	τ	r	N	ρ	τ	r	N	ρ	τ	r
TDFD	120	-0.125	-0.093	-0.175	67	-0.120	-0.104	-0.146	53	-0.144	-0.101	-0.239
		0.173	0.133	0.056		0.335	0.215	0.238		0.304	0.286	0.085
FD	85	-0.088	-0.072	-0.049	49	-0.093	-0.088	-0.088	36	-0.076	-0.060	-0.054
		0.425	0.327	0.656		0.523	0.370	0.548		0.661	0.605	0.754
TD	35	-0.183	-0.113	-0.248	18	-0.214	-0.163	-0.224	17	-0.140	-0.059	-0.238
		0.293	0.341	0.151		0.395	0.344	0.372		0.593	0.742	0.358

ρ: Spearsmans ρ
τ: Kendalls τ
r: Pearsons r

Table C.332 EW20 vs. $\log L_X 4$ (II)

	Ori A				ONC				L1641			
	N	ρ	τ	r	N	ρ	τ	r	N	ρ	τ	r
TDFD	92	-0.179	-0.126	-0.212	48	-0.152	-0.121	-0.175	44	-0.261	-0.185	-0.322
		0.088	0.074	0.042		0.302	0.227	0.234		0.088	0.077	0.033
FD	59	-0.155	-0.119	-0.107	32	-0.086	-0.073	-0.127	27	-0.316	-0.236	-0.266
		0.240	0.184	0.420		0.639	0.559	0.489		0.109	0.084	0.180
TD	33	-0.181	-0.106	-0.237	16	-0.215	-0.150	-0.220	17	-0.140	-0.059	-0.238
		0.313	0.386	0.184		0.425	0.418	0.413		0.593	0.742	0.358

ρ: Spearsmans ρ
τ: Kendalls τ
r: Pearsons r

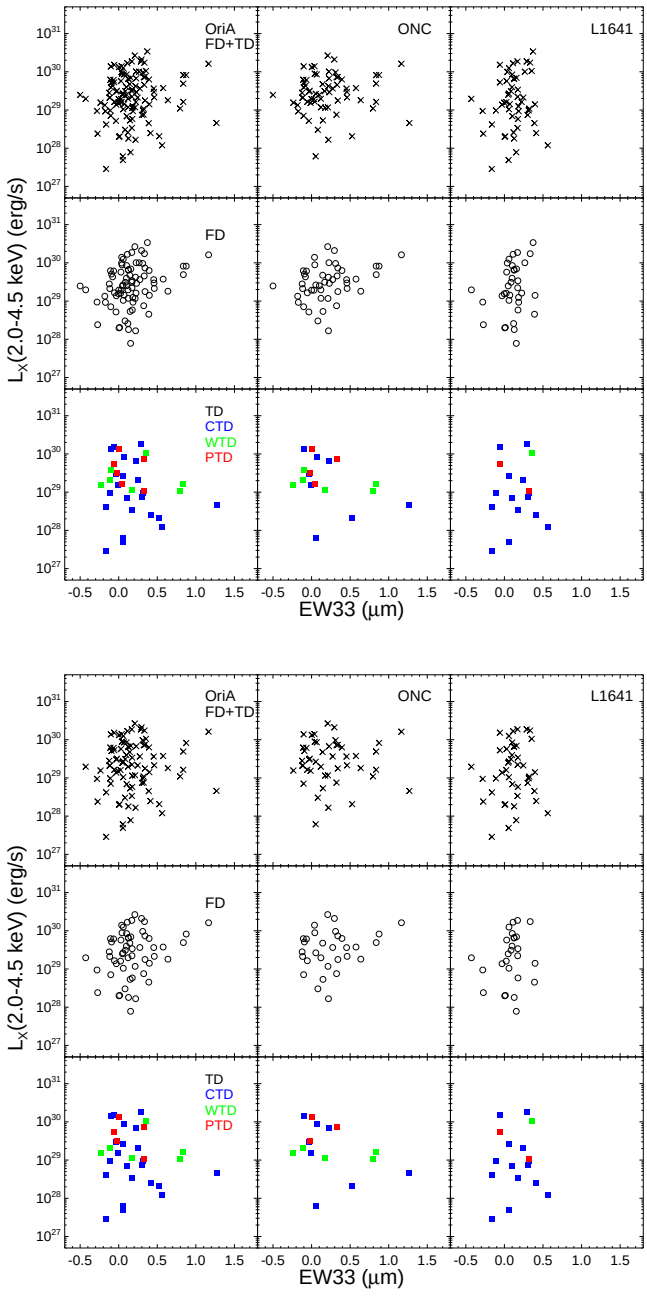


Figure C.167 EW33 vs. $\log L_X 4$. Upper panel: all available objects; Lower panel: objects with available spectral types only

Table C.333 EW33 vs. $\log L_X 4$ (I)

	Ori A				ONC				L1641			
	N	ρ	τ	r	N	ρ	τ	r	N	ρ	τ	r
TDFD	120	0.124	0.087	0.027	67	0.120	0.076	-0.011	53	0.117	0.092	0.128
		0.176	0.159	0.770		0.335	0.366	0.930		0.406	0.329	0.361
FD	85	0.274	0.184	0.055	49	0.300	0.196	0.029	36	0.204	0.162	0.247
		0.011	0.013	0.617		0.036	0.047	0.843		0.232	0.164	0.146
TD	35	-0.163	-0.108	-0.151	18	-0.379	-0.255	-0.359	17	0.071	0.052	0.055
		0.350	0.363	0.387		0.121	0.140	0.143		0.786	0.772	0.834

ρ: Spearsmans ρ
τ: Kendalls τ
r: Pearsons r

Table C.334 EW33 vs. $\log L_X 4$ (II)

	Ori A				ONC				L1641			
	N	ρ	τ	r	N	ρ	τ	r	N	ρ	τ	r
TDFD	92	0.078	0.057	0.074	48	0.026	0.017	0.042	44	0.105	0.079	0.082
		0.461	0.418	0.483		0.861	0.866	0.777		0.498	0.447	0.597
FD	59	0.222	0.153	0.228	32	0.209	0.137	0.262	27	0.232	0.180	0.193
		0.091	0.088	0.082		0.250	0.270	0.147		0.244	0.188	0.335
TD	33	-0.137	-0.089	-0.135	16	-0.368	-0.233	-0.351	17	0.071	0.052	0.055
		0.446	0.466	0.454		0.161	0.207	0.183		0.786	0.772	0.834

ρ: Spearsmans ρ
τ: Kendalls τ
r: Pearsons r

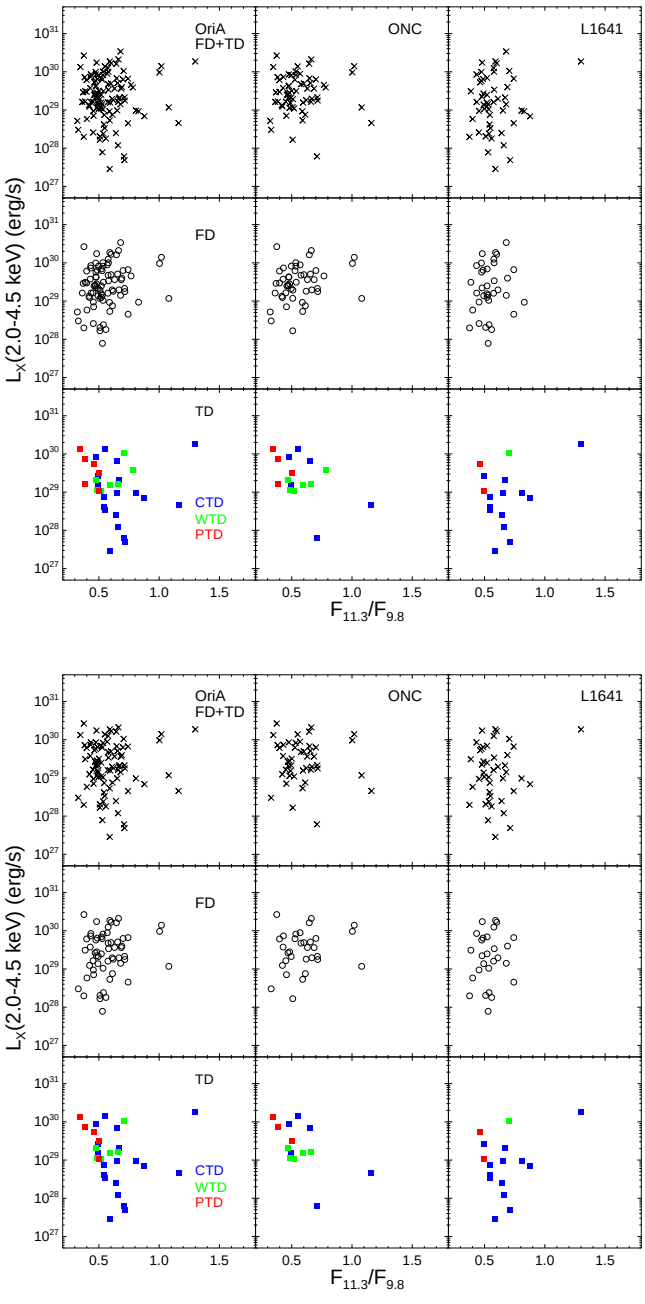


Figure C.168 $F_{11.3}/F_{9.8}$ vs. $\log L_X 4$. Upper panel: all available objects; Lower panel: objects with available spectral types only

Table C.335 $F_{11.3}/F_{9.8}$ vs. $\log L_X 4$ (I)

	Ori A				ONC				L1641			
	N	ρ	τ	r	N	ρ	τ	r	N	ρ	τ	r
TDFD	120	0.051	0.033	0.145	67	0.105	0.075	0.110	53	0.038	0.013	0.195
		0.578	0.589	0.114		0.399	0.372	0.376		0.788	0.890	0.162
FD	85	0.174	0.121	0.115	49	0.212	0.155	0.108	36	0.160	0.108	0.155
		0.111	0.101	0.295		0.144	0.117	0.460		0.352	0.354	0.367
TD	35	-0.071	-0.086	0.272	18	-0.170	-0.124	0.154	17	0.152	0.044	0.397
		0.683	0.469	0.114		0.499	0.472	0.542		0.560	0.805	0.115

ρ: Spearsmans ρ
τ: Kendalls τ
r: Pearsons r

Table C.336 $F_{11.3}/F_{9.8}$ vs. $\log L_X 4$ (II)

	Ori A				ONC				L1641			
	N	ρ	τ	r	N	ρ	τ	r	N	ρ	τ	r
TDFD	92	0.021	0.013	0.157	48	0.023	0.021	0.115	44	0.019	0.004	0.218
		0.839	0.855	0.135		0.875	0.831	0.436		0.900	0.968	0.155
FD	59	0.151	0.107	0.184	32	0.151	0.113	0.193	27	0.134	0.100	0.129
		0.253	0.231	0.163		0.408	0.364	0.290		0.506	0.466	0.521
TD	33	-0.097	-0.106	0.278	16	-0.232	-0.167	0.151	17	0.152	0.044	0.397
		0.593	0.386	0.117		0.387	0.368	0.577		0.560	0.805	0.115

ρ: Spearsmans ρ
τ: Kendalls τ
r: Pearsons r

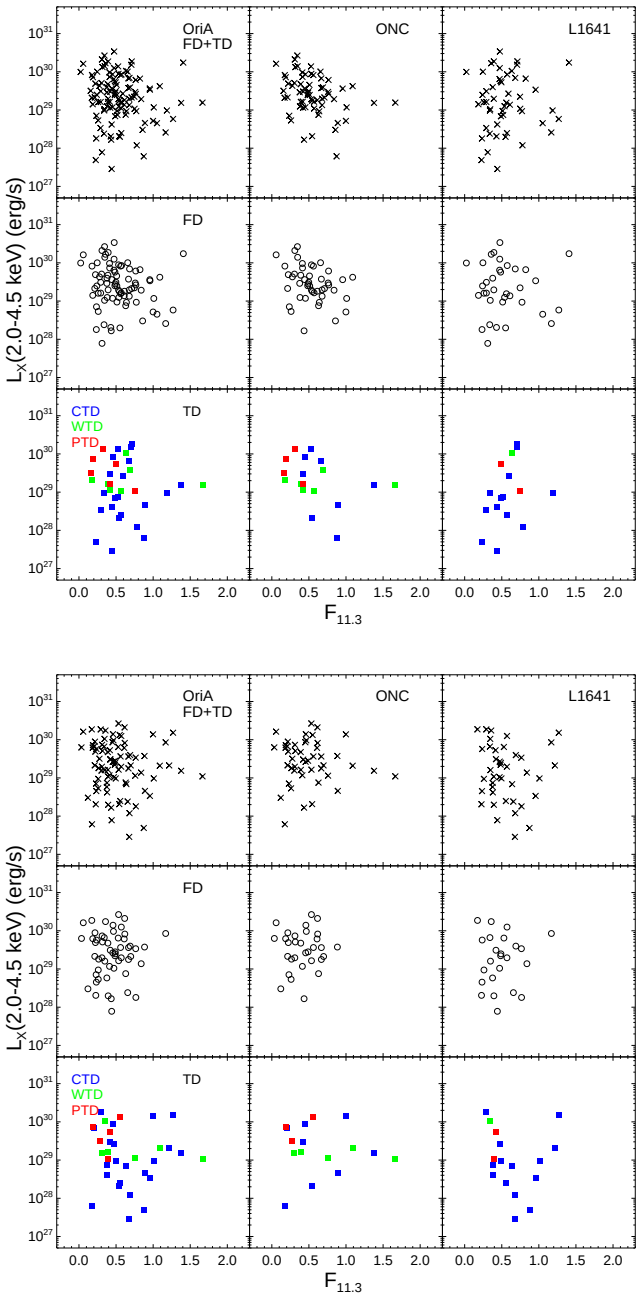


Figure C.169 $F_{11.3}$ vs. $\log L_X 4$. Upper panel: all available objects; Lower panel: objects with available spectral types only

Table C.337 $F_{11.3}$ vs. $\log L_X 4$ (I)

	Ori A				ONC				L1641			
	N	ρ	τ	r	N	ρ	τ	r	N	ρ	τ	r
TDFD	120	-0.032	-0.021	-0.069	67	0.086	0.054	0.098	53	-0.157	-0.105	-0.211
		0.732	0.737	0.454		0.488	0.516	0.430		0.261	0.266	0.129
FD	85	-0.053	-0.034	-0.073	49	-0.029	-0.020	0.006	36	-0.091	-0.059	-0.150
		0.631	0.646	0.507		0.844	0.836	0.967		0.596	0.613	0.383
TD	35	0.095	0.045	0.070	18	0.416	0.281	0.373	17	-0.167	-0.162	-0.170
		0.586	0.701	0.689		0.086	0.103	0.127		0.523	0.365	0.514

ρ: Spearsmans ρ
τ: Kendalls τ
r: Pearsons r

Table C.338 $F_{11.3}$ vs. $\log L_X 4$ (II)

	Ori A				ONC				L1641			
	N	ρ	τ	r	N	ρ	τ	r	N	ρ	τ	r
TDFD	92	-0.108	-0.073	-0.103	48	0.067	0.046	0.099	44	-0.269	-0.185	-0.269
		0.308	0.302	0.329		0.652	0.644	0.503		0.077	0.077	0.077
FD	59	-0.209	-0.135	-0.199	32	-0.121	-0.071	-0.030	27	-0.318	-0.217	-0.342
		0.113	0.132	0.131		0.510	0.570	0.871		0.106	0.113	0.081
TD	33	0.074	0.030	0.064	16	0.435	0.300	0.369	17	-0.167	-0.162	-0.170
		0.683	0.804	0.723		0.092	0.105	0.160		0.523	0.365	0.514

ρ: Spearsmans ρ
τ: Kendalls τ
r: Pearsons r

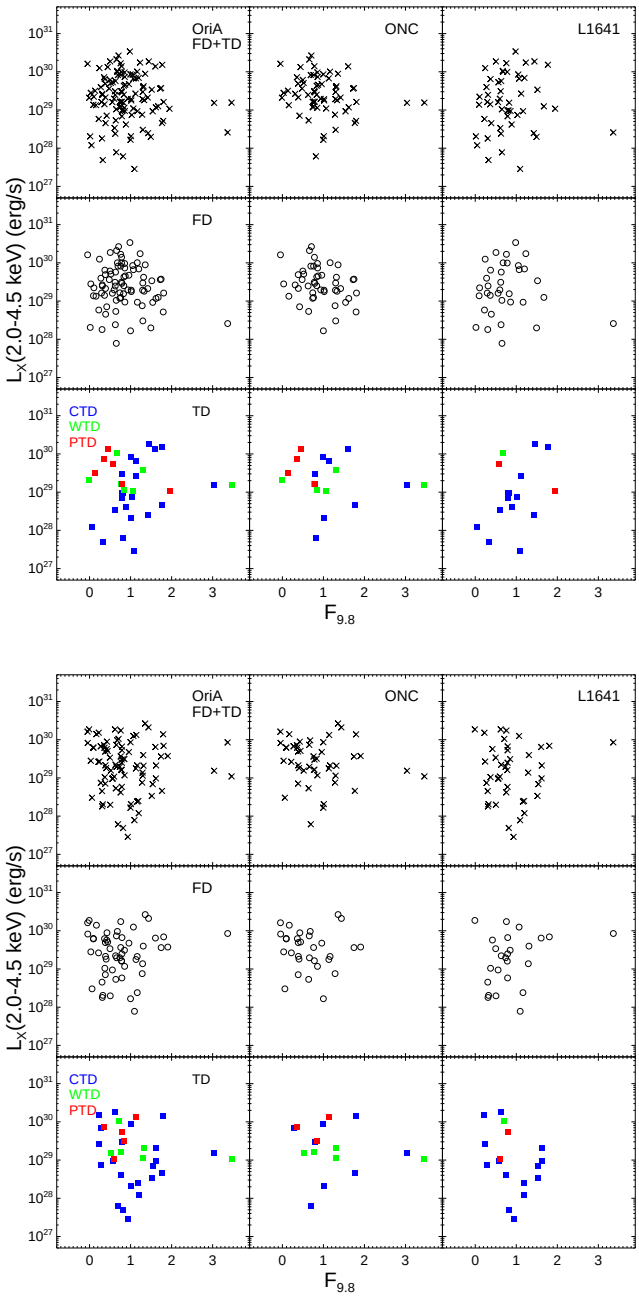


Figure C.170 $F_{9.8}$ vs. $\log L_X 4$. Upper panel: all available objects; Lower panel: objects with available spectral types only

Table C.339 $F_{9.8}$ vs. $\log L_X 4$ (I)

	Ori A				ONC				L1641			
	N	ρ	τ	r	N	ρ	τ	r	N	ρ	τ	r
TDFD	120	-0.074	-0.049	-0.037	67	0.025	0.016	0.094	53	-0.216	-0.144	-0.222
		0.424	0.427	0.688		0.842	0.846	0.449		0.121	0.129	0.110
FD	85	-0.121	-0.080	-0.146	49	-0.120	-0.082	-0.123	36	-0.141	-0.089	-0.183
		0.271	0.276	0.182		0.412	0.408	0.400		0.411	0.446	0.285
TD	35	0.148	0.106	0.161	18	0.486	0.359	0.432	17	-0.292	-0.206	-0.232
		0.397	0.371	0.356		0.041	0.037	0.073		0.256	0.249	0.370

ρ: Spearsmans ρ
τ: Kendalls τ
r: Pearsons r

Table C.340 $F_{9.8}$ vs. $\log L_X 4$ (II)

	Ori A				ONC				L1641			
	N	ρ	τ	r	N	ρ	τ	r	N	ρ	τ	r
TDFD	92	-0.112	-0.080	-0.046	48	0.071	0.047	0.132	44	-0.312	-0.220	-0.273
		0.286	0.258	0.663		0.630	0.637	0.371		0.039	0.035	0.073
FD	59	-0.239	-0.167	-0.232	32	-0.145	-0.109	-0.136	27	-0.335	-0.236	-0.305
		0.068	0.062	0.077		0.428	0.381	0.458		0.087	0.084	0.122
TD	33	0.143	0.106	0.164	16	0.532	0.417	0.456	17	-0.292	-0.206	-0.232
		0.426	0.386	0.362		0.034	0.024	0.076		0.256	0.249	0.370

ρ: Spearsmans ρ
τ: Kendalls τ
r: Pearsons r

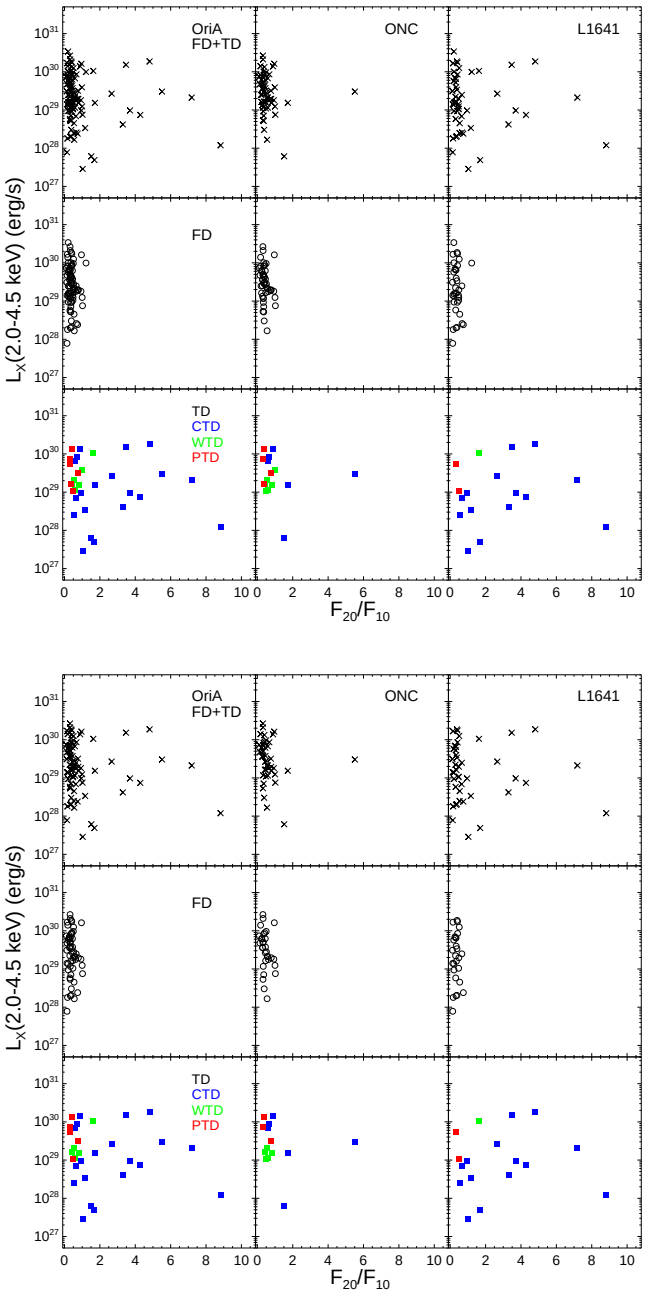


Figure C.171 F_{20}/F_{10} vs. $\log L_X 4$. Upper panel: all available objects; Lower panel: objects with available spectral types only

Table C.341 F_{20}/F_{10} vs. $\log L_X 4$ (I)

	Ori A				ONC				L1641			
	N	ρ	τ	r	N	ρ	τ	r	N	ρ	τ	r
TDFD	119	-0.223	-0.158	-0.176	66	-0.278	-0.202	-0.232	53	-0.174	-0.123	-0.107
		0.015	0.011	0.056		0.024	0.017	0.061		0.213	0.192	0.446
FD	85	-0.156	-0.119	-0.098	49	-0.293	-0.231	-0.240	36	-0.036	-0.035	-0.003
		0.154	0.106	0.372		0.041	0.019	0.097		0.835	0.764	0.986
TD	34	-0.200	-0.134	-0.157	17	-0.306	-0.206	-0.330	17	0.125	0.088	0.074
		0.258	0.266	0.375		0.232	0.249	0.196		0.633	0.621	0.778

ρ: Spearsmans ρ
τ: Kendalls τ
r: Pearsons r

Table C.342 F_{20}/F_{10} vs. $\log L_X 4$ (II)

	Ori A				ONC				L1641			
	N	ρ	τ	r	N	ρ	τ	r	N	ρ	τ	r
TDFD	91	-0.241	-0.166	-0.180	47	-0.376	-0.262	-0.257	44	-0.133	-0.089	-0.092
		0.021	0.020	0.088		0.009	0.009	0.081		0.388	0.396	0.553
FD	59	-0.145	-0.108	-0.105	32	-0.397	-0.294	-0.294	27	0.105	0.060	0.000
		0.274	0.226	0.429		0.024	0.018	0.102		0.602	0.662	1.000
TD	32	-0.191	-0.125	-0.150	15	-0.361	-0.238	-0.335	17	0.125	0.088	0.074
		0.294	0.315	0.413		0.187	0.216	0.222		0.633	0.621	0.778

ρ: Spearsmans ρ
τ: Kendalls τ
r: Pearsons r

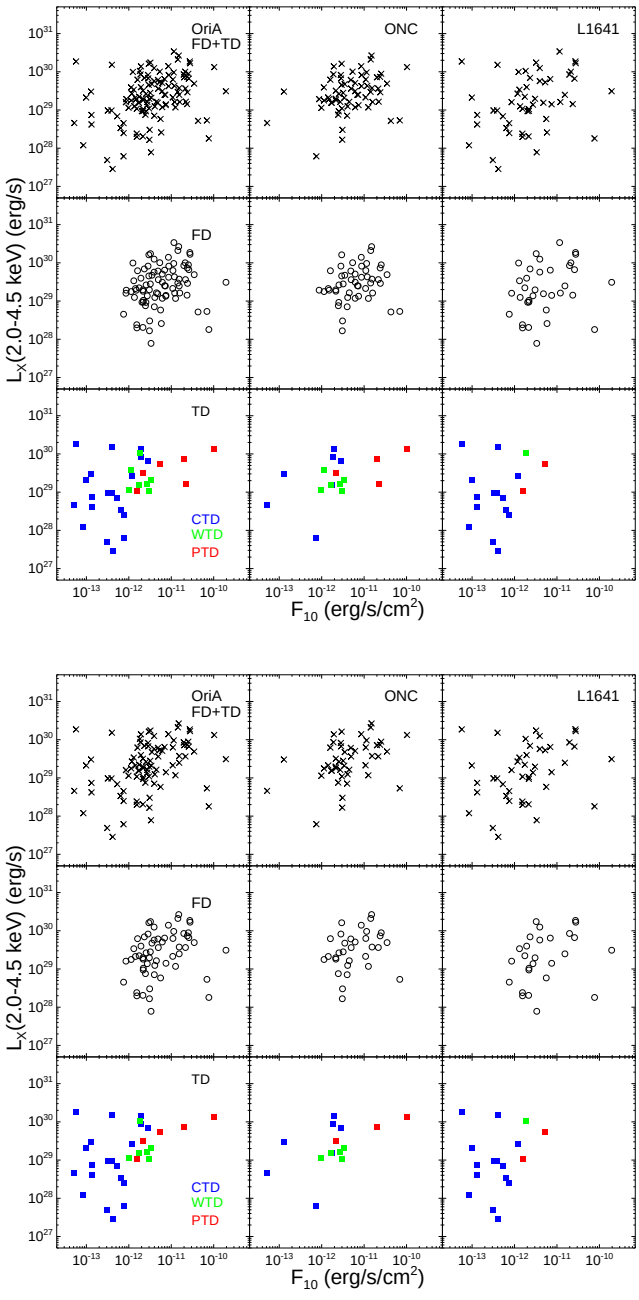


Figure C.172 $\log F_{10}$ vs. $\log L_X 4$. Upper panel: all available objects; Lower panel: objects with available spectral types only

Table C.343 $\log F_{10}$ vs. $\log L_X 4$ (I)

	Ori A				ONC				L1641			
	N	ρ	τ	r	N	ρ	τ	r	N	ρ	τ	r
TDFD	119	0.363	0.254	0.107	66	0.280	0.193	0.131	53	0.363	0.264	0.099
		0.000	0.000	0.247		0.023	0.022	0.294		0.008	0.005	0.481
FD	85	0.296	0.202	0.013	49	0.237	0.163	-0.068	36	0.325	0.238	0.059
		0.006	0.006	0.906		0.101	0.098	0.642		0.053	0.041	0.732
TD	34	0.444	0.326	0.286	17	0.456	0.338	0.376	17	0.164	0.118	0.321
		0.009	0.007	0.101		0.066	0.058	0.137		0.529	0.510	0.209

ρ: Spearsmans ρ
τ: Kendalls τ
r: Pearsons r

Table C.344 $\log F_{10}$ vs. $\log L_X 4$ (II)

	Ori A				ONC				L1641			
	N	ρ	τ	r	N	ρ	τ	r	N	ρ	τ	r
TDFD	91	0.433	0.310	0.126	47	0.392	0.282	0.202	44	0.380	0.280	0.099
		0.000	0.000	0.234		0.006	0.005	0.173		0.011	0.007	0.523
FD	59	0.379	0.262	0.024	32	0.326	0.242	0.007	27	0.389	0.299	0.060
		0.003	0.003	0.857		0.069	0.052	0.970		0.045	0.029	0.766
TD	32	0.445	0.335	0.293	15	0.532	0.410	0.400	17	0.164	0.118	0.321
		0.011	0.007	0.104		0.041	0.033	0.140		0.529	0.510	0.209

ρ: Spearsmans ρ
τ: Kendalls τ
r: Pearsons r

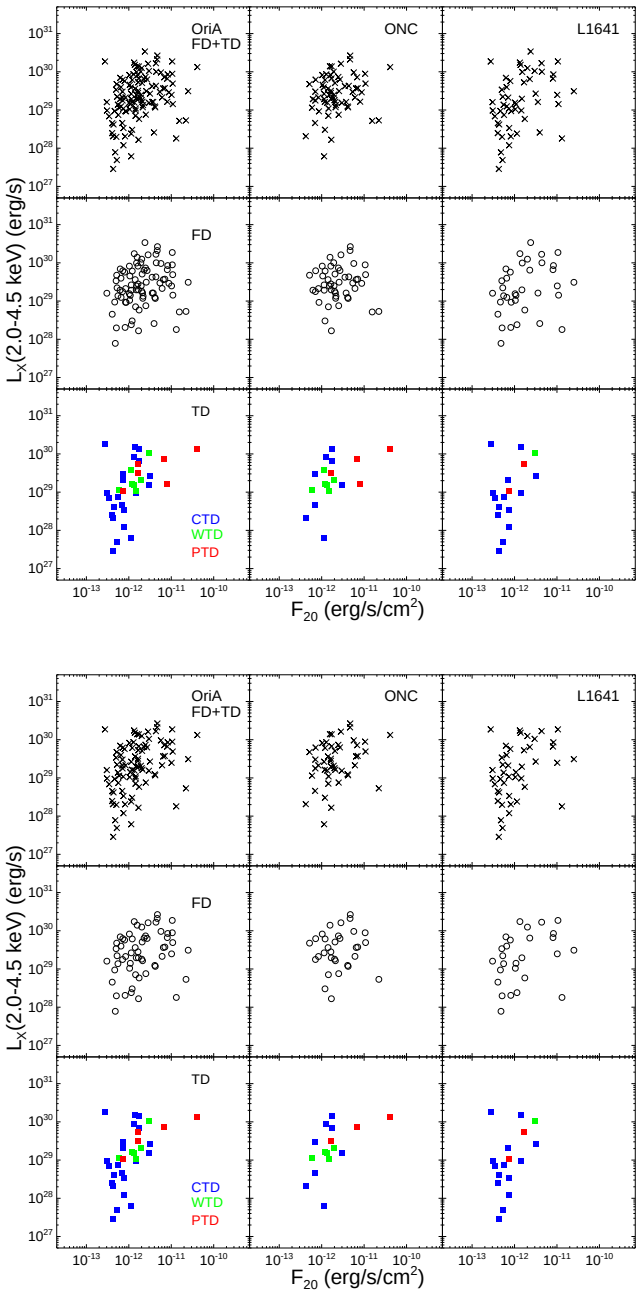


Figure C.173 $\log F_{20}$ vs. $\log L_X 4$. Upper panel: all available objects; Lower panel: objects with available spectral types only

Table C.345 $\log F_{20}$ vs. $\log L_X 4$ (I)

	Ori A				ONC				L1641			
	N	ρ	τ	r	N	ρ	τ	r	N	ρ	τ	r
TDFD	120	0.377	0.257	0.161	67	0.213	0.136	0.126	53	0.420	0.282	0.188
		0.000	0.000	0.079		0.084	0.103	0.310		0.002	0.003	0.178
FD	85	0.250	0.166	0.022	49	0.079	0.041	-0.124	36	0.366	0.248	0.130
		0.021	0.024	0.842		0.587	0.679	0.396		0.028	0.034	0.450
TD	35	0.559	0.402	0.306	18	0.540	0.386	0.378	17	0.348	0.235	0.476
		0.000	0.001	0.074		0.021	0.025	0.122		0.171	0.187	0.053

ρ: Spearsmans ρ
τ: Kendalls τ
r: Pearsons r

Table C.346 $\log F_{20}$ vs. $\log L_X 4$ (II)

	Ori A				ONC				L1641			
	N	ρ	τ	r	N	ρ	τ	r	N	ρ	τ	r
TDFD	92	0.446	0.308	0.209	48	0.337	0.223	0.190	44	0.427	0.292	0.215
		0.000	0.000	0.046		0.019	0.025	0.196		0.004	0.005	0.161
FD	59	0.324	0.224	0.081	32	0.147	0.093	-0.055	27	0.413	0.299	0.175
		0.012	0.012	0.542		0.421	0.456	0.765		0.032	0.029	0.383
TD	33	0.572	0.417	0.312	16	0.641	0.467	0.396	17	0.348	0.235	0.476
		0.001	0.001	0.077		0.007	0.012	0.129		0.171	0.187	0.053

ρ: Spearsmans ρ
τ: Kendalls τ
r: Pearsons r

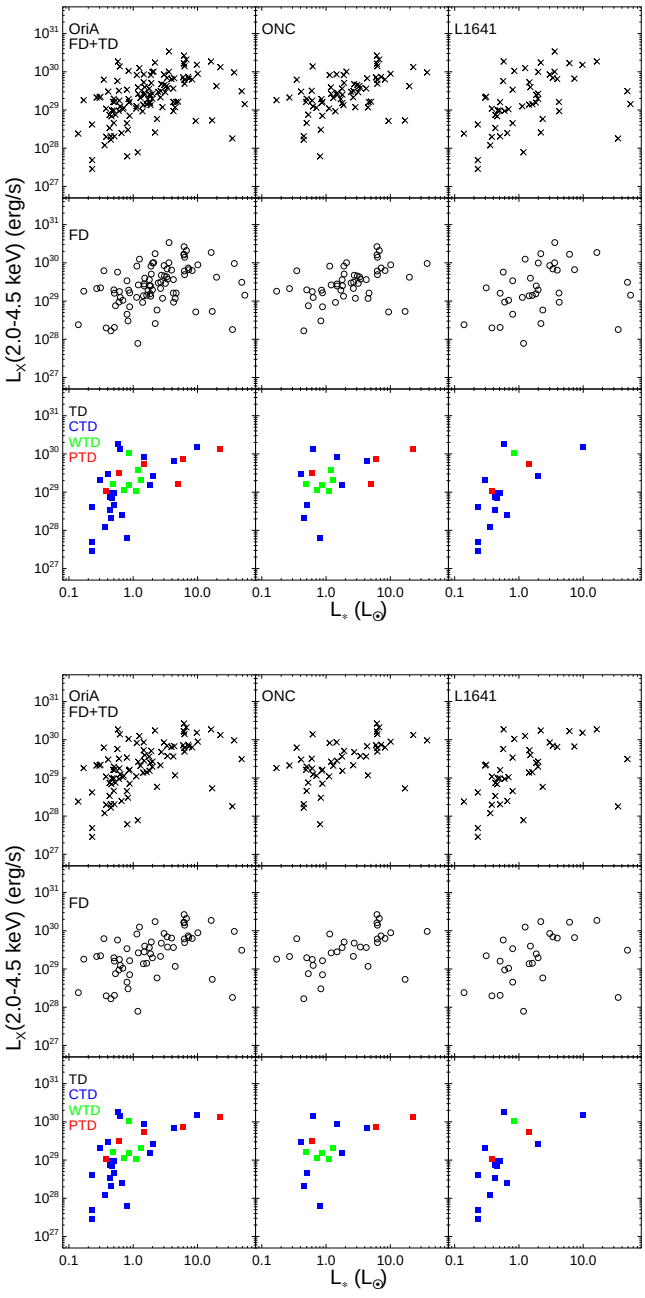


Figure C.174 $\log L_\star$ vs. $\log L_X 4$. Upper panel: all available objects; Lower panel: objects with available spectral types only

Table C.347 $\log L_\star$ vs. $\log L_X 4$ (I)

	Ori A				ONC				L1641			
	N	ρ	τ	r	N	ρ	τ	r	N	ρ	τ	r
TDFD	120	0.504	0.365	0.453	67	0.483	0.351	0.447	53	0.528	0.390	0.437
		0.000	0.000	0.000		0.000	0.000	0.000		0.000	0.000	0.001
FD	85	0.426	0.307	0.346	49	0.466	0.346	0.416	36	0.387	0.283	0.289
		0.000	0.000	0.001		0.001	0.000	0.003		0.020	0.015	0.087
TD	35	0.640	0.471	0.600	18	0.434	0.333	0.480	17	0.702	0.508	0.674
		0.000	0.000	0.000		0.072	0.053	0.044		0.002	0.004	0.003

ρ: Spearsmans ρ
τ: Kendalls τ
r: Pearsons r

Table C.348 $\log L_\star$ vs. $\log L_X 4$ (II)

	Ori A				ONC				L1641			
	N	ρ	τ	r	N	ρ	τ	r	N	ρ	τ	r
TDFD	92	0.584	0.425	0.517	48	0.576	0.425	0.529	44	0.593	0.440	0.484
		0.000	0.000	0.000		0.000	0.000	0.000		0.000	0.000	0.001
FD	59	0.535	0.383	0.434	32	0.586	0.432	0.520	27	0.483	0.351	0.354
		0.000	0.000	0.001		0.000	0.001	0.002		0.011	0.010	0.070
TD	33	0.638	0.472	0.618	16	0.409	0.317	0.520	17	0.702	0.508	0.674
		0.000	0.000	0.000		0.116	0.087	0.039		0.002	0.004	0.003

ρ: Spearsmans ρ
τ: Kendalls τ
r: Pearsons r

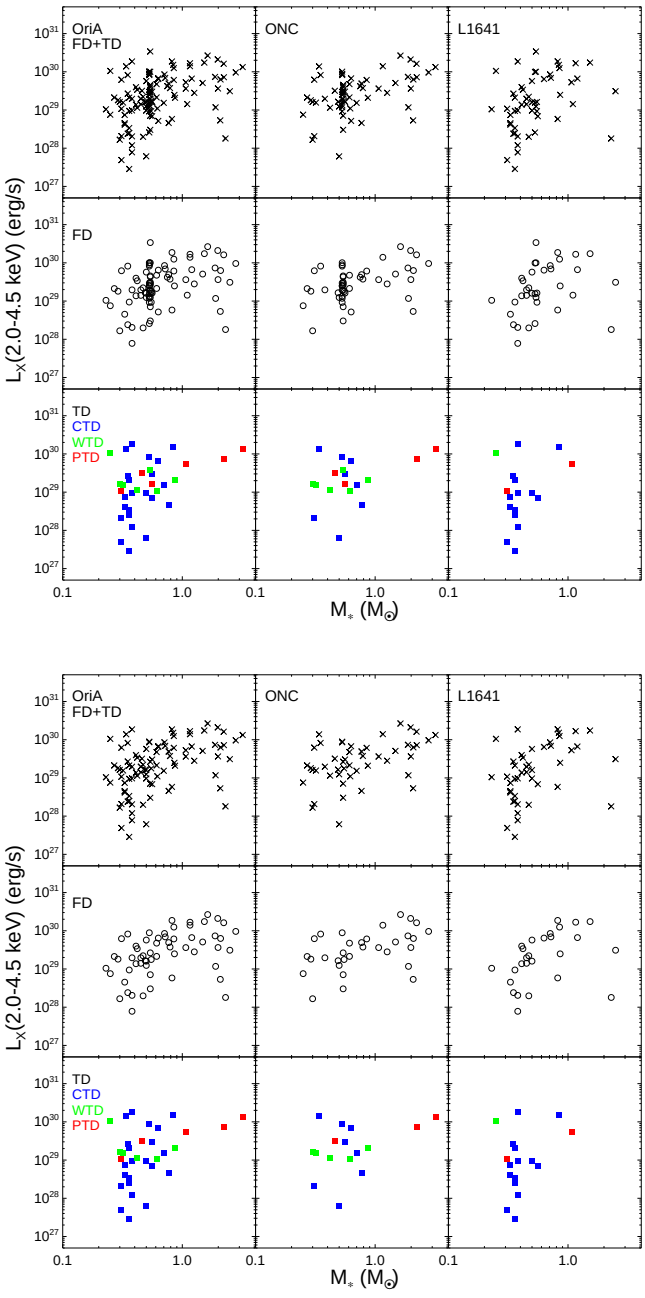


Figure C.175 $\log M_\star$ vs. $\log L_X 4$. Upper panel: all available objects; Lower panel: objects with available spectral types only

Table C.349 $\log M_\star$ vs. $\log L_X 4$ (I)

	Ori A				ONC				L1641			
	N	ρ	τ	r	N	ρ	τ	r	N	ρ	τ	r
TDFD	120	0.429	0.305	0.397	67	0.368	0.264	0.417	53	0.463	0.322	0.360
		0.000	0.000	0.000		0.002	0.002	0.000		0.000	0.001	0.008
FD	85	0.418	0.301	0.368	49	0.380	0.286	0.429	36	0.472	0.338	0.304
		0.000	0.000	0.001		0.007	0.004	0.002		0.004	0.004	0.071
TD	35	0.344	0.242	0.389	18	0.247	0.157	0.376	17	0.207	0.115	0.344
		0.043	0.041	0.021		0.324	0.362	0.124		0.426	0.519	0.176

ρ: Spearsmans ρ
τ: Kendalls τ
r: Pearsons r

Table C.350 $\log M_\star$ vs. $\log L_X 4$ (II)

	Ori A				ONC				L1641			
	N	ρ	τ	r	N	ρ	τ	r	N	ρ	τ	r
TDFD	92	0.473	0.334	0.438	48	0.452	0.321	0.449	44	0.481	0.346	0.396
		0.000	0.000	0.000		0.001	0.001	0.001		0.001	0.001	0.008
FD	59	0.489	0.355	0.431	32	0.468	0.344	0.465	27	0.548	0.428	0.376
		0.000	0.000	0.001		0.007	0.006	0.007		0.003	0.002	0.053
TD	33	0.322	0.229	0.389	16	0.250	0.167	0.384	17	0.207	0.115	0.344
		0.067	0.061	0.025		0.350	0.368	0.142		0.426	0.519	0.176

ρ: Spearsmans ρ
τ: Kendalls τ
r: Pearsons r

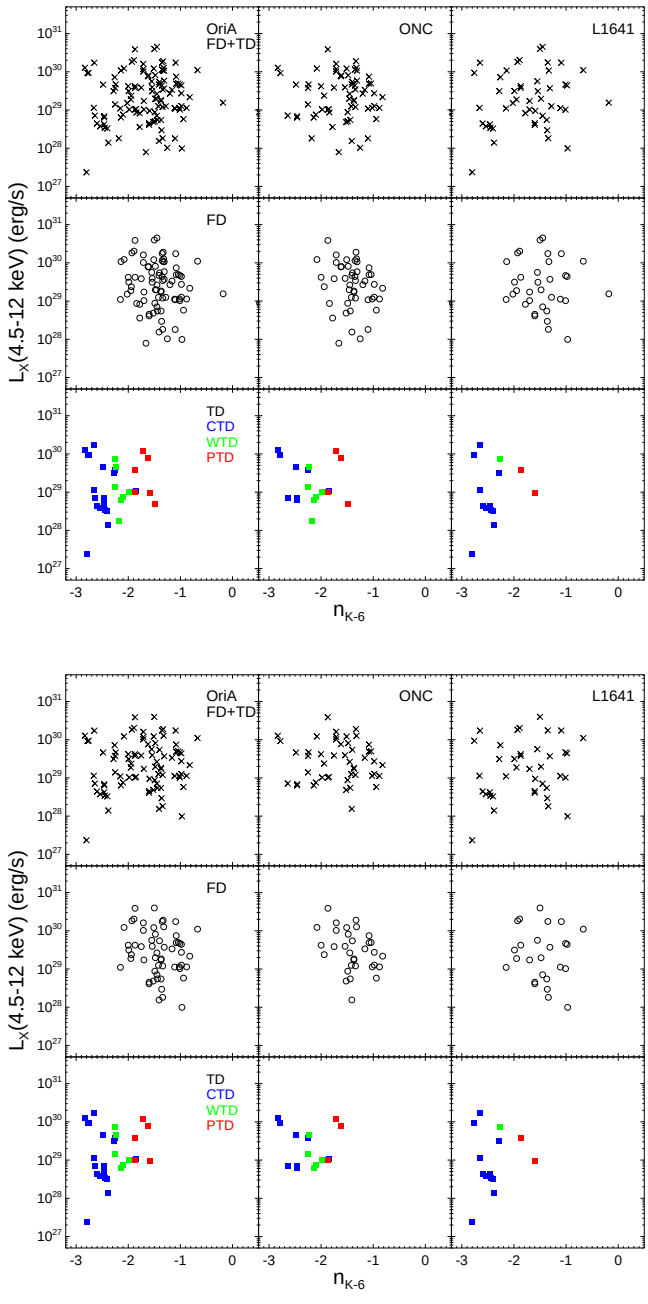


Figure C.176 n_{K-6} vs. $\log L_X 5$. Upper panel: all available objects; Lower panel: objects with available spectral types only

Table C.351 n_{K-6} vs. $\log L_X 5$ (I)

	Ori A				ONC				L1641			
	N	ρ	τ	r	N	ρ	τ	r	N	ρ	τ	r
TDFD	115	0.065	0.039	0.063	67	-0.013	-0.019	-0.071	48	0.170	0.104	0.187
		0.492	0.539	0.504		0.920	0.824	0.568		0.249	0.297	0.203
FD	83	-0.123	-0.091	-0.161	49	-0.196	-0.143	-0.220	34	-0.063	-0.059	-0.090
		0.267	0.222	0.146		0.177	0.148	0.129		0.725	0.623	0.613
TD	32	-0.009	-0.014	0.059	18	-0.181	-0.112	-0.170	14	0.077	-0.011	0.176
		0.961	0.909	0.748		0.473	0.517	0.500		0.794	0.956	0.547

ρ: Spearsmans ρ
τ: Kendalls τ
r: Pearsons r

Table C.352 n_{K-6} vs. $\log L_X 5$ (II)

	Ori A				ONC				L1641			
	N	ρ	τ	r	N	ρ	τ	r	N	ρ	τ	r
TDFD	87	0.073	0.044	0.104	48	-0.027	-0.028	-0.060	39	0.166	0.103	0.203
		0.504	0.546	0.338		0.858	0.782	0.685		0.312	0.357	0.215
FD	57	-0.170	-0.125	-0.197	32	-0.313	-0.227	-0.349	25	-0.084	-0.074	-0.086
		0.205	0.171	0.142		0.081	0.068	0.050		0.689	0.606	0.683
TD	30	0.053	0.037	0.134	16	-0.018	0.000	-0.061	14	0.077	-0.011	0.176
		0.779	0.774	0.480		0.948	1.000	0.822		0.794	0.956	0.547

ρ: Spearsmans ρ
τ: Kendalls τ
r: Pearsons r

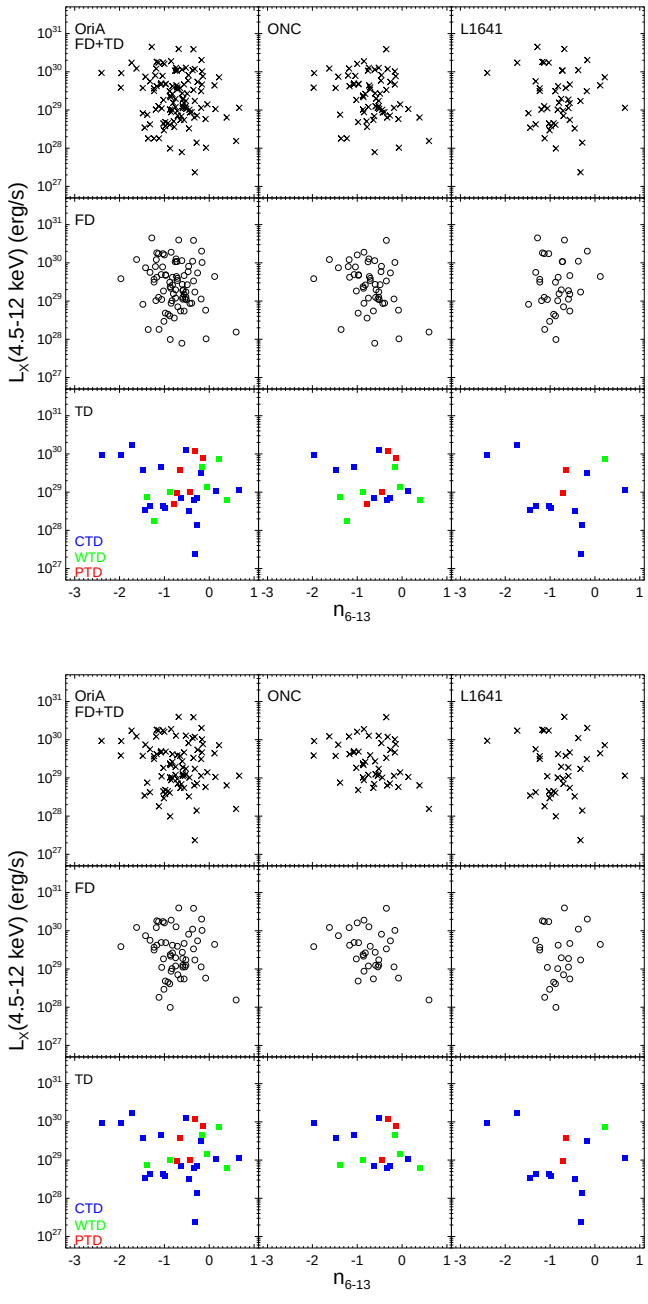


Figure C.177 n_{6-13} vs. $\log L_X 5$. Upper panel: all available objects; Lower panel: objects with available spectral types only

Table C.353 L_X5 vs. n_{6-13} (I)

	Ori A				ONC				L1641			
	N	ρ	τ	r	N	ρ	τ	r	N	ρ	τ	r
TDFD	115	-0.110	-0.075	-0.172	67	-0.212	-0.156	-0.259	48	-0.022	-0.008	-0.099
		0.241	0.233	0.066		0.085	0.061	0.034		0.881	0.936	0.503
FD	83	-0.121	-0.084	-0.166	49	-0.297	-0.218	-0.330	34	0.077	0.061	0.093
		0.277	0.261	0.134		0.039	0.027	0.021		0.664	0.612	0.601
TD	32	0.000	0.010	-0.163	18	0.005	-0.020	-0.096	14	-0.178	-0.099	-0.254
		0.999	0.935	0.373		0.984	0.910	0.705		0.543	0.622	0.381

ρ: Spearsmans ρ
τ: Kendalls τ
r: Pearsons r

Table C.354 n_{6-13} vs. $\log L_X5$ (II)

	Ori A				ONC				L1641			
	N	ρ	τ	r	N	ρ	τ	r	N	ρ	τ	r
TDFD	87	-0.121	-0.078	-0.193	48	-0.276	-0.197	-0.354	39	-0.022	0.003	-0.096
		0.264	0.283	0.073		0.058	0.049	0.014		0.893	0.981	0.561
FD	57	-0.110	-0.065	-0.156	32	-0.293	-0.204	-0.385	25	0.075	0.070	0.120
		0.414	0.472	0.247		0.104	0.100	0.030		0.721	0.622	0.568
TD	30	-0.063	-0.041	-0.212	16	-0.185	-0.167	-0.279	14	-0.178	-0.099	-0.254
		0.742	0.748	0.261		0.492	0.368	0.295		0.543	0.622	0.381

ρ: Spearsmans ρ
τ: Kendalls τ
r: Pearsons r

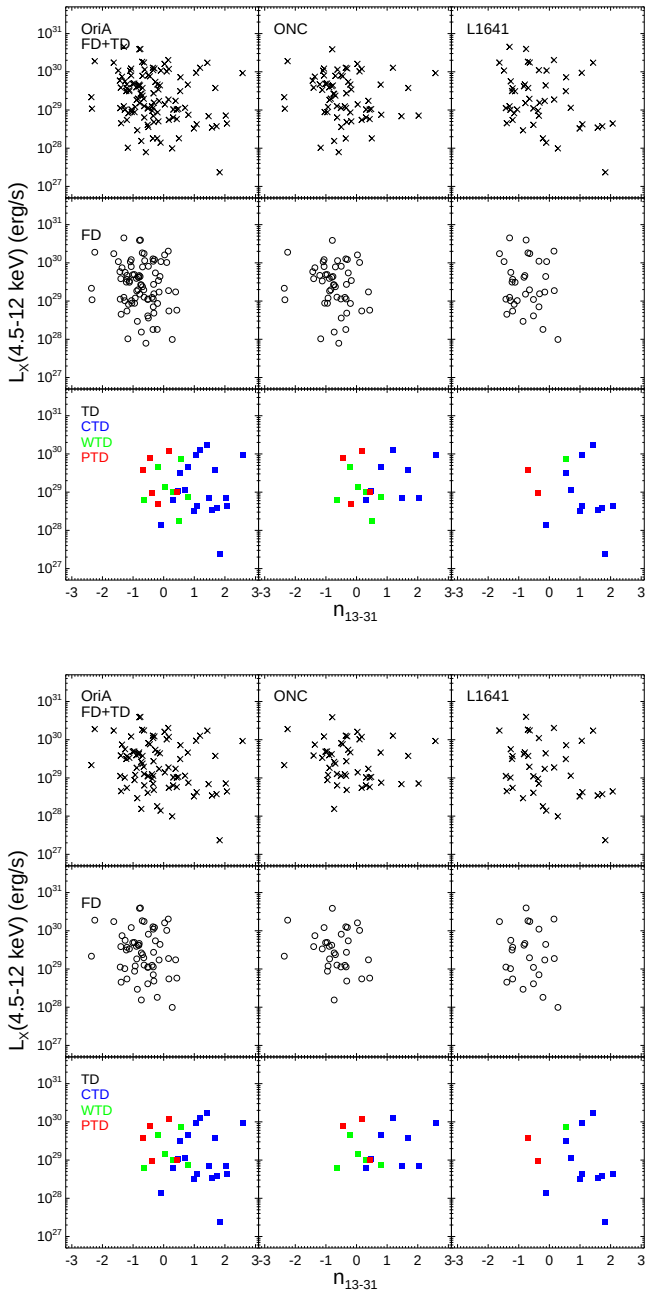


Figure C.178 n_{13-31} vs. $\log L_X 5$. Upper panel: all available objects; Lower panel: objects with available spectral types only

Table C.355 n_{13-31} vs. $\log L_X 5$ (I)

	Ori A				ONC				L1641			
	N	ρ	τ	r	N	ρ	τ	r	N	ρ	τ	r
TDFD	115	-0.213	-0.145	-0.219	67	-0.200	-0.131	-0.112	48	-0.265	-0.172	-0.329
		0.022	0.021	0.019		0.104	0.116	0.367		0.068	0.084	0.022
FD	83	-0.113	-0.078	-0.142	49	-0.165	-0.110	-0.149	34	-0.046	-0.034	-0.134
		0.310	0.296	0.200		0.258	0.265	0.307		0.797	0.777	0.450
TD	32	-0.113	-0.056	-0.089	18	0.112	0.059	0.172	14	-0.292	-0.165	-0.283
		0.537	0.650	0.628		0.657	0.733	0.495		0.311	0.412	0.327

ρ: Spearsmans ρ
τ: Kendalls τ
r: Pearsons r

Table C.356 n_{13-31} vs. $\log L_X 5$ (II)

	Ori A				ONC				L1641			
	N	ρ	τ	r	N	ρ	τ	r	N	ρ	τ	r
TDFD	87	-0.224	-0.155	-0.245	48	-0.219	-0.146	-0.156	39	-0.285	-0.187	-0.317
		0.037	0.034	0.022		0.135	0.142	0.290		0.078	0.094	0.049
FD	57	-0.117	-0.084	-0.171	32	-0.193	-0.135	-0.222	25	-0.062	-0.044	-0.124
		0.386	0.359	0.203		0.289	0.277	0.222		0.769	0.760	0.555
TD	30	-0.163	-0.090	-0.133	16	0.056	0.017	0.112	14	-0.292	-0.165	-0.283
		0.391	0.487	0.484		0.837	0.928	0.680		0.311	0.412	0.327

ρ: Spearsmans ρ
τ: Kendalls τ
r: Pearsons r

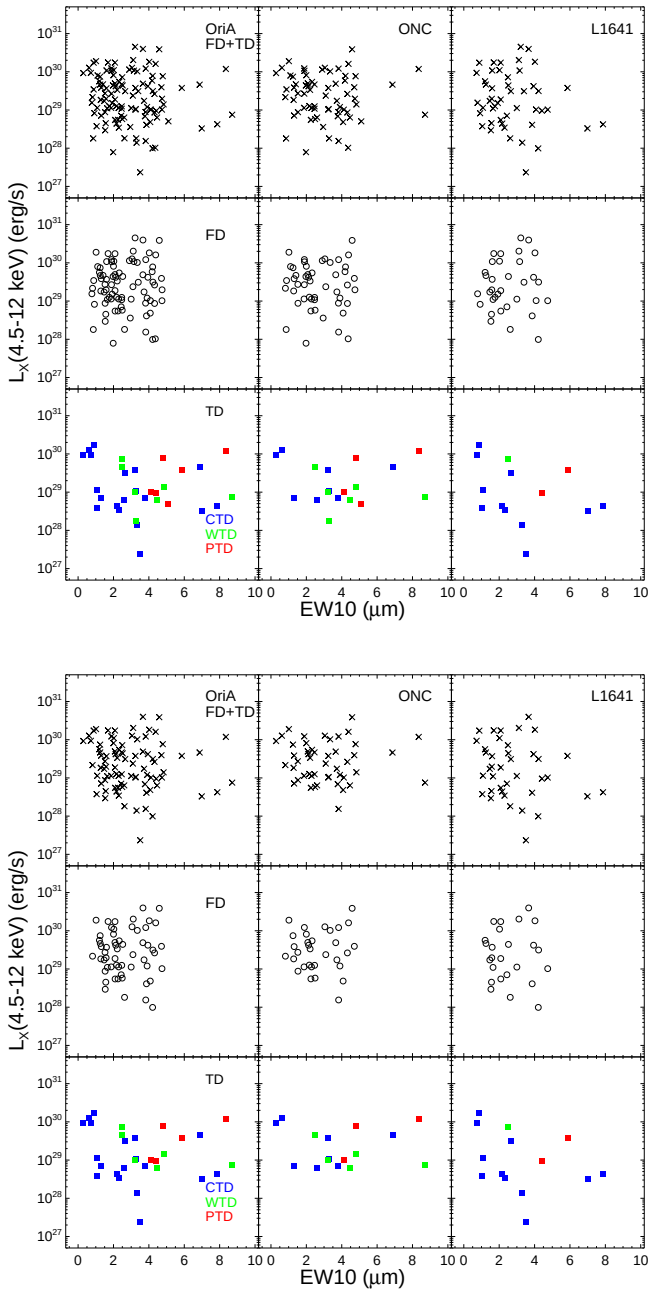


Figure C.179 EW10 vs. $\log L_X 5$. Upper panel: all available objects; Lower panel: objects with available spectral types only

Table C.357 EW10 vs. $\log L_X 5$ (I)

	Ori A				ONC				L1641			
	N	ρ	τ	r	N	ρ	τ	r	N	ρ	τ	r
TDFD	115	-0.137	-0.098	-0.108	67	-0.138	-0.107	-0.065	48	-0.145	-0.094	-0.176
		0.144	0.122	0.251		0.266	0.201	0.601		0.325	0.346	0.231
FD	83	-0.006	-0.010	0.008	49	-0.045	-0.043	-0.016	34	0.041	0.037	0.042
		0.960	0.894	0.943		0.761	0.660	0.913		0.817	0.756	0.814
TD	32	-0.237	-0.168	-0.142	18	-0.159	-0.118	-0.048	14	-0.446	-0.319	-0.308
		0.191	0.178	0.438		0.529	0.494	0.850		0.110	0.112	0.284

ρ: Spearsmans ρ
τ: Kendalls τ
r: Pearsons r

Table C.358 EW10 vs. $\log L_X 5$ (II)

	Ori A				ONC				L1641			
	N	ρ	τ	r	N	ρ	τ	r	N	ρ	τ	r
TDFD	87	-0.149	-0.107	-0.117	48	-0.118	-0.091	-0.048	39	-0.207	-0.144	-0.220
		0.169	0.142	0.280		0.423	0.359	0.746		0.206	0.196	0.178
FD	57	-0.021	-0.026	0.014	32	-0.001	-0.014	0.049	25	-0.039	-0.027	-0.032
		0.880	0.778	0.918		0.994	0.910	0.790		0.852	0.852	0.879
TD	30	-0.231	-0.152	-0.141	16	-0.104	-0.075	-0.057	14	-0.446	-0.319	-0.308
		0.220	0.238	0.457		0.700	0.684	0.834		0.110	0.112	0.284

ρ: Spearsmans ρ
τ: Kendalls τ
r: Pearsons r

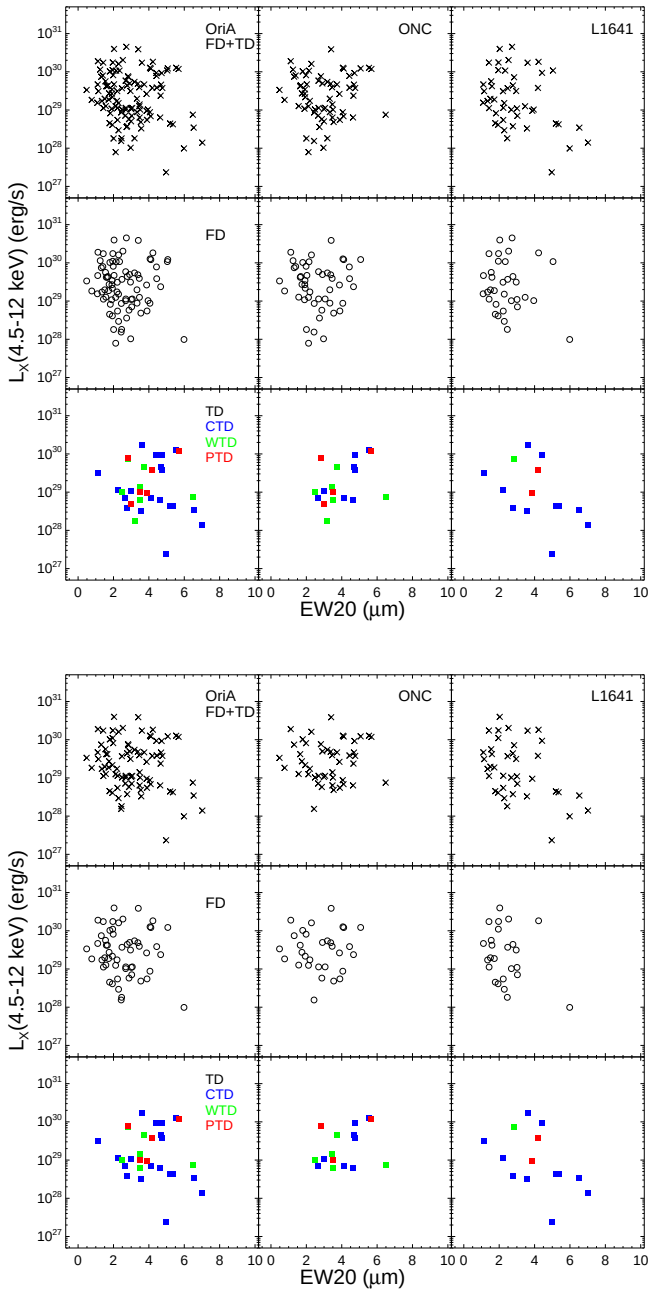


Figure C.180 EW20 vs. $\log L_X 5$. Upper panel: all available objects; Lower panel: objects with available spectral types only

Table C.359 EW20 vs. $\log L_X 5$ (I)

	Ori A				ONC				L1641			
	N	ρ	τ	r	N	ρ	τ	r	N	ρ	τ	r
TDFD	115	-0.142	-0.100	-0.156	67	-0.027	-0.026	-0.017	48	-0.279	-0.189	-0.369
		0.129	0.114	0.096		0.827	0.758	0.891		0.055	0.058	0.010
FD	83	-0.080	-0.054	-0.081	49	-0.088	-0.070	-0.062	34	-0.074	-0.052	-0.136
		0.469	0.472	0.467		0.549	0.480	0.672		0.678	0.667	0.443
TD	32	-0.077	-0.069	-0.133	18	0.408	0.294	0.423	14	-0.429	-0.319	-0.479
		0.675	0.581	0.468		0.093	0.088	0.080		0.126	0.112	0.083

ρ: Spearsmans ρ
τ: Kendalls τ
r: Pearsons r

Table C.360 EW20 vs. $\log L_X 5$ (II)

	Ori A				ONC				L1641			
	N	ρ	τ	r	N	ρ	τ	r	N	ρ	τ	r
TDFD	87	-0.166	-0.121	-0.200	48	-0.010	-0.025	-0.055	39	-0.359	-0.248	-0.444
		0.125	0.096	0.063		0.944	0.803	0.710		0.025	0.026	0.005
FD	57	-0.087	-0.059	-0.124	32	-0.063	-0.065	-0.111	25	-0.178	-0.127	-0.290
		0.521	0.518	0.358		0.730	0.604	0.545		0.395	0.375	0.160
TD	30	-0.130	-0.113	-0.189	16	0.335	0.233	0.346	14	-0.429	-0.319	-0.479
		0.493	0.382	0.317		0.204	0.207	0.189		0.126	0.112	0.083

ρ: Spearsmans ρ
τ: Kendalls τ
r: Pearsons r

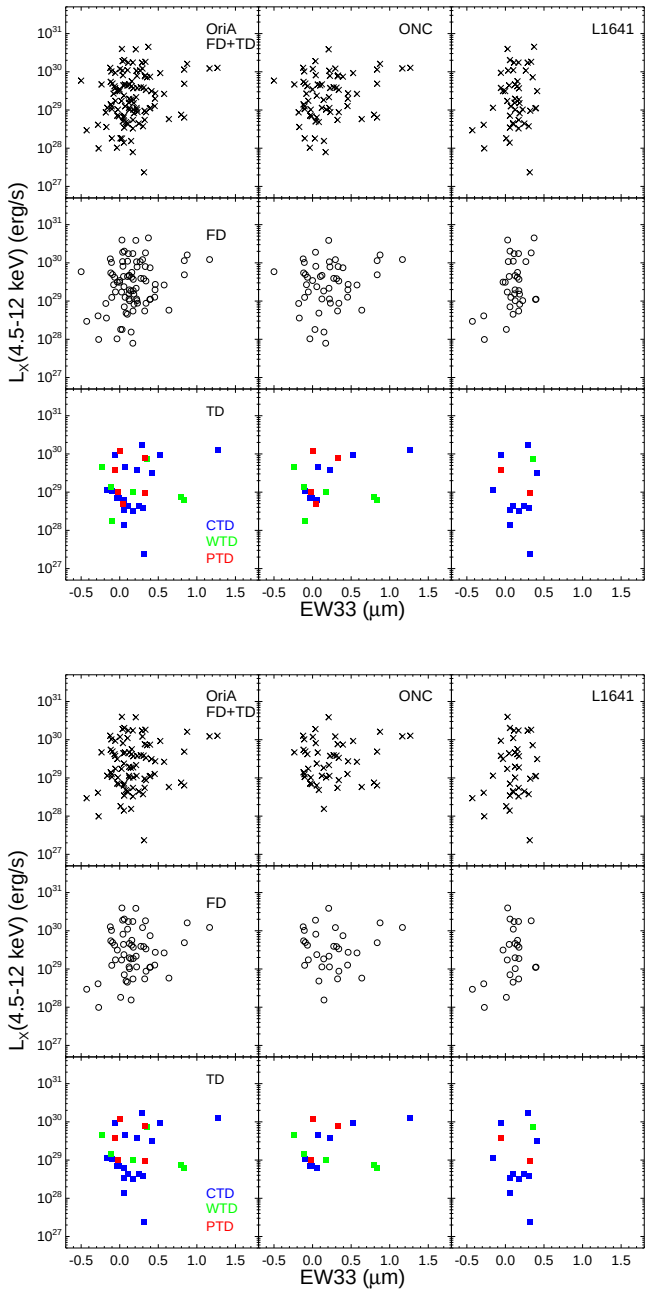


Figure C.181 EW33 vs. $\log L_X 5$. Upper panel: all available objects; Lower panel: objects with available spectral types only

Table C.361 EW33 vs. $\log L_X 5$ (I)

	Ori A				ONC				L1641			
	N	ρ	τ	r	N	ρ	τ	r	N	ρ	τ	r
TDFD	115	0.163	0.107	0.037	67	0.165	0.103	0.017	48	0.123	0.090	0.211
		0.081	0.089	0.695		0.182	0.219	0.891		0.407	0.368	0.150
FD	83	0.155	0.101	0.019	49	0.099	0.054	-0.018	34	0.223	0.152	0.428
		0.162	0.176	0.865		0.498	0.581	0.902		0.205	0.207	0.012
TD	32	0.059	0.010	0.167	18	0.199	0.124	0.299	14	0.007	0.044	-0.054
		0.748	0.935	0.361		0.428	0.472	0.228		0.982	0.826	0.855

ρ: Spearsmans ρ
τ: Kendalls τ
r: Pearsons r

Table C.362 EW33 vs. $\log L_X 5$ (II)

	Ori A				ONC				L1641			
	N	ρ	τ	r	N	ρ	τ	r	N	ρ	τ	r
TDFD	87	0.092	0.059	0.161	48	0.047	0.024	0.164	39	0.126	0.095	0.175
		0.395	0.415	0.136		0.753	0.810	0.265		0.443	0.396	0.287
FD	57	0.092	0.059	0.210	32	-0.039	-0.032	0.153	25	0.309	0.201	0.422
		0.496	0.517	0.117		0.833	0.795	0.403		0.133	0.160	0.036
TD	30	0.009	-0.023	0.123	16	0.121	0.050	0.221	14	0.007	0.044	-0.054
		0.964	0.858	0.517		0.656	0.787	0.411		0.982	0.826	0.855

ρ: Spearsmans ρ
τ: Kendalls τ
r: Pearsons r

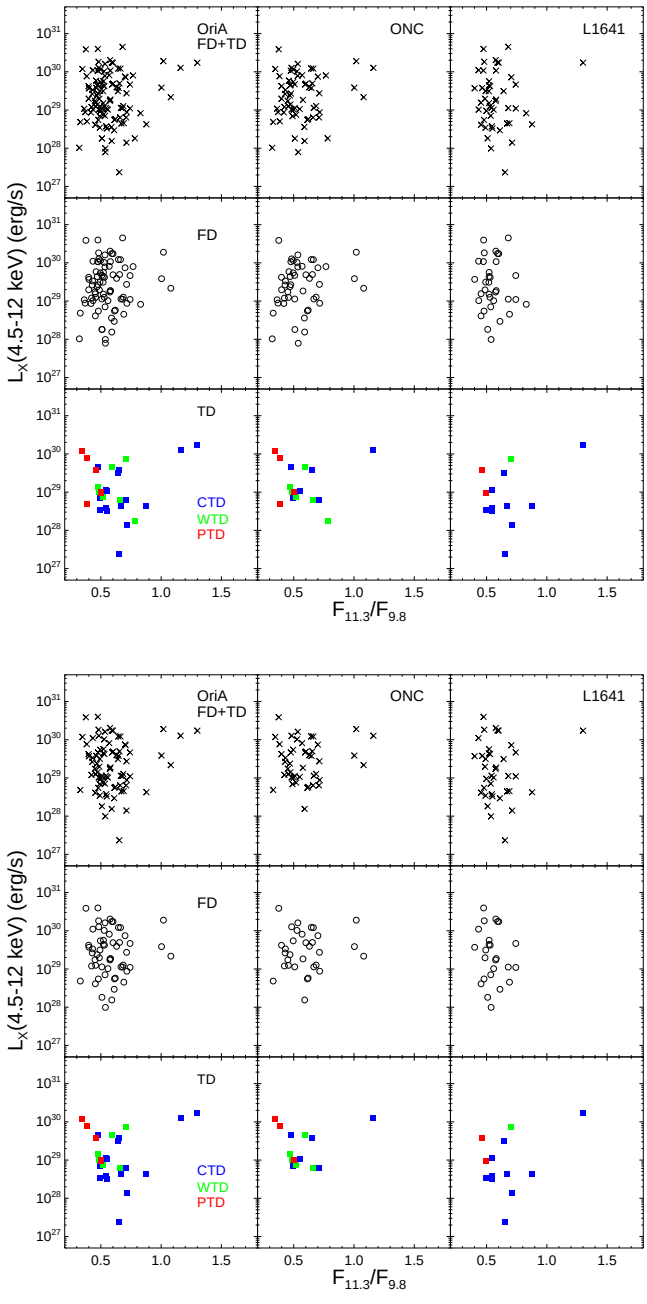


Figure C.182 $F_{11.3}/F_{9.8}$ vs. $\log L_X 5$. Upper panel: all available objects; Lower panel: objects with available spectral types only

Table C.363 $F_{11.3}/F_{9.8}$ vs. $\log L_X 5$ (I)

	Ori A				ONC				L1641			
	N	ρ	τ	r	N	ρ	τ	r	N	ρ	τ	r
TDFD	115	-0.017	-0.008	0.082	67	0.027	0.026	-0.079	48	-0.066	-0.053	0.143
		0.860	0.894	0.384		0.828	0.758	0.525		0.655	0.594	0.332
FD	83	0.068	0.054	0.090	49	0.184	0.146	0.147	34	-0.071	-0.052	-0.063
		0.539	0.472	0.418		0.205	0.138	0.313		0.688	0.667	0.723
TD	32	-0.151	-0.129	0.205	18	-0.366	-0.294	-0.281	14	0.235	0.143	0.379
		0.408	0.299	0.260		0.135	0.088	0.259		0.418	0.477	0.181

ρ: Spearsmans ρ
τ: Kendalls τ
r: Pearsons r

Table C.364 $F_{11.3}/F_{9.8}$ vs. $\log L_X 5$ (II)

	Ori A				ONC				L1641			
	N	ρ	τ	r	N	ρ	τ	r	N	ρ	τ	r
TDFD	87	-0.071	-0.052	0.087	48	-0.065	-0.053	-0.170	39	-0.078	-0.058	0.168
		0.512	0.475	0.423		0.658	0.594	0.248		0.635	0.603	0.307
FD	57	-0.039	-0.026	0.024	32	0.048	0.032	0.084	25	-0.138	-0.093	-0.137
		0.774	0.772	0.859		0.793	0.795	0.648		0.509	0.513	0.514
TD	30	-0.143	-0.131	0.200	16	-0.438	-0.350	-0.339	14	0.235	0.143	0.379
		0.449	0.309	0.289		0.090	0.059	0.199		0.418	0.477	0.181

ρ: Spearsmans ρ
τ: Kendalls τ
r: Pearsons r

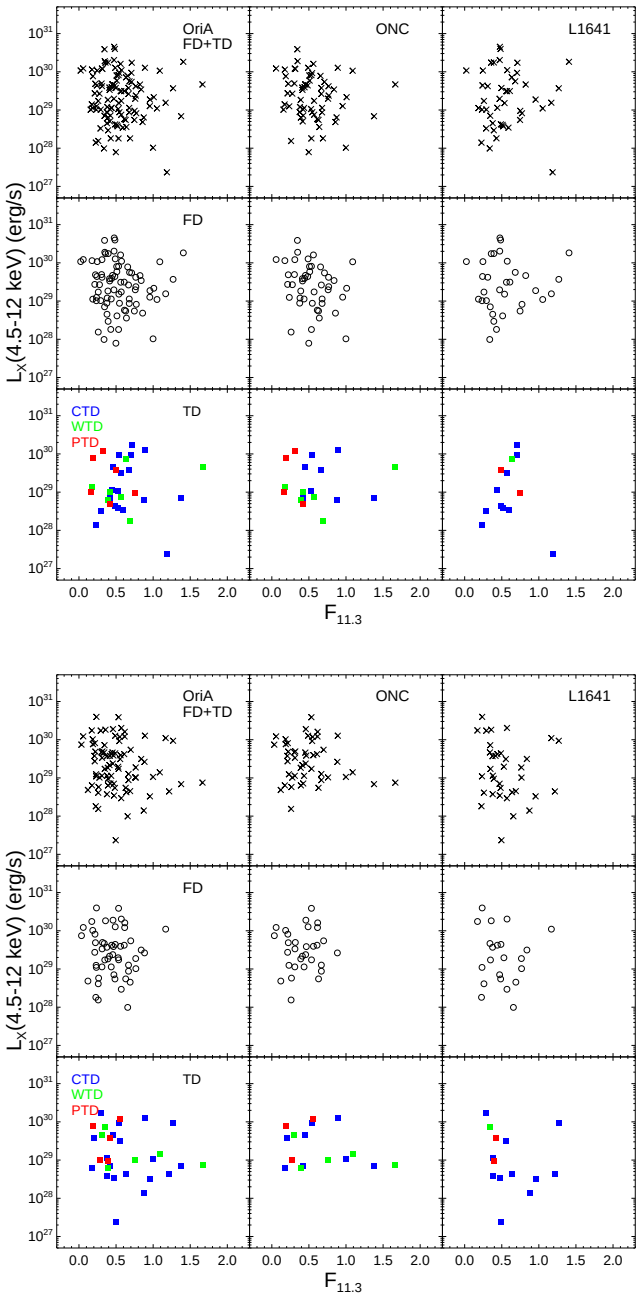


Figure C.183 $F_{11.3}$ vs. $\log L_X 5$. Upper panel: all available objects; Lower panel: objects with available spectral types only

Table C.365 $F_{11.3}$ vs. $\log L_X 5$ (I)

	Ori A				ONC				L1641			
	N	ρ	τ	r	N	ρ	τ	r	N	ρ	τ	r
TDFD	115	-0.164	-0.106	-0.162	67	-0.196	-0.137	-0.131	48	-0.145	-0.091	-0.201
		0.080	0.092	0.084		0.112	0.102	0.291		0.326	0.364	0.171
FD	83	0.014	0.009	0.019	49	-0.018	-0.017	0.024	34	-0.001	-0.002	0.014
		0.902	0.909	0.865		0.902	0.863	0.870		0.997	0.988	0.937
TD	32	-0.286	-0.194	-0.238	18	-0.302	-0.229	-0.269	14	-0.336	-0.231	-0.262
		0.113	0.120	0.190		0.223	0.185	0.280		0.240	0.250	0.366

ρ: Spearsmans ρ
τ: Kendalls τ
r: Pearsons r

Table C.366 $F_{11.3}$ vs. $\log L_X 5$ (II)

	Ori A				ONC				L1641			
	N	ρ	τ	r	N	ρ	τ	r	N	ρ	τ	r
TDFD	87	-0.202	-0.135	-0.200	48	-0.221	-0.153	-0.175	39	-0.213	-0.142	-0.242
		0.061	0.065	0.063		0.131	0.126	0.234		0.193	0.204	0.138
FD	57	-0.053	-0.045	-0.047	32	-0.031	-0.030	-0.008	25	-0.108	-0.087	-0.094
		0.696	0.620	0.728		0.865	0.808	0.965		0.608	0.544	0.655
TD	30	-0.271	-0.182	-0.231	16	-0.262	-0.183	-0.279	14	-0.336	-0.231	-0.262
		0.148	0.159	0.219		0.327	0.322	0.295		0.240	0.250	0.366

ρ: Spearsmans ρ
τ: Kendalls τ
r: Pearsons r

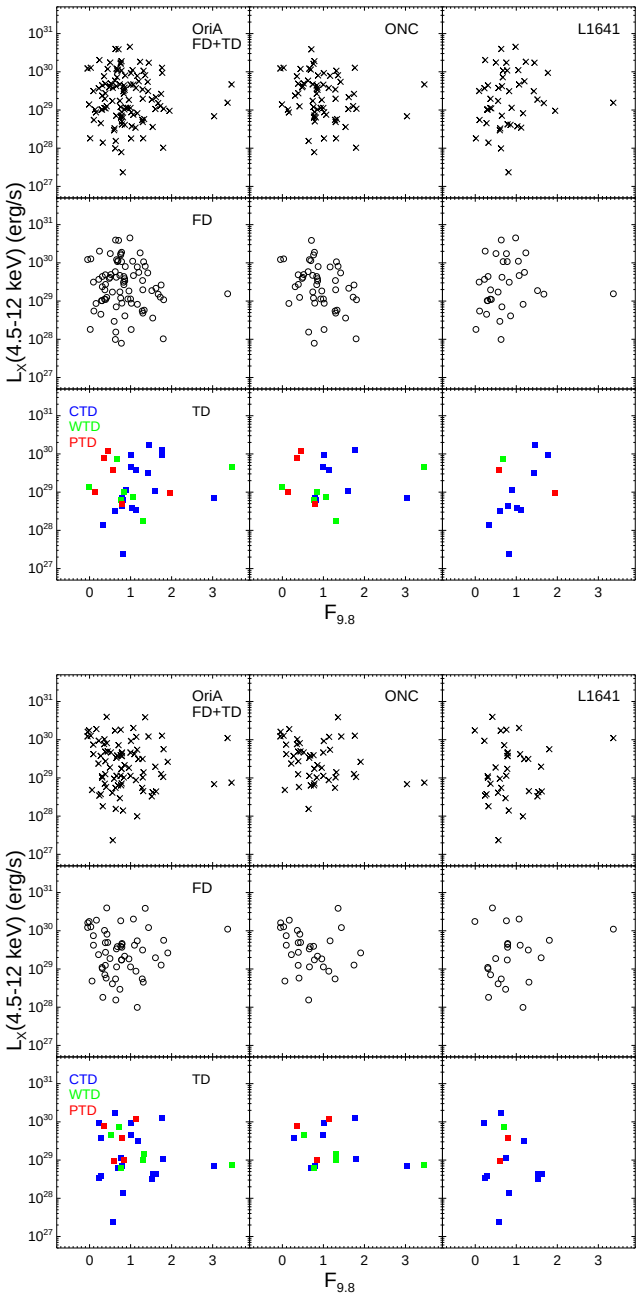


Figure C.184 $F_{9.8}$ vs. $\log L_X 5$. Upper panel: all available objects; Lower panel: objects with available spectral types only

Table C.367 $F_{9.8}$ vs. $\log L_X 5$ (I)

	Ori A				ONC				L1641			
	N	ρ	τ	r	N	ρ	τ	r	N	ρ	τ	r
TDFD	115	-0.154	-0.108	-0.113	67	-0.162	-0.116	-0.086	48	-0.161	-0.108	-0.181
		0.100	0.086	0.229		0.191	0.166	0.489		0.274	0.278	0.218
FD	83	-0.044	-0.036	-0.058	49	-0.116	-0.087	-0.096	34	0.036	0.034	-0.001
		0.690	0.626	0.602		0.427	0.379	0.512		0.839	0.778	0.996
TD	32	-0.188	-0.125	-0.083	18	-0.106	-0.072	0.007	14	-0.538	-0.407	-0.312
		0.304	0.315	0.652		0.675	0.677	0.978		0.047	0.043	0.277

ρ: Spearsmans ρ
τ: Kendalls τ
r: Pearsons r

Table C.368 $F_{9.8}$ vs. $\log L_X 5$ (II)

	Ori A				ONC				L1641			
	N	ρ	τ	r	N	ρ	τ	r	N	ρ	τ	r
TDFD	87	-0.143	-0.102	-0.101	48	-0.107	-0.074	-0.052	39	-0.231	-0.169	-0.211
		0.186	0.164	0.352		0.471	0.460	0.726		0.158	0.131	0.197
FD	57	-0.030	-0.026	-0.031	32	-0.024	-0.020	-0.025	25	-0.054	-0.040	-0.046
		0.824	0.772	0.819		0.897	0.871	0.892		0.798	0.779	0.827
TD	30	-0.176	-0.113	-0.076	16	-0.056	-0.033	0.008	14	-0.538	-0.407	-0.312
		0.351	0.382	0.690		0.837	0.857	0.977		0.047	0.043	0.277

ρ: Spearsmans ρ
τ: Kendalls τ
r: Pearsons r

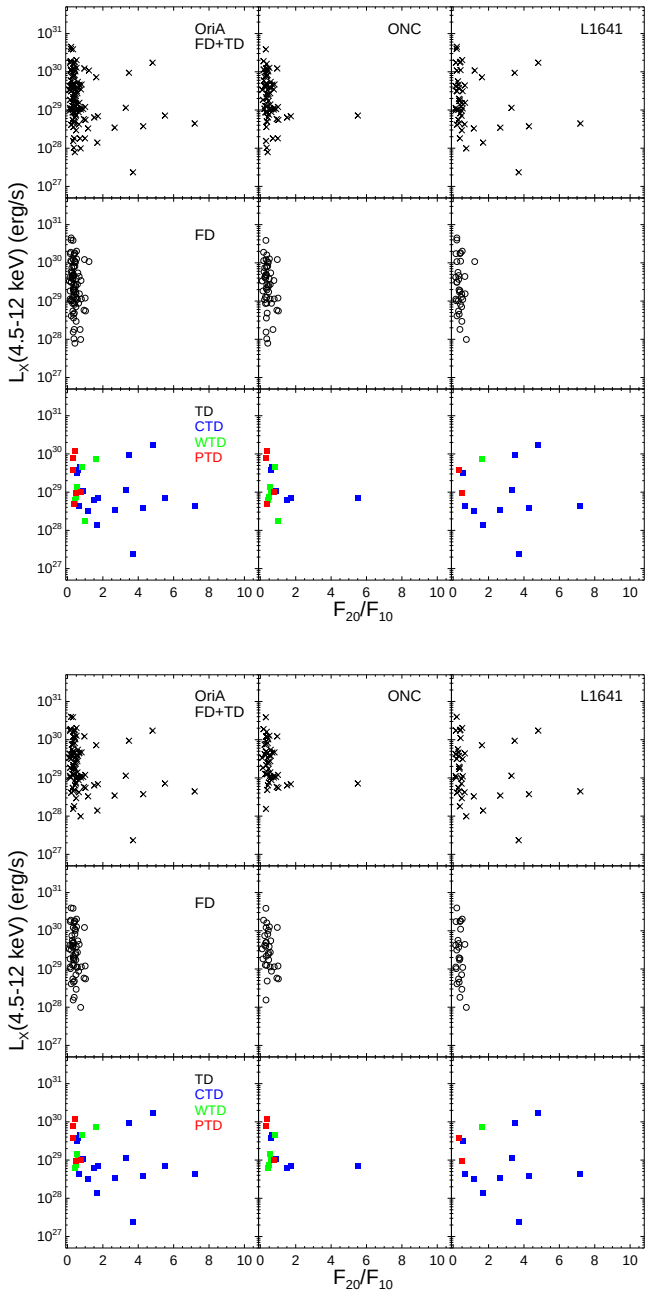


Figure C.185 F_{20}/F_{10} vs. $\log L_X 5$. Upper panel: all available objects; Lower panel: objects with available spectral types only

Table C.369 F_{20}/F_{10} vs. $\log L_X 5$ (I)

	Ori A				ONC				L1641			
	N	ρ	τ	r	N	ρ	τ	r	N	ρ	τ	r
TDFD	114	-0.282	-0.194	-0.064	66	-0.290	-0.192	0.062	48	-0.308	-0.218	-0.226
		0.002	0.002	0.499		0.018	0.023	0.621		0.033	0.029	0.122
FD	83	-0.201	-0.140	-0.176	49	-0.238	-0.158	-0.225	34	-0.172	-0.137	-0.113
		0.068	0.061	0.111		0.100	0.109	0.120		0.332	0.254	0.525
TD	31	-0.165	-0.097	0.111	17	-0.100	-0.044	0.320	14	-0.051	-0.033	-0.072
		0.376	0.444	0.552		0.701	0.805	0.211		0.864	0.870	0.807

ρ: Spearsmans ρ
τ: Kendalls τ
r: Pearsons r

Table C.370 F_{20}/F_{10} vs. $\log L_X 5$ (II)

	Ori A				ONC				L1641			
	N	ρ	τ	r	N	ρ	τ	r	N	ρ	τ	r
TDFD	86	-0.293	-0.201	-0.076	47	-0.349	-0.240	0.065	39	-0.299	-0.204	-0.217
		0.006	0.006	0.487		0.016	0.018	0.664		0.064	0.068	0.185
FD	57	-0.181	-0.122	-0.228	32	-0.307	-0.206	-0.297	25	-0.131	-0.107	-0.251
		0.179	0.182	0.088		0.087	0.098	0.099		0.533	0.455	0.226
TD	29	-0.191	-0.123	0.082	15	-0.171	-0.105	0.309	14	-0.051	-0.033	-0.072
		0.321	0.348	0.672		0.541	0.586	0.262		0.864	0.870	0.807

ρ: Spearsmans ρ
τ: Kendalls τ
r: Pearsons r

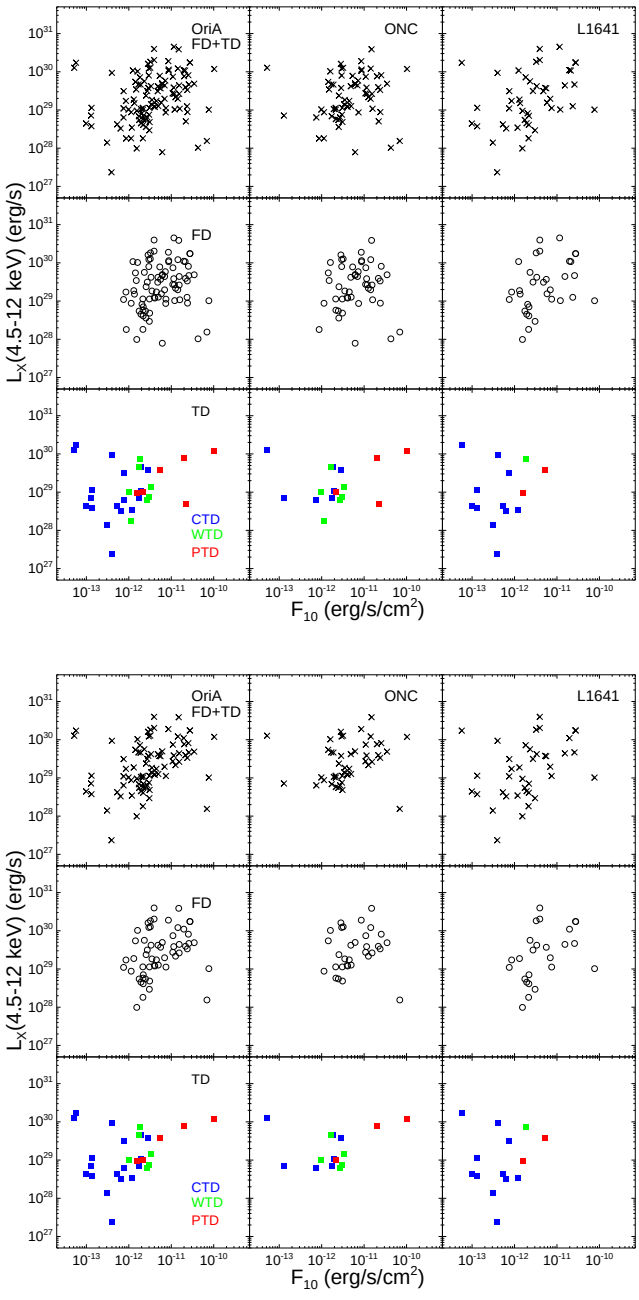


Figure C.186 $\log F_{10}$ vs. $\log L_X 5$. Upper panel: all available objects; Lower panel: objects with available spectral types only

Table C.371 $\log F_{10}$ vs. $\log L_X 5$ (I)

	Ori A				ONC				L1641			
	N	ρ	τ	r	N	ρ	τ	r	N	ρ	τ	r
TDFD	114	0.334	0.238	0.101	66	0.211	0.157	0.018	48	0.452	0.298	0.213
		0.000	0.000	0.285		0.089	0.062	0.886		0.001	0.003	0.146
FD	83	0.259	0.181	-0.042	49	0.098	0.073	-0.225	34	0.415	0.266	0.162
		0.018	0.016	0.706		0.501	0.459	0.120		0.015	0.027	0.360
TD	31	0.219	0.170	0.300	17	0.120	0.088	0.432	14	0.103	0.077	0.270
		0.237	0.179	0.101		0.646	0.621	0.083		0.725	0.702	0.351

ρ: Spearsmans ρ
τ: Kendalls τ
r: Pearsons r

Table C.372 $\log F_{10}$ vs. $\log L_X 5$ (II)

	Ori A				ONC				L1641			
	N	ρ	τ	r	N	ρ	τ	r	N	ρ	τ	r
TDFD	86	0.427	0.309	0.167	47	0.320	0.245	0.115	39	0.486	0.328	0.212
		0.000	0.000	0.124		0.028	0.015	0.441		0.002	0.003	0.195
FD	57	0.388	0.281	0.016	32	0.220	0.185	-0.178	25	0.555	0.373	0.173
		0.003	0.002	0.906		0.227	0.136	0.330		0.004	0.009	0.408
TD	29	0.260	0.212	0.323	15	0.211	0.162	0.503	14	0.103	0.077	0.270
		0.173	0.107	0.087		0.451	0.400	0.056		0.725	0.702	0.351

ρ: Spearsmans ρ
τ: Kendalls τ
r: Pearsons r

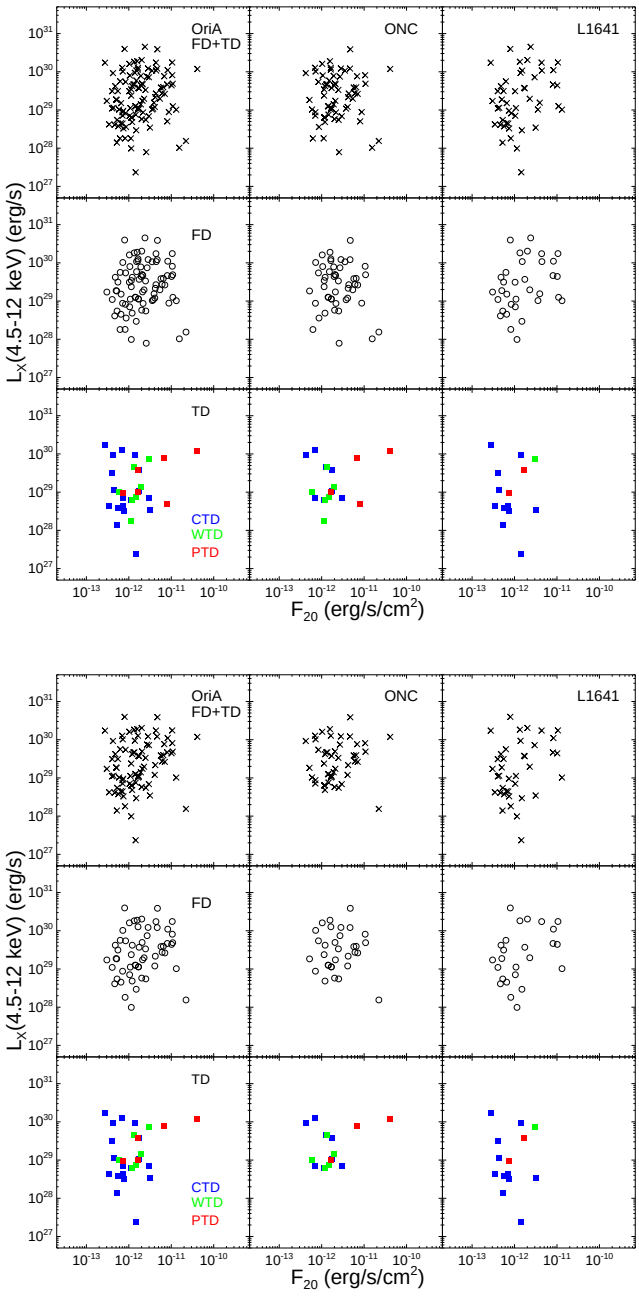


Figure C.187 $\log F_{20}$ vs. $\log L_X 5$. Upper panel: all available objects; Lower panel: objects with available spectral types only

Table C.373 $\log F_{20}$ vs. $\log L_X 5$ (I)

	Ori A				ONC				L1641			
	N	ρ	τ	r	N	ρ	τ	r	N	ρ	τ	r
TDFD	115	0.206	0.141	0.072	67	0.034	0.033	-0.006	48	0.300	0.181	0.231
		0.027	0.025	0.444		0.785	0.693	0.962		0.038	0.070	0.114
FD	83	0.172	0.120	-0.080	49	-0.035	-0.022	-0.273	34	0.326	0.201	0.206
		0.119	0.109	0.472		0.812	0.823	0.058		0.060	0.094	0.242
TD	32	0.089	0.073	0.264	18	0.018	0.033	0.364	14	-0.134	-0.099	0.065
		0.628	0.559	0.144		0.945	0.850	0.138		0.648	0.622	0.825

ρ: Spearsmans ρ
τ: Kendalls τ
r: Pearsons r

Table C.374 $\log F_{20}$ vs. $\log L_X 5$ (II)

	Ori A				ONC				L1641			
	N	ρ	τ	r	N	ρ	τ	r	N	ρ	τ	r
TDFD	87	0.269	0.186	0.159	48	0.113	0.089	0.087	39	0.262	0.150	0.280
		0.012	0.011	0.141		0.445	0.374	0.557		0.108	0.179	0.084
FD	57	0.269	0.188	0.027	32	0.068	0.044	-0.226	25	0.350	0.220	0.290
		0.043	0.039	0.842		0.712	0.721	0.214		0.086	0.123	0.160
TD	30	0.117	0.103	0.283	16	0.088	0.083	0.418	14	-0.134	-0.099	0.065
		0.537	0.422	0.130		0.745	0.653	0.107		0.648	0.622	0.825

ρ: Spearsmans ρ
τ: Kendalls τ
r: Pearsons r

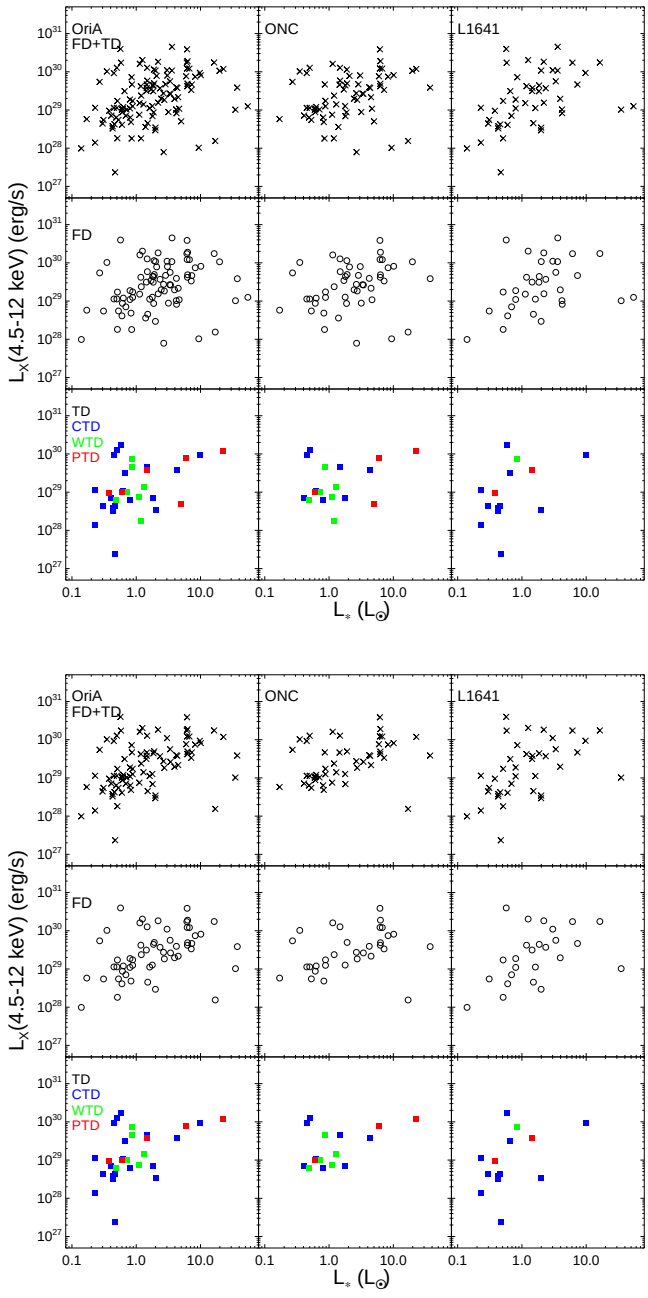


Figure C.188 $\log L_\star$ vs. $\log L_X 5$. Upper panel: all available objects; Lower panel: objects with available spectral types only

Table C.375 $\log L_\star$ vs. $\log L_X 5$ (I)

	Ori A				ONC				L1641			
	N	ρ	τ	r	N	ρ	τ	r	N	ρ	τ	r
TDFD	115	0.384	0.277	0.341	67	0.305	0.225	0.248	48	0.501	0.349	0.429
		0.000	0.000	0.000		0.012	0.007	0.043		0.000	0.000	0.002
FD	83	0.315	0.228	0.264	49	0.293	0.214	0.212	34	0.356	0.270	0.328
		0.004	0.002	0.016		0.041	0.030	0.144		0.039	0.025	0.058
TD	32	0.368	0.261	0.407	18	0.084	0.085	0.285	14	0.441	0.278	0.472
		0.038	0.036	0.021		0.742	0.622	0.252		0.115	0.166	0.088

ρ: Spearsmans ρ
τ: Kendalls τ
r: Pearsons r

Table C.376 $\log L_\star$ vs. $\log L_X 5$ (II)

	Ori A				ONC				L1641			
	N	ρ	τ	r	N	ρ	τ	r	N	ρ	τ	r
TDFD	87	0.477	0.355	0.445	48	0.408	0.323	0.372	39	0.558	0.394	0.496
		0.000	0.000	0.000		0.004	0.001	0.009		0.000	0.000	0.001
FD	57	0.423	0.319	0.383	32	0.406	0.327	0.322	25	0.468	0.355	0.444
		0.001	0.000	0.003		0.021	0.008	0.072		0.018	0.013	0.026
TD	30	0.466	0.337	0.486	16	0.262	0.233	0.443	14	0.441	0.278	0.472
		0.009	0.009	0.006		0.327	0.207	0.086		0.115	0.166	0.088

ρ: Spearsmans ρ
τ: Kendalls τ
r: Pearsons r

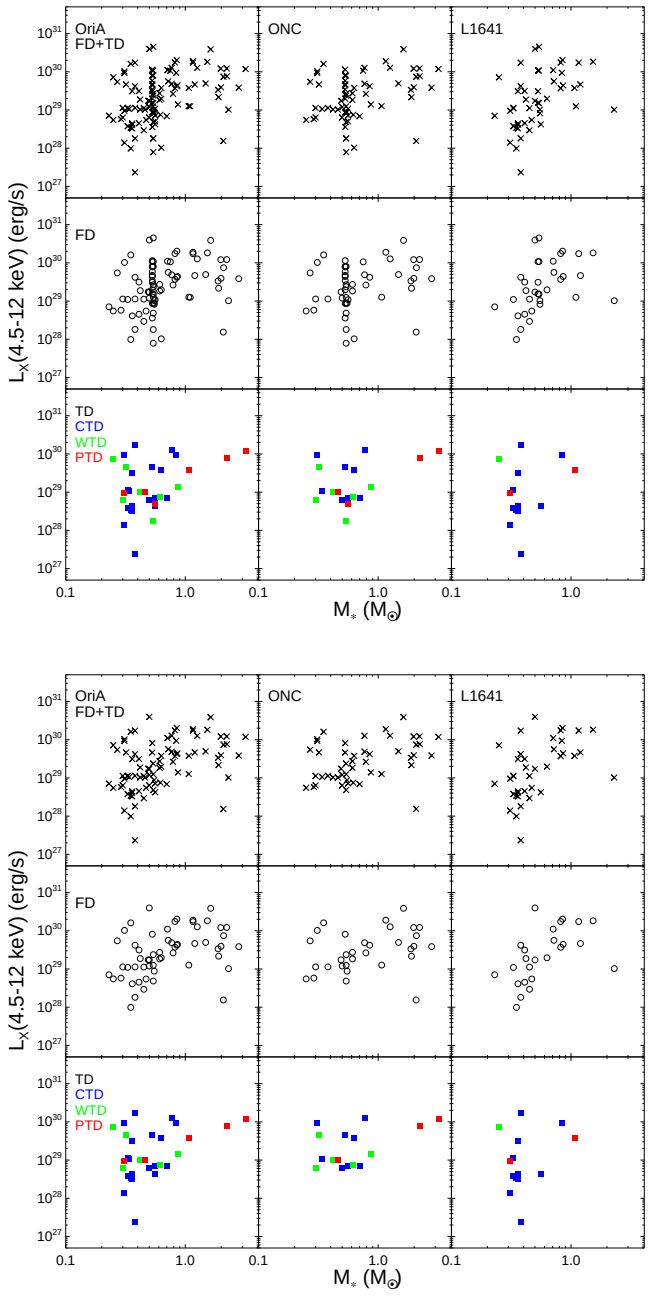


Figure C.189 $\log M_\star$ vs. $\log L_X 5$. Upper panel: all available objects; Lower panel: objects with available spectral types only

Table C.377 $\log M_\star$ vs. $\log L_X 5$ (I)

	Ori A				ONC				L1641			
	N	ρ	τ	r	N	ρ	τ	r	N	ρ	τ	r
TDFD	115	0.362	0.252	0.357	67	0.248	0.172	0.308	48	0.540	0.366	0.443
		0.000	0.000	0.000		0.043	0.040	0.011		0.000	0.000	0.002
FD	83	0.344	0.245	0.316	49	0.210	0.156	0.264	34	0.544	0.380	0.431
		0.001	0.001	0.004		0.148	0.113	0.067		0.001	0.002	0.011
TD	32	0.275	0.186	0.375	18	0.263	0.144	0.408	14	0.217	0.125	0.285
		0.128	0.136	0.034		0.291	0.403	0.093		0.456	0.533	0.323

ρ: Spearsmans ρ
τ: Kendalls τ
r: Pearsons r

Table C.378 $\log M_\star$ vs. $\log L_X 5$ (II)

	Ori A				ONC				L1641			
	N	ρ	τ	r	N	ρ	τ	r	N	ρ	τ	r
TDFD	87	0.447	0.320	0.422	48	0.375	0.270	0.357	39	0.568	0.397	0.494
		0.000	0.000	0.000		0.009	0.007	0.013		0.000	0.000	0.001
FD	57	0.447	0.331	0.395	32	0.342	0.275	0.300	25	0.655	0.474	0.534
		0.000	0.000	0.002		0.055	0.027	0.095		0.000	0.001	0.006
TD	30	0.320	0.214	0.398	16	0.338	0.183	0.445	14	0.217	0.125	0.285
		0.085	0.097	0.029		0.200	0.322	0.084		0.456	0.533	0.323

ρ: Spearsmans ρ
τ: Kendalls τ
r: Pearsons r

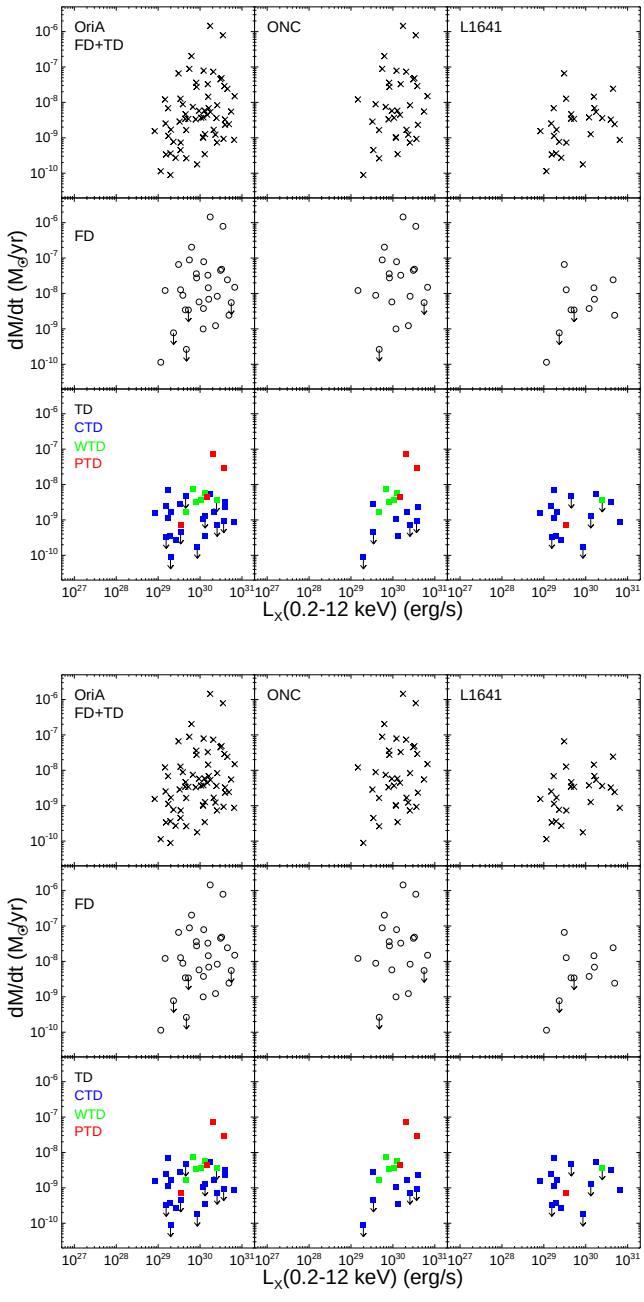


Figure C.190 $\log L_X 8$ vs $\log \dot{M}$. Upper panel: all available objects; Lower panel: objects with available spectral types only

Table C.379 $\log L_X 8$ vs $\log \dot{M}$ (I)

	Ori A				ONC				L1641			
	N	ρ	τ	r	N	ρ	τ	r	N	ρ	τ	r
TDFD	63	0.309	0.204	0.339	36	0.187	0.114	0.253	27	0.374	0.225	0.328
		0.014	0.018	0.007		0.275	0.327	0.137		0.054	0.100	0.095
FD	30	0.236	0.154	0.307	19	0.112	0.076	0.147	11	0.300	0.236	0.425
		0.209	0.232	0.099		0.647	0.649	0.548		0.370	0.312	0.193
TD	33	0.254	0.174	0.332	17	0.223	0.176	0.425	16	0.112	0.050	0.182
		0.153	0.154	0.059		0.390	0.323	0.089		0.680	0.787	0.500

ρ: Spearsmans ρ
τ: Kendalls τ
r: Pearsons r

Table C.380 $\log L_X 8$ vs $\log \dot{M}$ (II)

	Ori A				ONC				L1641			
	N	ρ	τ	r	N	ρ	τ	r	N	ρ	τ	r
TDFD	63	0.309	0.204	0.339	36	0.187	0.114	0.253	27	0.374	0.225	0.328
		0.014	0.018	0.007		0.275	0.327	0.137		0.054	0.100	0.095
FD	30	0.236	0.154	0.307	19	0.112	0.076	0.147	11	0.300	0.236	0.425
		0.209	0.232	0.099		0.647	0.649	0.548		0.370	0.312	0.193
TD	33	0.254	0.174	0.332	17	0.223	0.176	0.425	16	0.112	0.050	0.182
		0.153	0.154	0.059		0.390	0.323	0.089		0.680	0.787	0.500

ρ: Spearsmans ρ
τ: Kendalls τ
r: Pearsons r

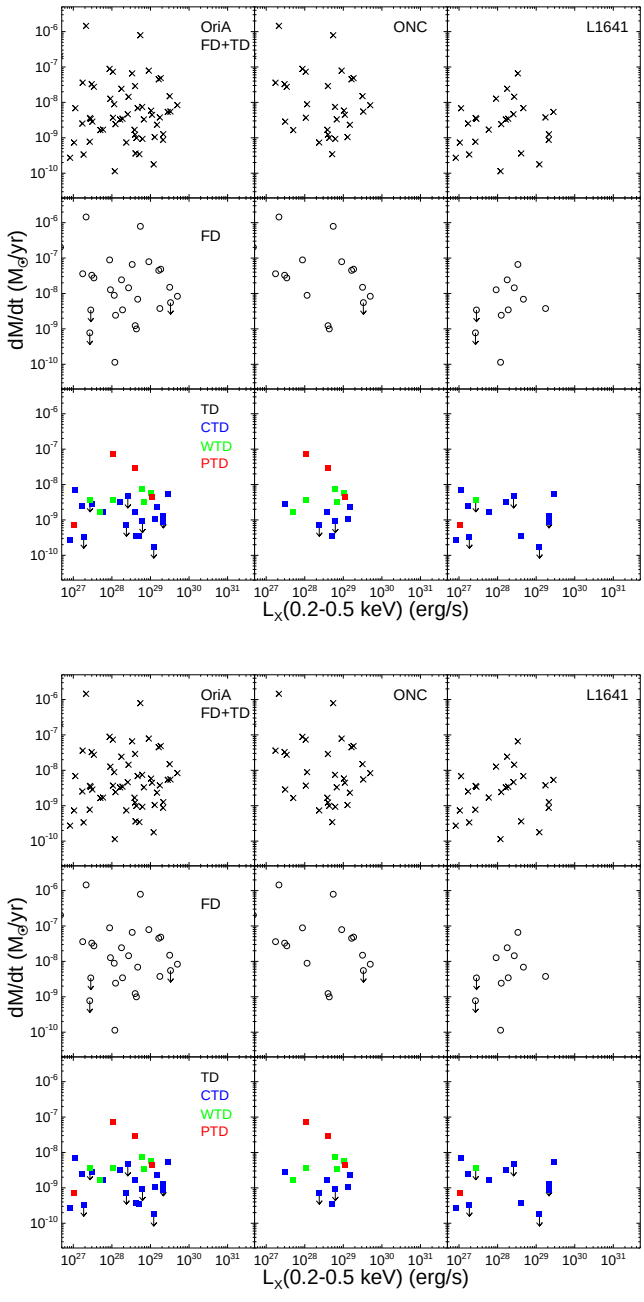


Figure C.191 $\log L_X 1$ vs $\log \dot{M}$. Upper panel: all available objects; Lower panel: objects with available spectral types only

Table C.381 $\log L_X 1$ vs $\log \dot{M}$ (I)

	Ori A				ONC				L1641			
	N	ρ	τ	r	N	ρ	τ	r	N	ρ	τ	r
TDFD	59	0.035	0.024	-0.010	32	-0.212	-0.149	-0.303	27	0.263	0.208	0.161
		0.793	0.789	0.940		0.244	0.230	0.092		0.186	0.128	0.422
FD	28	-0.089	-0.069	-0.118	17	-0.294	-0.250	-0.298	11	0.536	0.382	0.340
		0.652	0.607	0.550		0.252	0.161	0.245		0.089	0.102	0.306
TD	31	0.079	0.062	0.077	15	-0.039	-0.048	-0.151	16	0.097	0.083	-0.018
		0.674	0.622	0.681		0.889	0.805	0.591		0.721	0.653	0.947

ρ: Spearsmans ρ
τ: Kendalls τ
r: Pearsons r

Table C.382 $\log L_X 1$ vs $\log \dot{M}$ (II)

	Ori A				ONC				L1641			
	N	ρ	τ	r	N	ρ	τ	r	N	ρ	τ	r
TDFD	59	0.035	0.024	-0.010	32	-0.212	-0.149	-0.303	27	0.263	0.208	0.161
		0.793	0.789	0.940		0.244	0.230	0.092		0.186	0.128	0.422
FD	28	-0.089	-0.069	-0.118	17	-0.294	-0.250	-0.298	11	0.536	0.382	0.340
		0.652	0.607	0.550		0.252	0.161	0.245		0.089	0.102	0.306
TD	31	0.079	0.062	0.077	15	-0.039	-0.048	-0.151	16	0.097	0.083	-0.018
		0.674	0.622	0.681		0.889	0.805	0.591		0.721	0.653	0.947

ρ: Spearsmans ρ
τ: Kendalls τ
r: Pearsons r

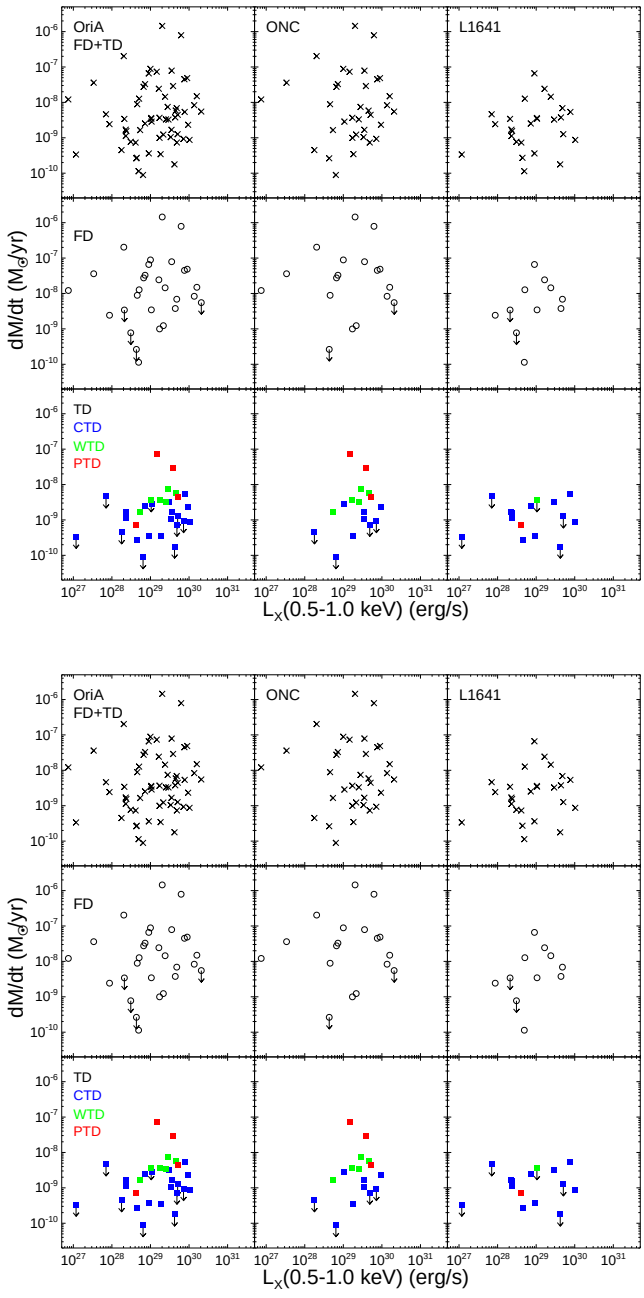


Figure C.192 $\log L_X 2$ vs $\log \dot{M}$. Upper panel: all available objects; Lower panel: objects with available spectral types only

Table C.383 $\log L_X 2$ vs $\log \dot{M}$ (I)

	Ori A				ONC				L1641			
	N	ρ	τ	r	N	ρ	τ	r	N	ρ	τ	r
TDFD	61	0.189	0.120	0.146	35	0.071	0.055	0.017	26	0.253	0.120	0.206
		0.144	0.171	0.262		0.683	0.639	0.923		0.213	0.390	0.313
FD	29	0.202	0.143	0.161	18	0.003	0.007	0.054	11	0.582	0.345	0.363
		0.292	0.277	0.404		0.990	0.970	0.831		0.060	0.139	0.273
TD	32	0.233	0.153	0.252	17	0.203	0.132	0.295	15	0.071	0.029	0.123
		0.200	0.218	0.164		0.434	0.458	0.250		0.800	0.882	0.662

ρ: Spearsmans ρ
τ: Kendalls τ
r: Pearsons r

Table C.384 $\log L_X 2$ vs $\log \dot{M}$ (II)

	Ori A				ONC				L1641			
	N	ρ	τ	r	N	ρ	τ	r	N	ρ	τ	r
TDFD	61	0.189	0.120	0.146	35	0.071	0.055	0.017	26	0.253	0.120	0.206
		0.144	0.171	0.262		0.683	0.639	0.923		0.213	0.390	0.313
FD	29	0.202	0.143	0.161	18	0.003	0.007	0.054	11	0.582	0.345	0.363
		0.292	0.277	0.404		0.990	0.970	0.831		0.060	0.139	0.273
TD	32	0.233	0.153	0.252	17	0.203	0.132	0.295	15	0.071	0.029	0.123
		0.200	0.218	0.164		0.434	0.458	0.250		0.800	0.882	0.662

ρ: Spearsmans ρ
τ: Kendalls τ
r: Pearsons r

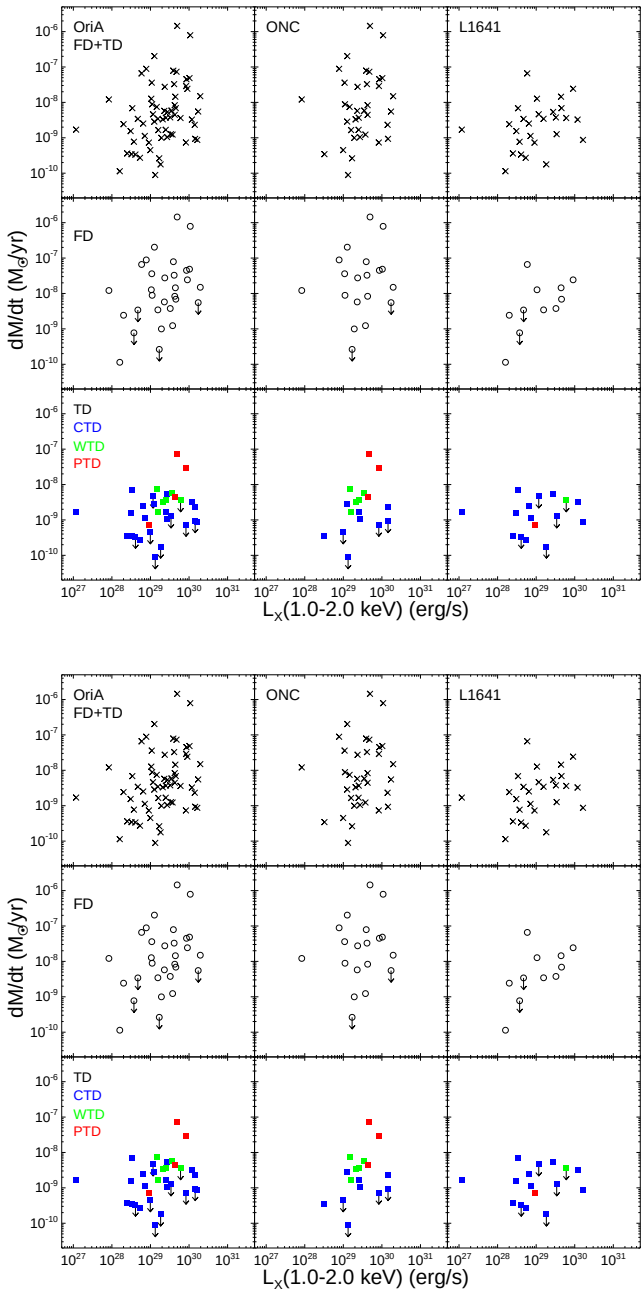


Figure C.193 $\log L_X 3$ vs $\log \dot{M}$. Upper panel: all available objects; Lower panel: objects with available spectral types only

Table C.385 $\log L_X 3$ vs $\log \dot{M}$ (I)

	Ori A				ONC				L1641			
	N	ρ	τ	r	N	ρ	τ	r	N	ρ	τ	r
TDFD	63	0.339	0.230	0.316	36	0.210	0.156	0.206	27	0.397	0.254	0.309
		0.007	0.008	0.012		0.219	0.182	0.228		0.040	0.064	0.117
FD	30	0.360	0.255	0.380	19	0.137	0.111	0.154	11	0.727	0.600	0.596
		0.051	0.048	0.038		0.576	0.506	0.529		0.011	0.010	0.053
TD	33	0.315	0.193	0.276	17	0.360	0.265	0.380	16	0.150	0.067	0.134
		0.074	0.114	0.120		0.155	0.138	0.132		0.579	0.719	0.621

ρ: Spearsmans ρ
τ: Kendalls τ
r: Pearsons r

Table C.386 $\log L_X 3$ vs $\log \dot{M}$ (II)

	Ori A				ONC				L1641			
	N	ρ	τ	r	N	ρ	τ	r	N	ρ	τ	r
TDFD	63	0.339	0.230	0.316	36	0.210	0.156	0.206	27	0.397	0.254	0.309
		0.007	0.008	0.012		0.219	0.182	0.228		0.040	0.064	0.117
FD	30	0.360	0.255	0.380	19	0.137	0.111	0.154	11	0.727	0.600	0.596
		0.051	0.048	0.038		0.576	0.506	0.529		0.011	0.010	0.053
TD	33	0.315	0.193	0.276	17	0.360	0.265	0.380	16	0.150	0.067	0.134
		0.074	0.114	0.120		0.155	0.138	0.132		0.579	0.719	0.621

ρ: Spearsmans ρ
τ: Kendalls τ
r: Pearsons r

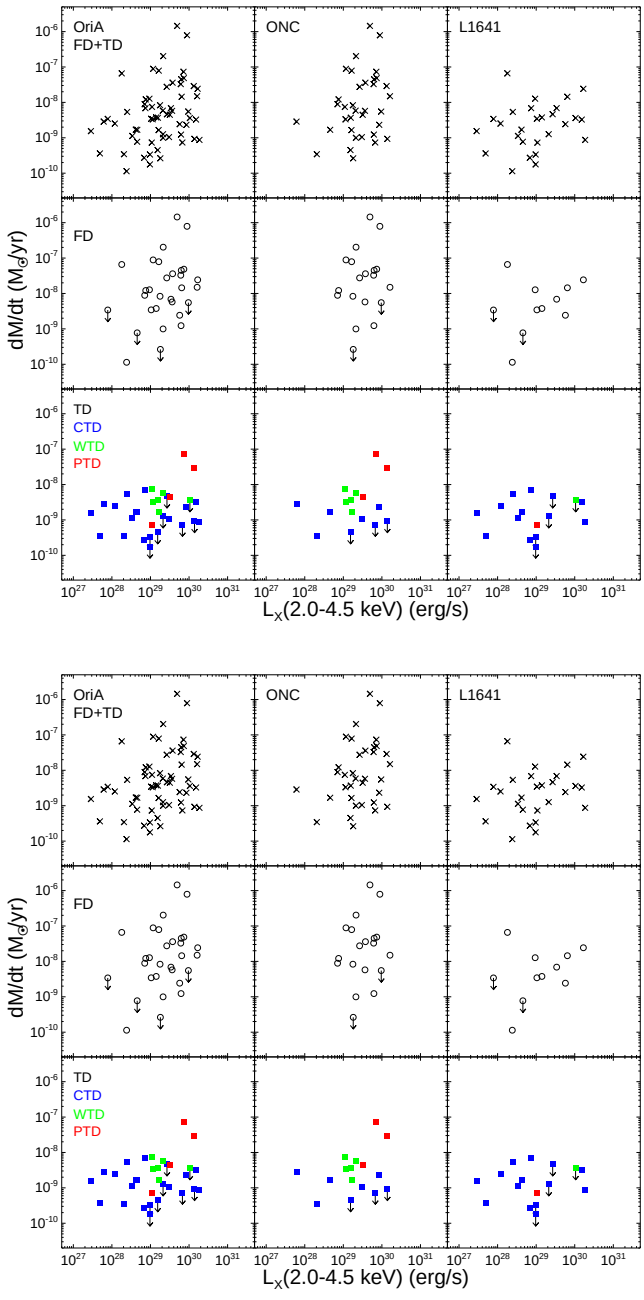


Figure C.194 $\log L_X 4$ vs $\log \dot{M}$. Upper panel: all available objects; Lower panel: objects with available spectral types only

Table C.387 $\log L_X 4$ vs $\log \dot{M}$ (I)

	Ori A				ONC				L1641			
	N	ρ	τ	r	N	ρ	τ	r	N	ρ	τ	r
TDFD	62	0.334	0.224	0.333	35	0.240	0.163	0.290	27	0.255	0.185	0.237
		0.008	0.010	0.008		0.164	0.168	0.091		0.200	0.175	0.234
FD	30	0.301	0.214	0.327	19	0.123	0.099	0.179	11	0.327	0.309	0.309
		0.106	0.097	0.078		0.616	0.552	0.463		0.326	0.186	0.355
TD	32	0.242	0.149	0.280	16	0.185	0.133	0.306	16	0.062	0.050	0.155
		0.182	0.230	0.121		0.492	0.471	0.249		0.820	0.787	0.567

ρ: Spearsmans ρ
τ: Kendalls τ
r: Pearsons r

Table C.388 $\log L_X 4$ vs $\log \dot{M}$ (II)

	Ori A				ONC				L1641			
	N	ρ	τ	r	N	ρ	τ	r	N	ρ	τ	r
TDFD	62	0.334	0.224	0.333	35	0.240	0.163	0.290	27	0.255	0.185	0.237
		0.008	0.010	0.008		0.164	0.168	0.091		0.200	0.175	0.234
FD	30	0.301	0.214	0.327	19	0.123	0.099	0.179	11	0.327	0.309	0.309
		0.106	0.097	0.078		0.616	0.552	0.463		0.326	0.186	0.355
TD	32	0.242	0.149	0.280	16	0.185	0.133	0.306	16	0.062	0.050	0.155
		0.182	0.230	0.121		0.492	0.471	0.249		0.820	0.787	0.567

ρ: Spearsmans ρ
τ: Kendalls τ
r: Pearsons r

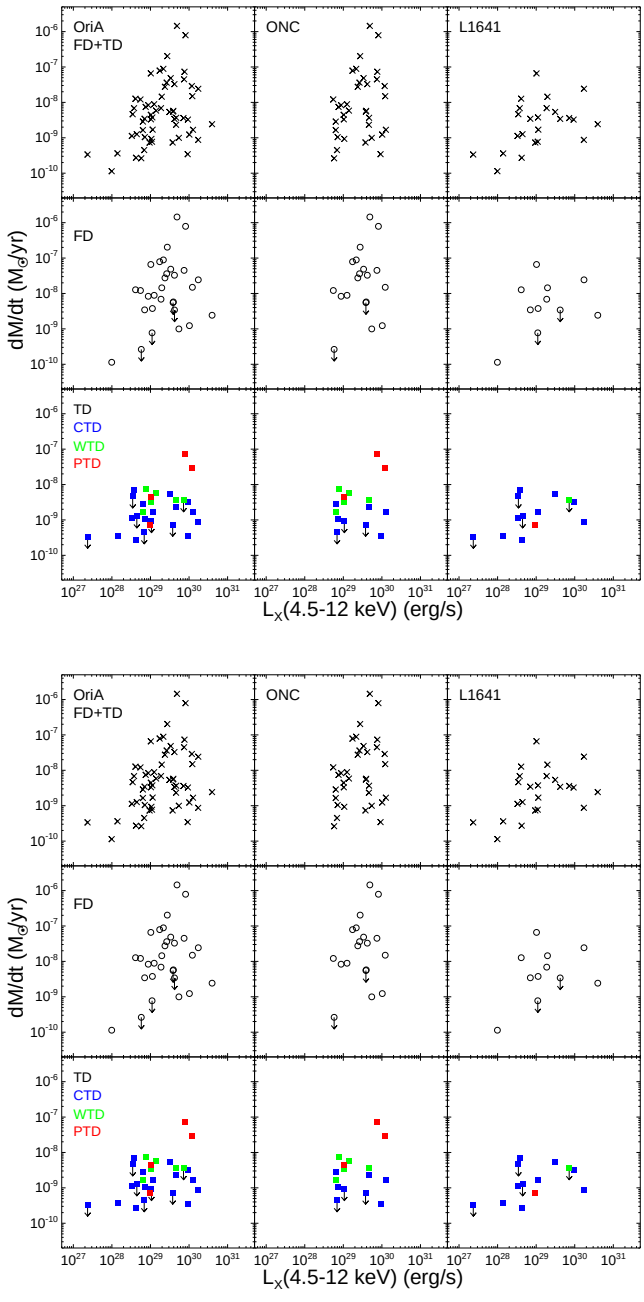


Figure C.195 $\log L_X 5$ vs $\log \dot{M}$. Upper panel: all available objects; Lower panel: objects with available spectral types only

Table C.389 $\log L_X 5$ vs $\log \dot{M}$ (I)

	Ori A				ONC				L1641			
	N	ρ	τ	r	N	ρ	τ	r	N	ρ	τ	r
TDFD	59	0.319	0.225	0.379	35	0.235	0.173	0.284	24	0.383	0.268	0.434
		0.014	0.012	0.003		0.174	0.144	0.098		0.064	0.066	0.034
FD	30	0.220	0.163	0.331	19	0.119	0.099	0.248	11	0.145	0.127	0.370
		0.242	0.205	0.074		0.627	0.552	0.306		0.670	0.586	0.263
TD	29	0.278	0.197	0.382	16	0.188	0.117	0.256	13	0.330	0.256	0.450
		0.144	0.133	0.041		0.485	0.528	0.339		0.271	0.222	0.123

ρ: Spearsmans ρ
τ: Kendalls τ
r: Pearsons r

Table C.390 $\log L_X 5$ vs $\log \dot{M}$ (II)

	Ori A				ONC				L1641			
	N	ρ	τ	r	N	ρ	τ	r	N	ρ	τ	r
TDFD	59	0.319	0.225	0.379	35	0.235	0.173	0.284	24	0.383	0.268	0.434
		0.014	0.012	0.003		0.174	0.144	0.098		0.064	0.066	0.034
FD	30	0.220	0.163	0.331	19	0.119	0.099	0.248	11	0.145	0.127	0.370
		0.242	0.205	0.074		0.627	0.552	0.306		0.670	0.586	0.263
TD	29	0.278	0.197	0.382	16	0.188	0.117	0.256	13	0.330	0.256	0.450
		0.144	0.133	0.041		0.485	0.528	0.339		0.271	0.222	0.123

ρ: Spearsmans ρ
τ: Kendalls τ
r: Pearsons r

C.2 Significant Correlations

Table C.391 Significance of correlations III: disks in ONC regardless of spectral type information

ONC	P01	P02	P03	P04	P05	P06	P07	P08	P09	P10	P11	P12	P13	P14	P15	p16	P17	P18	P19	P20	P21	P22	P23
P01		5			-1								5	1			5					1	
P02	5												1				1						
P03																							
P04																							
P05			-3	-3					1				-3										
P06			1								5	5											
P07																							
P08																							
P09																							
P10			-5		1	-5									-1								
P11			3			5				-5		5											
P12						5				-1	5												
P13	5														5		5						
P14	5	1															5						
P15			5		-1	5				-5	5	1					5						
p16			3			1					3		5				5						
P17	3				-1								1	1	3	1							
P18																							
P19																							
P20																							
P21																							
P22															3								
P23																							

Properties measured from Class II disks in ONC. Above diagonal is for FD's. Below diagonal is for TD's.
P1: $\log L_\star$; P2: $logM_\star$; P3: n_{K-6}; P4: n_{6-13}; P5: n_{13-31}; P6: $EW(10\mu m)$; P7: $EW(20\mu m)$; P8: $EW(33\mu m)$; P9: $F_{11.3}/F_{9.8}$; P10: F_{20}/F_{10}; P11: $F_{9.8}$; P12: $F_{11.3}$; P13: F_{10}; P14: F_{20}; P15: $\log F_{10}$; P16: $\log F_{20}$; P17: $\log \dot{M}$; P18: $\log L_X(0.2-12keV)$; P19: $\log L_X(0.2-0.5keV)$; P20: $\log L_X(0.5-1.0keV)$; P21: $\log L_X(1.0-2.0keV)$; P22: $\log L_X(2.0-4.5keV)$; P23: $\log L_X(4.5-12keV)$
Positive numbers indicate positive correlation; negative numbers indicate negative correlation.
5 or -5: Spearman's ρ, Kendall's τ, and Pearson's r are all greater than 0.5 and the probabilities that these correlations are generated from a random distribution are all less than 0.05.
3 or -3: Two among ρ, τ, and r are greater than 0.5 and the probabilities are all less than 0.05.
1 or -1: ρ, τ, and r are greater than 0.3 and the probabilities are all less than 0.05, but they cannot meet above two conditions.

Table C.392 Significance of correlations IV: disks in L1641regardless of spectral type information

L1641	P01	P02	P03	P04	P05	P06	P07	P08	P09	P10	P11	P12	P13	P14	P15	p16	P17	P18	P19	P20	P21	P22	P23
P01		5											5	5			5						
P02	1												3	3			5	1					1
P03															1	1							
P04		-3																					
P05			-1							1													
P06			1								5	5											
P07										1													
P08																							
P09																							
P10			-1		5	-5						-1											
P11			1			5				-5		5											
P12			1			5				-5	5												
P13	1															5							
P14	3																						
P15			5		-3	5				-5	5	5					1						
p16			1										3				1						
P17	3													1		1							
P18	5																						
P19																							
P20																							
P21	5			-1																			
P22	5			-3																			
P23																							

Properties measured from Class II disks in L1641. Above diagonal is for FD's. Below diagonal is for TD's.
P1: $\log L_\star$; P2: $logM_\star$; P3: n_{K-6}; P4: n_{6-13}; P5: n_{13-31}; P6: $EW(10\mu\mathrm{m})$; P7: $EW(20\mu\mathrm{m})$; P8: $EW(33\mu\mathrm{m})$; P9: $F_{11.3}/F_{9.8}$; P10: F_{20}/F_{10}; P11: $F_{9.8}$; P12: $F_{11.3}$; P13: F_{10}; P14: F_{20}; P15: $\log F_{10}$; P16: $\log F_{20}$; P17: $\log \dot{M}$; P18: $\log L_X(0.2-12keV)$; P19: $\log L_X(0.2-0.5keV)$; P20: $\log L_X(0.5-1.0keV)$; P21: $\log L_X(1.0-2.0keV)$; P22: $\log L_X(2.0-4.5keV)$; P23: $\log L_X(4.5-12keV)$
Positive numbers indicate positive correlation; negative numbers indicate negative correlation.
5 or -5: Spearman's ρ, Kendall's τ, and Pearson's r are all greater than 0.5 and the probabilities that these correlations are generated from a random distribution are all less than 0.05.
3 or -3: Two among ρ, τ, and r are greater than 0.5 and the probabilities are all less than 0.05.
1 or -1: ρ, τ, and r are greater than 0.3 and the probabilities are all less than 0.05, but they cannot meet above two conditions.

D Appendix to Chapter 6

D.1 Distribution of EW10, F_{10}, and $F_{11.3}/F_{9.8}$ by Distance from θ^1 Ori C

D.1.1 Histogram in subsections

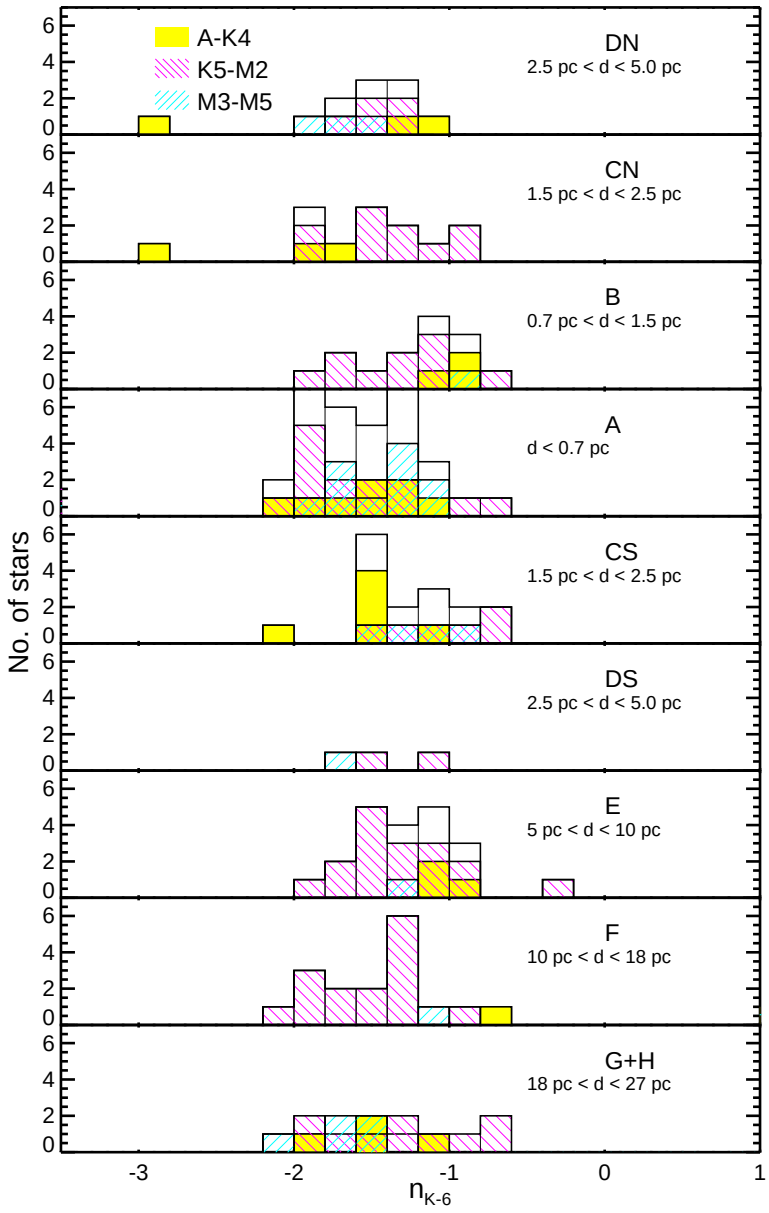


Figure D.1 distribution of nk6 by subsection

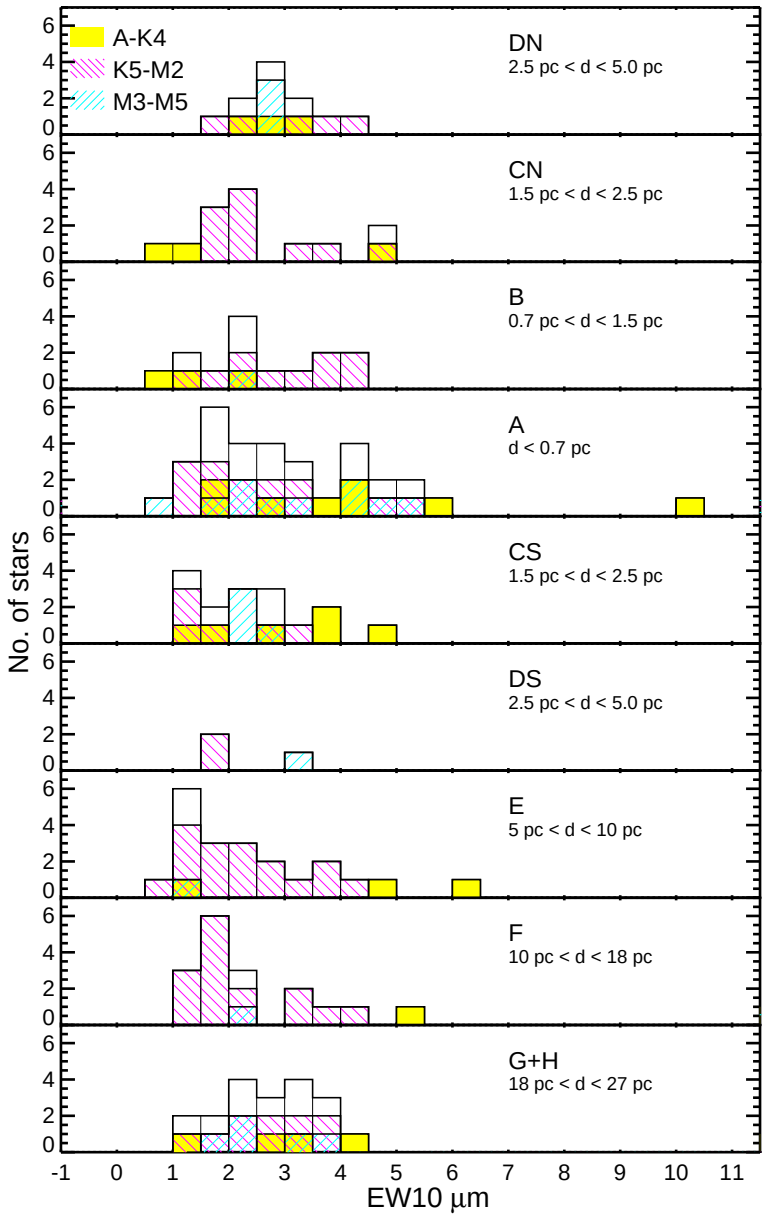


Figure D.2 distribution of EW10 by subsection

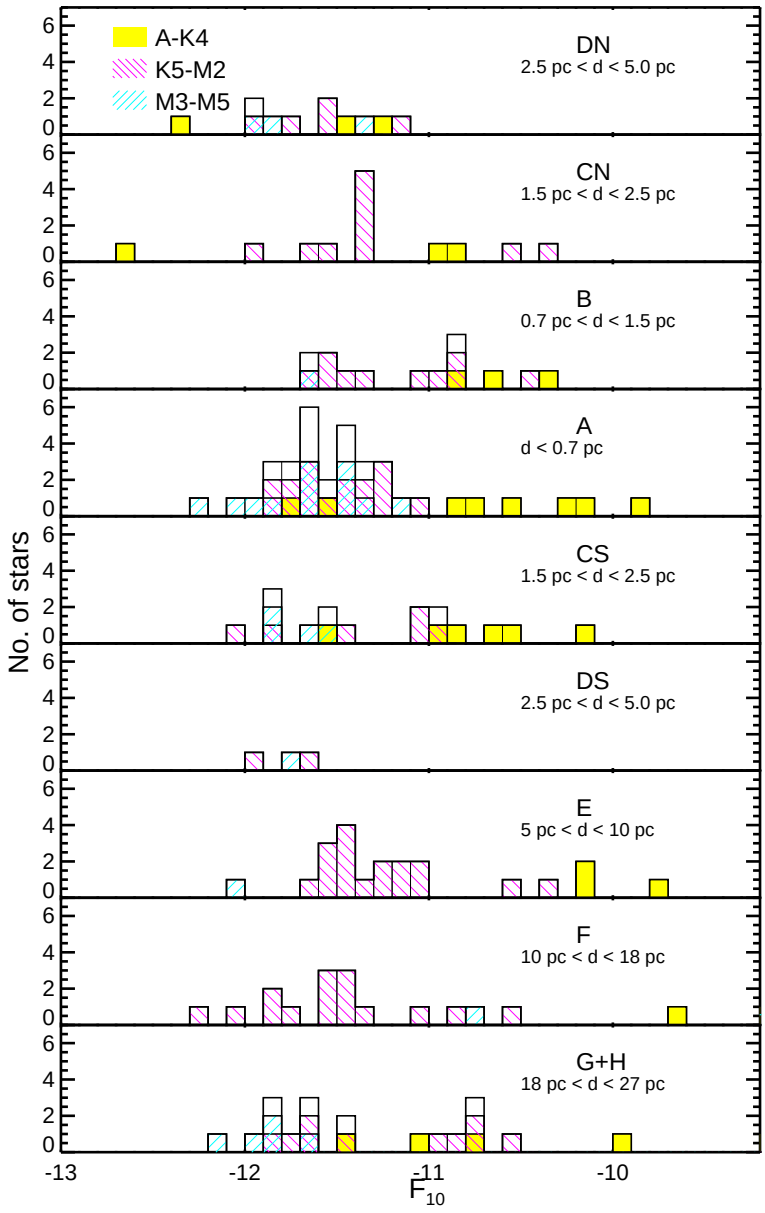


Figure D.3 distribution of F_{10} by subsection

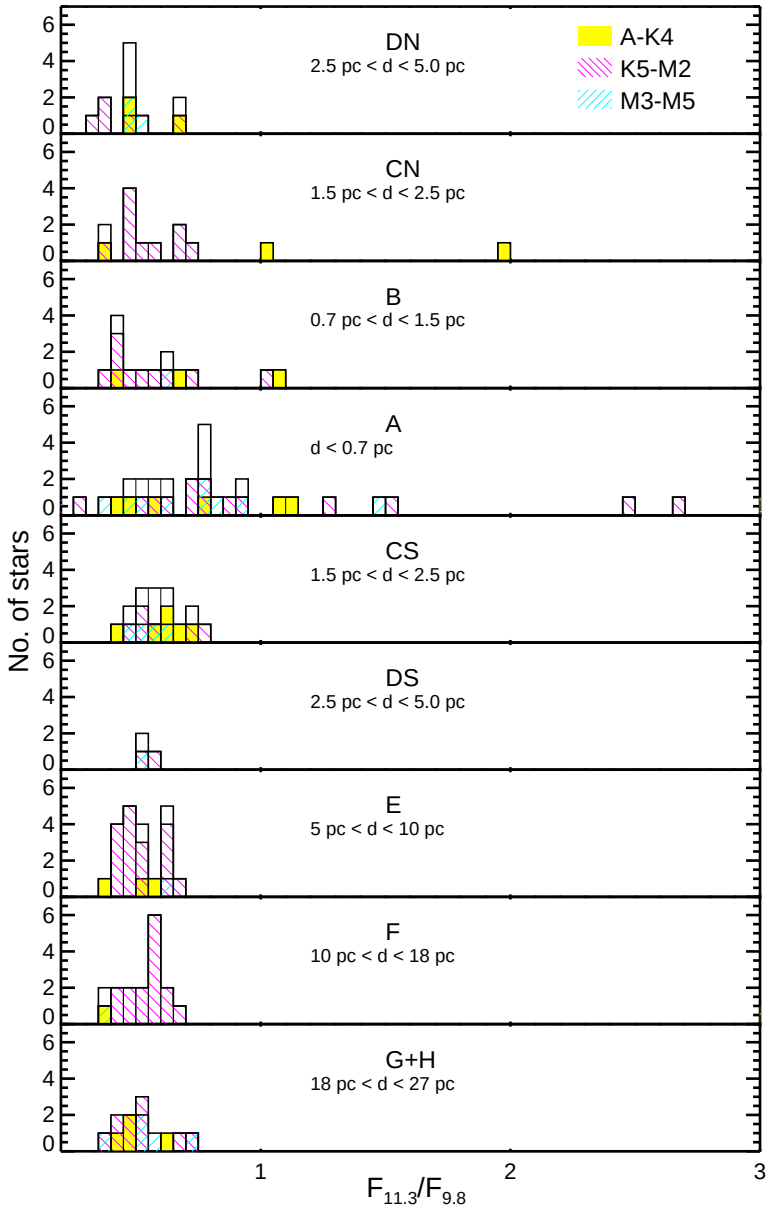


Figure D.4 distribution of $F_{11.3}/F_{9.8}$ by subsection

D.1.2 Variation of parameters via d

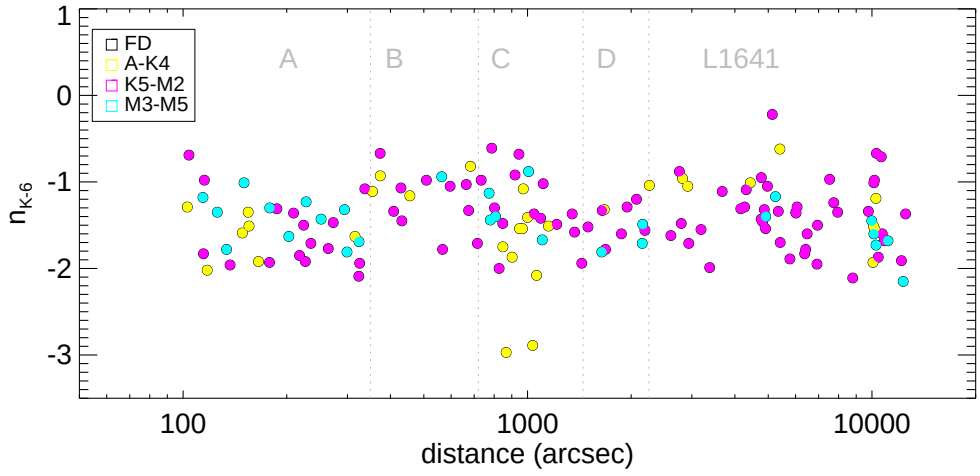


Figure D.5 Variation of n_{K-6} via distance from θ^1 Ori C.

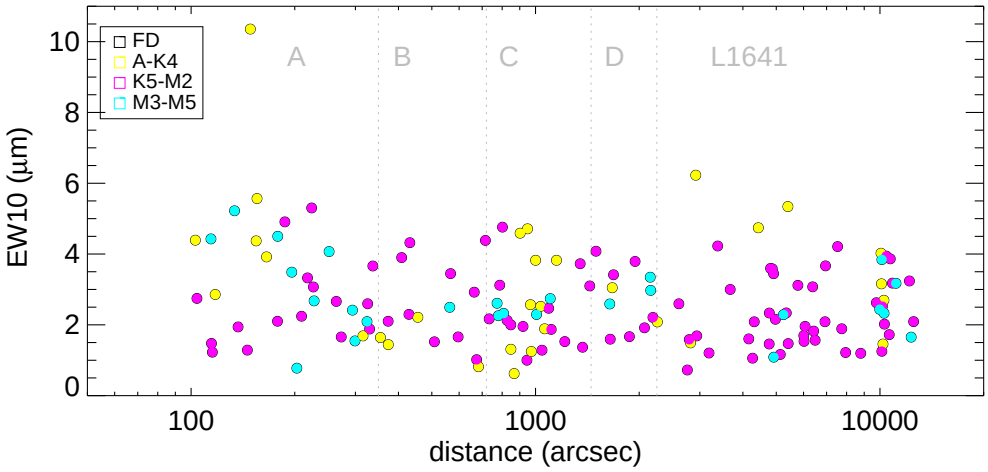


Figure D.6 Variation of EW10 via distance from θ^1 Ori C.

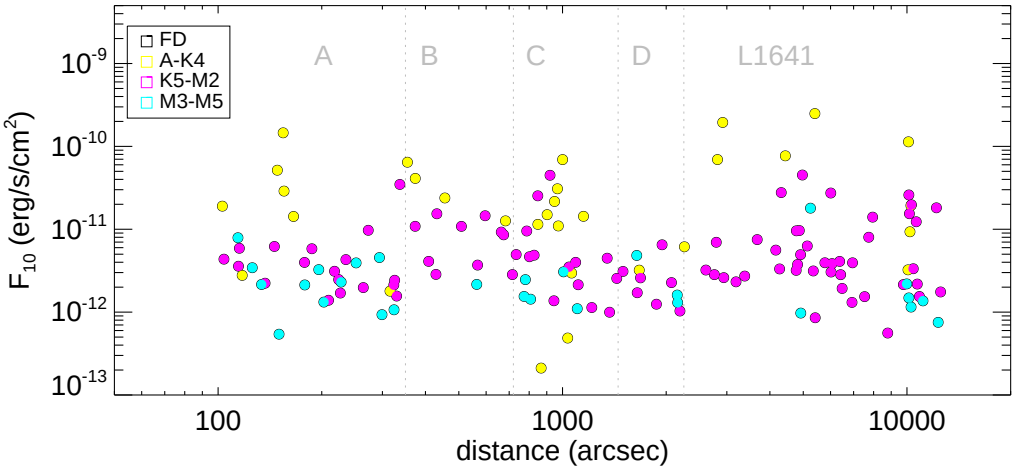


Figure D.7 Variation of F_{10} via distance from θ^1 Ori C.

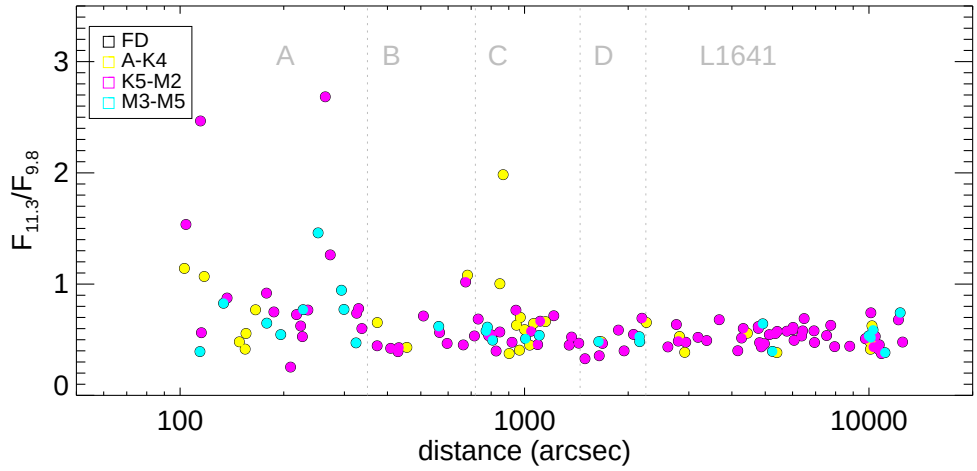


Figure D.8 Variation of $F_{11.3}/F_{9.8}$ via distance from θ^1 Ori C.

E Appendix to Chapter 7

E.1 Relative Integrated Fluxes vs. T_{eff} and Distance (d) from θ^1 Ori C

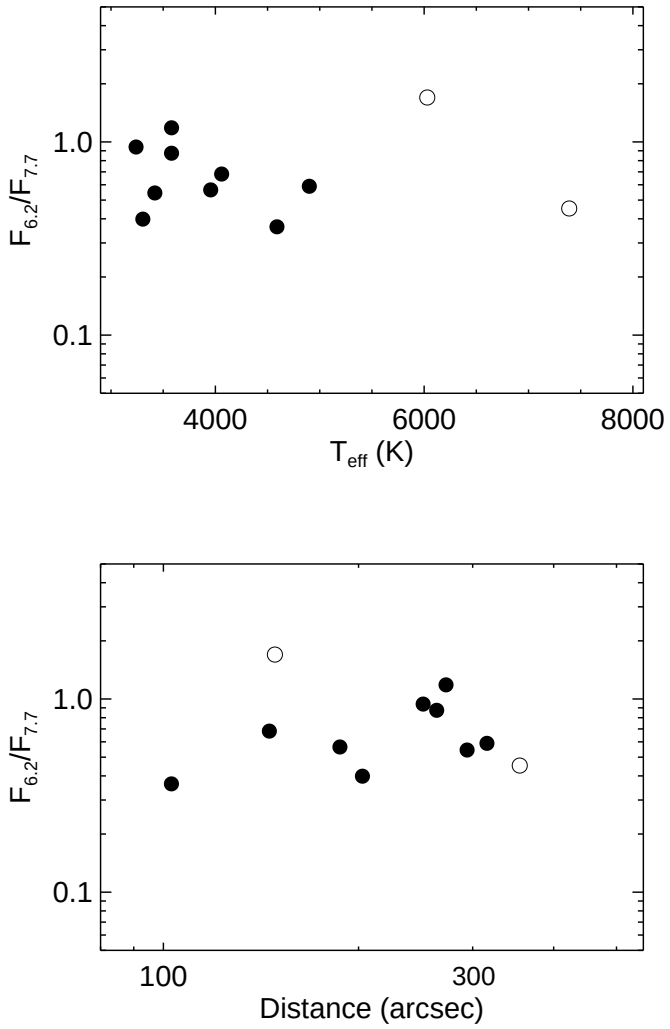


Figure E.1 $F_{6.2}/F_{8.6}$ vs. T_{eff} and distance from θ^1 Ori C.

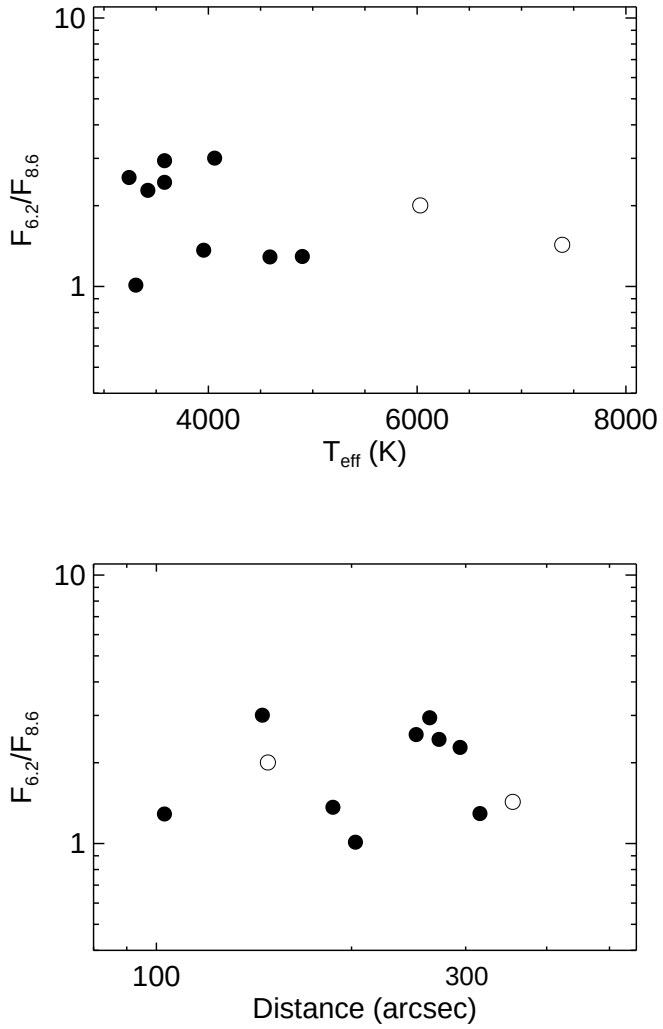


Figure E.2 $F_{6.2}/F_{8.6}$ vs. T_{eff} and distance from θ^1 Ori C.

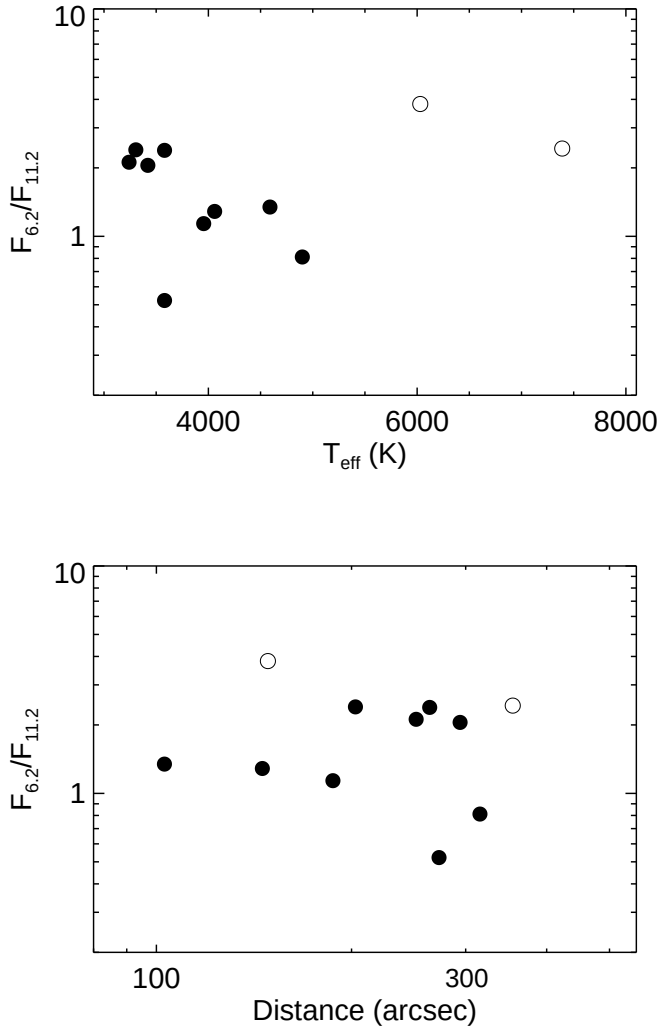


Figure E.3 $F_{6.2}/F_{11.2}$ vs. T_{eff} and distance from θ^1 Ori C.

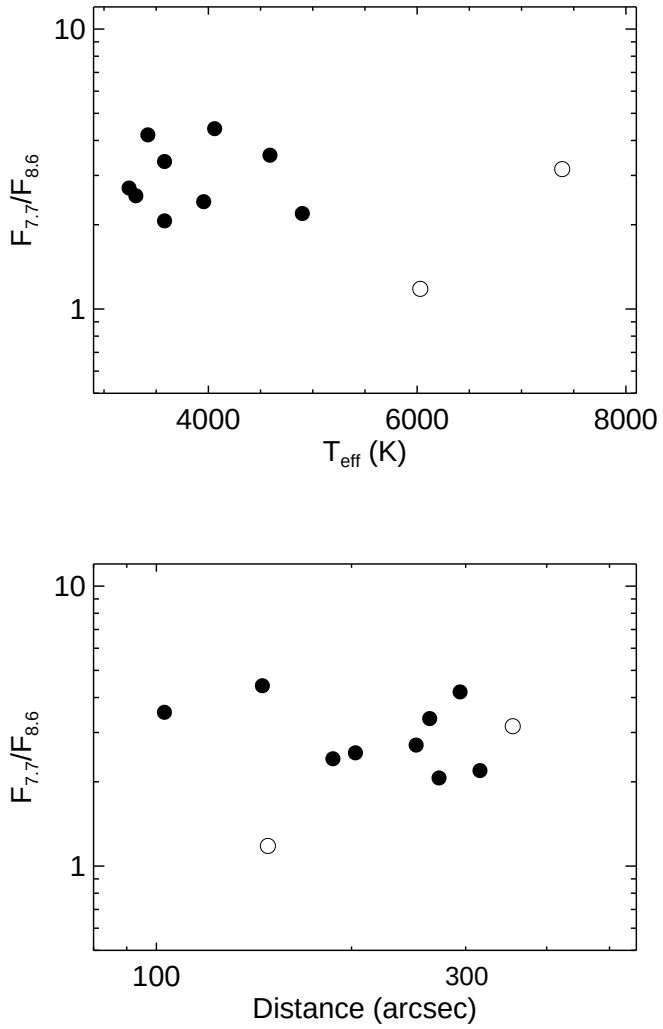


Figure E.4 $F_{7.7}/F_{8.6}$ vs. T_{eff} and distance from θ^1 Ori C.

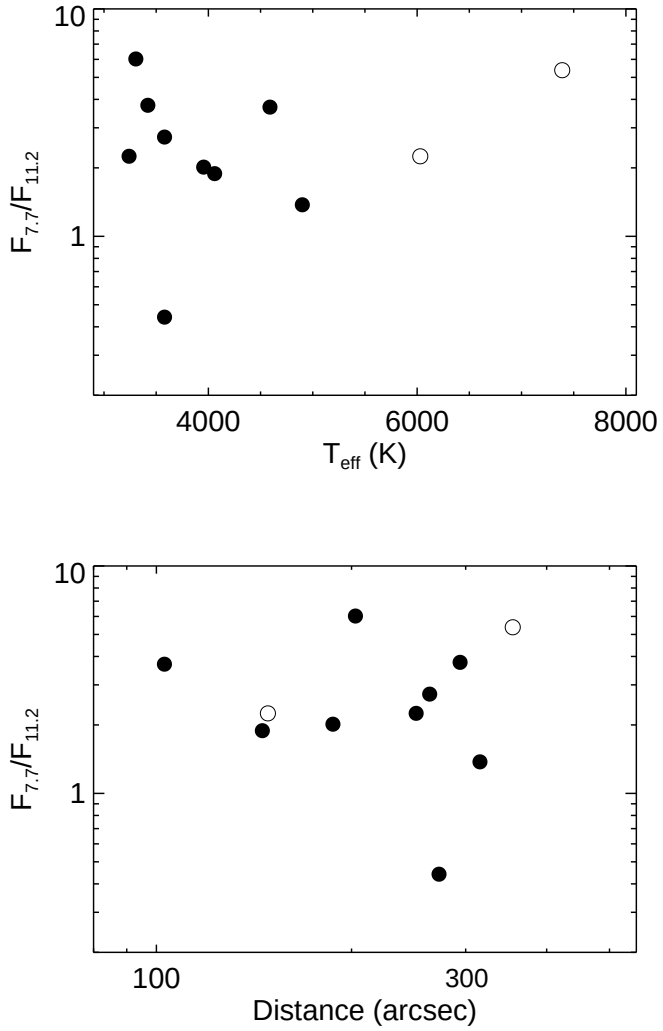


Figure E.5 $F_{7.7}/F_{11.2}$ vs. T_{eff} and distance from θ^1 Ori C.

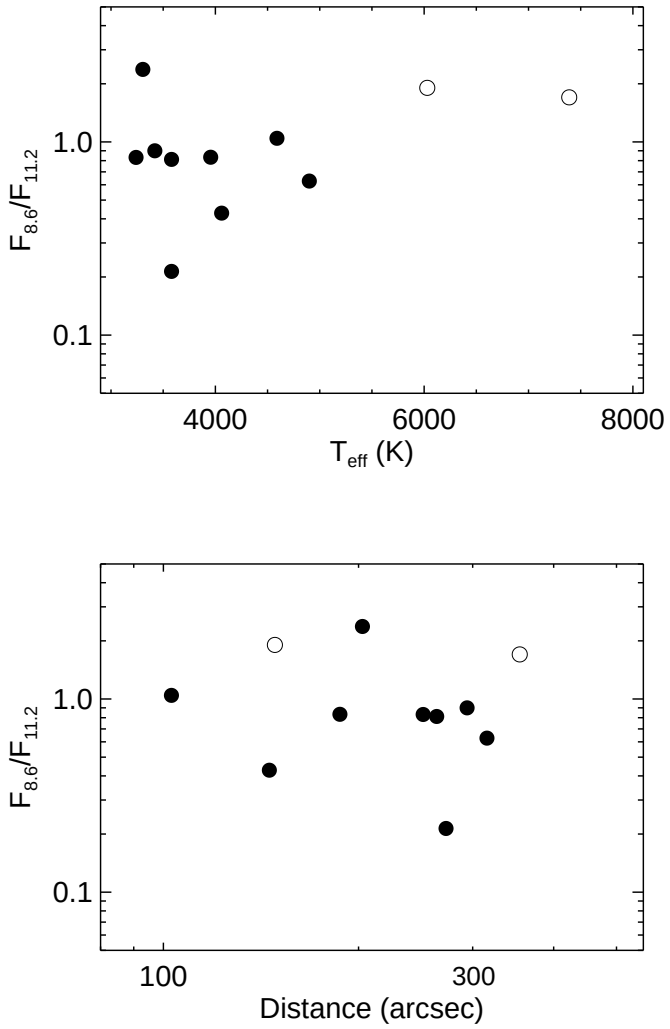


Figure E.6 $F_{8.6}/F_{11.2}$ vs. T_{eff} and distance from θ^1 Ori C.

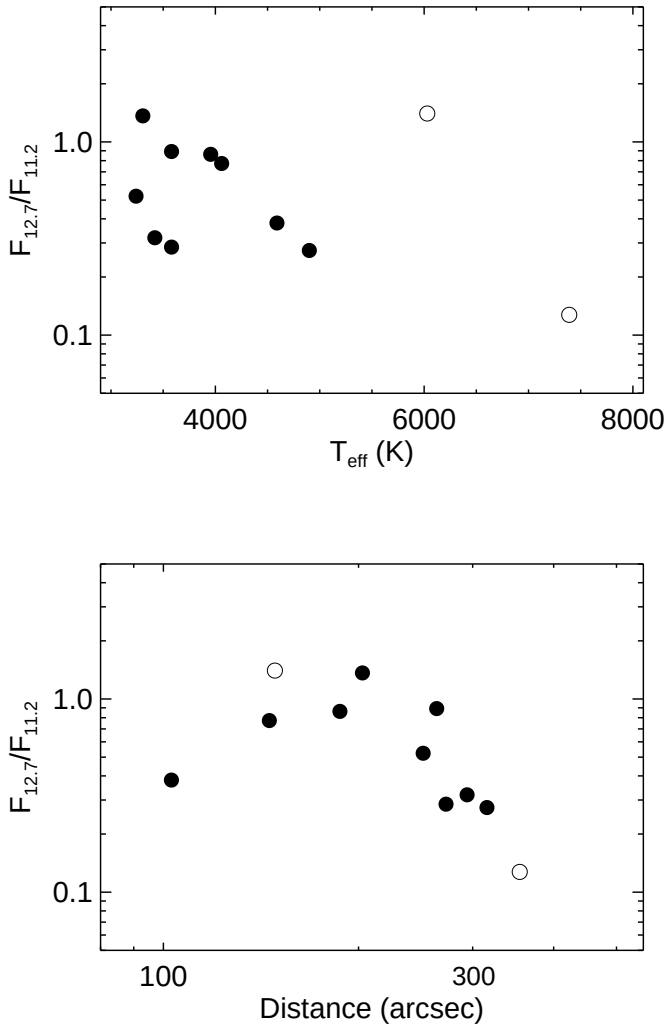


Figure E.7 $F_{12.7}/F_{11.2}$ vs. T_{eff} and distance from θ^1 Ori C.